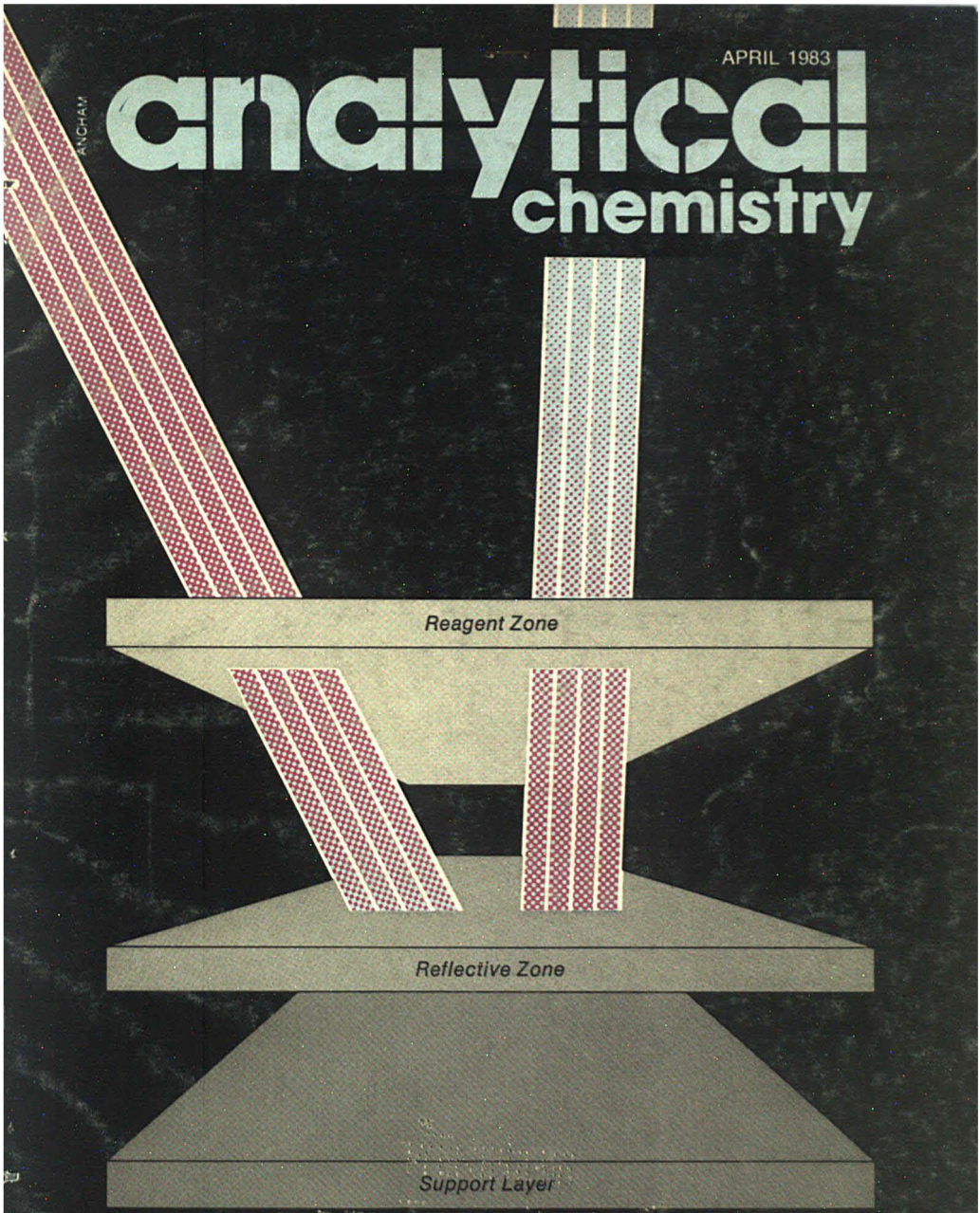
APRIL 1983

analytical chemistry

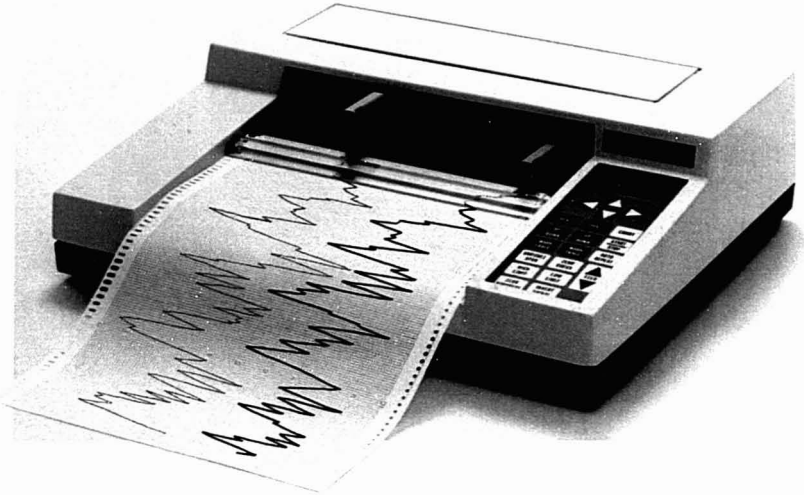


Dry Reagent Chemistries in Clinical Analysis

Report, Page 498 A

INTELLIGENT ANALOG STRIP-CHART RECORDER

The Houston Instrument Series 4500 MICROSCRIBE™



This New Cost Effective Recorder Has:

- Compact Size — yet a full 20 cm span width.
- Low Price* — yet provides 34 chart speeds, and 18 sensitivity ranges starting at 1 mv full scale.
- High Performance — from an improved servo system utilizing the time proven and patented Houston Instrument capacitive rebalance transducer. Fast 0.25 sec response.
- Clean Touch Control Panel — no knobs or switches to be disturbed.
- Dedicated microprocessor controls all functions and drives the LCD status display. Also runs continuous self test.
- Optional Digital Buss — enables your digitally-based system to remotely control all recorder functions.

These and many more advantages are yours in the new Houston Instrument Series 4500 Strip-Chart Recorder.

For the name, address and phone number of your nearest distributor, write Houston Instrument, 8500 Cameron Road, Austin, Texas 78753. Phone 512-835-0900, or 1-800-531-5205 if outside Texas. In Europe contact Bausch & Lomb Belgium NV., Rochesterlaan 6, 8240 Gistel, Belgium. Tel 059-27-74-45. Tlx 846-81399.

houston instrument

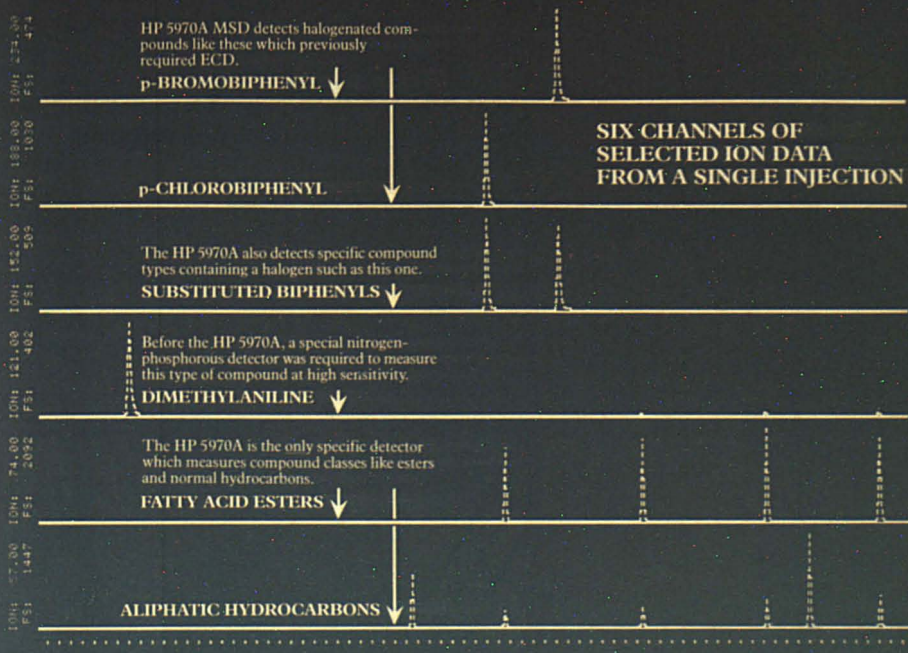
DIVISION OF **BAUSCH & LOMB**

*U.S. suggested list price: single pen $835, dual pen $1295.

4M009A

™ Microscribe is a Trademark of Houston Instrument.

CIRCLE 96 ON READER SERVICE CARD

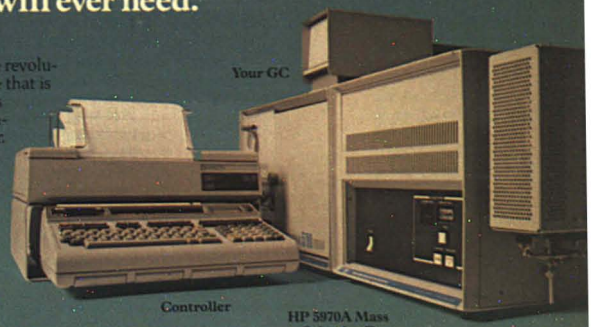


From now on, the new HP 5970A Mass Selective Detector may be the only capillary GC detector you will ever need.

Based on HP's proven quadrupole mass analyzer, the revolutionary HP 5970A is the first GC detector ever made that is both selective and universal. It permits unambiguous identification over almost the complete range of compounds a chromatographer will ordinarily encounter.

The HP 5970A can be mounted on either side of most capillary gas chromatographs. It is extremely compact, requires no special utilities and is as easy to use as any other selective GC detector.

For more information on this exciting breakthrough in detector technology, call your local Hewlett-Packard sales office and ask for an Analytical representative or write: Hewlett-Packard Co., Analytical Group, 1820 Embarcadero Rd., Palo Alto, CA 94303.



Circle 94 for literature. Circle 95 for an HP representative to contact you.

When performance must be measured by results

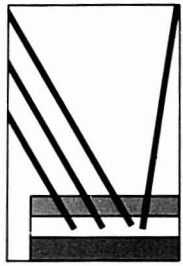
HEWLETT PACKARD

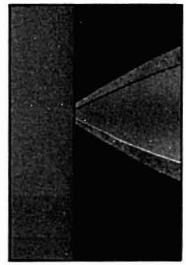
AG 04203A

analytical chemistry®

APRIL 1983

COVER FEATURE





REPORT

Dry reagent chemistries. Advances in dry reagent chemistries have made it possible to develop carriers for almost any chemical analysis. Bert Walter of Miles Laboratories describes the basic features and advantages of these carriers in clinical analysis

498 A

INSTRUMENTATION

Supersonic jet spectroscopy. The physics of cooling in supersonic expansions and the potential analytical applications are described by John Hayes and Gerald Small of Ames Laboratory–USDOE

565 A

FOCUS

Software secrets. A controversy has arisen as to whether instrument vendors are providing sufficient information about instrument-associated software to permit users to understand invisible data transformations going on inside the machine

519 A

Volume 55, No. 4
April 1983
ANCHAM
55(4) 469A–578A
593–816 (1983)
ISSN 0003 2700

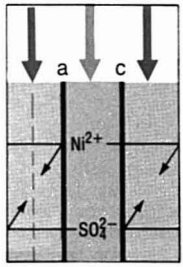
Registered in U.S. Patent and Trademark Office; Copyright 1983 by the American Chemical Society

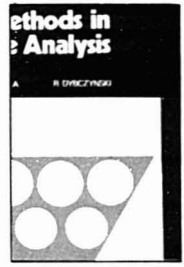
ANALYTICAL CHEMISTRY (ISSN 0003-2700) is published monthly with review issue added in April and Laboratory Guide in August by the American Chemical Society at 1155 16th St., N.W., Washington, D.C. 20036. Editorial offices are located at the same ACS address (202-872-4600). Second-class postage paid at Washington, D.C., and additional mailing offices. Postmaster: Send address changes to Membership & Subscription Services, P.O. Box 3337, Columbus, Ohio 43210.
Claims for missing numbers will not be allowed if loss was due to failure of notice of change of address to be received in the time specified; if claim is dated (a) North America: more than 90 days beyond issue date, (b) all other foreign: more than one year beyond issue date, or if the reason given is "missing from files."

Permission of the American Chemical Society is granted for libraries and other users to make reprographic copies for use beyond that permitted by Sections 107 or 108 of the U.S. Copyright Law, provided that the copying organization pays the appropriate per-copy fee through the Copyright Clearance Center, Inc., 21 Congress St., Salem, Mass. 01970 (617-744-3350). For reprint permission, write to Copyright Administrator, Books and Journals Division, ACS, 1155 16th St., N.W., Washington, D.C. 20036.

Advertising Management: Centcom, Ltd., 25 Sylvan Road South, Westport, Conn. 06881 (203) 226-7131

Technical Contents/Briefs ..... **474 A**
Letters ..... **490 A**
Call for Papers ..... **537 A**
Meetings ..... **538 A**
For Your Information ..... **538 A**
New Products ..... **546 A**
Chemicals ..... **548 A**
Manufacturers' Literature ..... **550 A**
Advertising Index ..... **576 A**
Author Index, Future Articles ..... **inside back cover**





NEWS

Fourier Transforms and Their Applications to Instrumental Analysis is the topic of this year's Summer Symposium on Analytical Chemistry, to be held June 21–23 in Lincoln, Neb.

531 A

THE ANALYTICAL APPROACH

Identification of a membrane foulant. Identification and/or removal of the compound causing the fouling is often an integral part of the overall recovery scheme in the disposal of nickel plating wastewater

551 A

BOOKS

Critical reviews. Books on analytical chemistry, inorganic trace analysis, and electroanalytical chemistry, and an audiovisual course on IR analysis are reviewed by R. A. Yost, Quintus Fernando, R. Mark Wightman, and Jack Koenig

559 A

EDITORS' COLUMN

Campus and company partnerships. Rapidly changing economic conditions have increased interest in mutually beneficial university–industry relationships

492 A

EDITORIAL

"Real" samples. Medical diagnosticians are already using a wide array of imaging techniques to extract information from the human body. It is now up to the imagination and ingenuity of analytical chemists to apply these techniques to complex and challenging analytical problems

593

1983 subscription rates include surface (and air freight) costs

Members	1 yr	2 yr
Domestic	18	30
Canada	37	68
Foreign	37 (113)	68 (220)
Nonmembers:		
Domestic	24	40
Canada	43	78
Foreign	67 (143)	120 (272)

Three-year and other rates contact: Membership & Subscription Services, ACS, P.O. Box 3337, Columbus, Ohio 43210, (614) 421-3776

Subscription orders by phone may be charged to Visa, MasterCard, Barclay card, or Access. Call toll free at (800) 424-6747 from anywhere in the continental U.S.; from Washington, D.C., call 872-8065. Mail orders for new and renewal subscriptions should be sent with payment to the Treasurer's Office at the Washington address.

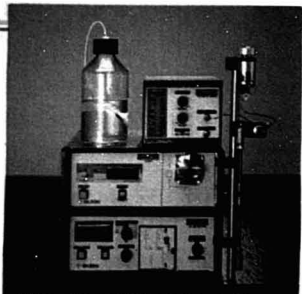
Subscription service inquiries and changes of address (include both old and new addresses with ZIP code and *recent mailing label*) should be directed to the ACS Columbus address noted above. Please allow six weeks for change of address to become effective.

ACS membership information: Ann Donahue, Washington address.

Single issues, current year, $6.00 except review issue and LabGuide, $7.25; **back issues and volumes and microform editions** available by single volume or back issue collection. For information or to order, call (800) 424-6747 or write the Sales Department at the Washington address.

Nonmember rates in Japan: Rates at left do not apply to nonmember subscribers in Japan, who must enter subscription orders with Maruzen Company Ltd., 3-10 Nihonbashi 2-chome, Chuo-ku, Tokyo 103, Japan. Tel: (03) 272-7211.

ห้องสมุดกรมวิทยาศาสตร์บริการ



Gilson Isocratic System *including precision pump, UV detector and column. This may be the only HPLC system you'll ever need. On the other hand, it could be just the beginning.*

GILSON's add-on approach to HPLC adds up to...

Look at it this way: we can tailor a system precisely for the separations you are doing right now. Later you can add on to change sample size, switch applications or expand in many other ways. Here's how it works. We design our HPLC systems so that you can add on at the level required to make the change you want without costly duplication of other components. For example, assume you've been doing analytical separations with a Gilson gradient system and you want to scale up to preparative. Add a new pump head, not a new pump; add a new flow cell, not a different detector; and to collect your fractions add our elevating kit, not a whole new fraction collector. You get the idea—adding on at the appropriate level without costly duplication: that's the Gilson approach.



Gilson Gradient Controller—*includes Apple II Plus microcomputer, software disks, Gilson Serial I/O Channel (GSIOC) interface and remote-control switching module; offers full gradient control of solvent composition and flow rate.*



Isocratic System *with a combination of UV and fluorescence detectors. A new configuration that is sparking a lot of interest.*

Looking at it another way, adding on with Gilson is a snap. Our hardware and software people design with your convenience in mind. Gilson's pump heads are called quick-change for good reason. And our software packages are designed to be cumulative so they can grow as your system does. For example, the Data Master disk contains a comprehensive program combining gradient control and data analysis software. To top it off, we build same-size, stackable modules whenever possible, so you can add on the space-saving, vertical way.



Data Master—*includes analysis module and software disk; uses Apple computer and NEC printer. Provides peak integration with multiple post-run analyses and baseline correction modes.*

Finally, look to the future because with Gilson there is more to come. We are hard at work developing new software, hardware and HPLC applications support. So take your pick—add on one at a time or all at once. For less than you might have thought possible. Send for our latest brochure or call to arrange for a demonstration... We'd like to hear from you.

Gilson—for the truly modular, cost-effective approach to HPLC.

Apple is a registered trademark of Apple Computer, Inc.

...the right system at the right price.



Going with Gilson can add up to this. *Gilson Gradient System with Apple-base gradient Controller, Data Master for peak analysis and programmable 201 fraction collector.*

*...all for less than $21,000.**

GILSON
INTERNATIONAL

Box 27, 3000 W. Beltline, Middleton, WI 53562
Telephone (608) 836-1551

B.P. No. 45, 95400, Villiers-le-Bel, France
Telephone (3) 990.54.41

**U.S. shipments only*

See us at FASEB Booths E-6, E-8, E-10 and F-5, F-7, F-9.
Circle #66 for literature. Circle #67, have your representative call on us.

Briefs

Aromatic Diesel Emissions as a Function of Engine Conditions 594

Concentrations of alkyl homologues of PAH and oxy-PAH on diesel particulates decrease as cylinder temperature increases. The degree of alkylation for the most abundant homologue increases by one to two carbons as the cylinder exhaust temperature decreases.

Trescott E. Jensen and Ronald A. Hites*, School of Public and Environmental Affairs and Department of Chemistry, Indiana University, Bloomington, Ind. 47405 *Anal. Chem., 55 (1983)*

Determination of Oxygenated Polycyclic Aromatic Hydrocarbons in Airborne Particulate Matter by Capillary Gas Chromatography and Gas Chromatography/Mass Spectrometry 599

Thirty-eight individual compounds, including ketones, quinones, anhydrides, coumarines, and aldehydes, are characterized by their retention indexes and mass spectra.

Johann König*, Eckhard Balfanz, Werner Funcke, and Thomas Romanowski, Fraunhofer-Institut für Toxikologie und Aerosolforschung, Nottulner Landweg 102, D 4400 Münster-Roxel, Federal Republic of Germany *Anal. Chem., 55 (1983)*

Spectrophotometric Determination of Atmospheric Nitrogen Monoxide and Nitrogen Dioxide after Collection with [*N,N'*-Ethylenebis(salicylideniminato)]cobalt 604

O_3, NH_3, SO_2, CO, and H_2O do not interfere under the usual sampling conditions. Detection limits are 2 ppb-h for NO and 1 ppb-h for NO_2.

Koichiro Ishii* and Kazuyuki Aoki, Tokyo Metropolitan Research Institute for Environmental Protection, Yurakucho 2-7-1, Chiyoda-ku, Tokyo 100, Japan *Anal. Chem., 55 (1983)*

Determination of Trace Quantities of Dimethyl Sulfide in Aqueous Solutions 608

Detection limit is 0.03 ng S (dimethyl sulfide), corresponding to a concentration of 0.3 ng L^{-1} for a 100-mL sample. Precision is 6.2%. Dimethyl sulfide is measured in a variety of natural waters.

M. O. Andreae* and W. R. Barnard, Department of Oceanography, Florida State University, Tallahassee, Fla. 32306 *Anal. Chem., 55 (1983)*

Simultaneous Determination of Hydrogen Peroxide, Peroxymonosulfuric Acid, and Peroxydisulfuric Acid by Thermometric Titrimetry 612

H_2SO_5, H_2O_2, and $H_2S_2O_8$ are determined in the range 100–1000 μmol. The method is based on differences between reaction rates and ΔH values in reactions of the peroxides with Fe^{2+}.

Phillippe E. A. Boudeville, Laboratoire Chimie Analytique, U.E.R. du Médicament, Faculté de Médecine et Pharmacie, 2, avenue du Professeur Léon Bernard, 35043 Rennes Cedex, France *Anal. Chem., 55 (1983)*

Generation of an Electrochemical Data Base for Pattern Recognition 615

Percent ethanol, pH, surfactant concentration, number of cycles, scan rate, and mercury hang drop time produce changes that are unique and reproducible in cyclic differential capacity curves and cyclic staircase voltammograms.

W. Arthur Byers and S. P. Perone*, Department of Chemistry, Purdue University, West Lafayette, Ind. 47907 *Anal. Chem., 55 (1983)*

Structural and Activity Characterization of Organic Compounds by Electroanalysis and Pattern Recognition 620

Structural classifications with 93.3% accuracy are possible using capacitive and Faradaic responses. Classifications of herbicidal activity are made for nitrodiphenyl ethers.

W. Arthur Byers, B. S. Freiser, and S. P. Perone*, Department of Chemistry, Purdue University, West Lafayette, Ind. 47907 *Anal. Chem., 55 (1983)*

Pattern Recognition for Identification and Quantitation of Complex Mixtures in Chromatography 626

Currently available chromatographic data systems are used to provide pattern recognition, quantitation, and elimination of interferences with simple programming techniques. PCB mixtures are determined.

Robert E. Lea, Entek, Inc., 1015 South Louisiana, Little Rock, Ark. 72202, and **Randall Bramston-Cook***, Varian Associates, Instrument Group, 9901 Paramount Boulevard, Downey, Calif. 90240, and **Janice Tschida**, Varian Associates, Instrument Group, 4665 Kipling Avenue, Wheatridge, Colo. 80033 *Anal. Chem., 55 (1983)*

Factor Analysis for Separation of Pure Component Spectra from Mixture Spectra 630

Normalization of spectra permits extension of the procedure to systems without fixed pathlength. Numerical examples, model spectra, and IR spectra illustrate the technique.

Paul C. Gillette, Jerome B. Lando, and Jack L. Koenig*, Department of Macromolecular Science, Case Western Reserve University, Cleveland, Ohio 44106 *Anal. Chem., 55 (1983)*

Abstract Factor Analysis of Solid-State Nuclear Magnetic Resonance Spectra 633

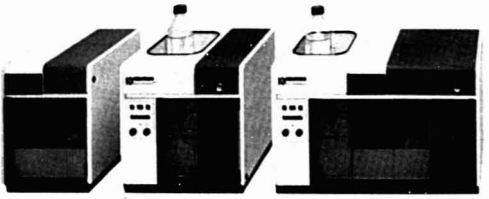
Differential cross-polarization (CP) rates are an experimental means to produce factor-analyzable "spin mixture" spectra. ^{31}P CP-magic-angle spinning spectra of octacalcium phosphate are analyzed to reveal three components.

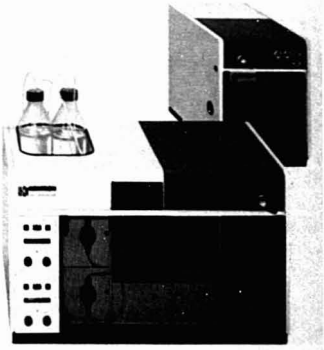
D. W. Kormos and J. S. Waugh*, Department of Chemistry, Massachusetts Institute of Technology, Cambridge, Mass. 02139 *Anal. Chem., 55 (1983)*

* Corresponding author

Looking for a compact AND flexible HPLC instrument?

HPLC 600





KONTRON
Your partner in modern HPLC

KONTRON
ANALYTICAL

Australia (Sydney)	(02) 9383433	Germany (Munich)	(08165) 771	Netherlands (Maarssen)	(03465) 60894
Austria (Vienna)	(0222) 670631	Great Britain (St. Albans)	(0727) 66222	Spain (Madrid)	(01) 7291155
Canada (Mississauga)	(416) 6781151	Italy (Milan)	(02) 50721	Sweden (Täby)	(08) 7567330
France (Vélizy)	(3) 9469722	Japan (Tokyo)	(03214) 5371	Switzerland (Zurich)	(01) 435 4111

U.S.A.: Kontron Electronics Inc., 630 Price Avenue, Redwood City/California 94063, (415) 3611012

Circle 121 for information. Circle 122 for a demonstration.

Briefs

Determining the Lowest Limit of Reliable Assay Measurement 638

Assay limit criteria formulas are derived for the heterogeneous variance situation. Widely disparate results can occur, depending on whether weights are employed and how they are selected.

Leonard Oppenheimer*, Thomas P. Capizzi, Roger M. Weppelman, and Hina Mehta, Merck Sharp & Dohme Research Laboratories, P.O. Box 2000, Rahway, N.J. 07065

Anal. Chem., 55 (1983)

Partial Least-Squares Method for Spectrofluorimetric Analysis of Mixtures of Humic Acid and Ligninsulfonate 643

Overlapping fluorescence spectra are resolved by the method of partial least squares in latent variables. Comparison is made with other numerical methods.

Walter Lindberg* and Jan-Åke Persson, Department of Analytical Chemistry, Unversity of Umeå, S-901 87 Umeå, Sweden, and **Svante Wold,** Research Group for Chemometrics, University of Umeå, S-901 87 Umeå, Sweden

Anal. Chem., 55 (1983)

Digital Smoothing of Noisy Spectra 648

The effect of smoothing on unknown spectral line properties such as shape, height, width, and position is considered theoretically to simplify the selection of filter types.

Manfred U. A. Bromba* and Horst Ziegler, FB 6—Angewandte Physik, Universität Paderborn, D-4790 Paderborn, West Germany

Anal. Chem., 55 (1983)

Phase-Plane and Guggenheim Methods for Treatment of Kinetic Data 653

The phase-plane method is more accurate than the Guggenheim method when the data are noisy, have a large baseline contribution, or are collected over less-than-optimum fitting regions.

J. Roger Bacon*, Chemistry Department, Western Carolina University, Cullowhee, N.C. 28723, and **J. N. Demas*,** Chemistry Department, University of Virginia, Charlottesville, Va. 22901

Anal. Chem., 55 (1983)

Kinetics of Extraction of Nickel with 8-Mercaptoquinoline 656

The rate-determining steps are the concurrent reactions of nickel(II) ion with neutral and anionic forms of 8-mercaptoquinoline in the aqueous phase.

Kensaku Haraguchi and Henry Freiser*, Department of Chemistry, University of Arizona, Tucson, Ariz. 85721

Anal. Chem., 55 (1983)

Determination of Partition Coefficient of Polar Organic Solutes in Octanol/Micellar Solutions 659

Shake-flask measurements of apparent partition coefficients of solutes in octanol/micellar solutions at several surfactant concentrations verify an equation derived for the simultaneous determination of partition coefficients in micelles/water and octanol/water.

G. M. Janini* and S. A. Attari, Department of Chemistry, University of Kuwait, Kuwait

Anal. Chem., 55 (1983)

Microemulsions in the Extraction of Gallium with 7-(1-Ethenyl-3,3,5,5-tetramethylhexyl)-8-quinolinol from Aluminate Solutions 662

The radius of microemulsion droplets is estimated to be 20–50 Å for the extraction of Ga with a butanol/carboxylate mixture. A large fraction of extractant is adsorbed on the droplets.

P. Fourré and D. Bauer*, Laboratoire de Chimie Analytique des Processus Industriels, 10, rue Vauquelin, 75231 Paris Cedex 05, France, and **Jean Lemerle,** Laboratoire de Polymères inorganiques, Université Pierre et Marie Curie, 8, rue Cuvier, 75230 Paris Cedex 05, France

Anal. Chem., 55 (1983)

Immobilized Morin as Fluorescence Sensor for Determination of Aluminum(III) 667

Response of the sensor is linear over the range 1×10^{-6}–1×10^{-4} M Al^{3+} at pH 4.8. Detection limit is 1×10^{-6} M, and response time is 1–2 min.

Linda A. Saari and W. Rudolf Seitz*, Department of Chemistry, University of New Hampshire, Durham, N.H. 03824

Anal. Chem., 55 (1983)

Laser Microprobe Mass Analysis of Asbestos Fiber Surfaces for Organic Compounds 671

Benzo[*a*]pyrene, benzidine, and oxidation products of *N,N*-dimethylaniline are detected on the surface of individual asbestos fibers under laser desorption conditions.

J. K. De Waele, E. F. Vansant, P. Van Espen, and F. C. Adams*, Department of Chemistry, Universitaire Instelling Antwerpen (U.I.A.), Universiteitsplein 1, B-2610 Wilrijk, Belgium

Anal. Chem., 55 (1983)

Determination of Chlorinated Pesticides in Urine by Molecular Neutron Activation Analysis 677

A solvent extraction/liquid chromatography separation is combined with neutron activation detection of ^{38}Cl to determine DDT and its metabolites in the ppb range. Confirmation analysis is made by mass spectrometry.

Laura R. Opelanio and Edward P. Rack*, Department of Chemistry, University of Nebraska—Lincoln, Lincoln, Neb. 68588-0304, and **Alan J. Blotcky,** Medical Research, Veterans Administration Medical Center, Omaha, Neb. 68105, and **Frank W. Crow,** Midwest Center for Mass Spectrometry, University of Nebraska—Lincoln, Lincoln, Neb. 68588-0304

Anal. Chem., 55 (1983)



A Class of One.

Whatman.
Glass microfibre filters.
Retention 0.7 μm to 2.7 μm;
high speed; high loading capacity.
The purity of borosilicate
glass. Nothing else. Consistent uniformity.
Grades for every application.
Circles and sheets.

From laboratory supply dealers worldwide.

For comprehensive technical literature, please write: *Whatman Laboratory Products Inc.*
Whatman Paper Division □ 9 Bridewell Place, Clifton, New Jersey 07014, Tel: (201) 773-5800.

ห้องสมุดกรมวิทยาศาสตร์บริการ

PAPER DIVISION

Whatman

See Us at FASEB, Booth Nos. G13 and G15.

Briefs

Determination of Arsenic, Molybdenum, Uranium, and Vanadium in Seawater by Neutron Activation Analysis after Preconcentration by Colloid Flotation 682

Hydrous iron(III) oxide is floated, in the presence of sodium dodecyl sulfate and tiny nitrogen bubbles, from 1 L of seawater at pH 5.7 ± 0.2. Recoveries of As, Mo, and V are better than 95% and recovery of U is about 75%.

R. S. Shreedhara Murthy and Douglas E. Ryan*, Trace Analysis Research Centre, Chemistry Department, Dalhousie University, Halifax, Nova Scotia B3H 4J1, Canada *Anal. Chem., 55 (1983)*

Raman Spectrometric Determination of Tribasic Sodium Phosphate Hydrolysis Quotient 684

The hydrolysis quotient ranges from near 0.004 M at phosphate concentrations above 0.01 M to 0.014 M at infinite dilution. The third dissociation constant of phosphoric acid is calculated as 7.1×10^{-13} M.

Allan G. Miller*, Analytical Laboratories, Rockwell Hanford Operations, Richland, Wash. 99352, and **John W. Macklin,** Department of Chemistry, University of Washington, Seattle, Wash. 98195 *Anal. Chem., 55 (1983)*

Atomic Fluorescence Spectrometry with Inductively Coupled Plasma as Excitation Source and Atomization Cell 688

Emission, excitation, and fluorescence analytical curves of growth are obtained along with vertical distributions for zinc atomic and calcium ionic fluorescence intensities. Limits of detection for 16 elements are compared to fluorescence detection limits using other radiation sources.

M. A. Kosinski, Hiroshi Uchida, and J. D. Winefordner*, Department of Chemistry, University of Florida, Gainesville, Fla. 32611 *Anal. Chem., 55 (1983)*

Furnace Atomic Absorption Spectrometry Atomizer with Independent Control of Volatilization and Atomization Conditions 692

Separate, optically sensed, temperature-feedback-controlled power supplies heat the atomization and vaporization zones. Some matrix interferences observed in analyses with conventional furnaces are reduced or eliminated.

Darryl D. Siemer, Exxon Nuclear Idaho Co., CPP 602, Idaho Falls, Idaho 83402 *Anal. Chem., 55 (1983)*

Differential Normal Pulse Voltammetric Oxidation of Mercury in the Presence of Iodide 698

Low iodide concentrations and small pulse widths limit surface coverage of adsorbed product to a small fraction of a full monolayer. Under these conditions, differential normal pulse responses are diffusion controlled and provide linear analytical working curves.

Timothy R. Brumleve, Robert A. Osteryoung, and Janet Osteryoung*, Department of Chemistry, State University of New York at Buffalo, Buffalo, N.Y. 14214 *Anal. Chem., 55 (1983)*

Faradaic Response in Derivative and Differential Normal Pulse Voltammetry 704

Peak-shaped voltammograms arising from differential pulse, differential normal pulse, and the normal pulse difference modes of pulse voltammetry are compared for reversible systems and for systems with heterogeneous charge transfer control.

Milivoy Lovrić, John J. O'Dea, and Janet Osteryoung*, Department of Chemistry, State University of New York at Buffalo, Buffalo, N.Y. 14214 *Anal. Chem., 55 (1983)*

Determination of Pertechnetate by Liquid Chromatography with Reductive Electrochemical Detection 708

The detection limit of 8.5×10^{-9} M allows determination of TcO_4^- (as both $^{99m}TcO_4^-$ and $^{99}TcO_4^-$) in $^{99}Mo/^{99m}Tc$ generator eluents. No sample pretreatment is necessary.

Jane Y. Lewis, Julius P. Zodda, Edward Deutsch, and William R. Heineman*, Department of Chemistry, University of Cincinnati, Cincinnati, Ohio 45221 *Anal. Chem., 55 (1983)*

Linearization of Electron Capture Detector Response to Strongly Responding Compounds 713

An alternate definition of response is described for a constant-current electron capture detector. With this response function, linear calibration curves are obtained for CCl_4 and $CFCl_3$ over the entire dynamic range of the instrument.

W. B. Knighton and E. P. Grimsrud*, Department of Chemistry, Montana State University, Bozeman, Mont. 59717 *Anal. Chem., 55 (1983)*

Automated Determination of Nickel and Copper by Liquid Chromatography with Electrochemical and Spectrophotometric Detection 718

The microprocessor-based monitoring system includes in situ formation of dithiocarbamate complexes, separation of complexes by reversed-phase LC, and dual electrochemical and UV/VIS spectrophotometric detection.

A. M. Bond* and G. G. Wallace, Division of Chemical and Physical Sciences, Deakin University, Waurn Ponds 3217, Victoria, Australia *Anal. Chem., 55 (1983)*

Speciation of Intermediate Polar Material in Coal Derived Process Solvents by Liquid Chromatography/Fourier Transform Infrared Spectrometry 723

Intermediate polar fractions contain predominantly aromatic cyclic secondary amines and highly hindered phenols. Nonhydrotreated coal-derived material contains more etheric species than the hydrotreated material.

Robert S. Brown and Larry T. Taylor*, Department of Chemistry, Virginia Polytechnic Institute and State University, Blacksburg, Va. 24061 *Anal. Chem., 55 (1983)*

UNSOLVABLE ANALYSIS PROBLEMS?



Dionex Ion Chromatography solves the tough ion analysis problems that HPLC, GC, AA, electrochemistry and wet chemistry just can't handle. No matter what the matrix, no matter what the class of ions, Dionex Ion Chromatography overcomes frustrating interference, speciation and detection problems. And it can generate a payback for many applications in just a few months.

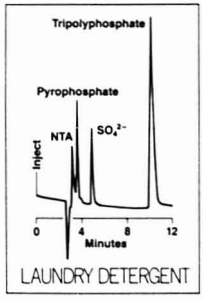
PROBLEMS

Here are just two examples.

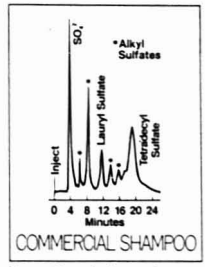
- Analysis of laundry powders is difficult because they are a complicated blend of polyphosphates, chelating agents and bleaching agents.
- Shampoo analyses involve complex mixtures of surfactants, soaps and dyes.

SOLUTIONS

Dionex Series 2000i Ion Chromatographs™ provide fast solutions to both types of problems. Just dilute the samples and inject. In less than 15 minutes, phosphates, sulfate, organophosphonates, EDTA and NTA in a commercial laundry powder may be accurately determined. Dionex Ion Chromatography also provides a definitive profile of the anionic surfactants in a shampoo, without interference from cationic and nonionic surfactants or common inorganic anions. And it can easily speciate organic sulfates from sulfonates.



LAUNDRY DETERGENT



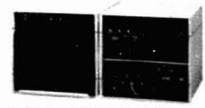
COMMERCIAL SHAMPOO

No matter what your ion problem – metals, inorganic or organic ions, or amino acids – Dionex has the solution.

LET'S GET STARTED

Call the nearest Dionex Regional Office today for a demonstration. Then calculate the payback for your *own* ion analysis problems!

Sunnyvale, CA
(408) 737-0700
Marlton, NJ
(609) 596-0600
Houston, TX
(713) 847-5652
Chicago, IL
(312) 860-1030
Camberley, England
0276-29771
Darmstadt, W. Germany
06150-12258



DIONEX CORPORATION
1228 Titan Way
Sunnyvale, CA 94086
U.S.A.

SERIES 2000i
DIONEX™
ION CHROMATOGRAPHS™

THE SOLUTION

CIRCLE 58 ON READER SERVICE CARD

Briefs

Equations for Calculation of Chromatographic Figures of Merit for Ideal and Skewed Peaks 730

Width and asymmetry factor (B/A) measurements at 10% peak height are recommended. Equations for the number of theoretical plates and variance are accurate to within ±1% for $1.00 \leq B/A \leq 2.76$.

Joe P. Foley and John G. Dorsey*, Department of Chemistry, University of Florida, Gainesville, Fla. 32611

Anal. Chem., 55 (1983)

Prediction of Gas Chromatographic Retention Indexes with Topological, Physicochemical, and Quantum Chemical Parameters 738

Retention behavior on apolar stationary phases is best explained by a combination of quantum chemically calculated electronic parameters and a topological parameter. Quantum chemical charge parameters related to local polarity describe retention behavior for polar stationary phases.

Lutgarde Buydens and Désiré L. Massart*, Vrije Universiteit Brussel, Farmaceutisch Instituut, Laarbeeklaan 103, B-1090 Brussel, Belgium, and, **Paul Geerlings**, Vrije Universiteit Brussel, Algemene Chemie, Faculteit Wetenschappen, Pleinlaan 2, B-1090 Brussel, Belgium *Anal. Chem., 55 (1983)*

Comparison of Gas Chromatography/High-Resolution Mass Spectrometry and Mass Spectrometry/Mass Spectrometry for Detection of Polychlorinated Biphenyls and Tetrachlorodibenzofuran 744

For a 10 μg/μL butyl stearate matrix, matrix effects increase the signal intensity by a factor of 17 for GC introduction of TCDF. The same sample analyzed by direct probe shows a loss in intensity relative to the nonmatrix standard.

Robert D. Voyksner and J. Ronald Hass*, National Institute of Environmental Health Sciences, P.O. Box 12233, Research Triangle Park, N.C. 27709, and **G. Wayne Sovocool**, U.S. Environmental Protection Agency, EMSL-LV, QAD, P.O. Box 15027, Las Vegas, Nev. 89114, and **Maurice M. Bursey**, Department of Chemistry, University of North Carolina, Chapel Hill, N.C. 27514 *Anal. Chem., 55 (1983)*

Thermospray Interface for Liquid Chromatography/Mass Spectrometry 750

LC effluents are thermosprayed directly into the ion source, and excess vapor is pumped away by an added mechanical pump. The system provides stable vaporization and ionization at flow rates up to 2 mL/min of aqueous mobile phase.

C. R. Blakley and M. L. Vestal*, Department of Chemistry, University of Houston, Houston, Tex. 77004

Anal. Chem., 55 (1983)

Nitrous Oxide as Reagent Gas for Positive Ion Chemical Ionization Mass Spectrometry 754

The low-energy NO^+ ion frequently gives M^+ or $(M + NO)^+$ ions for molecular weight determinations. The higher energy N_2O^+ ion gives significant amounts of fragmentation from dissociative charge exchange with aliphatic systems.

Charles W. Polley, Jr. and Burnaby Munson*, Department of Chemistry, University of Delaware, Newark, Del. 19711

Anal. Chem., 55 (1983)

Chemical and Toxicologic Characterization of Fossil Fuel Combustion Product Phenalen-1-one 758

Phenalen-1-one is differentiated from fluoren-9-one and benzo[c]cinnoline by GC/MS, high-resolution mass spectrometry, and LC with high-speed photometric detection. Retention data are reported for both gas and liquid chromatography.

Julie A. Leary, Arthur L. Lafleur, Howard L. Liber, and Klaus Biemann*, Department of Chemistry, Department of Nutrition and Food Science, and Energy Laboratory, Massachusetts Institute of Technology, 77 Massachusetts Avenue, Cambridge, Mass. 02139 *Anal. Chem., 55 (1983)*

Utilization of Natural Isotopic Abundance Ratios in Tandem Mass Spectrometry 762

This approach is applicable even to mixtures so complex that the characteristic isotope pattern cannot be recognized in the mass spectrum. General expressions are derived to predict expected isotopic abundance ratios for MS/MS spectra.

Kathleen E. Singleton and R. Graham Cooks*, Department of Chemistry, Purdue University, West Lafayette, Ind. 47907, and, **Karl V. Wood**, Engine/Fuels Laboratory, Institute of Interdisciplinary Engineering Studies, Chemistry Building, Purdue University, West Lafayette, Ind. 47907

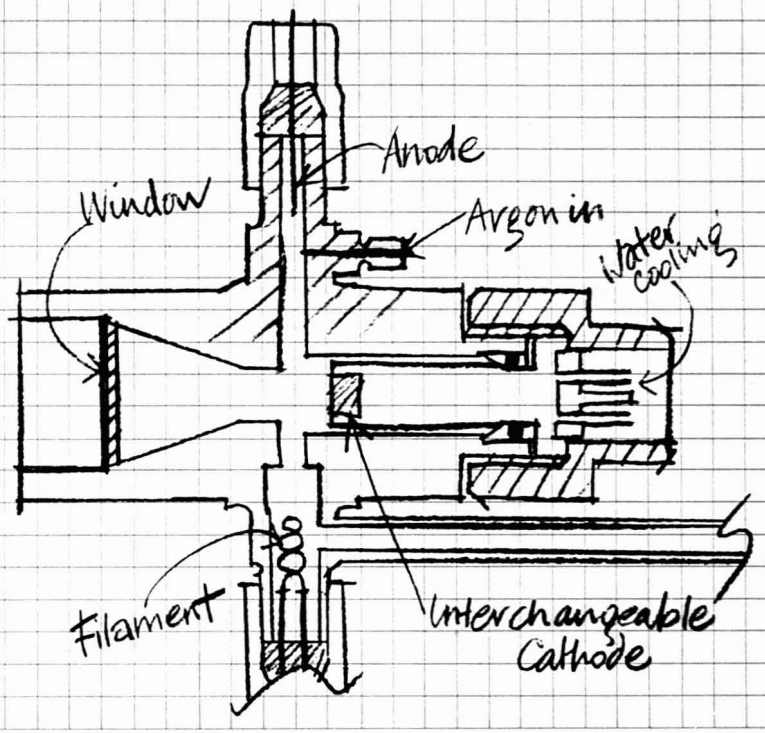
Anal. Chem., 55 (1983)

Atomic Ion Formation and Measurement with Resonance Ionization Mass Spectrometry 765

In the one-wavelength, two-photon ionization scheme, the first photon resonantly excites a bound transition in the near-ultraviolet region, and a second photon promotes the electron into the ionization continuum.

J. D. Fassett*, J. C. Travis, and L. J. Moore, Center for Analytical Chemistry, National Measurement Laboratory, National Bureau of Standards, Washington, D.C. 20234, and **F. E. Lytle**, Department of Chemistry, Purdue University, West Lafayette, Ind. 47907 *Anal. Chem., 55 (1983)*

From a brilliant idea to a brilliant lamp.

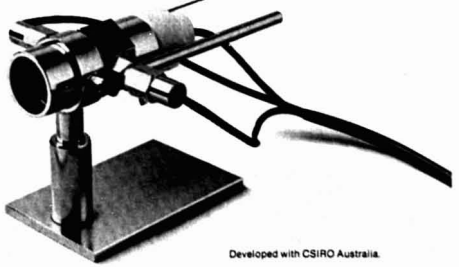


SGE's Demountable Cathode Lamp can be used for all AA analyses. It is no longer necessary to use a special spectral lamp for a particular element - now you can simply plug in an inexpensive interchangeable cathode. Less is suddenly a great deal more.

Not only does the SGE Demountable Cathode Lamp combine the performances of HCL's and EDL's, it also offers the advantages of rapid warm-up, high brightness, stability and narrow line width.

Rugged construction and low cost are good reasons why you should have this system, but other important factors are:

Single and multi-element cathodes can be changed quickly and without cross-contamination, multi-element cathodes can be made at short notice by SGE, or even by the user; and the lamp can be used for AA, fluorescence and emission.



Developed with CSIRO Australia.

Head Office and International Sales
Scientific Glass Engineering Pty Ltd
7 Argent Place Ringwood
Victoria 3134 Australia.
Telephone (03) 874 6333

UK Sales Office
Scientific Glass Engineering (UK) Ltd
Potters Lane Kiln Farm
Milton Keynes MK11 3LA Great Britain
Telephone (0908) 56 8844

U.S.A. Sales Office
Scientific Glass Engineering Inc
2007 Kramer Lane Suite 100
Austin Texas 78758 USA
Telephone (512) 837 7190

German (BRD) Sales Office
Scientific Glass Engineering GmbH
Fichtenweg 15
D-6108 Weiterstadt 1
Telephone (06150) 40662

SGE

CIRCLE 193 ON READER SERVICE CARD

MEMO

TO:

All Gas Chromatographers

FROM:

Instrumentation Gases Product Manager

SUBJECT:

Electron Capture Carrier Gases

A gas chromatograph equipped with an electron capture detector (ECD) is a very sensitive analytical instrument. It is a proven tool for analyzing electronegative functional groups such as halogenated compounds, but achieving optimum performance requires attention to detail.

The presence or introduction of electronegative impurities, e.g., oxygen and moisture, into the carrier gas has a detrimental effect on performance by increasing baseline noise and drift, while reducing sensitivity and linear range. You can minimize the risk of having these impurities jeopardize your results by using high purity carrier gases and the proper gas transport system between the cylinder and your instrument. For optimum performance in ECD-GC, Matheson offers 99.999% minimum purity Nitrogen and both Ultra P-5 and Ultra P-10 carrier gases. Blended to the most stringent specifications, Ultra P-5 and P-10 offer increased sensitivity and stability. Matheson also provides the Hydrox® Purifier which is capable of upgrading your standard P-5 or P-10 carrier gas by reducing the levels of oxygen and water to 0.1 ppm.

The key to a high purity transfer system is the Matheson 3104 pressure regulator. It features two stage design, a stainless steel diaphragm and a diaphragm packless valve. The stainless steel diaphragm and special high purity diaphragm packless valve protect against diffusion of impurities such as oxygen and water into the gas stream.

Matheson, the leader in specialty gases, is responsive to your instrument gas and accessory requirements. This is why we offer you more than one choice for better performance of your ECD.

For more information on electron capture and other applications of Matheson specialty gases in gas chromatography, please contact your nearest Matheson branch or circle the Reader Service Number below.

Matheson®

30 Seaview Drive, Secaucus, NJ 07094

CIRCLE 144 ON READER SERVICE CARD

Briefs

Kinetic and Equilibrium Studies of Insulin Immunoaffinity Chromatography 771

Computer simulation and experimental data demonstrate the contribution of nonspecific interactions with the support to the overall binding process. The rate of the antibody–antigen complex formation reaction is estimated.

J. Richard Sportsman, James D. Liddil, and George S. Wilson*, Department of Chemistry, University of Arizona, Tucson, Ariz. 85721 *Anal. Chem., 55 (1983)*

Determination of Rate Constants of Pseudo-First-Order Electrocatalytic Reactions from Overlapped Voltammetric Data 776

Nonlinear regression of overlapped voltammetric data gives more precise electrocatalytic rate constants than background subtraction. Deviation-pattern recognition distinguishes between catalytic and noncatalytic systems with severely overlapped voltammograms.

James F. Rusling* and Thomas F. Connors, Department of Chemistry, U-60, University of Connecticut, Storrs, Conn. 06268 *Anal. Chem., 55 (1983)*

Software for Quantitative Analysis by Carbon-13 Fourier Transform Nuclear Magnetic Resonance Spectrometry 782

Components of a high dynamic range mixture present at mole ratios of 88.83%, 5.59%, 1.08%, 0.27%, and 0.13% are determined as 87.50% (0.57), 5.43% (0.17), 1.04% (0.09), 0.28% (0.12), and 0.12% (0.07), respectively, with values in parentheses denoting ±1 SD.

Christopher H. Sotak, Charles L. Dumoulin, and George C. Levy*, NIH Resource for Multi-Nuclei NMR and Data Processing, Department of Chemistry, Syracuse University, Syracuse, N.Y. 13210 *Anal. Chem., 55 (1983)*

Correspondence

Study of Chromatographic Retention with Spectroscopic Bandwidths 787

Mary J. Wirth*, David A. Hahn, and Ronald A. Holland, Department of Chemistry, University of Wisconsin—Madison, Madison, Wis. 53706 *Anal. Chem., 55 (1983)*

Investigation of Adsorption of Benzene on Nickel(001) by Secondary Ion Mass Spectrometry 790

Nicholas Winograd* and E. J. Karwacki, The Pennsylvania State University, 152 Davey Laboratory, Department of Chemistry, University Park, Pa. 16802 *Anal. Chem., 55 (1983)*

Karl Fischer Titration Equation on Mass Basis 793

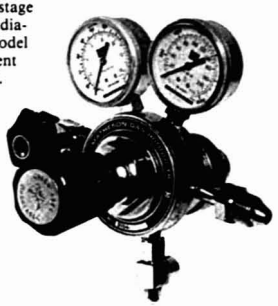
Frank E. Jones, Center for Chemical Engineering, National Engineering Laboratory, National Bureau of Standards, Washington, D.C. 20234 *Anal. Chem., 55 (1983)*

Special Matheson Products

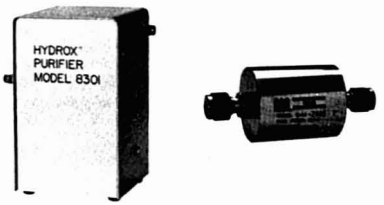
Improve GC Techniques

Pure Gases. Use the right gas! Don't use a welding grade of gas for a gas chromatograph. It can contain substantial amounts of water and oxygen. Matheson recommends UHP Helium or HP Helium for thermal conductivity detectors, a "zero gas" for FID and a special higher purity Ultra P-5 and Ultra P-10 for electron capture detectors. These are available from all Matheson plants. Circle No. 10

Use a Regulator Which Minimizes Diffusion. We recommend a two stage regulator with a metal diaphragm such as our Model 3104, which has excellent outlet pressure control. It minimizes inboard leakage of air or water from the atmosphere and does not outgas impurities into the carrier or fuel gas system as rubber diaphragm regulators can. Circle No. 11



Purifiers and Filters. Matheson supplies specially purified gases for GC, but we also recommend the addition of a filter or purifier to the system. Purifiers and filters remove trace water, oil, oxygen and particulates. In using such devices in our own laboratories, we find we can enhance the performance of our GC's. Circle No. 12



Calibration Standards. Sometimes called reference standards and span gases, these are gas mixtures and are the best means of calibrating a GC.

Matheson has prepared valuable tables and related information on Calibration Standards: "Gas Mixtures; Facts and Fables", and a wall chart entitled "How To Succeed At Gas Chromatography". These are available for the asking. Circle No. 13

Improve AA Techniques

Acetylene, 99.6% and Nitrous Oxide, 99.0%. Gases containing minimum impurities give less interference with final results. Matheson gases are specially purified for AA instrument use. Circle No. 14

Series 6103 Flash Arrestor. A flash arrestor is installed downstream after the regulator and cylinder. Should flashback occur, with the accompanying shock wave, the Matheson Flash Arrestor will seal off the path to both regulator and cylinder. This will prevent an explosion of greater magnitude in the regulator or cylinder. For more information, Circle No. 15

450 Purifier. The model 450 is a purifier with 454 activated charcoal filled replaceable cartridges. It is specially designed for controlling the acetone vapor from acetylene. It belongs in an AA system. Circle No. 16



Nitrous Oxide Heater. Because nitrous oxide, frequently used as an oxidizer gas in AA, is a liquefied gas, or a gas over liquid contents in a cylinder, it often cools or ices on expansion, causing problems in automatic control. The heater we offer is installed between cylinder and regulator and eliminates icing and allows for higher flows. Thermostatically controlled, the N_2O is not overheated and the flow can be left unattended. Works simply with 115 Vac. Circle No. 17



Automatic Regulators 1PA-150 and 1L-326. If you are using AA, choose the correct regulators. In the laboratory, use regulators designed for the specific gas. Information on these regulators can be obtained, Circle No. 18

Cylinder Scale, Model 8510. To judge accurately when a liquefied gas is nearing empty, Matheson has designed and sells a cylinder scale. We recommend this for nitrous oxide because it will let you know . . . and it's the only way . . . when the cylinder is empty. Invaluable! Circle No. 19

For further information, contact Matheson, 30 Seaview Drive, Secaucus, N.J. 07094.

Matheson®

Complete Chromatographic Media Selection

When separating components from a heterogeneous biological sample, it is important to utilize differences between the components of interest and its contaminants. The exploited difference may be charge, size, biological activity or other physical or chemical characteristic.

Pharmacia offers you a wide selection of innovative, high quality chromatographic media suited to virtually every separation problem. Select from over 30 gel filtration products. Purify your sample with the unique, high resolution technique Chromatofocusing, separating proteins according to their isoelectric point.

For your convenience, ready to use group specific affinity adsorbents as well as pre-activated media are available. Pharmacia supplies alternative protein separation media for hydrophobic interaction chromatography and metal chelate affinity chromatography. Write for complete information on our wide selection of chromatographic media today.



122

PHARMACIA FINE CHEMICALS
Division of Pharmacia, Inc.
Piscataway, NJ 08854
Orders Only: (NJ) 201-457-8150
800-526-3593
Information: 201-457-8000

Pharmacia Fine Chemicals

Visit us at Booths E35, 37, 39 & 41 at the FASEB Show.
CIRCLE 171 ON READER SERVICE CARD

Briefs

Comments on Sorption Capacities of Graphitized Carbon Black in Determination of Chlorinated Pesticide Traces in Water 793

Fabrizio Bruner*, Giancarlo Crescentini, and Filippo Mangani, Instituto di Scienze Chimiche, Universita di Urbino, Piazza Rinascimento, 6-61029 Urbino, Italy, and **Robert Petty*,** Marine Science Institute, University of California, Santa Barbara, Calif. 93106 *Anal. Chem., 55 (1983)*

Aids for Analytical Chemists

Semiquantitative Screening Test for Cocaine 795

Basil Travnikoff, P.O. Box 287, Lodi, Calif. 95241 *Anal. Chem., 55 (1983)*

Determination of Bromine in Blood Serum by Epithermal Neutron Activation Analysis 796

Zeev B. Alfassi*, Department of Nuclear Engineering, Ben-Gurion University of the Negev, Beer-Sheva 84121, P.O.B. 653, Israel, and **Nathan Lavi,** Soreq Nuclear Research Center, Yavne, Israel *Anal. Chem., 55 (1983)*

Determination of Quantum Yields of Fluorescence by Optimizing the Fluorescence Intensity 798

Clifford L. Renschler* and Larry A. Harrah, Sandia National Laboratories, Albuquerque, N.M. 87185 *Anal. Chem., 55 (1983)*

Hydrogen–Tritium Exchange between Glass-Fiber Filters and Tritiated Water 800

William P. Bryan, Department of Biochemistry, Indiana University School of Medicine, Indianapolis, Ind. 46223 *Anal. Chem., 55 (1983)*

Thermal Vaporization for One-Drop Sample Introduction into the Inductively Coupled Plasma 802

Eiichi Kitazume, Central Research Laboratory, Hitachi Ltd., Kokubunji, Tokyo 185, Japan *Anal. Chem., 55 (1983)*

Breath Analysis by Atmospheric Pressure Ionization Mass Spectrometry 805

Frank M. Benoit*, Environmental Health Directorate, Health and Welfare Canada, Tunney's Pasture, Ottawa, Ontario K1A 0L2, Canada, and **W. R. Davidson, A. M. Lovett, Sabatino Nacson, and Angie Ngo,** Sciex Inc., 55 Glencameron Road, Thornhill, Ontario L3T 1P2, Canada *Anal. Chem., 55 (1983)*

Modification of a Centrifugal Filtration Device for Direct Filtration into an Autosampler Vial 807

I. A. Eiseman and L. A. Pachla*, Warner-Lambert/Parke-Davis Pharmaceutical Research Division, Warner-Lambert Company, Ann Arbor, Mich. 48105 *Anal. Chem., 55 (1983)*

For $5890.00 you get Generations of Quality, Performance, Experience...

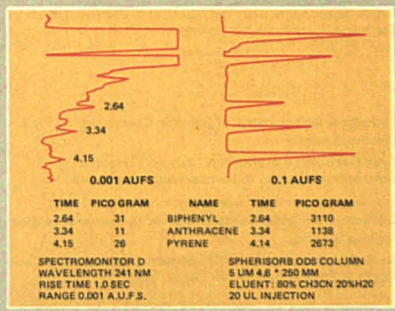


The new LDC/Milton Roy spectroMonitor®D variable wavelength detector.

On the outside, the newest variable wavelength detector from LDC/Milton Roy looks very much like its predecessors. But on the inside, *where it counts*, the spectroMonitor®D variable wavelength detector sets new industry standards for quality and performance.

LOWEST NOISE AND DRIFT

The new spectroMonitor D variable wavelength detector delivers the lowest noise (2×10^{-5} AU peak to peak) and drift (1×10^{-4} AU/hr.) specifications available today. Highly efficient dual beam optical system and state-of-the-art electronics make these specifications possible.



TIME	PICO GRAM	NAME	TIME	PICO GRAM
2.64	31	BIPHENYL	2.64	3110
3.34	11	ANTHRACENE	3.34	1138
4.15	26	PYRENE	4.14	2673

SPECTROMONITOR D
WAVELENGTH 241 NM
RISE TIME 1.0 SEC
RANGE 0.001 A.U.F.S.

SPHERISORB ODS COLUMN
5 UM 4.6 * 250 MM
ELUENT: 80% CH3CN 20%H20
20 UL INJECTION

Chromatogram illustrating detection limits with the spectroMonitor D.

HIGHEST EFFICIENCY AND SENSITIVITY - STANDARD

Our new max N™ series high efficiency, high pressure (1000 psi) fluid cell is a standard feature in the spectroMonitor D. The competition makes you pay extra for high efficiency. In addition, the max N series fluid cell has optimized flow dynamics and a *true* 10mm pathlength to maximize sensitivity according to Beer's Law. Others have tried to beat our noise and drift specifications by cutting cell pathlength, but in the process, they decreased sensitivity. With the spectroMonitor D you get it all - low noise, low drift *and* high sensitivity.

UV/VIS MEASUREMENTS

The spectroMonitor D also features absorbance measurements over the entire UV/VIS spectrum (190-700nm) *without* a lamp change. One 35-Watt deuterium lamp is all you need to buy or replace.

DIGITAL DIAGNOSTICS

New LED diagnostic circuitry, introduced in the spectroMonitor D, provides you with a switch selectable digital display of absorbance units, reference and sample energy in mV, lamp current in mA, and zero offset.

A TRADITION OF QUALITY AND PERFORMANCE

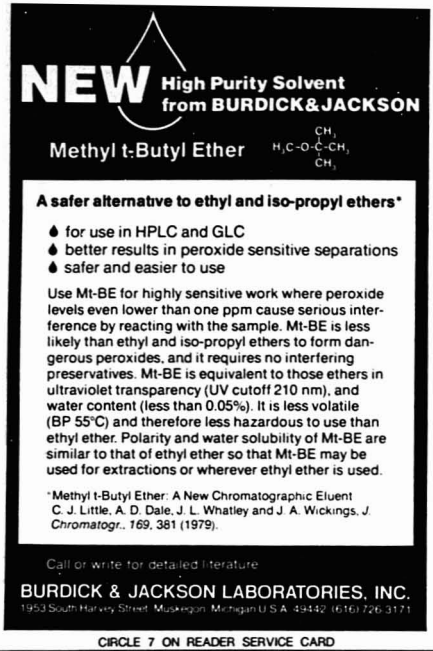
LDC/Milton Roy pioneered HPLC technology over a decade ago. We have put all of our technological experience and knowledge into making an instrument that is worth much more than its $5890.00 price. Let us show how the spectroMonitor D can work for you.

For further information call our Technical Representatives at **800-327-6182.**

LDC/Milton Roy

U.S. HEADQUARTERS, P.O. Box 10235, Riviera Beach, FL 33404 Toll-free: 800-327-6182, In Florida: (305) 844-5241 International Telex: 441098, Domestic Telex: 513479
SUNNYVALE OPERATION, 560 Oakmead Parkway, Sunnyvale, CA 94086 Toll-free: 800-538-1595, In California: (408) 736-0300
UNITED KINGDOM, LDC UK, Milton Roy House, 52 High Street, Stone, Staffordshire ST15 8AR England Phone: 785-81-3542 Telex: 36623
WEST GERMANY, Milton Roy (Deutschland) GMBH Johnstrasse 22-24 6467 Hasselroth 2, West Germany Phone: 6055-2031 (3366) Telex: 4184357
JAPAN, Milton Roy K.K., Takanawa Dai-Ichi Building 21-41, Takanawa 2-Chrome, Minato-Ku, Tokyo 108, Japan Phone: (03) 473-3181 Telex: 242-4296

CIRCLE 133 ON READER SERVICE CARD



CIRCLE 7 ON READER SERVICE CARD

"OUTSTANDING"

THE ATOMIC COMPLEX

by BERTRAND GOLDSCHMIDT

An accurate, complete and fascinating worldwide political history and personal memoir of nuclear energy — from the development of the bomb in World War II to today's nuclear energy complex and proliferation problems.

"READS EASILY"

Goldschmidt, a leading French scientist turned international statesman, reviews half a century of political moves, countermoves, international intrigue and manipulation. *The Atomic Complex* is a pragmatic look at the nuclear world today, carefully examining the terror nuclear weapons represent, but at the same time stressing the benefits of nuclear energy.

Order this 500 page best seller today.
$31 Hardbound $24 Softbound

American Nuclear Society
555 North Kensington Avenue
La Grange Park, IL 60525 USA

CIRCLE 4 ON READER SERVICE CARD

Briefs

Purification of Nitric Acid at Trace Metal Levels 808

Richard P. Maas* and Steven A. Dressing, Department of Environmental Sciences and Engineering, School of Public Health, University of North Carolina, Chapel Hill, N.C. 27514
Anal. Chem., 55 (1983)

Room-Temperature Gas Chromatography/Mass Spectrometry of Volatile Solids and of Volatiles Trapped in Solids 809

John R. Sutter*, James W. Wheeler, Arnold S. Collier, William M. Jackson, and Thomas Rush, Department of Chemistry, Howard University, Washington, D.C. 20059
Anal. Chem., 55 (1983)

Removal of Oxygen from Solvents for Liquid Chromatography with Electrochemical Detection 810

Fred Senftleber*, Daniel Bowling, and M. Sonia Stahr, Department of Chemistry, Murray State University, Murray, Ky. 42071
Anal. Chem., 55 (1983)

Determination of Lead in Plant Ash by X-ray Fluorescence Spectrometry 812

Mark L. Dietz and Stanford L. Tackett*, Department of Chemistry, Indiana University of Pennsylvania, Indiana, Pa. 15705
Anal. Chem., 55 (1983)

Mass Spectrometer Polymer Membrane Sample Introduction Device 813

George J. Kallos and Nels H. Mahle*, Analytical Laboratories, Dow Chemical U.S.A., Midland, Mich. 48640
Anal. Chem., 55 (1983)

Determination of Carbon Isotope Ratios in Plant Starch via Selective Enzymatic Hydrolysis 814

Arndt Schimmelmann* and Michael J. DeNiro, Department of Earth and Space Sciences, University of California, Los Angeles, Calif. 90024
Anal. Chem., 55 (1983)

Correction. Determination of Diffusion Coefficients by Flow Injection Analysis 816

Greg Gerhardt and Ralph N. Adams*, Department of Chemistry, University of Kansas, Lawrence, Kan. 66045

Correction. Circuit for Constant Current Operation of an Electron Capture Detector 816

W. B. Knighton and E. P. Grimsrud*, Department of Chemistry, Montana State University, Bozeman, Mont. 59717

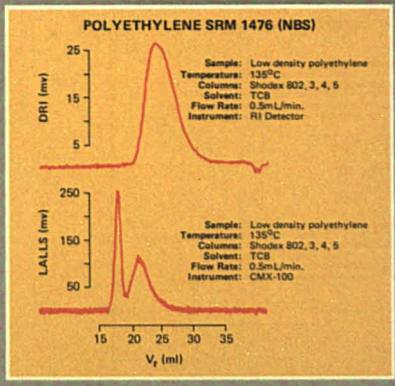
For Polymer Branching Information... Think Low Angle Laser Light Scattering



Chromatix® Low Angle Laser Light Scattering (LALLS) detectors and software give unique polymer branching data when coupled with Gel Permeation Chromatography (GPC).

RESULTS: NBS Polymer Standard SRM-1476 is known to contain branched material. The LALLS detector clearly indicates a high molecular weight fraction that is below the detection limit of the Differential Refractive Index (DRI) detector.

CONCLUSIONS: The CMX-100 LALLS detector is inherently sensitive to high $\bar{M}_w$ polymers and can yield unique results complementary to conventional GPC concentration detectors such as a differential refractive index unit (DRI). Only with LALLS can the polymer analyst realize the full potential of GPC for branched materials.



LALLS SOLVES PROBLEMS: It can easily detect the presence of that small concentration of high $\bar{M}_w$ polymer that would otherwise escape detection by using only a concentration detector. These unseen small concentrations of very high $\bar{M}_w$ branched polymers can dramatically alter the performance and processing characteristics of the material in many different applications. The production or end-use suitability of your polymer may be assured when LALLS data is used for routine quality control.

FAST AND EASY TO USE: The CMX-100 system is designed with unique features that save time and money:

- No GPC calibrations needed
- Absolute $\bar{M}_w$ for branched and linear polymers
- No lengthy and difficult post run calculations required

LDC/Milton Roy proprietary software dramatically extends the data generated by the CMX-100. It provides complete data formatting and many special calculation routines. All are available through easy-to-use-and-understand "menu"-driven prompting, specifically designed for the polymer chemist.

AFFORDABLE: The CMX-100 is designed to provide routine LALLS information to the polymer analyst at a surprisingly affordable price. The CMX-100 interfaces easily and quickly to your present GPC system and can operate at temperatures up to 150°C. It can be used with equal ease for aqueous and nonaqueous polymers.

COMPLETE SERVICE AND SUPPORT: Field service is now available through the extensive LDC/Milton Roy network. We maintain a complete applications laboratory to support your needs in GPC/LALLS. Call or write for additional information and the name of the nearest LDC/Milton Roy Sales/Service Representative.

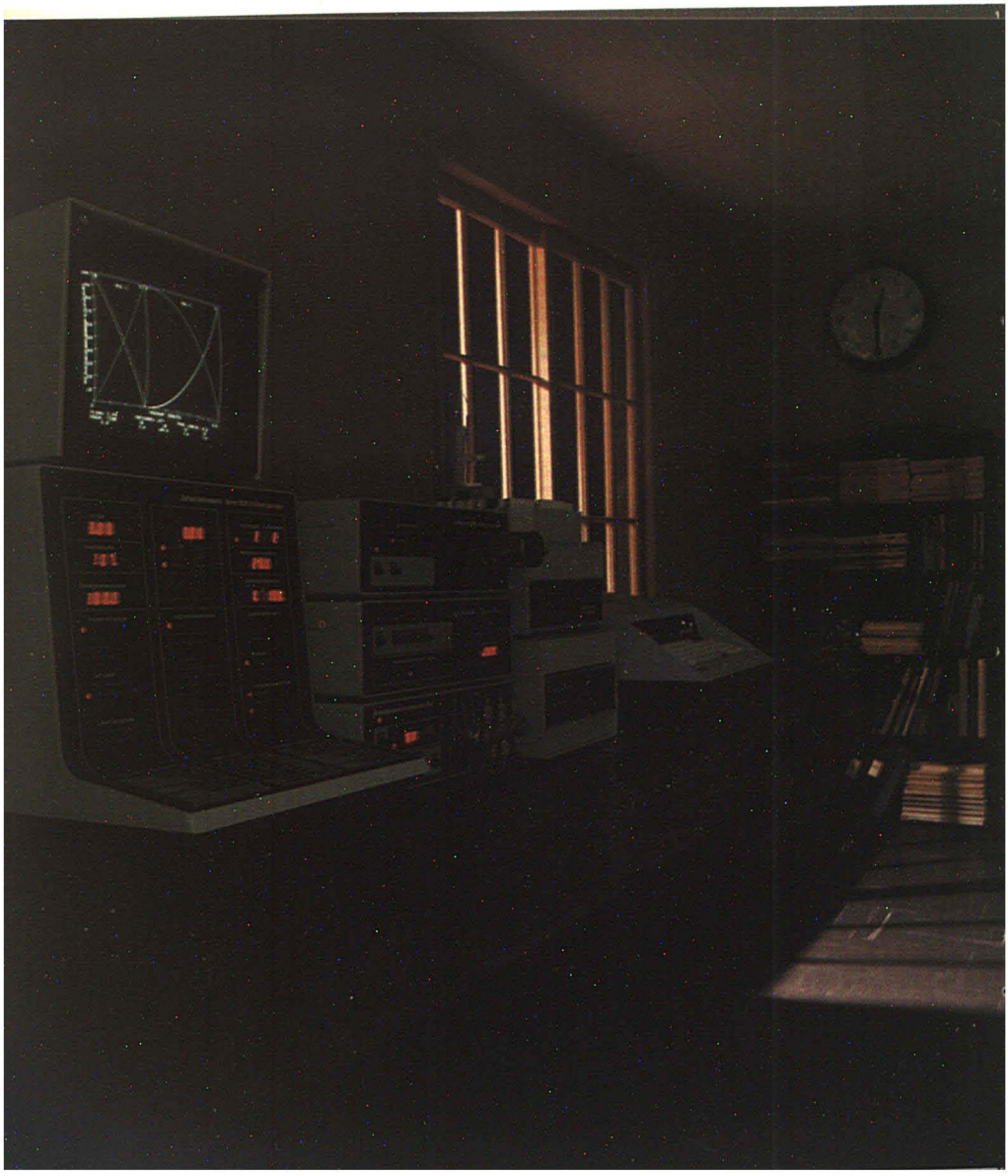
Chromatix® Product Manager
Toll Free 800-538-1595 or (408) 736-0300 (U.S.A. only)

LDC/Milton Roy

U.S. HEADQUARTERS, P.O. Box 10235, Riviera Beach, FL 33404 Toll-free: 800-327-6182, In Florida: (305) 844-8241 International Telex: 441098, Domestic Telex: 513479
SUNNYVALE OPERATION, 560 Oakmead Parkway, Sunnyvale, CA 94086 Toll-free: 800-538-1595, In California: (408) 736-0300
UNITED KINGDOM, LDC UK, Milton Roy House, 52 High Street, Stone, Staffordshire ST15 8AR England Phone: 785-81-3542 Telex: 36623
WEST GERMANY, Milton Roy (Deutschland) GMBH Jahnstrasse 22-24 6467 Hasselroth 2, West Germany Phone: 6055-2031 (3366) Telex: 4184357
JAPAN, Milton Roy K.K., Takanawa Dai-Ichi Building 21-41, Takanawa 2-Chome, Minato-Ku, Tokyo 108, Japan Phone: (03) 473-3181 Telex: 242-4296

CIRCLE 134 ON READER SERVICE CARD

DuPont's Sentinel works
It optimizes LC separations



even while you sleep. automatically in 12-24 hours.

DuPont's newest breakthrough frees you from the tedious calculations of methods development.

You can reduce methods development time to 12-24 hours with DuPont's Sentinel...rather than the weeks or month it can take with ordinary LC instruments. Sentinel, the first truly automated liquid chromatograph, uses the 4-solvent, 7-separation technique and gives you more time to concentrate on experimental design, make critical analytical decisions and evaluate your data.

Sentinel not only increases lab productivity, but frees you from the laborious and time-consuming methodology of optimizing complex LC separations. Sentinel improves the quality of your experiment to predict the values of the next one. It interacts with the chromatographic process and provides you with answers, not just data.

DuPont brings you this breakthrough by incorporating self-contained highly customized microprocessors in the Sentinel. These microprocessors automate the chromatographic procedures of L. L. Snyder and J. J. Kirkland involving the solvent selectivity triangle and the resulting 4-solvent, 7-step routine introduced by DuPont in 1981. There are five steps in Sentinel: "Sample," "Scout," "Search," "Separate" and "Sort."

Here's how they work:

In "Sample," you just enter column volume and retention desired, plus the number of vials to be used. Sentinel then provides autoinjection and autosampler functions, adjusts time sequences to fit your needs...and begins to complete the experiment you've created.

Next, "Scout" runs a routine standard gradient to determine if the separation can be run isocratically. Your time is not wasted. It also predicts the mobile phase concentration for the first isocratic experiment, to get desired retention time.

"Search" now runs the first experiment and compares the results with the predicted value. It learns from these results and corrects the mobile phase until results match your requirements. "Search" repeats this procedure as needed for each of the selectivity adjusting solvents defining the seven-step routine.

In "Separate," Sentinel now runs all seven experiments, which give you the needed data for optimization...saving more of your time.

"Sort" organizes and reports all the data gathered by "Separate." It automatically numbers all the peaks and highlights all changes in elution order.

Sentinel automated liquid chromatograph can be added to any DuPont 8800 HPLC System. It continues the DuPont philosophy of advancing instrumentation by add-on modules. Your HPLC system is never outmoded; it evolves with your growing needs.

Call us toll free, 800-441-9841, for more information, or write DuPont, Analytical Instruments Division, Room X39495, Wilmington, DE 19898.

Other offices throughout the United States and Canada; Netherlands; Stevenage, England; Bad Nauheim, Federal Republic of Germany; Paris; Milan; Mexico City; Caracas and Sao Paulo.

Compare technology and you will choose DuPont.

Analytical Instruments Division

DUPONT

Letters

Manufacturers' Software

Sir: I read with interest the Editorial on software and analytical instrumentation in the January 1983 issue of ANALYTICAL CHEMISTRY. The Perkin-Elmer Corporation has been in the forefront of the development of microcomputer-controlled analytical instrumentation. We are now developing analytical systems that include mini- and microcomputers as the controllers of the system. The expense of software engineering is approaching, and is about to exceed, the cost of the traditional mechanical and electrical engineering involved in analytical instrument development. Very often the product of several man-years of software engineering is a floppy disk containing applications software. Vendors of commercial instrumentation must be permitted to earn a profit on the development costs of such a product. The only way to do this is to ensure that the software is not copied.

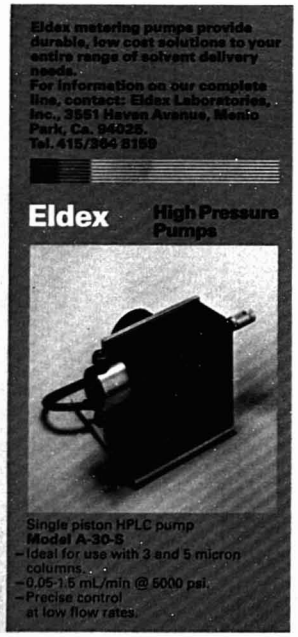
These proven software products are made available to users at a very reasonable price considering the time and resources involved in their development. Our customers generally recognize the value received compared to having to develop and debug the software themselves.

It is almost impossible to patent software, and copyright protection is usually very weak. If the source code is written in a high-level language, it could easily be modified to run on another computer that supports the same language. Thus the only opportunity is to treat the source code as a trade secret. The object code is usually specific for a certain hardware configuration; hence, its transportability is limited.

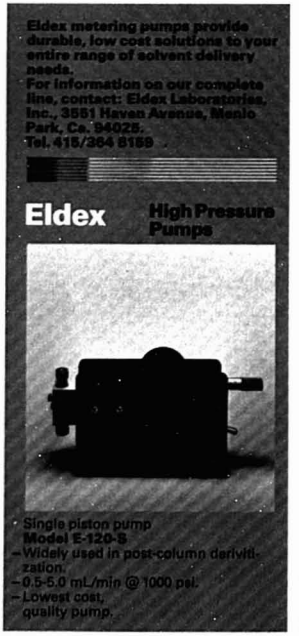
We agree that the purchaser should be able to understand the algorithms that are included in the software. In some cases, for example, the Sigma 10 and Sigma 15 Data Stations, we explain the algorithms in the manual. In other cases, however, we cannot explain the algorithms in detail because they would be easily translatable into programs by our competition and customers.

Software development consumes a very large portion of the expense of developing an instrument system. This investment must be protected to ensure that instrument manufacturers have the resources to pursue future research and development.

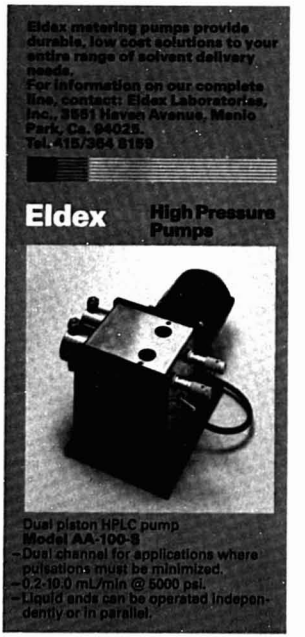
Melvin W. Redmond, Jr.
The Perkin-Elmer Corporation
Norwalk, Conn. 06856



CIRCLE 47 ON READER SERVICE CARD



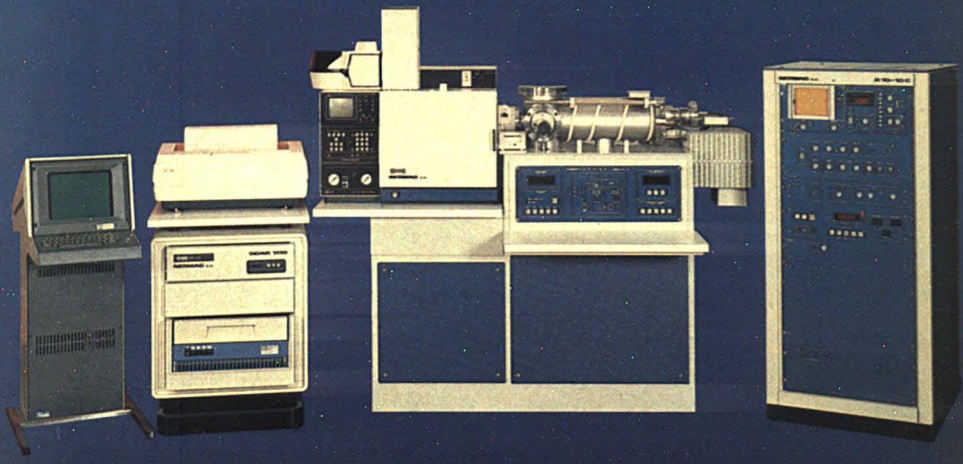
CIRCLE 48 ON READER SERVICE CARD



CIRCLE 49 ON READER SERVICE CARD

INTERESTING !

The time has come.
You may now select your mass spectrometer.



NERMAG GC/LC/MS/DS

ASK ABOUT OUR NEW LC/MS SYSTEM BASED ON DLI PRINCIPLE.
ALSO TAKE A LOOK AT OUR SIDAR 111 B.
DATA SYSTEM RUNNING ON A DEC® COMPUTER USING RS X 11 M® OPERATING SYSTEM.

S.N.G. NERMAG	NERMAG	NERMAG Ltd	NERMAG
49, quai du Halage	a division of DELSI Inc.	a subsidary of	a division of
92500 RUEIL MALMAISON	15423 Vantage Parkway, St. 100	DORAND ELECTRONICS Ltd	INTERSMAT Gmbh
FRANCE - Tél. (1) 732.92.05	HOUSTON Tx 77032	Poole, UK	Wuppertal, FRG
Télex 20.40.29 F	Tél. (713) 999 22 57	Tél. (0202) 62.20.06	Tél. (49)202.72.30.54

DEC and RSX11M are registered trade marks of Digital Equipment Corporation.

Our application labs are at your disposal in PARIS and HOUSTON. Please contact our sales engineers for a demonstration.

CIRCLE 155 ON READER SERVICE CARD.

Editors' Column

Campus and Company Partnerships

Rapidly changing economic conditions have increased interest in university–industry relationships within the academic and corporate communities. Programs such as Hewlett-Packard's contribution of analytical instrumentation to colleges and universities (*Anal. Chem.* **1983,** *55,* 47 A) and the Harvard–Monsanto and MIT–Exxon partnerships are examples of a 10-year upward trend in this activity, according to a report published by the National Science Board, the policy-making body of the National Science Foundation (NSF).

The report, entitled "University–Industry Research Relationships: Myths, Realities and Potentials," states that although most recent discussions attribute a base figure of between 3 and 4% of academic research and development to industrial sources, this is a significant underestimation due to several omissions, including the following:

- major research universities that do not report research and development expenditures from industrial sources,
- exclusion of industrial gifts and loans of scientific equipment from the data base,
- gifts from corporate-sponsored foundations not being counted as industrial support by many universities, and
- estimation of the portion of unrestricted corporate gifts of operating and capital funds that is spent on actual research expenses not being made.

The report states that "there are sound reasons to believe that we may be at the threshold of a permanent new state of corporate–academic research relationships." However, despite the likelihood of this trend increasing, it states that "all available evidence indicates that private industry has neither the resources nor the intention to compensate for any substantial cuts in publicly funded academic research. The implication is clear: If the present level of academic research is to be maintained, the principal burden will continue to fall upon the public purse, both federal and state governments."

The report identifies the mutual benefits as well as the difficulties and frictions involved in negotiating and conducting these partnerships. The innovative organizational experiments that the biotechnology field has given rise to are also discussed. In conclusion, it is suggested that the basis for a healthy strengthening of university–industry cooperation is not increased partnership, but increased understanding of each other's role.

The NSF report (038-000-00517-1) is available for $4.75 from the Superintendent of Documents, U.S. Government Printing Office, Washington, D.C. 20402.

Rani Anne George

Why are Milli-Q® owners switching to Gelman's Versacap?

Hundreds of lab water system users have switched to the Gelman Versacap capsule because it costs less, works better, lasts longer than any other final filtration unit available.



Versacap is available immediately from American Scientific Products, Fisher Scientific, VWR, CMS and A.H. Thomas. Order a capsule today and start saving money, time and trouble.

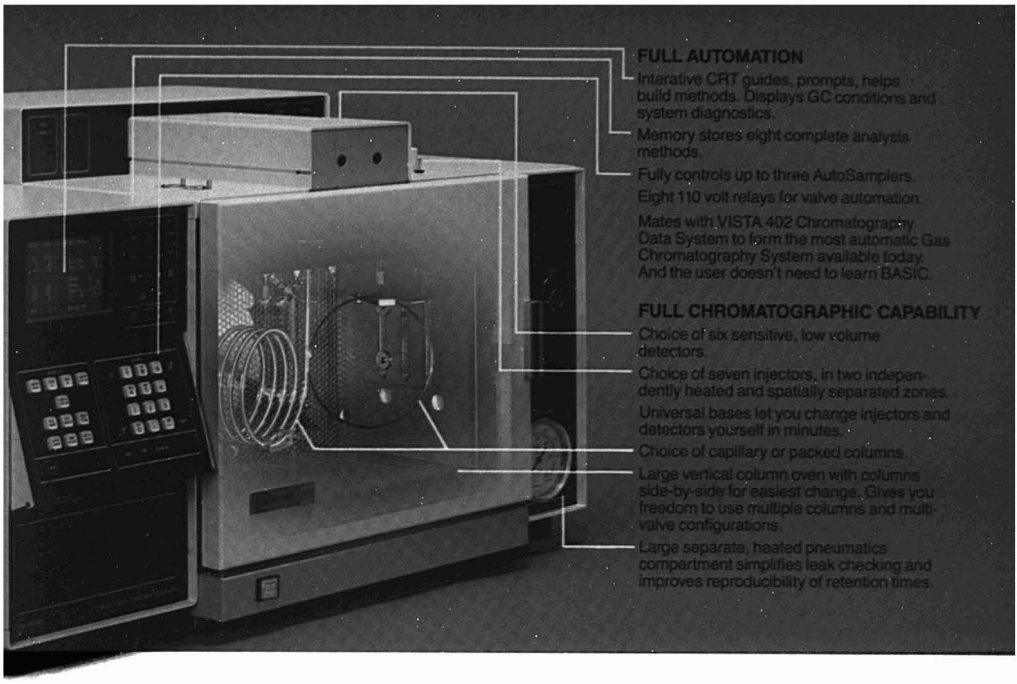
"Great flow; no drop in water quality." —G.S., Belchertown, MA

"Low operating pressure; works fine." —R.K., Longview, WA

"Lasted six weeks; no plugging, no cracking." —Y.F., Ann Arbor, MI

Gelman Sciences Inc.
600 South Wagner Road, Ann Arbor, Michigan 48106

CIRCLE 68 ON READER SERVICE CARD



So far ahead you can bet your future on it:

VISTA 6000 GC...from Varian.

With the VISTA 6000 you'll start ahead and stay ahead for years to come. And that's important. Because, odds are, ten years from now the gas chromatograph you buy today will still be in your lab.

You can handle more applications today and tomorrow. You can choose from seven state-of-the-art injectors, four capillary modes, and five sensitive, low-volume detectors. What's more, universal bases let you change injectors and detectors in minutes.

Intelligent, helpful automation. The 6000's interactive CRT gives you more intelligent help than any other. Makes it easier to set up methods. Easier to control and monitor analyses. And the memory stores eight analysis methods for key-touch callup.

The VISTA 6000 can fully control a dual-column satellite VISTA 6500. It will also control up to three AutoSamplers and eight external events. In addition, it combines with the VISTA 402 Chromatography Data System to form the most powerful fully automatic GC system.

Everything you need to succeed. Each VISTA 6000 is backed with full support: a broad curriculum of courses, local service, applications assistance, modular accessories and quick-delivery parts and supplies.

Ask us for full details on the VISTA 6000—the GC you can bet your future on. Call: Florham Park, NJ (201) 822-3700; Park Ridge, IL (312) 825-7772; Sugar Land, TX (713) 491-7330; or Los Altos, CA (415) 968-8141.

Circle Reader Service Number **219** for literature, or Number **220** to have a Varian Representative contact you.

611 Hansen Way, Palo Alto, CA 94303. In Europe: Steinhauserstrasse, CH-6300 Zug, Switzerland.



VISTA 6000 fully controls satellite dual-column Model 6500 GC.

varian

Intelligent chromatography... from Varian

Presenting the only chromatography data and automation system smart enough to handle both GC's and LC's—

The new VISTA 402...from Varian

The VISTA 402 is the only system that will fully control up to four GC's and/or LC's with AutoSamplers. And it will automate any analysis: routine repetitive assays and complex sets of samples while simultaneously calculating and reporting the data from any four GC and/or LC detectors. All this is accomplished by sophisticated multitasking software that addresses nearly five times as much memory as a standard 64K microcomputer.

The large, friendly CRT and simple keyboard make it easier to use.
You control and monitor the VISTA 402 through the interactive CRT and keyboard.

When you build a method the CRT guides you all the way step by step, line by line. For each entry, prompts tell you what settings or ranges can be entered.

The keyboard is in standard typewriter format. It also has nineteen self-explanatory special function keys which further simplify making entries and building methods.

Floppy disks provide over 819,000 bytes of mass storage and unique data handling capabilities.
Two 5.25 inch floppy disks, each with 409,600 bytes of storage, are available with the VISTA 402. Raw, digitized chromatographic data, as well as result data and methods, can be stored on the disks. For chromatograms with an average peak width at half height of 8 seconds, a two disk system can store about 20 hours of raw data. This is in addition to the VISTA 402's 144,000 bytes of RAM memory for about 18 methods and 2,200 peaks.

Advanced dual-channel printer/plotter produces clear, useful reports.
Fully and clearly annotated analysis reports are automatically produced by the VISTA 402's fast dual-channel printer/plotter. There is no overprinting of retention times and peaks are identified by compound name in both the chromatogram and the calculations report.

With dual channel, you can print two chromatograms side-by-side, e.g., to compare a sample with a stored standard from disk or to ratio the responses of two different detectors to the same sample.

And the printer/plotter saves you time because it is independent of the keyboard. It can be waiting for, or printing, data while you are editing programs on the CRT.

Accurately handles all peak geometries—automatically.
VISTA 402 software includes the most powerful and complete set of peak processing algorithms available. Every peak elution contingency can be handled correctly, most without recalculation. And this includes the narrowest, fastest capillary GC peaks. The VISTA 402 algorithms even handle the difficult end-of-peak region on the fly, in real time. You don't have to manually enter timed events to force proper peak integration.

Unique "learn mode" saves you time.
When you tell the VISTA 402 to "learn," it automatically determines the best peak processing parameters for each peak in a sample, even those as small as ½ second in width. You don't have to understand peak processing to do it right. Parameters such as slope sensitivity, are calculated for you, made part of your method and stored in memory for use on future samples.

The VISTA 402 can automatically plot every chromatogram with the baseline drawn in.
You can always confirm that the baseline is placed correctly because the VISTA 402 has the unique ability to automatically report every chromatogram in a run with the baseline drawn in.

Accurately corrects for drifting baseline.
The VISTA 402 is the only system to actually store a precise, point-by-point measurement of background as a part of your stored method and automatically subtract it from all sample runs. As a result, all peaks are presented on scale with true retention times and you have greater assurance that all peak areas are accurately integrated. This is especially critical for the narrow, closely spaced peaks of temperature-programmed GC runs.

A versatile, expandable, four-channel system.
VISTA 402 can increase the productivity of existing instruments. The four-channel data system will calculate the data and plot fully annotated chromatograms concurrently from any four gas and/or liquid chromatographs already in your laboratory.

For total automation of the entire chromatography process—full instrument control as well as data handling—VISTA 402 combines with up to four VISTA 6000 Gas Chromatographs and/or 5000 and 5500 Series Liquid Chromatographs. Then, methods you set in the 402 automatically control all instrument conditions as well as all data handling.

For completely automatic, unattended high-volume sample handling, as well as improved reproducibility, you can add up to four AutoSamplers, all simultaneously controlled by the VISTA 402.

The VISTA 402 will also send data to external computers, such as Apple //e and Digital Equipment VAX, for special handling and it will receive and print reports from them.

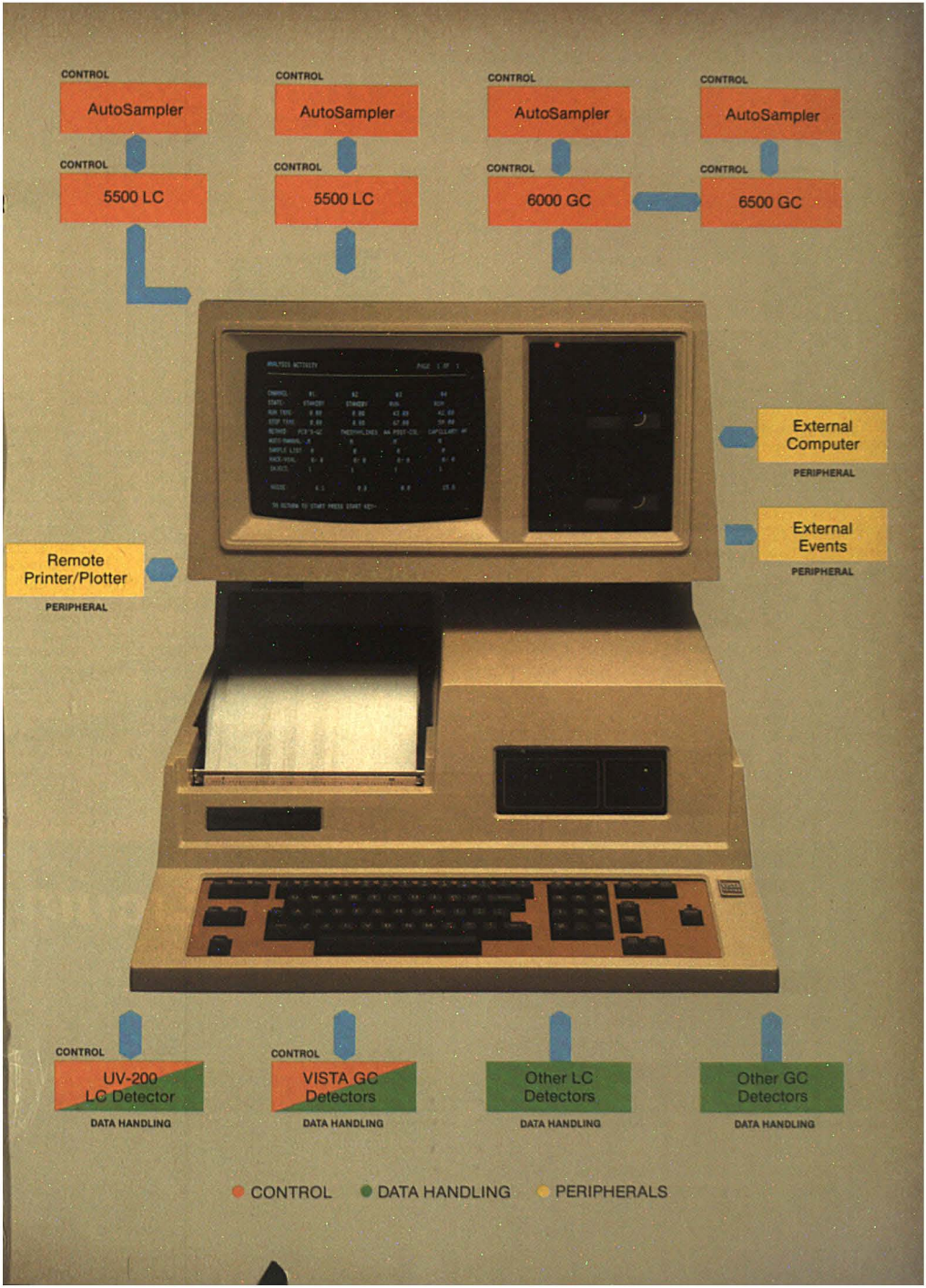
You can use the 402 to provide exactly the automation needed to increase the productivity of your lab.

For further information circle **Reader Service Number 200.** To have a Varian Representative contact you circle **Reader Service Number 201.**

For immediate assistance phone:
Florham Park, NJ (201) 822-3700; Park Ridge, IL (312) 825-7772; Sugar Land, TX (713) 491-7330; or write: 611 Hansen Way, Palo Alto, CA 94303. In Europe: Steinhauserstrasse, CH-6300 Zug, Switzerland.

varian

Intelligent chromatography . . . from Varian


CONTROL
AutoSampler
CONTROL
5500 LC
CONTROL
AutoSampler
CONTROL
5500 LC
CONTROL
AutoSampler
CONTROL
6000 GC
CONTROL
AutoSampler
CONTROL
6500 GC
External Computer
PERIPHERAL
External Events
PERIPHERAL
Remote Printer/Plotter
PERIPHERAL
CONTROL
UV-200 LC Detector
DATA HANDLING
CONTROL
VISTA GC Detectors
DATA HANDLING
Other LC Detectors
DATA HANDLING
Other GC Detectors
DATA HANDLING
CONTROL
DATA HANDLING
PERIPHERALS

This is what the future looks like in HPLC:

Memory stores up to nine complete methods.

Interactive CRT guides, prompts and displays conditions. Makes operation simple.

One simple CRT/keyboard controls entire HPLC system. There is a display for each major instrument function: Pump, Detectors, Scanning, Time-Relays, AutoSampler, Column Temperature, and Status. The Status display, presents a real-time readout of all operating conditions.

Chromatography keyboard. Each parameter has its own key. No computer jargon. One keystroke calls up the CRT for each function.

Proven reliable pump and hydraulics design eliminates inlet check valve failures. No need to degas.

Microstepped control provides precise, accurate flow rates for all modes: conventional, fast, semiprep and microbore HPLC.

Solvent proportioning for binary and ternary gradients is microprocessor controlled for precision and accuracy.

Any number of multilinear gradients can be created to handle the most difficult separation.

Convenient, enclosed, ventilated solvent compartment lets you use the standard bottles your solvent comes in as reservoirs. Saves time. Improves results.



The new Varian 5500 Liquid C

The new Varian 5500 Series offers more capability, and more potential for future growth, than any other liquid chromatograph.

To create it we took all the proven best from the 5000 Series, included all the newest LC advances and added many capabilities that are only beginning to be explored.

Advanced performance features include:

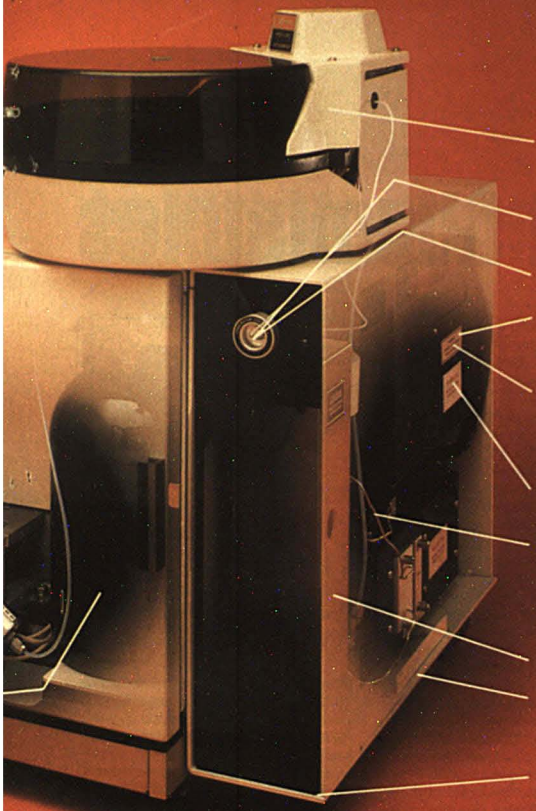
- Reproducible microstepped flow rates
- Fully integrated, intelligent control
- Programmable UV-Vis detection with scanning
- Microbore, ultra-fast and semiprep options
- Structured, upgradable software
- Complete stand-alone automation with built-in AutoSampler

Reliable, reproducible microstepped flow rates

The entire 5500 system is built to give you reliable, repeatable performance. The heart of it is the patented, single-pump ternary solvent system proven for reliability in the 5000 Series. A significant difference is the new microstep control that produces even smoother flow rates and gradients at higher pressures. It also allows the very slow flow rates you need for microbore LC.

Completely integrated for best synchronization of analysis actions

The 5500 is fully integrated both physically and operationally. Injectors, pump, detectors, column heaters, external events and serial communications are built in. Their operation and automation are controlled by a single method and clock for better reproducibility.



Integrated AutoSampler. Methods you set up in the 5500 control reproducible injections which can be automatically handled by different methods.

Choice of excellent injectors: manual loop valve, automatic loop valve, and AutoSampler.

Optional injectors available for microbore and fast LC

Choose any detector. Five excellent Varian detectors are offered: the built-in UV-200, UV-1 and UV-5, and the RI and Fluorichrom detectors.

UV-200 time-programmable UV-Vis (190 to 700nm) detector with scanning allows optimal detection of all components. You can also program baseline zeroing and attenuation.

Programmable scanning in the UV-200 helps you determine the best wavelengths for detection.

Large, accessible column/heater/detector compartment accepts 15 to 50 cm columns with or without heaters and allows installation of two detectors as shown here (UV-200 and UV-5) for dual wavelength detection and ratioing.

Column temperature control.

For total automation, including data handling, the 5500 combines with VISTA 402 to form the VISTA 55 Automated Liquid Chromatograph.

Saves space. Entire system as shown here, takes only 31 inches counterspace. Less than most component systems.

hromatograph

Simple, one-keyboard control
This synchronous, time-programmed control of all analysis components is through a single CRT and keyboard that simplifies operation.

Stand-alone automation
For completely automatic overnight operation, an AutoSampler can be added. Then methods set up in the 5500, and stored in its nine-method memory, will control injection and analysis of up to sixty samples.

Choice of 5500 configurations
Although fully integrated, the 5500 is modular. So, you can choose the best combination of injectors, detectors, heaters, columns and accessories for your specific needs. Even the software is structured for easy updating.

For full details, circle
Reader Service Number 223.
To have a Varian Representative contact you circle
Reader Service Number 224.

For immediate assistance phone:
Florham Park, NJ (201) 822-3700; Park Ridge, IL (312) 825-7772; Sugar Land, TX (713) 491-7330; or write: 611 Hansen Way, Palo Alto, CA 94303. In Europe: Steinhauserstrasse, CH-6300 Zug, Switzerland.

varian

Intelligent chromatography from Varian

Dry Reagent Chemistries

Recent advances in analytical methodology in clinical chemistry make use of reagents in a dry format for quantitative analysis. Providing a reagent in a dry format for rapid use is by no means new—a familiar example is litmus paper, which dates back to the 19th century. By introducing litmus, a colored extract from several lichens, into a paper matrix, the inventor provided a dry reagent chemistry for testing the alkalinity of a solution. This simple concept provided the user with a new dimension in routine analysis. Testing for alkalinity was made simple and rapid, and the dry reagent could be stored conveniently for later use. The litmus paper principle was the basis for other dry chemistries used in that century for qualitative analysis of glucose and other reducing sugars. Although not an analytical testing device, another noteworthy dry format chemistry that made its appearance in the 19th century was the photographic plate. It provided a dry format activated photochemistry capable of recording an object's image from its reflected light. Unlike litmus paper, the plate required treatment with liquid reagents to prepare the image. Like litmus paper, however, it introduced a previously unrealized dimension of convenience to the art of reproduction and documentation.

The first major impact dry format chemistries had on clinical testing was the appearance in the 1950s of Ames Clinistix urine reagent strips for testing urinary glucose. By comparing the color developed on the reagent strip with a color chart provided on the product label, the user got a rapid qualitative glucose analysis that otherwise would require a laboratory and skilled personnel. Clinistix reagent strips provided the groundwork for other reagent strips developed by Ames and other manufacturers for testing urine constituents. The appearance of Ames Dextrostix reagent strips in the 1960s for the semiquantitative analysis of blood sugar propagated the development of dry format chemistries for testing blood constituents. With the later introduction of instrumentation, the era of quantitative clinical analysis for glucose with reagent strips began.

In the 1970s, more sophisticated dry chemistries emerged for quantitative analysis of blood constituents. Whereas many of the clinical test formats available share the common trait of requiring reconstitution of reagents prior to use, either manually or automatically, the emerging reagents have a totally new format. In all cases, a complete chemistry is miniaturized into a dispensable dry format. No prior reconstitution of reagents is required, and many manipulations are replaced simply by applying the sample. An analysis is complete in 1–7 min. For simplicity, I will refer to these analytical elements as dry reagent chemistry carriers. Each such element contains all the chemical constituents required for a specific clinical analysis. The clinical sample is applied directly onto the carrier and, as with other chemistries, the analysis is usually monitored by instrumentation.

The development of dry reagent chemistries is the cumulation of several technologies. These technologies provided crucial knowledge on how to prepare quantitative chemistries in dry media such as thin films, paper matrices, and other synthetic porous materials. They also provided knowledge on how to cast thin films of desired porosity with high precision, how to make paper matrices and other porous matrices reproducibly with well-defined characteristics, and how to laminate various materials to each other. The photographic industry has made substantial contributions in advancing the technology of dry reagent chemistries (*1*). With the appearance of color photography, the industry had developed a technology that is based on conducting quantitative chemistries in discrete films arranged in multiple layers. This eventually resulted in instant photography. An instant color print may have as many as 15 layers of film, each with a specific chemical or physical function to perform in developing the photographic image. This very technology was used to develop several dry reagent chemistry formats for clinical testing. The coating and plastic industry provided a variety of techniques for precision casting of thin films (*2*), and it has developed lamination techniques frequently required for bonding various materials together. It also developed a variety of inert materials used in constructing dry reagent chemistries. The paper and fabric industries have developed techniques for making fibrous matrices with reproducible parameters to fit a variety of unique needs (*3*). Some of the parameters that can be controlled easily include matrix thickness, fiber density, and solvent absorbency, which are important in generating dry reagent chemistries.

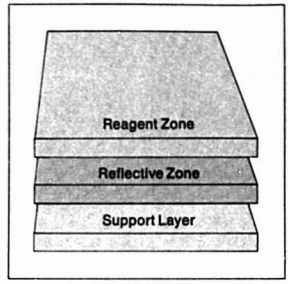


Figure 1. Basic components of dry reagent chemistry carriers

Contributions from these industries led to the evolution of dry reagent chemistries that can be adapted to meet any need in the clinical laboratory. The main focus of this text will be to describe some basic features governing the structure of these carriers, how chemical reactions are monitored, and what advantages these carriers provide for clinical chemistry analysis.

0003-2700/83/0351-498A$01.50/0
© 1983 American Chemical Society

Report

Bert Walter
Blood Chemistry Laboratory
Ames Division, Miles Laboratories, Inc.
Elkhart, Ind. 46515

in Clinical Analysis

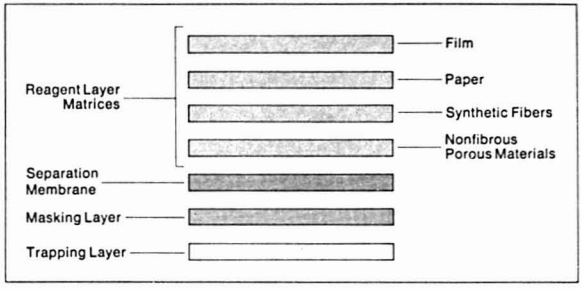


Figure 2. Basic constituents used in constructing carrier reagent zones

Contributions from several technologies have led to the development of sophisticated testing devices for clinical use. The technology of making dry reagent chemistries is sufficiently advanced that carriers can be developed for almost any chemical analysis. The dry reagent chemistry carrier contains all the reagents required to conduct an analysis. Separation steps required by conventional analysis are integrated into the analytical element. This offers several advantages to the user. The most obvious is the reduction of multiple-step procedures to one step. Only the sample need be applied to reconstitute the system and start the analysis. Hence, the skill of the user is less important. The waste of reconstituted but unused solutions is eliminated, providing for more efficient and cost-effective use of reagents. The small size of the carriers means little space is required for storage. Since the dry reagent chemistries are stored dry until use, their shelf life is prolonged beyond reconstituted conventional chemistries. The advantages provided by dry reagent chemistries will help ease the burden of quality control in operating laboratories.

Basic Structure of Dry Reagent Carriers

The common features of most dry reagent chemistry carriers monitored by diffuse reflectance methods are a support material, a reflective zone, and a reagent zone. This is illustrated schematically in Figure 1. In some carriers these three features are distinctly defined; in others, the reflective zone may coalesce with the reagent zone or the support zone, or both. The support material usually consists of a thin, rigid plastic or a plasticlike material that may be transparent or reflective. The support material serves as a building base for the reagent chemistry carrier. The major function of the reflective zone is to reflect to a detecting system any light not absorbed by the chemistry of the carrier. The reflective zone is usually constructed with pigments such as TiO_2 or $BaSO_4$ or reflective materials such as metal foils. Where paper constitutes the reagent zone, the paper matrix itself acts as a reflective layer. The primary requirement for the reflective material is that its absorbance of light in the visible range and, if possible in the UV, be negligible.

The reagent zone assembly contains all the reagents for a specific chemistry. This zone may be constructed with a paper matrix, a synthetic fiber matrix, film layers, other porous nonfibrous materials, or a hybrid of these. The reagent zone of the carrier is the most complex region of the carrier. In addition to the detecting chemistry, this zone may provide several additional functions as shown in Figure 2. It may include a separation membrane, a masking layer, or a trapping layer.

Two distinct approaches have been used to construct the layers containing the assay reagents. One approach makes use of film casting techniques. The layers are constructed by casting a porous film containing all the required assay components. For example, if the constituents have to be segregated before use, the reagents may be deposited in several films. Hence, a reagent zone may be constructed of multiple film layers, each containing portions of a specific detection chemistry. Separation membranes and trapping layers also can be introduced as necessary between reagent layers. The cross-sectional thickness of such a carrier may be less than 100 μm. The quantities of reagents made available during analysis are controlled by their concentration in the casting medium, the thickness of the cast film, and

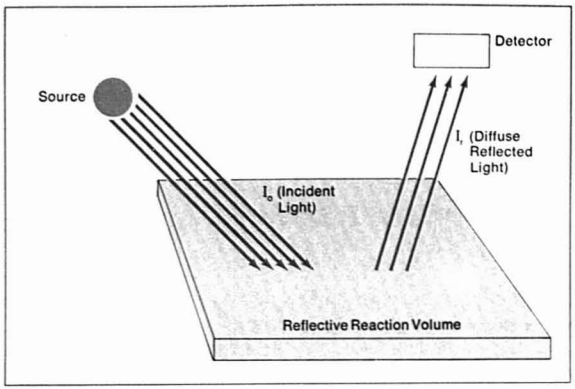


Figure 3. Principle of reflectance photometry

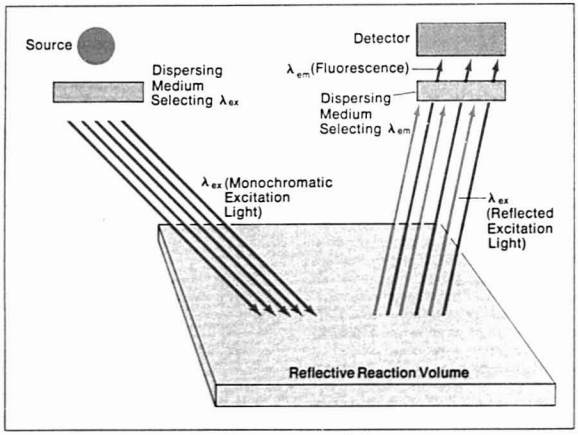


Figure 4. Principle of front-face fluorescence analysis

their solubility in the sample solvent. Film matrices commonly consist of such polymers as cross-linked gelatin, agarose, alginate, polyvinylalcohol, polyvinylpyrrolidone, and cellulose acetate. The porosity of the film is controlled by such factors as the molecular weight of the polymer, the degree of cross-linking, and the concentration of the polymer in the casting medium (*4*).

The second approach to constructing a reagent layer involves the use of a paper or a synthetic fiber matrix. The paper matrices commonly employed consist of pure α-cellulose with uniform fiber density and defined thickness. Reagents are introduced by saturating the matrix with reagent solutions followed by drying. Reagents can be introduced in a one-step saturation process or in multistep saturation processes. To prevent perturbation of reagents already deposited in multistep saturations, differential solubility techniques are used. The solvents for successive deposition of reagents are chosen so that reagents already laid down are not redissolved. The quantity of reagents made available during an assay is controlled by the reagent concentration in the saturation solution, the thickness of the matrix, the fiber density of the matrix, the absorptivity of the solution by the fibers, and the solubility of the reagents in the sample solvent. Typical thicknesses of reagent zones constructed with these matrices range from 0.2–0.5 mm. The porosity of the reagent zones may be further controlled by introducing a membrane layer on top of the paper matrix. To affix these matrices to other surfaces, various lamination techniques are employed, the most common of which make use of double-sided adhesive layers or a mesh overlayer to anchor the matrices to a given surface.

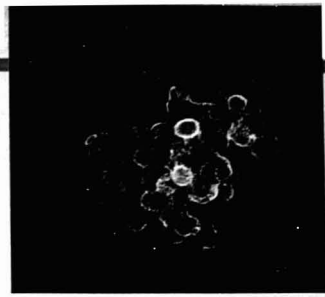
Instrumentation

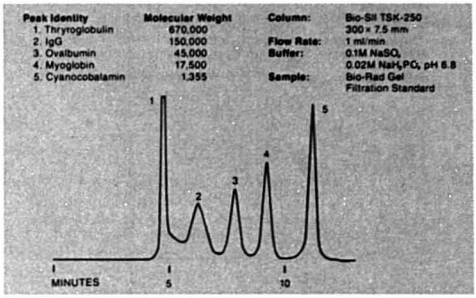
The chemical reactions occurring on dry reagent carriers usually are monitored by diffuse reflectance spectroscopy (*5*) and, to a lesser extent, by fluorescence (*6*). In discussing reflectance spectroscopy, two kinds of reflections must be considered. One is specular reflection, which is the mirrorlike reflection from a surface where the angle of incidence is equal to the angle of reflection. This type of reflection is of limited value in monitoring dry reagent chemistries. The second is diffuse reflection, which is a reflection from a matte surface. This is the predominant reflection of interest. Diffuse reflection may result from illumination of the reaction volume of the carrier with diffuse light or diffusion of light in the illuminated reaction volume. Diffuse reflectance is not a surface phenomenon, but the result of light interacting with various chemical and physical factors in the reaction volume of the carrier. These factors include the absorption, transmission, and scattering properties of the illuminated material. Figure 3 illustrates the general principle of reflectance spectroscopy. The reaction volume of the carrier, where a chromophore is either generated or degraded, is illuminated at a suitable wavelength. The amount of diffuse light recovered with the aid of the reflective layer is a measure of the progress of the reaction. The intensity of light reflected by the reaction media is determined relative to a known reflectance standard. The commonly used percent reflection (%R) can be expressed as:

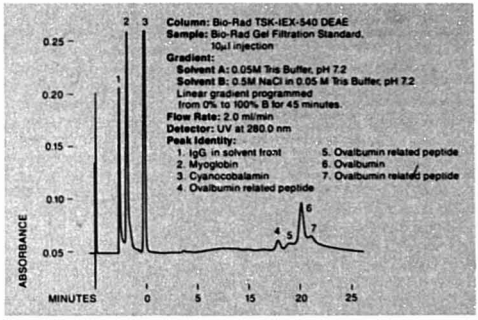
$$\%R = \frac{I_s}{I_r} \times R_r$$

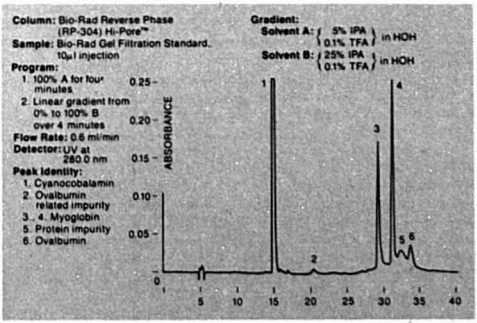
where I_s, I_r, and R_r represent the reflected light from the reagent carrier, the reflected light from the reference, and the percent reflectivity of the reference, respectively. The reflectance measurements are comparable to a transmittance measurement in absorption spectroscopy, where the con-

Applications Report: New Column Technology









New tools for protein separations.

New HPLC column technology from Bio-Rad gives researchers a number of worthwhile alternatives for protein separations.

For example, here are three separations of the same sample, using three different approaches — high performance gel filtration, our new high performance ion exchange column, and our new Hi-Pore™ reverse phase column.

Looking at those separations, it's apparent that these HPLC columns provide fast separations with excellent resolution. Not only that, certain compounds appear in the ion exchange and reverse phase separations that don't reveal themselves in the gel filtration separation. HPLC lets you "read between the peaks" with both speed and precision.

These new columns complement rather than compete with each other. Our HPLC ion exchange column for analysis of ionizable biochemical compounds is an excellent complement to our Bio-Sil gel filtration column. By using all three columns, better characterization of proteins (including large ones) may be obtained.

As always Bio-Rad is prepared to assist you in plotting an effective strategy for your protein separations, using any or all of these techniques. Give our applications staff a call, or contact us at

BIO-RAD

Bio-Rad Laboratories — Chemical Division
2200 Wright Avenue
Richmond, CA 94804
(415) 234-4130

Also in Rockville Centre, N.Y., Australia, Austria, Canada, England, Germany, Italy, Japan, The Netherlands, and Switzerland.

See us at FASEB Booths G-2, G-4, G-6, & G-8.

CIRCLE 23 ON READER SERVICE CARD

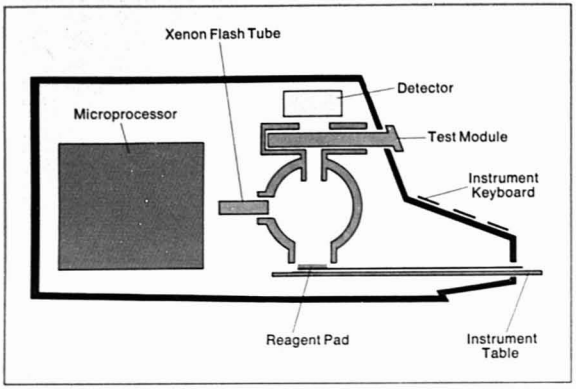


Figure 5. Cross-sectional diagram of the Seralyzer reflectance photometer (Ames Division, Miles Laboratories, Inc.)

centration of the absorbing component can be measured. As with transmittance, reflectance is not linear with concentration. To make the measurement useful and convenient, several algorithms are available to convert reflectance measurements to functions that are linear with concentration (7, 8). The specific algorithm employed depends on the nature of the illumination, the reflection characteristics of the dry reagent carrier, and the geometry of the instrument.

Reactions resulting in the appearance or disappearance of fluorescence are monitored by front-face analysis (9) in which irradiation and fluorescence are from the same surface of the carrier. The general principle of front-face fluorescence analysis is illustrated in Figure 4. For irradiation, a specific wavelength, dictated by the chemistry, is selected by passing light through a filter or light-dispersing device such as a monochromator. With the aid of the carrier's reflective layer, a portion of the total light (fluorescence + diffuse reflected excitation light) is collected by the detection system. The angle of irradiation is chosen so as to minimize specular reflection of the excitation light into the detector. The detection system segregates fluorescence from residual reflected excitation light by a filter or monochromator placed between the detector and the reaction surface. This allows the transmission of the fluorescence light only. Unlike reflectance, measured fluorescence is linear with fluorophore concentrations in the absence of self-quenching.

Instrumentation for dry reagent carriers ranges in size from hand-held dedicated devices to large freestanding instruments. Many of the hand-held instruments are designed to monitor a specific dry reagent chemistry. They are microprocessor controlled, allowing the user to store calibration curves and to time the chemical reaction on the carrier. They also provide the user with a clinical value after a measurement. Examples are the Glucometer reflectance photometer (Ames Division, Miles Laboratories, Inc.), the Accu-Chek bG (Boehringer Mannheim Corporation), the EasyTest (Australia Bio-Transducers), and the Hypo-Count IIB (Hypoguard, Ltd.) used in whole-blood glucose analysis.

For more general testing, bench top manual instrumentation is available for handling more than one chemistry. Figure 5 illustrates the basic components of one such instrument, the Seralyzer reflectance photometer (Ames Division, Miles Laboratories, Inc.). The instrument requires that each chemistry and sample be introduced individually onto the instrument's table by the operator. Each test has a specific module that contains part of the computer memory for the test, the algorithm, and the optical interference filter for that test. Analysis time may range from 30 s to 4 min, depending on the nature of the chemistry. After initial calibration for each chemistry of interest, a specimen can be tested for several analytes without recalibrating test modules. The instrument's microprocessor maintains control of several operations including temperature, timing of reactions, calculations, and display of clinical results. In addition, the system alerts the user to malfunctions and operator errors. The instrument can be updated easily as new test modules and dry reagent chemistries are made available.

Fully automated instrumentation is also available as exemplified by the Ektachem 400 Analyzer (Eastman Kodak). The operator need only provide the samples and select the desired tests. The instrument automatically selects the reagent carrier from a cassette, calibrates the selected chemistry, applies the sample, and reports the results. It is capable of more than 500 tests per h and can hold 1600 dry reagent chemistries. The instrument can be programmed to run any of 16 currently available tests and can be updated to run additional tests as they become available. The system reports malfunctions, diagnoses problems, and tells how the operator can correct them.

Dry Reagent Chemistries in Clinical Analysis

Dry reagent chemistries have been described for a variety of blood analytes. These include serum metabolites, enzymes, and serum electrolytes as well as therapeutic drugs. Many of these chemistries are available on the market and provide a unique approach to conducting quantitative analysis of serum analytes. Each dry reagent chemistry provides an integrated assay for a specific analyte that requires only the application of the serum sample. The structure and chemistry of a few representative carriers will be described to illustrate how several conventional steps have been integrated into a single-step procedure to provide a new concept in clinical analysis.

Blood Metabolites. Dry reagent chemistries are presently available for nearly all the commonly tested blood metabolites. These include glucose, blood urea nitrogen, uric acid, cholesterol, triglycerides, creatinine, bilirubin, ammonia, and calcium. Analysis of many of these metabolites by conventional means requires several steps that are done either manually or by automation. The integration of several steps into a single-step analysis is exemplified by the dry reagent chemistries developed for whole-blood glucose analysis. The cross sections of two such carriers developed by Boehringer Mannheim Corporation (BMC) and Ames Division, Miles Laboratories, Inc., are illustrated in Figures 6a and b, respectively. Glucose is detected by a glucose oxidase–peroxidase procedure. In both cases, approximately 50 μL of whole blood is applied to the surface of the carrier (approximately 0.5 cm × 1 cm), where plasma containing glucose is separated from red blood cells by the carrier matrix. After an allotted reaction

JUST ADD WATER

Versa-Bath provides everything else:

Economy

- Low-watt density heaters for efficient heat transfer and long service life.
- Gable covers that raise operating temperature by as much as 40°C — without using additional energy. And they're supplied *with the baths* — not as expensive accessories.
- Choice of 6-, 12-, 20- and 30-liter units.

Performance

- Temperatures from ambient to 60°C without a cover; ambient to 100°C with a cover; even below ambient with accessory cooling coils.
- ±0.25°C temperature uniformity and ±0.5°C accuracy.

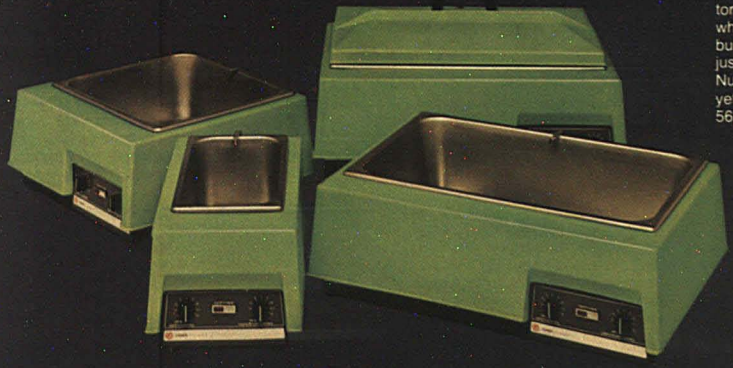
Safety

- Two adjustable thermostats (one primary/one backup Safety Sentinel) to prevent overheating, sample loss.
- Drain spouts on our 3 largest models eliminate the need to lift a full bath when it's time to change water.

Durability

- Housings and covers from a really tough, space age polymer that's extremely corrosion- and chemical-resistant (lightweight, too).
- One-piece stainless-steel chambers that won't rust or leak, and are easy to clean.

As versatile as the name implies, Fisher Versa-Bath fills a broad range of laboratory water bath needs. The whole story is in our new bulletin. For your free copy, just use the Reply Card Number below. Or better yet, call us at (412) 562-8543.



Fisher Scientific
An Allied Company

CIRCLE 52 ON READER SERVICE CARD

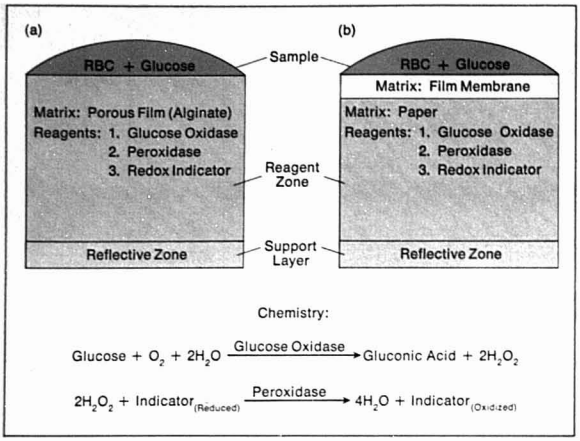


Figure 6. Cross section and chemistry of carriers for whole-blood glucose analysis, developed by (a) Boehringer Mannheim, Inc. and (b) Ames Division, Miles Laboratories, Inc.

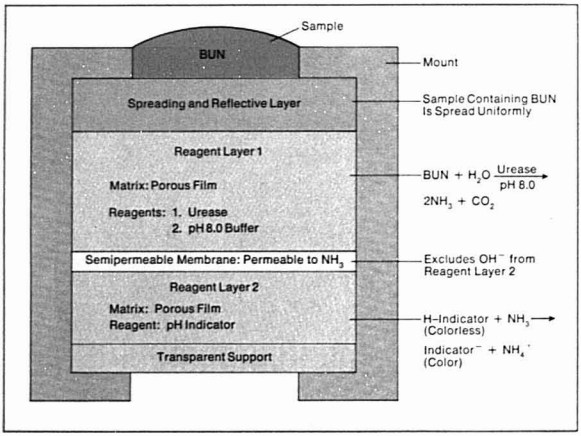


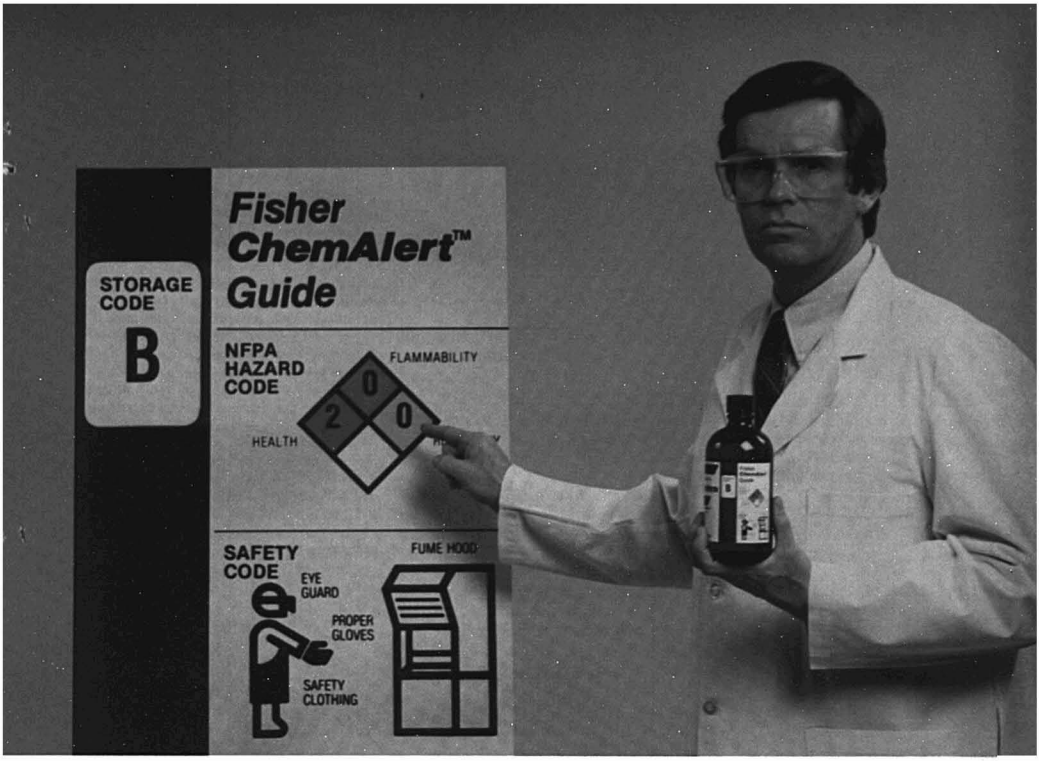
Figure 7. Cross section and chemistry of Eastman Kodak Ektachem slide for blood urea analysis

time (usually 1–3 min), the red blood cells are removed by washing or wiping, and the color developed is analyzed and translated to blood glucose concentrations. Both carriers consist of a support material that also incorporates the reflective zone. Both devices depend on a film layer to exclude red blood cells from the reagent zone and quantitatively meter a sample volume. In one case, the reagent zone is part of the film matrix (BMC); in the other, the reagent zone consists of a paper matrix with a membrane. Both devices have reduced the blood glucose analysis from a laborious effort of removing red blood cells, either by centrifugation or by precipitation prior to analysis, to one simple step.

Separation steps or immobilized catalytic centers also can be integrated into carriers at any reaction step of an analysis. An example of a dry reagent chemistry employing a separation step to isolate a product is the multilayer film chemistry (Ektachem slide) developed by Eastman Kodak for blood urea analysis. The cross section of the carrier is illustrated in Figure 7 (*10*). The carrier consists of a transparent support material, a reflective layer, and two reagent layers (film matrix) separated by a semipermeable membrane. A 10-μL sample of undiluted serum is applied to the reflective layer, which also acts as a spreading layer, to meter a uniform reaction volume. As the sample enters the first reagent layer, the urea is converted to ammonia and CO_2 by the enzyme urease. The semipermeable membrane acts as a barrier to hydroxyl ions and allows the diffusion of the ammonia into the second reagent layer where it deprotonates a pH indicator. The reaction is over in 7 min. The color developed is monitored by a reflectance meter from below the carrier, and the results are expressed as concentration of blood urea. The dimensions of the dry reagent carrier are 2.8 × 2.4 cm, with an application region of less than 0.8 cm^2. The thickness of the carrier is less than 100 μm.

Among the carriers incorporating catalytic centers is the dry reagent strip for blood urea analysis developed for the Seralyzer system by Ames. The cross section of the carrier is illustrated in Figure 8. The carrier consists of a support that incorporates a reflective zone and a paper matrix reagent layer that contains uniformly distributed cation exchange centers. Upon application, the sample is distributed into the reagent zone via capillary action; this solubilizes the reagents. The blood urea reacts with *o*-phthaldehyde to produce 1,3-dihydroxyisoindoline (DHI). The cation exchange centers catalyze the coupling of DHI to 3-hydroxy-1,2,3,4-tetrahydrobenzo(*h*)quinidine (HTBQ) to form a chromogen. The rate of color development, monitored by reflectance from above the carrier, is then converted into blood urea concentration units. The analysis requires 30 μL of solution after a threefold dilution of a serum sample with water (10 μL of undiluted serum is required per assay). The dimensions of the carrier are 0.5 × 1.0 cm, with a thickness of less than 0.5 mm.

Enzymes. As with serum metabolites, sophisticated dry reagent chemistries also are available for the analysis of serum enzymes. Dry reagent chemistries have been described for the analysis of creatine kinase, lactate dehydrogenase, aspartate transaminase, alanine transaminase, α-amylase, γ-glutamyltransferase, and alkaline phosphatase. Some of these carriers are available on the market. Determining enzyme activity in serum often involves complex and lengthy chemistries where several enzyme as-



Fisher ChemAlert™

NOTHING COULD BE SIMPLER

Laboratories have long depended on the Fisher reagent label. With its clear-cut purity grades, detailed analyses, applicable OSHA, DOT, and ANSI data, first aid instructions. Now this distinguished label becomes more useful than ever. Now it will also carry the Fisher ChemAlert Guide.

ChemAlert is an **instant** guide to storing and handling the reagent in question. A useful supplement to your regular safety program. It condenses a wealth of authoritative material into a uniquely simple three-part format.



☐ One part tells you, with a large uncluttered color bar, how to store the reagent. (For the color-blind, this bar also identifies itself by letter, i.e., for flammable storage it uses an "R" as well as the color red.)

☐ One part rates potential hazards numerically, inside a big bold NFPA "diamond," a symbol selected for its universality. (In fact, many industries, hospitals, and municipalities now require it.)

☐ One part demonstrates how to handle the reagent. What protective gear to wear. Whether to use a fume hood.

Right on the label — there's no more logical place to remind users — old and new — of the correct way to deal with chemicals.

ChemAlert was designed to do this reminding in the most **effective** way possible. Watch for it on your familiar Fisher reagents. Use it, for safety's sake.

For a detailed brochure on new ChemAlert, circle our number on the reply-card. Or give us a call at (412) 562-8543.

Fisher Scientific

An ALLIED Company

CIRCLE 53 ON READER SERVICE CARD

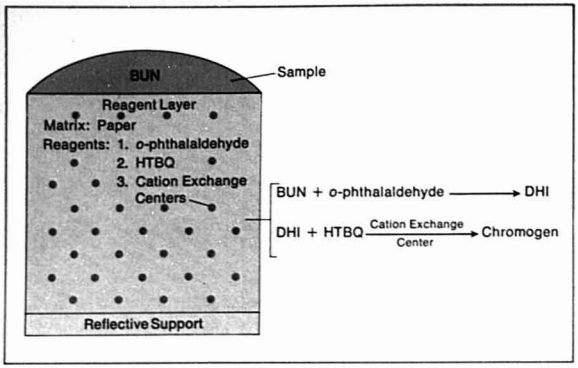


Figure 8. Cross section and chemistry of the Ames Division, Miles Laboratories, Inc., Seralyzer dry reagent strip for blood urea analysis

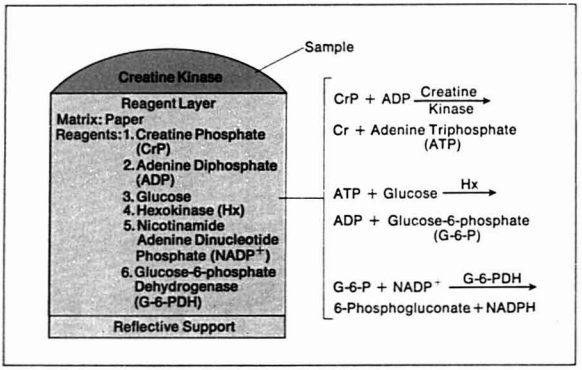


Figure 9. Cross section and chemistry of the Ames Division, Miles Laboratories, Inc., Seralyzer dry reagent strip for creatine kinase analysis

says must be coupled in order to conduct an analysis. The creatine kinase (CK) determination developed for the Seralyzer system by Ames is an example of a multiple-coupled-enzyme dry reagent strip chemistry. The cross section of the carrier is illustrated in Figure 9. The carrier consists of a paper matrix reagent zone fixed onto a reflective support. The chemistry is based on the Rosalki procedure (*11*), which couples a hexokinase and a glucose-6-phosphate dehydrogenase reaction to the ATP produced by creatine kinase to generate a creatine kinase assay. This results in the generation of NADPH that can be monitored at 340 nm by reflectance spectroscopy and converted into enzyme concentration units. The dry reagent carrier is 0.5 × 1.0 cm and 0.2 mm thick and requires 30 μL of solution derived from the ninefold dilution of a serum specimen (3.3 μL of undiluted serum is required per assay). The assay duration is 4 min, which includes a two-and-one-half-minute lag period.

Masking is another technique that allows several assay steps to be combined in an enzyme analysis. This procedure excludes undesirable absorbtion of light by reagents in the chemistry during an analysis. This is readily exemplified by an Ektachem slide for α-amylase analysis developed by Eastman Kodak. The cross section of such a carrier is illustrated in Figure 10. The element consists of a spreading layer containing a dye-bound amylopectin substrate followed by a masking layer to hide the dye. The masking layer also incorporates the reflective zone. Next to the masking layer is the registration layer, which rests on a transparent support. When a serum sample is applied to the carrier, the resulting hydrolysis of the substrate generates small molecular weight dye-bound starch units. Starch units containing fewer than 10 glucose units migrate through the masking layer into the registration layer where they become trapped. The dye is quantitated by reflectance spectroscopy at 540 nm. The quantity of dye appearing in the registration layer after a given time is proportional to the α-amylase concentration in the sample, and the results are expressed as enzyme concentration units. During the reaction, neither the enzyme nor the large molecular weight dye-bound substrate can diffuse into the registration layer. The masking layer separates and hides the dye-bound amylopectin from the instrumental measurement. This dry reagent chemistry requires 10 μL of an undiluted serum sample per analysis. The carrier is 2.8 × 2.4 cm, with an application region of less than 0.8 cm^2.

Electrolytes. Dry reagent chemistries developed for electrolyte analysis are based on ion-selective membranes using either electrochemical or spectroscopic principles for analysis. As with metabolites and enzyme chemistries, dry reagent chemistries for electrolytes are also small, disposable, and require a small sample volume. Figure 11 shows a diagram of the electrodes found in an Ektachem slide for K^+, a dry reagent electrochemistry carrier developed by Eastman Kodak for measuring serum K^+ concentrations (*12*). An ion-selective membrane is used to construct a K^+-specific electrode. The electrode consists of a support base and a silver and silver chloride layer that serves as the reference electrode. The salt bridge consists of KCl deposited in a film. The K^+-selective membrane, consisting of the ionophore valinomycin in a hydrophobic medium, resides on top. The dry reagent carrier consists of two such electrodes joined by a bridge, where only a portion of the ion-selective membrane is exposed. The sample is deposited in one opening and a reference KCl solution of known concentration is placed in the other. The K^+ concentration is determined from the potentiometric difference measured between the two electrodes in the carrier. Unlike conventional electrode measurements, the sample is referenced directly to a standard solution. The dimensions of the carrier are 2.8 × 2.4 cm, with a thickness of 150 μm requiring only 10 μL of sample and reference solution for a K^+ analysis. Similar dry reagent electrochemistries have been described for Na^+, Cl^-, and CO_2 analysis.

An electronic threat to the triple-beam

Tares in one second. Weighs in two. Without sliders, dials or weights.

The Fisher/Ainsworth SC-200. It may be the one electronic balance that can tempt you to replace your triple-beams. Unlike them, it has no bouncing beams, no sliders, no dials to twist, no weights to juggle. Yet it has the same rugged durability as the classic triple-beam, for day-in, day-out weighing. Plus a *very* affordable price tag.

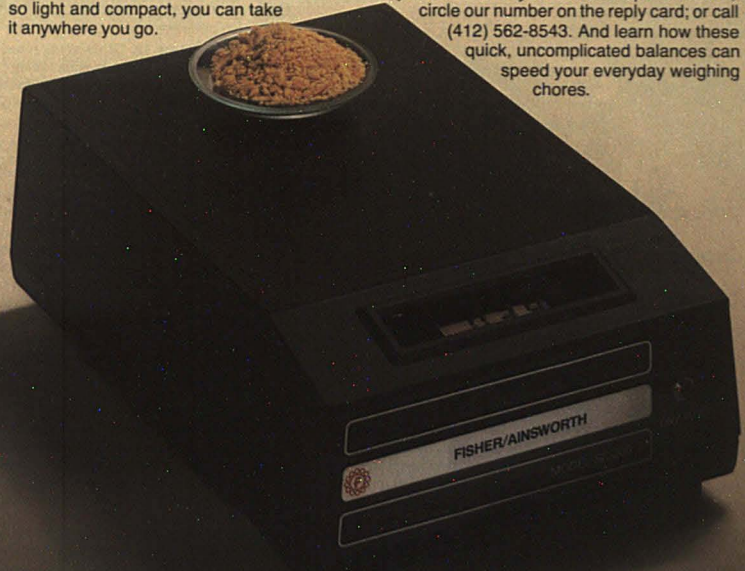
Consider the convenience. Just tap the toggle to turn it on; tap again for one-second taring, up to 49.9 grams. Weigh samples from 0.1 to 200 grams in two seconds flat. And with ±0.1 gram precision — thanks to the electronic filter that corrects automatically for environmental variables. *Including vibration.*

Examine the extras. The SC-200 is so light and compact, you can take it anywhere you go. And it operates on a single 9-volt battery, so it's independent of the power lines. Perfect for quality control right on the production line or weighing in the field. When you're finished, it turns itself off automatically to conserve the battery.

Now, enjoy the price. Just $349 for a full-featured electronic balance that can do the job of three mechanicals. *In less time.* And with absolutely no fuss.

Concerned about capacity? Meet the SC-2000. Same speed, portability and reliability as the SC-200. But with 2000 gram capacity, precision to ±1 gram. And only $449.

Weigh all the facts. For latest literature, just check with your Fisher Representative; circle our number on the reply card; or call (412) 562-8543. And learn how these quick, uncomplicated balances can speed your everyday weighing chores.



Fisher Scientific
An ALLIED Company

CIRCLE 54 ON READER SERVICE CARD

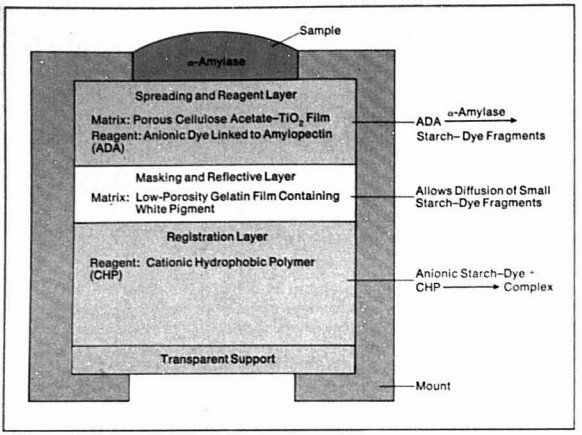


Figure 10. Cross section and chemistry of Eastman Kodak Ektachem slide for α-amylase analysis

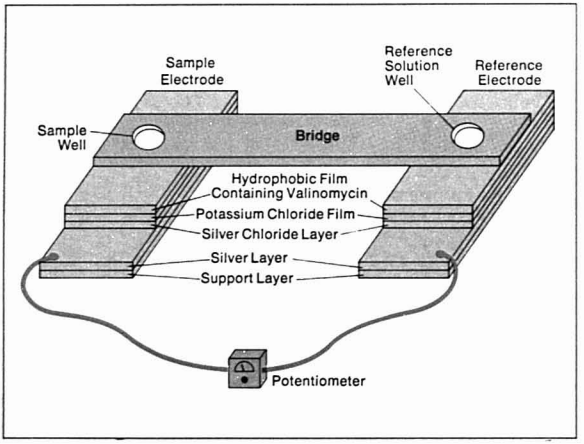


Figure 11. Diagram of Eastman Kodak Ektachem slide for potassium analysis by electrochemical means

Figure 12 illustrates the cross section of a dry reagent chemistry developed by Ames Division, Miles Laboratories, Inc., for K^+ determination by spectroscopic methods (*13*). The carrier consists of a support base with a reflective zone and an ion-selective membrane. The membrane consists of a nonpolar phase containing the ionophore valinomycin. A drop of sample mixed with an anionic dye is placed on the membrane. The ionophore transports K^+ into the nonpolar phase at a rate proportional to the K^+ concentration. To maintain charge neutrality, a dye molecule comigrates. At the end of the reaction period, the drop is removed by washing, and the K^+ concentration is determined from the quantity of dye in the nonpolar phase as measured by reflectance spectroscopy. The dimensions of the carrier are 1.0 × 0.5 cm and 100 μm thick. Only 15 μL of a serum sample is required per analysis.

Therapeutic Drugs. A more recent advance in dry reagent chemistries has been the development of carriers for the analysis of therapeutic drugs in serum. Figure 13 illustrates the cross

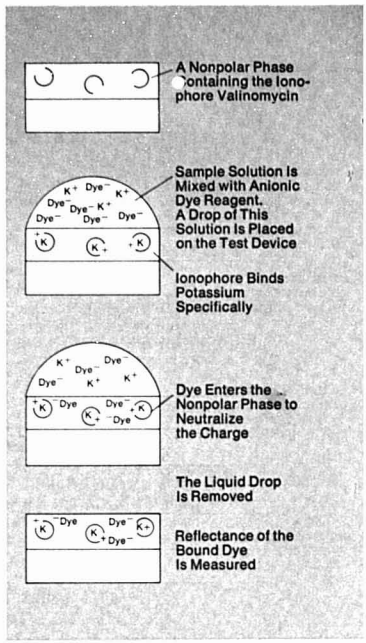


Figure 12. Cross section and chemistry of the Ames Division, Miles Laboratories, Inc., dry reagent strip for potassium analysis by reflectance photometry

section of a dry reagent strip developed by Ames Division, Miles Laboratories, Inc., for the detection of the antiasthmatic drug theophylline in serum (*14*). The chemistry is a competitive protein-binding assay based on the substrate-labeled fluorescence immunoassay (*15*). Upon placing the sample on the carrier, a competition for antibody-binding sites is established between the serum theophylline and the theophylline conjugate. The unbound conjugate remaining is proportional to the theophylline in the sample. The conjugate is monitored by fluorescence after the removal of the galactose moiety by the action of β-galactosidase. The conjugate, antibody, and enzyme are introduced in the paper matrix by differential solubility techniques. This prevents the premature interaction of the conjugate with the antibody or enzyme, yet provides a single-step, homogeneous assay. The dose response for such a carrier is illustrated in Figure 14, where the increase of fluorescence intensity is proportional to the theophylline concentration. Similar dry reagent chemistry



Your scientists will never be empty-handed...

if you rely on FASTBACK.®



It's our computerized ordering/inventory control system that took 15 years and millions of dollars to develop. We use it to handle more than half-a-billion dollars in sales a year. Now it's available as an invaluable service to Fisher customers.

FASTBACK is the sure-fire way to keep your inventory current — month after month, year after year. You have access to more than 80,000 items. And our on-line computer system instantly gives you up to the minute information on availability, quantity and price.

Your data terminal may already be suitable to plug into the FASTBACK system (if not, you can purchase the proper equipment inexpensively from Fisher). Place orders via your teleprinter and simplify recordkeeping with instantaneous print-outs. Forget about ordering errors, too — FASTBACK will immediately signal any mistake in catalog number, size, etc.

Whether you need glassware, reagents, instruments, furniture, apparatus or whatever, the FASTBACK system ties you into our central computer with access to all 28 strategically located Fisher distribution centers (and 33 million cubic feet of lab supplies). Delivery is guaranteed to be fast and dependable.

If storeroom space is a problem, take advantage of our Customer Reserve Quantity (CRQ) program in conjunction with FASTBACK. When you make a long-term order, we reserve the merchandise exclusively for you in the Fisher warehouse closest to your lab. You can forget about backorders — and empty-handed scientists.

FASTBACK is available as a service to Fisher customers at various levels of sophistication. You can benefit whether you're a crack computer expert or just starting out. For more information, just contact your Fisher rep or nearest branch. Or call (412) 562-8543. It's that simple.

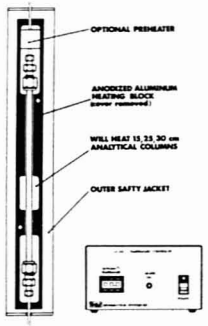
DMD DATA MANAGEMENT DIVISION

Fisher Scientific
An ALLIED Company

CIRCLE 55 ON READER SERVICE CARD

TEMPERATURE CONTROL FOR LC COLUMNS

Temperature control in liquid chromatography has generally been neglected. Improved resolution, efficiency, and precision often result from operation of LC columns at controlled temperatures above ambient.



Bioanalytical Systems offers a low cost column heating system based on a metal block heater and solid state controller. The versatile controller can be used with other heating elements and probes for a variety of laboratory applications.

BIOANALYTICAL SYSTEMS INC.

Purdue Research Park
1205 Kent Avenue
West Lafayette, IN 47906
(317) 463-2505

CIRCLE 31 ON READER SERVICE CARD

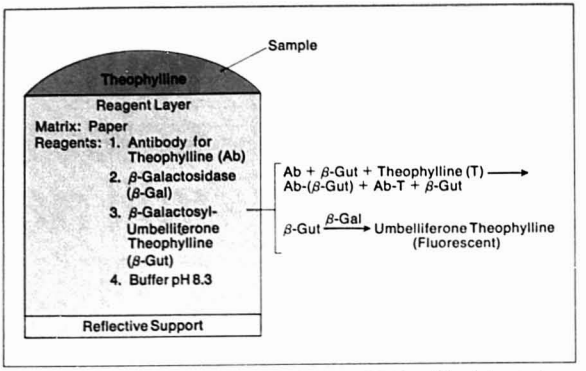


Figure 13. Cross section and chemistry of the Ames Division, Miles Laboratories, Inc., dry reagent strip for theophylline analysis

carriers have been described for the detection of antibiotics (gentamicin, amikacin, and tobramycin) and anticonvulsant drugs (carbamazepine, phenytoin, and primidone).

Performance

The fate of any new technology in the clinical chemistry community depends on its performance vis-á-vis established methodologies. Although space does not permit the comparison of every dry reagent chemistry with the various established methodologies, a few representative examples will illustrate that performance of dry reagent chemistries is comparable to established procedures. Table I summarizes the performance of the Eastman Kodak Ektachem slide for glucose analysis and compares it to the performance of the Du Pont Automatic Clinical Analyzer (ACA), a highly regarded comparative system. With the clinical decision level for upper normal being 120 mg/dL, the dry reagent carrier shows a dynamic range of 20–625 mg/dL glucose. Correlating the Ektachem slide with the ACA using 160 clinical samples yields a regression line $y_{\text{Ektachem}} = 0.9865x_{\text{ACA}} - 0.78$ mg/dL, a standard error of 4.4 mg/dL, and a correlation coefficient of 0.999 (*16*).

Dry reagent chemistries for clinical analysis of enzymes also demonstrate acceptable performance. Table II summarizes the performance of the Seralyzer dry reagent strip for CK analysis, developed by Ames, and compares it to the performance of the Du Pont ACA for CK. With a clinical decision level for upper normal of about 100 U/L at 37 °C, the dry reagent strip has a dynamic range of 0–1000 U/L of enzyme. Correlating the CK dry reagent chemistry with a commercially available automated analyzer using 87 clinical samples yields a regression line $y_{\text{reagent strip}} = 0.98x_{\text{Rosalki assay}} + 5.5$ U/L, a standard error of 16 U/L, and a correlation coefficient of 0.999.

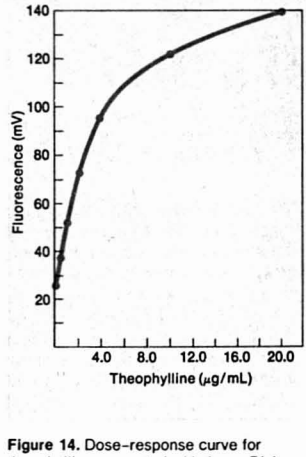
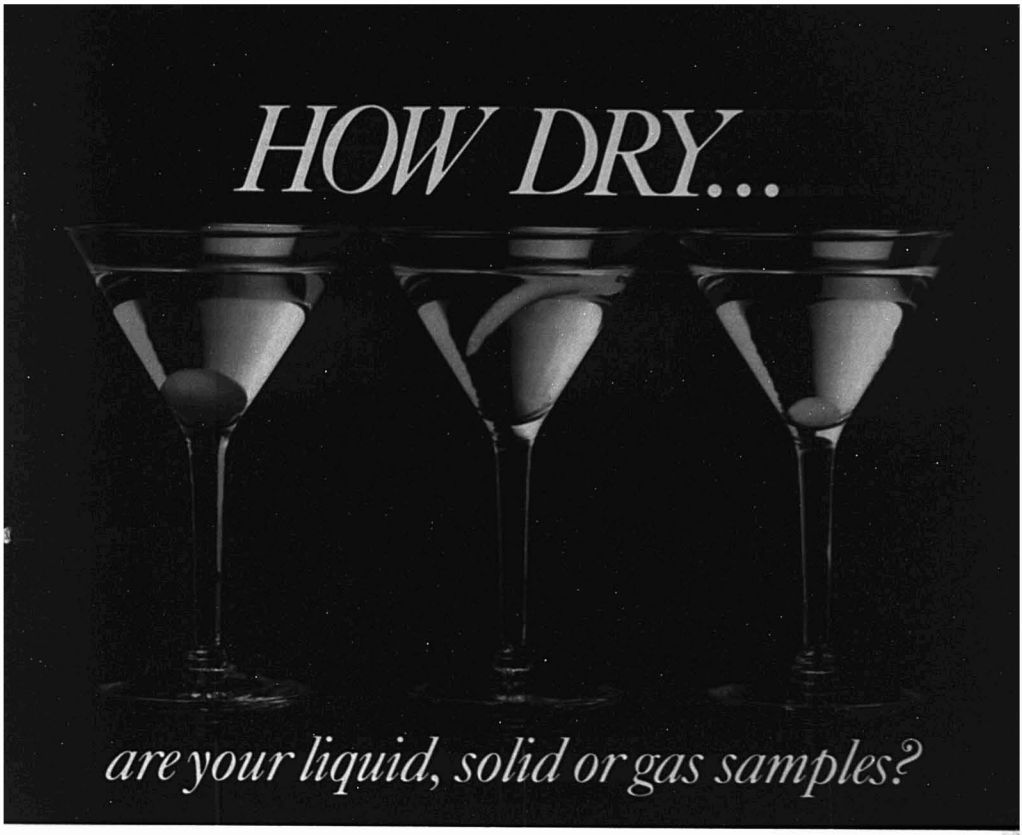


Figure 14. Dose–response curve for theophylline generated with Ames Division, Miles Laboratories, Inc., reagent strips for theophylline

Dry reagent chemistries for therapeutic drug analysis also compare favorably with established methodologies. Table III summarizes the performance of Ames dry reagent strips for theophylline determination and compares it to Syva's Enzyme Multiplied Immunoassay Technique—antiasthmatic drug (Emit-aad) procedure for



Fisher's Automatic K-F Titrimeter® provides the answers quickly and dependably. Performs precise volumetric moisture determinations with pushbutton ease. Results accurate to 1%.

System uses microprocessor-controlled digital buret and amperometric endpoint detection to provide sensitivity of 20μg H_2O. Features proportional endpoint approach. Automatic endpoint confirmation. Pushbutton solvent delivery and purging of waste from reaction vessel. Standard Karl Fischer reagent bottles attach directly without transfer. You can also use pyridine-free titrant (Hydranal*).

You're protected. Effectively sealed system safeguards operator and lab from toxic, noxious vapors.

Universal use. The Karl Fischer method is a world standard for moisture testing of a great variety of materials including:

Chemicals	Plastics	Petroleum derivatives
Cosmetics	Textiles	Pharmaceuticals
Foods	Tobacco	Paper products

Fisher applications engineers have developed specific time-saver moisture procedures including: Amines. Butter and margarine. Grain alcohol. Quench oils. Pharmaceutical tablets. Polyester resins. Tall oil. And more. Yours for the asking.

Flexible options. Simply plug-in our pre-programmed Calculator/Printer accessory for enhanced automation, documentation, automatic correction for parasitic reactions. Other modules open up a full range of titration capabilities.

You're supported. Design and manufacture by Fisher means you get immediate help when it's needed: equipment, literature, technical backup, supplies, service. As close as your Fisher branch.

*Hydranal is registered trademark of Riedel-deHaën AG.



For further information, circle reply card number shown, or phone (412) 562-8543.

Circle 56 for literature.
Circle 57 for a demonstration.

Fisher Scientific
An ALLIED Company

Table I. Comparison of Precision of the Dry Reagent Chemistry Ektachem for Glucose with the Du Pont ACA

System	Glucose (mg/dL)	n	Precision (%CV = SD/mean × 100) Within run	Day-to-day
Ektachem slide	68.5	174	0.91	1.42
for glucose	99.9	174	0.95	1.51
(Eastman Kodak)	296.1	161	0.66	1.32
Du Pont ACA[a]	106.1	20	1.6	—
	476.6	20	0.5	—
	105.1	20	—	1.9
	472.4	20	—	0.8

[a] Glucose test methodology for Du Pont ACA

Table II. Comparison of Precision of the Seralyzer Dry Reagent Strips for CK with the Du Pont ACA

System	Creatine kinase (U/L)	n	Precision (%CV = SD/mean × 100) Within run	Day-to-day
Seralyzer dry	58	180	6.3	—
reagent strip for CK[a]	158	180	3.1	—
	357	177	2.6	—
	58	60	—	6.5
	158	60	—	3.4
	357	59	—	2.8
Du Pont ACA[b]	161	20	2.4	—
	684	20	1.8	—
	133	20	—	3.2
	680	20	—	4.4

[a] Ames Division, Miles Laboratories, Inc., product package insert for CK reagent strips
[b] CK test methodology for Du Pont ACA

Table III. Comparison of Precision of Dry Reagent Strips for Theophylline Analysis with Syva's Emit-aad

System	Theophylline (μg/mL)	n	Precision (%CV = SD/mean × 100) Within run	Day-to-day
Ames dry reagent	5.0	30	8.4	—
chemistry for	15.0	30	3.8	—
theophylline[a]	25.0	30	3.6	—
	5.0	10	—	8.4
	15.0	10	—	3.7
	25.0	10	—	3.6
Syva Emit for theophylline[b]	10.0	20	<10%	—
	7.5	10	—	<15%
	25.0	10	—	<15%

[a] Reference 14
[b] Syva product package insert

theophylline. With the drug toxicity at levels greater than 20 μg/mL, the dry reagent strip has a dynamic range of 0–40 μg/mL theophylline. Correlating the dry reagent strips with the Emit procedure using 25 clinical samples yields a regression line $y_{\text{reagent strip}} = 1.06x_{\text{Emit-aad}} - 1.3$ μg/mL, a standard error of 1.9 μg/mL, and a correlation coefficient of 0.992.

Summary

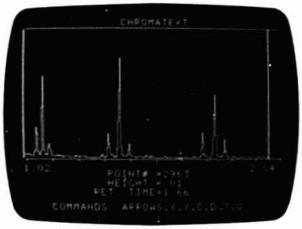
The small sample volumes needed to conduct an analysis make these chemistries suitable for clinical analysis of sera from geriatric and neonatal patients. Most of the dry reagent chemistries do not require more than 10 μL of serum or 30 μL of whole blood. Since infants have a small total blood volume, it is undesirable and difficult to extract a sufficient quantity of sample to conduct serum analysis by conventional methods (0.5–2.0 mL serum). Dry reagent chemistries are custom-made for conducting total serum profiles on a minimal sample volume. Hence, a serum profile of 15 tests requires only 150 μL of serum or about 300 μL of whole blood. In the long run, this will translate into better medical care for infants and the elderly.

The simplicity of using dry reagent chemistries and small instrumentation favors more decentralized clinical testing. Traditionally, laboratories for clinical analysis have been centralized in hospitals to serve the routine needs of wards and the specialized needs of intensive care wards and outpatient clinics. These services also were provided to small clinics and private practitioners. Private laboratories provided the same basic services, but usually at lower costs because of the larger customer base. Establishing and maintaining a central laboratory require a variety of often expensive automated instrumentation, reagents, and skilled operators. To make testing efficient and cost-effective, central laboratories depend on high-volume testing. Because of their stability and discrete formats, dry reagent chemistries allow cost-effective low-volume testing. This, in conjunction with the low cost of small instruments that have the capability of analyzing for a variety of chemistries, encourages decentralized clinical testing. For example, physicians could run in the office all the routine analyses that they would otherwise send to a laboratory. The advantage is a rapid analysis extracted from a freshly drawn blood sample. Further, dry reagent chemistries, by virtue of instrumentation, also can be used for high-volume testing in central laboratories, and they are sufficiently flexible to meet the needs of emergency and intensive care wards.

Probably the ultimate in decentralized testing is the home care front. With dedicated, inexpensive, handheld instruments, dry reagent chemistries can allow patients to monitor and control their own medication. One area where this has had a great impact is on the philosophy of treating the insulin-dependent diabetic. It is becoming clear to the medical profession that maintaining a well-regulated glucose level is a desirable way of dealing with diabetes. Now, insulin-dependent diabetic patients can control their blood glucose levels by appropriate insulin doses based on frequent blood glucose monitoring at home with available dry reagent chemistries. These patients often need fewer visits to the doctor and can lead more normal, productive lives. By controlling glucose levels many progressive aspects of the disorder (e.g., blindness, kidney failure, and circulatory problems) may be retarded or eliminated.

(*Continued on p. 514 A*)

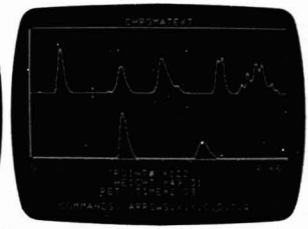
Your present GC or HPLC and ISAAC/Apple can do all this and more, within your budget, without programming.



Capture data.



Recall it.



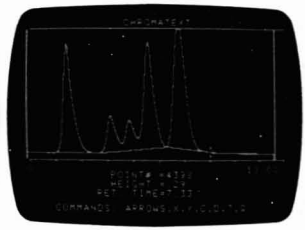
Integrate 2 channels.



Blow up peaks.



Ratio wavelengths.



Subtract baselines.



You don't have to be a computer expert to store and recall virtually unlimited numbers of chromatograms, and to manipulate your separations data the way you've always wanted to.

Not when you attach the new ISAAC/Apple Chromatography System to your GC or HPLC.

Because Chromatext software is menu-driven, you're led through every operation by clear, easy-to-understand instructions right on the screen. No new language to learn; no programming to do. Yet your system is powerful enough to expand as you do.

Installation is easy. Just detach your old strip chart recorder or integrator, and plug in your ISAAC/Apple. For hard copies, add the system printer. You'll be up and operational on day one.

For more information, phone toll-free, write, or check the Reader Service Number below.

Apple is a registered trademark of Apple Computer, Inc.
Cyborg is a registered trademark of Cyborg Corporation.
Chromatext is a trademark of Cyborg Corporation.

ISAAC

Cyborg® 55 Chapel Street, Newton, MA 02158 (617) 964-9020 toll-free (800) 343-4494

CIRCLE 34 ON READER SERVICE CARD

The Right GC For All Budgets



GOW-MAC GC's offer flexibility of detector from GC to GC rather than interchangeable detectors within a single instrument. By avoiding this expensive option, you get more GC for the dollar.

For example, you could buy a programmable thermal conductivity GC *and* a programmable FID GC from GOW-MAC for less than the cost of a combined FID/TCD instrument. That way either is available for ready use.

Learn the GOW-MAC story. Our small, dedicated GC's are not budget GC's: they are high quality instruments. For a free brochure describing GOW-MAC GC's, circle the Reader Service Number.

GOW-MAC INSTRUMENT CO.
PO Box 32, Bound Brook, New Jersey 08805

CIRCLE 69 ON READER SERVICE CARD

Until a cure for diabetes is developed, self-monitoring and adjustment of medication by the patient in conjunction with a physician is the therapy of choice.

Acknowledgment

The author would like to acknowledge Gary Shepherd, Steven C. Charlton, Alan McCleary, and Alfred C. Greenquist for valued comments and discussions.

References

(1) Duffin, G. F. "Photographic Emulsion Chemistry"; The Focal Press: New York, 1966.
(2) Deryagin, B. M.; Levi, S. M. "Film Coating Theory"; The Focal Press: London and New York, 1964.
(3) Clark, J. d'A. "Pulp Technology and Treatment of Paper"; Miller Freeman Publications, Inc.: San Francisco, 1978.
(4) Myers, R. R.; Long, J. S. "Film Forming Compositions"; Marcel Dekker, Inc.: New York, 1967, 1968, 1972; Vols. 1, 2, 3.
(5) Kortüm, G. "Reflectance Spectroscopy: Principles, Methods, Applications"; Springer-Verlag: New York, 1969.
(6) Pesce, A. J.; Rosén, C. G.; Pasby, T. L. "Fluorescence Spectroscopy"; Marcel Dekker, Inc.: New York, 1971.
(7) Kubelka, P.; Munk, F. *Z. Tech. Phys.* **1931,** *12*, 593.
(8) Williams, F. C.; Clapper, F. R. *J. Opt. Soc. Am.* **1953,** *43*, 595.
(9) Kuan, S. S.; Lau, H. K.; Guilbault, G. G. *Clin. Chem.* **1975,** *21*, 67.
(10) Spayd, R. W. et al. *Clin. Chem.* **1978,** *24*, 1343.
(11) Rosalki, S. B. *J. Lab. Clin. Med.* **1967,** *69*, 696.
(12) Curme, H. G. et al. *Clin. Chem.* **1979,** *25*, 1115.
(13) Charlton, S. C.; Zipp, A.; Fleming, R. L. *Clin. Chem.* **1982,** *28*, 1857.
(14) Walter, B.; Greenquist, A.; Howard, W. E. *Anal. Chem.*, in press.
(15) Burd, J.; Carrico, R.; Fetter, M.; Buckler, R.; Johnson, R.; Boguslaski, R.; Chistner, J. *Anal. Biochem.* **1977,** *77*, 56.
(16) Curme, H. G. et al. *Clin. Chem.* **1978,** *24*, 1335.



Bert Walter received his BA and PhD degrees in chemistry and biochemistry, respectively, from the University of Minnesota. He is currently a senior research scientist with Ames Division, Miles Laboratories, Inc. His research interests are in developing analytical assays for clinical testing and integrating multistep procedures to generate miniature single-step dry format reagent carriers.



SENSITIVITY SENSIBLY PRICED.

Leave it to American manufacturing know-how to combine lab grade sensitivity, workhorse dependability and a very sensible price in one versatile top loader—the Ohaus® Brainweigh® Model B300D electronic balance.

Priced at only $1,595 suggested list, this precision balance handles the most exacting measurements in the fine 30 g range with a readability of 0.001 g. It also provides big job capacity in the 300 g range with 0.01 g readability. All it takes is a touch of the switch.

In either range, readings are rock steady, thanks to advanced circuitry that virtually eliminates readout flutter caused by drafts or vibrations. Large, bright digits are easily readable from any operator position. And the balance can be quickly connected to all common computers, printers or other peripherals with your choice of five user-installable interfaces.

Compact as a desk telephone, the Model B300D tackles any lab work with legendary Ohaus dependability and traditional Ohaus value. For more information about the Model B300D and other Brainweigh electronic balances, contact Ohaus or your preferred Ohaus dealer.

OHAUS

BRAINWEIGH ELECTRONIC BALANCES

CIRCLE 156 ON READER SERVICE CARD

☐ I'd like some more sensible information about the Model B300D and the other Ohaus electronic balances.
☐ I'd also like to know about Ohaus mechanical balances.

Ohaus Scale Corporation
29 Hanover Road, Florham Park, NJ 07932
(201) 377-9000 Telex: 136518

AC-4/83

Name_____ Title_____

Organization_____ Address_____

City_____ State_____ Zip_____ Phone_____

© 1982 Ohaus Scale Corporation. Ohaus and Brainweigh are trademarks of Ohaus Scale Corporation. Prices and specifications are subject to change without notice.

NEW LOWER PRICES!

Man and Molecules

Dimensions in Science

Man and Molecules Cassettes:

An easy way to keep up with what's happening in science.

Outstanding scientists are interviewed in language that everyone can understand. Each cassette has two 15-minute programs.

Single Cassette	**$3.50**
Any Four — Nineteen Cassettes	**$3.00/Cassette**
Any 20 or more cassettes to one address	**$2.50/Cassette**

10% discount if payment accompanies order

California residents please add 6% State Use Tax.

Name _____

Address _____

_____

City _____

State _____ Zip _____

Annual Cassette Subscriptions also available

Select your choices and mail to:

American Chemical Society
1155 Sixteenth St., N.W.
Washington, D.C. 20036
Dept. M&M

Science and Society

☐ **World Energy** Dr. Glenn T. Seaborg
The Recycle Society Dr. Glenn T. Seaborg

☐ **Science and the Future** Dr. Linus Pauling
Society and the Future Dr. Linus Pauling

☐ **Chemrawn 2 — World Hunger Problems** Dr. Bryant Rossiter
Chemrawn 2 — World Hunger Solutions Dr. Bryant Rossiter

☐ **The Robots are Coming** Mr. R. Behler and Mr. R. Malczewski
The R&D Gap Dr. Herbert Striner and Rep. George Brown

☐ **Feeding the World** Dr. Norman Borlaug
Fighting World Famine Dr. Jean Mayer

☐ **Good News on Organic Farming** Dr. Garth Youngberg
Foods for the Future Dr. Robert Wiley

Health and Medicine

☐ **Vitamins — More is not Better** Dr. Victor Herbert
Evolution of the Human Diet Dr. Glynn Isaac

☐ **Sickle Cell Update** Dr. Clarice Reid
Antibiotics: The Vicious Circle Dr. Richard Novick

☐ **New Promise for Preemies** Dr. Shlomo Shinnar
New Developments in Dentistry Dr. Rayfael Bowen

☐ **Update on the Pill** Mr. Ward Rinehart
Ring Around the Collar Dr. Kay Obendorf

☐ **Rhythmic Humans I** Dr. Thomas Wehr
Rhythmic Humans II Dr. Thomas Wehr

☐ **The Organized Brain** Dr. Ronald MacGregor
Windows to the Brain Dr. Terry Bahill

☐ **The Science of Pain I** Drs. Edward Huskisson and William Beaver
The Science of Pain II Drs. John Bonica and Gerald Aronoff

☐ **The Frozen Cell: Cryobiology** Dr. Harold Meryman
How Blood Clots Dr. Russell Doolittle

☐ **Folk Medicine** Dr. Ned Heindel
Nuclear Medicine Dr. Ned Heindel

☐ **Vision and the Nervous System** Dr. Arthur Sanderson
Cataract: The Clouded Eye Dr. Abraham Spector

☐ **Trace Metals and Aging** Dr. Gunther Eichhorn
Diabetes: The Receptor Problem Dr. Jesse Roth

☐ **Halting Emphysema** Dr. James Powers
Pulmonary Fibrosis Dr. Ronald Crystal

☐ **The Stopped Heart: Assessing CPR** Dr. Myron Weisfeldt
Chemistry of the Sickled Cell Drs. Wm. Eaton and James Hofrichter

Science

☐ **Laser Age** Mr. John Walters
Verifying Art — It's a Science Dr. George Reilly

☐ **Delving Into Dreams** Dr. Robert McCarley
Earthquake Clues Drs. Mark Shapiro and Kate Hutton

☐ **Chemical Weapons** Dr. Arthur Westing
Tracing Breezes and Bombs Dr. Russell Dietz

☐ **Scientists Responsibility to Public** Dr. Harlyn Halvorson
Who Controls Scientific Data? Dr. Stephen Fienberg

☐ **Composite Materials** Prof. Byron Pipes
Fiber Optics Dr. Suzanne Nagel

☐ **Crime Fighting with Chemistry** Mr. Roger Aaron
Chemistry and Sherlock Holmes Dr. Samuel Gerber

☐ **Symmetry, Antimatter and the Big Bang** Drs. J. Cronin and B. Winstein
Atomic Movies Dr. Albert Crewe

The Natural World

☐ **Animals' Biological Compass** Dr. Joseph Kirschvink
The Horned Faced Bee Dr. Suzanne Batra

☐ **Bioluminescence** Dr. John Warner
Plants that Fight Back Dr. David Rhoades

☐ **A Sea of Chemicals** Dr. William Fenical
The Chemical Tree Dr. John Rowe

☐ **Animal Talk** Dr. Eugene Morton
The Defensive World of Insects Dr. Thomas Eisner

☐ **Problems in Weather Forecasting** Dr. Richard Somerville
Life on the Sea Floor Dr. Robert Hessler

☐ **The Unsteady Sun** Dr. J. Murray Mitchell
Climatic History On Ice Dr. Bruce Parker

☐ **Plants: Chemical Treasure Chest** Dr. Leon Zaikov
The Flowering Mystery Dr. Charles Cleland

☐ **Climate and Food** Dr. Wayne Decker
Plants and Temperature Dr. Judith St. John

Energy

☐ **More Energy from Less** Drs. Meyers, Harris, Meier
Alfalfa: Fuel and Food Dr. Bruce Dale

☐ **A New Look at Solar Economics** Mr. William Wilhelm
Water Weakens Glass Dr. Stephen Freiman

☐ **The Electric Car** Dr. John Hartman
Saving Energy with Batteries Mr. Kurt Kluner

☐ **Synfuels: The Uncertain Solution** Dr. Mark Hanson
Special Essay on Energy Essay Report

☐ **Saving Energy in Buildings** Mr. Christopher Flavin
The Sun's Heat Can Cool Mr. Dennis Schlepp

☐ **The New Age of Materials** Mr. Christopher Flavin
Synthetics: The Petroleum Connection Mr. Christopher Flavin

☐ **Solar Cells: Improving Materials** Mr. Donald Carmichael
Solar Cells: Performance Testing Mr. Donald Carmichael

Space

☐ **Cosmology by Experiment** Drs. Howell Pugh and Paul Richards
The Search for Gravity Waves Drs. Ronald Drever and Stanley Whitcomb

☐ **From Sputnik to Space Shuttle** Dr. Alan Needell
Landsat IV Dr. Vincent Salomonson

☐ **The Rings of Saturn** Dr. Larry Esposito
Saturn and its Moons Dr. Larry Esposito

☐ **Looking at Solar Explosions** Mr. Ken Frost
Jupiter and Beyond Dr. Edward Stone

☐ **Stars and the Elements** Dr. Michael Zeilik
Archaeoastronomy: Sky and Culture Dr. Edwin Kurpo

☐ **Universe of Questions** Dr. John Wheeler
Resources from Space Dr. James Arnold

☐ **The Expanding Universe** Dr. Victor Viola
Interstellar Molecules Dr. Eric Herbst

Environment

☐ **Acid Rain Update** Essay Report
Academia's Chemical Waste Dr. Jack Gerlovich

☐ **Coal Questions** Dr. K.P. Ananth
Fire Toxicity Mr. Gordon Vickery

☐ **Chemicals and Health: Biological Tests** Dr. Benjamin Barnhart Ms. Ann Grow
Chemicals and Health: Toxic Dumps Dr. William Lowrance

☐ **Taking the Hazard Out of Waste** Dr. Robert Pojasek
What to Do With Hazardous Wastes Mr. Thomas Williams

☐ **New Target in Water Pollution** Mr. Joseph Krivak
Environment Doctors Dr. Richard Perrine

☐ **Air Pollution: The Human Factor** Dr. Ralph Stacy
Indoor Air Pollution Mr. John Yocom

☐ **Water Weeds** Dr. Dean Martin
The Red Tide Dr. Dean Martin

☐ **Drinking Water Worries** Dr. John O'Conner
Water Chlorination Problems Dr. William Glaze

Popular Older Programs

☐ **The Vanishing Soil** Mr. Lester Brown
The Not So Limitless Oceans Dr. Joel Goldman

☐ **How Times Has Changed** Sir George Porter
Analyzing with Light Dr. Richard Nathan

☐ **Taking Earth's Temperature From Space** Dr. John Price
Probing the Earth's Magnetosphere Dr. Erwin Schmerling

☐ **Solar Thermal Energy** Mr. J.D. Walton
Coal Furnaces: Think Small Dr. Arthur Squires

☐ **Energy-Efficient Autos** Dr. Gene Mannella
Fuel Cells: Problems and Progress Dr. John Belding

☐ **New Light on Myasthenia Gravis** Dr. Daniel Drachman
Hormones and Aging Dr. George Roth

☐ **Nutrition and the Brain** Dr. John Fernstrom
Chemical Look at Mental Illness Dr. Seymour Kety

☐ **The Brain's Own Morphine** Dr. Solomon Snyder
Narcotics and the Brain Dr. Avram Goldstein

☐ **Plants and Air Pollution** Dr. Howard Heggestad
Particulate Air Pollution Dr. Glen Gordon

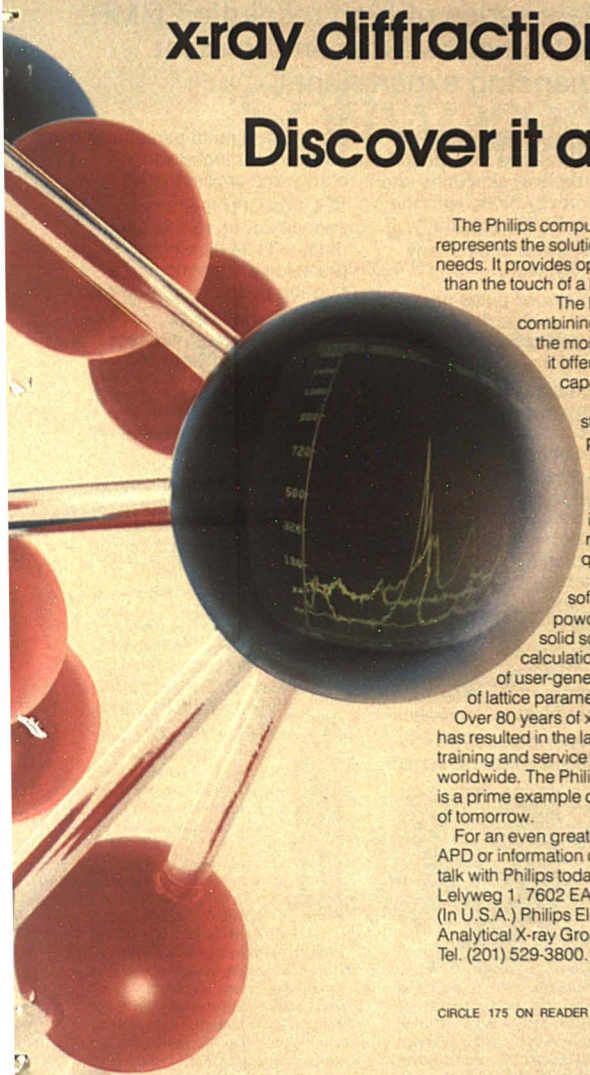
☐ **Genetic Engineering in Agriculture** Drs. P. Carlson and I. Zelitch
Jojoba Power Dr. Milton Harris

☐ **Chemistry of the Mind: Schizophrenia** Dr. Larry Stein
Chemistry of the Mind: Depression Dr. Joel Elkes

☐ **Cancer and Chemicals Part I** Dr. Charles Heidelberger
Cancer and Chemicals Part II Dr. Charles Heidelberger

Explore the advantage of the world's most sophisticated x-ray diffraction software.

Discover it at Philips.



The Philips computerized APD x-ray diffraction system represents the solution to an unparalleled range of analytical needs. It provides optimum results, yet requires little more than the touch of a button.

The Philips APD is totally user oriented. By combining a flexible hardware configuration with the most comprehensive software library available, it offers ease of operation and maximum system capability.

Interactive graphic operation guides the user step by step. In routine studies, a batch program automatically collects the data, then provides final analysis and a printout of identified phases or a calculation of concentrations. Unequaled accuracy in identification of phases is accomplished by a fast, automated search/match routine. A wide choice of algorithms provides for quantitative and profile analyses.

For more sophisticated applications, the APD software package includes programs for indexing powder patterns, isostructural searches aiding in solid solutions analysis, preferred orientation calculations, automated texture analysis, incorporation of user-generated patterns into a data base and calculation of lattice parameters to provide ultra-accurate 'd' spacings.

Over 80 years of x-ray experience on an international scale has resulted in the largest user base and a global network of sales, training and service personnel that meet our customers' needs worldwide. The Philips computerized APD x-ray diffraction system is a prime example of our unique ability to anticipate the technology of tomorrow.

For an even greater discovery of the capabilities of the APD or information on an upgrade of your present system, talk with Philips today. Contact: N.V. Philips Analytical X-ray, Lelyweg 1, 7602 EA Almelo, The Netherlands. Tel. (31) 5490-18291. (In U.S.A.) Philips Electronic Instruments, Inc., Analytical X-ray Group, 85 McKee Drive, Mahwah, NJ 07430. Tel. (201) 529-3800.

CIRCLE 175 ON READER SERVICE CARD

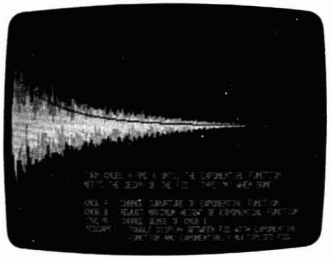
PHILIPS

Scientific & Analytical Equipment

PHILIPS

Introducing simplicity, versatility and productivity to NMR.

A new series of high resolution NMR spectrometers for even the most demanding experiments.



The unique features of the new AM Series provide truly new levels of simplicity and productivity along with the built-in Bruker versatility.

Check these against any other Supercon:

- Advanced pulse program system, with software designed specifically for simplicity and clarity.
- Complete microprocessor control of basic spectrometer functions, designed to simplify system set-up, lock operation and magnet shimming.
- Fast 8-color display processor for display of complex 2-D contour plots in seconds.
- Fourier transform array processor, with associated display and multi-pen plotter software for increased clarity and productivity.
- Large CPU memory capacity of up to 1 M word data, with 24 bit single precision arithmetic and a floating point instruction set.
- Extensive line of superconducting magnet systems from 200 to 500 MHz.
- Plus Bruker's flexible design concept, allowing for future upgrading.



So, if you want simplicity, versatility and productivity in your NMR work, write for complete information on the new AM Series or call a Bruker representative.

Bruker Instruments, Inc., Manning Park, Billerica, MA 01821. In Europe: Bruker GmbH, Silberstreifen, D-7512 Rheinstetten 4, West Germany.

With the new Bruker AM Series.



BRUKER *NMR Systems designed to solve problems.*

CIRCLE 21 ON READER SERVICE CARD

Software Secrets

Do analysts need to know more about the software that runs their instruments?

The most sophisticated of today's analytical instruments, and even many of the simpler ones, are connected to dedicated or stand-alone computers that control their operation and process the data they generate. As software-controlled instrument operation has become more and more commonplace, a thorny question has arisen: Is the analytical chemist being provided with sufficient information about *how* the software is actually transforming the data?

Many analysts would say no. They would prefer access to more detailed information on the computer programs that run their instruments. In some cases they are even asking for complete program listings so they can modify sections of code.

But the instrument manufacturers, afraid of software piracy by competitors and of ill-advised software modifications by users, seldom allow their customers access to program listings. Many vendors are reluctant even to disclose the algorithm, which describes the logical design of a computer program.

"It's very important for a user of an analytical instrument to understand the instrument," explains Allan Smith, a physical chemist at Drexel University. "That certainly means understanding the physical principles behind the measurement being made. But with the great tendency now to take those measurements and transform them mathematically in a whole variety of ways, it's also important to understand the transformations of data. Just as good instrument manufacturers will be pretty explicit about a mechanical part of the apparatus for those who really need to understand it, they should also be explicit about the software used to process the data.

If the scientific community is to benefit from the enormous amounts of effort that are put into software development, it has to be prepared to pay something for it.

At the very minimum, they should publish the details of the algorithm that was used, with some specific examples of how representative data are transformed."

Protecting Software

But with software development costs going through the roof, the vendors have little choice but to closely protect their investments. "I would say that the software for our data station has probably cost us in the area of $5 million," says Abraham Savitsky of Perkin-Elmer. "At the price this software is sold to the customer, we will barely recover the costs of development. If the scientific community is to benefit from the enormous amounts of effort that are put into software development, it has to be prepared to pay something for it. Otherwise, there's no justification for a commercial organization to put it out." [In this month's LETTERS column (p. 490 A), Melvin W. Redmond, Jr. of Perkin-Elmer expresses a similar opinion.]

"We have a big stake in our software," adds Glenn Ouchi of Nelson Analytical. "From our perspective, to make all the code available would be a mistake. You'd just be allowing the competition to catch up with you."

Many vendors would be happy to protect their software with patents instead of trade secrets. "Unfortunately," explains Savitsky, "the Patent Office has been sticky. Historically, they have insisted that software is not patentable. Patents are given on 'things,' and they have claimed that software is not a 'thing,' but an idea. Well, that's not really true, because software is the embodiment of an idea."

Some companies still do give their customers access to program listings. "We feel it's very important for people using computers to know how their data is being treated," explains Fred Putnam of Laboratory Technologies Corporation (*Chem. Eng. News* **1982**, *60* (37) 35–6). "For instance, subroutines that contain models for fitting peaks to data can be very easily supplied in FORTRAN source code. This allows users to read, understand, and even modify the program." And at Cyborg Corporation, "our philosophy has been to share software listings with our customers," says Nick Virca. "In fact, we have a user-contributed library based on customers sharing their program modifications back with us. Someone buying our ISAAC system has all this software available to them at no charge."

The major manufacturers have also devised various means of providing as much information as they possibly can without jeopardizing any of their trade secrets.

One approach is to provide part of the software in object code, which is undecipherable, and the rest in source code. Sections of code that are nonproprietary and that users are likely to

0003-2700/83/0351-519A$01.50/0
© 1983 American Chemical Society

PCR 81
82 PCR



PCR PRODUCTS

A general catalog listing physical properties and prices is available, free. This catalog lists:

Organofluorine Compounds
Organosilicon Compounds
Derivatizing Reagents
Mass Spec Standards
NMR Reference Compounds
Crown Ethers
Synthetic Reagents
Fine Organic Intermediates
Terpenes

If you are interested in any of the above products, you should have your own copy of our catalog.

Write or call for your free copy today.

PCR RESEARCH CHEMICALS, INC.
P.O. BOX 1778 GAINESVILLE, FLORIDA 32602 (904) 376-7522
SCM ORGANIC CHEMICALS DIVISION, SCM CORPORATION

CIRCLE 174 ON READER SERVICE CARD

FLOWMETERS

The Lab-Crest® Flowmeter Catalog (yours on request) is your guide to selection and application of the right flowmeter for your laboratory needs... from America's most experienced maker of variable-area flowmeters. Write, or call (215) 674-6610.



Lab-Crest®

Lab-Crest's new Corrosion-Resistant Rotameter employs *Teflon* end fittings and needle valve... does not require O-Ring Seals.

LAB-CREST SCIENTIFIC
A SUBSIDIARY OF FISCHER & PORTER
Warminster, Pa. 18974

CIRCLE 127 ON READER SERVICE CARD

want access to can be supplied in a high-level source language, such as FORTRAN, that users can read and modify. Company software maintenance is then usually based solely on the object-level code, so the manufacturer does not have to be concerned about the consequences of software modifications by users.

Nelson Analytical takes a slightly different approach to software protection. It supplies its software in high-level code, selected lines of which are replaced by dummy symbols when a user lists the program. "We secure the proprietary parts of the code only, about 10%. This means about 90% of the software can still be accessed by the user," explains Glenn Ouchi. "The customer can alter parts of the program if he wants to, and we still protect the code we've spent five or six man-years on." The policies of other manufacturers reflect many variations on this theme.

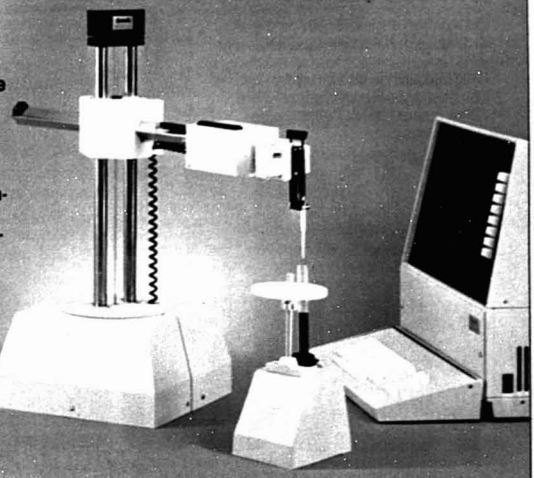
User Modifications

Donald Monn, director of electronic and computer services at Conoco, does not encourage his people to modify commercial software. "The first thing a user has to decide is whether he's got the technical and programming capability to make changes in turnkey systems," says Monn. "Our initial recommendation to someone who wants to buy a system and then modify it is, 'You probably don't want to do that.'

"But we also don't want to be in a situation where we've bought a black box with no editable code, and where we cannot get the kind of support we would like to have from the manufacturer," Monn continues. "If changes *are* going to be needed, we recommend our analytical people write a purchase agreement in which the vendor guarantees that changes can be made on the system itself. Most of the time we would like to be able to make changes ourselves, since it's very difficult to get the manufacturer to make specific changes. It's very expensive if it's not a change the vendor wants to include in all coming systems.

"For the most part we have gotten good cooperation from manufacturers," says Monn. "And obviously we're willing to pay for the capability to make changes, whether it be in terms of added hardware, or certainly in terms of purchasing the source documentation we may need. Occasionally, a manufacturer will say, 'No, that's proprietary; we use an algorithm we don't want to tell anybody about.' Our recommendation then is for the user to agree to sign a nondisclosure or secrecy agreement—whatever the ven-

The Amazing Zymate
Laboratory Automation System



Automate your laboratory sample preparation procedures. Free yourself from repetitive, tedious, step-by-step laboratory operations with the **Zymate** System for **Automated Sample Preparation and Analysis.**

The **Zymate** System combines robotics with state-of-the-art microprocessor technology to perform common laboratory operations — liquid handling, weighing, sample conditioning, and separations — even in hazardous areas.

A **Zymate** System will:

- Weigh, dilute, mix, and transfer samples to test tubes or vials for any chemical sample preparation procedure.
- Pipet, filter, and concentrate samples for chromatography or spectroscopy analysis.
- Homogenize, centrifuge, and extract samples for biological testing.

In short, for any operation you do in your laboratory, the **Zymate** Laboratory Automation System can help you do it better, safer, more economically, and with less chance for error. The System is well suited for **research & methods development, multiple analyses using several methods,** and **dedicated, routine analysis.**

Write or call today for complete information about automating your laboratory with the Zymate Laboratory Automation System.

Zymark

Zymark Corporation
Zymark Center, Hopkinton, Massachusetts 01748
(617) 435-9041

Laboratory Automation for Chemistry and Biotechnology

Zymark and **Zymate** are trademarks of the Zymark Corporation

CIRCLE 245 ON READER SERVICE CARD

If You Need An Explosion-Safe Refrigerator, Then You Need A Revco.

Revco's new line of Explosion-Safe Refrigerators (4°C) have these standard features:

- Audible and Visual Alarms for Low Voltage or Power Failure, Door Ajar or Unsafe Temperature Conditions.
- Continuous Temperature Display.
- Alarm Delays with Automatic and Manual Re-set Modes.
- Computer Connections for Automatically Collecting, Storing and Monitoring Temperature Data.
- Key Operated Master Switch for Maximum Protection.
- Stainless Steel Interior and Stainless Steel Wire Shelves.
- UL Rated Explosion-Proof Interior Motors.
- The Industry's Only 13 Month Full Warranty on both Parts and Labor.

Available in two convenient lab sizes: 23 and 50 cubic feet.

Write or call today for your free full-color catalog, or contact one of these nation-wide dealers: American Scientific Products, Curtin Matheson Scientific, Fisher Scientific, Sargent-Welch Scientific, Arthur H. Thomas Company and VWR Scientific.



REVCO

Rheem Manufacturing Company/Scientific Products Division
Aiken Road, Box 275, Asheville, N.C. 28804. Tel.: 704/658-2711. Telex: 57-7449.

CIRCLE 183 ON READER SERVICE CARD



Our .64m Monochromator performs like a 1m

The HR-640 Monochromator Spectrograph has the high aperture of smaller systems and the extended scanning range and resolution of larger spectrometers. A full line of multiport, computer interface and grating options gives the HR-640 unprecedented performance and flexibility. **Call or write ISA today!** 173 Essex Ave., Metuchen, N.J. 08840 201/494-8660. In Europe, 16-18 Rue du Canal 91160 Longjumeau, France, Tel. 909.34.93

JOBIN YVON Instruments SA, Inc.
J-Y Optical Systems Division

CIRCLE 104 ON READER SERVICE CARD

We don't want to be in a situation where we've bought a black box with no editable code, and where we cannot get the kind of support we would like to have from the manufacturer.

dor requires. If the vendor still says no, we recommend that the user look very carefully at another manufacturer's system."

Even though source listings cannot always be made available in this way, most users, and in fact many vendors, agree that at least the software algorithms should be available whenever possible. "It seems reasonable . . . to expect instrument vendors to share algorithms with users who want to be sure that the invisible data treatment being applied is appropriate to their requirements," wrote George H. Morrison in his January Editorial (*Anal. Chem.* **1983**, *55*, 1).

The manufacturers do make algorithms available whenever they can, but sometimes even this is not possible. For example, says Perkin-Elmer's Robert Hannah, "we have a transmittance-to-absorbance conversion that's part of our standard IR software package. That's highly proprietary, because it operates extremely fast. We're not willing to tell our competitors how we do that."

Publishing Software

Some argue that one root of the software problem is the refusal of journals such as ANALYTICAL CHEMISTRY to publish software. "Since software is not published," says Tomas Hirschfeld of Lawrence Livermore National Laboratory, "people do not make an effort to document it properly. When you want to follow a technique in the literature that is to any extent dependent on software written by the author, you will find that the author never wrote it up since no journal would accept it for publication. I think we're shooting ourselves in the leg on that one."

But publishing software is simply not practical for a number of reasons:



A shot in the arm

for forensic, pharmaceutical, pesticides and coatings analysis

Now it's possible to use infrared spectrophotometry to aid the identification of unknown materials with more speed, accuracy and flexibility than ever before – especially in the forensic and pharmaceutical fields.

Sargent-Welch's four new Infrared Library Search library packages provide a massive boost for users, forming probably the finest application-orientated libraries of such information available anywhere in the world.

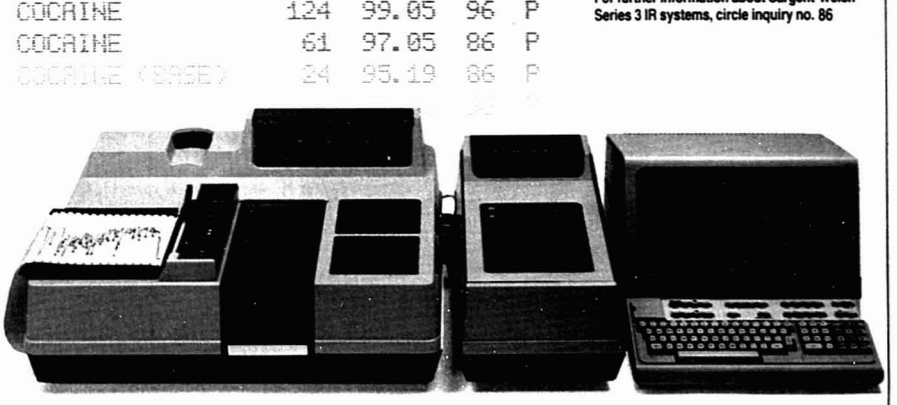
Most importantly, two new drugs libraries are introduced, each containing approximately 800 spectra. The drugs of abuse library classifies addictive drugs like amphetamines, barbiturates, opium derivatives and hallucinogens – and their fillers. There is also a drugs library classified according to therapeutic use, such as cardiac, bronchial, or nutritional fields. The classification also includes what the drug is used for – as a decongestant, for example.

For the agrochemical and food and hygiene industries, the new pesticides library includes herbicides, insecticides and fungicides – and some breakdown products. For the chemical, paints and plastics industries, the latest Coatings II library is the second edition, covering 1717 spectra. User-generated spectra may be added to any library.

Sargent-Welch's Library Search software, for use with Series 3 infrared spectrophotometry systems, is unique. Special algorithms have been used in the Library Search program to minimise any effects due to wavenumber shifts between unknown and reference spectra related to the spectrophotometer serviceability, resolution or the actual sample environment.

For further details about Sargent-Welch IR data handling and Library Search, circle inquiry no. 85

For further information about Sargent-Welch Series 3 IR systems, circle inquiry no. 86

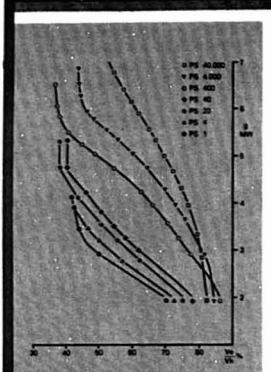


SARGENT-WELCH SCIENTIFIC COMPANY
7300 NORTH LINDER AVENUE, P.O. BOX 1026, SKOKIE, ILLINOIS 60077 Tel 312-677 0600

We're instrumental in your laboratory!

Anaheim, Baton Rouge, Birmingham, Cleveland, Dallas, Denver, Detroit, Skokie, Springfield NJ, Washington D.C.
Inquiries outside USA contact Pye Unicam Ltd, York Street, Cambridge, England CB1 2PX.

Polymer Analysis via HPLC



Prepacked HPLC columns with spherical 5&10 micron particles of LiChrogel™ PS

- For monomer, oligomer & polymer analysis
- Guaranteed performance of 40,000 & 25,000 N/m
- Pressure stable up to 2000 psi
- Fractionation range <100 to 50,000,000

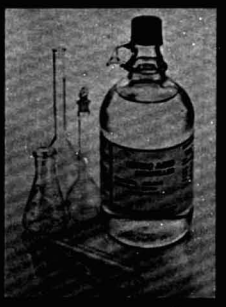
For complete information on these products write or call today.

The new dimension in lipophilic GPC

EM SCIENCE
A Division of EM Industries, Inc.
480 Democrat Road
Gibbstown, New Jersey 08027-9899
(609) 423-6300

Visit us at Booth #C21-C22 at FASEB
CIRCLE 64 ON READER SERVICE CARD

HIGH PURITY ACIDS



- **ACS REAGENT ACIDS**
- **REDISTILLED ACIDS**

Produced by taking ACS Reagent Grade acids and redistilling them in glass. This distallation yields high purity acids with very low or absent trace elements.

- **DOUBLE-DISTILLED ACIDS**

Manufactured by taking the already very pure redistilled acids and passing them through Vycor/Quartz stills twice. This process removes virtually all volatile and non-volatile impurities.

For details on the full line of GFS Chemicals High Purity Acids, circle the reader service number below.

GFS CHEMICALS

P.O. Box 23214 • Columbus, Ohio 43223 • (614) 881-5501

CIRCLE 65 ON READER SERVICE CARD

Focus

- How can journals afford to print programs that are, in some cases, thousands of lines in length?
- It is arguable whether a computer program truly represents analytical research.
- How do you subject a computer program to peer review? How many reviewers can devote the time needed to review the logic of a complex computer program for scientific accuracy and validity?

However, if development of a computer program is part of a research project, authors are expected to make the program available to readers by mail on request, or to submit the program listings as supplementary material. Supplementary material is not itself published, but an announcement on the nature of the material and instructions on how to order it appear along with the published manuscript in ANALYTICAL CHEMISTRY.

Meeting of Minds

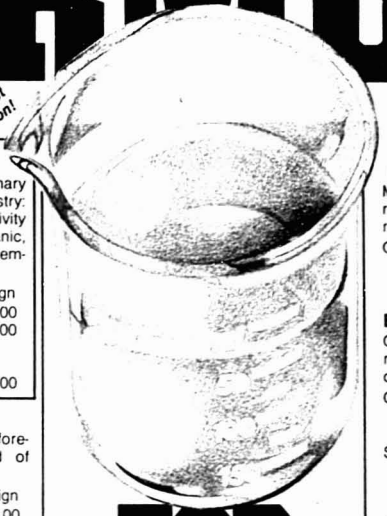
Ultimately, even the user who does not have a complete software description can fall back on his or her ability to determine if the software is behaving the way it's supposed to behave. "This software stuff is nothing more than electronics, soft electronics," says Bruce Kowalski of the University of Washington. "When you buy an instrument, you may not know beans about electronics. So you don't really understand how signals are being treated inside that instrument. But you can still run standards and test your instrument in all sorts of ways: linearity, signal-to-noise ratio, detection limits, calibration, etc. It's the same thing with software. So the company may refuse to tell you what the software is doing, but the instrument can still be checked as to what it's doing in the chemical world."

"A lot of hardware features of an instrument also have funny effects on the data," says Hirschfeld. "These funny effects were never properly documented by the manufacturers. We let them get away with this as long as they were making analog instruments. And they don't see why they should be penalized for making a better instrument."

"There's always a fine line," says Drexel's Smith. "You can't say nothing about a software package, or else people won't trust it. You can't say everything about a package, or people will copy it. Somewhere in between there has to be a meeting of minds between the people who build these instruments and the people who use them."

Stuart A. Borman

FORMULA FOR SUCCESS



Our Newest Publication!

ORGANOMETALLICS

Monthly journal with an interdisciplinary approach to organometallic chemistry: synthesis; structure and bonding; reactivity and mechanism; applications in organic, inorganic, polymer, and solid state chemistry, as well as materials science.

One Year Rate	U.S.	Foreign
ACS Members	$ 24.00	$ 40.00
Nonmembers	$180.00	$196.00
Supplementary material on microfiche	$ 35.00	$ 50.00

ANALYTICAL CHEMISTRY

This monthly journal is the world's foremost publication in the vital field of measurement science.

One Year Rate*	U.S.	Foreign
ACS Members	$ 18.00	$ 37.00
Nonmembers	$ 24.00	$ 67.00

Canada: Nonmember rate: $43.00

CHEMICAL AND ENGINEERING NEWS

Chemical newsweekly and the official publication of the ACS that all members receive as part of their dues.

One Year Rate*	U.S.	Foreign
Nonmembers	$ 34.00	$ 58.00

CHEMTECH

Stimulating, personal monthly helping chemists and engineers arrive at innovative solutions to real problems.

One Year Rate*	U.S.	Foreign
ACS Members	$ 22.00	$ 28.00
Nonmembers—Personal	$ 33.00	$ 39.00
Nonmembers—Institutional	$155.00	$161.00

ENVIRONMENTAL SCIENCE AND TECHNOLOGY

Monthly publication for chemists and engineers engaged in the study and maintenance of environment through the application of chemical principles.

One Year Rate*	U.S.	Foreign
ACS Members	$ 20.00	$ 30.00
Nonmembers—Personal	$ 25.00	$ 35.00
Nonmembers—Institutional	$110.00	$120.00

***There are multiple year rates available for *Chemical & Engineering News, Analytical Chemistry, Environmental Science & Technology*, and *CHEMTECH*. Details on request.**

ACCOUNTS OF CHEMICAL RESEARCH

Monthly publication offering short, critical reviews written by scientists active in the research described.

One Year Rate	U.S.	Foreign
ACS Members	$ 18.00	$ 23.00
Nonmembers	$ 79.00	$ 84.00

BIOCHEMISTRY

Offers results of original research in all recognized or developing areas of biochemistry. Biweekly.

One Year Rate	U.S.	Foreign
ACS Members	$ 49.00	$ 78.00
Nonmembers	$252.00	$281.00
Supplementary material on microfiche	$ 25.00	$ 35.00

CHEMICAL REVIEWS

Reviews of research in various areas of chemistry that eliminate the need to scan scores of articles concerning particular fields. Bimonthly.

One Year Rate	U.S.	Foreign
ACS Members	$ 17.00	$ 21.00
Nonmembers	$ 68.00	$ 72.00

22 publications from the American Chemical Society. From chemical news today to peer-reviewed research in print for the first time . . . ACS publishes worldwide developments in chemistry for you.

I&EC FUNDAMENTALS

Publishes, quarterly, original scientific papers dealing with the very frontiers of chemical engineering understanding.

One Year Rate	U.S.	Foreign
ACS Members	$ 11.00	$ 15.00
Nonmembers	$ 49.00	$ 53.00

Continued on next page

AMERICAN CHEMICAL SOCIETY, 1155 16th St., N.W., Washington, D.C. 20036 **1983**
CALL TOLL FREE 800-424-6747

Please enter a one-year subscription for the following publications:

PRICE PRICE

1. _____ 2. _____
3. _____ 4. _____
5. _____ 6. _____

Name _____ Position _____

Company _____ Address ☐ Home ☐ Business _____

City _____ State _____ Zip _____

☐ Payment enclosed _____ (Payable to American Chemical Society) ☐ Bill me ☐ **Bill company**

Charge my ☐ MasterCard ☐ VISA Account No. _____ Interbank No. _____ (MasterCard only)

Expire Date _____ Signature _____

Nature of Your Employer's Business: ☐ Manufacturing ☐ Government ☐ University

☐ Other (Please indicate) _____

☐ I am ☐ I am not an ACS member.

☐ Please send me information on how to become an ACS member.

Payment must be made in U.S. currency by international money order, UNESCO coupons, U.S. bank draft, or order through your subscription agency. For rates in Japan, contact Maruzen Co., Ltd.

Member rates are for personal use only.

Journal subscriptions start January 1983 and expire December 1983. Member subscriptions to *Analytical Chemistry, Environmental Science and Technology*, and *CHEMTECH* will start the month the order is placed and expire one year later unless subscriber requests a January start date.

2230M

AND DEVELOPMENT

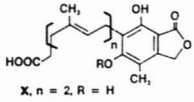
Quarterly contains original papers, and occasionally critical reviews, that present theoretical and experimental results relating to the development of processes and process equipment.

One Year Rate	U.S.	Foreign
ACS Members	$ 12.00	$ 16.00
Nonmembers	$ 58.00	$ 62.00
Supplementary material on microfiche	$ 8.00	$ 12.00

I&EC PRODUCT R&D

Publishes original research on broadly varied product related topics in an interdisciplinary manner. Quarterly.

One Year Rate	U.S.	Foreign
ACS Members	$ 12.00	$ 16.00
Nonmembers	$ 64.00	$ 68.00



X, n = 2, R = H

INORGANIC CHEMISTRY

Biweekly journal publishes fundamental studies, experimental and theoretical, in all phases of inorganic chemistry.

One Year Rate	U.S.	Foreign
ACS Members	$ 54.00	$ 79.00
Nonmembers	$273.00	$298.00
Supplementary material on microfiche	$ 50.00	$ 65.00

JOURNAL OF AGRICULTURAL AND FOOD CHEMISTRY

Bimonthly reporting of original research into the chemical aspects of agriculture and food.

One Year Rate	U.S.	Foreign
ACS Members	$ 17.00	$ 23.00
Nonmembers	$ 89.00	95.00
Supplementary material on microfiche	$ 10.00	$ 15.00



JOURNAL OF THE AMERICAN CHEMICAL SOCIETY

Most quoted biweekly journal of the widest possible interest to research workers and students in all areas of chemistry.

One Year Rate	U.S.	Foreign
ACS Members	$ 52.00	$ 93.00
Nonmembers	$253.00	$294.00
Supplementary material on microfiche	$ 50.00	$ 65.00

JOURNAL OF CHEMICAL AND ENGINEERING DATA

This quarterly journal is primarily concerned with the presentation of data of lasting value.

One Year Rate	U.S.	Foreign
ACS Members	$ 21.00	$ 25.00
Nonmembers	$115.00	$119.00
Supplementary material on microfiche	$ 8.00	$ 13.00

JOURNAL OF CHEMICAL INFORMATION AND COMPUTER SCIENCES

Quarterly reporting on new R&D, concepts, systems, and programs in all areas of information and computers relevant to chemistry and chemical technology.

One Year Rate	U.S.	Foreign
ACS Members	$ 13.00	$ 17.00
Nonmembers	$ 69.00	$ 73.00

Use the attached business reply card to order all the ACS publications you need to stay current in your profession!

MACROMOLECULES

Publishes monthly original material on all fundamental aspects of polymer chemistry.

One Year Rate	U.S.	Foreign
ACS Members	$ 32.00	$ 47.00
Nonmembers	$185.00	$200.00
Supplementary material on microfiche	$ 10.00	$ 14.00

JOURNAL OF MEDICINAL CHEMISTRY

Monthly journal concerned with the relationship of chemistry to biological activity, including rapid communication of major advances in drug design and development.

One Year Rate	U.S.	Foreign
ACS Members	$ 26.00	$ 35.00
Nonmembers	$135.00	$144.00
Supplementary material on microfiche	$ 15.00	$ 19.00



THE JOURNAL OF ORGANIC CHEMISTRY

Biweekly devoted to general organic chemistry offering critical accounts of original work and interpretative reviews of existing data that present new viewpoints.

One Year Rate	U.S.	Foreign
ACS Members	$ 38.00	$ 64.00
Nonmembers	$197.00	$223.00
Supplementary material on microfiche	$ 35.00	$ 50.00

THE JOURNAL OF PHYSICAL CHEMISTRY

Biweekly journal reporting experimental and theoretical research dealing with fundamental aspects of physical chemistry and chemical physics.

One Year Rate	U.S.	Foreign
ACS Members	$ 38.00	$ 58.00
Nonmembers	$226.00	$246.00
Supplementary material on microfiche	$ 30.00	$ 45.00

JOURNAL OF PHYSICAL AND CHEMICAL REFERENCE DATA

Quarterly published with AIP and NBS presenting critically evaluated data on physical and chemical properties.

One Year Rate	U.S.	Foreign
ACS, AIP Members and Affiliated Societies, Personal Use Only	$ 42.00	$ 48.00
Nonmembers	$170.00	$176.00

ACS SINGLE ARTICLE ANNOUNCEMENT

Semimonthly current awareness service reproduces contents pages of all ACS primary journals, except *C&EN*, so that you may order articles of your choice using a form provided.

One Year Rate	U.S.	Foreign
ACS Members	$ 25.00	$ 35.00
Nonmembers	$ 50.00	$ 60.00

NO POSTAGE NECESSARY IF MAILED IN THE UNITED STATES

BUSINESS REPLY CARD

FIRST CLASS PERMIT NO. 10094 WASHINGTON, D.C.

POSTAGE WILL BE PAID BY ADDRESSEE

AMERICAN CHEMICAL SOCIETY
Attn: Circulation Development
1155 Sixteenth Street, N.W.
Washington, D.C. 20036

A STANDARD REFERENCE IN THE FIELD OF ANALYTICAL CHEMISTRY. . .

FUNDAMENTAL REVIEWS



Chances are you've heard a lot about this special volume. And it's no wonder! For here, in some 400 pages, are authoritative, up-to-date surveys of the most recent literature, with the outstanding work cited and digested.

Below are just a few of the areas covered in the 1982 Fundamental Reviews issue: Analytical electrochemistry ■ Chromatography: gas, paper, thin-layer, liquid ■ Chemometrics ■ Kinetics ■ Surface analysis ■ Spectrometry: NMR, ESR, atomic, emission, IR, mass, X-ray ■ Nucleonics ■ Microscopy ■ Titrations

It's a portable library! And an enormous time-saver for any professional. Use the coupon below to order your copy today.

Distribution Center, American Chemical Society
1155 Sixteenth Street, N.W., Washington, D.C. 20036

☐ Yes! Send me **Fundamental Reviews.** I enclose $6 for each copy ordered.

Name_____

Address_____

City_____

State_____ Zip_____

B&J

Superior Purity Water Can Help Improve HPLC Results.

B&J Brand High Purity Water undergoes rigorous purification and quality control to guarantee lot-to-lot uniformity. That's your assurance of its superiority for:

- Reverse phase gradient separations.
- Applications that require purity higher than conventional lab water supplies.

What's more, negligible UV absorbance and extremely low organic carbon and particulates make it the best choice for your critical trace analysis requirements.

Improve your HPLC chromatograms with the consistent quality of B&J Brand High Purity Water. Call us today for a free copy of our high purity water data sheet or for the location of the nearest B&J Distributor. 616-726-3171.

BURDICK & JACKSON LABORATORIES, INC.

1953 South Harvey Street, Muskegon, Michigan U.S.A. 49442 (616) 726-3171
A Subsidiary of Hoffmann-LaRoche Inc.

CIRCLE 6 ON READER SERVICE CARD

READ JUST WHAT YOU NEED

Chemists agree that one hour in the library can save weeks in the lab. But why spend even an hour in the library when you could be reading CA SELECTS?

Each of the 133 CA SELECTS current-awareness publications cuts through stacks of scientific literature and brings you just the portion relevant to your work. That's why the world's chemists are reading CA SELECTS. Are you?

To find out how you can get out of the library and back to the lab—for less than $2.00 a week!—send for our 1983 catalog.

CA SELECTS®

Current-Awareness Publications from Chemical Abstracts Service

CA SELECTS

Tell me more about CA SELECTS! Send me your 1983 catalog.

Name_____

Address_____

_____

Return to Chemical Abstracts Service
Marketing Dept. 30883
P. O. Box 3012
Columbus, OH 43210 USA

CAS is a division of the American Chemical Society.
© 1983 by ACS

Here is the story of what chemistry is, what chemists do, and what the results have been.

And what a story it is! In "TAKING THINGS APART & PUTTING THINGS TOGETHER" you'll read the fascinating tales of cyclamates . . . anaesthetics . . . polio vaccine . . . radioactive waste disposal . . . and other exciting accounts.



TAKING THINGS APART & PUTTING THINGS TOGETHER is only $8.00 for the full-color soft cover version. Ridiculously low? We know!

Here is a unique and really remarkable book. Written in non-technical language and richly and attractively illustrated, this volume presents the story of chemistry in a concise, clear-cut, and easy-to-read manner.

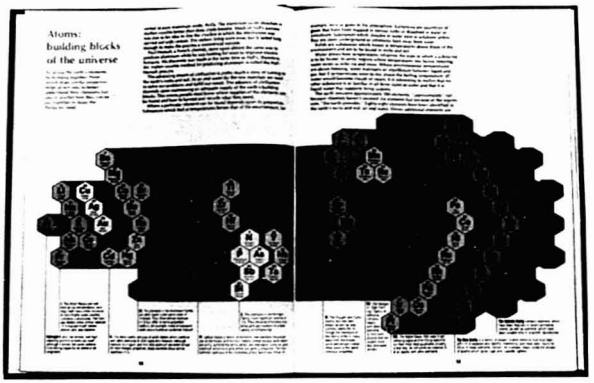
Five major areas of human activity are covered: HEALTH, FARMING, MATERIALS WE USE, ENERGY, AND COMMUNICATION. It starts with chemistry's miraculous "BUILDING BLOCKS" and ends with the choices we face in the future.

Besides the meatiness of its contents, its photographs, drawings, charts, cartoons, and watercolors make it a joy to own. The pages literally sing with color and bring the text to life.

For students, teachers, scientists, librarians, even chemists, you couldn't find a more welcome gift.



Trying to pick out just one illustration is a chore, but here is a sampling of one of the book's delightful graphic presentations.





Just like the illustration above, this book is bound to grow on you.

All you have to do is fill out the form below and mail it back to us today. After you receive your book, you are sure to order several more copies!

American Chemical Society, Distribution Office
1155 Sixteenth Street, N.W., Washington, D.C. 20036

Please send me _____ copies at $7.95 per copy of *"Taking Things Apart & Putting Things Together."*

Name _____

Address _____

City _____

State _____ Zip Code _____

Check must accompany order. Bulk rates available on request. 20

C-, S-, N_2-, O_2- and H_2-Analysis...



42-01.83.2

C-, S-, N_2-, O_2-, and H_2- in metals and other inorganic materials must be precisely and quickly, but also practically and economically analyzed in research and development laboratories as well as in incoming inspections and production control. The broad program of automatic analyzers that LEYBOLD-HERAEUS offers has the optimal practical solution for you. The following selection of compact apparatus is now available.

- Analyzers for C-, S-, N_2-, O_2-, and H_2- determination, and
- Analyzers for simultaneous C- and S-, or O_2- and N_2- analysis.

Everything runs automatically at the push of a button: integrated weighing, analyzing process, and data output.

The H_2-analyzers are complemented by the loss free sampler system with the patented disposable suction sampler (ESK).

LEYBOLD-HERAEUS is one of the world's largest producers of vacuum systems and vacuum process engineering. Our technological orientation and performance guarantee:

- Sofisticated analysis, e.g. with the highly sensitive gas specific IR photometer BINOS®
- Modern electronics, e.g. the 16 bit microprocessor in the 2003 series
- As well as the continuity of models, a worldwide service network, and, finally, qualified professional advice from our distribution engineers.

We'll inform you about our automatic C-, S-, N_2-, O_2-, and H_2-analyzers – precise – fast – reliable.
Write us, or just give us a call.

LEYBOLD-HERAEUS

LEYBOLD-HERAEUS GMBH
POB 1555 · D-6450 Hanau 1 · Tel.: 06181/364-273
Alpha Resources Inc.
P.O.Box 199 · Stevensville, MI 49127, USA,
Tel.: 616/4655559

...precise — fast — reliable: Analyzers from LEYBOLD-HERAEUS

CIRCLE 125 ON READER SERVICE CARD

Ultrospec
Simply more advanced

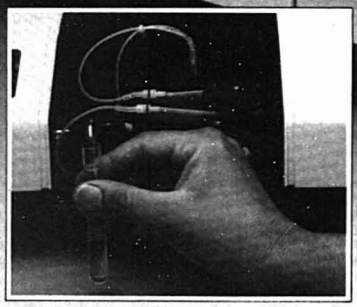
Ultrospec 4050 and 4051 These new generation single beam spectrophotometers fully utilising micro-processor technology are already establishing themselves as the most advanced instruments of their kind currently available. The advanced Ultrospec design is now complemented by the most complete range of accessories ever offered for an instrument of this type.

Sample handling: Easy with Ultrospec's exceptionally large cell compartment, so whatever your requirement, be it a test tube holder or an HPLC flowcell, there is sure to be an Ultrospec accessory to meet your needs.

Cells: A full range of high quality optical cells is available to match the wide range of applications to which the LKB 4050 & 4051 can be applied.

Autofill: For rapid handling of small volumes. Samples, after measurement, can either be returned to sample tube or to waste. Available either with or without a Peltier effect thermostatted cell holder (range 20°C-60°C). Includes programming for reaction rate measurements.





Computer systems: The linking of Ultrospec with mini computers via the built-in RS232C interface, greatly increases the scope of tasks for which Ultrospec may be used: to include:- automatic wavelengths scans with background correction; first and second derivative spectra; wavelength programming and reaction rate determinations.

More features than any other in its price range: finest after sales service too.

Easily the biggest advance in spectrophotometry

LKB
THE INCENTIVE GROUP

LKB BIOCHROM LTD, SCIENCE PARK, CAMBRIDGE CB4 4BH, ENGLAND.

Head office: LKB-Produkter AB, Box 305, S-161 26 Bromma, Sweden. Tel. 08-98 00 40, telex 10492
Main US sales office: LKB Instruments, Inc. 9319 Gaither Road, Gaithersburg, MD 20877, Tel. 301-963 3200, telex 64634
UK sales office: LKB Instruments Ltd., 232 Addington Road, S. Croydon, Surrey CR2 8YD, England. Tel. 01-657 8822, telex 264414
Other sales offices in: Athens (for Middle East), Copenhagen, Ghent, The Hague, Hong Kong, Munich, Paris, Rome, Turku, Vienna.

004

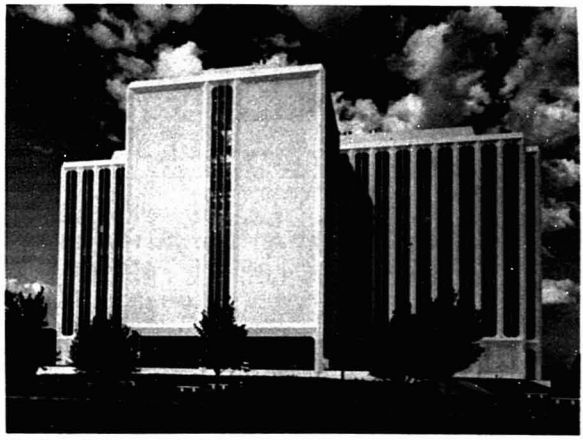
CIRCLE 129 ON READER SERVICE CARD

36th Annual Summer Symposium on Analytical Chemistry

Fourier Transforms and Their Applications to Instrumental Analysis

University of Nebraska, Lincoln, Neb. June 21–23, 1983

"Fourier Transforms and Their Applications to Instrumental Analysis" is the subject of the 1983 Summer Symposium of the ACS Division of Analytical Chemistry. The symposium will be held June 21–23, 1983, at the Lincoln Hilton Hotel and will be hosted by the University of Nebraska chemistry department. The program chairman is Peter R. Griffiths of the University of California—Riverside, and the general chairman is James D. Carr of the University of Nebraska. The symposium is sponsored by the ACS Division of Analytical Chemistry and ANALYTICAL CHEMISTRY.



Hamilton Hall houses the University of Nebraska chemistry department

About the University of Nebraska

The University of Nebraska is located in Lincoln, the state capital. It has a student population of 22 000, and its department of chemistry is comprised of 30 faculty members and 120 graduate students. Nebraska's Graduate College was the first to be established west of the Mississippi River. The university is the site of the NSF Midwest Center for Mass Spectrometry.

Travel

The Lincoln Municipal Airport is a few minutes' drive from the university campus and from downtown Lincoln; the Greyhound and Trailways bus stations and the Amtrak train station are within easy walking distance of the campus and the Lincoln Hilton Hotel. The downtown (I-180) exit from I-80 goes directly to the campus and to the Hilton, located on the southwest corner of 9th and P Sts.

Housing and Symposium Arrangements

Housing will be available at the Lincoln Hilton and at Smith Hall university dormitory. Rates in the dormitory are $12 and $18 per night for single and double rooms, respectively. Small children may stay in their parents' rooms without charge. Linens, pillows, and towels will be furnished in dorm rooms, and food will be available on a cash basis in the cafeteria. Free parking adjacent to the dormitory will be provided. Requests for dormitory housing should be made on the attached registration form and must be received by June 6. The dormitory is a 10–15-min walk from the Hilton.

Rates at the Hilton are $42 and $52 for single and double rooms, respectively. Those wishing accommodations at the Hilton should contact the hotel directly at 141 North 9th St., Lincoln, Neb. 68508; 402-475-4011 or 800-328-9155. Be sure to identify yourself as a participant in the Analytical Summer Symposium to get the special symposium rate noted above. Free parking is available to guests.

Registration and Social Gatherings

Registration will take place in the lobby of the Hilton Hotel on Monday, June 20, from 3:00 to 10:00 P.M., and on Tuesday, June 21, from 8:00 A.M. to 3:00 P.M. A reception will be held at 7:00 P.M. Monday. The registration fee of $65 includes admission to all technical sessions, symposium materials, and the banquet. The other meals listed on the registration form are optional and are not included in the registration fee. Indicate on the registration

form those functions and meals you wish to attend.

The student registration fee of $15 includes only admission to the technical sessions and the symposium materials. Students may order banquet tickets on the attached form. In addition, graduate credit may be granted for attendance at the symposium. Details are available from the general chairman, James Carr.

Family Activities

Although no organized family activities are planned, Lincoln offers a great many possibilities for family entertainment. Natural history and art museums and a planetarium are located on campus, and parks, swimming, tennis, and golf facilities are located close by. Immediately adjacent to the campus are downtown shopping areas, restaurants, and theaters. Intramural athletic facilities are available to all registrants and their families.

For further information about any aspect of the symposium, contact James D. Carr, Department of Chemistry, University of Nebraska, Lincoln, Neb. 68588; 402-472-3501.

Symposium Format

The symposium is divided into five half-day sessions dealing with Fourier transform spectrometry, data processing and applications, hyphenated techniques, surface analysis by FTIR, and kinetics and time-resolved spectrometry.

The following is the complete technical program for the symposium.

Program

Tuesday Morning, June 21

Fourier Transform Spectrometry

P. R. Griffiths, *Presiding*

8:30 Welcome and Introductory Statements

8:45 The Fourier Transform Algorithm. Alan G. Marshall, Ohio State U

9:30 FTIR and the Future of Infrared Spectrometry. Tomas Hirschfeld, Lawrence Livermore Labs

10:15 Atomic Spectrometry Using a High-Resolution Michelson Interferometer. Thomas M. Niemczyk, U of New Mexico; L. M. Faires, B. A. Palmer, and R. Engleman, Jr., Los Alamos National Lab

11:10 Introductory Theory and Instrumentation for FTMS. Sahba Ghaderi, Nicolet Instrument Corp.

11:45 Techniques for High-Resolution Measurements in FTMS. Michael L. Gross, U of Nebraska

Tuesday Afternoon

Data Processing and Applications

A. G. Marshall, *Presiding*

1:45 Smoothing and Deconvolution in the Fourier Domain. David G. Cameron, National Research Council of Canada

2:25 Fractal Analysis of Time Domain Data. James A. de Haseth, U of Alabama

3:00 Fourier Transforms in Electrochemistry. Donald E. Smith, Northwestern U

Registration Form

36th Annual Summer Symposium on Analytical Chemistry

Fourier Transforms and Their Applications to Instrumental Analysis

June 21–23, 1983 University of Nebraska, Lincoln, Neb.

Name (Print)_____

Title_____ Phone_____

Institution_____

Address_____

City_____ State_____ Zip_____

- ☐ I will arrange my own housing with the Lincoln Hilton
- ☐ I wish to stay in the university dormitory for the nights of:_____
  - ☐ Double room ($18/night)
  - ☐ Single room ($12/night)
  - ☐ I wish to share a room with:
    _____ ($9/person/night)
    (please be sure choice is mutual)
  - ☐ I wish to share a room with someone you assign ($9/person/night)
- ☐ I will arrange for housing other than the Hilton or dormitory

Sponsored by the ACS Division of Analytical Chemistry and *Analytical Chemistry*

	No Fee (Please check)	Fee
MONDAY, JUNE 20		
Reception (cash bar)	_____	
TUESDAY, JUNE 21		
Lunch, $7		$_____
Dinner, $10		$_____
WEDNESDAY, JUNE 22		
Lunch, $7		$_____
Banquet, $20	_____	$_____ (students and extra tickets)
THURSDAY, JUNE 23		
Lunch, $7		$_____
Registration Fee, $65		$_____
Student Registration, $15		$_____
Dormitory Housing Fee		$_____
TOTAL AMOUNT ENCLOSED		$_____

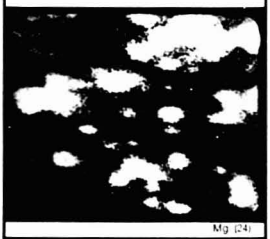
Return this form with a check made payable to the "University of Nebraska" for the total amount due to: Diane Stevens, Department of Chemistry, University of Nebraska, Lincoln, Neb. 68588-0304. Please send a registration form or photocopy for each registrant. **DO NOT SEND PAYMENT FOR THE HILTON TO THE CHEMISTRY DEPARTMENT.**

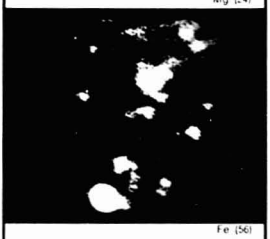
MIQ 156

SIMS

ion microprobe, the ideal source for material analyses.

The RIBER MIQ 156 is an ion microprobe which operates under UHV conditions, for enhanced sensitivity (residual gas pressure in 10^{-11} torr range).





Ion imaging of a clay sample, after injection of polymer and microtom slicing

problems : depth profiles, elemental map, mass spectra of polymers, biological samples, metals, glass, semiconductors,
geological samples ;
solution : ion microprobe MIQ 156

In one instrument, many capabilities :

- Analysis of materials, semiconductors, insulating materials.
- High sensitivity depth concentration profiles.
- High resolution images and profiles.
- Static SIMS.
- SIMS of high mass molecules and fragments.
- Hydrogen concentration profiles.

In North America :
Instruments S.A. Inc.
RIBER Division
173 Essex Avenue
Metuchen NJ 08840
tel. (201) 494-8660 - telex 844-516

Elsewhere :
ISA RIBER
BP 231 - 92503 Rueil Malmaison
France
tel. (1) 708-92-50 - telex 203 367 F

SURFACES
RIBER

CIRCLE 180 ON READER SERVICE CARD

LDC/Milton Roy
HPLC
Metering Pumps
Priced from $975



LDC/Milton Roy offers a complete family of precision metering pumps for high performance liquid chromatography (HPLC).

- **miniPump®** series metering pumps - The first metering pump manufactured and used for HPLC. Priced from $975.00. Single piston, 0-6000 psi, solvent delivery from 16-920 mL/hr, flow rate stability ± 0.3% per hour.
- **miniMetric™** series metering pumps - The newest addition to the LDC/Milton Roy family of metering pumps. Priced from $1752.* Fast-refill single sapphire piston, 0-6000 psi, pulseless solvent delivery from 50 μL – 5 mL/min, flow rate stability ± 0.3% per hour, gradient compatible.
- **constaMetric®** series metering pumps - The ultimate in pulseless flow performance. Priced from $2292.* Dual reciprocating sapphire pistons, 0-6000 psi, pulseless solvent delivery from 0.1 to 9.99 mL/min, flow rate stability ± 0.3% per hour, gradient compatible.

*When purchased with a gradient system.

For more information or to order call:
Toll Free: 800-327-6182
In Florida: (305) 844-5241

LDC/Milton Roy Analytical Instruments - a tradition of quality and performance.

LDC/Milton Roy

3661 Interstate Park Rd. N.
P.O. Box 10235
Riviera Beach, FL 33404

CIRCLE 135 ON READER SERVICE CARD

News

Program and General Chairmen



Peter Griffiths



James Carr

3:50 Fourier Transforms in Chromatography. Michael F. Burke, U of Arizona

4:25 Correlation and Fourier Transform Approaches to Time-Resolved Fluorescence Measurements. Joel M. Harris and Michael J. Pelletier, U of Utah

Wednesday Morning, June 22

Hyphenated Techniques

M. L. Gross, *Presiding*

8:45 Development and Application of GC/FTIR for Pollutant Analysis. Leo V. Azarraga, U.S. Environmental Protection Agency

9:30 GC/FTIR/FTMS. Charles L. Wilkins, U of California—Riverside

10:05 On-line Elemental Analysis by GC/FTNIR. Robert C. Fry, Kansas State U

10:55 HPLC/FTIR. Kiyokatsu Jinno, Toyohashi U of Technology

11:30 Nonroutine Applications of FTIR Evolved Gas Analysis. Charles A. Cody, Larry Di Carlo, and Bruce F. Faulseit, NL Industries/NL Chemicals

Wednesday Afternoon

Surface Analysis by FTIR

W. G. Fateley, *Presiding*

1:30 In Situ Studies of Catalyzed Reactions by Transmission FTIR Spectrometry. Alexis T. Bell, U of California—Berkeley

2:05 Photothermal FTIR Spectrometry for the Study of Surfaces. Edward M. Eyring, U of Utah

2:40 Surface Analysis by Diffuse Reflectance FTIR Spectrometry. Peter R. Griffiths, U of California—Riverside

3:15 Surface Analysis by Reflection-Absorption and Emission FTIR Spectrometry. David L. Allara, Bell Labs

4:05 Polarization Modulation Approach to Studying Adsorbates on Surfaces. Curtis Marcott, Procter and Gamble Corp.

Thursday Morning, June 23

Kinetics and Time-Resolved Spectrometry

J. D. Carr, *Presiding*

8:45 Studies of Collision-Induced Reactions by FTMS. Ben S. Freiser, Purdue U

9:20 Kinetics of Metal Cluster Reactions by FTMS. David H. Russell and D. J. Anderson, Texas A & M U

9:55 Vapor Analysis by FTIR in Atmospheric Photochemistry and Automobile Emission Studies. P. D. Maker, H. Niki, L. P. Breitenbach, and C. M. Savage, Ford Motor Co.

10:45 Kinetic and Structural Studies of Protein Adsorption from Blood, or "FTIR: Bloody but Unbowed." Robert J. Jakobsen, K. M. Burch, R. I. Leininger, and R. M. Gendreau, Battelle's Columbus Labs

11:20 Stroboscopic FTIR Spectrometry—Past, Present, and Future. William G. Fateley, Kansas State U

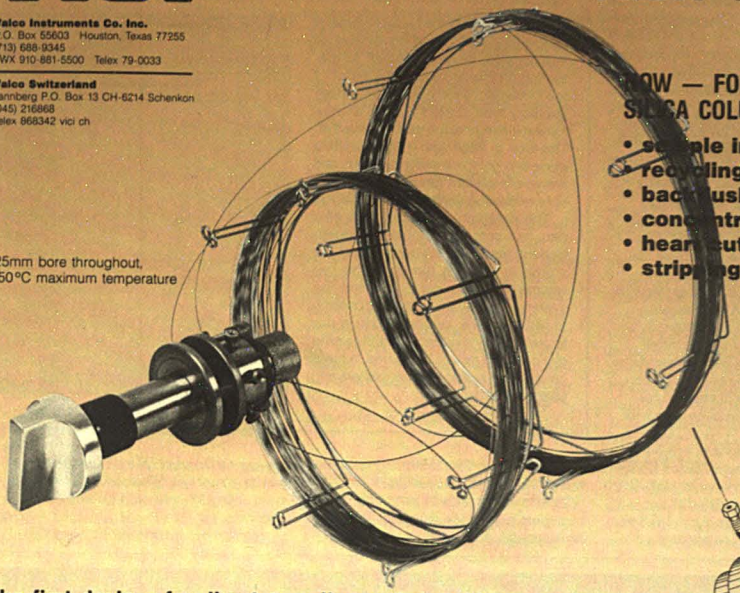
VICI

ANNOUNCING

NEW FOR GC

Valco Instruments Co. Inc.
P.O. Box 55603 Houston, Texas 77255
(713) 688-9345
TWX 910-881-5500 Telex 79-0033

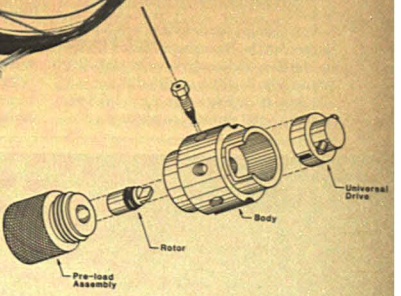
Valco Switzerland
Tannberg P.O. Box 13 CH-6214 Schenkon
(045) 216868
Telex 868342 vici ch



.25mm bore throughout,
350°C maximum temperature

NEW — FOR FUSED SILICA COLUMNS

- sample injection
- recycling
- backflushing
- concentration
- heart cutting
- stripping



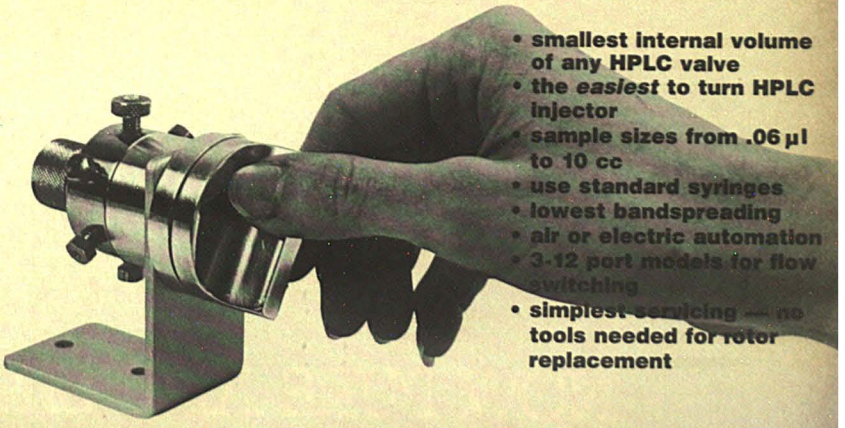
The first devices for direct sampling and switching of fused silica columns are now available from Valco and leading international dealers.

CIRCLE 226 ON READER SERVICE CARD

AND

NEW FOR HPLC

The most advanced "user friendly" HPLC sample injection and switching valves.



- **smallest internal volume of any HPLC valve**
- **the *easiest* to turn HPLC injector**
- **sample sizes from .06 µl to 10 cc**
- **use standard syringes**
- **lowest bandspreading**
- **air or electric automation**
- **3-12 port models for flow switching**
- **simplest servicing — no tools needed for rotor replacement**

CIRCLE 227 ON READER SERVICE CARD

13th Annual Symposium on the Analytical Chemistry of Pollutants May 16–18, 1983 Jekyll Island, Georgia

Analytical chemistry as a tool for gathering information on pollutants is attracting increasing interest as countries around the world confront environmental problems associated with the manufacture, use, and disposal of chemicals. The 13th Annual Symposium on the Analytical Chemistry of Pollutants, to be held May 16–18, 1983, on Jekyll Island, Ga., will bring together international experts in this important field. At the meeting, invited speakers from government, industry, and university laboratories will present the latest developments in the analysis of organic and inorganic pollutants and the validation of collected data. A poster session also will be held.

Symposium participants will be housed at the Buccaneer Motor Lodge by the Sea, 85 Beachview Dr., Jekyll Island, Ga. 31520; 912-635-2261 or 800-342-4620. Registrants should contact the hotel directly to arrange accommodations. The technical sessions will be held at the Buccaneer.

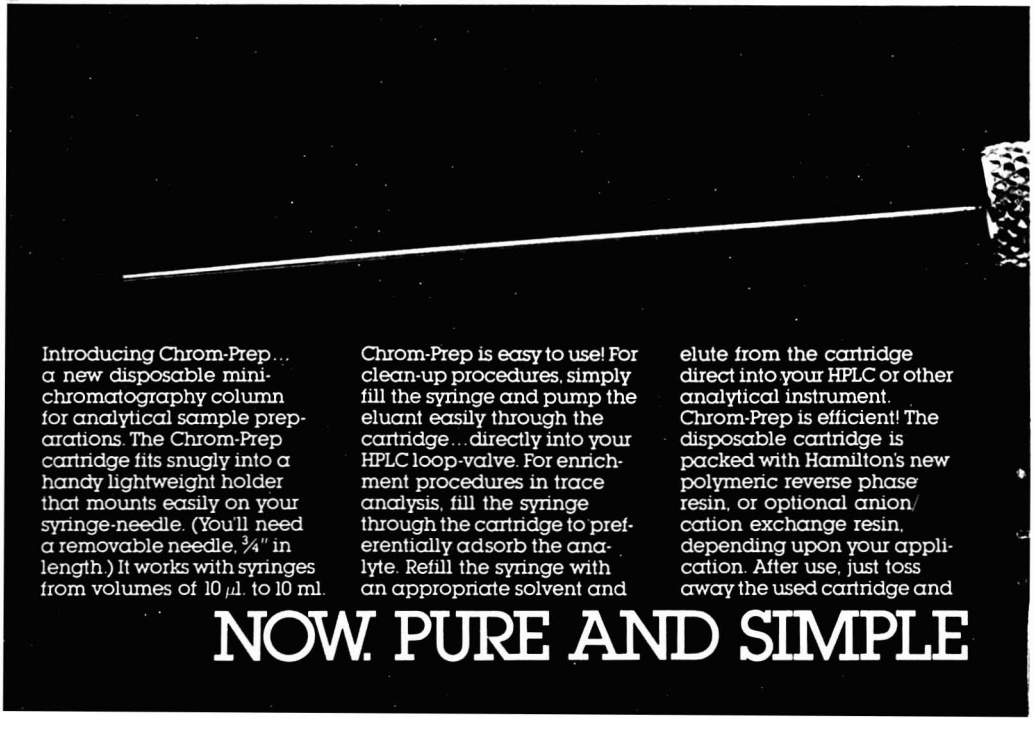
Chartered buses will be available to transport preregistrants from the Jacksonville, Fla., airport to the Buccaneer on Sunday, May 15, and back to the airport on Wednesday afternoon, May 18, and on Thursday morning, May 19.

For further information about the

Researchers at the Naval Research Laboratory (NRL) have developed an inexpensive, reusable sensor for detecting ammonia vapor. The heart of the detection system is a small, glass capillary tube coated with an ammonia-sensitive oxazine perchlorate dye. The tube is fitted with a light-emitting diode and phototransistor detector, and the whole system functions as a multiple reflecting waveguide device.

The detector, about the size of a pen, can detect ammonia in concentrations less than 60 ppm. When the ammonia vapor is removed, the dye returns to its normal color, and the system is ready for reuse. According to NRL's John F. Giuliani (right), there is preliminary evidence that the same dye can also detect hydrazine, a toxic gas used as a propellant in rockets and space vehicles.





symposium, including details on the technical program, reservations, transportation, special activities, and registration, contact: Elaine McGarity, U.S. Environmental Protection Agency, Environmental Research Laboratory, College Station Road, Athens, Ga. 30613; 404-546-3184.

Symposium on Analysis of Volatile Organic Chemicals in Water
May 17–18, 1983
Gaithersburg, Maryland

A symposium entitled "Analysis of Volatile Organic Chemicals in Water" will be held May 17–18, 1983, at the National Bureau of Standards in Gaithersburg, Md. Invited and submitted papers will be presented on sampling aspects and matrices, analytical methodology, and data interpretation and statistical analysis of results.

For information on registration and overnight accommodations, contact Harry Hertz, Organic Analytical Research Division, Center for Analytical Chemistry, National Bureau of Standards, Washington, D.C. 20234. The symposium is sponsored by the American Chemical Society's Committee on Environmental Improvement, the Environmental Protection Agency, the National Bureau of Standards, and the Chemical Manufacturers Association.

Nominations Sought for Benedetti-Pichler Award

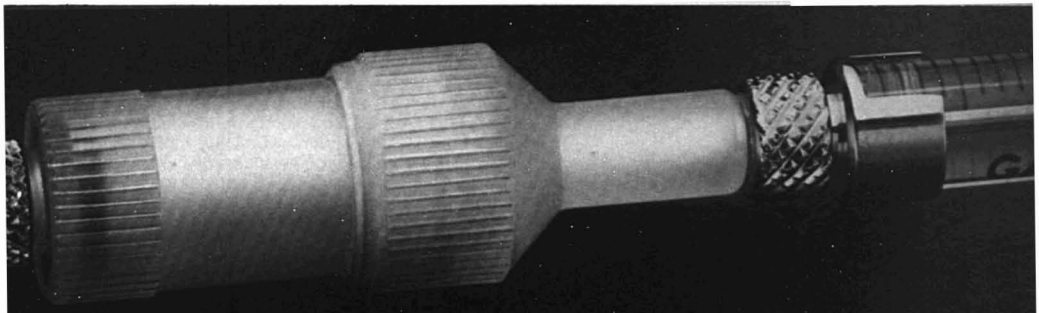
The American Microchemical Society is seeking nominations for the A. A. Benedetti-Pichler Award. Established in 1966, the award is given annually in recognition of service to microchemistry, including research, applications, administration, and teaching. Letters of nomination including citation of the nominee's work should be submitted by May 1 to Leonard C. Klein, FMC Corporation, P.O. Box 8, Princeton, N.J. 08540.

Call for Papers

32nd Annual Denver X-ray Conference and Summer Meeting of the American Crystallographic Association
Snowmass, Colo. Aug. 1–5. The joint meeting will emphasize X-ray diffraction and will include special sessions on fluorescence and diffraction. Papers for the special and general sessions will be presented in lecture or poster format. The deadline for submission of abstracts is May 1. For more information contact Mildred Cain, Denver Research Institute, University of Denver, Denver, Colo. 80208; 303-753-2141.

2nd International Symposium on Capillary Chromatography
Tarrytown, N.Y. Oct. 10–12. The symposium will consist of invited and submitted papers on all aspects of capillary chromatography and will include an exhibition of chromatographic instrumentation. Abstracts of 200 words should be submitted by May 2 to A. Zlatkis, Chemistry Department, University of Houston, Houston, Tex. 77004.

1983 Pacific Conference on Chemistry and Spectroscopy
Pasadena, Calif. Oct. 26–28. The conference is sponsored by the Northern



pop another into the holder. Chrom-Prep is currently available in two sizes: 20 μl and 320 μl. One is ideal for small sample clarification, the other is ideal for enrichment procedures.
And, Chrom-Prep is economical. A complete kit, including a cartridge holder and 30 disposable cartridges, has a recommended list price of $40.00.
Chrom-Prep...the simple, efficient, economical way to protect your costly HPLC columns, purify your samples, and enhance your trace analysis. For further information call toll-free 800-648-5950 for the dealer nearest you or write Hamilton Co., P.O. Box 10030, Reno, NV 89510.



HAMILTON

CIRCLE 99 ON READER SERVICE CARD

SAMPLE PREPARATIONS.

California Section of the Society for Applied Spectroscopy and the California Section of the American Chemical Society. Authors should submit 150–200-word abstracts to the ACS or SAS program chairman by June 15. To obtain forms and further information about the general and specific topic sessions, contact David L. Toppen, Program Chairman (ACS), Department of Chemistry, California State University, Northridge, Calif. 91330, 213-885-2064 or Robert Obremski, Program Chairman (SAS), Beckman Scientific Instrument Division, Campus and Jamboree, Irvine, Calif. 92713; 714-833-0751.

1984 Winter Conference on Plasma Spectrochemistry
San Diego, Calif. Jan. 2–6, 1984. The conference will feature developments in atomic plasma spectrochemical analysis by inductively coupled plasma, DC plasma, and microwave plasma excitation sources. Papers describing original work with atomic plasma spectrochemistry applications, fundamentals, and instrument development are solicited for lecture and poster sessions. Title and 50-word abstract are due July 1, 1983. For further information contact Ramon M. Barnes, 1984 Winter Conference, c/o ICP Information Newsletter, Department of Chemistry, GRC Towers, University of Massachusetts, Amherst, Mass. 01003-0035; 413-545-2294.

Meetings

The following meetings are newly listed in ANALYTICAL CHEMISTRY. *Other 1983 meetings are listed in the January, February, and March issues.*

■ **Symposium on the Applications of Chromatography.** June 16–17. New Haven, Conn. Sponsored by the Connecticut Chromatography Council. *Contact: Cs. Horvath, Yale University, Department of Chemical Engineering, P.O. Box 2159, Yale Station, New Haven, Conn. 06520*

■ **Symposium on Toxic Substances in the Environment II.** Sept. 9–10. Kingston, Ontario, Canada. *Contact: K. Nakatsu or J. F. Brien, Department of Pharmacology and Toxicology, Queen's University, Kingston, Ontario, Canada K7L 3N6; 613-547-3173 or 613-547-3223*

■ **Twenty-ninth Annual Conference on Bioassay, Analytical and Environmental Chemistry.** Oct. 12–13. Seattle, Wash. *Contact: Bob Robinson, Battelle, Pacific Northwest Laboratory, P.O. Box 999, 703/700, Richland, Wash. 99352*

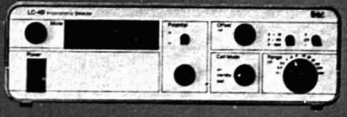
■ **Workshop on Handling of Environmental and Biological Samples in Chromatography.** Nov. 24–25. Lausanne, Switzerland. *Contact: R. W. Frei, The Free University of Amsterdam, Department of Analytical Chemistry, De Boelelaan 1083, 1081HV Amsterdam, The Netherlands*

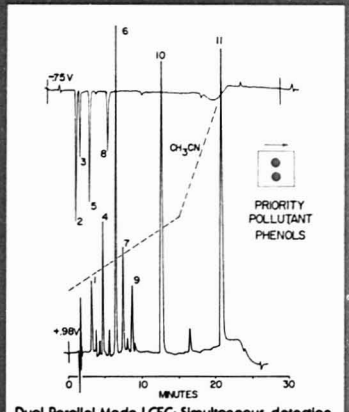
For Your Information

"Solvent Guide," 2nd ed., is a 150-page manual published by **Burdick & Jackson** designed as a reference source for chromatographers, spectroscopists, and laboratory chemists. It provides specifications, physical properties, safety data, typical UV ab-

electrochemical detectors for liquid chromatography

In 1974 BAS introduced the first commercial LCEC system. With over 5000 units installed and the largest research team to support them, it's not surprising that our nearest competitors are several generations behind us. Our thin-layer transducers lead the way with a wide selection of electrode materials in a variety of interchangeable configurations. The latest members of the family are revealed in the new LC4B/17 dual electrode amperometry package. Parallel and series amperometry can enhance selectivity, detection limits, speed and gradient compatibility. Let us show you how it's done, no one else can. Write or call for a detailed assessment of your trace analysis problem.





Dual Parallel Mode LCEC: Simultaneous detection of oxidizable and reducible components.

bas bioanalytical systems 1205 Kent Avenue, West Lafayette, IN 47906 (317) 463-2505 TLX 276141

JAPAN: Tokai Irika Co. (Tokyo) SWITZERLAND: Paul Bucher Co. (Basel) SWEDEN: Skandinaviska Genetec (Kungsbacka) KOREA: Ain Sung Scientific (Seoul) ITALY: Analytical Control Italia (Cinisello Balsamo) FRANCE: Biochrom s.a.r.l. (Vindelle) CANADA: Mandel Scientific (Rockwood, Ont.) U.K.: Anachem Ltd. (Luton) AUSTRALIA: Edwards Instruments (Moreltan) ISRAEL: Eldan Electronics (Jerusalem)

CIRCLE 30 ON READER SERVICE CARD

Here's why Perkin-Elmer had the biggest exhibit at the Pittsburgh Conference.

We had so much more to show, it took the biggest exhibit to cover everything. For example:

IR The new 1550 Fourier Transform IR with high-speed color graphics and on-the-fly GC and the new 780 Series of ratio recording IR spectrophotometers.

The new 7500 high-performance laboratory computer that has color graphics, soft keys, and a hard disk, and extends IR's line of data systems.

TA New software that expands our thermal systems' capabilities in R&D and quality control.

FL New software and a wide product range for simplified fluorescence spectroscopy.

LC A new series of optimized, dedicated, and general-purpose LC systems including the SERIES 10 low-cost gradient system, a new amino acid analyzer, the new Model LC 600 Autosampler, and significant improvements in LC column technology.

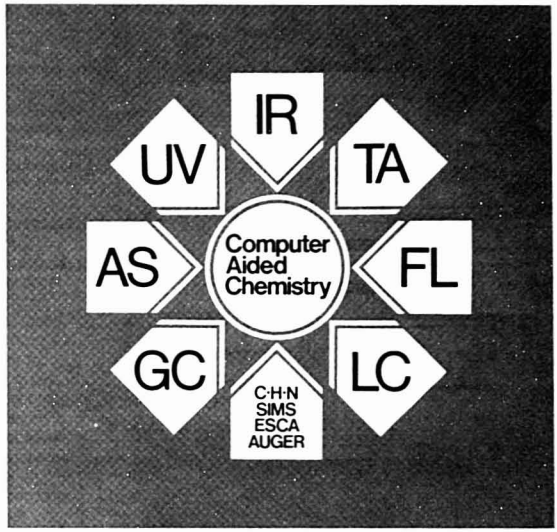
EA A most versatile Elemental (CHN) Analyzer and Data Station that handle more sample types.

ESCA A Surface Chemical Analyzer with ion scattering spectrometry and new automated sample advance.

GC The new SIGMA 300 Series of custom-built and preconfigured GC analyzers, the new AS-300 Autosampler and the new SIGMA 115 Air Monitoring System for continuous monitoring of workplace atmospheres.

The new HS-100 automatic headspace sampler.

AS The new sequential ICP/6000 system and 16-bit computer that determine 20 elements per minute, with color graphics and resident wavelength tables.



UV The new Model 553 fast-scan UV/VIS spectrophotometer with integral recording, overlaid spectra and double-beam optics for a superior price/performance ratio. The new Model R-100 microprocessor strip chart recorder.

Computer Aided Chemistry

The new LIMS/2000 Laboratory Information Management System and a new Chromatography Laboratory Automation software package (C/LAS) for multichannel data collection and reduction on Perkin-Elmer 32-bit superminicomputers.

The new, high-performance laboratory computer with bit-mapped color graphics, hard disk, and soft keys.

For details, contact your Perkin-Elmer representative or one of the offices below. Or phone toll-free **1-800-762-4000.**

Perkin-Elmer Corp., Analytical Instruments, Main Ave. (MS-12), Norwalk, CT 06856 U.S.A. Tel. (203) 762-1000. Telex 965-954

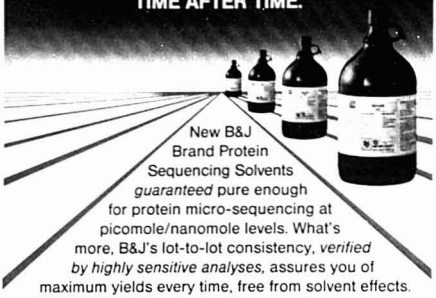
Bodenseewerk Perkin-Elmer & Co., GmbH, Postfach 1120, 7770 Ueberlingen, Federal Republic of Germany. Tel. (07551) 811

Perkin-Elmer Ltd., Post Office Lane, Beaconsfield, Bucks HP9 1QA, England. Tel. Beaconsfield (049 46) 6161

PERKIN-ELMER

Circle 162 For Literature. Circle 163 For Sales Call.

MAXIMUM PROTEIN SEQUENCING YIELDS. TIME AFTER TIME.



New B&J Brand Protein Sequencing Solvents *guaranteed* pure enough for protein micro-sequencing at picomole/nanomole levels. What's more, B&J's lot-to-lot consistency, *verified by highly sensitive analyses,* assures you of maximum yields every time, free from solvent effects.

Write or call today for our free brochure. It reveals how B&J Brand Ethyl Acetate, Butyl Chloride, Benzene, Heptane, and Ethylene Dichloride improve results by increasing PTH amino acid yields.

bj BURDICK & JACKSON LABORATORIES, INC.

1953 South Harvey Street, Muskegon, Michigan U.S.A. 49442 616-726-3171

A Subsidiary of Hoffmann-LaRoche Inc.

CIRCLE 8 ON READER SERVICE CARD

Cosa presents Mitsubishi moisture measuring instruments



Ushers in new standards of performance

The new Mitsubishi VA-02 Moisture Vaporizer offers shorter measuring time, greater range (starting at 5 ppm) and better reproducibility than conventional direct drying or indirect solvent extraction methods. Trace amounts of water in chips, powders, even solids, can be accurately measured by the VA-02. And it's totally unaffected by atmospheric humidity.

The CA-02 Moisture Meter employs the coulometry principle applied to Karl Fischer titration to eliminate the troublesome procedures involved in conventional titration. It's fully automatic and easy to use.

For complete information on both models, contact your nearby Cosa dealer. Or contact Cosa Instruments Corp., 70 Oak St., Norwood, N.J. 07648. Phone (201) 767-6600.

cosa

CIRCLE 35 ON READER SERVICE CARD



MANAGEMENT CONSULTANT 65¢

Want to get ahead? You couldn't pick a more valuable ally than **Chemical & Engineering News**

For $34 a year (just 65¢ per weekly issue), we'll turn you into a better informed, more valuable, more promotable employee.

Impress your boss by spotting trends that are going to impact your company's sales, production, construction, and prices. Earn management's respect with advance information on policy makers, legislation, and regulatory affairs. Move up by knowing what the competition's up to, how to use the latest technology, and where R&D dollars will be most productive.

Chemical & Engineering News *helps you take care of "number one" too, by examining employment prospects industry-wide. We give you special issues, packed with facts and figures you need to do a better job or get a better job.*

Our Key Chemicals column helps you keep track of world market conditions. And our crisp, comprehensive reporting makes us the one chemical publication that's absolutely indispensible to line professionals.

Why not call the toll-free number below, and give your career prospects a boost today.

Your very first issue will show you why people who are going places rely on us to help them get there.

To subscribe call:

(800) 424-6747 *(U.S. only)*

CHEMICAL & ENGINEERING

NEWS

sorbance curves, suggested applications, and selected technical references for 58 high-purity solvents. Copies can be obtained for $9.95 from Pat Kreiger, Burdick & Jackson Laboratories, Inc., 1953 South Harvey St., Muskegon, Mich. 49442.

Computer Sciences Corporation now provides user support activities for the **NIH/EPA Chemical Information System.** The system is a collection of data analysis computer programs and scientific and regulatory data bases. It includes the mass spectral search system, which contains spectra of more than 39 000 compounds. The user hotline number is 800-368-3432 (in Virginia call 703-237-2000).

Tracer Technologies, Inc. and VG Isogas, Ltd. have formed a joint venture to develop and validate **fully automated mass spectral analyzer systems** for clinical use in the nutrition field. The analyzers detect heavy isotopes of hydrogen, nitrogen, carbon, and oxygen, which are used diagnostically to follow fat, carbohydrate, and protein calorie utilization rates. For more information contact Alfred Ajami, Tracer Technologies, Inc., 225 Needham St., Newton, Mass. 02164.

Allied Corporation has acquired **Instrumentation Laboratory** (IL), a manufacturer of biomedical and analytical instruments located in Lexington, Mass. IL will become part of Allied's Health and Scientific Products Company, which was formed in late 1981 with the acquisition of Fisher Scientific Company. IL customers should refer questions to their closest Fisher branch or IL Regional Office.

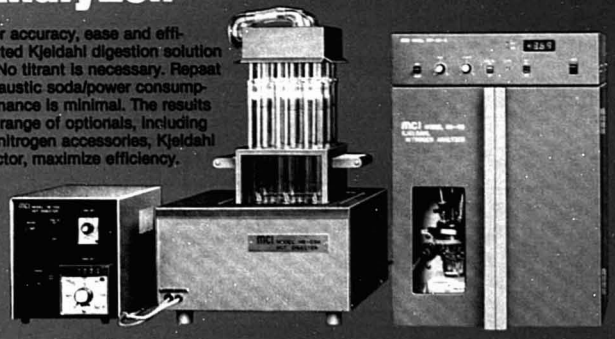
Water Quality Assessment of Toxic and Conventional Pollutants in Lakes, Streams, and Estuaries, a five-day workshop sponsored by EPA, will be held May 2–6 in Chicago, Ill. It is intended for engineers, chemists, biologists, and others involved in evaluating pollutant loadings and their effect on water quality. There is no fee for the workshop, and enrollment is limited to the first 75 registrants. For more information contact Virginia Hathaway, JACA Corporation, 550 Pinetown Rd., Ft. Washington, Pa. 19034.

Workshop on Enzyme and Protein Immobilization will be held June 13–15 at Tufts University. Hands-on laboratory sessions and lectures by experts in the field will be featured. The cost of the workshop is $1195 and includes lodging and meals. For more information contact Sean Callahan, Tufts University Conference Bureau, Medford, Mass. 02115; 617-381-3568.

The October 1982 issue of ***Chemistry International*** contains a five-page **bibliography of publications on chemical nomenclature.** The listing includes one section on nomenclature of chemical compounds and one on chemical terminology, units, symbols, and recommendations for presentation of results. Single copies are available at no charge; multiple copies may be purchased in lots of 10 at $4 per 10 copies. Orders (accompanied by a check payable to IUPAC) should be addressed to IUPAC Secretariat, 2-3 Pound Way, Cowley Centre, Oxford OX4 3YF, U.K.

HIGHER ACCURACY & AUTOMATIC EASE
MCI's New KN-03 Coulometric Kjeldahl Nitrogen Analyzer.

MCI's KN-03 introduces greater accuracy, ease and efficiency. Simple injection of diluted Kjeldahl digestion solution starts the automatic process. No titrant is necessary. Repeat measurements are possible. Caustic soda/power consumption are extremely low. Maintenance is minimal. The results are digitally displayed. A wide range of optionals, including the CP-02 Printer, ammonium nitrogen accessories, Kjeldahl digesters and waste gas collector, maximize efficiency. Write for complete details on the new high-precision KN-03 Coulometric Kjeldahl Nitrogen Analyzer today.



MITSUBISHI CHEMICAL INDUSTRIES LIMITED

Instruments Dept., Mitsubishi Bldg., 5-2, Marunouchi 2-chome, Chiyoda-ku, Tokyo, 100 Japan
Telex: J24901 Cable Address: MBISHICHEMICAL TOKYO

CIRCLE 141 ON READER SERVICE CARD

Our Second Skin can save your skin.





Second Skin is a clear high tensile plastisol skin which fits snugly over any glass bottle... just like a second skin.

It is applied to stock or custom glass with Wheaton's unique dipping process.

Second Skin has one major purpose. To keep dangerous liquids safely contained when the inner glass bottle is broken.

You see, chemically inert glass containers are absolutely necessary to safely carry and store acids, solvents, alcohols, alkalis, amides, esters, and surfactants. In fact, most anything dangerous and messy.

And Second Skin is absolutely necessary to contain the glass containers.

Second Skin is less slippery than glass. And is more resistant to impact.

But most of all, it stops glass shrapnel and splattered liquids when dropped. And it reduces contamination and clean up.

Because the whole mess is bottled up in Second Skin.

So on purchase orders, requisition slips and memos specify "Packaged in Wheaton's Second Skin."

Then when you drop the H_2SO_4 you'll know what Second Skin's for.

For more technical information, call Bob Norante or Vince Lisowski (609) 625-2291, (800) 257-7047.

WHEATON SAFETY CONTAINER CO.

A Division of Wheaton Industries
Mays Landing, New Jersey 08330



CIRCLE 234 ON READER SERVICE CARD

A STANDARD REFERENCE IN THE FIELD OF ANALYTICAL CHEMISTRY. . .

FUNDAMENTAL REVIEWS



Chances are you've heard a lot about this special volume. And it's no wonder! For here, in some 400 pages, are authoritative, up-to-date surveys of the most recent literature, with the outstanding work cited and digested.

Below are just a few of the areas covered in the 1982 Fundamental Reviews issue:

- Analytical electrochemistry
- Chromatography: gas, paper, thin-layer, liquid
- Chemometrics
- Kinetics
- Surface analysis
- Spectrometry: NMR, ESR, atomic, emission, IR, mass, X-ray
- Nucleonics
- Microscopy
- Titrations

It's a portable library! And an enormous time-saver for any professional. Use the coupon below to order your copy today.

Distribution Center
American Chemical Society
1155 Sixteenth Street, N.W.
Washington, D.C. 20036

Yes! Send me **Fundamental Reviews.**
I enclose $6 for each copy ordered.

Name_____

Address_____

City_____

State_____ Zip_____

APRIL 1983 VALID THROUGH AUGUST 1983

ADVERTISED PRODUCTS:

	7	8	9	10	11	12	13	14	15	16	17
18	19	20	21	22	23	24	25	26	27	28
29	30	31	32	33	34	35	36	37	38	39
40	41	42	43	44	45	46	47	48	49	50
51	52	53	54	55	56	57	58	59	60	61
62	63	64	65	66	67	68	69	70	71	72
73	74	75	76	77	78	79	80	81	82	83
84	85	86	87	88	89	90	91	92	93	94
95	96	97	98	99	100	101	102	103	104	105
106	107	108	109	110	111	112	113	114	115	116
117	118	119	120	121	122	123	124	125	126	127
128	129	130	131	132	133	134	135	136	137	138
139	140	141	142	143	144	145	146	147	148	149
150	151	152	153	154	155	156	157	158	159	160
161	162	163	164	165	166	167	168	169	170	171
172	173	174	175	176	177	178	179	180	181	182
183	184	185	186	187	188	189	190	191	192	193
194	195	196	197	198	199	200	201	202	203	204
205	206	207	208	209	210	211	212	213	214	215
216	217	218	219	220	221	222	223	224	225	226
227	228	229	230	231	232	233	234	235	236	237
238	239	240	241	242	243	244	245	246	247	248
249	250	251	252	253	254	255	256	257	258	259
260	261	262	263	264	265	266	267	268	269	270
271	272	273	274	275	276	277	278	279	280	281
282	283	284	285	286	287	288	289	290	291	292
293	294	295	296	297	298	299	300	301	302	303
304	305	306	307	308	309	310	311	312	313	314

NEW PRODUCTS:

401	402	403	404	405	406	407
408	409	410	411	412	413	414	415	416	417	418
419	420	421	422	423	424	425	426	427	428	429
430	431	432	433	434	435	436	437	438	439	440
441	442	443	444	445	446	447	448	449	450	451
452	453	454	455	456	457	458	459	460	461	462
463	464	465	466	467	468	469	470	471	472	473
474	475	476	477	478	479	480	481	482	483	484
485	486	487	488	489	490	491	492	493	494	495

TO VALIDATE THIS CARD, PLEASE CHECK ONE ENTRY FOR EACH CATEGORY BELOW:

Intensity of product need:
- ☐ 1. Have salesman call
- ☐ 2. Need within 6 mos.
- ☐ 3. Future project

Primary field of work:
- ☐ A. Energy
- ☐ B. Environmental
- ☐ C. Medical/Clinical
- ☐ D. Drug/Toiletries
- ☐ E. Forensic/Narcotic
- ☐ F. Biotechnology
- ☐ G. Metals
- ☐ H. Pulp/Paper/Wood
- ☐ I. Soaps/Cleaners
- ☐ J. Paint/Coating/Ink
- ☐ K. Electrical/Electronic
- ☐ L. Instrument Dev./Des
- ☐ M. Plastic/Polymer/Rub
- ☐ N. Agricultural/Food
- ☐ O. Inorganic Chemicals
- ☐ P. Organic Chemicals

Primary area of employment:
INDUSTRIAL
- ☐ A. Research/Development
- ☐ B. Quality/Process Contro

MEDICAL/HOSPITAL
- ☐ C. Research/Development
- ☐ D. Clinical/Diagnostic

GOVERNMENT
- ☐ E. Research/Development
- ☐ F. Regulate/Investigate

COLLEGE/UNIVERSITY
- ☐ G. Research/Development
- ☐ H. Teaching

INDEPENDENT/CONSULTING
- ☐ I. Research/Development
- ☐ J. Analysis/Testing

CIRCLE 314 FOR SUBSCRIPTION FORM TO ANALYTICAL CHEMISTRY

NAME: _____

TITLE: _____

FIRM: _____

STREET: _____

CITY: _____

STATE: _____ ZIP: _____

PHONE: (___ ___ ___) ___ ___ ___ ___

NEED MORE INFORMATION?
CIRCLE a key number. . .
SEND IN the postage paid reply card. . .
AND GET free data on any product advertised in this issue. . .

NO POSTAGE NECESSARY IF MAILED IN THE UNITED STATES

BUSINESS REPLY CARD
FIRST CLASS Permit #27346 Philadelphia, Pa.

POSTAGE WILL BE PAID BY ADDRESSEE

analytical chemistry
P.O. BOX #7826
PHILADELPHIA, PA 19101

NO POSTAGE NECESSARY IF MAILED IN THE UNITED STATES

BUSINESS REPLY CARD

FIRST CLASS Permit #27346 Philadelphia, Pa.

POSTAGE WILL BE PAID BY ADDRESSEE

analytical chemistry

P.O. BOX #7826
PHILADELPHIA, PA 19101

NEED MORE INFORMATION?
CIRCLE a key number. . .
SEND IN the postage paid reply card. . .
AND GET free data on any product advertised in this issue. . .

APRIL 1983

VALID THROUGH AUGUST 1983

ADVERTISED PRODUCTS:

7	8	9	10	11	12	13	14	15	16	17
18	19	20	21	22	23	24	25	26	27	28
29	30	31	32	33	34	35	36	37	38	39
40	41	42	43	44	45	46	47	48	49	50
51	52	53	54	55	56	57	58	59	60	61
62	63	64	65	66	67	68	69	70	71	72
73	74	75	76	77	78	79	80	81	82	83
84	85	86	87	88	89	90	91	92	93	94
95	96	97	98	99	100	101	102	103	104	105
106	107	108	109	110	111	112	113	114	115	116
117	118	119	120	121	122	123	124	125	126	127
128	129	130	131	132	133	134	135	136	137	138
139	140	141	142	143	144	145	146	147	148	149
150	151	152	153	154	155	156	157	158	159	160
161	162	163	164	165	166	167	168	169	170	171
172	173	174	175	176	177	178	179	180	181	182
183	184	185	186	187	188	189	190	191	192	193
194	195	196	197	198	199	200	201	202	203	204
205	206	207	208	209	210	211	212	213	214	215
216	217	218	219	220	221	222	223	224	225	226
227	228	229	230	231	232	233	234	235	236	237
238	239	240	241	242	243	244	245	246	247	248
249	250	251	252	253	254	255	256	257	258	259
260	261	262	263	264	265	266	267	268	269	270
271	272	273	274	275	276	277	278	279	280	281
282	283	284	285	286	287	288	289	290	291	292
293	294	295	296	297	298	299	300	301	302	303
304	305	306	307	308	309	310	311	312	313	314

NEW PRODUCTS:

408	409	410	411	412	413	414	415	416	417	418
419	420	421	422	423	424	425	426	427	428	429
430	431	432	433	434	435	436	437	438	439	440
441	442	443	444	445	446	447	448	449	450	451
452	453	454	455	456	457	458	459	460	461	462
463	464	465	466	467	468	469	470	471	472	473
474	475	476	477	478	479	480	481	482	483	484
485	486	487	488	489	490	491	492	493	494	495

TO VALIDATE THIS CARD, PLEASE CHECK ONE ENTRY FOR EACH CATEGORY BELOW:

Intensity of product need:
- ☐ 1. Have salesman call
- ☐ 2. Need within 6 mos.
- ☐ 3. Future project

Primary field of work:
- ☐ A. Energy
- ☐ B. Environmental
- ☐ C. Medical/Clinical
- ☐ D. Drug/Toiletries
- ☐ E. Forensic/Narcotic
- ☐ F. Biotechnology
- ☐ G. Metals
- ☐ H. Pulp/Paper/Wood
- ☐ I. Soaps/Cleaners
- ☐ J. Paint/Coating/Ink
- ☐ K. Electrical/Electronic
- ☐ L. Instrument Dev./Des
- ☐ M. Plastic/Polymer/Rub
- ☐ N. Agricultural/Food
- ☐ O. Inorganic Chemicals
- ☐ P. Organic Chemicals

Primary area of employment.
INDUSTRIAL
- ☐ A. Research/Development
- ☐ B. Quality/Process Control

MEDICAL/HOSPITAL
- ☐ C. Research/Development
- ☐ D. Clinical/Diagnostic

GOVERNMENT
- ☐ E. Research/Development
- ☐ F. Regulate/Investigate

COLLEGE/UNIVERSITY
- ☐ G. Research/Development
- ☐ H. Teaching

INDEPENDENT/CONSULTING
- ☐ I. Research/Development
- ☐ J. Analysis/Testing

CIRCLE 314 FOR SUBSCRIPTION FORM TO ANALYTICAL CHEMISTRY

NAME: _____

TITLE: _____

FIRM: _____

STREET: _____

CITY: _____

STATE: _____ ZIP: _____

PHONE: (___ ___ ___) ___ ___ ___ ___ ___ ___ ___

Space is Money

This publication is available in Microform.

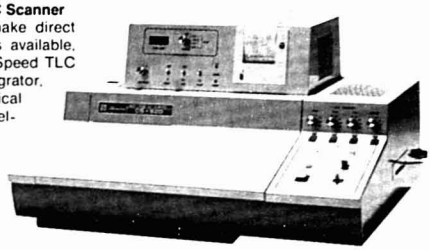
Call Toll Free
800-424-6747
for prices and information on American Chemical Society publications in microfilm and microfiche

American Chemical Society
1155 16th Street, N.W.,
Washington, D.C. 20036

Shimadzu data-processor equipped Densitometers for new dimensions in quantitative TLC.

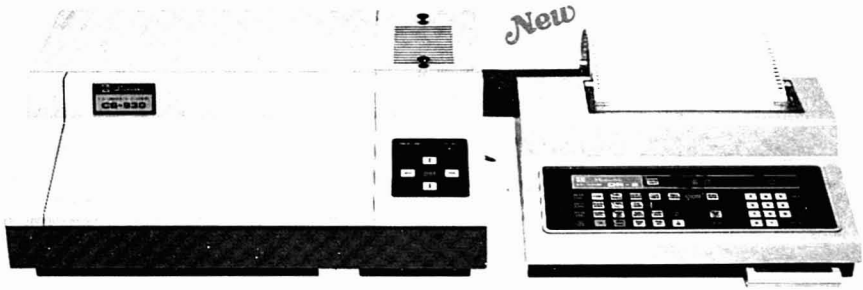
▶ CS-920 High-Speed TLC Scanner
The first instrument to make direct quantitation of TLC spots available, Shimadzu's CS-920 High-Speed TLC Scanner has a built-in integrator, printer and other technical refinements to ensure excellent quantitative analysis. Many valuable features:

- **The automatic lane changing mechanism permits rapid analysis of a large number of samples.** Up to seven samples a minute can be scanned.



- **The built-in microprocessor provides automatic detection of chromatogram spots.** Fused spots are separated and determined automatically.
- **Unique high-speed zigzag scanning, working curve linearization, background correction, and reflection absorption ensure concentration-linear output.** Thus excellent quantitativeness is provided.
- Quantitative calculation with either the external or internal standard method.
- **Direct printout of concentration values.**

CIRCLE 190 ON READER SERVICE CARD



▲ CS-930 Dual-Wavelength TLC Scanner
The Shimadzu CS-930 Dual-Wavelength TLC Scanner is a refined microcomputerized version of the Shimadzu CS-910 Dual-Wavelength Scanner—a winner of the 1977 I-R Competition. The CS-930 with parallel line printer is a low cost complete microprocessor controlled system for quantitative, highly sensitive, high-speed densitometry.
The features are outstanding:

- **Dual-wavelength method** eliminates baseline drifts caused by local irregularities of layer thickness.
- **Zigzag scanning method with a very small light beam** eliminates errors caused by irregular shape of developed spots.
- **Working curve linearization** according to the Kubelka-Munk's equations.

Built-in microprocessor provides:

- **Signal averaging-smoothing** permits the quantitation of nanogram quantity level.
- **Automatic lane changing** up to 30 lanes of chromatogram spots.
- **Automatic detection of chromatogram spots.**
- **Quantitative calculation** with the external or internal standard method. The concentration values are directly printed out.
- Storage of operational parameters.

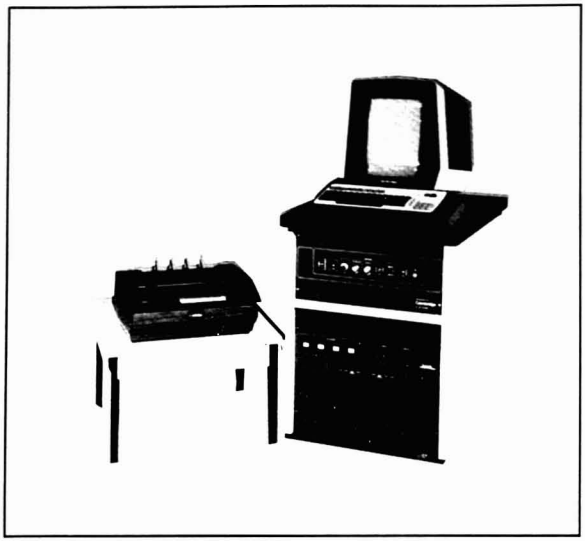
CIRCLE 191 ON READER SERVICE CARD

• Write today for more information on these and other Shimadzu instruments.

SHIMADZU
SCIENTIFIC INSTRUMENTS, INC.

SHIMADZU SCIENTIFIC INSTRUMENTS, INC. 9147 Red Branch Road, Columbia, Md. 21045, U.S.A. Phone: (301)997-1227 Fax: (301)730-1290
SHIMADZU (EUROPA) GMBH Acker Strasse 111, 4000 Düsseldorf, F.R. Germany Phone: (0211)666371 Telex: 08586839
SHIMADZU CORPORATION INTERNATIONAL MARKETING DIV. Shinjuku-Mitsui Building, 1-1, Nishishinjuku 2-chome, Shinjuku-ku, Tokyo 160, Japan. Phone: Tokyo 03-346-5641 Telex: 0232-3291 SHMDT J.

New Products



EDX X-ray Analysis System allows energy-dispersive and wavelength-dispersive analysis to be accomplished simultaneously, permitting detection of elements from atomic number 4 up to 92. A color video monitor displays the results obtained from the Stereoscan Scanning Electron Microscope. Cambridge Instruments, Inc. **403**

Pocket pH Meter

EC/105 Model 2A measures the full pH range from 0 to 14 and temperature from 0 to 80 °C. Results are indicated by a $3\frac{1}{2}$-digit LCD display. It weighs 10.6 oz and has an unbreakable electrode that requires no refilling. IBM **407**

Autoinjector Luminescence System

Model 20-031 Injector System for luminometers has reduced coefficients of variation to 1% or less, determined with ATP standards. Injector volume can be adjusted from 50 to 500 μL. Typical injection speed is less than 0.5 s. Up to three different reagents can be injected into one cuvette. With a count time of 15 s, more than 100 samples/h can be processed. Turner Designs **409**

Spectrofluorometer

Farrand System 3 incorporates digital displays, advanced electronics, the finest optical lens system available, a high-energy light source, a universal sample chamber, and data reduction capability. It will appeal to the researcher who needs to detect minute sample concentrations. Farrand Optical Company, Inc. **410**

Split-Field IR Video Microscope

KV-1 Microscope, primarily designed for transmission IR illumination, operates in the wavelength range between 8000 Å and 2.0 μm and is used for mask alignment on silicon, GaAs, inP, and other semiconductor materials and substrates. Magnifications may be set between 25X and 200X by changing objectives. Research Devices **411**

Crystal Growth Systems

Technology in both the CI-351 and CI-354 Systems is matched to industry requirements for large-area, circular, undoped GaAs wafers. Guaranteed to produce at least 50% yields, both machines are capable of continuous monitoring of crystal shape and have automatic diameter control. Most crystals can be grown in less than 36 h. Cambridge Instruments, Inc. **408**

GC Detector

Ion Trap Detector is both a universal and selective detector and is installable on any type of capillary GC. It enables the chromatographer to obtain positive identification of compounds in complex mixtures, in many cases with only a single analysis. The ITD delivers data in the form of chromatograms, selected mass chromatograms, mass spectra, and quantitation reports. Finnigan MAT **412**

Semimicro pH Electrode

Ross Model 81-03 electrode is designed for use in narrow test tubes and vials, with samples as small as 0.2 mL. The body is 6 mm in diameter and 140 mm long. Recommended for pH determinations in clinical, pharmaceutical, and food applications, it contains no silver precipitates to clog the junction or contaminate the sample. Orion Research Inc. **414**

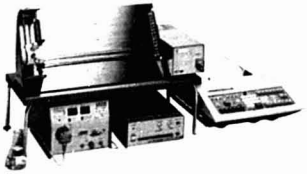
Spectrocolorimeter

CompuScan is designed to measure the reflected color of objects and, through a standard EIA RS 232-C (or 20-mA current loop) communications port, interfaces directly with the customer's computer. It performs continuous spectral scanning from 400–700 nm in 0.8 s and features fiber optic viewing of a fixed $1\frac{3}{4}$-in. sample illumination area. The optical sensor has 0°/45° circumferential geometry. Hunterlab **416**

For more information on listed items, circle the appropriate numbers on one of our Readers' Service Cards

Shimadzu's promise to liquid chromatography:

Modular design, versatile components and full automation



▲ LC-5A Microbore Column Liquid Chromatograph
A world-first to help you to reduce solvent consumption up to 95% and reach theoretical plate numbers higher than 200,000. The pump capacity of the Shimadzu LC-5A Microbore Column Liquid Chromatograph can be varied from 1 to 9900μl a minute, while the total system dead volume is only 2μl.

Circle 194



▲ SPD-M1A Photo-Diode Array Spectrophotometric Detector for LC
Designed for simultaneous quantitative and qualitative analyses, the Shimadzu SPD-M1A Photo-Diode Array Spectrophotometric Detector is a new type of detector offering the advantage of three-dimensional spectro-chromatograms, easily identifiable peaks, spectrum memory on-flow and single and double wavelength range chromatograms. The photo-diode array sensor covers the full UV and VIS spectrum range.

Circle 195

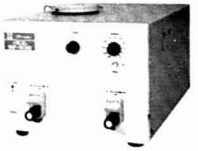
▼ LC-4A Liquid Chromatograph
Shimadzu's inexpensive ternary gradient liquid chromatograph offers microprocessor control over all system components, including liquid pump, sample injection and detectors. Operational conditions can be programmed and stored in up to 10 separate files, allowing analytical runs to be made automatically with different sets of operational conditions. Generous self-diagnostics are complemented by safety devices to protect against abnormal temperature, leaks and pressure. When linked with Chromatopac C-R2A which can offer true 2 channel operation, control may be made by user-defined BASIC programming.

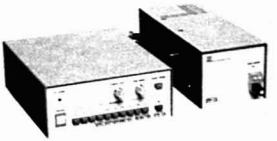
Circle 196



▼ RF-530 Fluorescence Spectromonitor for HPLC
Shimadzu's RF-530 Fluorescence Spectromonitor with xenon lamp and concave holographic gratings offers a wide range of excitation and emission wavelengths. The corrected excitation energy and sensitivity to give a detection limit for quinine sulphate is 0.45pg/12μl. An off-plane optical system and aberration-corrected concave holographic gratings decrease noise. All connections are made with standard 1/16" O.D. tubing for connection to all HPLC systems.

Circle 197





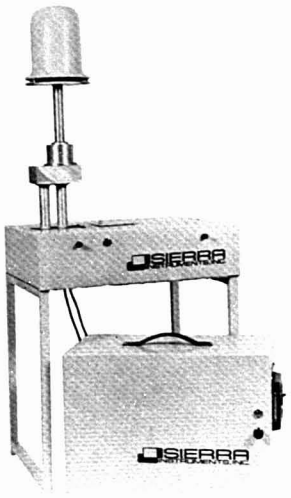
▲ SPD-2A UV Spectrophotometric Detector Series for HPLC
Shimadzu's SPD-2A is equipped with a high-performance grating monochromator having a wavelength range from 195 to 350nm. To ensure high stability, the SPD-2A has a double beam optical system which cancels drifts caused by fluctuation in the intensity of the light source. Available with 8μl flow cell and 0.5μl micro flow cell.

Circle 198

• Write today for more information on these and other Shimadzu instruments.

SHIMADZU
SCIENTIFIC INSTRUMENTS, INC.

SHIMADZU SCIENTIFIC INSTRUMENTS, INC. 9147 Red Branch Road, Columbia, Md. 21045, U.S.A. Phone: (301)997-1227 Fax: (301)730-1290
SHIMADZU (EUROPA) GMBH Acker Strasse 111, 4000 Düsseldorf, F.R. Germany Phone: (0211)666371 Telex: 08586839
SHIMADZU CORPORATION INTERNATIONAL MARKETING DIV. Shinjuku-Mitsui Building, 1-1, Nishishinjuku 2-chome, Shinjuku-ku, Tokyo 160, Japan. Phone: Tokyo 03-346-5641 Telex: 0232-3291 SHMDT J.



Model 245 Dichotomous Sampler features automatic changing of weighted disk filters. It samples particles smaller than 10 μm and separates the particles into two size fractions, "coarse" particles from 2.5 to 10 μm and "fine" particles smaller than 2.5 μm. Sierra Instruments, Inc. **404**

Multimeter

With 6.5-digit, 100-mV resolution, the 8505A Digital Multimeter measures dc volts at 10 ppm absolute accuracy (90 d, 18–23 °C). On the 10-V dc range, the meter increases its resolution to 7.5 digits. Up to 500 readings/s are possible in the dc-volts mode at 6.5-digit resolution and full accuracy. John Fluke Mfg. Co., Inc. **413**

Cryopumps

RPK series of cryopumps is available in 11 models with standard LF, CF, and ASA flanges with one-, two-, and three-stage cryogenerators. Pumping speeds range from 400 L/s to 10 000 L/s for N_2 or 1200 L/s to 40 000 L/s for H_2. The cryopumps require no liquid helium for operation and can be mounted in any position. Leybold-Heraeus **417**

Temperature Controller

Series 6000 controller incorporates two digital displays, touch-key operation, software linearized and stabilized thermocouple input with three-mode PID heating and cooling control, and dual alarms. Omega Engineering Inc. **422**

Soxhlet Extractor

Applications for the High-Pressure Soxhlet Extractor include: environmental research, food and flavor analysis, essence extraction, and pheromone analysis. Unit uses carbon dioxide, Freon, or other substances that liquefy at 0 to 20 °C and do not generate pressures exceeding 1500 psi. Kontes **415**

Airborne Particle Counters

Status 2000 and 5000 counters are suitable for lab or field use. Model 2000 measures two particle size ranges—0.5 and 5.0 μm—shown on a simultaneous three-digit display. Model 5000 measures five particle sizes—0.3, 0.5, 1.0, 2.0, and 5.0 μm—using a sequential five-digit display. Faley International Corp. **418**

Dew Point Meter

Protimeter chilled meter provides relative humidity readings to within ±1%. Depending on dew point temperature, the instrument cycles through dew point determinations every 2–5 min. The Protimeter is ideal for static air conditions, small enclosures, and immersion in products for measurement of equilibrium relative humidity where it will not affect the temperature being measured. Cosa Instrument Corp. **419**

Moisture and Temperature Test Set

Model HMP3 set consists of a hand-held electronic indicator with push-button activation, a sword-shaped sensor for insertion in cut stacks of paper or into granular solids, a calibration standard (the value for which is established by NBS), protective replaceable filters for testing chemically treated papers, and a nested carrying case. Beckman **421**

Moisture Vapor Analyzer

Analyzer is a portable instrument used to detect moisture in the ppm range up to approximately 17%. Applications include the food, drug, and cosmetic industries, and anywhere in quality control where the determination of water content is important. The instrument consists of a sample holder, an oven for heating the sample, a fractionating column, a detector, and a readout. Harvey Scientific Corp. **420**

Chemicals

Arsine Test Kit

Kit determines arsenic in accordance with Standard Methods for the Examination of Water and Wastewater. It includes all chemical solutions, glassware, and instructions needed for the test. Wheaton **425**

USP/NF/FCC-Grade Reagents

Reagents meet the strength, quality, and purity requirements of the U.S. Pharmacopeia, the National Formulary, and/or the Food Chemicals Codex. Some of the reagents now available include acetone, boric acid, glycerine, potassium iodide, sodium acetate, and zinc sulfate. Fisher Scientific Co. **426**

Wide-Pore HPLC Materials

Hypersil WP-300 300-Å wide-pore silica-based material is designed for separation of large molecules with HPLC. It is available in normal-phase, C_4, and C_8 materials. Particle sizes available are 5 μm and 10 μm. Shandon Southern Instruments, Inc. **424**



Sonifier Ultrasonic Laboratory System, for ultrasonic disintegration and homogenization, is suitable for lab, pilot, and production use and can handle most processes requiring high- or low-intensity ultrasonic energy. It delivers up to 350 W to the converter and can operate on a continuous or intermittent duty cycle on difficult or large-scale applications. Bronson Sonic Power Co. **402**

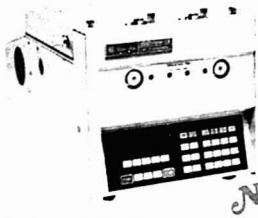
Shimadzu..... low cost alternative for quality GC.

ANNOUNCING ..... Split-splitless operation, full detector selection, full accessory availability and application support.

▼GC-MINI2
Gas Chromatograph
Compact and reliable, Shimadzu's GC-MINI2 Gas Chromatograph has a dual column flow system and on-column on-detector system. An optional temperature programmer is available for programming from the near ambient point. The three temperature sensors provide excellent repeatability in resetting initial column temperature.

Circle 202

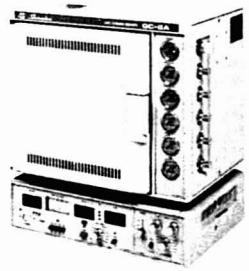




New

▲ GC-MINI3 Gas Chromatograph
The most compact microcomputerized GC with dual FID. A full performance new-generation GC with full keyboard operation. Features include an on-column on-detector system, multi-stage temperature-program capability with near ambient column temperature even with high injection port temperature.
Circle 204

▼ GC-8A Series Gas Chromatograph
A simple construction and low cost are the key features of Shimadzu's high-quality GC. The GC-8A Series offers digital temperature setting and digital temperature programming. An on-column on-detector system, FID, constant current TCD, FPD, and ECD models are available. Circle 205



▼ GC-6AM Series
Gas Chromatograph
The first modular designed system with sample injection port, column and detector combined into one cartridge unit—quick change of analytical conditions, elimination of cross contamination between samples and shorter down time. The only system with the complete analytical unit in the oven simultaneously. Circle 203





◀ GC-9A Series Gas Chromatograph
Shimadzu's GC-9A Series Gas Chromatograph with built-in microprocessor saves valuable laboratory time without loss of analytical excellence. It makes available easy user-defined programming, multiple files with linking, computer interface and generous self-diagnostics. Now available with full detector options (FID, TCD, ECD, FTD, FPD). Circle 206

AOC-9 Automatic Sampler for GC-9A
A new accessory designed to enlarge the capability of the GC-9A, the AOC-9 offers sequence control through the GC-9A keyboard. Sample volume is selectable in four steps of 10, 20, 40 and 80% of the plunger stroke; repeat sampling for up to a maximum of 10 samples; and sample vial detection eliminating the need for batch step sample placement. Circle 207

• Write today for more information on these and other Shimadzu instruments.

SHIMADZU
SCIENTIFIC INSTRUMENTS, INC.

SHIMADZU SCIENTIFIC INSTRUMENTS, INC. 9147 Red Branch Road, Columbia, Md. 21045, U.S.A. Phone: (301)997-1227 Fax: (301)730-1290
SHIMADZU (EUROPA) GMBH Acker Strasse 111, 4000 Dusseldorf, F.R. Germany Phone: (0211)666371 Telex: 08586839
SHIMADZU CORPORATION INTERNATIONAL MARKETING DIV. Shinjuku-Mitsui Building, 1-1, Nishishinjuku 2-chome, Shinjuku-ku, Tokyo 160, Japan. Phone: Tokyo 03-346-5641 Telex: 0232-3291 SHMDT J.

Manufacturers' Literature

UV/VIS Equipment. Application report UV-15 highlights the benefits of a design for research, as well as for routine repetitive measurements, and explains the philosophy behind the design. A hydrolysis of methyl salicylate covering a period of about one-and-one-quarter hours is described and graphed. 7 pp. Varian **433**

Turbomolecular Vacuum Pump. Brochure includes pump descriptions, dimensions, specifications, pumping speed curves, and information to assist the user in choosing the correct pump for each application. 12 pp. Sargent-Welch Scientific Co. **434**

Image Analysis System. IBAS system for automatic and interactive image analysis of microscopic, electron-microscopic, and macro samples is described. Illustrations of several image and data determinations as well as details of the system's many features are provided. 16 pp. Zeiss, Inc. **435**

Fused-Silica Capillary Columns. Selection guide covers 40 standard phases, 0.25 mm or 0.32 mm i.d., 25- or 50-m lengths; 13 popular and special-purpose columns; and contains information on custom columns manufactured to order. 6 pp. Chrompack, Inc. **436**

Materials Analyzer. Application note describes the use of the Model 740 Compact Materials Analyzer in determining the sulfur and ash content in pulverized coal samples in 1 min. When moisture content is known, BTU/lb values can be calculated. Columbia Scientific Industries Corp. **430**

AA Detection Limit Guide. Table allows comparison of detection limits for 71 elements between flame AA, furnace AA, and ICP spectroscopy. Optimal wavelengths for AA and ICP, AA lamp currents, and AA sensitivity values are also listed. Instrumentation Laboratory **431**

The Supelco Reporter. Vol. II, No. 1 includes articles on analyzing catecholamines on a 3-μm column packing, analyzing products of enzymatic reactions by HPLC, and analyzing benzodiazepines simultaneously by HPLC. 11 pp. Supelco, Inc. **438**

Chromatography Chambers. Booklet describes line of chromatography refrigerators (4 °C) with the Computron Control System, featuring multiple sensors for temperature control/uniformity and automatic, daily self-testing. Available in 23, 50, and 75 ft^3. 11 pp. Rheem Manufacturing Co. **437**

Catalogs

Tek Products. 1983 catalog features products from the company's design automation, information display, communications, and instrument systems divisions. 447 pp. Tektronix **449**

Nalgene Labware. 1983–84 catalog features filtration products such as a 30-mL sterilization filter unit, tissue culture sterilization units, and syringe filters with nylon membranes. 84 pp. Nalge Co. **444**

Research Products. Catalog describes liquid scintillation cocktails and chemicals, scintillation vials and nuclear accessories, radiochemicals, immunochemicals, and contamination/radiation survey instruments. 128 pp. Research Products International Corp. **445**

Chromatography. Catalog No. 50 introduces a range of computer products for chromatography. Also listed are new packing materials for HPLC. 300 pp. Alltech Associates Inc. **450**

Lab Chemicals. 1983 catalog/price list presents over 4000 currently offered chemicals along with some new products. 78 pp. Kodak **447**

Lab Stirrers. Catalog provides photos and complete specifications on 15 stirrer models and includes data on a variety of paddles, support stands, propellers, extension sleeves, extension bars, and precision chucks. Talboys Engineering Corp. **451**

Research Products. 1983 catalog/price list describes products for chromatography, electrophoresis, immunochemistry, and HPLC. 183 pp. Bio-Rad **446**

MS and GC Supplies. 1983–84 catalog features products for MS and GC, instrument cleaning, vacuum systems, linagraph paper, and tools. 120 p. Scientific Instrument Services, Inc. **448**

Chemicals. Lines of reagent acids, solvents, and specialty chemicals are covered. Specialized types such as semigrade reagents for the electronics industry and HPLC-grade solvents are also included. 6 pp. Corco Chemical Corp. **440**

Electrochemical Instruments. Major product offerings include polarographic and voltammetric analyzers, amperometric analyzers, EC detectors for LC, and specific analyzers for chlorine, peroxide, ozone, pH, and conductivity. 32 pp. IBM **441**

GC. Featured in the catalog are: MTBSTFA, a new dimension in silylation; Regisil, first choice for trimethylsilylation; GC/MS reagents; amino acid analysis standards and kits; and a guide to derivatization. 32 pp. Regis Chemical Co. **442**

Lab Instruments. A range of lab supplies is presented from filters to electrodes to weather instruments. 35 pp. ScienceMart **443**

For more information on listed items, circle the appropriate numbers on one of our Readers' Service Cards

H. C. Heller
V. Markovac
Engineering and Research Staff
Research
Ford Motor Company
Dearborn, Mich. 48121

The Analytical Approach

Edited by Jeanette G. Grasselli

Identification of a Membrane Foulant in the Electrodialytic Recovery of Nickel

Identification and/or removal of the compound causing the fouling often becomes an integral part of the wastewater recovery scheme

In recent years, economic and environmental pressures have made the disposal of nickel plating wastewater unacceptable. The price of nickel has been escalating, and severe restrictions have been placed on disposal of waste containing heavy metals into the environment (e.g., via landfilling). Several methods have been recommended for the recovery and/or recycling of nickel out of plating rinse water, including reverse osmosis and electrodialysis (*1*). These two recovery techniques usually involve use of organic membranes, which are often plagued by fouling, i.e., clogging of the transport pores. As a result, the process of identification and/or removal of the compound causing the fouling often becomes a necessary and integral part of the overall recovery approach.

Industrial nickel plating solutions contain three basic inorganic ingredients (nickel sulfate, nickel chloride, and boric acid) and several organic additives that are added to achieve bright, ductile, and leveled nickel deposits during plating. These organic additives, which are supplied as special formulations by several trade companies, usually contain sodium allyl sulfonate, saccharin, and some proprietary compounds. In our work evaluating the feasibility of nickel recovery by means of electrodialysis, we found that some component(s) present in additive formulation of a major supply company severely and rapidly fouled the electrodialytic membranes. For the sake of brevity, we shall designate this formulation by the letter "A." In this article, the work involved in removing, separating, and identifying the fouling species in A is described.

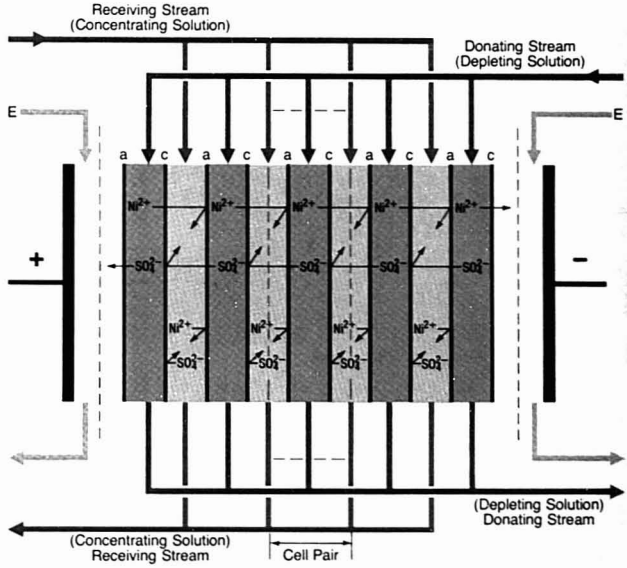


Figure 1. Multicompartment electrodialysis unit for concentrating $NiSO_4$ solutions
(a) and (c) represent anion- and cation-selective membranes, respectively. Reprinted with permission from Reference 3

Origin of the Problem

To understand more fully some of the reasoning behind the identification techniques adopted in this work, it is useful to start with a brief description of the electrodialytic recovery of nickel ions. More details on electrodialysis generally, as well as on recovery of nickel, may be found elsewhere (*2–4*). In the electrodialysis

0003-2700/83/0351-551A$01.50/0
© 1983 American Chemical Society

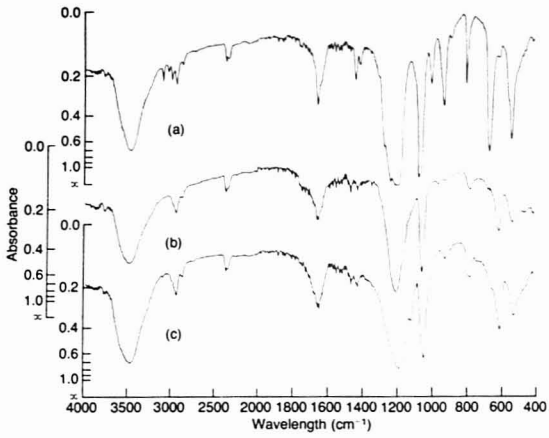


Figure 2. Infrared spectra of (a) Solid III (sodium allyl sulfonate), (b) Solid I (polyallyl sulfonate recovered via ion exchange), and (c) Solid II (polyallyl sulfonate obtained via methanol extraction)

process a number of alternately arranged cation- and anion-selective membranes are placed between two electrodes (Figure 1) (3). The anion-selective membranes are often vinyl copolymers with positively charged quaternary ammonium salt groups that pass their counterions (negatively charged anions) while repelling their coions (cations). Cation-selective membranes are usually copolymers containing negatively charged sulfonic-acid-type groups that pass their counterions (cations) but repel coions (anions). Solutions containing nickel ions flow in parallel channels between the membranes, forming alternately diluting (or donating) and concentrating (or receiving) streams. An electric field imposed across the electrodes causes an ionic current to pass through all streams and membranes. Thus, nickel cations are transferred through the cation-selective membranes toward the cathode, while anions (sulfate, chloride, etc.) migrate through the anion-selective membranes toward the anode. The net result is the transfer of nickel ions from the depleting streams to the concentrating streams. The concentrating process is repeated, if necessary, until the concentration of the receiving stream is near that of the nickel plating bath, after which the receiving stream can be recycled to the plating bath for reuse.

In our work, electrodialysis experiments were performed in an electrodialysis stackpack manufactured by Ionics, Inc. (Watertown, Mass.) containing anion-selective membranes (103.QZL.219) and cation-selective membranes (61.CZL.183). In general, a normal electrodialysis process unaffected by membrane fouling and operating under galvanostatic conditions (constant current density) can be maintained by voltage that varies little or not at all with time. For example, the concentration of a solution containing only the three inorganic ingredients (1000 ppm of nickel ions) with current density of 12.5 mA/cm^2 progressed smoothly for several hours with a constant voltage of 9.5 V. However, in a solution of identical nickel ion concentration obtained from post-plating rinse, and therefore also containing A, the voltage required to maintain 12.5 mA/cm^2 in the electrodialysis process rose rapidly from 14 to 40 V in less than 60 min. Clearly, fouling of the electrodialysis membranes was occurring. As a result, ionic transport through the membranes was impeded, requiring ever-increasing voltage to maintain it. The fouling could not have been caused by deposition of nickel hydroxide since the solutions had a pH < 4.8. Also, a careful postmortem examination of the disassembled electrodialysis membranes failed to reveal any traces of nickel hydroxide (light green) precipitate.

Removal of Fouling Species

Several methods were used in an attempt to remove the fouling species. These included filtration through 0.25-μm Millipore filters; adsorption on activated carbon, diatomaceous earth, and polymeric adsorbants; and removal with ion-exchange columns.

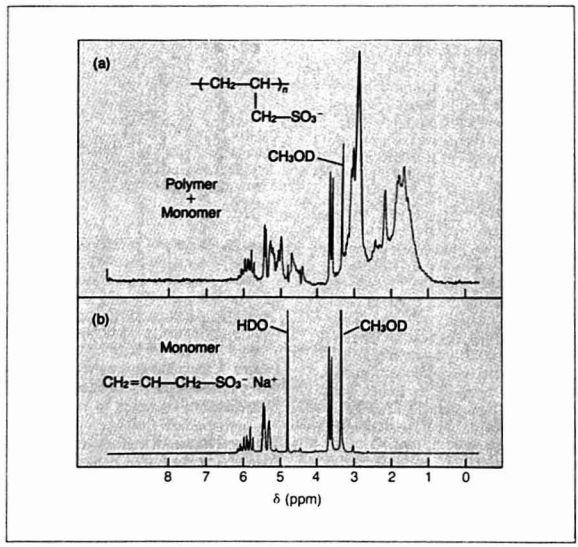
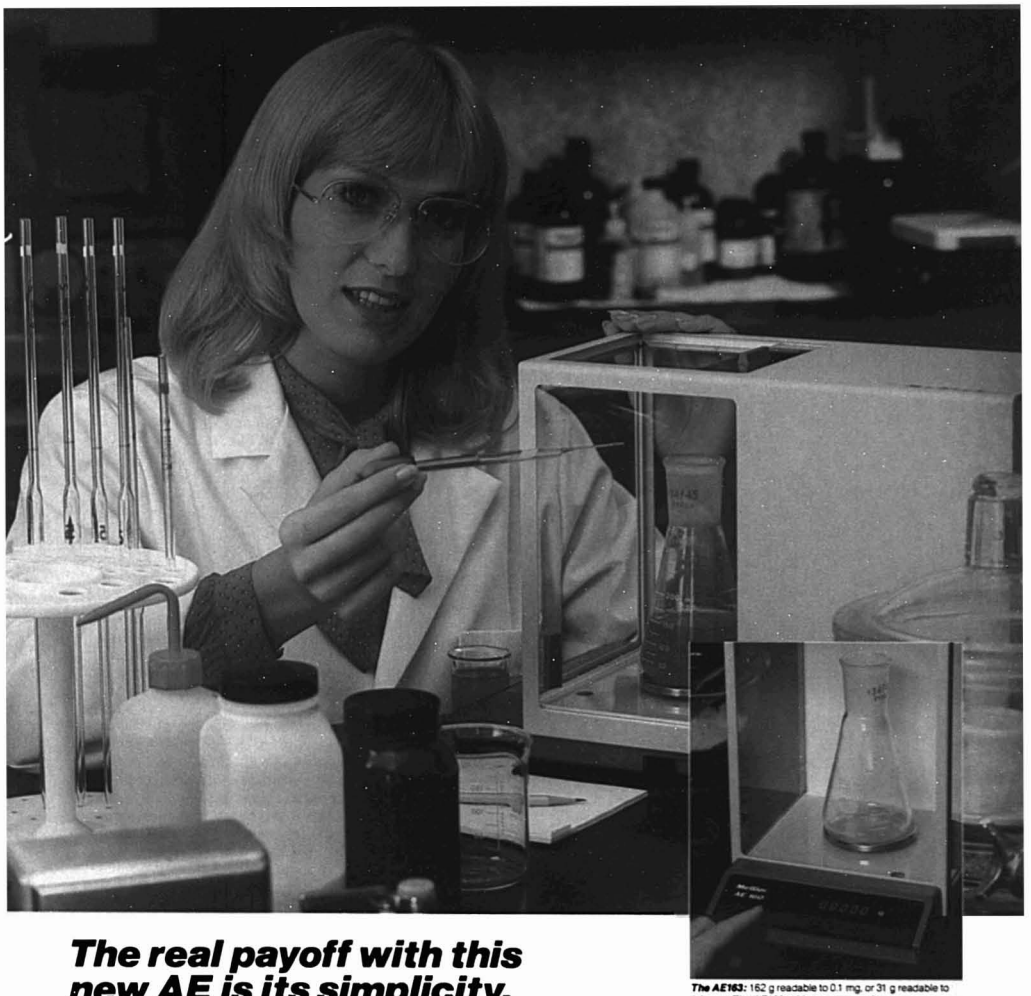


Figure 3. NMR spectra of (a) polyallyl sulfonate and (b) allyl sulfonate monomer



The real payoff with this new AE is its simplicity.

The AE163: 162 g readable to 0.1 mg, or 31 g readable to 0.01 mg. ***The AE160:*** 162 g readable to 0.1 mg.

One control bar on the new Mettler AE models puts you in touch with the simplest analytical balance you've ever used.

A touch locks in tare. You can calibrate the balance at a touch, in ten seconds or less. You can even adjust the balance to compensate for environmental factors (which might throw another balance off) at a touch of a single control bar.

Simple, therefore faster.
The new Mettler electronic balances are so simple to work with that weighings go three to four times quicker than they do with a mechanical analytical.* On the AE models, the top-loading weighing pan is stable. It doesn't swing back and forth. And it's just 55 mm above the lab bench's surface. The readout is right there, too. Big, bright, clear. The side doors slide easily. So does the one on top, which gives you easy access to the roomy weighing chamber.

Data transfer.
The simplicity of the AE also makes it easy to use with computers or other electronic peripherals. All you do is snap a Mettler optional data output device onto the back of the AE, and you're set to transfer weighing results. An automatic stability detector, within the balance, makes sure only stable values are transferred for data processing.

A simply great price.
The technology that has made this balance so simple to use has also reduced the number of parts in the AE, as compared to other electronic analytical balances. Fewer parts translate into a lower price. You can have this new Mettler electronic analytical balance for just about the same price as a mechanical analytical.

Write us for more information. We are Mettler Instrument Corporation, Box 71, Hightstown, NJ 08520.

*"A Comparison of Mechanical and Electronic Balances," Journal of Chemical Education, May 1982, P. 418. If you'd like a reprint, write to us.

Mettler

CIRCLE 140 ON READER SERVICE CARD

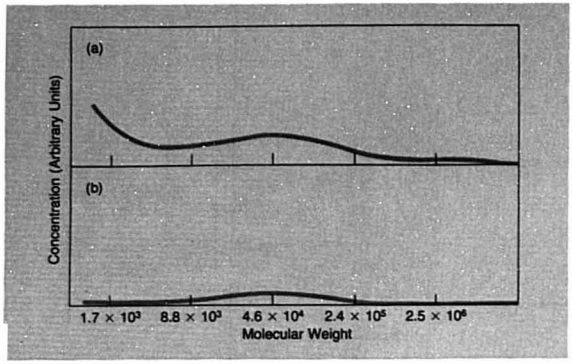


Figure 4. Gel permeation results for (a) Solid I and (b) Solid II

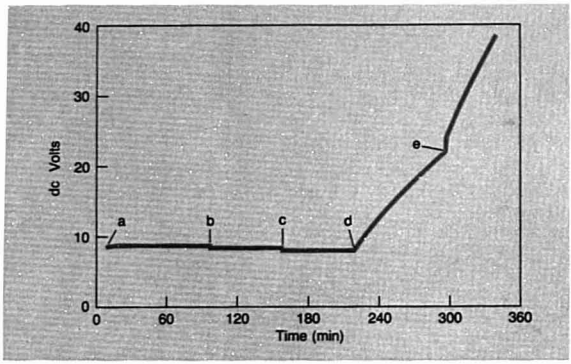


Figure 5. Voltage vs. time curve for a nickel plating rinse solution under galvanostatic conditions

Line a–b, after pretreatment with ion-exchange resin; lines b–c and c–d, after addition of 1 g each of sodium allyl sulfonate monomer (Solid III); and lines d–e and beyond e, after addition of 1 g each of polyallyl sulfonate (Solid I)

Treating plating rinse water by filtration or adsorption was unsuccessful. Activated carbon appeared to remove small amounts of the foulant, but its capacity for doing so was very limited, and it saturated rapidly. We achieved much better success by passing the rinse water through columns containing a number of anion-exchange resins (e.g., Rohm & Haas Amberlite-904 and Diamond Shamrock Duolite-A101D). Capacity for foulant removal varied from resin to resin, and only limited work was done to quantify it. As an example, 1000 mL of Duolite A101D resin completely removed the foulant concentration (undetermined) present in 4000–5000 L of rinse containing 1000 ppm of nickel and passing through the resin column at a rate of 20 bed-volumes/h. Ion-exchange columns saturated with the foulant could be regenerated to 90% or better of their original capacity by treatment with hydrochloric acid or sodium chloride methanol–water solution. Nickel rinse water containing A treated with the ion-exchange resin exhibited no fouling during electrodialysis (the voltage–time curve was constant with time).

Isolation and Identification

Separate electrodialysis experiments in which membranes were all either cation- or anion-transferring membranes showed that fouling occurred only with the latter. This strongly indicated that the foulant was an organic *anion*. The fact that the foulant exchanged with an anion-exchange resin further supported our hypothesis. Isolation and subsequent full identification of the foulant were achieved in two ways.

In the first method, nickel plating rinse water containing A was passed through an anion-exchange column that removed the foulant. The saturated column was then eluted with small amounts of methanol–water solution containing sodium chloride. The eluent consisted therefore of a relatively concentrated solution of the fouling species. This eluent was then evaporated to dryness and the solid residue (Solid I) was studied by IR and NMR techniques. IR spectra were recorded at room temperature on a Perkin Elmer No. 383 IR spectrophotometer. Samples studied were in the form of pressed KBr pellets containing small amounts of the solids being investigated. For NMR work, the solids were dissolved in D_2O and their NMR spectra recorded on a Jeolco 100-MHz spectrometer. Spectral results for Solid I are shown in Figures 2b and 3a.

Using the second method, we noticed that even fresh, preplating solutions containing A occasionally showed moderate fouling. The presence or absence of this moderate fouling varied from sample to sample. At our request, the vendor of A kindly supplied us with three individual components of the formulation.

One component (A-1) was basically a solution of sodium allyl sulfonate, $CH_2{=}CH{-}CH_2{-}SO_3^-Na^+$, the second was a saccharin solution, and the third a solution containing proprietary chemicals. Upon testing, only component A-1 was found to induce occasional fouling when added to solutions containing only inorganic ingredients. Pure sodium allyl sulfonate, obtained from a separate chemicals supplier or by purification in this laboratory, exhibited no fouling. It seemed, therefore, that the foulant was a large ionic molecule, perhaps an oligomer or polymer of the allyl sulfonate moiety, which is present in small amounts in component A-1.

Sodium allyl sulfonate is soluble in both water and methanol. Its polymer, which has been extensively studied only recently (*5*), is soluble in water only. Accordingly, a sample of solution A-1 was evaporated to dryness, and the residue was extracted with several portions of dry methanol. Most of the solid dissolved in the methanol except for a small amount of a gray–white tacky residue (Solid II). The IR spectrum of this gray–white residue is shown in Figure 2c. The extracted methanol solution was also evaporated to dryness, and the IR and NMR spectra of the resulting white solid (Solid III) are shown in Figures 2a and 3b.

The IR and NMR spectra of the





All the titration capability you need. The Mettler DL40RC MemoTitrator.

The MemoTitrator just got new remote control capability, improved software, a second titration head, an automatic sample transport module, and a new model designation: DL40RC. This single, improved instrument can handle all types of titrations. It stores up to 19 methods, performs endpoint, equilibrium and incremental titrations—links them—and prints out results in required units.

It's an all-purpose automatic titrator.

Plug in the Mettler RT40 Sample Transport peripheral and you can do a series of up to 16 samples. The RT40 can accept and store up to 50 sample weights from a connected balance.

It's a Karl Fischer titrator.

The DL40RC has improved software to handle the new two-component titrants. Dual titration heads allow you to work more efficiently by switching from one head to the other.

It's a nitrogen and protein analyzer.

You can connect a Kjeldahl/Nitrogen Analyzer to the DL40RC to quickly determine percent nitrogen or protein.

The new model DL40RC MemoTitrator is all the titration capability you need. For a demonstration or more information, complete the coupon and send it to us.

Mettler Instrument Corporation,
Box 71, Hightstown, NJ 08520-9944,
Phone (609) 448-3000

☐ Send me complete information on the new DL40RC MemoTitrator.
☐ I'd like a demonstration

Name _____
Company _____
Address _____
_____
City _____
State _____ Zip _____
Phone _____
(Area Code) (Number)

Mettler

CIRCLE 142 ON READER SERVICE CARD

methanol-extracted solid (Solid III), Figures 2a and 3b, are identical to those observed by Sasuga and coworkers for pure sodium allyl sulfonate monomer (5). Prominent IR features are the bands at 920, 998, and 3000–3100 cm^{-1}, which are due to stretch and deformation motions associated with the allylic double bond in $CH_2{=}CH{-}CH_2{-}SO_3^-$. Additional confirmation for the monomer is provided by the NMR data, where the chemical shift signals at 3.61–3.70, 5.15–5.30, and 5.80–6.15 ppm are due to the protons at $-CH_2-SO_3^-$, $CH_2=$, and $=CH$-groups, respectively.

The IR spectrum observed for the tacky gray-white solid (Solid II), Figure 2c, is identical to that obtained for the solid recovered from the ion-exchange column (Figure 2b). Moreover, these spectra are also similar to those obtained by Sasuga et al. (5) for a polymer they produced via high-energy radiation of sodium allyl sulfonate under pressure. The main spectral features that distinguish the polymer from the monomer are the absence of the bands due to the double-bond motions and a shift in the band at 660 cm^{-1} to 608 cm^{-1} in the former. The NMR spectrum provided additional evidence that the fouling species is a large molecule, i.e., a polymer. Figure 3a, obtained from Solid I, contains some narrow peaks at 3.5–6.1 ppm, due to some residual amounts of the allyl sulfonate monomer. However, the main intense peaks, situated at 1–3 ppm, are extremely broad and are characteristic of a large molecule in which restricted tumbling motion is not rapid enough to average out the anisotropic nuclear magnetic interactions in it.

Clearly, the spectral data strongly indicated that the foulant was a polymer, or more appropriately a polyelectrolyte of allyl sulfonate,

$$-\left(CH_2-\underset{\displaystyle CH_2-SO_3^-}{\underset{|}{CH}}\right)_n-$$

Molecular Weight Distribution

Some measure of the molecular weight distribution in the polymer was obtained from gel permeation chromatographic results. For this purpose small amounts of the gray-white residue (Solid II) and the white residue recovered from the ion-exchange elution (Solid I) were separately acidified with HCl and dissolved in *p*-dioxane. Aliquots of solutions of the solids were analyzed on a Waters Associates Ana-Prep chromatograph operating with *p*-dioxane as the solvent at 45 °C. A flow rate of 1 mL/min was maintained. Column arrangements consisted of

CHROMATOGRAM OF QUALITY

1 2 3 4 5 6

1. QUALITY
2. PRICES
3. SERVICE
4. AVAILABILITY
5. PRODUCT VARIETY
6. TECHNICAL SERVICE

Write or call today for our new 320 page chromatography catalog

ALLTECH ASSOCIATES

2051 Waukegan Road
Deerfield, Illinois 60015
(312) 948-8600

CIRCLE 5 ON READER SERVICE CARD



How to switch HPLC columns using valves.

Different analyses sometimes use different columns. But even when the same column can handle more than one kind of sample, many chemists dedicate a column to each analysis. This prolongs column life, reduces interferences, and eliminates equilibration delays.

Rheodyne's Technical Notes 4 tells how to use switching valves to connect as many as five columns to a chromatograph. Any column can be selected, while the off-line columns remain sealed at each end. The effect on resolution is shown to be negligible in most cases.

Send for Tech Note #4

For the well-illustrated tech note, contact Rheodyne, Inc., P.O. Box 996, Cotati, California 94928, U.S.A. Phone (707) 664-9050.

RHEODYNE
THE LC CONNECTION COMPANY

CIRCLE 185 ON READER SERVICE CARD

four columns in series with permeability limits designated as 10^2, 10^3, 10^4, and 10^5 Å. Polystyrene samples of narrow molecular weight distributions were used for calibration of the molecular weight scale (see Figure 4). The results obtained with Solid I are shown in Figure 4a; those obtained with Solid II are shown in Figure 4b. Interestingly, although both Solids I and II were shown to be polyallyl sulfonate by their IR spectra, they consist of different molecular weight distributions. Solid I, which originated from postplating rinse water, had a molecular weight distribution from 10^3 to 10^7 while Solid II, which came from fresh preplating solutions, exhibited a narrower molecular weight distribution, from 10^3 to 10^5. This suggested that small oligomers of allyl sulfonate present in the plating additives before the start of the nickel plating process may have grown in size during the plating process. However, attempts to determine whether nickel solutions containing purified sodium allyl sulfonate (without any oligomeric impurities) could be induced to polymerize via the plating process itself (at 65 °C and under air agitation) were inconclusive. Polymerization occurred in some samples but not in others.

To confirm the participation of the allyl sulfonate polyelectrolyte in the fouling process, we pretreated a nickel postplating rinse solution by passing it through an ion-exchange column, thus removing the foulant. This pretreated rinse was then processed by electrodialysis for 100 min under galvanostatic conditions. As seen in Figure 5, segments a–b, the electrodialysis proceeded without any sign of fouling. After 100 min (point b) and again after 160 min (point c), 1 g of purified sodium allyl sulfonate (Solid III) was added to the electrodialyzing solution. No fouling was observed, and the decrease in dc voltage was due to the slight increase in ionic concentration of the solution. One gram of polymeric allyl sulfonate (Solid I) was then added after 220 min (point d) and another gram after 280 min (point e). The result was a fast and dramatic increase in dc voltage, indicating an immediate and rapid fouling of the membranes.

Conclusion

We have identified polyallyl sulfonate as a foulant of ion-exchange membranes in the electrodialysis of some nickel plating solutions. It should be emphasized, however, that allyl sulfonate monomer does not cause any fouling. Indeed, a separate brightener formulation supplied by a different supplier and containing sodium allyl sulfonate exhibited no fouling. The presence of the polymeric allyl sulfonate in some proprietary formulations may be fortuitous, and the reasons for the polymer's formation and propagation are not clear at this point.

Acknowledgment

We wish to thank K. J. Tuite for assisting with some of the electrodialysis work. We also thank J. L. Parsons and M. Zinbo for obtaining the IR and gel permeation chromatographic spectra.

References

(1) "Technology Transfer," EPA 625/5-79-016, June 1979.
(2) Mason, E. A.; Kirkham, T. A. *Chem. Eng. Prog.* **1959**, *55*, 173.
(3) Markovac, V.; Heller, H. C. *Plating Surf. Fin.* **1981**, *68*, 66.
(4) Markovac, V.; Heller, H. C. *Plating Surf. Fin.* **1982**, *69*, 84.
(5) Sasuga, T.; Norishita, N.; Udagawa, A.; Kusama, Y.; Takehija, M. *J. Polym. Sci.* **1976**, *14*, 2575.

Part of the material in this paper was originally presented at the Electrochemical Society Meeting in Hollywood, Fla., Oct. 5–10, 1980, and appeared in the "Proceedings of the Symposium on Ion Exchange: Transport and Interfacial Properties"; 1981; Vols. 81 and 82, p. 367.

The Annual ACS LabGuide— the Definitive Source for

- Laboratory supply houses
- Sources for chemicals and instrumentation
- Meeting information
- Research and analytical services
- Trade names and new books

With the annual ACS LabGuide, the information is right where you need it—at your fingertips. It's most used because it's most useful! Use the coupon below to order your copy today.

Distribution Center, American Chemical Society
1155 Sixteenth Street, N.W., Washington, D.C. 20036

YES! Send me the annual ACS LabGuide. I am enclosing $6 for each copy ordered.

Quantity _____ Price _____ Total _____

California residents add 6% state use tax.

Name _____
Address _____
City _____
State _____ Zip _____



...the BEST in a HURRY

Burdick & Jackson local distributors will give you **fast delivery** on your HPLC solvents from **stock locations** in or near all these major cities:

East	Central	West
Boston	Detroit	Seattle
Philadelphia	Chicago	Portland
Atlanta	St. Louis	San Francisco
Pittsburgh	Denver	Los Angeles
	Houston	
	Minneapolis	

Call today for information: 616/726-3171

BURDICK & JACKSON LABORATORIES, INC.
1953 SOUTH HARVEY STREET • MUSKEGON, MICHIGAN 49442

CIRCLE 25 ON READER SERVICE CARD

Swagelok® "Keyed" Quick-Connects prevent accidental mixing of different fluids...



SWAGELOK "Keyed" Quick-Connects feature a positive mechanical lockout system which prevents coupling of unmatched stems and bodies. They are designed with eight separate keys, each one numbered and color-coded for your added convenience in making connections.

They are available from local distributors in brass and 316 stainless steel, with SWAGELOK or NPT end connections in 1/8", 1/4", 3/8" and 1/2" sizes. SWAGELOK ends are also available in 6mm, 10mm and 12mm sizes.

MATCHED "KEYS"— through flow

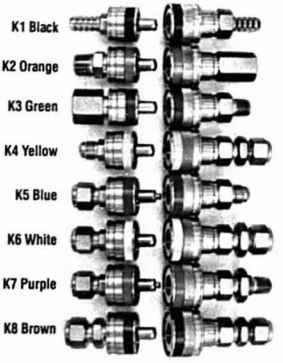


UNMATCHED "KEYS"— no flow



patented

Automatic shut off minimizes pressure or fluid loss during uncoupling. An attempt to connect unmatched "keys" **will not** open the shut-off valve and allow flow.



CRAWFORD FITTING COMPANY
29500 Solon Rd., Solon, OH 44139
Crawford Fittings (Canada), Ltd., Ontario

©1978, 1982 Markad Service Co., all rights reserved C-59

CIRCLE 32 ON READER SERVICE CARD

New Edition of a Classic Text

Fundamentals of Analytical Chemistry. 4th ed. Douglas Skoog, Donald West. xiv + 859 pp. W.B. Saunders Co., West Washington Square, Philadelphia, Pa. 19105. 1982. $29.95

Reviewed by Richard Yost, Department of Chemistry, University of Florida, Gainesville, Fla. 32611

This new edition of a classic will serve as an excellent text for an introductory analytical chemistry course for chemistry majors. The text complements two other Skoog and West texts: "Analytical Chemistry" (3rd ed., 1979), a simplified version of this text for nonchemistry majors, and "Principles of Instrumental Analysis" (2nd ed., 1980), for a second-term majors course.

The text is clearly written; its 31 chapters present a careful balance between theory and practice. An excellent discussion of stoichiometric and equilibrium calculations is now condensed into a single chapter. The authors have added new material throughout the text, detailing methods for problem solving. The reliance on fundamental concepts such as charge and mass balance and the clear handling of simplifying assumptions hopefully will influence other textbook authors. The chapter on data analysis includes new material on linear regression, as well as a section on significant figures, which is particularly welcome to those of us faced with calculator-wielding students who favor 10-digit answers. The electrochemistry chapters provide a comfortable transition from classical techniques to modern instrumental methods. These chapters have been trimmed to make room for more material on spectroscopy and chromatography. This includes discussion of ICP and molecular fluorescence, as well as a new chapter on HPLC. Following the coverage of spectroscopy are chapters on the analysis of "real" substances, preliminary steps of analysis, and sample preparation. These provide an unusually logical lead-in to the chapters on analytical separations. The book ends with chapters on laboratory techniques and experiments.

This edition contains a number of improvements. I applaud (as will those users of the third edition who suggested it) the abandonment of formal concentration and the introduction instead of the concept of molar analytical concentration. The often-confusing concepts of normality, equivalents, and titer are defined, but their use is minimized throughout the text. Similarly, activity coefficients are introduced in the discussion of solubility equilibria, and generally neglected thereafter. The new introductory chapters on electrochemistry, spectroscopy, and separations are a welcome addition. Finally, there are numerous worked-out examples throughout the text and a good selection of problems at the end of each chapter, half with numerical answers included.

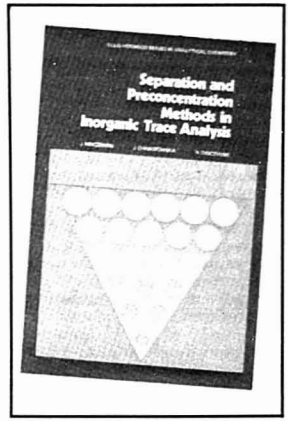
This reviewer finds only a few faults with the text. I dislike the term "neutralization titrations," which is used interchangeably with "acid–base titrations." I prefer use of the symbol e^- rather than e for the electron as an aid to students in balancing reactions. The new chapter on HPLC claims that most separations employ silica gel rather than the far more common bonded reversed-phase columns. I also dislike use of the term "sensitivity" to describe limits of detection (g/mL) for HPLC detectors. I was surprised to see UV and NMR spectrometers classed with MS and IR spectrometers as common GC detectors.

Overall, this is an excellent text, well suited for an introductory analytical chemistry course for majors. This edition covers this rapidly expanding field extremely well and contains significant improvements over previous editions.

Separation and Preconcentration Methods in Inorganic Trace Analysis. J. Minczewski, J. Chwastowska, R. Dybczynski, Eds. xi + 543 pp. John Wiley & Sons, Inc., 605 Third Ave., New York, N.Y. 10016. 1982. $85

Reviewed by Quintus Fernando, Department of Chemistry, University of Arizona, Tucson, Ariz. 85721

Analytical chemists involved in inorganic trace analysis will find this a useful and thoroughly documented reference work. In an excellent introductory chapter on working techniques, the authors deal effectively



with many of the experimental difficulties encountered in trace analysis. Many authors in this field have either ignored problems associated with sample handling and contamination or have been unaware of the importance of such mundane topics in the analysis of ppm or ppb levels. The bulk of the book is devoted to the theory and practice of liquid–liquid extraction and ion exchange chromatography. Reversed-phase chromatography, volatilization, precipitation, and coprecipitation are treated briefly. Although this book is not a comprehensive text that deals with all separation and preconcentration techniques in inorganic trace analysis, it is a valuable source of information for all chemists. The optimum conditions for numerous solvent extractions and ion exchange separations are listed in tabular form. These tables, together with the extensive and carefully compiled bibliography at the end of each chapter, are a lasting contribution to the literature in the field of trace analysis. Despite the absence of detailed experimental procedures, the information condensed in these tables will continue to be helpful in developing suitable separation schemes for specific inorganic determinations.

The translation of the text from Polish to English has resulted in awk-

ward phraseology in a few instances, but this does not detract from the book's scientific merit. This versatile reference work is a worthwhile addition to any library.

Electroanalytical Chemistry, Basic Principles and Applications. James Plambeck. xix + 404 pp. John Wiley & Sons, Inc., 605 Third Ave., New York, N.Y. 10016. 1982. $35

Reviewed by R. Mark Wightman, Department of Chemistry, Indiana University, Bloomington, Ind. 47405

This book is written as a textbook for advanced undergraduates or beginning graduate students. The author's goal is to provide a text that is also useful for those students who may have had only one year of general chemistry. The book is divided into three parts. The first concerns "basic information" and covers topics such as SI units, operational amplifiers, computer interfacing, measurement of electrical quantities, electrochemical cells, conductance, and interphases. The second part primarily concerns potentiometric measurements; the third part deals with coulometry, voltammetry, polarography, and amperometric titrations.

Because of the broad range of topics this book tries to encompass and because of its goal of serving a wide audience, many of the topics in the book are treated superficially, while others receive unnecessarily detailed treatment. For example, computers are discussed for nine pages, but four of these are devoted to details of the S100 bus, including pin connections. This discussion is in the first part of the book; unfortunately, none of the other sections point out the usefulness of computers in electrochemistry. It is distracting that many techniques are introduced only to be immediately characterized as archaic (e.g., electromechanical integrators and power supplies, metal–metal oxide electrodes and the quinhydrone electrode for the determination of pH, and high-frequency conductometric techniques).

The wide scope of topics covered means that chemical examples had to be kept to a minimum. However, the author cites the important and relevant works, so this book can be used as an introduction to the electrochemical literature. Useful discussions on SI units (which, unfortunately, are ignored by many electrochemists) and laboratory standards for electrical measurements are included. The concepts behind the rates of electrochemical reactions and the thermodynamics of electrochemical processes are both discussed; however, the two fundamental concepts are not tied together. Double-layer concepts are introduced at a level appropriate to this type of text; however, figures 5-3 and 5-4, models of the double layer, contain errors. The principles behind the functioning of ion-selective electrodes are presented in a somewhat elementary fashion; however, practical aspects of their use are described well.

The section on "nonequilibrium electroanalytical techniques" is not particularly well organized. Chronoamperometry, the simplest electrochemical technique with respect to understanding diffusion processes, is introduced after polarography and rapid-sweep techniques. The nomenclature used in this section of the book is somewhat unusual. What is commonly known as linear-sweep voltammetry is referred to as "chronoamperometry with linear sweep," and double potential step chronoamperometry is referred to as cyclic chronoamperometry. Although alternate names for these techniques are given, the ones that the author has suggested are certainly not the most common and will probably confuse beginning students.

I would not recommend this book for a graduate course in electroanalytical chemistry, unless the majority of students had never had freshman physics or undergraduate analytical chemistry. The author seems to have addressed this book to this rather unusual audience. Even for this audience, problems may occur with the use of this text because of its unique use of electrochemical nomenclature.

Principles of Infrared Quantitative Analysis. Program IR-101. 41 min. Savant, Sloane Audio Visuals for Analysis and Training, P.O. Box 3670, Fullerton, Calif. 92634. 1982. $220, slide/tape; $490, video.

Reviewed by Jack Koenig, Department of Macromolecular Science and Physical Chemistry, Case Western Reserve University, Cleveland, Ohio 44106

This audiovisual course is an excellent general introduction to quantitative IR analysis. The quality of the narration and slides is very high. The approach is limited to dispersive instruments with computers; FTIR is not mentioned. The facile interchange between transmission and absorbance spectra would lead one to believe that they are the simple inversions of each other and the significance of the baseline correction is lost. The method used to correct for the baselines is oversimplified. Recommendations for digital smoothing of data should be ignored. A straightforward approach to multicomponent analysis is well presented, but no caution about the problems of interaction of the components is given. Overall, for an elementary course, I thought it was well done and very informative. I recommend its use as an educational tool in this important area.

Books Received

Wilson & Wilson's Comprehensive Analytical Chemistry. Vol. 15 and Vol. 16. G. Svehla, Ed. 585 and 513 pp., respectively. Elsevier Science Publishing Co., Inc., 52 Vanderbilt Ave., New York, N.Y. 10017. 1982. $127.75 and $151, respectively

Evaluation of Analytical Methods in Biological Systems. Part A. Glen Baker, Ronald Coutts, Eds. xvi + 308 pp. Elsevier Science Publishing Co., Inc., 52 Vanderbilt Ave., New York, N.Y. 10017. 1982. $76.75

Methods for Analysis and Testing. Vol. 2. 41st annual ed. Pt. 1. xxviii + 313 pp. John Wiley & Sons, 605 Third Ave., New York, N.Y. 10016. 1982. $145

Introduction to Safety in the Chemical Laboratory. N. T. Freeman, J. Whitehead. ix + 244 pp. Academic Press, 111 Fifth Ave., New York, N.Y. 10003. 1982. $29

Correlation Analysis of Organic Reactivity. John Shorter. xi + 235 pp. John Wiley & Sons, 605 Third Ave., New York, N.Y. 10016. 1982. $41.95

Stereochemical Applications of NMR Studies in Rigid Bicyclic Systems. Alan Marchand. 231 pp. Verlag Chemie International Inc., 1020 N.W. 6th St., Deerfield Beach, Fla. 33441. 1982. $92.50

Developments in Atomic Plasma Spectrochemical Analysis. Ramon Barnes, Ed. xvii + 751 pp. John Wiley & Sons, 605 Third Ave., New York, N.Y. 10016. 1982. $21.95

Industrial Chemical Exposure: Guidelines for Biological Monitoring. Robert Lauwerys. 150 pp. Biomedical Publications, P.O. Box 495, Davis, Calif. 95616. 1983. $16.50

Electrophoresis. Z. Deyl, Ed. xiv + 462 pp. Elsevier Science Publishing Co., Inc., 52 Vanderbilt Ave., New York, N.Y. 10017. 1982. $104.75

Just published! *Just published!*

New techniques that can save you valuable time and money!

Essential state-of-the-art information for all scientists who use analytical techniques in their work!

INSTRUMENTATION IN ANALYTICAL CHEMISTRY, VOL. 2

Stuart A. Borman, *Editor*

An anthology of articles on developments in analytical techniques in the past ten years—from the volumes of *Analytical Chemistry*.

CONTENTS Signal Processing and Image Analysis • Computers and Laboratory Data Management • Atomic and Molecular Spectroscopy • Electroanalytical Chemistry • Gas and Liquid Chromatography • Hyphenated Methods • Mass Spectrometry • Surface Analysis • Nuclear Magnetic Resonance • Flow Methods • Laboratory Instrumentation
414 pages (1982) Clothbound
US & Canada **$31.95** Export **$38.95**
Special Student Paperbound Edition Available—Minimum Order 10 Copies
US & Canada **$14.95** Export **$17.95**

Multi-nuclei NMR, highest field NMR, NMR in solids, and more. . .

NMR SPECTROSCOPY: NEW METHODS AND APPLICATIONS

George C. Levy, Editor

Current work in new areas of NMR spectroscopy is treated in the comprehensive volume

CONTENTS Ultra High-Field NMR • NMR Spectroscopy at 600 MHz • Two-Dimensional Fourier Spectroscopy • Quadrupolar Metallic Nuclei • Deuterium NMR Spectroscopy • Metabolism of ^{13}C Labeled Substrates • Chemical Bond Labeling and Double-Cross Polarization NMR • NMR Spectroscopy at High Pressure • ^{13}C Cross Polarization Magic Angle Spinning NMR • NMR of Linear and Cyclic Peptides • ^{31}P NMR Studies • ^{13}C NMR Studies of DNA Dynamics • Photo-Chemically Induced Nuclear Polarization of Biological Molecules • ^{13}C NMR Characterization of Solid Fossil Fuels • Polyester Thermoplastic Elastomers • ^{23}Na NMR Studies
388 pages (1982) Clothbound
US & Canada **$49.95** Export **$59.95**

Up-to-date research results in this emerging interdisciplinary area of chemistry. . .

CHEMICALLY MODIFIED SURFACES IN CATALYSIS AND ELECTROCATALYSIS

Joel S. Miller, *Editor*

This book focuses on modification of materials for catalytic purposes and modification of organic and inorganic electrode materials for electrocatalytic and photoelectrochemical application.

CONTENTS Chemically Modified Surfaces in Catalysis • Poly(styrene-divinylbenzene)-Supported Catalysts • Homogeneous Rhodium (I) Catalyzed Alkene Hydrogenations • Reactive Organic Functional Groups • Polypyrrole Film Electrodes • Second Order EC Catalytic Mechanism • Semiconductor Photoelectrodes • Solution Reactivity Properties • Metallopolymer Films on Electrode Surfaces • Chemical Modification of TiO_2 Surfaces • Electrochemistry of Silane-Derivatized Iridium • Improvements in Photoelectrochemical and Electrochromic Reactions • Derivatized Layered M(IV) Phosphonates • Intercalation of Molecular Catalysts in Layered Silicates • Fischer-Tropsch Synthesis • Reactivity of Catalysts Derived from Organometallics • Silacrowns
301 pages (1982) Clothbound
US & Canada **$36.95** Export **$44.95**

An invaluable resource for all who use MS in their work.

MASS SPECTRAL CORRELATIONS, SECOND EDITION

F.W. McLafferty and R. Venkataraghavan, *Editors*

This volume is an invaluable resource for interpreting the copious spectral data generated in GC and MS investigations. Comprehensive tables show the most probable assignments for peaks in electron mass spectra of organic compounds. More than 3000 structures corresponding to 1500 elemental compounds are listed—several times the number in the first edition. Newcomers to the field will find this book indispensable. Seasoned professionals will find it a valuable timesaver in interpreting the spectrum of an unfamiliar compound when information on the history of the sample is lacking.
124 pages (1982) Clothbound
US & Canada **$24.95** Export **$29.95**

Mail to **Distribution Office Dept. 15, American Chemical Society, 1155 Sixteenth Street, N.W., Washington, D.C. 20036**
Please send me the books checked below:

	Quantity	Price	Total
Instrumentation in Analytical Chemistry, Vol. 2			
NMR Spectroscopy: New Methods and Applications			
Chemically Modified Surfaces in Catalysis and Electrocatalysis			
Mass Spectral Correlations, Second Edition			

California customers add 6% state use tax: _____
TOTAL: _____

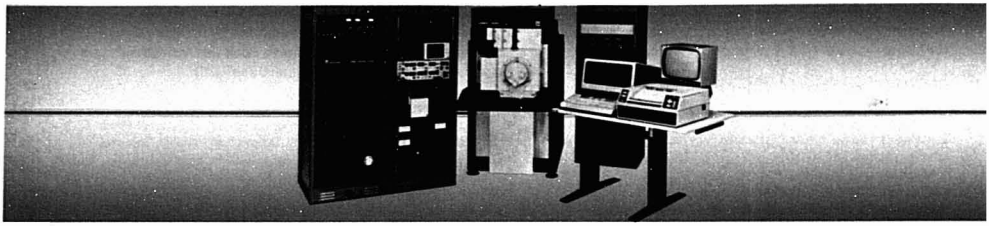
☐ **Payment enclosed.**
☐ **Purchase order enclosed.**
Charge my ☐ **MasterCard** ☐ **Visa.** Account No. _____
Expires _____ Interbank No. _____ (MasterCard only)
Signature _____
Ship to Name _____
Address _____
City, State, Zip _____

15

ORDERS MUST BE PREPAID. PLEASE ALLOW 4-6 WEEKS FOR DELIVERY. PRICES SUBJECT TO CHANGE WITHOUT NOTICE.

To charge books by phone, call (800) 424-6747.

Mass spec à la laser.



The Leybold-Heraeus LAMMA 1000 mass spectrometer for solids significantly advances your analytical and research technology.

The new perspective.

LAMMA 1000 is a consequent no-compromise development of the successful and well proven LAMMA 500.

The LAMMA 1000 opens the vast field of bulk solid samples to Laser Microprobe Mass Analyzer by operating in the incident laser irradiation mode.

Samples as large as 130 mm in diameter of almost any shape may be introduced and subjected to micro area analysis with a lateral resolution as small as 5 μm. A single laser pulse typically generates a crater of some fractions of a μm in depth. Several shots at the same spot result in a rough depth profile (Layer by Layer Analysis).

After loading, the sample is observed in situ through a powerful Light Microscope. Both the observation and ion extraction optics are arranged perpendicular to the sample ensuring good image quality and high detection sensitivity.

The proven principle.

LAMMA 1000 uses a frequency quadrupled Nd:YAG laser with an improved wide energy acceptance high resolution time-of-flight (TOF) mass spectrometer and a special optical system.

The high power pulsed laser beam is focused onto the sample down to a diameter of about 3 μm by a large working distance objective. By the interaction of UV laser light ($\lambda = 265$ nm) and matter, positive and negative ions are generated which are mass analyzed by the TOF mass spectrometer. A key feature is the continuously variable laser intensity which permits control of the total ion intensity and molecular fragmentation over a wide range.

LAMMA 1000 utilizes a transient recorder to output signals to either a strip chart recorder or a data system.

Although these operating principles are simplified, and understated, it's obvious LAMMA 1000 has created a new dimension in analyses capabilities.

Analyses results confirm that fact.

• Lateral resolution	<5 micron
• Depth of analysis	~0,1 micron
• Detection limit	$<10^{-17}$g
• Detectable concentration	ppm-range
• Mass resolution (lead isotopes)	m/Δm >500
• Speed of analysis	<1 s
• Sample changing time	<10 Min.

LAMMA 1000 performance characteristics are uncharacteristic.

Rapid, robust and reliable.

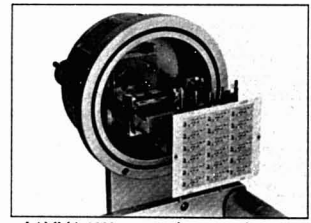
LAMMA 1000 requires virtually no sample preparation at all.

Samples of almost any shape may be accommodated either singly or in batches. Sample introduction typically takes about 10 minutes including pump down.

LAMMA 1000 makes extensive use of reliable and well proven units of the successful LAMMA 500:

- proven TOF
- proven Laser
- proven Electronics
- proven Optics

The special ion extraction optics and the improved wide energy acceptance TOF make LAMMA 1000 one of the most sensitive detection systems available today.



LAMMA 1000 manipulator/sample stage

If you think LAMMA 1000 is for you, we think you should contact us immediately to learn more about it. Please call or write for information, free demonstration or to arrange for analytical services in our Applications Laboratory.

LEYBOLD-HERAEUS

LAS GROUP
LEYBOLD-HERAEUS
VACUUM PRODUCTS INC.
5700 Mellon Road Export PA 15632
412 327 2022 TWX 510 468 5418

Worldwide except the United States and Canada
LEYBOLD-HERAEUS GMBH · WVA Group
Postfach 510760, D-5000 Köln 51
Telefon (221) 3701790, Telex 841·888·48120

CIRCLE 126 ON READER SERVICE CARD

John M. Hayes
Gerald J. Small
Ames Laboratory–USDOE and
Department of Chemistry
Iowa State University
Ames, Iowa 50011

Instrumentation

Supersonic Jets, Rotational Cooling, and Analytical Chemistry

Supersonic beams produce a vapor stream in which thermal broadening is dramatically reduced

Given a complex sample, such as shale oil or a biological specimen, which with slight exaggeration can be viewed as containing infinitesimal amounts of an infinite number of species, is it too much to ask for a *direct* quantitative analysis that affords selectivity and sensitivity? We think not and hope that this article will allow the reader to share our optimism.

To date the most widely used direct analysis technique for such samples has been capillary column/gas chromatography/mass spectroscopy (CC/GC/MS). Its success, of course, is due to the marriage of GC and MS, which serve, respectively, as fractionator and selective detector. A major problem, however, is that "dirty" samples cause rapid degradation of the capillary column. Thus, an extraction or prefractionation step frequently is used to clean up the sample prior to analysis. In addition, for isomeric species, CC/GC/MS must achieve chromatographic resolution to effect an analysis. Clearly, it is highly desirable to explore the utility of detectors that afford greater selectivity.

In principle, electronic absorption or emission spectroscopy is the basis for one such detector. This is because electronic–vibrational (vibronic) transition energies and relative intensities are extremely sensitive to subtle changes in molecular structure. For example, moving a methyl substituent from one skeletal position on a polycyclic aromatic hydrocarbon (PAH) to other symmetry-inequivalent positions produces vibronic energy shifts on the order of tens of cm^{-1}. Other substituents produce even larger shifts; the amino group, for example, affords shifts of hundreds of cm^{-1}. To be successful, however, optical spectroscopic methods must overcome severe degradation of spectral resolution caused, for example, by thermal broadening, collisions, and spectral congestion. Degradation in emission generally parallels that in absorption. In recent years several low-temperature solid-state laser-induced fluorescence techniques have been demonstrated to have the sensitivity and selectivity to be useful for direct analysis of PAHs in real complex mixtures (*1*, *2*). The use of low temperatures, 4–20 K, eliminates spectral congestion in absorption due to hot band transitions and minimizes thermal broadening of individual vibronic transitions.

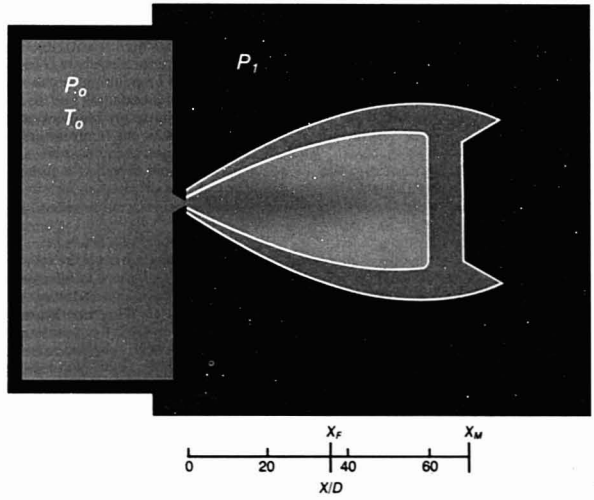


Figure 1. Diagrammatic representation of a supersonic expansion from a reservoir at initial temperature T_o and pressure P_o into a low-pressure region, P_1
Green region indicates shock wave around the jet. The location of the onset of free flow, X_F, and of the Mach disc X_M is indicated

0003-2700/83/0351-565A$01.50/0
© 1983 American Chemical Society

In addition, narrow band excitation with a laser can essentially eliminate site-inhomogeneous line broadening in fluorescence (the so-called fluorescence line-narrowing phenomenon).

Although such techniques are exceptionally sensitive and selective, they are limited to molecules with fluorescence quantum yields $\gtrsim 10^{-3}$ and by solid-state broadening effects that no amount of sorcery can eliminate. Unlike GC/MS they do not have an analogous prefractionation step. In one sense this is an advantage. However, for very complex mixtures in which, for example, complexation causes fluorescence quenching or broadening, sample cleanup is required. To couple an integral gas chromatographic step with selective detection of absorption or fluorescence would require that thermal broadening be eliminated in the vapor phase. For large molecules with boiling points > 100 °C, maintaining the sample as vapor and minimizing thermal broadening seem to be mutually exclusive. However, in the past few years, it has been demonstrated that supersonic molecular beams can be used to produce a vapor stream in which thermal broadening is dramatically reduced compared to that in static gas samples. Spectroscopic applications of this technique have grown rapidly. Reports of analytical applications have only recently appeared (*3–6*), although we are confident that they also will grow as the power of the technique becomes more widely known. In this paper we will attempt to explain the physics of cooling in supersonic expansions and to demonstrate the analytical potential of the technique by describing our work on analytical applications of supersonic expansions.

Broadening in Vapor-Phase Spectroscopy

Before proceeding to an explanation of the cooling observed in supersonic expansions, a brief summary of the extent and causes of broadening in the vapor phase will indicate under what conditions a supersonic expansion will eliminate broadening. Causes of broadening have been divided into two categories: intrinsic and trivial (i.e., extrinsic) (*7*). The distinction between the two is that given appropriate experimental conditions, trivial broadening can be eliminated, while intrinsic broadening cannot.

Thus, a supersonic expansion will not be useful in studying species whose absorption spectra are intrinsically broad. Fortunately, the examples of significant intrinsic broadening for the lowest excited singlet state of molecules are rare. For purposes of this discussion, the only important intrinsic broadening mechanism is intramolecular vibrational energy redistribution (IVER). This is the broadening that occurs when a molecule is excited to an energy above the zero-point vibrational level of the first excited state, at which the density of vibrational levels is high. Although only a single vibronic band may be optically active in this energy region, coupling between the vibrations results in the energy being redistributed among many vibrations. Spectroscopically, this manifests itself as band broadening. Since IVER only occurs at energies well above the zero-point level of the lowest excited state it usually will not prevent the observation of narrow absorptions, but will only limit the energy range over which such observations may be made. Thus, IVER will be a problem only for those molecules in which large geometry changes cause the low energy transitions to be Franck–Condon forbidden.

Trivial broadening is perhaps an unfortunate term: In principle, trivial broadening can be eliminated; in practice, this often has not been a trivial matter, requiring wizardry of the first order for solution. This is especially true if one requires high sensitivity, i.e., a high density for absorbers. The two major trivial broadening mechanisms, rotational broadening and vibrational broadening, are temperature dependent. Thus, as the temperature of a sample is raised to increase its vapor pressure, and thereby the number density of vapor-phase molecules, rotational and vibrational broadening blossom.

Rotational broadening arises because large molecules have large moments of inertia and hence minuscule energy spacings between rotational levels. Thus, at ambient temperatures many rotational levels are populated, and these levels usually cannot be resolved. Consequently, each vibronic absorption band exhibits a rotational contour rather than discrete rotational structure, and as the temperature is increased the width of the contour increases. By itself, however, rotational broadening would lead to bandwidths on the order of tens of cm^{-1}, sufficiently sharp that selective absorption could be accomplished in many cases.

The major cause of diffuseness in vapor absorption spectra is vibrational sequence congestion. This is a manifestation of the fact that at the temperatures required to obtain an appreciable vapor pressure, there is significant population of several low-lying vibrational levels of the ground state. For every principal or "cold" absorption band of the molecule, there will be associated bands for transitions from populated vibrational levels that terminate at corresponding levels in the excited state. The energies of these hot band transitions will differ from those of the principal transition by the difference in ground- and excited-state vibrational frequencies. These frequency differences are on the order of the rotational bandwidths, so that severe spectral congestion occurs.

The combination of rotational and vibrational broadening in favorable cases produces an absorption spectrum consisting of an unresolved broad background on which the fundamental absorption bands and the strongest sequence bands are superimposed. When such a spectrum can be obtained, it is only within a very restricted range of experimental conditions. In most cases, the spectra are far worse, exhibiting only broad diffuse features. For aromatic hydrocarbons, based on the known vibrational frequencies and computed densities of vibrational states, it has been predicted that with attainable experimental conditions, vibrational structure would be resolvable only in molecules with three or fewer rings (*7*).

Cooling in Supersonic Expansions

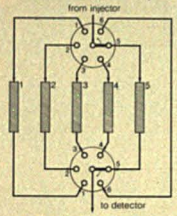
Let us see how the thermal broadening effects that make high-resolution spectroscopy of vapors of large molecules so difficult are essentially eliminated in a supersonic expansion. To understand the cooling that occurs in a supersonic molecular beam, and also to clarify the sometimes confusing nomenclature that is used, let us consider a molecular beam source (Figure 1). The source consists of a reservoir containing a gas at high pressure, P_o, and temperature, T_o, an orifice in the reservoir, and a low-pressure region downstream of the orifice. If the orifice diameter, D, is much smaller than the mean free path, λ_o, of the gas in the reservoir, then the flow from the reservoir into the low-pressure region is effusive. Alternatively, the orifice diameter may be much larger than λ_o, in which case the orifice acts as a supersonic nozzle or jet.

In the effusive case, because the orifice dimensions are less than the mean free path of the gas molecules, molecules pass from the reservoir into the low-pressure region without colliding with other gas molecules. The absence of collisions in and downstream of the orifice means that the velocity distribution of molecules in the low-pressure region will be a Maxwellian distribution characteristic of the reservoir temperature, T_o. In addition, the population of internal (rotational, vibrational) energy states will also be the same as in the reservoir.

In the case of supersonic flow, where $D \gg \lambda_o$, there will be many collisions in and downstream of the orifice. In particular, those collisions that

Plumber's helper. Switches LC columns without wrenches.

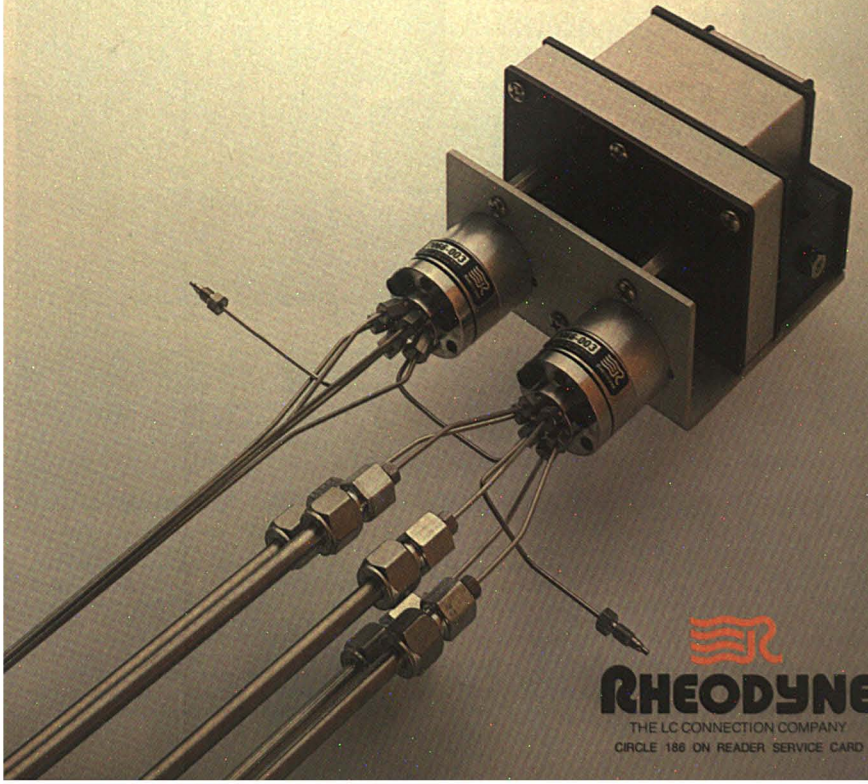
Rheodyne's newest valves make it unnecessary to disconnect the plumbing when you want to substitute one LC column for another. You need only turn a pair of tandem valves to select any column from as many as five.



Switching columns frequently is becoming a generally-accepted practice for several reasons. Often, you must switch to a different column to make a different analysis. But, even when switching columns is not essential, dedicating a separate column to each analysis eliminates column equilibration delays, reduces interferences, and prolongs column life.

Rheodyne's Model 7066 Tandem Column Selector connects any of up to five columns (or a bypass line) between the sample injector and the detector. Off-line columns are sealed at both ends, and no column need ever be exposed to a solvent intended for another.

Our Technical Notes 4 tells all about column selection with Model 7066 and other valves. To receive a copy, along with product literature, contact Rheodyne, Inc., P.O. Box 966. Cotati, California 94928, U.S.A. Phone (707) 664-9050.



RHEODYNE

THE LC CONNECTION COMPANY

CIRCLE 186 ON READER SERVICE CARD

Our evolutionary 3510 ICP is so fast and reliable, we could ask another $33,000.

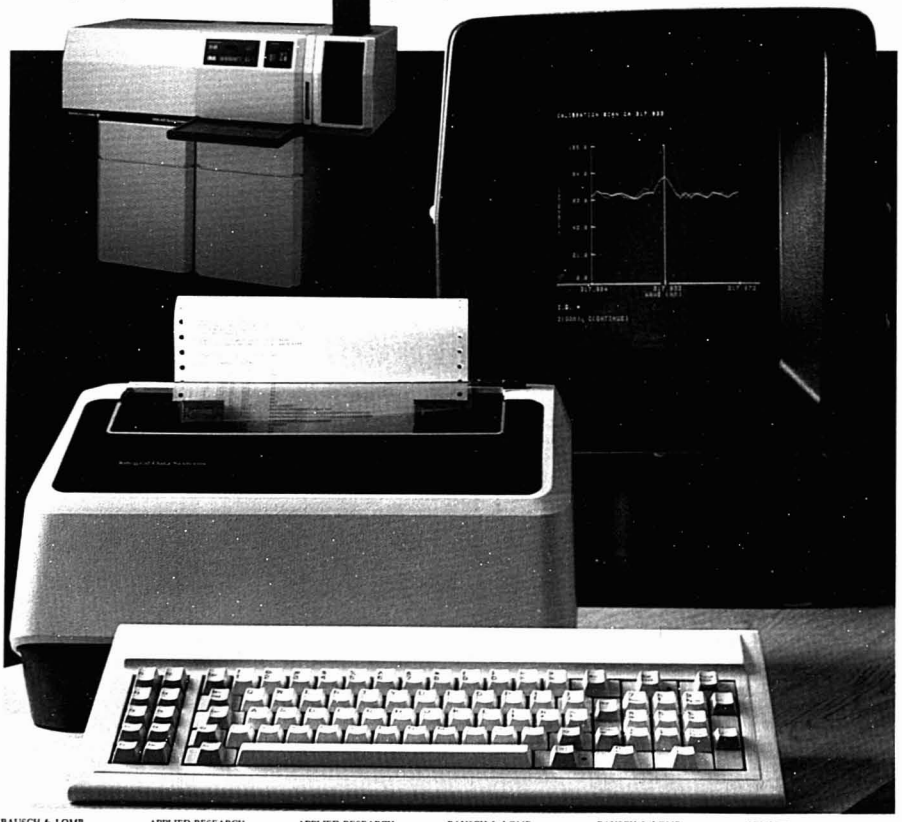
But we won't. Because Bausch & Lomb, whose 35000 ICP revolutionized sequential ICP spectrometry, has evolved an even more affordable instrument: the Model 3510 sequential ICP.

Its features quite simply outrank comparably priced systems:

Better, faster performance . . . means less total time per analysis, with new color graphics that speed and improve data accuracy and interpretation . . . high dispersion that minimizes and eliminates spectral interferences . . . and improved detection limits. *Increased reliability* . . . with more stable RF circuitry, laser pre-aligned optics and modular IC electronics throughout. *Greater operator convenience* . . . with optimum placement of controls.

All this, and more, for thousands of dollars less than you'd expect.

All you need to know is that the 3510 ICP's speed and reliability are ready for you now backed by Bausch & Lomb's world-wide service network. Call 800-828-6967 (in N.Y.S., call 716-338-8423), or write Bausch & Lomb, Instruments & Systems Division, P.O. Box 3807, Rochester, New York 14610.



BAUSCH & LOMB (AUSTRALIA) PTY. LTD.
North Ryde, N.S.W., Australia

APPLIED RESEARCH LABORATORIES
Wien, Austria

BAUSCH & LOMB BELGIUM NV
Gistel, Belgium

APPLIED RESEARCH LABORATORIES DIVISION of BAUSCH & LOMB CANADA, LTD.
Mississauga, Ontario, Canada

BAUSCH & LOMB S.A.
Le Mesnil Saint-Denis, France

APPLIED RESEARCH LABORATORIES GmbH
Duesseldorf, West Germany

BAUSCH & LOMB (HONG KONG) LTD.
Hong Kong

BAUSCH & LOMB (JAPAN) CO., LTD.
Tokyo, Japan

BAUSCH & LOMB INCORPORATED
Bosques de Echegaray, Est.
Mexico

APPLIED RESEARCH LABORATORIES B.V.
Heemstede, Holland

ARLABS (PTY.) LTD.
Rhodesfield, South Africa

BAUSCH & LOMB SINGAPORE (PTE) LTD.
Singapore

BAUSCH & LOMB INT'L, INC.
Madrid, Spain

ARL NORDISKA AKTIEBOLAG
Solna, Sweden

ARL S.A.
Ecublens, Switzerland

ARL LTD.
Luton, Bedfordshire, United Kingdom

BAUSCH & LOMB INCORPORATED
Instruments and Systems Division, Rochester, New York, United States

BAUSCH & LOMB

All you need to know

2H002

CIRCLE 24 ON READER SERVICE CARD

impart a large velocity component in the axial direction will be most effective in driving molecules from the reservoir. Thus there is a conversion of random molecular motion into directed mass flow along the beam axis.

This directed mass flow has three consequences: First, the peak of the velocity distribution of molecules along the axis is shifted to higher velocities and the distribution is narrowed. The narrowing of the distribution means that the characteristic temperature for the distribution has decreased. The increase in flow velocity, u, together with the decrease in the local speed of sound, a, as the gas expansion proceeds, means that the Mach number, $M = u/a$, increases. In an ideal nozzle, $M = 1$ at the most constricted point within the nozzle, and $M > 1$ downstream, hence the terms supersonic jet, supersonic nozzle, and supersonic expansion. A second consequence of the directed mass flow is that the density of molecules along the axis is much higher than for an effusive source. This increase in beam intensity was a primary motivation for the development of nozzle beam sources.

A third characteristic of supersonic expansions, and perhaps the most important for spectroscopic applications, is that the initial part of the expansion is isentropic, i.e., there is equilibration between the translational and the internal degrees of freedom. Thus in the isentropic core of the jet, the temperature characterizing rotational and vibrational energy distributions will decrease. As the collision frequency decreases, the vibrational temperatures and then the rotational temperatures begin to lag behind the translational temperature and at some point freeze. Eventually, the collision frequency becomes negligible and the beam enters the free molecular flow regime. In Figure 1, the point X_F marks the start of the free flow regime for typical expansion conditions. Beyond this point the beam constitutes an ideal spectroscopic medium: isolated molecules, rotationally and vibrationally cold, free of any matrix or collisional perturbations. Furthermore, the beam is protected from interactions with hot background molecules in the chamber by a shock wave that forms around the expansion. The shape of the shock wave is shown in the diagram. The leading edge of the shock wave is called the Mach disc and is at the point X_M in the figure.

The final temperatures attained in the expansion depend upon the properties of the gas being expanded. The lowest translational temperatures are obtained for monatomic gases that lack internal degrees of freedom. A monatomic gas can be seeded with a polyatomic species and, in the isentropic region, the polyatomic will also be in equilibrium with the monatomic. The final translational temperature obtained in a seeded expansion differs only slightly from that obtained in an expansion of the pure monatomic. The rotational temperature of the large molecule will then be on the order of 1–10 K. These remarkably low temperatures for vapor-phase species have resulted in the technique being called rotationally cooled spectroscopy. Vibrational cooling is by no means as extensive, being on the order of 30–100 K. However, with the larger energy spacings of vibrational levels, the excited vibrational states are almost completely depopulated. Even when some population remains in the lowest vibrational level, the narrowing of the rotational contour results in the hot band absorption being a well-resolved, weak spectral feature. Thus, vibrational sequence congestion, the most troublesome thermal-broadening mechanism, is virtually eliminated in a supersonic expansion.

A common misconception regarding supersonic expansions is that supersonic cooling is still difficult in practice, requiring very expensive and large vacuum systems. Although large systems with several stages of differential pumping are required with effusive sources and have been used with supersonic sources, they are not necessary for the latter. For a free jet expansion—a supersonic jet in which there are no downstream beam collimators—a chamber with a cross-sectional dimension of a few inches, pumped by a single high-throughput diffusion pump, is adequate. Indeed, supersonic cooling can be achieved using a mechanical pump with high pumping speed.

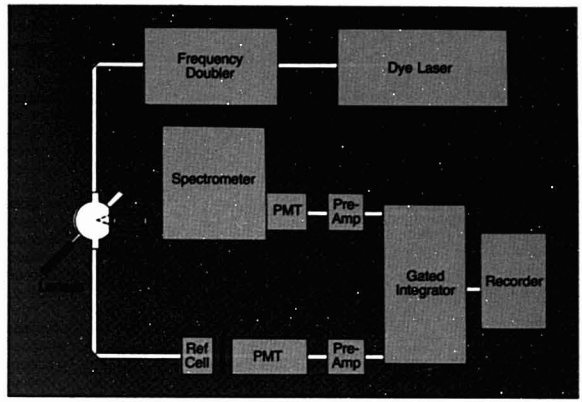


Figure 2. Block diagram of instrumentation used to obtain laser-induced photoexcitation and fluorescence spectra from a seeded supersonic beam

Spectroscopy of Supersonic Expansions

Having prepared a seeded supersonic beam, what can be done with it, and what are the analytical applications? Although the density of molecules of interest in the beam is much higher than in an effusive beam, the beam dimensions are small, so the spectroscopic interaction region will be small. For a beam seeded with a typical aromatic hydrocarbon ($\epsilon \sim 500$), under typical expansion conditions, the number density of absorbers in the beam will be $\sim 5 \times 10^{11}$ molecules cm^{-3}. Accounting for the angular divergence of the beam, at a distance from the nozzle of 1.0 cm, the optical pathlength will be ~0.5 cm. Under these conditions an absorbance $< 10^{-4}$ would be obtained. Thus, in general, direct absorption measurements on seeded beams are not feasible, although absorption measurements are possible on pure beams (*8*) or with slit nozzles (*6*).

By far the most common type of spectroscopy performed on seeded supersonic beams is laser-excited fluorescence. A block diagram of the equipment used to generate such spectra is shown in Figure 2. A frequency-doubled, Nd:YAG laser-pumped dye laser is used as a source of tunable ultraviolet radiation. This beam is focused onto the molecular beam axis through a quartz window and a set of light baffles, which minimize stray light reaching the detector. The laser beam crosses the molecular beam 2–10 mm downstream of the nozzle orifice. Fluorescence from the beam is

detected at right angles to both the molecular and the laser beams. The fluorescence is dispersed with a high-throughput medium-resolution monochromator and detected by a phototube. The phototube output is amplified, measured by a gated integrator, and divided by a reference signal proportional to the laser intensity to produce a normalized output. Using this arrangement, either photoexcitation spectra or fluorescence spectra can be obtained.

An example of a photoexcitation spectrum is shown in Figure 3. In this mode of operation, the dye laser wavelength is scanned while the detection monochromator is fixed at a wavelength at which the molecules of interest fluoresce. In the example shown, the sample is a mixture of naphthalene, α-methylnaphthalene, and β-methylnaphthalene. From left to right in the figure, the labeled bands are the S_1 origin of β-methylnaphthalene, the S_1 origin of α-methylnaphthalene, the S_1 origin of naphthalene, a 422-cm^{-1} vibration of α-methylnaphthalene, and a 438-cm^{-1} vibration of naphthalene. If the fluorescence quantum yield of each of the vibronic levels were equal, the photoexcitation spectrum would be equivalent to an absorption spectrum. In general this will not be the case. Nevertheless, the peak positions are invariant, and the photoexcitation spectrum serves as a fingerprint of the molecule in the expansion. It is clear from the figure that even with the moderate resolution (bandwidths are laser-limited, ~2 cm^{-1}) of this spectrum, the bands are well resolved and allow for easy identification of the three components of the sample. Thus, a qualitative analysis of a complex mixture can be obtained easily from the photoexcitation spectrum.

Bear in mind that in obtaining such a spectrum, photoexcitation peaks will be observed only for those molecules that emit in a spectral region within the bandpass of the detection monochromator. In the spectrum shown, the detection wavelength and bandpass were chosen so that all three molecules could be detected. If the bandpass were narrowed and a detection wavelength specific to one of the three molecules chosen, the photoexcitation spectrum of that single species would be obtained. When peaks due to each of the components of a mixture are resolvable there is no advantage to be gained by this procedure. However, if a component of the mixture absorbed in the same spectral region as other molecules of interest, but was intrinsically broadened (due to absorption into very high vibrational levels or into a higher excited state), then by a judicious choice of detection wavelength, the broad peaks could be eliminated from the spectrum.

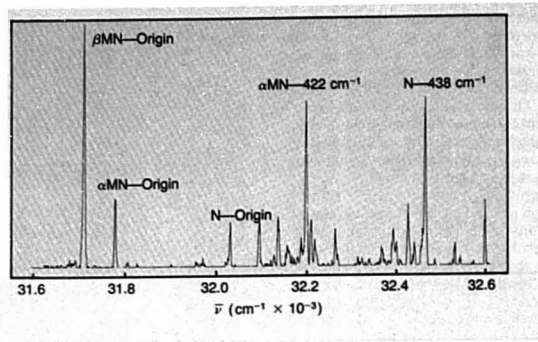


Figure 3. Laser-induced photoexcitation spectrum of a mixture of naphthalene (N), α-methylnaphthalene (αMN), and β-methylnaphthalene (βMN) seeded in a supersonic expansion of He

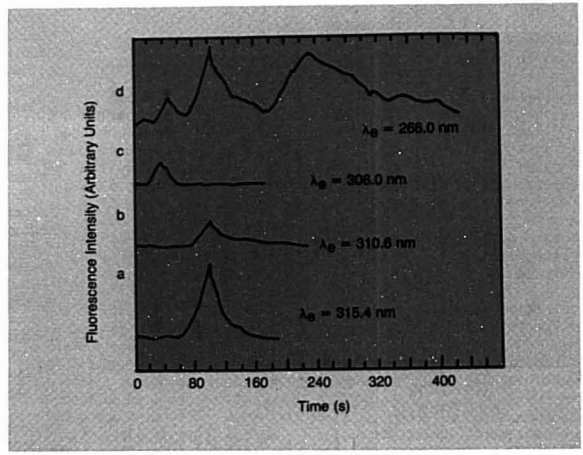


Figure 4. Analysis of a crude oil sample for naphthalene and methylnaphthalenes by rotationally cooled fluorescence

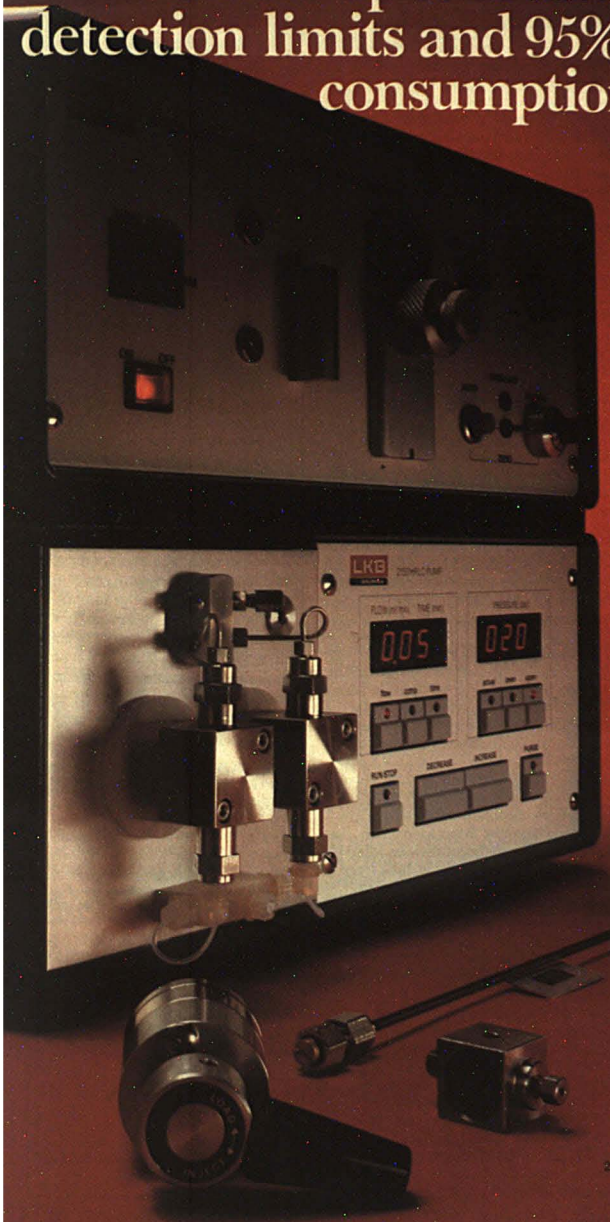
The traces a–c show chromatograms using selective excitation wavelengths for β-methylnaphthalene, α-methylnaphthalene, and naphthalene, respectively. Trace d shows a chromatogram using a nonselective excitation wavelength

The same apparatus used for obtaining photoexcitation spectra can be used for obtaining fluorescence spectra. In this case, the laser wavelength would be chosen to coincide with one of the bands in the photoexcitation spectrum and the monochromator would be scanned. In analytical applications, the fluorescence spectrum would be of use in determining the species responsible for the observed bands. For example, if one has obtained the photoexcitation spectrum of a supposedly pure substance, then the fluorescence spectrum from each band in photoexcitation should be analyzable in terms of the vibrations of that molecule. Bands that are not readily analyzable probably indicate impurities.

For many nonfluorescent species, spectra with the same resolution can be obtained via multiphoton ionization. This technique requires a more intense laser source to achieve ionization, but since in principle every ion is detectable whereas every photon is not, it can be as sensitive as fluores-

LKB's new Microbore HPLC System:

Offers up to 14 times lower detection limits and 95% less solvent consumption



Although microbore HPLC has attracted a great deal of interest from scientists and HPLC column manufacturers throughout the world, comparatively little attention has been paid to the specification of hardware capable of fully exploring the benefits of the technique —until now!

LKB, the world's leading manufacturer of high quality instrumentation for the biochemical research laboratory, has used experience gained in this field to develop the first commercially available HPLC system correctly specified for microbore applications.

The heart of LKB's new microbore system is the unique 2150 HPLC Pump. This is the only HPLC pump which can offer smooth, pulse-free and highly reproducible flow in the flow-rate range recommended for microbore applications: 10—150 µl/min.

Also included in LKB's microbore system is the 2151 Variable Wavelength Monitor with its unique microflow cell (0.8 µl, 3 mm pathlength), a low-volume injector for minimal pre-column diffusion, and a choice of glass-lined 1 mm I.D. microbore columns.

For full facts on our new microbore HPLC system don't hesitate to contact your local LKB representative.

LKB—the microbore specialists

LKB
BROMMA

Head office:
LKB-Produkter AB,
Box 305, S-161 26 Bromma, Sweden.
Tel. 08-98 00 40, telex 10492

Main US sales office:
LKB instruments, Inc.
9319 Gaither Road, Gaithersburg, Maryland 20877
Tel. 301-963-3200, telex 909870 (dom.), 64634 (intern.)

UK sales office:
LKB Instruments Ltd.,
232 Addington Road, S. Croydon, Surrey CR2 8YD, England
Tel. 01-657 8822, telex 264414

Other sales offices in:
Athens (for Middle East), Copenhagen, Ghent, Zoetermeer, Hong Kong, Luzern, Munich, Paris, Rome, Turku, Vienna

CIRCLE 131 ON READER SERVICE CARD

Key Chemicals & Polymers
New 5th Edition

One-page reviews packed with data on the current economic status and short-term outlook for 46 large-volume chemical industry products.

The 46 products are:

Acetone
Acrylic
Ammonia
Benzene
Butadiene
Carbon black
Carbon dioxide
Caustic soda
Chlorine
Cyclohexane
DMT/PTA
Epoxies
Ethanol
Ethylene
Ethylene oxide
Formaldehyde
High-density polyethylene
Lime
Low-density polyethylene
Methanol
Methylene chloride
Nitrogen
Nylon
Oxygen
Phenol
Penolics
Phosphoric acid
Phosphorus
Polyester
Polyesters
Polypropylene
Polystyrene
Polyvinyl chloride
Potash
Propylene
SBR
Soda ash
Styrene
Sulfur
Sulfuric acid
Titanium dioxide
Toluene diisocyanate (TDI)
Urea
Vinyl acetate
Vinyl chloride
***p*-Xylene**

Chemical & Engineering News
Distribution Dept.
1155 — 16th St., N.W.
Washington, D.C. 20036

Please send _____ copies of Key Chemicals & Polymers (5th Edition) at $5.00 per copy ($4.00 per copy for orders of more than 10.) On orders of $20 or less please send payment with order. California residents add 6% sales tax.

☐ Payment enclosed ☐ Bill me
Charge my ☐ MasterCard ☐ VISA

Card # _____
Interbank # _____
(MasterCard only)
Exp. date _____
Signature _____

Name _____
Address _____
City _____
State _____ ZIP _____

Call Toll Free 800-424-6747

cence detection. If the ion detector is also a mass detector, then mass-selective detector would be analogous to wavelength-selective fluorescence detection.

Quantitative Jet Spectroscopy

As described in the previous section, the dramatic narrowing of vibronic bands in a supersonic expansion makes qualitative analysis quite straightforward. A quantitative analysis is more difficult. The intensities of bands in the photoexcitation spectrum are proportional to the partial vapor pressure in the reservoir of the molecule causing the band. Therefore, obtaining quantitative data from band intensities requires knowing the partial pressure of each species in the reservoir. If the sample to be analyzed is a complex multicomponent mixture, these data would not be available.

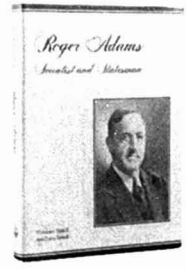
As an alternative to knowing all the partial pressures, one can set the reservoir temperature high enough that the analyte is totally vaporized and flows through the laser excitation region quickly. Then by fixing the excitation wavelength to an absorption of the species of interest and monitoring the fluorescence as a function of time, the area of a peak in the fluorescence vs. time graph will be proportional to the amount of absorbing material that passed through the excitation region. We have recently described how the reservoir of the supersonic nozzle can be converted to a simple GC to achieve quantitation in this manner (*4*).

In that work the reservoir was packed with GC packing material and heated to ~100 °C. A heated injection port was attached to the nozzle inlet. Solutions of analytes were then injected into the GC column. Figure 4 shows fluorescence vs. time graphs for a sample of dilute crude oil at several excitation wavelengths. The wavelengths of traces a–c correspond to strong absorption bands of β-methylnaphthalene, α-methylnaphthalene, and naphthalene. The peaks in each trace are due to the respective molecules, and the peak areas are proportional to the concentration of each species in the sample. The top trace, d, uses a nonselective wavelength and gives an indication of the complexity of the sample (only the low-melting compounds absorbing at 266 nm and emitting at 345 nm show up in this trace).

The limit of detection demonstrated in Reference 4 was $\sim 10^{-8}$ g. That work used a continuous-flow nozzle and a pulsed excitation laser. Thus, the duty factor was quite low, 10^{-7}. Use of a pulsed nozzle synchronized to the laser firing would result in an increase of duty factor and, hence, of limit of detection, by a factor of 10^3.

Roger Adams: Scientist and Statesman

by D. Stanley Tarbell and Ann Tracy Tarbell



Examines the life of Roger Adams — a man unparalleled in his contribution to the development of organic chemistry.

A comprehensive biographical sketch of Roger Adams, whose work was important in the development of American chemistry and chemical education. Adams's early years, education, and career achievements in academia, industry, research, and government are described. His contributions to Illinois chemistry in particular and the education of chemists are expounded.

CONTENTS

Introduction • Early Years and College • Germany and Harvard, 1912–16 • Illinois, 1916–26 • Academic Progress • Service and Research to 1942 • Government Service, 1940–48 • Illinois and Research, 1943–67 • Broader Horizons • Career Achievements of Roger Adams's Ph.D.s, 1918–58 • Career Achievements of Roger Adams's Postdoctorates, 1936–59

240 pages (1981) Clothbound
US & Canada **$13.95** Export **$16.95**
LC 81-17625 ISBN 0-8412-0598-1

240 pages (1981) Paper
US & Canada **$9.95** Export **$11.95**
LC 81-17625 ISBN 0-8412-0711-9

Order from:
American Chemical Society
Distribution Office — 16
1155 Sixteenth St., N.W.
Washington, D.C. 20036
or CALL TOLL FREE 800-424-6747
and use your credit card.

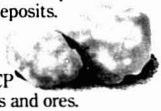
WITH OVER 400 JARRELL-ASH ICP'S INSTALLED WORLDWIDE, THERE'S BOUND TO BE AN APPLICATION JUST LIKE YOURS.

If you have a difficult applications problem, you may not care that Jarrell-Ash has the broadest line of ICP spectrometers. What you want to know is whether one of ours can be set up and run just to handle your individual analysis problem.

That's where experience counts. Jarrell-Ash experience. And technical expertise. Here's a sample of a few of our installations. See how close we come to yours.

1. GEOLOGICAL MAPPING. For the USGS, ICP analysis of mountain streams maps the location of mineral deposits.

2. MINERAL ASSAY. Mines use our ICP to assay minerals and ores.



3. CATALYTIC POISONS. Oil companies measure the levels of nickel and vanadium which inhibit the cracking process in crude oil.

4. SEWAGE. The State of New York looks for toxic metals in sewage and sludge using ICP.

5. DRY CELL BATTERIES. Manganese poisons nickel/cadmium and lead dry cells. Prest-O-Lite uses ICP to make sure that starting materials are manganese-free.

6. OIL EXPLORATION. Analysis of surface samples indicates the presence of oil hundreds of feet below the surface.

7. NUTRITION. ICP analysis of hair can diagnose the nutritional state of human subjects.

8. SOIL EVALUATION. Farmer's cooperatives measure the level of micronutrients in soil samples.



9. FOOD. The FDA uses ICP to measure mercury levels in fish.

10. CHEMICAL QUALITY CONTROL. Monsanto, Dow and Union Carbide check the purity of laboratory and industrial chemicals.

11. MEDICAL IMPLANTS. The FDA makes sure there there are no toxic metals in cardiac pacemakers, catheters and other implantables.

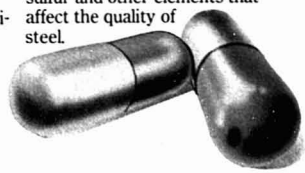
12. EXHAUST EMISSIONS. ICP helps engineers reduce the toxicity of exhaust at Ford.

13. WEAR METALS IN OIL. At McDonnell-Douglas and General Electric, analysis of engine lubricants tells which engine parts are wearing.



14. CERAMICS AND EPOXIES. Starting materials for s ceramic, epoxy and glassy carbon production can be measured for fracture-inducing elements.

15. SULFUR IN COAL. Steel mills assay coke for sulfur and other elements that affect the quality of steel.



16. DRUG EVALUATION. Hoffman-LaRoche checks drug purity with ICP.

17. INDUSTRIAL EMISSIONS. The EPA tests air quality with ICP.

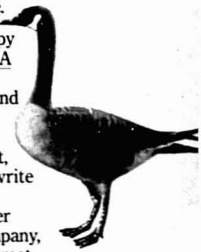
18. PLATING BATHS. ICP can measure the level of precious metals in plating baths.

19. BABY FOOD QUALITY. When Mead-Johnson certifies the nutritional element content of their baby foods, it's ICP results that stand by that guarantee.

20. PHOTOGRAPHIC MATERIALS. Kodak uses ICP to measure the levels of silver metal in film and paper.



21. BIOLOGICAL SUBSTANCES. Biologists and the USDA determine the migratory patterns of birds and insects by measuring the trace element composition of their tissue.

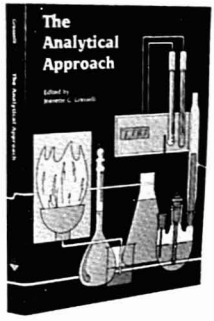


To get your copy of our PLASMA PRODUCTS BROCHURE and applications notes in your area of interest, please call or write Jarrell-Ash Division, Fisher Scientific Company, 590 Lincoln Street, Waltham, MA 02254. (617) 890-4300.

Jarrell-Ash
An ALLIED Company

CIRCLE 108 ON READER SERVICE CARD

The Analytical Approach



Jeanette G. Grasselli, *Editor*

Brings together 52 papers from *The Analytical Approach* column in ANALYTICAL CHEMISTRY. Provides unique approaches to analytical science and focuses on real-world problems. Discusses topical and interesting subjects such as the analysis of the JFK assassination bullets, Mt. St. Helens ash, flavor changes in food, and failure mechanisms in spacecraft parts. Written in a "popular" style yet is highly informative. Will serve as a teaching aid in higher education or as a guide in corporate training programs on analytical capabilities.

CONTENTS

Sections include:

- Production Processes
- Products
- Environmental
- Toxicity
- Forensic
- Miscellaneous

240 pages. (1983) Clothbound
LC 82-22618 ISBN 0-8412-0753-4
US & Canada **$29.95** Export **$35.95**
A paperbound student edition is available in bulk quantity. For price and ordering information, call toll free 800-424-6747.

Order from:
American Chemical Society
Distribution Office — 50
1155 Sixteenth St., N.W.
Washington, DC 20036
or CALL TOLL FREE 800-424-6747
and use your credit card.

Increasing the optical pathlength through the use of a slit nozzle (*6*) could also provide another order of magnitude increase in sensitivity.

Conclusion

The rapid growth in spectroscopic applications of supersonic nozzles can be demonstrated by considering that between 1974 and 1976 fewer than a half-dozen papers about this technique appeared, while in the past two years a noncomprehensive count indicated that well over 100 papers were published. A wide variety of uses are reported in these latter papers. Molecules as large as tetraphenylporphyrins have been studied (*9*), picosecond decays have been observed (*9*, *10*), and dimeric structures have been elucidated (*11*). Further applications and descriptions of the technique are contained in several review articles (*12*, *13*). Although this list of applications is by no means exhaustive, the variety of information available does explain the growing popularity of the technique.

Analytical applications have only begun to appear (*3–6*). Such a lag between fundamental studies and analytical applications is not unusual, and we are confident that as the simplicity, high selectivity, and sensitivity of this technique become more widely appreciated, the growth in analytical applications will mirror the rapid growth of the fundamental studies.

References

(1) Brown, J. C.; Duncanson, J. A.; Small, G. J. *Anal. Chem.* **1980**, *52*, 1711.
(2) Yang, Y.; D'Silva, A. P.; Fassel, V. A. *Anal. Chem.* **1981**, *53*, 894.
(3) Warren, J. A.; Hayes, J. M.; Small, G. J. *Anal. Chem.* **1982**, *54*, 138.
(4) Hayes, J. M.; Small, G. J. *Anal. Chem.* **1982**, *54*, 1202.
(5) Lubman, D. M.; Kronick, M. N. *Anal. Chem.* **1982**, *54*, 660.
(6) Amirav, A.; Even, U.; Jortner, J. *Anal. Chem.* **1982**, *54*, 1666.
(7) Byrne, J. P.; Ross, I. G. *Aust. J. Chem.* **1971**, *24*, 1107.
(8) Vaida, V.; McClelland, G. M. *Chem. Phys. Lett.* **1980**, *71*, 436.
(9) Even, U.; Jortner, J. *J. Chem. Phys.* **1982**, *77*, 4391.
(10) Felker, P. M.; Lambert, W. R.; Zewail, A. H. *Chem. Phys. Lett.* **1982**, *89*, 309.
(11) Levy, D. H. *J. Chem. Phys.* **1980**, *73*, 5380.
(12) Levy, D. H.; Wharton, L.; Smalley, R. E. In "Chemical and Biochemical Applications of Lasers"; Academic Press: New York, 1977; Vol. 2, Chapter 1.
(13) Levy, D. H. *Ann. Rev. Phys. Chem.* **1980**, *31*, 197.

Ames Laboratory is operated for the U.S. Department of Energy by Iowa State University under Contract No. W-7405-Eng-82. This research was supported by the Office of Health and Environmental Research, Office of Energy Research.



Gerald J. Small (left) is a professor of chemistry at Iowa State University and a senior chemist at the Ames Laboratory–USDOE. After obtaining a BSc degree in chemistry and mathematics from the University of British Columbia, he undertook graduate studies in chemical physics at the University of Pennsylvania, where he received his PhD in 1967. Following a two-year appointment as a research fellow at the Australian National University, he joined the faculty of Iowa State University in 1969. In addition to lasers in chemical analysis, his research interests include the photophysics and photochemistry of organic molecules and their solids, nonlinear optical phenomena, and electronic energy transfer in the condensed phase.

John M. Hayes is an associate chemist at the Ames Laboratory–USDOE. His undergraduate studies in chemistry were pursued at Providence College and the State College at Boston. He received his PhD in physical chemistry from Boston University in 1974. Analytical applications of laser spectroscopy and spectroscopic studies of structure and dynamics in gases and solids are among his research interests.

NEW FROM LECO®!

Energy instrumentation for coal and coke.



LECO's Family of Microprocessor, Energy Instrumentation:

- **AC-200** Automatic Calorimeter
- **MAC-400** Moisture • Ash • Volatiles • Fixed Carbon
- **CHN-600** Carbon • Hydrogen • Nitrogen
- **AF-500** Ash Fusibility
- **SC-132** Sulfur

FOR A DEMONSTRATION, CONTACT LECO® TODAY!

LECO®

LECO CORPORATION 3000 Lakeview Ave., St. Joseph, MI 49085-2396, U.S.A. Phone: (616) 983-5531

CIRCLE 130 ON READER SERVICE CARD

LABORATORY SERVICE CENTER

Acetylthiourea • 4-Aminoantipyrine • m-Aminophenol • Anisoin • Benzamide
1-Benzyl-4-piperidone • Bromoacetal • 5-Bromo-2-furoic Acid • Chalcone
Chloranilic Acid • Diacetylmonoxime • Dihydroxyacetone • Dimedone
2,2′ & 4,4′-Dihydroxydiphenyls • 2,3-Dimercaptosuccinic Acid • Dulcitol
Dodecyl Gallate • Ethanesulfonic Acid • Ethyl Pyruvate • Malonamide
Methylamine HCl • Nadic Anhydride • p-Nitrobenzaldehyde • Phloroglucinol
Potassium Acid Phthalate • Protocatechuic Acid • Rhamnose • Salicin
Tetrahydrofurfuryl Acetate • Tetraiodoethylene • iso-Vanillin • Xylose

Write for our Products List of over 3000 chemicals

Tel: 516-273-0900 • TOLL FREE: 800-645-5566 TWX: 510-227-6230

EASTERN CHEMICAL
A Division of UNITED-GUARDIAN, INC.
P. O. Box 2500
DEPT. AC
SMITHTOWN, N. Y. 11787

ANALYTICAL CHEMISTS
R&D positions are available in pharmaceutical and chemical companies nationwide through our specialized, free and confidential recruiting service.
Send your resume and job criteria to:
ROBERT WILKINSON ASSOCIATES
Box 300-500 Bradley Hill Road
Blauvelt, NY 10913

Laboratory Service Center (Equipment, Materials, Services, Instruments for Leasing). Maximum space — 4 inches per advertisement. Column width, 2-3/16″; two-column width, 4-9/16″. Artwork accepted. No combination of directory rates with ROP advertising. Rates based on number of inches used within 12 months from first date of first insertion. Per inch: 1″ — $107; 12″ — $105; 24″ —$101; 36″ — $98; 48″ — $96.

CALL OR WRITE BARBARA AUFDERHEIDE

ANALYTICAL CHEMISTRY
25 Sylvan Road South
P.O. Box 231
Westport, Ct. 06881
203-226-7131

USE LABORATORY SERVICE CENTER

INDEX TO ADVERTISERS IN THIS ISSUE

CIRCLE INQUIRY NO.	ADVERTISERS	PAGE NO.
5	Alltech Associates Chromad	556A
4	American Nuclear Society	486A
24	*B&L/Instruments & Systems Div. Blair Advertising	568A
27	**Beckman Instrument International	524P
30-31	*Bioanalytical Systems, Inc. Kissinger Advertising Assoc.	510A, 538A
23	*Bio-Rad Laboratories LaPointe, Schott & Smith, Inc.	501A
28-29	*Brinkmann Instruments Lavey/Wolff/Swift	OBC
21	*Bruker Instruments Techmarketing	518A
6-8, 25	*Burdick & Jackson Nordstrom/Cox Mkt.	486A, 527A, 540A, 557A
35	Cosa Corporation Jarman, Spitzer & Felix	540A
32	*Crawford Fitting Company Falls Advertising	558A
34	Cyborg Berenson & Isham, Inc.	513A
58	*Dionex Corporation Baxter, Gurian & Mazzei, Inc.	479A
xx	*Dupont Co./Liquid Chromatography N.W. Ayer ABH International	488A-489A
47-49	*Eldex Laboratories LaPointe, Schott & Smith, Inc.	490A
64	EM Science G&C Advertising	524A
52-57	*Fisher Scientific Company	503A, 505A, 507A, 509A, 511A
68	Gelman Sciences, Inc.	492A
65	*GFS Chemicals	524A
66-67	*Gilson Medical Electronics LaPointe, Schott & Smith, Inc.	472A-473A
69	Gow-Mac Instruments Kenyon Hoag Associates	514A
99	*Hamilton Company Mealer & Emerson	536A-537A
94-95	*Hewlett-Packard Company Pinne, Garvin & Hock	469A
96	Houston Instrument Div. of Bausch & Lomb Cooley & Shillinglaw	IFC
104	*Instruments SA, Inc. Kathy Wyatt & Associates	522A
108	Jarrell-Ash Buzzard Advertising	573A
121-122	*Kontron Analytical	475A
123-124	**Kontron Analytical Druckerei Schwarz	524D, 524F

INDEX TO ADVERTISERS IN THIS ISSUE

CIRCLE INQUIRY NO.	ADVERTISERS	PAGE NO.
127	*Lab-Crest Scientific Furlong Promotions	520A
133–135	LDC/Milton Roy HRS Communications	485A, 487A, 534A
130	Leco Corporation Leco Communications	575A
125	Leybold Heraus GmbH	529A
126	Leybold Heraus	564A
129	LKB Biochrom, Ltd.	530A
131	LKB-Produkter AB Marketing Service	571A
10–19, 144	*Matheson Kenyon Hoag Associates	482A, 483A
138	MCI/Link	578A
140, 142	Mettler Instrument McKinney, Inc.	553A, 555A
141	*Mitsubishi Chemical Global Advertising	541A
155	Nermag CD Communications	491A
156	*Ohaus Scale Corporation Jarman-Spitzer & Felix	515A
174	PCR Research Chemicals Media Marketing	520A
162–163	*Perkin-Elmer Corporation Marquardt & Roche	539A
171	*Pharmacia G&C Advertising	484A
175	*Philips Analytical STG Marketing	517A
83–84, 85–86	Pye/Sargent Connors Publicity, Ltd.	523A
70–82	**Pye Unicam, Ltd. Connors Publicity, Ltd.	524I–524J
183	Rheem Manufacturing Co. Carson Raichle & Assoc.	522A
185–186	*Rheodyne, Incorporated Bonfield Associates	556A, 567A
180	Riber Division/Instruments S.A. Kathy Wyatt & Associates	533A
192	**Schleicher & Schull Heinz Reise Werbung	524L
187	**Schott-Glasswerke Werbeagentur Frenz	524B
193	*Scientific Glass Engineering, Inc. Arden Advertising	481A
190–191, 194–198 202–207	Shimadzu Scientific Instruments General Adv-Sagami	545A, 547A, 549A
210	**Shimadzu Public-Werbung	524N
226–227	*Valco Instruments Technical Advertising Assoc.	535A
200–201, 219–220 223–224	*Varian Moran, Lanig & Duncan	493A–497A
221	VG Analytical** ICA Publicity, Ltd.	524G
xx	*Whatman Company J. S. Lanza & Associates	477A
234	Wheaton Safety Jonathan Advertising, Inc.	542A
245	*Zymark Corporation J. Balderson & Assoc.	521A

** See ad in ACS Laboratory Guide*

*** Company so marked has advertisement in Foreign Regional edition only.*

Advertising Management for the American Chemical Society Publications

CENTCOM, LTD.

Thomas N. J. Koerwer, President
James A. Byrne, Vice President
Alfred L. Gregory, Vice President
Clay S. Holden, Vice President
Benjamin W. Jones, Vice President
Robert L. Voepel, Vice President
Joseph P. Stenza, Production Director

25 Sylvan Rd. South
P.O. Box 231
Westport, Connecticut 06881
(Area Code 203) 226-7131
telex no. 643310

ADVERTISING SALES MANAGER
James A. Byrne

ADVERTISIING PRODUCTION MANAGER
Barbara Aufderheide

SALES REPRESENTATIVES

Philadelphia ... Dean A. Baldwin, Jerry Naab, CENTCOM, LTD., GSB Building, Suite 425, 1 Belmont Avenue, Bala Cynwyd, Pa. 19004. Telephone: 215-667-9666

New York ... Dean A. Baldwin, Don Davis, CENTCOM, LTD., 60 East 42nd St., 212-972-9660, New York, N.Y. 10165

Westport, CT ... Don Davis, CENTCOM, LTD., 25 Sylvan Rd. South, P.O. Box 231, Westport, Ct. 06881. Telephone: 203-226-7131, Telex 643310

Cleveland ... Bruce E. Poorman, CENTCOM, LTD., 17 Church St., Berea, Ohio 44017, 216-234-1333

Chicago ... Bruce E. Poorman, CENTCOM, LTD., 540 Frontage Rd., Northfield, Ill. 60093, 312-441-6383

Houston ... Dean A. Baldwin, CENTCOM, LTD., 215-667-9666

San Francisco, CA ... Paul M. Butts, CENTCOM, LTD., Suite 112, 1499 Bayshore Hwy, Burlingame, CA 94010. Telephone: 415-692-1218

Los Angeles ... Clay S. Holden, CENTCOM, LTD., Newton Pacific Center, 3142 Pacific Coast Highway, Suite 200, Torrance, CA 90505, 213-325-1903

Boston, MA ... Don Davis, CENTCOM, LTD. Telephone: 203-226-7131

Atlanta, GA ... Don Davis, CENTCOM, LTD. Telephone: 203-226-7131

Denver ... Clay S. Holden, CENTCOM, LTD., 213-325-1903

United Kingdom

Reading, England ... Malcolm Thiele, Technomedia Ltd., Wood Cottage, Shurlock Row, Reading RG10 OQE. Berkshire, England. Telephone: 0734-343302

Lancashire, England ... Technomedia Ltd., c/o Meconomics Ltd., Meconomics House, 31 Old Street, Ashton Under Lyne, Lancashire, England. Telephone: 061-308-3025

Continental Europe ... Andre Jamar, International Communications, Inc., Rue Mallar 1, 4800 Verviers, Belgium. Telephone: (087) 22-53-85, Telex #49263

Tokyo, Japan ... Shigeo Aoki, International Media Representatives Ltd., 2-29 Toranomon, 1-Chome Minato-ku Tokyo 105 Japan. Telephone: 502-0656

Microanalysis or image processing. We make it look too easy.

You won't impress anyone operating an MCI/Link microanalysis or image processing system if they see you at work.

Pushing a few buttons is anything but impressive.

Results are impressive. And easier to get than you need tell.

We believe that advanced systems and software shouldn't simply get the job done. But get the job done simply.

That's why ease of operation is meticulously designed into every MCI/Link system.

Precise Microanalysis

Detect. Process. Plot. Display. Analyze. The System 860 energy dispersive x-ray microanalyzer combines simplicity of operation with field-proven engineering and software.

It offers a total systems approach to precise element analysis.

Down to and including boron.

Another sophisticated development is our XR 500 energy dispersive x-ray fluorescence system.

It analyzes solid, liquid and powder samples down to less than 1mm in diameter.



System 860 energy dispersive x-ray microanalysis system.

Image Processing. At The Touch Of A Button.

Capture. Enhance. Analyze. Store. Retrieve. It's a push-button affair with the Intellect 100 desk-top image processing system.

From microscope image enhancement to robotic vision and on-line production monitoring, Intellect 100 provides standard software for the non-programmer.

And a program development system for experts.

Intellect 200 is a more powerful, fully modular version of Intellect 100. With capabilities such as hardware Fast Fourier Transform processing.



Intellect 100 image processing system.

Award-Winning Technology.

Behind every MCI/Link system is award-winning engineering for achievements in computer graphics, digital video processing, and other leading-edge technologies.

Including an Emmy Award for picture manipulation. The Montreux International Achievement Award for digital video developments. And more.

We make your results look easy. That makes us look good.

Call or write today for more information on the entire MCI/Link family of image processing and microanalysis products.

MCI/Link, Link Systems (U.S.A.), Inc., P.O. Box 50810, Palo Alto, CA 94303, (415) 856-2726, Telex: 334420.

MCI/LINK

CIRCLE 138 ON READER SERVICE CARD

Get the Best Readout with

analytical chemistry

Order your own monthly copy today!

1983	U.S.	Canada** (surface postage included)	Foreign** (surface postage included)
1 year			
ACS Members*	☐ $18.00	☐ $37.00	☐ $ 37.00
Nonmembers	☐ $24.00	☐ $43.00	☐ $ 67.00

☐ Payment Enclosed (Payable to American Chemical Society)
☐ Bill Me ☐ Bill Company
Charge my subscription to ☐ MasterCard ☐ VISA

Card # _____ Interbank # _____ (MasterCard only)

Exp. Date _____ Signature _____

or CALL TOLL FREE (800) 424-6747 (new orders)

Name _____
Job Title _____
Employer _____
Address ☐ Business ☐ Home _____
City _____ State _____ Zip _____
Employer's Business ☐ Manufacturing ☐ Academic ☐ Government ☐ Other _____
If manufacturing, type of products produced _____
☐ Check here if you wish subscription started with the January issue.

*Subscriptions at ACS member rates are for personal use only.
**Payment must be made in U.S. currency by international money order, UNESCO coupons, U.S. bank draft, or order through your subscription agency. For nonmember subscription rates in Japan, contact Maruzen Co., Ltd. Please allow 60 days for your first copy to be mailed.

560 2190K

MAIL THIS POSTAGE-PAID CARD TODAY!



Get the Best Readout with

analytical chemistry

Order your own monthly copy today!

1983	U.S.	Canada** (surface postage included)	Foreign** (surface postage included)
1 year			
ACS Members*	☐ $18.00	☐ $37.00	☐ $ 37.00
Nonmembers	☐ $24.00	☐ $43.00	☐ $ 67.00

☐ Payment Enclosed (Payable to American Chemical Society)
☐ Bill Me ☐ Bill Company
Charge my subscription to ☐ MasterCard ☐ VISA

Card # _____ Interbank # _____ (MasterCard only)

Exp. Date _____ Signature _____

or CALL TOLL FREE (800) 424-6747 (new orders)

Name _____
Job Title _____
Employer _____
Address ☐ Business ☐ Home _____
City _____ State _____ Zip _____
Employer's Business ☐ Manufacturing ☐ Academic ☐ Government ☐ Other _____
If manufacturing, type of products produced _____
☐ Check here if you wish subscription started with the January issue.

*Subscriptions at ACS member rates are for personal use only.
**Payment must be made in U.S. currency by international money order, UNESCO coupons, U.S. bank draft, or order through your subscription agency. For nonmember subscription rates in Japan, contact Maruzen Co., Ltd. Please allow 60 days for your first copy to be mailed.

560 2190K

MAIL THIS POSTAGE-PAID CARD TODAY!



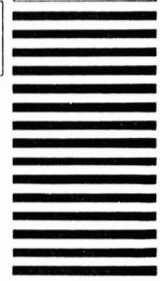
NO POSTAGE
NECESSARY
IF MAILED
IN THE
UNITED STATES

BUSINESS REPLY CARD

FIRST CLASS PERMIT NO. 10094 WASHINGTON, D.C.

POSTAGE WILL BE PAID BY ADDRESSEE

American Chemical Society
Circulation Dept.
1155 Sixteenth Street, N.W.
Washington, D.C. 20036





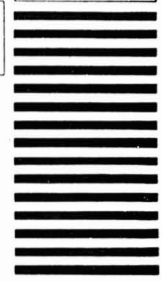
NO POSTAGE
NECESSARY
IF MAILED
IN THE
UNITED STATES

BUSINESS REPLY CARD

FIRST CLASS PERMIT NO. 10094 WASHINGTON, D.C.

POSTAGE WILL BE PAID BY ADDRESSEE

American Chemical Society
Circulation Dept.
1155 Sixteenth Street, N.W.
Washington, D.C. 20036



analytical chemistry

EDITOR: **GEORGE H. MORRISON**

EDITORIAL HEADQUARTERS
1155 Sixteenth St., N.W.
Washington, D.C. 20036
Phone: 202-872-4570 Teletype: 710-8220 151

Executive Editor: Josephine M. Petruzzi
Managing Editor: Barbara Cassatt
Associate Editor: Stuart A. Borman
Assistant Editors: Marcia S. Cohen, Rani A. George
Editorial Assistant: Louise Voress
Production Manager: Leroy L. Corcoran
Art Director: John V. Sinnett
Staff Artist: Linda M. Mattingly
Copy Editor: Gail M. Mortenson
Circulation Manager: Cynthia G. Smith

Journals Dept., Columbus, Ohio
Associate Head: Marianne Brogan
Associate Editor: Rodney L. Temos

Advisory Board: Joel A. Carter, Richard S. Danchik, Richard Durst, Dennis H. Evans, Jack W. Frazer, Helen M. Free, Shizuo Fujiwara, Roland F. Hirsch, Csaba Horvath, Wilbur I. Kaye, Thomas C. O'Haver, Janet Osteryoung, Herbert L. Retcofsky, Robert E. Sievers, Wilhelm Simon, Rudolph H. Stehl

Instrumentation Advisory Panel: Edward M. Chait, M. Bonner Denton, Raymond E. Dessy, Larry R. Faulkner, Martin S. Frant, Michael L. Gross, Fred E. Lytle, Curt Reimann, Andrew T. Zander

Contributing Editor, A/C Interface: Raymond E. Dessy

The Analytical Approach Advisory Panel: Edward C. Dunlop, Robert A. Hofstader, Wilbur D. Shults

Regulatory Affairs, Analytical Division Committee: Curt W. Reimann (Chairman)

Published by the
AMERICAN CHEMICAL SOCIETY
1155 16th Street, N.W.
Washington, D.C. 20036

Books and Journals Division
Director: D. H. Michael Bowen
Journals: Charles R. Bertsch
Production: Elmer Pusey, Jr.
Marketing & Sales: Claud K. Robinson
Research and Development: Seldon W. Terrant

Manuscript requirements are published in the January 1983 issue, page 171. Manuscripts for publication (4 copies) should be submitted to ANALYTICAL CHEMISTRY at the ACS Washington address.

The American Chemical Society and its editors assume no responsibility for the statements and opinions advanced by contributors. Views expressed in the editorials are those of the editors and do not necessarily represent the official position of the American Chemical Society.

"Real" Samples

Medical diagnosticians are the analytical chemists of the medical profession. They use a wide array of physical and chemical techniques to extract information from the human body. One of the most exciting recent developments in this field has been the rapid growth in imaging technology. This field, which was recently reviewed by Dr. C. Carl Jaffe [*Am. Sci.* **1982,** *70* (6), 576–85], is of considerable interest to those of us involved in imaging techniques for chemical analysis. Techniques discussed include film radiography, computed tomography, nuclear medicine (radioisotopes), positron emission tomography, ultrasonography, nuclear magnetic resonance, and digital radiography.

We chemists make use of some of these techniques in our study of physical and chemical systems; however, it is the use of these techniques in the imaging mode that suggests many exciting applications. All of the medical imaging techniques involve some form of radiation which is transformed into a visual pattern in a spatially well-defined manner. The energy may be either transmitted or reflected by structures deep inside the body. The use of imaging to study structure is obvious; however, a medical image can also serve as a physiological record that may be transient or permanent, depending on the medium and the problem to be addressed. Thus, both form and function can be studied. It is now possible to image blood flow and metabolic processes, as well as the structure of connective tissue and the sizes and configurations of organs.

The uses of these medical imaging techniques in the chemical analysis of nonmedical systems should be actively explored. For example, to properly sample a heterogeneous meteorite for the analysis of inclusions, Dr. James Arnold and his colleagues at La Jolla nondestructively probed the interior of this precious material by computed tomographic scanning (*Science* **1983,** *219*, 383–84). The tools for three-dimensional analysis exist. It is now up to the imagination and ingenuity of investigators to apply them to complex and challenging problems.

G. H. Morrison

Aromatic Diesel Emissions as a Function of Engine Conditions

Trescott E. Jensen and Ronald A. Hites*

School of Public and Environmental Affairs and Department of Chemistry, Indiana University, Bloomington, Indiana 47405

The abundance and distribution of the alkyl homologues of polycyclic aromatic hydrocarbons (naphthalene, fluorene, phenanthrene, pyrene, fluoranthene, and phenylnaphthalene) and oxygenated polycyclic aromatic hydrocarbons (naphthalenecarboxaldehydes, fluoren-9-one, biphenylcarboxaldehydes, phenanthrenecarboxaldehydes, and thioxanthen-9-one) in the organic extractables of particulates produced by a diesel engine are reported. Samples were obtained at three engine loads and at three fuel injection timing conditions. The concentrations of alkyl homologues of PAH and oxy-PAH on the particulates were found to decrease as cylinder exhaust temperature increased. The degree of alkylation for the most abundant homologue of these compounds increased by one to two carbons as the cylinder exhaust temperature was decreased.

Diesel soot production in the United States is estimated to be 10^{11} g annually. These particulates are predominantly carbon; however, 10–40% by weight can be extracted with organic solvents (*1*). The Ames' *Salmonella* assay has indicated that this organic soluble material is mutagenic (*2–4*), and consideration of this activity has prompted an evaluation of the possible human health effects of diesel particulates (*4–7*). Identification of the compounds responsible for the observed mutagenic activity has been necessary to provide information about the magnitude of the environmental impact of diesel particulates.

Information about the composition of organic extractables from diesel particulates is becoming more complete (*3, 4, 8–13*). Besides unburned fuel, diesel particulate extracts contain polycyclic aromatic hydrocarbons (PAH), oxygenated-PAH, a few sulfur and oxygen heterocyclic compounds, and nitro-PAH. Over 250 different aromatic compounds, including alkyl homologues, have been identified in diesel emissions (*3, 4, 8–13*). Naphthalene, fluorene, phenanthrene, phenylnaphthalene, pyrene, and fluoranthene are the major PAH. Ketone and aldehyde derivatives of these PAH are the predominant components of the oxy-PAH fraction. Hydroxy, dihydroxy, and dicarboxylic acid anhydride PAH have also been reported (*3*). Thioxanthen-9-one, dibenzothiophene, and xanthen-9-one are the major heterocyclic components. Nitropyrene, found in diesel emissions, has been the focus of many studies because of the high direct mutagenic activity of nitro-PAH in the Ames' *Salmonella* assay (*6, 13, 17*). A summary of all these compounds is given in Table I.

Even though nitropyrene and benzo[*a*]pyrene are known mutagens, another group of PAH found in diesel exhaust are also very biologically active. 1-Methylphenanthrene, 2-methylphenanthrene, and 9-methylphenanthrene have all been found in diesel exhaust and are active in a bacterial mutagenicity bioassay. Their specific mutagenicities are 0.2–0.5 times that of benzo[*a*]pyrene (*18*). 9-Methylfluorene is also in diesel exhaust and was reported to be 0.2 times as mutagenic as benzo[*a*]pyrene; its higher alkyl homologue, 1,9-dimethylfluorene, was found to be 0.6 times as active as benzo[*a*]pyrene (*19*). On the basis of these biological activity findings, the alkyl homologues of the PAH are important indicators of the environmental impact of diesel emissions. They are also more easily measured, because of their greater abundance (*3*) than are either benzo[*a*]pyrene or nitropyrene.

To decrease the potential impact of diesel exhaust on human health, engineering efforts have focused on improved fuel combustion. However, complete combustion has not been achieved. Many modern diesel engines burn 99.9% of their fuel (*20*). Thus, at least one thousandth of the fuel is discharged to the environment as partially burned or unburned material. Some improvement may yet be made that will increase fuel combustion efficiency, but it is not likely that exhaust emissions will be decreased significantly by using only this approach. Another approach would be the total removal of the soot from the exhaust. At the present time, however, the technology needed to remove all the particulates from diesel exhaust streams is neither economical nor practical.

Very little information is available concerning the effects of fuel composition, fuel to air ratio, fuel injection timing, injection pressure, engine combustion temperature, oil age, exhaust temperature, and other engine operating conditions on the trace organic species in diesel emissions. Thus, we have examined the alkyl homologues of PAH and oxy-PAH in the soluble organic extract of diesel particulates which were produced using different engine operating conditions.

EXPERIMENTAL SECTION

Cummins Engine Co. (Columbus, IN) provided diesel soot samples produced using a single cylinder test engine that burned no. 2 diesel fuel. On the basis of the data presented below, we judge this engine to be similar to multicylinder engines in its emission characteristics. Five samples were obtained at the following engine conditions: advanced timing at full load, normal timing at full load, retarded timing at full load, normal timing at half load, and normal timing at no load. Full load was set at 36 braking horse power; injection timing was retarded or advanced by 6° off the normal setting of 10° of rotation before top dead center cylinder stroke. The temperature was measured 1.5 ft (46 cm) down the exhaust manifold from the cylinder exhaust port. The exhaust temperature was 590 °C at full load, 470 °C at half load, and 190 °C at no load.

Exhaust was diluted about 14:1 with filtered air in a dilution tunnel. Particulates were collected on 47 mm diameter, Teflon-coated, glass fiber filters (Pallflex T60-A20 or Pallflex TX40). The temperature of the filter was about 50 °C. Filters were Soxhlet extracted for 24 h with 150 mL of methylene chloride. An internal standard was added to each extract before extractant volume reduction; it consisted of 200 ng each of fluorene-d_{10}, anthracene-d_{10}, pyrene-d_{10}, and perylene-d_{12} (Merck Sharp and Dohme Canada, Limited), and 320 ng of fluoren-9-one-d_8 which was synthesized from fluorene-d_{10} by oxidation with sodium dichromate in concentrated acetic acid.

Extraction solvent volume was reduced to about 1 mL with a rotovap unit, then to about 20 μL with dry nitrogen purging. Prior to fractionation, the methylene chloride was exchanged with hexane by adding 100 μL of hexane followed by nitrogen purging to a volume of about 20 μL, repeated four times. Crude extracts were separated into five fractions on silicic acid (5% deactivated) columns (5 cm × 0.8 cm). The sequence of the eluents was hexane (3 mL), 1:1 hexane:toluene (3 mL), toluene (3 mL), methylene chloride (3 mL), and methanol (3 mL). All solvents were pesticide grade or better and were checked for purity.

Gas chromatographic mass spectrometry (GC/MS) was done with a Hewlett-Packard 5985B mass spectrometer. A capillary

0003-2700/83/0355-0594$01.50/0 © 1983 American Chemical Society

Table I. PAH and Oxy-PAH Reported in Diesel Particulate Extracts

aromatic compound	alkyl homologue range reported	ref
naphthalene[a]	C_0-C_4	8, 14
fluorene[a]	C_0-C_4	8, 9
phenanthrene (and anthracene)	C_0-C_4	3, 8-11
phenylnaphthalene[a]	C_0-C_3	9
fluoranthene[a]	C_0-C_1	3, 8-11
pyrene[a]	C_0-C_1	3, 8-11
naphthalenecarboxaldehydes[a]	C_0-C_6	9-11
biphenylcarboxaldehydes[a]	C_0-C_2	9
phenanthrene (and anthracene[b]) carboxaldehydes[a]	C_0-C_2	3, 8-11
fluoren-9-one[a]	C_0-C_5	3, 8-11, 15
phenanthrone (and anthrone)	C_0-C_3	3, 10
4*H*-cyclopenta[*def*]phenanthren-4-one	C_0-C_2	8-11
fluorenequinone	C_0-C_2	3, 8
phenanthrene(and anthracene)quinones	C_0-C_2	3, 8-11
fluoranthene(and pyrene)quinones	C_0-C_1	3
hydroxyphenanthrenes	C_0-C_3	3
dihydroxyfluorenes	C_0-C_2	3
dihydroxyphenanthrenes	C_0-C_2	3
naphthalenedicarboxylic acids	C_0-C_2	3
naphthalenedicarboxylic acid anhydride	C_0-C_2	3, 8
dibenzothiophene	C_0-C_1	3, 9, 16
thioxanthen-9-one[a]	C_0-C_2	3, 10, 16

[a] Compounds discussed in this study. [b] Small abundance.

(30 m × 0.2 mm i.d.) fused silica column coated with a bonded silicone (J & W DB-5, equivalent to SE-54) stationary phase was used for GC separation. An injection of 1 μL at 30 °C was loaded splitless for 42 s. The initial temperature was held 4 min and then linear programming was begun at 4 °C/min to a final temperature of 280 °C and held for 55 min. Negative chemical ionization was done with methane as the reagent gas. All concentration values are reported as micrograms of component per gram of particulate. Concentrations were calculated by using the area for the mass chromatogram of the ions of interest, excluding interfering major components, ratioed to the appropriate internal standard. No attempt has been made to correct for the difference in mass spectrometer response factors for the higher alkyl homologues due to the lack of suitable standards.

The unsubstituted compounds were identified by comparison of the electron impact and negative chemical ionization mass spectra and gas chromatographic retention times with those of authentic compounds. Most of the methyl PAH and some of the methyl oxy-PAH were similarly identified. The other alkyl homologues were identified by a priori interpretation of their mass spectra and by extrapolation of their GC retention times obtained from mass chromatograms.

RESULTS AND DISCUSSION

Our analyses of the alkyl homologues in diesel particulates have focused on the hexane:toluene and toluene fractions. Both fractions have been examined by electron impact (EI) GC/MS, and the toluene fraction has also been studied with negative chemical ionization (NCI) GC/MS. The concentrations for naphthalene, fluorene, anthracene, phenanthrene, pyrene, fluoranthene, and phenylnaphthalene and their alkyl homologues are given in Table II. Table III lists concentration data for naphthalenecarboxaldehydes, fluoren-9-one, biphenylcarboxaldehydes, phenanthrenecarboxaldehydes, and thioxanthen-9-one and their alkyl homologues.

For full engine load samples, the fuel injection timing was either advanced, normal, or retarded. The cylinder exhaust temperature for full load was about 590 °C regardless of the timing. When the fuel injection timing is normal and the engine load is changed, the exhaust temperature varies from 590 °C for full load to 190 °C with no engine load. With this experimental design, it was possible to examine cylinder reaction products and compounds formed in the exhaust stream almost independently of each other. Unfortunately, there may be minor sources for the detected alkyl PAH compounds other than those desired. Potential sources are unconsumed fuel, lubricating oil, sample collection filter artifacts, and sample aging. For the purpose of this study, we believe these contributions are negligible.

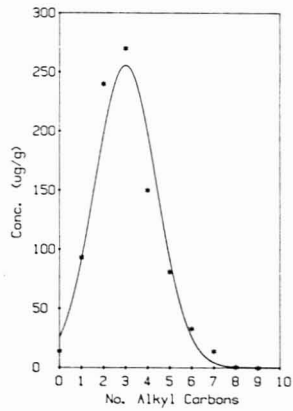


Figure 1. Concentration (in μg/g particulate) of the alkyl homologues of fluorenone as a function of the number of *alkyl* carbon atoms. The sample was emitted from a one cylinder diesel engine operating with normal timing and at no load. The curve is the best-fitting Gaussian function (average = 3.00, standard deviation = 1.40, normalization factor = 255.6).

Representation of the data in Tables II and III as plots of the number of alkyl carbons in the compound vs. the concentration of the homologue gives an alkyl homologue plot (see Figure 1 for an example). A Gaussian distribution can be fit to such data by calculating the first and second moments. The first moment gives the average number of alkyl carbons for a specific compound type, and the second moment gives a measure of the width of the distribution. These calculations give the curve shown in Figure 1. Similar calculations for each of the other 48 data sets gave the average

Table II. Amount of Unsubstituted PAH and its Alkyl Homologues Expressed as μg/g Particulate Found in the Hexane:Toluene Fraction

	sample (engine condition)				
compound	1 (advanced)[a]	2 (normal)[a]	3 (retarded)[a]	4 (half load)[b]	5 (no load)[b]
naphthalene (C_{10})	0	4.8	0	0	1.0
C_{11}	0	13	0	0.8	2.5
C_{12}	0	47	c	6.2	4.0
C_{13}	0	46	0.4	26	8.6
C_{14}	0	13	3.4	1.2	16
C_{15}	0	1.7	0.2	0	5.0
C_{16}	0	0	0	0	0
fluorene (C_{13})	0	2.9	0.2	0.4	0.3
C_{14}	0.2	4.9	1.5	18	1.2
C_{15}	0.4	13	7.8	62	3.8
C_{16}	2.3	14	12	63	42
C_{17}	1.4	5.6	2.3	10	56
C_{18}	0.3	0	0.1	c	15
C_{19}	0	0	0	0	3.1
C_{20}	0	0	0	0	0.8
C_{21}	0	0	0	0	0
anthracene (C_{14})	0	1.2	0.9	6.4	4.1
phenanthrene (C_{14})	8.3	91	86	110	140
C_{15}	35	180	150	340	160
C_{16}	50	120	120	170	310
C_{17}	16	33	32	43	290
C_{18}	0.4	9.1	7.2	11	110
C_{19}	0	1.8	1.3	9.8	8.6
C_{20}	0	0	0	0	0.2
C_{21}	0	0	0	0	0
pyrene (C_{16})	1.5	5.3	0.8	17	40
fluoranthene (C_{16})	43	39	24	28	35
C_{17}	4.0	6.7	3.2	6.0	79
C_{18}	0.4	0.7	0	0.1	55
C_{19}	0.1	0	0	0	31
C_{20}	c	0	0	0	15
C_{21}	0	0	0	0	2.3
C_{22}	0	0	0	0	0
phenylnaphthalene (C_{16})	3.1	9.1	6.6	13	12
C_{17}	9.5	20	13	15	92
C_{18}	4.5	8.5	7.7	7.4	110
C_{19}	0.2	3.2	0.9	1.8	74
C_{20}	0	0	0	0	22
C_{21}	0	0	0	0	5.7
C_{22}	0	0	0	0	0

[a] Full engine load. [b] Normal injection timing. [c] Alkyl homologue detected at a concentration <0.1 μg/g.

alkyl carbon numbers given in Table IV. In almost all cases, the second moment was about 1 alkyl carbon; thus, this parameter will not be discussed further.

Four trends are observed from the data given in Tables II and III and condensed in Table IV. First, with the possible exception of naphthalene and biphenylcarboxaldehydes, injection timing does not have an effect on the extractable component profiles of the reported compounds. Second, the most abundant alkyl homologue of the aromatic compounds reported, with the exception of phenanthrenecarboxaldehydes, extends to a greater number of carbons as the engine cylinder exhaust temperature decreases (decreased load). Third, there is an increase of the absolute concentration of all alkyl homologues, with the exception of naphthalene and fluorene, as the exhaust temperature decreases (decreased load). Fourth, the alkyl homologues of all compounds reported, except fluoranthene and thioxanthen-9-one, are more abundant than the unsubstituted aromatic compound. For fluoranthene and thioxanthen-9-one, the unsubstituted aromatic is less abundant than the methyl alkyl homologue for the no load sample.

Effect of Length of Combustion Time. For naphthalene, the shift from 2.4 to 4.0 alkyl carbons as the injection is retarded may be an artifact. Naphthalene and its smaller alkyl homologues have low boiling points (naphthalene, bp 218 °C, and 1-methylnaphthalene, bp 242 °C). The absence of these compounds in the extract may be due to the air flow through the sample filter, temperature of the filter, vapor particle partitioning, or loss during sample workup. Therefore, it is not possible to draw conclusions about the significance of the length of combustion time for the alkyl naphthalene series.

Combustion time *may* be a factor in the biphenylcarboxaldehydes alkyl homologue distribution. For the advanced injection timing sample for these compounds, the most abundant homologue is one carbon greater (2.4) than for normal or retarded injection timing (1.3). The absolute abundance of the alkyl biphenylcarboxaldehydes, however, is very small, and this difference may not be significant.

Since only two of the alkyl series appear to be influenced by length of cylinder reaction time, we conclude that formation of the remaining eight alkyl series is essentially complete irrespective of combustion time or are formed in the exhaust to a significant extent.

Effect of Exhaust Temperature. The most abundant alkyl homologue (for nine of the ten aromatics) extends to a greater number of carbons as the engine cylinder exhaust temperature decreases. Phenanthrenecarboxaldehydes alkyl homologues increase in absolute concentration as exhaust temperature decreases, but there is no shift observed at no load for the most abundant homologue (1.3 vs. 1.4 alkyl

Table III. Amount of Unsubstituted Oxy-PAH and Its Alkyl Homologues Expressed as μg/g Diesel Particulate Found in the Toluene Fraction

compound	sample (engine condition) 1 (advanced)[a]	2 (normal)[a]	3 (retarded)[a]	4 (half load)[b]	5 (no load)[b]
naphthalenecarboxaldehydes (C_{11})	0.8	0.9	1.8	6.3	0
C_{12}	1.3	1.2	2.0	33	0
C_{13}	1.2	0.9	1.3	50	20
C_{14}	0.3	0.3	1.1	26	84
C_{15}	0.1	0.1	1.0	12	44
C_{16}	c	0	0.5	3.7	9.1
C_{17}	0	0	0	0.3	5.7
C_{18}	0	0	0	0	0
fluoren-9-one (C_{13})	29	25	43	26	14
C_{14}	45	41	72	82	93
C_{15}	41	35	56	120	240
C_{16}	27	18	30	84	270
C_{17}	11	7.2	12	23	150
C_{18}	5	2.8	7.8	6.4	81
C_{19}	2.3	1.1	1.9	2.2	33
C_{20}	0.7	0.4	0.7	0.8	14
C_{21}	0	0	0	0	0.6
C_{22}	0	0	0	0	0
biphenylcarboxaldehydes(C_{13})	0.3	0.4	0.6	1.1	0.1
C_{14}	0.6	2.1	3.0	6.2	5.2
C_{15}	1.2	1.8	1.6	13	120
C_{16}	0.9	c	0.2	4.3	130
C_{17}	0.8	0	0	1.2	75
C_{18}	0.1	0	0	c	20
C_{19}	0	0	0	0	0
phenanthrenecarboxaldehydes (C_{15})	1.1	0.8	1.0	3.0	70
C_{16}	3.1	1.5	1.4	4.9	84
C_{17}	1.5	0.7	0.8	2.2	41
C_{18}	1.2	0.3	0.5	1.2	23
C_{19}	0.8	0.3	0.4	0.7	12
C_{20}	0.5	0.1	0.2	0.3	5.3
C_{21}	0	0	0	0	1.4
C_{22}	0	0	0	0	0
thioxanthen-9-one (C_{13})	4.9	3.1	7.1	15	58
C_{14}	4.1	2.1	4.3	12	87
C_{15}	1.6	0.8	1.9	3.2	37
C_{16}	0.9	0.2	0.5	0.4	7.7
C_{17}	0.2	0.1	0.2	0.2	2.9
C_{18}	c	0	0.1	0	1.1
C_{19}	0	0	0	0	0.6
C_{20}	0	0	0	0	0

[a] Full engine load. [b] Normal injection timing. [c] Alkyl homologue detected at a concentration of <0.1 μg/g.

carbons).

Homologue Concentration Inversely Related to Temperature. The total concentration of all of the alkyl homologues of a series increases as the cylinder exhaust temperature decreases. The no load sample has the greatest concentration (micrograms per gram of particulate) with the exception of naphthalene which was discussed previously.

Partitioning of fluoranthene and pyrene between the particulate and gas phase has been reported. At 37 °C, the median partitioning coefficients (particulate/gas-phase mass ratio) are 0.75 and 0.95 for pyrene and fluoranthene, respectively (*21*). For the samples in this study, the pyrene to fluoranthene ratio increases from 0.14 to 1.1 with decreasing cylinder exhaust temperature. A similar but smaller change is seen with the phenanthrene to anthracene ratio (0.013 to 0.029). Irrespective of the temperature or sample, the fluoranthene concentration is almost unchanged. From this we infer that fluoranthene is formed in the cylinder, and from the partition coefficient, we would expect to find most of the fluoranthene associated with the particulate.

For all compounds except fluorene, this third trend [a general increase of the absolute concentration of all alkyl homologues as the cylinder exhaust temperature decreases (decreased load)] is distinct. Fluorene, however, shows a decrease in concentration for the no load sample. At least two explanations for this observed difference in compound production are possible. Conversion of precursors to alkyl fluorenes may occur in the exhaust and is thermophilic, therefore, not occurring to a significant extent at a lower exhaust temperature. Alternatively, the alkyl fluorenes may be converted to alkyl fluorenones (*9*). The concentration of the alkyl fluorenones does increase and a homologue shift (1.7 to 2.1 to 3.0) does occur as engine temperature decreases.

The concentrations of alkyl homologues of most the compounds reported are exhaust temperature dependent. Unfortunately, our ability to describe the increase or decrease of these compounds as a function of formation, partitioning, or thermal stability is still limited.

Low Concentration of Unsubstituted Compounds. For all samples and for most compounds, the concentration of the unsubstituted PAH or oxy-PAH is lower than that for the alkyl homologues. There are several possible explanations for this distribution of homologues. (a) Formation of the unsubstituted compounds may not be favored. (b) Alkylation of the unsubstituted compound may be extensive. (c) Smaller (C_0–C_3) alkyl PAH may be more readily oxidized to oxy-PAH. Since the relative abundance of the oxy-PAH is about twice the concentration of the PAH, the oxy-PAH are probably more

Table IV. Average Number of Alkyl Carbons for Each Compound Type in Diesel Particulate Extracts as a Function of Operating Condition

	full load			normal timing	
compound	advanced	normal	retarded	half load	no load
naphthalene		2.4	4.0	2.8	3.4
fluorene	3.3	2.4	2.6	2.4	3.8
phenanthrene	1.7	1.3	1.3	1.3	2.1
pyrene and fluoranthene	0.1	0.2	0.1	0.2	1.6
phenylnaphthalene	1.1	1.1	1.1	1.0	2.1
naphthalenecarboxaldehydes	1.4	1.3	1.9	2.1	3.4
fluoren-9-one	1.8	1.7	1.7	2.1	3.0
biphenylcarboxaldehydes	2.4	1.3	1.3	1.9	3.0
phenanthrenecarboxaldehydes	1.9	1.5	1.7	1.4	1.3
thioxanthen-9-one	0.9	0.8	0.8	0.7	1.1

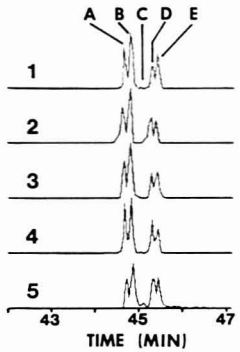


Figure 2. Mass chromatogram for methylphenanthrenes and methylanthracenes (peak A (3-methylphenanthrene), B (2-methylphenanthrene), C (2-methylanthracene), D (9-methylphenanthrene and 4-methylphenanthrene), and E (1-methylphenanthrene)) for hexane:toluene fraction of the advanced (1), normal (2), retarded timing (3), half load (4), and no load (5) samples.

stable in the exhaust or are formed in the exhaust. The low concentration of the unsubstituted compounds probably is not the result of exhaust temperature or boiling point of the compound because of the large range of exhaust temperatures and boiling points (naphthalene, bp 218 °C, and pyrene, bp 393 °C). At the lower engine exhaust temperature (no load), the amount of unsubstituted compound detected increased only for pyrene, phenanthrenecarboxaldehydes, and thioxanthen-9-one. For these compounds, the increase was 30 to 70 times the full load concentration but still not more than the alkyl homologues. Additional study will be required to more fully address this point.

CONCLUSIONS

Alkyl homologue analysis provides information about particulate bound diesel combustion products which are dependent on engine operating conditions. However, often only a few isomers of any single alkyl homologue have significant biological activity (*23*). Remembering that we desire to selectively decrease emission bioactivity as well as total extractable organics, we examined the individual methylphenanthrenes. The mass chromatograms for m/e 192 (methylphenanthrenes and methylanthracenes) of each sample are compared in Figure 2. Ratios for these alkyl homologue isomers do not indicate an obvious isomer specificity or dependence upon engine conditions. Thus, dependence of isomer concentration on engine condition is not a simple function of engine condition or is nonexistent.

The inverse relationship between engine temperature and production of extractable organics suggests one possible emission control strategy. Reduction of particulate associated organics might be achieved by a post combustion reactor. To evaluate the feasibility of such an engine design modification, both particulate and vapor emissions need to be collected simultaneously. This will allow proper correlation of particulate vapor partitioning with engine condition. Alkyl homologue analysis of diesel emissions provides information which may lead to selection of engine operating conditions that will reduce the environmental impact of diesel emissions.

ACKNOWLEDGMENT

We thank the Cummins Engine Co. for supplying the samples and Ming-Li Yu for helpful discussions.

Registry No. Naphthalene, 91-20-3; fluorene, 86-73-7; anthracene, 120-12-7; phenanthrene, 85-01-8; pyrene, 129-00-0; fluoranthene, 206-44-0; phenylnapthalene, 35465-71-5; naphthalenecarboxaldehyde, 30678-61-6; fluoren-9-one, 486-25-9; biphenylcarboxaldehyde, 55171-99-8; phenanthrenecarboxaldehyde, 77468-40-7; thioxanthen-9-one, 492-22-8.

LITERATURE CITED

(1) National Research Council "Diesel Cars Benefits, Risk, and Public Policy"; National Academy Press: Washington, DC, 1982; p 39.
(2) Huisingh, J.; Bradow, R.; Jungers, R.; Clayton, L.; Zweidinger, R.; Tejada, S.; Bumgarner, J.; Duffield, F.; Waters, M.; Simon, V. F.; Hare, C.; Rodriguez, C.; Snow, L. In "Application of Short-Term Bioassays in the Fractionation Mixtures"; Waters, M. D., Nesnow, S., Huisingh, J. L., Sandhu, S. S., Clayton, L., Eds.; Plenum Press: New York, 1979; pp 381–418.
(3) Schuetzle, D.; Lee, F. S.; Prater, T. J.; Tejada, S. B. *Int. J. Environ. Anal. Chem.* **1981**, *9*, 93–144.
(4) Rappaport, S. R.; Wang, Y. Y.; Wei, E. T. *Environ. Sci. Technol.* **1980**, *14*, 1505–1509.
(5) Barth, D. S.; Blacker, S. M. *J. Air Pollut. Control Assoc.* **1978**, *28*, 769–771.
(6) Santodonato, J.; Basu, D.; Howard, P. "Health Effects Associated with Diesel Exhaust Emissions"; U.S. Environmental Protection Agency: Washington, DC, 1978; EPA-600/1-78-063.
(7) National Research Council "Health Effects of Exposure to Diesel Exhaust"; National Academy Press: Washington, DC, 1981.
(8) Yergey, J. A.; Risby, T. H.; Lestz, S. S. *Anal. Chem.* **1982**, *54*, 354–357.
(9) Yu, M. L.; Hites, R. A. *Anal.* Chem. **1981**, *53*, 951–954.
(10) Choudhury, D. R. *Environ. Sci. Technol.* **1982**, *16*, 102–106.
(11) Newton, D. L.; Erickson, M. D.; Tomer, K. B.; Pellizzari, E. D.; Gentry, P. *Environ. Sci. Technol.* **1982**, *16*, 206–213.
(12) Pitts, J. N.; Lokensgard, D. M.; Harger, W.; Fisher, T. S.; Mejia, V.; Schuler, J. J.; Scorziell, G. M.; Kartzenstein, Y. A. *Mutat. Res.* **1982**, *102*, 241–249.
(13) Schuetzle, D.; Riley, T. L.; Prater, T. J.; Harvey, T. M.; Hunt, D. F. *Anal. Chem.* **1982**, *54*, 265–271.
(14) Karasek, F. W.; Smythe, R. J.; Laub, R. J. *J. Chromatogr.* **1974**, *101*, 125–136.
(15) Erickson, M. D.; Newton, D. L.; Pellizzari, E. D.; Tomer, K. B. *J. Chromatogr.* **1979**, *17*, 449–454.
(16) Prater, T. "Capillary Column GC/MS Characterization of Diesel Exhaust Particulate Extracts"; EPA Diesel Emission Symposium: Research Triangle Park, NC, Oct 1981.
(17) Rosenkrantz, H. S. *Mutat. Res.* **1982**, *101*, 1–10.
(18) Barfknecht, T. R.; Anden, B. M.; Thilly, W. G.; Hites, R. A. In "Polynuclear Aromatic Hydrocarbons"; Cooke, M., Dennis, A. J., Eds.; Battelle Press: Columbus, OH, 1981; pp 231–242.

(19) LaVoie, E. J.; Tulley, L.; Bedenko, V.; Hoffman, D. *Mutat. Res.* **1981**, *91*, 167–176.
(20) Yu, M. L., Cummins Engine Co., Columbus, IN, personal communication, 1982.
(21) Lee, F. S. C.; Schuetzle, D. In "Handbook of Polycyclic Aromatic Hydrocarbons"; Bjorseth, A., Ed.; Marcel Dekker: New York, 1982; Chapter 11.
(22) Schuetzle, D. *Environ. Health Perspect. J.*, in press.
(23) Kaden, D. A.; Hites, R. A.; Thilly, W. G. *Cancer Res.* **1979**, *39*, 4152–4159.

RECEIVED for review September 28, 1982. Accepted January 13, 1983. This work was supported by the U.S. Department of Energy (Grant No. 80-EV-10449).

Determination of Oxygenated Polycyclic Aromatic Hydrocarbons in Airborne Particulate Matter by Capillary Gas Chromatography and Gas Chromatography/Mass Spectrometry

Johann König,* Eckhard Balfanz, Werner Funcke, and Thomas Romanowski

Fraunhofer-Institut für Toxikologie und Aerosolforschung, Nottuiner Landweg 102, D 4400 Münster-Roxel, Federal Republic of Germany

By use of a two-step column chromatographic separation of crude extracts from airborne particulate matter, a special fraction was separated which contained mainly oxygenated polycyclic aromatic hydrocarbons (OXPAH). The analysis was made by capillary gas chromatography (GC) and capillary gas chromatography/mass spectrometry (GC/MS). A total of 38 individual compounds belonging to five different groups of substances (ketones, quinones, anhydrides, coumarines, and aldehydes) were characterized by their retention indexes and mass spectra.

In addition to the regular well-described polycyclic aromatic hydrocarbons (PAH), many oxygenated PAH (OXPAH) may be associated with particulate matter in ambient air. For instance, model experiments on chemical and, particularly, photochemical PAH stability suggest that several of the PAH that are emitted in sizable amounts from various natural and anthropogenic sources are degraded in the atmosphere by sunlight or by interactions with other reactive airborne species (*1–10*). To some extent, relatively stable oxidation products like quinones, ketones, aldehydes, coumarines etc. are generated by these reactions. Furthermore, analytical investigations of various source emissions have shown that oxygenated PAH may readily be formed by incomplete combustion of organic material (*11–18*). Recently, these compounds were investigated in more detail, particularly in the exhaust of diesel engines (*12–15*). Several components like quinones, ketones, dicarboxylic acid anhydrides, hydroxy compounds, etc. have been characterized. In spite of a variety of potential sources for these compounds, only a few OXPAH were actually detected, mostly associated with general airborne particulate matter (*19–24*). In most cases, they were not found as a result of systematic investigations but by chance. For instance, they were identified as part of the extract from airborne particulate matter in analyses of the polar fraction of the neutral portion collected by the classical extract separation into acidic, basic, and neutral portions (*23, 24*). By intent, only a few quinones of PAH in ambient air were investigated (*19*). Their concentrations were monitored over an extended period of time in order to assess the photochemical stability of the parent PAH by correlating the variations in concentration with meterological conditions. Obviously, a main reason for the lack of information on OXPAH in the atmosphere may be that, from the environmental hygiene point of view, these were not of special interest, up to now.

However, recent investigations on diesel exhaust have shown that the so-called moderately polar fraction, which normally contains the OXPAH, exhibits a considerable direct-acting Ames mutagenicity (*15*). In contrast to most of the mutagenic parent-PAH (*25*), these substances require no activation by mammalian enzymes to cause mutagenic responses. It is easy to imagine that similar compounds may also occur in association with general airborne particulate matter. Thus, it would be of special interest to determine their airborne concentration and the direct-acting mutagenic activity.

The aim of the work described here is to set the stage for such investigations by extracting airborne particulate matter and separating an extract fraction that contains, as far as possible, OXPAH only. In this fraction, as many substances as possible will be characterized.

EXPERIMENTAL SECTION

Particulate Collection and Extraction. Airborne particulate matter was collected during the months of February to April of 1982 on the flat roof of a house in the center of Duisburg (Ruhr area) approximately 15 m above street level. The sampling device was a high volume air sampler (type HV 100, manufactured by Sartorius, Göttingen) equipped with a filter head containing a glass fiber filter (type SM 13400, supplied by Sartorius, Göttingen) with a surface area of about 520 cm^2. The filters were replaced weekly after passage of about 8000 m^3 of air. Immediately following each collection period the filters with their deposits of particulate matter were subjected to a Soxhlet extraction by toluene for 8 h.

Liquid Chromatography. The extract contains various overlapping classes of substances, and the concentrations of oxygenated PAH are relatively low in comparison to substances of some other chemical groups in this fraction. Therefore, it is nearly impossible to characterize or identify more than a few, if any, individual substances without any further cleanup procedures. Thus, a two-step fractionation was performed prior to each analysis. For separating nonpolar substances like alkanes, PAH, etc. which are normally present in relatively high concentrations, the toluene extract was first prefractionated on a silica column (2.5 cm i.d., l = 20 cm; Kieselgel 60, 70–230 mesh, supplied by Merck, inactivated with 15% H_2O). For this purpose, 3 g of silica gel were added to the toluene extract. By rotary evaporation at 30 °C the solvent was removed under reduced pressure and the adsorbed residue was added to the top of the silica column. In the first step, the nonpolar substances were eluted with 450 mL of cyclohexane. Tests with several reference substances of the

0003-2700/83/0355-0599$01.50/0 © 1983 American Chemical Society

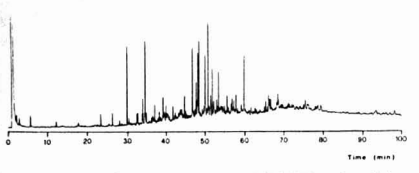


Figure 1. Typical GC trace of an isolated OXPAH-fraction utilizing a 25-m OV-73 glass capillary (conditions see text).

OXPAH group (9*H*-fluorene-9-one, anthracene-9,10-dione, benz[*a*]anthracene-7,12-dione, 11*H*-benzo[*a*]fluorene-11-one, 11*H*-benzo[*b*]fluorene-11-one, dibenzo[*a*,*h*]pyrene-7,14-dione) confirmed that these substances were not eluted during this step. After removal of the nonpolar substances, cyclohexane as the mobile phase was replaced by benzene because, in previous experiments, benzene proved to be the most suitable solvent for the elution of the moderately polar substances. About 220 mL of the benzene eluate was collected constituting the so-called moderately polar fraction. Mass spectrometric studies showed that, besides the OXPAH under consideration, numerous polar aliphatic and simple aromatic compounds were present in this fraction. Therefore, a further separation step with the chromatographic system Sephadex LH-20/2-propanol was necessary. This system not only facilitates the separation of aliphatic from aromatic compounds but elutes the aromatic substances in an order of increasing ring number (*27*, *28*). The solvent of the moderately polar fraction obtained in the first separation step was closely reduced to dryness by rotary evaporation. After about 1 mL of 2-propanol was added, the residue was fractionated by a Sephadex column (1.8 cm i.d., l = 28 cm; Sephadex LH-20, supplied by Deutsche Pharmacia, Freiburg; 2-propanol, 0.7 mL/min). After a prefraction of 59 mL, a so-called OXPAH fraction of 360 mL starting with 9*H*-fluorene-9-one and including at least compounds as large as the dibenzopyrenequinones was obtained. In addition, the chromatographic separation was monitored by means of a UV photometer at a wavelength of 281 nm.

Gas Chromatography/Mass Spectrometry. After addition of three internal standards (naphthalene, phenanthrene, and chrysene) and concentration of the sample by rotary evaporation, the OXPAH fraction was analyzed by means of a Perkin-Elmer gas chromatograph F22 equipped with a FID and connected to a Trilab computing integrator. With a 25-m glass capillary (0.32 mm i.d.) coated with 0.3 μm OV-73, the following chromatographic conditions were applied: oven temperature 4 min at 100 °C, 3 °C/min to 300 °C, hold at 300 °C; injector and detector temperature 300 °C; split 1:50; carrier gas helium at 1.2 bar. The substances separated so far were characterized by special retention indexes (cf. ref 29) as well as by runs of a modified Finnigan 4021 GC-MS system (*26*) equipped with a 30-m fused silica capillary (0.32 mm i.d.) coated with 0.25 μm SE-30. The following chromatographic conditions were used: linearly programmed oven temperature from 120 °C to 280 °C at a rate of 2 °C/min and hold at 280 °C; injector and interface temperature 300 °C; split 1:50; carrier gas helium at 0.6 bar. All mass spectrometric measurements were made in the EI mode at 70 eV with scanning from 50 to 400 amu every 1 s.

RESULTS AND DISCUSSION

All OXPAH fractions isolated from airborne particulate matter yielded qualitatively similar gas chromatograms. An example is shown in Figure 1. The reconstructed ion current (RIC), Figure 2, resulting from GC/MS analysis corresponds very well with the gas chromatograms obtained by FID. Thus an exact assignment of the individual substance peaks was feasible. By comparison of retention indexes and, mainly, by means of the mass spectra, 38 different consecutively numbered oxygenated PAH in the RIC were characterized in the OXPAH fraction in more detail. In addition to the OXPAH, some N-containing PAH were present in this fraction. Among these the most intensive peaks are marked a–d in Figure 2. Within the scope of this investigation, these compounds will not be further discussed. The peaks in Figure 2 marked by S2 and S3 correspond to phenanthrene (S2) and chrysene (S3), respectively. Both of these substances were added to the individual samples together with naphthalene in order to calculate the retention indexes. On the basis of the fragmentation patterns and of the molecular weights determined by mass spectrometry, the 38 characterized substances were divided into the following five classes of substances: ketones, quinones, anhydrides, coumarines, and aldehydes. A typical mass spectrum for each group is shown in Figure 3. The substances of all groups are specified in Table I.

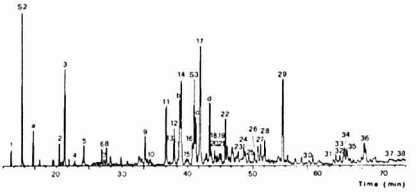


Figure 2. RIC for the GC/MS analysis of the OXPAH fraction utilizing a 30-m SE 30 fused silica capillary; numbered peaks are listed in Table I; for lettered peaks see text.

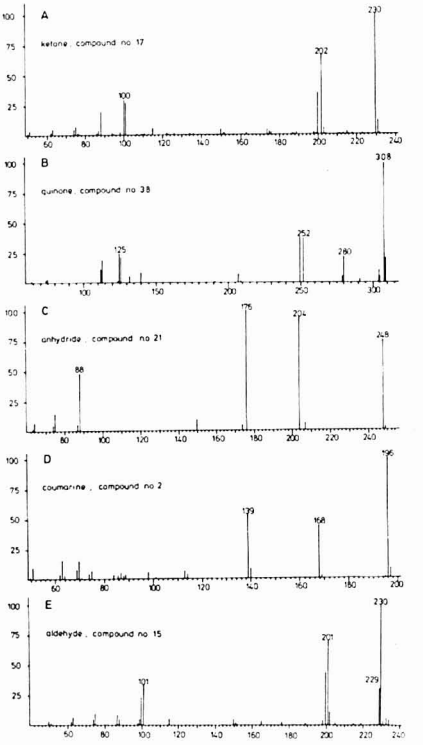


Figure 3. Typical examples for mass spectra of the compound classes found in the OXPAH fraction: (A) ketones, (B) quinones, (C) anhydrides, (D) coumarines, (E) aldehydes.

Table I. Compounds in the OXPAH-Fraction

no.	index	main fragments at 70 eV ionization energy [a]	proposed compd (index of ref subst)	concn range, ng·m^{-3}
		Ketones		
1	293.09	180 (100), 152 (50), 151 (10), 150 (10), 76 (29)	9*H*-fluorene-9-one (293.07)	0.06-0.60
5	342.87	204 (100), 176 (46), 174 (9), 88 (34)	ketone from a PAH with mol wt 190	<0.05-0.92
11	386.13	230 (100), 202 (27), 200 (26), 101 (27), 100 (17)	11*H*-benzo[*a*]fluorene-11-one [b] (385.96)	0.24-2.58
12	390.44	230 (100), 202 (80), 200 (38), 101 (30), 100 (30)	ketone from a PAH with mol wt 216	0.12-1.24
13	391.85	218 (100), 189 (72), 94 (57)	methyl from a ketone with mol wt 204	0.05-0.80
14	394.04	230 (100), 202 (32), 200 (27), 101 (26), 100 (11)	11*H*-benzo[*b*]fluorene-11-one [b] (394.08)	0.30-2.35
17	404.39	230 (100), 202 (67), 200 (36), 101 (21), 100 (36)	7*H*-benz[*de*]anthracene-7-one (404.27)	0.46-3.66
18	410.89	244 (100), 215 (41, 45, 59, 40),	methyl from ketones with mol wt 230 [c]	0.12-0.91
19	414.03	108 (7, 17, 20, 16)		0.09-0.51
20	414.50			0.05-0.40
23	423.43			0.05-0.42
26	430.96	254 (100), 226 (10, 17, 22, 47),	ketones from PAH with mol wt 240 [c]	0.06-0.47
27	434.17	225 (4, 12, 12, 0), 224 (29, 24, 22, 27)		0.06-0.58
28	436.52	113 (23, 26, 35, 57), 112 (21, 27, 22, 15)		0.09-0.74
29	446.00			0.40-3.11
31	469.51	280 (100), 252 (11, 12, 14),	ketones from PAH with mol wt 266 [c]	<0.05-0.36
32	471.16	250 (20, 20, 14), 126 (12, 13, 9),		0.06-0.60
34	474.45	125 (12, 18, 12)		0.11-0.76
35	476.96	278 (100), 250 (27), 248 (21), 125 (48), 124 (27)	ketone from a PAH with mol wt 264	0.07-1.03
36	485.11	280 (100), 252 (39), 250 (27), 126 (27), 125 (30)	ketone from a PAH with mol wt 266	0.06-0.95
		Quinones		
3	331.09	208 (100), 180 (97), 152 (95), 76 (87)	anthracene-9,10-dione (330.98)	0.22-1.89
6	352.74	222 (92), 207 (12), 194 (49), 165 (100)	methyl from anthracene-9,10-dione [d]	0.07-0.50
22	416.46	258 (100), 230 (37), 202 (77), 200 (32), 101 (49), 100 (12)	benz[*a*]anthracene-7,12-dione (416.38)	0.29-1.05
24	426.25	258 (100), 230 (31), 202 (54), 200 (28), 101 (28), 100 (14)	naphthacene-5,12-dione (426.23)	0.11-0.54
30	462.45	282 (100), 254 (35), 226 (16), 224 (19), 127 (10), 113 (21), 112 (17)	quinone from a PAH with mol wt 252	<0.05-0.38
37	496.63	308 (100), 280 (35, 20), 252 (60, 36),	quinones from PAH with mol wt 278 [c]	<0.05-0.37
38	[e]	250 (62, 35), 140 (11, 11), 126 (42, 19), 125 (42, 22)		<0.05-0.40
		Anhydrides		
4	341.19	198 (57), 154 (95), 126 (100), 63 (42)	naphthalene-1,8-dicarboxylic acid anhydride (341.25)	[f]
21	427.82	248 (75), 204 (93), 176 (100), 88 (46)	dicarboxylic acid anhydride from a PAH with mol wt 202	[f]
29	471.16	272 (49), 228 (53), 200 (100), 100 (54)	dicarboxylic acid anhydride from a PAH with mol wt 226	[f]
		Coumarines		
2	328.92	196 (100), 168 (43), 140 (9), 139 (52), 70 (16)	coumarine from a PAH with mol wt 178	<0.05-1.26
9	377.19	220 (100), 192 (19), 164 (8), 163 (43), 82 (34)	coumarine from a PAH with mol wt 202	0.11-1.33
21	415.75	246 (100), 218 (22), 190 (7), 189 (38), 94 (13)	coumarine from a PAH with mol wt 228	<0.05-0.35
		Aldehydes		
7	354.21	206 (100), 205 (28, 20), 178 (4, 29),	aldehydes from PAH with mol wt 178 [c]	<0.05-0.57
8	356.11	177 (36, 39), 176 (42, 52)		<0.05-2.05
10	379.15	218 (63), 217 (—), 189 (100), 94 (37)	methyl from an aldehyde with mol wt 204	<0.05-0.36
15	395.14	230 (100), 229 (46, 78), 202 (7, <1),	aldehydes from PAH with mol wt 202 [c]	<0.05-0.36
16	397.49	201 (72, 83), 200 (39, 31)		<0.05-0.63

[a] First fragment corresponds to the molecular ion peak; relative intensities are given in parentheses. [b] Reference substance was obtained by photooxidation of the corresponding benzofluorenes. [c] Compounds with similar mass spectra; in each case the M^+ peak is the base peak; the relative intensities given for the other fragment ions are listed along with the individual substances. [d] Due to the measured index 2-methylanthracene-9,10-dione can be excluded. [e] Index cannot be calculated; compound is eluted in the isothermal range. [f] Compound is not eluted quantitatively in the OXPAH fraction.

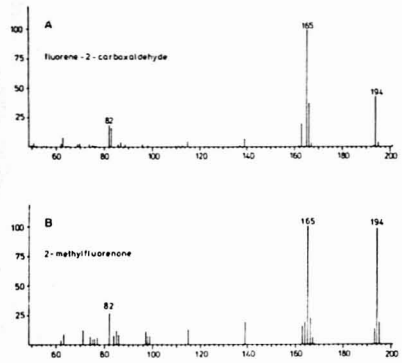


Figure 4. Mass spectra of a carboxaldehyde containing a CH_2 group and of a methylated ketone: (A) fluorene-2-carboxaldehyde, (B) 2-methylfluorenone.

The first column of the table shows the number of the individual substances according to the numbering in the RIC (Figure 2). The retention indexes of the characterized substances are tabulated in column 2. Due to the scarcity of reference compounds, further characterization by retention indexes was possible in only a few cases (see retention indexes in column 4). Thus, a precise nomenclature in column 4 is given only for these substances. Column 3 shows some main fragments from the mass spectra with their relative intensities in parentheses. The concentration range of the OXPAH given in column 5 is determined in relation to the internal chrysene standard without considering any response factors.

The main group of 20 substances is constituted of *ketones*. There was no problem in classifying the unsubstituted ketones. In some cases, these substances, by their molecular weight, could also be aldehydes of other parent PAH but this is not confirmed by the fragmentation in the mass spectra (compare Figure 3A and 3E). In the mass spectra of the unsubstituted ketones specified in Table I, the $[M - 1]^+$ peak as well as the $[M - 29]^+$ peaks (typical for aldehydes and normally uncommon for ketones) are missing. In contrast to the unsubstituted ketones, such classification is ambiguous for the substances **13**, **18**, **19**, **20**, and **23** denoted as methyl ketones. On the one hand, the aldehydes of PAH containing a CH_2 group, under certain circumstances give a $[M - 1]^+$ peak of relatively low intensity; see, e.g., fluorene-2-carboxaldehyde (Figure 4A).

On the other hand, methylated PAH ketones like 2-methylfluorenone (Figure 4B) show a very intensive $[M - 29]^+$ peak (*30*). Therefore, a classification as methyl ketones was based only on the fact that, in contrast to fluorene-2-carboxaldehyde, their molecular ion peak is the base peak as in the case for 2-methylfluorenone.

Only four of the ketones listed in Table I could be further identified by retention indexes of reference substances. The identity of the other compounds of this group is ambiguous, but the unsubstituted ketones will probably be 9*H*-cyclopenta[*def*]phenanthrene-9-one (**5**), 6*H*-benzo[*cd*]pyrene-6-one (**29**), and anellated derivatives of the following three different basic structures: 9*H*-fluorene-9-one, phenalene-1-one, and 9*H*-cyclopenta[*def*]phenanthrene-9-one.

Two of these compounds, 9*H*-cyclopenta[*def*]-phenanthrene-9-one and 6*H*-benzo[*cd*]pyrene-6-one, were already detected in carbon black (*17*, *31*) and the latter was also found in the emissions from peat and wood combustion (*16*). Of all the ketones in Table I, up to now only 9*H*-fluorene-9-one (*32*) and 7*H*-benz[*de*]anthracene-7-one (*22–24*, *33*) were detected in airborne particulate matter. On the other hand, some of the papers quoted above identified some other ketones in airborne particulate matter like phenalene-1-one, xanthene-9-one, and 7*H*-dibenzo[*c*,*h*]xanthene-7-one, which were not found in this study.

The second class of substances listed in Table I is made up of *quinones*. Their mass spectra generally show a typical 2-fold loss of carbon monoxide (see Figure 3B). With the exception of **6**, the molecular ion signal is observed to be the base peak. This indicates that all these substances are *p*-quinones, because in the case of *o*-quinones the $[M - 28]^+$ peak will normally constitute the base peak (*34*). The major signal which appears in the spectrum of **6**, presumably a methylated anthracene-9,10-dione, is observed at m/e 165. As proposed for the mass spectra of alkylfluorenones (*30*), this signal may arise from a substituted tropylium cation formed by successive loss of one hydrogen atom and two molecules of carbon monoxide. The amount of the quinones characterized in the present study is relatively small in comparison to the huge number of quinones that could result theoretically from PAH which, so far, have been identified in particulate matter from ambient air. Beside their relatively low concentration, the low volatility of these substances may be the main reason for the difficult gas chromatographic detection, especially of those quinones deriving from PAH with a molecular weight higher than 252. In the course of other investigations on airborne particulates, anthracene-9,10-dione and dibenzo[*cd*,*jk*]pyrene-6,12-dione (anthanthrone) were directly detected by gas chromatography (*24*). Furthermore, by means of other analytical methods, three isomeric quinones of benzo[*a*]pyrene and dibenzo[*b*,*def*]chrysene-7,14-quinone were identified (*19*).

Regarding the group of *anhydrides*, only three different compounds were detected. One of these compounds was identified by its retention index as naphthalene-1,8-dicarboxylic acid anhydride. The other two compounds are assumed to be oxidation products of PAH with a molecular weight of 202 (e.g., acephenanthrylene or aceanthrylene) and 226 (e.g., cyclopenta[*cd*]pyrene), respectively. Firstly, the five-membered ring of these compounds is readily oxidizable due to the outstanding olefinic nature of the existing carbon double bond, and, secondly, at least the pyrene-1,10-dicarboxylic acid anhydride as a possible derivative of the cyclopenta[*cd*]pyrene was identified not only on soot particles from diesel exhaust (*13*) but also in other environmental samples (*17*, *31*). In contrast to the oxygenation of a five-membered ring, an oxidative opening of an ortho-anellated terminal benzene ring of PAH with a molecular weight of 228 and 252, respectively, accompanied by the loss of a C_2 unit would also be a plausible way of formation of these two compounds. However, this way seems to be very unlikely. Up to now, it was observed only once during the photochemical degradation of anthracene on carbon microneedles of a field desorption mass spectrometer (*1*). In view of the fact that the anhydrides are not eluted exclusively into the OXPAH fraction (compare Table I), it is reasonable to assume that additional components of this group of substances may exist in ambient air. Although these PAH carboxylic acid anhydrides are obviously emitted by combustion processes (*15*), they were not detected in airborne particulate matter prior to this investigation.

Apart from the *coumarine* itself (*23*) which, however, cannot be incorporated in the group of OXPAH, up to now no other anellated compounds containing such a structural element were found in emissions and in airborne particulate matter. In the OXPAH fractions described here, three compounds are proposed to be coumarines. In view of the mass spectral fragmentation pattern (Figure 3D), substance no. 2 could be 9*H*-xanthene-9-one (xanthone) as well as benzo[c]coumarine,

which was found, for instance, among others during photochemical degradation of phenanthrene (*35*). However, the retention index of xanthone (313.67) indicates that it may be a coumarine. Lacking a corresponding reference substance, there is no proof that this compound is, in fact, benzo[*c*]-coumarine. The similarity of the mass spectra of the two compounds at choice may probably be one reason why, in contrast to this study, other authors have proposed the existence of xanthone in airborne particulate matter (*22*). Another reason may be that the library of spectra commonly used for the automatic interpretation of mass spectra normally contains the xanthone only and no benzocoumarine. As reasoned for **2**, substances **9** and **21** are proposed to be coumarines too, although it cannot be excluded that **21** may be an anellated xanthone.

Although numerous *aldehydes* were found in diesel exhaust, the five compounds in the aldehyde group of Table I are the first aldehydes detected in airborne particulate matter. With the exception of **10**, all compounds show a mass spectral fragmentation pattern typical for aldehydes (see Figure 3E). In contrast, to the other aldehydes, no $[M - 1]^+$ peak occurs in the mass spectrum of **10** and, thus, it could be a methylated ketone as well. Due to the fact, however, that the intensity ratio of the M^+ and $[M - 29]^+$ peak (base peak signal) was very similar to the ratio of these peaks observed in the mass spectrum of fluorene-2-carboxaldehyde (compare the discussion concerning the classification of the methylated PAH ketones), this compound was included in the aldehyde group.

Finally, considering the concentrations of the OXPAH as presented in column 5 of Table I, it becomes obvious that the concentrations of some of these compounds are undoubtedly comparable with those of benzo[*a*]pyrene observed in highly polluted areas (*36*). Therefore, in view of the direct-acting mutagenicity mentioned above, the OXPAH fraction may be of special interest from the environmental hygiene point of view.

ACKNOWLEDGMENT

The authors wish to thank W. Stöber for helpful discussion and aid in preparing the manuscript.

Registry No. **1**, 486-25-9; **3**, 84-65-1; **4**, 81-84-5; **11**, 479-79-8; **14**, 3074-03-1; **17**, 82-05-3; **22**, 2498-66-0; **24**, 1090-13-7.

LITERATURE CITED

(1) Barofsky, D. F.; Baum, E. J. *J. Am. Chem. Soc.* **1976**, *98*, 8286.
(2) Fatiadi, A. J. *Environ. Sci. Technol.* **1967**, *1*, 570.
(3) Fox, M. A.; Olive, S. *Science* **1979**, *205*, 582.
(4) Korfmacher, W. A.; Natusch, D. F. S.; Taylor, D. R.; Mamantov, G.; Wehry, E. L. *Science* **1980**, *207*, 763.
(5) Kortüm, G.; Braun, W. *Justus Liebigs Ann. Chem.* **1960**, *632*, 104.
(6) Kuratsune, M.; Hirohata, T. *Natl. Cancer Inst. Monogr.* **1962**, *9*, 117.
(7) Lane, D. A.; Katz, M. *Adv. Environ. Sci. Technol.* **1977**, *8* (Part 2), 137.
(8) Tebbens, B. D.; Mukai, M.; Thomas, J. F. *Am. Ind. Hyg. Assoc. J.* **1971**, *32*, 365.
(9) Pitts, J. N., Jr.; Van Cauwenberghe, K. A.; Grosjean, D.; Schmid, J. P.; Fritz, D. R.; Belser, W. L., Jr.; Knudson, G. B.; Hynds, P. M. *Science* **1978**, *202*, 515.
(10) Pitts, J. N., Jr.; Lokensgard, D. M., Ripley, P. S.; Van Cauwenberghe, K. A.; Van Vaeck, L.; Shaffer, S. D.; Thill, A. J.; Belser, W. L., Jr. *Science* **1980**, *210*, 1347.
(11) Pasternak, M.; Zinn, B. T. *Combust. Flame* **1981**, *41*, 335.
(12) Erickson, M. D.; Newton, D. L.; Pellizzari, E. D.; Tomer K. B. *J. Chromatogr. Sci.* **1979**, *17*, 449.
(13) Rappaport, S. M.; Wang, Y. Y.; Wei, E. T.; Sawyer, R.; Watkins, B. E.; Rapoport, H. *Environ. Sci. Technol.* **1980**, *14*, 1505.
(14) Schuetzle, D.; Lee, F. S.-C.; Prater, T. J.; Tejada, S. B. *Int. J. Environ. Anal. Chem.* **1981**, *9*, 93.
(15) Schuetzle, D. "Sampling of Vehicle Emissions for Chemical Analysis and Biological Testing", presented at the Karolinska Institute Symposium on Biological Tests in the Evaluation of Mutagenicity and Carcinogenicity of Air Pollutants, Stockholm, Sweden, Feb 8, 1982.
(16) Alsberg, T.; Stenberg, U. *Chemosphere* **1979**, *8*, 487.
(17) Stenberg, U. R.; Alsberg, T. E. *Anal. Chem.* **1981**, *53*, 2067.
(18) Herlan, A. *Staub-Reinhalt. Luft* **1978**, *38*, 276.
(19) Pierce, R. C.; Katz, M. *Environ. Sci. Technol.* **1976**, *10*, 45.
(20) Graedel, T. E. "Chemical Compounds in the Atmosphere"; Academic Press: New York, 1978.
(21) Jäger, J. *Z. Anal. Chem.* **1971**, *255*, 281.
(22) Epstein, S. S.; Mantel, N.; Stanley, T. W. *Environ. Sci. Technol.* **1968**, *2*, 132.
(23) Ketserides, G.; Hahn, J.; Jaenicke, R.; Junge, Ch. *Atmos. Environ.* **1976**, *10*, 603.
(24) Cautreels, W.; Van Cauwenberghe, K. *Atmos. Environ.* **1976**, *10*, 447.
(25) Salamone, M. F.; Heddle, J. A.; Katz, M. *Environ. Int.* **1979**, *2*, 37.
(26) Romanowski, T.; Funcke, W.; König, J.; Balfanz, E. *HRC CC, J. High Resolut. Chromatogr. Chromatogr. Commun.* **1981**, *4*, 209.
(27) Oelert, H. H. *Fresenius' Z. Anal. Chem.* **1969**, *224*, 91.
(28) Klimisch, H.-J. *Z. Anal. Chem.* **1973**, *264*, 275.
(29) Lee, M. L.; Vassilaros, D. L.; White, C. M.; Novotny, M. *Anal. Chem.* **1979**, *51*, 768.
(30) Yu, M.-L.; Hites, R. A. *Anal. Chem.* **1981**, *53*, 951.
(31) Gold, A. *Anal. Chem.* **1975**, *47*, 1469.
(32) Shultz, J. L. *Fuel* **1972**, *51*, 242.
(33) Pierce, R. C.; Katz, M. *Environ. Sci. Technol.* **1975**, *9*, 347.
(34) McCaustland, D. J.; Fischer, D. L.; Kolwyck, K. C.; Duncan, W. P.; Wiley, J. C., Jr.; Menon, C. S.; Engel, J. F.; Selkirk, J. K.; Roller, P. P. In "Carcinogenesis, Vol. 1. Polynuclear Aromatic Hydrocarbons: Chemistry, Metabolism and Carcinogenesis"; Freudenthal, R. I., Jones, P. W., Eds.; Raven Press: New York, 1976; p 349.
(35) Patel, J. R.; Politzer, I. R.; Griffin, G. W.; Laseter, J. L. *Biomed. Mass Spectrom.* **1978**, *5*, 664.
(36) Funcke, W.; König, J.; Balfanz, E.; Romanowski, T.; Grossmann, I. *Staub-Reinhalt. Luft* **1982**, *42*, 192.

RECEIVED for review October 4, 1982. Accepted December 13, 1982.

Spectrophotometric Determination of Atmospheric Nitrogen Monoxide and Nitrogen Dioxide after Collection with [*N*,*N*′-Ethylenebis(salicylideniminato)]cobalt

Koichiro Ishii* and Kazuyuki Aoki

Tokyo Metropolitan Research Institute for Environmental Protection, Yurakucho 2-7-1, Chiyoda-ku, Tokyo 100, Japan

A new method for sampling and determining NO and NO_2 in the atmosphere is investigated. Atmospheric NO and NO_2 are collected in a solution of [*N*,*N*′-ethylenebis(salicylideniminato)]cobalt (Co(salen)) in *o*-dichlorobenzene. NO reacts with Co(salen) reversibly yielding a nitrosyl complex (Co(salen)NO), which is converted to a nitro complex by air oxidation in the copresence of aminoethanethiol in an 83% yield. NO_2 is absorbed by Co(salen) solution irreversibly. The product compound can easily be decomposed by stripping with aqueous alkaline solution, yielding the NO_2^- ion quantitatively. The nitro compound and the NO_2^- were quantified spectrophotometrically with a Griess-type reagent. In usual sampling conditions, O_3, NH_3, SO_2, CO, and H_2O did not interfere with the present method. The detection limits were 2 ppb·h (NO) and 1 ppb·h (NO_2).

Nitrogen monoxide (NO) is emitted as exhaust gas from automobiles and industrial plants into the atmosphere, and is photooxidized to the more toxic nitrogen dioxide (NO_2) (*1–4*). Moreover, these nitrogen oxides as well as reactive hydrocarbons are known to cause photochemical smog formation (*1–3*).

Chemiluminescence methods (CLD) for the two oxides (*5*) in ambient air have been widely used because of their ability to detect NO and NO_x (NO + NO_2) even at low concentrations. However, no appropriate wet chemical techniques for direct measurement of NO have been developed. Only a modified Griess-Saltzman method for continuous NO_2 measurement is being used for continuous NO measurement (*6, 7*). In this conventional method, NO is indirectly determined by oxidizing it to NO_2, measuring the NO_2, and then converting the results to NO concentration. However, this oxidation step is not yet clarified, and various oxidizers such as CrO_3 have been tested (*8*).

Recently, Neadeau et al. (*9*) have reported a method for measuring NO by electron spin resonance (ESR) using a free radical reagent. A simultaneous measuring technique of NO and NO_2 has been tried by polarography under a nitrogen atmosphere using Fe(edta) (*10*). Much research has been done on the absorbing method of NO with use of metal complexes.

Among many such metal complexes, the authors have been interested in [*N*,*N*′-ethylenebis(salicylideniminato)]cobalt (Co(salen)) which was reported to take up NO irreversibly (*11*) and to take up O_2 reversibly (*12*). In an inert solvent such as chloroform, Co(salen) absorbs NO to form a five-coordinate nitrosyl compound (Co(salen)NO) (*11*). NO, coordinated to Co(salen) and its ring-substituted derivatives, is known to form nitro compounds by reaction with oxygen (*13*). This reaction needs bases

$$\text{Co(salen)NO} + {}^1/_2\text{O}_2 + \text{B} \rightleftharpoons \text{Co(salen)NO}_2 \quad (1)$$

where B represents a Lewis base such as pyridine or tributylphosphine. This reaction offers two suggestions for collection and determination of atmospheric NO, i.e., (1) Co(salen)NO formed in the absorbing solution disappears by reacting with oxygen catalyzed by basic substances in ambient air (generally NH_3), and (2) NO can be spectrophotometrically determined by a Griess-type reagent, by converting Co(salen)NO to a nitro compound.

The present authors have investigated the fundamental characteristics of Co(salen) and found that Co(salen) solution in *o*-dichlorobenzene (*o*-DCB) absorbs directly NO_2 as well as NO at approximately 100% efficiency without the influence of oxygen in air, and that NO and NO_2 can be simultaneously determined spectrophotometrically by using one absorber. The details of examination on the conditions and procedures for simultaneous determination of NO and NO_2 are presented.

EXPERIMENTAL SECTION

Reagents. Co(salen) was synthesized according to the method reported by Nishikawa and Yamada (*14*). The absorbing solution was prepared by dissolving 32.5 mg of Co(salen) in 0.1 L of *o*-DCB. The Griess-type reagent was made by dissolving 20 g of sulfanilamide, 50 mg of *N*-(1-naphthyl)ethylenediamine dihydrochloride, and 50 mL of phosphoric acid in 1 L of distilled water. The aminoethanethiol (AET) solution was prepared by dissolving 1 g of AET hydrochloride in 0.1 L of ethanol and standardized by iodometry. All reagents were of analytical reagent grade and used without further purification.

NO gas, NO_2 gas, and NO standard gas for calibration of a CLD NO_x analyzer (Bendix 8108-B) were supplied from gas cylinders (Takachiho). Ozone was generated from O_2 by a silent arc discharge instrument, diluted by air, and monitored with a Bendix O_3 analyzer.

Apparatus. In studying O_3 interference, NO in Co(salen)NO was determined by the system similar to that used by Cox (*15*). Nitrogen was used as a carrier gas. In the reaction vessel was placed 5 mL of *p*-toluenesulfonic acid solution in 1-butanol (2% (w/v)). A 0.1 mL sample was injected into the solution by means of a syringe. NO dissociated from Co(salen)NO and was measured by the NO_x analyzer (*15*). Quantitative evaluation of the samples was performed by comparison with the standard NO gas on the basis of peak areas.

The concentration of Co(II) was measured by a atomic absorption spectrometer (Seiko SAS727).

Absorption Experiment. Figure 1 shows a schematic diagram of the absorption apparatus. NO and NO_2 gases diluted by N_2 or air (0.5–10 ppm) were bubbled into the absorbing solutions (5 mL) in the absorbing vessel. The absorbing vessel is a test tube (25 mL) into which Teflon tubing (1 mm i.d.) is inserted. The concentrations of NO and NO_2 at the outlet of the absorbing vessel were monitored with the CLD NO_x analyzer. The gas flow rate could be conditioned by drawing N_2 or air at ca. 130 mL/min.

Air Sampling. A sampling train was assembled by connecting in series the absorbing vessel, a solvent trap, an orifice, an air pump, and a gas meter. Air was bubbled into the absorbing solution (5 mL) for 2 h at the rate of ca. 130 mL/min.

Equilibrium Measurement. In the absorption experiment system (Figure 1), N_2 was bubbled into the absorbing solution of known ratios of [Co(salen)]/[Co(salen)NO] (from 1/5 to 5/1). The output NO concentration was measured.

Analytical Procedure for Determination of NO_2. When sampling was completed, 0.1 mL of methanol was added to the absorbing solution. After 20 min, the solution was shaken strongly

0003-2700/83/0355-0604$01.50/0 © 1983 American Chemical Society

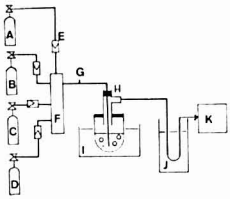


Figure 1. Schematic configurations of the apparatus for evaluation of NO and NO_2 absorption: (A) cylinder (NO in N_2), (B) cylinder (NO_2 in N_2), (C) cylinder (N_2), (D) cylinder (air), (E) orifice, (F) gas mixer, (G) hole for overiflow, (H) absorbing vessel, (I) thermostat, (J) ice trap, (K) CLD NO_x analyzer or both air pump and gas meter.

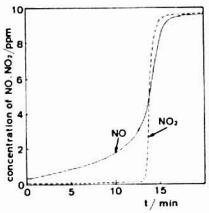


Figure 2. Concentration change of NO and NO_2 at the outlet of the absorbing vessel: inlet concentration, 9.8 ppm (NO and NO_2); concentration of Co(salen), 0.14 mM.

with 4 mL of $NaHCO_3$ solution (0.01 M) for 30 s. The aqueous layer was pipetted into a test tube (the organic layer was to be used for NO determination) and once washed with 2 mL of zinc diethyldithiocarbamate ($Zn(ddtc)_2$) solution in CCl_4 (0.5% (w/v)). To 3 mL of the washed aqueous layer, 2 mL of the Griess-type reagent was added. The absorbance was measured at 540 nm.

Analytical Procedure for Determination of NO. The organic layer from which NO_2 had been removed was shaken strongly with 5 mL of Micheal's buffer solution (pH 4, CH_3COOH–CH_3COONa) for 10 s. A small amount of anhydrous Na_2SO_4 was added to the washed organic layer for dehydration. Three milliliters of the dehydrated organic layer was pipetted into a centrifuge tube, and then 0.06 mL of *N*-ethylmorphorine solution in *o*-DCB (4% (v/v)) and 0.1 mL of AET solution were added. Twenty minutes were allowed for Co(salen)NO to react with AET, and then 4 mL of the Griess-type reagent was added. The mixture was shaken strongly for 30 s, was allowed to stand for more than 10 min, and was centrifuged (up 500*g*). The aqueous layer was carefully pipetted into an absorbing cell to measure the absorbance (at 540 nm).

The absorbed amounts of NO and NO_2 in the absorbing solution were calculated from the absorbance–concentration curves described below.

Calibration Curves. Known volumes of NO and NO_2 gases, adjusted to 0.5 ppm in nitrogen, were drawn through the absorbing solutions and the solutions were analyzed according to the analytical procedures. From the absorbances and the absorbed amounts of NO and NO_2, two absorbance–concentration curves were obtained.

RESULTS AND DISCUSSION

Absorption of NO and NO_2 by Co(salen) Solution. When 9.8 ppm of NO and NO_2 gases (in N_2) were separately passed into the system (Figure 1), the concentrations of NO and NO_2 at the outlet (C_{out} (ppm)) changed as shown in Figure 2. The same results were obtained in the case of air-diluted samples, meaning no influence of O_2. The efficiency of NO absorption decreased gradually according to the increasing amount of absorbed NO. The NO absorption efficiency (=1 − C_{out}/C_{in}, C_{in}: NO concentration (ppm) at the inlet of the absorbing vessel) can be related to NO vapor pressure (P_{NO} (atm)) and absorbed NO concentration, assuming the system is in equilibrium state

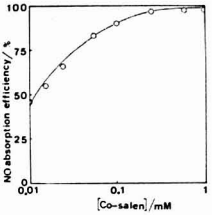


Figure 3. Relation between NO absorption efficiency (at $t \approx 0$, in Figure 2) and Co(salen) concentration: inlet concentration of NO, 9.8 ppm; volume of absorbing solution, 5 mL.

$$P_{NO} = C_{out}P_0 = \frac{[Co(salen)NO]}{[Co(salen)]_i - [Co(salen)NO]} \frac{1}{K_{P_{NO}}} \quad (2)$$

where P_0 denotes atmospheric pressure (atm), subscript i means initial state, and $K_{P_{NO}}$ is defined in eq 4. The relation between the efficiency of NO absorption (at $t \approx 0$, in Figure 2) and the concentration of Co(salen) solution is shown in Figure 3, at the rate of ca. 130 mL/min. The efficiency of NO absorption increases, when the concentration of Co(salen) increases. Because the solubility limit of Co(salen) in *o*-DCB is ca. 1 mM, the concentration of absorbing solution was set to be 1 mM. The NO absorption efficiency of the solution was at least 99% for sample gases containing 9.8–0.8 ppm NO.

On the other hand, the efficiency of NO_2 absorption was approximately 100%, independent of the amount of absorbed NO_2, until the Co(salen) solution was nearly saturated with NO_2, where the efficiency began to decrease rapidly (Figure 2).

NO- and NO_2–Co(salen) Complexes. The NO uptake by Co(salen) was found to be reversible by the following experimental results: (1) NO was regenerated by bubbling N_2 into or heating the Co(salen) solution saturated with NO, and (2) the Co(salen) solution, which had been once saturated with NO and heated to purge absorbed NO, absorbed again as the same amount of NO as in the former saturation.

On the other hand, the experiment with NO_2 was made in a similar way. As a result, it was found that 1 mol of NO_2 is irreversibly bound with 1 mol of Co(salen).

Stoichiometry and Equilibrium Constant of the Absorbing Reaction of NO. Since Hill's coefficient is 1, one molecule of NO binds with one molecule of Co(salen).

$$Co(salen) + NO \rightleftharpoons Co(salen)NO \quad (3)$$

The equilibrium constant $K_{P_{NO}}$, defined by eq 4, was determined in the temperature range of 35–65 °C.

$$K_{P_{NO}} = [Co(salen)NO]/([Co(salen)]P_{NO}) \quad (4)$$

Since the obtained $K_{P_{NO}}$ values were independent of N_2 flow rates, it could be concluded that this system was in equilibrium. $K_{P_{NO}}$ and enthalpy change ($\Delta H°$) of Co(salen)–NO, Co(salen)–O_2, and Fe(edta)–NO systems are summarized in Table I. Table I shows the following: (i) at room temperature, Co(salen) forms a more stable nitrosyl complex than Fe(edta) does, and (ii) theoretically, Co(salen) should absorb NO quantitatively even at the parts-per-billion level when the ratio of [Co(salen)NO]/[Co(salen)] is 0.01 or less.

Limit of Sampling Volume. Losses of NO from the absorbing vessel can be estimated by the following calculation: the concentration of Co(salen)NO in the absorbing solution is assumed to be represented by eq 5, where V_g, V_0, and V_l

$$[Co(salen)NO] = V_g C_{in}/(V_0 V_l) \quad (5)$$

Table I. Thermodynamic Data of NO and O_2 Coordination to Metal Complexes

system (metal complex-gas)	solvent	temp, °C	K_P, atm^{-1}	$\Delta H°$, kJ/mol
Co(salen)-NO	*o*-dichlorobenzene	35	4.5×10^7	−88.6
		50	1.1×10^7	
		65	2.4×10^6	
Co(salen)-O_2 (*16*)	pyridine	20	$>10^5$ [a]	−59
	dimethylformamide	20	640 [a]	−85
Co(salen)-O_2 (*17*)	0.1 M tetraethylammonium perchlorate	0	0.128 [b]	
		20	0.089 [b]	
Fe(edta)-NO (*18*)	water	60-70		−14.1 [c]
Fe(edta)-NO (*19*)	water	38.5	0.18×10^{-3} [d]	−15.8 [c]
		55.0	0.850×10^{-3} [d]	
		70.0	2.38×10^{-3} [d]	

[a] K ($L^4 \cdot mol^{-2}$) in eq 7. [b] In $torr^{-1}$. [c] In kcal/mol. [d] H/K_c.

denote volume of sampled air (L), molar volume (L), and volume of absorbing solution (L), respectively. Equation 6 is obtained from eq 4 and eq 5. The limiting volume of

$$C_{out}/C_{in} = V_g/(V_0(K_{P_{NO}}/P_0)V_l[\text{Co(salen)}]) \quad (6)$$

sampled gas, estimated with eq 6, is 125 L at 30 °C to maintain 99% absorption efficiency, theoretically.

Solvent. In polar solvents (*20*) such as pyridine, Me_2SO, and *N*,*N*-dimethylformamide, Co(salen) absorbs O_2 and consequently forms a dimeric μ-peroxo complex (*16*) which is less soluble and is likely to precipitate.

$$B + \text{Co(salen)} + O_2 \rightleftharpoons B\text{–Co(salen)}O_2 \quad (7)$$

$$B\text{–Co(salen)}O_2 + B\text{–Co(salen)} \rightleftharpoons B\text{–Co(salen)–O–O–Co(salen)–}B \quad (8)$$

Furthermore, this μ-peroxo species does not absorb NO.

On the contrary, in inert solvents (*20*) such as toluene, acetone, THF, 2,2′-dimethoxydiethyl ether, and benzene, Co(salen) neither absorbs O_2 nor forms a μ-peroxo complex (*16*). Among the most inert solvents, we selected *o*-DCB as the solvent, because its vapor pressure is low enough to minimize losses of solvent in air sampling.

It is recommended that fresh absorbing solution should be prepared at least every 2 weeks and that the stored absorbing solution should be heated to purge NO prior to use.

Determination of NO_2. Once NO_2 is collected in the absorbing solution, it remains stable at least for 24 h. Methanol was added so as to dissolve the precipitate formed by NO_2 absorption. To strip NO_2 into aqueous solutions, either $NaHCO_3$ solution (0.01 M) or NaOH solution (0.1 M) can be used. Absorbed NO_2 is stripped into the aqueous layer as NO_2^- in one shaking, and the absorbed NO remains in the organic layer. Next, for removal of any trace amount of Co(II), the aqueous layer was washed with $Zn(ddtc)_2$ solution.

A linear relationship was obtained between the absorbance of colored solution with the Griess-type reagent and the amount of absorbed NO_2. From this relation, and the volume change in the stripping operation together with molar absorptivity of NO_2^-, absorbed NO_2 was considered to be converted to NO_2^-, quantitatively.

Determination of NO. Once NO is collected in the absorbing solution, it disappears at the rate of 4%/day at 25 °C and of 2%/day at 0 °C. Remaining Co(salen), which interferes the development of color for determination of NO, has to be removed. When the organic layer containing Co(salen) and Co(salen)NO is washed with aqueous buffer solution (pH 4), 98% of the Co(salen) is removed from the organic layer; however Co(salen)NO remains in the organic layer. Though Co(salen)NO decomposes in a strong acid solution instantaneously, it does so very slowly (ca. 7%/h) at pH 4.

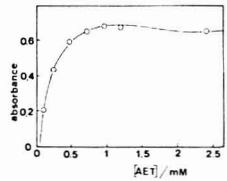


Figure 4. Relation between absorbance (at 540 nm) and AET concentration in *o*-DCB.

Since free AET is likely to suffer air oxidation, its hydrochloride was used and *N*-ethylmorphine was added as a neutralizer.

Oxidation of NO Group. It was not known until now how the NO group is oxidized with O_2 in the copresence of AET, but it seems to be similar to the mechanism reported by Clarkson and Basolo (*13*). In the case of using pyridine, which was used by Clarkson and Basolo (*13*) as a oxidation catalyst, in place of AET, oxidized Co(salen)NO solution did not make the Griess-type reagent color. Pyridine seems to prevent transference of the NO_2 group into the aqueous layer by coordinating the complex.

Appropriate Concentration of AET. The relation between AET concentration in the organic layer and the absorbance colored by the Griess-type reagent is shown in Figure 4. When the concentration of AET was higher than 1 mM, the absorbance was constant. In the lower concentration range of AET, the absorbance was lower because of incomplete oxidation of the NO group. From this result, the volume of AET solution (0.04 M) to be added to the organic layer (3 mL) was determined to be 0.1 mL.

Conversion Ratio of NO to NO_2^-. A linear relationship was obtained between the amounts of absorbed NO and the absorbances of color developed with the Griess-type reagent. The calibration curve varies with the volume of Griess-type reagent used (V). Moreover, the products of V and the absorbance (A) are not constant. Most of AET and Co(II) are extracted into the aqueous layer in this color development process. It was observed that the color development decreased according to the increasing concentrations of AET and Co(II) in the aqueous layer, i.e., the decreasing volume of the Griess-type reagent, V.

Values of $1/(AV)$, (mL^{-1}) obtained against V, (mL, in parentheses) were the following: 0.376 (4), 0.364 (5), 0.357 (6), 0.355 (7), 0.356 (8), 0.359 (9), 0.349 (10), 0.350 (13), 0.352 (17), and 0.345 (20). The relation between $1/(AV)$ and $1/V$ can be expressed as in eq 9, where $(AV)_0$ is the (AV) value

$$\frac{1/(AV)_0 - 1/(AV)}{1/(AV)} = \frac{k}{V} \quad (9)$$

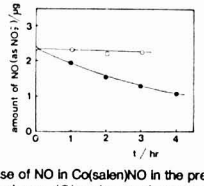


Figure 5. Decrease of NO in Co(salen)NO in the presence of NH_3: (O) under a N_2 atmosphere; (●) under an air atmosphere.

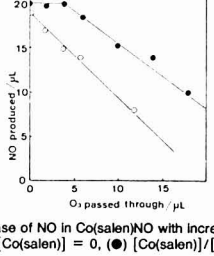


Figure 6. Decrease of NO in Co(salen)NO with increasing amount of O_3 passed: (O) [Co(salen)] = 0, (●) [Co(salen)]/[Co(salen)NO] = 1.

in the absence of AET and Co(II) and k is a constant. In this experiment, $(AV)_0$ was obtained as 0.340, which corresponded to 2.78 μg of NO_2^-. Since the absorbed amount of NO was 3.34 μg (as NO_2), it was concluded that 83% of NO was converted to NO_2^-.

Interferences. For the determination of ambient NO, the interfrences by possibly coexisting trace substances were studied.

(NH_3). One liter of N_2 containing 1250 ppm of NH_3 was bubbled into the absorbing solution containing Co(salen)NO (1.25 μmol/9 mL). Since the amount of NO did not decrease in a N_2 atmosphere, and decreased in an air atmosphere (Figure 5), NH_3 was considered to catalyze the oxidation by oxygen like pyridine. Clarkson and Basolo (*13*) analyzed the mechanism of reaction in eq 1. They showed that the rate of the reaction is first order in Co(salen)NO and that the rate constant can be expressed by [B] and [O_2]. When the concentration of B is low, the rate constant can be simplified as k[NH_3], where k is a constant. In this experiment, NH_3 concentration was low and $k_{obsd}/[Co(salen)NO]_i$ was obtained at 12%/h, where k_{obsd} is the rate constant and subscript i denotes initial state. In ambient air, the concentration of NH_3 is usually 10 ppb or less, the ratio becomes ca. 10^{-4}%/h. Therefore, the interference of NH_3 was negligible.

(O_3). One ppm of O_3 was bubbled into the absorbing solution containing a known amount of Co(salen)NO. Changes of the amount of NO against the amount of O_3 passed are shown in Figure 6. This shows that the reaction of O_3 with Co(salen)NO is equimolar, and that O_3 reacts with Co(salen) in preference to Co(salen)NO. In air sampling, the concentration of Co(salen) is much higher than that of Co(salen)NO, therefore no Co(salen)NO is lost.

(CO, SO_2, and Water). When CO (94 ppm) in air, SO_2 (16 ppm) in air, and humidified air were bubbled into the absorbing solutions containing a known amount of Co(salen)NO at the rate of 130 mL/min for 1 h, no significant interferences were found.

Mutual Interference of NO and NO_2. Absorption rate of NO_2 by the absorbing solution is higher than that of NO. NO (3.8 ppm), NO_2 (3.8 ppm), and the mixture of NO (3.8 ppm) and NO_2 (3.8 ppm) in air (1 L) were bubbled into three absorbing solutions, respectively. The absorbed amounts of NO and NO_2 in simultaneous absorption were equal to those in the separate experiments.

Therefore, the mutual interference was not observed up to 3.8 ppm of NO and 3.8 ppm of NO_2.

Table II. Comparative Studies of CLD with the Present Method

date	sampling time, Japan Mean Time	amt of NO, ppb·h CLD	amt of NO, ppb·h present method	amt of NO_2, ppb·h CLD	amt of NO_2, ppb·h present method
Sept 17, 1981	10-12	16	18	48	47
	12-14	9	12	41	41
	14-16	19	21	47	47
Sept 18, 1981	7-9	36	37	40	39
	9-11	21	25	51	46
	11-13	7	12	42	38
	13-15	10	13	44	40
Sept 22, 1981	9-11	19	22	51	49
	11-13	11	13	50	47
Sept 24, 1981	9-11	20	14	71	69
	11-13	44	31	45	44
Sept 25, 1981	13-14	49	49	42	45
	14-15	79	77	45	57
	15-16	56	56	50	60
Sept 28, 1981	10-13	13	22	50	55

Comparative Studies of CLD with the Present Method. Ambient air was introduced into the CLD NO_x analyzer and into the present absorbing solution, and NO and NO_2 were determined, respectively. Table II shows the comparisons of the present method with CLD measurement. These values are in good agreement. The mean squares of the differences between CLD and the present methods are 5 ppb-h both for NO and NO_2. The standard deviations of the blank measurements (n = 10) were 0.005 absorbance unit (NO) and 0.003 absorbance unit (NO_2). Therefore, the detection limits of NO and NO_2 are thought to be 2ppb-h and 1 ppb-h, respectively.

ACKNOWLEDGMENT

The authors are sincerely grateful to H. Sato of Yokohama National University for reading the manuscript, and to T. Aranoo and K. Yoshizumi of the Research Institute for assistance in preparing the manuscript.

Registry No. NO, 10102-43-9; NO_2, 10102-44-0; Co(salen), 14167-18-1.

LITERATURE CITED

(1) Leighton, P. A. "Photochemistry of Air Pollution"; Academic Press: New York, 1961; p 152.
(2) Tuesday, C. S. "Chemical Reactions in Urban Atmospheres"; Elsevier: New York, 1971; p 45.
(3) Altshuller, A. P.; Bufalini, J. J. *Environ. Sci. Technol.* **1971**, *5*, 39–64.
(4) "Air Quality Criteria for Nitrogen Oxides"; Environmental Protection Agency: Washington, DC, 1971.
(5) Fontijin, A.; Sabadell, A. L.; Ronco, R. J. *Anal. Chem.* **1970**, *42*, 575–579.
(6) Saltzman, B. E.; Mendenhall, A. L., Jr. *Anal. Chem.* **1964**, *36*, 1300–1304.
(7) Stern, A. C. "Air Pollution", 3rd ed.; Academic Press: New York, 1976; Vol. 3, p 267.
(8) Levaggi, D.; Kothny, E. L.; Belsky, T.; de Vera, E.; Mueller, P. K. *Environ. Sci. Technol.* **1974**, *8*, 348–350.
(9) Nedeau, J. S.; Treen, M. E.; Boocock, D. G. B. *Anal. Chem.* **1978**, *50*, 1871–1873.
(10) Hamamoto, O.; Uchiyama, S.; Nozaki, K.; Muto, G. *Bunseki Kagaku* **1979**, *28*, 118–121.
(11) Earnshaw, A.; Hewlett, P. C. Larkworthy, L. F. *J. Chem. Soc.* **1965**, 4718–4723.
(12) Tsumaki, T. *Bull. Chem. Soc. Jpn.* **1938**, *13*, 252–260.
(13) Clarkson, S. G.; Basolo, F. *Inorg. Chem.* **1973**, *12*, 1528–1534.
(14) Nishikawa, H.; Yamada, S. *Bull. Chem. Soc. Jpn.* **1964**, *37*, 8–12.
(15) Cox, R. D. *Anal. Chem.* **1980**, *52*, 332–335.

(16) Cesarotti, E.; Guliotti, M.; Pasini, A.; Ugo, R. *J. Chem. Soc., Dalton Trans.* **1977**, 757-763.
(17) Hammerschmidt, R. F.; Broman, R. F. *J. Electroanal. Chem.* **1979**, *99*, 103-110.
(18) Hasui, H.; Osuo, H.; Ohmichi, H.; Fukuzyu, Y.; Tarui, H. *Nippon Kagaku Kaishi* **1978**, 447-455.
(19) Hishinuma, Y.; Kaji, R.; Akimoto, H.; Nakajima, F.; Mori, T.; Kamo, T.; Akikawa, Y.; Nozawa, S. *Bull. Chem. Soc. Jpn.* **1979**, *52*, 2863-2865.
(20) Floriani, C.; Calderazzo, F. *J. Chem. Soc. A* **1969**, 946-953.

RECEIVED for review August 23, 1982. Accepted December 8, 1982.

Determination of Trace Quantities of Dimethyl Sulfide in Aqueous Solutions

M. O. Andreae* and W. R. Barnard

Department of Oceanography, Florida State University, Tallahassee, Florida 32306

A method is described for the determination of dimethyl sulfide (DMS) at the nanogram level in aqueous solutions. DMS is removed from aqueous samples by sparging with a He carrier gas stream. The volatile DMS is trapped cryogenically with liquid nitrogen on a chromatography column that serves as both the trapping and the separation mechanism. After controlled heating to separate DMS from interfering compounds, DMS is detected by a flame photometric detector. The detection limit is 0.03 ng of S (DMS), corresponding to a concentration of 0.3 ng L^{-1} for a 100-mL sample. Precision is 6.2%. Accuracy, sample storage, and stripping efficiency are also discussed. This procedure has been used to measure DMS in a variety of natural waters.

Models for the global mass balance of sulfur all indicate the need for a volatile, biogenically derived compound to transfer sulfur from the sea to the atmosphere in order to account for the total atmospheric sulfur content. Efforts to identify this compound have resulted in the measurement of several reduced-sulfur compounds including dimethyl sulfide, carbon disulfide, and carbonyl sulfide, in both the atmosphere and the oceans (*1-5*). The discovery that living organisms produce volatile, methylated sulfur compounds (*6*) has led to the investigation of the importance of dimethyl sulfide (DMS) in the transfer of sulfur from the sea to atmosphere (*1-3, 7-9*). Because of the need for a rapid, precise, and accurate method for the determination of trace amounts of DMS in seawater to help establish its role in the transfer of sulfur from sea to air, we have developed the method described below and tested it on over 200 seawater samples from various areas of the Atlantic Ocean and Gulf of Mexico.

DMS has been measured previously. Rasmussen (*5*) has measured DMS in pond waters by gas-liquid equilibration and GC-FPD determination. Another method involving extraction of DMS via CCl_4 and $HgCl_2$ from large volumes of seawater (15 L) has also been reported (*1*). DMS in the atmosphere has been preconcentrated on gold beads and analyzed using a similar detection system (*4*). Dimethyl sulfoxide (DMSO) has been determined as DMS after borohydride reduction by one of us (*10*), but improvements in the detection system have increased the sensitivity of the instrument by 2 orders of magnitude. The procedure detailed below represents the first report of a method for the determination of DMS in water samples that includes the analytical parameters accuracy, precision, detection limit, and a consideration of sample storage problems and interferences. Our method has several advantages over previous methods: it is rapid, accurate, and requires only small sample volumes. The instrument described below has also been used successfully aboard an oceanographic research vessel, eliminating the need for sample treatment to assure stability until samples can be analyzed onshore.

EXPERIMENTAL SECTION

Apparatus. The instrument configuration is depicted schematically in Figure 1. Known-volume sample loops of Teflon tubing are connected to an Altex series 202 six-way rotary sampling valve (Rainin Instrument Co., Woburn, MA). The He carrier gas stream passes through a 19-mm o.d., 36 cm long stainless steel pipe packed with a combination of activated charcoal (50-200 mesh, Fisher Scientific, Pittsburgh, PA) and molecular sieve (Union Carbide Type 4A, Fluka Chemical Co., Hauppauge, NY) to remove trace sulfur gases from the He carrier stream. From this scrubber the carrier is routed through the sample loop and the six-way valve and is used to inject the sample into the bubbling chamber through a glass frit at the base of the chamber. From the bubbling chamber, the carrier gas stream passes through a short length of Tygon tubing and into a 15 cm long, 12 mm o.d. Pyrex drying tube filled approximately two-thirds full with K_2CO_3 (Mallinckrodt, Inc., Analytical Reagent Grade) to remove moisture from the carrier gas stream. The gas stream then passes into a 6 mm o.d., 30 cm long glass U-tube filled with 15% OV3 on Chromosorb W AW-DMCS 60-80 mesh. This U-tube serves both as a trap and a separation column. About 2 m of 5 Ω m^{-1} Chromel wire is wound around the trap and connected to a variable transformer to allow controlled heating of the trap. The trap is connected to a Pyrex burner similar to that described by Braman et al. (*4*). Gas flow rates for this burner are 125 mL min^{-1} for air and 110 mL min^{-1} for H_2 and the He carrier gas flow is 100 mL min^{-1}. This burner is enclosed in an aluminum housing which is flanged to a photomultiplier system (9824A PMT and QL30F PMT housing, EMI GenCom Inc., Plainview, NY). Power for the PMT (700 V) is supplied by a Model 7101 high-voltage supply and the PMT current is measured by a Model 3A27 electrometer (both manufactured by Pacific Precision Instruments, Concord, CA). A Hewlett-Packard HP 3390A integrator is used to record and integrate the chromatographic peaks.

Standards. A gaseous diffusion tube with a known permeation rate was initially used to standardize the instrument. We used a wafer device with a nominal permeation rate of 2 ng of DMS/min (Metronics Assoc., Inc., Santa Clara, CA). This device was standardized against a gravimetrically calibrated permeation device by J. M. Ammons (1980, personal communication) and has an actual permeation rate of 2.84 ng of DMS/min at 30 °C. The wafer device was later replaced by liquid DMS standards which were prepared by dissolving liquid DMS (ICN Pharmaceuticals, Inc., Plainview, NY) in degassed ethylene glycol. Standards

0003-2700/83/0355-0608$01.50/0 © 1983 American Chemical Society

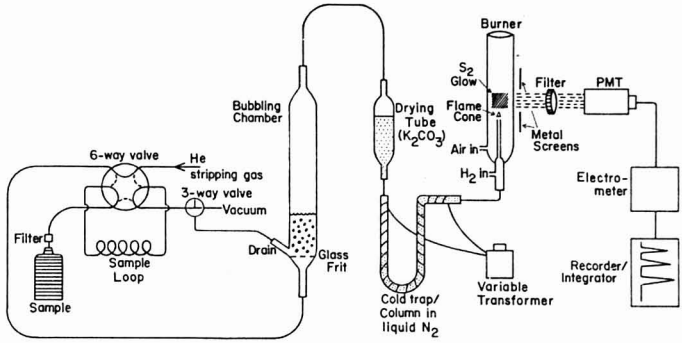


Figure 1. Sample degassing/flame photometric detection system for DMS determination.

prepared in this manner have been shown to have a number of desirable qualities for volatile organics (*11*). Primary standards were prepared by adding liquid DMS to a known weight of ethylene glycol and then weighing the total solution to determine the weight concentration of the standard. After the addition of DMS to the glycol the flask was immediately sealed and shaken for 15–20 min to ensure complete mixing. A working standard was prepared by injecting a few microliters of the primary standard into a weighed amount of degassed glycol. Working standards were prepared so that the concentration was in the range of 1–2 ng of S/μL of solution.

Analysis Procedure. Samples were loaded into the sample loop (5–37 mL depending on the concentration of the sample) via suction through the six-way valve. Once loaded, the six-way valve was switched to the inject position and the sample was forced out of the sample loop by the He carrier gas into the bottom of the bubbling chamber, through the fritted glass diffuser, and into the chamber itself. Immediately prior to injection of the sample the cold trap was immersed in liquid nitrogen. Once the sample is in the bubbling chamber, it is sparged by continuous purging with the He carrier gas for 20 min to remove the volatile DMS. After this the liquid nitrogen is removed and the cold trap is heated by switching on the variable transformer. The packed trap then serves as a very simple temperature-programmed gas chromatograph and separates the different sulfur compounds collected at the head of the packing. The DMS elutes in a sharp peak after 53 s, when a voltage of 19.5 V at a current of 6.5 A is applied to the heating coil. Following the analysis, the suction vacuum is applied to the drain outlet and the sample pumped out. Trap heating is continued until all water originally visible in the trap/column has evaporated.

RESULTS AND DISCUSSION

Analytical Parameters. *Accuracy.* One of the fundamental problems in the determination of many trace substances in natural matrices is the absence of certified standards, which makes it difficult to evaluate the accuracy of an analytical method. In order to minimize systematic errors, we base our calibration on gravimetric standards and the addition of standards to the natural matrix. We have not observed any differences between the results obtained by adding DMS standards to seawater samples which contain natural levels of DMS (method of standard additions) and those obtained by adding DMS standards to seawater from which DMS has been removed by gas stripping. For convenience reasons we normally follow the latter approach.

For calibration, we insert a glass T with an injection port between the six-way valve and the bubbler and inject microliter amounts of a solution of DMS in ethylene glycol into a volume of degassed seawater as it is being pushed from the sample loop to the bubbler. The calibration curve (log of peak area vs. log of the amount of S (DMS)) is linear from the detection limit of 0.03 ng of S (DMS) up to about 10 ng of S (DMS). It has a slope of about 1.8, somewhat dependent on the H_2-to-air ratio in the flame. Slopes somewhat below the theoretical value of 2.0 for the S_2 emission are typically observed with flame photometric detectors.

The accuracy of this calibration method is limited by that of the gravimetric preparation of the standard and by the accuracy of the microliter syringe used. Due to the inherent high accuracy of gravimetric procedures, the most important limitation to accuracy results from the syringe: typically ±2% when half of the maximum volume of the syringe is used. The calibration in terms of amount of DMS per analysis can therefore be performed with an accuracy of about ±2%. The sample volume measurement by the loop on the six-way valve is highly accurate; it can be calibrated gravimetrically by weighing the liquid delivered by a large number of injections.

In order to further assess the accuracy of our calibration, we compared the results of the method described above with the calibrations by injections of standards of DMS in glycol into a dry system, thereby eliminating the effects of matrix composition and stripping efficiency, and with a calibration of the detector alone, using a permeation tube standard.

Five replicate injections of 10 μL of DMS-in-glycol standard into the heated injection port without the simultaneous introduction of a water sample gave a result of 0.94 ± 0.06 ng of DMS. Injection of the same standard into a water sample followed by 20 min of stripping yielded a value of 0.93 ± 0.06 ng of DMS (n = 4). This difference is not statistically significant; the stripping process is therefore quantitative within the limits of analytical precision.

The accuracy of the glycol standards was checked against a permeation device standard (Metronics Assoc., Inc., Santa Clara, CA) with a known permeation rate of 2.84 ng/min at 30 °C. At long trapping times the agreement between the two standards was within the precision of the method. At shorter trapping times, discrepancies were found between the two standards. This discrepancy is due to the addition of a constant amount of DMS from the permeation device during the ~1 min peak elution time. When this amount is considered, the agreement between the two standards is better than 0.5%.

Precision. Table I represents the results of 12 duplicate sample determinations. These data were normalized by dividing the value of each determination by the mean for each pair of values. The precision (defined as the relative standard deviation of the normalized data) is 6.2%.

Detection Limit. When the detection limit is defined as the amount of analyte that produces a peak twice the height

Table I. Results of Duplicate Determinations

sample no.	amt of S found, ng L^{-1} 1st determination	2nd determination
9.10.80 1430Z	38.2	30.8
10.10.80 1220Z	46.3	41.3
11.10.80 0900Z	31.0	31.4
11.10.80 1000Z	35.5	32.1
11.10.80 1100Z	72.4	70.3
11.10.80 1500Z	80.0	79.4
18.10.80 SK-1	32.1	27.1
18.10.80 SK-2	16.8	13.9
18.10.80 SK-3	28.8	33.1
24.10.80 1000Z	30.5	26.7
M56-9-1	58.7	59.1
27.10.80 2100Z	16.1	14.8

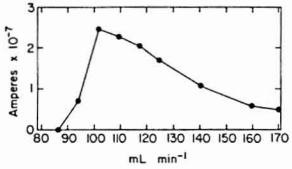


Figure 2. Instrument sensitivity response from 2.4 ng of S (DMS) as a function of air flow rate.

of the instrument noise, a detection limit of 0.03 ng of S (DMS) is obtained. This represents an improvement in detection limit of 2 orders of magnitude over our previous detection system (*10*). The major reasons for this improvement are modification of the burner housing and the installation of a head-on bialkali PMT rather than a side-on multialkali PMT. The bialkali PMT is better matched to the S_2 emission with higher sensitivity around 400 nm and lower sensitivity in the yellow and red regions than the multialkali PMT. The head-on geometry made it possible to move the active area of the tube closer to the flame and thereby increase the light yield. The burner housing has been modified so that an adjustable metal curtain can be moved up or down in front of the quartz burner, allowing a large fraction of the flame noise to be effectively screened out. This curtain results in an improvement by a factor of about 10 in the signal-to-noise ratio over our previous geometry (*10*).

The sensitivity of the instrument is also affected by variations in the burner gas flow rates. Our studies indicate that the sensitivity is greatly affected by variations in the air flow rate and less affected by variation in the H_2 flow. The change in response due to variations in the air flow rate is clearly seen in Figure 2. The change in sensitivity is dramatic below 100 mL min^{-1}. Changes in the H_2 flow rate with the air flow rate constant at 125 mL produced a similar shaped curve but the change in sensitivity was less pronounced. During actual analysis the air flow was not operated at the maximum sensitivity because of a persistent flame-out problem caused by water vapor condensation at the exit vent of the quartz burner and subsequent extinction of the flame by water droplets. Analyses were made with the air flow rate set slightly above the response maximum shown in Figure 2. This created a hotter flame which minimized condensation and only slightly decreased the instrument sensitivity.

Drying of the Gas Stream. Since the carrier gas passes through aqueous samples, a significant amount of moisture is carried along in the stream. It is necessary to remove most of the moisture from the gas stream to avoid clogging of the liquid nitrogen cold trap. This was initially accomplished by using a U-tube in a cold bath at −35 °C; however, for shipboard analyses we wanted to avoid using the bulky cryogenic unit necessary to cool the methanol in the cold bath. Several drying agents had been tried previously (*10*) but we eventually found that K_2CO_3 was effective and did not remove detectable amounts of DMS even after several hours of analysis. In order to examine the possibility of a loss of DMS to the K_2CO_3 drying tube, we injected DMS into the system between the six-way valve and the bubbler, which initially was kept dry. Then a fresh K_2CO_3 tube was added before the cold trap/column and several more aliquots of DMS were injected. For four replicate injections of 0.9 ng of S (DMS), the recovery was 97.7%, which is not significantly different from 100% at the stated precision of 6.2% relative standard deviation. Water was added into the bubbler and the system operated for 2 h to load the K_2CO_3 with water. Then, three replicate injections of 0.45 ng of S (DMS) were made. Recovery now was found to be 100.3%. From these results we conclude that no significant loss of DMS to the K_2CO_3 drying tubes occurs under the conditions used in our work. Furthermore, as we normally calibrate our system with aqueous standards, and with a K_2CO_3 tube in place, any such adsorption loss would be compensated for. The K_2CO_3 tubes must be replaced once they become saturated with water vapor since they can otherwise impede the carrier gas flow. This can usually be observed visually before it becomes a problem.

Table II. Retention Times (min)

	OV3[a] 9.9 V	TCP[b] 9.9 V	Carbopak[c] 11 V	PPQS[d] 17.8 V	PPQS/QF1[e] 17.8 V
air	0.37	0.35	0.64	0.85	0.89
COS	0.56	0.52	1.06	1.33	1.46
MeSH	0.94	2.27	1.29	1.90	1.95
CS_2	1.18	0.95	1.94	2.46	2.53
DMS	1.22	1.17	1.88	2.40	2.44
DMDS	1.99	2.64	3.09	3.84	3.84
SO_2				5.95	

[a] 15% OV3 on Chromosorb W AW DMCS 60-80 mesh. [b] 10% Tricresyl phosphate on Chromosorb W AW 80-100 mesh. [c] Carbopak B/1.5% XE60/1.0% H_3PO_4. [d] Porapak QS 80-100 mesh. [e] 5% DC-QF1 on Porapak QS, 80-100 mesh.

Interferences. Two types of potential interferences were considered in this study. One was a negative interference from adsorption of DMS by the glass container and tubing surfaces and the other was positive interference due to the elution of other sulfur compounds at the same time as DMS.

Adsorption of DMS by the glass and tubing surfaces was checked by injecting known amounts of DMS vapor (~5 ng) into the gas stream at various points and comparing the response with that obtained by injection directly before the cold trap. In all cases recovery was quantitative. All glass surfaces were silanized (SYLON-CT, Supelco, Inc.); this pretreatment has been found to minimize losses by deactivation of all surfaces that contact DMS vapor (*10*). Without surface deactivation the recoveries were substantially lower and highly variable. All connections between glass apparatus were made with short sleeves of Teflon tubing to minimize adsorptive losses (*10*).

Other reduced sulfur compounds were analyzed to determine whether their elution times coincided with DMS, resulting in a positive interference. We have investigated the retention characteristics of several short packed columns of the geometry described above. All columns were used both as cold trap and separating column. The results are summarized in Table II. OV3 gave the sharpest peaks and therefore the best detection limits. Figure 3 shows the separation on OV3 for the reduced sulfur compounds H_2S,

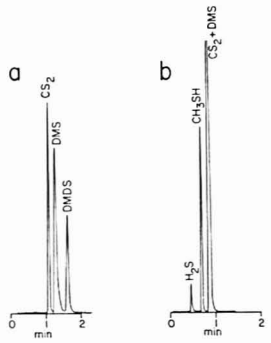


Figure 3. Peak separation of possible interfering reduced sulfur compounds: (a) with GC column conditioning at 100 °C in GC oven overnight; (b) after treatment of column with silanizing reagent.

CH_3SH, CS_2, $(CH_3)_2S$, and $(CH_3)_2S_2$. When the column was treated only by conditioning at 100 °C in a GC oven overnight, CS_2, DMS, and DMDS were well separated (Figure 3a). When we tried to remove the slight tailing of the DMS peak by treatment of the column with a silanizing reagent (Silyl-8, Pierce Chemical Co., Rockford, IL) at 150 °C in a GC oven, tailing of the DMS peak was indeed improved, but the CS_2 and DMS peaks were not separated any more (Figure 3b). In addition, the retention times were slightly reduced. H_2S, CH_3SH, and (DMS + CS_2) still showed excellent separation under these conditions. Thus, in the absence of CS_2, some improvement of peak shape can be attained by silane treatment. If the presence of CS_2 is suspected, however, exhaustive silanization of the packing used in this study must be avoided. The tricresyl phosphate column gives good separation of DMS and CS_2, but due to the broader peak shape the detection limit for DMS is about a factor of 4 lower on this column than it is using the OV3 column.

Commercial grades of helium contain small amounts of H_2S and DMS, their concentrations depending on the supplier and grade of the gas. This will result in a positive gas blank interference. This gas blank was eliminated by passing the carrier gas stream through a gas scrubber consisting of activated charcoal and molecular sieve.

When samples containing algal cells (e.g., unfiltered seawater) are introduced into the system, some algal material becomes trapped in the glass frit at the base of the purging unit. This material will continue to release DMS in significant amounts for long times (hours to days) and produce a system blank. This problem can be eliminated by including an in-line filter unit (2.5 cm diameter, Nuclepore Corp., Pleasanton, CA) with a glass fiber filter (GF/C, Whatman, Clifton, NJ) in the suction line through which the sample is introduced into the system. This filter has to be replaced after a few samples (depending on algal concentrations) to avoid cross-contamination.

Stripping Efficiency. We have also investigated the stripping rate of DMS from the sample by the carrier gas stream. The results of this study are shown in Table III. After 15–20 min the increase in measured DMS concentration is less than the instrument error. Immediately following these 15–20 min runs these same samples were stripped again for an identical time period. No detectable DMS was found in these second purges. We have fitted an exponential removal equation to these data and found that 99% of the DMS is removed from the solution after 19 min of purging. Consequently, all samples were stripped for 20 min to ensure complete recovery of dissolved DMS.

Table III. Results of Degassing of DMS via Carrier Gas Stream as a Function of Time[a]

time, min	concn of DMS (as ng of S (DMS) L^{-1})
5	34.8
10	45.2
15	47.4
20	47.7

[a] He flow rate: 100 mL min^{-1}, room temperature.

Table IV. Effects of Different Treatments on Sample Stability during Storage

initial concn	DMS concn [ng of S (DMS) L^{-1}] (0 h)
unfiltered	484.5
	484.2
filtered	454.6
	431.9

	DMS concn [ng of S (DMS) L^{-1}]		
sample treatment	12 h	24 h	48 h
UFUA	371.6	246.0	94.8
	432.7	321.1	19.2
UFUA R[a]	431.4	500.9	498.1
	518.3	448.0	511.6
UFA	306.4	383.7	453.9
	480.6	488.9	454.8
UFA R[a]	527.9	508.3	513.8
	503.7	566.3	464.2
FUA	382.0	341.5	57.3
	383.9	305.1	24.1
FUA R[a]	502.6	493.7	441.5
	516.4	476.1	495.8
FA	396.0	440.4	343.5
	404.0	419.5	356.6
FA R[a]	492.7	481.4	423.0
	459.4	464.2	450.8

[a] Sample refrigerated at 4 °C until analysis.

Sample Storage. A large volume of seawater was collected from a coastal location to study various methods of storing samples. Replicate 250-mL splits of this volume were stored in polyethylene bottles filled to the top to eliminate any headspace in an effort to minimize partitioning into the gas phase. These splits were then subjected to the following treatments: UFUA, unfiltered unacidified stored at ambient temperature; UFA, unfiltered acidified stored at ambient temperature; FUA, filtered unacidified stored at ambient temperature; FA, filtered acidified stored at ambient temperature. All filtered samples were filtered with a 2.5 cm diameter glass fiber filter (GF/C, Whatman, Clifton, NJ) connected in-line to a gravity feed line to avoid sample degassing. Samples were acidified with 2 mL of concentrated HCl (Mallinckrodt, Inc., Paris, KY). Additionally, duplicates of the above treatments were also stored in a refrigerator at 4 °C.

The results of this experiment are presented in Table IV. These results show no clear advantage to either filtered or acidifying samples. In fact, filtration tends to lower the concentration no matter how much care is used to avoid sample degassing. Refrigeration of samples, whether filtered or unfiltered, acidified or unacidified, tends to be the best way to maintain sample integrity at least for periods up to 48 h. We have adopted this sample storage strategy when immediate

Table V. DMS Concentrations in Some Natural Waters

sample	ng of S (DMS) L^{-1}
Elbe River Mouth (8 Oct 1980)	31.4
Dry Tortugas, Gulf of Mexico (8 April 1980)	28.0
North Sea (10 Oct 1980, 1050 GMT) 51°36.9′ N, 2°16.5′ E	58.0
Dover Straits (10 Oct 1980, 1600 GMT) 51°01.2′ N, 1°22.2′ E	76.6
English Channel (10 Oct 1980, 1800 GMT) 50°49.4′ N, 0°58.6′ E	116.4
Open Ocean Surface Seawater (N. Atlantic, 21 Oct 1980, 1000 GMT) 20°20.7′ N, 24°45.9′ W	62.5
Seawater Station M56-9 (23 Oct 1980, 1416 GMT) 11°28.8′ N, 28°03.5′ W	
5 m depth	100.1
35 m	76.1
70 m	38.3
100 m	21.3
130 m	15.5
200 m	5.7
300 m	8.8
500 m	8.1
1000 m	5.4
1500 m	2.5
2000 m	3.8
3000 m	3.8
4000 m	0.8
Open Ocean Surface Seawater (S. Atlantic, 28 Oct 1980, 0100 GMT) 5°50.5′ S, 33°53.7′ W	37.1
rain, N. Atlantic (18 Oct 1980) 30°58.5 N, 20°24.4′ W	10.4

analysis has proven impossible. In all cases samples have been analyzed within 36 h.

CONCLUSIONS

DMS has been determined in several types of natural waters, using the method described in this paper. Some results are presented in Table V. DMS is present even in samples taken from the deep oceans although there is a rapid decline in concentration below the euphotic zone. High levels of DMS tend to be found in productive areas of the ocean because of the algal production mechanism for DMS. Open ocean surface values are lower and show a narrow range of values for DMS and productivity.

ACKNOWLEDGMENT

We thank M. Dancy for her help with the preparation of the manuscript and graphics. J. M. Ammons is acknowledged for valuable discussions and for the cross calibration of the permeation tube standards. We thank W. Seiler for permission to participate in the cruise of the research vessel *Meteor*, during which some of the data presented in this paper were collected.

Registry No. DMS, 75-18-3.

LITERATURE CITED

(1) Nguyen, B. C.; Gaudry, A.; Bonsang, B.; Lambert, G. *Nature (London)* **1978**, *275*, 637.
(2) Lovelock, J. E.; Maggs, R. J.; Rasmussen, R. A. *Nature (London)* **1972**, *237*, 452.
(3) Maroulis, P. J.; Bandy, A. R. *Science* **1976**, *196*, 647.
(4) Braman, R. S.; Ammons, J. M.; Bricker, J. L. *Anal. Chem.* **1978**, *50*, 992.
(5) Rasmussen, R. A. *Tellus* **1974**, *26*, 254.
(6) Challenger, F. *Adv. Enzymol.* **1951**, *12*, 429.
(7) Sze, N. D.; Ko, M. K. *Atmos. Environ.* **1980**, *14*, 1223.
(8) Graedel, T. E. *Geophys. Res. Lett.* **1979**, *6*, 329.
(9) Cullis, C. F.; Hirschler, M. M. *Atmos. Environ.* **1980**, *14*, 1263.
(10) Andreae, M. O. *Anal. Chem.* **1980**, *52*, 150.
(11) Ramstad, T.; Nestrick, T. J.; Peters, T. L. *Am. Lab. (Fairfield, Conn.)* **1981**, *13*, 65.

RECEIVED for review April 2, 1981. Resubmitted October 12, 1982. Accepted January 14, 1983. This work was supported in part by the National Science Foundation Grant No. ATM 80-17574 and by a grant from The Florida State University Foundation.

Simultaneous Determination of Hydrogen Peroxide, Peroxymonosulfuric Acid, and Peroxydisulfuric Acid by Thermometric Titrimetry

Philippe E. A. Boudeville

Laboratoire Chimie Analytique, U.E.R. du Médicament, Faculté de Médecine et Pharmacie, 2, avenue du Professeur Léon Bernard, 35043 Rennes Cedex, France

An original method of determination by thermometric titrimetry (TT) of the amount of H_2SO_5, H_2O_2, and $H_2S_2O_8$ in a single sample within the range of 100–1000 μmol with Ce^{4+} and Fe^{2+} is described. This method uses the differences between reaction rates and enthalpy variations of reactions of these three peroxides with Fe^{2+}. For H_2SO_5, H_2O_2, and $H_2S_2O_8$, respectively, the values of the rate constants are fast, 187, and 8.5 L mol^{-1} s^{-1}, and those of the enthalpy variations are −366, −428, and −328 kJ mol^{-1} at 20.0 °C and with an ionic strength = 0.62 mol L^{-1}. These values have been determined by TT.

Peroxydisulfate ion is often used as an oxidizer or radical generator which is a good polymerization initiator. However, peroxydisulfuric acid is not stable in sulfuric media. It decomposes to give peroxymonosulfuric acid or hydrogen peroxide according to experimental conditions. It was interesting to rapidly determine the amount of these three peroxides and numerous papers (*1–9*) have already been published concerning different titration methods. The spectrophotometric methods (*6*, *7*) allow the determination of concentrations 2×10^{-5} M with good accuracy (2 to 3%). However they require three different samples: in the first sample, H_2O_2 is titrated by Ce^{4+} (λ = 320 nm) or Ti^{4+} (λ = 410 nm). In the second one, $H_2S_2O_8$ is titrated by Fe^{2+} (λ = 304 nm) in the presence of As_2O_3 and N_2. In the third one, the total amount of oxidant is titrated by Fe^{2+} (λ = 304 nm). The amount of H_2SO_5 is obtained by the difference. In the course of our kinetic study

0003-2700/83/0355-0612$01.50/0 © 1983 American Chemical Society

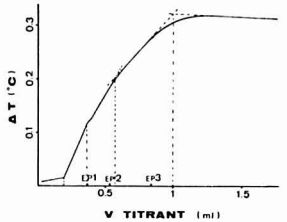


Figure 1. Thermogram for the titration of a mixture of H_2SO_5, H_2O_2, and $H_2S_2O_8$ by Fe^{2+}. EP1, EP2, and EP3 are the respective theoretical equivalent points.

of the reaction of iron(II) peroxydisulfate by thermometric titration (*10*), we have observed that H_2SO_5, H_2O_2, and $H_2S_2O_8$ react with Fe^{2+} with different rates and with different values of ΔH. The rate determining steps for these three reactions are

$$HSO_5^- + Fe^{2+} \xrightarrow{\text{fast}} HSO_5^{2-}\cdot + Fe^{3+}$$

$$H_2O_2 + Fe^{2+} \xrightarrow{k_1} OH\cdot + Fe^{3+} + OH^-$$

$$HS_2O_8^- + Fe^{2+} \xrightarrow{k_2} SO_4^{-}\cdot + Fe^{3+} + HSO_4^-$$

The values of the rate constants are, respectively, fast, $k_1 = 187 \pm 5$ L mol^{-1} s^{-1}, and $k_2 = 8.5 \pm 0.5$ L mol^{-1} s^{-1} and those of the enthalpy variations for the complete chemical reactions are −366, −428, and −328 kJ mol^{-1} at 200 °C and with an ionic strength = 0.62 mol L^{-1} (these values have been determined by TT). We have investigated the possibility of using these differences to effect a sequential titration of these three products on a single sample.

Indeed we can see on the thermogram (Figure 1) of the titration of a mixture of these three peroxides by a solution of Fe^{2+}, the three slopes corresponding respectively to H_2SO_5, H_2O_2, and $H_2S_2O_8$. While the first break in the curve gives a good result for the titration of H_2SO_5, this is not the case for the two others: a greater amount of peroxide than foreseen is obtained due to the fact that the reactions are slow. Therefore the direct titration by Fe^{2+} was not considered suitable.

Thermometric titrimetry (TT) is a method based on recording the temperature of the reaction mixture in the course of the titration of a reactant A by a titrating agent B (*11–14*). B is added to A at a regular rate and an excess of B is always added to A (which explains the presence of excess Ce^{4+} in the course of the titration of H_2O_2 in a mixture) so as to determine the equivalent point (EP) either by a sharp variation of the slope or by the intersection of extrapolations of the slopes before and after the more steeply curved portion.

Three kinds of curves are observed (Figure 2): Curve 1 corresponds to a fast and complete reaction; a sharp break represents the EP. Curve 2 corresponds to a fast but uncomplete reaction; we have a curvature and the EP is the point where the "extrapolation of the slopes" cross each other, depending on the K value (*15*, *16*). Curve 3 corresponds to a complete but slow reaction; we have a double curvature at the start and at the end and the point where the "extrapolation of the slopes" cross each other is higher than the equivalence (*10*, *17*).

EXPERIMENTAL SECTION

Instrumentation. The apparatus was described in ref 18. We have deliberately used the simplest possible conditions so as to facilitate repetitive titrations and eventually their automatization. Thus water was simply passed through an ion exchange resin

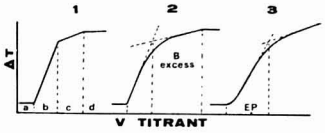


Figure 2. Theoretical thermograms (curves 1, 2, and 3): (a) base period, no titrant added; (b) reaction period, titrant added; (c) excess titrant period, titrant added; (d) posttitration period, no titrant added.

without distillation from permanganate and the thermometric titration system was not thermostated (except for measurements of rate constants and ΔH). All chemicals (Merck p.a., Prolabo R.P., or Carlo Erba RPE) were used as received.

Reagents and Standard Solutions. Solutions were prepared by dissolving the reactants in 0.5 M H_2SO_4 so as to obtain a constant ionic strength (μ = 0.62 mol L^{-1}) and to avoid precipitation of ferri hydroxide in the course of the titration. Peroxydisulfuric acid was prepared immediately before use (to avoid its hydrolysis to H_2SO_5 which occurs even in 0.5 M H_2SO_4 (*19*)) from ammonium peroxydisulfate. Peroxymonosulfuric acid was prepared by heating a solution of $H_2S_2O_8$ in 2 M H_2SO_4 for 4 h at 70 °C. Under these conditions some H_2O_2 was formed (*19*) and about 2% of the initial $H_2S_2O_8$ remained. The solution was diluted four times and kept away from light to avoid photolysis of H_2SO_5 to H_2O_2 (*20*). H_2O_2 was titrated spectrophotometrically in the presence of excess Ti^{4+} according to the method of Csanyi (*7*); it was generally 2 to 3%. $H_2S_2O_8$ was titrated according to our method. The total oxidizing capacity of each solution was determined for H_2O_2 solutions by direct titration with $KMnO_4$ and for H_2SO_5 and $H_2S_2O_8$ solutions by reaction with excess Fe^{2+} which was back-titrated with $KMnO_4$.

RESULTS AND DISCUSSION

Titration of the Products Alone. The titration of H_2O_2 at concentrations $\geq 10^{-4}$ M in an H_2SO_4 (0.5 or 5 M) medium was effected by Ce^{4+} (fast and complete reaction) with a precision of 1% (Table I). For concentrations lower than 10^{-4} M, Fe^{2+} was added first and the excess Fe^{2+} was then titrated by Ce^{4+}.

The titration of H_2SO_5 was effected by Fe^{2+} in 0.5 M H_2SO_4 in the presence of Ce^{3+} while keeping the ratio of $Ce^{3+}/H_2SO_5 \geq 4$ so as to avoid the decomposition of H_2SO_5 induced by Fe^{2+}. Under these conditions solutions having concentrations of about 5×10^{-5} M can be titrated with an accuracy of 2% (Table I).

The titration of $H_2S_2O_8$ was effected by adding an excess of Fe^{2+}, waiting 10 min, and then titrating the remaining Fe^{2+} by Ce^{4+}. An accuracy of 2.5% was obtained for solutions of about 5×10^{-5} M in 0.5 M H_2SO_4. In 5 M H_2SO_4, $H_2S_2O_8$ was hydrolyzed to H_2SO_5 but both were titrated (Table I).

Mixtures of Hydrogen Peroxide and Peroxydisulfuric Acid. H_2O_2 was first titrated by Ce^{4+}, allowing determination of the concentration of H_2O_2, and then the excess of Ce^{4+} was titrated by Fe^{2+}. The addition of Fe^{2+} was continued so as to reduce $H_2S_2O_8$ until there was an excess of Fe^{2+}. We waited 10 min and titrated the excess Fe^{2+} by Ce^{4+} (Table I). We were unable to use MnO_4^- instead of Ce^{4+} because titrations of H_2O_2 by MnO_4^- and of excess MnO_4^- by Fe^{2+} were tricky by TT and Mn^{2+} reacts slowly with $H_2S_2O_8$.

Mixtures of Peroxymonosulfuric Acid and Peroxydisulfuric Acid. Titration was effected by Fe^{2+} in 0.5 M H_2SO_4 in the presence of Ce^{3+} keeping the ratio $Ce^{3+}/H_2SO_5 \geq 4$. H_2SO_5 reacts first and the first break in the curve allows determination of its concentration. An excess of Fe^{2+} was then added, and after a wait of 10 min the excess Fe^{2+} was titrated with Ce^{4+}. This allows determination of the concentration of $H_2S_2O_8$. This titration can be done in 5 M H_2SO_5 but the amount of $H_2S_2O_8$ hydrolyzed to H_2SO_5 must be taken into account (Table I).

Table I. Titration of Mixtures of Peroxides

amt taken × 10^4, M				amt found,[a] % (std dev)				
H_2O_2	H_2SO_5	$H_2S_2O_8$	Ce^{3+}	H_2O_2	H_2SO_5	$H_2S_2O_8$	n	$[H_2SO_4]$, M
2				99.8 (0.8)			6	0.5
0.4				98.3 (2.7)			4	5
		9				99.8 (0.8)	5	5
		0.5				97.7 (2.2)	9	0.5
	10		0		80.3			5
	10		1		94.7			5
	10		10		98.1			5
	10		40		100.1			5
	10		80		99.8			5
	2		10		99.2 (0.8)		3	5
	0.2		10		98.1 (3)		3	5
	0.2	10	10		97.3 (4)	101.3 (0.4)	3	5
	8	8	40		99.1 (0.7)	98.8 (0.6)	2	0.5
9	2.1		40	101.3 (1.2)	99.9 (1.1)		4	5
1.8		1.4		99.4 (1.7)		100.5 (1.6)	4	5
4	9	8	40	100.2 (0.3)	99.1 (0.4)	100.6 (3.1)	4	5
2	9	20	40	104.1 (1.0)	98.8 (0.1)	100.3 (1.6)	2	5
9	9	4	40	98.3 (0.2)	96.8 (0.7)	103.5 (6.3)	2	5

[a] Each experimental result is expressed in % = experimental value × 100/theorical value. The data accuracy is given by the mean of the n values of a set and the precision by the standard deviation if there are more than three measurements or otherwise the deviation with respect to the average.

Mixtures of Hydrogen Peroxide and Peroxymonosulfuric Acid. There are two possible procedures, either the same as for the mixture $H_2SO_5 + H_2S_2O_8$ can be used when the amount of H_2O_2 is greater than that of H_2SO_5 (H_2O_2 playing the part of $H_2S_2O_8$) or the procedure using the first two steps of the titration of the mixture of the three peroxides in the other cases (Table I).

Mixtures of Hydrogen Peroxide, Peroxymonosulfuric Acid, and Peroxydisulfuric Acid. In order to avoid the reaction between H_2SO_5 and Ce^{4+} ($HSO_5^- + Ce^{4+} \rightleftarrows HSO_5\cdot + Ce^{3+}$), it was necessary to operate in a medium containing 4 to 5 M H_2SO_4 (6) and add Ce^{3+} so as to obtain a ratio $Ce^{3+}/H_2SO_5 \geq 4$. H_2O_2 was first titrated by Ce^{4+} (Figure 3, curve 1), and then excess Ce^{4+} and H_2SO_5 were titrated by Fe^{2+} (Figure 3, curve 2). An excess of Fe^{2+} was then added to reduce $H_2S_2O_8$, and we waited 10 min and titrated the excess Fe^{2+} by Ce^{4+} (Figure 3, curve 3).

Curve 2 (Figure 3) manifests two breaks (break (b) and (c) corresponding to the titration of Ce^{4+} and H_2SO_5, respectively) which indicate that the reaction of Fe^{2+} with Ce^{4+} is faster than with H_2SO_5. However break (b) did not allow determination of the excess Ce^{4+} since, at this point, a certain amount of H_2SO_5 had been reduced and an erroneously low result for H_2SO_5 would have been obtained. Break (c) allows us to know the sum of $Ce^{4+} + H_2SO_5$. Excess Ce^{4+} was determined by the difference between the total Ce^{4+} added and the amount of Ce^{4+} that had reacted with H_2O_2 (curve 1, break (a)). Thus the volume of Fe^{2+} which reacted with H_2SO_5 was easily determined. We found the amount of Fe^{2+} that had reacted with $H_2S_2O_8$ by the difference between the total Fe^{2+} added and the Fe^{2+} that had reacted with $Ce^{4+} + H_2SO_5$ and the one which had been oxidized by Ce^{4+} (curve 3, break (d)). When the amount of $H_2S_2O_8$ is greater than that of H_2SO_5, it is necessary to take into account the amount of $H_2S_2O_8$ hydrolyzed to H_2SO_5 (approximatively 2% for 10 min at 20 °C in 5 M H_2SO_4 whatever the initial concentration). The overall titration took 20 min.

Calculations are simple when we take the same concentration for the two titrants Ce^{4+} and Fe^{2+}.

Other Measurements. For this study we have tried other titrating agents like MnO_4^-, Ti^{4+}, and SCN^- already used by other authors for H_2O_2, Fe^{2+}, Ce^{4+}, and H_2SO_5, to see if the determination of the equivalent point by thermometric titrimetry instead of potentiometry or spectrophotometry gave better results. It was not the case. We have also studied the decomposition of H_2SO_5 which is induced by Fe^{2+}. Cerous ions inhibit this decomposition and this explains the necessity of always keeping a ratio of $Ce^{3+}/H_2SO_5 \geq 4$ as we can see in Table I: for the same concentration of H_2SO_5 if we increase the amount of Ce^{3+}, we obtain a good result when the ratio value is 4. All the results of these studies will be published subsequently.

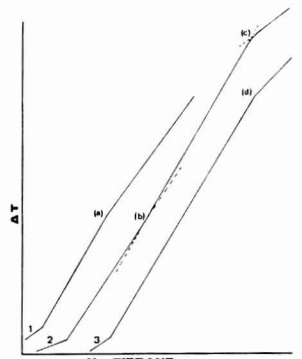


Figure 3. Thermogram for the titration by 0.19 M Ce^{4+} and 0.25 M Fe^{2+} of a mixture of 2 × 10^{-4} M H_2O_2, 9 × 10^{-4} M H_2SO_5, and 20 × 10^{-4} M $H_2S_2O_8$ in 5 M H_2SO_4 and with 40 10^{-4} M Ce^{3+}.

CONCLUSION

The results obtained by our method compare well with those obtained by the spectrophotometric method as to accuracy and limits of detection when the products are alone. In mixtures it is difficult to determine concentrations lower than 10^{-4} M for H_2O_2 and $H_2S_2O_8$ with good accuracy (spectrophotometry is better, 2 × 10^{-5} M). However this method seems the best for the determination of very small amounts of H_2SO_5 (10^{-5} M) whatever the concentration of H_2O_2 or $H_2S_2O_8$ (even when the ratio H_2SO_5/H_2O_2 or $H_2S_2O_8$ is lower than 10^{-2}) because H_2SO_5 can be determined in the first place whereas with other methods it is last and is obtained by

difference after two or three titrations. Other advantages of the TT method are the use of a single sample and the short time of analysis (under 20 min). Last, thermometric titrimetry is a linear method of titration and only requires knowledge of the concentration of the titrating agents which are generally stable for several days. This allows facile automation in cases of repeated measurements. In this respect, note that automatic apparatus for the titration by TT including microprocessor control data analysis are already available.

ACKNOWLEDGMENT

The author thanks J. L. Burgot for helpful suggestions and numerous informative discussions.

Registry No. H_2O_2, 7722-84-1; H_2SO_5, 7722-86-3; $H_2S_2O_8$, 13445-49-3.

LITERATURE CITED

(1) Kolthoff, I. M.; Belcher, R. "Volumetric Analysis"; Interscience: New York, 1957; Vol. III.
(2) Pascal, P. "Nouveau traité de Chimie Minérale"; Masson et Cie éditeurs: Paris, 1961; Vol. XII, p 1509.
(3) Pungor, E.; Schulek, E.; Trompler, J. *Acta Chim. Acad. Sci. Hung.* **1954**, *4*, 393–456.
(4) Csanyi, L. J.; Solymosi, F. *Acta Chim. Acad. Sci. Hung.* **1958**, *13*, 257–272.
(5) Csanyi, L. J.; Batyai, J. *Magy. Kem. Foly.* **1963**, *69*, 103–117.
(6) Mariano, M. H. *Anal. Chem.* **1968**, *40*, 1662–1667.
(7) Csanyi, L. J. *Anal. Chem.* **1970**, *42*, 680–682.
(8) Mariano, M. H. *Anal. Chem.* **1970**, *42*, 682–684.
(9) Schneider, J.; Nagy, L.; Csanyi, L. J. *Acta Chem. Acad. Sci. Hung.* **1976**, *89*, 15–21.
(10) Boudeville, P.; Burgot, J. L.; Chauvel, Y. *Thermochim. Acta* **1981**, *43*, 313–324.
(11) Tyrell, H. J. V.; Beezer, A. E. "Thermometric Titrimetry"; Chapman and Hall: London, 1968.
(12) Vaughan, G. A. "Thermometric and Enthalpimetric Titrimetry"; Van Nostrand-Reinhold: London, 1973.
(13) Jordan, J. "New Development in Titrimetry"; Marcel Dekker: New York, 1974; Vol. 2.
(14) Barthel, J. "Thermometric Titrations"; Wiley: New York, 1975.
(15) Tyrell, H. J. V. *Talanta* **1967**, *14*, 843.
(16) Bernard, M. A.; Burgot, J. L. *Talanta* **1981**, *28*, 945–949.
(17) Carr, P. W.; Jordan, J. *Anal. Chem.* **1973**, *45*, 634.
(18) Bernard, A. M.; Burgot, J. L. *Talanta* **1981**, *28*, 939–943.
(19) Schulek, E.; Punkor, E.; Trompler J. *Acta Chim. Acad. Sci. Hung.* **1954**, *4*, 429–444.
(20) Tsao, M. S.; Wilmarth, W. K. *J. Phys. Chem.* **1953**, *63*, 346–353.

RECEIVED for review May 10, 1982. Accepted December 13, 1982.

Generation of an Electrochemical Data Base for Pattern Recognition

W. Arthur Byers[1] and S. P. Perone*[2]

Department of Chemistry, Purdue University, West Lafayette, Indiana 47907

Instrumentation and methods are presented for determining the Faradaic and capacitive response of an analyte over a wide range of experimental conditions. Experiments were carried out by a fractional factorial design so that the best experimental conditions or changes in conditions for analyte identification could be determined in a later pattern recognition analysis. Percent ethanol, pH, surfactant concentration, number of cycles, scan rate, and mercury drop hang time all produced changes in cyclic differential capacity curves and cyclic staircase voltammograms which were unique and reproducible. Capacitive and Faradaic responses were determined independently for 19 nitro compounds under most experimental conditions.

Electroanalytical techniques have not often been used for elucidation of chemical structure. This is due in part to the fact that normally recorded organic electrochemical responses are usually complex functions of many variables such as electrode material, solution composition, and the time frame of the experiment. Theoretical expressions relating structure to electrochemical activity are valid under very restrictive conditions (*1*), and they are often difficult to evaluate (*2–4*).

An empirical approach such as computerized pattern recognition would seem to be the best solution for qualitative identification, and it has already been used with some success in electrochemistry (*5–8*). However, in order to use pattern recognition to assign an unknown to a specific structural class, one must first have a library of data for similar structures, obtained under conditions similar to those for the unknown. Although a vast amount of organic electrochemical data have been collected (*9*), only small subsets have been collected under conditions which are sufficiently similar for a pattern recognition analysis. Bugard and Perone (*10*) reported encouraging results for the analysis of 30 organics representing four structural classes, but better results might have been obtained if solution conditions had been varied.

Much of the complexity of an electrochemical response is due to the heterogeneous nature of the electron transfer. The interplay of adsorption and diffusion complicate the interpretation of current flowing due to electron transfer. It is common practice to use a solvent system such that adsorption effects are minimized. While this may improve peak shape for more accurate quantitation, one may be throwing away important structural information in the process. The strength and potential dependence of adsorption may indicate the presence of certain functional groups (*11*, *12*). π-electron interaction has a characteristic influence on the adsorption behavior of organics (*13*), and specific interactions between the analyte and some other molecule or ion within the double layer may also be helpful in identification (*14*, *15*). For these reasons we believe that structural classification might be made more reliably by using solution conditions where adsorption strongly affects electrochemical response.

The purpose of this work is to describe new methods and instrumentation which we have developed for producing a large body of electrochemical data and for determining the best measurements to be made for later pattern recognition analysis. The effects of seven different experimental variables on Faradaic and capacitive electrochemical responses have

[1] Present address: Westinghouse Electric Corp., 1310 Beulah Road, Pittsburgh, PA 15235.
[2] Present address: Chemistry & Materials Science Department, Lawrence Livermore National Laboratory, Livermore, CA 94550.

0003-2700/83/0355-0615$01.50/0 © 1983 American Chemical Society

Table I. Variable Levels

variable no.	variable	low level (−)	high level (+)
X_1	% ethanol	0.5%	9.5%
X_2	pH	8.0	5.1
X_3	surfactant concn	0	1.4×10^{-5} M
X_4	no. of cycles	1	2
X_5	scan rate	0.25 V/s	1.0 V/s
X_6	drop hang time	0.2 s	30 s
X_7	sampling time	30% of step ($\alpha' = 0.7$)	end of step ($\alpha' = 0.007$)

Table II. Fractional Factorial Design

experiment no.	variable						
	X_1	X_2	X_3	X_4	X_5	X_6	X_7
1	+	−	−	−	−	+	+
2	+	−	−	+	+	−	+
3	+	+	−	+	−	−	−
4	+	+	−	−	+	+	−
5(a)	+	+	+	+	+	+	+
6	−	−	+	+	−	−	+
7	−	−	+	−	+	+	+
8	−	+	+	−	−	+	−
9	−	+	+	+	+	−	−
10	−	−	−	+	+	+	−
11	−	−	−	−	−	−	−
12	−	+	−	−	+	−	+
13	−	+	−	+	−	+	+
14	+	−	+	−	+	−	−
15	+	−	+	+	−	+	−
5(b)	+	+	+	+	+	+	+
16	+	+	+	−	−	−	+

been examined. Initial results for several nitrodiphenyl ethers are reported and compared to other nitroaromatics. These compounds are important in agriculture because of their strong but selective herbicidal activity (*16*).

Electrode capacitance is related in a simple way to the degree of adsorption or surface excess (*17*). A number of methods are available for simultaneous recording of capacitive and Faradaic responses (*18–22*), one of the best having been recently reported by Elkin et al. (*23*). Elkin's semitrapazoidal wave form is optimal in terms of potentiostat stability but is difficult to generate experimentally. We have found that a simple staircase will produce excellent results while being easy to generate under computer control. Electrode capacitance is obtained by measuring the rate of charging current decay immediately after the step, while Faradaic currents are measured at the end of each step where capacitive contributions are minimal (*24*, *25*).

EXPERIMENTAL SECTION

Experimental Design. The seven variables which were investigated are listed in Table I. Performing a series of experiments in which one parameter is varied while all others are held constant at some arbitrary level would give a very narrow view of the effects of each parameter if there was any possibility of interaction between variables. To get a broader view of each variable effect, we conducted the experiments by use of a fractional factorial design (*26*). Two saturated fractions were run so that all main effects were dealiased from two-factor interactions (*27*). Higher order interactions could still be confused with the main effects, but in most cases, such interactions are relatively small in magnitude. The level of each variable in the 16 experiments is given in Table II. One experiment, no. 5, was repeated to test for reproducibility.

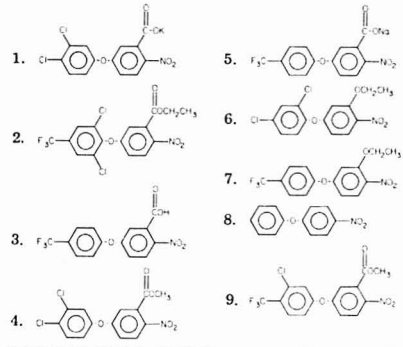
The main effects were explored with the aid of *variable effect curves*. These curves were constructed for each variable by summing point by point all responses obtained for those experiments in Table II where the variable was at its high level, and then subtracting all responses where the variable was at its low level. This approach is analogous to the method reported in ref 26 for extracting the contribution of each variable, free from the effects of other variables. Effect curves were plotted for both the Faradaic and capacitive responses.

Table III. Compounds Studied

Nitrobenzenes

1. *p*-nitrophenol
2. 1-chloro-2-nitrobenzene
3. *o*-nitrophenol
4. *m*-nitrophenol
5. *m*-nitrotoluene
6. 1-chloro-4-nitrobenzene
7. *p*-nitrotoluene
8. 2-6-dichloro-4-nitrophenol
9. *p*-nitroanisole
10. α-chloro-*m*-nitrotoluene

Nitrodiphenyl Ethers



Solution Preparation. Compounds analyzed in this study are listed in Table III. The diphenyl ethers were obtained from the Department of Botany and Plant Pathology, Purdue University. Purity was 95% or better. Other compounds were commercially available in pure form. Stock solutions were 2.0×10^{-3} M and were made by dissolving the compounds in 2.5 mL of ethanol and diluting to 50 mL with distilled water. The final concentration was 1.6×10^{-4} M after complete solution preparation.

Britton–Robinson buffers were used for pH control. These were made by adding reagent grade boric acid, sodium acetate, dibasic potassium phosphate, and potassium chloride either to distilled, deionized water or to a 10% ethanol solution so that each of the components was 0.2 F. The stock buffer solutions were stored in 5-gallon carboys and were delivered to the cell via deoxygenating columns and automatic pipets shown in Figure 1. The aqueous buffer was continuously irradiated with UV light to prevent the growth of bacteria. Purified nitrogen was used for deoxygenation. Stainless steel ac solenoid valves (ALCO 204CA1/453/32G) controlled the flow of solution through the pipets. The volume of solution delivered was set to 46.0 mL by adjusting the position of the pipets relative to the cell entry port. The standard deviation for three successive deliveries was found to be 0.02 mL.

Sodium lauryl sulfate, 1.85 M nitric acid, and the analyte were delivered to the cell by a Technicon Proportioning Pump (Model III) and latching three-way solenoid valves. The sodium lauryl sulfate (Merck) solution was 10^{-3} M and contained a mixture of alkyl sulfates, lauryl sulfate being the primary species. The valve used for control of the nitric acid flow was constructed from Teflon (General Valve 1-36) while the others were stainless steel (Angar Scientific Corp. 40L). Teflon tubing was used for the analyte, otherwise connections were made with Tygon tubing. The flow lines were terminated within the cell by glass nozzles which were rendered hydrophobic by immersion in dichlorodimethylsilane

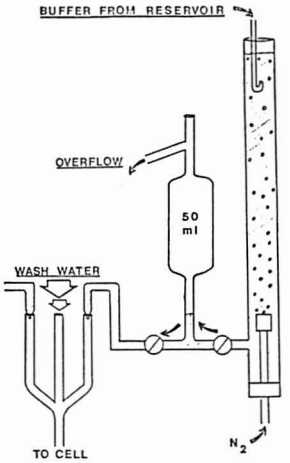


Figure 1. Solvent delivery system.

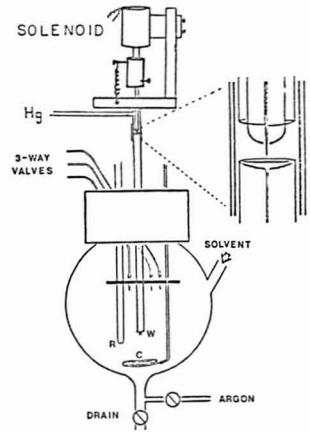


Figure 2. Cell design.

for 5 min. This treatment reduced the tendency of drops to hang from the nozzles after solution delivery.

The cell was made from a 100-mL round-bottom Pyrex flask to which a drain tube and solvent entry tube had been added (see Figure 2). The original 24/40 ground glass joint was replaced by a screwtop and Teflon cap. Holes of the appropriate size were drilled in the cap for the electrodes and pump lines.

An argon gas line which was attached to the bottom of the cell at the same point as the drain tube served several functions. The purified argon completed deoxygenation of the solution and mixed it thoroughly. Furthermore, the churning of the solution removed any drops remaining on the pumpline nozzles and aided in cleaning of the cell during the wash cycle.

All valves were operated under computer control. The TTL levels available at the computer interface were used to switch a bank of relays and dual peripheral driver chips which provided the necessary voltage levels. The peripheral drives (SN75450) were operated at 12 V. The relays (Sigma 70R4) switched 115 V ac. The 24 V dc required by the relay coils was provided with SN7407 gates.

Electrodes and Potentiostat. The mercury electrode was constructed in-house and could automatically deliver stationary drops with a mass range which was adjustable between 0.8 and 15 mg. The drop mass used in this work was 3.7 mg. Assuming a spherical drop, the drop area was 0.02 cm^2.

The reference electrode was a saturated calomel fiber tipped electrode (Coleman 3-710). The electrode was lengthened and bent slightly for positioning within the cell.

A large spiral of platinum wire was used for the counterelectrode. The spiral was 1.4 cm in diameter. A large electrode was used to make the potential gradient in the solution as uniform as possible.

The electrode placement is shown in Figure 2. A Teflon spacer within the cell served to hold the electrodes in position. A glass rod not shown in the figure was connected to the spacer. This rod was shaken by an electromechanical arm to dislodge mercury drops from the electrode after use.

A relatively fast potentiostat was needed to monitor the charging current decay accurately. Such a potentiostat was constructed from RCA 3140 operational amplifiers with conventional design (25). When a 10-mV step was applied to the potentiostat, the new potential (within 5%) was achieved at the reference within 5 μs, for a minimal cell time constant.

The gain of the current measurement circuitry could be adjusted manually or under computer control. The gain could be 1, 4, 8, or 32 times the manually selected gain. Automatic gain control was necessary so that accurate measurements could be made on both the charging current and the Faradaic current within the same step.

The potentiostat, cell, and solution mixing apparatus were all enclosed in a 32 × 22 × 18 in. acrylic box which was vented to a nearby hood. Aluminum sheet was fastened to the exterior of the box so that it also served as a Faraday cage for noise reduction. An external high current relay was used to turn off all ac power within the box while measurements were being made.

Computer Hardware. A Hewlett-Packard 2100S minicomputer with 32K words of core memory was used for generation of the staircase wave form, acquisition of data, and control of solution makeup. Peripherals included a general purpose interface, a paper tape punch and reader, a Tektronix 601 storage display monitor, and a TRS-80 Model II computer used as an intelligent terminal. A 16-bit optically isolated digital to analog converter was coupled to a sample and hold amplifier for production of a clean staircase which was free from DAC switching noise. Analog to digital conversion was accomplished with an Analog Devices ADC-1103 converter and a SHA-IA S/H amplifier. Timing for all operations was derived from a 20-MHz crystal clock which was scaled to a frequency appropriate for the task being executed.

The 2100S was linked to a HP 2117F minicomputer which was faster and had more extensive mass storage and graphics capabilities. Peripherals of the 2117 included a 5 MByte disk, a Tektronix 4012 graphics terminal, a Centronics 306 printer, and a Calcomp 565 digital plotter.

Experimental Timing. The staircase step height in all runs was 13.5 mV. The step length was adjusted to 13.5 or 54.0 ms to produce scan rates of 1.00 and 0.25 V/s. Two-hundred-fifty-six (256) steps were made on each cyclic staircase, scanning a potential of 0.00 to −1.73 V vs. SCE. Forty-five (45) current measurements were made on each step. The first 41 were recorded at a rate of 100 kHz starting 31.4 μs after the step using direct memory access. The final four measurements were made under program control at times which were dictated by the scan rate. When the san rate was 1.0 V/s the measurement times were 4.03, 4.13, 13.38, and 13.48 ms after the step. At 0.25 V/s, the times were 16.18, 16.28, 53.88, and 53.98 ms.

Two independent scans were averaged for each voltammogram. Before averaging was done, the scans were compared to make sure that no random noise spikes were present. They were also checked for ADC overflow and for the absence of a current spike after a step which would indicate the absence of a mercury drop. Whenever an error condition was detected, the solution was bubbled with argon for a few seconds and the mercury electrode was sent through a self-cleaning routine, after which the voltammogram was retaken.

Experiments were performed in the order in which they are listed in Table II. A new solution was created by adding components to the previous solution whenever possible. The cell was emptied and washed three times with deionized water after runs 5(a), 9, 13, and 16.

Hewlett-Packard BASIC was used to sequence the experiments and for operation I/O. Assembly subroutines were used for data acquisition and for all data manipulation done by the 2100 computer.

The 2100 computer sent the data block obtained from each experiment to the 2117 as soon as it was acquired. A FORTRAN program was run there to sort the Faradaic current from the data block and to calculate R_u and C_{dl}.

Faradaic Current Extraction. Current readings taken at the end of each step and at 30% of the step time were assumed to be predominantly Faradaic in nature. One of the two sampling times was selected as required by the factorial design. The two points which bracketed the desired time were averaged for signal to noise enhancement and stored in a permanent disk file:

Calculation of R_u and C_{dl}. The uncompensated resistance, R_u, and the double layer capacitance, C_{dl}, were calculated from the charging current decay data for each step. It was assumed that the Faradaic current remained constant over the time frame of the measurements and that it was equal to the current reading taken at the end of the previous step. Its contribution was subtracted from the charging current before further processing.

Taking the log of the familiar exponential decay equation allowed R_u and C_{dl} to be calculated by linear regression

$$\log (i) = \log (\Delta V/R_u) - t/R_uC_{dl} \quad (1)$$

An initial estimate of R_uC_{dl}, the cell time constant, was made by using only the first and twentieth point taken after the step. Six points at evenly spaced intervals were then selected to cover one time constant, and a second regression was done.

The time scale for the second regression was constructed by considering the peak of the charging current spike to be at time zero. This corrected for the dependence of the potentiostat's risetime on the capacitance of the double layer. Since the peak was not contained within the data, it was estimated from the following equation:

$$t_{peak(\mu s)} = 6.18C(\mu F) + 12.2 \quad (2)$$

The two-point estimate of C_{dl} was used in the equation. Oscilloscope measurements showed that this procedure gave peak times which were in error by no more than 2 μs for capacitances between 0.2 and 1.5 μF. Changes in R_u between 100 and 500 Ω had no effect on the peak time.

Blanks. A blank was recorded each time a new solution was made or the instrumentation was adjusted. Both the differential capacity blank and the Faradaic blank (primarily the reduction of water) were recorded and, at the operator's discretion, could be subtracted from the corresponding responses when the analyte was present.

RESULTS AND DISCUSSION

Dummy Cell Measurements. The accuracy of the double layer capacity and uncompensated resistance measurements was evaluated with a series of 15 dummy cells having time constants between 67 and 921 μs. Two percent plastic capacitors and 1% metal film resistors were used. The results are listed in Table IV. The standard error for R_u was 4.4 Ω and this error tended to be smaller for larger cell time constants. The standard error in C_{dl} estimation was 0.034 μF. It was relatively constant over the entire range of time constants examined.

Separation of Faradaic and Capacitive Currents. The accuracy of the dummy cell determinations can give an overly optimistic view of the error involved in double layer capacity measurements in real systems where Faradaic current is involved. Complete separation of Faradaic and capacitive currents can never be assumed (*28–30*). When trying to calculate the cell time constant from the step current decay, the presence of a rapid electron transfer reaction not only is an interference in itself but will also cause the flow of induced charging current which further complicates the calculation (*31*). Although simulation methods have been used to characterize the induced charging current caused by reversible electron transfer, no information is yet available for irreversible systems such as are being studied in this work.

Table IV. Dummy Cell Results

cell no.	R_u true	R_u experimental	C_{dl} true	C_{dl} experimental
1	175	183	0.382	0.35
2	175	180	0.765	0.71
3	175	180	1.15	1.10
4	175	179	1.53	1.51
5	175	176	2.29	2.23
6	301	305	0.382	0.35
7	301	306	0.765	0.76
8	301	303	1.15	1.13
9	301	303	1.53	1.50
10	301	302	2.29	2.26
11	402	410	0.382	0.36
12	402	405	0.765	0.77
13	402	401	1.15	1.12
14	402	400	1.53	1.50
15	402	399	2.29	2.28

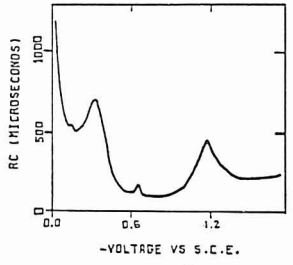


Figure 3. 0.05 M aniline and 8 × 10^{-5} M $Cd(NO_3)_2$ in 1.0 M KCl.

The presence of Faradaic interference in differential capacity curves can be recognized by unusually high capacity values near a redox couple's $E_{1/2}$. This effect is shown for a solution of aniline and cadmium nitrate in KCl (Figure 3). The shape of the curve agrees with literature values for the aniline–KCl system except for the potential region around –0.6 V vs. SCE where an extraneous peak is found. No distortion is seen at potentials somewhat anodic of $E_{1/2}$ or at potentials where the cadmium reduction is diffusion controlled. Similar results were observed with iron oxalate.

An effort was made to separate reversible Faradaic and capacitive responses by a curve-fitting technique. It was postulated that the step current response at early times could be represented by the sum of an exponential decay equation and a quadratic polynomial function representing both the Faradaic current and the induced charging current. This was found to be true for theoretical data generated by digital simulation, but fits to experimental data were not so successful. Curve fitting reduced the error in the cadmium–aniline system by 60%.

Fortunately the Faradaic current had little effect on differential capacity curves for most of the irreversible systems examined. The kinetics of oxygen reduction are slow (*32*), and the presence or absence of oxygen in the aniline solution had no effect on the differential capacity measurements. Figure 4 shows both responses for 1-chloro-2-nitrobenzene. No pseudocapacity peak was found in the region of the reduction

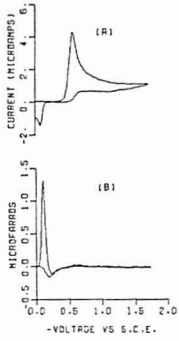


Figure 4. 1-Chloro-2-nitrobenzene response in experiment no. 1: (a) current, (b) differential capacity.

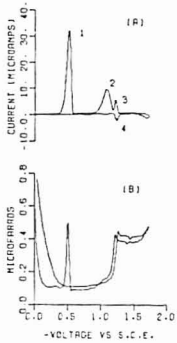


Figure 5. Response of ether 4 in experiment no. 4: (a) current; (b) differential capacity. Peaks 3 and 4 in graph (a) are due to capacitive effects. The sharp peak in graph (b) has both a capacitive and Faradaic component.

potential, −0.5 V vs. SCE. The same behavior was seen for all compounds with one benzene ring and for five of the nitrodiphenyl ethers. Faradaic interference peaks were found in the differential capacity curves for ethers 4, 6, 7, and 8 for the conditions of experiments 4 and 7 even though their reduction was irreversible. This is shown in Figure 5b. In such cases it is difficult to say whether the peak was totally due to Faradaic current or if it was due in part to a true change in capacity caused by the electron transfer reaction. The fact that there is a change in the limiting capacity on either side of the peak supports the latter view.

The contribution of charging current to the Faradaic measurements was very small in most cases. The average R_u for solutions in which ethanol was at its high level was 509 Ω. When ethanol was at its low level, the average R_u was 386 Ω. Since the average double layer capacitance was 0.37 μF, the first sampling of the Faradaic current was typically made at 24 cell time constants after the step. At 24 cell time constants, both step charging current and induced charging current should be insignificant (*31*).

The only anomalous Faradaic current measurements were observed for three of the nitrodiphenyl ethers. Voltammograms of ethers 1, 2, and 4 showed peaks which could not be explained by any reasonable Faradaic process (see Figure 5a). These peaks always occurred in regions where there was an abrupt change in differential capacity without a differential capacity peak and, thus, could be attributed to a very slow adsorption–desorption process.

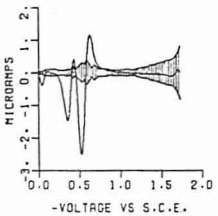


Figure 6. The effect of ethanol on the Faradaic response of 1-chloro-2-nitrobenzene. The shaded region represents the confidence interval for the effect. The effect curve is the average change in a staircase voltammogram when the percentage of ethanol in solution is changed from 9.5 to 0.5%.

Variable Effects. If a change in the level of a variable is to yield information which is useful in qualitative analysis, the change must be large enough to produce a response from the analyte which is significantly larger than the experimental noise. It would also be advantageous if each variable had a unique effect on the analyte's response so that no redundant information is collected.

The standard errors of the effects (*33*) for both the capacitive and Faradaic responses were calculated at each voltage for both compounds. The standard errors were then used to generate 95% confidence intervals which were superimposed on the plots of each effect. This is shown in Figure 6. Ninety-five percent of all variations due to experimental noise will fall within the shaded region. Any excursion of an effect curve beyond the shaded region representing the confidence interval can be considered significant.

All variables had a significant effect on the Faradaic response for both 1-chloro-2-nitrobenzene and ether 4. The magnitude of the effects decreased in the following order: pH > scan rate, ethanol, number of cycles > drop hand time > sampling time, surfactant. The shapes of all the effect curves were quite different for 1-chloro-2-nitrobenzene. For ether 4, the effect of scan rate and drop hang time were similar, but still differed from each other by more than a microamp in some places. The same was true for the effects of pH and ethanol.

The only variables which had a significant effect on the capacitive response of 1-chloro-2-nitrobenzene were pH, number of cycles, and ethanol. The effects of the number of cycles and pH were comparable in magnitude while the ethanol effect was much smaller. The shapes of each of the variable effect curves were different.

All of the variables except for the sampling time had a significant effect on the capacitive response of the strongly adsorbed ether 4. (The sampling time variable applies only to Faradaic measurements.) The magnitude of the effects decreased in the following order: number of cycles > pH > scan rate ethanol > hang time > surfactant. None of the effect curves showed much similarity in shape.

Since a possible sampling time effect on determination of capacity can be eliminated on first principles, an estimate can be made of the size of 3 factor interactions. The ethanol–number of cycles–scan rate, ethanol–pH–surfactant, and the pH–number of cycles–hang time interactions were confounded among themselves, but were free from any lower order effects. The capacitive response to these interactions was not significant at any voltage. This justifies our earlier assumption that high order interactions can be ignored in calculating the main effects, at least for the capacitive responses.

CONCLUSIONS

The methodology described here appears to provide a convenient, reliable means of generating an electrochemical data base appropriate for qualitative characterization of organic analytes. The variables chosen and the levels over which they were changed appeared to be appropriate for later pattern recognition analysis. The changes in all the experimental variables were large enough and reproducible enough to produce significant effects on both the Faradaic and capacitive responses of an analyte. The effect of each variable was unique, so that redundant information was not recorded. The information content appears to be large. Subsequent pattern recognition studies will be reported (*34*) to demonstrate applicability to computerized analyte classification.

ACKNOWLEDGMENT

The contribution of the diphenyl ethers by F. D. Hess is gratefully acknowledged.

Registry No. *p*-Nitrophenol, 100-02-7; 1-chloro-2-nitrobenzene, 88-73-3; *o*-nitrophenol, 88-75-5; *m*-nitrophenol, 554-84-7; *m*-nitrotoluene, 99-08-1; 1-chloro-4-nitrobenzene, 100-00-5; *p*-nitrotoluene, 99-99-0; 2,6-dichloro-4-nitrophenol, 618-80-4; *p*-nitroanisole, 100-17-4; α-chloro-*m*-nitrotoluene, 619-23-8; 5-(3,4-dichlorophenoxy)-2-nitrobenzoic acid potassium salt, 84132-82-1; 5-(2,6-dichloro-4-trifluoromethylphenoxy)-2-nitrobenzoic acid ethyl ester, 84132-83-2; 5-(4-trifluoromethylphenoxy)-2-nitrobenzoic acid, 84132-84-3; 5-(3,4-dichlorophenoxy)-2-nitrobenzoic acid methyl ester, 84132-85-4; 5-(4-trifluoromethylphenoxy)-2-nitrobenzoic acid sodium salt, 67815-55-8; 4-(2,4-dichlorophenoxy)-2-ethoxy-1-nitrobenzene, 33076-43-6; 2-ethoxy-1-nitro-4-(trifluoromethylphenoxy)benzene, 50594-37-1; 1-nitro-4-phenoxybenzene, 620-88-2; 5-(3-chloro-4-trifluoromethylphenoxy)-2-nitrobenzoic acid methyl ester, 84132-86-5.

LITERATURE CITED

(1) Zuman, P. "The Elucidation of Organic Electrode Processes"; Academic Press: New York, 1969; p 123.
(2) Wopschall, R. H.; Shain, I. *Anal. Chem.* **1967**, *39*, 1514.
(3) Peover, M. E.; Powell, J. S. *J. Electroanal. Chem.* **1969**, *20*, 427.
(4) Krygowshi, T. M.; Stencel, M.; Galus, Z. *J. Electroanal. Chem.* **1972**, *39*, 395.
(5) Sybrandt, L. B.; Perone, S. P. *Anal. Chem.* **1972**, *44*, 2331.
(6) Thomas, Q. V.; DePalma, R. A.; Perone, S. P. *Anal. Chem.* **1977**, *49*, 1376.
(7) DePalma, R. A.; Perone, S. P. *Anal. Chem.* **1979**, *51*, 829.
(8) Schachterle, S. D.; Perone, S. P. *Anal. Chem.* **1981**, *53*, 1672.
(9) Meites, L.; Zuman, P.; Rupp, E.; Fennor, T.; Spritzer, L., "CRC Handbook in Organic Electrochemistry"; CRC Press: Boca Raton, FL, 1978; Vol 1–4.
(10) Burgard, D. R.; Perone, S. P. *Anal. Chem.* **1978**, *50*, 1366.
(11) Damaskin, B. B.; Petrii, O. A.; Balrakov, V. V. "Adsorption of Organic Compounds on Electrodes"; Plenum Press: New York, 1971; p 40.
(12) Amadelli, R.; Daghetti, A.; Vergano, L.; DeBattisti, A.; Trasatti, S. *J. Electroanal. Chem.* **1979**, *100*, 379.
(13) Reference 11, p 39.
(14) Gupta, S.; Sharma, S. *Electrochim. Acta* **1965**, *10*, 151.
(15) Dutkiewicz, E.; Puzcz, A. *J. Electroanal. Chem.* **1979**, *100*, 947.
(16) Yih, R. Y.; Swithenbank, C., *J. Agric. Food Chem.* **1975**, *23*, 592.
(17) Bockris, J. O'M.; Reddy, A. K. N. "Modern Electrochemistry"; Plenum Press: New York, 1970; p 714.
(18) Valeriate, E. M. C.; Barradas, R. G. *J. Electroanal. Chem.* **1966**, *12*, 67.
(19) Barradas, R. G.; Kimmerle, F. M. *J. Electroanal. Chem.* **1965**, *9*, 483.
(20) Retajczyk, T. F.; Roe, D. E. *J. Electroanal. Chem.* **1968**, *16*, 21.
(21) Pilla, A. A.; Margules, G. S. *J. Electrochem. Soc.* **1977**, *124*, 1697.
(22) Ichise, M.; Yamagishi, H.; Oishi, H.; Kogima, T. *J. Electroanal. Chem.* **1980**, *106*, 35.
(23) Elkin, V. V.; Leutsner, B. I.; Abaterov, M. A.; Kuzmin, V. G. *J. Electroanal. Chem.* **1979**, *96*, 149.
(24) Ryan, M. D. *J. Electroanal. Chem.* **1977**, *79*, 105.
(25) Zipper, J. J.; Perone, S. P. *Anal. Chem.* **1973**, *45*, 452.
(26) Hendrix, C. D. *CHEMTECH* **1979**, *9*, 167.
(27) Box, G. E. P.; Hunter, W. G.; Hunter, J. S. "Statistics for Experimenters"; Wiley: New York, 1978; Chapter 12.
(28) Delahay, P. *J. Phys. Chem.* **1966**, *70*, 2373.
(29) Pilla, A. A. In "Electrochemistry, Calculations, Simulation and Instrumentation"; Mattson, Mark, MacDonald, Eds.; Marcel Dekker: New York, 1972.
(30) Fratoni, S. S., Jr.; Perone, S. P. *Anal. Chem.* **1976**, *48*, 287.
(31) Miaw, L. L.; Perone, S. P. *Anal. Chem.* **1979**, *51*, 1645.
(32) Delahay, P. "Double Layer and Electrode Kinetics"; Wiley-Interscience: New York, 1965; Chapter 10.
(33) Reference 27, p 319.
(34) Byers, W. A.; Freiser, B. S.; Perone, S. P. *Anal. Chem.*, following paper in this issue.

RECEIVED for review June 1, 1982. Accepted December 8, 1982. The authors express gratitude for the support of the Office of Naval Research.

Structural and Activity Characterization of Organic Compounds by Electroanalysis and Pattern Recognition

W. Arthur Byers,[1] B. S. Freiser, and S. P. Perone*[2]

Department of Chemistry, Purdue University, West Lafayette, Indiana 47907

Pattern recognition techniques were used to characterize organic electrochemical data. Studies included compounds of three structural classes all of which were reduced in the same potential range with four electrons. It was found that both capacitive and Faradaic responses were useful in characterization of the compounds. Structural classifications could be made with 93.3% accuracy using both types of responses. Classifications of herbicidal activity could also be made for nitrodiphenyl ethers.

The classification of chemical structure by using electrochemical techniques is a challenging problem. Although many organics of biological and commercial importance are electroactive, they generally produce electrochemical responses which consist of only a small number of peaks or waves. This lack of fine-structure makes fingerprinting difficult. The task of qualitative electroanalysis is made even more formidable from both a theoretical and experimental standpoint by the complex dependence of an electrochemical response on many variables. Electrode material and solution composition affect the nature of the electrode–solution interface and the characteristics of electron transfer in ways that are still not completely understood.

An empirical approach such as computerized pattern recognition would seem to be the best solution for qualitative identification. A computer using artificial intelligence methods can rapidly search large amounts of multivariate data for obscure relationships between structure and activity. Pattern recognition has already been used with success in determination of biological activity (*1*), and in spectral interpretation (*2*).

[1]Present address: Westinghouse Electric Corp., 1310 Beulah Road, Pittsburgh, PA 15235.
[2]Present address: Chemistry & Materials Science Department, Lawrence Livermore National Laboratory, Livermore, CA 94550.

0003-2700/83/0355-0620$01.50/0 © 1983 American Chemical Society

Within the field of electrochemistry, several pattern recognition studies have been done which have implications for qualitative electroanalysis. Schachterle and Perone (*3*) used pattern recognition to show that analysis of cyclic linear sweep voltammograms and cyclic staircase voltammograms yielded information which could be used to accurately classify the mechanism of an electrode reaction. Since similar structures can be expected to react by similar mechanisms, this approach should also be helpful in qualitative analysis.

Burgard and Perone (*4*), used staircase voltammetry to analyze 29 compounds belonging to four different electroactive group/skeleton combinations. The classes examined were aromatic–nitro, aliphatic–nitro, aromatic–aldehyde, and aromatic–aliphatic–ketone. These classes were almost completely separated on the basis of peak potential, but this feature alone cannot be considered sufficient for many identification problems. For this reason the voltammograms were examined for any shape information which might characterize a particular electroactive group or the skeleton to which it was attached. It was found that the change in peak shape with scan rate produced fair classification (70% correct) but that complete separation of the classes was not possible for the experimental conditions and compounds which were chosen. This result suggests that the information content of the electrochemical data base should be increased for more reliable structural classifications.

More information about the structure of an electroactive molecule may be gained by examination of its surface activity. The strength and potential dependence of adsorption may indicate the presence of certain functional groups (*5*, *6*). π-electron interaction with the electrode has a characteristic influence on the adsorption behavior of organics (*7*), and specific interaction between the analyte and some other molecule in the double layer may be helpful in identification (*8*, *9*).

Another potential source of structural information is the change in an analyte's electrochemical response caused by some chemical perturbation. Changes in solution conditions have been useful in the classification of electrode processes by traditional techniques (*10*) and for this reason would be expected to produce useful structural data as well.

The purpose of this paper is to evaluate the utility of pattern recognition in qualitative electroanalysis by using a data base which contains specific information on both adsorption and solution–analyte interactions. The optimization of experimental conditions for several classification problems will also be discussed.

EXPERIMENTAL SECTION

Forty-five (45) compounds representing three major structural classes were examined. All compounds were reduced between –0.3 and –0.8 V vs. SCE (pH 8) with four electrons. Large variations of reduction potential occurred within each class. The compounds and their class designations are listed in Table I. Class 1 consisted of 19 nitroaromatics containing a single benzene ring. Class 2 contains nine nitrodiphenyl ethers which were further subdivided as strong herbicides (class 2A) and those compounds which showed little or no herbicidal activity (class 2B). The criterion for the herbicidal class assignments was the Orr test (*11*). Class 3 consisted of 17 azo compounds which had hydroxy substituents ortho to the azo linkage. Most of the azo compounds contained at least one sulfonic acid group and naphthalene ring.

The nitrodiphenyl ethers were obtained from the Department of Botany and Plant Pathology, Purdue University. Purity was 95% or better. The azo compounds and most of the nitroaromatics were purchased from the Aldrich Chemical Co. in the purest form available.

Experimental conditions were varied in a fractional factorial design so that the effect of each of seven variables (*12*) could be independently determined. Sixteen different cyclic staircase voltammograms and cyclic differential capacity curves were obtained for every compound using instrumentation and techniques which have been described earlier (*12*).

Table I. Compounds Used and Class Designations

class	compound
1	4-nitrophenol
1	1-chloro-2-nitrobenzene
1	3-nitrophenol
1	nitrobenzene
1	4-nitrotoluene
1	2,6-dichloro-4-nitrophenol
1	4-nitroanisole
1	2-chloro-6-nitrophenol
1	α-chloro-3-nitrotoluene
1	1-chloro-4-nitrobenzene
1	methyl 2-nitrobenzoate
1	4-methyl-2-nitrophenol
1	5-chloro-2-nitro-1-(trifluoromethyl)benzene
1	3-methyl-4-nitrophenol
1	2-chloro-5-nitro-1-(trifluoromethyl)benzene
1	4-methyl-3-nitrophenol
1	5-chloro-2-nitrobenzoic acid
1	3-nitrotoluene
1	2-nitrophenol
2A	ethyl 5-(2-chloro-4-[trifluoromethyl]phenoxy)-2-nitrobenzoate
2A	methyl 5-(3,4-dichlorophenoxy)-2-nitrobenzoate
2A	2-chloro-1-(3-ethoxy-4-nitrophenoxy)-4-trifluoromethylbenzene
2A	methyl 5-(2-chloro-4-[trifluoromethyl]phenoxy)-2-nitrobenzoate
2B	potassium 5-(3,4-dichlorophenoxy)-2-nitrobenzoate
2B	5-(2-chloro-4-[trifluoromethyl]phenoxy)-2-nitrobenzoic acid
2B	sodium 5-(2-chloro-4-[trifluoromethyl]phenoxy)-2-nitrobenzoate
2B	1,3-dichloro-4-(4-nitrophenoxy)benzene
2B	4-phenoxy-1-nitrobenzene
3	Acid Orange 8
3	Brilliant Crystal Scarlet
3	Xylidine Ponceau 2R
3	Bordeaux R
3	Orange G
3	Erichrome Blue Black B
3	Sudan I
3	New Coccine
3	Acid Red 4
3	Chromotrope 2R
3	Crocein Orange G
3	Plasmocorinth B
3	Amaranth
3	Acid Red 88
3	Acid Red 8
3	Acid Alizarin N
3	Mordant Blue 79

The effect that each variable had on the Faradaic or capacitive response of an analyte was determined by calculation of a *variable effect curve*. This curve was constructed by summing point-by-point all responses obtained for those experiments where the variable of interest was at its high level and then subtracting out all responses where the variable was at its low level. Since the experiments were arranged according to a fractional factorial design (*13*), the effects of all other variables except the one of interest were randomized over each level and did not contribute to the effect curve.

Features for use in pattern recognition were extracted from each separate cyclic staircase voltammogram, cyclic differential capacity curve, and variable effect curve by the use of the fast Fourier transform. In each case, the cathodic and anodic portions of each curve were stored as one 256-point continuous response vs. time. The curve was scaled to cover a range of 0.0 to 1.0 and then rotated and translated in such a way that high frequency artifacts in the transform would be avoided (*14*). The transform was done with SUBROUTINE FORT (Purdue University Computer Center), and the first 64 coefficients were saved. Because

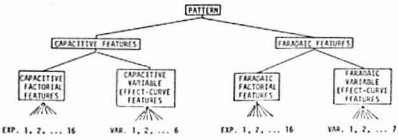


Figure 1. Feature sets.

of computer memory limitations, only the first 45 coefficients were used in later pattern recognition studies.

Figure 1 shows the breakdown of the data and the nomenclature used in referring to the different feature sets. Separate pattern recognition analyses were carried out by using the feature sets listed at the bottom of the diagram, each of which consisted of 45 Fourier coefficients.

The *Faradaic factorial features* were Fourier transform coefficients derived from individual staircase voltammograms in which the current had been sampled at the end of the step or after 30% of the step time had elapsed. There were 16 voltammograms for each compound, so 16 separate pattern recognition analyses were carried out with these features to determine which combination of experimental conditions produced voltammograms containing the most structural information.

Faradaic variable effect curve features were Fourier transform coefficients derived from Faradaic variable effect curves. Since there were seven variables in this study, seven Faradaic variable effect curves were calculated, each representing the average change in a staircase voltammogram when a variable was changed from its high to its low level. Seven separate pattern recognition analyses were carried out to determine if altering the level of any variable produced changes in a staircase voltammogram which were indicative of structure. In the same manner, *capacitive factorial features* and *capacitive variable effect curve features* were derived from the 16 differential capacity curves and six capacitive variable effect curves which were available for each compound. Only six capacitive variable effect curves were calculated since the sampling time variable applied only to measurements of Faradaic current.

Pattern recognition analyses were carried out on the various feature subsets using the k nearest neighbor (kNN) classifier with $k = 1$. Euclidian distance was used as the measure of nearness. Since the number of compounds in each class was small, the leave-one-out (LOO) procedure (*15*) was used to estimate the predictive information that was contained in each feature subset. The optimum feature combinations and weighting factors for each feature within each subset were determined by a feedback learning algorithm which used the nearest neighbor distance error (NNDE) as a performance criterion (*16*).

The feedback learning algorithm began by testing each of the 45 features in a subset to see which gave the lowest error alone. The best single feature was then combined sequentially with each of the remaining 44 features to determine the best feature pair. Each feature was assigned a weight factor to minimize the NNDE, and then the best three-feature combination was sought. This process was continued until neither adding another feature nor adjusting feature weights could reduce the NNDE.

RESULTS AND DISCUSSION

Faradaic Factorial Features. A pattern recognition analysis of the Faradaic factorial features gave classification accuracies for the 16 permutations of experimental variables. The most striking outcome of the analysis was the wide range of classification accuracies obtained, which varied between 91.1% and 68.9% over all classes. Within class 2 the classification accuracy varied between 33.3 and 100%. Obviously, the choice of experimental conditions has a strong effect on classification accuracy. The best conditions were for experiment no. 2 and 6, the worst was for no. 15. (See ref 12 for specific conditions.)

Some of the variability is undoubtedly due to experimental error. Confidence limits for the classification accuracies could have been calculated if the entire data set had been replicated, but this was not done because of the large amount of time and effort involved. A rough estimate of the error was made by comparing the results for two experiments which were run under the same conditons (*12*). Here, the total classification accuracy varied by 4.5% for the Faradaic factorial features. Thus, it is reasonable to assume that the large variations in classification accuracy with changes in experimental conditions were due to more than just random error.

Table II. Average Classification Accuracy at Each Variable Level for Faradaic Factorial Features, Classification of Structure

variable	average classification accuracy, high level	average classification accuracy, low level	effect
% ethanol	81.4	83.6	−2.2
pH	79.7	85.3	−5.6
surfactant	80.6	84.4	−3.8
no. of cycles	81.7	83.3	−1.6
scan rate	85.3	79.7	5.6
drop hang time	80.8	84.2	−3.3
sampling time	83.9	81.1	2.8

To see if it would be advantageous to hold any variable level consistently high or low in future studies, we calculated the average classification accuracy for each level of each variable. Subtraction of one average from the other gave the effect of that variable on total classification accuracy. The results for all seven variables are listed in Table II.

The two variables which had the greatest effect on the total classification accuracy were pH and scan rate. The best structural classifications were made when the pH was at 8.0 rather than 5.1, and when the scan rate was 1.0 V/s rather than 0.25 V/s.

The effect of pH on classification is most likely related to the presence of solvent reduction in the voltammograms obtained at the lower pH. Although the solvent reduction was largely eliminated through a blank subtraction, a good deal of error was involved in this process. Relatively small random changes in pH between the blank and the solution containing the analyte would cause measurable shifts in the solvent reduction. For this reason the base lines of voltammograms taken at pH 5 tended to fluctuate and degrade classification.

The better classifications obtained at the higher scan rate could be due to several causes. Increasing the scan rate would cause the differences between systems having different electrode kinetics to be accentuated. The contribution of adsorbed species to the total current would be greater at higher scan rates allowing for better distinction between molecules of high and low surface activity. Finally, the signal to noise ratio would be improved for all systems at higher scan rates.

Faradaic Variable Effect Curve Features. Previous work in this laboratory indicated that the changes in the shape of a voltammogram associated with scan rate variation contained structural information (*4*). In this study one of our goals was to confirm this finding and to see if changes in any other variable would also be helpful in structural classification. This goal can be achieved through the pattern recognition analysis of features derived from variable effect curves.

A Faradaic variable effect curve represents the average change in a staircase voltammogram when a variable is changed from one level to another. If a variable has no effect on a voltammogram, the entire effect curve should contain nothing more than random noise and be of no use in classification. Previous work (*12*) has shown that all of the variables listed in Table II produce statistically significant and reproducible changes in voltammetric wave shapes for a subset of the compounds considered in this study. Here we will consider whether or not any of these changes are good structural indicators.

Table III. Structural Classification by Using Faradaic Variable Effect Curve Features

variable effect curve	classification accuracy				no. of features
	total	class 1	class 2	class 3	
% ethanol	66.7	78.9	44.4	64.7	2
pH	84.4	94.7	44.4	94.1	5
surfactant	84.4	78.9	66.7	100	4
no. of cycles	93.3	94.7	88.9	94.1	5
scan rate	89.0	94.7	66.7	94.1	6
drop hang time	84.4	78.9	66.7	100	5
sampling time	75.6	63.2	88.9	82.3	4

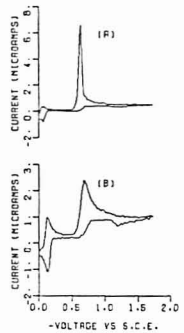


Figure 2. Second cycle staircase voltammograms of (a) Crocein Orange G and (b) 4-methyl-3-nitrophenol showing redox systems which appeared near −0.1 V vs. SCE with conditions of experiment 15 (ref 12).

Faradaic variable effect curves were calculated for each of the seven experimental variables. These curves were then analyzed in the same manner as the raw voltammograms. Fourier coefficients were extracted from the effect curves for each compound, and then an iterative feedback learning program was used to select and weight the coefficients to give the best possible classification accuracy. The results are listed in Table III.

The high classification accuracy obtained in the pattern recognition analysis of the scan rate effect curves confirms that changes in the shape of a voltammogram with scan rate are indeed useful in determination of structure. A total of 89.0% of the compounds examined were correctly classified by using scan rate effect curve features.

Even better classifications were made by using the "number of cycles" effect. A total of 93.3% of all compounds were correctly classified. This represents the highest total classification accuracy obtained for any set of Faradaic features.

The electrochemical generation of new electroactive species is a likely source of the structural information contained within the "number of cycles" effect curves. Both the nitro and the azo compounds undergo chemical reactions after electron transfer to create new redox systems which are found near −0.05 V vs. SCE. Figure 2 shows voltammograms from each group.

Another possible source of structural information is the change in the double layer between one scan and the next. Examination of differential capacity curves showed that there were often large changes in adsorption between cycles which would also be reflected in voltammetric responses.

Capacitive Factorial Features. The cyclic differential capacity curves were analyzed in the same manner as were the cyclic staircase voltammograms, obtaining classification accuracies for the 16 permutations of experimental variables. The capacitive factorial features appear to perform just as well as or better than Faradaic factorial features in classification of structure. The maximum classification accuracy was 93.3% for experiment no. 1 (see ref 12). This compares to 91.1% obtained with Faradaic features. The average total classification accuracy for all experiments was also higher. The average for the capacitive factorial features was 84.4%, while the average for the Faradaic factorial features was 82.1%.

Table IV. Average Classification Accuracy at Each Variable Level for Capacitive Factorial Features, Classification of Structure

variable	average classification accuracy		effect
	high level	low level	
% ethanol	87.4	81.1	6.3
pH	84.9	83.6	1.3
surfactant	87.1	81.4	5.7
no. of cycles	84.3	84.2	0.1
scan rate	83.7	84.7	−1.0
drop hang time	85.1	83.3	1.8

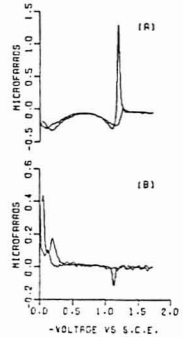


Figure 3. Blank-subtract differential capacity curves for (a) a nitrodiphenyl ether and (b) a single-ring nitroaromatic when both ethanol and surfactant were present. (Experiment no. 5, see ref 12.)

To see if classifications using capacitance data were consistently better at one level or another for the variables in Table II, we calculated the average classification accuracies for all the variable levels. Table IV lists the results. It is interesting to note that superior classifications were obtained when ethanol or sodium lauryl sulfate was present in solution. It seems that the presence of a surface active agent improved the classification of structure by increasing the differences between the responses of weakly and strongly adsorbed analytes. This was particularly true for the nitrodiphenyl ethers, where classifications were on the average 9% better when sodium lauryl sulfate was in solution.

Figure 3 compares the response of a nitrodiphenyl ether with that of another nitroaromatic when sodium lauryl sulfate was present. The nitrodiphenyl ethers had a positive differential capacity peak near −1.2 V indicating that they were strongly adsorbed at more anodic potentials. The nitroaromatics from class 1 had a negative peak in this region. The negative peak occurred because neither the surfactant (which caused a peak in the blank) nor the nitroaromatics were adsorbed on the electrode.

Capacitive Variable Effect Curve Features. Relatively poor results were obtained when capacitive variable effect curve features were used for classification of structure. The classification accuracies obtained for the variable effect curves

Table V. Structural Classification by Using Capacitive Variable Effect Curve Features

variable effect curve	classification accuracy total	class 1	class 2	class 3	no. of features
% ethanol	62.2	52.6	55.6	76.5	4
pH	71.1	68.4	66.7	76.5	4
surfactant	68.9	68.4	33.3	88.2	3
no. of cycles	75.6	68.4	77.8	82.3	3
scan rate	71.1	57.9	55.6	94.1	1
drop hang time	60.0	57.9	66.7	58.8	1

Table VI. Herbicide Analysis. Average MJEC at Each Variable Level by Using Faradaic Factorial Features

variable	average MJEC high level	low level	effect
% ethanol	0.1047	0.0848	0.0199
pH	0.1880	0.0015	0.1865
surfactant	0.1872	0.0023	0.1849
no. of cycles	0.0732	0.1164	−0.0432
scan rate	0.0732	0.1164	−0.0432
drop hang time	0.1155	0.0740	0.0415
sampling time	0.1050	0.0845	0.0205

are given in Table V. (The effect of sampling time is not included because it is not applicable to the capacitance measurement (*12*).)

The low signal to noise ratios in many of the effect curves are no doubt responsible for the poor classification accuracies. An earlier study showed that the differential capacity variable effects were too small to be distinguished from the noise for some weakly adsorbed compounds (*12*).

Determination of Herbicidal Activity. Some nitrodiphenyl ethers are potent herbicides. It has been proposed that the mechanism of herbicidal action within the class involves the formation of nitrodiphenyl ether free radicals which initiate destructive chain reactions with the polyunsaturated fatty acid moieties of phospholipid molecules making up cellular membranes (*11*). Since the first step in the reduction of most nitroaromatics at the mercury electrode also involves the formation of radical species (*17*), the electrochemical behavior and the herbicidal activity of the nitrodiphenyl ethers may be related. If this is true, then it might be possible to predict the herbicidal activity of a nitrodiphenyl ether from its voltammetric behavior using computerized pattern recognition.

The nitrodiphenyl ethers examined in this work can be divided into those which are strong herbicides (class 2A) and those which are weak herbicides or show no herbicidal action at all (class 2B). We have used computerized pattern recognition to search for electrochemical features which can distinguish between these classes.

The features which described the nitrodiphenyl ethers were divided into the same subsets which were used in the structural classification study. Analysis of the Faradaic and capacitive factorial features demonstrated that 100% classification accuracy could be achieved for over half of the experimental conditions examined using no more than two features in each case. The lowest accuracy obtained was 77.8%.

Although this result confirmed the hypothesis that voltammetric responses could be used to predict herbicidal activity, the fact that 100% classification accuracy was achieved so often made it difficult to draw any conclusions about the best experimental conditions for herbicidal analysis. For this reason another figure of merit for the performance of the pattern classifier, the modified Jurs criterion (MJEC) was used for selection of features and for evaluating experimental conditions. This figure of merit has been discussed briefly in an earlier work (*16*) and is calculated by the equation below:

$$\mathrm{MJEC} = \sum_{i=1}^{n} [R + R \tanh (\mathrm{DDS}/\mathrm{WDS})]^2 \qquad (1)$$

where n is the number of patterns, DDS is the distance to the kNN decision surface, WDS is the width of the decision surface, and R is used to weight correctly and incorrectly classified patterns. In the herbicide analysis, correctly classified patterns were given a weight of 0.1. Incorrectly classified patterns were given a weight of 1.0. A low MJEC value will indicate good class separation. Decision surfaces are usually not considered explicitly when using the kNN classifier, but their positions can be calculated if needed (*18*, *19*).

The results of the above analysis indicated that the best experimental conditions for herbicidal classification were no. 7, 11, 14, and 15 for Faradaic factorial features, and no. 4, 5, 7, 9, and 10 for capacitive factorial features. (See ref 12 for specific conditions.)

As was found before in the classification of structure, capacitive factorial features performed somewhat better than Faradaic factorial features. The mean MJEC was 0.125 for the Faradaic factorial features, but it was 0.049 for the capacitive factorial features.

The ability of capacitive factorial features to distinguish between classes 2A and 2B suggests that the hydrophobicity and/or the steric configuration of a nitrodiphenyl ether may play a very important role in determining its herbicidal activity.

It appeared that classifications of herbicidal activity using Faradaic factorial features could be improved considerably by working at high pH and by not using surfactant. Large increases in the modified Jurs error criterion were observed when either nitric acid or sodium lauryl sulfate was added to the solution being analyzed. This effect is shown in Table VI.

Table VII summarizes the results of the herbicide analysis using variable effect curve features. The modified Jurs error criterion has been listed as well as the total classification accuracy. Overall, features derived from variable effect curves did not do as well in the classification of herbicidal activity as did the features which were calculated directly from

Table VII. Results of Herbicide Analysis by Using Variable Effect Curve Features

variable	Faradaic variable effect curve features MJEC	% accuracy	no. of features	capacitive variable effect curve features MJEC	% accuracy	no. of features
% ethanol	0.0010	100	2	0.0027	100	2
pH	0.6939	77.8	2	0.4635	77.8	1
surfactant	0.0046	100	2	0.0039	100	2
no. of cycles	0.0015	100	2	0.6117	77.8	2
scan rate	0.0026	100	2	0.4075	77.8	1
drop hang time	0.5027	88.9	1	0.5009	88.9	1
sampling time	0.6877	77.8	1			

Table VIII. Overall Summary of Structural Characterization Studies

	parameters[a]			
	F_{fact}	C_{fact}	F_{ve}	C_{ve}
best overall % classfctn	91.1	93.3	93.3	75.6
no. of features	8	6	5	3
best classfctn by classes	89.4	100	94.7	68.4
	100	77.8	88.9	77.8
	82.3	94.1	94.1	82.3
most useful factors	high pH and scan rate	high % EtOH and surfactant	no. of cycles	no. of cycles

[a] F_{fact} = Faradaic factorial; C_{fact} = capacitive factorial; F_{ve} = Faradaic variable effects; C_{ve} = capacitive variable effects.

staircase voltammograms or differential capacity curves. Capacity effect curve features were particularly poor.

CONCLUSIONS

Computerized pattern recognition appears to be very useful in qualitative electroanalysis when the proper experimental conditions are chosen, as summarized in Table VIII. It was possible to distinguish between three structural classes with similar electrochemical characteristics. Even though nitrodiphenyl ethers, the nitroaromatics, and the azo compounds were reduced in the same potential region with the same number of electrons, 93.3% classification accuracy was achieved.

Pattern recognition appears to be useful in predicting herbicidal activity from electrochemical behavior. Herbicidally active and inactive nitrodiphenyl ethers were distinguished from each other with a classification accuracy of 100% over a wide range of experimental conditions. Although the small number of herbicides studied precludes too much optimism, it might be possible to use the methods described here to screen newly synthesized compounds within the same general structural class for herbicidal activity. Another important area of application would be identification of herbicides within the environment.

Perhaps the most significant result of the work reported here, however, is the demonstration that the information content of voltammetric data can be enhanced considerably by the systematic adjustment of experimental conditions. Moreover, it is clear that the interpretation objectives will dictate the choice of experimental conditions, and a well-designed study as described here is capable of specifying the most favorable choices. It is also interesting to observe that the most useful experimental variations are not necessarily those which are traditionally valued most highly in voltammetric studies—such as the enhancement of surface interactions. Thus, we hope the work described here will direct attention to the surprising amount of useful qualitative information available in voltammetry and to the effective tools for information enhancement and interpretation.

Registry No. 4-Nitrophenol, 100-02-7; 1-chloro-2-nitrobenzene, 88-73-3; 3-nitrophenol, 554-84-7; nitrobenzene, 98-95-3; 4-nitrotoluene, 99-99-0; 2,6-dichloro-4-nitrophenol, 618-80-4; 4-nitroanisole, 100-17-4; 2-chloro-6-nitrophenol, 603-86-1; α-chloro-3-nitrotoluene, 619-23-8; 1-chloro-4-nitrobenzene, 100-00-5; methyl 2-nitrobenzoate, 606-27-9; 4-methyl-2-nitrophenol, 119-33-5; 5-chloro-2-nitro-1-(trifluoromethyl)benzene, 118-83-2; 3-methyl-4-nitrophenol, 2581-34-2; 2-chloro-5-nitro-1-(trifluoromethyl)-benzene, 777-37-7; 4-methyl-3-nitrophenol, 2042-14-0; 5-chloro-2-nitrobenzoic acid, 2516-95-2; 3-nitrotoluene, 99-08-1; 2-nitrophenol, 88-75-5; ethyl 5-(2-chloro-4-[trifluoromethyl]phenoxy)-2-nitrobenzoate, 77207-01-3; methyl 5-(3,4-dichlorophenoxy)-2-nitrobenzoate, 84132-85-4; 2-chloro-1-(3-ethoxy-4-nitrophenoxy)-4-trifluoromethylbenzene, 42874-03-3; methyl 5-(2-chloro-4-[trifluoromethyl]phenoxy)-2-nitrobenzoate, 50594-67-7; potassium 5-(3,4-dichlorophenoxy)-2-nitrobenzoate, 84132-82-1; 5-(2-chloro-4-[trifluoromethyl]phenoxy)-2-nitrobenzoic acid, 50594-66-6; sodium 5-(2-chloro-4-[trifluoromethyl]phenoxy)-2-nitrobenzoate, 62476-59-9; 1,3-dichloro-4-(4-nitrophenoxy)benzene, 1836-75-5; 4-phenoxy-1-nitrobenzene, 620-88-2; acid orange 8, 5850-86-2; brilliant crystal scarlet, 2766-77-0; xylidine ponceau 2R, 3761-53-3; bordeaux R, 5858-33-3; orange G, 81604-88-8; erichrome blue black B, 3564-14-5; sudan I, 842-07-9; new coccine, 2611-82-7; acid red 4, 5858-39-9; chromotrope 2R, 4197-07-3; crocein orange G, 1934-20-9; plasmocorinth B, 1058-92-0; amaranth, 915-67-3; acid red 88, 1658-56-6; acid red 8, 4787-93-3; acid alizarin N, 2092-55-9; mordant blue 79, 3567-69-9.

LITERATURE CITED

(1) Chu, K. C.; Feldmann, R. J.; Shapiro, M. G.; Hazard, G. F.; Geran, R. I. *J. Med. Chem.* **1975**, *18*, 539.
(2) Abe, H.; Jurs, P. C. *Anal. Chem.* **1975**, *47*, 1829.
(3) Schachterle, S. D.; Perone, S. P. *Anal. Chem.* **1981**, *53*, 1672.
(4) Burgard, D. R.; Perone, S. P. *Anal. Chem.* **1978**, *50*, 1366.
(5) Damaskin, B. B.; Petrii, O. A.; Batrakov, V. V. "Adsorption of Organic Compounds on Electrodes"; Plenum Press: New York, 1971; p 40.
(6) Amadelli, R.; Daghetti, A.; Vergomo, L.; DeBattisti, A.; Trasatti, S. *J. Electroanal. Chem.* **1979**, *100*, 379.
(7) Reference 5, p 39.
(8) Gupta, S.; Sharama, S. *Electrochim. Acta* **1965**, *10*, 151.
(9) Dutkiewicz, E.; Puacz, A. *J. Electroanal. Chem.* **1979**, *100*, 947.
(10) Zuman, P. "The Elucidation of Organic Electrode Processes"; Academic Press: New York, 1969; Chapter 2.
(11) Orr, G. Ph.D. Thesis, Purdue University, 1981.
(12) Byers, W. A.; Perone, S. P. *Anal. Chem.*, preceding paper in this issue.
(13) Hendrix, C. D. *CHEMTECH* **1979**, *9*, 167.
(14) Hayes, J. W.; Clover, D. E.; Smith, D. E. *Anal. Chem.* **1973**, *45*, 277.
(15) Thomas, Q. V.; DePalma, R. D.; Perone, S. P. *Anal. Chem.* **1977**, *49*, 1376.
(16) Byers, W. A.; Perone, S. P. *Anal. Chem.* **1980**, *52*, 2173.
(17) Kastening, B.; Holleck, L. *J. Electroanal. Chem.* **1970**, *27*, 355.
(18) Byers, W. A. Ph.D. Thesis, Purdue University, West Lafayette, IN, 1981, SUBROUTINE HYPE.
(19) Batchelor, B. G. "Practical Approach to Pattern Classification"; Plenum Press: London, 1974.

RECEIVED for review June 1, 1982. Accepted December 8, 1982.

Pattern Recognition for Identification and Quantitation of Complex Mixtures in Chromatography

Robert E. Lea

Entek, Inc., 1015 South Louisiana, Little Rock, Arkansas 72202

Randall Bramston-Cook*

Varian Associates, Instrument Group, 9901 Paramount Boulevard, Downey, California 90240

Janice Tschida

Varian Associates, Instrument Group, 4665 Kipling Avenue, Wheatridge, Colorado 80033

Numerous applications in gas and liquid chromatography require the identification and quantitation of mixtures of compounds which together constitute a single entity. This analysis may be complicated by interference with one or more peaks by other compounds that ordinarily are not part of the mixture. A method is described which uses currently available chromatographic data systems to provide pattern recognition, quantitation, and elimination of interferences by simple programming techniques. The method is illustrated by identification and quantitation of some polychlorinated biphenyl (PCB) mixtures.

Both gas chromatography and liquid chromatography have been in routine use for determination of specific single components in a sample matrix. Concentrations are calculated by the ratio of standard responses of the detector to the response when the unknown sample is chromatographed

$$C_x = \frac{A_x C_s}{A_s} \tag{1}$$

where C_x is the concentration of a single unknown component and C_s is the known concentration of the single standard. A_x and A_s are the corresponding computed areas. Retention times are normally used to identify specific compounds in mixtures. If a chromatographic peak does not match the retention time of a known compound, the peak can neither be identified nor quantitated without severe assumptions on predicting retention times and detector responses (*1*, *2*).

By use of classical chromatographic methods in analyzing complex mixtures, each peak is required to be identified by retention time, and a standard must be created to calculate the unknown concentration by the equation

$$C_x = \sum_{i=1}^{n}\left(\frac{A_{xi}C_{si}}{A_{si}}\right) \tag{2}$$

where C_x is the total concentration of the mixture, C_{si} is the standard concentration for each component i, and A_{xi} and A_{si} are the computed areas for each unknown peak and its corresponding standard, respectively. This method requires extensive analysis of the mixture, frequently involving mass, infrared, or nuclear magnetic resonance spectrometries, and synthesis of pure standards of individual components (*3*). This complete analysis is often beyond the capabilities of many analytical laboratories. Even if this kind of analysis were undertaken, so many peaks may be involved that coelution of compounds may occur, prohibiting proper quantitations. Analysis would be improved significantly in gas chromatography with capillary columns, since peaks would be more fully resolved (*4*, *5*), and yet the analytical problem still would be very complicated since additional peaks would have to be identified and quantitated.

Another method used to quantitate mixtures is measuring total area of the standard mixture and comparing that total to the total area of the unknown to determine concentration (*2*)

$$C_x = C_s\left[\frac{\sum_{i=1}^{n} A_{xi}}{\sum_{i=1}^{n} A_{si}}\right] \tag{3}$$

This method assumes overlapping, unrelated peaks are absent—a difficult requirement in most analyses (*6*).

Both of these methods for mixtures require visual inspection of the chromatogram to determine the identity of the pattern prior to quantitation (*5*). This may require repeated injections at different attenuations to produce on-scale, significant peaks, even though no new quantitative data are generated by the data system.

The method described here is a straightforward, reliable mechanism for simultaneous identification and quantitation of mixtures without characterization of each component. This method reduces operator judgement in the identification of the mixture and properly eliminates interfering peaks due to possible contaminants. This simplified numerical pattern recognition is used to compare unknown mixtures to known standards. Individual chromatographic peak areas of the standard mixture are mathematically ratioed with the corresponding areas of the unknown peaks at the same retention times

$$C_{xi} = \frac{C_s A_{xi}}{A_{si}} \tag{4}$$

where C_s is the total concentration of the standard mixture. A perfect match of patterns would result when the reported ratios, C_{xi}, have consistent values for all peaks. The extent to which ratio values agree provides an objective measurement of the match. Statistical treatment of the results gives an assignment of a confidence level for the match. The resultant ratios would have a scattered distribution with no regions of consistency if the unknown mixture is not a match with the standard mixture. If a match is confirmed, concentration of the unknown mixture, $\bar{C}_x$, can be reported as the average of the reported values used in the match

$$\bar{C}_x = \frac{\sum_{i=1}^{n} C_{xi}}{n} \tag{5}$$

0003-2700/83/0355-0626$01.50/0 © 1983 American Chemical Society

If several complex mixtures have been combined, consistent ratios are observed in chromatographic regions that are unique to each mixture. Overlapping regions of peaks for both mixtures will have reported ratios that are inconsistent and meaningless. Examination of the unique regions permits combinations of mixtures to be both identified and quantitated.

EXPERIMENTAL SECTION

The Varian Vista 401 chromatographic data system (Varian Associates, Walnut Creek, CA) has been used to illustrate this simplified pattern recognition method. The demonstration has been performed both with synthetic chromatograms and with an authentic analytical problem.

In order to more readily illustrate the concept of this pattern recognition method, artificial chromatograms of mixtures had been created, using the base line subtraction routine of the data system. Manual entry of negative values at specific retention times, when subtracted from a flat base line, resulted in positive triangular peaks, suitable for controlled experiments.

Secondly, mixtures of PCB were analyzed with the Varian Vista 44 gas chromatographic system (Varian Associates) utilizing a 2-m stainless steel column, $^1/_8$ in. o.d. packed with 3% OV-101 on Chromosorb G-AW, 80/100 mesh. Detection was made by an electron capture detector with nitrogen as the carrier gas, set to a flow rate of 30 mL/min. Raw chromatographic data were stored on floppy disk for later recall and remanipulation.

The Varian CDS-111 (Varian Associates) has also been successfully programmed to perform this pattern recognition computation.

NUMERICAL PATTERN RECOGNITION

In the overall scheme for pattern matching, a method is created in the data system for each standard mixture. After the floppy disk containing the raw chromatographic data of each standard mixture is loaded into the data system, the "learn" mode is executed first, which automatically enters retention times of all peaks to be used in the matching process into the peak table for that method. The "learn" mode eliminates the necessity to manually enter peak retention times into the peak table.

To perform pattern recognition, peak areas from the standard mixtures are divided into the corresponding peak areas of the unknown with matching retention times. The computation is performed in two steps. The mathematical reciprocal of peak area is calculated for each peak of the standard mixture. The "calibration" mode in the data system is used to perform this step

$$R_i = \frac{1}{A_{si}} \tag{6}$$

where R_i becomes the reciprocal of the peak area for each component in the standard mixture.

When the areas from the unknown mixture are multiplied with the corresponding reciprocals using the "analysis" mode, a match will be confirmed if the reported ratios are consistent

$$C_{xi} = C_s R_i A_{xi} \tag{7}$$

Multiplication of the ratios by the total concentration of the standard mixture, C_s, results in concentration of the unknown mixture, C_{xi}, being reported.

Linkage of data system methods, each specific to individual standard mixtures, results in multiple reports being automatically generated. The report with consistent results for the most peaks in the unknown chromatogram provides identity of the match. Ratios may not be perfectly consistent due to sample or chromatography imperfections.

RESULTS AND DISCUSSION

Artificially created chromatograms to demonstrate the principle of this method are illustrated in Figure 1. Each of the three standard patterns (A, B, and C) yields a set of computed reciprocal values that are then stored in the method for that standard. When these reciprocals are multiplied with the corresponding areas of the "unknown" (Figure 2), 80% of the unknown peaks have very consistent reported ratios

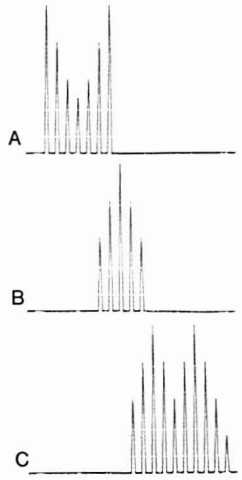


Figure 1. Artificially generated peak patterns illustrate the method of pattern recognition. Three standard patterns are used to compute retention times and factors to represent that mixture.

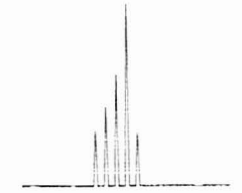


Figure 2. Computation of an unknown artificial sample against the standard patterns shown in Figure 1 results in consistent reported concentrations matching pattern B (except for one reported value). (See Table 1.)

Table 1. Results for Areas of the Unknown Artificial Sample Divided by Areas for Each Standard Pattern

peak no.	peak name	result ratio	time, min
	Pattern "A"		
1	six	0.49	3.50
2	seven	0.53	4.00
	Pattern "B"		
1	six	0.74	3.50
2	seven	0.71	4.00
3	eight	0.75	4.50
4	nine	1.63	5.00
5	ten	0.72	5.50
	Pattern "C"		
4	nine	2.45	5.00
5	ten	0.48	5.50

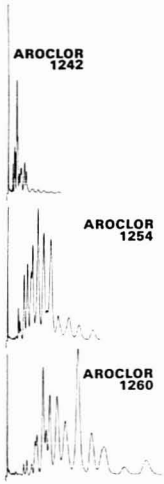


Figure 3. Standard mixtures of three common PCB mixtures are assigned individual data system programs. Retention times and response factors are determined for peaks in each mixture. These values are stored for later comparison with unknown samples.

when compared with pattern B (Table I); whereas, the other reports indicate inconsistent ratios (pattern C) or a small percentage of peaks (40%) that match in retention times (pattern A).

Several data treatments are tried on the ratios obtained from the matching comparisons. The objective is to reduce operator interpretation to confirm a match. To establish a basis for evaluating the validity of data obtained from these treatments, three major criteria are identified—reduction of operator judgement, proper elimination of interfering peaks due to possible contaminants, and assignment of a confidence level for a match.

A visual inspection of chromatograms for identification of mixtures does not fulfill these requirements. The matching is very dependent upon the operator's judgement. Major peaks will dominate the matching process. Multiple comparisons become tedious, and a numerical confidence value cannot be assigned.

Calculation of the relative standard deviation of the resultant ratios of peak areas from the pattern recognition results can relate the consistency of a match. If one peak ratio were eliminated from the comparison of the "unknown" with pattern B, a low relative standard deviation of 2% for the results indicates a match. Since the four matched peaks in the "unknown" corresponded in retention times to four of five peaks in pattern B, the two patterns must be a perfect match. Relative standard deviation levels required to indicate a match must be determined empirically from replicate analyses of standards and control samples to correct for experimental errors. A judgement level can then be assigned based on computations and not on operator bias.

Utilization of the "Q test" permits statistical elimination of a deviate ratio from the relative standard deviation calculation (7). Ratio of the deviation of the suspect value from its closest neighbor and the total range of all values (difference between the highest and lowest ratios) yields a value of 0.95 from results obtained with the comparison of the "unknown" with pattern B. This value is well above the rejection ratio

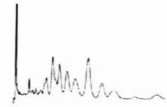


Figure 4. By computing concentrations for peaks found in an unknown sample from response factors of standards (determined from data in Figure 3), the unknown is matched with Aroclor 1260. (See Table II.)

Table II. Results for Comparison of the Unknown PCB Sample and the Three Standard Aroclor Mixtures

peak no.	result ratio, ppm	time, min
Unknown Sample vs. Aroclor 1242		
6	0.32	0.982
9	0.11	1.690
10	0.81	2.518
11	0.07	2.790
Unknown Sample vs. Aroclor 1254		
12	0.22	3.080
13	0.20	3.627
14	0.21	4.456
15	0.28	5.321
16	0.48	6.351
18	0.38	7.465
19	1.29	8.688
20	1.08	10.035
21	3.13	12.144
22	1.95	14.379
Unknown Sample vs. Aroclor 1260		
17	0.38	6.809
18	0.53	7.465
19	0.40	8.688
20	0.40	10.035
21	0.37	12.144
22	0.40	14.379
23	0.33	16.403
24	0.30	19.757
25	0.31	23.347

of 0.64, based on the averaging of five data points, as defined in the "Q test". This outside peak is simply dropped from the averaging and the reported mean concentration becomes more representative of the true value. This mathematical treatment of the data permits elimination of apparent ratio inconsistencies due to overlapping chromatographic interferences.

If too many inconsistent ratios are involved to be properly eliminated by the "Q test", a match could be determined by computing the percentage of peaks that are near the median value of the series of ratios. The median is the middle value of an ordered set of values. A large percentage of peaks close to the median value would confirm a match (8).

The above data treatments can be applied to the analysis problem of polychlorinated biphenyls (PCB). Figure 3 illustrates the chromatograms for three standard PCB mixtures (Aroclors 1242, 1248, and 1260). When the unknown sample (Figure 4) is ratioed with each of the three standards (Table II), the low relative standard deviation of 17% for the results with the Aroclor 1260 comparison indicates that the unknown is matched with this standard. Also indicative of a match is the high number (92%) of standard peaks found in the unknown sample. The other two comparisons (Aroclors 1242 and 1254) result in very high relative standard deviations (89% and 100%, respectively) and cannot be considered a possible match.

Crucial to the matching process is retention time repeatability. Slight shifts in retention time can cause mismatching of corresponding peaks and very inconsistent ratios. To

Table III. Results for Artificial Chromatogram Generated by Combining Two Standard Mixtures when Compared with Each Standard Pattern

peak no.	peak name	result ratio	time, min
	Pattern "A"		
1	six	0.67	3.50
2	seven	0.75	4.00
	Pattern "B"		
1	six	1.00	3.50
2	seven	1.00	4.00
3	eight	1.00	4.50
4	nine	1.67	5.00
5	ten	2.49	5.50
	Pattern "C"		
4	nine	2.50	5.00
5	ten	1.67	5.50
6	eleven	1.25	6.00
7	twelve	1.00	6.50
8	thirteen	1.00	7.00
9	fourteen	1.00	7.50
10	fifteen	1.00	8.00
11	sixteen	1.00	8.50
12	seventeen	1.00	9.00
13	eighteen	1.00	9.50

correct for minor shifts in retention time normally encountered in chromatography, major peaks can be identified as reference peaks. The data system assigns a reference peak as the largest peak within a specified time window of its expected retention time. Retention times for the rest of the peaks are then adjusted in the data system peak table to correct for small time shifts. This correction ensures proper peaks to be matched in the pattern recognition process.

Combinations of mixtures can be determined when reported ratios are consistent for regions unique to each mixture. An artificial chromatogram is shown in Figure 5. Table III shows consistent concentrations for regions unique to pattern B and to pattern C (see Figure 1). Reported peaks common to both mixtures have very inconsistent values compared with either standard and can be eliminated from the matching. Concentration for each mixture is then computed as the average of the consistent values.

Close examination of results for PCB's presented in Table II indicate consistent ratios near the beginning of the chromatogram that correspond to Aroclor 1254. A relatively low relative standard deviation of 33% for the six early peaks provides suspicion that the unknown mixture of PCB's contains both Aroclor 1254 and Aroclor 1260, with average concentrations of 0.38 ppm and 0.29 ppm, respectively.

CONCLUSION

This simplified numerical pattern recognition method can greatly assist in identifying complex mixtures which have consistent proportions of unidentified components. This method overcomes several difficulties with existing analytical procedures. Since both positive identification and quantitation are given in the same report, the chromatographer's interaction is greatly simplified. Judgements are based on objective results of numerical data. Reported concentrations are improved since the results become an average value. However, this method is not applicable when patterns are not consistent between standards and samples from preferential degradation of only a few of the components due to metabolism or volatility differences. The analyst must then revert to quantitation by the summation of individual component concentrations, since the pattern of the mixture cannot be identified.

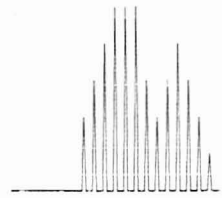


Figure 5. Computation of an unknown artificial sample against the standard patterns in Figure 1, results in two reports each with a region of consistent concentrations. Pattern B is consistent with early eluting peaks and pattern C is consistent with late eluting peaks. (See Table III.)

ACKNOWLEDGMENT

The authors extend appreciation to Anne Warner for the preparation of this manuscript.

LITERATURE CITED

(1) Gas Processors Association "Method of Analysis for Natural Gas and Similar Gaseous Mixtures by Gas Chromatography"; GPA: Tulsa, OK, 1972 (Revised); GPA Publication 2261–72 p 8.
(2) Association of Official Analytical Chemists "Official Methods of Analysis," 12th ed.; AOAC: Washington, DC, 1975; Chapter 29.
(3) Webb, T. G.; McCall, A. C. *J. Chromatogr. Sci.* **1973**, *11*, 366–373.
(4) Webb, R. G.; McCall, A. C. *J. Assoc. Off. Anal. Chem.* **1972**, *55*, 746–752.
(5) Gordon, R. J.; Szita, J.; Faeder, E. J. *Anal. Chem.* **1982**, *54*, 478–481.
(6) U.S. Environmental Protection Agency "Manual for Analytical Quality Control for Pesticides and Related Compounds"; National Technical Information Service, U.S. Department of Commerce: Springfield, VA, 1981; EPA 600/2 81-059.
(7) Waser, J. "Quantitative Chemistry"; W. A. Benjamin: New York, 1964; p 83.
(8) Lepisto, M.; Bramston-Cook, R., submitted for publication in *J. Forensic Sci.*

RECEIVED for review November 13, 1981. Resubmitted January 7, 1983. Accepted January 7, 1983. This work was presented at the 1981 Pacific Conference on Chemistry and Spectroscopy, Anaheim, CA, October 20, 1981.

Factor Analysis for Separation of Pure Component Spectra from Mixture Spectra

Paul C. Gillette, Jerome B. Lando, and Jack L. Koenig*

Department of Macromolecular Science, Case Western Reserve University, Cleveland, Ohio 44106

The use of factor analysis to extract pure component spectra from a series of infrared mixture spectra is described. This technique requires that each pure component spectrum have a nonoverlapped characteristic peak. Through the use of the cross product of eigenspectra it is possible to automatically identify key frequencies in the eigenspectra. Normalization of spectra permits extension of the procedure to systems in which the pathlength is not fixed. Numerical examples, model spectra, and actual infrared spectra are used to illustrate the technique.

In two previous papers the use of factor analysis to improve the signal to noise ratio (*1*) and the analysis of mixtures by searching spectral libraries was discussed (*2*). One is often confronted with systems in which it is not possible to prepare or isolate pure components. This situation is especially true in the spectrometric analysis of polymers where changes in conformation result in new crystal phases. The ratio method (*3*) provides one means of spectral separation, although its application is limited primarily to binary systems. During the course of factor analysis abstract "eigenspectra" are computed which contain all of the spectral features necessary to reconstruct the spectra of the mixtures. These same abstract "eigenspectra" can be combined to form the spectra of the pure components which form the mixtures (*4–11*).

EXPERIMENTAL SECTION

Instruments. Infrared spectra were collected on a Digilab FTS14 Fourier transform spectrometer equipped with a TGS detector using 10 scans of sample and reference at a resolution of 4 cm^{-1}. Spectra were transformed with zero filling by a factor of 1 with triangular apodization. Infrared spectra were then transferred to a DEC VAX 11/780 computer operating under VMS 3.0 for data processing.

Computer Programs. All calculations were performed by the FORTRAN 77 program FACANAL which contains ca. 5000 lines of source code exclusive of graphics routines. This program also incorporates facilities for target testing (*2*) of known spectra using the EPA spectral library and improvement (*1*) of individual S/N ratios in mixture spectra. Through the use of PARAMETER statements in INCLUDE files array dimensions may be readily changed to permit the analysis of high-resolution spectra or problems involving a large number of mixtures. Graphics output was displayed on a DEC VT100 with Retrographics (a terminal which emulates Tektronix 4010 series terminals) using Tektronix Plot10 software with hardcopy supplied by a Printronix P300 dot matrix line printer.

THEORY

Factor analysis generates two quantities which are essential in extracting the spectra of the pure components: abstract eigenspectra which contain all the spectral features necessary to construct the spectra of the pure components and eigenvectors which may be thought of as being abstract representations of the concentrations of the pure components within the mixtures. To obtain the pure component spectra it is necessary to rotate the abstract concentrations to obtain "real" concentrations. Unfortunately, both quantities are abstract in the sense that it is not possible to directly obtain the pure component spectra from this information alone. For most spectral techniques one can place some restrictions upon the pure spectra—for example in infrared spectrometry all absorbances must be greater than or equal to zero. The case in which each pure component spectrum has an absorbance which is unique to itself (i.e., a peak which is not overlapped) is a special one. If the positions of these peaks can be determined, then it is possible to set up a system of linear equations, the solution of which will provide the appropriate constants by which to multiply the abstract spectra to obtain pure component spectra.

Mathematically the preceding analysis is done by first constructing a covariance or correlation matrix as follows:

$$[C] = [D]^t[D] \tag{1}$$

where [C] = covariance/correlation matrix and [D] = mixture spectra matrix. (A correlation matrix requires that each spectrum be normalized by dividing by the square root of the sum of the squared absorbances.) The problem can then be expressed as an eigenvalue problem

$$[C][E] = [E][L] \tag{2}$$

where [C] = covariance/correlation matrix, [E] = eigenvector matrix, and [L] = eigenvalue matrix. (In this statement of the problem the eigenvectors are in columns of the [E] matrix.) Statistical methods which have been described elsewhere (*1*, *9*, *12–14*) permit one to establish the minimum number of eigenvalues/eigenvectors necessary to reconstruct the data matrix within the bounds of the experimental error. Eigenvalues/eigenvectors can then be assigned as being either "real" or "noise". Abstract "eigenspectra" are constructed by using the data matrix and the "real" eigenvectors in accordance with eq 3

$$[A] = [D][E'] \tag{3}$$

where [A] = abstract "eigenspectra" matrix, [D] = mixture spectra matrix, and [E'] = "real" eigenvector matrix. One desires to determine a transformation matrix [T] consisting of scaling coefficients by which to multiply the abstract eigenspectra to obtain the pure component spectra

$$[P] = [A][T] \tag{4}$$

where [P] = spectra of the pure components, [A] = abstract "eigenspectra", and [T] = transformation matrix. As mentioned previously, the restriction that each pure component spectrum contain a peak in a region where the other pure component spectra do not absorb enables one to devise a system of linear equations to calculate the transformation matrix [T]. Since every point in the calculated pure component spectra must be greater than or equal to zero, one has the following relationship for a binary system (*6–8*):

$$p_{ik} = t_{k1}a_{i1} + t_{k2}a_{i2} \geq 0 \tag{5}$$

Rearrangement of this equation permits one to establish ratio

0003-2700/83/0355-0630$01.50/0 © 1983 American Chemical Society

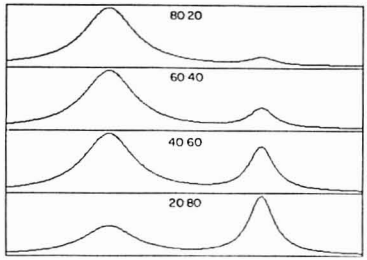


Figure 1. Model spectra generated by forming linear combinations of two Lorentzian peaks.

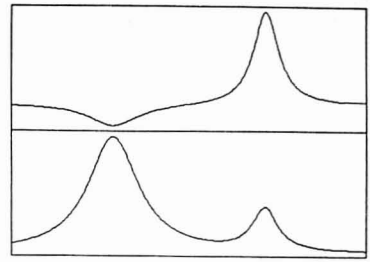


Figure 2. Abstract "eigenspectra" generated by using only two eigenvectors and Lorentzian model mixtures.

criteria in which the smallest minimum and positive ratios of the abstract eigenspectra establish boundary regions in which pure component spectra have negative absorbances. For spectra which are collected with a fixed pathlength cell and one is observing a system in which one component evolves as another is depleted, then the eigenvector pairs will fall on a straight line (*8*). The intersection of this line with the two boundary lines directly yields the coefficients by which to multiply the abstract spectra to obtain the pure component spectra.

Systems containing more than two pure components are somewhat more complicated and graphical methods cannot be utilized. By forming the ratios of all pairs of abstract eigenspectra, one can determine the locations of the characteristic points in the pure spectra. (Various combinations will produce the same points.) One can then use a modified form of eq 4 to determine the transformation matrix by arbitrarily setting the absorbances of the pure spectra to a square matrix of Kronecker deltas (i.e., a diagonal matrix with ones on the diagonal) and using only the absorbances in the abstract eigenspectra at the characteristic points. Rearrangement of eq 3 and 4 leads one to eq 6 in which the mixture spectra are defined in terms of the pure components.

$$[D] = [P]([T]^{-1}[E']^t) \qquad (6)$$

where [D] = mixture spectra matrix, [P] = spectra of pure components matrix, [T] = transformation matrix, and [E'] = "real" eigenvector matrix. The product of the inverse of the transformation matrix and the real eigenvectors represents the scaling coefficients by which to multiply the pure component spectra to obtain the mixture spectra. As such it is clearly related to the concentrations. For systems with more than two pure components it is necessary to standardize these coefficients by dividing by their sum for each mixture to obtain the relative concentrations within the mixtures. In this way the percentage contribution of the pure components to each mixture may be calculated. (All of the preceding steps are illustrated in great detail on a very simple problem in the Appendix.)

RESULTS AND DISCUSSION

As an illustration of pure component extraction by factor analysis, the four spectra in Figure 1 were generated by forming linear combinations of two Lorentzian peaks. Factor analysis of the covariance matrix indicated two pure components as anticipated. The two primary eigenvectors were then used to construct the abstract "eigenspectra" in Figure 2. A plot of the four ordered pairs of the two primary eigenvectors (Figure 3) clearly indicates a linear relationship between the eigenvectors. The points of intersection of this linear with the boundary region yield the coefficients by which to multiply the abstract eigenspectra to obtain the pure component

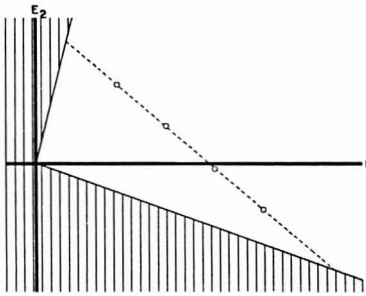


Figure 3. Plot of "real" eigenvectors—points in shaded region would produce pure component spectra with negative intensities.

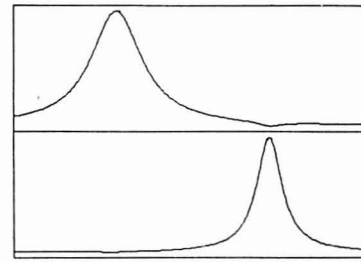


Figure 4. Extracted pure component spectra from Lorentzian model mixtures.

spectra. Depicted in Figure 4 are the spectra of the extracted pure components.

As an example of an application of the technique to actual spectral data, six mixtures of hexane and chloroform were prepared (Figure 5). For correction of differences in base lines which would result in an incorrect number of components a linear base line was removed as follows: A line was computed which passed through the minimum absorbances in the first and last 10% of the spectrum. This wedge was then subtracted and the entire spectrum shifted by a constant so that the minimum absorbance was 0. All forms of error analysis based on the magnitudes of the eigenvalues indicate two pure components. A plot of the primary eigenvectors generated by factor analysis of the covariance matrix fails to yield any apparent relationship between the eigenvectors (Figure 6). This is because the spectra are not in the same scale—a linear

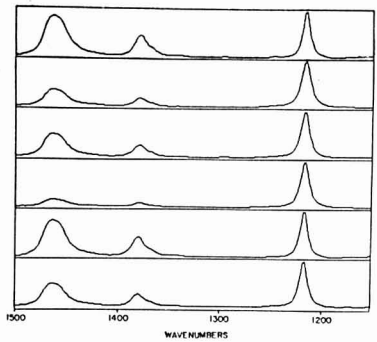


Figure 5. FTIR spectra of hexane/chloroform mixtures.

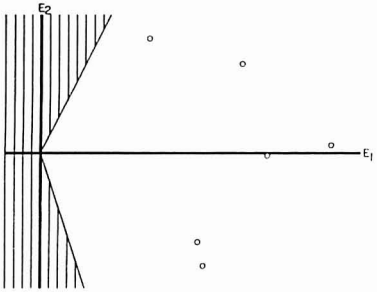


Figure 6. Plot of "real" eigenvectors based on factor analysis of the covariance matrix for hexane/chloroform mixtures.

relationship would have been observed if a fixed path cell had been used. Rather than attempting to scale the spectra with the use of an internal thickness band, it is much easier simply to normalize each spectrum by dividing it by the square root of the sum of the squared intensities (i.e., factor analysis on a correlation matrix.) A plot of primary eigenvectors exhibits a quadratic relationship between the eigenvectors (Figure 7). One encounters another problem in analyzing real spectral data: The forementioned procedure for establishing regions which would produce spectra having negative intensities does not always work due to noise. In regions where both abstract eigenspectra are of low intensity, the ratio represents little more than random noise and as such can produce spurious results. In practice the cross product of the abstract eigenspectra can provide the location of the points (Figure 8) to bound the concentration curve. A least-squares quadratic of the form $E_1 = aE_2^2 + bE_2 + c$ is fitted to the eigenvector pairs. Simultaneous solution of this equation in conjunction with boundary conditions imposed by the ratios of the abstract eigenspectra at the points defined by extremina in the cross product leads to the coefficients by which to scale the abstract eigenspectra produces two spectra which are virtually identical with those of chloroform and hexane (Figure 8). (The small anomaly in the spectrum of hexane at ca. 1220 cm^{-1} can be attributed to nonlinearity in Beer's law arising from the crude sample preparation used in collecting the infrared spectrum.)

APPENDIX

To illustrate the extraction of pure component spectra from mixtures, we generated three spectra by forming linear combinations of two pure component spectra. The solution for the pure component spectra follows:

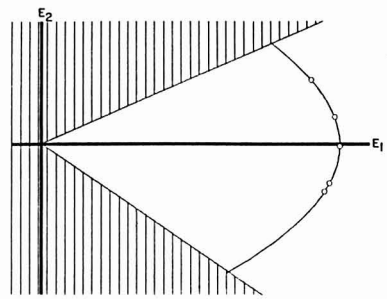


Figure 7. Plot of "real" eigenvectors based on factor analysis of the correlation matrix for hexane/chloroform mixtures.

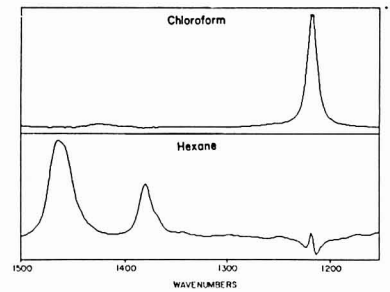


Figure 8. Pure component spectra extracted from hexane/chloroform mixtures using transformation matrix based on Figure 7.

The covariance matrix is calculated as: $[D]'[D] = [C]$

$$\begin{bmatrix} 0.26 & 0.20 & 1.60 & 0.12 \\ 0.22 & 0.40 & 1.20 & 0.14 \\ 0.14 & 0.80 & 0.40 & 0.18 \end{bmatrix} \times \begin{bmatrix} 0.26 & 0.22 & 0.14 \\ 0.20 & 0.40 & 0.80 \\ 1.60 & 1.20 & 0.40 \\ 0.12 & 0.14 & 0.18 \end{bmatrix} = \begin{bmatrix} 2.682 & 2.074 & 0.858 \\ 2.074 & 1.668 & 0.856 \\ 0.858 & 0.856 & 0.852 \end{bmatrix}$$

Solution of the eigenvalue problem $[C][E] = [E][L]$ yields:

$$\begin{bmatrix} 2.682 & 2.074 & 0.858 \\ 2.074 & 1.668 & 0.856 \\ 0.858 & 0.856 & 0.852 \end{bmatrix} \times \begin{bmatrix} 0.745 & -0.400 & 0.000 \\ 0.596 & 0.039 & 0.000 \\ 0.300 & 0.916 & 0.000 \end{bmatrix} = \begin{bmatrix} 4.688 & 0.000 & 0.000 \\ 0.000 & 0.514 & 0.000 \\ 0.000 & 0.000 & 0.000 \end{bmatrix} \times \begin{bmatrix} 0.745 & -0.400 & 0.000 \\ 0.596 & 0.039 & 0.000 \\ 0.300 & 0.916 & 0.000 \end{bmatrix}$$

The abstract eigenspectra are then readily solved as: $[A] = [D][E']$

$$\begin{bmatrix} 0.367 & 0.033 \\ 0.627 & 0.668 \\ 2.027 & -0.227 \\ 0.227 & 0.122 \end{bmatrix} = \begin{bmatrix} 0.26 & 0.22 & 0.14 \\ 0.20 & 0.40 & 0.80 \\ 1.60 & 1.20 & 0.40 \\ 0.12 & 0.14 & 0.18 \end{bmatrix} \times \begin{bmatrix} 0.745 & -0.400 \\ 0.596 & 0.039 \\ 0.300 & 0.916 \end{bmatrix}$$

Ratio of abstract 1/abstract 2

$$|0.367/0.033 \quad 0.627/0.668 \quad 2.027/-0.227 \quad 0.227/0.122| = |11.121 \quad 0.939 \quad -8.930 \quad 1.861|$$

Cross product of abstract 1 × abstract 2

$$|0.367*0.033 \quad 0.627*0.668 \quad 2.027*-0.227 \quad 0.227*0.122| = |0.012 \quad 0.419 \quad -0,460 \quad 0,028|$$

Line passing through (0.745, −0.400), (0.596, 0.039), (0.300, 0.916): $E_2 = -2.956E_1 + 1.802$.

In this example both the ratio and cross product indicate that the ratios corresponding to the second and third elements should be used to bound the concentration line. The line segment defining all possible concentrations of the two pure components is defined by that portion of the line $E_2 = -2.956E_1 + 1.802$ which is bounded by $E_2 \leq 8.930E_1$ and $E_2 \geq -0.939E_1$.

The transformation matrix [T] is solved for by simultaneous solution of $E_2 = -2.956E_1 + 1.802$ with $E_2 = -0.939E_1$ and $E_2 = 8.930E_1$

$$[P] = [A][T]$$

$$\begin{bmatrix} 0.10 & 0.30 \\ 1.00 & 0.00 \\ 0.00 & 2.00 \\ 0.20 & 0.10 \end{bmatrix} = \begin{bmatrix} 0.367 & 0.033 \\ 0.627 & 0.668 \\ 2.027 & -0.227 \\ 0.227 & 0.122 \end{bmatrix} \times \begin{bmatrix} 0.151 & 0.893 \\ 1.354 & -0.838 \end{bmatrix}$$

The concentrations of these pure components in the starting mixtures can be directly computed as

$$[K] = [T]^{-1}\ [E']^t$$

$$\begin{bmatrix} 0.20 & 0.40 & 0.80 \\ 0.80 & 0.60 & 0.20 \end{bmatrix} = \begin{bmatrix} 0.6276 & 0.6683 \\ 1.0135 & -0.1133 \end{bmatrix} \times \begin{bmatrix} 0.745 & 0.596 & 0.300 \\ -0.400 & 0.039 & 0.916 \end{bmatrix}$$

LITERATURE CITED

(1) Gillette, Paul C.; Koenig, Jack L. *Appl. Spectrosc.* **1982**, *36*, 535–539.
(2) Gillette, Paul C.; Koenig, Jack L. *Appl. Spectrosc.* **1982**, *36*, 661–665.
(3) Koenig, Jack L.; D'Esposito, L.; Antoon, M. K. *Appl. Spectrosc.* **1977**, *31*, 292–295.
(4) Knorr, F. J.; Futrell J. H. *Anal. Chem.* **1979**, *51*, 1236–1241.
(5) Ohta, N. *Anal. Chem.* **1973**, *45*, 553–557.
(6) Sylvester, E. A.; Lawton, W. H.; Maggio, M. S. *Technomet* **1974**, *16*, 353–368.
(7) Lawton, W. H.; Sylvester, E. A. *Technomet* **1971**, *13*, 617–633.
(8) Macnaughtan, D.; Rogers, L. B.; Wernimont, G. *Anal. Chem.* **1972**, *44*, 1421–1427.
(9) Malinowski, E. R.; Howery, D. G. "Factor Analysis in Chemistry"; Wiley: New York, 1980.
(10) Sharaf, Muhammad A.; Kowalski, Bruce R. *Anal. Chem.* **1982**, *54*, 1291–1296.
(11) Malinowski, Edmund R. *Anal. Chim. Acta* **1982**, *134*, 129–137.
(12) Malinowski, Edmund R. *Anal. Chem.* **1977**, *49*, 612–617.
(13) Malinowski, Edmund R. *Anal. Chem.* **1977**, *49*, 606–612.
(14) Malinowski, Edmund R. *Anal. Chim. Acta* **1978**, *103*, 339–354.

RECEIVED for review July 19, 1982. Accepted December 20, 1982. The authors express their gratitude to the National Science Foundation for support of this research under Grant DMR80-20245.

Abstract Factor Analysis of Solid-State Nuclear Magnetic Resonance Spectra

D. W. Kormos and J. S. Waugh*

Department of Chemistry, Massachusetts Institute of Technology, Cambridge, Massachusetts 02139

A method for component analysis of solid-state NMR spectra is described. By use of abstract factor analysis, AFA, simulated ^{13}C powder and magic angle spinning (MAS) spectra were utilized to establish *S/N* levels necessary for successful delineation of factors. Chemical shift tensor information for *p*-dimethoxybenzene, PMB, was used in the study. The use of differential cross-polarization (CP) rates was suggested and demonstrated as an experimental means to produce factor analyzable "spin mixture" spectra. ^{31}P CP-MAS spectra of octacalcium phosphate, OCP, were analyzed to reveal three components. Additional areas of application are noted.

Early work applying factor analysis to liquid-state NMR data focused on elucidating the number of physically significant factors which produce solvent shifts of solutes in solution. The work of Buckingham, Schaefer, and Schneider showed these shifts to be a linear sum of various contributions (*1*). Weiner, Malinowski, and Levinstone studied proton chemical shifts of substituted methanes in various media using factor analysis and concluded that three factors span the solvent-effect space (2). Using the published data of Abraham, Wileman, and Bedford, Malinowski found similar evidence for three factors for ^{19}F shifts of organofluorine compounds in nonpolar solvents (*3*). Factor analysis has also been used to study solvent shifts for ^{13}C and ^{29}Si resonances of Me_4Si (*4*) as well as ^{15}N resonances in amides (5). Two or three factors are generally found and are broadly ascribed to gas-phase chemical shifts, anisotropic solvent susceptibilities, and van der Waals effects. Factor analysis has also been used in attempts to elucidate the variables which intrinsically control chemical shifts. Studies of ^{13}C chemical shifts of aliphatic and aromatic halides suggest two principal factors and one smaller factor are needed to correlate collected data (*6*, *7*).

In this paper, we investigate the use of AFA to extract component information present in solid-state NMR spectra which exhibit overlapping powder patterns or, in the case of magic angle sample spinning, overlapping sets of spinning sidebands. Results of AFA applied to model and experimental solid-state NMR spectra are presented. The model simulations which were employed to probe the practical limitations of the technique include powder and magic angle sample spinning ^{13}C spectra for *p*-dimethoxybenzene, PMB. The four independent ^{13}C chemical shift tensors of PMB were combined in varying proportions to create chemical shift "spin mixtures". Random noise was systematically added to the spectra. In this way, the ability of AFA to predict the number of spectral components, or chemical shifts, underlying the spectra was assessed empirically as a function of signal to noise. We then

0003-2700/83/0355-0633$01.50/0 © 1983 American Chemical Society

report on the use of AFA in investigating experimental magic angle sample spinning, proton enhanced ^{31}P spectra of octacalcium phosphate or OCP. OCP was chosen not only because of its relevance in the study of calcified tissues but also because of its complex phosphate structure. Rothwell, Waugh, and Yesinowski have previously found evidence for two and perhaps three phosphate components each with high sensitivity to cross-polarization (CP) contact times (*8*). The ability to use distinct cross-polarization contact times of a single sample to create suitable factor analyzable chemical shift spin mixtures seemed an enticing possibility.

THEORY

Abstract Factor Analysis. Factor analysis is a multivariate statistical technique which consists of a series of operations. These operations are generally applied to data in matrix form which makes the method amenable to computerization. A prerequisite is that data must be expressible as a linear sum of product terms that relate, for example, to measurable quantities a and b

$$d_{ik} = a_{i1}b_{1k} + a_{i2}b_{2k} + \dots a_{in}b_{nk} = \sum_{j=1}^{n} a_{ij}b_{jk} \quad (1)$$

or in matrix form

$$[D] = [A][B] \quad (2)$$

Equation 2 may be rewritten with abstract row and column cofactor matrices, which reproduce the original data but are devoid of physical meaning

$$[D] = [R]_{abstract}[C]_{abstract} \quad (3)$$

Beyond AFA, one may seek an appropriate transformation matrix, [T], such that

$$[D] = \{[R]_{abstract}[T]\}\{[T]^{-1}[C]_{abstract}\} = [R]_{real}[C]_{real} \quad (4)$$

The $[R]_{real}$ matrix contains information about the factors (e.g., component spectra) and the $[C]_{real}$ matrix the contribution of the factors in the data (e.g., concentrations). Methods to find the [T] matrix go beyond AFA and will not be discussed here.

In the AFA of spectral mixture data, data matrices will generally be nonsquare and of the following form:

$$[D]_{raw} = \begin{bmatrix} d_{11} & d_{12} & \dots & d_{1y} \\ d_{21} & d_{22} & \dots & d_{2y} \\ \vdots & \vdots & & \vdots \\ d_{x1} & d_{x2} & \dots & d_{xy} \end{bmatrix} \quad (5)$$

where d_{11} through d_{x1} are the x sampled data points in each spectrum for each of the y mixture spectra. Data matrices can be pretreated in the first step of AFA according to the following linear equation:

$$[D] = [D]_{raw}[J] + [K] \quad (6)$$

In this work [J] and [K] were chosen to be the unit and null matrices, respectively, for covariance about the origin of factor space. This preserves the origin of the factor space and relative error and statistically weights the data points in proportion to their absolute value.

Construction of the covariance matrix, [Z], constitutes the second step of AFA. The [D] matrix is premultiplied by its transpose to obtain a square [Z] matrix

$$[Z] = [D]^t[D] \quad (7)$$

Standard eigenanalysis of the covariance matrix yields the eigenvalues and eigenvectors representing the data. Decision on the number of nonzero or insignificant eigenvalues composes the final step of AFA. The number of nonzero eigenvalues is equivalent to the rank of the covariance matrix. This is also the rank of the original data matrix. Determining the rank is the pinnacle of AFA since this is the determination of the number of factors or components, n. Knowledge of the eigenvalues and eigenvectors leads to the determination of $[R]_{abstract}$ and $[C]_{abstract}$ of eq 3.

A number of approaches have been suggested to find the least number of eigenvalues needed to represent the data being analyzed. A plot of the common logarithm of the eigenvalues vs. a component index as suggested by Ohta (*9*) is frequently used. A major break in the initial slope of such a curve signals the transition from significant to noise eigenvalues. Noise eigenvalues will be present in all real data. An empirical IND or factor indicator function has been shown by Malinowski (*3*) to reach a minimum at the correct number of factors. It has the following form for covariance about the origin:

$$IND_i = \frac{RE}{(y - i)^2} \quad (8)$$

$$RE = [\sum_{j=i+1}^{y} E_j/x(y - i)]^{1/2} \quad (9)$$

The IND value for each eigenvalue E_i ($i = 1$ to $y - 1$) is calculated as a function of the remaining smaller eigenvalues, E_j, using the residual error or RE. It is not defined for the smallest eigenvalue. Both of these methods will be utilized in the analyses presented here

Suitability of Solid-State NMR Spectra. In cross-polarization NMR, decoupled spectra can to a first approximation be written as a linear sum of product terms

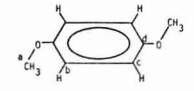
$$D_{CP}(i,\alpha,t) = \sum_{j=1}^{n} g(i,j)v(\alpha)c(j,\alpha)e(j,\alpha,t) \quad (10)$$

where the summation is over n spin components. $D_{CP}(i,\alpha,t)$ is the signal intensity of spin mixture α at frequency i with cross-polarization contact time t; $g(i,j)$ is a line shape function for the NMR signal of type j spins at frequency i; $v(\alpha)$ is the volume of spin mixture α; $c(j,\alpha)$ is the concentration of type j spins in mixture α, and $e(j,\alpha,t)$ is the cross-polarization efficiency for type j spins in mixture α with contact time t. For dilute, decoupled nonquadrupolar spins, $g(i,j)$ will be determined by the chemical shift Hamiltonian. The chemical shift parameters $\bar{\sigma}$, δ, and η will dictate the shape of $g(i,j)$ for static powder patterns. Magic angle sample spinning renders the Hamiltonian time dependent and introduces the rotor spinning speed, ω_R, as another parameter to the line shape. Maricq and Waugh have given the explicit form of $g(i,j)$ for static and spinning cases as a function of $\bar{\sigma}$, δ, η, and ω_R (*10*). A single spinning speed for all spectra is necessary in order that CP-MAS data matrices be factor analyzable.

It should be noted that the line shape function has in fact some dependence on contact time which will couple this term to the $e(j,\alpha,t)$ efficiency term. Consider the general case of an internuclear vector between an isolated I and S spin pair. When the angle between this vector and the applied static field approach the magic angle (54.7°), the cross-polarization efficiency is significantly diminished. A singularity would therefore be predicted to occur in the line shape function. Experimentally, anomalies of this type are rarely observed and for the purposes described here, we will consider eq 10 to be valid for CP data. This effect does not pertain to standard pulse experiments. Spectra obtained with these sequences should adhere to eq 10 with the deletion of the CP efficiency term. The spectra of spin mixtures resulting from such experiments should therefore also be factor analyzable.

Equation 10 reveals two approaches for preparing a set of spin mixture spectra. If the CP contact time is kept constant, varying the relative concentrations of each spin species is acceptable. If the concentration is fixed, varying the contact

Table I. PMB ^{13}C Shielding Tensors



	nucleus			
	a	b	c	d
σ_{11}(ppm)	-80.4	-193	-198	-230
σ_{22}(ppm)	-71.5	-134	-136	-162
σ_{33}(ppm)	-16.1	-12.0	-23	-74
$\bar{\sigma}$ (0 ppm = TMS)	-56	-113	-119	-155.3

time will produce a set of spin mixture spectra. In this case eq 10 reduces to

$$D_{CP}(i,t) = \sum_{j=1}^{n} g(i,j)c'(j)e(j,t) \qquad (11)$$

where $c'(j)$ is a constant spin concentration for each spin species. If a single sample is used, $v(\alpha)$ is a constant and is accounted for in the $c'(j)$'s. Equation 11 predicts that if different spin species have sufficiently distinct cross-polarization characteristics, CP-MAS intensities can be influenced to create chemical shift spin mixture spectra from a single sample. Spin mixtures can be produced from a single molecular species as well as from physical mixtures of distinct molecules in this way. An analysis of polarization transfer and CP efficiencies for CP-MAS NMR is given by Stejskal, Schaefer, and Waugh (*11*).

EXPERIMENTAL SECTION

Instrumentation. A Digital Equipment Corp. LSI-11 computer was used for all calculations including spectral stimulation and factor analyses. All programs were written in FORTRAN. The computer, an integral part of a home-built 250-MHz proton spectrometer, was interfaced to an Analogic AP400 array processor for Fourier transformation and other manipulations of data sets. An Oxford Instruments widebore superconducting magnet (5.872 T) was used with a double resonance single coil probe for ^{31}P operation at 101.2 MHz with ^{1}H decoupling.

OCP Spectra. ^{31}P NMR spectra of OCP were obtained by using the technique of cross-polarization combined with magic angle sample spinning and high power ^{1}H decoupling (CP-MAS). The decoupling field was 8 G. Principles of CP-MAS NMR and applications to solids are given by Pines, Gibby, and Waugh (*12*) and by Schaefer and Stejskal (*13*). Cross-polarization was done for signal enhancement and to decrease signal averaging recycle times. A Delrin sample rotor of Beams design was spun at 1201 Hz. The ^{1}H spin temperature was cyclically alternated during half of the cross-polarization contacts to minimize zero frequency spectral artifacts (*14*). Zero-filling of the 1K sampled points to 2K was done. With a spectral window of 40 kHz, an appropriate line-broadening function was used to apodize the data. All OCP spectra were the result of 100 accumulations at room temperature. Nine contact times incremented by 0.25 ms from 0.5 ms to 2.5 ms were used to create the OCP spin mixture spectra used for the factor analysis experiment.

Computer PMB Simulations. The simulated ^{13}C PMB static powder pattern spectra were computed by use of the tabulated PAS frame tensor elements for the four chemical shifts observed in the solid. The shielding tensors values are summarized in Table I. A prescription detailed by Mehring (*15*) with an approximation to the needed elliptic integrals given by Abramowitz and Stegun (*16*) was employed to do the calculations. The chemical shift line shapes obtained were weighted, suitably broadened, and added to obtain a powder pattern for the molecule. Various weighting factors corresponding to CP efficiencies were employed to simulate 10 cross-polarization spin mixtures. This modeled the effect of distinct CP efficiencies. The ratio of b to c efficiencies was kept

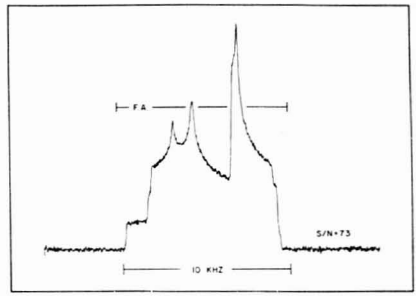


Figure 1. Model *p*-dimethoxybenzene static ^{13}C spectrum.

constant partly to simulate the fact that their true CP efficiencies should be quite similar and also as an added test for AFA to detect only three chemical shift components in spin mixtures displaying shielding information for four tensors. The b and c spins should therefore be detected as only a single component.

Magic angle sample spinning simulations for ^{13}C spectra of PMB were computed with the tensor information contained also in Table I for a spinning speed of 1000 Hz. A procedure described by Maricq and Waugh (*10*) was used to calculate the spinning sideband line shape for each of the four shielding tensors. For each of the Euler angles (α, β, γ), 5° steps were used to obtain an orientation-averaged complex signal for one rotor period ($2\pi/\omega_R$). This time domain signal was replicated to fill a 1024-point complex buffer to form a train of rotational spin echoes, suitably line broadened, zero-filled to 4096 data points and Fourier transformed to give magic angle spinning line shapes. The line shapes were again weighted in the manner used for the preceding static case and combined to form 10 simulated CP-MAS spin mixtures. For both the spinning and static CP model mixtures, no line shape anomalies due to contact time dependencies were simulated.

To further simulate real spectra, artificial random noise was added to each calculated spin mixture spectrum. Sets of spectra with S/N ratios from approximately 30 to 300 were created. The S/N was defined as

$$S/N = \frac{I_{max}}{2(\sum_{i=A}^{B}(I_i - \bar{I})^2/N)^{1/2}} \qquad (12)$$

where

$$I_{max} = I_{maxpeak} - \bar{I} \qquad (13)$$

$$\bar{I} = (\sum_{i=A}^{B} I_i)/(N+1) \qquad (14)$$

I_{max} is the difference between the peak maximum intensity and the average base line intensity, $\bar{I}$, defined for N points from spectral points A to B where no significant spectral features are seen.

RESULTS AND DISCUSSION

Simulated Spectra. Typical static and magic angle spinning ^{13}C model spectra for PMB are shown in Figures 1 and 2. The spectra shown are composed of equally weighted contributions of each of the four chemical shift tensors of the molecule. They represent spin mixture 1 of Table II. For the static powder case, the number of chemical shift components is not obvious from the spectrum itself. The previously defined S/N ratios are also given. The region of each spectrum encompassed for factor analysis is indicated. For the static case, 520 data points were used in the analysis. For the magic angle spinning case, 600 data points were used.

The results of AFA applied to 8 sets of model PMB ^{13}C static spin mixture spectra are summarized in Figure 3.

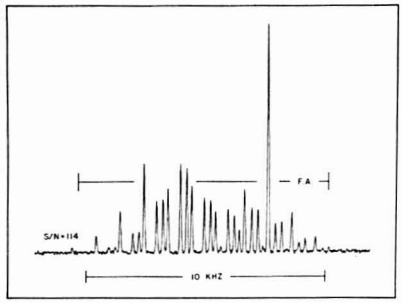


Figure 2. Model *p*-dimethoxybenzene magic angle spinning ^{13}C spectrum.

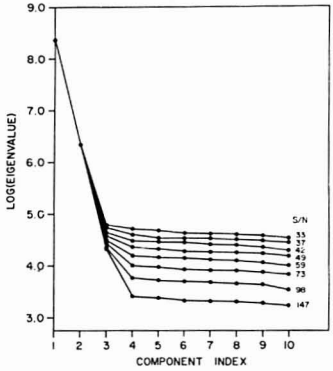


Figure 3. AFA eigenvalue results for model ^{13}C PMB static spin mixture spectra. Three components are indicated.

Table II. CP Efficiency Factors for Spin Mixture Calculations

spin mixture	nucleus a	b	c	d
1	1.0	1.0	1.0	1.0
2	1.0	0.9	0.9	0.8
3	1.0	0.9	0.9	0.7
4	1.0	0.9	0.9	0.6
5	1.0	0.8	0.8	0.6
6	1.0	0.8	0.8	0.6
7	1.0	0.7	0.7	0.6
8	1.0	0.7	0.7	0.5
9	1.0	0.5	0.5	0.4
10	1.0	0.4	0.4	0.2

Plotted as the common logarithm of the determined eigenvalues vs. component index, a number of features appear. S/N values simulated range from 33/1 to 147/1 and differentiate the data sets. The highest S/N data consists of eigenvalues which level off at a component index of 4, indicating the clear presence of three factors or component spectra. These eigenvalues are distinguished in the figure from the remaining seven noise on zero eigenvalues. This is the expected result since the ratio of b to c spin species was kept constant in the spin mixture simulation (see Table II). As the S/N decreases, a steady, uniform increase in eigenvalue magnitudes is noted

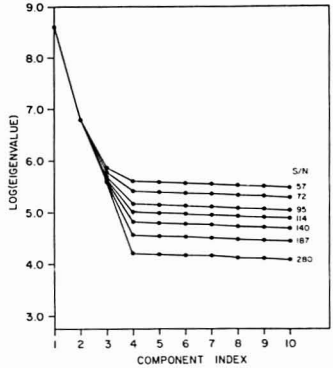


Figure 4. AFA eigenvalue results for model ^{13}C PMB magic angle spinning spin mixture spectra. Three components are indicated.

Table III. AFA Results of OCP Spin Mixture Spectra

component index	log (eigenvalue)	IND
1	12.95	250.21
2	11.58	79.56
3	10.08	75.79
4	9.56	91.31
5	9.33	121.44
6	9.06	195.38
7	8.97	376.27
8	8.69	1430.9
9	8.60	

for the noise eigenvalues. A smaller, consistent increase is observed for the smallest real eigenvalue. The result is a small dispersion in this eigenvalue for the data sets. The third eigenvalue is seemingly lost in the noise eigenvalues at a S/N value of 33/1.

Similar eigenvalue results for AFA of model ^{13}C PMB MAS spin mixture spectra are shown in Figure 4. As for the static case, S/N values differentiate the seven data sets and range from 57/1 to 280/1. Three factors are again shown to characterize the data sets. A similar trend is noted with decreasing S/N values. The third factor's eigenvalue is still perceptible at a S/N of 57/1 but with lower S/N its recognition would be doubtful.

These studies for PMB spin mixtures indicate a minimum S/N of approximately 75/1 is necessary for a successful application of AFA. This requirement is rigorously applicable only to the mixture compositions modeled here and to the AFA of whole spectral regions. We suggest that AFA of MAS spectra will in general be more successful than for powder spectra.

OCP Spectra. Representative cross-polarization, magic angle spinning ^{31}P NMR spectra of octacalcium phosphate are presented in Figure 5. Spectra taken with four contact times are shown with the spectral region used for AFA indicated. The chemical shifts of the central peaks are 3.2 ± 0.2, 1.8 ± 0.2, and −0.7 ± 0.2 ppm relative to an 85% H_3PO_4 reference. Differing cross-polarization efficiencies are responsible for the intensity changes in the central and sideband peaks. The average S/N of the nine spectra used in the AFA was 95/1.

Tabulated eigenvalue and factor indicator function values in an AFA of nine OCP CP-MAS spectra are presented in

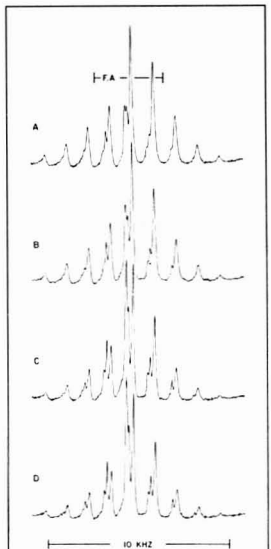


Figure 5. Experimental ^{31}P CP-MAS spectra of OCP. Contact times used were as follows: (A) 0.5 ms, (B) 0.75 ms, (C) 1.75 ms, and (D) 2.0 ms.

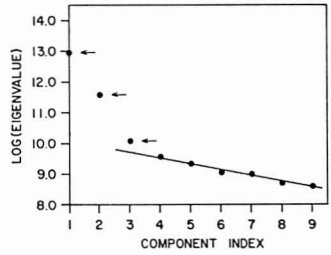


Figure 6. AFA eigenvalue results for nine OCP spin mixture spectra. Three components are indicated with arrows.

Table III. Nine contact times ranging from 0.5 to 2.5 ms were used to collect the CP-MAS spin mixture spectra used in the analysis. A spectral region containing the zero- and first-order sidebands spanning 195 data points was used. The IND values reach a minimum at three components before turning up. This result is corroborated by an eigenvalue plot shown in Figure 6. A straight line can be drawn through the seven noise eigenvalues (n = 0.9894). It is useful in distinguishing the nearly constant difference in noise eigenvalues from the substantially larger difference between the third, smallest eigenvalue and the noise eigenvalues. In comparison to the model studies, the noise eigenvalues appear to fall on a line with a much larger negative slope. This may be attributed to small errors in peak phasing or base line artifacts not present in the simulated spin mixture spectra.

A previous ^{13}P NMR study of solid calcium phosphates by Rothwell, Waugh, and Yesinowski has indicated a tricomponent nature for octacalcium phosphate (*8*). This finding is substantiated here both by the observed CP-MAS spectra (at higher resolution than the previous report) and by the use of AFA. The observed chemical shifts here are in basic agreement with their values. We accept the assignment of the high field peak (–0.7 ppm) to the acidic HPO_4^{2-} groups, the low field peak (3.2 ppm) to the "apatitic layer" PO_4^{3-} groups, and the middle peak (1.8 ppm) to PO_4^{3-} groups near hydrated sites or adjacent HPO_4^{2-} groups.

Applications. Abstract factor analysis has been successfully applied to model and experimental solid-state NMR spectra. The method offers an unbiased procedure for extracting additional information useful in characterizing complex overlapping powder or magic angle sample spinning sideband spectra. The number of isotropic chemical shifts is in many cases apparent in spectra. In cases where it is not, AFA may provide the information. In cases of coincidental near overlap of chemical shifts, detection of hidden resonances may be achieved. Entire spectral regions may be quickly analyzed subject only to data processing limitations.

Observations using model data, although an exhaustive study was not attempted, are the following: Reasonably high S/N spectra are necessary in order that eigenvalues, small in magnitude, are not lost in noise eigenvalue background. This establishes a practical limitation especially for broad powder pattern spectra of isotopically dilute spin species. Similar reasoning suggests very small but real eigenvalues will commonly fall into the noise background. Such conditions imply that AFA will reveal only the minimum number of factors needed to reproduce the experimental data.

Cross-polarization efficiencies, through the use of varied contact times, have been shown to be a convenient and powerful method to produce chemical shift spin mixture spectra which are factor analyzable. The spin mixture spectra need not result from molecular mixtures but also from single compounds containing different chemical shift species. A limitation is inherent for spin species with similar cross-polarization characteristics. These species will most likely be seen as a single component. The PMB model simulation has shown this clearly.

We believe that there is substantial potential for factor analysis in solid-state NMR. Additional methods to clarify and extract new information from many varieties of solid-state NMR spectra are still needed. The complexity of coal, wood, and many biological solid sample spectra are but a few areas where AFA may be applied for component analysis. AFA might also supplement information in phase transition studies. The method as outlined here is not limited to chemical shift spectra and could easily be expanded to include other inhomogeneous interactions in NMR such as weak quadrupole or heteronuclear dipolar coupled spectra. In addition to AFA, the future application of spectral isolation procedures using factor analysis described by Malinowski and others (*17–19*) holds much promise in solid-state NMR and in other spectroscopies as well.

ACKNOWLEDGMENT

The authors wish to acknowledge W. E. Brown of the National Bureau of Standards, Washington, DC, for the octacalcium phosphate sample used in this investigation.

Registry No. PMB, 150-78-7; OCP, 13767-12-9.

LITERATURE CITED

(1) Buckingham, A. D.; Schaefer, T.; Schneider, W. G. *J. Chem. Phys.* **1960**, *32*, 1227–1233.
(2) Weiner, P. H.; Malinowski, E. R.; Levinstone, A. R. *J. Phys. Chem.* **1970**, *74*, 4537–4542.
(3) Malinowski, E. R. *Anal. Chem.* **1977**, *49*, 612–617.
(4) Bacon, M. R.; Maciel, G. *J. Am. Chem. Soc.* **1973**, *95*, 2413–2426.
(5) Martin, G. J.; Bertrand, T.; Le Botlan, D.; Letourneux, J. *J. Chem. Res., Synop.* **1979**, *12*, 408–409.
(6) Wiberg, K. B.; Pratt, W. E.; Bailey, W. F. *J. Org. Chem.* **1980**, *45*, 4936–4947.

(7) Bailey, W. F.; Cioffi, E. A.; Wiberg, K. B. J. Org. Chem. 1981, 46, 4219-4225.
(8) Rothwell, W. P.; Waugh, J. S.; Yesinowski, J. P. J. Am. Chem. Soc. 1980, 102, 2637-2643.
(9) Ohta, N. Anal. Chem. 1973, 45, 553-557.
(10) Maricq, M. M.; Waugh, J. S. J. Chem. Phys. 1979, 70, 3300-3316.
(11) Stejskal, E. O.; Schaefer, J.; Waugh, J. S. J. Magn. Reson. 1977, 28, 105-112.
(12) Pines, A.; Gibby, M. G.; Waugh, J. S. J. Chem. Phys. 1973, 59, 569-590.
(13) Schaefer, J.; Stejskal, E. O. J. Am. Chem. Soc. 1976, 98, 1031-1032.
(14) Stejskal, E. O.; Schaefer, J. J. Magn. Reson. 1975, 18, 560-563.
(15) Mehring, M. "High Resolution NMR Spectroscopy in Solids"; Springer-Verlag: New York, 1976; Chapter 2.
(16) Abramowitz, M.; Stegen, I. "Handbook of Mathematical Functions"; Dover: New York, 1965; p 591.
(17) Malinowski, E. R. Anal. Chim. Acta 1982, 134, 129-137.
(18) Howery, D. G. In "Chemometrics: Theory and Application"; Kowalski, B. R., Ed.; American Chemical Society: Washington, DC, 1977; ACS Symp. Ser. No. 52, pp 73-79.
(19) Malinowski, E. R.; Howery, D. G. "Factor Analysis in Chemistry"; Wiley-Interscience: New York, 1980; Chapter 3.

RECEIVED for review October 12, 1982. Accepted December 22, 1982. This work was supported in part by the National Science Foundation [Grant No. 8111180-CHE] and in part by the National Institutes of Health [Grant No. GM 16552].

Determining the Lowest Limit of Reliable Assay Measurement

Leonard Oppenheimer,* Thomas P. Capizzi, Roger M. Weppelman, and Hina Mehta

Merck Sharp & Dohme Research Laboratories, P.O. Box 2000, Rahway, New Jersey 07065

The use of external standards to determine the lowest limit of reliable assay measurement is commonly used to evaluate the limitations of a particular analytical technique and to make comparisons between different procedures. All previously developed criteria have assumed a constant variance over the entire concentration range of interest. Assay limit criteria formulas have been developed for the heterogeneous variance situation. Widely disparate results can be obtained depending on the choice of criteria, whether a uniform variance or a nonuniform variance analysis is employed, the method used to select the weights, the models and/or transformations utilized, and experimental design considerations. These issues are examined by using data from an analytical procedure developed to monitor tissue residues for Ivermectin, an antiparasitic agent.

The "lowest limit of reliable assay measurement" (LLORAM) is often used in analytical work since it makes a succinct statement about the limitations of an assay and allows for meaningful comparisons between different assays. It expresses how effectively one can distinguish between a measurement made when true activity is zero and one made when true activity is greater than zero. All too often the LLORAM is determined intuitively which compromises its utility. However, even an objective, well-defined criterion may be deficient if the statistical methodology used in its determination is inappropriate.

Previous work on LLORAM determination (*1–6*) has assumed that the response variance was constant and thus independent of the response's magnitude. In this case (the unweighted case) all values used for calculating the standard curve can be treated equally and results can be obtained by using ordinary least squares. However constant variance is probably not attained by most assays. For example, many assays involve transferring constant volumes of solutions containing variable quantities of the material to be assayed. The variance of the volumes transferred can reasonably be expected to be constant, but clearly the variance in the amount of material transferred will depend on its concentration in the solution, i.e., the percent error will be constant and thus the variance will be proportional to the predicted response squared. This general point has been recognized by Smith and Mathews (*7*) who stated that for "typical chemical application, the experimental conditions are controlled so as to make the percentage error a constant." This structure with variance proportional to the square of the predicted value may also have application in atomic absorption spectrometry and anodic stripping voltammetry (*8*). Other structures are also possible, for assays based on Poisson distributed counting measurements (either photon or radioactive) the variance may be proportional to its predicted value (*9*, *10*) rather than its square. Garden, Mithcell, and Mills (*11*) have a less sanguine view: "It is reasonable to expect that much analytical data will not show constant variance nor would we expect the variance to be a simple function of concentration."

The issue of nonconstant variance and the weighted least-squares approach in obtaining standard curves has been previously addressed (*7–13*), but this work has not been extended to determining assay measurement limits. This report describes the derivation of appropriate expressions for obtaining various types of assay limits under the more general conditions of heterogeneous variances. The results have been illustrated by using data from an assay developed to monitor tissue residues of Ivermectin, an antiparasitic agent, potent at very low doses. Rather dramatic differences have been observed depending on whether a valid weighted or an inappropriate unweighted analysis is used. In addition, related issues which also affect assay limit determinations are discussed and illustrated using the tissue residue data. These issues include the method used to select the variance weights, alternative models which transform the variance structure of the responses, and experimental design considerations used in obtaining the standard curve.

EXPERIMENTAL SECTION

Data Description. A newly developed analytical procedure (*14*) was employed to analyze spiked tissue samples (fat, kidney, liver, muscle) at various concentrations (9.7 to 100 ppb) in four species (cattle, swine, horses, sheep). The tissues were spiked with Ivermectin, a broad spectrum antiparasitic agent. The analytical procedure was based upon the detection of a fluorescent derivative of Ivermectin following high-performance liquid chromatography. For each combination of animal species and target tissue, multiple samples were assayed for at least four concentration residue levels which were believed to be in the linear range (observed response vs. concentration). Table I indicates the distribution of independently performed assays among species–tissue–concentration combinations. An assay which will be acceptable to governmental regulatory agencies must be able to reliably discriminate the marker residue response from the target tissue background at very

0003-2700/83/0355-0638$01.50/0 © 1983 American Chemical Society

Table I. Available Data: Number of Observations

	concentration, ppb										
animal tissue	9.7	10	19	19.4	20	29	41	46	50	97	100
swine											
muscle		3			3				3		3
liver		3			3				3		3
kidney		3			3				3		3
fat		3			3				3		3
horse											
muscle	3		3		2		3			3	
liver	3		3		2		3			3	
kidney	3		3		1		3			3	
fat	3		3		1		3			3	
sheep											
muscle	3		3				3			3	
liver	3		3				3			3	
kidney	3			3			3			3	
fat	3		3				3			3	
cattle											
muscle	3	2			2			3	2	2	
liver	3	2	3		3	1	3		3	3	
kidney	3						3		4	3	
fat	3							3	4	3	

low concentrations, i.e., the lowest limit of reliable assay measurement must be below a designated safe tissue residue level.

Computation. All the computations discussed below, both weighted and unweighted regression analysis, and graphics have been computer generated by using the data management, graphics, and statistical package SAS (statistical analysis system), Helwig and Council (*15*).

RESULTS AND DISCUSSION

Assessment Criteria. Altshuler and Pasternack (*1*) initially used the statistical concepts of a type I and type II error to obtain more objective criteria to calculate the lowest limit of reliable measurement for an analytical procedure. A type I error is to falsely conclude there is sample activity when there is none (a false positive), while a type II error is to falsely conclude there is no activity in the sample when there is some (a false negative). Since then a plethora of criteria have been introduced, none of which are totally unique, inviolate, or universally appropriate. For example, some of the criteria are only concerned with type I errors and not type II (*2, 6*), some criteria use two-sided test statistics rather than one sided (*4*), some criteria use linear calibration curves (*5*), some more complicated logistic curves (*12*), while others are model free (*4*). Whichever definition and method are employed, it is essential to specify the exact criteria, all required assumptions, and the method of analysis. This is especially important because of the often deceptive and conflicting terminology that has been employed.

The three different assessment criteria introduced by Currie (*3*) are extended to the nonuniform variance situation, i.e., (i) the critical level, (ii) the detection level, and (iii) the determination level. The notation, assumptions, derivation, and results are given in the Appendix, Figures 1 and 2 for the weighted case. Currie's (*3*) unweighted results are then a special case of this more general formulation and can be obtained by setting all the weights equal, i.e., $k_i = 1$ for all i. The *critical level* (L_{Cw}), eq 2, is the assay response above which an observed response is reliably recognized as detected, i.e., the response at which one may decide whether or not the result of an analysis indicates the presence of a residue. The *detection limit* (L_{Dw}), eq 3, is the actual net response which may be a priori expected to lead to detection. The *determination limit* (L_{Qw}), eq 4, is the level at which measurement precision will be satisfactory for quantitative determination, i.e., a result which is satisfactorily close to the limiting expected value. In general, we have that $L_{Cw} \leq L_{Dw} \leq L_{Qw}$. Note that even for a specified criteria, results will vary depending on the probability levels chosen for committing a type I (α) or type II (β) error, whether a one-sided or two-sided test statistic is employed, and the measurement precision required.

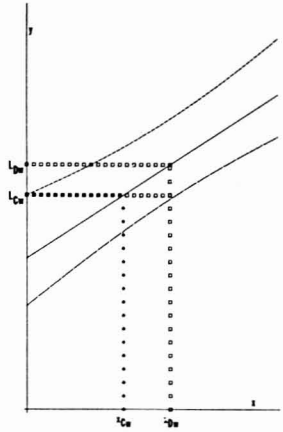


Figure 1. The critical level (L_{Cw}, x_{Cw}) and the detection level (L_{Dw}, x_{Dw}) defined. Includes the predicted calibration curve (—) with its upper $(1 - \alpha)$ (---) and lower $(1 - \beta)$ (– –) confidence intervals for a predicted observation. The horizontal x axis refers to concentration and the vertical y axis to the assay response.

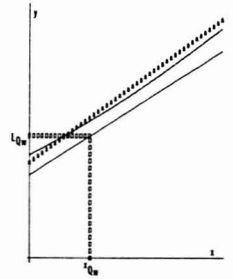


Figure 2. The determination level (L_{Qw}, x_{Qw}) defined, i.e., the coefficient of variation of the predicted value at x_{Qw} is sufficiently small, i.e., equal to the quantity C; also includes the predicted calibration curve (—) and the predicted calibration curve plus one standard error for a predicted observation (---) and $(1 + C)$ times the predicted value (*). The horizontal x axis refers to concentration and the vertical y axis to the assay response.

Unweighted Analysis. The LLORAM estimates for the various tissues and species were similar and hence only overall results (combining all the observations) have been reported. Table II presents summary statistics for the assay response by spiked tissue concentrations. Assay limits were computed by using eq 2, 3, and 4 in the Appendix for ordinary (unweighted, $k_i = 1$ for all i) least squares both with and without the inclusion of the high concentration (97–100 ppb) and are reported in Table III. Examination of Figure 3 and Table II indicates that the variability is not homogeneous but increases along with the spiked concentration levels. When the high concentration (97–100 ppb) results are omitted from the analysis the overall standard deviation drops by one-third (4.70 to 3.07) and so do the various LLORAM estimates, x_{Cw}, x_{Dw}, x_{Qw} (respectively, 9.3 to 6.0, 18.7 to 12.0, 28.2 to 18.2). The

Table II. Summary Statistics by Concentration

concn, ppb	no. of observns	mean	std dev	coeff of variation
9.7	36	7.68	0.93	12.0
10.0	16	8.59	1.21	14.1
19.0	24	16.33	1.57	9.7
19.4	3	16.67	1.53	9.2
20.0	23	17.35	1.82	10.5
29.0	1	25.00		
41.0	30	32.93	2.89	8.8
46.0	6	37.33	5.47	14.6
50.0	25	43.68	5.70	13.0
97.0	35	80.71	8.27	10.2
100.0	12	83.83	8.28	9.9

reason for the drop is that in the unweighted analysis all observations are weighted equally and thus observations at 100 ppb, far removed from the region of interest, have the same influence on the results as observations made at 10 ppb. Note the 3-fold spread for these different assay limit criteria, and also that $x_{Cw} \leq x_{Dw}$ as required and that $x_{Dw} \leq x_{Qw}$ as expected.

Weighted Analysis. Earlier work on assay detection limits, including Currie's results (*3*) have all assumed a constant variance around expected values, for the entire range of responses considered, i.e., $k_i = 1$ for all i. There are many situations when such an assumption is untenable. For example, the plot of residuals from fitting an unweighted least-squares line vs. predicted values (Figure 3) indicates a funnel shape, i.e., increasing variability with increasing magnitude of response. Ordinary (unweighted) least squares treats all observations equally but is not appropriate when heterogeneity exists. In that case, weighted least squares is used which gives observations with a large variance, less weight in fitting the model, than observations with smaller variance. Weighted regression equations, when the variance associated with the ith observation is proportional to the quantity k_i and not all the k_i are equal, are presented in the Appendix with corresponding LLORAM expressions denoted by x_{Cw}, x_{Dw}, x_{Qw} given by eq 2, 3, and 4, respectively. Weighted least squares would not be expected to alter the slope estimate, b, a great deal but it will have a large effect on the estimate of precision, s, especially at the lower concentrations (*11*), where more precise results are required. Thus a dramatic effect on the resulting detection limit estimates x_{Cw}, x_{Dw}, x_{Qw} can readily occur.

Empirical Weights. In order to apply a weighted least-squares analysis one must assign weighting values, k_i, to the various observations. In most applications the true k_i values

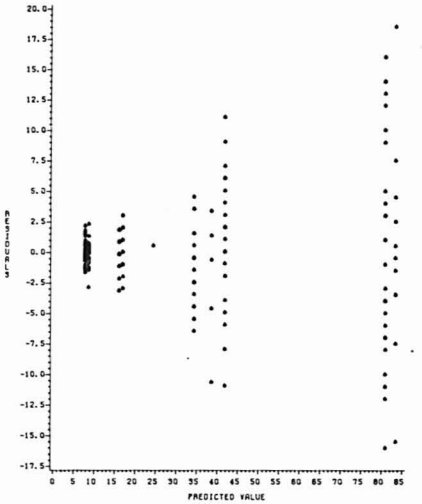


Figure 3. Residuals from the unweighted least-squares analysis vs. predicted values indicating variance heterogeneity.

are not known. With sufficient replication at each concentration, at least 10 replicates (*11*), an empirical estimate of k_i from the observed data can be obtained, i.e.

$$\text{weight} = 1/(\text{estimated } k_i) = 1/(\text{observed sample variance})$$

This weighting scheme will give more variable observations lower weight than less variable observations. In order to have more precise variance estimates, with at least 9 degrees of freedom (*11*), nearby concentrations have been pooled whenever possible as indicated in Table II.

Table III indicates the substantial reduction in the assay limits by employing a weighted least-squares analysis. In this case, omitting the high concentration does not alter results much, since even when these observations were included they had a small weight and little influence on the results. Although the slope and intercept estimates, (a, b), have not changed much from the unweighted analysis, the estimate of precision at the lower concentrations is dramatically affected (*11*) and this accounted for the change in assay limits. The

Table III. Results for Different Situations

situations considered			model fitting					assay limits by criteria		
models	weighting	high concn included	intercept a	slope b	std deviation	k	lack of fit statistic	critical[a] x_C	detection[b] x_D	determination[c] x_Q
$y = A + Bx$	none	yes	0.099	0.834	4.70	n/a[d]	0.89[e]	9.3	18.7	28.2
$y = A + Bx$	none	no	−0.177	0.846	3.07	n/a	2.72[f]	6.0	12.0	18.2
$y = A + Bx$	empirical	yes	−0.067	0.836	1.00	1.0	n/a	2.1	4.2	6.0
$y = A + Bx$	empirical	no	−0.083	0.837	1.00	1.0	n/a	2.1	4.2	6.0
$y = A + Bx$	modeled	yes	−0.195	0.844	1.01	1.0	n/a	2.1	4.2	6.0
$y = A + Bx$	modeled	yes	−0.195	0.844	1.01	0.0109	n/a	1.2	2.4	1.0
$y = A + Bx$	modeled	no	−0.312	0.854	1.00	1.0	n/a	2.1	4.2	6.0
$y = A + Bx$	modeled	no	−0.312	0.854	1.00	0.0109	n/a	1.2	2.5	1.0
$y = Ax^B$	none	yes	0.810	1.007	0.116	n/a	2.23[f]	1.2	2.4	1.8
$y = Ax^B$	none	no	0.787	1.017	0.121	n/a	2.58[f]	1.2	2.5	1.8

[a] $\alpha = 0.05$, one sided test statistic. [b] $\alpha = \beta = 0.05$, one sided test statistic. [c] $C = 0.10$. [d] Not applicable. [e] Not statistically significant, $P > 0.05$. [f] Statistically significant lack of fit, $P < 0.05$.

weighted analysis uses a more appropriate estimate of precision which reflects the actual situation at the lower concentrations. Note that the overall standard deviation, s, for the weighted analysis is constrained to unity (within rounding error) by the choice of weights used. (This may not be true for other weighting schemes.)

The expressions for determining the assay limits for a weighted analysis are a function of the variance at the assay limit. Thus the initial term under the radical sign, k_0, k_{Dw}, and k_{Qw} in eq 2, 3, and 4 would generally not be known. In this case we have set $k = 1$ since this makes the variance equal to that observed at the lowest experimental concentration, 10 ppb (refer to Table II). This is probably a conservative approach since we would expect the variance to continue to decrease as the concentration went below 10 ppb. Note that a certain amount of restraint is required with these assay limits since the results involve an extrapolation below observed experimental results, i.e., below 9.7 ppb.

Modeled Weights. An alternative to using the reciprocal of the computed variance as weights is to model the variance as a function of concentration. The model may be a theoretical construct, e.g., count response follows a Poisson distribution for which the variance is proportional to the mean, or it may be an empirical model which is fit to the data. Empirical models which have been considered for radioligand assays (*12*, *13*) and may be appropriate in other general situations are as follows:

$$\sigma_x^2 = A(x + 1)^B \text{ (power function)}$$

$$\sigma_x^2 = C_0 + C_1x + C_2x^2 \text{ (quadratic function)}$$

The power function model has been fit to the tissue residue data by using ordinary least squares with resulting estimates: $a = 0.0109$, $b = 1.9186$. This is quite close to a quadratic fit (1.9186 vs. 2). To avoid the unrealistic assumption of zero variance at zero concentration, $(x + 1)$ rather than the usual x was used in specifying the model. This model was then used to estimate the expected variance at various concentrations, and the reciprocals of these estimated variances were used as weights.

Once more the initial term under the radical sign, k, in eq 2, 3, and 4 is required to calculate the assay limits. With a model for the variance structure we could now iterate to obtain an explicit solution. In Table III we have presented results using two values of k: (i) $k = 1$, and (ii) $k = 0.0109$. The first is chosen so that results can be compared to the conservative (upper bound) empirical weighting results. Not surprisingly these two results are very similar. Alternatively, the choice of $k = 0.0109$ is a lower bound and corresponds to the variance that would be estimated when the concentration is zero. Using $k = 0.0109$ gives x_{Cw}, x_{Dw} estimates which are almost half $k = 1.0$ results; however, the x_{Qw} result has been reduced even more, by a factor of 6.

Our experience indicates that results from a single assay, without supplementary information, rarely contain enough information to adequately model the variance structure. In fact, more data may be required to model the variance function than is needed to establish the form of the calibration curve. Finney and Phillips (*13*) have obtained poor results in attempts using sophisticated statistical methodology to fit either the quadratic or power functions to data from a number of radioimmunoassay experiments from a single laboratory.

Alternative Models and/or Scale Transformations. Statistical tests of model validity (lack of fit tests) can be performed since replicate results are available at several concentrations (*16*). For the linear model, observed assay response vs. spiked concentration, lack of fit exists when the high concentration is excluded (Table III). Adequate fit with all concentrations included is somewhat deceptive in that the "pure error" term (*16*) used in the statistical test of fit is artificially inflated due to the inclusion of the high concentration.

Alternative models might provide an improvement in fit. A linear model of the form log observed assay response vs. log spiked concentration was also examined (Table III) which is equivalent to the following

$$\text{assay response} = A(\text{concentration})^B$$

Note that the log transformation has the added advantage of stabilizing the variance, and thus unweighted least squares can be used to obtain estimates of A and B. The estimates obtained (a and b) are similar with or without the inclusion of the high concentration and indicate that the assay detects about 80% of the spiked residue concentration, i.e., $a = 0.80$, $b = 1.0$, approximately.

Since the model is now fit using log concentration rather than concentration, the intercept occurs when $x = 1$ not $x = 0$. This may have an effect on LLORAM estimates when the assay limits turn out to be extremely low. A solution to this numerical anomaly would be to change scales to parts per trillion (pptr) from parts per billion in order to remove results from the region near the intercept.

Design Considerations. The following experimental aspects are controllable: (a) the total number of standards (spiked tissue samples) to be used; (b) the range of the concentration of standards; (c) the spacing of the concentrations and the number of replicates at each concentration; and (d) the number of unknowns examined.

The strategy is to manipulate these aspects so as to minimze the x_{Cw}, x_{Dw}, x_{Qw} estimates given in the Appendix. Hubaux and Vos (*5*) have examined selected design aspects for the homogeneous variance case while Franke et al. (*8*) considered improvements in the method of standard addition when a constant coefficient of variation exists.

In addition to optimality considerations the experimental design should permit the assumptions required in the analysis to be checked and allow for remedial actions if necessary. For the tissue residue example the availability of multiple concentrations with replicate observations (at least eight to ten replicates) at each concentration allowed for checking variance homogenity and the application of a weighted least-squares analysis as well as the ability to check model adequacy. However, it would have been beneficial to have additional data at lower concentrations so that less extrapolation would be required both for the variance structure and for the actual estimates obtained. The availability of enough concentrations to allow for the examination of several models, other than just linear relationships, is to be encouraged.

CONCLUSIONS

A cautious and conservative attitude toward assumptions, methodology, and extrapolation seems warranted. In our illustrative example, even using well-defined objective criteria we obtained a wide range of results for LLORAM estimates (1.0–28.2) and found that many basic assumptions were not satisfied. The experimental design should allow for the ability to check required assumptions, and low concentrations should be included so as to preclude the necessity of undue extrapolation. Whichever LLORAM definition is used, it is essential to specify the exact criteria, all required parameters (α = type I error rate, β = type II error rate, one or two sided test statistics, C = measurement precision required, etc.), and the estimation methodology employed.

For the tissue residue data examined a LLORAM estimate of 4.2 seems appropriate. This is obtained by using the detection limits for a weighted least-squares analysis, using the empirical weights, and setting $k = 1$. Detection limits L_{Dw} and x_{Dw} are recommended since they offer protection against

both types of error, a type I error which concludes there is a residue present when there is none and a type II error which concludes there is no residue present when there is some. Setting the probability of committing a type I error equal to that of committing a type II error (say at $\alpha = \beta = 0.05$) and using one sided test statistics would be reasonable.

The variance heterogeneity has to be addressed through either a weighted least-squares approach or by using an appropriate (e.g., log) transformation. Since a test of the log transformed model indicated lack of fit, the weighted least-squares approach seemed preferable. The approach of using empirical weights and setting $k = 1$ (a conservative choice) was selected rather than a modeled variance structure with an alternative choice of k since there would be less chance of bias caused by a poor fitting variance structure model and less extrapolation beyond observed experimental results.

APPENDIX

Statistical Notation, Assumptions, and Formulas.

Linear model:

$$y_i = A + Bx_i + \epsilon_i \quad i = 1, 2, ..., N \tag{1}$$

Assumptions: ϵ_i values are independent, identically distributed normal random variables with variance $(\epsilon_i) = k_i\sigma^2$. Unweighted least squares applies when $k_i = 1$ for all i. Weighted least squares applies when not all the k_i's are equal. Estimated linear model:

$$\hat{y}_{wi} = a_w + b_w x_i$$

with

$$\text{slope} = b_w = \sum[(x_i - \bar{x}_w)y_i/k_i]/\sum[(x_i - \bar{x}_w)^2/k_i]$$

and

$$\text{intercept} = a_w = \bar{y}_w - b_w\bar{x}_w$$

where

$$\bar{y}_w = \sum[y_i/k_i]/\sum[1/k_i]$$

$$\bar{x}_w = \sum[x_i/k_i]/\sum[1/k_i]$$

$$s_w^2 = \sum[(y_i - \hat{y}_{wi})^2/k_i]/(N - 2)$$

is the weighted residual variance.

$t_{(1-\alpha)}$ is the upper α percentage point of the Student t distribution with $(N - 2)$ degrees of freedom.

Estimated variance for a predicted value, $\hat{y}_{wj}$, is as follows:

$$\text{variance}\,(\hat{y}_{wj}) = s_w^2\left\{k_j + \frac{1}{\sum(1/k_i)} + \frac{(x_j - \bar{x}_w)^2}{\sum(x_i - \bar{x}_w)^2/k_i}\right\}$$

Upper $(1 - \alpha)\%$ confidence interval for $\hat{y}_{wj}$, i.e., predicted value at a concentration x_j is as follows:

$$\hat{y}_{wj} + t_{(1-\alpha)}\sqrt{\text{variance}(\hat{y}_{wj})}$$

Refer to Draper and Smith (*16*) for additional clarification and details.

Critical Level: L_{Cw}, x_{Cw}. *Definition*: The upper $(1 - \alpha)\%$ confidence interval for a predicted value of an individual observation at a blank value, i.e., $x = 0$ (see Figure 1). The type I error rate = α, i.e., reject a blank when it is really a blank $\alpha\%$ of the time.

$$L_{Cw} = a_w + t_{(1-\alpha)}s_w\sqrt{k_0 + \frac{1}{\sum(1/k_i)} + \frac{\bar{x}_w^2}{\sum[(x_i - \bar{x}_w)^2/k_i]}}$$

$$x_{Cw} = (L_{Cw} - a_w)/b_w \tag{2}$$

where k_0 = value of k_i when $x = 0$.

Detection Level: L_{Dw}, x_{Dw}. *Definition*: The value $x = x_{Dw}$ [corresponding value $L_{Dw} = \hat{y}(x_{Dw})$] such that the lower β confidence interval for the predicted value of an individual observation at x_{Dw} equals L_{Cw} (see Figure 1), i.e.

$$L_{Cw} = \hat{y}(x_{Dw}) - t_{(1-\beta)}s_w\sqrt{k_{Dw} + \frac{1}{\sum(1/k_i)} + \frac{(x_{Dw} - \bar{x}_w)^2}{\sum(x_i - \bar{x}_w)^2/k_i}}$$

implies

$$L_{Dw} = L_{Cw} + t_{(1-\beta)}s_w\sqrt{k_{Dw} + \frac{1}{\sum(1/k_i)} + \frac{(x_{Dw} - \bar{x}_w)^2}{\sum(x_i - \bar{x}_w)^2/k_i}}$$

Since

$$\frac{(x_{Dw} - \bar{x}_w)^2}{\sum[(x_{Dw} - \bar{x}_w)^2/k_i]} < \frac{\bar{x}_w^2}{\sum[(x_{Dw} - \bar{x}_w)^2/k_i]}$$

and also is much less than $k_{Dw} + 1/\sum(1/k_i)$, then a computationally simpler but adequate approximation for L_{Dw} is as follows:

$$L_{Dw} = L_{Cw} + t_{(1-\beta)}s_w\sqrt{k_{Dw} + \frac{1}{\sum(1/k_i)} + \frac{\bar{x}_w^2}{\sum[(x_i - \bar{x}_w)^2/k_i]}}$$

$$x_{Dw} = (L_{Dw} - a_w)/b_w \tag{3}$$

where k_{Dw} = value of k_i at $x = x_{Dw}$. Note that the approximation will provide a conservative estimate, i.e., it will increase the assay limit. However, since the $|k_{Dw} + 1/\sum(1/k_i)|$ term will tend to dominate the expression under the square root radical, the effect of the substitution should be minimal. The type II error rate = β, i.e., will accept a blank when $x = x_{Dw}$ only $\beta\%$ of the time.

Determination Limit: L_{Qw}, x_{Qw}. *Definition*: Find the value $x = x_{Qw}$ [corresponding value $L_{Qw} = \hat{y}(x_{Qw})$] such that the coefficient of variation of $\hat{y}(x_{Qw})$ is sufficiently small, e.g., equals the quantity C (see Figure 2). Thus

$$\frac{\sqrt{\text{Variance}[\hat{y}(x_{Qw})]}}{\hat{y}(x_{Qw})} = C, \text{ say, } 0.10$$

implies

$$\hat{y}(x_{Qw}) = (1/C)\sqrt{\text{Variance}[\hat{y}(x_{Qw})]}$$

and thus

$$L_{Qw} = \left(\frac{s_w}{C}\right)\sqrt{k_{Qw} + \frac{1}{\sum(1/k_i)} + \frac{(x_{Qw} - \bar{x}_w)^2}{\sum[(x_i - \bar{x}_w)^2/k_i]}}$$

As for the detection limits, a computationally simpler, but adequate approximation for L_{Qw} is as follows:

$$L_{Qw} = \left(\frac{s_w}{C}\right)\sqrt{k_{Qw} + \frac{1}{\sum(1/k_i)} + \frac{(\bar{x}_w)^2}{\sum[(x_i - \bar{x}_w)^2/k_i]}}$$

$$x_{Qw} = (L_{Qw} - a_w)/b_w \tag{4}$$

where k_{Qw} = value of k_i at $x = x_{Qw}$.

Registry No. Ivermectin, 70288-86-7.

LITERATURE CITED

(1) Altshuler, B.; Pasternack, B. *Health Phys.* **1963**, *9*, 293–298.
(2) St. John, P. A.; McCarthy, W. J.; Winefordner, J. D. *Anal. Chem.* **1967**, *39*, 1495–1497.
(3) Currie, L. A. *Anal. Chem.* **1968**, *40*, 586–593.
(4) Gabriels, R. *Anal. Chem.* **1970**, *42*, 1439–1440.

(5) Hubaux, A.; Vos, G. Anal. Chem. 1970, 42, 849-855.
(6) Ingle, J. D. J. Chem. Educ. 1974, 51, 100-105.
(7) Smith, E. D.; Mathews, D. M. J. Chem. Educ. 1967, 44, 757-759.
(8) Franke, J. P.; de Zeeuw, R. A.; Hakkert, R. Anal. Chem. 1978, 50, 1374-1380.
(9) Schwartz, L. M. Anal. Chem. 1977, 49, 2062-2068.
(10) Schwartz, L. M. Anal. Chem. 1979, 51, 723-727.
(11) Graden, J. S.; Mitchell, D. G.; Mills, W. N. Anal. Chem. 1980, 52, 2310-2315.
(12) Rodbard, D. Anal. Biochem. 1978, 90, 1-12.
(13) Finney, D. J.; Phillips, P. Appl. Statistics 1977, 26, 312-320.
(14) Twsy, P. C.; Wood, J. S., Jr.; Downing, G. V. J. Agric. Food Chem. 1981, 29, 1059-1063.
(15) Helwig, J. T.; Council, K. A. "SAS Users Guide"; SAS Institute: Raleigh, NC, 1979.
(16) Draper, N. R.; Smith, H. "Applied Regression Analysis", 2nd ed.; Wiley: New York, 1981; pp 33-42.

RECEIVED for review September 20, 1982. Accepted January 6, 1983.

Partial Least-Squares Method for Spectrofluorimetric Analysis of Mixtures of Humic Acid and Ligninsulfonate

Walter Lindberg* and Jan-Åke Persson

Department of Analytical Chemistry, University of Umeå, S-901 87 Umeå, Sweden

Svante Wold

Research Group for Chemometrics, University of Umeå, S-901 87 Umeå, Sweden

Quantitative determinations of multicomponent fluorescent mixture have been made. The test substances used were humic acid, ligninsulfonate, and an optical whitener from a detergent. The fluorescence spectra from these substances have similar features with severe overlap in the whole wavelength region. For resolving these spectra and quantifying the substances, we used a numerical method, the partial least squares in latent variables (PLS). The results of its application and the theory of the method are presented and a comparison is made with other numerical methods.

Molecular fluorescence has attained popularity as an analytical technique due to its high sensitivity and relative selectivity. In complex samples, however, spectral overlap is often a serious limitation. In order to avoid time-consuming cleanup procedures, attempts to resolve complex spectra by using instrumental approaches (*1*) or various numerical methods have been made. The numerical methods used can be divided into two classes depending on whether all substances in the sample are known or not. If all substances in the sample are known and no interactions causing nonlinearities occur, then multiple regression (*2, 3*) is applicable. Individual contributions from each substances to a spectrum can be obtained and thereby their concentrations can be determined. However, usually these conditions are not fulfilled for unknown samples. In such cases, principal component analysis (*4*) has been employed for resolving the spectra obtained. With a related method called the partial least-squares models in latent variables (PLS) developed by Wold and co-workers (*5*), a new approach to the multivariate calibration problem is demonstrated. This method is preferable to principal component analysis since it not only describes the emission matrix but also at the same time correlates the measured intensities with the concentrations of each substance in the standard solutions.

Ligninsulfonate, a compound released into water from sulfite pulp mills, contributes to the general pollution of seawaters and may be fatal to fish resources. This compound has earlier been determined with some success by using fluorescence spectrometry (*6*). With this method, possible interferences arise from humic acid and detergents containing optical whiteners. Emission spectra of these compounds are severely overlapped and no spectral region with a single emitting compound can be found. The aim of this work was to evaluate the prospectives of the PLS method for quantitative determinations in various mixtures of these compounds.

MATHEMATICAL METHODS

Problem Formulation and Notation. We use boldface capital letters for matrices, e.g., $\mathbf{X}$ and $\mathbf{Y}$, primes for transposed matrices, e.g., $\mathbf{X}'$, boldface small characters for vectors, $\mathbf{x}$, $\mathbf{x}_i$, and $\mathbf{y}_m$, and italic small characters for scalars, e.g., s, p_a, and x_{ik}.

The samples are divided into two matrices, the calibration matrix, the training set, and the test matrix, the validation set. We use the first set containing the samples 1, 2,..., i,..., n to establish a calibration model which relates the measured concentrations y_{ik} of the constituents 1, 2,..., k,..., m to the measured spectroscopic data x_{ij} (wavelength j = 1, 2,..., p).

As a first step we subtract the means $\bar{x}_j$ and $\bar{y}_k$ from the data x_{ij} and y_{ik}, respectively, and then scale each variable $\mathbf{x}_j$ and $\mathbf{y}_k$ to unit variance. The thus centered and normalized data are collected in the $n \times p$ matrix $\mathbf{X}$ and the $n \times m$ matrix $\mathbf{Y}$. The centering makes the following computations numerically well conditioned. The normalization gives each variable (i.e., emission wavelength) equal influence in the initial stage of the data analysis. If prior information about the information content of the variables is at hand, this can be utilized by weighting the variables proportionally to this information. We note that this is *not* directly related to the precision of the variables, but rather a function of the degree of "nonoverlap" between the chemical constituents in the variable in combination with its precision. A priori information about this information content was not at hand in the present example and hence the variables were normalized to unit variance.

Assuming that the spectroscopic data, $\mathbf{X}$, and the concentrations, $\mathbf{Y}$, are linearly related, we have the calibration model (Figure 1) with the $m \times p$ coefficient matrix $\mathbf{C}$ still to be

0003-2700/83/0355-0643$01.50/0 © 1983 American Chemical Society

$$\mathbf{Y} = \mathbf{X}\mathbf{C}' + \mathbf{E}_p$$

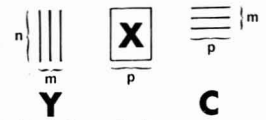


Figure 1. The data for the n calibration samples are contained in the spectroscopic matrix **X** and their concentrations in matrix **Y**. The calibration coefficients **C** are to be determined by the statistical analysis.

$$\mathbf{X} = \mathbf{T}\mathbf{B} + \mathbf{F}$$



Figure 2. The matrix **X** is decomposed as a product of two matrices **T** and **B** plus "random" errors contained in **F**.

determined (**E** contains the "random" residuals not explained by the systematic model).

Traditional Methods. If the variables $\mathbf{x}_j$ were independent of each other (i.e., little correlated) and the number of samples, n, was large compared to the number of wavelengths, p, the estimation of **C** is best made by ordinary least squares (OLS) with multiple regression (MR). However, in the present type of problems, the x variables are strongly correlated. This is so because each constituent in the samples emits light over the whole spectral range, i.e., influences all x variables. Hence these variables all go up and down when the concentration of one constituent changes. Moreover, the number of wavelengths, p, is much larger than the number of major constituents in the samples (2 or 3) which also makes the effective rank of **X** much smaller than p.

These correlations among the x variables make the OLS solution, which requires the inversion of **X'X**, almost infinite which, in turn, gives the calibrated model bad prediction properties.

The best solution to this statistical–numerical problem is to represent **X** by a product of two small matrices, **T** and **B**, of dimensions $n \times a$ and $a \times p$, respectively, with $a \ll n$ and $a \ll p$ (Figure 2). Here **F** is a matrix of "small" and "random" errors. The columns in **T** are mutually orthogonal as are the rows in **B**.

The dimensionality, a, is selected to make **TB** represent **X** as close as possible in some statistical sense (*5*, *7*, *8*).

In numerical analysis this representation of **X** as **TB** is called singular value decomposition (*9*), in statistics, principal components analysis (*10–12*), and in electrical engineering, the Karhunen–Loeve expansion (*13*). In chemistry, for some reason, the names rank annihilation (*4*), eigenvector projection (*14*), and factor analysis (*8*) are common for the same analysis.

The analysis has a nice geometrical representation as a linear projection of the p-dimensional **X** space down on the a-dimensional plane **T** using the projection matrix **B**. Since **T** has orthogonal columns, these can be used as new variables in the regression model, leading to the inversion of **T'T** instead of **X'X** giving the coefficients **G** instead of **C**. Because **T** is defined as **XB'**, biased estimates of **C** are given as **BG'**.

Predictions. For new samples (with data x_i) in the test set the predictions of **Y** are x_iC' by MR and $x_iB'G'$ ($= t_iG'$) for principal components regression (PCR).

PLS (the Present Method). The PLS solution is similar to PCR except that the projection **T** is computed *both* to model **X** *and* to correlate with **Y**, while the PCR, **T** is computed only to model **X** (*5*, *15*). This is accomplished by introducing a weight matrix **W** and a set of latent variables for **Y** denoted by **U** with the corresponding loading matrix $\mathbf{B}_y$.

This makes the PLS solution have equal or better predictive properties for **Y**; better in the case when the information in **X** about **Y** appears among the later singular vectors of **X** (corresponding to small singular values).

The PLS algorithm is described below. We note that if differs from PCR also in the prediction phase since no explicit regression step is given in the method. It is also much faster than PCR.

Table I. Compositions of the Calibration Solutions (μg mL^{-1})

calibration set I		calibration set II		
humic acid	lignin-sulfonate	humic acid	lignin-sulfonate	detergent
1.24	0.111	3.01	0	0
4.12	0.099	0	0.401	0
1.52	0.492	0	0	90.6
3.05	0	1.48	0.158	40.0
0	0.390	1.12	0.410	30.4
2.25	0.148	3.40	0.303	50.8
2.33	0.219	2.43	0.298	70.6
1.34	0.134	4.02	0.115	89.4
0.931	0.263	2.28	0.504	81.8
3.68	0.312	0.959	0.145	101
1.40	0.415	3.19	0.253	120
2.94	0.305	4.13	0.569	118
3.50	0.341	2.16	0.436	27.6
3.02	0.671	3.09	0.247	61.7
		1.60	0.286	109
		3.16	0.701	60.0

EXPERIMENTAL SECTION

Apparatus. A Perkin-Elmer Model 512 double beam fluorescence spectrometer was used for all measurements. Emission spectra were measured in the ratio mode with both excitation and emission slits set at 20 nm. The SIMCA-3B BASIC program Package for 8-bit microcomputers (ABC-80 and CP/M) was used for the data evaluation. The package is available from S. Wold.

Reagents. Sodium ligninsulfonate was obtained from the Finnish Paper and Pulp Research Institute and humic acid from K&K Laboratories (Plainview, NY). A commercial detergent was used as a standard for the optical whitener.

Procedure. Two sets of multicomponent calibration solutions were prepared according to Table I. In the measurements, excitation was made at 300 nm and emission spectra were recorded between 320 and 540 nm. From these spectra emission intensities at 27 equidistant wavelengths were used. In this way a signal concentration matrix that could be subjected to data analysis was obtained. All calibration solutions were measured in a random order so that experimental errors due to drift were not introduced.

RESULTS AND DISCUSSION

For this investigation, three substances that can be found in natural water samples were chosen, namely, humic acid, ligninsulfonate, and an optical whitener contained in a commercial detergent. The concentrations of these species were taken to reflect the ranges that normally can be found in Swedish seawaters (*16*). When fluorescence spectrometry is utilized for determination of such samples, all of these species emit light over the same spectral region. Of the three substances, the strongest emissions will be obtained from humic acid as it can be found in high concentrations in waters. The difficulties that arise when mixtures of these compounds are to be determined are realized by studying the individual emission spectra shown in Figure 3. The similarities between the spectra are strong and no wavelength can be found where any of the substances is the only emitter. This means that

Table II. Results ($\mu g\ mL^{-1}$) for Mixtures with Two Substances Calibrated with Set I

	humic acid		ligninsulfonate		
sample no.	actual concn	prediction error[a]	actual concn	prediction error[a]	dissimilarity factor[b]
1	4.02	−0.13	0.507	−0.062	0.36
2	2.48	0.10	0.266	−0.004	0.42
3	4.26	−0.12	0.364	−0.005	0.54
4	0.997	−0.11	0.203	0.049	0.79
5	2.96	0.64	0.116	−0.082	0.94
6	1.14	0.0	0.404	0.087	0.65
7	5.08	0.0	0.209	−0.155	1.03
8	4.99	−0.34	0	0.075	1.08
9	0	0.30	0.723	−0.119	5.30
$\left(\frac{\Sigma(y_{true} - y_{calcd})^2}{n}\right)^{1/2}$		0.27		0.085	

[a] Equals predicted minus actual concentration. [b] Equals $s/s_a(E_x)$. Thus if the dissimilarity factor exceeds $F^{1/2}$, then the sample is dissimilar to the calibration set.

Table III. Results ($\mu g\ mL^{-1}$) for Mixtures with Three Substances Calibrated with Set II

	humic acid		ligninsulfonate		detergent		
sample no.	actual concn	prediction error[a]	actual concn	prediction error[a]	actual concn	prediction error[a]	dissimilarity factor[b]
10	2.44	0.08	0.289	0.042	80.2	0.9	1.29
11	4.08	0.07	0.361	−0.058	88.5	−14.4	3.51
12	1.06	0.09	0.234	0.024	69.2	−1.2	0.74
13	3.32	0.07	0.123	−0.059	40.1	16.3	1.29
14	0.998	0.08	0.416	0.059	30.7	−3.0	0.92
15	2.98	−0.10	0.403	0.074	120	2.4	1.39
16	5.13	−0.32	0.229	−0.015	49.0	14.8	2.22
17	5.06	−0.20	0	−0.017	51.1	−12.4	1.85
18	0	−0.49	0.735	0.688	99.6	−31.9	21.3
$\left(\frac{\Sigma(y_{true} - y_{calcd})^2}{n}\right)^{1/2}$		0.22		0.234		14.4	

[a,b] See Table II.

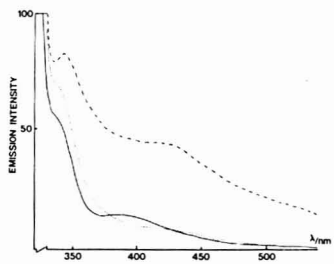


Figure 3. Emission spectra obtained for 0.88 $\mu g\ mL^{-1}$ of humic acid (– –), 0.1 $\mu g\ mL^{-1}$ of ligninsulfonate (—), and 25 $\mu g\ mL^{-1}$ of a detergent (• • •).

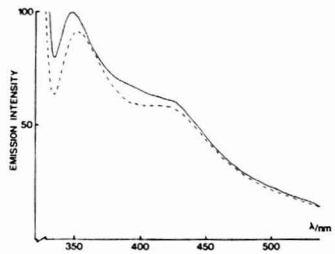


Figure 4. Emission spectra obtained of numerically added signals from pure substances (—) and for a mixture of the three solutes (– – –). Concentrations: humic acid, 4.4 $\mu g\ mL^{-1}$; ligninsulfonate, 0.5 $\mu g\ mL^{-1}$; detergent, 100 $\mu g\ mL^{-1}$.

conventional calibration procedures cannot be used for quantitative determinations. Determinations are further complicated by interactions within the solutions. This is seen in Figure 4, where an emission spectrum obtained for a mixture with all three substances is compared with the spectrum expected from the mixture, i.e., a summation of the individual spectra. In the figure, it is seen that these spectra differ in both intensity and shape. This means that the relationship between signal intensity and concentration is nonlinear.

Evaluation of the PLS Algorithms for Resolving Overlapped Spectra. The use of the partial least-squares model in latent variables (PLS) for resolving overlapped spectra was examined by selecting test and calibration sets so that different levels of complexity could be investigated. In order to account for interaction processes, all standards were prepared as mixtures of the substances used. The data set obtained is imbalanced as humic acid emits more strongly than the others. Hence, the number of significant dimensions in the model tends to be underestimated. Consequently we have regarded the dimensionality estimated by cross validation as a lower limit and used a dimension number of 2–4 higher. As long as the used dimensionality is not larger than a third of the number of variables (frequencies) in the calibration set, this will not affect the statistical stability of the results (*17*). The results obtained are presented in Tables II–V.

In Table II predicted concentrations in sample mixtures containing humic acid and ligninsulfonate are shown. In the test set, concentrations of these substances were varied so that the contribution to the total signal from humic acid varied

Table IV. Results ($\mu g\ mL^{-1}$) for Mixtures with Three Substances Calibrated with Set II but Only Two Dependent Variables (Humic Acid and Ligninsulfonate)

	humic acid		ligninsulfonate		
sample no.	actual concn	prediction error[a]	actual concn	prediction error[a]	dissimilarity factor[b]
10	2.44	0.04	0.289	0.016	1.31
11	4.08	0.12	0.361	−0.100	3.51
12	1.06	0.04	0.234	0.044	0.75
13	3.32	0.07	0.123	−0.024	1.12
14	0.998	0.11	0.416	0.037	0.95
15	2.98	−0.10	0.403	0.010	1.55
16	5.13	−0.22	0.229	−0.109	2.20
17	5.06	−0	0	−0.017	1.80
18	0	−0.35	0.735	0.532	18.5
$\left(\frac{\Sigma(y_{true} - y_{calcd})^2}{n}\right)^{1/2}$		0.15		0.185	

[a, b] See Table II.

Table V. Results ($\mu g\ mL^{-1}$) for Mixtures with Two Substances Calibrated with Set II

	humic acid		ligninsulfonate		detergent		
sample no.	actual concn	prediction error[a]	actual concn	prediction error[a]	actual concn	prediction error[a]	dissimilarity factor[b]
1	4.02	−0.32	0.507	−0.409	0	−12.4	5.17
2	2.48	0.05	0.266	0.005	0	−11.6	1.02
3	4.26	−0.11	0.364	−0.086	0	−7.06	5.63
4	0.997	0.12	0.203	−0.067	0	−11.7	1.29
5	2.96	0.41	0.116	0.053	0	−7.11	1.29
6	1.14	0.06	0.404	0.023	0	−6.51	1.02
7	5.08	−0.30	0.209	0	0	−9.73	5.63
8	4.92	−0.40	0	0.126	0	−16.4	5.54
9	0	−0.16	0.723	0.229	0	0.18	13.0
$\left(\frac{\Sigma(y_{true} - y_{calcd})^2}{n}\right)^{1/2}$		0.25		0.098		10.2	

[a, b] See Table II.

from 50 to 100%, except for sample no. 9. In the predictions, both the mean errors and the standard deviation obtained can be regarded as acceptable. As an example, the mean error for the minor substance in the mixtures, ligninsulfonate, was $-0.024\ \mu g\ mL^{-1}$ corresponding to a standard deviation of $0.085\ \mu g\ mL^{-1}$. By addition of a commercial detergent with an optical whitener to these mixtures, a more complex situation was obtained. In Table III it can be seen that, in this situation, the accuracy of the predictions for humic acid and ligninsulfonate equals those for the simpler case shown in Table II. At the same time an equally good estimation of the concentration of the detergent could be obtained. However, to obtain these results for the three-component mixture, the model used had to involve an increased number of dimensions. This indicates that when the detergent is introduced into the system, the number of interactions within the solution also increases. To investigate how PLS works in the case when the calibration is made with respect to a few "known" substances in a complicated mixture, we also used set II (with all three substances) as a calibration set for only humic acid and ligninsulfonate. Thus the presence of detergent was considered as an unknown disturbance. Table IV shows the observed and predicted values for humic acid and ligninsulfonate in "test" samples 10–18 (same as in Table III). It is seen that actually the prediction errors go down in comparison with Table III. This is because fewer dimensions are needed in the model and therefore the results are more stable.

In the tables it can also be seen that errors in the predictions tend to be large for samples with large differences in the concentrations of the species and for those with concentrations near the outer limits of the calibration set used. In such cases, the uncertainty of the predicted concentrations and hence the standard deviation can be expected to be large. However, this is an inherent property with this as well as with all other calibration procedures.

One of the main advantages with the PLS model is the fact that a criterion reflecting the simlarity between standards and samples is obtained. In the tables this is called the dissimilarity factor. If an attempt is made to determine a sample which cannot be accurately described with the set of standards used for calibration, the prediction is accompanied by a high figure in the dissimilarity factor. In this way the analyst can judge whether the determination is reliable or not. As an example, the concentrations of ligninsulfonate in samples no. 9 and 18 are higher than in any of the standards used. Due to this, erratic results with high values of the dissimilarity factor are obtained. If calibration models for different types of samples are determined, the dissimilarity factor can be used to classify a sample as similar to one of the calibration models.

In all quantifications, random and systematic errors arise when concentrations in unknown samples are predicted. Random errors are mainly due to experimental uncertainties and the noise level of the analytical method used. The chemical reactions involved in the method and the statistical model used for evaluation can in turn introduce systematic errors. However, errors caused by the chemistry can usually be compensated for with appropriate standardization. In statistical models, the sign and magnitude of the error will depend on where the unknown sample is situated in the calibration space. When calibration with three substances (set II) was used for the determination of the nine samples without any detergent (no. 1–9), a situation was obtained where all of the samples were situated in the same region of the calibration space. The results presented in Table V show that a systematic error was obtained when the concentration of the detergent was predicted. the mean error was $-9.15\ \mu g$

mL^{-1}. In comparison with the concentrations of the detergent used in the calibration set, this error can be regarded as acceptable. However, with calibration set II, both humic acid and ligninsulfonate could be determined with the same precision as if calibration set I had been used (Table II). This cannot be stated as a general conclusion since the possibility for interactions within the solutions increases with the number of substances added. If samples of less complexity than the standards are determined, errors can be introduced due to differences in the interactions that can occur. This means that a careful examination of the standardization procedure has to be made in each case, if erratic results are to be avoided. Humic acid and ligninsulfonate are ill-defined compounds and the fluorescence properties of these compounds can change with time. This means that if these substrates are to be determined in natural waters, extensive work has to be done in order to isolate appropriate standards. However, this problem is the same with any calibration method; PLS can no more than other methods compensate for ill-designed calibration sets.

CONCLUSION

Severely overlapped spectra can be resolved with the PLS algorithm and individual concentrations in mixtures can be determined. Compared with other approaches, the PLS algorithm has the followed advantages: (*i*) the information from the calibration solutions is better used. If the signals contain structure which has predictive relevance for the concentrations in the calibration mixtures, this will appear in the PLS solution. This is not necessarily the case for multiple regression, principal component, and ridge regression methods. (*ii*) When the PLS model is determined, a criterion reflecting the dissimilarity of new samples to the calibration set is obtained. This means that one gets information if the calibration set is qualified or not to determine the composition of a sample. This type of information is not given by other methods. (*iii*) The PLS method can, like other methods related to principal components analysis, compensate for unidentified fluorescent species in the solution. (*iv*) The computation time is much shorter than that for multiple regression. (*v*) The algorithms are easy to program for microcomputers.

THE PLS METHOD FOR MULTIVARIATE CALIBRATION

I. The Calibration Phase. A. Center and normalize **X** and **Y** (see section 1 in mathematical methods). In case prior information exists about the importance of individual variables, scale proportionally to this information.

B. For dimension $h = 1, 2, ..., a$.

1. Starting values $u_{ih} = Y_{il}$. In case of a single **Y** variable ($m = 1$) $\mathbf{u}_h \equiv \mathbf{y}$.

2. Weights for the **X** variables $\mathbf{w}_h = \mathbf{u}_h'\mathbf{X}$. Normalize **w** to $\|\mathbf{w}\| = 1$.

3. Latent variable $\mathbf{t}_h = \mathbf{X}\mathbf{w}_h'$. In case of a single **Y** variable the algorithm continues with step 7, otherwise:

4. Loading for the **Y** variables $\mathbf{b}_y = \mathbf{t}_h'\,\mathbf{Y}$.

5. New latent variable values for the **Y** matrix $\mathbf{u}_h = \mathbf{Y}\mathbf{b}_y'$.

6. If $\|\mathbf{u} - \mathbf{u}_{old}\| > 10^{-6}\|\mathbf{u}\|$ then back to step 2, else convergence is reached and step 7 is taken next.

7. Compute the coefficient v_h which relates the latent variable of **X** to the latent variable of **Y**

$$\mathbf{u}_h = v_h \cdot \mathbf{t}_h + d$$

$$v_h = \mathbf{t}_h'\mathbf{u}_h / \|\mathbf{t}_h\|^{1/2}$$

8. Compute the loading for **X**, $\mathbf{b}_{hx}$

$$\mathbf{b}_{hx} = \mathbf{t}_h'\mathbf{X}$$

9. Compute residuals

$$\mathbf{E}_x = \mathbf{X} - \mathbf{t}_h\mathbf{b}_{hx}$$

$$\mathbf{E}_y = \mathbf{Y} - v_h\mathbf{t}_h\mathbf{b}_{hy}$$

10. For the next dimension, use $\mathbf{E}_x$ instead of **X** and $\mathbf{E}_y$ instead of **Y**. Start again with step 1 above.

II. The Number of Dimensions, *a*. The number of significant dimensions, *a*, is determined by cross validation. A quarter of the calibration samples is kept out of the calculations in the *h*th dimension. The **Y** values of these samples are then predicted as $\mathbf{t}_h\mathbf{b}_{hy} \cdot \mathbf{v}_h$ by the calculated model and the partial sum of squares (SS) of the differences between predicted and actual values are formed. Another quarter of the sample is then kept out, a second partial SS computed, etc., until each calibration sample has been kept out once and only once.

If the resulting SS (sum of the four partial SS) is smaller than the residual SS (of Y) before the *h*th dimension, the *h*th dimension has predictive relevance and is deemed to be statistically significant. The procedure is continued until a dimension $(a + 1)$ is nonsignificant.

III. Predictions of y_i from the Calibrated Model and a "New" Sample Data Vector, $\mathbf{x}_i$. (*i*) *Degree of Fit.* The fit of the "new" sample to the model is measured as the SD (standard deviation) of the residual **e**

$$\mathbf{e}_i = \mathbf{x}_i - \mathbf{x}_i\mathbf{B}'\mathbf{B} \qquad (\mathbf{x}_i\mathbf{B}' = t_i)$$

$$s^2 = \|e\|/(p - a)$$

If the fit is acceptable, i.e., $s^2 < s_a^2(\mathbf{E}_x)\cdot F$, the predicted values **y** can be reliably computed by the algorithm shown below. Here $s_a^2(\mathbf{E}_x)$ is the residual SD of the **X** matrix after dimensions *a* and *F* the *F* statistic at probability level α and $(p - a)/2$ and $(p - a)(n - a - 1)/2$ degrees of freedom.

Algorithm for Prediction. 1. Scale and center **X** as in the calibration.

2. $h = 0$ $\mathbf{y} = \bar{\mathbf{y}}$ (average)

3. $h = h + 1$

$$t_h = \mathbf{x}\mathbf{w}_h'$$

$$\mathbf{y} = \mathbf{y} + v_h t_h \mathbf{b}_{hy}$$

$$\mathbf{x} = \mathbf{x} - t_h\mathbf{b}_{hx}$$

4. If $h > a$, then terminate (step 5) or else go back to step 3.

5. The predicted values of **y** are now obtained in scaled and centered form. They are transformed back to the original coordinates by applying the reverse of the centering and scaling done in the calibration phase.

Registry No. H_2O, 7732-18-5; ligninsulfonic acid, 8062-15-5.

LITERATURE CITED

(1) "Modern Fluorescence Spectroscopy 4;" Plenum Press: New York, 1981.
(2) Warner, I. M.; Davidson, E. R.; Christian, G. D. *Anal. Chem.* **1977**, *49*, 2155.
(3) Gold, H. S.; Rechsteiner, C. E., Jr.; Buck, R. P. *Anal. Chim. Acta* **1978**, *103*, 167.
(4) Ho, C.-N.; Christian, G. D.; Davidson, E. R. *Anal. Chem.* **1980**, *52*, 1071.
(5) Wold, S.; Wold, H.; Dunn, W. J., III; Ruhe, A. Report UMINF-83, Deptment of Chemistry, University of Umeå, Sweden, 1980.
(6) Almgren, T.; Josefesson, B.; Nyquist, G. *Anal. Chim. Acta* **1975**, *78*, 411.
(7) Wold, S. *Technometrics* **1978**, *20*, 397.
(8) Malinowski, E. R.; Howery, D. G. "Factor Analysis in Chemistry"; Wiley: New York, 1980.
(9) Golub, G. H.; Kahan, W. *J. Numer. Anal.* **1965**, *B2*, 205.
(10) Kruskal, J. "Factor Analysis and Principal Component Analysis, The Bilinear Methods"; Encyclopedia of Statistics; The Free Press: New York, 1978.
(11) Gnanadesikan, R. "Methods for Statistical Data Analysis of Multivariate Observations"; Wiley: New York, 1977.
(12) Draper, N.; Smith, H. "Applied Regression Analysis", 2nd ed.; Wiley: New York, 1981.
(13) Kanal, L. *IEEE Trans. Inform. Theory* **1974**, *IT-20*, 697.
(14) Massart, D. L.; Dijkstra, A.; Kaufman, L. "Evaluation and Optimization of Laboratory Methods and Analytical Procedures"; Elsevier: Amsterdam, 1978.

(15) Wold, S.; Martens, H.; Wold, H. In "Proceedings on the Symposium Matrix Pencils, Piteå 1982"; Ruhe, A., Kågström, B., Eds.; Lecture Notes in Mathematics. Springer Verlag: Berlin and Heidelberg, in press.
(16) Nyquist, G. Ph.D. Dissertation, University of Gothenburg, Sweden, 1979.
(17) Wold, S.; Sjöström, M. In "Chemometrics: Theory and Application;" Kowalski, B. R., Ed.; American Chemical Society: Washington, DC, 1977; ACS Symposium Series, No. 52.

RECEIVED for review September 13, 1982. Accepted December 6, 1982.

Digital Smoothing of Noisy Spectra

Manfred U. A. Bromba* and Horst Ziegler

FB 6—Angewandte Physik, Universität Paderborn, D-4790 Paderborn, West Germany

It is shown what properties a digital low-pass filter should possess if only a few very general common features like symmetry, positivity, and monotonicity of the individual spectral lines are known a priori. The effect of smoothing on such unknown line properties as shape, height, width, and position is considered theoretically to simplify the selection of suitable filter types in view of a good compromise between noise reduction and signal deformation.

Usually random noise is a permanent but nevertheless unpleasant component of all kinds of spectra since it may alter important quantities such as the position, the height, or the width of a spectral line in an unpredictable way. Even spurious lines may be created by random noise.

One way to simplify the interpretation of noisy spectra is smoothing by digital filtering. Besides deconvolution (resolution enhancement) and differentiation, smoothing seems to be the most frequent used type of filtering. The price to be paid for the reduction of noise (and hence a reduction of random errors) is the introduction of a systematic (predictable) line deformation error. There are numerous criteria concerning the total error (systematic & random) which allow the theoretical design of an optimal filter. Sometimes a parameter of a class of filters (e.g., Savitzky–Golay smoothing filters of fixed degree 2M (*1–4*)) may be adjusted to minimize the total error. Usually this parameter is called "filter width" and, in principle, controls the degree of smoothing. However, all these criteria need detailed a priori information about the signal, especially the line shape and the line width. (As a rule, line height and line position need not be considered because of the linearity and the translational (or time) invariance of our filters.) Also some noise properties should be known. While in most cases the assumption of white noise meets the real world sufficiently well, the line width may vary over a wide range, dependent on the physics of the line, the scan speed, and the sampling rate. Different line shapes and line widths may even occur in the same spectrogram, thus making the choice of an optimal filter impossible. Furthermore, in several cases an a priori determination of the line shape and the line width is very difficult or time-consuming so that trial-and-error methods have gained a great popularity.

The intention of this paper is to show what properties a digital filter should or should not possess if only a few very general common properties of the individual lines of a spectrum are known a priori. Lines having these properties will be called "spectrometric functions" throughout this paper.

We only consider the effect of smoothing on single lines. Since digital filters are linear and translationally invariant, it suffices to treat centered lines of unit height. Thus we define (sampled) Gaussians g and Lorentzians h (of width $\beta > 0$) by ($k = 0, \pm1, \pm2, ...$)

$$g[k] = \exp\left(-\frac{k^2}{\beta^2}\right) \tag{1}$$

$$h[k] = \left(1 + \frac{k^2}{\beta^2}\right)^{-1} \tag{2}$$

Most spectral lines can be represented fairly well by Gaussians and Lorentzians. The Fourier transform and further formulas concerning sums and square sums of these functions are reviewed in the Appendix.

We have chosen the following common properties of Gaussians ($f = g$) and Lorentzians ($f = h$), which are valid for every width $\beta > 0$, to define a spectrometric function f:

(a) f is symmetric

$$f[k] = f[-k] \quad \text{every } k \tag{3}$$

(b) f is absolutely summable

$$\|f\|_1 = \sum_{k=-\infty}^{\infty} |f[k]| < \infty \tag{4}$$

(c) f is strictly monotonic

$$f[k] > f[k+1] \quad \text{every } k \geq 0 \tag{5}$$

(d) The Fourier transform of f is strictly positive

$$\mathcal{F}f(\omega) = \sum_{k=-\infty}^{\infty} f[k] \exp(-i\omega k) > 0 \quad \text{every } |\omega| \leq \pi \tag{6}$$

From properties (a)–(d) we can deduce further properties of spectrometric functions:

(e) f is strictly positive

$$f[k] > 0 \quad \text{every } k \tag{7}$$

(f) $\mathcal{F}f$ has a maximum at $\omega = 0$

$$\mathcal{F}f(0) > \mathcal{F}f(\omega) \quad (0 < |\omega| \leq \pi) \tag{8}$$

(e) is a direct consequence of (a)–(c). (f) results from (e) and can be shown using eq 6 to establish the low-frequency character of spectrometric functions. Moreover, regarding elementary properties of alternating series, we can derive the following inequalities from eq 6:

$$f[0] - 2f[2] < \mathcal{F}f(\pi/2) < f[0] \tag{9}$$

0003-2700/83/0355-0648$01.50/0 © 1983 American Chemical Society

$$f[0] - 2f[1] < \mathcal{F}f(\pi) < f[0] \tag{10}$$

It is important to know that additions and convolutions of spectrometric functions also are spectrometric functions. This includes, e.g., the Voigt profiles (*5*).

We note that the strict positivity of spectrometric functions also holds true for shifted lines and additions of any number of shifted lines. This feature can be applied with success as a "positivity constraint" to modify the Van Cittert resolution enhancement algorithm (*6*) toward a considerably improved noise behavior (*7–11*).

Although we have not defined a width for general spectrometric functions, it is intuitively clear that the extreme cases of infinite and minimum width are the constant background and the delta impulse (eq 20). We note that these two cases do not represent spectrometric functions since one is not absolutely summable while the other fails to be strictly positive. However, they may serve for the consideration of the cases of strong and weak filtering, respectively.

THEORY

As in a previous paper (*4*), we describe a general digital filter operator A by

$$Af[k] = \sum_{n=-\infty}^{\infty} a[n]f[k-n] \tag{11}$$

where f is the unfiltered signal (e.g., a spectrometric function), a is the filter function, and Af corresponds to the filtered signal ($k = 0, \pm1, \pm2, ...$). Assuming stationary white noise, the noise amplification (*12*) is given by the square root of the sum of squares of the filter function. We use the abbreviation

$$\|a\|_2 = \sqrt{\sum_{n=-\infty}^{\infty} (a[n])^2} \tag{12}$$

In this paper, a digital low-pass with filter function a is defined to have a noise amplification smaller than 1

$$\|a\|_2 < 1 \tag{13}$$

Furthermore, the filter function must be symmetric (eq 3). At last, a normalization to unit area (moment)

$$\mu(a) = \sum_{n=-\infty}^{\infty} a[n] = 1 \tag{14}$$

is introduced to ensure comparability. In the frequency domain the convolution of a with f, eq 11, simply appears as a pointwise multiplication of the frequency response $\mathcal{F}a$ with the Fourier transform of the signal

$$\mathcal{F}Af(\omega) = \mathcal{F}a(\omega)\mathcal{F}f(\omega) \tag{15}$$

An additional restriction leads to a class of low-passes which we shall call "smoothing filters", according to a suggestion of Schoenberg (*13*)

$$\mathcal{F}a(\omega) < 1 \ (0 < |\omega| \leq \pi) \tag{16}$$

A smoothing filter is said to be a "strict smoothing filter" if

$$\mathcal{F}a(\omega) \geq 0 \tag{17}$$

for every ω. The motivation for these restrictions will be given in the subsequent discussions. It should be remarked that the moment (area) of a function equals its Fourier transform at zero. Thus eq 14 is equivalent to $\mathcal{F}a(0) = 1$.

Line Conservation. It is a well-established fact that spectrometric functions cannot be low-pass-filtered without line deformation. This is easily seen by the following consideration. Suppose the spectrometric function f is filtered without error. Then we have

$$Af = f \tag{18}$$

or, by Fourier transform of eq 18

$$\mathcal{F}Af = \mathcal{F}a \cdot \mathcal{F}f = \mathcal{F}f \tag{19}$$

Since $\mathcal{F}f$ is strictly positive by assumption (e), the second equation of eq 19 can only be fulfilled if $\mathcal{F}a(\omega) = 1$ for every $|\omega| \leq \pi$. Thus, a must be the filter function of the identity filter which is the delta impulse d

$$a[n] = d[n] = \begin{cases} 1 & n = 0 \\ 0 & \text{else} \end{cases} \tag{20}$$

However, the identity ("do nothing"-) filter is not a low-pass in the sense of our definition since its noise amplification equals 1. We note that there exist functions f which fulfill eq 18, e.g., polynomials (*4*) or band-limited signals (by eq 6 and 7, a spectrometric function is neither band limited nor time limited). Spectrometric functions can be represented by such functions only approximately, in agreement with the fact that line conservation is not realizable with low-passes.

There are several criteria to describe the unavoidable line deformation. The most popular one seems to be the sum of error squares which is given by

$$\epsilon_2 = \|f - Af\|_2 \tag{21}$$

If the shape and the width of the line f are known, ϵ_2 can be minimized subject to the constraints of a fixed noise amplification and eq 14. Since we did not make assumptions on these quantities, we cannot find an optimum filter. However, the question "Given a digital low-pass, can this low-pass be improved in such a way that it becomes better with regard to ϵ_2 for *every* spectrometric function?" may be posed. The answer will be "yes" in at least the following (unfavorable) cases: (i) The frequency response $\mathcal{F}a$ exhibits regions of negative values. (ii) $\mathcal{F}a(\omega)$ exceeds 1 in certain frequency ranges. (iii) $a[0]$ is not the greatest coefficient of the filter function a. (Proof: By the Parseval theorem, eq 21 can be expressed as

$$\epsilon_2^2 = \frac{1}{2\pi} \int_{-\pi}^{\pi} (1 - \mathcal{F}a(\omega))^2 (\mathcal{F}f(\omega))^2 \, d\omega \tag{22}$$

Applying the Parseval theorem also to the noise amplification, it is seen that the replacement of $\mathcal{F}a$ by the positive frequency response $|\mathcal{F}a|$ does not affect the noise amplification and eq 14 but reduces ϵ_2 for *every* spectrometric function f, if $\mathcal{F}a$ has regions of negative values. Similarly, if $\mathcal{F}a(\omega)$ exceeds 1 in certain regions, we may replace $\mathcal{F}a(\omega)$ by $1 - |1 - \mathcal{F}a(\omega)|$ to get the same error but a smaller noise amplification. If the frequency response $\mathcal{F}a$ is positive, $a[0]$ must be the maximum of the filter function. Conversely, if $a[0]$ is not a maximum, $\mathcal{F}a$ must have negative regions and case (iii) can be reduced to case (i).)

A further criterion is the maximum error:

$$\epsilon_\infty = \|f - Af\|_\infty = \sup_k |f[k] - Af[k]| \tag{23}$$

Usually this criterion is mathematically cumbersome to handle—except for the case where $\mathcal{F}a(\omega) \leq 1$ for every ω, since ϵ_∞ then reduces to the peak height error ϵ_0 which is discussed later

$$\epsilon_\infty = \epsilon_0 = f[0] - Af[0] \tag{24}$$

(The proof uses the inverse Fourier transform and shows that

$$\begin{aligned} (f - Af)[k] &= \frac{1}{2\pi} \int_{-\pi}^{\pi} (1 - \mathcal{F}a(\omega))\mathcal{F}f(\omega) \cos(\omega k) \, d\omega \\ &\leq \frac{1}{2\pi} \int_{-\pi}^{\pi} (1 - \mathcal{F}a(\omega))\mathcal{F}f(\omega) \, d\omega \\ &= (f - Af)[0] \end{aligned} \tag{25}$$

for every $k = 0, \pm1, \pm2, ...$)

Since exact line conservation (which is the strongest possible constraint) cannot be achieved with low-passes, we may look for the conservation of weaker line characteristics. This we shall do in the following.

Area. Because our low-passes are normalized to have filter functions of unit area ($\mu(a) = \mathcal{F}a(0) = 1$), exact line area conservation is attained for every spectrometric function f in the sense of

$$\mu(Af) = \mu(f) \tag{26}$$

At the same time our normalization ensures the exact conservation of constant backgrounds.

Unfortunately the moment μ is no practicable measure because of its infinite summation (see eq 14). If we replace $\mu(f)$ by a finite sum, exact conservation for *every* spectrometric function cannot be achieved any more (*14*). It should be noted that a second error caused by sampling arises, when the area is originally defined by the integral of the unsampled (continuous) line; compare eq 40 and 41 with eq 44 and 45. This error can only be avoided by suitable prefiltering methods.

Symmetry. By the symmetry of our low-pass filter functions, the symmetry (or antisymmetry) of an arbitrary signal is conserved exactly. (We note that symmetric filters are a subclass of linear phase filters (*15*).) Symmetry conservation is a fundamental requirement for the conservation of peak positions.

Positivity. By eq 11, strict positivity (property (e)) is conserved for *every* spectrometric function, if the filter function a is positive

$$a[n] \geq 0 \quad \text{every } n \tag{27}$$

This condition is necessary and sufficient, if conservation for *every* spectrometric function is required. We note that low-passes with positive filter functions always are smoothing filters.

To conserve the positivity of the Fourier transform of an arbitrary signal, the positivity of the frequency response is an indispensable condition; see eq 15.

Invertibility. Since the Fourier transform of a spectrometric function is strictly positive (property (d)), the pointwise inverse $1/\mathcal{F}f(\omega)$ can be formed to serve as the frequency response of a deconvolution filter which narrows a fixed spectrometric function f to a delta impulse. Therefore it may be desirable in specific cases to conserve strictly positive Fourier transforms. This can only be achieved with a strictly positive frequency response $\mathcal{F}a$ (which belongs to an invertible low-pass). Every positive frequency response can be made strictly positive by adding an arbitrarily small positive number to $a[0]$ and then renormalizing the filter function a for unit area. However, the exact conservation of invertibility is of doubtful value since a filter with $(\mathcal{F}f)^{-1}$ as frequency response usually exhibits a very large noise amplification, dependent on the width of f.

Position. As has been already pointed out, an indispensable precondition for the conservation of the line position is the symmetry of the filter function. Here we assume that the position of a spectrometric function is given by the location of its maximum (in contrast to, e.g., the location of the center of gravity). The symmetry of the filter function guarantees the conservation of signal symmetry. However, for a unique definition of a maximum of the filtered line, symmetry is not sufficient. For example, it is no problem to construct a smoothing filter A that "duplicates" a spectrometric function f in such a way that Af is symmetric but exhibits 2 maxima at equal distance to the origin (where f has its unique maximum).

Perhaps the most reliable method to ensure position conservation is to conserve strict monotonicity for *every* spectrometric function. A necessary and sufficient way to accomplish this is to use a monotonic ($a[n] \geq a[n+1]$ for every $n \geq 0$) filter function. (This may be shown step by step with the aid of the inequality

$$\alpha_1\beta_1 + \alpha_2\beta_2 \geq \alpha_1\beta_2 + \alpha_2\beta_1 \tag{28}$$

which holds if $\alpha_1 > \alpha_2$ and $\beta_1 \geq \beta_2$.)

Though a monotonic filter function prevents the generation of nonexisting peaks even when a linear background is superimposed, monotonicity over the whole interval $-\infty \ldots \infty$ sometimes is too severe and may be replaced by weaker conditions if small side lobes can be tolerated. (For example, monotonicity excludes the use of Savitzky–Golay smoothing filters of degree two and greater.) Such a criterion which ensures the conservation of a unique *global* maximum is

$$Af[0] > Af[k] \tag{29}$$

for every $k \neq 0$ and every spectrometric function f. Inequality 29 is fulfilled if the frequency response of the low-pass A is positive. This follows directly from the inversion formula of the Fourier transform which can be expressed as

$$f[k] = \frac{1}{2\pi}\int_{-\pi}^{\pi} \mathcal{F}f(\omega)\cos(\omega k)\,\mathrm{d}\omega \tag{30}$$

for symmetric f. However, the positivity of the frequency response seems to be too restrictive. The authors intuitively feel that the position of the global peak maximum is uniquely conserved also with Savitzky–Golay smoothing filters of any degree 2M, though these in general have neither a monotonic filter function nor a positive frequency response (*4*, *16*). Here further theoretical investigations are necessary.

Conversely, if inequality 29 is fulfilled for every spectrometric function f, it follows that

$$a[0] \geq a[n] \tag{31}$$

for every n since f may be chosen arbitrarily close to the delta impulse ($Ad = a$). Inequality 31 may be viewed as a necessary condition but unfortunately it is not sufficient. It is easy to construct a filter function of a smoothing filter (which may even be positive) that meets inequality 31 but disobeys inequality 29 for certain spectrometric functions. A better criterion will probably require that the side lobes of a filter function are smaller in area than the main lobe.

Height. A peak height conservation for *every* spectrometric function is not achievable with the same low-pass. So we consider the peak height error ϵ_0 which is defined by the second equation of eq 24 and can be expressed as (Parseval equation)

$$\epsilon_0 = \frac{1}{2\pi}\int_{-\pi}^{\pi} (1 - \mathcal{F}a(\omega))\mathcal{F}f(\omega)\,\mathrm{d}\omega \tag{32}$$

(Obviously, when inspecting eq 32, peak height conservation ($\epsilon_0 = 0$) is achievable for a *known* spectrometric function and requires that $\mathcal{F}a(\omega)$ exceeds 1 in a limited region. This implies that the filter function must have negative values. The optimal finite filter function is given by eq 9 of a paper by Hnatowicz (*17*), except for his normalization to zero area.)

Note that ϵ_0 can only be interpreted as peak height error, if Af obeys inequality 29. Again the question arises: "Given a digital low-pass, can this low-pass be improved in such a way that it becomes better (now with regard to ϵ_0!) for *every* spectrometric function?" Such an improvement will be indeed realizable in at least the following cases: (i) The frequency response has negative regions. (ii) $a[0]$ is not the greatest value of the filter function a. (iii) The filter function is not monotonic within the interval of nonzero values beyond the origin.

Case (iii) only applies to finite filter functions. (The proof of (i) and (ii) will be as in the ϵ_2 case. As for (iii), ϵ_0 can be reduced for *every* spectrometric function f if we permute the values $a[n]$, $n \neq 0$, of a finite filter function in such a way

Table I. Conservation Properties, Signal to Noise Behavior, and Features of Some Special Digital Low-Passes[a]

	$a[k] \geq a[k+1]$	$a[k] \geq 0$	$\lvert\mathcal{F}a(\omega)\rvert \leq 1$	$\mathcal{F}a(\omega) > 0$	$\mathcal{F}a(\omega) \geq 0$	$a[0] \geq a[k+1]$
$Af[k] > Af[k+1]$	ns	n	n			n
$Af[k] > 0$	s	ns	n			
$\lvert\mathcal{F}Af(\omega)\rvert \leq \lvert\mathcal{F}f(\omega)\rvert$	s	s	ns			
$\mathcal{F}Af(\omega) > 0$				ns	n	n
$\mathcal{F}Af(\omega) \geq 0$				s	ns	n
$Af[0] > Af[k+1]$	s			s	s	n
$\chi(a,f)$	+	+	+		+	+
$\epsilon_0 = f[0] - Af[0]$	(+)	−	−		+	+
$\epsilon_2 = \lVert f - Af\rVert_2$			+		+	+
WILP						×
NER						×
SGS			×			×
SGS²			×		×	×
MAXFLAT			×		×	×
ILP*			×		×	×
MA	×	×	×			×
MA²	×	×	×		×	×
BINOMINAL	×	×	×		×	×
GAUSSIAN*	×	×	×	×	×	×

[a] Asterisk (*), not realizable; n, necessary condition; s, sufficient condition; +, enhances corresponding quantity; −, deteriorates corresponding quantity; (+) see text.

within the support interval $-N \leq n \leq N$ that they decrease monotonically beyond the origin, possibly assuming negative values. This can be shown with the aid of successive applications of inequality 28. The permutation does not change the area and the square sum (noise amplification) of the filter function.)

Directly related to the peak height error at constant noise amplification is the signal to noise ratio (SNR) when it is defined by the quotient of the peak height $f[0]$ and the standard deviation (σ) of the noise. After filtering the SNR is equal to $Af[0]/(\lVert a\rVert_2\sigma)$ if we assume white noise and the validity of inequality 29. $Af[0]$ can be written as a scalar product

$$Af[0] = \langle a,f\rangle = \sum_{n=-\infty}^{\infty} a[n]f[n] \tag{33}$$

We introduce the quantity

$$\chi(a,f) = \frac{\langle a,f\rangle}{\lVert a\rVert_2\lVert f\rVert_2} \tag{34}$$

and call it "efficiency". The efficiency is a normalized measure for the SNR enhancement when filtering a noisy spectrometric function f using the filter function a. By the Schwarz inequality, the efficiency cannot exceed 1. The maximum is obtained when the filter function a equals the signal f except for a positive constant factor. The corresponding filter is called a "matched filter" (*18*). Due to the infinity of a spectrometric function (property (e)), a matched filter cannot be realized exactly. It can be shown that the optimal finite approximation is simply the truncated spectrometric function. We do not further extend the consideration of SNR maximization since this requires the a priori knowledge of the line shape and line width and so does not meet our intention to make statements which are valid for unknown spectrometric functions.

"Can a given low-pass be improved to give more efficiency for *every* spectrometric function?" The answer is affirmative in the following cases: (i) The filter function has negative values. (ii) The filter function is not monotonic. (iii) The frequency response has negative regions. (iv) The frequency response exceeds 1.

(The proof is similar to the preceding cases except for the lucky circumstance that the normalization $\mu(a) = 1$ does not influence the efficiency: (i) replace a by $|a|$; (ii) permute $|a|$ for monotonicity; (iii) replace $\mathcal{F}a$ by $|\mathcal{F}a|$; (iv) a exhibits negative values, replace a by $|a|$. We note that (ii) is even true if $a[0]$ is not the maximum of a and therefore a permutation does not deliver complete monotonicity. This can be shown, e.g., by the successive equalization of the central value $a[0]$ and its neighbors until the resulting filter function is monotonic.)

If the chosen low-pass has a monotonic filter function a and a positive frequency response, no further improvement to *every* spectrometric function is possible: Let f be a spectrometric function and let $\alpha > 0$. Then $a + \alpha f$ is a spectrometric function and may serve as a possible signal so that $\chi(a, a + \alpha f)$ can be made arbitrarily close to 1 as $\alpha \to 0$.

Width. The conservation of line width largely depends on the width criterion. If the width criterion is the second moment, divided by the area, exact conservation is achievable even with smoothing filters (e.g., Savitzky–Golay smoothing filters of degree 2). Unfortunately, not every spectrometric function possesses a finite second moment (Lorentzians, e.g.). Conversely, the full width at half maximum (fwhm), though it may not be defined exactly for discrete functions, has the advantage of being very practicable. As a result, it is nearly intractable in theory. A third measure for the line width of spectrometric functions f is the equivalent width (*19, 20*) which is given by $\mu(f)/f[0]$. After filtering, replacing f by Af, we obtain $\mu(Af)/\langle a,f\rangle = \mu(f)/\langle a,f\rangle$ as new equivalent width. Thus a decrease in peak height (eq 33) is interpreted as an increase in equivalent width and the discussions for peak height conservation are applicable. Obviously, for a *known* spectrometric function, a low-pass can be designed which even reduces the equivalent width. The frequency response of such a filter increases beyond the origin and then falls off rapidly. It is evident that smoothing filters always increase the equivalent width.

Range. The conservation of the range of values of arbitrary signals may be useful in hardware implementations. It can be shown that

$$\lVert Af\rVert_\infty \leq \lVert a\rVert_1\lVert f\rVert_\infty \tag{35}$$

for every bounded function f. Thus a conservation of range is equivalent to $\lVert a\rVert_1 = 1$ which for our low-passes again is equivalent to the positivity of the filter function a. If the filter function is positive, also the range of values of the Fourier transform is conserved since then $|\mathcal{F}a(\omega)| \leq 1$ for every ω (the

converse is not true). We note that the condition $|\mathcal{F}a(\omega)| \leq 1$ (with equality only if $\omega = 0$) enables multiple filtering without artifacts such as Slutsky–Yule oscillations (*4*).

RESULTS AND DISCUSSION

The main results of this paper are listed in Table I. The column inequalities represent the constraints on the filter function a or the frequency response $\mathcal{F}a$ of a low-pass A and are assumed to be valid for every $k \geq 0$ or $|\omega| \leq \pi$, respectively. The rows of Table I are divided into three main parts.

The upper part contains inequalities which describe the conservation properties in the following order: strict monotonicity, strict positivity, Fourier transform range, strict positivity of Fourier transform, positivity of Fourier transform, position of unique global maximum. This part of the table gives necessary and/or sufficient conditions for the row inequalities to hold for *every* spectrometric function f and *every* $k \geq 0$ ($|\omega| \leq \pi$, respectively).

In the following three rows the influence of the column inequalities on the efficiency (relative SNR improvement), the peak height error ϵ_0 (at constant noise amplification), and the sum of error squares (at constant noise amplification) is given. A plus (+) sign indicates that a filter function not having the corresponding property can be improved for *every* spectrometric function f. (To avoid misunderstandings, it must be remarked that for a *known* spectrometric function and a given filter function which does not satisfy the column inequality, there exist arbitrarily many filter functions which do satisfy it but show a greater error (at the same noise amplification) or smaller SNR improvement.) A minus (−) sign indicates the violation of the corresponding property (inequality) by every low-pass which is optimized for an arbitrary *known* spectrometric function in the sense of the corresponding criterion. The + sign in parantheses indicates the restriction of the column inequality to the interval $-N \leq k \leq N$ if a is a finite filter function with nonzero values only on this interval.

In the lower part of Table I several well-known examples of low-passes (all normalized to $\mu(a) = 1$) are listed together with their features. WILP is a low-pass obtained by windowing an ideal low-pass (*12*) by using the customary windows (*15*). NER (nearly equiripple frequency response) is a special case of WILP, using a Kaiser window (*21*). SGS is a Savitzky–Golay smoothing filter of degree $2M = 2$ and filter width $N > 1$ (*1–4*). (SGS^2 denotes twice filtering by SGS). The MAXFLAT filters (*21*, *22*) stand out for a monotonically decreasing frequency response with maximally flat pass-band and stop-band. ILP is the (nonrealizable) ideal low-pass. It follows the moving average MA and the BINOMIAL filter (*22–24*), the latter of which is a special case of MAXFLAT. The GAUSSIAN filter is named by its filter function. Due to the infinity of Gaussians, GAUSSIAN filters are not realizable.

Obviously, the ILP is not optimal in our applications. This is also true when the spectrometric function is known a priori. One reason for this drawback is the frequency response cutoff which is too sharp for spectrum smoothing purposes. (A sharp cutoff is advantageous especially in applications where signal and noise are distributed over disjoint frequency ranges.) A similar argumentation applies to the filter function of the MA, although its monotonicity is a favorable feature. Double filtering (MA^2) eliminates the MA-drawback of negative side lobes in the frequency domain (at the expense of a larger number of computations at the same noise amplification).

It must be emphasized that part three of Table I is not suitable to judge the low-passes in question for at least three reasons. First, the decision for a filter to get an "×" usually depends on infinitesimally small quantities. The table gives no information on how *much* a filter violates a condition. Evidently, "small" violations are of no practical account. How much violation can be tolerated ultimately depends on the special application and the intention of the user. It should be realized that the WILP and the NER filter can be designed to approach the missing properties arbitrarily well.

Second, the computational requirements have not been taken into account until now. We have shown how to improve a given low-pass for *every* spectrometric function. However, such an improvement may result in an increase in the number of nonzero filter coefficients $a[n]$. Especially a positive frequency response usually is only achievable at the expense of a larger number of computations when a fixed noise amplification is considered. (For example, a finite filter function which is SNR optimized for a known spectrometric function may have negative regions in its Fourier transform. This is not true if the constraint of finiteness is dropped.) Improvements which directly refer to the filter function (positivity, monotonicity) do not increase the number of coefficients. We note that the filters SGS, SGS^2, MA and MA^2 have the additional advantage of being realizable recursively (*2*), thus saving much computation time in the case of larger filter widths.

Third, "for every digital filter there is a criterion so that this filter is optimal". However, the choice of the criterion to be preferred often is a matter of philosophy of life and is thus directed by the filter type one favors rather than by practical requirements.

The list of advantageous filter properties could be enlarged if further restrictions on the signal are imposed. One such restriction could be a monotonically decreasing Fourier transform, possibly leading to the preference of monotonically decreasing frequency responses. Conversely, several conditions can be weakened if there is a minimal nonzero line width. Such a restriction is reasonable especially in view of the aliasing error (*16*) and allows a more unpretentious stop-band behavior of the frequency response since $\mathcal{F}f$ may be viewed as a weighting function in eq 22 and 32.

APPENDIX

The Fourier transforms of discrete Gaussians g and Lorentzians h as defined in eq 1 and 2 are given by

$$\mathcal{F}g(\omega) = \pi^{1/2}\beta \exp(-(\beta\omega/2)^2) + 2\pi^{1/2}\beta \sum_{n=1}^{\infty} \exp(-\beta^2(\omega^2 + 4\pi^2n^2)/4) \cosh(\beta^2\pi\omega n) \quad (36)$$

and

$$\mathcal{F}h(\omega) = \pi\beta \cosh((\pi - |\omega|)\beta)/\sinh(\pi\beta) \quad (37)$$

(Proof: Poisson summation formula (*25*) and/or eq 17.3.7 of ref 26.) The deviation of eq 36 and 37 from the continuous Fourier transforms is an effect of aliasing which always occurs when a non-band-limited function is sampled (*16*). However, if the width β is great enough ($\beta > 10$), the continuous Fourier transforms are approached sufficiently well

$$\mathcal{F}g(\omega) \approx \pi^{1/2}\beta \exp(-(\beta\omega/2)^2) \quad (38)$$

$$\mathcal{F}h(\omega) \approx \pi\beta \exp(-|\omega|\beta) \quad (39)$$

Further exact formulas concerning the sum and the square sum are seen to be

$$\mu(g) = \pi^{1/2}\beta + 2\pi^{1/2}\beta \sum_{n=1}^{\infty} \exp(-\beta^2\pi^2n^2) \quad (40)$$

$$\mu(h) = \pi\beta \coth(\pi\beta) \quad (41)$$

$$\|g\|_2^2 = (\pi/2)^{1/2}\beta + (2\pi)^{1/2}\beta \sum_{n=1}^{\infty} \exp(-\beta^2\pi^2n^2/2) \quad (42)$$

$$\|h\|_2^2 = \pi\beta(\coth(\pi\beta) + \pi\beta/(\sinh(\pi\beta))^2)/2 \quad (43)$$

The approximations for large β ($\beta > 1$) are given by

$$\mu(g) \approx \pi^{1/2}\beta \quad (44)$$

$$\mu(h) \approx \pi\beta \quad (45)$$

$$\|g\|_2^2 \approx (\pi/2)^{1/2}\beta \quad (46)$$

$$\|h\|_2^2 \approx \pi\beta/2 \quad (47)$$

where the right-hand sides represent the results obtained by integration of the continuous lines. The full width at half maximum is

$$\text{fwhm} = 2(\ln 2)^{1/2}\beta \quad (48)$$

in the Gaussian case and

$$\text{fwhm} = 2\beta \quad (49)$$

for Lorentzians.

LITERATURE CITED

(1) Savitzky, A.; Golay, M. J. E. Anal. Chem. 1964, 36, 1627-1638.
(2) Bromba, M. U. A.; Ziegler, H. Anal. Chem. 1979, 51, 1760-1762.
(3) Ziegler, H. Appl. Spectrosc. 1981, 35, 88-92.
(4) Bromba, M. U. A.; Ziegler, H. Anal. Chem. 1981, 53, 1583-1586.
(5) Korb, J.-P.; Maruani, J. J. Magn. Reson. 1981, 46, 514-520.
(6) Van Cittert, P. H. Z. Phys. 1931, 69, 298-308.
(7) Schafer, R. W.; Mersereau, R. M.; Richards, M. A. Proc. IEEE 1981, 69, 432-450.
(8) Mersereau, R. M.; Schafer, R. W. Proc. 1978 IEEE Int. Conf. ASSP 192-195.
(9) Mersereau, R. M.; Schafer, R. W. Proc. 1978 IEEE Europ. Conf. CT & D 404-411.
(10) Richards, M. A.; Schafer, R. W.; Mersereau, R. M. Proc. 1979 IEEE Int. Conf. ASSP 401-404.
(11) Youla, D. C. IEEE Trans. Circuits Syst. 1978, CAS-25, 694-702.
(12) Hamming, R. W. "Digital Filters"; Prentice-Hall: Englewood Cliffs, NJ, 1977.
(13) Schoenberg, I. J. Quart. Appl. Math. 1946, 4, 45-99.
(14) Tominaga, H.; Dojyo, M.; Tanaka, M. Nucl. Instrum. Methods 1972, 98, 69-76.
(15) Rabiner, L. R.; Gold, B. "Theory and Application of Digital Signal Processing"; Prentice-Hall: Englewood Cliffs, NJ, 1975.
(16) Willson, P. D.; Edwards, T. H. Appl. Spectrosc. Rev. 1976, 12, 1-81.
(17) Hnatowicz, V. Nucl. Instrum. Methods 1976, 133, 137-141.
(18) Turin, G. L. Proc. IEEE 1976, 64, 1092-1112.
(19) Lam, R. B.; Isenhour, T. L. Anal. Chem. 1981, 53, 1179-1182.
(20) Bracewell, R. N. "The Fourier Transform and Its Applications", 2nd ed.; McGraw-Hill: New York, 1978; Chapter 8.
(21) Kaiser, J. F.; Reed, W. A. Rev. Sci. Instrum. 1977, 48, 1447-1457.
(22) Bromba, M. U. A.; Ziegler, H. Electron. Lett. 1980, 16, 905-906.
(23) Arsenault, H. H.; Marmet, P. Rev. Sci. Instrum. 1977, 48, 512-516.
(24) Marmet, P. Rev. Sci. Instrum. 1979, 50, 79-83.
(25) Edwards, R. E. "Fourier Series", 2nd ed.; Springer: New York, 1979; p 182.
(26) Hansen, E. R. "A Table of Series and Products"; Prentice-Hall: Englewood Cliffs, NJ, 1975.

RECEIVED for review August 19, 1982. Accepted December 6, 1982.

Phase-Plane and Guggenheim Methods for Treatment of Kinetic Data

J. Roger Bacon*

Chemistry Department, Western Carolina University, Cullowhee, North Carolina 28723

J. N. Demas*

Chemistry Department, University of Virginia, Charlottesville, Virginia 22901

A common kinetic problem is the analysis of data which are exponential decays on constant, but unknown, base lines. Most commonly, data treatment is by the Guggenheim method. A new phase-plane (PP) method is developed. The two methods are compared experimentally and by digital simulations. The PP method is insensitive to the nature of the noise and, unlike the Guggenheim method, does not require operator adjustments to fitting parameters. For good data measured under optimum conditions, the PP and Guggenheim methods are comparable in accuracy and precision. The PP method is more accurate than, and not susceptible to the computational failures of, the Guggenheim method where the data are noisy, have a large base line contribution, or were taken over other than the optimum fitting regions. Therefore, the PP method is ideal for use in automated instruments or with samples where multiple runs cannot be made to optimize measurement parameters.

Evaluation of kinetic parameters from experimental data is a pervasive and important problem in mechanistic chemical studies (*1*, *2*), luminescence spectrometry (*3*), and a variety of kinetic chemical analyses (*4*). The most common systems involve first- or pseudo-first-order kinetics which yield exponential decays. When the base line is stable and noise free, the standard and most accurate approach to evaluating the decay parameters is to subtract the base line and fit the resultant curve by a linear least-squares fit to the semilogarithmic plot of the data vs. time.

Frequently, however, a good stable noise-free base line is unavailable. This may be due to irreproducible solvent blanks in luminescence, instrument base line drift (*3*), or too short a data acquisition time to permit the signal to decay to the base level (*1*, *2*). Further, if a noisy base line is available (e.g., stopped flow), attempts to subtract the base line can yield increased noise levels on the decays and, in extreme cases, negative base line corrected signals. Under these conditions the signal is given by

$$D(t) = K \exp(-t/\tau) + B \quad (1)$$

where $D(t)$ is the decay vs. time t, K is the proportionality constant, and B is the base line.

The solution of eq 1 where $B = 0$ can be by the Guggenheim method (*1-3*, *5*), Mangelsdorf method (*5*, *6*), or nonlinear least squares (*5*, *7*). By far the most popular approach is the Guggenheim method. In the Guggenheim method one linearizes the function by first taking the differences of $D(t)$ and $D(t + \Delta t)$

$$Y = A_0 + A_1 t \quad (2a)$$

0003-2700/83/0355-0653$01.50/0 © 1983 American Chemical Society

$$Y = \ln [D(t) - D(t + \Delta t)] \quad (2b)$$

$$A_0 = \ln \{K[1 - \exp(-\Delta t/\tau)]\} \quad (2c)$$

$$A_1 = -1/\tau \quad (2d)$$

A plot of Y versus t is linear. τ and K can then be derived from the slope and intercept respectively. The selection of Δt can be a problem. Δt should, in general, be at least $2-3\tau$ (2). If the data acquisition period is shorter than $2-3\tau$, smaller Δt values of course, must be used.

The Guggenheim method is popular because it eliminates the need for acquiring a base line, gives accurate measurements, and is simple. At least for phosphorescence decay measurements it is more precise than Mangelsdorf's method (3). It is much simpler to program and faster computationally than nonlinear least squares. However, the Guggenheim method has several disadvantages. The fitting region and Δt must be properly selected for accurate results; improper selection can yield negative $[D(t) - D(t + \Delta t)]$ values which are computationally unacceptable in eq 2b. Depending on the fitting range and Δt selected, only part of the data may be used in the fit (5). The Guggenheim method does not directly fit $D(t)$ and reconstruction of $D(t)$ using the best fit parameters and eq 1 is complicated since B is not directly available.

We wish to report a new method for treating kinetic data of the form of eq 1. The method is based on the phase-plane (PP) method which was originally developed for evaluation of simple exponentials ($B = 0$) (8, 9). It was subsequently extended to the treatment of luminescence lifetime measurements involving the deconvolution of exponential decays from data taken with a finite flash (10, 11) and with scattered light (12, 13). It also has been extended to decays involving Förster kinetics (14).

We will show that the modified PP method is simple and permits direct calculation of K, B, and τ. Further, the PP method is more forgiving in the fitting ranges and the noise levels than the Guggenheim method. Additionally, the PP method requires no operator selection of optimum fitting parameters (i.e., Δt and fitting region) which makes it particularly amenable to automated analytical instruments. Unlike nonlinear least squares, no initial guesses of the parameters are required.

THEORY

The PP solution to eq 1 is developed by integrating eq 1 over the limits 0 to t to yield

$$D(t) = A_0 + A_1 X(t) + A_2 t \quad (3a)$$

$$X(t) = \int_0^t D(t)\, dt \quad (3b)$$

$$A_0 = B + K \quad (3c)$$

$$A_1 = -1/\tau \quad (3d)$$

$$A_2 = B/\tau \quad (3e)$$

$D(t)$ is now a linear function of the variable $X(t)$ and t. $X(t)$ is readily derived from $D(t)$ by numerical integration. The desired system parameters B, K, and τ are then readily computed from the coefficients of the linear equation.

One can obtain A_0, A_1, and A_2 by standard linear least-squares fitting. In an unweighted least-squares sense one strives to minimize

$$\sum [D(t_i) - [A_0 + A_1 X_i + A_2 t_i]]^2 \quad (4)$$

where X_i is $X(t)$ evaluated at t_i. The summation is over all data points used in the fit. The resultant normal equations for this minimization are

$$\begin{pmatrix} \Sigma 1 & \Sigma X_i & \Sigma t_i \\ \Sigma X_i & \Sigma X_i & \Sigma X_i t_i \\ \Sigma t_i & \Sigma X_i t_i & \Sigma t_i^2 \end{pmatrix} \begin{pmatrix} A_0 \\ A_1 \\ A_2 \end{pmatrix} = \begin{pmatrix} \Sigma D(t_i) \\ \Sigma D(t_i) X_i \\ \Sigma D(t_i) t_i \end{pmatrix} \quad (5)$$

Solution of these equations yields the best A_0, A_1, and A_2 which, from eq 3c, d, and e, yield K, B, and τ. By use of the least-squares A_0, A_1, and A_2, $D(t)$ can be simply and rapidly calculated from eq 3 for comparison with the original decay. For real data $X(t)$ is derived by numerical integration. We use the trapezoidal rule which yields

$$X_i = \int_0^t D(t)\, dt \approx (\Delta t/2) R_i \quad (6a)$$

$$R_i = D(t_i) + D(t_{i-1}) + R_{i-1} \quad i \geq 1 \quad (6b)$$

$$\Delta t = t_{i+1} - t_i \quad (6c)$$

$$R_0 = 0 \quad (6d)$$

Note that the Δt used here is the time between points and bears no relationship to the Δt used in the Guggenheim method. For most experimental data with a reasonably small Δt relative to τ, any errors associated with the trapezoidal rule integration will be insignificant.

EXPERIMENTAL SECTION

Materials. The $K_3Co(CN)_6$ from Alpha Chemical Co. was recrystallized once from water. Its absorption and emission spectra matched the literature results (15).

Lifetime Measurements. Luminescence decay time measurements were made with a Tektronix 7912 ultrahigh speed transient digitizer interfaced to an Altair 8800B microcomputer. The system is described elsewhere (16).

Simulations. Because noise on experimental data can possess widely varying properties, we deemed it necessary to ensure that the results of our simulations were not sensitive to the detailed noise characteristics. We have used two different noise types, amplitude dependent Poisson noise and amplitude independent noise. These mimic experimentally observed noise. In both cases the noise distribution was assumed to be normal or Gaussian. Synthetic noisy data were generated by

$$D_P(t) = D(t) + ND(t)^{1/2} \quad (7a)$$

$$D_C(t) = D(t) + ND(0)^{1/2} \quad (7b)$$

Where $D(t)$ is given by eq 1 and N is a random Gaussian number with a mean of zero and standard deviation of unity. N was derived from our computer's uniformly distributed random number generator using the algorithm outlined by Knuth (17). $D_P(t)$ is $D(t)$ with superimposed Poisson noise which has a standard deviation equal to the square root of $D(t)$. For large values (>25) $D_P(t)$ is the same as single photon counting statistics which arise in single photon counting nanosecond fluorimeters or shot noise in photomultiplier signals. It also is similar to the noise encountered in a variety of instruments, such as spectrofluorimeters, where the magnitude of the noise increases with signal strength, but the fractional component of the noise decreases. $D_C(t)$ exhibits constant amplitude noise independent of $D(t)$. The signal from a stopped flow or flash photolysis instrument generally exhibits similar behavior.

In order to simulate varying noise levels, we varied $(K + B)$ which is $D(0)$ in eq 7b. For $(K + B) = 10^4$, the data are similar to good analog or single photon counting data with a peak noise level of 1% of full scale. A $(K + B)$ of 10^3 corresponds to reasonably noisy data and $(K + B) = 10^2$ yields very noisy experimental data. The typical quality of data exhibiting Poisson noise (peak values of 100 and 10^4) are shown in ref 11.

For the digital simulation, ten simulated $D_P(t)$'s or $D_C(t)$'s were generated for every K, B, and τ with 201 evenly spaced points in each decay. Each decay was reduced by the Guggenheim and by the PP methods. For each set of calculations, we evaluated the relative error (RE) and relative standard deviation (RSD) in

$$RE = [(\bar{\tau} - \tau)/\tau] \times 100\% \quad (8a)$$

$$RSD = (\sigma/\tau) \times 100\% \quad (8b)$$

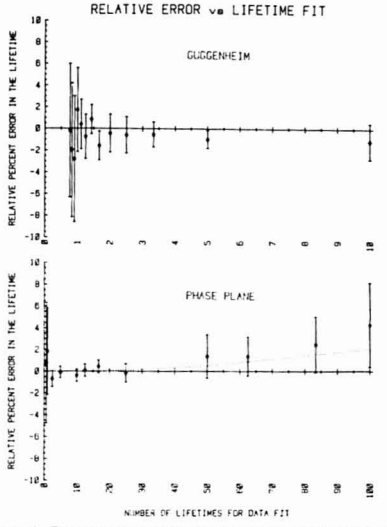


Figure 1. Effect of fitting region on the accuracy and precision of the Guggenheim (upper) and phase-plane (lower) methods. The asterisks indicate the RE in τ for ten runs and the error bars are ± 1 RSD. In all cases the noise was Poisson with $K = 8000$ and $B = 2000$. Note that the fitting scales differ for the two plots.

$\bar{\tau}$ and σ are the average τ and standard deviation in $\bar{\tau}$ calculated for the set of simulations.

RESULTS AND DISCUSSION

Effect of Noise Types. All of the simulations reported below are for Poisson noise. For constant noise, the results were comparable. All the RSD's were larger, however, due to the greater overall noise levels. With constant noise the Guggenheim method failed more often because of its sensitivity to the noise level.

Choice of Δt in the Guggenheim Method. The optimum choice in Δt is not clearly defined in the literature. Laidler (2) recommends $\Delta t > 2\text{–}3\tau$. We opted to resolve the question by simulations. We selected a transient spanning 5τ's with $K = 8000$ and $B = 2000$. This corresponds to reasonable quality data with the transient decaying to within 1% of the terminal base line. Using Poisson noise we then evaluated RE and RSD for different Δt values by using the Guggenheim method. The maximum possible data range was used in the fits. The RSD's exhibited a broad minimum for $2.5\tau < \Delta t < 3.7\tau$. For larger or smaller Δt's, RSD increased rapidly. For all further Guggenheim simulations we used Δt corresponding to 65% of the signal measurement period.

Effect of Varying the Fitting Region. Figure 1 shows the effect of varying the range over which the data were acquired in units of τ. The RE in τ is plotted along with error bars corresponding to ± 1 RSD. In all cases $(K + B) = 10^4$. For both the Guggenheim and the PP methods, the RSD's increase rapidly if too small or too large a fitting range is used. This occurs either because there is insignificant decay in $D(t)$ or τ is so short that there are few points on the decaying portion of the transient. Note the differences in fitting scales for the Guggenheim and the PP methods. The Guggenheim method failed for sample periods $>10\tau$ or $<0.7\tau$ because the $[D(t) - D(t + \Delta t)]$ term becomes negative, but the PP method was unconditionally stable for all fitting regions. For the optimum fitting region of 5τ, the Guggenheim and the PP methods yield very similar results. As the fitting region deviates from the optimum, however, the RSD's for the Guggenheim method increase much more rapidly than those for the PP method.

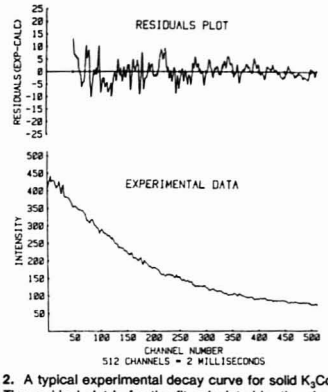


Figure 2. A typical experimental decay curve for solid $K_3Co(CN)_6$ at 77 K. The residual plot is for the fit calculated by the phase-plane method using the data from points 50–511.

For very large fitting ranges the accuracy of the PP method begins to fall in a small but systematic fashion. The errors arise from the use of the trapezoidal rule with too low a density of points. The dotted line of Figure 1 shows the error curve for noise-free data. Therefore, even for very long fitting periods the accuracy of the PP method is limited only by the accuracy of the numerical integration used.

Effect of Varying the Noise Level. To vary the noise level, we varied $(K + B)$ from 100 to 10^4. We carried out an extensive series of simulations similar to those in Figure 1 with $B/K = 1/4$ and a fitting range of 5τ. For relatively noise-free data (peak counts >1000), the PP and Guggenheim methods are essentially equivalent. For noisy data, however, the PP method yields significantly better RE's and RSD's than the Guggenheim method. Indeed, the Guggenheim method failed for $(K + B) \leq 200$ due to the appearance of negative $D(t) - D(t + \Delta t)$ terms. The PP method was unconditionally stable and yielded usable results even with $(K + B) = 100$.

Effect of Varying the Base Line. To test the effect of base line variation, we carried out extensive simulations with $(K + B) = 10^4$ and base line contributions ranging from 0 to 95%. Again the fits were made by using a 5τ range. For small base line contributions (<25%) the two solutions are comparable. For larger base line corrections, however, the PP method yielded significantly better RSD's. It was not even possible to use the Guggenheim method for base line contributions above 80% due to the generation of negative $D(t) - D(t + \Delta t)$ terms.

Experimental Results. Figure 2 shows a typical luminescence decay for solid $K_3Co(CN)_6$ at 77 K. We evaluated the lifetimes for 10 different measurements by using the Guggenheim and the PP methods as well as the standard semilogarithmic method. Each entry was obtained from 10 different measurements. For the semilogarithmic method, a separate instrument base line was measured and subtracted from the decay and an unweighted linear least-squares fit was made to the ln $[D(t)]$ vs. t plot. The results are summarized in Table I.

The Guggenheim and PP methods were equally satisfactory in this case as the experimental range was near optimum for

Table I. Lifetimes of $K_3Co(CN)_6$ at 77 K Measured by Different Methods

method	lifetime,[a] μs
semilogarithmic plot[b]	657 ± 3
phase plane method	666 ± 8
Guggenheim method	661 ± 8

[a] Mean and standard deviation for ten determinations. All data are fit from point 50 to 511. [b] Determined from a linear least-squares fit to the semilogarithmic plot of the base line corrected decay vs. time.

both. The semilogarithmic approach was better as judged by the standard deviation, but this is not surprising as more experimental information was included in these calculations. Figure 2 also shows the residual plot for the PP best fit using eq 3 to regenerate $D(t)$. The fit is satisfactory. The lifetime apparatus used exhibits noise which more closely approximates a Poisson distribution than an amplitude independent constant noise level.

While the residuals plot provides all of the visual information necessary to judge the quality of the fit, it is less conventional than the traditional linear semilogarithmic or Guggenheim plots. The PP relationship of eq 3 is, however, a linear function of two variables and readily lends itself to linearized plots suitable for inspection. For a simple exponential decay, a plot of $[D(t) - (B/\tau)t]$ vs. $X(t)$ will be linear with an intercept of $B + K$ and a slope of $(-1/\tau)$. Similarly, a plot of $[D(t) + (1/\tau)X(t)]$ vs. t will be linear with a slope of B/τ and an intercept of $B + K$. For the data of Figure 2, both presentations yield excellent linear plots.

CONCLUSIONS

Our simulations and experimental analyses reveal the following features. If an accurate, relatively noise free base line is available, base line subtraction followed by a least-squares fit to the ln $[D(t)]$ vs. t plot is the most accurate approach. If the optimum range of data acquisition for the Guggenheim method can be used, the data are relatively noise free, and the base line contribution is relatively small, then the Guggenheim and PP methods will be equivalent. Even under these ideal conditions, however, the PP approach readily permits direct comparison of the original raw data with the best least-squares fit while the Guggenheim method does not.

The PP method has clear advantages over the Guggenheim method whenever the signal noise level is large, the base line is a large percentage of the peak signal, or the optimum fitting conditions have not been, or cannot be, selected. The PP method is then more precise and works for data which fails with the Guggenheim method. Finally, because of its overall accuracy and forgivingness to measurement parameters, the PP method is ideal for automated instruments or in measurements where making replicate runs to optimize the fitting parameters is either very time-consuming or impossible. The latter case could arise due to sample loss or destruction (e.g., flash photolysis). Further, the PP method is simpler to program and about 5–10 times faster than a nonlinear least-squares algorithm based on the Marquardt method (*18*).

The improved dynamic range of the PP method would simplify and increase the accuracy of automated data acquisition schemes where widely varying data are acquired in a single series of experiments. In fluorescence quenching methods, for example, both τ and the $(K + B)$ can vary dramatically.

LITERATURE CITED

(1) Friess, S. L.; Lewis, E. S.; Weissberger, A. "Technique of Organic Chemistry"; Wiley: New York, 1963; Vol VIII, Part II.
(2) Laidler, K. J. "Chemical Kinetics", 2nd ed.; McGraw-Hill: New York, 1965; Chapter 1.
(3) Cline Love, L. J.; Skrilec, Marie *Anal. Chem.* **1981**, *53*, 2103.
(4) Mottola, H. A.; Mark, H. B., Jr. *Anal. Chem.* **1982**, *54*, 62R.
(5) Alcock, R. M.; Hartley, F. R.; Rogers, D. E. *J. Chem. Soc., Dalton Trans.* **1978**, 123.
(6) Mangelsdorf, P. C. *J. Appl. Phys.* **1959**, *30*, 443.
(7) Wentworth, W. E. *J. Chem. Educ.* **1965**, *42*, 96.
(8) Bernalte, A.; LePage, J. *Rev. Sci. Instrum.* **1969**, *40*, 2463.
(9) Huen, T. *Rev. Sci. Instrum.* **1969**, *40*, 106.
(10) Demas, J. N.; Adamson, A. W. *J. Phys. Chem.* **1971**, *75*, 2463.
(11) Greer, J. M.; Reed, F. W.; Demas, J. N. *Anal. Chem.* **1981**, *53*, 710.
(12) Jezequel, J. Y.; Bouchy, M.; Andre, J. C. *Anal. Chem.* **1982**, *54*, 2199.
(13) Love, J. C.; Demas, J. N., submitted for publication in *Rev. Sci. Instrum.*
(14) Love, J. C.; Demas, J. N., unpublished results, University of Virginia, 1982.
(15) Crosby, G. A. *J. Chim. Phys. Phys.-Chim. Biol.* **1967**, *64*, 160.
(16) Turley, T. J. M.S. Thesis, University of Virginia, 1979.
(17) Knuth, P. E. "Seminumerical Algorithms. The Art of Computer Programming"; Addison-Wesley: Reading, MA, 1969; Vol. 2.
(18) Marquardt, D. W. *J. Soc. Ind. Appl. Math.* **1963**, *6*, 431.

RECEIVED for review August 13, 1982. Accepted December 6, 1982. We gratefully acknowledge support by the donors of the Petroleum Research Fund, administered by the American Chemical Society, the Air Force Office of Scientific Research (Grant 78-3590), and the National Science Foundation (CHE 82-06279). All calculations were carried out on a Hewlett-Packard 85A computer purchased with a Department of Energy SERI Grant, DE-FG02-CS84063. All lifetime measurements were carried out on the University of Virginia laser facility purchased in part with NSF Grant CHE 77-09296.

Kinetics of Extraction of Nickel with 8-Mercaptoquinoline

Kensaku Haraguchi[1] and Henry Freiser*

Department of Chemistry, University of Arizona, Tucson, Arizona 85721

The kinetics and mechanism of solvent extraction of nickel(II) ion with a chloroform solution of 8-mercaptoquinoline (HL) has been studied in the pH range of 5.9–6.8 at ionic strength 0.1 and 25 °C. The rate expression for the extraction of nickel by 8-mercaptoquinoline can be described as

$$-\frac{d[Ni^{2+}]}{dt} = \left\{k_{HL} + k_L \frac{K_{a_2}}{[H^+]}\right\} \frac{[Ni^{2+}]\,[HL]_0}{K_D}$$

which supports the hypothesis that the rate-determining steps are the concurrent reactions of nickel(II) ion with neutral and anionic forms of 8-mercaptoquinoline in the aqueous phase. The rate constants k_{HL} and k_L are $(2.8 \pm 0.4) \times 10^3$ M^{-1} s^{-1} and $(2.7 \pm 0.7) \times 10^5$ M^{-1} s^{-1}, respectively.

8-Mercaptoquinoline, the S-analog of 8-quinolinol, is a very

[1] On study leave from Government Industrial Development Laboratory, Hokkaido, Sapporo, Japan.

0003-2700/83/0355-0656$01.50/0 © 1983 American Chemical Society

useful analytical reagent, in that it is a more selective metal ion extractant and is also capable of removing metal ions from more strongly acidic solutions than does 8-quinolinol (*1*). Fundamental studies have adequately described the molecular structural influences on equilibrium aspects of this interesting reagent (*2*). In order to more fully understand the reaction of 8-mercaptoquinoline with metal ions, so as to provide a rational basis for optimizing existing analytical methods based on its use as well as to enable the development of new analytical methodology, we decided to undertake the study of the kinetics and mechanism of solvent extraction of nickel(II) by this reagent into chloroform, using the high-speed stirring apparatus developed in this laboratory (*3*).

EXPERIMENTAL SECTION

Reagents. 8-Mercaptoquinoline was obtained from Sigma Chemical Co. (St. Louis, MO) as the hydrochloride. A 1.00×10^{-2} M stock solution was prepared by dissolving this reagent in 3 M hydrochloric acid. This stock solution was stable at least 2 weeks, as described previously (*4*). The chloroform solution of 8-mercaptoquinoline was prepared just before each kinetic run by extracting the reagent from aqueous media at pH 5.0 with acetate buffer solution. The concentration of the reagent was checked by measuring the absorbance at 325 nm as previously reported (*5*). A 1.00×10^{-2} M nickel stock solution was prepared by dissolving reagent grade nickel perchlorate in 10^{-2} M perchloric acid. The concentration of nickel was determined by complexometric titration with EDTA. All aqueous nickel solutions for kinetic runs were prepared daily from stock solution. The initial concentration of nickel in the aqueous phase was 2.00×10^{-5} M and ionic strength was adjusted to 0.1 with sodium perchlorate and pH adjustment was made with a 1×10^{-2} M phosphate buffer solution.

Apparatus. The extraction kinetic apparatus has been described previously (*3*). Nickel was determined with a Varian AA-6 atomic absorption spectrophotometer at 232 nm with an air–acetylene flame. UV and VIS absorbances were measured with a Perkin-Elmer 552 spectrophotometer using 10-mm quartz cells. All pH measurements were made with an Orion 701 pH meter calibrated before each measurement by using pH 4.00 and 7.00 standard buffer solutions.

Kinetic Procedure. The procedure was similar to that described previously (*3*, *6–8*). Preliminary spectrophotometric equilibrium experiments showed that the nickel(II) in the aqueous phase is completely extracted into the chloroform phase as a 1:2 chelate (NiL_2) under the conditions employed in the kinetic runs. The kinetic runs were carried out under pseudo-first-order conditions, 8-mercaptoquinoline in the organic phase being in large excess over nickel ion in the aqueous phase. A 100-mL aliquot of aqueous solution containing 2.00×10^{-5} M of nickel ion and an equal volume of reagent solution were each carefully transferred into the 500-mL reaction flask. The reaction was begun by starting the high-speed stirring motor. Experiments were carried out in the "plateau" region, i.e., where a further increase of stirring speed had no effect on the rate of extraction. At predetermined time intervals, samples were delivered into test tubes by means of positive nitrogen pressure and then immediately centrifuged to separate the phases. The concentration of nickel in the aqueous phase was determined by means of atomic absorption spectrophotometry.

The observed pseudo-first-order rate constants, k_{obsd}, were determined from

$$\ln ([Ni^{2+}]_{t=0}/[Ni^{2+}]_t) = k_{obsd}t \qquad (1)$$

where t is the reaction time, $[Ni^{2+}]_{t=0}$ and $[Ni^{2+}]_t$ are the concentrations of nickel in aqueous phase at reaction time 0 and t, respectively. All experiments were carried out at 25 °C.

RESULTS AND DISCUSSION

It should be remembered that the extraction technique for measuring kinetics of reactions occurring in the aqueous phase is based on several assumptions: (1) The rates of mass transfer are very rapid, i.e., on the order of a second or less. This assumption is assured by the use of the high-speed stirring apparatus. Further, the half-lives of the extractions under study are in excess of several minutes. (2) The concentration of intermediate complexes, unless they react slowly (*3*), cannot build up in the aqueous phases, nor can the fully formed chelate, because it is instantly extracted into the organic phase.

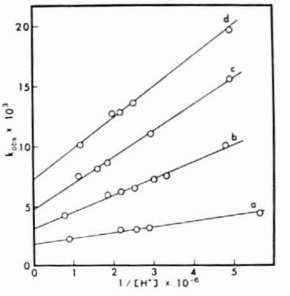


Figure 1. Rate of extraction of nickel with 8-mercaptoquinoline as a function of $1/[H^+]$. [HL]: (a) 2.34×10^{-4} M, (b) 4.67×10^{-4} M, (c) 7.01×10^{-4} M, (d) 9.34×10^{-4} M. Solid lines are obtained from least-square treatment of the data.

Plots of $\ln ([Ni^{2+}]_{t=0}/[Ni^{2+}]_t)$ against reaction time, t, were linear and through the origin. The slopes of the linear plots give pseudo-first-order rate constants, k_{obsd}, and are shown in Table I.

The simple slope analysis from plots of $\log k_{obsd}$ vs. $\log [HL]_0$ exhibited first-order dependence with respect to the reagent but the fractional order pH dependence of $\log k_{obsd}$ suggested that the reaction mechanism of the present system is different from those of dithizone and its substituted analogues (*9–11*) in which only the ligand anion is involved. This system is similar to those of nickel extraction with 8-quinolino (*12*) and 2-(2-thiazolylazo)-4-methylphenol (*13*), in which two concurrent 1:1 nickel chelate formation steps controlled the rate of extraction.

Since the major forms of ligand present in aqueous phase in the range of pH studied are HL and L^- ($pK_{a1} = 2.16$, $pK_{a2} = 8.38$ (*2*)), the equilibria and the reactions involved in the formation of mononickel chelate are shown in eq 2–7, where subscript (o) indicates organic phase. K_D is the distribution constant of the ligand and k_{HL} and k_L represent the rate constants of respective reaction steps.

$$HL_{(o)} \rightleftharpoons HL \quad K_D = [HL]_o/[HL] \qquad (2)$$

$$HL \rightleftharpoons H^+ + L^- \quad K_{a2} = [H^+][L^-]/[HL] \qquad (3)$$

$$Ni^{2+} + HL \xrightarrow{k_{HL}} NiL^+ + H^+ \qquad (4)$$

$$Ni^{2+} + L^- \xrightarrow{k_L} NiL^+ \qquad (5)$$

$$-\frac{d[Ni^{2+}]}{dt} = k[Ni^{2+}] = k_{HL}[Ni^{2+}][HL] + k_L[Ni^{2+}][L^-] \qquad (6)$$

$$k = \left\{k_{HL} + k_L\frac{K_{a2}}{[H^+]}\right\}\frac{[HL]_o}{K_D} \qquad (7)$$

The plots of k_{obsd} against $1/[H^+]$ at various $[HL]_o$ gave linear relations having intercepts as shown in Figure 1. Both the values of intercepts and slopes of these lines were proportional to the concentration of 8-mercaptoquinoline in organic phase $[HL]_o$. The slopes of the resulting linear plots give the values of k_{HL} and k_L. The values of k_{HL} and k_L thus obtained are $(2.8 \pm 0.4) \times 10^3$ M^{-1} s^{-1} and $(2.7 \pm 0.7) \times 10^5$ M^{-1} s^{-1}, respectively, where values of $pK_{a2} = 8.38$ (*2*) and $k_D = 372$ (*14*) were employed.

Table I. Summary of Extraction Kinetics of Nickel by 8-Mercaptoquinoline at 25 °C, $[Ni^{2+}]_{t=0} = 2.00 \times 10^{-5}$ M and $I = 0.1$

$10^4[HL]_o$, M	pH	10^3k, s^{-1}	$10^4[HL]_o$, M	pH	10^3k, s^{-1}
2.34	5.95	2.22	7.01	6.06	7.50
	6.34	3.08		6.21	8.10
	6.41	3.15		6.27	8.62
	6.46	3.28		6.47	11.00
	6.75	4.40		6.69	15.40
4.67	5.90	4.30	9.34	6.08	10.10
	6.27	5.88		6.30	12.70
	6.34	6.30		6.34	12.80
	6.40	6.38		6.40	13.50
	6.48	7.15		6.69	19.60
	6.52	7.94			
	6.68	9.94			

Table II. Rate Constants of NiL' Formation Determined by Solvent Extraction at 25 °C and $\mu = 0.1$

ligand	$-\log (K_a/K_D)$	k_{HL}, M^{-1} s^{-1}	k_L, M^{-1} s^{-1}	ref
diarylthiocarbazones				
aryl = phenyl	10.21	6.1×10	6.1×10^3	11
			1.1×10^3	10
	10.18[a]		1.3×10^3 [a]	9
p-fluorophenyl	9.72		2.7×10^3	10
p-chlorophenyl	10.73		1.2×10^4	11
			3.3×10^3	10
p-bromophenyl	11.06		5.3×10^4	11
			2.0×10^4	10
p-iodophenyl	11.44		3.5×10^5	11
			1.3×10^5	10
p-methylphenyl	11.89		2.4×10^4	10
o-methylphenyl	12.00[a]		5.2×10^3 [a]	11
p-methoxyphenyl	11.26		1.2×10^3	10
p-*m*-trifluoromethyl	10.36		4.5×10^2	10
p-tolyl	12.40		4.7×10^5	11
o-tolyl	12.13		1.0×10^4	11
2-naphthyl	12.30[a]		1.3×10^4 [a]	9
LIX 65N	13.30		7.9×10^5	7
1-(2-thiazolylazo)-2-naphthol	14.15		2.5×10^6	20
2-(2-thiazolylaxo)-4-methylphenol	12.74	3.3×10^2	2.2×10^4	20
8-quinolinol	12.34	3.6×10^3	5.4×10^5	12
8-mercaptoquinoline	10.95	$(2.8 \pm 0.4) \times 10^3$	$(2.7 \pm 0.7) \times 10^5$	*b*

[a] Ionic strength $I = 0.3$. [b] This work.

It should be kept in mind that although 8-mercaptoquinoline exists in aqueous media predominantly (>96%) in the zwitter ionic form (*2*, *5*, *15*), the value for k_{HL} is of the same order of magnitude for the values observed for nickel ion with 8-quinolinol by solvent extraction (see Table II) and stopped-flow technique ($k_{HL} = 1.3 \times 10^3$ M^{-1} s^{-1} (*16*)), which is predominantly in the neutral (i.e., not dipolar) form. The close agreement of the values of k_{HL} among these systems strongly supports our conclusion that the rate-determining steps are 1:1 chelate formation steps in the aqueous phase in the present system, since the experiment by stopped-flow technique (*16*) has been done in aqueous solution under conditions where only 1:1 chelate formation is favored.

The rate constant for anionic form of 8-mercaptoquinoline is much higher than that expected from the normal Eigen mechanism which involves a diffusion-controlled outer sphere complex formation between the reacting metal ion and the ligand followed by the rate-determining dissociation of the inner-sphere coordinated solvent molecule (*17*). This is not the first system in which a rate constant higher than expected from the Eigen dissociation mechanism has been observed. In 1966, Rorabacher (*18*) called attention to anomalously large formation rate constants for nickel ion and ethylenediamine and related ligands. The enhanced rate was attributed to an outer-sphere hydrogen bonding between the ligand and a coordinated water molecule. If this were the predominant factor here, we should expect the rate of the anionic form of 8-mercaptoquinoline to be far lower than that for 8-quinolinolate ion since the proton affinities of N and S^- in the 8-mercaptoquinolate ion are each several orders of magnitude lower than those of N and O^- in 8-quinolinolate. Furthermore, the values of k_{HL} for both 8-mercaptoquinoline and 8-quinolinol, corresponding to that for protonated ethylenediamine, are close to that for ammonia with nickel ion and not abnormally small as is the case with protonated ethylenediamine, which Rorabacher et al. (*19*) attributed to an intramolecular hydrogen bond. There is a strong intramolecular hydrogen bond for 8-quinolinol, whereas there is none in 8-mercaptoquinoline. Hence, some other factor may be operating to affect k_{HL} and k_L in the present system. It is noteworthy that 2-(2-thiazolylazo)-4-methylphenol reacts with nickel ion more slowly than 8-mercaptoquinoline and 8-quinolinol (*13*). Further work remains to be done to elucidate the interesting variation of rate constants observed with certain ligands in metal complex formation.

Registry No. Nickel, 7440-02-0; thiooxine, 491-33-8.

LITERATURE CITED

(1) Bankovskii, Yu. A. "Chelate Chemistry of 8-Mercaptoquinoline and Its Derivatives"; Izdatelstvo Zinatne: Riga, USSR, 1978, and literature cited therein.
(2) Kealey, D.; Freiser, H. *Anal. Chem.* **1966**, *38*, 1577.

(3) Carter, S. P.; Freiser, H. *Anal. Chem.* **1979**, *51*, 1100.
(4) Bankovskii, Yu. A.; Chera, L. M.; Ievin'sh, A. F.; Luksha, E. A. *J. Gen. Chem. USSR (Engl. Transl.)* **1958**, *28*, 2310.
(5) Bankovskii, Yu. A.; Chera, L. M.; Ievin'sh, A. F. *Zh. Anal. Khim.* **1963**, *18*, 668.
(6) Carter, S. P.; Freiser, H. *Anal. Chem.* **1980**, *52*, 511.
(7) Bag, S. P.; Freiser, H. *Anal. Chim. Acta* **1982**, *134*, 333.
(8) Akiba, K.; Freiser, H. *Sep. Sci. Technol.* **1982**, *17*, 745.
(9) McClellan, B. E.; Freiser, H. *Anal. Chem.* **1964**, *36*, 2262.
(10) Oh, J S.; Freiser, H. *Anal. Chem.* **1967**, *39*, 295.
(11) Ohashi, K.; Freiser, H. *Anal. Chem.* **1980**, *52*, 767.
(12) Yamada, K.; Nakagawa, K.; Haraguchi, K.; Ito, S. *Nippon Kagaku Kaishi* **1975**, 294.
(13) Yamada, K.; Nakagawa, K.; Haraguchi, K.; Ito, S. *Nippon Kagaku Kaishi* **1975**, 1431.
(14) Reference 1, p 98.
(15) Kawase, K.; Freiser, H. *Anal. Chem.* **1966**, *38*, 1577.
(16) Johnson, W. A.; Wilkins, R. G. *Inorg. Chem.* **1970**, *9*, 1917.
(17) Eigen, M.; Tamm, K. *Z. Elektrochem.* **1962**, *66*, 107.
(18) Rorabacher, D. B. *Inorg. Chem.* **1966**, *5*, 1891.
(19) Taylor, R. W.; Stephen, H. K.; Rorabacher, D. B. *Inorg. Chem.* **1974**, *13*, 1282.
(20) Ito, S.; Haraguchi, K.; Nakagawa, K.; Yamada, K. *Nippon Kagaku Kaishi* **1973**, 948.

RECEIVED for review May 5, 1982. Resubmitted October 12, 1982. Accepted December 13, 1982. This work was supported by the National Science Foundation.

Determination of Partition Coefficient of Polar Organic Solutes in Octanol/Micellar Solutions

G. M. Janini* and S. A. Attari

Department of Chemistry, University of Kuwait, Kuwait

A shake-flask method is presented for the determination of the partition coefficients involved in the distribution of polar solutes between octanol and aqueous micellar solutions. An equation is derived for the simultaneous determination of the partition coefficients of solutes between octanol and water and between micelles and water from simple measurements of the apparent partition coefficients of solutes in octanol/aqueous micellar solutions at different surfactant concentrations. By application of basic chromatographic theory this treatment is readily extended to account for the partitioning behavior of solutes eluted with micellar mobile phases in reversed-phase liquid chromatography. The advantages and limitations of this method are discussed.

The partition coefficients of organic chemicals in octanol/water serve as an empirical measure of the hydrophobicity of these substances in biomedical and pharmacological systems (*1*). They have been used for the estimation of bioconcentration of organic pollutants in trout muscle (*2*), for correlations with basic solvent properties (*3*, *4*), and for determination of retention in reversed-phase high-pressure liquid chromatography (*5*). On the other hand, the partition coefficient of solutes in micelles/water is useful in the research areas of oil recovery (*6*) and micellar catalysis, enzymes, and biological membranes (*7*–*9*).

It is well established that retention in reversed-phase liquid chromatography depends upon the partitioning characteristics of the solute between the aqueous mobile phase and the hydrophobic stationary phase. The addition of surfactants to the mobile phase affects the partitioning process significantly. Liquid chromatographic separations utilizing aqueous micellar mobile phase, whereby significant partitioning of solute occurs to discrete aggregates dissolved in the mobile phase, have resulted in a degree of selectivity not shared by conventional pure or mixed solvents (*10*). As articulated by Armstrong and Nome, the partition coefficients involved include that of a solute between the stationary phase and water, between the stationary phase and the micelles, and between the micelles and water. A high-pressure liquid chromatography (HPLC) method for the calculation of these partition coefficients has been outlined by the above authors (*10*).

In this work an analogous treatment of the partitioning of solutes between aqueous micellar solutions and octanol is presented. An equation is derived which accounts for all possible equilibria for such systems. Data are obtained by the shake-flask technique, where solute concentration in octanol and in the aqueous micellar phase is determined by HPLC. The method is tested by using sodium dodecyl sulfate (SDS) surfactant and dihydroxybenzene solutes.

THEORY

The octanol/water partition coefficient, K_{OW}, is defined as the ratio of molar concentration of solute (S) in octanol saturated with water, C_S^O, to its concentration in water saturated with octanol, C_S^W, under equilibrium conditions.

$$K_{OW} = C_S^O / C_S^W \tag{1}$$

The concentration of solute in the two phases will bear a constant ratio as long as their activity coefficients remain relatively constant. In many instances solute molecules may participate in different equilibria in the two phases, thus complicating the partition process. Here we consider the partition of solute between octanol and an aqueous micellar solution. The three equilibria involved are schematically represented in Figure 1.

For such a system an apparent partition coefficient, K_{app}, may be defined as

$$K_{app} = \frac{(m_S^M + m_S^W)/(V_M + V_W)}{m_S^O / V_O} \tag{2}$$

where m denotes number of moles, V denotes volume, and the numerator is the total concentration of solute in the aqueous phase (bulk water + micelles).

Utilizing the definition of $K_{MW} = (m_S^M/V_M)/(m_S^W/V_W)$, it could be easily shown by algebriac rearrangement that

$$(m_S^M + m_S^W)/(V_M + V_W) = \frac{m_S^W}{V_W}\left[K_{MW}\left(\frac{V_M}{V_M + V_W}\right) + 1 - \frac{V_M}{V_W}\right] \tag{3}$$

0003-2700/83/0355-0659$01.50/0 © 1983 American Chemical Society

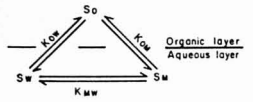


Figure 1. A schematic representation of the equilibria involved in the partition of solutes between octanol and micellar solutions (S = solute; O = octanol; W = water; M = micelles; $K_{OW} = C_S^O/C_S^W$; $K_{MW} = C_S^M/C_S^W$, $K_{OM} = C_S^O/C_S^M$).

Here, one should first fractionate the left-hand side of eq 3 and then expand the fraction $M_S^W/(V_M + V_W)$ in a power series neglecting second and higher terms, where it is assumed that $(V_M/V_W) \ll 1$. As will be shown later, this assumption is valid for dilute micellar solutions.

Introducing C_M as the concentration of micellar surfactant which is equal to the total surfactant concentration minus CMC, the critical micelle concentration, and $\bar{V}$ as the partial specific volume of the surfactant in the micelle we have

$$C_M\bar{V} = \frac{V_M}{V_M + V_W} \simeq \frac{V_M}{V_W} \tag{4}$$

Here, the units of C_M should be the reciprocal of the units of $\bar{V}$ so as to obtain dimensionless volume fraction.

Substituting eq 4 and 3 in eq 2 we have

$$K_{app} = \frac{(M_S^W/V_W)[C_M\bar{V}(K_{OW} - 1) + 1]}{M_S^O/V_O} \tag{5}$$

Substituting the expression for K_{OW} and rearranging we get

$$K_{app} = \frac{\bar{V}(K_{MW} - 1)}{K_{OW}}C_M + \frac{1}{K_{OW}} \tag{6}$$

By plotting K_{app} vs. C_M in the surfactant concentration range where eq 6 is valid, one should obtain a straight line. K_{OW} is obtained from the intercept and K_{MW} is obtained from the ratio of the slope to the intercept.

The maximum error introduced by assuming that $V_M \ll V_W$ is estimated as follows:

The maximum surfactant concentration used in this study is 3.58×10^{-3} g/mL and the CMC of SDS is 2.3×10^{-3} g/mL (*11*). Hence the maximum micellar surfactant concentration is 3.35×10^{-2} g/mL. Assuming a value of 0.862 mL/g for the specific volume, $\bar{V}$, of micellar SDS (*12*), then the volume fraction of micelles in the aqueous phase according to eq 4 would be $(3.35 \times 10^{-2}$ g/mL)(0.862 mL/g) $= 2.89 \times 10^{-2}$. The numerical value of the quantity $\bar{V}C_M$ is the same whether it refers to the surfactant or to the micelle aggregates. In the later case $\bar{V}$ would be the molar volume of aggregates in liters per mole and C_M would be the concentration of aggregates in the mobile phase in moles per liter. Thus for a solution containing 1 mL of water $V_M = 2.97 \times 10^{-2}$ mL and V_M/V_W is larger than $V_M/(V_M + V_W)$ by less than 3%. The larger the surfactant concentration becomes, the higher is the error introduced by this approximation.

Finally, for an HPLC column with octanol stationary phase (s) and a micellar mobile phase (m) the basic chromatographic equation is

$$V_e = V_m + K_{sm}V_s \tag{7}$$

where V_e is the elution volume of solute, V_m is the void volume of the column, V_s is the volume of the stationary phase in the column, and K_{sm} is the reciprocal of K_{app} as defined in eq 2.

Substituting the value of K_{app} from eq 6 and eq 7 and rearranging, we get Armstrong and Nome's expression (*10*)

$$\frac{V_s}{V_e - V_m} = \frac{\bar{V}(K_{MW} - 1)}{K_{SW}}C_M + \frac{1}{K_{SW}} \tag{8}$$

Table I. Partition Coefficients of Dihydroxybenzenes between Octanol and Aqueous Micellar Solutions as a Function of Micellar Surfactant Concentration

concn of micellar surfactant (C_M, g/mL)[a]	K(aqueous/octanol) resorcinol	catechol	hydroquinone
0	0.255[b]	0.203[b]	0.349[b]
0.0067	0.274	0.228	0.381
0.0156	0.330	0.264	0.421
0.0335	0.402	0.335	0.512

[a] $C_M = C$ − CMC, where C is the total surfactant concentration and CMC is the critical micelle concentration, which for sodium dodecyl sulfate is equal to 2.3×10^{-3} g/mL (*11*). [b] These values represent the inverse of the octanol/water partition coefficient.

As was stated by Armstrong and Nome, the value of K_{MW} represents the partition coefficient between micelle and water per monomer of surfactant. To get the value per micelle, K_{MW} must be multiplied by the surfactant's aggregation number which is 62 for pure SDS aqueous micelles. It is to be noted that in the present treatment, the aqueous phase is not a pure SDS micelle system because some octanol will be solubilized in the micelles as a cocomponent. Furthermore, surfactant and possibly reversed micelles may be present in the organic phase. Consequently, values of K_{MW} obtained from partition experiments would not be the same as those obtained by reversed-phase HPLC.

EXPERIMENTAL SECTION

Shake-Flask Equilibrations. For each equilibration about 10 mL of water or micellar solution and about 10 mL of the organic phase were placed in a 25-mL sample vial and closed with a Teflon-lined cap. The organic phase was a 0.5% (by weight) octanol solution. The volume ratio of the organic phase to the aqueous phase was chosen so as to facilitate the accurate determination of solute concentration in both phases. The flasks were gently inverted 100 times in about 5 min at ambient temperature (*1*). Vigorous agitation was avoided in order to prevent emulsion formation. After centrifugation (PR 6000 Refrigerated Centrifuge by Damon/IEC Division, at 1200 rpm) a sample of the equilibrated aqueous phase was transferred to a 10-mL vial with a Pasteur pipet. Thirty-microliter samples were then withdrawn from the vial for direct HPLC analysis. Samples from the organic phase were directly withdrawn from the equilibration vial.

Materials. The solutes were analytical grade (Aldrich Chemical Co.) and were used without further purification. SDS was purchased from Sigma Chemical Co. Water was double distilled and acetonitrile was glass-distilled Burdick and Jackson product.

HPLC Analysis. The liquid chromatograph used for the analysis of solute concentration was assembled from a laboratory Data Control Constamertic I and II pumps and gradient master, a Chromatronix dual-channel UV absorbance detector set at 280 nm, a Rheodyne sample injector equipped with a 50-μL injection loop, and a Fisher Recordall series 5000 strip-chart recorder with 10 mV input. Retention times and peak areas were automatically fed to a 3352 A Laboratory Data System (Hewlett–Packard) linked to the UV detector output through a Hewlett-Packard 1865 A/D converter. The output from the data system was recorded on a 9866A thermal line printer (Hewlett-Packard). The RP-18 reversed-phase column was 250 mm × 4.6 mm prepacked with 10-μm particle size material (Waters Associates). Experiments were run at ambient temperature with a 25% acetonitrile/water mobile phase at a flow rate of 1.2 mL/min. To avoid excess deposition of octanol the column was periodically washed with pure acetonitrile and then reequilibrated with the mobile phase.

Analysis for solute concentration in each phase was done in triplicate. The precision of the numerical area measurement as determined from the reproducibility of the numerical area printout

Table II. Partition Coefficients K_{MW} and K_{OW} for Dihydroxybenzenes

					K_{OW}		
solute	slope	intercept	corr coef.	K_{MW}	1/ intercept	exptl	range of lit. values[a]
resorcinol	4.52 ± 0.32	0.25 ± 0.006	0.995	19.4	3.80	3.92	3.72-6.31
catechol	3.96 ± 0.03	0.202 ± 0.001	0.999	23.7	4.95	4.92	1.62-10.72
hydroquinone	4.86 ± 0.09	0.348 ± 0.002	0.999	17.2	2.87	2.87	2.45-3.89

[a] Reference 1.

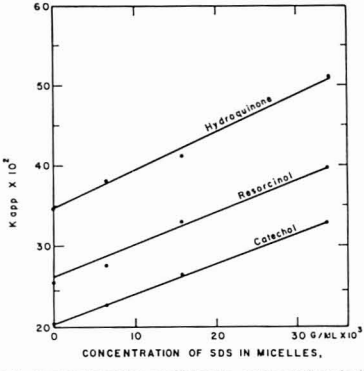


Figure 2. Apparent partition coefficient vs. concentration of micellar surfactant for dihydroxybenzene solutes.

with repeated injection of 30 μL each was within 2%.

The apparent partition coefficient for each solute was calculated as the ratio of the molar concentration of solute in the aqueous phase to its molar concentration in the organic phase.

RESULTS AND DISCUSSION

To test the validity of eq 6 and of the underlying assumptions, we measured the partition coefficients of resorcinol, hydroquinone, and catechol between octanol and micellar solutions of different concentrations of SDS in water. The data are presented in Table I. Plots of K_{app} vs. C_M are shown in Figure 2. The results of linear regression analysis on the data as well as the values for K_{MW} and K_{OW} are presented in Table II. The fact that the plots in Figure 2 are linear with correlation coefficients near unity and that the reciprocals of the intercepts are equal to the respective K_{OW} values is a strong indication of the validity of the theoretical treatment. Our experimental K_{OW} values differ considerably from literature values (*1*). We believe that our analytical method has the advantage that solute concentrations were measured in both phases and that impurities, if present, were separated and therefore did not interfere with the evaluation of the partition coefficients. The analytical procedure was simple and accurate because the values of the octanol/water partition coefficients of the solutes studied ranged from 2.87 to 4.92. The method is best suited for solutes with K_{OW} values in the range 1–10. For $K_{OW} < 1$, most of the solute is already extracted in the aqueous phase prior to the addition of surfactant. For solutes with K_{OW} values >10 the larger the value of K_{OW}, the higher the demand on the accuracy of the analytical determination of solute concentration in the aqueous phase. Furthermore experimental artifacts such as the formation of emulsions and adsorption of solute onto surfaces of transfer vessels may only be reduced at a cost of inconvenience and increased analysis time.

Registry No. Octyl alcohol, 111-87-5.

LITERATURE CITED

(1) Leo, A.; Hansch, C.; Elkins, D. *Chem. Rev.* **1971**, *71*, 525–616.
(2) Neely, W.; Branson, D.; Blau, G. *Sci. Technol.* **1974**, *8*, 1113–1115.
(3) Watarai, H.; Tanaka, M.; Suzuki, N. *Anal. Chem.* **1982**, *54*, 702–705.
(4) Watarai, H.; Suzuki, N. *Bull. Chem. Soc. Jpn.* **1980**, *53*, 1848–1852.
(5) Karger, B. L.; Snyder, L. R.; Eon, C. *Anal. Chem.* **1978**, *50*, 2126–2136.
(6) Doe, P. H.; Wade, W. H.; Schechter, R. S. *J. Colloid Interface Sci.* **1977**, *59*, 525–531.
(7) Fendler, J. H. "Membrane Mimetic Chemistry"; Wiley: New York, 1982.
(8) Bunton, C. A. *Prog. Solid State Chem.* **1973**, *8*, 239–281.
(9) Cordes, E. H.; Gitlar, C. *Prog. Biorg. Chem.* **1973**, *2*, 1–53.
(10) Armstrong, D. W.; Nome, F. *Anal. Chem.* **1981**, *53*, 1662–1666, and references therein.
(11) Mysels, K. J.; Princen, L. H. *J. Phys. Chem.* **1959**, *63*, 1696–1701.
(12) Mukerjee, P. *J. Phys. Chem.* **1962**, *66*, 1733–1735.

RECEIVED for review November 1, 1982. Accepted December 30, 1982. This research was sponsored by the Research Council of Kuwait University.

Microemulsions in the Extraction of Gallium with 7-(1-Ethenyl-3,3,5,5-tetramethylhexyl)-8-quinolinol from Aluminate Solutions

P. Fourré and D. Bauer*

Laboratoire de Chimie Analytique des Processus Industriels, 10, rue Vauquelin, 75231 Paris Cedex 05, France

Jean Lemerle

Laboratoire des Polymères Inorganiques, Université Pierre et Marie Curie, 8, rue Cuvier, 75230 Paris Cedex 05, France

The extraction rate of gallium from aqueous NaOH and Al(III) solutions with 7-(1-ethenyl-3,3,5,5-tetramethylhexyl)-8-quinolinol in kerosene is increased by addition of an alcohol together with the sodium salt of a long chain carboxylic acid. It has been shown that the organic phase of this system is a water-in-oil microemulsion. This result has been obtained by the determination of water and metal solubilized in the organic phase and by means of ultracentrifugation experiments. The amount of water solubilized in the organic phase may reach 9 M. The radius of microemulsion droplets has been estimated to be 20–50 Å for the extraction of gallium with a mixture (butanol + carboxylate). At a constant concentration ratio of octanoate to butanol, it decreases as the octanoate concentration increases. Preparative ultracentrifugation experiments have shown that a large fraction of the extractant was adsorbed on the droplets.

Microemulsions according to Schulman appellation (*1*), or swollen micellar solutions according to Shinoda appellation (*2*), are optically transparent and thermodynamically stable oil–water dispersions. They can be formed spontaneously by adding to an oil–water mixture quantities of a surfactant and a cosurfactant, usually an alcohol. Water-in-oil microemulsions are usually described as a dispersion in oil of droplets of water surrounded by a shell of molecules of surfactant and cosurfactant, and vice versa for oil-in-water microemulsions. The size range of the droplets is 50–1000 Å. Microemulsions constitute a phase existing alone or in equilibrium with an excess of aqueous phase or an excess of organic phase or with an excess of each of these two phases. Microemulsions have attracted considerable interest (*3*) because of their applications in various areas such as enhanced recovery of oil (*4*) and microdispersions of drugs, cosmetics, etc. Several books have been published during the last 5 years that deal with the structure and applications of such phases (*5*, *6*).

Additionaly, it is well-known that systems involving micelles influence separation methods (*7*) as TLC (*8*) and liquid–liquid extraction (*9–13*). In solvent extraction, a fast rate transfer may be obtained by the use of surface active agents, the role of which has not been clearly established. Nyman and Hummelstedt (*14*) have shown that the addition of (dinonylnaphthalene)sulfonic acid increases the rate of Ni(II) and Co(II) extraction with LIX 70-Versatic 10 mixtures. Similarly, Osseo-Azare et al. (*15*, *16*) have studied the extraction of Ni(II) with LIX 63, in the presence of long chain sulfonic acids. The authors attributed the enhancement of the extraction rate to the micellar aggregation of *surfactant* molecules, the effect of which is to concentrate the reactants and to make them more accessible to one another. This concentrative effect of micelles has also been proposed by Robinson et al. who have studied the reaction between Ni^{2+} and ligands in aqueous micellar solutions of sodium alkyl sulfate (*17–19*) and in reversed micelles of Aerosol-OT in heptane (*20*).

Table I. Similarity between a Microemulsion System and the Extraction System of Gallium

microemulsion system	extraction system of gallium[a]
brine	aqueous phase: Al(III) 1.5 M and Ga(III) 0.004–0.012 M in NaOH 3.5 M
oil	kerosene
cosurfactant	long chain alcohol
surfactant	sodium salt of a long chain carboxylic acid

[a] Extractant RHOx.

Although the difference between microemulsions and micellar solutions is very narrow and consists mainly in the size range of the droplets, the quantity of trapped water and the surfactant concentration range, the name "microemulsion" is not previously mentioned in the literature concerning surfactant enhanced extraction. The similarity of composition between microemulsions and typical liquid–liquid extraction systems is illustrated in Table I. Chin-Kwang et al. (*21*) have already shown the existence of water-in-oil microemulsions in some extraction systems. In their systems, the surfactant was the extractant itself, and the microemulsion was subsequently destroyed when the metal was extracted. One of us has recently shown rates of extraction of Ge(IV), Fe(III), and Ni(II) with "Kelex 100", Al(III) and Ni(II), with HDEHP, and Ni(II) with LIX 70-Versatic 911 mixture were greatly enhanced by the use of a microemulsion instead of a classical organic phase. Typically, the time was reduced from 20 min to several hours without any additive to 1 min in the microemulsion extraction system (*22–24*).

Now we are faced with the problem of elucidating the role of microemulsions, especially the presence of water swollen micelles in the organic phase, in the mass transfer process from a kinetics point of view. What is the effective water–oil interfacial area in such a case? Is the rate enhancement induced by an increase of the interfacial area or by a modification of the mass transfer mechanism, or by both? How is it possible to give experimental evidence for the role of the tensioactive species?

In this paper, we present the results of analytical and preparative ultracentrifugation experiments, with regard to the composition of the micelles. The chosen example is the Ga(III) extraction from strongly basic solutions (NaOH 3.5 M) with the 7-(1-ethenyl-3,3,5,5-tetramethylhexyl)-8-quinolinol (RHOx) into kerosene (*25*). The extraction rate of gallium, at constant interfacial area, may be increased up to 20 times

0003-2700/83/0355-0662$01.50/0 © 1983 American Chemical Society

by adding a long chain alcohol and the sodium salt of a long chain carboxylic acid to the extraction system (*26–29*). We present here the results of our investigations which provide evidence for the existence of a microemulsion (*28*) and give the partition of RHOx between the droplets and the continuous organic phase of the microemulsion. (In this paper, we call "continuous organic phase" the organic phase which surrounds the droplets. The water trapped in these droplets is called "dispersed aqueous phase". They constitute together the microemulsion phase, which is in equilibrium with the aqueous phase of the extraction systems, which is called "continuous aqueous phase" or "outer aqueous phase".) These results have been obtained by measuring the amount of water solubilized in the microemulsion, studying the solubilization of metallic salts in the "dispersed aqueous phase" (secondary solubilization), and performing analytical and preparative ultracentrifugations.

EXPERIMENTAL SECTION

(1) Methods. (a) Analytical ultracentrifugation. Organic phases used in the ultracentrifugation studies were prepared by mixing 10 mL of an aqueous phase with 7.5 g of an organic mixture containing kerosene, 5% by weight of RHOx, with variable quantities of sodium carboxylate and butanol. Systems were left standing overnight to obtain transparent organic and aqueous phases.

Sedimentation velocities were measured at 20 °C in a Beckman Model E ultracentrifuge equipped with Schlieren optics. Kel-F single sector cells were used. For large amounts of solubilized water, a 1° positive wedge window was used in order to have the whole cell image on the photographic plate. All runs were performed at 56000 rpm.

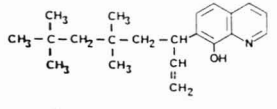
(b) Preparative ultracentrifugation experiments were performed at 52000 rpm during the time necessary to obtain a sufficient displacement of the boundary of water droplets. This time ranged from 4 to 36 h. About 0.1 mL of pure organic continuous phase was then withdrawn at the surface of the centrifuge tube which initially contained 5 mL of organic phase.

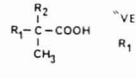
This continuous phase was diluted in a solution of octanol in decane, 8:92 by volume. The diluted solution was shaken with an equal volume of 9 M HCl. The UV–visible spectrum of the organic phase was recorded with a Varian 634 S spectrophotometer. The RHOx concentration was determined by comparison with calibrated curves established at 358 nm ($\epsilon = 2.15 \times 10^3$ M^{-1} cm^{-1}).

(c) The amount of water solubilized in the organic phases was determined by Karl-Fisher titration. The aluminum concentration in the organic phases was measured by atomic absorption spectrophotometry (309.2 nm) in a nitrous oxide–acetylene flame (Varian AA6 spectrophotometer) after stripping with 1 M H_2SO_4.

(2) Reagents. The 7-(1-ethenyl-3,3,5,5-tetramethylhexyl)-8-quinolinol (RHOx) was a pure material synthesized on our demand as described in ref 30. It is an extractant analogous to the industrial extractant "Kelex 100", the active product of which is the 7-undecyl-8-quinolinol. The carboxylic acids "Cekanoic 10" (dimethyloctanoic acid) and "Versatic 10" were, respectively, supplied by PCUK and Shell Co. Gallium oxide was supplied by Rhône-Poulenc Co.

RHOx





Kerosene and octanoic acid were obtained from Fluka ("purum" quality). Sodium hydroxide (Merck) and the other reagents (PROLABO) were all analytical grade.

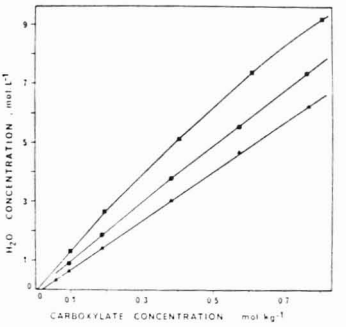


Figure 1. Amount of water solubilized in the microemulsion vs. the concentration of a few carboxylates at constant ratio [carboxylate]/[butanol]: (■) sodium octanoate, (●) sodium "Cekanoate 10", (▲) sodium "Versatate 10"; organic mixture (7 g) kerosene, RHOx 0.16 mol·kg^{-1}, [carboxylate]/[butanol] = 0.223; aqueous phase, NaOH 3.5 M; V = 10 mL.

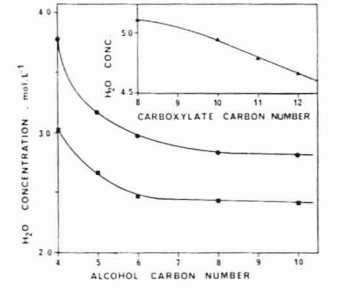


Figure 2. Amount of water solubilized in the microemulsion vs. the hydrocarbon chain length of linear alcohols and carboxylates: organic mixture (7 g) kerosene, RHOx 0.16 mol·kg^{-1} (▲); butanol 1.80 mol·kg^{-1} and carboxylate 0.402 mol·kg^{-1} (●, ■); alcohol 1.70 mol·kg^{-1}, sodium "Cekanoate 10" (●); and sodium "Versatate 10" (■) 0.380 mol·kg^{-1}; aqueous phase (10 mL) NaOH 3.5 M.

RESULTS AND DISCUSSION

Solubilization of Water in the Organic Phase. The addition of an alcohol and a sodium salt of a long chain carboxylic acid allows the solubilization of large amounts of water in the organic phase: about ten molecules of water per molecule of surfactant when butanol is the alcohol. The quantity of water solubilized is smaller with branched-chain carboxylates ("Cekanoate 10" and "Versatate 10") than with linear carboxylates (sodium octanoate) (Figure 1). It decreases as the hydrocarbon chain length of the carboxylate or the alcohol increases (Figure 2). The variation seems to be in relation with the space occupied by the alcohol and the carboxylate. This space increases with branching or increasing the hydrocarbon chain length of the alcohol and carboxylate and thus varies in inverse ratio to water solubility.

At constant concentration of octanol, the water content of the organic phase depends on "Cekanoate 10" (CK 10) concentration (Figure 3) in the following way:

$$[H_2O] = a[CK\ 10]^2 + b[CK\ 10] + [H_2O]_0$$

where a and b are constants and $[H_2O]_0$ the water concentration in the absence of "Cekanoate 10". To a first approximation, $[H_2O]_0$ may be attributed to water solubilized

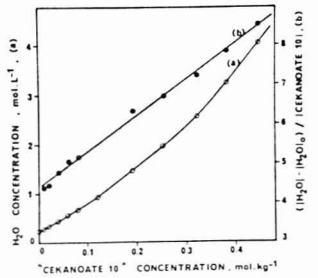


Figure 3. Amount of water solubilized in the microemulsion (a) and of the ratio ($[H_2O] - [H_2O]_0$)/[CK 10] (b) vs. the "Cekanoate 10" concentration at constant octanol concentration: organic mixture (7 g) kerosene, RHOx 0.16 mol·kg^{-1}, octanol 0.85 mol·kg^{-1}; aqueous phase (10 mL) NaOH 3.5 M.

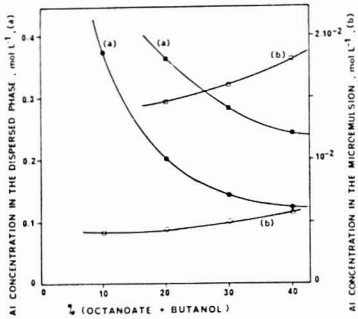


Figure 4. Al(III) concentration in the dispersed phase (a) and in the microemulsion (b) vs. the percentage of (octanoate + butanol) in the organic mixture: organic mixture (20 g) kerosene, [octanoate]/[BuOH] = 0.112 (■, □) and 0.0558 (●, ○); aqueous phase (25 mL) NaOH 3.5 M, Al(III) 1.5 M, and Ga 0.0143 M.

in the continuous organic phase whereas the major portion of solubilized water ($[H_2O] - [H_2O]_0$) is contained in the microemulsion droplets.

Secondary Solubilization of Al(III) and Ga(III) in the Organic Phase. At zero concentration of RHOx, salts of Al(III) and Ga(III) only exist in the "dispersed" and "outer" aqueous phase (NaOH 3.5 M, Al(III) 1.5 M, and Ga 0.0143 M) since the carboxylate anions do not complex Al or Ga in our systems. This was verified by separating the continuous organic and dispersed phases by preparative ultracentrifugation and determining that the Al and Ga concentrations were zero. The partition coefficients of gallium and aluminum between the dispersed and the outer aqueous phases are always less than unity and are greatly dependent upon the composition of the organic mixtures. Thus, curves (a) of Figure 4 show that the Al(III) concentration in the dispersed aqueous phase ($[Al(III)]_{disp.aq.}$) decreases as the percentage of sodium octanoate + butanol in the organic mixture increases. Curves (b) of Figure 5 show a gradual increase of Al(III) concentration in the microemulsion ($[Al]_{\mu E}$), i.e., in the dispersed aqueous phase + the continuous organic phase, with increasing percentage of (octanoate + butanol). As Al(III) in the microemulsion (volume $V_{\mu E}$) is only trapped in the dispersed aqueous phase (volume $V_{disp.aq.}$), its total quantity satisfies the relation

$$[Al(III)]_{\mu E} V_{\mu E} = [Al]_{disp.aq.} V_{disp.aq.}$$

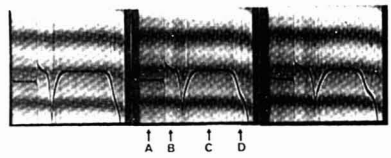


Figure 5. Typical ultracentrifugation patterns, system III of Table II.

We observe here that $[Al(III)]_{\mu E}$ increases and $[Al(III)]_{disp.aq.}$ decreases as the percentage of (sodium octanoate + butanol) mixture increases. The above equality requires that, at constant $V_{\mu E}$, $V_{disp.aq.}$ increases more strongly than $[Al(III)]_{disp.aq.}$ decreases.

Analytical Ultracentrifugation. Ultracentrifugation has been used by a few authors (*30–33*) to demonstrate the existence of a microemulsion and determine the size of the droplets of dispersed phase. During ultracentrifugation, spherical droplets of mass m, hydrodynamic radius r_h, and density ρ_d move in the continuous phase of density ρ_c and viscosity η. They are submitted to the four following forces:

Centrifugal force

$$F_c = m\omega^2 R = \rho_d \frac{4}{3}\pi r_h^3 \omega^2 R$$

where R is the distance of the droplet to the rotation axis and ω the angular speed.

Archimedes force

$$F_A = -\rho_c \frac{4\pi}{3} r_h^3 \omega^2 R$$

Frictional force

$$F_f = -6\pi\eta r_h \frac{dR}{dt}$$

where dR/dt is the migration velocity of the droplet.

Diffusion force.

In our experiments, which were carried out at high speed and with particules of sufficient mass, diffusion may be neglected. By use of the Stokes formula for the laminar flux of hard spheres, the hydrodynamic radius of droplets can be obtained

$$r_h^2 = \frac{9}{2}\frac{\eta S_0}{\rho_g - \rho_c}$$

where $S_0 = (1/\omega^2 R)(dR/dt)$ is the sedimentation coefficient at infinite dilution.

When subjected to the centrifugal field, droplets move and a boundary is formed between the region cleared of droplets and the region where the initial microemulsion subsists. This sedimentation front is characterized by an abrupt variation of the refractive index n. As the ultracentrifuge was equipped with Schlieren optics, giving the variation $dn/dR = (\partial n/\partial C)(\partial C/\partial R)$ (C, droplet concentration) vs. the distance R to the axis of rotation, the front appears as a peak. Peaks lie under the horizontal base line showing that $\partial n/\partial C$ is negative, so the organic phase of extraction is a water-in-oil microemulsion.

From the typical ultracentrifugation patterns (Figure 5), five regions can be distinguished:

The peak represents the sedimentation boundary. It is attributed to water droplets surrounded by a mixed film of carboxylate and alcohol molecules. These droplets, the density of which is higher than that of the continuous phase, move outward toward the bottom of the cell. Because the droplets have a smaller refractive index than that of the organic phase ($\partial n/\partial C < 0$) the peak is inverted.

Table II. Analytical Ultracentrifugation of Organic Phases [a]

	sodium octanoate						"Versatate"	"Cekanoate"
	I	II	III	IV	V	VI	VII	VIII
carboxylate, mol·kg^{-1}	0.603	0.603	0.402	0.201	0.100	0.201	0.380	0.380
water solubilized, M	5.22	7.33	5.11	2.67	1.33	2.45	3.02	3.78
S (svedbergs)	0.50	0.90	1.9	4.05	7.2	1.35	0.90	0.94

[a] Aqueous phase (10 cm^3): NaOH 3.5 M, Al(III) 1.5 M in system I; NaOH 3.5 M, Ga 0.0043 M in the other systems. Organic mixture (7.5 g): kerosene, RHOx 5% by weight; [carboxylate]/[butanol] = 0.112 in system VI and 0.223 in the other systems. Rotation speed: 56000 rpm. Temperature: 293 K.

Region A corresponds to the air present in the cell.

In region B, between the meniscus and the peak, no water droplets exist, but only the continuous organic phase.

Region C, after the peak, nearly corresponds to the initial microemulsion.

Region D is a region rich in droplets.

The analysis of the centrifugation patterns has given apparent sedimentation coefficients S varying from 0.5 to 7 S (Table II). It is difficult to relate S to the droplet radius r_h. Indeed, it is necessary to determine η, ρ_d, ρ_c, and the sedimentation coefficients S_0 at zero concentration of droplets. One must isolate some of the continuous organic phase in order to measure some of these quantities. But this continuous phase is very complex: it contains butanol, solubilized water, and RHOx in various forms (neutral, basic, or as complexes with gallium and aluminum). For this reason, the dilution procedure used by Taupin et al. (*31*) is not applicable here. So we have prepared a small quantity of the continuous phase of system (IV) of Table II by use of preparative ultracentrifugation. The organic phase is centrifuged for 5 h and some continuous phase is withdrawn above the sedimentation boundary. The solution thus obtained is not exactly the true continuous organic phase because molecules of extractant (mol wt = 311) move slowly toward the bottom of the cells and after 5 h the RHOx concentration is about 7% less than the initial RHOx concentration; however, the solution obtained is very close to the true continuous organic phase. The organic phase was then diluted with the continuous phase thus obtained. Only a slight decrease representing 10% of the sedimentation coefficient obtained without dilution has been observed while the microemulsion was diluted four times. So variations of the sedimentation coefficient may not be attributed to variations of the concentration of (carboxylate + butanol) mixture but to changes of droplets structure. For a given system, the sedimentation coefficient at zero concentration of droplets is approximately equal to the apparent sedimentation coefficient. The quantities η, ρ_d, and ρ_c remain unknown because we cannot, even by preparative ultracentrifugation, separate sufficient quantities of the continuous organic phase to perform measurements of viscosity and density. On the other hand, it is also impossible to have "pure droplets" without some continuous organic phase. Values η and ρ_c may be estimated by considering synthetic organic phases containing kerosene, RHOx 0.16 mol·kg^{-1}, and butanol in various concentrations. These organic phases were equilibrated with NaOH 3.5 M. For instance, we have obtained at 293 K, $\eta = 2.0 \times 10^{-2}$ P and $\rho_c = 0.795$ g/mL with butanol 2.68 mol·kg^{-1}. So we have chosen the following approximate values: $\eta = 1.5$ to 2×10^{-2} P and $\rho_c \simeq 0.79$ g/mL. The droplets contain butanol, carboxylate, RHOx, and core of aqueous phase. Hence, a range of ρ_d values from 0.9 to 1 g/mL seems reasonable. The major error on the droplet radius comes from this estimation of ρ_d. It may be limited by considering that the proportion of aqueous phase in the droplet and thus ρ_d increases as the droplet radius increases. So, we have chosen values of ρ_d close to 0.9 g/mL for the smallest radius and close to 1 g/mL for the greatest radius. With this range of values for η, ρ_c, and ρ_d, we obtain values for the droplet radius of 20 to 50 Å.

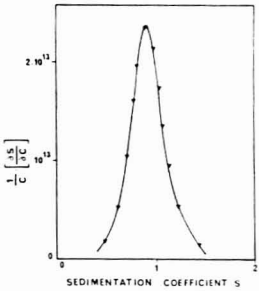


Figure 6. $(1/C)(\partial S/\partial C)$ vs. the sedimentation coefficient, system VIII of Table II.

With the same concentration of sodium octanoate and butanol, the sedimentation coefficient obtained with the aqueous phase (3.5 M NaOH and 1.5 M Al(III)) is nearly half than that obtained with the aqueous phase (3.5 M NaOH, 0,0043 M Ga). This fact may be explained by the difference of salinities between the two phases since the electrolyte has a screening effect on the repulsion of the charged polar heads of sodium octanoate. At a lower salinity, the repulsion is stronger, leading to a tendency to form droplets of greater radius.

At a constant ratio of octanoate concentration to butanol concentration, (systems II, III, IV, and V of Table II), the sedimentation coefficient and thus the droplet radius decrease as the percentage of the (octanoate + butanol) mixture increases. This fact is in good agreement with the variation of the Al(III) concentration in the aqueous dispersed phase (Figure 4a). As the droplet radius decreases, Al(III) is more excluded from the droplet.

At constant concentration of sodium octanoate, the sedimentation coefficient decreases as the alcohol concentration increases.

Salts of branched chain carboxylic acids "Versatic 10" and "Cekanoic 10" give similar values of S, values which are significantly smaller than that obtained with octanoate under the same conditions.

The mass distribution of droplets has been evaluated from the sedimentation coefficient distribution (Figure 6). It has been found that the distribution was rather symmetrical and homogeneous with a ratio (width at half height/mean sedimentation coefficient) between 0.3 and 0.4.

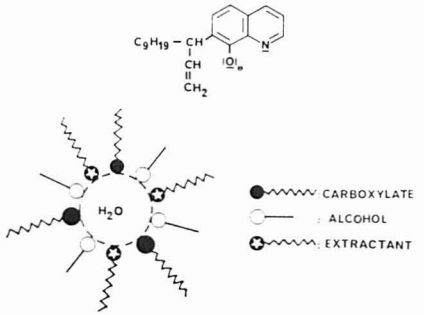
Preparative Ultracentrifugation Experiments. In our systems, the water-in-oil microemulsion is essentially built by

Table III. Variation of Fraction f_d of RHOx Adsorbed on Droplets and of RHOx Concentration ($[RHOx]_d$) on Droplets vs. Octanoate Concentration [a]

[octanoate], mol·kg^{-1}	$[RHOx]_{\mu E}$, M	$[RHOx]_{c\phi}$, M	volume fraction α	f_d	$[RHOx]_d$, M
0.06	0.127 ± 0.001	0.108 ± 0.003	0.045 ± 0.005	0.19 ± 0.04	0.5 ± 0.15
0.12	0.125 ± 0.001	0.080 ± 0.003	0.090 ± 0.009	0.42 ± 0.035	0.5 ± 0.1
0.24	0.124 ± 0.001	0.074 ± 0.002	0.165 ± 0.017	0.50 ± 0.035	0.3 ± 0.05

[a] [Octanoate]/[butanol] = 0.112; aqueous phase, NaOH 3.5 M.

the introduction of a long chain carboxylate and an alcohol. However, the molecule of extractant also exhibits an amphiphile behavior, especially in its basic form (ROx^-) which predominantly exists under the working conditions.



Thus some extractant may be included in the organic shell of the droplets along with carboxylate and alcohol. We have performed preparative ultracentrifugation experiments to study the localization of RHOx.

To take into account the slow migration of isolated RHOx molecules, two experiments were carried out for each system, one with the microemulsion system and one with the same system but without carboxylate (that is to say with a classical organic phase). From these two experiments, it was possible to determine the extractant concentration in the continuous organic phase. The balance of RHOx is given by the following relation:

$$[RHOx]_{\mu E} = [RHOx]_{c\phi}(1 - \alpha) + \alpha[RHOx]_d \quad (1)$$

where $[RHOx]_{\mu E}$, $[RHOx]_{c\phi}$, and $[RHOx]_d$ are respectively the concentrations of RHOx in the whole microemulsion, in the continuous organic phase, and in the droplets; α is the volume fraction of droplets in the microemulsion. $[RHOx]_d$ and the fraction f_d of RHOx adsorbed on droplets may be deduced from (1)

$$[RHOx]_d = \frac{[RHOx]_{\mu E} - [RHOx]_{c\phi}(1 - \alpha)}{\alpha}$$

$$f_d = \frac{\alpha[RHOx]_d}{[RHOx]_{\mu E}} = \frac{[RHOx]_{\mu E} - [RHOx]_{c\phi}(1 - \alpha)}{[RHOx]_{\mu E}}$$

The volume fraction f_d of droplets (aqueous core + organic shell composed of octanoate, butanol, and RHOx) has been calculated by assuming that the droplets contain almost all of the carboxylate and half of the butanol (that has been found by titration of the continuous organic phase of system IV of Table II). After a first determination of f_d, α was recalculated to take into account the contribution of RHOx. We have voluntarily taken a large relative error of 10% on the obtained values of α. That means for instance, that an error of 20% on the proportion of butanol adsorbed on the droplets is

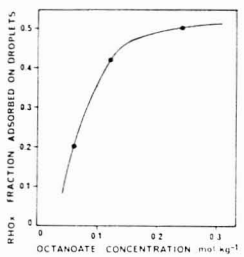


Figure 7. Fraction of RHOx adsorbed on droplets vs. the octanoate concentration at constant ratio [octanoate]/[butanol]: organic mixture (7 g) kerosene, RHOx 0.16 mol·kg^{-1}; [octanoate]/[butanol] = 0.112; aqueous phase (10 mL) NaOH 3.5 M.

tolerated (butanol represents less than half of the droplet constituants). Values reported in Table III show the concentrative effect of microemulsion droplets on RHOx which is two to four times as concentrated in the droplets as in the bulk organic phase. At constant concentration ratio of octanoate to butanol, the fraction of RHOx incorporated in the organic shell of droplets greatly increases with the concentration of sodium octanoate at low concentration, and then, seems to reach a limiting value slightly greater than 0.5 (Figure 7). That may be explained by a greater difficulty for RHOx to be adsorbed on the droplets because of a more compact occupation of the droplet surface by the octanoate and butanol molecules as the concentration of sodium octanoate increases. It is thus more difficult for the extractant RHOx to be adsorbed on the droplets.

Registry No. Ga, 7440-55-3; Na, 7440-23-5; RHOx, 29171-27-5; sodium octanoate, 1984-06-1; butanol, 71-36-3; aluminum sodium oxide, 11138-49-1.

LITERATURE CITED

(1) Stoeckenius, W.; Schulman, J. H.; Prince, L. M. *J. Phys. Chem.* **1959**, *63*, 1677.
(2) Shinoda, K.; Kunieda, H. *J. Colloid Interface Sci.* **1973**, *42* (2), 381.
(3) Rosoff, M. *Prog. Surf. Membr. Sci.* **1978**, *12*, 405.
(4) Healy, R. N.; Reed, R. L.; Carpenter, C. W., Jr. *Soc. Pet. Eng. J.* **1975**, 87.
(5) Mittal, K. L. "Micellisation, Solubilization and Microemulsions"; Plenum Press: New York, 1977; Vol. 2.
(6) Friberg, S. "Microemulsions, Theory and Practice"; Academic Press: New York, 1977.
(7) Hinze, W. L. In "Solution Chemistry of Surfactants"; Mittal, K. L., Ed.; Plenum: New York, 1979; Vol. 1.
(8) Armstrong, D. W.; Terrill, R. Q. *Anal. Chem.* **1979**, *51* (13), 2160.
(9) Markovits, G. Y.; Choppin, G. R. In "Ion Exchange and Solvent Extraction"; Marinsky, J. A.; Marcus, Y., Eds.; Marcel Dekker: New York, 1973; Vol. 3, p 51.
(10) Morris, D. F. C. *J. Colloid Interface Sci.* **1975**, *51*, 52.
(11) Van Dalen, A.; Gerritsma, K. W. "Solvent Extraction, Proceedings of the International Solvent Extraction Conference, The Hague"; Society of Chemical Industry: London, 1971; Vol. 2, p 1096.
(12) Van Dalen, A.; Wijkstra, J.; Gerritsma, K. W. *J. Inorg. Nucl. Chem.* **1978**, *40* (5), 875.
(13) Wang, S. M.; Chuang, H. C.; Tseng, C. L. *J. Inorg. Nucl. Chem.* **1975**, *37*, 1983.
(14) Nyman, B. G.; Hummelstedt, L. "Proceedings of the International Solvent Extraction Conference, Lyon"; Society of Chemical Industry: London, 1974; Vol. 1, p 669.

(15) Osseo-Azare, K.; Keeney, M. E. "International Solvent Extraction Conference, [Proceedings], Liege"; 1980; Vol. 1, Paper 80–121.
(16) Osseo-Azare, K.; Keeney, M. E. *Sep. Sci. Technol.* **1980**, *15* (4), 999.
(17) Robinson, B. H.; James, A. D. *J. Chem. Soc., Faraday Trans 1* **1973**, *74*, 10.
(18) Robinson, B. H.; White, N. C. *J. Chem. Soc., Faraday Trans 1* **1978**, *74*, 2625.
(19) Reinsborough, V. C.; Robinson, B. H. *J. Chem. Soc., Faraday Trans. 1* **1979**, *75*, 2395.
(20) Robinson, B. H.; Steytler, D. C.; Tack, R. D. *J. Chem. Soc., Faraday Trans. 1* **1979**, *75*, 481.
(21) Chin-Kwang, W.; Hung-Chang, K.; Tien, C.; Seng-Chung, L.; Tien-Chu, K.; Kwang-Hsien, H. "International Solvent Extraction Conference, [Proceedings], Liege"; 1980; Vol. 1, Paper 80–23.
(22) Komornicki, J. Thesis, Paris, France, 1981.
(23) Bauer, D.; Komornicki, J.; Tellier, J. French Patent Appl. No. 81.24.267.
(24) Bauer, D.; Komornicki, J.; Tellier, J. French Patent Appl. No. 82.03.231.
(25) Helgorsky, J.; Leveque, A. "CIM Special Volume"; Canadian Institute of Mining and Metallurgy: Montreal, 1979; No. 21, Vol. 2, p 439.
(26) Leveque, A.; Helgorsky, J. European Patent No. 29.70 Rhône-Poulenc Co.
(27) Fourre, P.; Bauer, D. *C. R. Hebd. Seances Acad. Sci. II* **1981**, *292*, 1077.
(28) Bauer, D.; Fourre, P.; Lemerle, J. *C. R. Hebd. Seances Acad. Sci. II* **1981**, *292*, 1019.
(29) Fourre, P.; Bauer, D., unpublished work, Paris, France.
(30) Buddle, W. M., Jr.; Hartlage, J. A. U.S. Patent 3 637 711, 1972.
(31) Bowcott, J. E.; Schulman, J. H. *Z. Elektrochem.* **1955**, *59*, 283.
(32) Dvolaitzky, M.; Guyot, M.; Lagues, M.; Le Pesant, J. P.; Ober, R.; Sauterey, C.; Taupin, C. *J. Chem. Phys.* **1978**, *69* (7), 3279.
(33) Hwan, R. N.; Miller, C. A.; Fort, T., Jr. *J. Colloid Interface Sci.* **1979**, *68* (2), 221.
(34) Jorpes-Friman, M. *Finn. Chem. Lett.* **1979**, *7–8*, 240.

RECEIVED for review May 24, 1982. Accepted December 14, 1982.

Immobilized Morin as Fluorescence Sensor for Determination of Aluminum(III)

Linda A. Saari and W. Rudolf Seitz*

Department of Chemistry, University of New Hampshire, Durham, New Hampshire 03824

We have prepared a sensor for Al^{3+} based on fluorescence. Morin is immobilized on cellulose powder and attached to the end of a bifurcated fiber optic. When the immobilized morin is placed in a solution containing Al^{3+}, fluorescence is observed from the Al^{3+}–morin complex. Response is linear from 1×10^{-6} to 1×10^{-4} M Al^{3+} at pH 4.8. At this pH the binding constant for the Al^{3+}–immobilized morin complex is 1.7×10^4. Response time is 1–2 min. The detection limit is 1×10^{-6} M. The detection limit is established by variations in background signal which is comprised of detector dark current and background fluorescence. Under conditions of this study, the sensor extracts about 1% of the aluminum in the sample when operating in the range of linear response.

The development of sensors based on immobilized fluorogenic reagents is a subject of growing interest. We have previously reported a pH sensor based on immobilized fluoresceinamine (*1*). Other research in this area has been described in the Focus section of ANALYTICAL CHEMISTRY (*2*).

These sensors offer two important advantages relative to conventional solution fluorescence measurements: they can measure concentrations without significantly perturbing the sample, and they can be used for continuous sensing.

In this report we describe the characteristics of a sensor for Al^{3+} based on immobilized morin (3,5,7,2′,4′-pentahydroxyflavone). Morin is only weakly fluorescent by itself but forms highly fluorescent complexes with Al^{3+}. It has been widely used as a reagent for fluorometric analysis of aluminum and other metals as well as for spectrophotometric analysis of metals that do not form fluorescent complexes (*3–5*).

THEORY

This section develops theory to describe the relative response of the immobilized morin sensor as a function of aluminum ion concentration. It is assumed that the total number of immobilized morin molecules, C, is much less than the number of aluminum ions in solution. Under these conditions the insertion of the sensor will not significantly affect the aluminum ion concentration in solution.

The equilibrium constant for aluminum binding to immobilized morin can be represented (assuming a 1:1 complex)

$$K = M_{Al}/Ma_{Al} \quad (1)$$

where M is the number of immobilized morin ligands not associated with aluminum, M_{Al} is the number of immobilized morin ligands associated with aluminum ion, a_{Al} is the aluminum metal ion activity in solution, and K is the equilibrium constant.

Because the total number of immobilized morin molecules, C, is fixed:

$$C = M + M_{Al} \quad (2)$$

Since morin is essentially nonfluorescent by itself and the morin–aluminum complex is fluorescent, the fluorescence signal will depend on the amount of aluminum bound to the morin

$$I = kM_{Al} \quad (3)$$

where I is the fluorescence intensity and k is a proportionality constant relating fluorescence intensity to the amount of aluminum bound to morin. It is assumed that the conditions are such that intensity is proportional to the number of sites (i.e., no inner filter effects).

By substituting eq 2 into eq 1 and rearranging, it is possible to express M_{Al} in terms of C, a_{Al}, and K

$$M_{Al} = a_{Al}KC/(1 + a_{Al}K) \quad (4)$$

By substituting eq 4 into eq 3, an expression for fluorescence intensity as a function of aluminum ion activity is obtained

$$I = kKCa_{Al}/(1 + a_{Al}K) \quad (5)$$

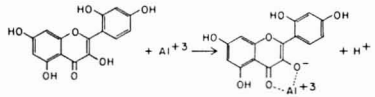
To determine K for the sensor a linear form of eq 5 can be used

$$a_{Al}/I = a_{Al}/kC + 1/kCK \quad (6)$$

A plot of a_{Al}/I vs. a_{Al} will be linear with a slope of $1/kC$ and an intercept of $1/kCK$.

0003-2700/83/0355-0667$01.50/0 © 1983 American Chemical Society

The experimental equilibrium constant, K, is a conditional constant that depends on pH because Al^{3+} displaces hydrogen ion when binding to morin as shown below.



In addition, hydrolysis of Al^{3+} will affect K.

EXPERIMENTAL SECTION

Apparatus. The filter fluorometer used to measure the fluorescence of the immobilized Al^{3+}–morin complex has been described previously (*1*). The excitation wavelength was selected with a 2 in. × 2 in. interference filter from Oriel with maximum transmittance at 420 nm and a 10-nm bandwidth at half maximum transmittance. The emission wavelength was selected by a 1 in. × $^1/_2$ in. interference filter from Edmund Scientific with maximum transmittance at 488 nm and a bandwidth of 7 nm at half maximum transmittance. The bifurcated fiber optic from Fiber Optics Technology is glass with a diameter of $^3/_{16}$ in.

Excitation spectra of the immobilized morin and its aluminum complex on the optic surface were measured with an SLM 8000 spectrofluorometer equipped with an MC 300 manual monochromator. Measurements were made by attaching the excitation and emission arms of the bifurcated fiber optic to the source and detector lens housings in the sample chamber by means of light-tight aluminum fittings.

pH was measured with an Orion Digital Ionalyzer/501. Fluorescence excitation and emission solution spectra were measured on a Perkin-Elmer 204 spectrofluorometer. UV-VIS absorbance measurements were made on a Bausch and Lomb Spectronic 200 UV spectrometer.

Reagents. Morin and cyanuric chloride were purchased from Aldrich. Powdered cellulose (microcrystalline for TLC, through 60 sieve, Baker) was used as the cellulose support.

Immobilization Procedure. Morin was immobilized on powdered cellulose, using cyanuric chloride according to a previous procedure (*1*). The concentration of the cyanuric chloride solution was 0.14 M in acetone and the concentration of morin was 0.0076 M in acetone. The product was washed with acetone, dried by suction, and stored at room temperature. A single batch of immobilized morin was used for all characterization studies.

Morin was also immobilized as its Al^{3+} complex, because this should prevent the functional groups involved in complexation from reacting with cyanuric chloride. The soaking solution consisted of acetone–water (3:2) 0.0021 M in morin and 0.014 M in Al^{3+}. For comparison a batch of uncomplexed morin was immobilized under the same conditions, but omitting the aluminum. The morin bound uncomplexed gave slightly higher intensity then the morin bound complexed when both were saturated with aluminum, and consequently, morin bound in the uncomplexed form was used for all experiments. The amount of morin bound per gram of cellulose was found to be slightly greater when morin was bound as the complex. Thus, it is not clear why this preparation failed to respond more sensitively to Al^{3+}. This is an interesting question but was not pursued.

Determination of Amount Bound. The amount of morin bound/gram of cellulose was found by stripping the morin from the cellulose in 1 M KOH and measuring the morin concentration by spectrophotometry. Weighed amounts (0.0311 g and 0.0356 g) of the immobilized morin were soaked in 1 M KOH solutions (10.00 mL) until the cellulose lost color (4 h). The absorbance of 1:10 dilutions of the soaking solutions was measured at 405 nm along with morin standards in 1 M KOH. Absorbance spectra were measured for the standards and soaking solutions from 350 to 600 nm.

The amount of active aluminum binding sites contained/gram of cellulose was determined by two methods. The first method consisted of soaking weighed amounts (0.0077 g and 0.0115 g) of the immobilized morin in solutions of aluminum sulfate (5.45×10^{-4} M, 0.400 mL) at pH 5.1 for 15 min. The decrease in aluminum concentration of the soaking solutions was then determined by taking 0.100 mL of each soaking solution, adding morin (0.00683 M, 0.175 mL), diluting to 25 mL with pH 5.1 acetate buffer, and measuring the fluorescence intensity using the SLM 8000 spectrofluorometer. The excitation wavelength was set at 420 nm and the emission wavelength was selected by using the 488 nm interference filter. Standards of varying aluminum concentration, of the same pH, acetate concentration, and morin concentration were used to determine aluminum concentration. Since this method involves the morin–Al^{3+} system at equilibrium, the equilibrium constant for binding at pH 5.1 (Table I) was used in calculating the number of active sites from the decrease in aluminum concentration.

Table I. Experimental Values of the Conditional Equilibrium Constant, K, for Aluminum Binding to Immobilized Morin

pH	K	pH	K
3.8	4×10^3	5.1	3.3×10^4
4.1	1.2×10^4	5.5	2.8×10^4
4.6	1.4×10^4	5.9	3×10^4
4.8	1.7×10^4	6.5	1.8×10^4

In the second method used to determine the amount of active aluminum binding sites contained/gram of cellulose, weighed amounts (0.0215 g and 0.0197 g) of the immobilized morin were each soaked in a solution of aluminum sulfate (7.56×10^{-4} M) at pH 4.8 for 0.5 h. This concentration of aluminum is sufficient to saturate all binding sites. The excess solution was washed away with four 10-mL portions of distilled, deionized water on a sintered glass funnel. In deionized water the kinetics of complex dissociation are so slow that the washing step may be completed without significant dissociation of the complex. The cellulose was then soaked in 10 mL of 20% acetic acid for 1 h. The cellulose was fluorescent under UV light after the aluminum soaking and washing, but nonfluorescent after the acetic acid treatment indicating that all the aluminum was stripped off. The solution was poured off and the cellulose was rinsed with 5 mL of distilled water, making 15 mL of solution. The pH was adjusted to 4.7 with KOH and the solutions were analyzed for aluminum by adding morin (0.1 mL of 0.00777 M) and measuring the fluorescence intensity with the fiber optic fluorometer. Standards of varying aluminum concentration, of the same pH, acetate concentration, and morin concentration were used to determine the aluminum concentration.

Fluorescence Measurements. To determine the wavelengths for excitation and emission, fluorescence spectra were measured on the morin–Al^{3+} complex in solution by use of the Perkin-Elmer 204 spectrofluorometer.

Fluorescence measurements on the immobilized morin (i.e., the sensor) were made by attaching the immobilized morin to the end of the fiber optic and immersing the optic in acetate buffer solution. A thin layer of the cellulose support was spread on a piece of cellophane tape (Scotch brand) and the tape was held in place on the end of the optic by a piece of Tygon tubing. This has been described previously (*1*). The tape is not entirely satisfactory because it becomes cloudy when wet with reduced transmittance and significant scattering. Because of the limitations of the tape, collodion was also tried. A small amount of the collodion was spread on the end of the optic and allowed to become sticky and then the powder was applied as a thin layer. This was not found to be satisfactory because it was difficult to form a thin, uniform layer. The collodion also loses its adhesive properties with time.

Aluminum concentration was varied both by adding known amounts of aqueous standard solutions of aluminum sulfate to the same solution and by immersing the sensor in buffered solutions of varying aluminum concentrations. The solution was stirred as measurements were taken.

The effect of pH on the response to aluminum was studied by using acetate buffers of varying pH in the range 2.9 to 6.5. Interferences were studied by adding various ions separately to the immobilized morin sensor when it was responding to aluminum. Metal ions tested were iron(III), cobalt, copper(II), beryllium, calcium, and magnesium.

The reversibility of the sensor response was determined by adding aluminum ion to the sensor in buffer solution until the response was constant and then immersing the sensor into a buffer

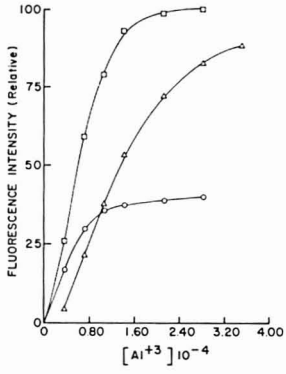


Figure 1. Relative fluorescence intensity of the immobilized morin sensor as a function of Al^{3+} concentration at pH 3.8 (Δ), pH 4.8 (□), and pH 5.9 (○).

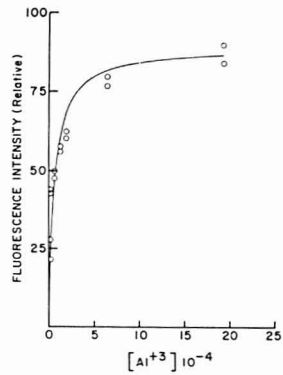


Figure 2. A plot of the theoretical response of the sensor (curve) represented by eq 5 and experimental points (○) at pH 4.8.

solution without aluminum. The sensor was then submerged into a fresh buffer solution and more aluminum was added. The aluminum was also stripped by immersing the sensor in a solution of EDTA (0.0255 M at pH 7) and washing with water.

Excitation spectra of the immobilized morin and its aluminum complex were measured at a fixed emission wavelength of 488 nm at a pH of 4.8 using the SLM 8000 spectrofluorometer.

Measurements were made on morin in solution for comparison to the immobilized morin. The fluorescence of the morin–Al^{3+} complex, the effect of pH, and the effect of interferences on the morin–Al^{3+} complex were studied. The excitation spectra of morin and its aluminum complex in solution were measured with the SLM 8000 spectrofluorometer. The concentration of morin used in the solution study was 8.00×10^{-5} M.

RESULTS AND DISCUSSION

Response to Aluminum. The fluorescence of the sensor based on immobilized morin increases with aluminum concentration as shown in Figure 1. This is expected since aluminum forms a fluorescent complex with morin. The response is linear from 10^{-6} M to 10^{-4} M aluminum concentration. Above 10^{-4} M there is a change in slope and the response levels off. This leveling off is due to saturation of the morin with aluminum. The same type of response is observed for morin in solution.

The fluorescence intensities and aluminum concentrations were plotted in the form of the theoretical linear equation modeling the system (see eq 6). The linear model is adequate for the system at the 95% confidence level as shown by the appropriate regression analysis. From the slope and intercept, values for the conditional binding equilibrium constant, K, were determined by the immobilized morin in solutions of varying pH. The results are shown in Table I. These values reflect changes in protonation of the immobilized morin and formation of hydroxide complexes of aluminum. At low pH the formation constant decreases because protons tend to displace Al^{3+}. At high pH the formation constant decreases because more of the aluminum is in the form of hydroxide complexes. The binding constant for aluminum ion to morin in solution has been reported as 2.96×10^6, but the pH is not specified (*3*, *5*).

By use of the slope and intercept of the linear plot at pH 4.8, the theoretical equation to describe the response of the sensor (eq (5) is plotted in Figure 2. Since the data are represented adequately by the theory for a 1:1 morin–aluminum complex, this suggests that the complex is primarily in this form.

Determination of Amount Bound. The amount of morin bound/gram of cellulose is 4.2×10^{-5} mol as determined by measuring the amount of morin stripped off the cellulose in strong base by spectrophotometry. The absorbance spectra are identical for the morin in base and the solutions containing the stripped morin. This indicates that treatment with base yields free morin rather than a morin–cyanuric chloride conjugate.

The number of moles of active complexing sites/gram is 26% of the number of moles of morin bound/gram (1.1×10^{-5} mol of Al^{3+}/gram of immobilized morin as determined by the two methods which are in agreement). That the number of active sites is less than the total shows that the group responsible for complexation is probably tied up in the immobilization procedure. It is not known which of the morin phenolic sites the cyanuric chloride binds to, but the product is most likely a mixture with the cyanuric chloride bound to different sites.

Operating Characteristics. The optimum pH for the sensor is 4.8. The response to aluminum at various pH values is shown in Figure 1. At low pH the kinetics of the response are very slow and the intensity is low. At higher pH values the fluorescence intensity is low due in part to the hydrolysis of aluminum ion. Fluorescence intensity vs. time data at different pH values are shown in Figure 3. The response time for the sensor is 1–2 min to a change in aluminum concentration. When the sensor is saturated and placed in a buffer solution without aluminum, the fall time is about 3 min. The response time when immobilized reagent is inserted into solution for the first time is 3–4 min.

Measurements were made with 1 mg of derivatized support on the optic surface. This corresponds to 4.2×10^{-8} mol of morin on the optic surface as determined by absorbance measurements.

With the following relationship which is valid at any aluminum level:

$$\text{no. of Al ions bound/total no. of sites} = \text{intensity/intensity at saturation}$$

it is possible to show that only 1% of the aluminum ion is extracted from solution when operating in the region of linear response to aluminum. This supports the assumption in the Theory section that insertion of the sensor does not significantly affect concentration.

The excitation spectra of the immobilized morin (i.e., background), its aluminum complex, and the morin–Al^{3+}

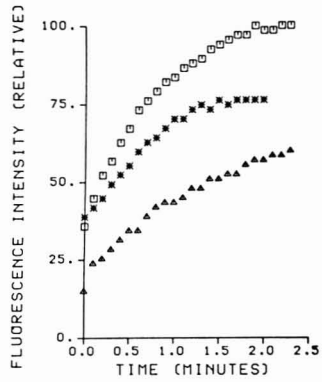


Figure 3. Response to added Al^{3+} as a function of time for the immobilized morin sensor at pH 3.5 (Δ), pH 4.8 (□), and pH 6.5 (*). The Al^{3+} concentration was 7.2×10^{-5} M.

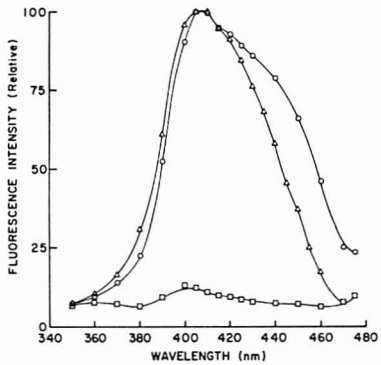


Figure 4. Excitation spectra (uncorrected) of the morin–Al^{3+} complex in solution (Δ), the immobilized morin–Al^{3+} complex (○), and the immobilized morin without aluminum (□) at pH 4.8. The spectra for immobilized morin with and without Al^{3+} are drawn to the same scale. The spectrum for the complex in solution is normalized to have the same maximum value as the spectrum for the immobilized complex. The Al^{3+} concentration was 1.0×10^{-4} M for the spectra of the complexes.

complex in solution are shown in Figure 4. The spectra of the immobilized complex and the complex in solution are similar with the spectrum of immobilized complex showing a slight broadening. The excitation spectrum of the immobilized morin shows a small peak similar in shape to the spectrum of the complex superimposed on a flat continuous background. This indicates that the background includes both a contribution from weak morin fluorescence plus a signal due to reflected and scattered excitation radiation.

The signal to background ratio is 2.5:1 at aluminum concentrations of 1×10^{-3} M. Dark current represents 50% of the background with the remainder due to scattered and reflected light plus residual morin fluorescence. The signal to background ratio can be improved to 7:1 at 1×10^{-3} M aluminum, using the SLM spectrofluorometer as source and detector with dark current representing 25% of the background. The detection limit for the sensor, as the concentration equivalent to 2 times the standard deviation of the background signal, is 1×10^{-6} M Al^{3+} (0.027 ppm). Because the background is quite stable, we are able to measure small signals superimposed on a relatively large background.

Table II. Effect of Interferences on the Al^{3+} Response of the Immobilized Morin Sensor

interference	concn, M	signal	signal with interference	% change
Ca^{2+}	3.32×10^{-3}	0.088	0.090	+2[a]
Mg^{2+}	2.83×10^{-3}	0.108	0.118	+9[a]
Be^{2+}	3.19×10^{-5}	0.084	0.103	+23[a]
	4.73×10^{-4}	0.084	0.153	+82[a]
Co^{2+}	3.75×10^{-4}	0.097	0.097	+0[a]
	2.93×10^{-3}	0.097	0.080	−18[a]
Cu^{2+}	7.64×10^{-5}	0.134	0.108	−19[b]
	7.59×10^{-4}	0.134	0.039	−71[b]
Fe^{3+}	3.27×10^{-5}	0.162	0.138	−15[b]
	4.87×10^{-4}	0.162	0.020	−88[b]

[a] $[Al^{3+}] = 3.59 \times 10^{-5}$ M. [b] $[Al^{3+}] = 7.18 \times 10^{-5}$ M.

Interferences. Because beryllium, calcium, and magnesium form fluorescent complexes with morin (*3–5*) they were tested as interferences. The optimum pH for formation of these complexes, however, is above 7 (*3, 4*). Iron(III), copper(II), and cobalt are all heavy metal ions and could quench fluorescence by complexation or by the heavy atom effect in solution. The effect of these ions in the aluminum response is shown in Table II. The major interferences are beryllium which increases the signal and iron(III) and copper(II) which quench fluorescence to an appreciable extent. Copper(II) causes the signal due to aluminum to decrease, but the sensor still responds to further increases in aluminum concentration. The quenching by copper(II) may be due to ions in solution or to weak complexation, rather than due to strong complex formation as in the case of iron(III). After being quenched by the addition of iron, the sensor no longer responds to added aluminum. To use the sensor in the presence of iron, it would be necessary to reduce iron to the ferrous form and tie it up as a complex.

Morin in solution behaves in a similar manner when subjected to the ions tested.

Registry No. Aluminum, 7429-90-5; morin, 480-16-0; cellulose, 9004-34-6.

LITERATURE CITED

(1) Saari, L. A.; Seltz, W. R. *Anal Chem.* **1982**, *54*, 821–823.
(2) Borman, S. A. *Anal Chem.* **1981**, *53*, 1616A–1618A.
(3) Katyal, M.; Prakash, S. *Talanta* **1977**, *24*, 367–375.
(4) Katyal, M. *Talanta* **1968**, *15*, 95–106.
(5) Nevskaya, E. M.; Nazarenko, V. A. *J. Anal. Chem. USSR (Engl. Transl.)* **1972**, *27*, 1544–1561.

RECEIVED for review September 13, 1982. Accepted December 20, 1982.

Laser Microprobe Mass Analysis of Asbestos Fiber Surfaces for Organic Compounds

J. K. De Waele, E. F. Vansant, P. Van Espen, and F. C. Adams*

Department of Chemistry, Universitaire Instelling Antwerpen (U.I.A.), Universiteitsplein 1, B-2610 Wilrijk, Belgium

Laser microprobe mass analysis was applied for the analysis of organic impurities at the surface of asbestos fibers. Benzo[*a*]pyrene was adsorbed from the gas phase and from a benzene solution, benzidine from aqueous solution and *N,N*-dimethylaniline from benzene. By use of laser desorption conditions these compounds, and in the case of *N,N*-dimethylaniline its oxidation products, such as Methyl Violet, could easily be detected. It appeared that the asbestos samples used contain organic contaminants at the surface.

Asbestos is becoming more and more of a concern to scientists, the construction industry, and the general public because there is reason to believe that exposure to the fiber, under some circumstances, is associated with lung cancer, asbestosis, and other diseases (*1*).

From the biochemical and environmental standpoint, fine respirable asbestos fibers of high surface area have considerable capacity to adsorb other substances. They may therefore selectively adsorb the constituents of living cells and thereby upset the delicate balance of cell reproducibility, but they may also adsorb pollutants from the atmosphere to be transported to the lung and deposited in the tissue (*2*).

Because of the hypothesis that the toxicity of the asbestos fibers is correlated with the adsorption power of pollutants (*3–6*), the intention of this paper is to characterize the surface of asbestos. Therefore, organic impurities were adsorbed onto the asbestos surface by using a gas adsorption process (*7*) or through equilibration of the fibers with a benzene or water solution.

A rapidly increasing number of publications illustrate the usefulness of laser microprobe mass spectrometry in single particle analysis (*8–11*). The primary utility of the method in this application appears to lie in the areas of quick routine qualitative and semiquantitative analysis of individual particles of micrometer size for minor and in some conditions trace level inorganic constituents (*12, 13*). At the same time there is evidence that by use of the technique as a variable ionization source for mass spectrometry, information can be gained regarding the presence of molecular inorganic and organic species present in the microscopical objects (*14*). In this paper we want to report preliminary results which show that laser microprobe mass analysis (LAMMA) can detect sensitively chemical impurities present at the asbestos fiber surface.

EXPERIMENTAL SECTION

The LAMMA Instrument. For a full description of the LAMMA-500 instrument (Leybold-Heraeus, GmbH, Köln, FRG) we refer to other publications (*12, 15, 16*).

The most attractive features of the LAMMA instrument are spatial resolution to 1 μm, high collection efficiencies (10–50%), and ease of operation and simplicity. On the other hand, the mass resolution of 700–800 is marginally adequate for inorganic analysis and for the characterization of fingerprint organic spectra.

The laser energy on the sample can be varied with a set of attenuating filters. It is monitored by an energy meter. Laser energy is adjusted either to provide complete vaporization of a micrometer size sample of the fiber or else to give the lowest energy which provides a mass spectrum. Adsorbed impurities onto the fiber surface can be detected in this laser desorption (LD) operation mode (*17*). In the LD mode a rather small number of ions are formed belonging to a limited number of ion species that are in most cases directly related to the molecular structure of the material analyzed, often with a high yield of the parent molecular ions (M^+), protonated $(M + 1)^+$, or cationized species $(M + Na)^+$ or $(M + K)^+$ (*17–19*). When laser desorption is applied to asbestos, the fibers remain intact and the characteristic mass spectrum of the material vanishes to an insignificant intensity.

Reagents: benzo[*a*]pyrene (BaP), 99+%, Gold Label, Aldrich-Europe, Belgium; benzene, 99+%, spectrophotometric grade, Gold Label, Aldrich-Europe, Belgium; benzidine dihydrochloride, >99, Fluka AG, Buchs, FRG; *N,N*-dimethylaniline (DMA), 99%, Aldrich-Europe, Belgium; hydrogen chloride (0.1 N), Titrisol, Pro Analysis, Merck, FRG; Methyl Violet 2B, certified (Basic Violet 1), Aldrich-Europe, Belgium.

Materials. UICC (Union Internationale Contre le Cancer) standard asbestos of crocidolite and amosite from South Africa, Canadian (Type B) and Rhodesian (Zimbabwe) (type A) chrysotile, and Finnish anthophyllite were used (*20–22*). The UICC has sponsored the preparation and distribution of standard reference samples of each class of asbestos, and these samples have been employed in inhalation, ingestion, inoculation, and in vitro experiments. Other applications are in identification of asbestos type in aerosols and tissues, standardization of conventional fiber counting, development and calibration of techniques and instruments for fiber assessment, and studies on influence of fiber size and shape on inhalation and retention (*23*).

All filtrations were carried out by means of Schleicher & Schüll filter paper, no. 589[1] Schwarzband, ϕ 110 mm.

For introduction of asbestos into the LAMMA instrument for analysis, a standard copper electron microscopy grid, coated with a Formvar film, is brought into contact with the fibers. A number of them stick to the grid coating. Fibers large enough to be detectable with the optical microscope can be selected for individual analysis.

RESULTS AND DISCUSSION

Adsorption of Benzo[*a*]pyrene on Crocidolite. *Procedure.* Benzo[*a*]pyrene (BaP) was adsorbed onto the UICC standard of crocidolite using two methods:

Adsorption from a Benzene Solution. To a 30-mg crocidolite sample, 20 mL of a 10^{-3} M BaP solution in benzene is added. The suspension is refluxed at a temperature of 60 °C for 15 h. The asbestos is filtered over a Schleicher & Schüll filter and rinsed twice with a pure benzene solution.

Gas-Phase Adsorption. Gas-phase adsorption is performed with an apparatus for vapor-phase adsorption of polycyclic organic matter, designed by Korfmacher et al. (*24*), and Miguel and Natusch (*7*). Approximately 30 mg of asbestos is weighted into an expanded-bed adsorption tub. The expanded-bed is heated to a temperature of ca. 150 °C. The BaP vapor in nitrogen gas is passed over the material until equilibrium adsorption is obtained as indicated by fluorescence measurements of the effluent. The adsorption bed is then cooled rapidly (*7*).

Whereas at high laser energy above 1 μJ, pure BaP gives rise to a fragmentation pattern, at lower energy the spectrum

0003-2700/83/0355-0671$01.50/0 © 1983 American Chemical Society

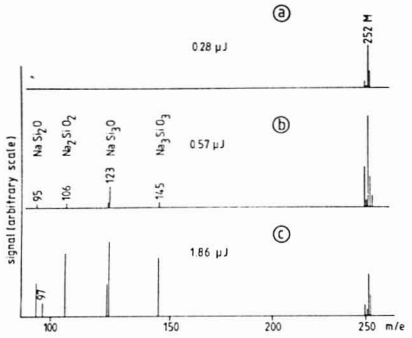


Figure 1. Positive laser mass spectra of benzo[*a*]pyrene (BaP) adsorbed from solution onto separate crocidolite fibers for three laser energies.

is considerably simpler: the fragmentation peaks become negligible and the molecular ion peak becomes more intense. Below 0.35 μJ, the latter becomes the only detectable mass spectral component. The negative mass spectrum, even when collected at very low laser energy, provides an intense fragmentation pattern C_nH^- with n even for the most abundant peaks. The intensity of mass peaks around the molecular mass of BaP is much lower than that for the positive spectra and consists of major peaks at m/e = 251 and 253.

The positive spectrum of the solution doped crocidolite samples shows the presence of the characteristic BaP desorption spectrum at low laser energy. Figure 1 gives three examples. At low laser energy the molecular ions at m/e = 252 and 253 are the only features of the mass spectrum. They are detected on more than 90% of the fibers analyzed. Their intensity is maximum around 0.5 μJ. At still higher energy the intensity starts leveling off and the inorganic cluster ions of crocidolite become the dominant peaks in the spectrum. The BaP doped crocidolite mass spectrum does not correspond entirely with that obtained from pure crocidolite fibers at a similar laser energy. The Mg^+ and Fe^+ elemental ions are considerably decreased in intensity sometimes even entirely absent from the spectra taken at low energy. Figure 2a,b illustrates this peculiar behavior which is presently unexplained.

When subsequent laser shots of comparable energy are directed at the same location of a fiber, the organic fragments gradually disappear from the spectra and at the same time the intensity of the crocidolite substrate increases but remains distorted compared to an undoped sample. Figure 2c shows a typical example of a spectrum taken after removal of most of the adsorbent through two previous laser shots. These observations indicate that LAMMA can be used as a rather crude depth probing device.

Negative spectra taken in similar conditions do not lead to a ready detection of the adsorbent. The spectra correspond closely with those obtained for pure crocidolite.

Gas-phase adsorption provided a bulk concentration of 580 μg g^{-1} of BaP as determined with gas chromatography. LAMMA analysis of the doped samples indicates an inhomogeneous distribution on the fibers. Indeed, a fraction of them give rise to the BaP molecular ions in the positive spectrum, another fraction not (ca. 25% and 75%, respectively). In the latter case several other peaks appear consistently in the spectra. Figure 3 shows a characteristic example of each of the two typical LD spectra obtained. It can be assumed that the mass spectral components at m/e = 348,

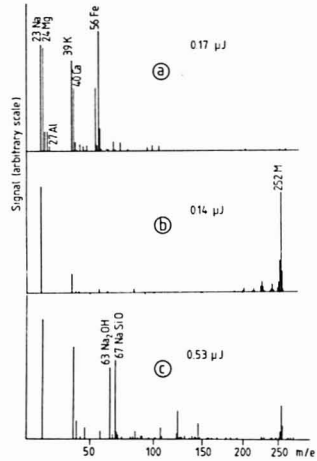


Figure 2. Positive laser mass spectrum of an untreated crocidolite fiber (a), a fiber doped with BaP from solution (b), and a fiber which was subjected to two previous laser shots (c).

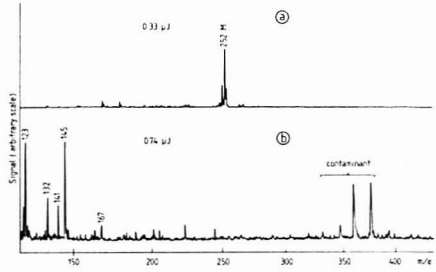


Figure 3. Typical positive laser desorption (LD) spectra of gas-phase BaP doped crocidolite: BaP containing fiber (a); fiber containing an accidental surface impurity (b).

360, and 376 ± 1 result from an organic surface contaminant present at the UICC crocidolite before the adsorption experiment, which inhibits further adsorption of the polyaromatic compound. Separate experiments proved the presence of the impurity on crocidolite when the material was stored into closed polyethylene bags of the same origin as the one used for the adsorption experiment.

It has been reported previously that the UICC asbestos standards are often contaminated by storage in polyethylene bags (25, 26). Bulk analysis has proved the presence of 3,3′,5,5′-tetra-*tert*-butyldiphenoquinone (molecular mass = 408) resulting from the presence of antioxidants in the polythene packing material (25). The absence of the molecular ion at m/e = 408 suggests the presence of other compounds in this particular sample. We are presently working on the elucidation of the component and several other contaminants in asbestos samples. Results will be published elsewhere.

Adsorption of Benzidine on UICC Asbestos. Benzidine was adsorbed onto the five UICC standards from an aqueous solution. This compound has been previously adsorbed onto clay minerals such as montmorillonite (27) and sepiolite and laponite (28). It gives rise to a good adsorption and to intense

Table I. Intensity Ratios of Different Elemental Ion Peaks to ^{23}Na for Benzidine Treated and Untreated Anthophylite Fiber Fibers

laser energy, μJ		relative intensity to ^{23}Na												
		^{24}Mg		^{27}Al		^{28}Si		^{39}K		^{40}Ca		^{56}Fe		benzidine m/e = 184
pure	treated	pure	treated	pure	treated	pure	treated	pure	treated	pure	treated	pure	treated	
0.37	0.39	20	50	9	5	<0.05	5	60	50	0.6	<1	3	7	60
0.45	0.45	20	10	3	0.3	0.02	0.3	35	2	0.6	0.3	1.1	2	1.3
0.68	0.63	50	20	1.1	1.3	0.1	0.4	1.2	0.2	4	0.8	2	7	0.03
0.88	0.92	50	7	1.3	0.1	5	1.0	0.5	0.04	0.7	0.3	3	1.5	0.009
1.14	1.13	30	5	0.8	0.09	10	0.3	0.5	0.003	2	0.3	3	1.5	0.001

Table II. Intensity Ratios of Different Elemental Ion Peaks to ^{23}Na for Benzidine Treated and Untreated Chrysotile A Fiber Fibers

laser energy, μJ		relative intensity to ^{23}Na												benzidine m/e = 184
		^{24}Mg		^{27}Al		^{28}Si		^{39}K		^{40}Ca		^{56}Fe		
pure	treated	pure	treated	pure	treated	pure	treated	pure	treated	pure	treated	pure	treated	
0.29	0.27	1300	0.01	40	0.02	20	0.01	4	0.05	12	0.01	20	0.01	2
0.49	0.52	300	0.1	14	0.01	3	0.002	1	0.2	25	0.02	20	0.1	0.2
1.01	1.05	50	1.0	10	0.005	6	0.01	2	0.03	2	0.1	4	0.3	0.1
1.17	1.14	30	1.5	9	0.2	12	0.3	0.2	0.07	0.5	0.2	3	0.7	0.001

coloration through the formation of radicals (*29*).

Procedure. A 70-mg asbestos sample is treated with 25 mL of 10^{-3} M benzidine dihydrochloride in bidistilled water. The slurry is stirred and heated to 60 °C during 19 h. The asbestos is filtered off with a Schleicher & Schüll filter and washed twice with bidistilled water. No coloration of asbestos is observed. The concentration of benzidine at the asbestos surface is roughly 1000 μg g^{-1} as determined by spectrophotometry.

LD conditions at laser energy down to 0.01 μJ provide intense positive and negative spectra of pure benzidine which are characterized by molecular ion peaks (M^+ = 184 and 185 in the positive spectrum, $(M-1)^-$ and $(M-2)^-$ in the negative. The mass peaks are ca. 3 times less intense in the negative spectra than in the positive. Higher masses derived, e.g., from the dihydrochloride are undetectable.

The positive mass spectra of benzidine adsorbed onto asbestos follows a similar behavior as a function of laser energy as those obtained for BaP on crocidolite. Figure 4 shows the results for chrysotile A. At the lowest laser energies used (<0.1 μJ) benzidine becomes detectable in nearly every fiber analyzed. No organic contaminants of the standard samples were detected because storage in polythene bags had been prevented. The intensity of the benzidine molecular ion peak again passes through a maximum (around 0.25 μJ) and the spectra obtained at higher laser energies contain a rapidly increasing contribution of the asbestos substrate. The intensity of the benzidine molecular peak is considerably lower for anthophyllite than for the other samples. This behavior is in accordance with the results of Markham and Wosczyna (*30*) who also obtained minimal adsorption of Aluminon (aurintricarboxylic acid, triammonium salt) for this type of asbestos.

The mass spectrum of the asbestos substrate obtained on the treated samples is again different from that obtained for the pure specimen. In general, in accord with the results for BaP, a reduction of apparent magnesium and iron intensity is obtained for crocidolite. Selected semiquantitative results obtained at closely similar laser energy for anthophyllite and chrysotile A are summarized in Tables I and II. They are expressed as intensity ratios to Na to take into account the inherent irreproducibility of the method. In general the ratios remain comparable between treated and untreated samples

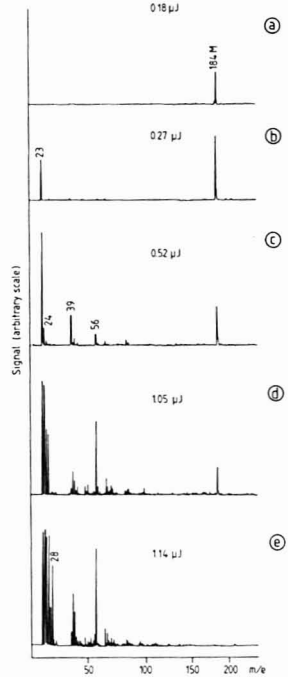


Figure 4. Positive mass spectra of benzidine adsorbed onto chrysotile A as a function of laser energy.

for anthophyllite, except for the anomalous behavior of the K/Na ratio. This is the result of the large and unexplained differences obtained for the K elemental ion intensities as a

function of laser energy. Repeated measurements indicate that its intensity is extremely high at very low laser energy of 0.1 μJ. It then drops, becomes systematically very high again between 0.35 and 0.50 μJ, and then drops again.

Compared to anthophyllite the differences between asbestos spectra of treated and untreated samples are very important for chrysotile A. These results cannot be explained by bulk leaching of the samples during treatment (*31*) as was verified by electron microprobe microanalysis nor by a different laser interaction process because of the presence of the organic material.

We assume that the difference could be explained by alterations of the chrysotile A fibrils to a state in which chemical changes occur in the outer layer. The brucite ($Mg(OH)_2$) external layer might be completely lost with a decrease of surface magnesium. The fact that above 1 μJ the magnesium intensity becomes comparable to that in the untreated sample would then imply that sufficient material becomes removed by the later interaction to reach the Mg atoms in the second layer about 1 nm below the surface. For the other elements listed in Table II, the general trend is the same, a loss in intensity, hence concentration, at the surface.

All this is quite speculative and needs further evidence from another surface analytical technique. We are presently using secondary ion mass spectrometry to obtain real depth profile information. If this evidence supports the explanation given, it indicates that LAMMA at low laser energy can provide surface and limited depth information. Significant in this context is that chrysotile samples containing the brucite outer layer provide a positive LD spectrum which contains an intense peak at $m/e = 41$, due to $MgOH^+$.

In the negative mass spectra, the benzidine molecular peaks are completely absent. The magnesium-containing ion clusters, e.g., $MgSiO_3^-$ at $m/e = 100$ and $MgSiO_4^-$ at $m/e = 116$ are considerably reduced in intensity compared to the untreated asbestos spectra, for the two chrysotile asbestos types. The decrease of Fe-containing clusters is less easy to quantitate as Fe- and Si-containing mass peaks interfere in the mass spectra (e.g., FeO_2^- and $Si_2O_2^-$ at $m/e = 88$).

Adsorption experiments were repeated for amosite at a concentration of benzidine of 0.15 M in a 0.03 M HCl solution. The suspension became slightly pink colored rapidly after the addition of the amosite to the solution. The intensity of the molecular ion at $m/e = 184$ was considerably higher than in the previous experiments. Also, it appeared that it persisted up to a laser energy in excess of 1 μJ. No asbestos-catalyzed reaction products of benzidine could be detected in the mass spectra.

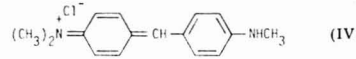
Adsorption of *N,N*-Dimethylaniline on UICC Standards. The oxidation of *N,N*-dimethylaniline (DMA) by various oxidation agents (e.g., cupric sulfate) and the formation of, e.g., Methyl Violet is a well-known process in the manufacturing of the dye. Also, coloration of synthetic Laponite by DMA has been studied with visible and infrared spectra (*32*). The coloration has been described by the following stages: (A) sorption of DMA, (B) oxidation by atmospheric oxygen into *N,N*-dimethyl-*N'*-methylbenzidine and bis[4-(*N,N*-dimethylamino)phenyl]-4-[(*N'*-methylamino)phenyl]-methane, and (C) further oxidation in an acidic environment to a blue quinoid cation or its protonated yellow component and to Methyl Violet. The reactions can be summarized as follows (*32*):

$$C_6H_5N(CH_3)_2 + [O] \rightarrow C_6H_5NHCH_3 + HCHO \quad (I)$$

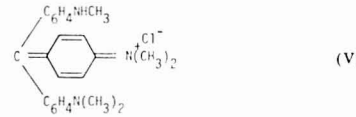
$$HCHO + C_6H_5NHCH_3 + C_6H_5N(CH_3)_2 \rightarrow HOH + (CH_3)_2NC_6H_4CH_2C_6H_4NHCH_3 \quad (II)$$

$$(CH_3)_2NC_6H_4CH_2C_6H_4NHCH_3 + C_6H_5N(CH_3)_2 + [O] \rightarrow HOH + [(CH_3)_2NC_6H_4]_2CHC_6H_4NHCH_3 \quad (III)$$

Further oxidation of (II) and (III) in HCl environment results in the formation of (IV) and (V), respectively:

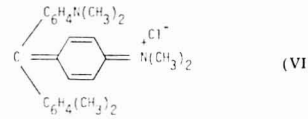


(IV)



(V)

Krüger et al. (*33*) suggested that the reaction of DMA with kaolinite resulted also in the formation of Crystal Violet (VI)



(VI)

N,N-Dimethylaniline was adsorbed onto acid treated UICC standards, which became intensely colored (blue-violet). We hence assumed that the oxidation reaction sequence derived for Laponite also proceeds for the asbestos.

Procedure. The samples are acid-treated by adding 40 mL 0.1 N HCl to 200 mg of UICC asbestos at room temperature. The mixture is stirred and warmed to between 80 and 90 °C under reflux for 24 h. The fibers are then filtered on a Schleicher & Schüll filter and washed five times with bidistilled water. The fibers are dried at 65 °C in a drying kiln.

A solution of 10 mL of DMA at variable concentration up to 5% in benzene and an equivalent amount of 0.1 N HCl are added to 20 mg of the acid-treated asbestos at room temperature. The mixture is stirred and warmed up to 80–90 °C under reflux for 5 h. Then the solution is evaporated to almost dry and the asbestos is recovered for analysis.

DMA adsorbed at various concentrations on the crocidolite asbestos fibers shows the following behavior in the negative spectra. At DMA concentration of up to 2%, elemental and molecular clusters of the asbestos substrate are present and fragments of the organic material occur at $m/e = 26, 42, 48, 49, 50, 72, 73$, and 74. At a 5% concentration, a characteristic pattern occurs. Figure 5a–c gives typical examples taken at ca. 2 μJ. When the laser energy is increased, the spectrum becomes complicated by the occurrence of peaks due to the asbestos substrate and by increased fragmentation, as shown in Figure 5d. As appears from Figure 6, the spectrum corresponds with the one obtained for Methyl Violet, although the abundance of the pattern around $m/e = 163$ is lower. When repeated spectra are taken at a particular location on a fiber, the asbestos mass spectrum is first absent and then starts dominating without a significant decrease of the organic components. This is demonstrated in Figure 7.

Positive mass spectra also show considerable amounts of information on reaction products of DMA. For pure Methyl Violet the most intense mass peaks obtained correspond with the molecular ions $(M - Cl^+)$ and $(M + CH_2 - Cl)^+$ at $m/e = 358$ and 372, respectively. A systematic feature is also that at lower m/e values fragments occur which are 14 amu below the most intense peak. When Methyl Violet is adsorbed onto crocidolite from a 5×10^{-4} M solution in water, spectra of the type shown in Figure 8a are obtained which show clearly the presence of the Methyl Violet fingerprint. As follows from Figure 8, the same peaks also occur at low intensity in positive

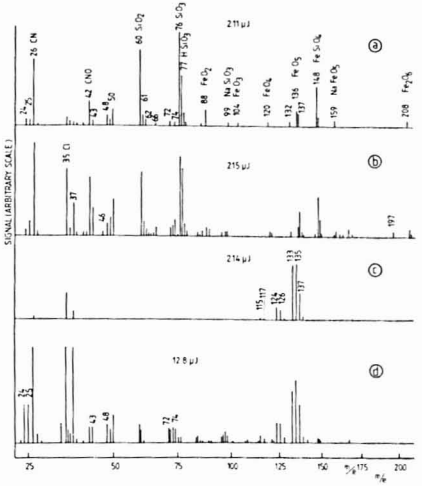


Figure 5. Negative mass spectra of *N,N*-dimethylaniline (DMA) adsorbed onto acid-treated crocidolite: (a) DMA concentration 0.1%; (b) 2%; (c) 5%, low laser energy; (d) 5%, high laser energy.

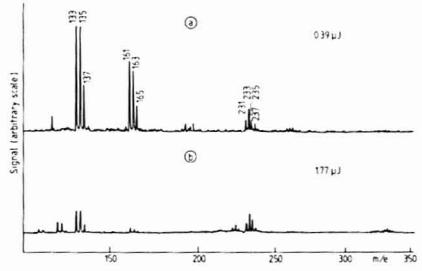


Figure 6. Negative mass spectra of pure Methyl Violet (a) and of 5% DMA/HCl treated crocidolite (b).

mass spectra of 5% DMA/HCl-treated crocidolite. Other characteristic peaks at m/e = 134, 239, and 253 are due to the fragments also shown in Figure 8. The small fragment at m/e = 121 is probably the DMA molecular ion.

It appears that several of the major catalytic oxidation products of DMA (*34*, *35*) which have previously been identified on bulk clay minerals (*32*), are clearly detectable on single crocidolite fibers. When DMA is adsorbed at a concentration of 5% on crocidolite fibers without the HCl treatment, none of the oxidation products can be detected. This again is in accordance with previous literature data (*32*). The positive and negative mass spectra of Crystal Violet are distinctly different from those of Methyl Violet. This compound was never detected in the 5% DMA/HCl treated asbestos.

The other UICC standards behave differently from crocidolite. Figure 9 shows typical positive spectra for chrysotile B, amosite, and anthophyllite. The spectra for chrysotile and amosite show the presence of Methyl Violet but the other fragments detected in treated crocidolite are now absent or barely detectable. The conclusion is that the oxidation re-

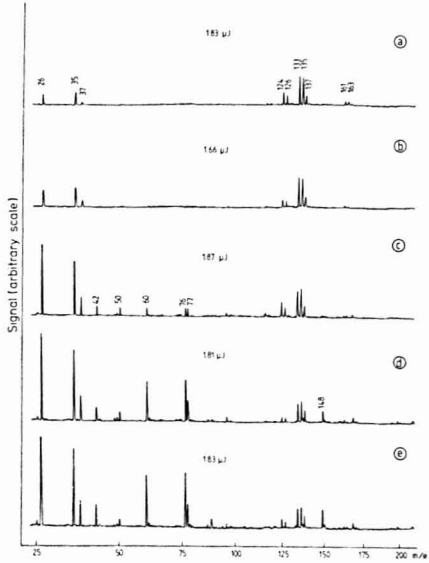


Figure 7. Negative spectra of five sequential laser shots on a single 5% DMA/HCl treated crocidolite fiber.

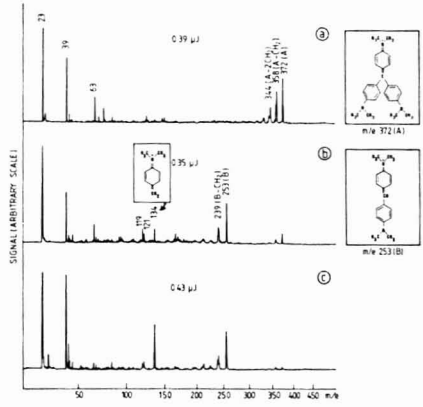


Figure 8. Positive LD mass spectrum of Methyl Violet adsorbed on crocidolite (a) and two characteristic LD mass spectra of 5% DMA/HCl onto crocidolite (b and c).

actions proceed more fully on these fibers. Another chrysotile sample, chrysotile A, gave similar results. In the spectra shown in Figure 9a,b, a number of barely detectable fragments around m/e = 446, 460 and 474 systematically occur, which indicates that probably further oxidation products have been formed. Anthophyllite does not show the presence of DMA nor any oxidation products (Figure 9c), which again proves the lesser reactivity of this asbestos variety.

The reproducibility of the mass spectra of individual fibers is in general excellent. Table III shows relative intensity ratios

Table III. Relative Negative Ion Intensity Ratio to m/e = 135 for Pure Methyl Violet and the DMA Treated Asbestos

	relative intensity				
m/e	methyl violet	crocidolite	amosite	chrysotile A	chrysotile B
124	21 ± 2	33 ± 4	36 ± 10	37 ± 7	22 ± 4
126	16 ± 2	26 ± 3	25 ± 6	29 ± 6	19 ± 3
128	3.4 ± 0.7	7.2 ± 0.9	7.0 ± 1.6	4.6 ± 1.0	4.1 ± 0.6
133	98 ± 2	96 ± 3	112 ± 3	105 ± 2	106.3 ± 1.9
135	100	100	100	100	100
137	37.0 ± 1.3	36 ± 1.6	35 ± 1.9	32.9 ± 0.9	31.7 ± 0.9
139	5.2 ± 0.3	5.1 ± 0.9	6.6 ± 0.6	5.2 ± 0.3	4.8 ± 0.7
161	78 ± 7	8.0 ± 0.9	1.4 ± 0.3	4.0 ± 0.6	3.6 ± 0.6
163	70 ± 6	8.2 ± 1.3	1.2 ± 0.2	4.1 ± 0.9	3.3 ± 0.5
165	23 ± 2	2.6 ± 0.5	0.7 ± 0.2	0.9 ± 0.2	1.4 ± 0.2
167	2.6 ± 0.3	1.1 ± 0.2	0.6 ± 0.2	0.4 ± 0.1	0.7 ± 0.1
222	2.1 ± 0.5	13.6 ± 0.9	17 ± 3	14.6 ± 1.6	12.7 ± 1.6
224	3.4 ± 0.8	21.3 ± 1.3	21 ± 4	20 ± 3	16.8 ± 1.9
226	2.4 ± 0.5	10.1 ± 0.9	13 ± 2	11.5 ± 1.3	8.9 ± 1.3
228	1.0 ± 0.2	4.0 ± 0.6	3.1 ± 0.8	3.7 ± 0.7	2.4 ± 0.6
231	15 ± 0.9	43 ± 4	44 ± 3	43 ± 3	46 ± 4
233	27 ± 1.6	78 ± 6	66 ± 4	64 ± 5	75 ± 7
235	19 ± 1.3	58 ± 5	38 ± 2	37 ± 3	50 ± 5
237	6.8 ± 0.4	16 ± 2	12 ± 1.6	11.4 ± 0.9	16 ± 1.6
239	1.7 ± 0.3	5.1 ± 0.9	3.3 ± 0.7	3.3 ± 0.7	2.7 ± 0.4
329	0.8 ± 0.2	7.1 ± 0.8	7.8 ± 0.9	11.0 ± 1.6	8.9 ± 1.3
331	1.7 ± 0.2	18 ± 2	18 ± 2	24 ± 3	21 ± 3
333	2.2 ± 0.3	22 ± 2	18.7 ± 1.9	22.1 ± 1.9	21.8 ± 3
335	1.5 ± 0.2	13.4 ± 1.6	10.4 ± 0.9	12.7 ± 1.3	12.5 ± 1.6
337	0.7 ± 0.2	6.1 ± 0.9	3.3 ± 0.6	4.5 ± 0.7	4.7 ± 0.7
339	0.6 ± 0.2	1.6 ± 0.5	1.1 ± 0.4	1.6 ± 0.4	4.7 ± 0.3

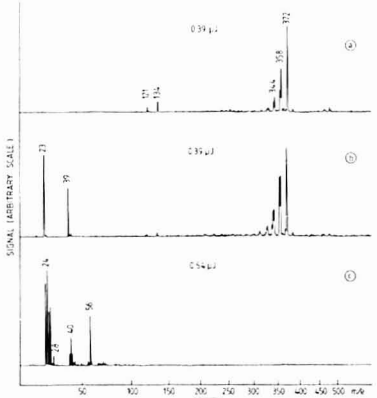


Figure 9. Positive LD spectra of 5% DMA/HCl on chrysotile B (a), amosite (b), and anthophyllite (c).

of a number of molecular fragments to the peak at m/e = 135 for three different asbestos types and Methyl Violet. All spectra were collected in similar conditions at a laser energy of ca. 1 μJ. Anthophyllite did not yield detectable mass peaks. As indicated earlier the pattern at m/e = 161, 163, 165, and 167 is considerably reduced in intensity in relation to the reference compound. Also, for other groups there are statistically significant differences in relative intensity between the Methyl Violet spectra and the treated asbestos fibers. The reasons for these differences are presently unknown. The mass spectra of the two chrysotile varieties are closely similar, which stresses again their similarity in adsorption and reaction behavior. The amphiboles crocidolite and amosite give rise to a different intensity distribution. Only the pattern between

Table IV. Relative Intensity Distribution of Elemental Ion Peaks for Pure, Acid Treated, and DMA + Acid Treated Crocidolite

	rel intens ratio to Na^+ (std dev)		
element	pure	HCl treated	5% DMA/HCl treated
Mg	0.073 ± 0.018	0.059 ± 0.009	0.022 ± 0.004
Al	0.013 ± 0.004	0.0031 ± 0.0008	0.0030 ± 0.0005
Si	0.084 ± 0.022	0.08 ± 0.03	0.019 ± 0.009
K	0.35 ± 0.05	0.013 ± 0.002	0.024 ± 0.008
Ca	0.063 ± 0.019	0.018 ± 0.003	0.020 ± 0.008
Mn	0.006 ± 0.002	0.0008 ± 0.0002	0.0006 ± 0.0003
Fe	0.51 ± 0.05	0.60 ± 0.06	0.13 ± 0.02

m/e 161 to 167 is significantly different for these two asbestos types.

The asbestos spectra of 5% DMA/HCl-treated fibers are significantly different from those obtained for the raw standard fibers and acid treated fibers. Relative intensity ratios to Na^+ are summarized in Table IV for crocidolite for measurements at a laser energy of 0.8 μJ. The results corroborate earlier conclusions for benzidine and benzo[*a*]pyrene.

Registry No. BaP, 50-32-8; DMA, 121-69-7; benzidine, 92-87-5; methyl violet, 8004-87-3; crocidolite, 12001-28-4; anthophyllite, 17068-78-9; chrysotile, 12001-29-5.

LITERATURE CITED

(1) Bowen, M. D. H. *Environ. Sci. Technol.* **1970**, *4*, 727.
(2) Hodgson, A. A. *Phil. Trans. R. Soc. London, Ser. A* **1977**, *286*, 611–624.
(3) Harington, J. S. *Ann. N.Y. Acad. Sci.* **1965**, *132*, 31–47.
(4) Jaurand, M. C.; Bignon, J.; Sebastien, P.; Goni, J. *Environ. Res.* **1977**, *14*, 245.
(5) Kohyama, N.; Kawai, K.; Alta, S.; Puzuki, M.; Hayashi, H. *Ind. Health* **1977**, *15*, 159.
(6) Morgan, A.; Davies, P.; Wagner, J. C.; Berry, G.; Holmes, A. *Br. J. Exp. Pathol.* **1977**, *58*, 465.
(7) Miguel, A. H.; Natusch, D. F. S. *Anal. Chem.* **1975**, *47*, 1705–1707.
(8) Wieser, P.; Wurster, R.; Seiler, H. *Atmos. Environ.* **1980**, *14*, 485–494.
(9) Wieser, P.; Wurster, R.; Haas, U. *Fresenius' Z. Anal. Chem.* **1981**, *308*, 260–269.

(10) Adams, F.; Bloch, P.; Natusch, D. F. S.; Surkyn, P. Proceedings of the International Conference on Environmental Pollution, Thessaloniki, Greece, Anagnostopoulos, A., Ed.; Thessaloniki University, 1982; pp 122-142.
(11) Surkyn, P.; De Waele, J.; Adams, F. *Environ. Anal. Chem.*, in press.
(12) Denoyer, E.; Van Grieken, R.; Adams, F.; Natusch, D. F. S. *Anal. Chem.* **1982**, *54*, 26A-41A.
(13) Spurny, K. R.; Schörmann, J.; Kaufmann, R. *Fresenius' Z. Anal. Chem.* **1981**, *308*, 274-279.
(14) De Waele, J.; Van Espen, P.; Vansant, E.; Adams, F. "Proceedings of the 17th Annual Conference on Microbeam Analysis, Washington, DC, Aug 9-13, 1982; Heinrich, K. F. J., Ed.; San Francisco Press. Inc.: San Francisco, CA, 1982; pp 371-377.
(15) Kaufmann, R.; Hillenkamp, H.; Wechsung, R. *Med. Prog. Technol.* **1979**, *6*, 109-120.
(16) Vogt, H.; Heinen, M. J.; Meier, S.; Wechsung, R. *Fresenius' Z. Anal. Chem.* **1981**, *308*, 195-200.
(17) Heinen, M. J.; Meier, S., Vogt, H., Wechsung, R. *Fresenius' Z. Anal. Chem.* **1981**, *308*, 290-296.
(18) Busch, K. L.; Unger, S. E.; Vincze, A.; Cooks, R. G.; Keough, T. *J. Am. Chem. Soc.* **1982**, *104*, 1507-1511.
(19) Balasanmugam, K.; Fuan Anh Dang, R. J.; Hercules, D. M. *Anal. Chem.* **1981**, *53*, 2296-2298.
(20) Timbrell, V.; Rendall, R. E. G. *Powder Technol.* **1971/1972**, *5*, 279-287.
(21) Timbrell, V. Pneumoconiosis, Proceedings of the International Conference, Johannesburg, 1969; pp 28-36.
(22) Timbrell, V.; Gilbson, J. C.; Webster, I. *Int. J. Cancer* **1968**, *3*, 406-408.
(23) Timbrell, V. "Biological Effects of Mineral Fibers"; Wagner, J. C., Ed.; IARC Scientific Publications: Lyon, 1980; No. 30, Vol. 1, pp 127-142.
(24) Korfmacher, W. A.; Miguel, A. M.; Mamamtov, G.; Wehry, E. L.; Natusch, D. F. S. *Environ. Sci. Technol.* **1979**, *13*, 1224.
(25) Commins, B. T.; Gibbs, G. W. *Br. J. Cancer* **1969**, *23*, 358-362.
(26) Hibborn, J.; Thomas, R. S.; Lao, R. C. *Sci. Total Environ.* **1974**, *3*, 129-140.
(27) Lahav, N., Raziel, S. *Isr. J. Chem.* **1971**, *9*, 683.
(28) Furukawa, T.; Brindley, G. W. *Clays Clay Miner.* **1973**, *21*, 279.
(29) Yariv, S.; Lahav, N.; Lacher, N. *Clays Clay Miner.* **1976**, *24*, 51.
(30) Markham, M. C.; Wosczyna, K. *Environ. Sci. Technol.* **1976**, *10*, 930-931.
(31) Chowdhury, S. *J. Appl. Chem. Protechnol.* **1975**, *25*, 347-353.
(32) Vansant, E. F.; Yariv, S. *J. Chem. Soc., Faraday Trans. 1* **1977**, *73*, 1815-1824.
(33) Kruger, D.; Oberlies, F. *Naturwissenschaften* **1943**, *31*, 92.
(34) Noller, C. R. " Textbook of Organic Chemistry", 3rd ed.; Saunders: Philadelphia, PA, 1966.
(35) Feigl, F. "Spot Tests in Organic Analysis", 7th ed.; Elsevier: Amsterdam, 1966.

RECEIVED for review September 21, 1982. Accepted December 15, 1982. This research was funded by the EEC through research Grant No. ENV-486-BCN and by the Interministrial Commission for Science Policy, Belgium, through research grant 80-85/10. J.K.D.W. is indebted to the "Instituut tot Aanmoediging van het Wetenschappelijk Onderzoek in Landbouw en Nijverheid (IWONL)" for financial support.

Determination of Chlorinated Pesticides in Urine by Molecular Neutron Activation Analysis

Laura R. Opelanio and Edward P. Rack*

Department of Chemistry, University of Nebraska—Lincoln, Lincoln, Nebraska 68588-0304

Alan J. Blotcky

Medical Research, Veterans Administration Medical Center, Omaha, Nebraska 68105

Frank W. Crow

Midwest Center for Mass Spectrometry, University of Nebraska—Lincoln, Lincoln, Nebraska 68588-0304

A molecular neutron activation analysis (MoNAA) procedure employing solvent extraction and high-performance liquid chromatography separation techniques with subsequent irradiation of the eluted fractions and radioassay for ^{38}Cl activity is applied to the determination of trace quantities of DDT and its metabolites DDA [bis(*p*-chlorophenyl)acetic acid], DDD [1,1-dichloro-2,2-bis(*p*-chlorophenyl)ethane], and DDE [1,1-dichloro-2,2-bis(*p*-chlorophenyl)ethylene] in urine. Data and confirmation analyses using mass spectrometry are presented.

The toxic nature and unknown long term effects of chlorinated pesticides to living organisms necessitate the need to evaluate continually their presence in the environment. While the trichlorobis(*p*-chlorophenyl)ethane family of compounds (DDT) have been banned from use in many countries, they are still widely used in many Third World countries, and thus their continued use can constitute a serious problem for the global population (*1*). The urinary excretion of bis(*p*-chlorophenyl)acetic acid (DDA), a metabolite of DDT, can be used as an indicator of exposure to DDT (*2-5*).

The current Environmental Protection Agency (EPA) procedure available for the determination of DDA involves chemical derivatization and gas chromatographic separation employing a ^{63}Ni electron capture detector (*6*, *7*). Unlike previous procedures, where chemical derivatization is employed prior to GC separation, this study develops a method of separating out, and then determining DDT and its metabolites, DDA, DDD, and DDE by means of instrumental neutron activation analysis—simultaneously with minimum interference from other chlorinated hydrocarbons. Separation is performed by high-performance liquid chromatography (HPLC) with subsequent neutron activation of the collected eluent and radioassay for ^{38}Cl activity. It is important to realize that if one is analyzing urine for trace DDA by neutron activation analysis, all chemical separations must be performed prior to neutron irradiation rather than after activation. By virtue of the (n,γ) reaction on ^{37}Cl, the emission of the prompt γ-rays creates an energetic ^{38}Cl recoil atom which breaks greater than 99% of the original chlorine bonds. The recoil ^{38}Cl atom undergoes new chemical reactions with its environment; thus it finds itself in a different chemical form than originally present in the urine sample. Our confirmation analysis is not an automated LC/MS approach (*8*), but an

0003-2700/83/0355-0677$01.50/0 © 1983 American Chemical Society

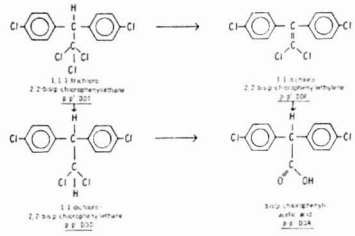


Figure 1. Chemical structures and metabolic pathways of DDT and its metabolites.

off-line LC/MS technique involving an independent collection of HPLC fractions followed by mass spectrometric analysis. This approach has a distinct advantage of giving those workers in the field choices in undertaking their DDA determinations.

DDT has an affinity for lipid tissues in animals since it is fat soluble. Ingestion, even in trace amount, results in storage and concentration in fatty tissues, where it is slowly dehydrochlorinated to DDE and/or DDD and ultimately excreted as DDA in urine. Figure 1 illustrates the structures of DDT and its metabolites. Urine is a complex matrix for analysis, regardless of the technique employed, because of the number of ions and molecular compounds present. The presence of radioactivable sodium and chloride ions in urine presents a severe problem in neutron activation analysis. In a recent study we developed a procedure for trace level determination of iodoamino acids and hormonal iodine in a urine matrix employing a combined HPLC/NAA technique which is a form of what we term "molecular neutron activation analysis" (MoNAA) (*9*). Our procedure requires that the compounds of interest contain radioactivable atoms that have high neutron cross sections and that form radionuclides of suitable half-lives for radioassay. It is also important that these compounds be in a form amenable to chemical separation without prior irradiation. No acid digestion procedure can be employed, since this can change the identity of the trace compounds. Since chlorinated compounds, such as plasticizers and pesticides, are ubiquitous in nature, their potential interference can make the analytical task for specific identification, especially at the trace level, very difficult. For this reason, analysts have employed various cleanup techniques, such as column adsorption, prior to a gas or liquid chromatographic step (*3*, *10*).

EXPERIMENTAL SECTION

Reagents and Solvents. Burdick and Jackson Laboratories, Inc. (Muskegon, MI), HPLC-grade hexane and methanol were used without further purification. ACS reagent-grade glacial acetic acid from Fisher Scientific, Inc. (Fairlawn, NJ), was used as received. Solvent mixtures were degassed under vacuum prior to use. For preparation of spiked urine, 1,1,1-trichloro-2,2-bis-(*p*-chlorophenyl)ethane (or p-p'DDT), 1,1-dichloro-2,2-bis(*p*-chlorophenyl)ethylene (or p-p'DDE), 1,1-dichloro-2,2-bis(*p*-chlorophenyl)ethane (or p-p'DDD), and bis(*p*-chlorophenyl)acetic acid (or p-p'DDA) from Aldrich Chemical Co., Inc. (Milwaukee, WI), were used. Triply distilled water, showing negligible activity after a 140-min reactor irradiation, was used in all phases of the procedure.

Pre-HPLC Sample Preparation. The solubility of DDT and its metabolites in organic solvents allows their extraction from urine, using 2% glacial acetic acid in hexane. For each determination, one urine blank and one urine sample spiked with a known amount of DDA, DDD, DDT, and DDE were used, employing the same extraction procedure for both.

Twenty milliliters of urine (raw or spiked) was diluted with 20 mL of distilled deionized water and extracted twice with 10 mL of 2% glacial acetic acid in hexane for a maximum extraction yield. It was necessary to acidify the urine during solvent extraction to keep the DDA in the acid form and hence to obtain a maximum extraction recovery. Although urine contains a large amount of radioactivable sodium and chlorine, removal of these contaminants was afforded by the solvent extraction procedure. The chlorinated compounds of interest are insoluble in the aqueous phase, while inorganic salts, such as those of sodium and chlorine, are highly soluble. The extracts were combined and centrifuged at 3300 rpm for 45 min to break the emulsion formed by shaking the sample. The hexane layer was evaporated to dryness with nitrogen gas, to allow a change of solvent into the reversed-phase elution solution—consisting of a 60 + 20 + 20 (v/v) methanol–water–acetic acid mixture ready for injection into the liquid chromatograph.

HPLC Instrumentation, Columns, and Separation. An ISCO Model 1440 liquid chromatograph equipped with a Model 314 metering pump and a Model UA-5 absorbance monitor with built-in recorder was used. The eluent was collected employing an ISCO Model 328 fraction collector (collecting 1 mL volume in polystyrene Autotechnicon vials). Two reversed-phase Whatman columns were evaluated: 6.35 × 250 mm Partisil 5-ODS and Partisil 10/C_8. Both columns were protected with a 7 cm × 2.1 mm i.d. guard column dry-packed with Whatman Co:Pell ODS (25–37 m). The Partisil 5-ODS column afforded the better separation for DDT and its metabolites, as seen in Table I. The solvent reservoir, guard column, and the column itself were operated at ambient temperature. The mobile phase consisted of 60 + 20 + 20 (v/v) methanol–water–glacial acetic acid mixture was maintained at a flow rate of 1 mL/min and a pressure of 2100 psi. The mobile-phase solvent was degassed prior to use, and isocratic elution was employed. The ultraviolet detection was set at a wavelength of 254 nm. Two separate HPLC runs were made, one of the spiked urine and the other of the blank urine sample. The fractions in which the chlorinated compounds of interest elute were combined and subjected to neutron activation and radioassay. Samples for confirmation analysis by mass spectrometry were subjected to exactly the same solvent extraction and liquid chromatographic procedures. The HPLC fractions containing the chlorinated compounds were evaporated to dryness with dry nitrogen gas and brought up to 1-mL volume with methanol for DDA, and with hexane for the fractions containing DDD, DDT, and DDE.

Neutron Irradiation. Glassware, polystyrene, and polyethylene collection vials were all acid-washed with nitric acid and rinsed with distilled deionized water to remove possible radioactivable contaminants. Irradiation was done in the Omaha VA Medical Center TRIGA Mark I Reactor operating at a thermal-neutron flux of 1×10^{11} neutrons cm^{-2} s^{-1}. The samples were irradiated in the rotary specimen rack of the facility for 140 min and allowed to decay for 5 min before conventional radioassay.

Radioassay. γ-Ray spectrometry was conducted with a 60-cm^3 coaxial lithium-drifted germanium detector (Princeton Gamma Tech) and a Nuclear Data ND 600 4096-channel analyzer, or two each 3 in. × 3 in. NaI(Tl) detectors in parallel and an ND 2400 2096-channel analyzer. The Ge(Li) system had a resolution of 2.0 kV (fwhm), a peak-to-Compton ratio of 37:1, and a relative peak efficiency of 11.3% for the 1.332 MeV γ of ^{60}Co.

Mass Spectrometric Conditions and Instrumentation. Solid probe analysis of DDA was performed on a Kratos MS-50 (Manchester, England) double-focusing high-resolution mass spectrometer. The instrument was operated in the electron-impact mode, with a source temperature of 250 °C and an electron energy of 70 eV. Samples were introduced via solids inlet probe and volatilized by heating the probe. The molecular ion peaks at m/z 280 and m/z 282 were monitored via a multiple ion monitor peak switch unit (*11*). The instrument was operated at a resolution of 20 000 to avoid interference peaks resulting from sample contamination. Data for these two ions were stored in a Nicolet (Madison, WI) signal averager and processed by a computerized quantitative analysis program written to operate in the Kratos DS-55 data system.

DDD, DDT, and DDE were determined employing a Kratos MS-80 medium-resolution mass spectrometer (ultimate resolution 20 000) equipped with a five-channel multiple peak monitoring (MPM) device. The instrument was directly coupled with a Carlo Erba gas chromatograph operating with a SE-54 fused silica

Table I. Retention of DDT and Its Metabolites with LC Columns

column	solvent for standard	mobile phase	DDA		DDD		DDT		DDE					flow rate, mL/H
			t_R(A),[a] min	W_b,[b] min	t_R(B), min	W_b, min	t_R(C), min	W_b, min	t_R(D), min	W_b, min	$\alpha_{B/A}$[c]	$\alpha_{D/B}$	$\alpha_{D/C}$	
Partisil 10/C_8	B[d]	A[d]	4.3	2.1	4.9	3.6	4.5	3.6	4.2	3.4	1.14	0.86	0.93	52
	B	A	3.4	0.4			13.4	3.4						90
	B	95A:5C	6.4	1.2	4.2	2.5	4.4	2.4	4.1	3.0	0.66	0.98	0.93	52
	D × A	A	27.8	5.0										60
	D × A	A	24.1	5.2			3.0	2.0						90
Partisil 5-ODS	A	A	17.6	2.4										60
	B × B	B	11.4	2.6			5.4	1.2						60
	B	A			13.4	0.8	14.2	0.8						90
	B	A	25.2	2.6	4.2	4.0	4.6	4.0	4.6	4.3	0.17	1.10	1.00	52
	B	85A:15C	4.3	3.1	4.2	5.5	4.4	4.0	4.0	3.4	0.98	0.95	0.91	52
	B S D	B			5.6	2.2	5.0	1.6	5.2	2.2		0.93	1.04	52
	90A:10C	B	9.6	0.9	1.6									52
	90D:10E	90A:10E	5.7	0.9			3.2	1.8						130
	90A:10C	90D:10C	9.8	1.2										52
	90A:10C	90A:10C	4.4	1.6										130
	90A:10C	90A:10C	7.7	4.2	2.6	1.0	2.7	1.3			0.34			90
	60D:20F:20G	60D:20F:20G	3.5	2.1	8.4	2.5	12.5	2.5	15.5	4.0	2.47	1.81	1.25	60

[a] Retention time. [b] Base width. [c] Separation factor. [d] A = heptane, B = hexane, C = butanol, D = methanol, E = 2-butanol, F = water, G = glacial acetic acid, H = propionic acid; S = saturated with, X = extracted with.

capillary column (0.25 mm × 30 m). The gas chromatograph (GC) was operated employing a helium carrier gas with a linear velocity of ~35 m/s, an injector temperature of 250 °C, and a detector temperature of 275 °C. The oven temperature was programmed from 200 °C to 280 °C at 5 °C/min during the analysis. A split injection technique was used. The mass spectrometer was operated in the electron-impact mode, with a source temperature of 250 °C and an electron energy of 70 eV at a resolution of 3000. The peak profiles were acquired at an amplifier bandwidth of 30 000 Hz. MPM was used to monitor the following ions: m/z 317.9352 (molecular ion + 2) for DDE, m/z 237.0052 (fragment ion) for DDD and for DDT as well. The instrument was tuned by using m/z 280.9824 of perfluorokerosene (PFK), which was also used as a check mass during the analysis. The output was recorded on a Linear Model 595 three-pen strip chart recorder.

RESULTS AND DISCUSSION

Several methods have been developed for the routine determination of DDA excretion levels in urine. Cueto et al. (7) employed a colorimetric procedure after DDA recovery from urine by using an ion exchange resin. The method which has been adopted by the Environmental Protection Agency involves derivatization with boron trifluoride in methanol after a solvent extraction step, ultimately followed by a gas chromatographic separation utilizing ^{63}Ni electron-capture detection. No attempt has been made, prior to the present work, to approach the problem via a liquid chromatographic route. While an electron capture detector may be a thousand times as sensitive as the conventional HPLC ultraviolet detector, neutron activation analysis can be employed as a specific HPLC detector for compounds having radioactivable atoms in their structures. It was our main intent to develop a combined HPLC/NAA procedure for the quantitation of DDA in a urine matrix in the presence of the other metabolites and of DDT itself. The presence of radioactivable chlorine atoms in the structures of DDT and its metabolites makes them eligible for determination by neutron activation.

Solvent Extraction Procedure. Solvent extraction is the technique of choice for preparing pesticide samples, prior to chromatographic separation, because of the major advantages it offers, such as concentration of the sample, removal of aqueous radioactivable contaminants (such as sodium and chlorine), and its inherent simplicity. Since our MoNAA procedure involves a radioassay of ^{38}Cl activity, it is important that all the reagents and solvents to be used be evaluated for their chlorine content and for other possible radioactivable interferences. Jacobs et al. (12) conducted a study on the trace element composition of some commonly used organic solvents and concluded that HPLC-grade solvents do not necessarily have lower trace element contents than reagent grades. We used instrumental neutron activation analysis as employed by Jacobs et al. to determine the possible radioactivable elements in all our solvents and reagents. A low but significant ^{38}Cl activity was observed in methanol, thus causing an increase in the detection limit of our MoNAA technique. We did not see such contribution from hexane, glacial acetic acid, and distilled water when subjected to the same analysis.

Because it is highly possible for DDA to be excreted in urine as conjugates of amino acids (10), we incorporated a digestion step into our solvent extraction procedure to evaluate this possibility. We added 9 M sulfuric acid into the raw or spiked urine and performed a digestion, at ambient temperature prior to the solvent extraction step, by shaking the mixture in an automatic shaker for 30 min. However, the sulfuric acid digestion resulted in a gross enhancement in the DDA recovery, with concomitant decrease in the yields of DDT, DDD, and DDE. Apparently the sulfuric acid digestion facilitates the conversion of DDT and lower metabolites to DDA. Since we were using a reversed-phase HPLC, it was necessary to evaporate the hexane layer to dryness, using nitrogen gas, and

Table II. Efficacy of the Method

amt expected,[a] μg/mL	MoNAA result, μg/mL	MS result,[b] μg/mL
DDA 0.57	0.51 (88.8%)[c]	0.52 (91.0%)[c]
DDD 4.10	3.76 (91.6%)	3.77 (92.0%)
DDT 1.49	1.29 (86.7%)	1.20 (80.5%)
DDE 1.78	1.70 (95.4%)	1.68 (94.4%)

[a] The number of micrograms of compound per milliliter of urine. [b] The mass spectrometry result for DDA was obtained by using the solid probe technique, while results for DDD, DDT, and DDE were obtained by GC/MS. Mass spectrometric conditions are given in the Experimental Section. [c] The recoveries have been found to be reproducible within 5% variation and independent of the trace molecular concentrations in the range studied. Yields can be determined by employing spiked samples.

then dissolve and adjust the residue to volume with the HPLC elution solution so that it was ready for injection into the liquid chromatograph.

Extraction recovery of the chlorinated compounds was investigated by doing solvent extraction on urine spiked with DDT and its metabolites in the sub-parts-per-million range. The combined extracts (hexane layer from the first and second extractions) were irradiated with neutrons and radioassayed for ^{38}Cl activity. Extraction recoveries obtained for all the compounds were nearly 100%.

High-Performance Liquid Chromatography Separation Procedure. Table I shows the retention times of DDT and its metabolites, as well as the mobile phases and flow rates employed. Both normal and reversed-phase elution modes were considered and evaluated. The Partisil $10/C_8$ column afforded poor resolution for the polychlorinated compounds. For all compounds and conditions, the chloride ion eluted almost immediately and was separated before the appearance of any of the polychlorinated compounds. The Partisil 5-ODS column gave the best separation for DDT and its metabolites with the solvent system consisting of 60 + 20 + 20 (v/v) methanol–water–acetic acid. DDA contains a carboxyl group and undergoes a normal chemical equilibrium based on ionization. Separations of ionizable species in conventional reversed-phase HPLC would ordinarily result in poor retention and peak tailing. However, by suppressing the ionization, that is, by having a mobile phase with a low pH of about 2 to 3, retention would be increased and peak symmetry improved (*12–15*). The acetic acid ($pK_a = 4.76$) in the solvent mixture served this purpose. The reproducibility of the separation was also enhanced by the presence of acetic acid in the mobile phase. Because of the multiplicity of the polychlorinated biphenyls (PCBs) and other related pesticides, such as 2,4D, the mere separation of the DDT and its metabolites may not be sufficient as a criterion for their identification. Polychlorinated biphenyl mixtures, Arochlor 1254 and Arochlor 1242, interfere sufficiently with the HPLC separation of DDT, DDE, and DDD but not of DDA. However, 2,4D or any other substituted acetic acid analogue will interfere with the determination of DDA without any previous derivatization or separation employing Florisil. An ultraviolet detector (UV) with a fixed wavelength at 254 was used on all chromatographic runs. It can be seen from Figure 2 (upper figure), which illustrates the UV detector response at 254 nm with respect to the elution volume containing urine from the solvent extraction procedure discussed in the previous section, that human urine contains compounds, probably amino acids, which would interfere in the determination of DDA. It would then be a difficult task to distinguish between these compounds and DDA just by relying on the UV detector response; hence, it becomes necessary to use neutron activation analysis as a detection device in lieu of the built-in UV detector. DDT

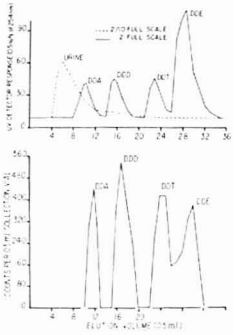


Figure 2. Chromatograms of human urine (---) and human urine spiked with 1.0 ppm of the chlorinated compounds (—) after a solvent extraction step (upper figure), employing a neutron activation detection of ^{38}Cl after a solvent extraction step (lower figure).

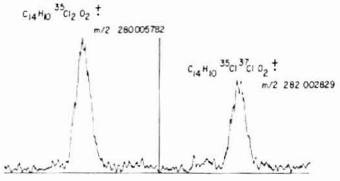


Figure 3. Selected ion high-resolution (R = 20 000) mass spectra for 100 ng of DDA. Each scan window is 300 ppm wide.

and its metabolites contain chlorine (24.23% chlorine-37), which when irradiated with neutrons in the nuclear reactor produces ^{38}Cl with a half-life ($T_{1/2}$ = 37.3 min) and radioemanations suitable for γ-ray spectrometry. Neutron activation of HPLC fractions where DDT and its metabolites elute is highly specific and sensitive in analyzing for the ^{38}Cl activity. Illustrated in Figure 2 (upper figure) is a typical HPLC chromatogram of 1000 ppb spiked DDT, DDD, DDE, and DDA in an urine matrix. The dotted lines represent the chromatogram of a blank urine sample, showing a peak which is not DDA but probably due to amino acids in urine. The radioassay responses of the chlorinated compounds are shown in Figure 2 (lower figure).

Mass Spectrometry. Confirmation analysis for DDA was performed employing a double-focusing high-resolution mass spectrometer monitoring molecular ion peaks at m/z 280 and m/z 282 (Figure 3) at 20 000 resolving power. Solid probe analysis may also be performed on DDE, which gives intense molecular ion peaks at m/z 318 and m/z 320. However, DDT is expected to interfere because it gives small fragment ions in the region of m/z 320. DDD and DDT have very similar electron-impact fragmentation patterns, both giving significant fragment ions at m/z 235 and no molecular ion. Therefore, the distinction between DDD and DDT could not be made by using the solid probe technique. However, these three chlorinated compounds, DDD, DDT, and DDE, could be distinguished based on their GC retention data. By employing gas chromatographic mass spectrometry, the molecular ion peaks of DDE could be monitored without any interference from DDT. Also, DDD and DDT could now be monitored at m/z 235. The gas chromatograms of DDD, DDT, and DDE are shown in Figure 4.

Detection Limits. Detection limits afforded by the MoNAA procedure are quite dependent on the neutron flux of

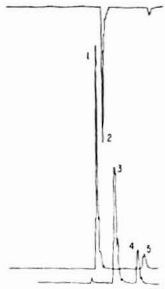


Figure 4. GC/MS selected ion chromatograms of the chlorinated compounds DDD, DDT, and DDE using a three-pen strip chart recorder. Peaks shown correspond to DDE, (1) and (2); DDD, (3); and DDT, (4) and (5). The masses monitored were m/z 317.9352 for DDE and m/z 237.0052 for DDD and DDT.

Table III. Limits of Detection by Molecular Neutron Activation Analysis

	limit, ng/mL of urine[a]	
	Ge(Li) detector[b]	NaI(Tl) detector
1×10^{12} thermal-neutrons cm^{-2} s^{-1}		
DDA	10.6	2.1
DDD	7.0	1.4
DDT	6.0	1.2
DDE	6.4	1.3
1×10^{13} thermal-neutrons cm^{-2} s^{-1}		
DDA	1.1	0.2
DDD	0.7	0.1
DDT, DDE	0.6	0.1
1×10^{14} thermal-neutrons cm^{-2} s^{-1}		
DDA	0.11	0.02
DDD	0.07	0.01
DDT, DDE	0.06	0.01

[a] Detection limit—minimum detectable concentrations that will give a signal exceeding critical level 95% of the time. [b] In comparing the efficiencies of the two detectors, it was found that the Ge(Li) detector is 19.98% as efficient as the NaI(Tl) crystal for ^{38}Cl activity.

the nuclear reactor. Presented in Table III are the limits of detection for the reactor procedure employing both Ge(Li) and NaI(Tl) detectors. It is quite apparent from inspection of Table III that for the determination of chlorinated pesticides in urine in the parts-per-billion range a nuclear reactor with a neutron flux of at least 1×10^{12} neutrons cm^{-2} s^{-1} must be employed. By employing urine samples that have been spiked with sub-parts-per-million concentrations of the chlorinated compounds, we found, in general, relative standard deviations of about ±5%. This study demonstrates the feasibility of nuclear activation as a specific HPLC detector for compounds having radioactivable atoms in complex biological samples such as urine or serum.

Presented in Table IV are the limits of detection of the chlorinated pesticides employing mass spectrometry. The same procedure leading up to neutron activation and radioassay was employed in preparing samples for mass spectrometry. As can be seen in Table IV, the limits of detection are sufficiently low to allow routine analysis for any of the chlorinated pesticides by the described procedure. It appears that the mass spectrometry procedure would allow routine analysis of urine samples processed by the solvent extraction–HPLC steps.

Table IV. Limits of Detection by Mass Spectrometry

	limit,[a] ng/mL of urine	S/N[b]	resolution
DDA (solid probe technique)	0.35	2:1	20 000
DDD (GC/MS)	0.003	2:1	3 000
DDT (GC/MS)	0.013	2:1	3 000
DDE (GC/MS)	0.001	2:1	3 000

[a] For this limit of detection, 20 mL of urine is extracted into the n-hexane solvent according to the procedure described in the Experimental Section. [b] Signal to noise ratio.

ACKNOWLEDGMENT

The assistance of N. C. A. Weerasinghe with the GC/MS analysis is greatly appreciated.

Registry No. DDT, 50-29-3; DDA, 83-05-6; DDD, 72-54-8; DDE, 72-55-9.

LITERATURE CITED

(1) *Business Week* June 12, 1978, p 152.
(2) Fiorentina, D. H.; De Graeve, J.; Grogna, M.; De Wiest, F. *J. Chromatogr.* **1978**, *157*, 421.
(3) Durham, W. F.; Armstrong, J. F.; Quinby, G. E. *Arch. Environ. Health* **1965**, *11*, 76.
(4) Laws, F. R.; Curley, A.; Biros, F. J. *Arch. Environ. Health* **1967**, *15*, 766.
(5) Wolfe, H. R.; Durham, W. F.; Armstrong, J. F. *Arch. Environ. Health* **1970**, *21*, 711.
(6) Cranmer, M. F.; Carroll, J. J.; Copeland, M. F. *Bull. Environ. Contam. Toxicol.* **1969**, *4*, 214.
(7) Cueto, C.; Barnes, A. G.; Mattson, A. M. *J. Agric. Food Chem.* **1956**, *4*, 943.
(8) Guiochon, G.; Arpino, P. J. *Anal. Chem.* **1979**, *51*, 682A.
(9) Firouzbakht, M. L.; Garmestani, S. K.; Rack, E. P.; Blotcky, A. J. *Anal. Chem.* **1981**, *53*, 1746.
(10) Enos, E. F.; Biros, F. S.; Gardner, D. T.; Wood, J. P. Presented at the 154th National Meeting of the American Chemical Society, Chicago, IL, Sept 10–15, 1967, Ag. and Food Section.
(11) Crow, F. W.; Giblin, D. E. Presented at the 29th Annual Conference on Mass Spectrometry and Allied Topics, ASMS, Minneapolis, MN, May 24–29, 1981.
(12) Jacobs, F. S.; Ekambaram, V.; Filby, R. H. *Anal. Chem.* **1982**, *54*, 1240.
(13) Horvath, C.; Melander, W. *J. Chromatogr. Sci.* **1977**, *9*, 393.
(14) St. Claire, R. L., III; Ansari, G. A. S.; Abell, C. W. *Anal. Chem.* **1982**, *54*, 186.
(15) Majors, R. E. "High Performance Liquid Chromatography, Advances and Perspectives"; Horvath, C., Ed.; Academic Press: New York, 1980; Vol. 1, p 95.

RECEIVED for review November 10, 1982. Accepted January 3, 1983. This research was supported by the Division of Chemical Sciences of the U.S. Department of Energy (Contract No. DE-A502-76ER01617.0A004), Medical Research Service of the Veterans Administration, and a University of Nebraska Research Council NIH Biomedical Research Support Grant.

Determination of Arsenic, Molybdenum, Uranium, and Vanadium in Seawater by Neutron Activation Analysis after Preconcentration by Colloid Flotation

R. S. Shreedhara Murthy and Douglas E. Ryan*

Trace Analysis Research Centre, Chemistry Department, Dalhousie University, Halifax, Nova Scotia B3H 4J1, Canada

Colloid flotation of arsenic, molybdenum, uranium, and vanadium on hydrous iron(III) oxide permits rapid collection of the precipitate for neutron activation analysis. The precipitate is floated, in the presence of sodium dodecyl sulfate and tiny nitrogen bubbles, from 1 L of seawater at pH 5.7 ± 0.2. Except for uranium, recoveries are better than 95%; about 75% of the uranium was recovered. Selenium(IV) and tungsten(VI) can be similarly collected but their natural concentration levels in seawater are below detection limits for 1 L volumes.

Among the various techniques for the preconcentration of trace elements from aqueous solutions onto a solid phase (*1*), adsorbing colloid flotation (ACF) is simple and rapid and permits the determination of several elements in seawater (*2–10, 12, 13, 15–18*), river and tap water (*11, 14*), and acid solution (*20*). Most of the early work involved the preconcentration of a single element but simultaneous separation of many elements has been done recently (*13, 15, 20*). These procedures required the dissolution of the floated precipitate for determination by spectrophotometry (*2–4, 10, 12, 18*), atomic absorption spectrometry (*5, 7–9, 11, 13, 14, 16, 17, 20*), or inductively coupled plasma atomic emission spectrometry (*15*) and sometimes required further separation by ion-exchange (*6, 20*) or solvent extraction (*3, 5, 12*). This paper gives the results obtained by neutron activation after collection of the precipitate by an extremely simple and rapid procedure.

Hydrous iron(III) oxide was used in the present study because it has been shown to collect from acid solution many elements present as anionic species (*2–8, 11, 20*) thus separating them from other metals present as cations in natural waters. In addition, ^{59}Fe (half-life, 45.1 days) produced by activation of hydrous iron oxide is very insensitive and hence does not produce high matrix activity.

EXPERIMENTAL SECTION

Materials and Equipment. A 0.1 M iron(III) solution was prepared by dissolving reagent grade ferric chloride in 0.1 M hydrochloric acid. The surfactant was a 0.1% solution of sodium dodecyl sulfate in 50% ethanol. Solution standards of the elements contained 1 mg/mL. Gelman Metricel membrane filters, because of their low bromine content, were used to prevent interference of the 554-keV γ-peak of ^{82}Br with the 559-keV peak of ^{76}As.

Artificial seawater was prepared with analytical grade chemicals (*19*) and deionized, distilled water. Natural seawater (filtered through a sand bed before entering the building) from the Northwest Arm, Halifax, Nova Scotia was collected directly from the taps in the oceanography laboratory of the university.

Samples were irradiated in the Dalhousie University SLOWPOKE-2 reactor at a neutron flux of 5×10^{11} n cm^{-2} s^{-1} for three different irradiation, decay, and counting times (Table I). The activated samples were counted on a 60-cm^3 Ge(Li) detector attached to a Tracor Northen TN-11 Model 16K pulse height analyser.

Flotation Procedure. One liter of seawater was transferred into a 1-L beaker and 2.0 mL of 0.1 M iron(III) solution was added.

Table I. Irradiation Conditions and Nuclides Used

nuclide	half-life	γ energy used, keV	sensitivity, counts/μg	detection limit, μg
60 s Irradiation, 10 s Decay, 60 s Count				
^{77m}Se	17.5 s	162	2.15×10^3	0.02
5 min Irradiation, 1 Min Decay, 5 Min Count				
^{239}U	23.54 min	74	1.88×10^4	0.007
^{52}V	3.75 min	1434	1.27×10^4	0.02
16 h Irradiation, 2 day Decay, 30 min Count				
^{76}As	1.096 days	559	6.38×10^4	0.06
^{99}Mo	2.758 days	140	2.88×10^3	0.8
^{187}W	0.996 day	686	5.06×10^4	0.014
^{59}Fe	45.1 day	1099	6.8×10^{-1}	

The pH was adjusted to 5.7 resulting in the formation of hydrous iron(III) oxide. After the mixture was stirred for 10 min, 1.0 mL of 0.1% sodium dodecyl sulfate solution was added, stirring was stopped, and nitrogen was passed through the solution from a porosity F frit at a flow rate of 10 ± 5 mL/min for 5 min. After flotation, the nitrogen flow was stopped and the precipitate was transferred onto a Gelman Metricel membrane filter (0.45 μm pore size, 47 mm diameter) placed inside a Nuclepore filter funnel assembly (No. 411800) (Figure 1). The filter funnel assembly was tilted at an angle to collect only the foam containing the precipitate. The precipitate was washed with deionized distilled water and the wet membrane folded before transferring to an irradiation vial. Hydrous iron(III) oxide precipitate, prepared from 2.0 mL of 0.1 M iron(III) solution in 50 mL of deionized distilled water at pH 5.7 and filtered through a membrane filter, was used as a blank. Appropriate concentrations of elements obtained by fresh dilution of 1 mg/mL standards were spotted onto another set of precipitate blanks and used as neutron activation standards.

Optimization of Experimental Conditions. Studies were initially done to determine the trace level impurities in the iron(III) solution used. Blanks were made by precipitation of hydrous iron(III) oxide from solutions containing 2 mL of the Fe(III) standard in 50 mL of deionized distilled water and filtration through membrane filters. Lesser amounts of trace impurities present in the iron(III) solution were collected at pH >7; it was therefore necessary to make the hydrous iron(III) oxide blanks at the same pH (5.7) as in the collection process. Iron(III) solutions obtained from various salts and even from 99.99% pure iron wire contained low levels of arsenic, molybdenum, and vanadium.

Figure 2 shows the effect of pH variation on the collection process. Except for uranium, there is no variation in recovery, up to pH 6, for arsenate, molybdate, selenate, tungstate, and vanadate. Contrary to an earlier report (*5*), vanadium collection by the procedure used here is not sensitive to pH and molybdenum is collected over a wider range than previously reported (*2*). Since the addition of 2.0 mL of the 0.1 M iron(III) solution to 1 L of seawater lowered the pH to 5.7 with the precipitation of hydrous iron oxide, the pH chosen for studies was 5.7 ± 0.2. Variations in the amount of iron(III) solution added (1–4 mL) have no effect on collection and 2.0 mL was used to provide a manageable amount of precipitate and minimum matrix activity.

Variations in stirring time (from 10 to 45 min) had no effect on the collection. One milliliter of 0.1% sodium dodecyl sulfate

0003-2700/83/0355-0682$01.50/0 © 1983 American Chemical Society

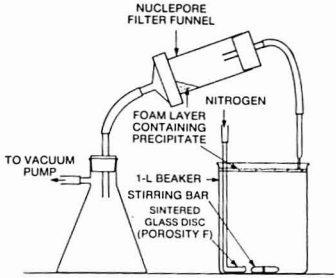


Figure 1. Apparatus for adsorbing colloid flotation and collection of precipitate.

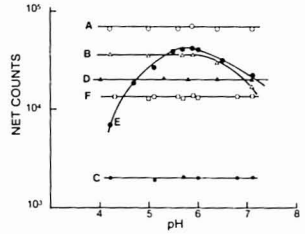


Figure 2. Effect of pH on the collection of arsenic (A), molybdenum (B), selenium (C), tungsten (D), uranium (E), and vanadium (F).

and a nitrogen flow rate of 10 ± 5 mL/min produced sufficient foam to support the precipitate formed and to float it to the surface in less than 5 min. Increase of surfactant or gas flow resulted in too much frothing which made washing of the precipitate difficult. Organic solvents (acetone or ethanol) could not be used to collapse the foam as they dissolved the membrane filter.

If care was exercised not to wet the membrane completely before all the foam was transferred, the filter funnel assembly (Figure 1) was very convenient to transfer the precipitate in less than a minute onto the membrane filters. Although each sample requires 25 min for pH adjustment, flotation, collection, and washing of precipitate, many samples can be simultaneously processed.

Recovery Studies. The floated hydrous iron(III) oxide has been collected either by manually scooping the foam (*2–6, 10, 20*) or by filtering the entire volume of sample (*7–9, 11*). The complete collection of foam is sometimes difficult (*21*); studies were therefore made to check the recovery of added iron(III) by the developed flotation and precipitate collection procedure. Replicate flotations from 1 L of seawater were done and, after removal of foam, the samples were filtered through a membrane filter to recover any unfloated precipitate. The area under the 1099-keV γ-peak of ^{59}Fe was measured for both the floated and filtered samples. Comparison with precipitate blanks made by filtration of hydrous iron(III) oxide from 50 mL of deionized distilled water showed a recovery of 95 ± 3% by flotation and 3–5% by filtration. Therefore, the area under the 1099-keV γ-peak of ^{59}Fe was always measured and used to normalize data due to any variations in the recovery of foam or sample geometry.

RESULTS AND DISCUSSION

Table I shows the nuclides, irradiation conditions, γ-peaks used, and the detection limits obtained based on counting statistics ($2 \times (\text{background})^{1/2}$) of precipitate blanks. The lead shield around the Ge(Li) detector was removed when counting for ^{239}U to eliminate interference from the lead X-ray at 74 keV. At least 2 days of decay was given after the 16-h irradiation to allow ^{99m}Tc (half-life 6.02 h) daughter nuclide from ^{99}Mo to reach equilibrium; this also removed all the activity from ^{56}Mn (half-life 2.576 h) produced by fast neutron reaction with ^{56}Fe and substantially decreased activity from ^{24}Na (half-life 15 h).

Table II. Recovery Studies[a]

element	% recovery from artificial seawater	% recovery from natural seawater
arsenic(V)	96 ± 4	97 ± 5
molybdenum(VI)	99 ± 3	100 ± 4
selenium(IV)	99 ± 3	98 ± 3
tungsten(VI)	98 ± 4	99 ± 4
uranium(VI)	74 ± 5	72 ± 4
vanadium(V)	100 ± 2	100 ± 3

[a] Mean ± standard deviation from four replicates.

Table III. Analysis of Seawater[a]

element	concn (μg/L) found by ACF-NAA	concn (μg/L) found by adsorption on activated carbon-NAA (ref)
arsenic	1.04 ± 0.01	
molybdenum	10.1 ± 0.3	10.3 ± 0.4 (*25*)
uranium	3.08 ± 0.07	3.10 ± 0.05 (*23*)
vanadium	1.22 ± 0.02	1.23 ± 0.02 (*24*)

[a] Mean ± standard deviation from four replicates.

Table II shows the percent recovery of arsenic(V), molybdenum(VI), selenium(IV), tungsten(VI), uranium(VI), and vanadium(V) from artificial and natural seawater samples. The studies, using inactive spikes for selenium, uranium, and vanadium and radioactive tracers for arsenic, molybdenum, and tungsten, show >95% recovery for all the elements except for uranium from both artificial and natural seawater; 72 ± 4% of the uranium was recovered. Contribution to the 140-keV γ-peak of ^{99}Mo from the 143-keV peak of ^{59}Fe was negligible compared to blank levels for molybdenum. However, the production of ^{99}Mo from the fission of ^{235}U was expected. Its contribution was obtained by irradiating and counting 3 μg (concentration expected from 1 L of seawater) of uranium(VI) (of natural isotope abundance) added onto hydrous iron(III) oxide blanks. The area under the 140-keV γ-peak (which was 2.3 times higher than the blanks not containing uranium) was used to calculate the correction factor for the blank level of molybdenum due to the presence of uranium.

Table III shows the results of analysis of seawater for arsenic, molybdenum, uranium, and vanadium; these agree with those obtained after preconcentration by adsorption of oxine or APDC complex onto activated carbon. The natural concentration levels of selenium and tungsten in seawater were below detection limits.

The present work, by using the solid phase for direct neutron activation analysis (NAA), has utilized the advantages of adsorbing colloid flotation for rapid preconcentration of trace elements from large sample volumes. Although sample handling becomes more difficult, flotation and collection of precipitate for NAA can be done for up to 4-L sample volumes. Other solid phases suitable for ACF-NAA are now being investigated.

Registry No. Hydrous iron(III) oxide, 1309-33-7; sodium dodecyl sulfate, 151-21-3; arsenic, 7440-38-2; molybdenum, 7439-98-7; uranium, 7440-61-1; vanadium, 7440-62-2; selenium(IV), 7782-49-2; tungsten(VI), 7440-33-7; water, 7732-18-5.

LITERATURE CITED

(1) Shreedhara Murthy, R. S.; Holzbecher, J.; Ryan, D. E. *Rev. Anal. Chem*; in press.
(2) Kim, Y. S.; Zeitlin, H. *Sep. Sci.* **1971**, *6*, 505.

(3) Kim, Y. S.; Zeitlin, H. *Anal. Chem.* **1971**, *43*, 1390.
(4) Chaine, F. E.; Zeitlin, H. *Sep. Sci.* **1974**, *9*, 1.
(5) Hagadone, M.; Zeitlin, H. *Anal. Chim. Acta* **1976**, *86*, 289.
(6) Tzeng, J.; Zeitlin, H. *Anal. Chim. Acta* **1978**, *101*, 71.
(7) Nakashima, S. *Anal. Chem.* **1979**, *51*, 654.
(8) Nakashima, S. *Bull. Chem. Soc. Jpn.* **1979**, *52*, 1844.
(9) Nakashima, S. *Fresenius' Z. Anal. Chem.* **1980**, *303*, 10.
(10) Kim, Y. S.; Zeitlin, H. *Sep. Sci.* **1972**, *7*, 1.
(11) Nakashima, S. *Analyst (London)* **1978**, *103*, 1031.
(12) Leung, G.; Kim, Y. S.; Zeitlin, H. *Anal. Chim. Acta* **1972**, *60*, 229.
(13) Hiraide, M.; Yoshida, Y.; Mizuike, A. *Anal. Chim. Acta* **1976**, *81*, 185.
(14) Mizuike, A.; Hiraide, M.; Kanematsu, T. *Bunseki Kagaku* **1977**, *26*, *137*. *Chem. Abstr.* **1978**, *88*, 83049p.
(15) Hiraide, M.; Ito, T.; Baba, M.; Kawaguchi, H.; Mizuike, A. *Anal. Chem.* **1980**, *52*, 604.
(16) Voyce, D.; Zeitlin, H. *Anal. Chim. Acta* **1974**, *69*, 27.
(17) Rothstein, N.; Zeitlin, H. *Anal. Lett.* **1976**, *9*, 461.
(18) Sekine, K. *Mikrochim. Acta* **1975**, 313.
(19) Kester, D. R.; Duedall, I. W.; Connor, D. N.; Pytkowicz, R. M. *Limnol. Oceanogr.* **1967**, *12*, 176.
(20) DeCarlo, E. H.; Zeitlin, H.; Fernando, Q. *Anal. Chem.* **1981**, *53*, 1104.
(21) Robberecht, H. J.; van Grieken, R. E. *Anal. Chem.* **1980**, *52*, 449.
(22) Ryan, D. E.; Stuart, D. C.; Chattopadhyay, A. *Anal. Chim. Acta* **1978**, *100*, 87.
(23) Holzbecher, J.; Ryan, D. E. *Anal. Chim Acta* **1980**, *119*, 405.
(24) van der Sloot, H. A.; Das, H. A. *J. Radioanal. Chem.* **1977**, *35*, 139.
(25) van der Sloot, H. A.; Wals, G. D.; Das, H. A. *Anal. Chim. Acta* **1977**, *90*, 193.

RECEIVED for review November 1, 1982. Accepted January 3, 1983. This work was supported by a grant from the Natural Sciences and Engineering Research Council of Canada.

Raman Spectrometric Determination of Tribasic Sodium Phosphate Hydrolysis Quotient

Allan G. Miller*[1]

Analytical Laboratories, Rockwell Hanford Operations, Richland, Washington 99352

John W. Macklin

Department of Chemistry, University of Washington, Seattle, Washington 98195

The hydrolysis quotient of tribasic sodium phosphate has been determined over the 0.001 to 0.4 M phosphate concentration range in order to establish hydroxide concentration limits for the quantitative determination of PO_4^{3-} in aqueous solutions by laser Raman spectrometry. Concentrations of phosphate species in the hydrolysis equilibrium were measured by laser Raman spectrometry and hydroxide concentrations were determined by both pH measurement and a titrimetric method. The hydrolysis quotient ranged from near 0.004 M at phosphate concentrations above 0.01 M to 0.014 M at infinite dilution. This corresponds to a thermodynamic equilibrium constant 7.1×10^{-13} M, for the third dissociation of phosphoric acid. These results are compared with those of the only previous Raman spectrometric investigation of the HPO_4^{2-}–PO_4^{3-} equilibrium.

Raman spectrometry is a suitable technique for quantifying orthophosphate as described previously (*1*). The application is, however, hindered by the spectral complications of more than one phosphate species resulting from phosphoric acid dissociation and dimerization equilibria (*2*, *3*). Phosphate is essentially 100% PO_4^{3-} in the presence of greater than about 0.3 M hydroxide allowing direct spectrometric analysis. Below this hydroxide concentration, the analytical determination is complicated by the presence of protonated phosphate species. So that we can establish this lower hydroxide concentration limit better, the hydrolysis quotient, Q_h, was measured for the 0.001 to 0.4 M PO_4^{3-} concentration range, and consequently, K_3, the third dissociation constant of phosphoric acid. Although the literature contains many values of K_3 from which Q_h can be calculated (*4*, *5*), they range over 2 orders of magnitude.

A determination of Q_h by Raman spectrometry is more direct than many methods and involves the same measurements as the Raman analytical method for PO_4^{3-} (*1*). Other methods such as titrimetry are nonspecific and may suffer from difficulties such as the insensitivity of the pH electrode at the high pH levels necessary.

The Raman and infrared spectra of aqueous orthophosphate solutions have been studied and assigned (*6*, *7*), and equilibrium investigations by Raman spectrometry have recently been reported by Preston and Adams (*2*, *3*, *8*). They also determined Q_h for the HPO_4^{2-}–PO_4^{3-} equilibrium; however, their experimental procedure does not include carbon dioxide control or an internal standard. The work described here includes these controls along with independent measurements of each constituent in the hydrolysis equilibrium in order to establish Raman spectrometrically measured values of Q_h that can be confidently used in the quantitative determination of PO_4^{3-} and to estimate the third dissociation constant, K_3 of phosphoric acid.

EXPERIMENTAL SECTION

Solutions. A 1.001 M phosphate stock solution was prepared by dissolving undried, assayed $NaH_2PO_4 \cdot H_2O$ (Mallinkrodt, analyzed reagent) in distilled, deionized water. The phosphate solution was filtered through a Millipore BDWP 0.4-μm filter. Similarly filtered, distilled, and deionized water was used in all subsequent preparations. All vessels were rinsed with the filtered water. A 0.049 95 M dilution by weight of the stock solution was prepared.

Solutions for Raman studies with the following approximate concentrations were prepared: 0.4, 0.1, 0.05, 0.02, 0.01, 0.005, 0.002, 0.001, and 0.0005 M. Weighed aliquots of the appropriate phosphate solution and 1.00 mL of 2.50 M sodium nitrate internal standard solution were added to water in individual 25-mL volumetric flasks. Subsequent preparation steps for these test solutions were carried out in a gloved gas bag purged with nitrogen to provide a carbon dioxide free atmosphere. In addition, beakers containing dilute sodium hydroxide were kept in the gas bag for waste and as getters for CO_2. Calculated amounts of either 4.3 or 19.3 M NaOH were added to each solution to obtain approx-

[1] Present address: United States Testing Laboratories, Richland, WA 99352.

0003-2700/83/0355-0684$01.50/0 © 1983 American Chemical Society

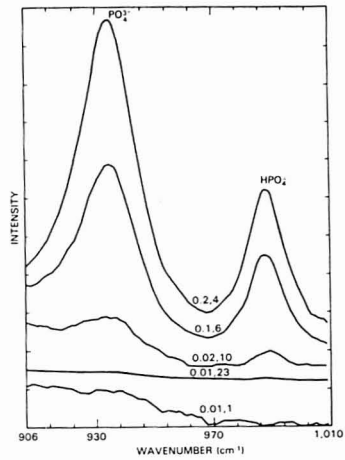


Figure 1. Averaged spectra for solutions of various phosphate concentrations. Spectra are identified by total phosphate molarity and number of spectra averaged, respectively.

imately equal concentrations of HPO_4^{2-} and PO_4^{3-} (around pH 12.3). The solutions were diluted to 25 mL and stirred before pH measurements were performed within in the gas bag with a Beckman 0-14 pH electrode and an Orion Model 901 "Ionalyzer" pH meter. Reference pH solutions were 1.00 and 0.1 M NaOH and Beckman pH 10 buffer.

Raman Spectra. Spectra were taken at 2 to 2.5 W of 514.5-nm radiation from a CR-6, Coherent Radiation argon laser. The spectrometer system is a Spex Industries Ramalog-5 equipped with 1800 grove/mm holographic gratings, a photon counting system, and slits set to provide a spectral band-pass of 6 cm^{-1}. Spectra were accumulated in 1-cm^{-1} increments with 1-s integration time. Glass capillary spectrometer cells were loaded inside the gas bag. Raman spectra were taken from 890 to 1095 cm^{-1} to include the 936, 990, and 1048 cm^{-1} A_1 analytical lines of PO_4^{3-}, HPO_4^{2-}, and NO_3^- ions, respectively, at 22 °C. The capillary cells were positioned perpendicular to the vertical laser beam and the scattered light was collected at 90°. Laser heating of the sample was measured with a thermocouple to be about 3 °C. Up to 110 spectra of each solution were collected and averaged to provide improved signal-to-noise ratios. The number of spectra averaged was increased as phosphate concentration decreased. Examples of spectra showing only the phosphate peaks and the benefit of averaging multiple spectra are shown in Figure 1. Computer control and data acquisition were accomplished with a Data General Nova 840 minicomputer.

Computer Techniques. The Data General Nova minicomputer was used to normalize and subtract interfering spectral lines and the solvent background contribution from the spectra. The background subtraction routine subtracts a chosen reference spectrum until zero is obtained as determined from a plot of the net peak. Net peaks were integrated by summing the residual counts in the spectrum segment. Accurate subtractions frequently could not be obtained at the lower concentrations because noise and small differences between reference and sample spectra prevent zeroing of the difference spectrum on both sides of the peak. In these cases, peak areas were adjusted by manually zeroing the peaks in plots of difference spectra followed by cutting and weighing. Computerized plotting permits appropriate magnification of difference spectra.

Analysis. Reagent analysis was performed by back-titration with 0.0496 M ± 0.28% NaOH from a 10-mL microburet to end points between 6 and 8 pH units. Standard 1.002 M HNO_3 and 19.23 M NaOH were prepared by the chemical standards laboratory of Rockwell Hanford Operations. Characterization of these

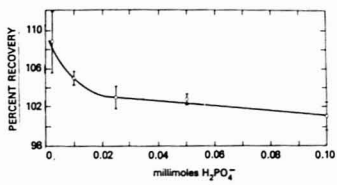


Figure 2. Bias in $LaPO_4$ precipitation, reverse titration method for aqueous hydrogen ion.

solutions was based on National Bureau of Standards tris(hydroxymethyl)aminomethane. Stoichiometry of the $NaH_2PO_4{\cdot}H_2O$ was determined to be 100.0 ± 1.8% by analysis of solutions of the salt by magnesium ammonium phosphate precipitation and weighing magnesium pyrophosphate (*9*).

Quantification of HPO_4^{2-} and PO_4^{3-} anions in the test solutions was derived from the Raman intensities using 0.1 M NO_3^- as an internal standard. The ratio of integrated intensities of phosphate A_1 analytical lines to that of nitrate is related to concentration through calibration curves.

A volumetric method for determining free hydroxide in the presence of varying concentrations of di- and tribasic phosphate was devised. The method involves a back-titration in which a sample aliquot is added to excess standard acid so that carbon dioxide absorption does not contribute error during room atmosphere titrations. Aliquots of acidified sample are titrated with 0.0496 M NaOH to end points between 6 and 8 pH units. Phosphate is titrated by precipitation of $LaPO_4$ simultaneously with titration of the excess acid and acid released from HPO_4^{2-} and $H_2PO_4^-$ when $LaPO_4$ is precipitated. Residual phosphate concentrations were detected by the size of the pH drop with additions of the stoichiometric volume of 0.1 M $LaCl_3$. The concentration of free hydroxide in the original test solution can be calculated from the added amount of standard acid, the titrant volume, aliquot sizes, and the Raman spectrometrically measured concentration of HPO_4^{2-}. Initial evaluation of the method with standard NaH_2PO_4 indicated 100.7% recovery with lanthanum additions at pH less than 4. Analysis of solutions and further evaluation of the method were performed with lanthanum additions made at pH levels between 4 and 6 for better sensitivity of the phosphate end point. According to the evaluation results shown in Figure 2, a phosphate dependent bias occurs. Test solution results were corrected for this bias.

RESULTS AND DISCUSSION

Hydrolysis Equilibria. At pH levels greater than 10, tribasic orthophosphate hydrolyzes according to the following reaction:

$$H_2O + PO_4^{3-} \rightleftharpoons HPO_4^{2-} + OH^- \qquad (1)$$

Preston and Adams (*3*) studied the equilibrium by dissolving various concentrations of tribasic sodium or potassium orthophosphate in water and determining the concentration of HPO_4^{2-} from hydrolysis by Raman spectrometry. The concentrations of HPO_4^{2-} and hydroxide were assumed equal and the concentration of PO_4^{3-} was obtained by difference. The resulting values permitted calculation of the concentration hydrolysis quotient, Q_h, according to the following equation:

$$K_h = \frac{a_{HPO_4^{2-}} a_{OH^-}}{a_{PO_4^{3-}}} = \frac{\gamma_{HPO_4^{2-}} \gamma_{OH^-}}{\gamma_{PO_4^{3-}}} \frac{[HPO_4^{2-}][OH^-]}{[PO_4^{3-}]} = Q_\gamma Q_h \qquad (2)$$

where a_i is activity, [i] is concentration in molarity, γ_i is the activity coefficient of species i, and K_h is the thermodynamic hydrolysis quotient.

In our work the orthophosphate hydrolysis equilibrium was studied by an independent analysis method that features several differences from the hydrolysis method in order to achieve an analytically applicable measurement of Q_h and

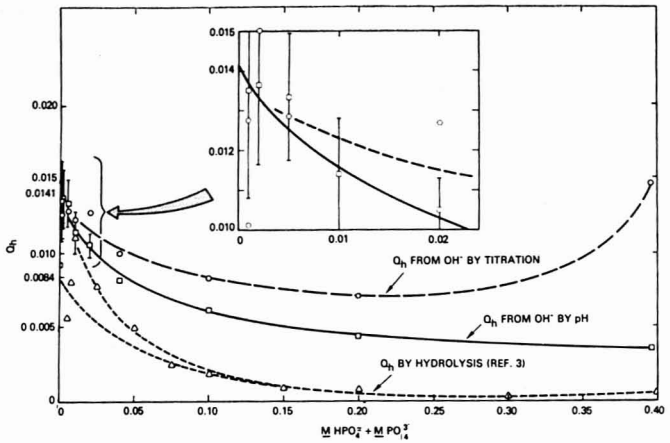


Figure 3. Hydrolysis quotient for PO_4^{3-} vs. concentration.

estimation of the thermodynamic hydrolysis constant, K_h. Preston and Adams point out that the reliability of their results is limited to above 0.02 M phosphate because of the lack of "computer time averaging" and the resulting imprecision at lower concentrations. Therefore, our experiments to determine K_h include computer acquisition and averaging of multiple spectra in order to extend the measurable concentration range and to improve the reliability of results. All operations which might permit significant absorption of carbon dioxide by the alkaline solutions were performed under a nitrogen atmosphere, since absorption of carbon dioxide may significantly lower pH and yield high results for Q_h, especially at low phoshate concentrations. The hydrolysis method for measuring Q_h is insensitive at low concentrations where nearly all phosphate is HPO_4^{2-}. The theoretical lower limit is where all phosphate is HPO_4^{2-}, near 0.0001 M, but the practical limit is much higher because the uncertainty of the HPO_4^{2-} determination must be much less than the total PO_4^{3-} concentration for meaningful results. In this study, all solutions were prepared to pH levels where the HPO_4^{2-} and PO_4^{3-} concentrations would be similar. All three constituents of the equilibrium expression, eq 2, have been determined to constitute the aforementioned independent analysis method. The internal standard that was incorporated may be an improvement over the external standard used by Preston and Adams because it cancels any changes in refractive index over the large concentration range studied.

Analyses. Peak area measurements for the A_1 lines of HPO_4^{2-} and PO_4^{3-}, that were straightforward for the solutions of higher concentration, were difficult at lower concentrations where the match between sample and reference spectra failed. Refinement of computer-determined peak areas by cutting and weighing was only partially effective because the real limitation is low peak-to-background ratio when quantifying peaks zeroed on only one side. Tiny mismatches between sample background and reference spectra become large errors in the difference spectrum as the peak-to-background ratio approaches zero. Table I contains the measured concentrations for each test solution. The combined uncertainty of measurements at the lower concentrations is near 13% relative standard deviation.

Accurate measurement by hydroxide concentrations was expected to be the most difficult aspect of the independent analysis method because of problems in obtaining accurate pH measurements at low hydrogen ion concentrations and because of phosphate interference in titration methods. Therefore, pH measurements were taken at completion of solution preparation and a volumetric method for determining hydroxide in phosphate solutions was devised to provide a second determination which was independent of pH measurements. With PO_4^{3-} removed from solution as $LaPO_4$, a sharp acid–base end point occurs. This precipitation–titrimetric method was evaluated for standard recovery of 0.0025 to 0.1 mmol of phosphate with a precision of 1.6% relative standard deviation. Corrections for greater than 100% recoveries, indicated in Figure 2, were applied to the test solution analyses as a function of total phosphate. Since lanthanum additions were made at pH levels greater than 4, it seems likely that a finite amount of lanthanum hydroxide forms to cause the high results. Lanthanum additions at lower pH levels may eliminate this complication. Hydroxide concentrations measured by both pH and titration methods are included in Table I. Agreement between the two methods is reasonable at low phosphate concentrations, but the disparity increases with increasing phosphate.

Table I. Analytical Molar Concentrations of HPO_4^{2-}–PO_4^{3-} Equilibrium [a]

total phosphate, M	$10^3[HPO_4^{2-}]$, M	$10^3[PO_4^{3-}]$, M	$[OH^-]$, M by pH	$[OH^-]$, M by titration
0.3959	82	302	0.0126	0.0533
0.1994	49	149	0.0132	0.0216
0.0995	28	67	0.0145	0.0195
0.0402	10.6	27	0.0204	0.0249
0.0199	5.9	12	0.0219	0.0264
0.00987	3.2 ± 0.6	6.1 ± 1.2	0.0219	0.0216
0.00498	1.5 ± 0.2	3.4 ± 0.4	0.0311	0.0300
0.00197	0.60 ± 0.03	1.2 ± 0.2	0.0282	0.0311
0.00100	0.28 ± 0.02	0.7 ± 0.2	0.0347	0.0323
0.000497		0.4 ± 0.1	0.0302	0.0292

[a] Lower phosphate concentrations are the mean of multiple measurements. Uncertainties are the standard deviations of those measurements.

Hydrolysis Quotient. Hydrolysis quotients calculated from the data in Table I are listed in Table II and plotted in

Table II. Hydrolysis Quotients (Q_h) for the HPO_4^{2-} Dissociation Equilibrium

total phosphate molarity	$10^3 Q_h$ [a] [OH^-] by pH	[OH^-] by titration	uncertainty, [b] %
0.3959	3.4	14.5	
0.1994	4.3	7.1	
0.0995	6.1	8.2	
0.0402	8.1	9.9	
0.0199	10.5	12.7	
0.00987	11.4	11.2	±19
0.00498	13.4	12.9	±12
0.00197	13.1	15.0	±14
0.00100	13.5	12.6	±21
0.000497	7.6	7.3	±21

[a] Values calculated from mean of analytical measurements. [b] Uncertainty calculated as standard deviation of multiple measurements.

Figure 3. The disparity in Q_h, depending on the source of hydroxide concentration values, is larger at the higher phosphate concentrations. Since the disparity is greatest there, a greater phosphate interference than indicated by the Figure 2 corrections is suggested. The Q_h values calculated from pH measurements show less scatter in Figure 3 than the Q_h values calculated from volumetrically measured hydroxide concentrations. Therefore, pH measurements appear to provide more accurate data throughout the concentration range for calculating Q_h.

The extrapolation of Q_h to zero concentration provides an estimate of K_h, the thermodynamic hydrolysis quotient for the HPO_4^{2-} dissociation, to be 0.0141 ± 0.00015 M. The uncertainty estimate was obtained by shifting the curve of the line through the range of values permitted by the error bars in Figure 3. An extrapolation of the Q_h values obtained from the volumetric titrations also intersects the ordinate near Q_h = 0.014 M.

The independent analysis method implemented in this work provides independent checks on the accuracy of results. The phosphate material balance can be seen from Table I to be mostly in the 90–100% range. Two methods, independent of each other, for determining hydroxide provide a check on possible errors and biases. For example, the pH results verify a problem with the volumetric method at the higher concentrations.

The results of Preston and Adams (*3*) and their extrapolation to zero concentration at Q_h = 0.0084 M are also plotted in Figure 3. They did not claim reliability for their results below 0.02 M phosphate. If their Q_h values for less than 0.01 M phosphate concentrations are ignored, their data seem to extrapolate to near Q_h = 0.014 M. Figure 3 shows smooth curves drawn through the Preston and Adams data and extrapolated to both Q_h = 0.0084 and toward 0.014 M. Preston and Adams also presented results for the hydrolysis of potassium orthophosphate. These results are not included in Figure 3 for reasons of clarity, but they also extrapolate to near Q_h = 0.014 M at zero concentration if Q_h values for less than 0.01 M concentrations are omitted.

The greatest difference between the results of Preston and Adams and those presented here is in the values obtained for Q_h at concentrations above 0.01 M. This disparity, on the order of a factor of 10 for the higher concentrations, is very large, especially when the results extrapolate to the same intercept value. The checks in the independent analysis method discussed above instill confidence in the reliability of the results reported here.

The value of K_h = 0.0141 ± 0.0015 M leads to the third dissociation constant of phosphoric acid, $K_3 = 7.1 \times 10^{-13}$ M at 25 °C. This is compared to quoted values of 2.2×10^{-13} (*10*) and 4.8×10^{-13} M (*11*). The former appears to be the smallest in the literature, while 7.9×10^{-11} M (*5*) and 5.6×10^{-12} M (*4*) seem to be the two largest values. The Raman value for K_3 from this work is toward the small end of the range of literature values. The value for K_3 estimated by Preston and Adams is 1.2×10^{-12} M (*3*). While Raman spectrometry can only detect phosphates at moderately low concentrations, the data in Figure 3 go to a low enough concentration to show that an intercept of 0.020 or more ($K_3 < 5 \times 10^{-13}$ M) is not probable.

Partially neutralized phosphoric acid species may form dimers by means of multiple hydrogen bonds according to the model presented by Preston and Adams (*3*). According to spectra which they report, such dimerization of HPO_4^{2-} increases with concentration and amounts to only a small part of the total phosphate at concentrations near 0.1 M. Since the highest HPO_4^{2-} concentration in the test solutions is 0.028 M (Table I), any effect due to dimerization is likely negligible. In addition, the HPO_4^{2-} calibration likely compensates for any dimerization effects on the results reported here.

The previously discussed advantages of this method for measuring the hydrolysis quotient of orthophosphate are real, but some disadvantages are significant. Analysis of test solutions for three constituents instead of one means more sources of error. Use of an internal standard means a more complex spectrum. At low concentrations where peak areas must be manually determined, the determination of background is more difficult because of HPO_4^{2-} and PO_4^{3-} lines coexisting with the strong nitrate internal standard A_1' line. While the utilization of computer-acquired and -averaged spectra was helpful and permitted extension of the study to lower concentrations, it is not a cure-all. The ability to make measurements in low peak-to-background situations is governed by the molar intensities of the species being studied as well as by the number of spectra averaged.

ACKNOWLEDGMENT

The work of S. W. Dodd in the characterization of $NaH_2PO_4 \cdot H_2O$, and the experimental contributions of S. W. Dodd and B. K Miewald in conceptualizing this study are appreciated.

Registry No. PO_4^{3-}, 14265-44-2; Na_3PO_4, 7601-54-9.

LITERATURE CITED

(1) Miller, A. G. *Anal. Chem.* **1977**, *49*, 2044.
(2) Adams, W. A.; Preston, C. M.; Chew, H. A. M. *J. Chem. Phys.* **1979**, *70*, 2074.
(3) Preston, C. M.; Adams, W. A. *J. Phys. Chem.* **1979**, *83*, 814.
(4) "Stability Constants"; Chemical Society: London; Spec. Publ.—Chem. Soc. No. 17.
(5) Ghosh, A. K.; Ghosh, J. C.; Prasad, B. J. *Indian Chem. Soc.* **1980**, *57*, 1194. *Chem. Abstr.* **1981**, *94*, 53800H.
(6) Chapman, A. C.; Thirlwell, L. E. *Spectrochim. Acta* **1964**, *20*, 937.
(7) Steger, V. E.; Herzog, K. *Z. Anorg. Allg. Chim.* **1964**, *331*, 169.
(8) Preston, C. M.; Adams, W. A. *Can. J. Spectrosc.* **1977**, *22*, 125.
(9) "Scott's Standard Methods of Chemical Analysis", 5th ed.; D. Van Nostrand: New York, 1939; Vol. 1, p 696.
(10) "Handbook of Chemistry and Physics", 58th ed.; Chemical Rubber Company Press: Cleveland, OH, 1977; p D-151.
(11) Van Wazer, J. R. "Phosphorus and Its Compounds"; Interscience: New York, 1958; Vol. 1, p 481.

RECEIVED for review March 2, 1982. Resubmitted November 8, 1982. Accepted December 9, 1982. Prepared for the United States Department of Energy under Contract DE-AC06-77RL01030. Presented to the 36th Northwest Regional Meeting of the American Chemical Society, Bozeman, MT, June 17–19, 1981.

Atomic Fluorescence Spectrometry with Inductively Coupled Plasma as Excitation Source and Atomization Cell

M. A. Kosinski, Hiroshi Uchida,[1] and J. D. Winefordner*

Department of Chemistry, University of Florida, Gainesville, Florida 32611

A novel approach is presented in which two inductively coupled plasmas (ICPs) are used in an atomic fluorescence system. One ICP is used as the excitation source and the second ICP is used as the atomization cell. Emission, excitation, and fluorescence analytical curves of growth, and vertical distributions for zinc atomic and calcium ionic fluorescence intensities are obtained. Limits of detection for 16 elements are compared to fluorescence detection limits using other radiation sources. Interelement effects, spectral interferences, and noise sources are also discussed.

The inductively coupled plasma (ICP) has long been used as an effective vaporization, atomization, excitation, and ionization (VAEI) cell for emission spectrometry (*1*). Many physical parameters of the ICP have been investigated and a review by Barnes (*2*) contains references covering the various operating principles of the ICP. However, in emission, inherently complex spectra are produced, resulting in the need of a high-resolution monochromator to isolate the analytical lines of interest.

Xenon arc lamps (*3*), electrodeless discharge lamps (EDLs) (*4*), boosted hollow cathode lamps (HCLs) (*5*), ICP emission (*6*), and dye lasers (*7*) have all been previously used as excitation sources for flame atomic fluorescence spectrometry (AFS). However, in flames, chemical and ionization interferences along with quenching effects of fluorescence by flame gas molecules are a major concern. The use of the ICP as an atomization cell for AFS should be beneficial due to its high volatilization and quantum efficiency (*8*).

The first use of the ICP as an excitation source for flame AFS was reported by Hussein and Nickless (*9*). Relatively poor detection limits were obtained, though. Since then, improvements in the sample introduction and the plasma stability have resulted in the increasing use of the ICP as an excitation source for flame AFS. Epstein et al. (*6*) have shown the advantage of the ICP as compared to other AFS sources is its flexibility with respect to the available intense atomic and ionic line radiation. Changing from one element to the next is simply done by aspirating a different solution into the source ICP.

Omenetto et al. (*10*) have examined ICP emission profiles by using the resonance monochromator method. In this method, a low concentration of analyte is aspirated into a flame and increasing concentrations of the analyte are aspirated into the ICP. The resulting fluorescence from the flame is monitored, allowing certain limiting characteristics of the ICP emission profile to be inferred.

The properties of high intensity, long-term stability, narrow line width, and freedom from self-reversal all contribute to the ICP being an excellent excitation source for AFS. Also, due to the narrow line width of spectral lines in the ICP, spectral interferences are insignificant.

[1] On leave from Industrial Research Institute of Kanagawa Prefecture, Yokohama 236, Japan.

In this work, the utilization of the ICP as an excitation source for atomic and ionic fluorescence in a second ICP was investigated (ICP-ICP-AFS). Emission, excitation and fluorescence analytical curves of growth were obtained and, from these, further information about the line profile of the ICP was revealed. For the conventional emission curve of growth, the emission from the source ICP was plotted vs. concentration. For the excitation curve of growth, a fixed, low concentration of the analyte was aspirated into the atomization ICP, while increasing concentrations were introduced to the source ICP.

Thirdly, the fluorescence analytical curve of growth was obtained by aspirating a fixed high concentration (20 mg mL^{-1}) into the source ICP while increasing concentrations of the analyte were introduced to the atomization ICP. Vertical distributions of atomic and ionic species densities were obtained and detection limits for 16 elements are compared to other ICP techniques. Further, a few examples of chemical and spectral interferences were examined. Finally, the noise sources limiting the measurements were investigated and suggested improvements are discussed.

EXPERIMENTAL SECTION

Instrumentation. A block diagram of the experimental system is shown in Figure 1.

The source ICP (Model 2500K, Plasma-Therm, Kresson, NJ) utilized a conventional short torch (Model T1.0, Plasma-Therm). The normal operating conditions were 2.0 kW RF power, 15 L min^{-1} plasma support argon flow rate, and 20 psig nebulizing gas pressure. A 20 mg mL^{-1} analyte excitation solution was used. Two exceptions, however, were aluminum and sodium. Aspiration of 20 mg mL^{-1} solutions of aluminum and sodium clogged the pneumatic nebulizer (Model PN5601, Plasma-Therm) after only a few minutes of operation. For these elements, a 10 mg mL^{-1} excitation solution was used and a nebulizer gas pressure of 40 psig was used to avoid clogging.

The atomization ICP (Model 1500D, Plasma-Therm, Kresson, NJ) utilized an extended-sleeve torch (Baird Corp., Bedford, MA) and was operated at 0.7 kW for the atomic lines and 1.0 kW for the ionic lines of nonrefractory elements, as well as the atomic and ionic lines of refractory and rare earth species. The only exception in this case was vanadium for which 1.2 kW was used. The observation height in the atomization ICP for the atomic lines of nonrefractory elements was 40 mm above the top of the extended-sleeve torch. This position corresponded to a height of 80 mm above the load coil since the outer sleeve of the torch extends for 40 mm beyond the top of the load coil. The observations height for all other lines was 20 mm above the top of the torch (60 mm above the load coil). The plasma support argon flow rate was 15 L min^{-1}, with no auxiliary argon flow being used, and the nebulizer gas pressure was 35 psig (Model T-230-Ae, J. E. Meinhard Assoc., Santa Ana, CA).

The source radiation obtained (10–30 mm above the load coil) by aspirating 20 mg mL^{-1} aqueous solutions of the analyte into the source ICP was chopped at a frequency of 550 Hz (Model 7500, Rofin-Math Assoc., Great Neck, NY) and focused onto the atomization ICP through the use of spherical quartz S1-UV grade lenses (50 diameter, 75 mm focal length). The resultant fluorescence was observed at a 90° angle through the use of a 350 mm focal length monochromator (Model EU-700, Heath Co., Benton Harbor, MI; now GCA Corp., McPherson Instruments,

0003-2700/83/0355-0688$01.50/0 © 1983 American Chemical Society

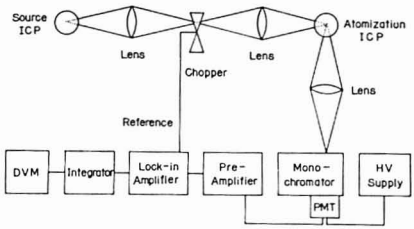


Figure 1. Block diagram of the ICP-ICP-AFS system.

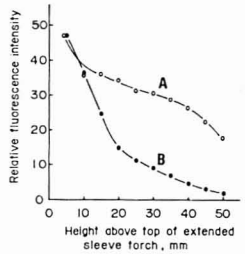


Figure 2. Vertical distributions of fluorescence intensities for (A) Zn(I) at 213.9 nm, 1 μg mL^{-1} atomization, 20 mg mL source ICP, and (B) Ca(II) at 393.4 nm, 1 μg mL^{-1} atomization, 20 mg mL source ICP. RF powers: 2.0 kW source ICP, 0.7 kW (Zn), and 1.0 kW (Ca) atomization ICP.

Acton, MA). The entrance and exit slit widths were 1 mm and the slit height was 10 mm. The photomultiplier tube (Model R928, Hamamatsu, Inc., Middlesex, NJ) was operated at −1000 V (Pacific Precision Instruments H.V. Supply, Concord, CA). The output was preamplified (Model 427, Keithley Instruments, Inc., Cleveland, OH) and fed to a lock-in amplifier (Dynatrac 391, Ithaco Inc., Ithaca, NY). The resulting signal was fed to a laboratory constructed integrator. The 10-s integrations were displayed on a digital voltmeter (Model 8000A, John Fluke Mfg. Co., Inc., Seattle, WA). For the spectral inteference studies, the output of the lock-in was fed to a chart recorder (Model 5000, Fisher Scientific Co., Pittsburgh, PA). Neutral density filters allowed verification of the linearity of the fluorescence and emission photomultiplier response.

Chemicals. Stock solutions of 20 mg mL^{-1} were prepared from the pure metal when possible or from reagent grade chemicals, dissolved in the minimum amount of acid, and successively diluted with distilled/deionized water.

RESULTS AND DISCUSSION

Vertical Distributions of Atomic and Ionic Fluorescence Intensities. In Figure 2, vertical distributions are given for zinc atomic and calcium ionic fluorescence intensities. The fluorescence intensity at 5 mm above the top of the extended-sleeve torch was taken to be the same for both elements. However, the signal-to-noise ratio was found to be poor at this height. Consequently, an observation height of 40 mm above the top of the extended-sleeve torch (80 mm above the load coil) was adopted for zinc and was also found to be optimal for the other atomic lines of nonrefractory elements investigated. It can be seen from Figure 2 that beyond 40 mm above the top of the extended-sleeve torch, the zinc fluorescence intensity drops off rapidly due to quenching by air entrainment in the plasma (*8*).

For ionic, all other lines, a 20 mm observation height above the top of the extended-sleeve torch (60 mm above the load coil) was adopted. Above this height, the fluorescence intensity for these lines became very weak due to the decrease in temperature of the plasma (*11*) and air entrainment (*8*).

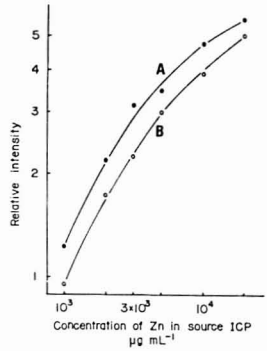


Figure 3. Excitation and emission curves of growth for zinc atom at 213.9 nm (RF powers: 2.0 kW source ICP, 0.7 kW atomization ICP): (A) excitation curve of growth, 40 mm observation height above the top of the extended-sleeve torch (80 mm above the load coil), 1 μg mL^{-1} zinc aspirated into atomization ICP; (B) emission curve of growth, 20 mm observation height above the load coil (conventional short torch).

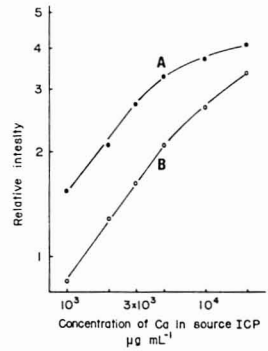


Figure 4. Excitation and emission curves of growth for calcium ion at 393.4 nm (RF powers: 2.0 kW source ICP, 1.0 kW atomization ICP): (A) excitation curve of growth, 20 mm observation height above the top of the extended-sleeve torch (60 mm above the load coil) 1 μg mL^{-1} calcium aspirated into atomization ICP; (B) emission curve of growth, 20 mm observation height above the load coil (conventional short torch).

Curves of Growth. In Figures 3 and 4, the emission and excitation curves of growth for zinc and calcium are shown. As previously shown for both elements in ICP-excited flame-AFS (*10*), the emission curves of growth for both elements yield a limiting slope of unity at low atom densities in the source ICP and a slope of 0.5 at high atom densities. Also, the excitation curves of growth yield a limiting slope of unity at low atom densities in the source ICP and a slope approaching zero at high atom densities. The limiting slopes of Figures 3 and 4 agree well with theory (*10*) and show that self-reversal is absent in the ICP under the conditions used in these analysis. In Figure 5, fluorescence analytical curves of growth are given for calcium and zinc; these curves show that at low atom densities in the atomization ICP, a limiting slope of unity is obtained while at high atom densities a slope

Table I. Limits of Detection

species	ex λ/fl λ,[a] nm	limits of detection, ng mL^{-1} ICP-ICP-AFS	ICP-flame-AFS[c]	laser-excited ICP-AFS[d]	HCL-ICP-AFS[e]
Al I	309.278	8000	1000		
	394.401/396.152			5	
Ca I	422.673	60	4	100	0.08
Ca II	393.366	2		1	
Co I	240.725	40	11		5
Co II	228.616	300			
Cr I	357.869	900	2		10
Cr II	205.552	2000			
Cu I	324.754	30	2		1
Fe I	248.327	1300	6		10
Fe II	259.940	100			
Mn I	279.482				0.3
	279.827	150	2		
Mn II	257.610	9			
Mo I	313.259				30
	386.411	1500		100	
Mo II	202.030	12000			
Na I	588.995	100			0.5
Nd II	430.358	N.D.[b]			
Ni I	232.003	380			10
Ni II	231.604	100			
Sm II	363.429	30000			
Tb II	350.917	N.D.[b]			
V I	411.178	8000	400		90
V II	309.311	1000			
	390.326/290.882			10000	
Yb I	398.799	150			
Yb II	369.419	30			
Zn I	213.856	6	0.5		0.5
Zn II	206.200	600			

[a] Excitation λ/fluorescence λ, if different from excitation wavelength. [b] Not detectable. [c] Reported by Epstein et al. (*6*). [d] Reported by Kosinski et al. (*11*). [e] Reported by Demers and Allemand (*13*).

of −0.5 is obtained. According to theory (*10*), the source ICP is acting as a "line" excitation source compared to the absorption profile in the atomization ICP; this occurs even though the higher temperature of the source ICP (2.0 kW RF power, short torch) would seem to cause the Doppler half-width to be larger than that of the cooler atomization ICP (<1.2 kW RF power, extended-sleeve torch). It has been previously shown (*11*) that the temperature of the plasma using an extended-sleeve torch is about 1000–1500 K less than the plasma using a short torch, depending on the RF power and observation height.

The temperatures of the atomization ICP were obtained at the two heights and three RF powers using a three-line slope calculation by measuring iron atomic emission lines at 382.0 nm, 382.4 nm, and 382.6 nm. Spectral data with respect to these lines have been summarized previously (*12*). The temperatures were found to be: (i) 3290 K (0.7 kW, 40 mm observation height above the top of the extended-sleee torch); (ii) 3540 K (1.0 kW, 20 mm observation height); (iii) 3810 K (1.2 kW, 20 mm observation height).

Limits of Detection. As shown in Table I, limits of detection for many of the elements investigated are within 1 order of magnitude for the best reported values using the ICP as an excitation source for flame AFS (*6*). Also presented are some detection limits obtained by laser-ICP-AFS (*11*) and HCL-ICP-AFS (*13*).

Chemical Interferences. In Figure 6, chemical interferences observed on calcium ionic fluorescence at 393.4 nm are shown (atomization ICP: 1.0 kW, 20 mm observation height above the top of the extended-sleeve torch). It can be seen that there is an enhancement in calcium fluorescence with the addition of aluminum and sodium possibly due to a change in the atom and ion distributions in the plasma in both cases. The distribution of refractory elements is known to change

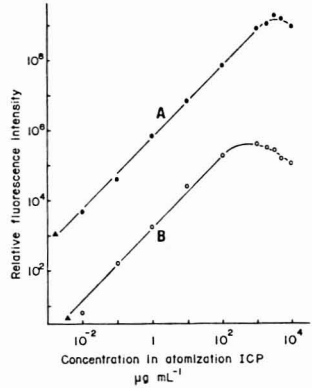


Figure 5. Fluorescence analytical curves of growth for calcium ion at 393.4 nm and zinc atom at 213.9 nm (RF powers: 2.0 kW source ICP, 0.7 kW (Zn) and 1.0 kW (Ca) atomization ICP): (A) Ca(II), 20 mm observation height above the top of the extended-sleeve torch (60 mm above the load coil), 20 mg mL^{-1} calcium aspirated into source ICP; (B) Zn(I), 40 mm observation height above the top of the extended-sleeve torch (80 mm above the load coil), 20 mg mL^{-1} zinc aspirated into source ICP.

by the addition of aluminum in a flame because of the formation of monoxides (*14*). Further, the change in the atom and ion distributions in the plasma in the presence of sodium has been reported in a capacitively coupled plasma (*15*). This change could also be the result of an aerosol ionic redistri-

Table II. Spectral Interferences for ICP-ICP-AFS

mixture	species/concn in source ICP	species/concn in atomization ICP	wavelength of fluorescence (nm)	fluorescence intens (rel)
Zn-Cu	Zn/20 mg mL^{-1}	Cu/5000 μg/mL^{-1}	213.9	0.30
		Zn/10 μg mL^{-1} + Cu/5000 μg/mL^{-1}		100
Ni-Co	Co/20 mg mL^{-1}	Co/1000 μg mL^{-1}	231.2[a]	100
		Ni/1000 μg mL^{-1}		4.5
		Co/1000 μg mL^{-1} + Ni/1000 μg mL^{-1}		99
	Ni/20 mg mL^{-1}	Ni/1000 μg mL^{-1}	231.2	100
		Co/1000 μg mL^{-1}		2.0
		Ni/1000 μg mL^{-1} + Co/1000 μg mL^{-1}		97

[a] Taken on a 10 times more sensitive scale than Ni.

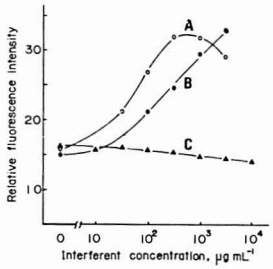


Figure 6. Effect of coexisting aluminum, sodium, and phosphorus on 1 μg mL^{-1} calcium ionic fluorescence intensities at 393.4 nm: RF powers, 2.0 kW source ICP, 1.0 kW atomization ICP; observation height, 20 mm above the top of the extended-sleeve torch (60 mm above the load coil); interferent, (A) aluminum, (B) sodium, (C) phosphoric acid.

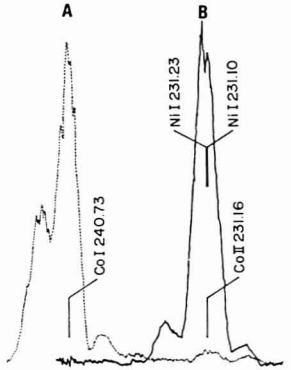


Figure 7. Fluorescence spectra for a 1000 μg mL^{-1} Co–1000 μg mL^{-1} Ni solution: RF powers, 2.0 kW source ICP, 0.7 kW atomization ICP; observation height, 40 mm above the top of the extended-sleeve torch (60 mm above the load coil); (A) 20 mg mL^{-1} cobalt excitation, (B) 20 mg mL^{-1} nickel excitation. Spectral band-pass was 1 nm.

bution effect (*16*). Similar enhancements with the addition of sodium were observed at high carrier flow rates (>1.0 L min^{-1}) at 15 mm above the load coil with a conventional short torch in the ICP (*12*). The signal suppression at high aluminum concentrations is due to the increase in sample solution viscosity.

In combustion flames, the presence of phosphorus in the analyte matrix or flame gases results in the formation of refractory compounds (*17*). This formation results in a consequent decrease in the fluorescence signal. In Figure 6, the effect of the presence of phosphorus on calcium ionic fluorescence is shown. The intensity was slightly suppressed by the presence of phosphorus, possibly due to the increase in sample solution viscosity (*18*, *19*).

Spectral Interferences. One of the advantages in ICP-ICP-AFS should be relative freedom from spectral interferences due to the narrow bandwidth of spectral lines in the source and atomization ICPs. Here, we investigated spectral overlap in two cases: (i) Zn (213.856 nm) and Cu (213.853 nm); (ii) Co (231.160 nm) and Ni (231.096, 231.234 nm). The results obtained are summarized in Table II.

Difficulty is encountered in the measurement of zinc in a copper matrix by atomic absorption of ICP atomic emission spectrometry (ICP-AES) since the zinc resonance line at 213.856 nm is subject to direct interference from the copper nonresonance line at 213.853 nm. This interference has been reported (*20*) for flame atomic absorption analysis and requires elaborate procedures to remove the copper prior to analysis. Even with an echelle spectrometer (spectral band-pass = 0.003 nm), this line pair has been shown to exhibit an overlap (*21*).

The measurement of a 10 μg mL^{-1} zinc solution in a 5000 μg mL^{-1} copper matrix using a 20 mg mL^{-1} zinc solution for excitation resulted in no significant excitation of copper fluorescence using a monochromator spectral band-pass of 2 nm. This is both because the radiation emitted by the source ICP is in the form of sharp lines and because the copper nonresonance transition at 213.853 nm (11203–57949 cm^{-1}) is difficult to excite due to the excited lower level of this transition.

Nickel and cobalt are also subject to spectral interference problems in the wavelength region of 231 nm. The radiation emitted from the source ICP while aspirating a 20 mg mL^{-1} cobalt solution was used to excite a solution containing 1000 μg mL^{-1} nickel and 1000 μg mL^{-1} cobalt. On the other hand, the radiation emitted from a 20 mg mL^{-1} nickel solution was also used to excite this same solution. As can be seen from Table II, no significant nickel fluorescence results when cobalt excitation is used and, conversely, no significant cobalt fluorescence is seen with nickel excitation. Also, Figure 7 shows the simplified fluorescence spectra obtained with a monochromator spectral band-pass of 1 nm.

Noise Considerations and Scatter Interferences. In order to determine the principle source of noise in this technique and to see if scattered radiation from the source ICP was present, a noise study was carried out for zinc at 213.9 nm and sodium at 589.0 nm. This study enabled an estimate of noise in the ultraviolet and visible regions of the spectrum to be obtained.

The analytical precision (4 s time constant, 10 s integration time, with 16 consecutive readings) for the measurement of high concentration solutions was on the order of 2% for zinc and 10% for sodium and was limited to some extent by the source ICP stability. Other researchers (*22*) have reported

ICP emission precision to be limited by the fluctuations in sample transport and nebulization to about 1%. It is reasonable, therefore, that the precision is slightly worse with two ICPs. The long-term stability of the ICP provides an advantage over other sources used for AFS such as electrodeless discharge lamps, which must be carefully thermostated (23), and the Eimac short-arc xenon lamp (24), which has a lower intensity in the ultraviolet. Also, there was no significant difference in the precision when the measurements for zinc and sodium were carried out in a matrix containing 10 mg mL^{-1} calcium. However, there was an increase in scattered radiation.

The precision for the measurement of low concentration solutions was about 3-4 times worse than that for high concentration solutions. The scatter signal due to the calcium matrix at the zinc and sodium lines resulted in a 2-5 times increase in signal over the blank level, respectively. Even though scatter was observed due to the calcium matrix, it did not act as a significant noise source. The precision for the low concentration analysis was about the same with and without the 10 mg mL^{-1} calcium matrix. Consequently, if present, scatter can be subtracted out by using the two-line technique (20), assuming that the scatter level does not change appreciably in the wavelength vicinity of the atomic fluorescence line.

While the fluorescence detection system is well optimized for a background shot-noise limited system, the optical transfer of radiation from the source ICP to the atomization ICP could be improved by at least an order of magnitude through the use of an ellipsoidal reflector (25, 26) placed behind the plasma to collect a much larger solid angle of emission. Indeed, based upon solid angle considerations, we are presently collecting less than 1% of the source radiation using 50 mm diameter lenses. Also, a mirror placed behind the atomization ICP in the direction of the fluorescence monochromator might improve detection powers by two times and aspiration of higher concentration excitation solutions could also be used to increase the source intensity in some cases. However, clogging of the nebulizer and aerosol tube of the torch may result as was noticed in this work for aluminum and sodium. The use of demountable torches with large diameter aerosol tubes might improve the situation.

ACKNOWLEDGMENT

The authors wish to thank Nicolo Omenetto of the University of Pavia, Pavia, Italy, and Edward Voigtman, Benjamin Smith, and Gary Long (University of Florida) for their helpful discussions and comments during this work.

Registry No. SO_2, 7446-09-5; $BaSO_4$, 7727-43-7; V_2O_5, 1314-62-1; SiO_2, 7631-86-9; copper, 7440-50-8.

LITERATURE CITED

(1) Fassel, V. A.; Kniseley, R. N. *Anal. Chem.* **1974**, *46*, 1110A.
(2) Barnes, R. M. *Crit. Rev. Anal. Chem.* **1978**, *7*, 203.
(3) Demers, D. R. *Appl. Spectrosc.* **1988**, *22*, 797.
(4) Mansfield, J. M., Jr.; Bratzel, M. P., Jr.; Norgordon, H. O.; Knapp, D. O.; Zacha, K. E.; Winefordner, J. D. *Spectrochim. Acta, Part B* **1968**, *23B*, 389.
(5) Lowe, R. M. *Spectrochim. Acta, Part B* **1971**, *26B*, 201.
(6) Epstein, M. S.; Nikdel, S.; Omenetto, N.; Reeves, R.; Bradshaw, J.; Winefordner, J. D. *Anal. Chem.* **1979**, *51*, 2071.
(7) Fraser, L. M.; Winefordner, J. D. *Anal. Chem.* **1971**, *43*, 1693.
(8) Uchida, H.; Kosinski, M. A.; Omenetto, N.; Winefordner, J. D. *Spectrochim. Acta*, in press.
(9) Hussein, Ch. A. M.; Nickless, G. Paper presented at the 2nd ICAS, Sheffield, England, 1969.
(10) Omenetto, N.; Nikdel, S.; Bradshaw, J.; Epstein, J. S.; Reeves, R. D.; Winefordner, J. D. *Anal. Chem.* **1979**, *51*, 1521.
(11) Kosinski, M. A.; Uchida, H.; Winefordner, J. D. *Talanta*, in press.
(12) Uchida, H. *Spectrosc. Lett.* **1981**, *14*, 665.
(13) Demers, D. R.; Allemand, C. D. *Anal. Chem.* **1981**, *53*, 1915.
(14) West, A. C.; Fassel, V. A.; Kniseley, R. N. *Anal. Chem.* **1973**, *45*, 1587.
(15) Murayama, S. *Spectrochim. Acta, Part B* **1970**, *25B*, 191.
(16) Borowiec, J. A.; Boorn, A. W.; Dillard, J. N.; Cresser, M. A.; Browner, R. F.; Matteson, M. J. *Anal. Chem.* **1980**, *52*, 1054.
(17) Alkemade, C. Th. J.; Voorhuis, M. H. *Fresenius' Z. Anal. Chem.* **1958**, *163*, 91.
(18) Greenfield, S.; McGeachin, H. M.; Smith, P. B. *Anal. Chim. Acta* **1967**, *84*, 76.
(19) Uchida, H.; Matsui, H. *Bunko Kenkyu* **1978**, *27*, 110.
(20) Larkins, P. L.; Willis, J. B. *Spectrochim. Acta, Part B* **1974**, *29B*, 319.
(21) Zander, A. T.; O'Haver, T. C.; Keliher, P. H. *Anal. Chem.* **1977**, *49*, 838.
(22) Boumans, P. W. J. M.; DeBoer, F. J. *Spectrochim. Acta, Part B* **1977**, *32B*, 365.
(23) Browner, R. F.; Batel, B. M.; Glenn, T. H.; Rietta, M. E.; Winefordner, J. D. *Spectrosc. Lett.* **1972**, *5*, 311.
(24) Cochran, R. L.; Hieftje, G. M. *Anal. Chem.* **1977**, *49*, 2040.
(25) Shull, M.; Winefordner, J. D. *Anal. Chem.* **1971**, *43*, 799.
(26) Benetti, P.; Omenetto, N. O.; Rossi, G. *Appl. Spectrosc.* **1971**, *25*, 57.

RECEIVED for review November 5, 1982. Accepted December 20, 1982. This work was supported by AFOSR-F-49620-80-C-0005.

Furnace Atomic Absorption Spectrometry Atomizer with Independent Control of Volatilization and Atomization Conditions

Darryl D. Siemer

Exxon Nuclear Idaho Co., CPP 602, Idaho Falls, Idaho 83402

A graphite furnace atomizer featuring independent control of the temperatures of both an atomization zone and a spatially separate volatilization zone was constructed and characterized. Separate optically sensed temperature feedback controlled power supplies were employed to heat both zones. A number of previously documented matrix interference problems observed in analyses performed with furnaces of conventional construction were found to be greatly reduced or eliminated with this system.

Recent work in this laboratory has been directed toward the improvement of the routine reliability ("ruggedness") of trace element determinations in complex samples by graphite furnace atomic absorption spectrometry (GFAAS). These projects have included the modification of furnace power supplies to incorporate temperature feedback control (1); a study of the biases that the "slow" electronic signal processing circuitry commonly found in AAS spectrometers primarily designed for flame AAS impose onto GFAAS signals (2); and, finally, the modification of the atomizers themselves in order to increase the effective gas-phase temperatures experienced by volatile analyte elements "atomized" in several versions of Varian Techtron's carbon rod atomizer (CRA).

0003-2700/83/0355-0692$01.50/0 © 1983 American Chemical Society

The first approach to modified atomizers involved a version of the "cup-in-flame" technique described by L'vov (*3*). This technique is not really GFAAS because the CRA cup is only used to selectively volatilize the analyte into the flame which actually serves as the atomization volume. (See ref 2 for an example of this work.)

The second approach involved "end-heating" of an elongated CRA atomizer tube using four rods pinched in pairs across the ends of the tube (*4*). The next modification involved a simple change in heating rod placement with respect to a CRA cup's optical axis: instead of placing rods in the conventional across-the-bottom configuration, the rods were clamped across the top of the cup (*5*). A final paper described the development of both "cup" and "tube-cup" variations of the CRA featuring atomization temperatures for volatile analytes approximately a thousand degrees higher than are attainable with the standard design (*6*).

All of these modified furnaces significantly reduced the gas phase related "matrix effects" observed in the analysis of the types of samples for which they were designed. However, they also all share two drawbacks. First, they were deliberately designed so that the point within the atomizer upon which the sample is deposited heats more slowly than does the portion of the atomizer optically sampled by the AAS spectrometer. An unavoidable consequence of this is that the sample deposition point never achieves as high a temperature as it does in the standard furnace configurations. This restricts these furnaces to the determination of *only* volatile analytes and, in some instances, permits the buildup of an undesirably large amount of involatile matrix salt if the atomizer is used for a long series of determinations.

A second problem is one shared by both these atomizers and the "L'vov platform–Massmann furnace" system suggested by L'vov (and subsequently popularized by the Perkin-Elmer Corp.). This weakness is that in order to significantly increase effective atomization temperatures, the maximum possible furnace heating rate must be used. When this is done, careful control of the volatilization process is lost. Consequently, there is often an increase in the degree of overlap between the volatilization profiles of the analyte and the matrix which serves to counteract the beneficial effects of raising the atomization temperature (*7*).

Both this writer's previous efforts and the pioneering work of L'vov (*3*) and, later, that of Lundgren and Johansson (*8*), clearly indicated that a truly "rugged" and flexible GFAAS atomizer would have to feature atomization conditions truly independent of volatilization conditions. Physically, this means that the atomizer must possess two distinct zones and that each be heated independently of the other.

This paper describes an updated version of Lundgren and Johannson's basic furnace design possessing some new features likely to enhance its practical value. These features include a completely isothermal atomization zone (both spatially and temporally), temperature feedback control of both power supplies, an overall physical size compatible with most AAS spectrometers, and a simple design that does not require any part of the furnace to be moved during an analysis.

EXPERIMENTAL SECTION

Furnace. The graphite working parts of the furnace consist of a Massmann tube furnace (atomization zone) with a carbon rod atomizer (CRA) cup (volatilization zone) inserted into an access hole drilled in the center of the tube (Figure 1). The tube and cup were machined from 6.2 mm diameter AFX5Q graphite rod (Poco, Decatur, TX). Standard CRA rods (the same rods used with the Varian Techtron CRA 63/90 atomizer series) were used with the cups.

The central portion of the Massmann tube possesses a greater wall thickness than does the rest of the tube. Additionally, two relatively large oblong holes (end holes) were drilled through the

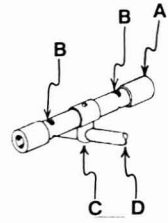


Figure 1. Graphite parts of the atomizer: (A) 6.2 mm outer diameter tube ends which are clamped into the electrode blocks; (B) holes limiting the length of the atomization zone; (C) CRA cup machined to fit into a 4.1-mm hole in the bottom of a Massmann tube; (D) CRA rods.

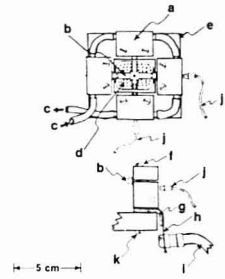


Figure 2. (Top) Top view of atomizer: (a) electode blocks; (b) Massmann tube; (c) water cooling lines; (d) holes in bottom of inert gas sheath system; (e) base plate. (Bottom) Detail of an electrode block (for the Massmann tube): (f) steel screw to clamp the graphite tube into place; (g) neoprene rubber gasket; (h) copper foil; (i) no. 4 welding cable to the power supply; (j) optical temperature sensor (of the CRA power supply); (k) nylon screw.

tube vertically (parallel to the axis of the CRA cup) 8 mm from the center of the tube at both ends. The variation in wall thickness and the presence of the holes serve to balance the I^2R heat-producing phenomena with the conductive heat loss to the ends of the tube and, therefore, provide a spatially isothermal atomization zone between the end holes.

Volatilized analyte is swept out of the light path at these end holes by an argon (or argon/propane mixture) gas stream directed vertically upward through holes in a perforated plate situated under the graphite parts. In practice, therefore, the spacing between these end holes defines the effective length of the optical path (in this instance 1.6 cm). The tube was designed in this way to give a high (and unambiguous) effective optical-path temperature and to prevent the "double peaking" often observed in conventional Massmann tube furnaces (*9*).

The graphite parts were clamped in electrode blocks machined from 19 mm thick aluminum plate. These four electrode blocks were mounted onto a 12.7 mm thick rectangular aluminum base plate with nylon screws (see Figure 2(top) for a top view of the system). Holes in the electrode blocks were drilled to accommodate the tube (or rods), hold-down screws (in which case the holes were then tapped), the cooling water passage, and the optical probe. Then each block was sawed laterally across the center line of the rod (or tube) hole to permit ready replacement of the graphite parts. Figure 2(bottom) is a side view of one these electrode blocks showing the power cable connection and an optical temperature sensing probe.

Electrical power connections to each block were made with three 2.2 cm wide, 0.127 mm (0.005 in.) thick strips of heavy copper foil sandwiched between the block and the 2 mm thick soft neoprene rubber gasket which serves to electrically insulate the block from the base plate. The rubber gasket–nylon screw combination also serves to allow the electrode blocks enough flexibility to prevent breakage of the graphite parts when they expand upon

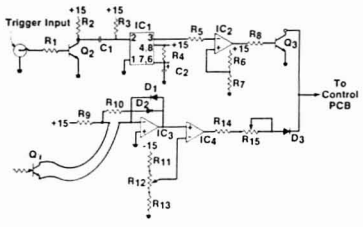


Figure 3. Schematic of the modification to the M63 power supply: Q_1, HEP 312 phototransistor; IC_1, SNE555; IC_2–IC_4, 741 operational amplifier; Q_2, 2N3904; D_{1-3}, 1N4007; R_1, R_3, R_{5-8}, 20 kΩ; R_2, 10 kΩ; R_4, 1 MΩ, R_9, 1 kΩ; R_{10}, 20 MΩ; R_{11}, 3 20 kΩ; R_{12}, 10 kΩ ten-turn; R_{13}, 5.1 kΩ; R_{14}, 12 kΩ; R_{15}, 25 kΩ one-turn; C_1 0.001 μF; C_2 10 μF.

heating. The center line of the CRA rod holes is 7 mm below that of the Massmann tube.

Power Supplies. The power supply used to heat the CRA cup during the "dry", "ash", and "volatilize" stages is a Varian Techtron M63 CRA power supply modified to provide both optical feedback control of the volatilization temperature and an interface with the power supply used to heat the Massmann tube. In operation, only the CRA power supply is "on" during the "dry" and "ash" portions of the experimental cycle. At the end of the "ash" cycle, the Massmann tube's power supply is turned "on" and the CRA supply is shut "off". When the Massmann tube reaches its preset atomization zone temperature, the CRA supply is turned back on to volatilize the sample. Both the heating rate and the final temperature of the CRA cup are essentially independent of the temperature of the Massmann tube.

The circuitry added to the M63 power supply necessary to implement the desired functions is shown in Figure 3. It incorporates the simple, optically sensed, temperature feedback control circuitry described in a previous report (ref 1) with a triggerable switching circuit; this circuit prevents the CRA cup from being heated until the Massmann tube's power supply outputs a signal indicating that the atomization zone's temperature is at the desired level. The four integrated circuit "chips" and the associated discrete circuitry were all mounted in a small prototype "bread board" and connected to the rest of the internal circuitry with jumper wires as described in ref 1.

A schematic diagram of the power supply used to heat the Massmann tube is give in Figure 4. Because the supply serves only one function (i.e., to heat the Massmann tube to a desired temperature for a fixed time), it is very simple. Basically it consists of a 2.4 KVA 10:1 step-down transformer (Signal Transformer Co., Inwood, NY) and a 25 A, 400 V, triac. Switching current to this triac is supplied by an optically coupled, zero-crossing trigger integrated circuit "chip" (IC 1). This IC is, in turn, controlled by a circuit similar to that added to the CRA 63 power supply described above. The control circuitry functions as follows: When the triggerable monostable multivibrator IC (SNE 555) is triggered "on" (by a negative-going pulse output from the CRA 63 power supply at the end of its "ash" cycle), its output goes "high" and drives current (through R_5) to the photodiode within the triac trigger IC. This IC then turns on the triac in series with the primary winding of the power transformer. However, when the temperature of the tube becomes so high that the output of the logarithmic amplifier (IC_3) becomes negative with respect to the setpoint of potentiometer R_{12}, the comparator (IC_4) will "short" the output of the timer IC to ground with transistor Q_2, thereby shutting "off" the power supply until the temperature of the graphite falls below the desired level.

Some hysteresis (overshoot) was added to the temperature setpoint comparator circuit (with R_9) in order to prevent the supply from "locking in" to the 60 Hz mains frequency and possibly switching significantly more mains power half-cycles of one polarity than the other through the primary of the transformer. (If this should happen, the transformer core will saturate which results in overheating and/or a "blown" circuit breaker.)

Pieces of fine-bore ceramic tubing (of the sort usually used as high-temperature insulation for thermocouple wires) blackened

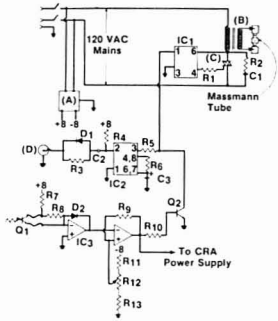


Figure 4. Schematic of Massmann tube power supply: (A) ±8 V logic power supply; (B) 2.4 KVA transformer; (C) GE SC260 D triac; (D) trigger input from CRA power supply: IC_1, MOC 3031; IC_2, SNE555; IC_{3-4}, 741 operational amplifier; R_1, 56 Ω; R_2, 100 Ω; R_3, 1 MΩ; R_4, 75 kΩ; R_5 Ω; R_8, 5.1 MΩ; R_7, R_{10}, 1 kΩ R_8, 20 MΩ; R_9, 2 MΩ; R_{11}, 18 kΩ; R_{12}, 2 kΩ ten-turn; R_{13}, 510 Ω; C_1, 0.01 μF 400 V; C_2, 0.1 μF; C_3, 1 μF; Q_1, HEP 312 phototransistor; Q_2, 2N3904; $D_4$007.

with "Aqua Dag" (a suspension of colloidal graphite powder in ammonia water) were inserted through holes drilled in the electrode blocks to act as simple "light pipes" for the phototransistors used as temperature sensors (see Figure 2). The front ends of these tubular "light pipes" were placed approximately 0.5 cm from the graphite surface whose temperature was to be regulated. The phototransistors were attached to the other end of the ceramic tubes with several sizes of black plastic "heat shrink" electrical insulation. To extend the range of temperature regulation upward, the effective apertures of these "light pipes" were reduced by inserting pieces of electrical insulation stripped from 28 gauge wire into the "cool" ends of the ceramic tubes.

Instrumentation. The same atomic absorption spectrometer (Varian Techtron AA6 optical components with electronically "fast" homemade analog signal processing circuitry), Hewlett-Packard computer data acquisition and display system, Thermodot optical pyrometer, and homemade gas regulation equipment described in the previous papers was used for this project (*2*, *5*, *6*).

Reagents and Supplies. All solutions used were prepared with doubly deionized water and reagent grade (or better) chemicals. Solutions were manually pipetted with Oxford micropipets. These pipets feature uniform diameter plastic capillary tubing tips instead of the more common conical plastic variety. Micropipets featuring conical tips are *not* suitable because the sample aliquots must be placed into the CRA cup *through* the entire diameter of the Massmann tube. To do this with a conical tipped pipet would require a sample access hole so large that significant analytical sensitivity would be lost.

RESULTS AND DISCUSSION

The temperature setting potentiometers of the power supplies were calibrated by directing the light (temperature) sensors at the Massmann tube and recording the voltage output of the logarithmic amplifier circuits in the temperature control circuits while that tube was heated. (This is done with the same programmable DVM–computer system used to measure the analytical signals.) The temperature–time response of the Massmann tube upon heating was established by similarly recording the output of the optical pyrometer aimed at the same point. A correlation of the temperatures indicated by the optical pyrometer with the voltages of the logarithmic amplifier at various points in time allowed the corresponding potentiometer voltages to be assigned definite temperature values.

The range of temperatures controllable by the power supplies (as configured for this paper) was from 1250 to 2750 K

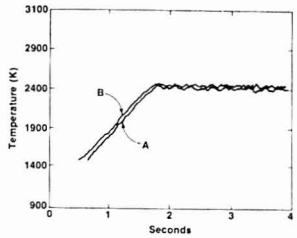


Figure 5. Heating rate of atomization zone (A) at the center and (B) at the end.

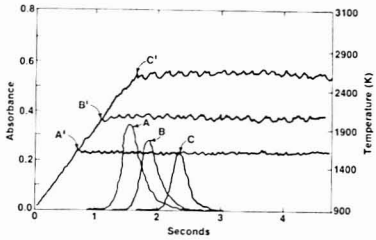


Figure 6. Cadmium signals observed at different atomization temperatures: (A) signal seen at 1640 K; (B) signal seen at 2104 K; (C) signal at 2632 K. The primed letters depict the point in time and the tube temperature at which the volatilization power supply was turned on in each case.

for the Massmann supply and from 1200 to 2550 K for the CRA system. These control ranges can be readily adjusted in either direction by changing the effective aperture of the ceramic light pipes.

Figure 5 shows the heating rates measured at the center (A) and at the inner edge of one of the end holes (B) in the Massmann tube. The hysteresis deliberately added to the power supply control circuitry is responsible for the approximately 40 K of "jitter" in the setpoint temperatures at the top of the plateaus. On these plateaus, the power supply periodically turns itself "on" and "off" to maintain the desired temperature and "overshoots" about 20 K each time it switches.

A series of experiments which illustrate the degree of independence achievable between the volatilization and atomization processes are depicted in Figure 6 In this and all other figures in this paper showing actual "raw" analytical data, the computer's data acquisition cycle was initiated at the instant that the Massmann furnace started to heat up. The signals shown in all of the figures were not subjected to any digital "smoothing routine" and represent unbiased instrument responses. In this particular experiment, 20 pg samples of cadmium were volatilized into the Massmann tube preheated to three different temperatures. The same volatilization power supply program was used in each case, viz., a temperature ramp at about 1 K/ms to a final, stable, CRA cup temperature of 2000 K. It is important to remind the reader that this CRA volatilization program does not begin until the Massmann tube has reached the desired atomization zone temperature (at the times indicated by the letters A′, B′, and C′ on the temperature–time traces in Figure 6). The atomic absorbance signals observed at the three successively increasing atomization temperatures are correspondingly labeled A, B, and C.

As expected the magnitudes of the analytical responses decrease as the temperature of the atomization zone increases.

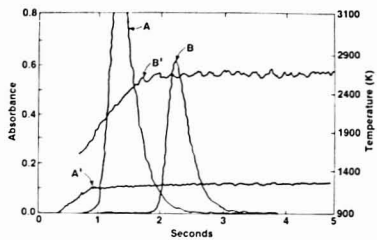


Figure 7. Mercury signals at different atomization temperatures: (A) signal seen at 1279 K; (B) signal seen at 2641 K.

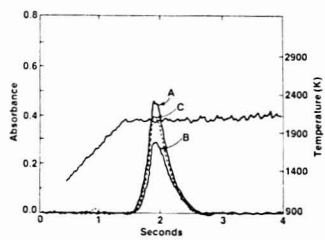


Figure 8. Signal transients observed for lead at three spectral lines arising from different energy levels: (A) 100 ng of lead at 368.3 nm; (B) 100 ng at 280.2 nm; (C) 1 ng of lead at 283.3 nm.

This is due to the fact that each individual atom spends less time within the tube at higher temperatures (residence time is diffusion controlled and gaseous diffusion constants are inversely related to temperature).

Please note that in each instance, the interval between the initiation of the volatilization heating program and the appearance of the atomic absorption signal is essentially independent of the temperature of the atomization zone. This degree of independence is possible because the CRA rods clamped onto the cup act as efficient "heat sinks" preventing the volatilization zone from being significantly heated either by radiation from the tube or by conduction along the walls of the cup itself.

Figure 7 shows the results of a similar experiment performed with mercury. Two-microliter aliquots of a 10 mg/L mercury solution (stabilized with 1% nitric acid and 0.01% sodium dichromate) were atomized at either 1280 K (A′, A) or 2640 K (B′, B). Figures 6 and 7 demonstrate that, with this furnace, an analyst has the freedom to choose atomization conditions based on whether achieving the maximum possible sensitivity (compatible with a cool atomization zone featuring long individual atomic residence times) or the greatest assurance of freedom from gas-phase interferences (hot atomization zone) is more important for solving the problem at hand. The flame spectroscopist routinely makes the same decision for similar reasons in choosing which flame to use.

The gas-phase temperatures experienced by analyte atoms were independently determined by a "two-line" spectroscopic method using lead as the test element. The detailed procedure for doing this has been described in previous papers (*5*, *6*). The results of a typical experiment are shown in Figure 8. The larger of the two absorption transients denoted by the solid lines is the signal seen from 100 ng of lead using the 368.3-nm line (originating from an energy state 7819 cm^{-1} above ground) and the smaller is the response seen for the same amount of lead at the 280.2-nm line (10 650 cm^{-1} above ground). The dashed line is the signal seen from 1 ng of lead

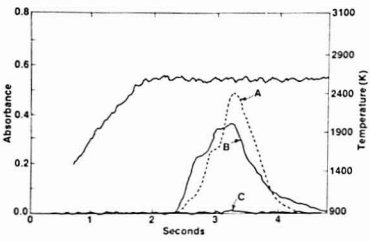


Figure 9. Signal transients for lead in both dilute nitric acid and a "hard water" matrix: (A) in nitric acid; (B) in 5 μL of matrix (51 μg of mixed salt); (C) matrix alone.

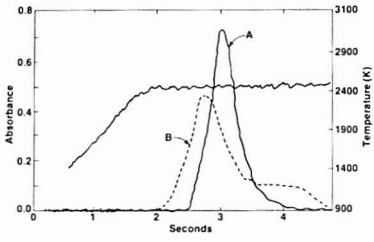


Figure 10. Thallium in both nitric and perchloric acid: (A) 2.5 ng of Tl in 0.16 M HNO_3; (B) 2.5 ng of Tl in 0.5 M $HClO_4$.

observed at the 283.3-nm resonance line (ground state). The spectroscopic temperature (based on the relative sizes of the two nonresonance line signals) was 2060 K, which is in good agreement with the 2100 K temperature setpoint of the Massmann furnace. Similar experiments at other nominal temperature setpoints gave equally good agreement with measured graphite temperatures.

In order to demonstrate the practical analytical advantages of this atomizer, a series of signal recovery studies were performed for several volatile analyte metals in matrices which have been reported to cause severe problems with conventional furnaces. In the following examples, the comparisons made between the new furnace and conventional systems were based on published reports of what this writer considers to be reliable research performed by experienced workers able to get the best possible performance from the particular atomizer used for the work. The general conclusions drawn about any particular manufacturer's product will apply with equal force to other basically similar systems.

Figure 9 depicts a complete, representative experiment showing the analytical signals seen from 2.5 ng of lead in either (a) 1% nitric acid or (b) an acidified "hard water" matrix. The matrix chosen was similar to those studied by Manning and Slavin in their 1979 paper describing the advantages of using a L'vov platform in the Perkin-Elmer HGA 500 version of the Massmann furnace (*10*). The matrix solution used for this example actually represents a "worst case" and contains all of the concomitants at the maximum levels of the range of concentrations listed in Manning and Slavin's paper (Ca, 800 mg/L; Mg, 800 mg/L; SO_4, 5000 mg/L; Cl, 100 mg/L as well as 973 mg/L of sodium and 2650 mg/L of nitrate added in salt form). This solution was acidified with nitric acid to the 1% (v/v) level usually recommended for trace element studies. Five-microliter aliquots of the solution were used (a total of 51 μg of mixed salts) in the experiment. The furnace heating program consisted of a 40-s "dry" cycle at 95 °C, a 10 s "ash" cycle at approximately 400 °C, and a final CRA volatilization temperature of 2100 K. The temperature of the Massmann tube was 2700 K.

The recovery of lead from the hard water matrix was 99.7% in this experiment. (This is based on the relative sizes of the *integrated* signals after correction for the small reagent blank.) The mean recovery for five replicates of the experiment was 100.4%.

The *shapes* of the analytical signals are not identical; nor is it reasonable to expect them to be so. The shapes of GFAAS signals are largely determined by the volatilization characteristics of the analyte. These characteristics are in turn determined by the physical and chemical state of the analyte at the end of the "ash" stage. However, because the individual atomic residence times within the atomization zone of this furnace are independent of the volatilization characteristics of the analyte, the time integrated atomic absorbance signals are *not* different. In other words, it is not necessary to experiment with different "matrix modifiers" and "ash" programs until a set of conditions are found under which the analyte in both the sample and the standard *volatilizes* in exactly the same way in order to get an unbiased analytical result.

Koirtyohann, Glass, and Lichte (*11*) recently reported that the use of perchloric acid in sample preparation caused essentially total suppression of thallium signals (as well as those of some other metals) when analyses were attempted with a conventional Massmann furnace (a Perkin-Elmer HGA 2100).

Figure 10 depicts analytical signals seen with the dual-power supply furnace for thallium in both 0.16 M nitric acid and 0.5 M perchloric acid. A 10-s "ASH" program at about 250 °C was used prior to volatilizing the analyte into the preheated Massmann tube (2540 K). A 25:1 argon to propane gas mixture at a flow rate of 8 L/min was used to sheath the graphite parts.

As was the case for lead in the experiment described above, differently *shaped* atomic absorption signals are observed for thallium in the two different sample matrices. However, as explained previously both in this paper and in Sturgeon's review article (*12*), the best measure of analytical response in isothermal furnaces is the integral, not the peak height.

The mean recovery of thallium from the perchloric acid relative to from the nitric acid (three replicates of each experiment) was 103%. The pooled relative standard deviation for the experiments was 4.1% which makes a definite statement about the existence (or absence) of a matrix effect difficult to justify: if there *is* one, it is small.

When the experiment was repeated with argon alone as the sheath gas, the apparent recovery of thallium in the perchloric acid dropped from 103% to 77%. The reason for this is unproven but is probably due to the presence in the CRA cup of an oxygen and/or chlorine residue formed when perchloric acid is evaporated from graphite (*13*). The covolatilization of this material with the analyte during the ensuing "atomize" cycle would explain the reported signal suppressions. The pyrolysis products of the propane used in the first set of experimental conditions are good "scavengers" for both chlorine and oxygen (the carbonaceous moiety for oxygen and the hydrogen for chlorine).

The recovery of thallium signals from sample solutions containing $MgCl_2$ was studied by Manning and Slavin using an HGA 2200 furnace modified so that samples were introduced into it on a tiny coil of tungsten wire inserted *after* the furnace had achieved thermal equilibrium (*9*). These experiments were repeated with this furnace with the results shown in Figure 11. A $MgCl_2$ concentration of 4% (200 μg of the salt) was necessary to reduce the thallium signal recovery by 50% when an atomization zone temperature of 2650 K was used. This concomitant concentration is 20-fold higher than that which the *temporally* isothermal system described

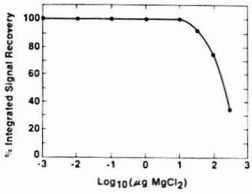


Figure 11. Percent integrated thallium signal recovery as a function of the amount of $MgCl_2$ present in the sample aliquot.

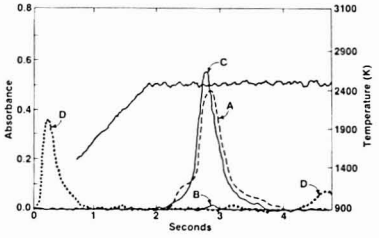


Figure 12. Cadmium signal recovery in a raw urine matrix: (A) cadium in 0.01% HNO_3; (B) urine alone; (C) urine "spiked" with cadmium; (D) background "smoke" signals from urine (dotted line).

by Manning et al. could accommodate, even when their furnace was used at a nominal atomization temperature of 2973 K (*9*). The probable reason for the difference in performance is that the Massmann atomizer tube used in this study is *spatially* as well as *temporally* isothermal. In contrast, the HGA 2200 furnace, as do most commercial versions of the basic Massmann design, possesses cool ends through which the cloud of volatilized sample must pass when the furnace is used in the "gas stop" mode usually recommended when a "platform" or "probe" is to be used. Analyte atom–matrix concomitant chemical association occurs at these cool zones reducing the atomic absorption signals seen when matrix is present. Another consequence of the cool tube ends is that some of the molecular species which cause much of the nonatomic absorption background signal are also formed there. With the furnace described in this paper, these "background" signals are often much smaller than those observed in conventional Massmann furnaces.

A graphic example of the practical utility of this furnace is depicted in Figure 12. Basically, what the figure demonstrates is a signal recovery of 97% when a 50-pg "spike" of cadmium was added directly to a 5-μL aliquot of a pooled "raw" human urine specimen. (The mean recovery for six such experiments was 99.2% with a relative standard deviation of 3.4%.) No "matrix modification" or elaborate prior chemical or thermal sample pretreatment procedure was used. The sample aliquot was simply dried at about 95 °C, "ash"ed for 10 s at approximately 300 °C in order to drive some of the more volatile organic compounds out of the cup, and finally volatilized into the preheated atomization zone (2500 K). The temperature of the CRA cup was raised at a rate of approximately 300 K/s to a final temperature of 1500 K. The dotted line on the figure is the nonatomic background absorbance signal measured with the hydrogen continuum lamp. The initial "smoke" peak occurs when the matrix material volatilized from the CRA cup (and then condensing in the Massmann tube) during the "dry" and "ash" cycles is revolatilized as the tube's temperature starts to rise. The final nonatomic absorbance peak is probably due to the bulk of the matrix salts volatilizing after the cadmium has left the tube.

The preceding examples demonstrate the relative "ruggedness" of determinations performed with this furnace as compared to those done with systems which do not permit independent control of volatilization and atomization conditions. In the examples shown, no extensive effort was expended in attempting to discover the "optimum" set of analytical conditions for each analysis because the additional effort would not have resulted in significantly improved analytical results. When conventional atomizers are used for analysis, it is usually the research effort necessary to find a satisfactory set of experimental parameters (suitable "matrix modifier(s)" and "ash" program) that makes the overall procedure tedious and "difficult" . . . not the final determination itself.

The extremely high prices of the latest commercial GFAAS systems can be largely attributed to the degree of automation incorporated into them in order to make these "in situ" sample preparation steps less tedious and more precise.

This furnace in its present state of development represents only the writer's first attempt at implementing control of both of the fundamental processes taking place in GFAAS determinations. However, it does combine the stable, high-temperature, atomization environment seen in L'vov (*3*, *14*) and Woodriff (*15*, *16*) furnaces with the useful "in situ" thermal sample pretreatment capability and volatilization control characteristics of the commercially available furnaces.

The following changes would further enhance the practical utility of this furnace. First, the electrode blocks should be made of nickel-plated brass instead of aluminum (which tends to oxidize). Second, the addition of temperature feedback control circuitry to the "ash" stage of the CRA power supply would be desirable. Third, the Massmann tube should be heated during the "ash" stage to prevent volatilized matrix material from condensing there. Fourth, and finally, better temperature regulation (±10 K) of the Massmann tube would permit the accurate routine analysis of a number of metals using nonresonance atomic lines (*17*).

ACKNOWLEDGMENT

The author thanks both Norm Graham and Harry Brinkley for help in the construction of the atomizer. He also thanks L. C. Lewis for providing both the helpful advice and moral support necessary for the continuation of this line of research.

LITERATURE CITED

(1) Siemer, D. D. *Appl. Spectrosc.* **1979**, *33*, 613.
(2) Siemer, D. D.; Baldwin, J. M. *Anal. Chem.* **1980**, *52*, 295.
(3) L'vov, B. V. *Spectrochim. Acta, Part B* **1978**, *33B*, 153.
(4) Siemer, D. D. *Anal. Chem.* **1982**, *54*, 1659.
(5) Siemer, D. D. *Appl. Spectrosc.*, in press.
(6) Siemer, D. D.; Lewis, L. C. *Anal. Chem.* **1983**, *55*, 99.
(7) Czobik, E. J.; Matousek, J. P. *Anal. Chem.* **1977**, *50*, 2.
(8) Lundgren, G.; Johansson, G. *Talanta* **1974**, *21*, 257.
(9) Manning, D. C.; Slavin, W.; Myers, S. *Anal. Chem.* **1979**, *51*, 2375.
(10) Manning, D. C.; Slavin, W. *Anal. Chem.* **1979**, *51*, 261.
(11) Koirtyohann, S. R.; Glass, E. D.; Lichte, F. E. *Appl. Spectrosc.* **1981**, *35*, 22.
(12) Sturgeon, R. E. *Anal. Chem.* **1977**, *49*, 1255A.
(13) Slavin, W.; Manning, D. C. *Prog. Anal. At. Spectrosc.* **1982**, *5*, 243.
(14) L'vov, B. V. "Atomic Spectroscopy"; Isreal Program for Scientific Translation: Jerusalem, 1969.
(15) Hagemann, L.; Mubarek, A.; Woodriff, R. *Appl. Spectrosc.* **1979**, *33*, 226.
(16) Hagemann, L.; Nichols, H. A.; Viswandham, P.; Woodriff, R. *Anal. Chem.* **1979**, *51*, 1406.
(17) Siemer, D.; Stone, R. *Appl. Spectrosc.* **1975**, *29*, 240.

RECEIVED for review September 23, 1982. Accepted January 12, 1983.

Differential Normal Pulse Voltammetric Oxidation of Mercury in the Presence of Iodide

Timothy R. Brumleve,[1] Robert A. Osteryoung, and Janet Osteryoung*

Department of Chemistry, State University of New York at Buffalo, Buffalo, New York 14214

The technique of differential normal pulse voltammetry with alternating sign of the second pulse is applied to the determination of iodide at a static mercury drop electrode. The greatest analytical utility is found for low iodide concentrations and small pulse widths, which limit the surface coverage of adsorbed product to a small fraction of a full monolayer. Under these conditions the differential normal pulse responses are diffusion controlled and provide linear analytical working curves. A diffusion-controlled, partial electron-transfer adsorption mechanism is developed which accounts for the observed behavior at small coverage.

The technique of differential normal pulse (DNP) voltammetry employs a wave form which is a hybridization of the differential pulse (DP) and normal pulse (NP) wave forms. The working electrode spends most of the time at an initial potential, E_i, and the faradaic reaction takes place during the application of double potential pulses of short duration (typically 1–500 ms). The resulting voltammetric response is the differential display of currents sampled near the end of each step of the double pulse. This technique thus provides the advantage of peak shaped voltammograms (as obtained in DP voltammetry) while limiting the extent of the faradaic reaction (as in NP voltammetry).

Recently DNP voltammetry has been applied to reversible reactions at mercury electrodes (*1*) and irreversible reactions at solid electrodes (*2*). A certain sequence of pulse application (referred to as the alternating pulse mode (*1–3*)) has been found to be advantageous for improving the voltammetric peak shape and reducing background responses. The alternating pulse modification involves subtraction of the voltammograms obtained from differential (second) pulses of alternating sign and yields symmetric (*1*) or nearly symmetric (*2, 3*) voltammetric peaks. This procedure resembles techniques involving differencing of NP responses (*4, 5*), and equivalent information may result (at least in cases where kinetic complications are absent). The truly differential forward and reverse DNP responses, however, provide additional diagnostic information not available with subtractive NP methods.

This paper is concerned with the application of the DNP technique in the alternating pulse mode of the determination of I^- at a static mercury drop electrode (SMDE). While a number of cathodic stripping techniques for iodide and other halides have been reported (*6–11*), direct pulse voltammetric determinations have received little attention (*12*). Although direct pulse methods cannot be expected to attain the detection limits of cathodic stripping techniques (see especially ref 6)), they offer the advantages of fast analysis and freedom from such interferences as slow halide exchange reactions encountered in simultaneous halide stripping determinations (*7, 8*). Although this study does not treat rigorously the subject of detection limits and chemical interferences, the applicability of the DNP technique is demonstrated at I^- concentrations as low as 9.7 μM (1.2 ppm).

[1] Present address: Anderson Physics Laboratories, 406 N. Busey Av., Urbana, IL 61801.

At low I^- concentrations (<100 μM), and with symmetrical double pulses ($t_1 = t_p = 50$ ms), the DNP technique in the alternating pulse mode shows distinct advantages over NP voltammetry in terms of peak-shaped nature of the responses. In this range (which corresponds to <6% of full monolayer product coverage) linear analytical calibration curves result, and the responses are diffusion controlled. However, for I^- concentrations above 100 μM (or for pulse widths greater than $t_1 = t_p = 50$ ms) the calibration curves become nonlinear, and an abrupt change in mechanism is suggested by the changes in the dependence of the peak currents and peak potentials on pulse width.

The ideal, low-coverage responses are interpretable in terms of a diffusion-controlled adsorption mechanism. The results of this analysis indicate that the adsorbed product undergoes only partial (noninteger) electron transfer, in agreement with previous work on underpotential deposition and electrosorption on similar systems (*13, 14*). The results of the mechanistic analysis then permit development of a quantitative criterion for the combination of I^- concentration and pulse widths for which the ideal, low-coverage behavior is observed. The abrupt change in mechanism at larger concentrations and pulse widths is interpreted as a change in stoichiometry of the electrode reaction: from the adsorption of partially discharged iodide at low coverage, to the deposition of a complete monolayer (or monolayers) of Hg_2I_2.

EXPERIMENTAL SECTION

The computer-controlled pulse voltammetric instrument has been described previously (*1*). Currents were measured by gated integration over a time period t_4.

All experiments on the I^- system were conducted with a EG&G/PARC Model 303 static mercury drop electrode (SMDE) as the working electrode. The small drop size (area 0.0104 cm^2) was used for all experiments. The internal Ag/AgCl reference electrode provided with the SMDE was removed and a conventional SCE/salt bridge arrangement was substituted. The Pt wire provided with the SMDE was used as the auxiliary electrode. Analyte solutions were throughly degassed with purified argon. All chemicals were reagent A.C.S. grade. Distilled water was repurified with a Millipore Milli-Q filtration system.

The 0.5 M CH_3COOH/0.5 M CH_3COONa buffer system (pH 4.7) was chosen as the supporting electrolyte for control of pH conditions. Previous studies of I^- oxidation on mercury (*6, 15*) have indicated that acidic conditions prevent formation of HgO and HgI_2 deposits. In addition to the acetate buffer, a preliminary evaluation of two other supporting electrolyte systems was conducted: 0.1 M KNO_3 adjusted to pH 2 with HNO_3, and neutral 0.1 M $NaClO_4$. NP or DNP voltammetric responses for 0.1 mM iodide were essentially the same in all supporting electrolytes, although the potential for anodic oxidation of mercury differed in the three media.

An initial (or delay) potential, E_i, of –0.8 V vs. SCE was chosen for all pulse voltammetric experiments. This is the potential at which each Hg drop grows and stabilizes and is the base line from which the DNP double pulses are applied (see Figure 1). This value (–0.8 V) is 0.5 V more negative than the most negative peak potential or half-wave potential observed. In order to evaluate the possible interference of specific adsorption of undischarged I^- on the observed anodic responses, preliminary studies were conducted in which both the initial potential, E_i, and the delay time at this potential, t_i, were varied. Both the NP and DNP

0003-2700/83/0355-0698$01.50/0 © 1983 American Chemical Society

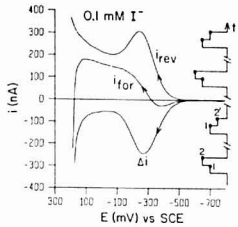


Figure 1. Forward (i_{for}), reverse (i_{rev}), and alternating pulse difference (Δi) DNP voltammograms for the oxidation of 0.1 mM I^-. The alternating pulse DNP wave form is illustrated schematically at the right. Experimental parameters are as follows: $t_1 = t_p = 50$ ms; $t_s = 16.7$ ms; $\Delta E = 50$ mV; $t_i = 0.4$ s.

voltammetric responses for 0.1 mM I^- were independent of these parameters in the range $-0.7 \leq E_i \leq -1.0$ V vs. SCE and $0.4 \leq t_i \leq 2.0$ s.

RESULTS AND DISCUSSION

Figure 1 illustrates the alternating pulse DNP wave form and the voltammetric response of 0.1 mM I^- in 0.5 M CH_3COOH/0.5 M CH_3COONa at the SMDE. A complete discussion of the DNP wave form and associated timing parameters and current sampling modes may be found in the literature (*1*). The following discussion summarizes the features of the wave form relevant to the present case.

Most of the time is spent at an initial potential, E_i, and as in NP voltammetry, successively larger pulses to a potential E_1 are applied for time t_1. At time t_1 a small differential pulse of magnitude ΔE is imposed for time t_p. In the alternating pulse mode the sign of ΔE is changed on alternate double pulses. The forward current is the differential display of the currents sampled at points 2 and 1 (at potentials E_2 and E_1), $i_{for} = i_2 - i_1$. The reverse current is similarly obtained from currents sampled at points 2′ and 1 (at $E_{2'}$ and E_1), $i_{rev} = i_{2'} - i_1$. The alternating sign difference current, $\Delta i = i_{for} - i_{rev}$, is computed experimentally as $\Delta i = i_2 - i_{2'}$ to avoid introduction of noise by subtraction of successive values of i_1.

In the present case at the SMDE, a new stationary Hg drop is dispensed at the end of each double pulse (after current sampling at points 2 and 2′ of Figure 1). The discontinuities in the wave form (broken lines) indicate a delay time, $t_i = 0.4$ s, at the initial potential ($E_i = -800$ mV) between application of the double pulses. This allows each Hg drop to grow and stabilize at the initial potential (with zero faradaic current) before the double pulses are applied.

The voltammetric response illustrated in Figure 1 contains a number of distinctive features. The reverse current (i_{rev}) exhibits a large cathodic peak at about −250 mV whereas only a small anodic peak appears in the forward current (i_{for}). Both forward and reverse currents show a sloping current–voltage response in the region from −100 to +100 mV. The resulting difference current, Δi, has an asymmetrical anodic peak and does not return to zero current in the region −100 to +100 mV. (This is not background current, as shown below.) These features are inconsistent with the behavior of simple reversible or irreversible electrode reactions (*1–3, 16*). This fact and the experimental results which follow clearly suggest a mechanism in which the product of the electrode reaction is adsorbed totally and reversibly on the Hg surface. The proposed mechanism for small surface coverage is discussed in more detail below.

Concentration Dependence. Figures 2 and 3 illustrate the Δi and NP voltammetric responses of the I^- system in the concentration range 0.0097 to 1.7 mM. The NP response is

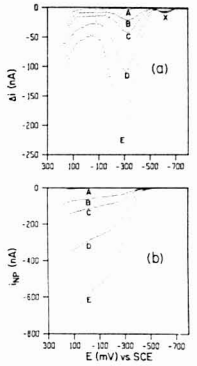


Figure 2. (a) Alternating pulse DNP voltammograms (Δi) and (b) normal pulse voltammograms (i_{NP}) for low I^- concentrations. NP responses are acquired simultaneously with the DNP responses. All parameters are the same as those given in Figure 1 except I^- concentration (μM): (A) 0, (B) 9.7, (C) 19, (D) 47, (E) 89.

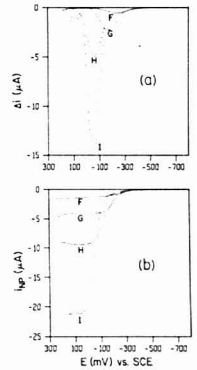


Figure 3. (a) Alternating pulse DNP voltammograms and (b) NP voltammograms for high I^- concentrations. All parameters are the same as those given in Figure 1 except I^- concentration (mM): (F) 0.18, (G) 0.44, (H) 0.87, (I) 1.7. In (a) parts of curves H and I (at potentials less than −150 mV) have been omitted for clarity.

always obtained simultaneously with the DNP wave form and is simply the current sampled at time t_1. The Δi voltammograms of Figure 2a for very low I^- concentrations (curves B–D) show no significant shift in peak potential ($E_p = -320$ mV) or change in peak shapes as the I^- concentration is increased. The Δi response of curve E (89 μM) begins to deviate from that of curves B–D, and the peak potential is shifted by about 40 mV to $E_p = -280$ mV. (The peak labeled × in Figure 2a is due to an impurity in the supporting electrolyte, probably Cd^{2+} which is being plated in at $E_i = -800$ mV and anodically stripped. The analogous wave is also present in the NP responses but does not appear in Figure 1b because positive currents were not plotted.)

The NP voltammograms of Figure 2b exhibit similar behavior in that waves B–D are all isomorphic; curve E deviates only slightly in shape. All of the NP voltammograms exhibit a sloping current–voltage response in the range −100 to +100 mV. This is not an additive background effect (note back-

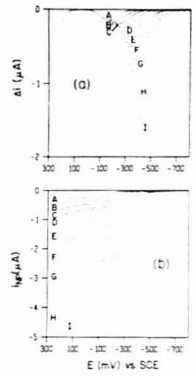


Figure 4. Pulse width dependence of (a) Δi voltammograms and (b) NP voltammograms for the oxidation of 0.1 mM I^-. All parameters are the same as those given in Figure 1 except pulse widths and sampling times, $t_1 = t_p = 3t_s$ (ms): (A) 500, (B) 200, (C) 100, (D) 50, (E) 20, (F) 10, (G) 5, (H) 2, (I) 1. In (a) parts of curves B–I (at potentials positive of the peak potentials) have been omitted for clarity.

ground scan, curve A). The lack of a well-defined NP limiting current in this concentration range severely limits the analytical utility of the NP wave form. In contrast, the Δi responses of Figure 2a show well-defined, easily measured peak currents. The poorly defined NP limiting currents are manifest in the Δi response only as a nonzero current (near 0.0 V) with slight asymmetry of the peak.

Figure 3 illustrates the Δi and NP responses for high I^- concentrations (0.18–1.7 mM, curves F–I). As the I^- concentration is increased, the Δi responses show a drastic shift in peak potential (from $E_p = -230$ mV for curve F to $E_p = -65$ mV for curve I), with a corresponding decrease in peak width at half height ($W_{1/2} = 200$ mV for curves B–F, to $W_{1/2} = 105$ mV for curve I). Peaks F–H are more symmetric than those of Figure 2a and return to zero current in the vicinity of +100 mV. The NP voltammograms (F–I) now exhibit well-defined limiting currents and show increasingly sharper waves (e.g., decreasing $E_{3/4} - E_{1/4}$) with a shift of $E_{1/2}$ to more positive potentials as the I^- concentration is increased.

The peak currents (Δi_p) of Figures 2a and 3a, measured from the zero concentration curve, A, and given together with the corresponding concentration of iodide are (μA, mM): B (0.0209, 0.0097), C (0.0417, 0.0185), D (0.109, 0.0462), E (0.219, 0.0882), F (0.481, 0.176), G (2.26, 0.436), H (4.86, 0.864), I (14.9, 1.69). These points, if plotted as a calibration curve, show excellent linearity for low concentrations (A–D: slope = 2.37 μA/mM with $r = 0.9997$). This is exactly the range for which NP voltammetry is unsuitable due to poorly defined limiting currents. Above about 100 μM the working curve becomes markedly nonlinear.

The range of greatest analytical utility for determination of iodide is the linear region of the calibration curve, which for this particular choice of timing parameters occurs for concentrations below about 100 μM. All of the behavior noted above for concentrations higher than this (i.e., changes in peak potential and shape and nonlinear working curves) suggests that the oxidation of Hg in the presence of iodide involves a transition between two distinct mechanisms involving surface products of different stoichiometry. A more complete description of the mechanism and a general expression for the maximum concentration for which a linear calibration curve results is given below.

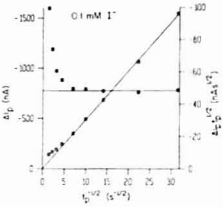


Figure 5. Test of diffusion control of peak current (Δi_p) for the 0.1 mM I^- responses of Figure 4a. Open squares (□) are a plot of Δi_p vs. $t_p^{-1/2}$ (left-hand axis). Solid line is the linear least-squares fit to the five shortest pulse widths (E–I). Dark squares (■) are a plot of $\Delta i_p t_p^{1/2}$ vs. $t_p^{-1/2}$ (left-hand axis). Constant line is best fit to the five shortest pulse widths (E–I).

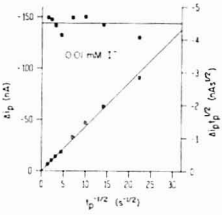


Figure 6. Test of diffusion control of the peak currents for 0.01 mM I^- (raw data not illustrated). All parameters are the same as those given in Figure 4 (data for $t_p = 1$ ms was not obtained). Regressions and symbols are given in Figure 5. Linear and constant curve fitting employed all data points in each plot.

Pulse Width Dependence. Figure 4 illustrates the effect of variation of pulse width on the Δi and NP responses for oxidation of 0.1 mM I^-. The most striking feature of Figure 4 is the shift in Δi peak potentials and NP half-wave potentials to more negative values as pulse width is decreased. This is exactly the opposite of the behavior observed for slow electron transfer kinetics (for which peak potentials would shift to more positive values for an oxidation) and indicates the product adsorption mechanism detailed below.

In order to clarify further the oxidation mechanism and to provide a quantitative description of the parameters required for linear Δi_p analytical working curves, we consider the range of diffusion control of the peak currents. Figure 5 (open squares) shows a plot of Δi_p vs. $t_p^{-1/2}$ for the responses of Figure 4a for 0.1 mM I^-. Good linearity (and zero intercept) is observed for the five shortest pulse widths (curves E–I of Figure 4a), but significant deviations are apparent for longer t_p (curves A–D of Figure 4a. These deviations are even more apparent in the plot of $\Delta i_p t_p^{1/2}$ vs. $t_p^{-1/2}$ (dark squares) where significant deviations from the constant product appear for pulse widths greater than or equal to $t_1 = t_p = 50$ ms. In contrast, a similar series of experiments for 0.01 mM I^- (Figure 6) shows complete diffusion control of the Δi_p currents over the complete range of pulse widths considered.

Figure 7 illustrates the dependence of the peak potentials, E_p, of Figure 4a on the log of the pulse width, $t_p = t_1$. Two distinct regions of different slope are indicated by (a) and (b). The solid lines are linear least-squares fits (a) to points F–I of Figure 4, and (b) to points A–E for Figure 4. The abrupt change in slope occurs between pulse widths of $t_p = 10$ and t_p 20 ms, which is about the same point at which deviations from the constant $\Delta i_p t_p^{1/2}$ product were noted in Figure 5. A similar regression for 0.01 mM I^- gives a single straight line with slope (27.4 mV) quite close to slope (a) of Figure 7 (29.1

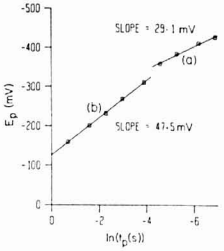


Figure 7. Peak potential vs. ln (pulse width) for the data of Figure 4a. Solid lines are linear least-squares fit to (a) the four shortest pulse widths (F–I) and (b) the five longest pulse widths (A–E). Linear least-squares slopes are indicated adjacent to each fit.

mV) for short t_p. A detailed mechanistic treatment which accounts for these results is presented below.

Mechanism. It is clear from the nature of the concentration and pulse width dependence noted above that a simple unified mechanism for I^- oxidation on Hg may be very difficult to elucidate for the whole range of experimental parameters considered. While a great deal of excellent work has been done on the electrochemical kinetics of halide film formation on mercury (*17–19*), most treatments have been concerned with high bulk halide concentrations and with the growth of multiple layers. Since the DNP technique finds greatest analytical utility at low iodide coverages, it is worthwhile to consider some plausible mechanisms for this limiting case.

It should be noted that the stoichiometry of the reaction at low coverages is not even known, although the following two electrode reactions appear to be the most probable alternatives. For halide X^-

$$Hg + X^- \rightarrow HgX(s) + e^- \quad (1)$$

$$2Hg + 2X^- \rightarrow Hg_2X_2(s) + 2e^- \quad (2)$$

Note that these reactions would be indistinguishable in terms of the faradaic n-value (n_f = moles of e^-/moles of X^-). Although the two possible products are indicated as solids, they may just as easily be envisioned as adsorbed species.

Full monolayer coverage for reaction 1 is most logically approximated from the total number of Hg^0 sites available for I^0 adsorption. From the bulk density and molecular weight of Hg, full monolayer coverage by HgI corresponds to 190 $\mu C/cm^2$ (or 1.96×10^{-9} mol/cm^2 of Hg sites). For reaction 2 full monolayer coverage is most logically approximated from the bulk density of Hg_2I_2, giving 118 $\mu C/cm^2$ (or 6.13×10^{-10} mol/cm^2 of Hg_2I_2).

To verify that all of the oxidation product remains on the electrode surface, and that no solution-soluble species (such as Hg_2I_2(aq) or HgI_4^{2-}(aq)) are formed, double potential step chronocoulometric experiments such as that illustrated in Figure 8 were performed. (Similar soluble species have been postulated in the anodic formation of calomel (*20, 21*).) The response to the first pulse potential (+0.1 V vs. SCE) from 0 to 100 ms is a typical diffusion-controlled response, and a plot of q vs. $t^{1/2}$ is linear, with slope = 8.8×10^{-7} C s$^{-1/2}$ (steps to smaller values of the first pulse potential in the range–0.2 to –0.5 V vs. SCE do not yield linear q vs. $t^{1/2}$ responses. This is a manifestation of the diffusion-controlled adsorption mechanism outlined below (as described by integrating eq 7 below with respect to time) and reflects the time dependence of the surface activity of the adsorbed product. (Analogous nonlinear chronoamperometric responses have been observed in metal deposition experiments (*22*).) When the potential is stepped back to the initial value (–0.8 V) the q vs. t response

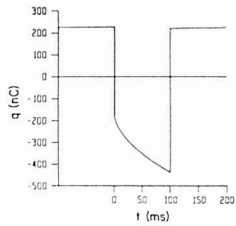


Figure 8. Double potential step chronocoulometric response for 0.18 mM I^-. Initial potential is –0.8 V vs. SCE. First pulse potential (0–100 ms) is +0.1 V vs. SCE. Second pulse potential (100–200 ms) is –0.8 V vs. SCE.

of Figure 8 from 100 to 200 ms is absolutely constant, and the value of q returns to the initial value (which is the value of q_{dl} in the acetate buffer at –0.8 V vs. SCE). All of the oxidation product is therefore on the electrode surface and is instantaneously reduced back to I^- when the potential is reset to the initial value.

The simplest treatment for the NP voltammetric responses involves a Nernstian boundary condition, and for reaction 1 we may write

$$E = E^0 - (1/nf) \ln (a_X - a_{Hg}/a_{HgX}) \quad (3)$$

where E^0 is the standard reduction potential for reaction 1, a_{X^-}, a_{Hg}, and a_{HgX} are the surface activities of X^-, Hg, and HgX, $f = F/RT$, and $n = 1$ in the present case. For submonolayer coverages ($\theta < 1$) one may assume that the HgX activity is proportional to surface coverage

$$a_{HgX} = \theta = \Gamma_{HgX}/\Gamma_{max} \quad (4)$$

and that the activity of the metal is given by

$$a_{Hg} = 1 - \theta \simeq 1 \quad (5)$$

where Γ_{max} is full monolayer coverage (mol/cm^2). With the additional simplification of constant ionic strength, the surface activity of X^- is directly proportional to $C_X°$, i.e., $a_{X^-} = \gamma_X C_X°$ where γ_X is a constant (cm^3/mol). Equations 3–5 then become the limiting equilibrium form of the general kinetic equation considered applicable to single-state adsorption (see eq 2 and 3 of ref 23). For very low coverages one may make the further simplification that $a_{Hg} = 1$. Similar assumptions have been employed in the equilibrium analysis of submonolayer metal deposition (*24*).

Since all of the adsorbed product remains on the electrode surface

$$\Gamma_{HgX} = -(q(t) - q_{dl})/n_f FA = -\int_0^t \{i(t)/n_f FA\}\, dt \quad (6)$$

where $q(t)$ is the faradaic charge passed during each NP potential step of duration t. When the assumption of semiinfinite linear diffusion is applied to the NP experiment in which the potential E is stepped from an initial potential where no faradaic reaction occurs (–0.08 V vs. SCE in this case) to successively more positive values, then standard Laplace transform techniques yield

$$i_{NP}/i_d = 1 - \sqrt{\pi} z F(z) \quad (7)$$

$$z = \xi\sqrt{Dt}\,/(\gamma_X \Gamma_{max}) \quad (8)$$

$$\xi = \exp(-nf(E - E°)) \quad (9)$$

$$i_d = -n_f FAC_X{}^b\sqrt{D/\pi t} \quad (10)$$

$$F(z) = \exp(z^2)\ \mathrm{erfc}\ (z) \quad (11)$$

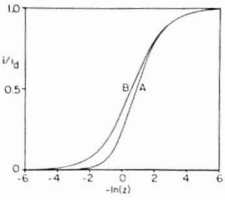


Figure 9. Theoretical predictions of eq 7 (curve A, exact solution) and of eq 12 and 16 (curve B, approximate solutions) for diffusion-controlled adsorption at low coverage.

where t is the measurement time for the NP responses, C_X^b is the bulk concentration of halide, and the other symbols have their usual significance. This result has been derived and employed repeatedly in many contexts: originally for diffusion-controlled adsorption of reactant by Delahay and Trachtenberg (25) and Reinmuth (26), as well as in the context of metal deposition (21, 22, 27). Reinmuth and Balasubramanian (28) have also developed a generalized theoretical framework for reversible, diffusion-controlled adsorption reactions. The present case of deposition of insoluble species is also treated, and if a linear adsorption isotherm is assumed a solution equivalent to eq 7–11 above results.

Equation 7 predicts the NP voltammetric wave shape illustrated in Figure 9. A plot of the limiting form of eq 7 for small z

$$i/i_d = 1/(1 + \sqrt{\pi}z) \tag{12}$$

is also shown in Figure 9 for comparison. The wave shape for this limiting form is identical with that of a reversible electrode reaction with solution-soluble product.

By evaluating eq 7 for $i/i_d = 0.5$ it is found that $z = 0.43$ and hence

$$E_{1/2} = E^\circ - (1/nf) \ln (0.43\gamma_X\Gamma_{max}/\sqrt{Dt}) \tag{13}$$

This treatment thus predicts no shift in the NP $E_{1/2}$ with concentration, and a shift in $E_{1/2}$ to more negative potentials with decreasing pulse width, in qualitative agreement with the behavior observed experimentally in Figures 2b and 4b.

It is useful to note that a much simpler approximate result for the same case may be obtained by a diffusion layer treatment by assuming

$$C_X^\circ = C_X^b + i\delta/n_tFAD \tag{14}$$

$$q = -n_tFA\delta(C_X^b - C_X^\circ) \tag{15}$$

which yields (when the approximation $\delta = \sqrt{\pi Dt}$ is made)

$$E = E^\circ - (1/nf) \ln (\gamma_X\Gamma_{max}/\sqrt{\pi Dt}) - (1/nf) \ln ((i_d - i)/i) \tag{16}$$

This result is identical with the limiting case for small z given by eq 12 and plotted in Figure 9. The dependence on half-wave potential is thus given by

$$E_{1/2} = E^\circ - (1/nf) \ln (0.56\gamma_X\Gamma_{max}/\sqrt{Dt}) \tag{17}$$

again predicting no concentration dependence and the same pulse width dependence as eq 13.

The diffusion layer treatment above has been included to suggest the validity of a similar treatment of reaction 2. The assumptions are

$$E = E^\circ - (1/nf) \ln (a_X^{-2}/a_{Hg_2X_2}) \tag{18}$$

and equations identical with eq 14 and 15. In eq 18, E° is the standard reduction potential of reaction 2 and $n = 2$. The diffusion layer result then becomes (when $\delta \simeq \sqrt{\pi Dt}$

$$E = E^\circ - (1/nf) \ln (2\gamma_X^2\Gamma_{max}C_X^b/\sqrt{\pi Dt}) - (1/nf) \ln ((i_d - i)^2/ii_d) \tag{19}$$

and

$$E_{1/2} = \text{const} - (1/nf) \ln (\gamma_X^2\Gamma_{max}C_X^b/\sqrt{Dt}) \tag{20}$$

(An exact NP treatment of reaction 2 (invoking activity concepts similar to those of eq 4 and 5) is possible, and involves expressing i/i_d as a power series in $(\xi\sqrt{Dt}/\gamma_X^2\Gamma_{max}C_X^b)^{1/2}$. The predictions of the exact theory for the functional dependence of $E_{1/2}$ are identical with those of the diffusion layer treatment above.)

The stoichiometry of reaction 2 thus predicts a shift to more negative values of the NP $E_{1/2}$ as bulk I^- concentration is decreased. This does not agree with the experimental results of Figure 2b which show invariant wave shapes and $E_{1/2}$ values at low concentration. We may thus rule out reaction 2 for low coverages.

The absence of concentration dependence at low coverage thus indicates that reaction 1 (and the exact result of eq 7) is a step in the right direction. Clearly, however, the NP wave shapes of Figure 2b bear little resemblance to the theoretical prediction of Figure 9. In addition, eq 13 predicts that the slope of a plot of $E_{1/2}$ vs. ln (t_p) should be equal to $1/2nf$, whereas the observed low concentration slope for E_p vs. ln (t_p) noted in Figure 7 is equal to about twice this value.

These inconsistencies can be rationalized by invoking the concept of partial electron transfer, in which a nonintegral number of electrons, λ, is transferred

$$Hg + X \leftrightarrow MX_{(ads)}^{(\lambda-1)} + \lambda e^- \tag{21}$$

This concept has been applied extensively in the interpretation of adsorption phenomena involving anions, cations, and neutral molecules at a wide variety of metal/solution interfaces. Much of this work has been summarized in two excellent reviews by Schultze and Vetter (13) and Schultze and Koppitz (14).

The partial electron transfer coefficient, λ, is not an experimentally measurable quantity (13). The electrosorption valency, γ, however, is experimentally accessible and, for ionic adsorption, can be approximated by (14)

$$\gamma = gz - \lambda(1 - g) \tag{22}$$

where g is a geometric factor describing the depth of penetration of the adsorbate into the compact double layer ($0 < g < 1$) and $z = -1$ for halide adsorption. All three quantities (γ, λ, and g) may exhibit potential dependence.

The electrosorption valency, γ, is a therodynamically defined quantity and is totally analogous to the Nernst valency for equilibrium electrode reactions (13). It is thus possible to derive the NP voltammetric responses predicted by reaction 21 above simply by substituting $-\gamma$ for n in the derivation of eq 3–11 above. (The minus sign on γ arises because n does no generally include sign, whereas γ is negative for oxidations and positive for reductions.) The result for the pulse width dependence of the half-wave potential then becomes

$$E_{1/2} = E^\circ - (1/(-\gamma f)) \ln (0.43\gamma_X\Gamma_{max}/\sqrt{Dt}) \tag{23}$$

Since the alternating pulse DNP peak potential, E_p, tracks the NP $E_{1/2}$ (i.e., $E_p = E_{1/2} + \text{const}$), eq 23 provides a reasonable explanation for the pulse width dependence of E_p noted in Figure 7 (slope (a)). By use of the slope (27.4 mV) for 0.01 mM I^-, eq 23 yields a value of $\gamma = -0.47$. This is in

good agreement with the value of $\gamma_N = -0.45$ reported by Schultze and Koppitz (*14*) based on analysis of Grahame's (*29*) original differential capacitance data for I^- adsorption on mercury. ($\gamma_N = \gamma$ at the point of zero charge (pzc)).

The thermodynamic definition of γ also predicts that the faradaic n_f of eq 6 and 11 should be replaced by γ when partial electron transfer operates (*13*). If γ were potential independent and equal to −0.47 over the whole potential range, the expected NP wave shape would still resemble Figure 9 (with n replaced by $-\gamma$ in the definition of z in eq 8 and 9). As noted above, however, the NP curves of Figure 2b for low coverage do not show well-defined limiting currents, and exhibit nearly linear current–voltage responses in the range −200 to +100 mV vs. SCE. (This effect is manifested in the derivative-like Δi responses of Figure 2(a) as asymmetric peaks which do not return to the base line.) These effects must thus be caused totally by the potential dependence of γ in this potential range.

For the low-coverage responses of Figure 2b a plot of $i_{NP}\sqrt{\pi t}/FAC_X{}^b\sqrt{D}$ vs. E is fairly linear with slope $\partial\gamma/\partial E = -0.55\ V^{-1}$ in the range −200 +100 mV vs. SCE. (A value of $D = 2.0 \times 10^{-6}$ cm^2/s was calculated from the well-defined NP limiting current of curve I of Figure 3b with $n_f = 1$.) Thus γ grows linearly with potential, from a value of −0.47 near the DNP peak potential of −320 mV to increasingly negative values at more positive potentials. Even at +100 mV, γ does not reach the faradaic value of $-\gamma = n_f = 1$ as is evidenced by comparison of $-\gamma = i_{NP}\sqrt{\pi t}/FAC_X{}^b\sqrt{D}$ for curve D ($-\gamma = 0.6$) and curve I ($-\gamma = n_f = 1.0$) of Figures 2b and 3b.

That γ should become increasingly negative at more positive potentials is physically consistent with the increasingly positive electrode charge. (The pzc in the acetate buffer system employed here is at about −0.5 V vs. SCE.) In terms of eq 22, the increasingly negative γ may be due to either an increase in g (because of increasing electrostatic attraction of the partially discharged adsobate), to an increase in λ itself, or to both. These effects are not easily separated (*13*).

A similar potential dependence of γ has been noted by Schultze and Vetter (*13*) in their analysis of Grahme's data for the Hg/I^- system, and a value of $\partial\gamma/\partial E = -0.18\ V^{-1}$ reported. The potential range considered, however, was restricted to potentials close to the pzc (such that $E - E_{pzc} \leq 0.25$ V) (*13*, *29*) whereas the value of $\partial\gamma/\partial E = -0.55\ V^{-1}$ reported above corresponds to the range $+0.3 \leq E - E_{pzc} \leq +0.6$ V, a range inaccessible to differential capacitance measurements in pure concentrated (>0.01 M) I^- solutions.

In concluding the low-coverage analysis we note that the peak width ($W_{1/2}$) of the alternating pulse DNP responses of Figure 2a is $W_{1/2} \simeq 200$ mV. If the approximate NP wave shape (eq 16) is invoked, then the Δi responses will be proportional to the derivative of the NP wave for small pulse height, ΔE, as in the case of reversible reactions (*1*). The peak width will then be given by $W_{1/2} = 90/n$ mV at 25 °C. Since we can replace n by $-\gamma$, the value of $\gamma = -0.47$ calculated from the pulse width dependence predicts $W_{1/2} = -90/\gamma$ (mV) = 191 mV, in good agreement with the experimental value of 200 mV noted above. The alternating pulse DNP peak width thus provides further verification of the partial electron transfer mechanism and a particularly simple method for approximating γ.

On the basis of the diffusion-controlled adsorption mechanism outlined above it is possible to develop a quantitative criterion for the combination of bulk concentration and timing parameters for which the responses are analytically useful and exhibit ideal, low-coverage behavior. Invoking the diffusion layer approach of eq 14–17 (with n_f replaced by $-\gamma$), one can calculate the charge density from eq 15 (for $C_X{}^o = 0$) at $t = t_p$. In particular, the voltammetric responses deviate from ideality at curve E of Figure 2a ($q/A = -7\ \mu C/cm^2$), at $t_p = 50$ ms in Figure 5 ($q/A = -8\ \mu C/cm^2$), and at $t_p = 20$ ms in Figure 7 ($q/A = -5\ \mu C/cm^2$). All of these data indicate deviations at about the same point ($q/A \leq -5\ \mu C/cm^2$), which corresponds to about 6% of the full monolayer coverage (89 $\mu C/cm^2$) calculated on the basis of reaction 21 with $\gamma = -0.47$. From eq 15 it follows that the criterion for ideal low-coverage behavior and linear working curves is (for $t_1 = t_p$)

$$\sqrt{t_p}C_X{}^b \leq 5\ \mu C/cm^2/(-\gamma F\sqrt{\pi D}) \quad (24)$$

or

$$\sqrt{t_p}C_X{}^b \leq 1.4 \times 10^{-8}\ M\ s^{1/2} \quad (25)$$

As a final note we consider a possible mechanistic explanation for the dramatic shifts in peak and wave shape and position when the bulk concentrations or pulse widths are increased above the limits specified by eq 24 and 25. Clearly, at high enough concentration or large enough pulse width, full monolayer coverage will be exceeded, and the expected electrode reaction is that of reaction 2 above, in which the activity of the Hg_2I_2 deposit is unity. Under these conditions the NP voltammetric response should give a linear plot of ln $(i_d - i)$ vs. E with a slope of $-f$ (*29*). When the NP data of curve I of Figure 3b (1.7 mM I^-) are analyzed in this fashion, a nonlinear curve is obtained with a linear portion of slope $-0.9f$ resulting only in the region $i/i_d \geq 0.67$. From the integrated Cottrell equation (and the value of D noted above), the charge density accumulated on each NP pulse in the limiting current region is calculated to be 170 $\mu C/cm^2$ (using an effective NP pulse width of $t_1 - t_s/2 = 0.042$ s). This is higher than the full monolayer coverage value of 118 $\mu C/cm^2$ for reaction 2 noted above. This is sufficient to account for the nonlinearity of the ln $(i_d - i)$ vs. E regression at values of $i/i_d < 0.67$, since less than a full monolayer is present at these smaller currents. Further increases in I^- concentration or in pulse width lead to ill-defined and irreproducible NP and DNP voltammetric responses, presumably due to passivation and fouling of the electrode surface. (Similar effects have been noted in DC polarographic studies (*30*).)

Transitions from low-coverage to high-coverage behavior have recently been investigated for the related Hg/S^{2-} system by Peter et al. (*31*). A similar underpotential deposition (or adsorption) mechanism was found at low coverage, followed by a first-order phase transition and nucleation and growth of multiple layers. The results clearly indicate, however, that the dramatic shifts in peak and wave slope and position are consistent with a change in stoichiometry of the electrode reaction: from the partial electron transfer adsorption process of reaction 21 at low coverages to the formation of mono- or multilayers of Hg_2I_2 described by reaction 2.

In the above the DNP technique, by virtue of providing a fixed potential where no reaction occurs as in NP voltammetry, but also yielding a differential response, has proven useful for both analysis and elucidation of mechanism. The results indicate that the technique should be valuable in the study of other adsorption and passivation phenomena.

ACKNOWLEDGMENT

The authors thank John J. O'Dea for technical assistance and helpful discussions.

Registry No. Hg, 7439-97-6.

LITERATURE CITED

(1) Brumleve, T. R.; O'Dea, J. J.; Osteryoung, R. A.; Osteryoung, Janet *Anal. Chem.* **1981**, *53*, 702–706.
(2) Brumleve, T. R.; Osteryoung, R. A.; Osteryoung, Janet *Anal. Chem.* **1982**, *54*, 782–787.
(3) Brumleve, T. R.; Osteryoung, Janet *Anal. Chem.* **1981**, *53*, 988–991.
(4) Anderson, J. E.; Bond, A. M. *Anal. Chem.* **1981**, *53*, 504–508.
(5) Lane, R. F.; Hubbard, A. T. *Anal. Chem.* **1976**, *48*, 1287–1293.

(6) Propst, R. C. Anal. Chem. 1977, 49, 1199-1205.
(7) Colovos, G.; Wilson, G. S.; Moyers, J. L. Anal. Chem. 1974, 46, 1045-1050.
(8) Colvos, G.; Wilson, G. S.; Moyers, J. L. Anal. Chem. 1974, 46, 1051-1054.
(9) Perchard, J. P.; Buvet, M.; Molina, R. J. Electroanal. Chem. 1967, 14, 57-74.
(10) Kemula, W.; Kublik, Z.; Taraszewska, J. Microchem. J. Symp. Ser. 1962, 2, 865-877.
(11) Shain, I.; Perone, S. P. Anal. Chem. 1961, 33, 325-329.
(12) Turner, J. A.; Abel, R. H.; Osteryoung, R. A. Anal. Chem. 1975, 47, 1343-1347.
(13) Schultze, J. W.; Vetter, K. J. J. Electroanal. Chem. 1973, 44, 63-81.
(14) Schultze, J. W.; Koppitz, F. D. Electrochim. Acta 1976, 21, 327-336.
(15) Boult, E. H.; Thirsk, H. R. Trans. Faraday Soc. 1954, 50, 404-412.
(16) Aoki, K.; Osteryoung, Janet; Osteryoung, R. A. J. Electroanal. Chem. 1980, 110, 1-18.
(17) Bewick, A.; Fleischmann, M.; Thirsk, H. R. Trans. Faraday Soc. 1962, 58, 2200-2216.
(18) Fleischmann, M.; Thirsk, H. R. J. Electrochem. Soc. 1963, 110, 688-698.
(19) Fleischmann, M.; Thirsk, H. R. Electrochim. Acta 1964, 9, 757-771.
(20) Armstrong, R. D.; Fleischmann, M.; Thirsk, H. R. Trans. Faraday Soc. 1965, 61, 2238.
(21) Thirsk, H. R.; Harrison, J. A. "A Guide to the Study of Electrode Kinetics"; Academic Press: New York, 1972; pp 115-135.
(22) Astley, D. J.; Harrison, J. A.; Thirsk, H. R. J. Electroanal. Chem. 1968, 19, 325-334.
(23) Conway, B. E.; Angerstein-Kozlowska, H. Acc. Chem. Res. 1981, 14, 49-56.
(24) Delahay, P. "New Instrumental Methods in Electrochemistry"; Interscience: New York, 1954; pp 278-281.
(25) Delahay, P.; Trachtenberg, I. J. Am. Chem. Soc. 1957, 79, 2355-2362.
(26) Reinmuth, W. H. J. Phys. Chem. 1961, 65, 473-476.
(27) Armstrong, R. D.; Harrison, J. A. J. Electrochem. Soc. 1969, 116, 328-331.
(28) Reinmuth, W. J.; Balasubramanian, K. J. Electroanal. Chem. 1972, 38, 271-281.
(29) Grahame, D. C. J. Am. Chem. Soc. 1958, 80, 4201-4210.
(30) Kolthoff, I. M.; Lingane, J. J. "Polarography"; Interscience: New York, 1952; Vol. II, pp 577-581.
(31) Peter, L. M.; Reid, J. D.; Scharifker, B. R. J. Electroanal. Chem. 1981, 119, 73-91.

RECEIVED for review July 21, 1982. Accepted January 5, 1983. This work was supported in part by the National Science Foundation under Grant No. 7917543.

Faradaic Response in Derivative and Differential Normal Pulse Voltammetry

Milivoy Lovrić, John J. O'Dea, and Janet Osteryoung*

Department of Chemistry, State University of New York at Buffalo, Buffalo, New York 14214

The peak-shaped voltammograms arising from differential pulse, differential normal pulse, and normal pulse difference modes of pulse voltammetry are compared for reversible systems and for systems with heterogeneous charge transfer control. The effects of variation of kinetic parameters, k_s and α, and the dependence on experimental parameters of time and potential are examined. For the reversible case the current-potential curves are the same for the appropriate choice of experimental parameters. For quasi-reversible cases the differences depend strongly on kinetic parameters. Maximum differences are obtained for the totally irreversible case. The differences between the differential normal pulse and normal pulse difference currents are less significant than the striking relative diminution of the differential pulse response for irreversible systems.

The advent of computer-controlled experiments has made possible and encouraged the proliferation of potential-time wave forms and current measurement schemes in pulse voltammetry. Variations on normal pulse voltammetry are especially interesting, for in the normal pulse mode the indicator electrode is maintained most of the time at a potential at which no faradaic reaction occurs. Thus for each pulse the same initial conditions obtain at the time of pulse application. A "derivative" voltammogram can be obtained by using the difference between the currents arising from successive pulses. This option was available on the PARC Model 170 electrochemical system (*1*). Auerbach et al. did the same in the form of "incremental derivative polarography" (*2*). Jackson et al. (*3*) and Abel at al. (*4*) have described modifications of the PARC Model 174 polarographic analyzer which also have this feature. Lane and Hubbard employed essentially the same technique but called it "differential double pulse voltammetry" (*5*). Albery et al. have presented an extensive theoretical description of charge-transfer irreversibility for "differential double pulse" (*6*). Anderson and Bond have described "pseudoderivative normal-pulse polarography", again a technique in which the normal pulse wave form is used but the currents are subtracted in a fashion which produces a peak-shaped current-potential response (*7*). In an elaboration of this work Evans and Hanck have verified again the simple theory for the reversible case and presented an example of the response for an irreversible case (*8*). In all of this work, the current response arises from application of a series of single pulses, each applied from the same initial conditions.

In contrast with these approaches, a differential technique may be used to give a peak-shaped response. So-called differential normal pulse voltammetry, in which a series of double pulses are applied, is an example (*9-13*). Traditional differential pulse voltammetry developed by Barker (*14*) is from the theoretical viewpoint a special case of differential normal pulse voltammetry in which the time duration of the first pulse is long in comparison with the time duration of the second pulse. The result of subtracting currents from successive double pulses gives peak-shaped voltammograms which resemble the various derivative normal pulse responses described above (*10*, *12*, *13*).

There are several factors which should influence the choice of pulse wave form and current measurement scheme for either analytical or mechanistic studies. The pulse wave form should control conditions at the electrode surface to enhance reproducibility, discriminate against unwanted capacitative or faradaic currents, and provide sensitivity appropriate for the application. Differential normal pulse voltammetry and normal pulse voltammetry have in common the characteristic that most of the time is spent at a potential at which no current flows. This potential may be chosen to affect adsorption or, especially at solid electrodes, surface reactions.

0003-2700/83/0355-0704$01.50/0 © 1983 American Chemical Society

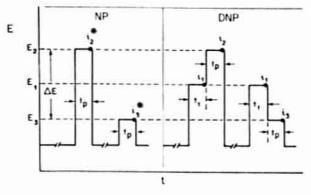


Figure 1. Potential–time wave forms and current-measurement schemes in the normal pulse (NP) and differential normal pulse (DNP) modes. The current is measured at potentials and times indicated by the filled circles.

The differential normal pulse wave form was developed in part to achieve finer control of conditions at the electrode surface than that provided by the normal pulse wave form.

The current measurement scheme which gives rise to the actual current–potential response should be selected to produce the most revealing and easily obtained diagnostic information, or the best analytical signal. The current-sampling mode in differential normal pulse voltammetry has been selected to provide a symmetrical peak-shaped response which is easily analyzed (*10*, *11*). In contrast with the peak arising from differencing the normal pulse current, the peak in differential normal pulse voltammetry occurs at the half-wave potential, and the peak position is independent of differential pulse amplitude.

The single pulse techniques have the great advantage of simplicity of theory. The development of differential pulse voltammetry has been hindered by the complexity of its theoretical description for all but the simple reversible case (*9*, *13*, *15*). Numerical methods pioneered by Nicholson (*16*) have proven the most efficient way to calculate the response for the theoretically intractable double pulse techniques, but the time scale employed in differential pulse voltammetry makes this approach cumbersome in that case also.

The differential normal pulse wave form is a reasonable model for differential pulse voltammetry (*15*). Anderson and Bond allege that the response in differential pulse and "pseudoderivative normal pulse" (i.e., the normal pulse difference current) is nearly identical for reversible and irreversible electrode processes (*7*). It should be obvious from the principle of superposition that the response is identical for reversible systems provided that the equivalent parameters are chosen correctly. For irreversible systems the response must differ.

Accordingly, in this paper we compare the faradaic response for differential normal pulse voltammetry and for the difference current in normal pulse voltammetry for the case of heterogeneous charge transfer control. The differential normal pulse wave form includes the special case of conventional differential pulse voltammetry.

EXPERIMENTAL SECTION

Voltammograms were calculated by numerical integration, using techniques previously described (*17*). The slow heterogeneous charge transfer case corresponds to the boundary condition

$$i(t) = (nFAk_c^{\ominus}/D_O^{(1-\alpha)/2}D_R^{\alpha/2}) \exp(-\alpha nF(E - E_{1/2})/RT) \times [\sqrt{D_O}C_O(0,t) - \epsilon\sqrt{D_R}C_R(0,t)]$$

where $k_c^{\ominus}$ is the standard heterogeneous rate constant referred to the reversible formal potential, $E^{\ominus}$, $\epsilon = \exp(nF(E - E_{1/2})/RT)$, and the other symbols have their usual meaning.

RESULTS AND DISCUSSION

The potential–time wave forms under consideration are presented in Figure 1. The normal pulse current is i^* and the normal pulse difference current is $i_2^* - i_3^* = \Delta i_{NP}$. In the differential normal pulse mode the corresponding current response is given by $i_2 - i_3 = \Delta i_{DNP}$. The differential pulse current is given by $\Delta i_{DP} = i_2 - i_1$ for the case $t_1 \gg t_p$.

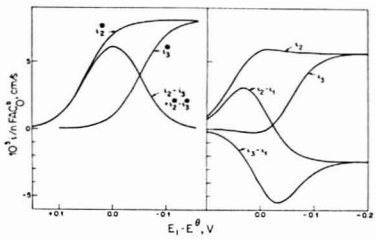


Figure 2. Current–potential response for the potential–time wave forms and current measurement schemes of Figure 1 for the reversible case $k_c^{\ominus} = 1$ cm/s, $\alpha = 0.5$, $D = 10^{-5}$ cm^2/s) with $\Delta E = 100$ mV, $E_2 - E_1 = 50$ mV, $t_1 = t_p = 50$ ms.

There is some ambiguity in choosing the set of parameters for a proper comparison of these current differences. However, for the reversible case (*10*) for the reduction of O to R involving n electrons

$$(i_2 - i_3)/i_d = 1/(1 + \epsilon\zeta_2) - 1/(1 + \epsilon\zeta_3) \qquad (1)$$

where $i_d = nFAC_O^b\sqrt{D/\pi t_p}$, $\epsilon = \sqrt{D_O/D_R}$, $\zeta_i = \exp[nf(E_i - E^{\ominus})]$ for $i = 2$ or 3 and the other symbols have their usual meaning. Thus $(i_2 - i_3)/i_d$ depends only on the choice of t_p, E_2, and E_3 and therefore $i_2^* - i_3^* = i_2 - i_3$ when these quantities are the same for the two cases. As eq 1 shows, this is true independent of the value of t_1. Thus in all of the following we choose only the case illustrated in Figure 1 for which $E_1 - E_2 = E_3 - E_1 = \Delta E/2$. For convenience we choose the case $t_1 = t_p$ to illustrate the differential normal pulse response. Conventional differential pulse voltammetry is represented by differential normal pulse voltammetry with $t_1 \geq 10t_p$. However, the DNP response with which we wish to compare the DP response is not $i_2 - i_1$, but rather $i_2 - i_3$. Thus the appropriate potential difference is ΔE rather than $\Delta E/2$.

Figure 2 shows the currents which arise from these potential–time wave forms and current measurement schemes for the case in which the charge transfer process is much faster than diffusion. The current is expressed in units of cm/s, $i/nFAC_O^b$, here and throughout. The currents of Figure 2 are actually calculated by the method described above for heterogeneous charge transfer control with appropriate choice of parameters to give the result for a diffusion-controlled system. Curves i_2^* and i_3^* are the same currents simply offset on the potential axis by the amount ΔE. The normal pulse difference current, Δi_{NP}, is $i_2^* - i_3^*$, as shown. Notice that the index potential is chosen to be E_1. This makes Δi_{NP} have its maximum value, $(\Delta i_{NP})_p$, at the potential value $E_p = E^{\ominus}$. The right-hand side of Figure 2 shows the individual and both differential DNP responses. The difference $i_2 - i_3 = \Delta i_{DNP}$ is exactly the same as Δi_{NP}, as predicted by the superposition principle. Again, the index potential is E_1.

The DP response is the current $i_2 - i_1$ for the case $t_1 > 10t_p$. For $E_1 \ll E^{\ominus}$, a diffusion-limited current is reached. This current is proportional to $1\sqrt{1 + t_1/t_p} - 1\sqrt{t_1/t_p}$. When $t_1 = t_p$ this time function has the value −0.29 and the curve for $i_2 - i_1$ on the right-hand side of Figure 2 is obtained. As t_1/t_p increases, the maximum value of $i_2 - i_1$ increases, and the diffusion-controlled tail decreases in magnitude. For $t_1 \geq 19t_p$, the function of time given above is 0.006, the diffusion-controlled current is nearly zero, and the curve has the same shape as that of $i_2 - i_3$. For $\Delta E = 100$ mV, with index potential E_1,

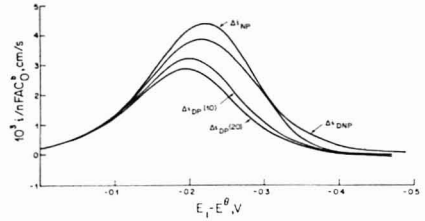


Figure 3. The currents Δi_{NP}, Δi_{DNP}, and Δi_{DP} expressed as $\Delta i/nFAC_O^b$ for $k_c^\theta = 10^{-4}$ cm/s, $\alpha = 0.5$, $n = 1$, $D = 10^{-5}$ cm^2/s and $\Delta E = 0.1$ V. For Δi_{NP} and Δi_{DNP}, $t_p = t_1 = 50$ ms; for $\Delta i_{DP}(10)$ and $\Delta i_{DP}(20)$, $t_1/t_p = 10$ and 20, respectively.

and for $t_1 \geq 19t_p$, the differential pulse response, Δi_{DP}, is identical with the curve $i_2 - i_3$ within the accuracy of the graph. Note that typically the index potential for DP is taken as E_3 (cf. Figure 1), and therefore the peak for a reversible system lies at $E^\theta - \Delta E/2$. Here, for the purposes of comparison, we use E_1 as the index, and the peak current is attained at E^θ.

Typical behavior for an irreversible case is illustrated in Figure 3. Here, as is generally true, the differential normal pulse response appears to be "less reversible" than the normal pulse difference current. Although the widths of the peaks at half height are nearly identical, the peak current, $(\Delta i_{DNP})_p$, is less than $(\Delta i_{NP})_p$, and Δi_{DNP} displays an extended tail for $E \ll E^\theta$. Qualitatively Δi_{DNP} is more profoundly influenced by charge transfer kinetics, and therefore DNP is possibly a better wave form for the determination of kinetic parameters. This is intuitively reasonable, for in DNP the differential pulses are applied in both the forward and reverse directions. Correspondingly, to the extent that Δi_{NP} responds less to charge-transfer kinetics, it should be favored for analytical work.

The DP response is also shown in Figure 3 for two values of the ratio t_1/t_p. The current response is significantly less than that for Δi_{DNP}, the peak potential is shifted to more positive values with respect to that for Δi_{DNP}, and there is a strong time dependence. The peak current, $(\Delta i_{NP})_p$, is about 60% greater than the peak current $(\Delta i_{DP}(20))_p$. This is substantially different rather than "nearly identical" as claimed without supporting evidence by Anderson and Bond (*7*). The dependence of Δi_{DP} on t_1/t_p has been discussed elsewhere (*13*). The numerical integration procedure used to calculate Δi_{DP} takes an inordinate amount of time for large values of t_1. Therefore below we discuss only the case $t_1/t_p = 10$ (with $t_1 = 500$ ms). The value of t_p for the PARC 174A polarographic analyzer is 48 ms, and other instruments have comparable values. The smallest value of t_1 available on the PARC 174 is 500 ms. Therefore the following representative calculations conservatively understate the magnitude of the difference between Δi_{DP} and Δi_{NP} which would be observed in normal practice.

The theory for single potential step chronoamperometry under conditions of semiinfinite linear diffusion with Butler–Volmer boundary conditions is well-known, and the current–potential curves at a specific time are readily calculable. Thus the voltammograms Δi_{NP} can be obtained in a straightforward manner. The same is not true for the double potential step case. Although analytical solutions exist (*9*, *11*, *13*), the calculations required are complicated. The most efficient way to calculate the voltammograms Δi_{DNP} and Δi_{DP} is to use numerical integration, as mentioned above. In the material following all calculated curves have been obtained by numerical integration. The method of calculation was checked by comparing the results obtained from programs

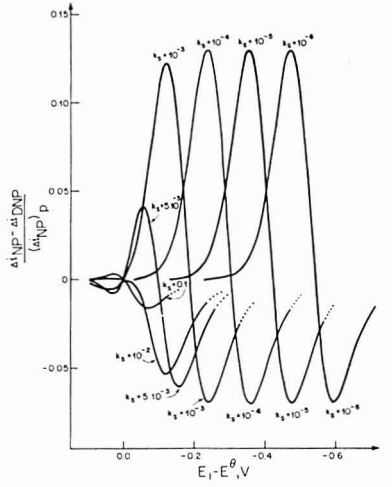


Figure 4. Normalized differences of difference currents, $(\Delta i_{NP} - \Delta i_{DNP})/(\Delta i_{NP})_p$, vs. $E_1 - E^\theta$ for k_s $(= k_c^\theta)$ as indicated and other quantities as in Figure 3.

which were written independently and by comparing results of the numerical integration procedure with these obtained by direct calculation from the analytical solution. Because we are interested in the details of the response rather than only gross measures such as peak height and width, the results are presented in the form of figures which show the difference between the Δi_{NP} voltammogram and either Δi_{DP} or Δi_{DNP}. Because the Δi_{NP} voltammogram itself changes over the pertinent range of kinetic parameters, the differences have been normalized by dividing by the Δi_{NP} peak current, $(\Delta i_{NP})_p$. We consider first the i_{DNP} voltammograms.

As might be expected, the difference $\Delta i_{NP} - \Delta i_{DNP}$ depends on the choice of kinetic parameter. A shown in Figure 4, the relative magnitude of the difference is a strong function of kinetic parameter in the quasi-reversible region but becomes independent of potential for totally irreversible reactions, for which the wave shapes are invariant and only the peak potential changes with change in k_c^θ.

Because peak shape is a much stronger function of α than of k_c^θ, one might expect the difference between response in the two modes to be a strong function of α, and that is the case as illustrated in Figures 5 and 6. Again the normal pulse difference current is less sensitive to kinetic effects, and the magnitude of the differences and the shapes of the current–voltage curves depend strongly on α. Figure 5 illustrates the behavior in the quasi-reversible region. The differences are fairly small, but the morphology of the curves is quite complex and sensitive to the magnitude of α. For more irreversible reactions the differences are more pronounced, but the relative shapes of the curves do not change markedly with change in the value of α.

The dependence on ΔE is not strong. For example, for the parameters of Figure 4 with $k_c^\theta = 10^{-3}$ cm/s, the maximum difference changes only from 12.3% to 13.2% in going from $\Delta E = 100$ mV to $\Delta E = 10$ mV. This is quite instructive, for it emphasizes the general observation concerning pulse techniques that although the current is a strong function of ΔE, there is almost no kinetic information in that dependence. Since the difference in the response $\Delta i_{NP} - \Delta i_{DNP}$ is entirely

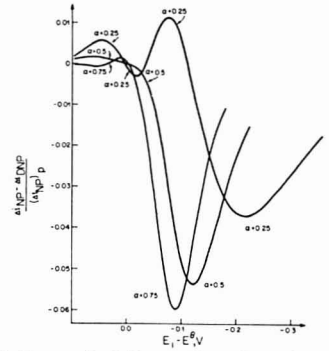


Figure 5. The normalized difference $(\Delta i_{NP} - \Delta i_{DNP})/(\Delta i_{NP})_p$ vs. $E_1 - E^\ominus$ for α as indicated with $k_c^\ominus = 10^{-2}$ cm/s and the other quantities as in Figure 3.

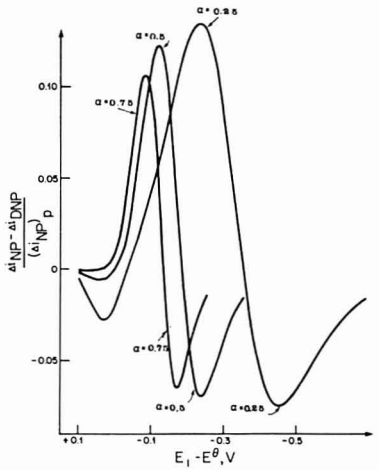


Figure 6. The normalized difference $(\Delta i_{NP} - \Delta i_{DNP})/(\Delta i_{NP})_p$ vs. $E_1 - E^\ominus$ as in Figure 5 except $k_c^\ominus = 10^{-3}$ cm/s.

a kinetic phenomenon, that difference depends only weakly on ΔE.

Figures 4, 5, and 6 have illustrated the normalized current difference $(\Delta i_{NP} - \Delta i_{DNP})/(\Delta i_{NP})_p$. Figures 7, 8, and 9 illustrate the corresponding differences $(\Delta i_{NP} - \Delta i_{DP})/(\Delta i_{NP})_p$. As shown in Figure 7 for the timing parameters chosen the maximum difference for a totally irreversible reaction is 37%. Because of the small negative limiting current for Δi_{DP}, the negative differences of Figure 4 do not appear. The curves of Figure 8 share with those of Figure 5 the characteristic that the nature of the difference depends strongly on the value of α. And finally, Figure 9 illustrates the quite substantial dependence of the difference on the value of α at smaller values of $k_c^\ominus$. Over the change from $\alpha = 0.75$ to $\alpha = 0.25$, the maximum relative difference changes from 25 to 48%, or a change of 92%. This change is in the direction one would expect, as again it reflects a kinetic effect. The case $\alpha = 0.25$ is the least reversible and exhibits the greatest difference. In going from $\alpha = 0.75$ to $\alpha = 0.25$ the peak current $(i_{NP})_p$ decreases by 40%,

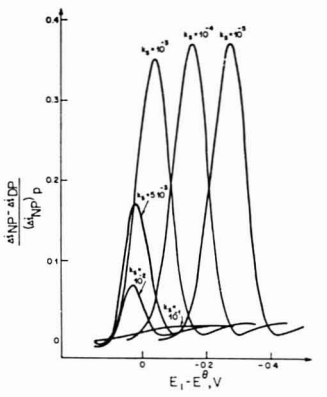


Figure 7. The normalized difference $(\Delta i_{NP} - \Delta i_{DP})/(\Delta i_{NP})_p$ vs. $E_1 - E^\ominus$ for the parameters of Figure 4, but with $t_1 = 500$ ms.

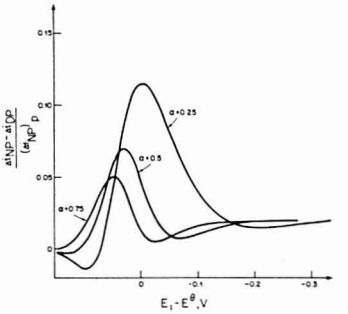


Figure 8. The normalized difference $(\Delta i_{NP} - \Delta i_{DP})/(\Delta i_{NP})_p$ vs. $E_1 - E^\ominus$ for the parameters of Figure 5, but with $t_1 = 500$ ms.

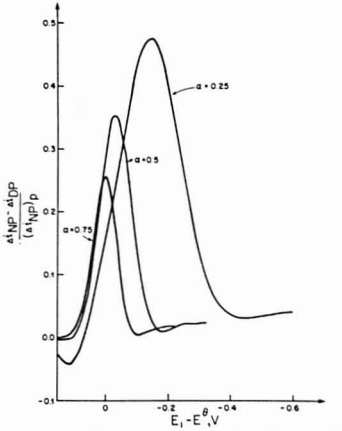


Figure 9. The normalized difference $(\Delta i_{NP} - \Delta i_{DP})/(\Delta i_{NP})_p$ vs. $E_1 - E^\ominus$ for the parameters of Figure 6, but with $t_1 = 500$ ms.

so the absolute diminution in current for i_{DP} is even more striking.

The differences in current response illustrated above serve as a guide to the behavior to be expected in practical experimental cases. In general the current Δi_{NP} gives the largest value of peak current and therefore the greatest analytical sensitivity. Correspondingly the current Δi_{DP} is by far the worst in sensitivity, and the effect is greater the slower the reaction until the limiting value is reached for total irreversibility. The effects of irreversibility on the current Δi_{DP} are more pronounced for greater values of the time t_1, and the representative calculations given here are at the short end of the time range normally employed. Thus they understate the effect of slow heterogeneous charge transfer kinetics on the differential pulse response. The shape of the Δi_{DNP} voltammogram is the most sensitive to changes in kinetic parameters in the quasi-reversible region.

ACKNOWLEDGMENT

The authors express their thanks to Robert deLevie whose thoughtful questions prompted this work initially. They also thank Robert Osteryoung for helpful comments.

LITERATURE CITED

(1) "Instruction Manual. Electrochemical System Model 170"; Princeton Applied Research Corp.: Princeton, NJ, 1970.
(2) Auerbach, C.; Finston, H. L.; Kissel, G.; Glickstein, J. *Anal. Chem.* **1961**, *33*, 1480-1484.
(3) Jackson, L. L.; Yarnitzky, Ch.; Osteryoung, R. A.; Osteryoung, Janet *Chem. Biomed. Environ. Instrum.* **1980**, *10*, 175-188.
(4) Abel, R. H.; Christie, J. H.; Jackson, L. L.; Osteryoung, Janet; Osteryoung, R. A. *Chem. Instrum. (N.Y.)* **1976**, *7*, 123-138.
(5) Lane, R. F.; Hubbard, A. T. *Anal. Chem.* **1976**, *48*, 1287-1293.
(6) Albery, W. John; Beck, T. W.; Brooks, William N.; Filienz, Marianne. *J. Electroanal. Chem.* **1981**, *125*, 205-217.
(7) Anderson, J. E.; Bond, A. M. *Anal. Chem.* **1981**, *53*, 504-508.
(8) Evans, Otis M.; Hanck, Kenneth W. *Anal. Chim. Acta* **1981**, *129*, 79-86.
(9) Aoki, Koichi; Osteryoung, Janet; Osteryoung, R. A. *J. Electroanal. Chem.* **1980**, *110*, 1-18.
(10) Brumleve, Timothy R.; O'Dea, John; Osteryoung, R. A.; Osteryoung, Janet *Anal. Chem.* **1981**, *53*, 702-706.
(11) Brumleve, Timothy R.; Osteryoung, Janet *Anal. Chem.* **1981**, *53*, 988-991.
(12) Brumleve, Timothy R.; Osteryoung, R. A.; Osteryoung, Janet *Anal. Chem.* **1982**, *54*, 782-787.
(13) Lovrić, Milivoy; Osteryoung, Janet *Electrochim. Acta* **1982**, *27*, 963-968.
(14) Barker, G. C.; Gardner, A. W. AERE Harwell C/R 2297, 1955.
(15) Aoki, Koichi; Osteryoung, Janet *J. Electroanal. Chem.* **1980**, *110*, 19-36.
(16) Nicholson, R. S.; Olmstead, M. L. In "Electrochemistry: Calculations, Simulation and Intrumentation"; Mattson, J. S., Mark, H. B., MacDonald, H. C., Eds.; Marcel Dekker: New York, 1972; Vol. 2..
(17) O'Dea, John; Osteryoung, Janet; Osteryoung, R. A. *Anal. Chem.* **1981**, *53*, 695-701.

RECEIVED for review September 8, 1981. Resubmitted August 3, 1982. Accepted January 10, 1983. This work was supported by the National Science Foundation under Grant No. CHE 7917543.

Determination of Pertechnetate by Liquid Chromatography with Reductive Electrochemical Detection

Jane Y. Lewis, Julius P. Zodda, Edward Deutsch, and William R. Heineman*

Department of Chemistry, University of Cincinnati, Cincinnati, Ohio 45221

A method utilizing liquid chromatography with electrochemical detection has been developed for the determination of total TcO_4^- ($^{99m}TcO_4^-$ and $^{99}TcO_4^-$) in $^{99}Mo/^{99m}Tc$ generator eluents. Pertechnetate, which is the starting material for the preparation of many diagnostic radiopharmaceuticals, is generally present in these eluents in the concentration range of 5×10^{-8} M to 5×10^{-6} M. No sample pretreatment is necessary since impurities and other components are separated by the HPLC NH_2-bonded column. By use of both static mercury drop (SMDE) and solid electrode detectors, in conjunction with rigorous deoxygenation procedures, total TcO_4^- in generator eluents is readily determined. A severe electrode fouling phenomenon limits the use of solid electrode detectors to TcO_4^- concentrations less than 10^{-7} M, the working range for a carbon electrode being 8.5×10^{-8} to 1.0×10^{-7} M. The working range for the SMDE is 2.1×10^{-8} to 1.0×10^{-4} M TcO_4^-.

In diagnostic nuclear medicine, a particular chemical form of a γ-ray-emitting isotope is introduced into the body so that the isotope localizes in the organ of interest. A scan obtained with a γ-ray camera then provides valuable diagnostic information about the organ (*1*). In this essentially noninvasive technique, nearly 80% of the clinically used radiopharmaceuticals incorporate ^{99m}Tc because it is an isotope that has ideal nuclear properties, has diverse chemistry, and is readily available. ^{99m}Tc in the form of $^{99m}TcO_4^-$ is supplied by a $^{99}Mo/^{99m}Tc$ generator which utilizes the following decay scheme:

$$^{99}Mo \xrightarrow[66\ h]{\beta^-} {}^{99m}Tc \xrightarrow[6\ h]{\gamma} {}^{99}Tc$$

^{99}Mo in the form of $^{99}MoO_4^{2-}$ is adsorbed on alumina and packed in a column at a reactor site. It is then shipped to the hospital packaged in lead. Each morning an aliquot of saline is drawn through the generator eluting the -1 charged TcO_4^- (both $^{99}TcO_4^-$ and $^{99m}TcO_4^-$) and leaving the -2 charged $^{99}MoO_4^{2-}$ on the column. TcO_4^- is then mixed with a reductant, a ligand which will confer some desirable biological properties on the final complex, and a stabilizer to form the final radiopharmaceutical mixture (*1*). In order to understand the chemistry and kinetics of this preparation scheme, the total pertechnetate concentration (i.e., both $^{99}TcO_4^-$ and $^{99m}TcO_4^-$) in the original generator eluent must be known (*2*). The current method for determining total TcO_4^- is to measure the ^{99m}Tc activity with a γ counter. Given certain assumptions about the history of the generator, $[^{99}TcO_4^-]$ can then be calculated. However, these assumptions have never been validated, and the calculated results have never been experimentally verified.

Recently, a liquid chromatography method utilizing UV detection (LCUV) at 254 nm has been developed in this

0003-2700/83/0355-0708$01.50/0 © 1983 American Chemical Society

laboratory for determining total TcO_4^- in $^{99}Mo/^{99m}Tc$ generator eluents (*3, 4*). This HPLC procedure involves a simple NH_2-bonded phase separation in acetate buffer and has a detection limit of 6.4×10^{-8} M TcO_4^-. It is convenient, inexpensive, and readily applicable to generator samples as interferences are easily overcome by the HPLC separation. It was found that $^{99}Mo/^{99m}Tc$ generators typically yield eluents containing pertechnetate in the concentration range of 5×10^{-8} M to 5×10^{-6} M. The LCUV method can be used to monitor the majority of such eluents, the major exceptions being the second of two consecutive elutions performed within a short time period or samples drawn late in the generator life. Thus, in order to monitor all generator eluents a more sensitive detection method is needed. In addition, it is of interest to monitor radiopharmaceutical mixtures for any remaining, unreacted TcO_4^-, since the presence of this species is almost always detrimental to the quality of the γ-ray image. Because the major fraction of radiopharmaceutical mixtures contains Tc in a reduced form, the concentration of TcO_4^- in these mixtures is very low, and again a very sensitive detection system is required.

In this work, liquid chromatography/electrochemistry (LCEC) is applied to the determination of total TcO_4^- in generator eluents as LCEC is known to be one of the most sensitive HPLC methods (*5*). TcO_4^- contains the most oxidized form of Tc (i.e., the VII oxidation state), and therefore reductive LCEC is necessary. There have been several papers in the literature recently that report the use of LCEC in the reductive mode. Though reductive LCEC is not a new technique (*6–9*), this trend reflects development of the method into a highly sensitive analytical tool with a wide range of applications. These include the determination of organics (*10–15*), organometals (*16*), and metal ions (*14, 17, 18*). State-of-the-art developments have been reviewed (*11, 19*). Many of the typical problems associated with reductive LCEC were encountered while developing the method for the determination of TcO_4^-. These include difficulties associated with electrode fouling, the necessity of detecting at somewhat large negative potentials, and interferences from dissolved O_2. However these problems were overcome to the extent that generator eluent levels of TcO_4^- could be readily detected.

EXPERIMENTAL SECTION

Apparatus. Voltammograms were obtained with a Bioanalytical Systems, Inc. (BAS), CV-1A or CV-1B potentiostat, a Hewlett-Packard 7015-B x-y recorder, and a Keithley 178 digital multimeter. The standard bulk solution voltammetry cell with glassy carbon working (area = 9.1 mm^2), Ag/AgCl (3 M NaCl) reference, and Pt auxiliary electrodes was from BAS.

Differential pulse polarography was performed at a EG&G Princeton Applied Research (PAR) Model 303 static mercury drop electrode (SMDE), which incorporates a Ag/AgCl (3 M NaCl) reference electrode and a Pt auxiliary electrode. Large drops (surface area of 2.7 mm^2) were used. A PAR 174A polarographic analyzer controlled the SMDE.

Chromatograms were obtained with a liquid chromatograph that could be connected to either a thin-layer detector with a glassy carbon electrode or a mercury drop detector. The BAS liquid chromatography system, depicted in Figure 1(A–E), is a LC-304 apparatus which includes a LC-22 temperature controller, a mobile phase deoxygenation system as recommended by BAS, a PM-30 dual piston pump, a TL-5 electrochemical cell, an LC-4 amperometric controller (time constant = 0.5 s), and a Houston Instruments Omniscribe strip-chart recorder. The TL-5 thin-layer cell contains a glassy carbon working electrode (area = 8.0 mm^2) and a 5-mil Teflon spacer. The Ag/AgCl (3 M NaCl) reference and stainless steel auxiliary electrodes are located downstream. No pulse dampener was used since it proved to be unnecessary.

Detection at a mercury drop electrode was accomplished by replacing the BAS detection system with an EG&G PAR Model 310/174A SMDE system (time constant in the sampled DC mode = 16.7 ms). This is depicted in Figure 1; again parts A–D are used, except that the TL-5 thin-layer cell in D is replaced by F, and detector E is replaced by detector G. The SMDE system utilizes a mercury drop assembly that is coupled to the column outlet tubing by an LC adapter body. The adapter body as well as the Ag/AgCl reference electrode, and Pt auxiliary electrode are suspended in a 50-mL bulk flow cell. Medium drops with a surface area of 1.7 mm^2 were used.

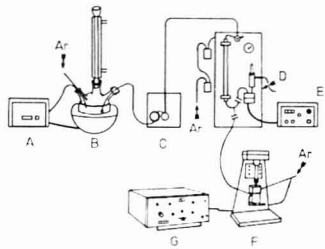


Figure 1. LCEC apparatus: (A) temperature controller; (B) solvent reservoir; (C) pump; (D) BAS LC component rack which holds (clockwise from left) analytical column, injection valve, pressure gauge, and TL-5 thin-layer cell, left of the rack are two vials for deoxygenating sample with Ar (lower and upper contain water and sample, respectively); (E) BAS amperometric controller; (F) EG&G PAR SMDE; (G) EG&G PAR polarographic analyzer.

The HPLC Knauer column (25 cm × 4.6 mm i.d.) from Unimetrics was packed in our laboratory with 5-μm NH_2-bonded Spherisorb from Jones Chromatography, Inc. A guard column of 10-μm Amino Spheri-5 material from Brownlee Labs was installed between the injection valve and the analytical column; this column is located behind the component rack and thus is not depicted in Figure 1D.

Deoxygenation Requirements. Detection in the reductive mode at potentials in excess of −1.0 V required rigorous deoxygenation procedures. These include adaptations recommended by BAS: a reflux apparatus for deoxygenating the mobile phase; lines from the Ar tank that are $^1/_8$ in. copper tubing with brass fittings (no further purification of the Ar proved necessary); and exclusive use of 316 stainless steel tubing and fittings between the reflux apparatus and the electrochemical cell. Additionally, an Ar line was extended to the SMDE electrochemical cell and fitted to a fine porosity glass dispersion tube. This tube was passed through the spiking hole in the side of the SMDE electrode support block as shown in Figure 1.

The deoxygenation procedures were as follows: (a) The appropriate aqueous mobile phase was placed in a 2-L flask and refluxed at 100 °C for 1 h (using the LC-22 temperature controller and probe) while being purged with Ar. The temperature was then allowed to drop to 45 °C, and, with Ar flowing over the solution, the mobile phase was pumped directly from this vessel through stainless steel tubing. If the LC had been exposed to O_2 in the meantime, the deoxygenated mobile phase was pumped through it overnight to purge all O_2 from the porous packing material. Our system incorporated two such apparatuses so that shut-down time for deoxygenating was eliminated. This procedure is essentially that described by Bratin and Kissinger (*11*). (b) The SMDE flow cell was rinsed with distilled, deionized H_2O each day. The trap was then filled with Hg and the cell was filled with nondeoxygenated buffer that was being used as the mobile phase. Deoxygenation was accomplished by purging with Ar through the porous glass frit for 45–60 min. The 310 is equipped with an Ar inlet so that Ar continuously flows over the solution to prevent O_2 from reentering the cell. Thus, once purged, the cell may be operated with no further deoxygenation. If this cell is not deoxygenated sufficiently, not only does the magnitude of the base line current rise but the peak-to-peak base line noise increases. (c) If the BAS solid electrode system was used, only the mobile phase was deoxygenated; there are no special requirements for the flow cell. (d) The sample solution was deoxygenated by purging with an Ar stream (that had been saturated with H_2O) for 2–5 min (Figure 1D). Immersing the inlet of the injection valve

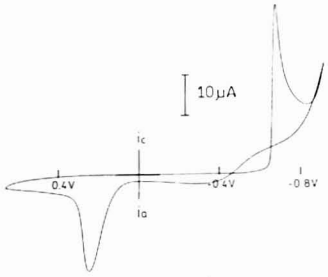


Figure 2. Cyclic voltammogram of 10^{-3} M $KTcO_4$ in 0.1 M, pH 5 acetate buffer, glassy carbon electrode, scan rate = 25 mV/s.

in the sample solution, a syringe was used to pull an aliquot into the 20-μL loop with no exposure to air (*11*). Available sample volumes were large enough (0.5 to 2.0 mL) that this deoxygenation procedure was adequate.

Reagents and Materials. Instrument mercury (A.C.S. grade, Bethlehem Apparatus Co., Inc.) was used without further purification. Acetate buffer was prepared from reagent grade acetic acid and concentrated NaOH. Phosphate buffer was prepared from HPLC grade KH_2PO_4 and reagent grade concentrated NaOH. All water had a resistivity of at least 17 MΩ cm and was obtained from a Sybron/Barnstead system. Technetium-99, obtained from Oak Ridge National Laboratory in the form of $NH_4^{99}TcO_4$, was converted to $K^{99}TcO_4$ by metathesis with KOH, and this material was used for preparing standard solutions. Pertechnetate generator samples were eluted from a commercial $^{99}Mo/^{99m}Tc$ generator; these samples were the same as those used in previous studies (*3*). All solvents were filtered through a 0.2-μm Gelman Metricel GA-8 membrane filter.

RESULTS AND DISCUSSION

Voltammetry. A cyclic voltammogram of 10^{-3} M $^{99}TcO_4^-$ in pH 5 acetate buffer at a glassy carbon electrode is shown in Figure 2. The voltammogram (initiated at 0.0 V in the negative direction) exhibits highly irreversible behavior with a reduction wave at −0.68 V and an oxidation wave at 0.25 V. The symmetry of the latter indicates that it could be a stripping wave. Further experiments employing the technique of anodic stripping voltammetry confirm this; i.e., the height of this wave is linearly dependent on TcO_4^- concentration and on the time spent in the deposition step (during which stirring occurred).

One further notable feature of Figure 2 is the appearance of a poorly defined cathodic wave at −0.57 V. This occurs while scanning in the positive direction and indicates that there is some alteration of the electrode surface following reduction of TcO_4^-. Figure 3 shows the results of further experiments designed to elucidate this phenomenon. With the same conditions as before, scans were initiated at 0.0 V in the negative direction. Voltammogram A exhibits the normal behavior that is also seen in Figure 2. If the positive scan is then reversed at 0.0 V instead of scanning through the stripping wave, voltammogram B (Figure 3) is obtained. There is an obvious distortion in the voltammogram exemplified by a shift toward positive potentials of both the TcO_4^- reduction wave and the H_2 evolution background wave. Voltammogram C is obtained after holding the potential at −0.9 V for approximately 2 min. Clearly the electrode characteristics have changed; most likely the electrode no longer has just a carbon surface but consists of a technetium film on the carbon surface. This same phenomenon was observed on gold, platinum, wax-impregnated graphite, hanging mercury drop, and Au amalgam electrodes. A detailed analysis of this phenomenon is complicated by the proximity of the TcO_4^- reduction wave

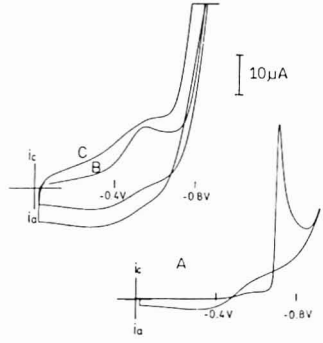


Figure 3. Cyclic voltammograms of 10^{-3} M $KTcO_4$ in 0.1 M, pH 5 acetate buffer, glassy carbon electrode, scan rate = 25 mV/s: (A) initial scan, (B) second scan (inner tracing), (C) third scan (following the application of E = −0.9 V for 2 min).

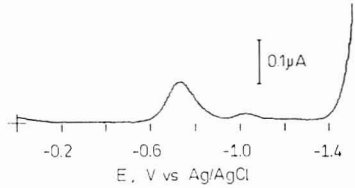


Figure 4. Differential pulse polarogram of 10^{-5} M $KTcO_4$ in 0.05 M, pH 6 phosphate buffer: SMDE, scan rate = 10 mV/s, 1 drop/s, modulation amplitude = 25 mV.

to the H_2 evolution wave; this creates difficulties in the LCEC application.

A differential pulse polarogram of TcO_4^- using the static mercury drop electrode is shown in Figure 4. It has been reported in the literature that TcO_4^- has a well-behaved, diffusion-controlled, polarographic wave corresponding to three electrons at approximately −0.7 V in pH 7 phosphate buffer (*20*). Figure 4 shows that this same wave occurs in pH 6 phosphate buffer. At pH 5.3, it is still present, along with waves at −1.05 V and −1.35 V. Thus the potential of this peak is independent of pH over this range. More importantly, this peak is well removed from the H_2 evolution wave, a fact that simplifies the LCEC analysis.

Liquid Chromatography/Electrochemistry. LCEC generally employs either solid electrodes or a dropping mercury electrode. Solid electrodes used for reductive processes commonly are either carbon or a Au amalgam, and in the absence of adsorption problems these electrodes can be used for routine analyses with minimal daily preparation; they are simple to use and inexpensive. Solid electrodes, however, are subject to passivation, and considerable effort has been expended to circumvent this limitation (*21–23*). These effects can be avoided by the use of a dropping mercury electrode which presents a renewable surface to the electroactive solution. The dropping mercury electrode also has a large negative potential range and a uniform surface that is not subject to inhomogeneities associated with the surfaces of solid electrodes. On the other hand, dropping Hg electrodes can be somewhat inconvenient because they require more operator attention. Since it is evident from the data in Figure 3 that reduction of 10^{-3} M TcO_4^- on a carbon surface involves a serious adsorption problem, two approaches have been taken

Table I. Linear Least-Squares Analysis for $K^{99}TcO_4$ Standard Curves[a]

	slope	Y intercept	corr coeff
SMDE detector	12.80 ± 0.04	0.16 ± 0.01	0.9989
glassy carbon electrode detector	1.47 ± 0.01	−0.0069 ± 0.0002	0.9996
SMDE detector under generator working conditions	11.68 ± 0.02	0.18 ± 0.01	0.9995

[a] At least three sample injections were made at each concentration; the mean value of i in nA was plotted vs. concentration TcO_4^- in μM. Y values are weighted in the least-squares analysis as $1/\sigma_m^2$ where σ_m = the standard deviation of the mean.

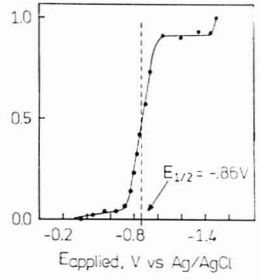


Figure 5. Hydrodynamic voltammogram of 10^{-6} M $KTcO_4$: i^* = normalized current, mobile phase = 0.01 M, pH 5.7 phosphate, SMDE, sampled DC mode, 1 drop/s, flow rate = 1.0 mL/min.

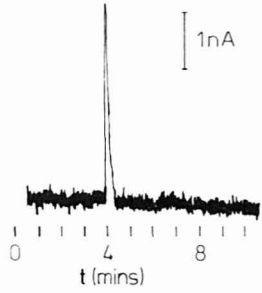


Figure 6. Chromatogram of 2.6×10^{-7} M standard $KTcO_4$ solution: mobile phase = 0.01 M, pH 6.0 phosphate, SMDE, sampled DC mode, $E_{applied}$ = −1.1 V, 1 drop/s, flow rate = 1.0 mL/min.

to circumvent the associated difficulties. First, a static mercury drop electrode has been employed for use with higher concentrations of TcO_4^-, and, second, a glassy carbon electrode has been employed to detect those levels of TcO_4^- (i.e. less than 1×10^{-7} M) that do not give extensive adsorption effects.

SMDE Detection. Figure 5 shows a hydrodynamic voltammogram constructed from chromatographic data using 0.01 M phosphate buffer (pH 5.7) as a mobile phase. This was done in the sampled DC mode by making successive TcO_4^- injections at increasingly negative potentials. Current was measured at each potential and normalized by dividing all values by the largest current value (at E = −1.50 V). A plot of E vs. $i_{normalized}$ yields $E_{1/2}$ = −0.86 V. Any potential ≥−1.0 V results in a current equal to the limiting current, thus producing maximum sensitivity. All further analyses are conducted at E = −1.10 V.

Three different modes of detection were employed to determine the optimum type of analysis, i.e., differential pulse, normal pulse, and sampled DC detection. On the basis of the peak heights, normal pulse gives the maximum current response (i.e., a factor of 1.5 greater than that observed in DC detection), followed by sampled DC, and then differential pulse. However, the signal to noise ratio is essentially the same for all three modes; thus, sampled DC is used for the analysis since the regular base line associated with this mode facilitates peak height measurements.

Peak response is directly dependent on Hg drop area; however, if the drop is too large, the surface can be distorted by the eluent flow. Thus, a medium drop was used which provided both sensitivity and reproducibility. A 1-s drop time proved advantageous for two reasons: first, electrode alteration problems late in the drop life are avoided and, second, sufficient data points during a peak (i.e., 30 drops/peak) are obtained. Figure 6 shows a typical chromatographic peak obtained with these parameters and a mobile phase of 0.01 M phosphate (pH 6). Thoroughly deoxygenating the sample ensures the absence of an O_2 peak. Table I shows the calibration data obtained under these optimal conditions. With 14 different pertechnetate concentrations, linearity extends over 4 orders of magnitude from 2.1×10^{-8} M to 1.0×10^{-4} M TcO_4^-. Response may continue to be linear above 1.0×10^{-4} M TcO_4^-, but these levels were not investigated. The detection limit, defined as a peak height that is twice base line peak-to-peak noise, is 2.1×10^{-8} M ±8.3%. Three repetitive injections were made at each concentration, and precision is reported as the percent relative standard deviation (% rsd) between the three measured current values. Precision varied over the range from 8.3% at the detection limit to 0.2% at the high end of the range.

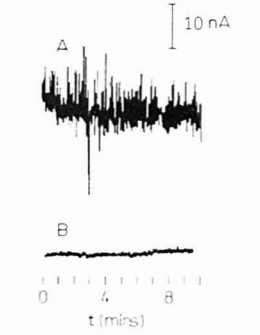


Figure 7. Chromatographic background: (A) flow cell not deoxygenated, (B) flow cell deoxygenated; mobile phase = 0.01 M, pH 5.3 phosphate, SMDE, sampled DC mode, $E_{applied}$ = −1.1 V, 1 drop/s, flow rate = 1.0 mL/min.

As mentioned in the Experimental Section, the presence of O_2 is a significant problem in reductive LCEC. This has been solved in many cases by simple purging of the mobile phase and sample; in other cases it has been solved by more novel approaches (*17*, *18*, *24*, *25*). Nonetheless, detection limits have generally been dependent on the magnitude of the base line peak-to-peak noise which in turn has been found to be

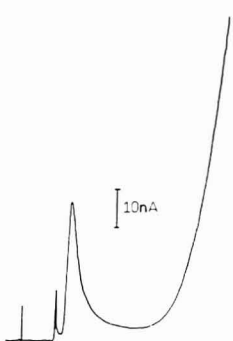


Figure 8. Chromatogram of 10^{-7} M $KTcO_4$, mobile phase = 0.1 M, pH 5 acetate buffer, glassy carbon electrode, $E_{applied}$ = −0.9 V, flow rate = 1.0 mL/min.

directly dependent on the amount of dissolved O_2 both in the mobile phase and in the flow cell. Deoxygenation of the latter is a special requirement when using the static mercury drop electrode and cannot be simply accomplished by deoxygenation of the mobile phase; contrary to what is stated in the manufacturer's literature this is not a negligible problem (*26*). Figure 7 shows a comparison of the peak-to-peak base line noise in a deoxygenated flow cell vs. that in a nondeoxygenated flow cell. Following the deoxygenation procedure previously described, peak-to-peak base line noise of 1.0 nA can be routinely achieved; the lowest level observed throughout this study was 0.2 nA. The magnitude of base line offset required is likewise dependent on the amount of dissolved O_2. Thus not only does deoxygenation effectively minimize the peak-to-peak noise, but it reduces the overall base line offset required such that the limits of detection that one would expect for this type of instrumentation are readily achieved.

One further interesting point is that O_2 in the analyte solution has not proven to be a severe problem. This is because O_2 is somewhat retained on the NH_2-bonded phase column, eluting at ca. 6.2 min. The retention time of this peak is not affected by mobile phase conditions (i.e., pH, ionic strength, particular buffer used, etc.) but is affected when a column is repacked with new NH_2-bonded phase material. These observations are presumably due to the fact that O_2, being a small molecule, is able to diffuse into the porous packing material. Thus, even though there is no chemical interaction between O_2 and the column material, O_2 experiences a larger effective void volume than TcO_4^-. On the basis of this fixed retention time for O_2, TcO_4^- can be readily separated from O_2 by adjusting such mobile phase conditions as pH and ionic strength which do affect the retention time of TcO_4^-.

Solid Electrode Detection. The second approach employed to overcome electrode fouling alteration involves amperometric detection at a solid electrode, as in Figure 1(A–E), but using only very low levels of TcO_4^-. The severity of the adsorption problem at a carbon electrode is illustrated by the following chromatographic experiment. Using a mobile phase of pH 5 acetate buffer, a 20-μL aliquot of 10^{-6} M TcO_4^- was injected, yielding a clean chromatogram with TcO_4^- eluting at 4.3 min. A subsequent 20-μL injection of 10^{-7} M TcO_4^- yields the chromatogram shown in Figure 8 again with TcO_4^- eluting at 4.3 min. The large peak at 6.2 min corresponds to O_2 in the $KTcO_4$ sample as discussed earlier. The most notable feature in this second chromatogram is the dramatic rise in base line beginning at approximately 17 min. This results from alteration of the electrode surface following TcO_4^- reduction and makes subsequent detection on the particular electrode impossible without a lengthy cleanup procedure. However, if the TcO_4^- concentration is kept at levels $\leq 10^{-7}$ M, this phenomenon is not observed. With a mobile phase of 0.01 M phosphate buffer (pH 6.0) and a potential of −1.0 V, a calibration curve was constructed, the data for which are given in Table I. A detection limit of 8.5×10^{-9} M TcO_4^- was obtained with a precision of 4.5% rsd. The worst precision encountered was 16.3% at 9.4×10^{-9} M TcO_4^-. With 10 different $KTcO_4$ concentrations, this calibration curve extends to 1.0×10^{-7} M TcO_4^-; six repetitive injections were made at this level with no evidence of electrode fouling. Therefore, the detection limit of the LCEC analysis using solid electrode detection is ca. a factor of 5 better than that using SMDE detection. This occurs because of the very low level base line peak-to-peak noise found with the BAS solid electrode system. However, fouling of the solid electrode at high TcO_4^- concentrations allows a working range of little more than 1 order of magnitude.

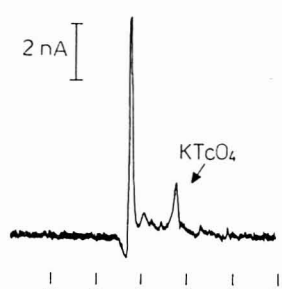


Figure 9. Chromatogram of a $KTcO_4$ sample from a $^{99}Mo/^{99m}Tc$ generator: mobile phase = 0.1 M, pH 5.3 phosphate, SMDE, sampled DC mode, $E_{applied}$ = −1.1 V, 1 drop/s, flow rate = 1.0 mL/min.

Application to Generator Samples. Previous work in our laboratory (*4*) has shown that $^{99}Mo/^{99m}Tc$ generator samples typically contain 5×10^{-8} M to 5×10^{-6} M TcO_4^-. These concentrations fall readily within the determined working range of the polarographic detector. To analyze actual generator eluents, mobile phase conditions had to be adjusted such that TcO_4^- would be separated from some early eluting interferences. By use of 0.01 M phosphate (pH 5.3), standard $KTcO_4$ samples were found to elute with a retention time of 5.1 min. Figure 9 shows a chromatogram of a typical generator sample analyzed under these same conditions; in this sample TcO_4^- elutes at approximately 5.5 min and is free from interferences. There is a slight discrepancy (i.e., 5.1 vs. 5.5 min) in retention times between the standard sample and the generator sample. This was investigated by conducting matched matrix experiments in which an aliquot of standard TcO_4^- solution was added to (a) a sample of the generator background solution (i.e., 0.15 M NaCl) and (b) a generator TcO_4^- sample. In both these samples, TcO_4^- eluted at 5.5 min, indicating that the observed discrepancy in retention time is thus a result of matrix effects.

Table I gives the standard calibration data obtained from injecting six different concentrations from 4.2×10^{-8} M to 6.3×10^{-6} M TcO_4^-, i.e., the working range for most generators. A detection limit of 4.2×10^{-8} M TcO_4^- was obtained with a precision of 2.0% rsd; the worst observed precision is 2.7% rsd at 6.3×10^{-8} M TcO_4^-.

The variation in total TcO_4^- levels from day to day over the lifetime of a given generator has been investigated; however, these results will be published elsewhere.

CONCLUSIONS

SMDE detection is applicable to most $^{99}Mo/^{99m}Tc$ generator eluents, i.e., other electroactive components are readily separated by the NH_2-bonded column, and the majority of generator eluents contain TcO_4^- within the established working concentration range. For those generator eluents drawn late in the generator life or resulting from second elutions, solid electrode detection (i.e., glassy carbon electrode) may have to be employed. With these two detection schemes, this method should be applicable as well to determining TcO_4^- in other sample matrices such as environmental samples, biological samples, and actual radiopharmaceutical preparations. This developed procedure constitutes an example of the capabilities of reductive LCEC for determining ionic inorganic species. More generally, however, it illustrates the versatility that can be achieved in an LCEC system; i.e., the capability of performing analyses in either the oxidative or reductive mode is realized with this system (even though the oxidative mode was not required for the TcO_4^- determination), as well as the capability of obtaining qualitative information on low-level components by constructing hydrodynamic voltammograms.

ACKNOWLEDGMENT

The authors gratefully acknowledge T. William Gilbert, Peter T. Kissinger, Karl Bratin, and Kenneth R. Wehmeyer for helpful discussions and assistance.

Registry No. Technetate, 23288-61-1.

LITERATURE CITED

(1) Saha, G. P. "Fundamentals of Nuclear Pharmacy"; Springer-Verlag: New York, 1979; pp 33-94.
(2) Deutsch, E. In "Radiopharmaceuticals II"; Proceedings of the 2nd International Symposium on Radiopharmaceuticals; Society of Nuclear Medicine: New York, 1979; p 129.
(3) Deutsch, E.; Heineman, W. R.; Zodda, J. P.; Gilbert, T. W.; Williams, C. C. *Int. J. Appl. Radiat. Isot.* **1982**, *33*, 843-848.
(4) Zodda, J. P.; Heineman, W. R.; Gilbert, T. W.; Deutsch, E. *J. Chromatogr.* **1982**, *227*, 249-255.
(5) Kissinger, P. T. *Anal. Chem.* **1977**, *49*, 447A-456A.
(6) Kemula, W. *Rocz. Chem.* **1952**, *26*, 281.
(7) Blaedel, W. J.; Todd, J. W. *Anal. Chem.* **1958**, *30*, 1821-1825.
(8) Rebertus, R. L.; Cappell, R. J.; Bond, G. W. *Anal. Chem.* **1958**, *30*, 1825-1827.
(9) Tustanowski, S. *J. Chromatogr.* **1967**, *31*, 266-268.
(10) Funk, M. O.; Keller, M. B.; Levison, B. *Anal. Chem.* **1980**, *52*, 771-773.
(11) Bratin, K.; Kissinger, P. T. *J. Liq. Chromatogr.* **1981**, *4* (Suppl. 2), 321-357.
(12) Samuelsson, R.; Osteryoung, J. *Anal. Chim. Acta* **1981**, *123*, 97-105.
(13) Vohra, S. K.; Harrington, G. W. *J. Chromatogr. Sci.* **1980**, *18*, 379-383.
(14) Lyle, S. J.; Saleh, M. I. *Talanta* **1981**, *28*, 251-254.
(15) Wightman, R. M.; Paik, E. C.; Borman, S.; Dayton, M. A. *Anal. Chem.* **1978**, *50*, 1410-1414.
(16) MacCrehan, W. A.; Durst, R. A.; Bellama, J. M. In "Trace Organic Analysis: A New Frontier in Analytical Chemistry"; Proceedings of the 9th Materials Research Symposium; NBS: Gaithersburg, MD, 1978; pp 57-63.
(17) Maitoza, P.; Johnson, D. C. *Anal. Chim. Acta* **1980**, *118*, 233-241.
(18) Buchanan, E. B., Jr.; Bacon, J. R. *Anal. Chem.* **1967**, *39*, 615-620.
(19) Štulík, K.; Pacáková, V. *J. Electroanal. Chem.* **1981**, *129*, 1-24.
(20) Magee, R. J.; Cardwell, T. J. In "Encyclopedia of Electrochemistry of the Elements"; Bard, A. J., Ed.; Marcel Dekker: New York, 1974; Vol. II, pp 161-162.
(21) Van Rooijen, H. W.; Poppe, H. *Anal. Chim. Acta* **1981**, *130*, 9-22.
(22) Johnson, D. C. "Applications of Pulse Techniques to EC Detection"; presented at the LCEC Symposium on Environmental and Industrial Applications of LCEC and Voltammetry, May 17-19, 1981, Indianapolis, IN, Abstract No. 2.
(23) Miner, D. J.; Bopp, R. J. "The Reproducibility of Measurements by LCEC"; presented at the LCEC Symposium on Environmental and Industrial Applications of LCEC and Voltammetry, May 17-19, 1981, Indianapolis, IN, Abstract No. 25.
(24) Hanekamp, H. B.; Voogt, W. H.; Bos, P.; Frei, R. W. *Anal. Chim. Acta* **1980**, *118*, 81-86.
(25) Larochelle, J. H.; Johnson, D. C. *Anal. Chem.* **1978**, *50*, 240-243.
(26) EG&G Princeton Applied Research Model 310 Polarographic Detector Operating and Service Manual, p 10.

RECEIVED for review September 28, 1982. Accepted December 20, 1982.

Linearization of Electron Capture Detector Response to Strongly Responding Compounds

W. B. Knighton and E. P. Grimsrud*

Department of Chemistry, Montana State University, Bozeman, Montana 59717

An extended means of processing the signal of a constant-current electron capture detector (CC-ECD) is proposed. This new response function provides a significant improvement in quantitative analysis by the ECD because it provides linear calibration curves for strongly electron attaching molecules over the entire dynamic range of the instrument. This refinement in the ECD response occurs because it accounts for the alteration of the analyte concentration in the detector by the electron capture process, itself. The theoretical basis and experimental support for the proposed EC response function are presented where CCl_4, $CFCl_3$, and $CHCl_3$ are used as test compounds.

The electron capture detector (ECD) is widely used in gas chromatography (GC) for the analysis of numerous environmentally important compounds because of its unsurpassed sensitivity often permitting detection at the femtogram level (*1*). Unfortunately quantitation with this detector has often been difficult because of nonlinear and unpredictable relationships between the measured response and analyte concentration. During its early use the ECD was operated in the direct current (DC) or the fixed frequency (FF) pulsed modes of operation where the change in current (ΔI) was taken as the response. Detectors operated in either of these two modes yielded linear calibration curves only over the initial 10% of the entire response range. In 1967 Wentworth and Chen (*2*) showed that if the analytical response in the fixed frequency mode was taken as $(I^\circ - I)/I$, where I° is the measured standing current in the absence of sample and I is the cell current measured continuously during the chromatogram, that linear calibration curves could be obtained up to and exceeding 90% of detector saturation. A practical limitation of this mode

0003-2700/83/0355-0713$01.50/0 © 1983 American Chemical Society

of signal processing is its requirement for unusually clean chromatographic conditions so that a high standing current with long pulse periods can be achieved. In 1971 Maggs et al. (*3*) proposed operating the ECD in the frequency modulated or constant current (CC) mode of operation. In this case a feedback network maintains the magnitude of the measured current constant and equal to a preselected reference value by control of the pulsing frequency. As an electron capturing compound passes through the cell the frequency of pulsing increases by an amount required to keep the current constant. The analytical response is taken as the increase in frequency of pulsing. The constant current ECD has been shown to yield responses to many compounds which are linear with sample concentration up to 99% of detector saturation. The present acceptance of this mode of ECD operation is evidenced by the fact that it is now the standard offering of commercial vendors of gas chromatographs.

Ironically, with all the above advances in the operation of the ECD, this detector is still not expected to provide linear responses to those compounds (such as highly halogenated hydrocarbons) for which it is most sensitive. The lack of linear responses to this important group of compounds is not due to instrumental deficiencies but is attributed to the alteration of the analyte concentration within the detector by the electron attachment process, itself. Nonlinear responses of this type have been previously described and explained (*4–6*). Briefly, this behavior of strongly responding compounds is explained as follows. At low sample concentrations a significant fraction of the analyte is destroyed by the electron capture reaction because the EC rate constant and the average electron density are both large. Under this low sample concentration condition an approximately linear response is observed as long as the electron population remains high and relatively constant, causing the same fraction of analyte molecules to be reacted over this limited sample concentration range. However, as the concentration of the sample increases, a smaller population of electrons consumes a successively smaller fraction of the analyte entering the cell. The monitored responses for ECDs operated in either the $(I^\circ - I)/I$ or CC mode are directly proportional to the instantaneous concentration of the analyte within the detector. Therefore, the response cannot also be linearly related to the analyte concentration entering the cell over the entire dynamic range of the detector.

One approach to minimizing this problem is to make the detector volume very small or make the carrier flow rate very fast. The residence time of the analyte in the cell is then very short and little destruction of the sample by the EC reaction is allowed. The small detector approach has been demonstrated by Patterson (*7*), where the active volume of a small cell was made effectively smaller by use of a displaced coaxial anode. Alternatively, high flow rates are easily obtained through the addition of makeup gases. The compromise inherent in these approaches is that while only partially improving the quantitative response to strongly responding compounds the sensitivity to weakly and moderately responding compounds will be proportionately reduced.

In this paper a new means of ECD signal processing is described by which a linear response over the entire dynamic range is achieved for strongly responding compounds, using a detector of any size or design with conventional flow rates. This is made possible by combining the usual constant current mode of control with an extended definition of the processed response. This improvement occurs because any alteration of analyte concentration by the attachment of electrons is accounted for and incorporated into this response function. Following its theoretical description, experimental support for this refinement of the ECD response is provided by using the strongly electron attaching compounds, $CFCl_3$ and CCl_4, as test compounds. This choice of test compounds is made because the electron capture reactions of these will occur with a one-to-one electron-to-analyte stoichiometry (*8*). Complications which might be expected from more complex EC reactions as well as those caused by physical effects of the ion–electron dynamics of an ECD are briefly discussed at the conclusion of this article.

THEORY

It is appropriate to first describe how the measured response is related to sample concentration in the usual CC-ECD. The reactions occurring within the ECD which are of primary significance include the following:

$$\text{neutrals} \xrightarrow{S} P^+ + e^- \quad (1a)$$

$$A + e^- \xrightarrow{k_A} \text{negative ions} + \text{neutrals} \quad (1b)$$

$$B + e^- \xrightarrow{k_B} \text{negative ions} + \text{neutrals} \quad (1c)$$

$$P^+ + e^- \xrightarrow{R} \text{neutrals} \quad (1d)$$

$$P^+ + \text{negative ions} \rightarrow \text{neutrals} \quad (1e)$$

Where reaction 1a represents the production of positive ions (P^+) and electrons (e^-) by the ionizing radiation (usually provided by ^{63}Ni) with S being the first-order ion–electron pair production rate constant. The electron loss pathways are given by reactions 1b–1d. Electron capture by the electron attaching sample (A) is given by reaction 1b where k_A is the second-order rate constant for electron capture. Loss of electrons by attachment to carrier gas impurities and column bleed (B) is combined into a single reaction 1c with a rate constant, k_B. The final electron loss mechanism is recombination of positive ions (P^+) with electrons (e^-). Reaction 1e is the recombination of positive ions with negative ions to form neutrals. For the above reactions the change in electron density with time can be expressed as a simple differential equation of the form

$$dN_e/dt = S - LN_e \quad (2)$$

where $L = (Rn_+ + k_B n_B + k_A n_A)$ is a first-order rate constant which represents the sum of all the electron loss rates and N_e is the instantaneous electron population. Positive ion concentration, n_+, is assumed to be relatively constant throughout a ^{63}Ni ECD (*9*) (the validity and implications of this assumption are further discussed at the conclusion of this paper). Since n_A and n_B can be assumed constant over the short time of a period between pulses, the entire term, L, can be treated as a constant independent of the variable, N_e. Integration of eq 2 and evaluation at time $t = T$, the pulse period, yields the following expression for N_e^T, the population of electrons at the instant prior to a pulse.

$$N_e^T = (S/L)(1 - e^{-LT}) \quad (3)$$

Given that the level of demanded current $I = K'N_e^T/T$, where K' is a proportionality constant somewhat less than unity that accounts for the perturbation in the observed current by the arrival of positive ions at the anode between pulses (*9*), eq 4 is obtained.

$$I = (K'S/LT)(1 - e^{-LT}) \quad (4)$$

Inspection of the above equation reveals that the magnitude of the current can remain constant as the input of analyte changes only if the values of L and T vary in a definite manner such that the product of L and T remains constant at all times. Therefore the entire term, $(1 - e^{-LT}) = Z$, must also be a constant. Realizing that frequency of pulsing, f, is equal to

the reciprical of T, eq 5 is obtained. In the constant current

$$f = (I/K'SZ)L \tag{5}$$

ECD the response is taken as the change in frequency $f - f°$ where $f°$ and f correspond to the frequency of pulsing in the absence ($L = Rn_+ + k_Bn_B$) and presence ($L = Rn_+ + k_Bn_B + k_An_A$) of sample, respectively. The usual response of the CC-ECD defined as the frequency increase is then given by eq 6, where $G = Ik_A/K'SZ$. This response function is seen

$$f - f° = (I/K'SZ)k_An_A = Gn_A \tag{6}$$

to be linearly related to the *instantaneous concentration* of analyte within the detector. This response will also be linearly related to the amount of material entering the detector from the GC provided the concentration of the analyte is not significantly perturbed by the EC process itself. This condition is met only for compounds which have low to moderate electron capture rates.

For molecules which have fast electron attachment rates the concentration of analyte entering the cell is not the same as the instantaneous average concentration within it. For these cases it is necessary to relate the analyte concentration which is entering the cell (the quantity sought) to the instantaneous concentration in the cell (the quantity sensed by the normal CC-ECD). In eq 7 three terms account for the change of analyte concentration with time. The first term is ventilation

$$dn_A/dt = Fn_A°/V - k_An_A\bar{N}_e/V - Fn_A/V \tag{7}$$

into the cell where F is carrier gas flow rate, V is the detector volume, and $n_A°$ is the concentration of the analyte entering the cell. The second term is the electron capture term where n_A is the instantaneous concentration of sample and $\bar{N}_e$ is the average electron population over several pulse periods. The final contribution is ventilation out of the cell. Because gaseous diffusion is fast relative to the flow rates used here, it is reasonable to assume that the ECD is a well-mixed reactor with respect to the distribution of analyte within it. A steady-state approximation is then valid and eq 7 can be set equal to zero. Solving for n_A and substituting into eq 6 yields eq 8. The time-averaged electron population, $\bar{N}_e$, is equivalent

$$f - f° = (I/K'SZ)\left(\frac{1}{(k_A\bar{N}_e/F) + 1}\right)k_An_A° \tag{8}$$

to N_e^T only if the period between pulses is unusually long so that an equilibrium between the production and loss of the electrons is established. In the CC-ECD considerably faster pulsing is normally used and then, $\bar{N}_e = K''N_e^T$ where K'' is a proportionality constant between 0.5 and 1.0 (the proportionality constant can be evaluated from the general expression $K'' = (1 - e^{-LT})^{-1} - (LT)^{-1}$) which accounts for the reduced value of the average electron population compared with the maximum instantaneous electron population just prior to a pulse. Combined with the affect of the positive ion contribution on the measured current, the measured current can be redefined as $I = K\bar{N}_e/K''T$. Substituting $\bar{N}_e$ obtained from this expression and $T = 1/f$ into eq 8 results in eq 9, where

$$f - f° = Gn_A°/((H/f) + 1) \tag{9}$$

again, $G = Ik_A/K'SZ$ and $H = Ik_AK''/FK'$. Equation 9 is of the same form as eq 6 except for the denominator, $(H/f) + 1$, which accounts for the alteration of analyte concentration by the EC reaction. Most importantly, $n_A°$, the quantity desired in the analytical measurement, rather than n_A occurs as the independent variable in eq 9. In the case where the electron capture rate constant is small the term H/f becomes negligible and eq 9 reduces to eq 6. A slight rearrangement of eq 9 yields our final result, eq 10. This expression more

$$(f - f°)(H + f)/f = Gn_A° \tag{10}$$

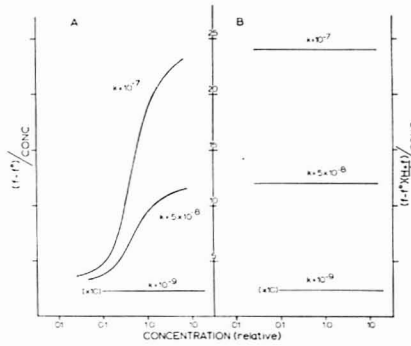


Figure 1. Synthesized molar response curves predicted from (A) the conventional response function calculated from eq 9 and (B) the extended response function calculated from eq 10, for three analytes of differing electron capture rate constants.

conveniently describes the response of the CC-ECD than does eq 6, because the response is linearly related to $n_A°$, the analyte concentration eluting from the GC into the detector, rather than the instantaneous concentration within the cell.

Simulated responses derived from eq 9 and 10 and from reasonable approximations of G and H are shown in Figure 1 for two relatively strongly responding compounds and one moderately responding compound. The following are the values used to determine H: $K' = 0.75$ (for detectors of concentric coaxial design about 25% of the positive ions arrive at the anode between pulses (*9*)); $I = 7 \times 10^{-9}$ A (the value for the reference current used in experiments to be reported here); $F = 0.5$ mL/s (a typical volume flow rate); and $K'' = 0.5$ (the time averaged electron density is about half of the maximum instantaneous electron population when relatively fast pulsing is used). With the above estimates, $H = 6000$, 3000, and 60 s^{-1} for EC rate constants of 1×10^{-7}, 5×10^{-8}, and 1×10^{-9} mL/s, respectively. The shape of the response curves is dependent only on the values of H and the base frequency of pulsing in the absence of sample. A value of $f° = 1000$ s^{-1} is chosen here to mimic our experimental conditions. The constant G contains many of the terms previously determined for the constant H. However, it is also dependent on values of the constants S and Z, both of which are more difficult to evaluate. Fortunately, the magnitude of G determines only the relative amplitude of the response curves and has no effect on their shape. Because the shape of the response curves is of primary concern here values for G have been selected rather arbitrarily. For the rate constants of 1×10^{-7}, 5×10^{-8}, and 1×10^{-9} mL/s the corresponding values of G assigned were 24 000, 12 000, and 240 concentrations^{-1} s^{-1}, respectively. Figure 1 is divided into two parts. In part A response curves are predicted for the usual response, $f - f°$, and in part B for the newly developed response function, $(f - f°)(H + f)/f$. In part A only the response associated with the small EC rate constant is linear with concentration. This is expected because H is then small compared with f for all concentrations. The response curves corresponding to the values of $k = 10^{-7}$ and 5×10^{-8} are S-shaped. This behavior is expected for any case in which $H/f > 1$ in the low concentration region. It is interesting to note that when the analytical signal is processed as $(f - f°)$, halving the EC rate constant such that G and H are halved results in a halving of the molar response only in the high concentration region and not over the entire response range. In the low concentration region the molar responses of the imagined compounds

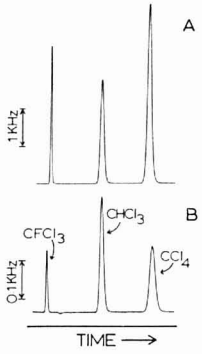


Figure 2. Typical chromatograms of standards containing $CFCl_3$, $CHCl_3$, and CCl_4. Concentrations are (A) 3.8 ppb $CFCl_3$, 48 ppb $CHCl_3$, and 9.5 ppb CCl_4 and (B) 0.38 ppb $CFCl_3$, 4.8 ppb $CHCl_3$, and 0.95 ppb CCl_4.

tend to converge to a similar value. When the response function as defined in part B is used, the predicted response curves are linear with concentration over the entire response range regardless of the rate of the electron attachment reaction.

EXPERIMENTAL SECTION

The gas chromatograph and constant current ECD used in this study were both home built. The ECD is of concentric coaxial design with an internal volume of 1.5 mL where the cylindrical walls are formed by a 15 mCi ^{63}Ni plated on Pt foil. The electronics which operate the ECD in the constant current mode have been previously described (*10*). This electronics package allows for the selection of any desired reference current and provides a dynamic range of up to 100 kHz. For all the experiments performed here a reference current of 7.08 nA was used. The value of the current was selected so as to give a base line frequency of 1000 Hz. Each pulse was of 1 μs duration and 50 V in amplitude. The output signal, a voltage proportional to frequency, was monitored on a strip chart recorder.

Samples were introduced via a 2-mL gas sampling loop (Carle 8030) onto a 10 ft × $^1/_8$ in. packed column containing 10% SF-96 on Chromosorb W. The oven was operated at ambient temperature. The detector temperature was 150 °C. A carrier gas flow of 30 mL/min of 10% methane in Ar which was first passed through oxygen and water traps was used. Samples were prepared by dilution of the neat liquid or gas into nitrogen by use of airtight containers which were held at above ambient pressure. Final dilutions and transfer of the sample to the gas sampling valve was done with a 100-mL gas tight syringe. Typical chromatograms thus obtained are shown in Figure 2.

In order to compare the molar responses of different compounds introduced by gas chromatography, it is necessary to account for analyte broadening within the column. Use of the term relative flux, which is proportional to the rate of entry of the analyte into the detector at a point corresponding to the center of the peak, accounts for this analyte broadening and is obtained by dividing the known concentration of analyte by its corresponding chromatographic peak width at half height. A low concentration chromatogram is chosen for the half-width measurement to ensure that the molar ECD sensitivity for the given compound will be constant over the entire chromatographic peak. The relative molar responses of all compounds is then determined by the peak height response divided by relative flux.

To process data in accordance with the proposed response function, $(f - f^\circ)(H + f)/f$, the value of H must first be determined. While various methods for this can be envisioned, the following procedure was used here. For both $CFCl_3$ and CCl_4, H was determined from two selected points on their response curves. Two

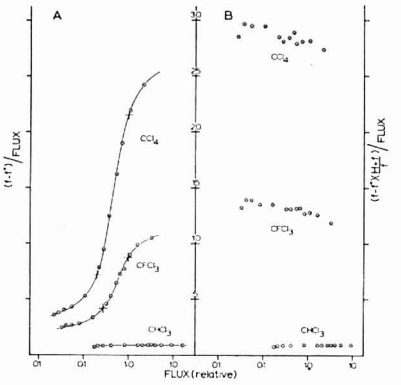


Figure 3. Measurements of relative molar responses vs. relative input rate (flux) for halogenated methane standards, where the response has been measured by using (A) the conventional response function and (B) the extended response function.

points are required because the response function $(f - f^\circ)(H + f)/f = Gn_A^\circ$ contains two unknowns, G and H. From two simultaneous equations representing points on a calibration curve, H can be determined according to

$$H = \left[f' \frac{n_A^{\circ\prime\prime}}{n_A^{\circ\prime}} - \frac{(f'' - f^\circ)f'}{(f' - f^\circ)} \right] \Bigg/ \left[\frac{(f'' - f^\circ)f'}{(f' - f^\circ)f''} - \frac{n_A^{\circ\prime\prime}}{n_A^{\circ\prime}} \right] \qquad (11)$$

The superscripts of one prime and two primes designate the appropriate frequency and concentration terms for the different points. The points chosen for the determination of H are represented by the crosses on the response curves of $CFCl_3$ and CCl_4 in part A of Figure 3. The portion of the response curves from which the values are taken to determine H is somewhat arbitrary. The best values of H, i.e., those which give the most linear response curves in part B, were obtained by chosing points from within the steeply rising section of the molar response curves. By use of the marks designated on the response curves of $CFCl_3$ and CCl_4 in part A of Figure 3, values of H = 4600 and 7200 s^{-1} for these two compounds, respectively, are obtained. For weakly responding compounds such as $CHCl_3$ for which linear response curves are obtained when the response is taken $(f - f^\circ)$ the value of H is assigned to be zero. The response curves in part B of Figure 3 were then determined by using these values of H in conjunction with the normal responses for the three compounds.

RESULTS AND DISCUSSION

The analyses of samples containing CCl_4, $CFCl_3$, and $CHCl_3$ over a wide range of concentrations are shown in Figure 3. This figure is constructed in the same format as Figure 1. On the left side, part A, the molar responses for the three compounds are plotted as $(f - f^\circ)$/flux, and on the right side, part B, the response is taken as $((f - f^\circ)(H + f)/f)$/flux. The abscissa, relative flux, is a measure of analyte input rate to the detector and has been defined (see Experimental Section) so that the relative molar responses for the different compounds can be directly compared. In Figure 3 CCl_4 is seen to be the most strongly responding compound followed by $CFCl_3$ and $CHCl_3$, respectively. Comparison of the theoretical curves shown in Figures 1 with those in Figure 3 indicates considerable similarity. The response curves for $CFCl_3$ and CCl_4 in part A of Figure 3 are seen to be nonlinear with concentration of analyte entering the cell and are similar in shape to the synthesized response curves in part A of Figure 1 for $k = 10^{-7}$ and 5×10^{-8}. With the extended definition of

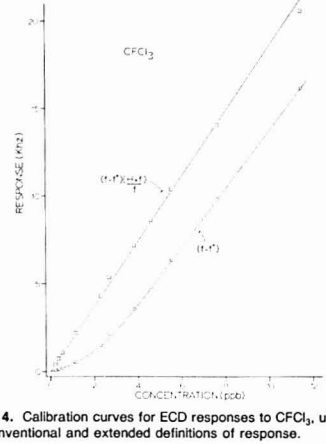


Figure 4. Calibration curves for ECD responses to $CFCl_3$, using both the conventional and extended definitions of response.

total EC response given by eq 10, the relative molar responses shown in part B of Figure 3 are obtained for the three test compounds. The improvement in linearity of the response to CCl_4 in part B relative to that in part A is quite dramatic. When the CCl_4 response is taken as $(f - f^\circ)$ the relative molar response changes by about a factor of 6 over the dynamic range whereas, with the extended definition of response, only a 10% variation in molar response is observed over the same concentration range. The overall molar response for $CFCl_3$ appears to be about half of that of CCl_4. This rate of attachment to $CFCl_3$ is, however, still large large enough so that its $(f - f^\circ)$ response in part A varies by a factor of 4 over the sample concentrations examined. Again, the molar response for $CFCl_3$ in part B is seen to remain relatively constant with concentration. The response curves for $CHCl_3$ are seen to be linearly related to concentration in both parts A snd B of Figure 3. This result occurs because the rate of electron capture for $CHCl_3$ is only moderately fast such that H/f is small for all concentrations. In this case the response defined in part B becomes equivalent to the usual response in part A.

The superior characteristics of the newly defined response function are further illustrated in Figure 4 where the same data for $CFCl_3$ have been plotted as response vs. sample concentration. This figure shows two calibration curves in which the response is taken as either $(f - f^\circ)$ or $(f - f^\circ)(H + f)/f$. The calibration curve obtained by using the conventional response shows considerable curvature and requires the use of at least several data points to be adequately defined. However, the calibration curve using the proposed response function is a straight line passing through the origin. With this extended response function it is possible to define a useful calibration curve with as little as a single data point, provided the value of H is known for the compound of interest.

In use of the proposed response function for quantitative analysis, it is necessary to know the value of H associated with each compound of interest. Determination of H can be accomplished from as little as two measurements, of high and low concentration samples. However, if greater precision is required a larger number of standards can be analyzed. Once values of H have been determined for a given detector temperature, these values should be valid in subsequent analyses even if different chromatographic conditions exist. This follows because H is only dependent on the reference current, I, the flow rate, F, and the second-order electron capture rate constant, k_A, all of which are either constant or easily measured and incorporated into the value of H.

The use of the proposed response function will be further facilitated by an associated data system. The analytical signal can then be determined in real time, in terms of the new function $(f - f^\circ)(H + f)/f$ as well as the conventional $(f - f^\circ)$ method. This would allow chromatograms to be processed in either or both modes. The new response function will allow peak areas as well as peak heights to be used as a measure of concentration of strongly responding compounds (peak areas obtained from any responses which are nonlinear are complicated and probably meaningless because the molar response is not constant over the concentration variation occurring during a single chromatographic peak).

While the above describes and accounts for a major cause of the nonlinearity in the EC response of strongly responding compounds, additional complicating influences on the total quantitative response of the ^{63}Ni ECD have not yet been fully characterized. For certain compounds, the mechanism of electron capture will be more complex than the relatively well-behaved cases of $CFCl_3$ and CCl_4 studied here. In our laboratory, alone, we have observed several such cases in which the EC responses to alkyl chlorides (*11*), anthracene (*12*), and methyl iodide (*6*) cannot be explained by a single reaction between an electron and the analyte molecule but require the addition of other chemical steps to the total response mechanism. Also, in the cases of large highly halogenated molecules, for which the ECD is often used, further electron capture by products generated from the original EC reaction seems probable. In addition to such chemical effects another complexity is presented by the possible failure of our earlier assumption made in eq 2 that positive ion density is constant throughout the ECD under all conditions of sample concentration and pulsing frequency. This question has been previously addressed by Wentworth and Chen (*13*), but for the quite dissimilar tritium source of plane parallel design. In several studies in our own laboratory (*9*, *14*, *15*) positive ion concentration within ^{63}Ni sources of cylindrical geometry have been directly measured with the assistance of atmospheric pressure ionization mass spectrometry. In these studies it was found that positive ions are formed relatively evenly throughout a typical cylindrical ^{63}Ni ECD (*15*) and that the positive ion concentration at a given location is relatively independent of pulsing frequency (*9*). Perhaps the most significant variation in positive ion density was observed when the ionization cell was saturated with an electron capturing compound. The positive ion density was then found to increase 50% relative to the sample free condition (*16*). This observation can be explained if the rate constant for the recombination of positive ions with negative ions is somewhat smaller than the corresponding rate constant for positive ion–electron recombination. The effects of these additional contributions to the quantitative response of the ^{63}Ni ECD are presently being individually investigated in our laboratory. Preliminary indications are that, although measurable, these latter considerations are not nearly as significant to the response of strongly responding molecules as the effect characterized in this paper.

LITERATURE CITED

(1) Corkill, J. A.; Kuttab, S. H.; Giese, R. W. *Anal. Chem.* **1982**, *54*, 481.
(2) Wentworth, W. E.; Chen, E. J. J. *Gas Chromatogr.* **1967**, *5*, 170.
(3) Maggs, R. J.; Joynes, P. L.; Davies, A. J.; Lovelock, J. E. *Anal. Chem.* **1971**, *43*, 1966.
(4) Sullivan, J. J.; Burgett, C. A. *Chromatographia* **1975**, *8*, 176.
(5) Lovelock, J. E.; Watson, A. J. J. *Chromatogr.* **1978**, *158*, 123.
(6) Grimsrud, E. P.; Knighton, W. B. *Anal. Chem.* **1982**, *54*, 565.
(7) Patterson, P. L. J. *Chromatogr.* **1977**, *134*, 25.
(8) Grimsrud, E. P.; Kim, S. H. *Anal. Chem.* **1979**, *51*, 537.
(9) Gobby, P. L.; Grimsrud, E. P.; Warden, S. W. *Anal. Chem.* **1980**, *52*, 473.

(10) Knighton, W. B.; Grimsrud, E. P. Anal. Chem. 1982, 54, 1892.
(11) Grimsrud, E. P.; Miller, D. A. J. Chromatogr. 1980, 192, 117.
(12) Grimsrud, E. P.; Miller, D. A.; Stebbins, R. G.; Kim, S. H. J. Chromatogr. 1980, 197, 51.
(13) Wentworth, W. E.; Chen, E. C. M. J. Chromatogr. 1979, 186, 99.
(14) Grimsrud, E. P.; Kim, S. H.; Gobby, P. L. Anal. Chem. 1979, 51, 223.
(15) Grimsrud, E. P.; Connolly, M. J. J. Chromatogr. 1982, 239, 397.
(16) Miller, D. A.; Grimsrud, E. P. Anal. Chem. 1979, 51, 851.

RECEIVED for review October 25, 1982. Accepted December 27, 1982. This work is supported by the National Science Foundation under Grant No. CHE-8119857.

Automated Determination of Nickel and Copper by Liquid Chromatography with Electrochemical and Spectrophotometric Detection

A. M. Bond* and G. G. Wallace

Division of Chemical and Physical Sciences, Deakin University, Waurn Ponds 3217, Victoria, Australia

A microprocessor-based instrumental method for automated monitoring of nickel and copper in a wide variety of matrices found in industrial plant situations has been developed. In situ formation of dithiocarbamate complexes, separation of complexes by high-performance reversed-phase liquid chromatography, and dual electrochemical and UV/visible spectrophotometric detection are included as integral components of the monitoring system. The unusual versatility associated with the separation and detection system provides the analyst with methodology to determine nickel and copper down to trace levels and with extremely large variation in concentration ratio. Data obtained during the trial period of operation suggest that matrix and other interferences are likely to be minimal after appropriate choice of operating parameters.

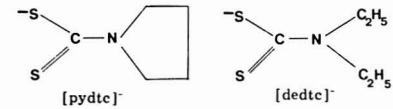
Continuous determination of concentrations of chemical species is often required in quality control or effluent monitoring programs associated with industrial plants. If it is necessary to collect a sample from the plant, transport it to the laboratory, and finally undertake the determination, the time lag induced between collection and any appropriate action being taken may lead to a costly and inefficient operation. Furthermore, staff may not be available in the analytical laboratory 24 h a day. The absence of data at these times could lead to delays in detecting a safety or environmental hazard.

Many on-line automated analytical systems have been devised. These have been based on various chemical principles as perusal of ref 1 to 8 would indicate. Recently, many refinements have been made to electrochemically based flow through systems, particularly in the area of cell design (*9–11*). These developments and the use of microprocessor-based equipment to apply potential wave forms and collect and process the relevant data (*12–15*) have substantially aided the ease of automation.

Despite these advances, the application of automated "on-line" electrochemical methods is still limited. This is because of the need, in many cases, for extensive sample pretreatment prior to a determination (*16–19*). Often removal of metals, organics, or even oxygen (*20, 21*) is necessary to avoid interference effects. Overlapping electrochemical or spectral parameters have frequently restricted the use of electrochemical or spectrophotometric detectors respectively and variable matrix effects also cause difficulties.

In this work, a system is described which is applicable to the automated "on line" determination of nickel and copper. A chemical reaction step and a separation stage are included prior to the determinations in the flow through electrochemical and/or UV–visible absorption spectrophotometric cells to provide specificity and minimize problems associated with a variable matrix (see later). A microprocessor-based system controls most of the experimental variables, generates the electrochemical wave form, and collects, stores, and analyzes the data. The system for monitoring copper and nickel has been tested on a wide range of industrial effluents and industrial plant liquors to demonstrate the reliability of the system.

The chemical step, and separation stage, included in this new automated system is based on the kinetically rapid formation of a metal–dithiocarbamate complex. Both ammonium pyrrolidine dithiocarbamate (I) $[pydtc]^-$ and sodium diethyldithiocarbamate (II) $[dedtc]^-$ are considered. The ability



I or II = $[dtc]^-$

of these ligands to stabilize high oxidation states allows monitoring of the oxidation rather than the reduction process of the metal dithiocarbamate complex formed in situ in the liquid chromatographic system (*22, 23*) and the difficulty in removing oxygen, as required with reduction processes is therefore eliminated. The amenability of metal–dithiocarbamates to chromatographic separation (*24–28*) is the basis of the separation stage. The UV–visible absorption characteristics of metal–dithiocarbamates has led most workers to develop separations using normal-phase chromatography with UV/visible spectrophotometric detection (*29–32*). In the automated system developed, both spectrophotometric and electrochemical detectors are considered with high-performance reversed-phase rather than normal-phase liquid chromatography. The new feature enabling continuous on-line monitoring is the inclusion of the ligand, $[dtc]^-$, in the solvent (*22*) and complex formation occurs in situ rather than externally to the system. All stages of the experiment are

0003-2700/83/0355-0718$01.50/0 © 1983 American Chemical Society

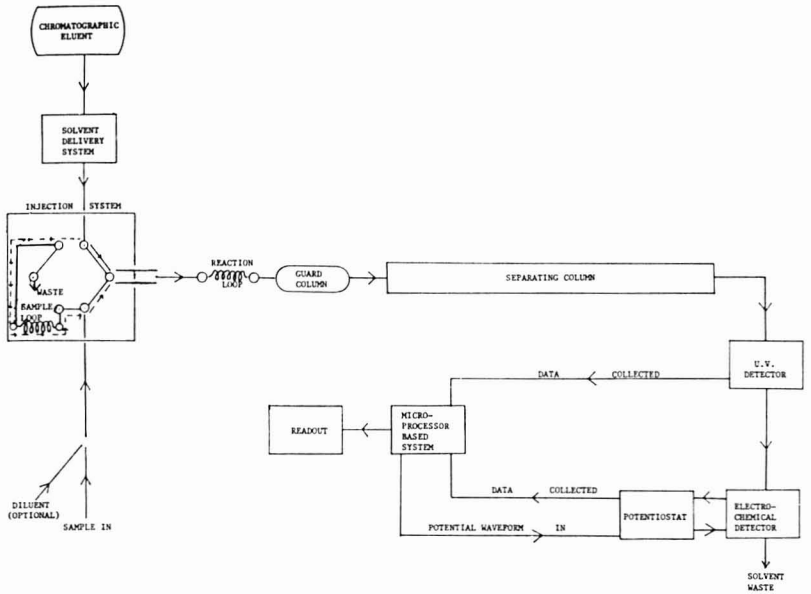


Figure 1. Schematic diagram of the automated system: separation stage, injection stage. Sample loop size is variable.

compatible with control and data acquisition by microprocessor-based technology.

EXPERIMENTAL SECTION

Reagents and Standard Solutions. All chemicals used were of A.R. grade purity, unless otherwise stated. Sodium diethyldithiocarbamate and ammonium pyrrolidine dithiocarbamate were purified by recrystallization from ethanol. Distilled, deionized water was used in preparation of acetate buffer, all standards, and stock solutions.

Acetate buffer was prepared as described by Vogel (*33*).

Acetonitrile was LC grade obtained from Waters Associates, Methanol was AR grade obtained from Ajax Chemicals.

Calibration was undertaken in all work with standard aqueous copper and nickel solutions prepared from high purity metals or $Cu(NO_3)_2{\cdot}3H_2O$ or $NiCl_2{\cdot}6H_2O$.

Instrumentation. Figure 1 shows a schematic diagram of the automated "on-line" system. In previous work (*22*, *23*) a Model 6000A solvent delivery pump was employed in conjunction with a Model U6K universal injector both obtained from Waters Associates (Milford, MA). In the automated system the manual injector is replaced by its automatic counterpart, e.g., Model 7126 Automatic Sample Injector from Rheodyne Inc. (Cotati, CA).

The "reaction coil" is 20 cm of coiled stainless steel capillary tubing. The guard column which protects the more expensive column (length = 1.5 cm, inside diameter = 3.9 mm) is packed with silica-based C-18 material. The C-18 reversed-phase separating column (length = 30 cm, inside diameter = 3.9 mm) was obtained from Waters. Two electrochemical detector cells were used in the development work: (i) Model TL-5 detector cell obtained from Bioanalytical Systems, West Lafayette, IN; (ii) Model EA 1096 wall jet detector cell obtained from Metrohm (Herisau, Switzerland).

Working electrodes made from glassy carbon were supplied by the detector cell manufacturers. The auxiliary electrode was made from glassy carbon and the reference electrode was Ag/AgCl (3 M NaCl). Electrodes were cleaned as recommended by the manufacturers once per week provided potentials less positive than 0.9 V vs. Ag/AgCl were being used. The need for maintenance became more frequent if more positive potentials were used.

A Model 450 variable wavelength UV/visible detector from Waters Associates was used as the spectrophotometric detector. The microprocessor-based equipment is based on that described in detail elsewhere (*12*, *13*). The microprocessor generates all wave forms for applying the potential, collects, stores and calculates data from the results, and can be used to control all other steps of the experiment if required. The potentiostat was built in these laboratories but other commercially available potentiostats are adequate (*13*).

Atomic absorption measurements were performed in an off-line mode on a Varian Techtron (Springvale, Australia) Model AA6 atomic absorption spectrometer. An air–acetylene flame was used and copper or nickel hollow cathode lamps (λ = 324.7 nm for Cu, λ = 341.5 nm for Ni) were used as the light source. The atomic absorption results were used for verifying the results obtained via the new method.

RESULTS AND DISCUSSION

Chromatographic Eluent. The solvent composition 70%:30% acetonitrile: acetate buffer (0.02 M, pH 6) gives adequate separation of $Cu(dtc)_2$ and $Ni(dtc)_2$. The 0.005–0.01 M $NaNO_3$ is added to the solvent to provide adequate conductivity for electrochemical detection. In most work the solvent contained between 10^{-3} and 10^{-4} M $[dtc]^-$. Addition of ligand to the solvent did not affect the retention volumes of these compounds.

The selectivity (resolution), with respect to nickel and copper, could be increased by replacing acetonitrile with methanol in the running solvent. Methanol has the added advantage of being a less expensive solvent; however the overall efficiency (plate count) of the chromatographic system is decreased by using this solvent.

Complex Formation. Both copper and nickel react very rapidly with either $[dedtc]^-$ or $[pydtc]^-$ to form the corresponding metal–dithiocarbamate. Work in a conventional electrochemical cell (*13*, *21*, *22*) indicated that a 10-fold excess

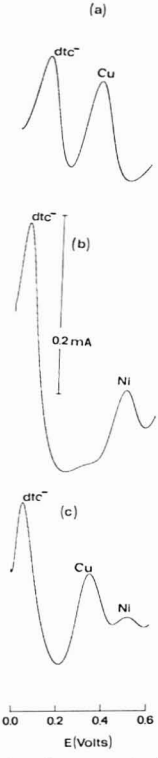


Figure 2. Differential pulse voltammogram showing oxidation of $M(dtc)_2$ at a glassy carbon electrode: delay between pulses = 0.5 s, pulse amplitude = 100 mV, scan rate = 5 mV/s; (a) 5 ppm copper added to 5×10^{-4} M $[dedtc]^-$ in 70%:30% acetonitrile:acetate buffer (0.02 M) pH 6, (0.1 M $NaNO_3$), (b) 5 ppm nickel added to $[dedtc]^-$ solution, (c) 5 ppm nickel + 5 ppm copper added to $[dedtc]^-$ solution.

of ligand was required for fast complete complex formation. Results showed these complexes to be stable in acetonitrile or methanol for at least 12 h. It was also shown that quantitative complex formation was possible within the automated system when the required ligand is included in the chromatographic eluent. A short length of coiled tubing (10–30 cm), inserted between injector and guard column, allows sufficient time for complete reaction (Figure 1).

In general the linear range of calibration curves and retention volumes of the $M(dtc)_2$ (M = Cu, Ni) complexes are decreased by using $[pydtc]^-$ as opposed to $[dedtc]^-$ in the solvent.

Electrochemical Detection. Figure 2, shows voltammograms of $Cu(dtc)_2$ and $Ni(dtc)_2$ in a conventional cell in the presence of excess ligand. While it would be possible to simultaneously determine copper and nickel in a conventional cell, only limited concentration ratios would be available. At around 0.1 V vs. Ag/AgCl oxidation of the free ligand occurs to produce thiuram disulfide (*34*), dtc-dtc.

$$2dtc^- \rightarrow 2dtc\cdot + e^- \quad (1)$$

$$2dtc\cdot \rightarrow dtc\text{-}dtc \quad (2)$$

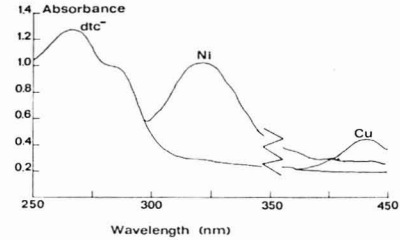


Figure 3. UV/visible absorbance spectra of free ligand (5×10^{-4} M $[dedtc]^-$), 10^{-4} M $Cu(dedtc)_2$ and 10^{-4} M $Ni(dedtc)_2$ in 70%:30% acetonitrile:acetate buffer.

At more positive potentials, the following overall reactions have been shown to occur on oxidation of $M(dtc)_2$ (*35*, *36*).

$$Cu(dtc)_2 \rightleftharpoons [Cu(dtc)_2]^+ + e^- \quad (3)$$

$$3Ni(dtc)_2 \rightarrow 2[Ni(dtc)_3]^+ + Ni^{2+} + 4e^- \quad (4)$$

Mercury, gold, platinum, and glassy carbon working electrodes were considered with glassy carbon proving optimum for multielement analysis (*23*). A glassy carbon electrode was used to obtain all electrochemical data reported in this work.

Recording of voltammograms in the flow through electrochemical cell, after chromatographic separation, gave the expected results. That is, a $M(dtc)_2$ oxidation response appeared at the retention volume of the complex. However, additionally, a shift in peak potential position (Ni and Cu) and increase in magnitude of current (Ni only) of the free ligand wave at the retention volume of the $M(dtc)_2$ complex was observed. This leads to a method of determining the metals indirectly by monitoring the free ligand oxidation response.

In view of the above, application of a DC wave form at various potentials, or different types of pulse wave form, will produce varying sensitivities and selectivity for each element. This is a valuable aid when applying this system to an applied industrial problem and readily implemented because the microprocessor can be used to generate any required wave form.

The electrochemical wave forms considered in this paper are (i) DC [+0.20 V vs. Ag/AgCl], (ii) normal pulse [−0.10 to +0.25 V vs. Ag/AgCl], (iii) DC [+0.70 V vs. Ag/AgCl], and (iv) differential pulse [+0.40 to +0.48 V vs. Ag/AgCl]. Wave form (i) has a relatively low background current since the oxidation of free ligand occurs to only a limited extent. This method is more sensitive for nickel than copper. Wave form (ii) has an even lower background current since at the rest potential *no* oxidation of free ligand occurs. Wave form (iii) is equally sensitive to both nickel and copper but a higher background current from ligand oxidation decreases the signal to noise ratio. Wave form (iv) is chosen to specifically determine copper. Even in the presence of extremely large excesses of nickel, only a response for copper is observed.

UV–Visible Spectrophotometric Detection. Figure 3 shows UV-visible spectra for $[dedtc]^-$; also $Ni(dedtc)_2$ and $Cu(dedtc)_2$ are shown in the presence of excess $[dedtc]^-$. Absorption due to the free ligand is well removed from the absorption associated with $Cu(dedtc)_2$ (λ_{max} = 423 nm) and $Ni(dedtc)_2$ (λ_{max} = 320 nm). Hence selective determination of each metal is possible. Alternatively, simultaneous determination of both metals is possible by suitable choice of wavelength. The two detection systems are readily used in series and both can be "tuned" to handle the required problem.

Table I. Comparison of Electrochemical and Spectrophotometric Detectors[a]

	spectrophotometric			electrochemical[b]		
	λ = 423 nm	λ = 400 nm	λ = 320 nm	normal pulse (−0.10 to +0.25 V)	DC (+0.20 V)	DC (+0.70 V)
Nickel						
detection limit (ng)	2.0	0.5	0.2	0.1	0.2	0.1
linear response range (ng)	0-150	0-150	0-150	0-50	0-50	0-100
Copper						
detection limit (ng)	0.4	0.8	1.0	1.0	1.0	0.2
linear response range (ng)	0-150	0-150	0-150	0-50	0-50	0-100

[a] Injection volume = 10 μL. Solvent flow rate = 1 mL/min. Solvent system: 70%:30% acetonitrile:acetate buffer (0.02 M), pH 6, 0.01 M $NaNO_3$, 2×10^{-4} M $[dedtc]^-$. [b] Potentials, V, vs. Ag/AgCl (3 M NaCl). Detection limits and dynamic ranges for TL-5 thin layer cell. Linear response range increased in Metrohm wall jet detector (lower RC), although detection limits not as low.

Table II. Determination of Nickel and Copper by Liquid Chromatographic Technique and Atomic Absorption Spectrometry

	atomic absorption spectrometry[a]		liquid chromatography electrochemical detection[b]		liquid chromatography spectrophotometric detection (λ = 400 nm)	
sample	amt of Ni, ppm	amt of Cu, ppm	amt of Ni, ppm	amt of Cu, ppm	amt of Ni, ppm	amt of Cu, ppm
drinking water	0.05 ± 0.01	0.85 ± 0.05	0.05 ± 0.01	0.80 ± 0.03	0.05 ± 0.01	0.82 ± 0.03
Urn water	0.05 ± 0.01	0.05 ± 0.01	0.05 ± 0.01	0.06 ± 0.01	0.05 ± 0.01	[c]
industrial effluent	0.50 ± 0.02	0.25 ± 0.02	0.50 ± 0.03	0.23 ± 0.02	0.50 ± 0.02[d]	0.22 ± 0.02[d]
copper refinery[e] 1	[f],[c]	4100 ± 100	[f],[c]	4200 ± 100	[f],[c]	4200 ± 100
copper refinery[e] 2	[f],[c]	1200 ± 50	[f],[c]	1250 ± 50	[f],[c]	1200 ± 50
copper refinery[e] 3	[f],[c]	2100 ± 50	[f],[c]	2200 ± 50	[f],[c]	2100 ± 50

[a] Air–acetylene flame, λ = 341.5 nm for Ni, λ = 327.4 nm for Cu. [b] DC potential monitored at +0.70 V. Identical results (within experimental error) were obtained for DC = +0.20 V or normal pulse (−0.10 to +0.25 V) (monitoring of ligand wave), for all samples. Differential pulse mode for determining copper in copper refinery samples also provided results quoted. [c] Not determined. [d] λ = 423 nm for Cu determination. λ = 320 nm for Ni determination. [e] Sample diluted 100-fold prior to determination. [f] Problem involved determination of copper in presence of very large excess of nickel (e.g., nickel 20 g L^{-1}). Nickel concentration not determined. On-line method based on liquid chromatography used same conditions and solvent system as for Table I except for copper refinery samples where 55%:45% acetonitrile:acetate buffer or 70%:30% methanol:acetate buffer was used instead of 70%:30% acetonitrile:acetate buffer.

Comparison of Spectrophotometric and Electrochemical Detection. Figure 4 shows the excellent separation of copper and nickel with this system with electrochemical detection. It is also clear that simultaneous determination of both elements can be achieved with spectrophotometric detection.

With both detectors connected in series (Figure 1) calibration curves were obtained in order to determine detection limits and linear dynamic range. Table I summarizes the results. The electrochemical detector was generally more sensitive and by application of the correct wave form more selective. However, less maintenance was associated with the spectrophotometric detector and day to day reproducibility was higher with this form of detection.

The linear calibration range attainable with a spectrophotometric detector is greater than that obtained when the thin layer (TL-5) electrochemical detector is employed. However, use of another cell with lower resistance (e.g., Metrohm wall jet) expands the range attainable with an electrochemical detector.

Determination of Copper and Nickel in Industrial Plant Solutions. Table II shows results obtained when a variety of samples obtained from industrial plant solutions were determined for nickel and copper by using the automated system. Results obtained with the newly developed system also are compared with data from off-line experiments using atomic absorption spectrometry and excellent agreement is observed. A pilot plant situation similar to that described in ref 3 was used for the "on-line" monitoring. Results for copper and nickel could be obtained at 6-min intervals in a typical experiment.

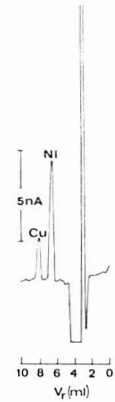


Figure 4. Chromatogram showing separation of nickel and copper as dithiocarbamates: chromatographic eluent, 70%:30% acetonitrile:acetate buffer (0.02 M) pH 6, 0.005 M $NaNO_3$, 10^{-4} M $[dedtc]^-$; flow rate, 1 mL/min; detection, the DC response was monitored at +0.75 V vs. Ag/AgCl; injection, 10 μL of sample containing 2 ppm of nickel and 2 ppm of copper.

Figure 5 shows the readout obtained with the new system

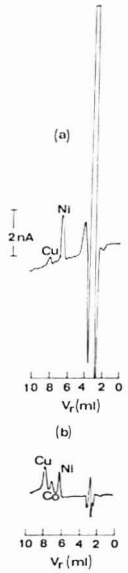


Figure 5. Determination of copper and nickel in an industrial effluent sample (see Table II): injection volume = 10 μL; readout obtained for (a) electrochemical detection (conditions as in Figure 4), (b) UV detection, λ = 400 nm (solvent and other chromatographic conditions as in Figure 4).

for injection of industrial effluent. In addition to the detection of copper and nickel, the presence of a response for $Co(dtc)_3$ is noted with the spectrophotometric detector. Atomic absorption spectrometry measurements confirmed the presence of cobalt. Previous work (*23*) has shown that $Co(dtc)_3$ does form in situ but a fairly positive potential (+1.00 V vs. Ag/AgCl) must be applied to detect it electrochemically and is therefore not observed with electrochemical detection under the conditions of Figure 5.

Figure 6 shows typical results from samples obtained from the purification plant of a copper refinery (*3*). A large excess of nickel is present at this stage of the plant purification procedures (e.g., 20 g L^{-1}). Use of the solvent 70%:30% acetonitrile: acetate buffer makes accurate determination of copper difficult with the very high nickel concentrations using spectrophotometric and some forms of electrochemical detection [Figure 6a,b (i)(ii)]. Use of a different solvent (e.g., 55%:45% acetonitrile:buffer or 70%:30% MEOH:buffer) provides adequate separation (Figure 6c). However an alternative approach to this problem is the use of a differential pulse wave form. Figure 6b(iii) shows the differential pulse output for a sample with very high nickel concentration which produces a clearly defined copper response void of any interference from the nickel. This example confirms that if complete resolution is not obtained with the chromatographic stage, then added selectivity can be obtained by "tuning" the detector(s) and or solvent composition.

In the past 18 months the automated system described above has been applied to a substantial number of industrial situations. In all cases, the extreme versatility available with a separation scheme and two forms of detection, each with their own set of variables, has enabled a system of continuous monitoring to be developed.

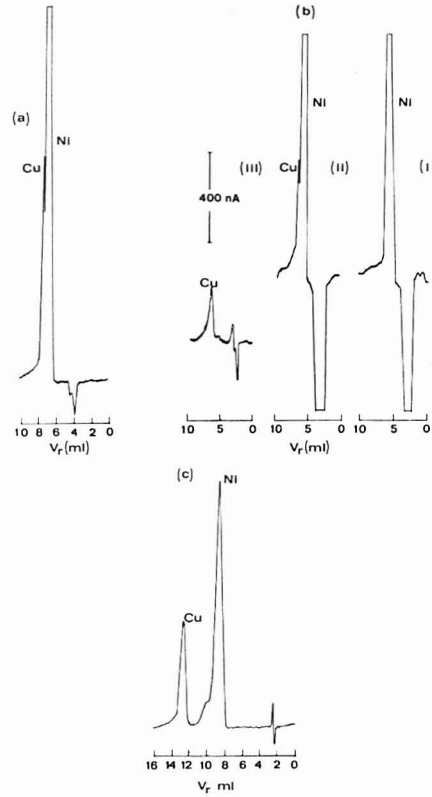


Figure 6. Determination of copper in sample number 2 from a copper refinery (see Table II): (a) UV detection (λ = 420 nm, solvent and other chromatographic conditions as in Figure 4, injection volume = 10 μL); (b) electrochemical detection applying a pulse wave form (initial potential = 400 mV, final potential = 480 mV, delay between pulses = 1 s, pulse duration = 0.40 s; (i) DC component, (ii) pulse component, (iii) differential pulse component; injection volume = 10 μL); (c) UV detection (λ = 420 nm, same conditions as in Figure 4 except that acetonitrile has been replaced by methanol and the injection volume = 3 μL).

ACKNOWLEDGMENT

Extensive and valuable discussions with L. McLachlan and T. Crosher, Ordnance Section, Maribyrnong, Victoria, Australia, and H. R. A. Exelby, Copper Refineries, Townsville, Queensland, Australia, were held throughout the duration of this project.

Registry No. Ni, 7440-02-0; Cu, 7440-50-8; $Co(dtc)_3$, 13963-60-5; Co, 7440-48-4; $Cu(dedtc)_2$, 13681-87-3; $Ni(dedtc)_2$, 14267-17-5; $[pydtc]^-NH_4^+$, 5108-96-3; $[dedtc]^-Na^+$, 148-18-5; water, 7732-18-5.

LITERATURE CITED

(1) Mottola, H. A. *Anal. Chem.* **1981**, *53*, 1312A–1316A.
(2) Snyder, L. R. *Anal. Chim. Acta* **1980**, *114*, 3–18.
(3) Bond, A. M.; Hudson, H. A.; van den Bosch, P. A.; Walter, F. L. Exelby, H. R. A. *Anal. Chim. Acta* **1982**, *136*, 51–59.
(4) Landis, J. B. *Anal. Chim. Acta* **1980**, *114*, 155–163.

(5) Ruckl, R. J. *Talanta* **1980**, *27*, 147-156.
(6) Tóth, K.; Géza, N.; Tehér, Z.; Horval, G.; Pungor, E. *Anal. Chim. Acta* **1980**, *114*, 45-58.
(7) Ivaska, A.; Franklin Smyth, W. *Anal. Chim. Acta* **1980**, *114*, 283-291.
(8) Booth, M. D.; Fleet, B.; Win, S.; West, T. S. *Anal. Chim. Acta* **1969**, *48*, 329-337.
(9) Bond, A. M.; Hudson, H. A.; van den Bosch, P. A. *Anal. Chim. Acta* **1981**, *127*, 121-133.
(10) Mason, W. D. *J. Pharm. Sci.* **1973**, *62* (6), 999-1001.
(11) Lown, J. A.; Koile, R.; Johnson, D. C. *Anal. Chim. Acta* **1980**, *116*, 33-39.
(12) Anderson, J. E.; Bagchi, R. N.; Bond, A. M.; Greenhill, H. B.; Henderson, T. L. E.; Walter, F. L. *Am. Lab. (Fairfield, Conn.)* 1981, *13* (2), 21-32.
(13) Anderson, J. E.; Bond, A. M.; Heritage, I. D.; Jones, R. D.; Wallace, G. G. *Anal. Chem.* **1982**, *54*, 1702-1705.
(14) Kryger, L. *Anal. Chim. Acta* **1981**, *133*, 591-602.
(15) Anderson, J. E.; Bond, A. M. *Anal. Chem.* **1981**, *53*, 1394-1398.
(16) Bond, A. M. In "Modern Polarographic Methods in Analytical Chemistry"; Marcel Dekker: New York, 1980.
(17) Flato, J. B. *Anal. Chem.* **1972**, *44* (11), 75A-87A.
(18) Brezonik, P. L.; Brauner, P. A.; Stumm, W. *Water Res.* **1976**, *10*, 605-612.
(19) Bond, A. M.; Heritage, I. D.; Briggs, M. H. *Anal. Chim. Acta* **1981**, *127*, 135-145.
(20) Trojanek, A.; Holub, K. *Anal. Chim. Acta* **1980**, *121*, 23-28.
(21) Hanekamp, H. B.; Voogt, W. H.; Bos, P.; Frei, R. W. *Anal. Chim. Acta* **1980**, *118*, 81-86.
(22) Bond, A. M.; Wallace, G. G. *Anal. Chem.* **1981**, *53*, 1209-1213.
(23) Bond, A. M.; Wallace, G. G. *Anal. Chem.* **1982**, *54*, 1706-1712.
(24) Lehotay, J.; Kisken, O.; Brandstetorá, E.; Guiochen, G. *J. Chromatogr.* **1979**, *172*, 379-383.
(25) Ballschmiter, K. *Z. Anal. Chem.* **1971**, *254*, 348-353.
(26) Schwedt, G. *Chromatographia* **1978**, *11* (3), 145-148.
(27) Schwedt, G. *Z. Anal. Chem.* **1979**, *295*, 382-387.
(28) Schwedt, G. *Chromatographia* **1979**, *12* (5), 289-293.
(29) Liska, O.; Lehotay, J.; Brandstetorá, E.; Guiochon, G.; Colin, H. *J. Chromatogr.* **1979**, *172*, 384-387.
(30) Merlyasu, M.; Hashimah, Y. *Anal. Lett.* **1978**, *A11* (7), 593-602.
(31) O'Laughlin, J. W.; O'Brien, T. P. *Anal. Lett.* **1978**, *A11* (10), 829-844.
(32) Gaetani, E.; Laureri, C. F.; Mangia, A. *Ann. Chim. (Rome)* **1979**, *69*, 181-187.
(33) Vogel, A. "A Textbook of Quantitative Inorganic Analysis"; Longman: London, 1968; p 689.
(34) Cauquis, G.; Lachenal, D. *J. Electroanal. Chem. Interface. Chem.* **1973**, *43*, 205-213.
(35) Hendrickson, A. R.; Martin, R. L.; Rohde, N. M. *Inorg. Chem.* **1976**, *15*, 2115-2119.
(36) Hendrickson, A. R.; Martin, R. L.; Rohde, N. M. *Inorg. Chem.* **1975**, *14*, 2980-2985.

RECEIVED for review October 5, 1982. Accepted December 6, 1982. This project was supported by Research Grants provided by Ordnance, Factory, Maribyrnong, Victoria, Australia, and Copper Refineries, Townsville, Queensland, Australia. A provisional patent on this automated system has been granted.

Speciation of Intermediate Polar Material in Coal Derived Process Solvents by Liquid Chromatography/Fourier Transform Infrared Spectrometry

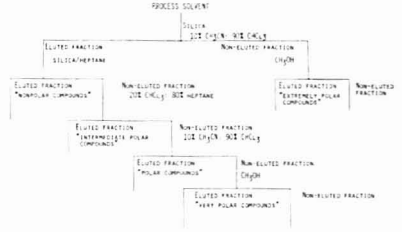
Robert S. Brown and Larry T. Taylor*

Department of Chemistry, Virginia Polytechnic Institute and State University, Blacksburg, Virginia 24061

Intermediate polar coal-derived material eluted initially from a silica column with heptane/20% $CHCl_3$ has been identified via high-performance liquid chromatography coupled with Fourier transform infrared spectrometry. Chemically bonded silica (mixed amino and cyano) has been employed with isocratic chloroform elution and UV detection. For FTIR on-line detection, $CDCl_3$ was employed in order to expand the available infrared spectral window region. The intermediate polar fractions contain predominantly aromatic cyclic secondary amines and highly hindered phenols. Nonhydrotreated coal derived material, based on this analysis, contains more etheric species than the hydrotreated material. Modeling with a variety of amines and phenols has been performed.

Process solvents play a key role in the conversion chemistry leading from coal to coal liquid products. The effects of various heteroatom-containing components in the process solvent on liquefaction behavior is only just beginning to be understood and explored. Certain model nitrogen-containing compounds have recently been shown to greatly enhance conversion to pyridine and toluene soluble products (*1*, *2*). The overall detailed composition of process solvents, however, is poorly known and this has hampered an understanding of the complex chemistries which occur during coal liquefaction. Clearly, more specific analytical techniques for process solvent characterization are needed. This report addresses in part this problem.

Scheme I. Preparative Scale Separation of Process Solvents



Liquid chromatography (LC) is an obvious means to separate the nonvolatile components in process solvents. Early attempts at characterizing the whole solvent by normal-phase LC were frustrated by the wide polarity range of components and the low concentration level of the more polar, yet more interesting components. Gradient elution reversed-phase (RP) chromatography (*3*, *4*), which can handle wide polarity ranges, has been investigated as a partial solution to this problem. However, RP chromatography does not separate by chemical class, and conventional LC detectors (UV, RI) give little more than retention time data which are of limited use in highly complex mixture analysis. Furthermore, solubility of process solvents is a problem with the H_2O-based solvent systems normally employed in RP chromatography. Employment of

0003-2700/83/0355-0723$01.50/0 © 1983 American Chemical Society

information-specific detectors (infrared and ^1H nuclear magnetic resonance) is hampered by the fact that the solvents used in RP chromatography are for the most part incompatible with these spectroscopic modes.

One solution in our laboratory to both of the above process solvent analytical problems (wide polarity range, low heteroatom content) has been a preliminary preparative LC separation on silica into several fractions prior to analytical scale LC. This separation, which has been described previously (*5, 6*) (see Scheme I), allows concentration of the more polar components (~20% of the total) into several fractions. The polarity range of the components contained in each fraction is also limited which simplifies subsequent analysis under isocratic normal-phase LC conditions.

Given the simpler, more concentrated fractions, we have found that the samples, nevertheless, remain complex. Conventional modes of detection (UV, RI) remain relatively uninformative as to species. Since we are interested in identifying the heteroatom-containing species in process solvents, Fourier transform infrared spectrometry (FTIR) appears to have great potential as a detection mode in this regard. Many heteroatom-containing compounds exhibit characteristic absorbances in the infrared region (*7*), thereby making FTIR an extremely specific functionality detector. The rapid scan rate of FTIR also makes it attractive as an LC detector and enables "on-the-fly" spectra to be obtained for compound identification.

This report deals with the analysis of the "intermediate polar" fraction (heptane/20% $CHCl_3$ eluted) arising from the previously mentioned preparative separation of both a hydrogenated and nonhydrogenated process solvent by LC/FTIR employing a chemically bonded phase silica column and $CDCl_3$ elution.

EXPERIMENTAL SECTION

A Varian Model 5060 ternary solvent liquid chromatograph (Walnut Creek, CA) was employed equipped with a Rheodyne Model 7125 injector (50-μL loop) and standard fixed wavelength (254 nm) UV detector. Solvents were Burdick and Jackson Laboratories Inc. (Muskegon, MI) preservative-free chloroform and Aldrich (Milwaukee, WI) 99.6+ atom % deuterated chloroform. Two Whatman Partisil-10 Polar Amino Cyano (PAC) bonded phase columns (25 cm × 4.6 cm i.d.; 10 μm particles) were employed. One was equilibrated in chloroform and was used for methods development with the UV detector, while the other was equilibrated in deuteriochloroform and used with FTIR detection.

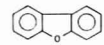
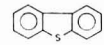
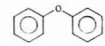
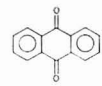
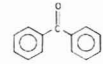
A Nicolet 6000 FTIR (Madison, WI) with a cooled MCT-B detector was employed as a LC detector. A directly coupled flow cell obtained from Nicolet Instrument Corp. was employed. This cell which had a 3-mm circular aperture and a fixed 1-mm pathlength had an effective cell volume including transfer tubing of 23 μL. FTIR file spectra were obtained by coadding eight "on-the-fly" spectra taken at 4 cm^{-1} resolution and ratioing these vs. 32 coadded background files. This amounted to storage of a file spectrum every 6.2 s during an LC run.

Two process recycle solvents (boiling range: 400–800 °F) originating at the SRC-I pilot plant (approximately 3 years ago) in Wilsonville, AL, were obtained from Mobil Research and Development Corp., Central Research Division, Princeton, NJ (*8*). One process solvent (92-26-019) had been previously hydrotreated by the Conoco Co. and contained 9.6% hydrogen. The other process solvent (92-03-035) was not hydrotreated and contained 8.15% hydrogen. Each solvent was separated into fractions of varying polarity as outlined in Scheme I. The second fraction from this preliminary separation, termed "intermediate polar", was subjected to further analysis by LC/FTIR.

RESULTS AND DISCUSSION

Background. From earlier work (*7*), it was originally thought that the "intermediate polar" (IP) fraction would be rich in such oxygen-containing functionalities as ethers and carbonyls. With this in mind, 10 model compounds containing

Table I. Elution Behavior of Intermediate Polar Models

	name	structure formula	R_T,[a] min
1.	dibenzofuran		3.45
2.	dibenzothiophene		3.50
3.	diphenyl ether		3.55
4.	anisole		4.15
5.	di-*tert*-butyl ketone		4.95
6.	anthraquinone		6.10
7.	benzophenone		6.35
8.	phenyl acetate		6.55
9.	cyclohexyl acetate		7.05
10.	hydrocoumarin		10.05

[a] Flow rate = 1 mL/min.

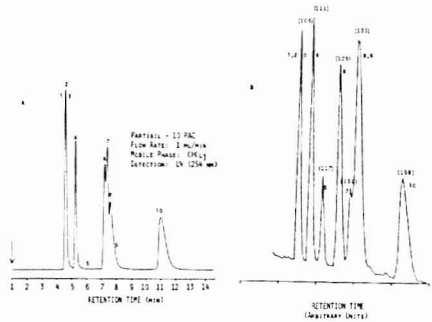


Figure 1. Chromatogram of the separation of IP models on Partisil-10 PAC: (A) UV (254 nm) detection, $CHCl_3$ elution, 1 mL/min; (B) Gram–Schmidt reconstruction, FTIR detection, $CDCl_3$ elution, 1 mL/min.

the above functionalities were chosen and a separation was developed by the use of $CHCl_3$ on a PAC column. These compounds are tabulated along with their retention times in Table I. It can be seen that a variety of ethers, ketones, esters, and lactones elute under these conditions over a fairly broad range. Figure 1 shows the separation achieved by using UV detection (254 nm). Ethers initially elute followed by ketones. Cyclic esters elute last preceded by linear esters. The totally aliphatic *tert*-butyl ketone and cyclohexyl acetate have no UV absorption. Figure 1B represents the IR reconstructed

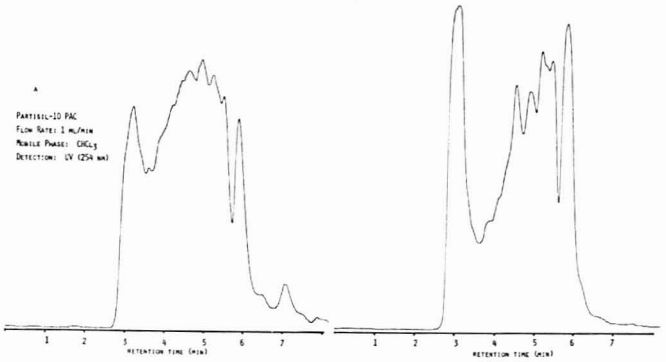


Figure 2. Chromatogram of the separation of the IP fraction of (A) HPS and (B) PS: UV (254 nm) detection; $CHCl_3$ elution, 1 mL/min.

chromatogram (based on the Gram–Schmidt algorithm) of these same models employing the IR flow cell and $CDCl_3$ elution. The slight difference here in resolution is due to the superior dryness of the $CDCl_3$ relative to $CHCl_3$ which causes the PAC column to be more activated. It is apparent that a better separation is obtained in the latter case. Identification of chromatographic peaks was made by comparing file spectra obtained during the separation with the solution spectrum of each model compound.

After this preliminary work, the two IP fractions generated from the hydrogenated (92-026-019) (HPS) and nonhydrogenated (92-03-035) (PS) process solvents were chromatographed first using $CHCl_3$ dried over molecular sieves on a PAC column with UV detection. Figure 2 shows the chromatograms obtained for PS and HPS. As can be seen, the UV-absorbing components elute almost identically over the same time range (3–8 min) as the models. This result, without a more specific detector, might lead one to believe that these fractions are truely rich in aromatic ethers and carbonyls. In addition, the compositional differences between PS and HPS are not apparent from this experiment. The UV mode of detection also provides no information regarding non-aromatic-containing moieties. Clearly a more detailed picture of each fraction is needed.

Prior to separation, both IP fractions were subjected to solution "static" IR analysis (Figure 3). Noticeable differences are observed in the two spectra. First, the ratio of the CH aliphatic (3000–2800 cm^{-1}) to CH aromatic (3100–3000 cm^{-1}) absorbance is drastically increased upon hydrogenation as would be expected. Secondly, the carbonyl stretching region around 1700 cm^{-1} shows very weak absorption indicating little of this functionality is present in these fractions. Thirdly, ether related absorbance bands appear between 1250 cm^{-1} and 1100 cm^{-1}. Since ethers have IR absorbance bands which greatly depend on substitution, the type of ether is debatable. The most distinctive bands, which are most prevalent in the IP fraction of HPS but also present in the IP fraction of PS, occur between 3600 and 3400 cm^{-1}. These absorbances are very indicative of alcohols/phenols and amines. This analysis of the IR spectra of the IP fractions of PS and HPS indicates that our initial choice of models based totally on known chromatographic elution behavior with UV detection was incorrect. Although small amounts of carbonyl compounds and ethers are present in each IP fraction, major constituents containing –OH and –NH functionalities appear.

LC/FTIR of Intermediate Polar Fraction. Preliminary Analysis. The suggested presence of –OH and –NH

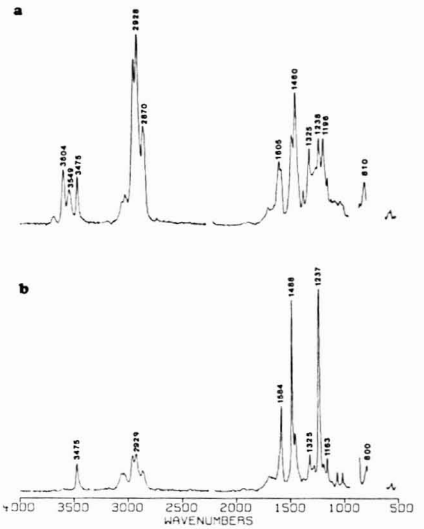
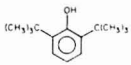
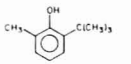
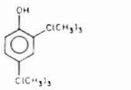
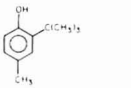
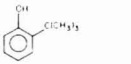
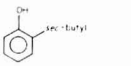
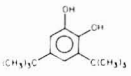
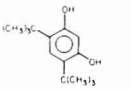


Figure 3. Infrared spectrum of the whole IP fraction of (A) HPS and (B) PS: in $CDCl_3$; 0.2-mm pathlength cell.

functionalities in both IP fractions was puzzling since we had previously found that simple alcohols–phenols–amines do not elute off of a PAC column (UV detection) with $CHCl_3$ as the mobile phase. FTIR has been employed as a mode of detection with $CDCl_3$ elution to better understand the species being separated. The employment of $CDCl_3$ in place of $CHCl_3$ enabled the C–H stretching region to be monitored. Preliminary analysis of "on-the-fly" IR spectra generated during the $CDCl_3$ separation of the IP fraction of HPS and PS indicated that indeed a wide range of –OH and –NH materials elute, but their identities were still a question. With the realization that certain –NH and –OH compounds in each IP fraction were being chromatographed, we searched further for acceptable models. The –OH/–NH compounds which were discovered to elute with 100% $CHCl_3/CDCl_3$ on a PAC column are tabulated in Tables II and III along with their re-

Table II. Elution Behavior of Selected Phenols

compound	structural formula	R_T,[a] min
2,6-di-*tert*-butylphenol		3.45
2-*tert*-butyl-6-methylphenol		4.56
2,4-di-*tert*-butylphenol		6.45
2-*tert*-butyl-4-methylphenol		7.23
2-*tert*-butylphenol		8.47
2-*sec*-butylphenol		11.83
3,5-di-*tert*-butylcatechol		not eluted
4,6-di-*tert*-butylresorcinol		not eluted

[a] Flow rate = 1 mL/min.

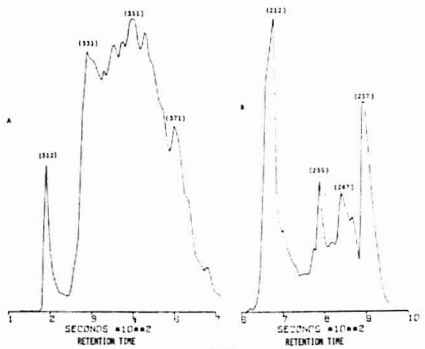
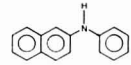
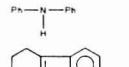
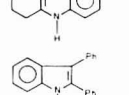
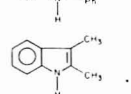
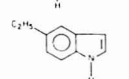
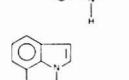
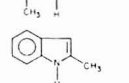
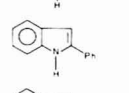
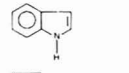
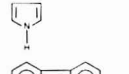
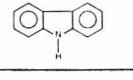
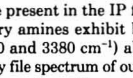


Figure 4. Chromatogram of the separation of the IP fraction of (A) HPS and (B) PS: Gram-Schmidt reconstruction; FTIR detection; $CDCl_3$ elution, 1 mL/min.

tention times. A wide range of alcohols and phenols were chromatographed but only compounds having very hindered –OH groups eluted. With the exception of diphenylamine and *N*-phenyl-2-naphthylamine, both aromatic substituted secondary amines, only "indole-like" heterocyclic secondary amines were found to elute. Interestingly, no aromatic primary amines (e.g., aniline) were found to be chromatographable

Table III. Elution Behavior of Selected Amines

compound	structure	R_T, min
N-phenyl-2-naphthylamine		3.95
diphenylamine		4.25
1,2,3,4-tetrahydrocarbazole		5.05
2,3-diphenylindole		5.20
2,3-dimethylindole		5.90
5-ethylindole		6.42
7-methylindole		6.60
2-methylindole		7.35
α-phenylindole		7.45
indole		7.80
pyrrole		7.85
carbazole		8.00

under our conditions. None are present in the IP fraction of either HPS or PS since primary amines exhibit both symmetric and asymmetric (~3450 and 3380 cm^{-1}) absorbance bands which do not appear in any file spectrum of our samples. This preliminary analysis narrows down the possible compound classes which can be present in the IP fraction and will aid greatly in the analysis of the individual file spectra.

Hydrotreated Process Solvent. Figure 4A represents the Gram–Schmidt reconstructed chromatogram of the IP fraction of HPS. Note the similarity of it with the UV trace in Figure 2A. The comparison is fairly good with the exception of the early eluting peak which is not present in the UV trace (retention time ~3 min, file spectrum no. 312). This no doubt is due to the non-UV absorbing nature of this component. File spectrum no. 312 is shown in Figure 5A. As is evidenced by the lack of aromatic C–H absorbance band at 3150–3000 cm^{-1} and phenyl ring absorbance bands ~1600 cm^{-1}, this component is not aromatic and hence non-UV absorbing. Analysis of the spectrum shows that it is a siloxane-like material with associated characteristic absorbance bands. A spectrum of poly(dimethylsiloxane) appears to match our unknown very

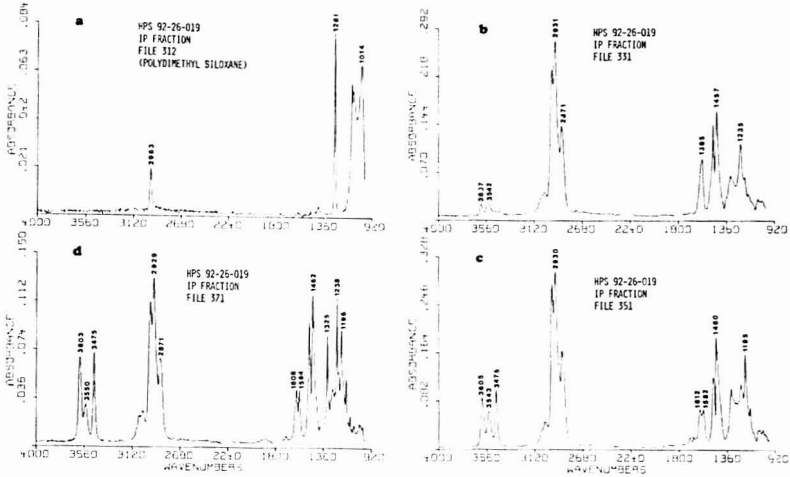


Figure 5. Infrared spectra of file 312, 331, 351, and 371. See Figure 4 for chromatography conditions.

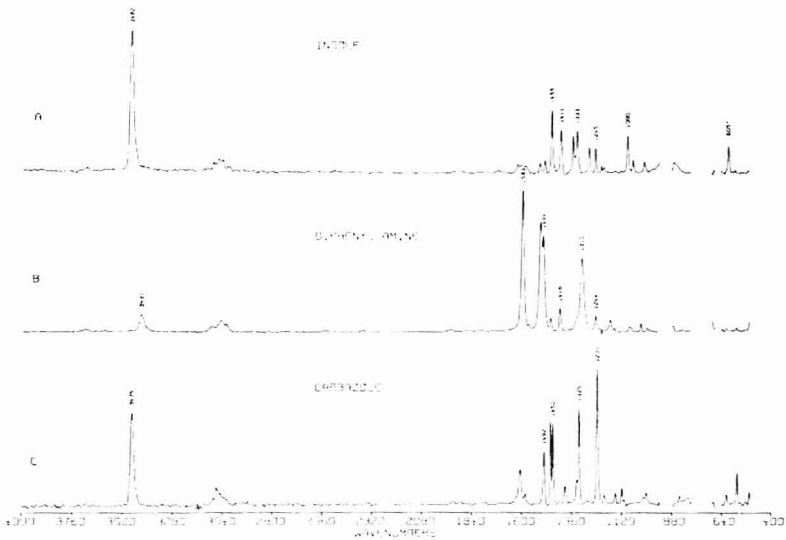


Figure 6. Infrared spectra of (A) indole, (B) diphenylamine, and (C) carbazole each dissolved in $CDCl_3$, 0.2-mm pathlength cell.

well. This material is believed to be a contaminant from the silicone rubber septums employed in the storage of the sample. Different septums are currently used which do not seem to produce this problem.

What appears to be small amounts of mixed aromatic and aliphatic ethers elute between files 312 and 331. These are in low concentration and are not retained sufficiently to be resolved chromatographically. The next significant eluting species appear in file spectrum 331 (Figure 5B) which shows four prominent bands between 3600 and 3400 cm^{-1} which are indicative of –OH and –NH functionality. These bands are more prevalent in HPS as compared to PS. The weak absorbance band at ~3420 cm^{-1} is assignable to a secondary amine such as diphenylamine (Figure 6A) which elutes in this region of the chromatogram (see Table III). Nonheterocyclic secondary aromatic amines, however, are a minor component class which elute only in files 330–340 in the IP fraction of HPS.

The absorbance band at ~3475 cm^{-1} in file spectrum 351 (Figure 5C) is due to ring –NH such as is found in indole

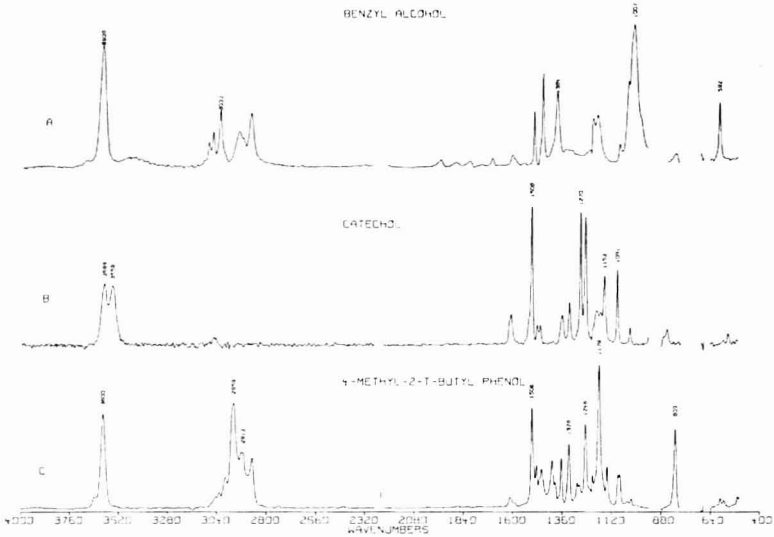


Figure 7. Infrared spectra of (A) benzyl alcohol, (B) catechol, and (C) 4-methyl-2-*tert*-butylphenol each dissolved in $CDCl_3$, 0.2-mm cell pathlength.

(Figure 6B). This class of compound elutes over almost the entire chromatographic region (Table III) depending upon substitution and is a major constituent of the IP fraction eluting from files 330–396. These cyclic aromatic secondary amines are not sufficiently resolved chromatographically (from the –OH components in the fraction and each other) to identify any specific compounds.

The final two IR bands (3601 and 3536 cm^{-1}) represent –OH functionalities. Chromatographically, only highly hindered phenols (Table II) elute under the given conditions. Figure 7C shows a spectrum of 4-methyl-2-*tert*-butylphenol. Its –OH absorbance band at 3600 cm^{-1} is similar to the band seen in files 338–396 (Figure 5D) and its chromatographic retention time (Table II) is consistent with the components suspected in this fraction. Unhindered phenols do not elute. Alcohols and hindered phenols have a tendency to have slightly higher energy O-H stretching absorbance bands. 2,6-Di-*tert*-butylphenol has an absorbance band at ~3640 cm^{-1}, while benzyl alcohol (Figure 7A) exhibits an absorbance band at 3609 cm^{-1}. These absorbance bands are similar to those briefly observed in the earlier files such as file 334. Later in the separation this absorbance band shifts to ~3600 cm^{-1} which is more indicative of phenols. To date, no model alcohols have been found to elute from the PAC column. Hindered "benzyl alcohol like" compounds could be present but the 3600-cm^{-1} band is most likely a hindered phenol.

The absorbance band around 3536 cm^{-1} may originate from polyphenolic material. For example, bands at ~3545 cm^{-1} and 3600 cm^{-1} are observed in the $CDCl_3$ solution FTIR spectrum of catechol (Figure 7B). These two bands are probably due to the symmetric and asymmetric stretching vibrational modes of the two adjacent –OH groups. Again, catechol itself is too strongly retained to chromatographically elute under our conditions, but a hindered catechol might elute similarly to a hindered phenol. This combination of bands (3545 cm^{-1} and 3600 cm^{-1}) occurs in files 328–392 with the relative intensities of the two varying. This could be due to overlap of a "phenol-type" absorbance band (at 3600 cm^{-1} only)

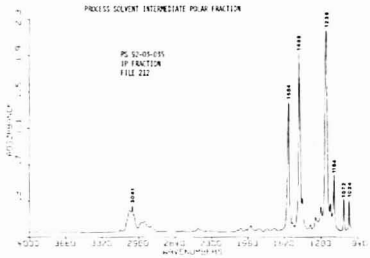


Figure 8. Infrared spectrum of file 212. See Figure 4 for chromatography conditions.

with a "catechol-like" absorbance band since the 3600-cm^{-1} band is almost always more intense than the 3545-cm^{-1} band. Figure 5C,D shows two file spectra (351 and 371) taken during the chromatographic run which illustrates this comparison.

Generally, all files show very strong aliphatic absorbance bands (3000–2800 cm^{-1}) as one would expect for a hydrotreated sample. Better fractional separation is needed to identify individual components. This is more easily accomplished in the IP fraction of PS which appears to contain fewer –OH/–NH components (vide infra).

Nonhydrogenated Process Solvent. Figure 4B shows the Gram–Schmidt reconstructed chromatogram for the separation of the IP fraction of PS. Several distinctions can be made between the hydrotreated and nonhydrotreated fraction. There is a notable absence of the siloxane component in the nonhydrogenated sample indicating that the IP fraction of PS is much less corrosive to the septums used in storage. The separation, as can be seen in the reconstructed chromatogram, is nevertheless dominated by an early eluting peak. Examination of the file spectrum (no. 212) taken at the maximum of the first peak reveals a significant concentration of ethers

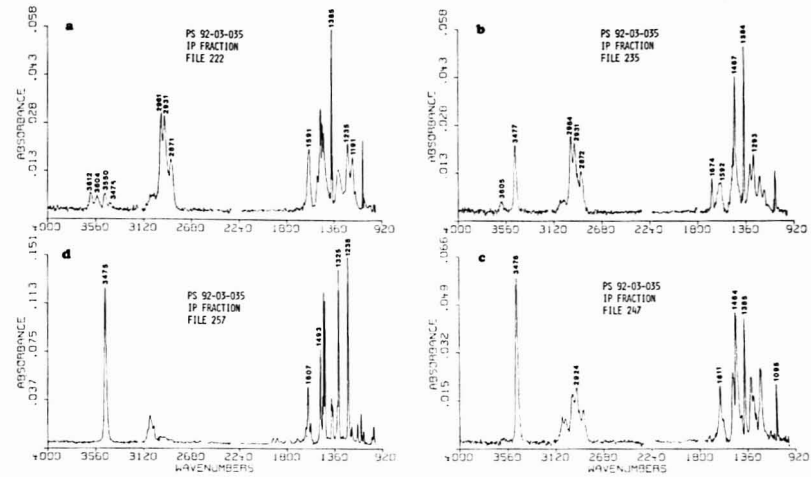


Figure 9. Infrared spectra of file 222, 235, 247, and 257. See Figure 4 for chromatography conditions.

(Figure 8). The eluting components are highly aromatic in nature with a much lower level of aliphatic –CH absorbance than was seen in the hydrotreated sample. The band at 1230 cm^{-1} is characteristic of aromatic ethers, while the smaller bands at ~1000 cm^{-1} could be due to aliphatic ethers. The complicated overtone pattern between 1800 and 2000 cm^{-1} is characteristic of several types of substituted benzenes.

File spectrum 222 (Figure 9A) shows the four distinctive bands above 3300 cm^{-1} due to –OH and –NH as was seen in the hydrotreated fraction. Note also the reversal from file 212 to a considerably higher –CH aliphatic/–CH aromatic absorbance ratio, although not as high as for the IP fraction of HPS. The assignments of the –OH and –NH bands are believed to be the same as in the HPS sample, except that there is much less (weaker absorbance) phenol and amine material than was found in the hydrotreated sample.

The IP fraction of PS appears to have more well-defined chromatographic peaks due to a fewer number of components than exist in the IP fraction of HPS. A well-defined peak (Figure 9B) is reflected in file spectrum 235. Here we see that the –NH band at ~3420 cm^{-1} has disappeared as well as the –OH band at 3540 cm^{-1} that was present through most of the chromatography of the hydrotreated fraction. In addition, the 3600-cm^{-1} band due to phenols is very weak. The major "indole-like" band at ~3575 cm^{-1} dominates the spectrum at this point. Additionally, a carbonyl band at 1675 cm^{-1} is apparent in files 227–242, which is probably an aromatic ketone (such as benzophenone). This band was not in the IP fraction of HPS to as great an extent.

By file spectrum 247 (Figure 9C), the third major chromatographic peak, only the band at ~3475 cm^{-1} is present in the –OH/–NH region. It is most probably a highly aliphatic substituted (note the 3000–2800 cm^{-1} absorbance) indole. Finally, file spectrum 257, which is the maximum of the last chromatographic peak, is due to the elution of a single component, Figure 9D. This spectrum can readily be identified as carbazole. See Figure 6B which is a spectrum of sublimed carbazole dissolved in $CDCl_3$ taken in our laboratory.

In conclusion, the effect of hydrotreating a sample can be seen not only in the increased –CH aliphatic/–CH aromatic IR absorbance ratio but also in the smaller amounts of ethers present. It appears that ether material may be readily converted to hydroxyl-containing components upon hydrotreating with the result that highly hindered phenols are produced. Hindered dihydroxy components may also be produced in hydrotreating, possibly from ether-substituted phenols. Additional monophenols may also be produced by hydrotreating but they should appear in later fractions of our preparative-scale separation. The presence of very small amounts of carbonyl-containing compounds may be due to sample oxidation which is a problem with coal-derived products. If this is the case, then this method would also lend itself to monitoring the integrity of the sample vs. time. We have reanalyzed this fraction after 1 year and have found no evidence of sample change. Work is under way in our laboratory to develop separations of the more polar fractions of the two process solvents with FTIR detection in order to test this hypothesis. Work with a microbore LC system to reduce solvent consumption and to enhance the separation and sensitivity is currently being performed.

ACKNOWLEDGMENT

The assistance of John W. Hellgeth in providing the intermediate polar fraction of coal derived process solvent is greatly appreciated.

Registry No. 1, 132-64-9; 2, 132-65-0; 3, 101-84-8; 4, 100-66-3; 5, 815-24-7; 6, 84-65-1; 7, 119-61-9; 8, 122-79-2; 9, 622-45-7; 10, 119-84-6; 2,6-di-*tert*-butylphenol, 128-39-2; 2-*tert*-butyl-6-methylphenol, 2219-82-1; 2,4-di-*tert*-butylphenol, 96-76-4; 2-*tert*-butyl-4-methylphenol, 2409-55-4; 2-*tert*-butylphenol, 88-18-6; 2-*sec*-butylphenol, 89-72-5; 3,5-di-*tert*-butylcatechol, 1020-31-1; 4,6-di-*tert*-butylrescorcinol, 5374-06-1; *N*-phenyl-2-naphthylamine, 135-88-6; diphenylamine, 122-39-4; 1,2,3,4-tetrahydrocarbazole, 942-01-8; 2,3-diphenylindole, 3469-20-3; 2,3-dimethylindole, 91-55-4; 5-ethylindole, 68742-28-9; 7-methylindole, 933-67-5; 2-methylindole, 95-20-5; α-phenylindole, 948-65-2; indole, 120-72-9; pyrrole, 109-97-7; carbazole, 86-74-8.

LITERATURE CITED

(1) Derbyshire, F. J.; Odoerfer, G. A.; Rudnick, L. R.; Varghese, P.; Whitehurst, D. D. "Fundamental Studies in the Conversion of Coals to Fuels of Increased Hydrogen Content", EPRI Ap-2177, 1981; Vol. 1.
(2) Carver, J. M.; Gir, S.; Paranjape, A. S. Proceedings of the 7th EPRI Contract's Meeting, Palo Alto, CA, May 1982.

(3) Amateis, P. G.; Taylor, L. T., submitted to *J. Chromatogr.*
(4) Schabron, J. F.; Hurtubise, R. J.; Silver, H. F. *Anal. Chem.* **1979**, *51*, 1426.
(5) Brown, R. S.; Heilgeth, J. W.; Taylor, L. T. Presented at the 8th FACSS Meeting, Philadelphia, PA, Sept 1981.
(6) Johnson, C. C.; Taylor, L. T. *Anal. Chem.*, in press.
(7) Brown, R. S.; Hausler, D. W.; Taylor, L. T.; Carter, R. C. *Anal. Chem.* **1981**, *53*, 197.
(8) Rudnick, L. R.; Whitehurst, D. D. *ACS Symp. Ser.* **1981**, *No. 169*, 153.

RECEIVED for review September 8, 1982. Accepted December 22, 1982. The financial assistance provided by Department of Energy Grant DE-FG22-81PC40799 and the Commonwealth of Virginia is gratefully appreciated.

Equations for Calculation of Chromatographic Figures of Merit for Ideal and Skewed Peaks

Joe P. Foley and John G. Dorsey*

Department of Chemistry, University of Florida, Gainesville, Florida 32611

By use of the exponentially modified Gaussian (EMG) as the skewed peak model, empirical equations based solely on the graphically measurable retention time, t_R, peak width at 10% peak height, $W_{0.1}$, and the empirical asymmetry factor, B/A, have been developed for the accurate and precise calculation of parameters (termed chromatographic figures of merit (CFOMs)) characterizing both ideal (Gaussian) and skewed chromatographic peaks. These CFOMs include: the number of theoretical plates (observed efficiency), N_{SYS}; the maximum efficiency attainable if all asymmetry is eliminated, N_{MAX}; the EMG peak parameters, t_G, σ_G, and τ; the first through fourth statistical moments; the peak skew and peak excess, γ_S and γ_E; and two new CFOMs—the relative system efficiency, RSE, and the relative plate loss, RPL. Equations for the number of theoretical plates and the second central moment (variance) are accurate to within ±1.5% for $1.00 \leq B/A \leq 2.76$. Width and B/A measurements at 10% peak height are recommended.

In recent years there has been considerable interest in the characterization of experimental chromatographic peaks. Presented in Table I are the names, symbols, and general expressions that have evolved for the parameters used in chromatographic peak characterization. It is proposed that these parameters be referred to collectively as chromatographic figures of merit (CFOMs).

These CFOMs have been estimated either by hand (manual) calculation using graphical measurements made directly from the chromatogram or by a computer following data acquisition. Both methods have advantages and disadvantages.

Manual methods were used exclusively at first and are employed quite extensively today. For arbitrary peak shapes, they are accurate for only five CFOMs: t_R, B/A, h_P, W_b, and W_a. If a Gaussian peak shape is assumed, however, then $M_1 = t_R$, and M_2 is only a function of W_b, W_a, or M_0, and N may be subsequently calculated. Except for higher *even* central moments, the remaining CFOMs are zero for Gaussian peaks.

For real chromatographic peaks, it is almost always a mistake to assume a Gaussian peak shape. Experimentally these ideal symmetric peaks are rarely, if ever, observed due to various intracolumn and extracolumn sources of asymmetry (*1–13*). Pauls and Rogers, for example, have shown that the variance of an asymmetric peak can be underestimated by more than 50% (*9*) if the Gaussian width at half-height equation is used. Kirkland et al. have demonstrated that the plate count can be overestimated by as much or more than 100% if any of the three most common Gaussian-based equations are employed (*10*).

Computer estimation methods are more accurate than common manual methods for a given CFOM but are not available to every chromatographer. The general approach taken has been one of peak statistical moment analysis (*3, 7, 10, 11, 14, 15*). Via relatively simple algorithms all the CFOMs may be determined quite accurately, though the precision of the second and higher central moments is seriously affected by base line noise (*16*).

The failure of the Gaussian function as a peak shape model for real chromatographic peaks led to the search for a more accurate model and the eventual acceptance of the exponentially modified Gaussian (EMG). The development, characterization, and theoretical and experimental justification of this model has been thoroughly reviewed (*9, 11, 14, 17*).

Application of the EMG peak model yields a new set of CFOMs given in Table II; this set consists of fundamental and derived EMG parameters, the latter containing explicit expressions for the first through fourth statistical moments defined previously in Table I. Included among the new CFOMs are the following: the retention time, t_G, and standard deviation, σ_G, of the associated parent Gaussian peak from which the skewed EMG peak is derived; the exponential modifier, τ; the fundamental ratio, τ/σ_G, which characterizes peak asymmetry; the observed efficiency (number of theoretical plates) of a given (asymmetric) chromatographic system, N_{SYS}; the maximum efficiency a given system could achieve, N_{MAX}, if all sources of asymmetry were eliminated; and finally, two CFOMs proposed originally in this work which demonstrate dramatically how peak asymmetry drastically reduces chromatographic efficiency—the relative system efficiency, RSE, and the relative plate loss, RPL.

Adoption of the EMG peak-shape model has improved the estimation of the CFOMs. A new algorithm for the computer-based peak moment analysis has been derived (*17*) and tested (*11*) which is less sensitive to base line noise and the uncertainty of peak start/stop assignments. More recently, Barber and Carr described a manual method for CFOM quantitation which requires the graphically measurable retention time t_R, peak width W_a, empirical asymmetry factor B/A, and successive interpolations from three large-scale, universal calibration curves (*18, 19*).

The purpose of the present work was to develop accurate equations for CFOM calculation dependent solely on t_R, $W_{0.1}$, and B/A. The need for computerized data acquisition is thus circumvented, and, in addition, this method is faster and

0003-2700/83/0355-0730$01.50/0 © 1983 American Chemical Society

Table I

Common Chromatographic Figures of Merit

parameter	symbol	general expression
theoretical plates	N	(retention time)²/variance
retention time	t_R	peak maximum
	M_1	peak centroid
	t_m	peak median
empirical asymmetry factor	B/A	see Figure 1
peak height	h_p	
peak width at specified height	W_α	α denotes peak height fraction
peak width at base	W_b	tangents drawn from inflection points
peak shape function	$h(t)$	

Statistical Moments and Related Quantities

zeroth (peak area)	M_0	$\int_{-\infty}^{\infty} h(t)\,dt$
first (peak centroid)	M_1	$\int_{-\infty}^{\infty} th(t)\,dt/M_0$
2nd central moment (variance)	$\bar{M}_2$	$\int_{-\infty}^{\infty} (t - M_1)^2 h(t)\,dt/M_0$
nth central moment	$\bar{M}_n$	$\int_{-\infty}^{\infty} (t - M_1)^n h(t)\,dt/M_0$
peak skew	γ_S	$\bar{M}_3/\bar{M}_2^{3/2}$
peak excess	γ_E	$\bar{M}_4/\bar{M}_2^2 - 3$

Table II. Chromatographic Figures of Merit Based on Exponentially Modified Gaussian Model

Fundamental

$$t_G,\ \sigma_G,\ \tau,\ \tau/\sigma_G$$

Derived

$$N_{SYS} = t_R^2/(\sigma_G^2 + \tau^2)$$

$$N_{MAX} = (t_G/\sigma_G)^2$$

$$RSE = \frac{N_{SYS}}{N_{MAX}}\left(\frac{t_G}{t_R}\right)^2 = \frac{\sigma_G^2}{\bar{M}_2}$$

$$RPL = \left(\frac{N_{MAX} - N_{SYS}}{N_{MAX}}\right)\left(\frac{t_G}{t_R}\right)^2 = 1 - RSE = \frac{\tau^2}{\bar{M}_2}$$

$$M_1 = t_G + \tau$$

$$\bar{M}_2 = \sigma_G^2 + \tau^2$$

$$\bar{M}_3 = 2\tau^3$$

$$\bar{M}_4 = 3\sigma_G^4 + 6\sigma_G^2\tau^2 + 9\tau^4$$

$$\gamma_S = \bar{M}_3/\bar{M}_2^{3/2}$$

$$\gamma_E = \bar{M}_4/\bar{M}_2^2 - 3$$

somewhat more precise than the other accurate manual method since no graphical interpolation is required.

DERIVATIONS

If a Gaussian peak shape equation G is used to approximate the true value T of a CFOM for an asymmetric peak, the relative error RE which results is defined as

$$RE = (G - T)/T \tag{1}$$

which can be rearranged to give

$$T = G/(RE + 1) \tag{2}$$

Thus, the true value T and the Gaussian approximation G for the CFOM are related by the correction term (RE + 1) in the denominator of eq 2.

Kirkland et al. have shown that

$$RE = f(\tau/\sigma_G) \tag{3}$$

for the three popular Gaussian-based methods for determining plate counts of a system (*10*). Equation 3 should hold, in fact, for any CFOM for which a Gaussian approximation exists except t_G. Since Barber and Carr have shown (*18*) that

$$\tau/\sigma_G = f(B/A) \tag{4}$$

successive substitution of eq 3 and 4 into eq 2 yields

$$T = G/[f(B/A) + 1] \tag{5}$$

Although the exact form of $f(B/A)$ is unknown, a least-squares curve fitting of an RE vs. B/A plot can suffice as an approximation.

The above approach was used for calculation of N_{SYS}, σ_G, and $\bar{M}_2$. Following this, τ was calculated (see sixth equation, Table II) by

$$\tau = \sqrt{\bar{M}_2 - \sigma_G^2} \tag{6}$$

For determination of t_G, the universal relationship

$$(t_R - t_G)/\sigma_G = f(\tau/\sigma_G) \tag{7}$$

previously described (*18*) was rearranged and combined with eq 4 to give

$$t_G = t_R - \sigma_G f(B/A) \tag{8}$$

where $f(B/A)$ was approximated by a least-squares fit of $(t_R - t_G)/\sigma_G$ vs. B/A.

Since t_R, B/A, and $W_{0.1}$ are graphically measurable, all the remaining CFOMs can be calculated once the fundamental parameters σ_G, τ, and t_G have been determined.

EXPERIMENTAL SECTION

Apparatus. An Apple II Plus 48K microcomputer was programmed in BASIC for EMG peak generation. A curve-fitting program available from Interactive Microware with linear, geometric, exponential, and polynomial capabilities was used for the unweighted least-squares fitting of various data sets.

EMG Peak Generation. An exponentially modified Gaussian peak can be given (*14*) by

$$f(t) = \frac{A^*\sigma_G}{\tau\sqrt{2}} \exp\left[\left(\frac{\sigma_G}{\tau}\right)^2 \frac{1}{2} - \frac{(t - t_G)}{\tau}\right] \int_{-\infty}^{Z} \exp[-x^2]\,dx \tag{9}$$

where

$$Z = [(t - t_G)/\sigma_G - \sigma_G/\tau]/\sqrt{2} \tag{10}$$

Via change of variable the integral in eq 9 is transformed to

$$\sqrt{\pi} \int_{-\infty}^{Z\sqrt{2}} \frac{\exp[-y^2/2]}{\sqrt{2\pi}}\,dy$$

and the EMG function can now be written as

$$f(t) = \frac{A^*\sigma_G}{\tau}\sqrt{\frac{\pi}{2}} \exp\left[\left(\frac{\sigma_G}{\tau}\right)^2 \frac{1}{2} - \frac{(t - t_G)}{\tau}\right] \int_{-\infty}^{Z\sqrt{2}} \frac{\exp[-y^2/2]\,dy}{\sqrt{2\pi}} \tag{11}$$

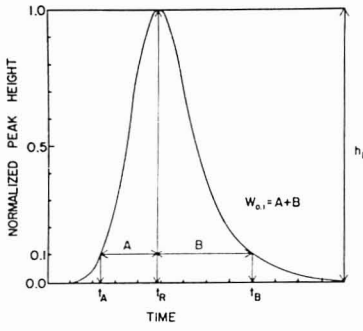


Figure 1. Measurement of retention time, t_R; peak width, $W_{0.1}$; and asymmetry factor, B/A, at peak height fraction $\alpha = 0.1$ required for equations in Table III. Analogous measurements at $\alpha = 0.3$, 0.5 are needed for equations in Tables IV and V, respectively. Except for A, B, and B/A at $\alpha = 0.1$, all width-related measurements are subscripted with the value of α to prevent ambiguity.

where A^* is the peak amplitude, τ is the exponential modifier, σ_G and t_G are the standard deviation and retention time, respectively, of the parent Gaussian, and y is a dummy variable of integration. For fixed A^*, τ, σ_G, and t_G, $f(t)$ is defined over an infinite continuum of time. Calculation of $f(t)$ was facilitated by use of a polynomial approximation $P(Z2^{1/2}, Z2^{1/2} \geq 0)$ in error by less than 7.5×10^{-8} for the integral in eq 11 (*20*). When $Z2^{1/2} < 0$, the integral may be calculated from $1 - P(-Z2^{1/2})$.

Procedure. Except as otherwise noted, values of $A^* = 1$, $t_G = 100$, and $\sigma_G = 5$ were used in eq 11 for EMG peak generation. The τ/σ_G ratio was varied from 0.1 to 3 in 0.05 increments producing data equivalent to 59 peaks. The times for t_R, t_A, and t_B (see Figure 1) at $\alpha = 0.1$, 0.3, and 0.5 for each of the 59 peaks were determined to within 0.001, using a simple search algorithm; corresponding values of W and B/A were then computed. When values for $W_{0.1}$, B/A, and $(t_R - t_G)/\sigma_G$ for the 59 peaks were compared with analogous data obtained elsewhere (*19*), the maximum relative average deviations observed were 25 ppm, 405 ppm, and 668 ppm, respectively.

Textfiles of RE (N_{SYS}, $\bar{M}_2$, σ_G) vs. $(B/A)_{0.1,0.3,0.5}$, $(t_R - t_G)/\sigma_G$ vs. $(B/A)_{0.1,0.3,0.5}$, and RSE vs. B/A were made for $0.1 \leq \tau/\sigma_G \leq 3$. The Gaussian relations $\sigma_G = W_{0.1}/4.291932$ and $\bar{M}_2 = (W_{0.1}/4.291932)^2$ were used in the calculation of the Gaussian approximations for N_{SYS}, σ_G, and $\bar{M}_2$ at $\alpha = 0.1$. Similar equations were used for $\bar{M}_2$ and σ_G at $\alpha = 0.3$, 0.5. The true values of N_{SYS}, σ_G, $\bar{M}_2$, and RSE were computed from the known values of τ, σ_G, t_G, and t_R for a given peak. Although the least-squares fittings of the various B/A textfiles were initially judged by visual inspection and the coefficient of determination, their final evaluation was based on the accuracy and simplicity of the resulting CFOM equations.

The relationship between several quantities [e.g., RE(N), $(B/A)_a$, W_a] and τ/σ_G has been shown previously (*10*, *18*) to be nonlinear for $0 < \tau/\sigma_G < 0.5$ and nearly linear for $0.5 \leq \tau/\sigma_G \leq 3$. Because similar relationships were observed in some of the textfiles above, least-squares fitting was limited to about the same τ/σ_G range 0.5–3 ($1.09 \leq B/A \leq 2.76$) except for the RSE vs. B/A textfile where the complete set of values was used in the regression analysis.

For ease of use, the CFOM equations were simplified first by algebraic factorization and cancellation and then by successive rounding of numerical coefficients. The occasional nearness of the decimal coefficients to whole numbers was exploited. For example, if $f(B/A) = 1.02(B/A) + 0.69$, then for $1.09 \leq B/A \leq 2.76$ the much simpler function $f(B/A) = B/A + 0.72$ is approximately the same (exactly if $B/A = 1.5$) and the accuracy of this function is not significantly affected.

All CFOM equations were simplified as much as possible—any more rounding of the coefficients will result in appreciably greater error.

The accuracy of the CFOM equations was evaluated in terms of four parameters, listed in decreasing order of importance: the percent relative error limits (%RELs) which represent the maximum possible error of the CFOM equations within the specified B/A range; the mean percent relative error or bias $\%\overline{RE} \equiv \sum \%RE/n$; the average magnitude of the percent relative error $\sum|\%RE|/n$; and the standard deviation of the percent relative error. The last three parameters are not specified for each CFOM in this report but may be obtained upon request.

The precision of the empirical, EMG-based CFOM equations and three Gaussian CFOM equations was calculated via error propagation theory (*21*) and is reported as percent relative standard deviation (%RSD). The required precision estimates of t_R, W_a, and $(B/A)_a$ [the graphically measurable quantities] were obtained by using data from a previous study (*19*).

RESULTS AND DISCUSSION

Listed in Table III are the empirical CFOM equations based on t_R, $W_{0.1}$, and B/A measurements (see Figure 1) which we recommend.

Accuracy. By use of eq 1 in Table III, the true efficiency of a chromatographic system, N_{SYS}, *may be estimated to within ±1.5% for both Gaussian and exponentially tailed peaks* within the asymmetry range $1.00 \leq B/A \leq 2.76$. Equations for $\bar{M}_2$, t_G, and M_1 also achieve this accuracy and range.

All CFOMS except RPL, $\bar{M}_3$, γ_S, and γ_E can be estimated to within ±5% for $1.09 \leq B/A \leq 2.76$, the asymmetry range over which most of the curve fitting was performed.

All CFOM equations are accurate to within ±5% for $1.19 \leq B/A \leq 2.76$, and 18 out of 21 are accurate to within ±2%.

Except for eq 11b, 13b, and 14b which had biases of +0.976%, +0.820%, and +1.111%, respectively, the bias for every equation given in Tables III, IV, and V was less than ±0.6%.

Precision Summary. For the equations in Table III, the estimated relative standard deviation (RSD) limits obtained via propagation of error theory for N_{SYS}, $\bar{M}_2$, σ_G, N_{MAX}, and RSE were all less than or equal to ±4.5%. RSD limits for t_G and M_1 were ±0.2%.

The precision of the EMG equations in Table III, the width-based Gaussian equations, and the calibration curve method of Barber and Carr (*18*) is compared for N_{SYS}, $\bar{M}_2$, and σ_G in Table VI. The results shown for the Gaussian equations are valid for 50%, 30%, and 10% width measurements because $RSD(W_{0.5}) = RSD(W_{0.3}) = RSD(W_{0.1})$. The slightly greater imprecision observed for the EMG equations is due to uncertainty in the B/A measurement not required for the Gaussian equations. The somewhat larger %RSDs for the method of Barber and Carr are probably due to interpolation uncertainties (from the calibration curves) unique to this method.

The precision of the remaining CFOMs in Table III was found to be highly dependent on the peak shape. Rather than reporting RSD limits, the RSD for several CFOMs or groups of CFOMs has been plotted vs. B/A in Figure 2.

Other Equations. Listed in Table IV and V are smaller sets of CFOM equations developed *only* for use in determining if a real chromatographic peak is well-modeled by an EMG peak and should *not* be used to routinely calculate any CFOM (including N_{SYS}) since they are usually less accurate, less precise, and more complex than the analogous equations in Table III. However, the accuracy and precision for $\bar{M}_2$, σ_G, t_G, and τ at $\alpha = 0.3$ and 0.5 is still sufficient to permit peak modeling decisions to be made.

Detailed Discussion of Precision. Shown in Table VII are the precision data for t_R, W_a, and $(B/A)_a$ used in this study. The RSD results were obtained by converting previously reported raw precision data (*19*) to the form appropriate for error propagation analysis for the conditions specified in

Table III. Recommended Equations for Chromatographic Figures of Merit[a]

no.	equation	asymmetry range (B/A)	% rel error limits	% RSD limits
1	$N_{SYS} = \frac{41.7\,(t_R/W_{0.1})^2}{B/A + 1.25}$	1.00-2.76 2.77-4.00	−1.5, +1 −10, −1.5	±2.5
2a	$\overline{M}_2 = \frac{W_{0.1}^2}{1.764(B/A)^2 - 11.15\,(B/A) + 28}$	1.00-2.76	−1.5, +0.5	±2.2
2b	$\overline{M}_2 = t_R^2/N_{SYS}$	1.00-2.76	−1, +1.5	±2.4
3	$\sigma_G = \frac{W_{0.1}}{3.27\,(B/A) + 1.2}$	1.09-2.76	−1, +0.5[b]	±2.0
4a	$\tau = \sqrt{\overline{M}_2\ (\text{eq 2a}) - \sigma_G^2}$	1.09-2.76	−1, +3.5[c]	[f]
4b	$\tau = \sqrt{\overline{M}_2\ (\text{eq 2b}) - \sigma_G^2}$	1.09-2.76	−0.5, +5[c]	[f]
5a	$\frac{\tau}{\sigma_G} = \frac{\tau\ (\text{eq 4a})}{\sigma_G}$	1.09-2.76	−1, +4.5[c]	[f]
5b	$\frac{\tau}{\sigma_G} = \frac{\tau\ (\text{eq 4b})}{\sigma_G}$	1.09-2.76	−0.5, +6[c]	[f]
6	$t_G = t_R - \sigma_G[-0.193\,(B/A)^2 + 1.162\,(B/A) - 0.545]$	1.00-2.76	±0.5[d]	±0.2
7	$N_{MAX} = \left(\frac{t_G}{\sigma_G}\right)^2$	1.09-2.76	−0.5, +1[d]	±2.0
8	$RSE = 0.99\,(B/A)^{-2.24}$	1.00-2.76	±2	±4.5
9	$RPL = 1 - RSE$	1.09-2.76	−6, +1.5[c]	[f]
10	$M_1 = t_G + \tau$ (eq 4a or eq 4b)	1.00-2.76	±1[d]	±0.2
11a	$\overline{M}_3 = 2\tau^3{}_{\text{eq 4a}}$	1.09-2.76	−2.5, +10.5[c]	[f]
11b	$\overline{M}_3 = 2\tau^3{}_{\text{eq 4b}}$	1.09-2.76	−1.5, +16[c]	[f]
12a	$\overline{M}_4 = 3\sigma_G{}^4 + 6\sigma_G{}^2\tau_{4a}{}^2 + 9\tau_{4a}{}^4$	1.09-2.76	−3, +1.5	[f]
12b	$\overline{M}_4 = 3\sigma_G{}^4 + 6\sigma_G{}^2\tau_{4b}{}^2 + 9\tau_{4b}{}^4$	1.09-2.76	−2, +3.5	[f]
13a	$\gamma_S = \frac{\overline{M}_3\ (\text{eq 11a})}{\overline{M}_2{}^{3/2}\ (\text{eq 2a})}$	1.09-2.76	−1, +10[c]	[f]
13b	$\gamma_S = \frac{\overline{M}_3\ (\text{eq 11b})}{\overline{M}_2{}^{3/2}\ (\text{eq 2b})}$	1.09-2.76	−0.5, +14.5[e]	[f]
14a	$\gamma_E = \frac{\overline{M}_4\ (\text{eq 12a})}{\overline{M}_2{}^2\ (\text{eq 2a})} - 3$	1.09-2.76	−1.5, +14[c]	[f]
14b	$\gamma_E = \frac{\overline{M}_4\ (\text{eq 12b})}{\overline{M}_2{}^2\ (\text{eq 2b})} - 3$	1.09-2.76	−0.5, +19.5[e]	[f]

[a] Based on t_R, $W_{0.1}$, and B/A measurements depicted in Figure 1. B/A measurements should be made to two decimal places. Numerical coefficients should not be rounded further (see Procedure). [b] Error limits are −4%, −1% for $1.00 \leq B/A \leq 1.09$. [c] Error limits are ±2% or less for $1.19 \leq B/A \leq 2.76$. [d] Error limits reported for $t_G/\sigma_G = 20$. For $t_G/\sigma_G > 20$, the error limits will be smaller than those reported. [e] Error limits are between ±2% and ±5% for $1.19 \leq B/A \leq 2.76$. [f] Precision of this CFOM is a function of peak shape. See plot of %RSD vs. B/A in Figure 2.

Table IV. Equations for Use Only in Peak Modeling[a]

equation	% rel error limits[b]	%RSD limits[b]
$N_{SYS} = \frac{6.88\,(t_R/W_{0.3})^2}{(B/A)_{0.3} - 0.3}$	±2	±4.0
$\overline{M}_2, a = \frac{W_{0.3}^2}{-3.85\,(B/A)_{0.3}^3 + 23\,(B/A)_{0.3}^2 - 47.9\,(B/A)_{0.3} + 38.7}$	−0.5, +1	±4.0
$\overline{M}_2, b = t_R^2/N_{SYS}$	±2	±4.1
$\sigma_G = \frac{W_{0.3}}{2.8\,(B/A)_{0.3} + 0.48}$	−2, +1	±2.5
$\tau, a = \sqrt{\overline{M}_2, a - \sigma_G^2}$	−0.5, 6[c]	[d]
$\tau, b = \sqrt{\overline{M}_2, b - \sigma_G^2}$	−1.5, +9.5[e]	[d]
$t_G = t_R - \sigma_G(0.6\,(B/A)_{0.3}^2 + 2.58\,(B/A)_{0.3} - 1.58)$	±0.5[f]	±0.2

[a] Based on t_R, $W_{0.3}$, and $(B/A)_{0.3}$ measurements. $(B/A)_{0.3}$ measurements should be made to two decimal places. Numerical coefficients should not be rounded further (see Procedure). [b] Valid for $1.09 \leq (B/A)_{0.1} \leq 2.76$. [c] Error limits are −0.5%, +2% for $1.19 \leq (B/A)_{0.1} \leq 2.76$. [d] Precision ranges from ±13.9% at $(B/A)_{0.1} = 1.09$ to ±2.0% at $(B/A)_{0.1} = 2.76$ in a manner similar to the $\tau, \tau/\sigma_G$ curve shown in Figure 2. [e] Error limits are −1.5%, +4% for $1.19 \leq (B/A)_{0.1} \leq 2.76$. [f] Error limits reported for $t_G/\sigma_G = 20$ for $t_G/\sigma_G > 20$, the error limits will be smaller than those reported.

Table VII. Data excluded in the previous study for $(B/A - 1)_a$ was also excluded in this analysis. The RSDs of t_R, W_a, and $(B/A)_a$ for individual peak shapes (at a given peak height fraction) were averaged as done previously, thereby implicitly

Table V. Equations for Use Only in Peak Modeling[a]

equation	% rel error limits[b]	% RSD limits[b]
$N_{SYS} = \frac{1.83(t_R/W_{0.5})^2}{(B/A)_{0.5} - 0.7}$	±2	±9.4
$\bar{M}_2,a = \frac{W_{0.5}^2}{-8.28\,(B/A)_{0.5}^3 + 41.8\,(B/A)_{0.5}^2 - 72.3\,(B/A) + 44.6}$	−1, +2	±7.7
$\bar{M}_2,b = t_R^2/N_{SYS}$	±2	±9.4
$\sigma_G = \frac{W_{0.5}}{2.5\,(B/A)_{0.5}}$	±2	±3.2
$\tau,a = \sqrt{\bar{M}_2,a - \sigma_G^2}$	−1, +5.5[c]	*d*
$\tau,b = \sqrt{\bar{M}_2,b - \sigma_G^2}$	−1, +2.5	*d*
$t_G = t_R - \sigma_G(-1.46\,(B/A)_{0.5}^2 + 5\,(B/A)_{0.5} - 3.14)$	±0.5[c]	±0.2

[a] Based on t_R, $W_{0.5}$, and $(B/A)_{0.1}$ measurements. $(B/A)_{0.5}$ measurements should be made to two decimal places. Numerical coefficients should not be rounded further (see Procedure). [b] Valid for $1.09 \leq (B/A)_{0.1} \leq 2.76$. [c] Error limits are −1%, +2% for $1.19 \leq (B/A)_{0.1} \leq 2.76$. [d] Precision ranges from ±24.5% at $(B/A)_{0.1} = 1.09$ to ±3.2% at $(B/A)_{0.1} = 2.76$ in a manner similar to the τ, τ/σ_G curve shown in Figure 2. [e] Error limits reported for $t_G/\sigma_G = 20$. For $t_G/\sigma_G > 20$, the error limits will be smaller than those reported.

Table VI. Precision[a] Comparison of Three Graphical Methods for Estimating N_{SYS}, $\bar{M}_2$, and σ_G

CFOM/ method	Gaussian eqs	empirical eqs, Table III, this work	calibration curve method reported previously (*18*)
N_{SYS}	±2.0	±2.5	±5
$\bar{M}_2$	±2.0	±2.4	±3
σ_G	±1.0	±2.0	±3

[a] Reported as percent relative standard deviation (%RSD). Precision of equations estimated via error propagation, using data of Table VII.

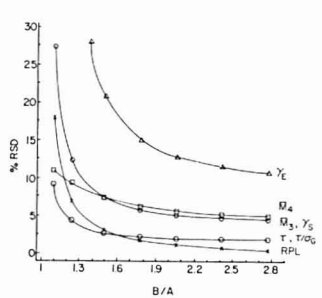


Figure 2. Dependence of precision on peak asymmetry for several CFOMs. The precision of all other CFOMs (N_{SYS}, $\bar{M}_2$, etc.) is essentially independent of peak shape and is included in Tables III–VI.

assuming the independence of the RSDs on peak shape.

The RSDs for t_R, W_α, and $(B/A - 1)_\alpha$ for individual peak shapes were originally reported relative to σ_G, σ_G, and $(B/A - 1)_\alpha$, respectively. Multiplication by σ_G/t_R, σ_G/W_α, and $(B/A - 1)_\alpha/(B/A)_\alpha$ converted them to the appropriate form.

Since the RSDs of t_R, W_α, and $(B/A)_\alpha$ were assumed to be independent of peak shape, intuitively it might seem that this should also be true for the RSD of any calculated CFOM. This is not the case, however. For one group of CFOMs (N_{SYS}, $\bar{M}_2$, σ_G, t_G, N_{MAX}, RSE, and M_1), a slight to moderate variation in RSD with $(B/A)_\alpha$ was observed. This can be explained by examining the random error propagation in the general empirical equation

$$N_{SYS} = \frac{C_1(t_R/W_\alpha)^2}{(B/A)_\alpha + C_2}$$

Assuming negligible covariances, RSD(N_{SYS}) is given by

$$\mathrm{RSD}\,(N_{SYS}) = \Bigg[\underbrace{4\left(\frac{\sigma_{t_R}}{t_R}\right)^2}_{1} + \underbrace{4\left(\frac{\sigma_{W_\alpha}}{W_\alpha}\right)^2}_{2} + \underbrace{\left(\frac{\sigma_{(B/A)_\alpha}}{(B/A)_\alpha}\right)^2}_{3}\underbrace{\left(\frac{(B/A)_\alpha}{(B/A)_\alpha + C_2}\right)^2}_{4}\Bigg]^{1/2} \quad (12)$$

Even when terms 1–3 in eq 12 are constant, RSD(N_{SYS}) will vary somewhat with $(B/A)_\alpha$ because of term 4. Clearly this variation will be greatest for $-(B/A)_\alpha \leq C_2 \leq 0$. Additionally, as $C_2 \to -(B/A)_\alpha$, RSD(N_{SYS}) $\to \infty$. For $C_2 \approx 0$, RSD(N_{SYS}) is essentially independent of $(B/A)_\alpha$. Finally, for $C_2 > 0$, a negligible to slight variation of RSD(N_{SYS}) with $(B/A)_\alpha$ may be observed, depending on the magnitude of terms 1 and 2 relative to the product of terms 3 and 4. Except for the first

Table VII. Suggested Chromatographic Measurement Conditions and the Relative Standard Deviations of t_R, W_α, and $(B/A)_\alpha$ Achieved

Conditions

1. Chromatogram recording rate: 1 cm/σ_G ($W_{0.1} \geq 4.3$ cm)
2. Ruler resolution: ±0.2 mm
3. Minimum retention distance, $(t_R)_{MIN}$: 10 cm
4. Minimum peak height, $(h_p)_{MIN}$: 10 cm

Results[a,b]

CFOM	%RSD (α = 0.1)	%RSD (α = 0.3)	%RSD (α = 0.5)
t_R	±0.2	identical	identical
W_α	±1.0	±1.0	±1.0
$(B/A)_\alpha$	±2.0	±2.5	±3.0

[a] Data obtained from ref 19 and subsequently converted (see Detailed Discussion of Precision) for α = 0.1, 0.5—results interpolated for α = 0.3. [b] %RSD (t_R) rounded to nearest 0.1%; %RSDs for W_α, $(B/A)_\alpha$ rounded to nearest 0.25%.

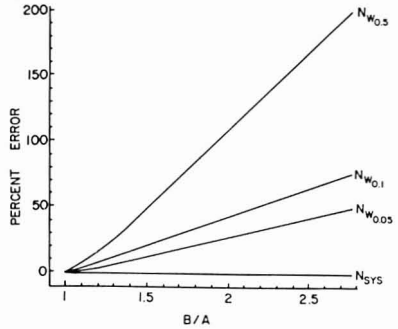


Figure 3. Relative error in plate count of three Gaussian equations (based on the indicated peak width measurements) and the EMG-based N_{SYS} equation (Table III, eq 1) for ideal and skewed peaks.

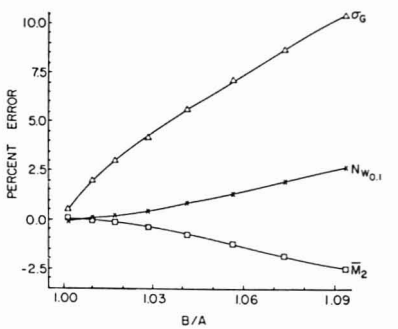


Figure 4. Relative error in the Gaussian standard deviation, plate count, and second central moment for Gaussian equations based on t_R, $W_{0.1}$ measurements for ideal and slightly skewed peaks.

three equations in Table V, the RSDs of N_{SYS}, $\bar{M}_2$, σ_G, t_G, N_{MAX}, RSE, and M_1 calculated via equations in Tables III, IV, and V varied by less than 0.5% for $1.00 \leq B/A \leq 2.76$.

The remaining CFOMs (τ, τ/σ_G, RPL, $\bar{M}_3$, γ_S, γ_E) comprise a second group whose RSDs are moderate to strong functions of peak shape as Figure 2 shows. In every instance the imprecision is largest for the least asymmetric peaks and smallest for the most highly skewed peaks. Analysis of the error propagation equations shows that one or more terms within the equations gets very large as the peak shapes become symmetric (22).

Why Measure at 10%? For reasons listed below, the recommended CFOM equations in Table III are based on (in addition to t_R) the measurement of W and B/A at 10% peak height rather than at other peak height fractions such as 50%, 30%, or 5%:

1. Examination of Tables III, IV, and V shows that many CFOM equations at 10% are clearly superior to the corresponding ones at 30% and 50% in terms of:
   (a) precision (lowest RSD limits)
   (b) widest working range for equivalent accuracy
   (c) simplicity for M_2 (path a)
2. The N_{SYS} equation at 10% peak height is more accurate for Gaussian and near-Gaussian peaks than other N_{SYS} equations developed at 50%, 30%, or 5% (22).
3. In a previously reported graphical measurement study (19), statistically significant positive and negative biases were detected in the measurement of $A_{0.5}$ and $B_{0.5}$, respectively, resulting in a consistent underestimation of $(B/A)_{0.5}$. No such biases were detected for $A_{0.1}$ and $B_{0.1}$, and only a slight underestimation was observed for $(B/A)_{0.1}$.
4. It is likely that $RSD(W_{0.05}) > RSD(W_{0.1})$, since in going from $W_{0.1}$ to $W_{0.05}$ the magnitude of the slope of the peak (on either side) decreases much more rapidly than the peak width increases. Thus the precision for the 5% CFOM equation would be poorer [assuming $RSD(W_{0.05})$ contributes substantially to the total uncertainty].
5. Superior resolution between overlapping peaks is required for measurements at 5% peak height than at 10%.
6. As exemplified in Figure 3 for N_{SYS}, Gaussian CFOM equations based on width measurements at 10% are much less inaccurate (though still exceedingly in error) for asymmetric peaks than the corresponding Gaussian equations at 50% (shown) and 30% (not shown). That is, the slope of the RE vs. $(B/A)_\alpha$ (shown for $\alpha = 0.1$) plots is smaller; thus the approximate RE correction function in the denominator of eq 2 and 5 (text) will be less sensitive to the measurement imprecision of $(B/A)_\alpha$.
7. The sensitivity of the RE correction functions to the $(B/A)_\alpha$ measurement imprecision is only slightly lower at 5% than at 10% peak height (see Figure 3) and is insufficient to warrant CFOM estimation at 5%.
8. The RSE can be calculated much more accurately by using an equation of the form of eq 8, Table III at 10% than at 50%, 30%, or 5%. In addition, the RSD limits are much lower at 10% than at 50% or 30% and are comparable to those at 5% (22).
9. The empirical asymmetry factor measurement, B/A, was introduced at 10% peak height rather than at 50% or 30% because peak tailing is much more apparent at 10%. Since then almost all empirical measurements of asymmetry have been reported at this peak height fraction; these data will be of little value in later years if the B/A peak height fraction is redefined.
10. It is easier to mentally compute 10% of an arbitrary peak height than 50%, 30%, or 5%.

Taken collectively, the above arguments indicate that *the best CFOM estimation is obtained from graphical chromatographic measurements at 10% peak height.*

What Type of Peak Shape? Chromatographic peaks should be examined for their resemblance to Gaussian, EMG, or other peak shapes, first by visual inspection and then from the asymmetry factor measurement. In the unlikely event that $B/A \approx 1$, the validity of the Gaussian model can be checked by comparing the measured peak width ratios $W_{0.5}:W_{0.3}:W_{0.1}$ to the theoretically predicted ratios 0.5487:0.7231:1. For $B/A \geq 1.09$, the validity of the EMG model can be judged by the agreement of values of σ_G, $\bar{M}_2$, and/or τ and t_G determined from both B/A and W measurements at $\alpha = 0.1$, 0.3, and 0.5 (see Tables III, IV, and V).

For slightly asymmetric chromatographic peaks, the assignment of peak shape models may be ambiguous due to the imprecise measurement of B/A (e.g., is a peak with $B/A = 1.03 \pm 0.02$ Gaussian?). Insofar as accuracy and precision are concerned, does it matter if EMG-based equations are used with Gaussian peaks or vice versa? As seen from Table III, the EMG base equations for N_{SYS}, $\bar{M}_2$, and σ_G are accurate to within ±1.5%, ±1.5%, and ±4%, respectively, over the asymmetry range $1.00 \leq B/A \leq 1.09$. Figure 4 shows the accuracy of the Gaussian based equations ($\alpha = 0.1$) over this same range. Clearly, little error in the estimation of $\bar{M}_2$, N_{SYS}, and σ_G will result from peak model misassignments at low asymmetries ($1.00 \leq B/A \leq 1.09$) due to B/A imprecision, though for $B/A \geq 1.04$ the EMG equations are more accurate. Furthermore, as seen from Table VI, the change in the precision of CFOM estimation resulting from peak model mis-

assignment would be less than 1%.

General Aspects of the Method. The universality of the relative error approach (introduced in the Derivations section above) was checked by the independent variation of t_G and σ_G over the t_G/σ_G range of 10 to 5000. The generality was confirmed by identical statistical results (%RELs, etc.) over a given B/A range (e.g., 1.09–2.76) for all CFOMs calculated from this approach.

As an additional check on the experimental work, $\bar{M}_2$ and N_{SYS} were calculated by statistical moment analysis (*10*), using the same t_R search algorithm as before (see Procedure). The agreement among the true, moment, and manual values for both $\bar{M}_2$ and N_{SYS} was within ±1% for $1.00 \leq B/A < 2.05$ with very little bias present in either approximation. At higher asymmetries ($2.05 \leq B/A \leq 2.76$), the manual values remained with ±1.5% of the true values, but the corresponding moment values showed a significant positive bias ranging from +1.5% to +5.5%. An even greater bias of +4.4% at $B/A = 2.05$ ($\tau/\sigma_G = 2$) reported elsewhere (*10*) was attributed to arbitrary data truncation. This was probably the source of bias in our statistical moment method as well, but regardless of the source of bias, the same conclusion may be drawn: at high asymmetries ($2.05 \leq B/A \leq 2.76$) the manual CFOM equation method is more accurate than the moment method.

Working Range of the Equations. The EMG-based equations were expected to be accurate over the asymmetry range used for the least squares curve fitting of the $f(B/A)$ approximations. Thus, except for eq 8, the accurate working range was thought to be $1.09 < B/A < 2.76$. Nevertheless, eq 1, 2(a,b), 6, 7, and 10 allow accurate estimation of N_{SYS}, $\bar{M}_2$, t_G, N_{MAX}, and M_1, respectively, for Gaussian shaped peaks ($B/A = 1.00$). Although somewhat surprising, this is explained by the near convergence of these EMG equations to Gaussian ones when the substitution $B/A = 1.00$ is made in the former. The N_{SYS} equation in Table III, for example, becomes

$$N_{SYS} = 18.53(t_R/W_{0.1})^2 \quad (13)$$

which is within +0.6% of the Gaussian formula

$$N_{W_{0.1}} = 18.42(t_R/W_{0.1})^2 \quad (14)$$

CFOM equations could have been developed for asymmetries greater than $B/A = 2.76$ ($\tau/\sigma_G = 3$), but a sacrifice of simplicity, accuracy, or both would have been required. More importantly, however, it was felt that nearly all peaks reported in the literature exhibit B/A's ≤ 2.76. Indeed, a chromatographic system producing peaks with B/A's > 2.76 is operating at a relative system efficiency of less than 10%.

When the EMG N_{SYS} equation was tested for asymmetries higher than those for which it was developed, the %RE varied between −1.5% and −10% for $2.77 \leq B/A \leq 4.00$, compared to the %RE range of +70% to +110% for the Gaussian 10% equation ($N_{W_{0.1}}$).

Real vs. Ideal CFOMs; Column Characterization. Given that peak asymmetry is (almost) always present in any real chromatographic system, N_{SYS}, $\bar{M}_2$, and t_R represent the experimentally observed chromatographic efficiency, peak variance, and retention time, respectively. The corresponding CFOMs N_{MAX}, σ_G^2, and t_G represent idealized chromatographic parameters which would describe the system if all sources of asymmetry could be eliminated. If all or nearly all asymmetry is extracolumn in origin, then for a given set of conditions N_{MAX}, σ_G^2, and t_G are valid descriptors of the efficiency, band-broadening, and retention characteristics of the *column*.

Pluralism of the Method. As might be surmised from Table III, there is more than one way to calculate several of the CFOMs. The variance, for example, can be calculated via eq 2a from measurements of $W_{0.1}$ and B/A or via eq 2b from t_R and N_{SYS} (eq 1). Generally, CFOM estimates via the "b" equations are simpler, faster, equally precise, but less accurate than estimates via the "a" equations. This trade-off of accuracy for simplicity and speed is slight, however; in most cases much time can be saved with little sacrifice in accuracy if the "b" equations are employed.

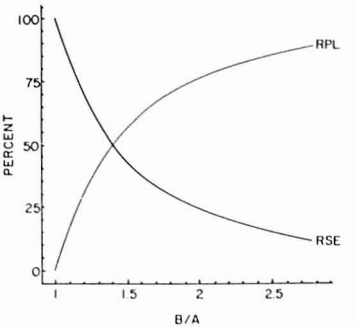


Figure 5. Relative system efficiency, RSE, and relative plate loss, RPL, for ideal and skewed peaks.

Only the simplest and most accurate methods are given in Table III. Therefore, while N_{SYS} could be calculated from its components t_R, σ_G, and τ (see N_{SYS} equation in Table II), this method was not reported since it would be much more time-consuming, tedious, and in all likelihood less accurate and less precise than the "wholistic" N_{SYS} equation in Table III.

Usefulness of RSE, RPL. The relative system efficiency (RSE) and relative plate loss (RPL), two new parameters defined in Table II, are dualistic CFOMs. First, they can be interpreted intuitively as N_{SYS}/N_{MAX} and $(N_{MAX} - N_{SYS})/N_{MAX}$, respectively, with a corrective retention factor $(t_G/t_R)^2$ applied. Alternatively, RSE and RPL can be viewed as the relative contributions of symmetrical (σ_G^2) and asymmetrical (τ^2) band-broadening processes to the total system band-broadening ($\bar{M}_2$, the total variance). If $(t_G/t_R)^2$ can be neglected because of its nearness to unity, the former intuitive expressions for RSE and RPL become particularly useful. For example, the best possible efficiency, N_{MAX}, can be related very simply to the true chromatographic efficiency, N_{SYS}, by

$$N_{MAX} = N_{SYS}/\text{RSE} \quad (15)$$

In fact, this approximation is good to within +2% with an RSD limit of ±5% (for $1.00 \leq B/A \leq 2.76$) whenever N_{MAX} (calculated via eq 15) > 4000. Thus, eq 15 can serve as a useful estimation of N_{MAX} for moderate to high efficiency chromatographic systems.

Although B/A, RSE, and RPL are mutually interdependent (i.e., once B/A has been measured RSE and RPL may be calculated), *the specification of RSE, RPL, or both* in addition to the reporting of B/A *greatly enhances the qualitative description of a chromatographic system.* Thus, while $B/A = 1.30$ indicates that a given peak is asymmetric, the corresponding RSE = 55% or RPL = 45% provides a clearer indication of the actual efficiency and how much room for improvement exists.

Figure 5 shows the exponential-like relationship of RSE and RPL with B/A. Chromatographic systems with asymmetries of 1.00 and 1.10 are operating at much different relative efficiencies, while two systems operating at $B/A = 2.00$ and 2.10 are realizing nearly the same relative efficiencies.

Alternative Derivations. Two other approaches for deriving CFOM equations were not as successful as that already

described. In the first attempt, a modification of the Carr graphical method, three universal calibration curves were approximated by linear or quadratic polynomials. This approach yielded equations for σ_G, τ, t_G, and the remaining CFOMs in terms of $W_{0.1}$, B/A, and t_R, but is unsatisfactory for three reasons: (a) an accurate but simple approximation of τ/σ_G in terms of B/A cannot be obtained for the range $1.00 \leq B/A \leq 2.76$ because the relationship between them changes at $B/A = 1.36$ from a decidedly nonlinear one to an almost perfectly linear one; (b) the errors introduced by the polynomial approximations tend to accumulate slightly rather than cancel; and (c) the equations derived for all the CFOMs except, τ, σ_G, and t_G are extremely unwieldly, e.g.

$$N_{SYS} = (t_R/W_{0.1})^2[g(B/A)/h(B/A)] \qquad (16)$$

where g and h are second degree polynomials of B/A. A variation of this same approach in which B/A was substituted for the original abscissa τ/σ_G in the latter two calibration curves made little difference.

Another try, a variation of the relative error approach utilizing $(B - A)$ as the approximation G in eq 5 for τ, failed because the simplest $f(B/A)$ approximation required for sufficient accuracy was too complex.

CFOM Units. For ease of interlaboratory comparison, all nonunitless CFOMs should be reported in time units; if units of length are chosen instead, the recorder chart speed should be specified to permit conversion to time units.

Superiority of EMG-Based Equations. Although Gaussian-based equations are somewhat simpler than their EMG counterparts in Table III (compare eq 14, text, with eq 1, Table III), the EMG equations are to be much preferred. They exhibit comparable precision (see Table VI) and are equally accurate for Gaussian (or near-Gaussian) peaks and considerably more accurate for skewed (EMG) chromatographic peaks. Adoption of the equations in Table III, especially

$$N_{SYS} = \frac{41.7(t_R/W_{0.1})^2}{B/A + 1.25}$$

is strongly urged.

LITERATURE CITED

(1) Snyder, L. R.; Kirkland, J. J. "Introduction to Modern Liquid Chromatography", 2nd ed.; Wiley: New York, 1979.
(2) Giddings, J. C. *Anal. Chem.* **1963**, *35*, 1999–2002.
(3) Kucera, E. *J. Chromatogr.* **1965**, *19*, 237.
(4) Karger, B. L.; LePage, J. N.; Tanaka, N. "High Performance Liquid Chromatography, Advances and Perspectives"; Horvath, C., Ed.; Academic Press: New York, 1980; Vol. 1, pp 119–121.
(5) Schmuach, L. J. *Anal. Chem.* **1959**, *31*, 225–230.
(6) Johnson, H. W., Jr.; Stross, F. H. *Anal. Chem.* **1959**, *31*, 357–365.
(7) Sternberg, J. C. "Advances in Chromatography"; Giddings, J. C., Keller, R. A., Eds.; New York: Marcel Dekker: 1966; Vol. 2, pp 205–270.
(8) McWilliam, I. G.; Bolton, H. C. *Anal. Chem.* **1969**, *41*, 1755–1770.
(9) Pauls, R. E.; Rogers, L. B. *Sep. Sci.* **1977**, *12*, 395–413.
(10) Kirkland, J. J.; Yau, W. W.; Stoklosa, H. J.; Dilks, C. H. *J. Chromatogr. Sci.* **1977**, *15*, 303–316.
(11) Pauls, R. E.; Rogers, L. B. *Anal. Chem.* **1977**, *49*, 625–628.
(12) Haddad, P. R.; Keating, R. W.; Low, K. C. *J. Liq. Chromatogr.* **1982**, *5*, 853–867.
(13) Maynard, V.; Grushka, E. *Anal. Chem.* **1972**, *44*, 1427–1434.
(14) Grushka, E.; Myers, N. M.; Schettler, P. D.; Giddings, J. C. *Anal. Chem.* **1969**, *41*, 889–892.
(15) Chesler, S. N.; Cram. S. P. *Anal. Chem.* **1971**, *43*, 1922–1933.
(16) Yau, W. W. *Anal. Chem.* **1977**, *49*, 395–398.
(17) Grushka, E. *Anal. Chem.* **1972**, *44*, 1733–1738.
(18) Barber, W. E.; Carr, P. W. *Anal. Chem.* **1981**, *53*, 1939–1942.
(19) Carr, P. W., University of Minnesota, Minneapolis, Minnesota, personal communication, supplementary material from ref 18.
(20) Abramowitz, M., Stegun, I. A., Eds. "Handbook of Mathematical Functions"; National Bureau of Standards: Washington, DC, 1964; Applied Mathematics Series No. 55, p 932.
(21) Bevington, P. F. "Data Reduction and Error Analysis for the Physical Sciences"; McGraw-Hill: New York, 1969; pp 56–64.
(22) Foley, Joe P.; Dorsey, John G., unpublished work, 1982.

RECEIVED for review August 13, 1982. Accepted December 22, 1982. This work was presented in part at the 184th National Meeting of the American Chemical Society, in Kansas City, MO, on Sept 5, 1982.

Prediction of Gas Chromatographic Retention Indexes with Topological, Physicochemical, and Quantum Chemical Parameters

Lutgarde Buydens and Désiré L. Massart*

Vrije Universiteit Brussel, Farmaceutisch Instituut, Laarbeeklaan 103, B-1090 Brussel, Belgium

Paul Geerlings

Vrije Universiteit Brussel, Algemene Chemie, Faculteit Wetenschappen, Pleinlaan 2, B-1090 Brussel, Belgium

Gas chromatographic retention indexes on stationary phases of different polarity are related to structural parameters by means of multiple regression and factor analysis. Combinations of topological, physicochemical, and quantum chemically calculated electronic parameters are used. The data set consists of the retention indexes of mono- and bifunctional molecules on stationary phases of different polarity. The retention behavior on the apolar stationary phases is best explained by a combination of a topological parameter and quantum chemically calculated electronic parameters. For the polar stationary phases the retention behavior is best described by quantum chemical charge parameters related to the local polarity.

Gas chromatographic behavior of molecules results from the interaction forces between the stationary phase and the molecules. Earlier attempts have been made to predict and/or explain gas chromatographic retention indexes by means of structural and physicochemical parameters (*1–6*). These studies proved the validity of the molecular connectivity parameters in predicting gas chromatographic retention indexes on apolar stationary phases and in data sets consisting of molecules belonging to one chemical family. On polar stationary phases and for data sets consisting of molecules of different chemical families, a combination of these molecular connectivity terms with some electronical parameters is necessary. Combination of the molecular connectivity terms with the Hansch constant π and the Hammet constant σ has been investigated (*7*). These combinations describe rather well the interactions even on polar phases for a data set consisting of monofunctional molecules from different chemical families. The regression indexes of molecules with more than one functional group (i.e., an alcohol and a keto group) in the same molecule are not well predicted by the regression line describing the chromatographic behavior of the molecules.

Therefore we wanted to investigate if better results would be obtained by combinations of the molecular connectivity terms with a set of parameters, related in a more direct way to the molecular electronic structure, such as the molecular dipole moment, in order to describe the chromatographic behavior of these bifunctional molecules. Due to the lack of suitable experimental data we have chosen to take values resulting from quantum chemical calculations, which moreover offer the possibility of obtaining electronic structural parameters not directly obtainable from experiments, e.g., atomic charges.

THEORY

Topological Parameters. Topological parameters describe the general size and volume of the molecules. They are derived from the topological or neighborhood matrix. The parameters used here are the molecular connectivity terms, the Wiener number, W, and the Hosoya index, Z. The equations necessary to calculate them can be found in ref 8–13:

Molecular Connectivity Terms. To calculate the connectivity parameters, we write the molecule in skeletal form. To each of the atoms "i" a value δ_i is attributed, according to the difference between the number of valence electrons and the number of hydrogen atoms suppressed. An example (2-methyl-1-butanol) is given in Figure 1. The respective connectivity indexes are calculated by means of the following equations.

Zero-order term ($^0\chi$)

$$^0\chi = \sum(1/\delta_i)^{-1/2} \tag{1}$$

The δ_i values are the δ values of the atom i, for example, 2-methyl-1-butanol

$$^0\chi = \frac{2}{\sqrt{1}} + \frac{2}{\sqrt{2}} + \frac{1}{\sqrt{3}} + \frac{1}{\sqrt{5}} = 4.439 \tag{2}$$

First-order term $^1\chi$

$$^1\chi = \sum_{l=1}^{N}\left(\frac{1}{\delta_i\delta_j}\right)_l^{-1/2} \tag{3}$$

δ_{ij} are the δ values of the adjacent atoms i and j and N is the number of bonds in the molecule. For 2-methyl-1-butanol

$$^1\chi = \frac{1}{\sqrt{1\times 2}} + \frac{2}{\sqrt{2\times 3}} + \frac{1}{\sqrt{1\times 3}} + \frac{1}{\sqrt{2\times 5}} = 2.417 \tag{4}$$

Second-order term ($^2\chi$)

$$^2\chi = \sum_{q=1}^{M}\left(\frac{1}{\delta_i\delta_j\delta_k}\right)_q^{-1/2} \tag{5}$$

$\delta_{i,j,k}$ are the δ values of the atoms of two adjacent bonds, and M is the number of two adjacent bonds in the molecule. For 2-methyl-1-butanol

$$^2\chi = \frac{1}{\sqrt{1\times 2\times 3}} + \frac{1}{\sqrt{2\times 3\times 1}} + \frac{1}{\sqrt{1\times 3\times 2}} + \frac{1}{\sqrt{3\times 2\times 5}} + \frac{1}{\sqrt{2\times 2\times 3}} = 1.699 \tag{6}$$

The third-order term: there are two possibilities, namely, a path and a cluster term.

(a) Path term ($^3\chi_p$)

$$^3\chi_p = \sum_{q=1}^{P}(\delta_i\delta_j\delta_k\delta_l)_q^{-1/2} \tag{7}$$

$\delta_{i,j,k,l}$ are the δ values for the atoms of three adjacent bonds

0003-2700/83/0355-0738$01.50/0 © 1983 American Chemical Society

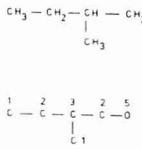


Figure 1. δ values for 2-methyl-1-butanol; the δ values are given just above the respective atoms.

forming a chain, in this case the butane skeleton (C–C–C–C), and P is the number of these three sets of adjacent bonds. For 2-methyl-1-butanol

$$^3\chi_p = \frac{1}{\sqrt{1\times2\times3\times1}} + \frac{1}{\sqrt{1\times2\times3\times2}} + \frac{1}{\sqrt{2\times3\times2\times5}} + \frac{1}{\sqrt{1\times3\times2\times5}} = 1.009 \quad (8)$$

(b) Cluster term ($^3\chi_c$)

$$^3\chi_c = \sum_{q=1}^{Q} (\delta_i\delta_j\delta_k\delta_l)_q^{-1/2} \quad (9)$$

$\delta_{i,j,k,l}$ are the δ values for the atoms of three adjacent bonds forming a star, in this case the isobutane skeleton, and Q is the number of isobutane skeletons in the molecule. For 2-methyl-1-butanol

$$^3\chi_c = \frac{1}{\sqrt{2\times3\times2\times1}} = 0.289 \quad (10)$$

The Wiener number, W, and Hosoya's index, Z, are also topological parameters. Formulas to calculate them can be found in ref 9 and 13.

Physicochemical Parameters (*8*, *9*, *12*). *Hansch's Constant, π.* Hansch's constant, π, is defined as the logarithm of the distribution coefficient of the molecule between water and octanol. It can be calculated by means of fragmental constants, π_f, defined as

$$\pi_f = \log \frac{P_x}{P_0}$$

P_0 is the distribution constant (octanol/water) of the parent molecule without fragment x. P_x is the distribution constant (octanol/water) of the parent molecule with the fragment x.

π_f is thus the contribution of fragment x to the total π value. Summation of the π_f constants over the relevant fragments, constituting the molecule, yields the π value. This parameter is a mixed parameter, related to the polar characteristics and to the general size and volume of the molecules.

Hammet's Constant, σ. Hammet's constant, σ, is an electronic parameter. It is related to the polar characteristics of the molecules. It can be calculated in a way analogous to that for π. Because the molecules considered here are all aliphatic, the σ scale, derived from the hydrolysis of aliphatic acids, is used.

Quantum Chemical Parameters. Out of the vast amount of electronic structure parameters, which can be obtained from a standard quantum chemical calculation, the following parameters were chosen: DM, the magnitude of the dipole moment; QT, the sum of absolute values of the charges in a given molecule; QA, the sum of absolute values of the charges of the atoms constituting the functional group, when a monofunctional molecule is considered and the atoms in α position of this functional group. When a bifunctional molecule is considered, QA is the sum of the quantities computed in this manner for both functional groups; QB, QA + the absolute value of the charges on the atoms in β position; QT2, the sum of squares of the absolute charges of all the atoms in the molecule; QA2, the sum of squares of the charges considered in QA; QB2, the sum of squares of the charges considered in QB; DM2, the square of the magnitude of the molecular dipole moment. (All charge parameters are given in atomic units, one atomic unit being the elementary charge.)

This set of parameters was chosen because it could be hoped that they would prove efficient in describing as accurately as possible the interactions of the molecules with polar phases. For this purpose the polar characteristics of this molecule should be invoked.

DM and QT describe the global polarity of the molecules. However, one can expect that the specific interactions between the stationary phases and the molecules should even more depend upon the local polarity of these molecules. To account for these local effects, one may introduce bond dipole moments. However, as it is rather time-consuming to calculate this parameter, we have chosen, as a first approximation to this quantity, the parameters QA and QB. Indeed, these parameters describe only the charges in and near the functional groups, which, in a classical point charge model, are directly related to the bond dipole moment.

As, in the dipole dipole interaction, which is one of the possible interaction mechanisms between polar molecules, the energy of interaction is proportional to the squares of dipole moments (*14*), we also included the square terms of the different parameters: QA2, QB2, QT2, DM2.

EXPERIMENTAL SECTION

All these parameters are calculated for a data set consisting of molecules with two functional groups such as an alcohol and a keto group or two keto groups. A list of the included molecules can be found in Table I. The same parameters are also calculated for a data set consisting of monofunctional molecules. A list of these molecules can be found in Table II.

The molecular connectivity terms are calculated on a UNIX PDP 11/70 computer with a program developed by us.

The quantum chemical parameters are calculated by using the CNDO/2 method (*15*). This semiempirical approximate molecular orbital method, in which only the valence electrons are considered explicitly, is an approximation to the full Hartree–Fock–Roothaan equations (*16*). Calculations were performed with the standard parameterization.

Since especially in the case of bifunctional molecules the quantum chemically calculated properties may strongly depend on the molecular conformation, all calculations are carried out for two conformations in these cases. For the first conformation we have chosen the most stable conformation for molecules in the gaseous phase (*17*). The second one is the cis conformation in which the two functional groups point to the same direction. As in the latter case a simultaneous energetically favored interaction of both functional groups with the stationary phase can occur, we expect that the cis conformation will be the one taken by the molecule upon interaction with the stationary phase.

The retention indexes are considered on four stationary phases of different polarity (Table III) (*18*).

Multiple regressions and correlations are calculated by using the BMDP79 program (*19*). The BMDP subprogram P9R chooses the subset of variables which results in the best regression. The different regression equations are evaluated to their Mallow's c_p (*19*). This is

$$c_p = \frac{RSS}{s^2} - (N - 2p') \quad (11)$$

The "best" subset is the one that minimizes the Mallow's c_p. RSS is the residual sum of squares of the considered subset.

s^2 is the residual mean square based on the regression of all independent variables.

N is the total number of independent variables.

p' is the number of independent variables used in the subset being tested.

The resulting multiple correlation R is a measure of the goodness of fit. The multiple correlation coefficient is the cor-

Table I. Bifunctional Molecules

2-propyn-1-ol	3-hydroxy-2-butanone
2-butene-1-ol	4-hydroxy-2-butanone
3-butene-2-ol	1-hydroxy-2-methyl-3-butanone
1-pentene-3-ol	2-hydroxy-2-methyl-3-butanone
1-butene-4-ol	2-methoxyethanol
2-methyl-3-butene-2-ol	2-ethoxyethanol
2-methyl-3-butyn-2-ol	2-butoxyethanol
3-butene-2-one	2-ethoxy-1-propanol
2,3-butanedione	4-methoxy-4-methyl-2-pentanol
2,3-pentanedione	1-ethoxy-3-pentanol
2,4-pentanedione	

Table II. Monofunctional Molecules

butyl methyl ether	isobutyraldehyde
diethyl ether	propionaldehyde
isopropyl propyl ether	2-pentanone
propyl ether	2-methyl-2-propanol
methyl propyl ether	2,3-dimethyl-2-butanol
methyl formate	ethyl propionate
ethyl formate	methyl propionate
isopropyl formate	3-methyl-2-butanol
propyl acetate	3,3-dimethyl-2-butanol
isopropyl acetate	2-propanol
butyraldehyde	2-butanol

Table III

(a) Correlation Coefficients: Bifunctional Molecules, CIS Conformation

	π	σ	$^0\chi$	$^1\chi$	$^2\chi$	$^3\chi_p$	$^3\chi_c$	$^3\chi_T$	QT	QT2	QA	QA2	QB	QB2	DM	DM2
π	1.00	−0.56	0.28	0.44	0.26	0.30	0.06	0.22	−0.34	−0.44	−0.12	−0.45	−0.43	−0.44	−0.62	−0.69
σ	−0.56	1.00	0.16	0.12	0.17	0.12	0.13	0.14	0.65	0.62	0.44	0.61	0.67	0.62	0.26	0.39
$^0\chi$	0.28	0.16	1.00	0.86	0.87	0.88	0.50	0.83	0.57	0.52	0.43	0.52	0.50	0.52	0.56	0.23
$^1\chi$	0.44	0.12	0.86	1.00	0.76	0.91	0.23	0.69	0.60	0.51	0.50	0.50	0.53	0.50	−0.19	−0.06
$^2\chi$	0.26	0.17	0.87	0.76	1.00	0.84	0.80	0.98	0.57	0.53	0.40	0.51	0.48	0.52	0.25	0.29
$^3\chi_p$	0.30	0.12	0.88	0.91	0.84	1.00	0.41	0.85	0.59	0.53	0.43	0.52	0.52	0.52	0.06	0.13
$^3\chi_c$	0.06	0.13	0.50	0.23	0.80	0.41	1.00	0.83	0.25	0.26	0.12	0.23	0.18	0.25	0.44	0.39
$^3\chi_T$	0.22	0.14	0.83	0.69	0.98	0.85	0.83	1.00	0.50	0.47	0.34	0.45	0.42	0.47	0.30	0.30
QT	−0.34	0.65	0.57	0.60	0.57	0.59	0.25	0.50	1.00	0.98	0.69	0.97	0.99	0.97	0.23	0.44
QT_2	−0.44	0.62	0.52	0.51	0.53	0.53	0.26	0.47	0.98	1.00	0.64	1.00	0.98	1.00	0.36	0.56
QA	−0.12	0.44	0.43	0.50	0.40	0.43	0.12	0.34	0.69	0.64	1.00	0.64	0.67	0.64	−0.04	0.11
QA_2	−0.45	0.61	0.52	0.50	0.51	0.52	0.23	0.45	0.97	1.00	0.64	1.00	0.98	1.00	0.36	0.56
QB	−0.43	0.67	0.50	0.53	0.48	0.52	0.18	0.42	0.99	0.98	0.67	0.98	1.00	0.98	0.27	0.49
QB_2	−0.44	0.62	0.52	0.50	0.52	0.52	0.25	0.47	0.97	1.00	0.64	1.00	0.98	1.00	0.37	0.56
DM	0.62	0.26	0.16	−0.19	0.25	0.06	0.44	0.30	0.23	0.36	−0.04	0.36	0.27	0.37	1.00	0.95
DM_2	−0.69	0.39	0.23	−0.06	0.29	0.13	0.39	0.30	0.44	0.56	0.11	0.56	0.49	0.56	0.95	1.00

(b) Correlation Coefficients: Bifunctional Molecules, CIS Transformation

π	1.00	−0.56	0.06	0.33	0.17	0.30	0.06	0.12	−0.52	−0.51	−0.47	−0.52	−0.54	−0.52	0.21	0.15
σ	−0.56	1.00	0.35	0.22	0.30	0.12	0.13	0.29	0.65	0.59	0.67	0.60	0.62	0.59	−0.25	−0.09
$^0\chi$	0.06	0.35	1.00	0.86	0.79	0.74	0.13	0.79	0.50	0.50	0.55	0.50	0.45	0.49	0.03	0.20
$^1\chi$	0.33	0.22	0.86	1.00	0.79	0.87	0.09	0.73	0.47	0.43	0.54	0.44	0.40	0.43	−0.16	0.03
$^2\chi$	0.17	0.30	0.79	0.79	1.00	0.87	0.65	0.98	0.52	0.53	0.54	0.53	0.45	0.52	0.27	0.43
$^3\chi_p$	0.30	0.12	0.74	0.87	0.87	1.00	0.41	0.87	0.43	0.41	0.47	0.42	0.37	0.40	−0.01	0.13
$^3\chi_c$	0.06	0.13	0.13	0.09	0.65	0.41	1.00	0.65	0.19	0.22	0.15	0.21	0.14	0.22	0.56	0.59
$^3\chi_T$	0.12	0.29	0.79	0.73	0.98	0.87	0.65	1.00	0.47	0.47	0.48	0.47	0.40	0.46	0.26	0.40
QT	−0.52	0.65	0.50	0.47	0.52	0.43	0.19	0.47	1.00	0.90	0.93	0.90	0.84	0.90	−0.15	0.09
QT_2	−0.51	0.59	0.49	0.43	0.53	0.41	0.22	0.47	0.90	1.00	0.96	1.00	0.90	1.00	0.04	0.24
QA	−0.47	0.67	0.55	0.54	0.54	0.47	0.15	0.48	0.93	0.96	1.00	0.97	0.91	0.96	−0.16	0.08
QA_2	−0.52	0.60	0.50	0.44	0.53	0.42	0.21	0.47	0.90	1.00	0.97	1.00	0.90	1.00	0.00	0.20
QB	−0.54	0.62	0.45	0.40	0.45	0.37	0.14	0.40	0.84	0.90	0.91	0.90	1.00	0.90	−0.13	0.06
QB_2	−0.52	0.59	0.49	0.43	0.52	0.40	0.22	0.46	0.90	1.00	0.96	1.00	0.90	1.00	0.03	0.23
DM	0.21	−0.25	0.03	−0.16	0.27	−0.01	0.56	0.26	−0.15	0.04	−0.16	0.00	−0.13	0.03	1.00	0.95
DM_2	0.15	−0.09	0.20	0.03	0.43	0.13	0.59	0.40	0.09	0.24	0.08	0.20	0.06	0.23	0.95	1.00

Table IV. Stationary Phases

SE-30	apolar
squalane (SQUAL)	apolar
poly(ethylene glycol) (PEG)	medium polar
diethylene glycol succinate (DEGS)	polar

relation coefficient of the dependent variable with the predicted values of this variable from the regression equation considered. R^2 is the part of the total variance corrected for the mean explained by the regression equation.

RESULTS AND DISCUSSION

To find out the relationship between the different parameters, we calculated the correlation coefficients. The correlation matrix is shown in Table III. From these results one can see that the topological parameters are highly intercorrelated. There is also some correlation between the quantum chemical parameters, except for the dipole moment. DM and DM2 are different from these two groups, since their correlation coefficients with the other parameters are almost zero.

To see which parameters are important in describing the gas chromatographic behavior, we calculated the multiple regression equations. The regression equation is of the form

$$RI_i = ax_{1i} + bx_{2i} + cx_{3i} + \ldots nx_{ni}$$

where x_{1i} is one of the parameters for component i, RI_i is the retention index for component i, and n is the number of parameters considered.

The regression equations are calculated by using the best subset of variables and by means of a stepwise entry of the variables. The results are shown in Tables V–VII.

For the monofunctional molecules we came to the conclusion that for the apolar stationary phases the topological parameter can explain a great part of the total variance (2, 7). For the polar stationary phases a combination of topological and electronic parameters is necessary. σ (and to a smaller extent π) were chosen for this purpose in our earlier work (7). When the quantum chemical electronic parameters are included in the regressions, they are preferred to the experimental σ parameter.

For the bifunctional molecules we came to the conclusion that no parameter combination was really efficient enough to describe the specific interactions on the polar phases, since they were outliers of the regression equation (7). Therefore we considered these molecules in a separate data set. The results, including the quantum chemical parameters are shown in Tables VI and VII.

The results for the trans conformation (Table VI) show that the chromatographic behavior on apolar phases can still be explained, at least partially, by means of topological parameters. Indeed the topological parameter $^1\chi$ enters first the regression equation in the stepwise method. $^1\chi$ is also chosen as topological parameter in subsets with only a few parameters. Once a topological parameter is included in the regression, the next parameters entered are quantum chemical, describing the polarity of the molecules. This means that the retention indexes on these phases are largely proportional to the general size and volume of the molecules, described by their topological parameters. This feature is undoubtedly due to the

Table V. Monofunctional Molecules

										R
(a) SQUAL										
$^0\chi$										0.86
$^0\chi$	$^3\chi_p$									0.89
$^0\chi$	$^1\chi$	$^3\chi_p$								0.91
π	$^0\chi$	$^1\chi$	$^3\chi_p$							0.93
π	$^0\chi$	$^1\chi$	$^3\chi_p$	QA2						0.94
π	$^0\chi$	$^1\chi$	$^3\chi_p$	QA2	DM					0.96
π	$^0\chi$	$^1\chi$	$^2\chi$	$^3\chi_p$	QA2	DM				0.98
π	σ	$^0\chi$	$^1\chi$	$^2\chi$	$^3\chi_p$	$^3\chi_t$	QT2	QA	DM	0.997
(b) SE-30										
$^0\chi$										0.78
$^0\chi$	$^3\chi_p$									0.82
$^3\chi_p$	$^0\chi$	σ								0.84
$^0\chi$	$^3\chi_p$	σ	DM							0.91
$^0\chi$	$^3\chi_p$	σ	DM	QA2						0.91
$^0\chi$	$^1\chi$	$^3\chi_p$	σ	DM	QA2					0.93
$^0\chi$	$^1\chi$	$^2\chi$	$^3\chi_p$	σ	DM	QA2				0.97
$^0\chi$	$^1\chi$	$^2\chi$	$^3\chi_p$	σ	DM	QA2	π			0.99
(c) DEGS										
$^3\chi_t$										0.26
π	$^3\chi_t$									0.45
π	$^3\chi_t$	$^1\chi$								0.58
π	$^3\chi_t$	$^3\chi_p$	QA							0.71
π	$^0\chi$	$^1\chi$	$^3\chi_t$	QA						0.75
π	$^0\chi$	$^1\chi$	$^2\chi$	$^3\chi_t$	QA					0.80
π	$^0\chi$	$^1\chi$	$^2\chi$	$^3\chi_t$	QA	D				0.87
π	$^0\chi$	$^1\chi$	$^2\chi$	$^3\chi_t$	$^3\chi_p$	QA	D			0.95
π	$^0\chi$	$^1\chi$	$^2\chi$	$^3\chi_p$	$^3\chi_t$	QA	DM	QT2	σ	0.95
(d) PEG										
$^2\chi$										0.38
$^2\chi$	π									0.64
$^2\chi$	π	QA2								0.69
$^2\chi$	π	QA2	DM							0.74
π	$^0\chi$	$^2\chi$	QA2	DM						0.87
π	$^0\chi$	$^1\chi$	$^2\chi$	QA2	DM					0.91
π	σ	$^0\chi$	$^1\chi$	$^2\chi$	$^3\chi_p$	QA2	DM			0.94

Table VI. Bifunctional Molecules—TRANS

						R
			(a) SQUAL			
$^1\chi$						0.82
$^1\chi$	QA2					0.88
π	$^3\chi_p$	QA				0.92
π	$^3\chi_p$	$^3\chi_t$	QA			0.94
π	$^3\chi_p$	$^3\chi_t$	QA	QT		0.95
π	$^3\chi_p$	$^2\chi$	W	QT2	QA2	0.95
			(b) SE-30			
$^1\chi$						0.73
$^1\chi$	QA2					0.85
π	QT2	QA2				0.90
π	W	QT2	QA2			0.91
π	$^3\chi_p$	$^3\chi_t$	QT2	QA2		0.92
π	σ	$^3\chi_p$	$^3\chi_t$	QA2	QT2	0.94
			(c) DEGS			
QA						0.41
QA	QT					0.44
QA	QT	σ				0.59
QA2	QT2	σ	π			0.61
QA2	QT2	σ	π	$^1\chi$		0.69
			(d) PEG			
QA						0.27
QA	QT					0.43
$^3\chi_p$	QT	QA				0.46
π	QT2	$^1\chi$	QA2			0.52
π	$^1\chi$	QT2	QA2	σ		0.67

predominant role of the London dispersion forces in the intermolecular interaction in these cases (*14*). When this effect is filtered out of the total variance, the residual variance is due to polarity effects, most adequately described by the quantum chemical parameters QA, QA2, and QT2, accounting for both local and global polarity.

The results for the polar stationary phases are shown in Tables VIc and Vd. Here the first parameter entered in the two regression methods is the quantum chemical parameter QA, describing the local polarity. The next parameter entered is QT. Both parameters together explain about 45% of the total variance of the two polar stationary phases PEG and DEGS. The topological parameters are entered after the effect of polarity is filtered out of the total variance. This means that specific interactions are the most important on these polar stationary phases. The effect of the global size and volume of these molecules is clearly of less importance here than for the monofunctional molecules. These results indicate also that the specific interactions for bifunctional molecules are much better described by the quantum chemical parameters than by σ, since σ is of little importance in these regression equations. The reason for this failure could be due to nonadditivity of the used σ values.

The results for the cis conformations (Table VII) are analogous. For the apolar stationary phases the topological parameters are again the most important ones. For the polar stationary phases the quantum chemical parameters explain the most important part of the variance. The dipole moment and squared dipole moment are here more important than for the trans configuration as they are included in nearly all the best subsets. Since, in the set of parameters used the change of conformation is almost exclusively reflected in the dipole moments, the choice of the dipole moment or squared dipole moments in the regressions can be due to the fact that the cis conformation is the most logical conformation when interaction with the stationary phase takes place. The quantitative results, as reflected by the R or R^2, are however about the same for the two conformations. If the cis conformation is the most probable conformation, one could expect that the quantum chemical parameters for the cis conformation should be more efficient and so result in better correlation coefficients for the regression equations. The reason that this trend is not found could be due to the fact that the parameters describing the local polarity (QA, QA2, QB, QB2) are still much more important than the dipole and squared dipole moment. Since the quantum chemical calculations indicate that the influence of conformation on these parameters is almost negligible, the quantitative results for the regressions are about the same.

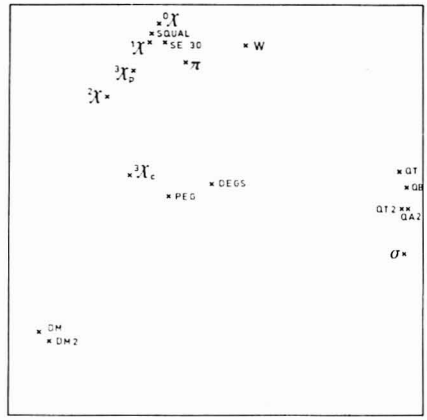


Figure 2. Factor analysis of the data set consisting of monofunctional molecules.

To confirm these results, we carried out factor analysis. To find out the intercorrelations in the system factor analysis reduces the total amount of variables to a few fundamental or latent variables. These latent variables are a linear combination of the original variables explaining as much as possible of the total variance.

In the three data sets (monofunctional, bifunction-trans, bifunctional-cis) the factor analysis results in the extraction of three important factors, explaining together about 85–90% of the total variance. In Figures 2–4 one can see that the topological parameters, the quantum chemical parameters QA, QB, and QT, the apolar stationary phases, and the polar stationary phases form clusters. This means they are related to each other. The cluster of the topological parameters is in all three data sets in the neighborhood of the apolar stationary phases. For the monofunctional molecules (Figure 2), these parameters form even one cluster.

For the monofunctional molecules one can see that the apolar stationary phases contain very analogous information, since they are situated in the same cluster. The parameter σ is related to the quantum chemical parameters QA to QT, while the dipole and the squared dipole moment are rather distant from all the clusters.

For the bifunctional molecules (Figures 3 and 4), the clusters of the quantum chemical parameters are much closer to the cluster of the polar stationary phases. They even form nearly one cluster. The difference between the trans and cis conformation is mainly situated in the localization of the dipole and squared dipole moment. These parameters are closer to the polar stationary phases for the cis conformation than for the trans conformation. This is in agreement with the fact that these parameters are more important in the cis than in the trans conformation in the regressions. One can also see

Table VII. Bifunctional Molecules—CIS

								R
				(a) SQUAL				
$^1\chi$								0.82
$^1\chi$	QA2							0.89
$^1\chi$	QA2	π						0.91
$^1\chi$	QA2	QT2	π					0.92
$^1\chi$	$^3\chi_p$	QA2	QT2	π				0.94
$^2\chi$	$^3\chi_t$	W	QT	QB	π			0.96
DM2	π	$^3\chi_p$	W	QT	QB	DM		0.97
DM	π	$^3\chi_p$	W	QT	QA2	QB	DM2	0.98
				(b) SE-30				
$^1\chi$								0.73
$^1\chi$	QA2							0.86
$^1\chi$	QA2	π						0.88
$^1\chi$	QA2	QT2	π					0.90
$^1\chi$	$^3\chi_p$	QA2	QT2	π				0.91
DM	W	QT	QB	DM2	π			0.94
DM	W	QT	QB	DM2	π	QA2		0.96
DM	W	QT	QB	DM2	π	QA2	$^1\chi$	0.97
DM	π	$^2\chi$	$^3\chi_t$	W	QT	QA2	QB DM2	0.98
				(c) DEGS				
QB								0.44
DM2	QA2							0.48
π	QT	QB						0.57
π	QT	QB	σ					0.63
π	QT	QB	σ	DM2				0.63
DM	π	QA2	σ	$^2\chi$	DM2			0.74
DM	π	σ	$^0\chi$	QT2	QA2	DM2		0.82
				(d) PEG				
QB								0.30
QB	DM2							0.37
QA2	DM	DM2						0.58
DM2	QB	QT	DM					0.63
DM2	π	QT	QB	DM				0.73

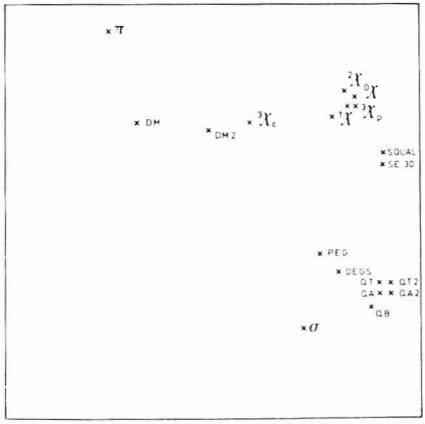


Figure 3. Factor analysis of the data set consisting of bifunctional molecules in the trans conformation.

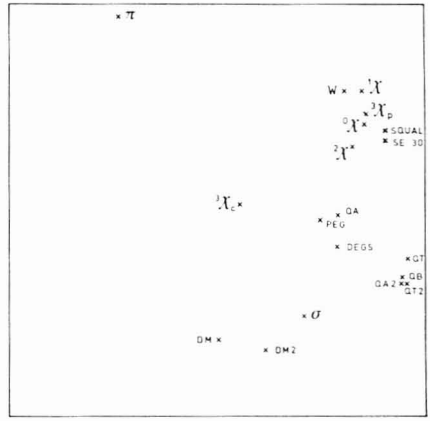


Figure 4. Factor analysis of the data set consisting of bifunctional molecules in the cis conformation.

that the other quantum chemical parameters are still more related to the polar stationary phases, than DM and DM2.

The retention indexes used were not corrected for adsorption so that some of the variance may be due to the fact that we did not only consider partition between the gas and the liquid phase but mainly partition and (perhaps) some adsorption. This is a not unusual approach with parameters, taken to a large degree from pharmacology such as π, σ, etc. Indeed pharmacological activity usually is determined by many different mechanisms (resorption from the gastrointestinal tract, transport, interaction with the receptor, etc.).

ACKNOWLEDGMENT

The authors thank L. Maes for technical assistance.

LITERATURE CITED

(1) Michotte, Y.; Massart, D. L. J. Pharm. Sci. 1977, 66, 1630-1632.
(2) Buydens, L.; Massart, D. L. Anal. Chem. 1981, 53, 1990-1993.
(3) McGregor, T. R. J. Chromatogr. Sci. 1979, 17, 314-316.
(4) Millership, J. S.; Woolfson, A. D. J. Pharm. Pharmacol. 1978, 30, 483-485.
(5) Chrétien, J. R.; Dubois, J. E. Anal. Chem. 1977, 49, 747-756.
(6) Chrétien, J. R.; Dubois, J. E. J. Chromatogr. 1978, 158, 43-56.
(7) Buydens, L.; Coomans, D.; Vanbelle, M.; Massart, D. L. J. Pharm. Sci., in press.
(8) Hansch, C. In "Drug Design"; Ariens, E. J., Ed.; Academic Press: New York, 1971; Chapter 2.
(9) Martin, Y. C. "Quantitative Drug Design"; Marcel Dekker: New York and Basal, 1978.
(10) Kier, L. B.; Hall, L. H. "Molecular Connectivity in Chemistry and Drug Research"; Academic Press: New York, 1976.
(11) Kier, L. B.; Hall, L. H. J. Pharm. Sci. 1981, 70, 583-584.
(12) Shorter, J. In "Correlation Analysis-Recent Advances"; Chapman, N. B., Shorter, J., Ed.; Plenum Press: New York, 1978.
(13) Amidon, G. L.; Anik, S. T. J. Pharm. Sci. 1976, 65, 801-806.
(14) Atkins, P. W. "Physical Chemistry"; Oxford University Press: Oxford, 1978.
(15) Pople, J. A.; Beveridge, D. L. "Approximate Molecular Orbital Theory"; McGraw-Hill: New York, 1970.
(16) Roothaan, C. C. J. Rev. Mod. Phys. 1951, 23, 69-89.
(17) Pople, J. A.; Gordon, M. J. J. Am. Chem. Soc. 1976, 89, 4253-4261.
(18) McReynolds, W. O. "Gas Chromatographic Retention Data"; Preston Technical Abstracts Co.: IL, 1966.
(19) Engleman, L.; Frane, J. W.; Jennrich, R. I. In "BMDP-79"; Dixon, W. J., Brown, M. B., Eds.; University of California Press: Berkeley-Los Angeles-London, 1979.

RECEIVED for review July 19, 1982. Accepted December 15, 1982. The authors thank F.G.W.O. for financial support.

Comparison of Gas Chromatography/High-Resolution Mass Spectrometry and Mass Spectrometry/Mass Spectrometry for Detection of Polychlorinated Biphenyls and Tetrachlorodibenzofuran

Robert D. Voyksner[1] and J. Ronald Hass*

National Institute of Environmental Health Sciences, P.O. Box 12233, Research Triangle Park, North Carolina 27709

G. Wayne Sovocool

U.S. Environmental Protection Agency, EMSL-LV, QAD, P.O. Box 15027, Las Vegas, Nevada 89114

Maurice M. Bursey

Department of Chemistry, University of North Carolina, Chapel Hill, North Carolina 27514

Mass spectral techniques for environmental samples which receive little cleanup were evaluated. Analyses on identical samples of PCB's and TCDF by mass spectrometry/mass spectrometry (MS/MS) and gas chromatography/high-resolution mass spectrometry (GC/HRMS) were compared. For the TCDF samples the use of GC/MS/MS was also compared with these two techniques. On comparison of the quantitative results, the direct probe MS/MS analysis was 2-10 times higher than the GC/HRMS or GC/MS/MS values. Matrix effects, for a 10 μg/μL butyl stearate matrix, were shown to increase the signal intensity by a factor of 17 for GC introduction of TCDF while the same sample by the direct probe showed a loss in intensity relative to the nonmatrix standard. The advantages and limitations of the methods, the necessity of multiion or reaction detection to ensure specificity, the ability to detect interferences, and the validity of the methodologies are discussed.

The validity of a technique for environmental analysis is dependent on its ability to obtain adequate sensitivity to detect the analyte and enough specificity to ensure the absence of interferences. This criterion is often impossible to satisfy because sensitivity is limited and the nature of possible interferences is unknown. The evaluation of a new technique can be based on the less rigorous criterion that another independent technique gives the same results. Though this approach is fallible (both procedures could detect the same interferences) it is useful in evaluating different methodologies for complex sample characterization.

Most environmental analyses involving mass spectrometry as the detection method use one of two general approaches: (a) to employ extensive cleanup procedures which minimize the need for mass spectral selectivity (*1*, *2*), (b) to use specific mass spectral techniques to minimize the effect of interferences. The latter approach has the advantages of speed, smaller sample volumes, and fewer possibilities for analyte loss. These specific mass spectral techniques include chemical ionization (CI) mass spectrometry (*3*, *4*), atmospheric pressure ionization mass spectrometry (*5*), mass spectrometry/mass spectrometry (MS/MS) (*6-8*), gas chromatography/low- or high-resolution mass spectrometry (GC/LRMS or GC/HRMS) (*9-11*), and gas chromatography/mass spectrometry/mass spectrometry (GC/MS/MS) (*12*).

The capability of MS/MS for structural elucidation and quantitative analysis has been investigated (*6-8*, *13*, *14*). The first analyzer provides nominal mass separation of the analyte from the matrix. The selected ion undergoes collisional activation (CA) to form structurally relevant fragments. The main advantage is fast analysis time; probe samples can take from a fraction of a minute to a few minutes. The analyses of cocaine in leaves; benzoylecgonine, cocaine, hippuric acid, and glucose in urine; and methylnaphthalenes, anthracene, quinoline, tetrahydroisoquinoline, and other polycyclic compounds in coal tar have been reported in recent literature (*13-16*). The initial mass analysis and the precursor/daughter

[1] Also at the University of North Carolina, Chapel Hill, NC.

0003-2700/83/0355-0744$01.50/0 © 1983 American Chemical Society

identification eliminate most of the chemical noise present and permit low nanogram to picogram detection limits. These advantages have made MS/MS an attractive technique for environmental analysis.

GC/HRMS analysis provides an initial separation of the analyte from matrix by differences in the partition coefficient of the components between stationary and mobile phases, rather than by mass. This type of separation provides isomer information that would be lost if separation were based on mass alone. The HRMS detection adds specificity to the analysis by requiring the signal recorded to have the exact mass, within a narrow range, corresponding to the analyte. The removal of chemical noise by HRMS permits picogram detection limits.

The GC/MS/MS analysis has all the advantages discussed for MS/MS, except for short analysis time. The use of the GC as the means of sample introduction increases specificity of the analysis with a sacrifice in time and is only appliable to gas chromatographable compounds. The specificity requirements are that if a compound in a certain retention time window shows a particular parent–daughter ion relationship, the technique should provide a valid environmental analysis.

This paper compares the advantages and disadvantages of quantitative analysis by MS/MS and GC/HRMS of polychlorinated biphenyls (PCB's) and tetrachlorodibenzofuran (TCDF) in fat, blood, or oil matrix. For the TCDF sample GC/MS/MS analysis was performed for further evaluation of the mass spectrometric techniques.

Polychlorobiphenyls are a widespread environmental contaminant detected in various biological fluids and tissues (*17–19*). These compounds and their associated impurities, polychlorodibenzofurans (*20–22*) have been investigated to determine their toxicological effects on humans. These samples provide a challenging test for the above MS techniques, because several types of interferences have been reported in GC/LRMS analysis (*23–25*).

The methodology evaluated for the analyses was based on optimizing the mass spectral techniques to provide the best sensitivity and specificity. Since both classes of compounds gave intense molecular ions under electron impact (EI) conditions and many biological molecules do not, EI was chosen over CI as the mode of ionization. The GC/HRMS analysis was performed by monitoring the $[M]^{+\cdot}$ and $[M + 2]^{+\cdot}$ ions while observing the exact mass, retention time, and $[M]^{+\cdot}/[M + 2]^{+\cdot}$ ratio. Deviations from the standard values indicated the presence of interferences. The MS/MS analyses carried out on the same samples monitored the loss of one and two chlorine atoms from the $[M]^{+\cdot}$ ion for PCB's and the loss of ·COCl and Cl· for TCDF. The analyses demanded that the ratio of the two observed losses be the same as that of a standard in order to demonstrate the presence of the analyte and the absence of interferences.

Quantitation of PCB's has always presented problems (*24–27*). It is reasonable to assume that PCB quantitation will become validated when each relevant isomer is synthesized and its relative response measured. Such an undertaking is out of the scope of this paper. Rather, Aroclor 1254 standards were used because they resembled the isomer distribution of the fat samples. The TCDF sample presented no quantitation problems since only the one isomer (the 2,3,7,8 isomer) is present and the standard was available for it.

EXPERIMENTAL SECTION

To facilitate comparisons the same standards and samples were analyzed by each technique within days of each other and kept cold between analyses. The blood samples were extracted with hexane, the animal fat samples with benzene, and the human fat samples with ether. All samples were further purified by gel permeation chromatography. Each sample was evaporated to low volume then diluted with a known volume (0.1–1.0 mL) with the respective solvent. Monsanto Aroclor 1254 was used for the PCB standards, which ranged from 1 pg/μL to 100 ng/μL. The TCDF sample in an oil matrix, used for animal feed studies, was made from a certified isomeric pure 2,3,7,8-TCDF standard and had a known concentration of 2 ng/μL. Standards ranging from 200 pg/μL to 13 ng/μL were made by spiking various amounts of pure 2,3,7,8-TCDF into the blank and diluting to volume with toluene. Aliquots of 0.5–2.0 μL were used in the analyses.

Analyses were performed on the VG Micromass ZAB-2F mass spectrometer equipped with a Finningan-INCOS 2300 data system.

GC/HRMS Analysis. The samples were analyzed by on-column injection on a 20 M, OV-1 (Supelco, Inc.) or a 20 M, SE-30 (J+W Scientific) fused silica column inserted directly into the mass spectrometer source. After the solvent front eluted, the temperature was programmed ballistically to 150 °C and then programmed to 250 °C at 8 °C/min. The acquisition started 4 min after the temperature program was initiated. The mass spectrometer was operated at 5000 or 10 000 resolution (10% valley), at 200 μA trap current, 8 keV accelerating voltage, 70 eV electron energy, and a source temperature of 220–240 °C. Either the C_6F_{11} ion (for PCB's) or the C_7F_{11} ion (for TCDF) of PFK was used as the lock mass for the VG digital multiple ion detection (MID) unit. The accelerating voltage scan of the MID unit was synchronized by a start of scan pulse from the data system (*28, 29*). A 200–300 ppm window was scanned for each monitored ion and the resulting signal stored in profile mode at a rate of 75 μs/point. The positions of the centroids for the peak within the window enabled the determination of the exact mass of the signal.

The MS/MS Analysis. The magnetic field was set to pass $[M]^{+\cdot}$ ions of either m/z 358 (PCB's) or 304 (TCDF). The electrostatic analyzer (ESA) was scanned to observe the transitions $[M]^{+\cdot} \rightarrow [M - Cl]^{+}$ and $[M]^{+\cdot} \rightarrow [M - 2Cl]^{+\cdot}$ for the hexachlorobiphenyls and for TCDF the $[M]^{+\cdot} \rightarrow [M - Cl]^{+}$ and $[M]^{+\cdot} \rightarrow [M - COCl]^{+\cdot}$ transitions. The mass spectrometer was operated at a primary ion resolution of 800, 200 μA trap current, 7 kV accelerating voltage, 70 eV electron energy, and at a source temperature of 200–240 °C. Helium was used as the collison gas at an analyzer gauge pressure of 1.5×10^{-7} torr which was about 2×10^{-4} torr in the collision cell (*30*).

The GC/MS/MS Analysis. This analysis was performed under the same conditions described for the MS/MS analysis, but only the COCl loss was observed. The TCDF was chromatographed on a DB-5, 20 M fused silica column (J+W Scientific), which was coupled directly into the mass spectrometer source. The column was temperature programmed from 200 to 280 °C at 16 °C/min. Acquisition began 3.5 min after the temperature program started.

The HRMS Analysis. This analysis was performed under the same conditions as described for the GC/HRMS except the blood samples were introduced by direct probe. The C_9F_{13} ion of PFK was used as the lock mass for the MID unit, and a 200 ppm window, centered on the exact mass for the $[M]^{+\cdot}$ and $[M + 2]^{+\cdot}$ ions of hexachlorobiphenyl, was scanned in 0.2 s for a total scan time of 0.7 s.

RESULTS AND DISCUSSION

PCB Analysis. The GC/HRMS analysis was performed by monitoring the $[M]^{+\cdot}$ and the $[M + 2]^{+\cdot}$ ions for the tetra-, penta-, and hexachlorobiphenyls. Each window was observed for 0.2 s with a total scan time of 1.68 s. The isomer resolution (Figure 1) for the Aroclor standards and samples permited quantitation of the individual isomers, but for this comparison only the total hexachlorobiphenyl concentration was determined. The amounts of the various hexachlorobiphenyls in Aroclor 1254 have been determined (*31*), enabling the use of the Aroclor for a standard. The areas of all the hexachlorobiphenyls were summed and the $[M]^{+\cdot}/[M + 2]^{+\cdot}$ ratio was checked to confirm the expected ratio for a compound containing six chlorines. The quantitative results must depend on the similarity of the blood and fat samples to the Aroclor standard, because of different responses for the various isomers. This assumption was reasonable for the fat samples but not for the blood samples. The calibration curve was linear

Table I. Quantitative Results for the Hexachlorobiphenyl Analysis[a]

	MS/MS		GC/HRMS		HRMS	
sample	amt, μg/g	$[M - 2Cl]^{+\cdot}/[M - Cl]^{+}$	amt, μg/g	$[M]^{+\cdot}/[M + 2]^{+\cdot}$	amt, μg/g	$[M]^{+\cdot}/[M + 2]^{+\cdot}$
fat no. 1	40.5	1.5	16.5	0.53		
fat no. 2	35.9	1.7	14.5	0.50		
fat no. 3	58.6	1.4	14.9	0.53		
fat no. 4	15.6	1.1	1.7	0.50		
blood no. 1	0.05	2.4	0.003	0.50	0.02	0.47
blood no. 2	0.02	1.2	0.006	0.56	0.01	0.50
H-fat no. 1	0.53	1.7	0.10	0.53		
standards		2.1		0.51		0.52

[a] The standard deviations for direct probe work are usually less than 20% of the value and those for GC work are less than 5% of the value.

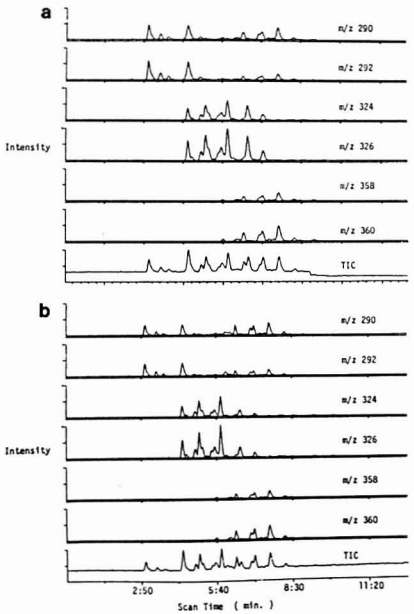


Figure 1. Reconstructed ion chromatograms for the $[M]^{+\cdot}$ and $[M + 2]^{+\cdot}$ windows for the tetra-, penta-, and hexachlorobiphenyls: (a) response for the 1 ng standard of Aroclar 1254; (b) response for a fat sample.

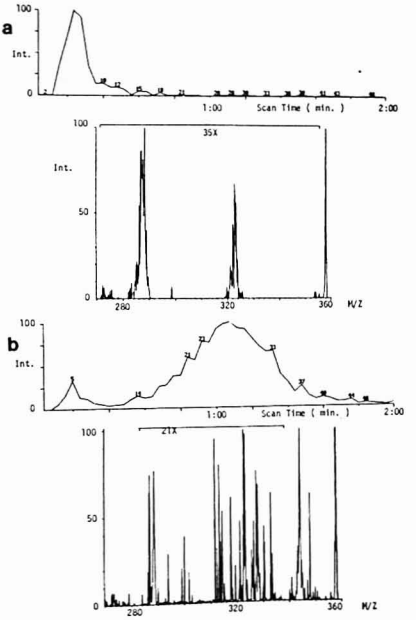


Figure 2. The total ion current and peak profile for the loss of Cl· and 2Cl· from the molecular ion of hexachlorobiphenyl: (a) trace for 10 ng of Aroclor 1254 standard; (b) response for a blood sample.

from 100 ng to 20 pg, with a correlation coefficient of 0.998. The detection limits were determined to be about 2 pg in each case. The summary of the quantitative results is given on Table I. The similarity of the peak ratios and the lack of interfering signals in the 300 ppm window indicate that there were no interferences in the analysis.

In the MS/MS analysis the m/z 358 ion of hexachlorobiphenyl was selected and the ESA was scanned to cover the mass range from 270 to 360 in 2.7 s. No information about the various isomers could be obtained since there is no way to resolve them. This presents problems if the quantity of a particular isomer is desired in a matrix of many isomers. The standards gave no signals other than the $[M]^{+\cdot} \rightarrow [M - Cl]^{+}$ and $[M]^{+\cdot} \rightarrow [M - 2Cl]^{+\cdot}$ transitions (Figure 2). The calibration was linear from 100 ng to 100 pg with a correlation coefficient of 0.995. The detection limits of 50 pg could be lowered to 10 pg when a 2 mass unit wide window was scanned in 0.5 s for each loss. The peak width was ignored because the kinetic energy release (KER) has been shown to depend on the chlorine substitution pattern of the biphenyls (32) and thus would vary because of different isomer content between samples and standards. Rather, the $[M]^{+\cdot} \rightarrow [M - 2Cl]^{+\cdot}/[M]^{+\cdot} \rightarrow [M - Cl]^{+}$ ratio was taken to detect interferences and measure similarity of the isomer content in the sample with the standard. Ratios different than the standard ratio indicate there is an interference or a dissimilarity in isomer content between sample and standard. The ratio of $[M]^{+\cdot} \rightarrow [M - 2Cl]^{+\cdot}/[M + 2]^{+\cdot} \rightarrow [M - 2Cl]^{+\cdot}$ has been proposed to be more suitable for the detection of interferences since this ratio should remain independent of the hexachlorobiphenyl isomer distribution. In principle it is straightforward to switch

primary ion beams by alteration of the accelerating and electric sector potentials at fixed magnetic field strength to perform this multiple reaction monitoring (*33*). This type of switching only requires a few milliseconds and there is no increase in analysis time. While at first thought, this would seem to add specificity to the assay, it is not the case when you consider the probability that an interfering substance would be present which gave an $[M - Cl]^+$ and $[M - 2Cl]^{+\cdot}$ peak. It is very unlikely any compound not containing Cl would give both those daughter ion peaks. Thus, if the first criteria were met, the compound would likely also give appropriate signals from the ion 2 daltons higher in mass. Therefore, the increase in experimental complexity would result in a reduction of *S:N* (one must decrease the dwell time to increase the number of different masses monitored) with the only apparent gain being that the analysis is independent of the hexachlorobiphenyl isomer distribution. The samples show a completely different elution profile (Figure 2) with possible interferences in the analyte windows. The comparison of the results (Table I) shows the values by MS/MS are 2 to 10 times larger than the GC/HRMS values. The results obtained by direct probe HRMS on the blood samples are higher than those obtained by GC/HRMS. This might indicate that the majority of the interferences are removed by the high-resolution techniques with prior chromatographic separation. These results suggest that the direct probe HRMS and MS/MS techniques are detecting more interferences, possibly due to aliphatics (cholesterol, etc.) in blood and fat (large $[M - CH_3]^+$ present) or from hepta-, octa-, nona-, and decachlorobiphenyls. These higher mass compounds can undergo fragmentation in the source to produce ions that coincide with the molecular ion of hexachlorobiphenyl (m/z 358$^+$). These ions are transmitted through the magnet and if they undergo the same dissociation as the $[M]^{+\cdot}$ ion of hexachlorobiphenyl, the loss of Cl and 2Cl, they can cause interferences in the analyses. For example an octachlorobiphenyl shows EI fragment, $[M - 2Cl]^{+\cdot}$, ions of m/z 358$^+$ in the source. This fragment is transmitted through the magnet and undergoes the subsequent dissociations $[M - 2Cl]^{+\cdot} \rightarrow [M - 3Cl]^+$ and $[M - 2Cl]^{+\cdot} \rightarrow [M - 4Cl]^{+\cdot}$ which will cause interferences in the hexachlorobiphenyl analysis. The GC/HRMS is presumed to be the more accurate method since it gave lower quantitative results, which indicates less influence from the matrix. The accuracy of the analysis cannot be checked since the true levels in the samples are not known a priori.

Analysis of TCDF. The GC/HRMS analysis of TCDF in oil at 10 000 resolution monitored the 200 ppm $[M]^{+\cdot}$ and $[M + 2]^{+\cdot}$ windows along with the PFK lock mass of 292.9824. The total scan time was 0.73 s. The retention time observed from the SE-30 column was 8.1 ± 0.07 min (N = 15) after the temperature program initiation. In this time window there were no interferences or other isomers detected. The $[M + 2]^{+\cdot}/[M]^{+\cdot}$ ratio was 1.3 ± 0.05 (N = 15) which is the expected chlorine isotopic ratio for an ion with four chlorines. The centroid for the $[M]^{+\cdot}$ and $[M + 2]^{+\cdot}$ signals, calculated to be 303.9016 and 305.8986, respectively, did not deviate by more than 10 ppm from these values for all the runs (Figure 3). The calibration curve was linear from 200 pg to 13 ng, with a correlation coefficient of 0.996. The concentration of TCDF determined by this analysis was 2.1 ± 0.1 ng/μL (N = 3), in agreement with the known spiked concentration.

The MS/MS analysis observe the $[M]^{+\cdot} \rightarrow [M - Cl]^+$ and $[M]^{+\cdot} \rightarrow [M - COCl]^{+\cdot}$ transitions to give a total scan time of 1.45 s. The sample and standards produced similar recordings (Figure 4), but the sample eluted over a longer time span. The TCDF $[M]^{+\cdot} \rightarrow [M - COCl]^{+\cdot}/[M]^{+\cdot} \rightarrow [M - Cl]^+$ ratio for the standards had the value 1.4 ± 0.1 (N = 17). The sample ratio was 1.7 ± 0.1 (N = 3) and, therefore, indicated

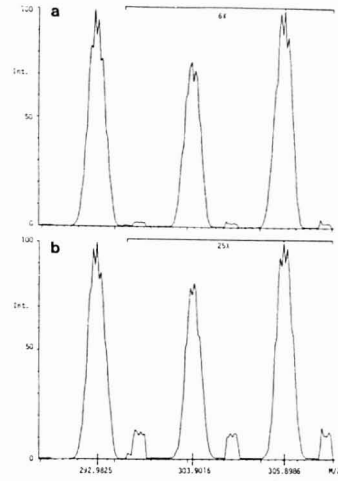


Figure 3. GC/HRMS peak profiles for the $[M]^{+\cdot}$ ions of TCDF at 10 000 resolution: (a) 4 ng of standard; (b) the sample.

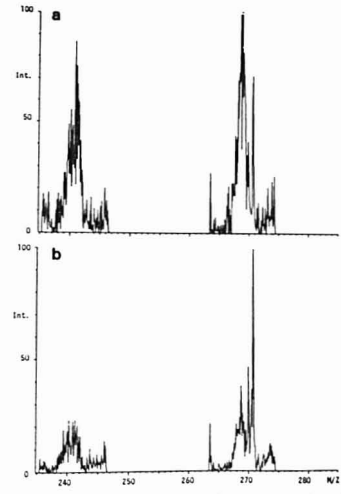


Figure 4. The total ion current for $[M]^{+\cdot} \rightarrow [M - Cl]^+ [M]^{+\cdot} \rightarrow [M - COCl]^{+\cdot}$ transitions of TCDF from the probe: (a) 4 ng standard; (b) the sample.

the presence of interferences. The KER's at half height (*34*) for the loss of Cl and COCl were 66 and 140 ± 5 meV (N = 6), respectively, for the TCDF standards. The sample showed a KER of 71 and 134 ± 6 meV (N = 3). The calibration over the same concentration range was linear with a correlation coefficient of 0.998. The results of the determination showed the concentration to be 3.4 ± 0.3 ng/μL (N = 3) and to differ significantly from those of the GC/HRMS determination.

These differences in the determined concentrations for the GC sample introduction as oppossed to the direct probe

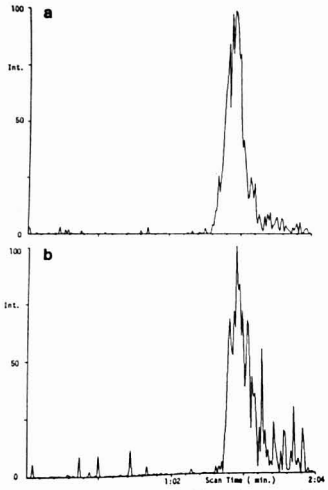


Figure 5. GC/MS/MS profile for the $[M]^{+\cdot} \rightarrow [M - COCl]^{+}$ transition of TCDF: (a) 4 ng of standard; (b) the sample.

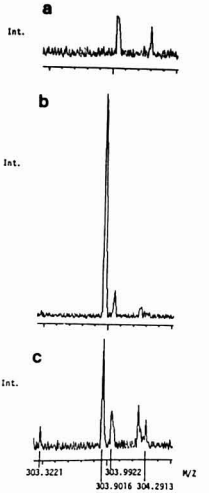


Figure 6. High-resolution (10 000) scan over the mass window transmitted dby MS/MS for the molecular ion of TCDF: (a) blank; (b) 4 ng of TCDF spiked into blank; (c) sample.

technique leave questions about the validity of the latter. To validate a technique, by the criterion defined above, the analysis was repeated by GC/MS/MS. Only the $[M]^{+\cdot} \rightarrow [M - COCl]^{+\cdot}$ transition was observed to reduce the scan time to 0.61 s. The retention time for TCDF from a DB-5 column was 4.9 ± 0.08 min (N = 15). The KER for the sample was 136 meV, which compared favorably with the standards (140 meV). Examination of the spectra did not reveal evidence of interference (Figure 5). The standard calibration curve was linear with a correlation coefficient of 0.997. From the calibration the concentration of TCDF was determined to be 1.9 ± 0.15 ng/μL (N = 3). This value is in agreement with the GC/HRMS, and both are lower by a factor of 1.7 than the MS/MS value.

Matrix Effects and Interferences. The validity of MS/MS for environmental analysis can be questioned in the limited number of cases examined. The advantages of speed and little sample preparation are, in our opinion, outweighed by the fact that the results were consistently and unpredictably high and did not agree with other techniques. It is not our opinion that GC/HRMS or GC/MS in void of interferences, but it seems clear that GC introduction reduces the probability of encountering interferences compared to direct probe techniques. The variance of the $[M]^{+\cdot} \rightarrow [M - COCl]^{+\cdot}/[M]^{+\cdot} \rightarrow [M - Cl]^{+}$ ratio for TCDF by MS/MS analysis indicated that an interference was present and that the analysis needed to be performed by another method. The high resolution (10000) observation of the mass window 303.4 to 304.4, which includes the mass range that would be selected by the first analyzer in MS/MS, reveals at least seven ions (Figure 6). The peaks at 303.9922 and 304.3082 are present in the blank. The 303.9016 ion is due to 2,3,7,8-TCDF present in the sample. The four peaks at 303.3221, 304.2513, 304.2883, and 304.2913 are interferences present in the sample but not found in the spiked blank.

The GC/HRMS technique proves to be more analyte specific by comparison since it has been demonstrated that components 20 ppm apart can be distinguished (*35*). The specificity of HRMS can be shown by the fact there are 72 elemental compositions which satisfy the valence laws, contain four chlorines, and are composed of C, H, N, O, and S within 20 ppm of TCDF. This number is reduced to 20 when the compositions that give the proper $[M + 2]^{+\cdot}/[M]^{+\cdot}$ ratio for a four chlorine compound are considered. On the other hand, the specificity of MS/MS analysis is partly dependent upon the particular instrumentation used in the analysis. For example in MIKES analysis, the daughter ion resolution, for the reaction $304^{+} \rightarrow 241^{+}$ of TCDF, is approximately 4 mass units wide. It is reasonable to assume that instrumentation which is capable of unit mass resolution of both parent and daughter ion (such as a triple quadrupole or BE linked scan techniques) would be subject to fewer interferences. Interferences also exist from high molecular weight matrix components undergoing metastable decompositions in the first field region and the flight tube. There are hundreds of compounds and metastable ions that could be within the unit mass window of TCDF that contain chlorine and oxygen. There is a high probability that these compounds will show losses of Cl and COCl similar to TCDF. Thus, it is speculated that there is a lower probability of exact mass interferences when compared to the probability of interference with separation based on reactions. The specificity of MS/MS should be enhanced by GC sample introduction because the analyte must now show a particular retention time and fragmentation reaction.

The inability to obtain a true blank can greatly change the results for a direct probe analysis. Recent work showed the m/z 320 to m/z 257 transition for TCDD was reduced by one-third when 1 μg of methyl stearate was added to 100 pg of sample (*36*). Another example showed a decrease of the m/z 322 ion current of TCDD by 85% with the addition of 25 μg of squalane to the probe cup (*37*). Our results (Table II) showed a slight depression of ion current when 10 μg of butyl stearate was added to the cup with TCDF. The sample blank showed a drop in response of almost 50% compared to the standard in pure solvent. These matrix effects do no apply only to probe work but also to GC analysis as well: the sample blank (oil) doubled the response (area) of the TCDF signal over the response of TCDF in toluene (Table II). The most significant change recorded was the peak height. The butyl

Table II. Matrix Effects Observed for Both Mass Spectral Techniques for 4 ng of TCDF

matrix	MS/MS area	GC/HRMS rel area	GC/HRMS rel peak height
toluene (no matrix)	1.0	1.0	1.0
10 μg of butyl stearate	0.85	2.0	17.5
10 μg of oil	0.56	2.0	2.3

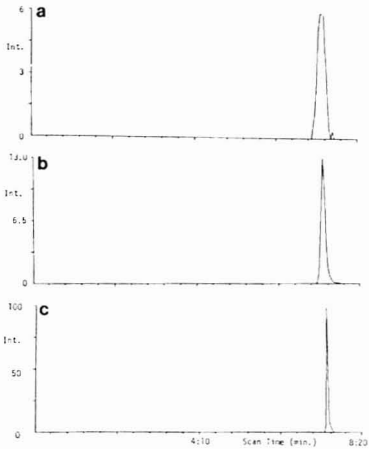


Figure 7. The matrix effects observed for a 4 ng TCDF sample from the column: (a) no matrix; (b) spiked blank (oil matrix); (c) 10 μg of butyl stearate.

stearate, which elutes seconds before the TCDF, seems to carry the analyte through the column, reducing chromatographic band spread and enhancing peak height (Figure 7). This Grob type effect of chromatographic band narrowing was also noticed to a lesser extent for the oil matrix. Few components of the matrix elute from the column before the TCDF, and this observation may possibly explain the smaller enhancement for the TCDF. These observations indicate the importance of obtaining an accurate blank, the use of isotopically labeled internal standards, or the use of standard addition methods for quantitative analyses.

ACKNOWLEDGMENT

We are grateful to Donald J. Harvan for his insight into the instrumental aspects of the analysis.

Registry No. TCDF, 30402-14-3; hexachlorobiphenyl, 26601-64-9; tetrachlorobiphenyl, 26914-33-0; pentachlorobiphenyl, 25429-29-2.

LITERATURE CITED

(1) Langhorst, M. L.; Shadoff, L. A. *Anal. Chem.* **1980**, *52*, 2037–2044.
(2) Lamparski, L. L.; Nestrick Y. J. *Anal. Chem.* **1980**, *52*, 2045–2054.
(3) Jennings, K. R. "Gas Phase Ion Chemistry"; Academic Press: New York, 1979; Vol. 2, 123–151.
(4) Hunt, D. F.; Harvey, T. M.; Russell, J. W. *J. Chem. Soc., Chem. Commun.* **1975**, *5*, 151.
(5) Mitchum, R. K.; Molec, G. F.; Korfmacher, W. A. *Anal. Chem.* **1980**, *52*, 2278–2282.
(6) Kondrat, H. W.; Cooks, R. G. *Anal. Chem.* **1978**, *50*, 51A–92A.
(7) McLafferty, F. W.; Bockhoff, F. M. *Anal. Chem.* **1978**, *50*, 69–75.
(8) Yost, R. A.; Enke, C. G. *Anal. Chem.* **1979**, *51*, 1251A–1264A.
(9) Gross, M. L. "High Performance Mass Spectrometry: Chemical Applications"; American Chemical Society: Washington, DC, 1978; pp 120–149.
(10) Kimble, B. J.; Gross, M. L. *Science* **1980**, *207*, 59.
(11) Tindall, G. W.; Wininger, P. F. *J. Chromatogr.* **1980**, *196*, 109–119.
(12) Harvan, D. J.; Hass, J. R.; Schraeder, J. L.; Corbett, B. J. *Anal. Chem.* **1981**, *53*, 1755–1759.
(13) Kondrat, R. W.; McClusky, G. A.; Cooks, R. G. *Anal. Chem.* **1978**, *50*, 2017–2021.
(14) Kruger, T. L.; Litton, J. F.; Kondrat, R. W.; Cooks, R. G. *Anal. Chem.* **1976**, *48*, 2113–2119.
(15) Zakett, D.; Shaddock, V. M.; Cooks, R. G. *Anal. Chem.* **1979**, *51*, 1849–1852.
(16) McClusky, G. A.; Kondrat, R. W.; Cooks, R. G. *J. Am. Chem. Soc.* **1978**, *100*, 6045–6051.
(17) Wasserman, M.; Wisserman, D.; Cycos, S.; Miller, H. J. *Ann. N.Y. Acad. Sci.* **1979**, *320*, 69–124.
(18) Kutz, F. W.; Strassman, S. C. Proceedings of the National Conference on Polychloronated Biphenyls Nov 19–21, 1975, Chicago, IL, pp 139–143.
(19) Risebrough, R. W.; Rieche, P.; Peakall, D. B.; Herman, S. G.; Kirven, M. N. *Nature (London)* **1968**, *220*, 1098.
(20) Goldstein, J. A.; Hass, J. R.; Linko, P.; Harvan, D. J. *Drug Metab. Dispos.* **1978**, *6*, 258–264.
(21) Buser, H. R.; Rappe, C.; Gara, A. *Chemosphere* **1978**, *7*, 439–449.
(22) Poland, A.; Glover, E.; Kende, A. S.; DeCamp, M.; Giandomenica, C. M. *Science* **1976**, *194*, 630.
(23) Ast, T.; Bozorgzadeh, M. H.; Wiebers, J. L.; Beynon, J. H.; Brenton, A. G. *Org. Mass Spectrom.* **1979**, *14*, 313–318.
(24) Cairns, T.; Siegmund, E. G. *Anal. Chem.* **1981**, *53*, 1183A.
(25) Albro, P. W.; Parker, C. E. *J. Chromatogr.* **1980**, *197*, 155–169.
(26) Albro, P. W.; Parker, C. E. *J. Chromatogr.* **1979**, *169*, 161–166.
(27) Eichelberger, J. W.; Harris, L. E.; Budde, W. L. *Anal. Chem.* **1974**, *46*, 227–231.
(28) Harman, D. J.; Hass, J. R.; Wood, D. *Anal. Chem.* **1982**, *54*, 332–334.
(29) Weiss, M.; Harvan, D. J.; Hass, J. R. 28th Annual Conference on Mass Spectrometry and Allied Topic, New York, NY, May 25–30, 1980, RPMP-6, p 602.
(30) Murgan, R. P.; Beynon, J. H.; Bateman, R. H.; Green, B. N. *Int. J. Mass. Spectrom., Ion Phys.* 1978, 28, 171–191.
(31) Albro, P. W.; Corbett, J. T.; Schroeder, J. L. *J. Chromatogr.* **1981**, *205*, 103–111.
(32) Hass, J. R.; Bursey, M. M.; Levy, L. A.; Harvan, D. J. *Org. Mass Spectrum.* **1979**, *14*, 319–325.
(33) Kondrat, R. W.; McClusky, G. A.; Cooks, R. G. *Anal. Chem.* **1978**, *50*, 2017–2021.
(34) Cooks, R. G.; Beynon, J. H.; Caprioll, R. M.; Lester, G. R. "Metastable Ions"; Elsevier: New York, 1973; pp 97–128.
(35) Hass, J. R.; Tondeur, Y., unpublished work NIEHS. Research Triangle Park, NC, 1981.
(36) Harvan, P. J.; Hass, J. R.; Busch, K. L. 27th Annual Conference on Mass Spectrometry and Allied Topics, Seattle, WA, June 3–8, 1979; RAMOC-10, pp 529–530.
(37) Baughman, R.; Meselson, M. "Chlorodioxins-Origin and Fate"; Blair, E. H., Ed.; American Chemical Society: Washington, DC, 1973; Chp. 10.

RECEIVED for review July 19, 1982. Accepted January 6, 1983.

Thermospray Interface for Liquid Chromatography/Mass Spectrometry

C. R. Blakley and M. L. Vestal*

Department of Chemistry, University of Houston, Houston, Texas 77004

The latest version of the thermospray LC/MS interface has been installed on a Biospect quadrupole mass spectrometer. This interface requires only minor modification of the commercial instrument with a single mechanical vacuum pump required in addition to the pumping system normally used for CI operation. It appears that this LC interface can readily be adapted to other quadrupole mass spectrometers. LC effluents are thermosprayed directly into the ion source and the excess vapor pumped away by the added mechanical pump which is directly coupled to the ion source through a port opposite the electrically heated thermospray vaporizer. This system provides stable vaporization and ionization at flow rates up to 2 mL/min of aqueous mobile phase. When used with mobile phases containing significant concentration of ions in solution (ca. 10^{-4} to 1 M) no external ionizing source is required to achieve detection of many nonvolatile solutes at the subnanogram level. With weakly ionized mobile phases a conventional electron beam is used to provide gas-phase reagent ions for chemical ionization of solute molecules.

During the past decade several laboratories have worked on the development of combined LC/MS systems; the results of these efforts have been amply reviewed (*1*, *2*). Much of this work has focused on dealing with the fact that the mass flows involved in conventional HPLC (ca. 1 g/min) are 2 or 3 orders of magnitude larger than can be accommodated by conventional mass spectrometer vacuum systems. The status of various approaches to overcoming the apparent incompatibility between liquid chromatography and mass spectrometry has recently been summarized by Arpino (*3*, *4*).

Our original approach to LC/MS employed laser heating to rapidly vaporize both the solvent and sample and molecular beam techniques to transport and ionize the sample while minimizing contact of the sample molecules with solid surfaces (*5*). The original apparatus used a large and expensive vacuum system and a 50-W CO_2 laser. Later we developed a greatly simplified version of this system by using oxy–hydrogen flames to vaporize the LC effluent and a substantially less elaborate vacuum system (*6*).

The earlier systems were designed to efficiently transfer the sample to either an electron impact (EI) or chemical ionization (CI) source while vaporizing and removing most of the solvent. In the latter version more than 50% of the sample was transferred to the CI ion source with only about 5% of the solvent vapor. This system gave satisfactory performance for a number of relatively nonvolatile samples and was used successfully with reversed-phase separations employing aqueous buffers at flow rates as high as 1 mL/min. The major problem with this system was that the vaporizer was difficult to control properly which often caused uncontrolled fluctuations in performance and some times frustrated attempts at application of the system to real analytical problems.

In the course of this work it was found that, under certain conditions, ions were produced even though the hot filament normally used to produce the primary ionizing beam was turned off (*7*). Initial measurements of mass spectra produced from nonvolatile compounds such as peptides, nucleosides, and nucleotides showed that the spectra were quite different from those obtained by chemical ionization and were, in fact, most similar to those obtained by field desorption.

Our recent efforts have focused on developing an electrically heated vaporizer which would allow more precise control of the solvent vaporization. This has recently been accomplished; the present version allows the stable vaporization of virtually any solvent including aqueous buffers at flow rates up to at least 2 mL/min. The use of this electrically heated vaporizer has greatly improved the stability and reproducibility of the vaporization of solvents and nonvolatile samples and it is now possible to predict with confidence the conditions appropriate for a particular solvent composition and flow rate. The availability of a stable, reproducible vaporizer has also allowed more definitive studies of the vaporization and ionization mechanisms to be conducted. The results of these studies have led to some further modifications of the apparatus which both improve the performance and further simplify the construction. the present system is readily adapted to any commercial quadrupole mass spectrometer equipped with a vacuum system suitable for CI operation. The only addition to the vacuum system is a single stage mechanical vacuum pump of moderate capacity (ca. 300 L/min).

Initially we used the electrically heated vaporizer with differential pumping of the vaporizer housing, but more recently we have obtained improved performance by vaporizing the total LC effluent directly into the ion source with the mechanical vacuum pump connected opposite the vaporizer. With this system any solvent can be accommodated at flow rates up to 2 mL/min. It now appears that the apparent incompatibility between LC and MS has been successfully overcome and that a truly practical LC/MS has been developed.

EXPERIMENTAL SECTION

Apparatus. A schematic diagram of the "thermospray" system presently in use is shown in Figure 1. This interface and ion source are much simpler than the earlier versions and require only minor modification of a commercial quadrupole mass spectrometer. The present version of the vaporizer consists of a few centimeters of 0.015 mm i.d. by 1.5 mm o.d. stainless steel tubing (Handy and Harmon, Morris Town, PA) which is brazed at one end into a copper block. The block is heated by two commercial 100-W cartridge heaters (Watlow, St. Louis, MO) normally operated at substantially below their rated power. A thermocouple is imbedded in the copper block to monitor the temperature of the vaporizer and may be used in conjunction with a proportioning controller to maintain the temperature of the block constant. The length of tubing immersed in the block is not particularly critical, but lengths on the order of 3 cm are presently used. It is very important that the stainless tube be in good thermal contact with the copper block; the brazed joint is essential. The vaporizer produces a supersonic jet of vapor, normally containing a mist of fine particles or droplets. This jet traverses the ion source of the mass spectrometer and enters directly into a 1 cm diameter pumping line which is connected to a 300 L/min mechanical vacuum pump. Modifications to the ion source include the use of a conical ion exit aperture (as shown in Figure 1) and high

0003-2700/83/0355-0750$01.50/0 © 1983 American Chemical Society

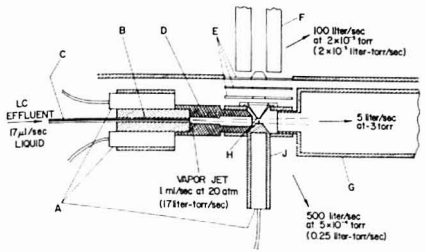


Figure 1. Schematic diagram of thermospray apparatus using electrically heated vaporizer: (A) 100-W cartridge heater; (B) copper block brazed to stainless steel capillary; (C) 1.5 mm o.d. × 0.15 mm i.d. stainless steel capillary; (D) thick-walled copper tube; (E) ion lenses; (F) quadrupole mass filter; (G) pump out line to mechanical pump; (H) ion exit aperture; (J) source heater.

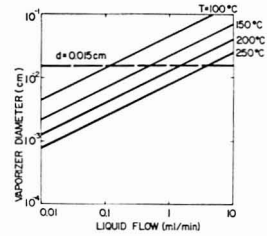


Figure 2. Relationship between vaporizer diameter and liquid flow rate for steady vaporization of water at the indicated vapor temperatures. The horizontal dashed line corresponds to the capillary nozzle used in the present work and the intersection with the isotherms gives the expected flow rate for steady vaporization at that temperature.

capacity source heater consisting of an 100-W cartridge heater imbedded in a copper rod which extends into the ion source cavity but does not intersect the main part of the jet. Except for the vaporizer, pump-out line, and source block, the thermospray LC/MS system is a commercial quadrupole mass spectrometer equipped for CI operation (Biospect, Scientific Research Instruments, Baltimore, MD).

At first it is somewhat surprising that this system can accommodate vaporizing up to 2 mL/min of liquid directly into the ion source without overloading the pumping systems since this corresponds to a gas flow which is about 100 times larger than that used with the mass spectrometer operated in the conventional CI mode. The addition of the mechanical vacuum pump connected directly to the source would only account for about 1 order of magnitude of increased capacity normally, but locating the pumping line directly opposite the thermospray vaporizer allows the supersonic jet to act as its own ejector pump. Thus the conductance of the pumping aperture is about 10 times as high as normal due to the highly directed flow of the jet. We have found that a 300 L/min mechanical pump is more than adequate to maintain stable performance at flow rates to 2 mL/min. It is essential that the pump be operated with gas ballast to avoid excess accumulation of liquid in the pump oil. Even then, it is important to service the pump frequently (usually daily) to drain out solvent and add pumping fluid.

RESULTS AND DISCUSSION

Design and Performance of the Vaporizer. The maximum velocity with which a superheated liquid may vaporize is given by

$$v_V = \left(\frac{m}{2\pi kT}\right)^{1/2} \frac{P_V(T)}{\rho L} \qquad (1)$$

where $P_V(T)$ is the vapor pressure at temperature T, m is the molecular mass, ρ is the density of the liquid, k the Boltzmann constant, and L is Avagodro's number. For steady vaporization from the capillary nozzle the vaporization velocity given by (1) must be equal to the velocity of the liquid flow in the capillary tube. Assuming that sufficient heat is supplied, the pressure and temperature of the vapor emerging from a given diameter capillary nozzle are determined by (1) and the liquid flow rate. This relationship is illustrated for water vapor in Figure 2. At a flow rate of 1.0 mL/min of water through the 0.015 cm i.d. capillary presently in use, steady vaporization produces vapor at approximately 183 °C and at a pressure of about 10.5 atm. Measurement of liquid pressures and temperatures in the jet confirm that the behavior is approximately as predicted by the model.

In the thermospray vaporizer the temperature of the copper block coupling the heaters to the stainless steel capillary is monitored by a thermocouple. For stable operation it is essential that good thermal contact be maintained between the copper block and the capillary; this is accomplished by brazing them together with a suitable silver alloy (e.g., 56% silver, cadmium free). The heat transfer from the copper block to the flowing fluid is then determined almost entirely by the temperature drop in the capillary tubing and at the solid–liquid interface. If the temperature were uniform over the length of the vaporizer, L, then for the cylindrical geometry used the resistance to heat flow is given by

$$R = \frac{1}{2\pi L}\left[\frac{\ln (b/a)}{k_s} + \frac{2}{nk_f}\right] \qquad (2)$$

where a and b are the inner and outer diameter, respectively, of the capillary tube, k_s is the thermal conductivity of the stainless steel tube ($k_s = 0.16$ W/(cm °C)) and k_f is the thermal conductivity of the liquid (for water $k_f = 6 \times 10^{-3}$ W/(cm °C)), and n is the Nusselt number for the liquid solid interface (8). Equation 2 is a rather crude approximation to the actual case because, while the temperature of the outer surface is essentially constant over the length of the vaporizer, the temperature of the fluid varies along the length from that of the liquid at ambient to that of the vapor at the exit. In any case the heat flow, h, is related to the temperature drop between the copper block and the fluid by an equation of the form

$$h = (T - T_f)/R \qquad (3)$$

where T is the temperature of the copper block and T_f is the average temperature of the fluid in the vaporizer which we approximate by the arithmetic mean between the entrance and exit temperatures. If just enough heat is supplied to completely vaporize the liquid as it passes through the vaporizer, then the total heat transferred must be equal to the heat required to convert liquid to vapor at the exit temperature and pressure.

If the temperature of the heater is higher than the minimum required for steady vaporization, then the necessary heat can be supplied in a length shorter than the length of the heater and vaporization will tend to occur inside the capillary; on the other hand, if insufficient heat is supplied, superheated liquid will emerge and begin to vaporize only after exiting the capillary. From correlation of visual observation of the vaporizer jet in the laboratory with the behavior of the vaporizer installed in the mass spectrometer, it appears that the best performance probably corresponds to nearly complete vaporization occurring a short distance back inside the vaporizer. Since heat is supplied to the liquid primarily by conduction from the walls, the vaporization of the liquid near the axis of the capillary will tend to lag behind that near the walls.

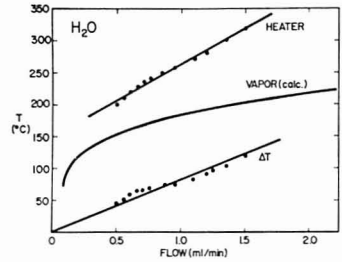


Figure 3. The upper curve (heater) gives the measured temperature of the vaporizer heater block required to produce a fine dry mist when thermospraying water in the laboratory atmosphere. The middle curve gives the calculated vapor temperature according to the steady vaporization model for the 0.015 cm diameter capillary used in this work. The lower curve (ΔT) is the difference between the upper and middle curves and corresponds to the temperature drop in the stainless steel capillary and the solid–liquid interface.

If the nominal liquid–vapor interface is near the exit of the vaporizer, this portion of the liquid emerges as a visible mist entrained in the vapor jet. At slightly higher vaporizer temperatures the mist dissapears and a hot, dry, very intense vapor jet emerges from the capillary, presumably with sonic velocity at the exit.

The vaporizer temperature for the best performance in the mass spectrometer can be correlated with the performance of the vaporizer in the laboratory atmosphere. The conditions for maximum ion current production in the mass spectrometer correspond (in the laboratory atmosphere) to the production of a jet containing visible, very fine droplets which produce a visible spot upon striking a room temperature surface but which vaporize on impact leaving no accumulation of liquid on the surface. The vaporizer temperature at which this behavior is observed for water is plotted as a function of flow rate in Figure 3, where it is compared with the calculated vapor temperature by using the steady vaporization model. Also shown in Figure 3 is the difference between the vaporizer temperature and the calculated vapor temperature. This difference is approximately proportional to the flow rate. If we assume that the temperature of the liquid entering the vaporizer is about 30 °C, these results correspond to a thermal resistance of about 3.2 °C/W. The resistance corresponds to a value of the convection coefficient, n, in eq 2 of ca. 7 which implies that about 80% of the thermal resistance is due to the solid–liquid interface. With the thermal resistance of the vaporizer known, the vaporizer temperature necessary to produce steady vaporization of any liquid can readily be calculated.

The efficiency of thermospray ionization is very sensitive to vaporizer conditions. Total ion currents obtained from thermospray ionization of 0.1 M aqueous ammonium acetate measured as a function of vaporizer temperature and flow rate are summarized in Figure 4. These results were obtained by operating the quadrupole with only RF excitation so as to transmit all of the ions and by collecting the ions on a Faraday cup at the quad exit. No external source of ionization was used for these experiments and no electrical fields were employed inside the ion source. These results were obtained for positive ions, but approximately equal intensities of negative ions are also produced and their behavior with temperature and flow rate is similar.

These results correlate well with our visual observations. The maximum current corresponds to production of a relatively dry mist in an intense vapor jet; the temperatures corresponding to the maxima in Figure 4 are in excellent

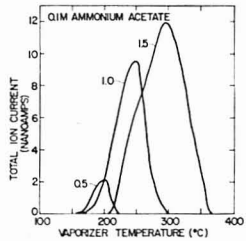


Figure 4. Total ion current produced by thermospray ionization of 0.1 M aqueous ammonium acetate as a function of vaporizer temperature. The flow rates in mL/min are as indicated.

agreement with the optimum temperature vs. flow rate results obtained visually (Figure 3). Also, the temperature at which the current vanishes on the high temperature side correlates with disappearance of the mist, while the low temperature threshold for current production correlates with the minimum temperature for jet formation. Mass spectra obtained by thermospray ionization of aqueous ammonium acetate show that the positive ion spectra consist almost entirely of NH_4^+ and its clusters with water, ammonia, and acetic acid while the negative ion spectra consist of the acetate ion clustered with one or two acetic acid molecules.

Mechanism of Thermospray Ionization. Studies of the mechanism of thermospray ionization are still in progress, but the major features are now fairly well understood (*9*). Briefly, it appears that the process begins with nearly complete vaporization of the liquid at the rate with which it is supplied to the vaporizer to produce a superheated mist carried in a supersonic jet of vapor. Nonvolatile molecules are preferentially retained in the droplets of the mist. The droplets of the mist are charged positively or negatively according to statistical expectations for random sampling of a neutral fluid containing discrete positive and negative charges as described by Dodd (*10*). Molecular ions clustered with a few solvent molecules evaporate from the superheated droplets assisted by the high local electrical fields generated by the charge on the droplet. The initially formed cluster ions rapidly equilibrate with the vapor in the ion source to produce the degree of solvation appropriate to the temperature and pressure of the vapor in the source. Ion–molecule reactions will occur if exothermic channels are available. Finally, the ions present in the source diffuse to the sampling aperture and are transmitted to the mass analyzer. While some details of this proposed mechanism remain somewhat speculative at present, all of our observations to date are compatible with it.

Thermospray ionization appears to provide intact molecular ions for any molecule which is ionized in solution and the efficiency of producing these ions seems nearly independent of the molecular weight and volatility of sample. As an example, a spectrum of the tetradecapeptide renin substrate is shown in Figure 5. This is the largest molecule which has been successfully detected by using thermospray ionization to date and is near the upper mass limit of our quadrupole as presently configured. The mass resolution is too low and the mass scale calibration too uncertain in this high mass range to assign with certainty the peaks corresponding approximately to doubly and triply charged ions. From recent results on field desorption of large peptides with multiply ionizable side chains (*11*), we tentatively suggest that these are probably doubly and triply protonated molecules. Similar results have been obtained on other molecules with molecular weights in excess of 1000 amu including vitamin B_{12}, grammicidin, and several peptides.

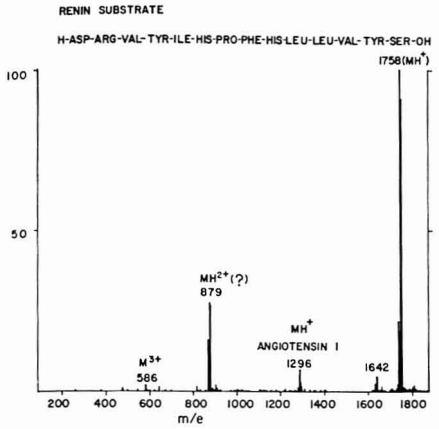


Figure 5. Thermospray ionization mass spectrum of renin substrate obtained from 10 μg injected into 0.1 M ammonium acetate flowing at 1 mL/min. The peak at m/e 1296 is tentatively identified as due to angiotensin I present as an impurity in the sample while the peaks at approximately 879 and 586 are probably due to multiply protonated molecules.

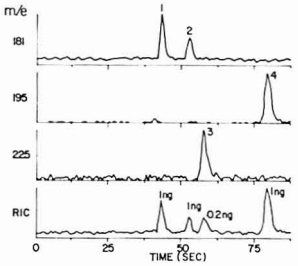


Figure 6. LC/MS analysis of a mixture of xanthine derivatives: 1, theobromine; 2, theophylline, 3, β-hydroxyethyltheophylline; 4, caffeine. Obtained with a 3-μm Ultrasphere (Altex) ODS column and mobile phase consisting of 12% acetonitrile in 0.1 M ammonium acetate at a flow rate of 1.5 mL/min. MS obtained with thermospray ionization of the total LC effluent; sample quantities are indicated on the figure.

We have not succeeded in obtaining molecular ions for large nonvolatile molecules which are neutral in solution; however molecules which are slightly voltatile and thermally stable can be ionized by ion–molecule reactions with reagent ions either produced by thermospray from the buffer or by gas-phase processes initiated by electron ionization. The behavior of the system in this operating mode is very similar to that obtained by so-called "desorption chemical ionization" (*12, 13*).

Performance as a Detector for HPLC. Most of our work on applying the thermospray system to analyses by LC/MS has focused on reversed-phase chromatography with ammonium acetate buffer with either methanol or acetonitrile as organic modifer with flow rates between 1 and 2 mL/min. An example of a chromatogram obtained on a test mixture is shown in Figure 6. Several features of the performance of the system are illustrated by these results. The response is quite dependent on the properties of the sample molecule, and it is not yet possible to predict reliably the relative response of similar molecules. For example, the sensitivity for β-hydroxyethyltheophylline is about five times that for theophylline.

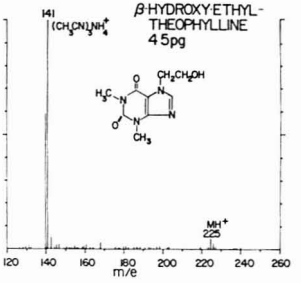


Figure 7. Mass spectrum obtained from 45 pg of β-hydroxyethyltheophylline injected on column. Chromatographic conditions are as given in the preceding figure. Peaks other than the MH^+ ion at m/e 225 are due to the solvent.

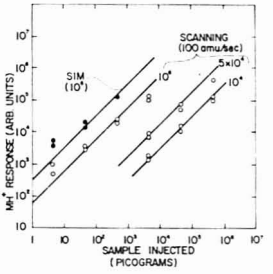


Figure 8. MH^+ response as a function of sample of β-hydroethyltheophylline injected. The parameter labeling the lines corresponding to the expected linear response is the approximate electron multiplier gain used.

The peaks in the chromatogram shown in Figure 6 are between 2 and 3 s wide FWHM; the caffeine peak corresponds to an overall efficiency of about 10^4 theoretical plates. Any contribution to band broadening by the mass spectrometer is undetectable. Regular oscillations in the background intensity, for example at m/e 181, which occurs with a period of about 3.5 s are due to flow fluctuations introduced by the HPLC pump. These oscillations in flow are only about 2% of the nominal flow but because of the strong dependence of ion intensities on liquid flow rate these oscillations are amplified to about 20% in the signal. At present this oscillation due to flow fluctuation is primarily responsible for setting the noise level.

A typical spectrum for one of these test compounds at trace levels is shown in Figure 7. In this example, the MH^+ ion intensity produced by an injection of 45 pg is the largest peak above m/e 141. The integrated response at MH^+ (m/e 225) is shown as a function of sample injected on column in Figure 8. Duplicate measurements were run on each sample; where only a single point is shown the difference between the two results was smaller than the width of the dot used in the plot. The detection limit (S/N = 2) is about 5 pg both for SIM and for full scans and the mean difference in response between duplicate runs is approximately 20%. Both short-term reproducibility and detection limit are primarily set by pump induced flow fluctuations. By changing the multiplier gain to avoid saturation of the amplifier, the response is linear over

6 orders of magnitude from the low picogram to the low microgram range.

The development of the thermospray technique has reached the point that it appears to be a useful analytical tool both for producing spectra of nonvolatile, thermally labile molecules and for use in an on-line LC/MS system. Results similar to those presented here have been obtained for a variety of other classes of compounds including amino acids, small peptides, nucleosides, and antibiotics. Despite these successes, some additional research is required to develop a system which is routinely applicable to a broad range of analytical problems. Many details of the mechanism of ionization are not yet well understood and the optimum configuration of the vaporizer and ion sampling have not yet been established. Major limitations on the technique at present are the difficulties with day-to-day reproducibility of ionization efficiency and fragmentation patterns and the rather severe dependence of the ion intensities on the liquid flow.

ACKNOWLEDGMENT

We thank C. R. Hsieh for preparing the figures for publication and H.-Y. Kim for assistance in obtaining some of the data presented.

LITERATURE CITED

(1) Arpino, P. J.; Guichon, G. *Anal. Chem.* **1979**, *51*, 682A.
(2) McFadden, W. H. *J. Chromatogr. Sci.* **1979**, *17*, 2.
(3) Arpino, P. J. *Trends Anal. Chem.* **1982**, *1*, 154.
(4) Arpino, P. J. *Biomed. Mass Spectrom.* **1982**, *9*, 176.
(5) Blakley, C. R.; McAdams, M. J.; Vestal, M. L. *J. Chromatogr.* **1978**, *158*, 261.
(6) Blakley, C. R.; Carmody, J. J.; Vestal, M. L. *Anal. Chem.* **1980**, *52*, 1636.
(7) Blakley, C. R.; Carmody, J. J.; Vestal, M. L. *J. Am. Chem. Soc.* **1980**, *102*, 5931.
(8) Sissom, L. E.; Pitts, D. R. "Elements of Transport Phenomena"; McGraw-Hill: New York, 1972; pp 488–496 and 673–675.
(9) Vestal, M. L. *Int. J. Mass Spectrum. Ion Phys.* **1983**, *46*, 193.
(10) Dodd, E. E. *J. Appl. Phys.* **1953**, *24*, 73.
(11) Katakuse, I.; Matsuo, T.; Wollnik, H.; Matsuda, H. *Org. Mass Spectrom.* **1979**, *14*, 457.
(12) Cotter, R. J. *Anal. Chem.* **1980**, *52*, 1589A.
(13) Carroll, D. I.; Nowlin, J. G.; Stillwell, R. N.; Horning, E. C. *Anal. Chem.* **1981**, *53*, 2007.

RECEIVED for review October 12, 1982. Accepted December 13, 1982. This work was supported by the Institute of the General Medical Sciences (NIH) under Grant GM 24031.

Nitrous Oxide as Reagent Gas for Positive Ion Chemical Ionization Mass Spectrometry

Charles W. Polley, Jr., and Burnaby Munson*

Department of Chemistry, University of Delaware, Newark, Delaware 19711

Nitrous oxide may be an analytically useful chemical ionization reagent gas for positive ion as well as negative ion analyses. The low-energy NO^+ ion frequently gives M^+ or $(M + NO)^+$ ions for molecular weight determination. The higher energy N_2O^+ ion gives significant amounts of fragmentation from dissociative charge exchange with aliphatic systems.

Nitrous oxide, N_2O, has the potential of being a very useful reagent gas in chemical ionization mass spectrometry (CIMS). Its use in mixtures with hydrocarbons to produce OH^- for negative CIMS has been demonstrated (*1–4*). Nitrous oxide is somewhat unusual as a reagent gas in that reactions occur between negative ions from the sample and N_2O (*1*). Reactions of O^- ions from N_2O have also been studied with organic compounds (*5*, *6*). Little work has been reported on the positive ion chemistry of N_2O with complex organic molecules. It has been reported that NO^+ and N_2O^+ were stable in N_2O at usual CI pressures, although some clustering is observed at high pressures (*7*, *8*). Since the ionization energy of N_2O is 12.9 eV and IE(NO) = 9.27 eV (*9*) there is an energetic reactant ion, N_2O^+, which can produce structurally useful fragment ions and a low energy ion, NO^+, which may give ions in the molecular weight range from hydride or electron transfer reactions. Nitrous oxide, then, may give CI spectra similar to those obtained previously with N_2/NO mixtures (*10*, *11*) without the complications of handling NO mixtures. In addition, these may be reactions of positive ions with N_2O analogous to the reactions with negative ion reported previously (*1*).

EXPERIMENTAL SECTION

The majority of these spectra were obtained with a CEC (Du Pont) 21-110B mass spectrometer which has been described previously (*12*, *13*). The compounds used in these experiments were obtained from several commercial sources and were used without further purification. The nitrous oxide and nitrogen/10% nitric oxide mixtures were obtained from Matheson, East Rutherford, NJ. The volatile liquids were introduced into the hot (200–250 °C) mass spectrometer source from a conventional heated oven or from a gas chromatograph. Solid samples were vaporized into the source from a glass capillary in the well of a separately heatable glass probe. N_2O and N_2/10% NO CI spectra were obtained at 0.5 ± 0.1 torr and an electron energy of approximately 600 eV. The precision in the relative abundances of ions in the spectra is ±20%. Electron ionization (EI) spectra were obtained with conventional low pressure sources.

The major fragment ions of N_2O (N_2^+, N^+, and O^+) react rapidly with N_2O. The dominant ions in the high-pressure spectra of N_2O are NO^+ (33% of ionization) and N_2O^+ (63% of ionization). The relative abundances of these two ions are essentially constant from about 0.1 torr to the highest pressure used, 0.6 torr. Small, variable abundances were noted for an ion of $m/z = 45$, presumably HN_2O^+ formed from reaction of N_2O^+ with ever present traces of water or with the samples. The association ions, $NO^+ \cdot N_2O$ and $N_2O^+ \cdot N_2O$ were not detected at the high temperatures of these experiments. These observations are in agreement with earlier reports for large negative temperature coefficients for the formation of these cluster ions (*8*). The ratio, NO^+/N_2^+, in the N_2/10% NO mixtures was approximately 3.

RESULTS AND DISCUSSION

Spectra were obtained for several classes of compounds with N_2O and N_2/10% NO as the reagent gases for comparison with

0003-2700/83/0355-0754$01.50/0 © 1983 American Chemical Society

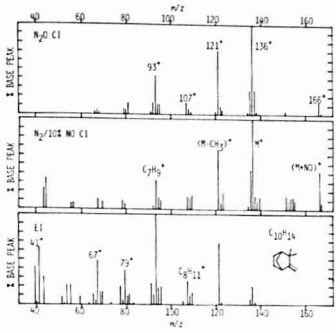


Figure 1. A comparison of the EI, N_2/10% NO, and N_2O CI mass spectra of camphene.

their electron ionization spectra. The N_2O and N_2/10% NO spectra of *n*-octadecane contained almost exclusively alkyl ions, but the extent of fragmentation was large: $(M - H)^+$ = 2% of sample ionization and 8% of the base peak, $C_4H_9^+$, with N_2O and 15% sample ionization and 83% of the base peak, C_5H_{11}, with N_2/10% NO. This abundance of $(M - H)^+$ is much lower than the abundance of $(M - H)^+$ in the NO CI spectra of alkanes (70–80% of the total ionization) (*14*) and also lower than the relative abundance of $(M - H)^+$ ions in the CH_4 CI spectra of *n*-alkanes (25–40% of total ionization) (*15*). For both N_2O and N_2/10% NO the abundance of $(M - H)^+$ ions is sufficiently high that the ion can be readily recognized. Significant amounts of $(M - 3)^+$ and $(M - 2 + NO)^+$ were not observed with either of these reagent gases. The relative abundances of these ions have been reported to decrease with increasing temperature with pure NO as a reagent gas and also to decrease as the NO is diluted with N_2 (*14*). The absence of these ions in the N_2O spectrum supports the idea that they are formed by reactions with NO. There are no products which suggest reactions of alkyl ions with N_2O.

Figure 1 shows the EI, N_2/10% NO CI, and N_2O CI spectra of camphene, $C_{10}H_{14}$. The N_2O spectrum contains no unexpected ions when compared with the EI and N_2/10% NO CI spectra. However, the adduct ion $(M + NO)^+$ is not the dominant ion of the spectrum in contrast with the NO CI spectra of terminal olefins (*16*). Perhaps this smaller $(M + NO)^+/M^+$ ratio results from the higher temperatures of these experiments than those reported previously. The presence of small amounts of $(M - CH_3 + NO)^+$ ions (m/z = 151) in the N_2O CI spectrum (as well as in the N_2/10% NO) suggests that some of these ions are formed by decomposition of $(M + NO)^+$ ions. The larger abundance of these and related ions in the N_2/10% NO spectra suggests reactions of sample ions with NO. Similar spectra were observed for the isomeric compound *d*-limonene, for which the most abundant ion is M^+, not $(M - H)^+$ or $(M + NO)^+$.

Table I shows the N_2O CI spectra of two isomeric octenes. The compounds are easily differentiable. Again, M^+ is the abundant species, not $(M - H)^+$ or $(M + NO)^+$ in contrast to the NO CI spectra of these two compounds (*16*). The very abundant M^+ ions in these spectra are perhaps produced by electron transfer of N_2O^+ in which some of the excited molecular ions, M^{+*}, are stabilized by collision. Alternatively, it may be that at these higher temperatures, the $(M + NO)^+$ ions dissociate to give M^+ ions. No products are observed that suggest reactions of sample ions with N_2O.

Table II shows partial mass spectra of three polynuclear aromatic hydrocarbons. The NO CI spectra of aromatic hydrocarbons and their derivatives contain predominantly M^+ and $(M + NO)^+$ ions (*17*, *18*). It has also been noted that the ratio, $(M + NO)^+/M^+$, decreases with decreasing ionization energy of the aromatic species: $(M + NO)^+$ is the dominant species for benzene and M^+ is the dominant species for naphthalene (*18*). Since the ionization energies of anthracene and phenanthrene are lower than the ionization energy of naphthalene, one would expect electron transfer reactions to NO^+ to be rapid and essentially no adduct formation will be observed. The ratios of ionic abundances, 179/178 and 193/192, for the N_2O CI spectra are significantly higher than the ratio expected for ^{13}C only. These ratios for the EI spectra are approximately the correct values for ^{13}C isotopes. Consequently, some proton transfer reactions must be occurring, probably from the hydrogen-containing impurity ions among CI reactant ions. One observation that is potentially very important analytically is the observation of the small amount of $(M + O)^+$ ions for the two anthracenes and the absence of this ion for methylphenanthrene. One short experiment showed that the $(M + O)^+/M^+$ ratio for anthracene was essentially constant as the entire sample was evaporated from a probe. This experiment suggests that the two ions originate

Table I. N_2O CI Spectra of Isomeric Octenes

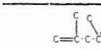
	% sample ionization	
		
41	2.0	2.1
55	2.2	1.5
56	3.9	2.0
57 $C_4H_9^+$	69.4	35.6
58	0.8	0.3
69	0.5	1.6
70		4.0
97	2.0	17.9
111 $(M - H)^+$	1.5	
112 M^+	17.1	36.3
130	0.7	

Table II. Partial Spectra of Some Polynuclear Hydrocarbons

	% sample ionization		
	N_2O CI	N_2/10% NO CI	EI
Anthracene, $C_{14}H_{10}$			
167	0.7	1.0	0.5
176			5.8
177		1.7	3.0
178 M^+	74.7	82.7	40.4
179	20.4	13.8	6.1
180	2.1	0.8	0.4
194 $(M + O)^+$	0.6		
195	0.2		
9-Methylanthracene, $C_{15}H_{12}$			
189			6.8
190			2.6
191		9.8	15.9
192 M^+	69.5	75.3	30.8
193	19.0	13.4	4.7
194	2.6	1.4	4.7
208 $(M + O)^+$	0.7		
1-Methylphenanthrene, $C_{15}H_{12}$			
189			7.6
190			3.7
191		9.9	14.4
192 M^+	71.2	74.6	34.7
193	23.9	14.1	5.3
194	2.0	1.4	0.4

from anthracene. This $(M + O)^+$ ion may result from reactions of M^+ from anthracene with N_2O or from an O^+ transfer reaction of N_2O^+. One notes here that N_2O would be better than N_2/10% NO (and NO) for quantitation of complex mixtures of polynuclear aromatic hydrocarbons because of the lower abundance of the $(M - H)^+$ ions.

The spectra of long chain halides contain mostly hydrocarbon fragment ions. These spectra are, however, readily differentiable from the spectra of alkanes by the presence of significant concentrations of even mass olefin ions at each carbon number. Cyclic halonium ions, $C_4H_8X^+$ and $C_5H_{10}X^+$, are also observed in these charge exchange spectra. $(M - X)^+$ ions are present of 1–2% of total ionization, possibly as the result of X^- abstraction reactions of NO^+. $(M - HX + NO)^+$ ions are also observed at approximately 1% of total ionization, perhaps from dissociation of $(M + NO)^+$ or perhaps from addition of NO^+ to the small amounts of neutral olefins produced by thermal decomposition of the alkyl halides. These spectra contain only very small amounts of $(M - H)^+$ ions, 0.2–0.3% of total ionization. Characterization of the halides from these N_2O CI spectra, however, is difficult.

Spectra of alcohols can be more readily used for identification. The N_2O CI spectrum of 1-octadecanol contains the $(M - H)^+$ ion as the base peak, 14% of total ionization, with another major ion at $(M - OH)^+$, 6%. The $(M - H_2O)^+$ ion is only present at 0.7% of the total ionization. Additional ions occur at each carbon number with masses nominally assigned as $C_nH_{2n-2}^+$, $C_nH_{2n-1}^+$, $C_nH_{2n}^+$, and C_nH_{2n+1} with the most abundant ion in each cluster being $C_nH_{2n-1}^+$ and the most abundant cluster at C_6. One unusual ion is observed at m/z = 241 which is also observed in the N_2/10% NO CI spectrum but not in the EI spectrum. Precise mass measurements have not been made for any of these ions. For comparison, the EI spectrum of 1-octadecanol contains essentially no M^+ and only a low abundance of $(M - H_2O)^+$ ions, 0.5%.

The N_2O CI spectrum of the unsaturated steroidal alcohol, cholesterol is a simple one: M^+, 30% of the total ionization as the base peak; $(M - H_2O)^+$, 10%; $(M - OH)^+$, 10%. The next most significant fragment ion is at m/z = 301, $(M - C_6H_{13})^+$, which is also abundant in the EI mass spectrum. There is virtually no fragmentation of the steroidal nucleus. The abundant M^+ ion for this alcohol results from ionization of the double bond. The much greater abundance of the $(M - H_2O)^+$ ion in this spectrum compared with the spectrum of 1-octadecanol is another reflection of the stability of the steroidal nucleus. It should be mentioned that the EI spectrum of cholesterol also contains a very abundant M^+ ion for molecular weight identification.

The N_2O CI spectra of 1- and 2-adamantanol shown in Figure 2 (like their EI spectra) are readily differentiable. The most abundant ion in the spectrum of 1-adamantanol is the $(M - OH)^+$ ion, 61% of sample ionization. This ion is presumably formed by abstraction of the tertiary hydroxyl group by NO^+ since it is abundant in the N_2/10% NO CI spectrum and minor in EI spectrum. The $(M - H)^+$ ion is a minor one, about 0.7% of the total ionization. For 2-adamantanol, the $(M - OH)^+$ ion is still the base peak, 28% of the total ionization, but the $(M - H)^+$ ion is now a major one, 25% of total ionization. This difference is readily explained in terms of a greater ease of abstraction of a tertiary than of a secondary hydroxyl group and of a strong preference for abstraction of the hydrogen of the substituted carbon in preference to all others. These observations for the reactions of NO^+ are consistent with early conclusions from the NO CI spectra of alcohols (*19, 20*). Dissociative charge transfer from N_2O^+ to 1-adamantanol produces $C_6H_7O^+$, 18%, the major ion in the EI spectrum. Dissociative charge transfer from N_2O^+ to 2-adamantanol produces $(M - H_2O)^+$, 9%, and the C_6 and C_7

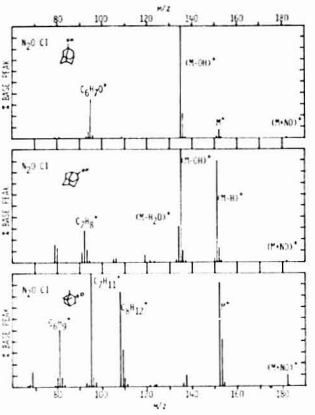


Figure 2. A comparison on N_2O CI spectra of isomeric compounds, $C_{10}H_{16}O$.

hydrocarbon ions, all of which are abundant fragment ions in the EI spectrum of 2-adamantanol.

The N_2O CI spectra of *n*-heptaldehyde contains the $(M - H)^+$ ion as the base peak (30% of the total ionization) and essentially no $(M + NO)^+$ ions from reactions of NO^+. The electron transfer reactions of N_2O^+ give almost exclusive decomposition to hydrocarbon fragment ions. The aromatic aldehyde, *p*-methylbenzaldehyde, also contains the $(M - H)^+$ ion as the base peak (76% of total ionization), some M^+ (3%), and only traces of $(M + NO)^+$ (0.5%). Since the $(M - H)^+$ ion is an abundant ion in the EI spectrum of the aromatic aldehyde, but not the aliphatic aldehyde, we cannot distinguish between hydride transfer to NO^+ and dissociative electron transfer to N_2O^+ as the dominant method of formation. Small amounts of ions at m/z = 91 (4.8%) and 92 (3.6%) are also observed, probably formed by dissociative electron transfer to N_2O^+ because $C_7H_7^+$ is the base peak in the EI spectrum of *p*-methylbenzaldehyde. Small amounts of a product from attack on the aromatic ring are observed at m/z = 136 (1%), perhaps $(M + O)^+$.

Benzil, $C_6H_5COCOC_6H_5$, gives a simple N_2O CI spectrum with a base peak at m/z = 105, 71% of total ionization, $C_6H_5CO^+$. M^+ ions (8%) and $(M + NO)^+$ ions (1%) are also observed. The aryl alkyl ketone $C_6H_5COC_9H_{19}$ also has a simple spectrum with N_2O as the CI reagent gas. Approximately equal abundances of M^+ and $(M - H)^+$ ions are observed, 12% and 11%, as well as an abundant $(M + NO)^+$ ion, 16%. The two abundant fragment ions, $C_6H_5CO^+$ at 105 and $C_6H_5COCH_3^+$ at 120, are the most abundant ions, 24% and 20%, respectively. These fragment ions are the dominant species in the N_2/10% NO and EI spectra, as well.

The N_2O spectrum of the cylic ketone, camphor, is shown in Figure 2 with the spectra of the isomeric alcohols. The ketone is readily distinguished from the alcohols by the abundant M^+ ion and the relatively abundant $(M + NO)^+$ ion. The fragment ions that are observed are also present in the EI spectrum of the compound.

For decanoic acid, the abundant high mass ion is $(M - OH)^+$, 25% of the sample ionization; however small amounts of $(M - H)^+$, 2%, and M^+, 1%, are also observed. Hydrocarbon and oxygen-containing fragment ions are present as well, presumably from dissociative electron transfer reactions of N_2O^+ since these ions (43, 60, and 73) are also present in the EI spectrum of decanoic acid. None of the oxygenated

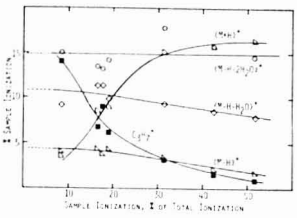


Figure 3. Sample ion/sample molecule reactions in N_2O CI spectra of 1,8-octanediol.

ions obviously reacts with or is produced by reaction of another ion with N_2O.

For some simple nitrogen-containing aromatic compounds (benzamide, carbazole, *p*-dimethylaminobenzaldehyde, *N*-phenylglycine), M^+ is always one of the major ions in the mass spectra. The fragmentation products can generally be rationalized readily in terms of abstraction by NO^+ of small groups to give stable ions or by decomposition of excited M^+ ions according to mechanisms that are well established from low-pressure electron ionization studies.

These N_2O CI spectra of polar organic compounds have an artifact that is characteristic of charge exchange or electron transfer spectra obtained with other reagent gases. The abundances of what should be the ^{13}C isotope of M^+ ions are almost always too high. These anomalously high isotope ratios result from ion/molecule reactions of hydrogen-containing ions in the reagent gas plus sample. With sufficiently small samples, sample ion/sample molecule reactions can be reduced to essentially zero. However, in routine spectra it is likely that isotope ratios of M^+ ions will be high. Figure 3 illustrates this point dramatically for 1,8-octanediol. The major high mass ions, $(M - H)^+$, $(M - H - H_2O)^+$, and $(M - H - 2H_2O)^+$ change only slightly with increasing sample size. The relative abundance of the $(M + H)^+$ ions increases significantly with increasing sample size. The increasing gas-phase concentration of sample is indicated by the increase in the ratio of the sum of all sample ions to the sum of sample and reagent ions. The relative abundance of the propyl ion shows a marked decrease from a proton transfer reaction with 1,8-octanediol. These reactions can be very useful for confirmation of molecular weights, but they can create significant confusion in molecular weight and structure determination if their occurrence is not considered.

N_2O as a reagent gas for positive ion CIMS has advantages over NO or N_2/NO mixtures in ease of handling. The spectra appear to be reasonably useful for characterization and N_2O may replace N_2/NO mixtures. N_2O may be particularly useful for instruments for which positive and negative ion spectra may be easily obtained. Additional experiments are planned to see if the suggested reactions with polynuclear aromatic hydrocarbons are analytically useful.

ACKNOWLEDGMENT

The authors are grateful to Patrick Rudewicz for obtaining some of these spectra.

Registry No. N_2O, 10024-97-2; N_2O^+, 12269-46-4; 2,4,4-trimethylpentene, 25167-70-8; 2,4,4-trimethyl-2-pentene, 107-40-4; anthracene, 120-12-7; 9-methylanthracene, 779-02-2; 1-methylphenanthrene, 832-69-9; 2,2-dimethyl-3-methylenenorbornane, 79-92-5; 1-adamantanol, 768-95-6; 2-adamantanol, 700-57-2; 1,7,7-trimethyl-2-norbornanone, 76-22-2.

LITERATURE CITED

(1) Smit, A. L. C.; Field, F. H. *J. Am. Chem. Soc.* **1977**, *99*, 6471–6483.
(2) Bruins, A. P. *Anal. Chem.* **1979**, *51*, 967–972.
(3) Sieck, L. W.; Jennings, K. R.; Burke, P. D. *Anal. Chem.* **1979**, *51*, 2232–2235.
(4) Hunt, D. F.; Shabanowitz, J.; Giorgani, A. B. *Anal. Chem.* **1980**, *52*, 386–390.
(5) Harrison, A. G.; Jennings, K. R. *J. Chem. Soc., Faraday Trans. 1* **1976**, *72*, 1601.
(6) Gregor, I. K.; Jennings, K. R.; Sharma, D. K. S. *Org. Mass Spectrom.* **1977**, *12*, 93–97.
(7) Derwish, G. A.; Galli, A.; Giardini-Guidoni, A.; Volpi, G. G. *J. Chem. Phys.* **1964**, *40*, 3450–3451.
(8) Sieck, L. W.; Gorden, R., Jr.; Ausloos, P.; Lias, S. G.; Field, F. *Radiat. Res.* **1973**, *56*, 441–459.
(9) Rosenstock, H. M.; Draxl, K.; Steiner, B. W.; Herron, J. T. *J. Phys. Chem. Ref. Data* **1977**, *6*, Suppl. No. 1.
(10) Jelus, B. L.; Munson, B.; Fenselau, C. *Biomed. Mass Spectrom.* **1974**, *1*, 96–102.
(11) Jelus, B. L.; Munson, B.; Fenselau, C. *Anal. Chem.* **1974**, *46*, 729–730.
(12) Hatch, F.; Munson, B. *Anal. Chem.* **1977**, *49*, 169–174.
(13) Hatch, F.; Munson, B. *Anal. Chem.* **1977**, *49*, 731–733.
(14) Hunt, D. F.; Harvey, T. M. *Anal. Chem.* **1975**, *47*, 1965–1969.
(15) Field, F. H.; Munson, M. S. B.; Becker, D. A. *Adv. Chem. Ser.* **1966**, *No. 58*, 167–192.
(16) Hunt, D. F.; Harvey, T. M. *Anal. Chem.* **1975**, *47*, 2136–2141.
(17) Hunt, D. F.; McEwen, C. N.; Harvey, T. M. *Anal. Chem.* **1975**, *47*, 1730–1734.
(18) Einolf, N.; Munson, B. *Int. J. Mass Spectrom. Ion Phys.* **1972**, *9*, 141–160.
(19) Hunt, D. F.; Ryan, J. F. *J. Chem. Soc., Chem. Commun.* **1972**, 620–621.
(20) Jelus, B. L.; Munson, B.; Babiak, K. A.; Murray, R. K., Jr. *J. Org. Chem.* **1974**, *39*, 3250–3254.

RECEIVED for review October 12, 1982. Accepted January 13, 1983.

Chemical and Toxicologic Characterization of Fossil Fuel Combustion Product Phenalen-1-one

Julie A. Leary, Arthur L. Lafleur, Howard L. Liber, and Klaus Biemann*

Department of Chemistry, Department of Nutrition and Food Science, and Energy Laboratory, Massachusetts Institute of Technology, 77 Massachusetts Avenue, Cambridge, Massachusetts 02139

In the course of analysis of the combustion products of fossil fuels, phenalen-1-one has been identified as one of the components. It was differentiated from fluoren-9-one and benzo[*c*]cinnoline, all of which exhibit very similar mass spectra, by gas chromatographic mass spectrometry, high-resolution mass spectrometry, and high-performance liquid chromatography with high-speed spectrophotometric detection. Ultraviolet spectra are reported along with retention data for both gas and liquid chromatography. Mutagenic activity was determined in *Salmonella typhimurium*, using resistance to the purine analogue 8-azaguanine as a genetic marker. Phenalen-1-one was found to be a potent mutagen, while benzo[*c*]cinnoline was six times less active. Fluoren-9-one was completely inactive as a bacterial mutagen.

The chemical analysis of the combustion products of fossil fuels has become of increasing importance because of the concern that some of the components of these complex mixtures may be toxic, mutagenic, or both. The identification of the constituents is usually accomplished by gas chromatography (GC) either alone or in conjunction with mass spectrometry (GC/MS). Although mass spectra in general contain a high degree of structural information, they often lack the capability to differentiate certain aromatic isomers or, in the case of low-resolution mass spectrometry, even isobars. Fortunately, their GC retention behavior is often sufficiently different to allow identification, if such data are available in the literature or can be determined with an authentic sample. If this is not possible other methods must be employed and we have found a combination of conventional capillary GC-MS, high resolution mass spectrometry (HRMS), and high-performance liquid chromatography coupled to a fast recording UV spectrophotometer (HPLC/UV) to be particularly useful for this purpose, eliminating the need for laborious isolation of the pure component.

In this paper we report methodology for the identification of combustion products of fossil fuels employing a combination of techniques rather than GC/MS alone. This is particularly important for compounds which are mass spectrometrically difficult to differentiate. As an example, the unambiguous identification of phenalen-1-one is discussed in detail. This compound is present in the combustion products of No. 2 fuel oil (*1*) and was subsequently also identified in the same way in the effluent of a fluidized bed combustor burning bituminous coal (*2*). Phenalen-1-one turned out to be quite mutagenic and may have been previously misidentified as benzo[c]cinnoline (*3, 4*), a compound which exhibits a much lower mutagenicity.

EXPERIMENTAL SECTION

Apparatus. The gas chromatographic mass spectrometer used was a Finnigan-MAT Model 212 double-focusing instrument interfaced to a Varian SS-200 data system running on a Digital Equipment Corp. PDP 11/34A computer. Coupled to the mass spectrometer through a capillary interface was a Varian Model 3700 gas chromatograph. It was equipped with a 15-m DB-5 fused silica capillary column with an internal diameter of 0.32 mm and a film thickness of 0.25 μm (J & W Scientific, Rancho Cordova, CA) and an on-column injector.

The high-resolution mass spectrometer was a CEC 21-110B instrument of the Mattauch-Herzog type. Spectra were recorded on IONOMET evaporated silver bromide plates and measured with a computer-controlled microdensitometer.

The liquid chromatographic system employed was a Varian Model 5060 ternary gradient pumping system with a Model UV-1 fixed wavelength (254 nm) detector (Varian/Instrument Group, Palo Alto, CA). The spectrophotometric system consisted of a Hewlett-Packard Model 8450A diode-array UV-Vis spectrophotometer with 32K word memory, Model 7225B graphics plotter, and adjustable flow cell holder (Hewlett-Packard Corp., Palo Alto, CA). The spectrophotometer flow cell had a 1.0 mm diameter circular aperture and a volume of 8 μL (Hellma Cells Inc., Forest Hills, NY). The spectrophotometer flow cell was coupled in series with the fixed wavelength detector. The following HPLC columns were used: (1) For reversed-phase analysis of the chloroform fractions Apex octadecylsilyl-bonded silica columns were employed. The columns had an internal diameter of 4.6 mm and a length of 250 mm. The packing material consisted of spherical totally porous particles 5 μm in diameter. (2) Preparative separations were performed by using a 250-mm column with an internal diameter of 10.0 mm packed with 10-μm Spherisorb ODS. (Both obtained from Jones Chromatography, Columbus OH.)

Chemicals. Mobile phases used in the column fractionation of the combustion effluent and in the HPLC analysis were HPLC grade solvents obtained from Burdick and Jackson Laboratories, Muskegon, MI. The neutral aluminum oxide used in the column chromatography (Brockman Activity I, 80–200 mesh) was purchased from Fisher Scientific. Reference samples of benzo[c]-cinnoline [230-17-1] and phenalen-1-one [548-39-0] (also called perinaphthenone), were obtained from Aldrich Chemical, Milwaukee, WI. Fluoren-9-one [486-25-9] was obtained from Chem Service, Inc., West Chester, PA. All chemicals used in preparing the NADPH generating system were purchased from Sigma Chemical Co. The postmitochondrial supernatant (PMS) used in the assay was obtained from Litton Bionetics. (Numbers in brackets are Chemical Abstracts Service Registry Numbers.)

Sample Collection and Preparation. The combustion products from No. 2 fuel oil fired in a hot air furnace operating at smoke number 5 (Bacharach scale) were obtained by sampling in an adsorbent collection train equipped with Teflon-coated glass fiber filters and XAD-2 sorbent resin. The system used was based on a design previously reported (*5*). The total sampling time was approximately 50 h, after which the filters and XAD-2 resin were extracted with dichloromethane in a Soxhlet extractor. The extracts were evaporated to dryness and weighed. Portions of both the filter (52 mg) and XAD-2 (207 mg) extracts were separately fractionated by gravity column liquid chromatography on neutral alumina according to previously published methods (*6, 7*) although the procedure employed here varied slightly from those. During elution with chloroform, two fractions of approximately 40 mL each were collected instead of one large 80-mL fraction (X-3(1) and X-3(2) for the XAD-2 extract and F-3(1) and F-3(2) for the filter extract). The four chloroform fractions were then concentrated by evaporation under nitrogen and analyzed by the methods outlined below.

Gas Chromatographic Mass Spectrometry. Approximately 0.5 to 1.0 μL of sample was injected into the GC/MS. The column was held isothermal at 45 °C for 45 s and then programmed at

0003-2700/83/0355-0758$01.50/0 © 1983 American Chemical Society

Table I. HRMS Data of Components with Molecular Weight 180 from Fractions 3(1) and 3(2)

fraction	determined mass	calcd mass	difference, mmu	elemental compn
3(1)	180.0562	180.05752	1.3	$C_{13}H_8O$
3(2)	180.0552	180.05752	2.3	$C_{13}H_8O$
		180.06874	13.5	$C_{12}H_8N_2$

4 °C/min to 280 °C and held for 2 min. The mass spectrometer operating conditions were as follows: 70 eV electron energy, 4.5 A filament current, 3000 V accelerating voltage, and an ion source temperature of 200 °C. The resolution was 1:1000 and the range from m/z 50 to 500 was scanned in 2 s with an interscan period of 0.8 s.

High-Resolution Mass Spectrometry. The high-resolution instrument was set for 8000 V accelerating potential, 70 eV electron energy, 2.0 mA emission current, and 3.0 A filament current while the ion source temperature was maintained at 200 °C and the resolution 1:12 000. Mass spectra were recorded on vacuum-deposited silver bromide photoplates (IONOMET, Lincoln, MA) for a 1-min exposure and developed photoplates were measured on a computer-controlled microdensitometer.

Liquid Chromatography. Analytical scale HPLC was performed with the Apex ODS column described above. The mobile phase consisted of acetonitrile and water at a flow rate of 1.2 mL/min. For the complete HPLC analysis of the chloroform fraction, the following mobile phase program was employed: 0–40 min, 50:50 acetonitrile/water; 40–60 min, 50% to 100% acetonitrile; 60–80 min, 100% acetonitrile. The absorbance signal represents the integrated absorbance between 252 and 256 nm. For the comparison of HPLC chromatograms of the standards with the chloroform fraction, the HPLC was operated isocratically at 1.0 mL/min with a mobile phase composition of 1:1 acetonitrile/water. The detection parameters were the same as above.

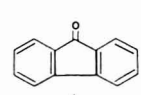
Bioassay. The mutagenicity of phenalen-1-one, fluoren-9-one, and benzo[c]cinnoline was determined in *S. typhimurium* utilizing 8-azaguanine resistance as the genetic end point (*8*, *9*). Frozen aliquots of strain TM677 were grown in minimal media supplemented with 2% brain heart infusion and treated for 2 h at 37 °C in a liquid suspension with both compounds at concentrations of 0–200 μg/mL. This was done in both the presence and absence of a 5% (v/v) aroclor-induced rat liver postmitrochondrial supernatant (PMS). Cultures treated with PMS contained an NADPH generating system. Stock solutions were prepared in Me_2SO and a 10 μL aliquot was added to 0.99 mL of bacteria with or without PMS and the NADPH generating system.

Bacteria were plated in triplicate on minimal agar plates in the presence or absence of 50 μg/mL of 8-azaguanine (8AG), incubated at 37 °C, and counted 2 days later. The number of mutant colonies observed divided by the plating efficiency of the culture times the dilution factor yielded an estimate of the mutant fraction (MF). The operational definition of a bacterial mutagen in this type of assay is a sample which induces a response greater than the 99% upper confidence limit for the background. The level of significance is the concentration at which the dose response curve crosses that limit. The batch of bacteria used in these experiments has an average background of $(10.2 \pm 5.1) \times 10^{-5}$ and therefore, the upper 99% confidence limit is 23.5×10^{-5}.

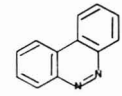
RESULTS AND DISCUSSION

In the course of our studies of the chemical identification of combustion products of fossil fuels, we are turning our attention more and more toward heteroatom-containing polyaromatic systems because of the likelihood that they could contribute considerably to the mutagenicity of these products. In the course of that work we have found in a number of sources the presence of two compounds of molecular weight 180 which are well separated by gas chromatography. One elutes before and the other after phenanthrene and both have practically identical mass spectra. From the mass chromatogram of m/z 180, one can conclude that the abundance ratio of these two components is 2:1.

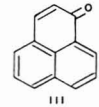
Computer comparison of each of the two with the NIH/EPA collection of 38 000 mass spectra retrieved in both cases fluoren-9-one (I) and benzo[c]cinnoline (II) as the two closest matches. The gas chromatographic retention behavior of the



I



II



III

first peak agreed with that of I but the value for II was not known and therefore this parameter could not be used to confirm the identity of the second component. The presence of II could be compatible with the fact that the component in question appeared in the more polar fraction in which oxygen- and nitrogen-containing heterocyclic compounds elute. Furthermore, this compound has been previously reported to be present in the effluent from a domestic oil burner (*3*) as well as in the extractable portion of diesel particulate matter (*4*).

In an effort to confirm the identity of the earlier eluting compound of molecular weight 180 as I and to definitely identify the later eluting component, a larger sample was obtained by collection of the effluent from a dosmestic oil burner. It was fractionated on alumina by batch elution with hexane, benzene, chloroform, and methanol, respectively. The chloroform fraction which elutes oxygen- and nitrogen-containing aromatic systems was collected in two portions when it was observed that a yellow band migrated down the column with the solvent. When the two filter fractions (3(1) and 3(2)) were subjected to GC/MS, it was found that the component eluting earlier from the gas chromatograph was in the first fraction while the fraction which included the yellow band contained the compound with the longer retention time. Figure 1 represents the total ion chromatogram and the mass chromatogram of m/z 180 for fraction 3(1) (top) and 3(2) (bottom). The mass spectra of these two components are practically identical (Figure 2).

The presence of a compound containing two nitrogen atoms (such as II) would be of particular interest because it might imply interaction of molecular nitrogen with a polycyclic aromatic hydrocarbon during combustion. In order to positively confirm or rule out the presence of a nitrogen-containing molecule, high-resolution spectra of fractions 3(1) and 3(2) were obtained. Exact mass measurement (Table I) revealed that both components were of the composition $C_{13}H_8O$. The $C_{12}H_8N_2$ combination was clearly eliminated because the mass calculated for this compound was well outside the limits of error (±0.003 amu) for the experimentally determined value.

Since the compound in fraction 3(2) was determined not to be II, it remained to be determined which isomer of I this compound represented. Clearly, this question could not be answered by either low- or high-resolution mass spectrometry but required a technique than can differentiate isomeric

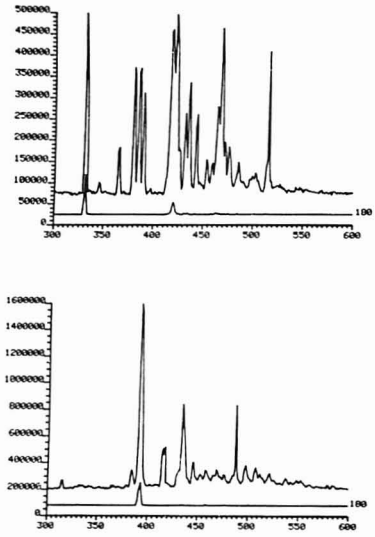


Figure 1. Total ion plots and mass chromatogram of m/z 180 for fraction 3(1) (top) and fraction 3(2) (bottom).

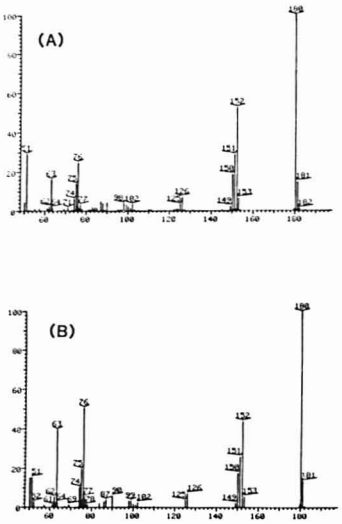


Figure 2. Mass spectra of components with molecular weight 180 (A) from fraction 3(1) and (B) from fraction 3(2).

aromatic systems. For this reason fraction 3(2) was separated by HPLC using a continuously recording UV detector which allowed the acquisition of the complete UV spectrum of this component during the separation. The resulting spectrum was then compared with the UV spectra of compounds of the elemental composition $C_{13}H_8O$, and it was found that it

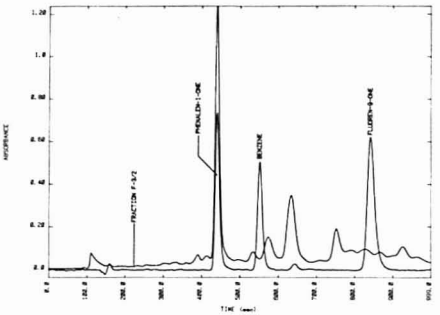


Figure 3. HPLC trace of fraction 3(2) superimposed on that of three standards: phenalen-1-one, benzene, and floren-9-one.

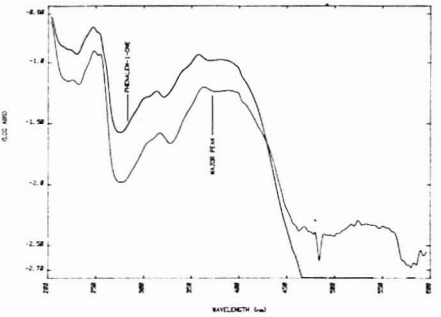


Figure 4. UV spectra of authentic phenalen-1-one superimposed on that of the major component in fraction 3(2).

matched quite closely that of phenalen-1-one (III). An authentic sample of III, which is commercially available, was acquired, and a mixture of II, III, and benzene was separated under identical conditions by HPLC and the UV spectra recorded. The resulting chromatogram (Figure 3) is shown superimposed on that of fraction 3(2) demonstrating the same retention behavior of authentic III. As expected, the UV spectrum recorded for authentic III showed a high degree of correspondence with that of the unknown as shown in Figure 4.

The identity of the two isomers was also checked by comparing the gas chromatographic retention indexes (*10*) with those of the compounds present in fractions 3(1) and 3(2). Authentic standards of I, II, and III were obtained and their gas chromatographic retention indexes calculated. Five measurements were made and mean values of 294.20, 320.52, and 323.50 obtained with standard deviations of 0.02, 0.07, and 0.10 for I, III, and II, respectively. The values for the compounds eluting in fraction 3(1) and 3(2) were 294.41 and 320.53 and therefore matched that of fluoren-9-one and phenalen-1-one. It turns out that the retention indexes of II and III are quite close and III could well be misidentified as II unless one coinjects the standard and sample on a capillary column. Because of this coincidence and the fact that the mass spectrum of III is not contained in the NIH/EPA collection of mass spectra, it is not unlikely that the previous identification of II (*3, 4*) may well have been in error. Since both II and III are commercially available, coinjection is the simplest

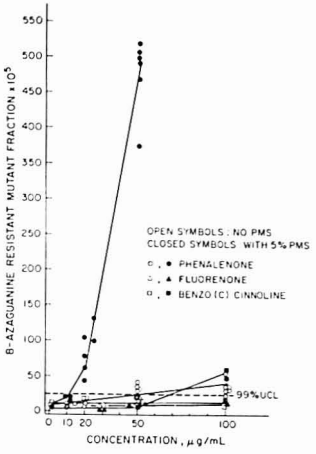


Figure 5. Mutagenicity data for phenalen-1-one, fluoren-9-one, and benzo[*c*]cinnoline with and without postmitochondrial supernatant activation.

check to determine which one of the two, or both, are present.

The identification of III as a combustion product of fossil fuels became even more significant when a sample of III was tested for mutagenicity. From Figure 5 it can be seen that I is completely inactive as a bacterial mutagen. II is weakly mutagenic in the presence of PMS and inactive in the absence of metabolic activation at the concentrations tested. III is mutagenic both with and without metabolic activation and is clearly more active after metabolism with PMS, since the dose response curve crossed the 99% upper confidence level for the background at 10 μg/mL with PMS and 50 μg/mL without PMS.

Although only the chloroform fractions of the filter extract are discussed here, compounds I and III were also found in the same 2:1 abundance ratio in the corresponding fractions of the XAD-2 extract. In the experiments described in this paper, both compounds appear in both extracts. One has to keep in mind, however, that the distribution of the combustion products between filter and XAD-2 trap depends to a great extent on the temperature at which the filter is held. Methods are currently being developed to quantitate both compounds at several different temperatures and smoke number.

ACKNOWLEDGMENT

For the fuel oil combustion sample, the authors are indebted to William A. Peters who directs the domestic oil burner project with the assitance of Edward Kruzel. We also thank Joan Jackman, Rita Klibanov, and Greg Vasquez for carrying out the mutagenicity tests.

Registry No. Fluoren-9-one, 486-25-9; benzo[*c*]cinnoline, 230-17-1; phenalen-1-one, 548-39-0.

LITERATURE CITED

(1) Leary, J. A.; La Fleur, A. L.; Peters, W. A.; Kruzel, E. L.; Longwell, J. P.; Biemann, K. "Polycyclic Aromatic Hydrocarbons", 7th International Symposium; Battelle Press: Columbus, OH, in press.
(2) Chiu, K. S.; Walsh, P. M.; Bier, J.; Biemann, K. "Polycyclic Aromatic Hydrocarbons", 7th International Symposium; Battelle Press: Columbus, OH, in press.
(3) Suprenant, N. F.; Hall, R. R.; McGregor, K. T.; Werner, A. S. "Emissions Assessment of Conventional Stationary Combustion Systems; Volume I. Gas- and Oil-fired Residential Heating Sources"; U.S. Environmental Protection Agency, Report No. EPA-600/7-79-029b, May 1979.
(4) Yergey, J. A.; Risby, T. H.; Lestz, S. S. *Anal. Chem.* **1982**, *54*, 354–357.
(5) Strup, P. E.; Giammar, R. D.; Stanford, T. B.; Jones, P. W. "Carcinogenesis—A Comprehensive Survey"; Freudenthal, R.I., Jones, P.W., Eds.; Raven Press: New York, 1976; Vol 1, pp 241–251.
(6) Schiller, J. E.; Mathiason, D. R. *Anal. Chem.* **1977**, *49*, 1225–1228.
(7) Later, D. W.; Lee, M. L.; Bartle, K. D.; Kong, R. C.; Vassilaros, D. L. *Anal. Chem.* **1981**, *53*, 1612–1620.
(8) Skopek, T. R.; Liber, H. L.; Krolewski, J. J.; Thilly, W. G. *Proc. Natl. Acad. Sci. U.S.A.* **1978**, *75*, 410–414.
(9) Skopek, T. R.; Liber, H. L.; Kaden, D. A.; Thilly, W. G. *Proc. Natl. Acad. Sci. U.S.A.* **1978**, *75*, 4465–4469.
(10) Lee, M. L.; Vassilaros, D. L.; White, C. M.; Novotny, M. *Anal. Chem.* **1979**, *51*, 768–773.

RECEIVED for review December 6, 1982. Accepted January 14, 1983.

Utilization of Natural Isotopic Abundance Ratios in Tandem Mass Spectrometry

Kathleen E. Singleton and R. Graham Cooks*

Department of Chemistry, Purdue University, West Lafayette, Indiana 47907

Karl V. Wood

Engine/Fuels Laboratory, Institute of Interdisciplinary Engineering Studies, Chemistry Building, Purdue University, West Lafayette, Indiana 47907

Isotope abundance ratios in various types of mass spectrometry/mass spectrometry (MS/MS) spectra (parent, daughter, and neutral loss scans) are used to facilitate identification of halogenated components in simple and complex mixtures. By monitoring reactions due to the several isotopic constituents of an ion, one can use the characteristic signal intensity ratio, with the mass data, to identify the type and number of polyisotopic elements in the ion. This information is contained independently in the parent, neutral loss, and daughter scans. This approach is even applicable to mixtures so complex that the characteristic isotope pattern cannot be recognized in the mass spectrum. General expressions have been derived to predict the expected isotopic abundance ratios for MS/MS spectra.

Mass spectrometry/mass spectrometry (MS/MS) is suited to the analysis of complex mixtures as it requires little or no sample preparation (*1-5*). Several MS/MS scanning modes can be used in such work. Parent and neutral loss spectra both characterize sets of compounds with specified properties, whereas daughter spectra identify individual constituents (*6, 7*). Specificity can be further increased by using ancillary techniques (*8*) in conjunction with the two stages of mass analysis inherent in MS/MS. These techniques include selective methods of ionization (*9*), collision-induced dissociation accompanied by charge inversion (*10*), chemical derivatization of the bulk sample prior to MS/MS (*11*), and preseparation during evaporation of the sample into the ion source (*11*).

The value of MS/MS scanning modes is enhanced by considering isotopic abundance ratios when analyzing spectra. When ions containing polyisotopic elements are considered, not only is it necessary for particular peaks to be present in the spectra but they must exhibit appropriate intensity ratios. This additional restriction permits greater certainty in the identification and/or confirmation of components present in a mixture. Isotopic patterns in MS/MS spectra are different from those of mass spectra. This can facilitate spectral interpretation as has already been shown for the case of daughter scans (*12*). This paper illustrates, extends and applies these ideas in examining both simple and complex mixtures using several MS/MS scan procedures.

EXPERIMENTAL SECTION

MS/MS spectra were obtained at low (20 eV) ion energy on a Finnigan triple quadrupole mass spectrometer equipped with an INCOS data system (*13*). Mass spectra were recorded by scanning the third quadrupole (Q3) and setting the first and second quadrupoles (Q1 and Q2, respectively) to pass all ions. MS/MS scanning utilized the second quadrupole in the rf-only mode as a combined focusing device and collision cell. Q2 passed all ions generated by collision activated dissociation (CAD) of a specified precursor ion. Daughter spectra were obtained by setting Q1 to pass an ion of selected m/z ratio and scanning Q3 to record the fragment ions produced by CAD in Q2. Parent spectra were obtained by setting Q3 to pass a selected ion and scanning Q1, thus characterizing the set of parent ions which produce a specified daughter on CAD in Q2. Neutral loss spectra were obtained by simultaneously scanning Q1 and Q3 with a mass offset characteristic of a particular functional group, so as to screen a mixture for constituents containing this functional group.

Solid samples were introduced into the mass spectrometer via a direct insertion probe. Liquid samples were introduced via the solid probe inlet, and regulated with a Granville-Phillips valve to maintain a constant sample pressure in the ion source of ca. 3×10^{-5} torr. The axial kinetic energy of ions entering the collision quadrupole (the difference between the potential of Q2 and the grounded ion source) was 20 eV. The potential of Q3 relative to Q2 was -2 eV. The offset potential of Q1 was set to optimize ion beam intensity. Argon was used as the collision gas at a pressure of ca. 2.3×10^{-3} torr. The ion source was operated in the electron impact mode, with the temperature maintained at ca. 550 K. All compounds were purchased commercially and used without further purification. The nitrogen bases extract was provided by Chuck Schmidt of the Pittsburgh Energy Technology Center.

RESULTS AND DISCUSSION

The use of isotope ratios will first be illustrated with reference to neutral loss scans. Particular cases of each scan type will be considered before the general cases are described. Consider two successive neutral loss scans taken with the mass difference set to correspond to loss of a fragment which includes an atom of the stable isotope of interest. For chlorine-containing mixtures, the mass offsets chosen can be 35 amu and 37 amu, corresponding to the loss of ^{35}Cl and ^{37}Cl, respectively, or a higher mass fragment containing one chlorine atom may be selected (vide infra). Any ion appearing in both scans with the appropriate $^{35}Cl/^{37}Cl$ isotope ratio can be confirmed as originating from a chlorine-containing compound. For any monochlorinated fragment lost from any chlorinated precursor this ratio (^{35}Cl:^{37}Cl or the corresponding higher fragments) is 3:1; in the general case of a polychlorinated neutral fragment the ratio of peak heights *between* the several neutral loss scans will always have the normal isotopic abundance signature characteristic of the neutral fragment. This is illustrated in Figure 1 which shows the neutral loss scans obtained from mixtures containing chlorinated and brominated compounds. The two spectra associated with bromine loss give ions of approximately equal abundance, corresponding to the ^{79}Br:^{81}Br ratio of 1.02 (1.11 ± 0.03) while ions in the spectrum associated with chlorine loss approximate the ^{35}Cl:^{37}Cl ratio of 3.08 (3.16 ± 0.36).

The main source of error was sample pressure regulation during the course of the two successive neutral loss scans. One can also consider relative peak intensities *within* neutral loss spectra. In the case at hand, no characteristic multiplets are present, demonstrating that all halogenated components are

0003-2700/83/0355-0762$01.50/0 © 1983 American Chemical Society

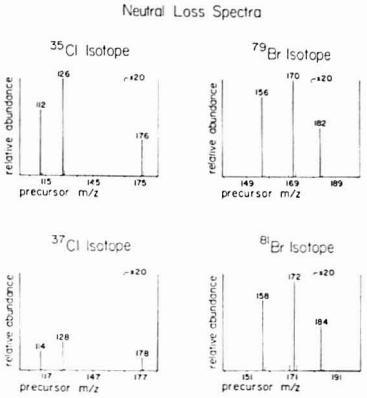


Figure 1. Neutral loss (35 amu and 37 amu) spectra of a mixture containing chlorinated compounds and spectra due to loss of 79 amu and 81 amu for a mixture containing brominated compounds. The chlorine and bromine spectra were normalized independently.

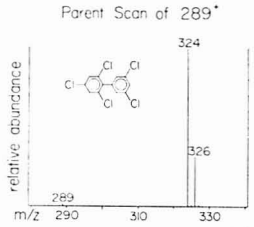


Figure 2. Parent scan of m/z 289 from 2,4,6,3′,5′-pentachlorobiphenyl.

monochlorinated or monobrominated. In fact, the chlorine compound mixture consisted of chlorobenzene (mol wt 112), benzyl chloride (mol wt 126), and 1-(chloromethyl)naphthalene (mol wt 176). The bromine compounds were bromobenzene (mol wt 156), *o*-bromotoluene (mol wt 170), and *β*-bromostyrene (mol wt 182).

An additional or alternative method for confirming the presence of components containing a stable isotope is a parent scan, which records all precursors of a given fragment ion. In contrast to the neutral loss experiments, ion abundance ratios *within* a scan are now of primary interest. A fragment ion resulting from the loss of an atom of the stable isotope, for example, $(M - Cl)^+$, is selected. A parent scan of this ion should show two molecular ions corresponding to the ^{35}Cl and ^{37}Cl constituents in the usual isotopic ratio. This is illustrated in Figure 2, which is the parent scan of m/z 289, the $(M - Cl)^+$ ion of 2,4,6,3′,5′-pentachlorobiphenyl. The parent spectrum contains the parent ions, m/z 324 and m/z 326, in a 3:1 ratio. This characteristic chlorine ratio is obtained in spite of the fact that the isotopic intensity ratio for the m/z 324 and m/z 326 ions of pentachlorobiphenyl is 1:1.6. The 3:1 ratio results because the fragment ion chosen, m/z 289, is produced by the loss of a single chlorine atom from the molecular ion, thus the observed isotopic abundance is 3:1, characteristic of a single chlorine atom. Selection of any other isotopic variant of the $(M - Cl)^+$ ion gives the *same* ion abundance ratio in the parent scan. Thus, it is the isotopic distribution in the neutral fragment which determines the ratio of peak intensities recorded within a parent spectrum.

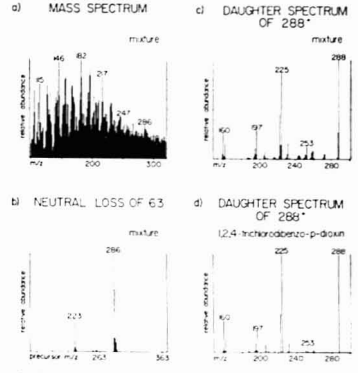


Figure 3. (a) Electron impact mass spectrum, (b) neutral loss 63 amu spectrum, (c) daughter spectrum, m/z 288, from a nitrogen bases extract from a solvent refined coal mixture spiked with 150 ppm 1,2,4-trichlorodibenzo-*p*-dioxin, and (d) daughter spectrum of m/z 288 derived from authentic 1,2,4-trichlorodibenzo-*p*-dioxin.

For the third type of scan, daughter scans, it is again ion abundance ratios *within* individual spectra which are of primary interest. These spectra display all fragment ions derived from a chosen precursor. In these spectra the fragment ions have isotope ratios which reflect the number of atoms of the polyisotopic element in the neutral fragment, as well as the chosen isotopic version of the parent ion. An extreme case is the choice of an isotopically homogeneous ion, e.g., containing six ^{35}Cl atoms, which can only give singlets in the daughter spectrum. The general case of mixed isotopes and loss of various numbers of atoms of the polyisotopic element has been discussed by McLafferty and co-workers (*12*).

These examples show the ease with which multiple MS/MS scans can be used to glean compositional information on simple mixtures. The same procedures are also applicable to the analysis of constituents in complex mixtures where the isotope abundance ratios are masked by interfering ions in the mass spectrum. In this case, neutral loss scans can be used to screen for the presence of specific functional groups or molecules. A neutral loss 35 amu scan may be chosen to screen for chlorine-containing molecules whereas a neutral loss 63 amu scan (loss of COCl, characteristic of chlorinated dibenzo-*p*-dioxins (*14–18*)) will screen specifically for chlorinated dibenzo-*p*-dioxins. An application of these scanning modes to a complex mixture is illustrated in Figure 3. The complex mixture consists of a nitrogen bases extract from solvent refined coal spiked with 1,2,4-trichlorodibenzo-*p*-dioxin at ca. 150 ppm. It is not possible to identify the molecular ion or the characteristic isotope cluster (m/z 286, 288, 290) of 1,2,4-trichlorodibenzo-*p*-dioxin in the mass spectrum, Figure 3a, due to interference from other constituents of the complex mixture. By scanning for neutral loss 63 amu (loss of COCl), Figure 3b, the precursor ions at m/z 223 and 286 are clearly identified. The isotope ratios of these ions show the characteristic signatures for one and two chlorines, respectively. In selecting the mass offset to be 63 amu, a ^{35}Cl atom is specified in the neutral fragment, therefore the precursor ions must actually contain two and three chlorines, respectively. This information can be confirmed by taking daughter scans. When this is done for the second ion, $(M + 2)^+$, in the isotope cluster selected from the neutral loss scan, examination of the ratio $(M + 2 - 35)^+/(M + 2 - 37)^+$ provides a rapid means

Table I. Isotopic Abundance Ratios in MS/MS Spectra

scan type	between spectra	within a spectrum
parent	$(a + b)^{n-z}$	$(a + b)^z$
daughter	$(a + b)^n$	${}^{n-i}C_{z-x} \cdot {}^iC_x$
neutral loss	$(a + b)^z$	$(a + b)^{n-z}$
mass spectrum		$(a + b)^n$

for determining the number of chlorine atoms present in the fragment ion. (Ratios of 0:1, 1:1, 2:1, or 3:1..., correspond to the presence of 0, 1, 2, or 3... chlorine atoms.) For example, in the daughter spectrum of 288$^+$ (Figure 3c), the 253:251 ratio is 2:1, indicating that these ions contain two chlorine atoms. This again indicates the presence of three chlorine atoms in the m/z 288 ion. This information is also evident in the 2:1 ratio of abundances for 225:223. In the case where the (M + 2)$^+$ ion selected is from the molecular ion isotope cluster, comparison of this daughter spectrum to the daughter spectrum of the same ion in a standard can be used to identify the given constituent (see Figure 3d), in spite of the massive interference evident in the mass spectrum.

Generalized equations have been derived to give the various abundance relationships for polyisotopic species examined by the several MS/MS spectra (Table I). Chlorine is chosen as the polyisotopic atom; however, the equations are applicable to any compound containing a polyisotopic element. For these equations, the terms are defined as follows: a and b represent the relative isotopic abundances of ^{35}Cl and ^{37}Cl, respectively, n is the number of chlorine atoms in the precursor ion, i is a term number in the isotope cluster of the precursor ion, z is the number of chlorine atoms in the neutral fragment, and x ranges from 0 to z (each value of x representing a term number in the fragment ion cluster). The following descriptions of these expressions first refer to ion abundance ratios *within* individual scans.

The relative abundances of peaks in a given isotope cluster *within* a daughter spectrum are described by the expression

$$\frac{(n - i + 1)!(i - 1)!}{[n - i + 1 - (z - x)]!(z - x)!(i - 1 - x)!\, x!} = {}^{n-i}C_{z-x} \cdot {}^iC_x$$

It should be noted that the expression is independent of the natural isotopic abundances and dependent only on the number of polyisotopic atoms present. For a case in which $n = 6$, $i = 4$, and $z = 3$, the peaks in the daughter spectrum are given by the ratio 1:9:9:1. The $x = 0$ term represents the loss of ^{35}Cl. In a case such as $n = 6$, $i = 4$, and $z = 4$ where it is not possible to lose four ^{35}Cl, the value at $x = 0$ is undefined, and the cluster begins at $x = 1$ with the loss of three ^{35}Cl and one ^{37}Cl. In contrast, the ratios of total ion abundances *between* daughter spectra are given simply by the binomial expansion $(a + b)^n$.

For ion abundances *within* parent spectra, the isotope cluster ratio is described by the binomial expansion $(a + b)^z$. For example, the parent scan of (M − 70)$^+$ (70 = $^{35}Cl_2$) for a compound containing four chlorine atoms will show a cluster characteristic of two chlorines. The same spectrum will be generated for each choice of daughter ion. However, when comparisons are made *between* parent spectra, total abundances will be in a ratio given by the relative natural abundances of the various selected ions, viz., $(a + b)^{n-z}$.

The isotope cluster ratios *within* neutral loss spectra can be described by the binomial expansion $(a + b)^{n-z}$. For example, the neutral loss 72 amu spectrum of a compound containing three chlorine atoms will show a cluster characteristic of one chlorine. (Note the isotope cluster would be the same, as would the masses at which it is observed, for neutral loss 70 amu and 74 amu from a three chlorine-containing compound.) Similarly, the ratio of intensities *between* neutral loss spectra representing the various isotopic choices can be described by the coefficients of the binomial expansion $(a + b)^z$.

Summarizing, there are two sets of ion abundance ratios of interest for each type of scan: those *within* a particular scan and those *between* the various isotopically distinct scans of the same type. The former are of chief interest for parent and daughter scans, while both types are useful for neutral loss scans. The ratios of ion abundances for each of the six scan types is summarized in Table I.

CONCLUSION

MS/MS neutral loss, parent, and daughter scanning modes can be used to assist in analyzing complex mixtures through recognition of specific classes of compounds as evident from isotopic abundance ratios. The several isotopic versions of each spectrum are identical in appearance (but not intensity) for the neutral loss and for the parent scans. However, for daughter spectra the particular isotopic version of the parent ion which is selected determines the appearance of the spectrum. Isotopic abundance ratios *within* and *between* individual parent, neutral loss and daughter scans occur as given in Table I.

LITERATURE CITED

(1) Cooks, R. G.; Glish, G. L. *Chem. Eng. News* **1981**, Nov 30, 40.
(2) Kondrat, R. W.; Cooks, R. G. *Anal. Chem.* **1978**, *50*, 81A.
(3) Maugh, T. H. *Science* **1980**, *209*, 675.
(4) McLafferty, F. W. *Science* **1981**, *214*, 280.
(5) Yost, R. A.; Enke, C. G. *Anal. Chem.* **1979**, *51*, 1251A.
(6) Ciupek, J. D.; Cooks, R. G.; Wood, K. V.; Ferguson, C. R. *Fuel*, in press.
(7) Zakett, D.; Schoen, A. E.; Kondrat, R. W.; Cooks, R. G. *J. Am. Chem. Soc.* **1979**, *101*, 6781.
(8) McLuckey, S. A.; Cooks, R. G. In "Tandem Mass Spectrometry"; McLafferty, F. W., Ed.; Wiley: New York, in press; Chapter 15.
(9) Ciupek, J. D.; Zakett, D.; Cooks, R. G.; Wood, K. V. *Anal. Chem.* **1982**, *54*, 2215.
(10) Bowie, J. H.; Blumenthal, T. *J. Am. Chem. Soc.* **1975**, *97*, 2959.
(11) Zakett, D.; Cooks, R. G. In "New Approaches in Coal Chemistry"; Blaustein, G. D., Bockrath, B. C., Friedman, S., Eds.; American Chemical Society: Washington, DC, 1981; ACS Symp. Ser., Chapter 16.
(12) Todd, P. J.; Barbalas, M. P.; McLafferty, F. W. *Org. Mass Spectrom.* **1982**, *17* (2), 79.
(13) Slayback, J. R. B.; Story, M. S. *Ind. Res./Dev.* **1981**, (Feb), 129.
(14) Buser, H. *J. Chromatogr.* **1975**, *107*, 295.
(15) Buser, H.; Rappe, C. *Chemosphere* **1978**, *2*, 199.
(16) Mahle, N. H.; Shadoff, L. A. *Biomed. Mass Spectrom.* **1982**, *9*, 45.
(17) Plimmer, J. R.; Ruth, J. M.; Woolson, E. A. *J. Agric. Food Chem.* **1973**, *21*, 90.
(18) Safe, S.; Jamieson, W. D.; Hutzinger, O.; Pohland, A. E. *Anal. Chem.* **1975**, *47*, 327.

RECEIVED for review October 27, 1982. Accepted January 18, 1983. This research was supported with funds from NSF (CHE-8011425). K.E.S. acknowledges the support of CONOCO through a grant to the Purdue Coal Research Center.

Atomic Ion Formation and Measurement with Resonance Ionization Mass Spectrometry

J. D. Fassett,* J. C. Travis, and L. J. Moore

Center for Analytical Chemistry, National Measurement Laboratory, National Bureau of Standards, Washington, D.C. 20234

F. E. Lytle

Department of Chemistry, Purdue University, West Lafayette, Indiana 47907

Resonance ionization mass spectrometry has been used to study the formation of the atomic ions of molybdenum, rhenium, and vanadium. A one-wavelength, two-photon ionization scheme was used that is potentially applicable to nearly 50 elements. The first photon resonantly excites a bound transition in the near-ultraviolet region and a second photon promotes the electron into the ionization continuum. Wavelength-dependent ion formation from a thermally produced atom reservoir was demonstrated for these elements by scanning a Nd/YAG-pumped tunable dye laser across specific resonant electronic transitions and recording the mass-selected ion intensities in a single magnetic sector mass spectrometer. Limitations on potential analytical sensitivity and selectivity appear to result from two-photon backgrounds of atomic and molecular ions and from the appearance of untabulated spectral features.

Resonance ionization mass spectrometry (RIMS) is a new technique combining mass spectrometry with laser photoionization to produce ions selectively and sensitively from a gas-phase reservoir of atoms (*1–5*). The technique exploits both the limited bandwidth and intense photon flux inherent to laser-produced radiation. By tuning the laser to discrete, resonant electronic transitions of an element, the ionization probability becomes increased manyfold due to the stepwise absorption of photons. The technique differs from other spectroscopic methods in that the absorption or emission of photons is not directly measured. Only the mass selected ions that are produced are measured. Thus, there exists a combined selectivity: elemental selectivity in ionization and isotopic selectivity in measurement.

An early demonstration of RIMS utilized a thermally produced potassium reservoir (*1*). RIMS has been recently applied to the selective photoionization of rare earth elements (*2, 3*) and U and Pu (*4*) where the atom reservoirs again were produced by thermal vaporization. RIMS of ion sputtered In has also been demonstrated (*5*).

Resonance ionization spectroscopy (RIS) has been studied predominantly in ionization chambers without mass selected measurement and then only for a limited number of elements, although Hurst et al. have published schemes for resonance ionization of a majority of elements in the periodic table (*6*). Single atom detection has been demonstrated in RIS (*7*), thus illustrating the potential ultimate sensitivity. The process requires atom reservoirs and thus would appear to be ideally suited for analytical techniques that produce atoms in the gas phase such as secondary ion mass spectrometry, laser ablation, or thermal ionization mass spectrometry where atomization occurs incidental to the desired ionization process. The application of RIMS to basic investigations of atomization processes in spectroscopic techniques, such as furnace atomic absorption spectrometry (*8*), as well as ionization techniques is also suggested.

Table I. Atoms Amenable to Resonance Ionization by $A(2W_1 2W_1 e^-)A^+$ Process and Nd:YAG/Tunable Dye Laser System, 260–355 nm

Al	Eu	Ir	Ni	Sc	Ti
Ba	Gd	Fe	Nb	Na	W
Bi	Ga	Pb	Os	Sr	U
Ca	Ge	Li	Pd	Ta	V
Cr	Au	Lu	Pt	Tb	Yb
Co	Hf	Mg	Re	Th	Y
Dy	Ho	Mn	Rh	Tm	Zr
Er	In	Mo	Ru	Sn	

Langmuir vaporization has been used extensively and successfully in making highly precise and accurate isotope ratio measurements by thermal ionization mass spectrometry (TIMS) and, combined with isotope dilution mass spectrometry (IDMS), highly precise and accurate analytical measurements. Because of its inherent accuracy, IDMS has been used to certify the concentrations of a broad range of elements at ultratrace and macro levels in a wide variety of matrices (*9*). Furthermore, IDMS has been used as a definitive method to referee other analytical procedures (*10, 11*). RIMS has the potential to be applied to TIMS problems where either sensitivity (inability to produce ions) and/or selectivity (isobaric interferences) present fundamental measurement limits.

A critical part of evaluating and controlling systematic errors in IDMS and related applications is the ability to understand and control mass discrimination effects that occur in the process of ion formation in the ionization source. Although limited theoretical and empirical studies have been pursued (*12–14*) there has been little attention devoted to experimental diagnostic studies to understand the processes by which compounds evaporate and form atomic ions in the Langmuir vaporization conditions of thermal ionization sources. Resonant and nonresonant multiphoton ionization can be employed to selectively ionize gas-phase atoms and molecules to assist in characterizing the transition from condensed phase to gaseous ion in analytical systems.

For the purpose of studying RIMS, a tunable ultraviolet laser system has been combined with a magnetic sector mass spectrometer containing a suitably modified thermal source. This system is capable of ionizing more than 47 elements. Initially the spectral properties of V, Mo, and Re have been investigated.

THEORY

Hurst and co-workers (*6*) have proposed five basic types of resonance ionization schemes to cover the majority of elements in the periodic table. The scheme used in this study, $A(2\omega_1 2\omega_1 e^-)A^+$, can be considered a subset of Hurst's type I, the absorption of two photons of equal wavelength, $A(\omega_1\omega_1 e^-)A^+$, which requires that the resonant level is more than

This article not subject to U.S. Copyright. Published 1983 by the American Chemical Society

halfway to the ionization continuum. With this approach the 47 elements listed in Table I are amenable to resonance ionization, using the laser system described. The specific exclusion of the resonance ionization scheme employed here from the five types originally defined (*6*) resulted from criteria designed to assure maximum ion yield with minimal spectral distortion due to power broadening. However, state-of-the-art, frequency-doubled tunable laser systems are now capable of producing maximum ion yield, and the requirements for spectral selectivity are reduced by the mass spectrometer in RIMS.

The formation of atomic ions by using resonance ionization requires a source of neutral atoms. Conventional single and multiple filament assemblies that are normally used in TIMS can also be used for the efficient formation of neutral atom reservoirs. Customarily, ions are produced from single filament surfaces at a temperature that is high enough to effect any preliminary molecular decomposition and to remove an electron to form the final ion product. For elements that do not efficiently produce atomic ions, multiple filament assemblies permit a further refinement in the overall vaporization–ionization process. In multiple filament assemblies the compound containing the analyte is vaporized as molecules (chiefly monomers) from the lower temperature surface and at a higher temperature second surface the molecules are dissociated into their constituent atoms and ionized. Mechanisms for atom reservoir formation include:

Type Ia

$$M^0(s) \rightarrow M^0(g)$$

Type Ib

$$MX(s) \rightarrow M^0(s) + X^0(s) \rightarrow M^0(g) + X^0(g)$$

Type II

$$MX(s) \rightarrow MX(g) \rightarrow M^0(g) + X^0(g)$$

where the type I mechanisms occur on single filaments and type II on multiple filament thermal ionization sources. Examples of type Ia are electrodeposited metals such as Cu or Re. Type Ib can occur either by reduction at the metal surface, or, in the case of encapsulated samples, by reduction below the surface with diffusion controlling transport of metal atoms to the filament surface (*15*). Examples of type II are rare earth halides and related high molecular weight inorganic compounds of alkaline earth elements, such as $M_xRe_yO_z(g)$ which dissociate and form $M^0(g)$ atoms and, at sufficiently high filament temperatures, M^+ ions.

When the assumption is made that the only species leaving the filament are positively charged and neutral species of an element, the Saha–Langmuir equation may be applied, where

$$n^+/n^0 \propto \exp(W - \mathrm{IP})/kT$$

and n^+/n^0 is the ratio of ions to neutral atoms evaporated from the surface, W is the work function of the filament (5 eV for rhenium), k is the Boltzmann constant, T is temperature in K, and IP is the ionization potential of the element n. Although the Saha–Langmuir relationship is not applicable to complex chemical systems, the relationship qualitatively predicts the relative thermal ionization efficiencies for elements. For high ionization potential elements, the ion/neutral ratio is so small that improvement in absolute ionization efficiencies and sensitivities are potentially achievable by using resonance ionization, even considering the low duty cycles of pulsed lasers. The elements in Table I have ionization potentials ranging from 6.0 eV (Al) to 9.2 eV (Au).

The duty cycle of a resonance ionization system which uses a pulsed laser and a thermal source to produce a continuous

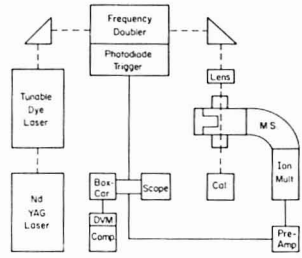


Figure 1. Block diagram of RIMS system.

reservoir of neutral atoms can be defined as the fraction of atoms traversing the laser focal volume which are irradiated. This duty cycle will be determined by the diffusion time of the atoms, the size of the laser focal volume, and the repetition rate of the laser. With diffusion times on the order of 10^5 cm/s and a laser beam with a width of several millimeters, a laser with a repetition rate of nearly 10^6 pulses/s is required to produce a 100% duty cycle. A 10-Hz laser capable of ionizing all the atoms in the focal volume on every pulse would thus improve the absolute ion yield for an n^+/n^0 ratio less than 10^{-5}.

EXPERIMENTAL SECTION

Figure 1 schematically illustrates the experimental system which consists of three basic components: a laser system capable of producing tunable ultraviolet radiation, a magnetic sector mass spectrometer with a suitably modified thermal source, and a detection and measurement circuit capable of quantifying the pulsed ion currents produced in the experiment.

Laser. The laser system consists of a Molectron Corp. MY-34 Nd:YAG laser, capable of producing 225 mJ/pulse at 532 nm, which was used to pump a Molectron Corp. DL-18 tunable dye laser. This laser produces 4-ns pulses at 10 Hz. Three dyes were used in this study: Rhodamine 640 and DCM to access the wavelength region 608–632 nm and Rhodamine 610 to access the wavelength region 587–618 nm.

The dye laser output is directed to a frequency doubler (Inrad 512) which uses an angle-tuned second harmonic generating crystal (KDP). The tunable ultraviolet light with a bandwidth of 0.25 Å is directed into the source of the mass spectrometer parallel to the sample filament and focused by a 30-cm focal length lens. The radiation continues out the exit window of the mass spectrometer and is directed onto a calorimeter for energy measurements. Operating the Nd:YAG at 100 mJ/pulse, with 20–30% conversion efficiencies by the dye laser and 10% conversion efficiency in frequency doubling, typical ultraviolet energy is 2 mJ/pulse. To study the ionization signal vs. laser power dependence a polarizing filter is inserted in the unfocused ultraviolet beam. This filter attenuates the light as a function of the square of the cosine of the polarizing angle and thus provides a reliable factor of 10 attenuation.

Mass Spectrometer. The mass spectrometer is a 60°, 6-in. magnetic sector instrument originally designed for use in thermal ionization mass spectrometry and high-precision isotope ratio measurement (*16*). The source chamber was modified by the insertion of sapphire entry and exit windows for the laser radiation. The thin-lens ion source was also modified by increasing the distance between the shield and draw-out plates in order to accommodate the laser beam and sample filament which is inserted into this region. The focused laser beam enters and exits the mass spectrometer without interaction with any solid surface, except the windows.

The laser beam is focused 2–3 mm in front of and parallel to the thermal ionization sample filament, a ribbon of rhenium 0.76 mm wide and 6.35 mm long. The ion optics of the mass spectrometer and the laser focal volume were optimized together. This procedure discriminates against ions produced at the filament. The temperature of the filament is controlled by a solid-state dc

Table II. Instrument Conditions for RIMS of V, Mo, and Re

	vanadium	molybdenum	rhenium
sample form	V_2O_3	Mo	Re
sample size, μg	1	1	
analysis temp, °C	1275	1590	1800
accelerating potential, V	6940	6940	4000
magnetic field, G	5589	7838	8160
time of flight, μs	8	12	23

power supply of NBS design and is measured by use of an optical pyrometer which views the back of the heated filament. Temperatures quoted in this study are uncorrected for emissivity of the filament material or transmission of the viewing window. Instrument pressure was maintained at 3×10^{-8} torr.

Ion Measurement. Detection of the laser-produced ions is accomplished with a 17-stage electron multiplier (EM) with the "Rajchman" structure and a Cu/Be conversion dynode. The EM is operated at 1600–2000 V which provides a linear signal output at modest gain (10^4–10^5) with a dynamic range spanning several orders of magnitude. Because of the 10-Hz repetition rate of the laser, pulse counting was not attempted.

The output of the EM is directed into a 10^5 V/A preamplifier which also stretches the signal pulses to 500 ns. The preamplifier output is split into an oscilloscope and the gated integrator of a boxcar averager (EG&G Princeton Applied Research Models 162 and 163). The trigger is provided by a photodiode which senses reflected light from the frequency doubler. The acceptance window of the boxcar averager is typically set at 200 ns and manually optimized. The integrated output of the boxcar is directed into a Hewlett-Packard 5328A digital voltmeter connected via an IEEE-488 interface to a Hewlett-Packard 9845A calculator which controls signal processing and provides graphics.

Samples. Molybdenum, vanadium, and rhenium vapor-phase atom reservoirs were produced by Langmuir vaporization from rhenium filaments. Molybdenum samples were prepared by the reduction of molybdic acid in a hydrogen atmosphere directly on the filament substrate (*17*). Vanadium samples were prepared by drying a drop of vanadium oxychloride (50 μg/g in 10% HCl) in air on the filament which produced a black oxide, presumably V_2O_3. Although the latter samples might be expected to produce primarily a vanadium oxide signal, it has been demonstrated, using thermal ionization, that a suitable V^+ signal is generated. From this demonstration the generation of a corresponding V^0(g) beam has been inferred. Support of this inference comes from Knudsen cell investigations where the formation of vanadium atomic beams from vanadium oxide (*18*) has been shown. The vapor-phase atom reservoir of rhenium was produced by the direct sublimation from the rhenium filament substrate material, although a procedure has been developed to analyze microgram quantities of rhenium by thermal ionization (*19*) and could equally well have been utilized.

The instrumental parameters established to produce and detect Mo, V, and Re are summarized in Table II. Care was taken to provide atom reservoirs of the elements under equilibrium conditions determined by the temperature of the filament. In all cases constant signals of sufficient intensity were easily maintained over several-hour periods indicating that little sample depletion occurred at the analytical temperatures chosen and permitting extensive spectroscopic study.

Spectroscopy. RIMS spectra were obtained by manually stepping the laser wavelength and manually optimizing the double efficiency. The resultant data spacing was typically 0.5 Å in the region between major features and 0.1 Å across the features. Each point represents the average of 20 s of integration and each spectrum was normalized to the strongest spectral feature.

RESULTS AND DISCUSSION

Three representative elements which are difficult to ionize with conventional methodology were investigated in this study: Re (IP 7.9 eV), Mo (IP 7.1 eV), and V (IP 6.7 eV). Production of vapor-phase atom reservoirs for Mo and Re was by the previously designated type Ia mechanism. Production of the vapor-phase atom reservoir for V was a type Ib mechanism requiring reduction of vanadium oxide at the filament surface. Ground-state absorption transitions examined in the tunable wavelength regions of the dyes used were selected from Meggers (*20*). These transitions are summarized in Table III.

Table III. Ground-State-Connected Transitions Observed in this Study

element	wavelength, Å	excited state: designation	excited state: J	tabulated intens[a]
Mo	3002.21	y^5P^o	2	190
	3112.12	z^7D^o	4	1400
	3132.59	y^7P^o	4	14000
Re	2976.29	y^6P^o	$1^1/_2$	310
	2992.36	z^6D^o	$2^1/_2$	1800
V	2942.39	w^4D^o	$1^1/_2$	230
	2943.20	w^4D^o	$^1/_2$	230

[a] Reference 20.

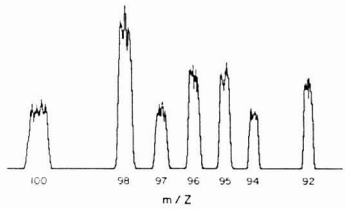


Figure 2. Resonance ionization mass spectrum of molybdenum, 3132.6 Å; magnetic field scanning, 1 s per point and 500 s total scan time.

The mass spectrometer was initially optimized for each element by measurement of the dc signal produced by thermal ionization from the filament. The output of the EM was directed to a vibrating reed electrometer with a 10^{10} or 10^{11} Ω input resistor, and the output of the EM was then switched to the pulse measurement circuitry for manual laser alignment. The mass spectrometer was refocused by use of the resonance ionization signal, since optimization of the ion optics requires compensation for the two differing positions of ionization. Figure 2 illustrates the resonance ionization mass spectrum of molybdenum which is comparable to a thermal spectrum in terms of both peak shape and peak resolution.

Care was taken in optical focusing to avoid formation of ablated ions produced by the interaction of the laser with the solid surface of the filament. These ions are easily identified: they are produced independent of both wavelength of the laser and temperature of the filament. Furthermore, these ions have a longer time-of-flight and can be resolved in time on the oscilloscope. Also, the temperature of the sample filament was controlled to avoid a large, thermally produced ion current which potentially could saturate the pulse detection system. Thermal ions, randomly produced in time, were occasionally observed on the oscilloscope, even though ions produced at the surface are discriminated against by the ion optics of the mass spectrometer.

The pulsed ion beam produced by the laser has a time-of-flight from formation to detection in the mass spectrometer proportional to the square root of the ratio of mass to accelerating potential. Thus, the instrument possesses dual mass selectivity due to magnetic and time filtering. The two mass filtering processes are complementary in the experiment. The magnetic sector filters out all thermally produced ions except

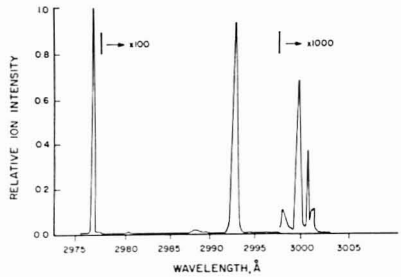


Figure 3. Relative $^{187}Re^+$ ionization signal vs. wavelength, 2975–3005 Å; laser energy nominally 2 mJ.

a single m/e, thus eliminating a potential dc background to a time-of-flight mass spectrometer. The time-of-flight filters out the dc background, or thermally produced ions, at the desired m/e position. The experimental times-of-flight corresponding to the 135-cm flight path and accelerating potentials used are listed in Table II.

For all three elements, the resonance ionization signal was measured as a function of filament temperature. The log I vs. $1/T$ linear behavior, predicted by the Clausius–Clapeyron relationship, was observed for all elements. The slope of the line relating log I to $1/T$ equals the value for the heat of vaporization of an element, although this technique for determining the heat of vaporization is prone to systematic errors (*21*) presumably due to complex surface/sample interactions.

Spectroscopy. *I. Re.* The wavelength region 2975–3005 Å was examined, yielding the data shown in Figure 3. The two ground-state-originating transitions occurring within this range (2976.3 and 2992.4 Å) both produced strong RIMS signals. Additionally, at least one, and perhaps two, excited-state-originating transitions were present. The appearance of a signal from this latter type of transition would require that the atom be thermally excited at or near the filament to an energy state which is sufficiently metastable not to depopulate during the approximately 500 ns required to drift into the excitation volume. The weak line at 2999.6 Å corresponds to a tabulated transition connecting the $a^6D_4J = 4^1/_2$ level (11 754.5 cm^{-1}) with the $y^6F_4J = 5^1/_2$ level (45 082.63 cm^{-1}). Although a definite assignment is difficult to make, the very weak line at 3001.1 Å does correspond to a tabulated transition connecting the $a^4G_4J = 2^1/_2$ level (14 621.46 cm^{-1}) with the $y^6F^o_4J = 3^1/_2$ level (47 932.55 cm^{-1}). The two remaining lines at 2997.8 and 3000.6 Å lines do not correspond to tabulated transitions for rhenium. The wavelength regions between the above spectral features contain a flat background signal with a quadratic laser power dependence. Ubiquitous to all of the RIMS experiments, this off-resonance interference was very small with rhenium and occurred only when maximum focused laser power was utilized.

Throughout the RIMS experiments the measured widths of the resonance lines were found to be directly related to the tabulated line intensities. Thus the rhenium 2976.3-Å line with an intensity of 310 is laser-limited at 0.25 Å wide, while the 2992.4-Å line with an intensity of 1800 is 0.6 Å wide. This observation can be qualitatively explained by the relative degree of coupling to the photon field which in turn controls the power broadening. As a result, the more analytically selective transitions may be those having weaker absorption cross sections. The observed degree of broadening is roughly consistent with theoretical expectations as discussed by Shimoda (*22*). For strong transitions, the spectral irradiance of the focused laser is some 7 orders of magnitude above that

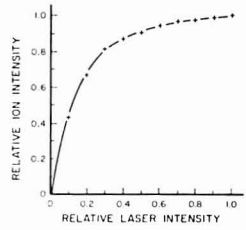


Figure 4. Relative $^{187}Re^+$ ionization signal vs. relative laser energy, 2976.3 Å.

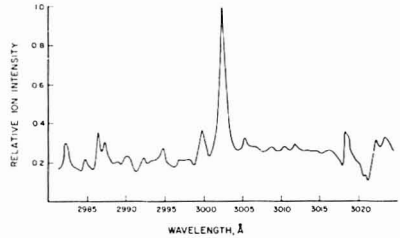


Figure 5. Relative $^{98}Mo^+$ ionization signal vs. wavelength, 2980–3025 Å; laser energy nominally 2 mJ.

required to optically saturate the transition, broadening the homogeneous (natural) component of the line width by the square root of 10^7 (*22*). Since photoionization cross sections are typically 3 orders of magnitude smaller than strong absorption cross sections (*6*), the resonant transition must be saturated by at least this amount for complete ionization using the described two-photon scheme. Replacing the lens with a beam reducing telescope would probably provide an optimal spectral irradiance to yield complete ionization with laser limited line widths. For the only excited state line that could be assigned with any certainty, 2999.6 Å, the relationship also seems to hold, i.e., a tabulated intensity of 5500 and a width of 0.6 Å.

The variation of the RIMS signal with laser power should show three consecutive types of behavior. At very low power the two sequential steps in the process should generate a second order dependence. When the power is increased sufficiently to begin to saturate the process, and all ions are collected, the dependence should become 3/2 (*23*). Finally, as the laser saturated excitation volume grows comparable in size to the focal volume of the mass spectrometer, the power dependence will decrease to zero (*24*). Figure 4 shows that the 2976.3-Å radiation can completely saturate the focal volume of the mass spectrometer with the approximate 2 mJ of laser energy available per pulse since the laser power dependence is less than 3/2 and approaches zero. The corresponding data for the 2992.4-Å line resembles the rapidly rising portion of Figure 4. The power dependence was less than second order indicating some degree of saturation, but at a level insufficient to fill the focal volume at the same energy per pulse. However, the 0.6-Å peak width indicates that the first optical step is saturated, with the photoionizing step being rate limiting.

II. Mo. The wavelength region 2980–3025 Å was examined with approximately 2 mJ of energy per pulse, yielding the data shown in Figure 5. The single ground-state-originating transition occurring within this range (3002.2 Å) produced a strong RIMS signal. Additionally, there was an equally strong

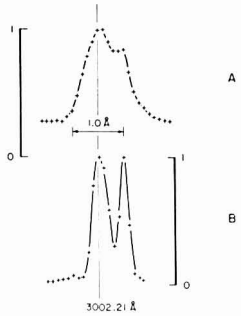


Figure 6. Relative $^{98}Mo^+$ ionization signal vs. wavelength, high resolution wavelength scan of 3002.2 Å line: (a) laser energy nominally 2 mJ; (b) laser energy nominally 0.2 mJ.

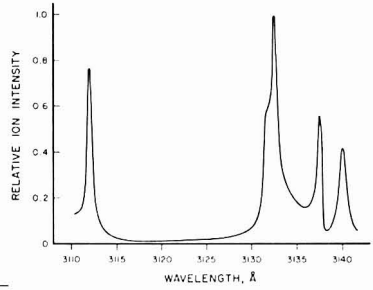


Figure 7. Relative $^{98}Mo^+$ ionization signal vs. wavelength, 3110–3142 Å; laser energy nominally 0.15 mJ.

peak occurring at 3002.7 Å which does not correspond to a tabulated line for molybdenum. As a final complication there was a moderate strength background signal with a quadratic laser power dependence. The major peaklike features in this continuum were reproducible and not due to large signal fluctuations. Again, none could be assigned to known transitions.

A factor-of-ten decrease in laser power significantly reduced the percentage of the signal due to the background continuum. In addition, the reduction in power broadening allowed good resolution of the two overlapping, strong spectral features. These effects are shown in Figure 6.

The wavelength region 3110–3142 Å was examined with approximately 150 μJ of energy per pulse, yielding the data shown in Figure 7. The two ground-state-originating transitions occurring within this range (3112.1 and 3132.6 Å) both produced strong RIMS signals. Additionally, there were strong peaks occurring at 3131.9, 3137.6, and 3140.1 Å, and the possibility of three weaker peaks each shifted about 1 Å lower in wavelength than these values. None of these lines correspond to tabulated values for molybdenum. However, the 3140.1-Å line agrees energetically with a transition connecting the $a^5G_4J = 5$ level (16 784.6 cm^{-1}) with the $x^3H^o_4J = 4$ level (48 622.1 cm^{-1}). Since the transition does not appear among those tabulated, such an assignment would be tenuous. The background signal was small due to the low laser power used in this spectral region although the quadratic dependence on laser power persisted.

Again the line widths were directly related to the tabulated line intensities. The peak at 3002.2 Å with an intensity of 190

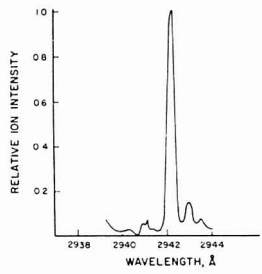


Figure 8. Relative $^{51}V^+$ ionization signal vs. wavelength, 2939–2944 Å; laser energy attenuated as described in text.

is 0.35 Å wide, that at 3112.1 Å with an intensity of 1400 is 0.5 Å wide, while that at 3132.6 Å with an intensity of 14 000 is 0.6 Å wide. The power dependence of the 3112.1 Å RIMS signal was similar to the rhenium data shown in Figure 4.

III. V. The wavelength region 2939–2949 Å was examined with approximately 2 mJ of energy per pulse. The result was a very strong, noisy looking RIMS signal with quadratic dependence on laser power. The spectrum was composed of an essentially flat background on which was superimposed reproducible, though unassignable, peaklike features. In an attempt to reduce this interference, the laser power was cut by eliminating the YAG amplifier and by a simultaneous ×10 attenuation in the ultraviolet excitation beam. This change in conditions produced a spectrum in which the vanadium 2942.4-Å ground-state-originating transition could be observed above the background. Finally, the focusing lens was removed to further decrease the power density in the sample irradiation region. The resultant spectrum from 2939.2–2944.1 Å is shown in Figure 8. Note that both ground-state-originating transitions (2942.4 and 2943.2 Å) are now observed. The laser power dependence of the RIMS signal was less than 1.5.

During mass scanning it was observed that there existed a relatively large VO^+ signal ($VO^+/V^+ = 25$) produced by laser ionization (IP of VO = 8 ± 1 eV). The ratio of thermal VO^+/V^+ was 5 at the same fixed temperature. With the same laser intensity as that employed to obtain the V^+ data of Figure 8, the VO^+ spectrum resembled the noisy looking background previously described for V^+ and 2 mJ of energy per pulse. The VO^+ RIMS signal most likely results from a two-photon ionization of VO thermally produced from the filament. Unfortunately, a laser power dependence of 1.76 for the data cannot substantiate the point (*23*). It is intriguing to hypothesize that the large nonresonance ionization background for V^+ is due to photodissociation of VO^+. To test this hypothesis will require a thermal vaporization source for vanadium from which oxide formation is avoided. Such a source is presently being developed.

CONCLUSIONS

Hurst has discussed the loss of selectivity attendant with a one-color, two-photon scheme (*6*). The basic problem is that when the laser is sufficiently powerful to saturate the overall process, it is usually many times more powerful than that required to saturate the bound transition. Thus, when the laser is tuned relatively far from the line center, the element can still produce a strong RIMS signal. This loss of spectroscopic selectivity is not as critical in RIMS as in RIS because of the elemental selectivity provided by the mass spectrometer. Only selectivity between elements with common isobars is critical in RIMS. Thus, the resonance ionization scheme used here is analytically very useful because of the range of elements that can be ionized by a single laser.

For the three elements studied, it has been shown that the tabulated intensities for the lines are unrelated to the magnitude of the RIMS signal: e.g., compare the values in Table III for molybdenum and the resulting spectral data. As a result, the transitions that are weakly coupled with the ground state may provide the best combination of sensitivity and selectivity, while simultaneously greatly broadening the choice of transitions for chemical analysis.

Although the necessity for spectral selectivity is reduced in RIMS, the appearance of excited-state-originating transitions and untabulated lines with significant intensities increases the probability of spectral interferences. Furthermore, the presence of a two-photon ionization continuum background also will reduce selectivity between elements with isobars. The experimental situation presented here illustrates the interesting behavior that the signal-to-background ratio can be increased by decreasing the laser power. The appearance of this ionization continuum seems to be inversely related to the ionization potential, although its production via the decomposition of a molecular species cannot yet be ruled out.

For the experimental RIMS system used here, the 10-Hz repetition rate of the laser provides a significant limitation to sensitivity. However, the sensitivity per pulse allows Langmuir vaporization systems to be studied at lower temperatures than required to achieve significant thermal ionization. As a result, RIMS has the potential to analyze very small amounts of high ionization due to the typical rapid depletion of the sample. Although the experimental determination of absolute measurement sensitivities was not attempted, the RIMS signal should have been comparable to the thermal ion signal for these elements at the temperatures studied due to the relatively large neutral-to-ion ratios as defined by the Saha–Langmuir equation. Ideally, as an analytical technique, the highest sensitivity requires matching the laser duty cycle with pulsed atomization sources such as laser probe or pulsed sputtering sources. Or, alternatively, the use of lasers with repetition rates required to provide a 100% effective duty cycle would also provide the highest sensitivity. The commercial introduction of such lasers is expected.

Although the experiments reported here were done with a single filament source, the generic nature of the vaporization processes in the single and multiple filament sources is extremely important for the broad utilization of RIMS in analytical measurements. It should be emphasized that while the current experiments focused on metal atoms such as those that result from molecular decomposition, the other atomic decomposition products are equally important. For example, in the second step of the type Ib and in the final step of the type II mechanisms, the production of $X^0(g)$ also occurs. This offers a completely unexplored potential for the RIMS analysis of different classes of elements, such as the halides. Based in part on previous theoretical and experimental investigations (*12*, *14*) and on a broad base of studies of high temperature phenomena (e.g., ref 25), it is possible to conclude that, in principle, these vapor sources can be tailored to produce atom reservoirs for any element in the periodic table that can exist as part of a condensed-phase compound under vacuum.

These experiments demonstrate that by combining optical spectroscopy and mass spectrometry the fundamental processes involved in each are more readily accessible and understood. It is the understanding of these fundamental processes that allows the ultimate exploitation of an analytical technique.

LITERATURE CITED

(1) Beekman, D. W.; Callcott, T. A.; Kramer, S. D.; Arakawa, E. T.; Hurst, G. S. *Int. J. Mass Spectrom. Ion Phys.* **1980**, *34*, 89–97.
(2) Donahue, D. L.; Young, J. P.; Smith, D. H. *Int. J. Mass Spectrom. Ion Phys.* **1982**, *43*, 293–307.
(3) Miller, C. M.; Nogar, N. S.; Gancarz, A. J.; Shields, W. R. *Anal. Chem.* **1982**, *54*, 2377–2378.
(4) Donahue, D. L.; Young, J. P. *Anal. Chem.*, in press.
(5) Winograd, N.; Baxter, J. P.; Kimock, F. M. *Chem. Phys. Lett.* **1982**, *88*, 581–584.
(6) Hurst, G. S.; Payne, M. G.; Kramer, S. D.; Young, J. P. *Rev. Mod. Phys.* **1979**, *51*, 767.
(7) Hurst, G. S.; Nayfeh, M. H.; Young, J. P. *Appl. Phys. Lett.* **1977**, *30*, 229.
(8) Styris, D. L.; Kaye, J. H. *Anal. Chem.* **1982**, *54*, 864.
(9) Barnes, I. L.; Garner, E. L.; Gramlich, J. W.; Moore, L. J.; Murphy, T. J.; Machlan, L. A.; Shields, W. R.; Tatsumoto, M.; Knight, R. J. *Anal. Chem.* **1973**, *45*, 880.
(10) Cali, J. P.; Mandel, J.; Moore, L. J.; Young, D. S. *NBS Spec. Publ. (U.S.)* **1972**, *No. 260–36*.
(11) Gramlich, J. W.; Machlan, L. A.; Brletic, K. A.; Kelly, W. R. *Clin. Chem. (Winston-Salem, N.C.)* **1982**, *28*, 1309.
(12) Moore, L. J.; Heald, E. F.; Filliben, J. J. *Adv. Mass Spectrom.* **1978**, *7A*, 448.
(13) Kanno, H. *Bull. Chem. Soc. Jpn.* **1971**, *44*, 1808.
(14) Moore, L. J.; Heald, E. F., unpublished work, NBS 1982.
(15) Rec, J. R.; Myers, W. G.; White, F. A. *Anal. Chem.* **1974**, *46*, 1243.
(16) Shields, W. R., Ed. *NBS Tech. Note (U.S.)* **1966**, *No. 277*.
(17) Moore, L. J.; Machlan, L. A.; Shields, W. R.; Garner, E. L. *Anal. Chem.* **1974**, *46*, 1082.
(18) Edwards, J. W.; Johnston, H. L.; Blackburn, P. E. *J. Am. Chem. Soc.* **1951**, *73*, 4727.
(19) Gramlich, J. W.; Murphy, T. J.; Garner, E. L.; Shields, W. R. *J. Res. Natl. Bur. Stand., Sect. A* **1973**, *77A*, 691.
(20) Meggers, W. F.; Corliss, C. H.; Scribner, B. F. "Tables of NBS Spectral Line Intensities Part I-Arranged by Elements", 2nd ed.; U.S. Department of Commerce, National Bureau of Standards: Washington, DC, 1975; NBS Monograph 145.
(21) Hultgren, R.; Desal, P. D.; Hawkins, D. T.; Gleiser, M.; Kelley, K. K.; Wagman, D. "Selected Values of the Thermodynamic Properties of the Elements"; Am. Soc. for Metals: Metals Park, OH, 1973.
(22) Shimoda, K. In "High-Resolution Laser Spectroscopy"; Shimoda, K., Ed.; Springer-Verlag: New York, 1976; Chapter 2.
(23) Speiser, S.; Jortner, J. *Chem. Phys. Lett.* **1976**, *44*, 399.
(24) Eichelberger, T. S.; Fisanick, G. J. *J. Chem. Phys.* **1981**, *74*, 5962.
(25) Hastie, J. W. "High Temperature Vapors"; Academic Press: New York, 1975.

RECEIVED for review October 25, 1982. Accepted December 13, 1982. F. E. Lytle wishes to acknowledge partial support of this work by the National Science Foundation. J. C. Travis wishes to acknowledge support by the Defense Nuclear Agency. In order to describe adequately experimental procedures, it is necessary to identify commercial products by manufacturer's name or label. In no instance does such identification imply endorsement by the National Bureau of Standards nor does it imply that the particular products or equipment are necessarily the best available for that purpose.

Kinetic and Equilibrium Studies of Insulin Immunoaffinity Chromatography

J. Richard Sportsman, James D. Liddil, and George S. Wilson*

Department of Chemistry, University of Arizona, Tucson, Arizona 85721

The kinetic and equilibrium characteristics of the interaction of insulin with a specific antibody immobilized on silane-treated controlled pore glass beads have been evaluated by using the technique of "high-performance immunoaffinity chromatography" (HPIC). A previously described equilibrium model was verified and used to establish the equilibrium constants for the reaction of the immobilized antibody with insulin in the mobile phase. Computer simulations and experimental data were used to demonstrate the contribution of nonspecific interactions with the support to the overall binding process. An estimate is also made of the rate of the antibody–antigen complex formation reaction, and its effect on immunochromatographic investigations is discussed.

Immunoaffinity chromatography is a widely used technique for the purification of antibodies and antigens (*1*). A column consisting of covalently immobilized antibody or antigen ("immunosorbent") allows the convenient and selective sorption of the soluble component (ligate). It specifically binds to the immunosorbent from a mixture of contaminants which are washed away prior to recovery of the ligate through desorption by some change in mobile phase composition, typically a change in pH (*1*). In a previous report (*2*) we demonstrated that antibodies immobilized on silane-treated porous glass could be used as immunosorbents at relatively high flow rates. Thus we designated the technique high-performance immunoaffinity chromatography (HPIC). The application of HPIC to rapid immunoassays and protein purification requires that limitations imposed by the kinetics and thermodynamics of interphase interactions be assessed. It has been shown that the limit of detection in radioimmunoassays is on the order of $0.1K_0^{-1}$ where K_0 is the average affinity constant of the antiserum (*3, 4*). By similar arguments it can be shown that the performance of purification schemes based on immunoaffinity chromatography will depend on the relative magnitudes of the affinities and concentrations of the substances involved. The kinetics of these systems will also be important to optimization of experimental conditions.

It was shown previously that the binding of antigen by an HPIC column could be described in terms of an apparent binding constant, K', and an apparent total binding site concentration $(Ab)_t$, whose values could be determined by assessing the extent of antigen binding as a function of concentration according to quasi-equilibrium arguments (*2*). The values of K' were shown to vary inversely with flow rate.

Given these observations, we decided to investigate whether an increase in concentration of antibody binding sites would show up as a corresponding increase in the value of (Ab), and whether this would affect the value of K'. Since the value of K' appears to change with flow rate and hence residence time of antigen in the column, we also undertook kinetic studies to further elucidate this phenomenon.

We report results here which demonstrate the kind of behavior predictable by such an equilibrium treatment. For this study we have elected to use the binding of the antigen insulin by an antiserum exhibiting high affinity in order to be able to investigate the behavior of the system down to subnanomolar antigen concentrations.

EXPERIMENTAL SECTION

Materials. Lichrospher SI 1000 (10 μm diameter microporous silica of 100 Å pore size) was obtained from MC/B Manufacturing Chemists, Inc., Cincinnati, OH. Glycidoxypropyltrimethoxysilane (GOPS) was obtained from Petrarch Systems, Inc., Levittown, PA. Crystalline bovine zinc insulin was the gift of Mary Root of Lilly Research Laboratories, Indianapolis, IN. [^{125}I]insulin (porcine), 130 μCi/μg, was obtained from New England Nuclear, Inc., Boston, MA, and was purified by gel filtration on Sephadex G-75F (Pharmacia, Inc., Piscataway, NJ) (50 cm × 1 cm), using the second hot peak material (*5*) which comprised antigen of high (>90%) immunoreactivity. Competitive binding studies of this material with subnanomolar concentrations of unlabeled insulin showed that labeling did not significantly affect binding characteristics and demonstrated the similar high affinity of the antiserum for both porcine and bovine insulin.

Lyophilized antisera to porcine insulin, raised in the capybara, were the gift of Ernest C. Adams of Miles Laboratories, Inc., Elkhart, IN, and were received as lyophilized whole sera (*5*). The globulin fraction of the reconstituted antisera was prepared by precipitation with Na_2SO_4 three times, followed by dialysis against 0.2 M borate buffered saline, 0.85%, pH 9.0 (BBS). The specific antibody was shown to comprise 7% of the total globulin protein by a Scatchard plot of binding data obtained originally in the form of a competitive binding assay standard curve for insulin in the region of nanomolar concentrations. The hyperbolic shape of the Scatchard plot suggested that the native antiserum exhibited affinities for the antigen in the range of 10^7–10^{10} L/mol. Bovine serum albumin (BSA), "RIA grade", was obtained from Sigma Chemical Co., St. Louis, MO. Normal guinea pig serum gamma globulin, purified by preparative isoelectric focusing, was the gift of Perry Cole of the V.A. Hospital, Tucson, AZ. This was used as a control for nonimmunospecific binding since normal capybara globulin was not available. The close immunochemical similarity of capybara and guinea pig gamma globulin has been reported (*5*).

The silanization of the silica support by aqueous GOPS to give a diol bonded phase was performed as previously described (*2*). This bonded silica was given the designation "G23".

The capybara immune globulin or normal guinea pig gamma globulin (NGPG) was then attached to this support by reductive alkylation as also described in ref 2. Analysis of the resulting capybara globulin immunosorbent by hydrolysis in 6 N HCl (*2*) followed by Folin-Lowry protein assay (*6*) gave a value of 6.3 mg of protein/g of glass (dry weight basis). The antiserum as supplied was labeled "CAPY. 2". The resulting immunosorbent was given the abbreviated designation "CP2-G23".

Apparatus. Spectral measurements were made with a Cary 219 UV-VIS spectrophotometer. Counting of [^{125}I]insulin was done on a Nuclear Chicago Model 4454 gamma well counter. The liquid chromatograph used was a SpectraPhysics Model 8700 solvent delivery system. The column used for HPIC work is shown in Figure 1. It consists of a Swagelok ZDV $^1/_4$ in. to $^1/_{16}$ in. reducing union with a 2-μm stainless steel frit secured into the bottom. The actual "column" consists of 50–70 mg of derivatized silica support material. A silanized glass wool plug takes up any dead space between the column head and the special inlet fitting, which is made by silver-soldering a $^1/_{16}$ in. (0.002 in. i.d.) 316 stainless steel (SS) tube into a $^1/_4$ in. i.d. (0.2 cm i.d.) 316 SS sleeve

0003-2700/83/0355-0771$01.50/0 © 1983 American Chemical Society

Table I. Effect of Immunosorbent Concentration on Observed $[Ab]_t$ and K' as Determined by HPIC[a]

immunosorbent added, mg	added $[Ab]_t$,[b] M	obsd $[Ab]_t$,[c] M	% active[d]	K_L',[e] M^{-1}	$(B/F)_0$[f]
1.8	3.8×10^{-7}	4.9×10^{-9}	12.9	1.1×10^{7}	0.51
8.8	1.9×10^{-6}	1.5×10^{-7}	7.9	2.1×10^{7}	3.6
23.0	4.9×10^{-6}	4.3×10^{-7}	8.8	3.6×10^{6}	6.9
58	1.2×10^{-5}	1.1×10^{-6}	9.2	7.5×10^{5}	7.1
0[g]					0.17

[a] Conditions: 0.4 mL/min flow rate; antigen, insulin with [^{125}I]insulin as tracer in 0.2% BSA/PB; volume injected, 0.050 mL; elution scheme, see text. [b] Determined from volume of immunosorbent suspension added to suffcient diol bonded silica to make 70 mg of mixture and from known protein content of immunosorbent. [c] Determined from extrapolation of Scatchard plots. [d] Ratio of experimental $[Ab]_t$ to added $[Ab]_t$. [e] Determined from the limiting slope of line from Scatchard plot used to calculate $[Ab]_t$. [f] B/F ratio at zero unlabeled antigen concentration. [g] Column consists only of diol bonded phase.

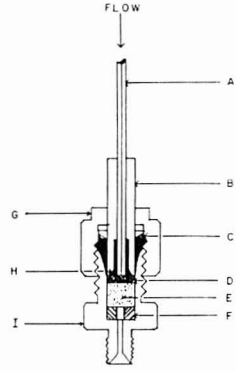


Figure 1. Column for HPIC studies: (A) $^1/_{16}$ in. o.d., 0.002 in. i.d., 316 stainless steel (SS) tubing; (B) $^1/_4$ in., 2.2. mm i.d. SS tubing; (C) $^1/_4$ in. ferrules; (D) glass wool plug; (E) immunosorbent; (F) 5-μm frit; (G) $^1/_4$ in. Swagelok nut; (H) silver solder seal; (I) ZDV reducing union.

as shown. Thus the column dimensions are 6 mm i.d. × 0.5 cm length. It was found that such columns are best packed by slurrying the immunosorbent in 0.1 M phosphate buffer with 0.8% NaCl (PBS) and allowing the particles to settle by gravity.

In the quantitative study of the effect of variation of antibody binding sites in HPIC, a series of columns as described above were packed with sorbents consisting of various microliter volumes of immunosorbent suspension (100 mg/mL) added to 70 mg of diol bonded phase. The mixture was ultrasonicated and then packed as described.

Binding measurements by HPIC were performed by making appropriate dilutions of antigen with 0.1% (w/v) BSA in PBS, adding [^{125}I]insulin to give an activity of 10 000 counts/min per 100 μL, and then injecting 50-μL samples onto the column at a given flow rate. At this point, the mobile phase is 0.1 M phosphate, pH 7.0. After 2 mL, including the "free" fraction (F), had been collected at the column outlet, the mobile phase is changed to 0.1 M sulfamic acid, pH 1.2, whereupon antigen bound to the antibody on the column is displaced (*2*). Eluting antigen is again collected as a 2-mL fraction (fraction B for "bound"). The ^{125}I activity of each fraction is then determined. Recoveries of activity were always above 95%. The temperature of the column was maintained at 33 °C by a thermostated water bath.

Binding data were evaluated as described in ref 2. It was shown previously that an apparent binding constant could be calculated by determining the ratio of bound to free antigen (B/F) and plotting this value against the concentration of bound antigen, for several initial concentrations of antigen (*2*). The method for determining equilibrum constants as given by Scatchard (*7*) is rearranged to give

$$B/F = [Ab]_t K' - [B]K' \quad (1)$$

Thus K' is determined from the slope of the plot, and $[Ab]_t$, the total binding site concentration, is given by the intercept on the abcissa. Since only the labeled antigen is directly measured, it is necessary to assume essential identity of labeled and unlabeled antigen, as in ordinary cold competition binding assays (*8*).

Method for HPIC Kinetic Measurements. The kinetics of insulin HPIC were studied at 33 °C by measuring the extent of binding of G-75 fractionated [^{125}I]insulin, the concentration of which was 0.05 ng/mL as calculated from the specific activity (130 μCi/μg) after allowing for isotopic decay time and counter efficiency. Aliquots of 50 μL were injected and "bound" and "free" fractions were collected as before.

Batch Kinetics. The kinetics of a batch mode binding of [^{125}I]insulin to immunosorbent were studied at 33 °C by adding 0.15 mL of [^{125}I]insulin (approximately 30 000 counts/min or 0.05 ng/mL) to 0.25 mL of a suspension of CP2-G23 in 1.5-mL microcentrifuge tubes (precoated with 1% BSA for 2 h, followed by rinsing and drying). The CP2-G23 suspension had 1.0 mg of immunosorbent/mL of BSA buffer.

The mixture was agitated at once and continuously until the desired time elapsed, at which point the tube was centrifuged at 12000*g* for 3 min, effectively stopping the reaction. The supernatants were decanted and the pellets counted.

RESULTS AND DISCUSSION

According to the previously developed model it might be predicted that increasing the antibody content of the HPIC column would affect only the parameter $[Ab]_t$ (eq 1), while the slope of the Scatchard plots would remain the same.

The results of varying the specific immunosorbent concentration of an HPIC column are summarized in Table I. The values of the parameter $[Ab]_t$ were determined by extrapolation of the Scatchard plots to the abscissa as in ref 2. A linear correlation exists between the weight of immunosorbent added and the value of $[Ab]_t$ subsequently observed in accordance with expected behavior.

The lower limiting slope of the extrapolated line in the Scatchard plot should be a measure of the lower limit of apparent binding constant K_L' for an immunosorbent exhibiting heterogeneity of binding affinities (*9*). In Table I it may be seen that these limiting affinities appear to decrease with increasing immunosorbent concentration.

The fact that the values of $[Ab]_t$ are ten-fold less than the amount of globulin protein known to be immobilized on the immunosorbent could be taken to support earlier conclusions that the immoblization of an antibody results in significant loss of activity (*2*, *10*). However, antibody comprised only about 7% of the total protein in the immune serum globulin. Thus when the expected 80%–90% loss of activity upon immobilization is taken into account, a value for the percent activity of less than 1.5 should be obtained instead of the higher values shown in Table I. This led us to suspect that the matrix of the immunosorbent might be contributing to the binding of the antigen through nonspecific interactions. Batch experiments run with unmodified diol bonded phase

Table II. Simulation of Equilibrium Binding of Antigen by a Support Material Exhibiting 3-Fold Heterogeneity[a]

simulation	$[Ab]_t$ actual, M	$[Ab]_t$ apparent, M	K_L', M^{-1}
1	2×10^{-9}	3.3×10^{-8}	3.5×10^{7}
2	2×10^{-8}	2.5×10^{-7}	5.6×10^{6}
3	1×10^{-7}	2.2×10^{-6}	9.3×10^{6}
4	2×10^{-7}	9.6×10^{-6}	6.4×10^{5}

[a] A support with components B1, B2, and B3 having equilibrium constants K_1, K_2, and K_3 reacts to equilibrium with monovalent antigen: $K_1 = 10^{10}$, $K_2 = 10^{8}$, and $K_3 = 10^{2}$ L/mol; $[B3] = 1 \times 10^{-3}$ M; $[B1] = [B2]$ and $[B1] + [B2] = [Ab]_t$ actual in all simulations. In all cases the range of antigen concentration [Ag] is from $5([B1] + [B2]) > [Ag] > 0.05([B1] + [B2])$.

and with immobilized NGPG showed a binding affinity for insulin of 10^2 to 10^4, indicating that nonspecific adsorption of the antigen is a significant process.

Computer simulation of the equilibrium binding of an antigen to a heterogeneous antibody was then undertaken to see whether the discrepancy of values for $[Ab]_t$ in Table I might be explained by invoking the presence of low affinity nonspecific interactions. Scatchard plots for hypothetical antigen–antibody binding experiments were generated. Here, antibody heterogeneity was mimicked by assuming the existence of a mixture of two discrete antibody populatons, each with its own affinity constant and concentration. The antibodies were assumed to be of two discrete types, having binding constants K_1 and K_2 of 1×10^{10} and 1×10^{8} L/mol, respectively. Their concentrations B1 and B2 were assumed to be equal. The third interaction was then assumed to involve sites on a diol bonded phase with a binding constant K_3 of 1×10^{2} and a concentration B3 equal to that of the diol moieties on the bonded phase (viz., approximately 100 μmol/g). This translates into an effective column concentration of diol of about 1×10^{-3} M. The monovalent antigen (Ag) was then assumed to react to equilibrium with all binding sites. Such a model can be represented by the relationship

$$[Ag]_b = \frac{[Ag]_f[B1]K_1}{[Ag]_fK_1 + 1} + \frac{[Ag]_f[B2]K_2}{[Ag]_fK_2 + 1} + \frac{[Ag]_f[B3]K_3}{[Ag]_fK_3 + 1} \quad (2)$$

where $[Ag]_b$ and $[Ag]_f$ represent bound and unbound antigen concentrations, respectively, at equilibrium. Concentrations of the antigen and antibodies in the simulated experiments were chosen to cover the ranges studied in the actual experiments. The results of several simulations are reported in Table II.

As can be seen, the presence of a high concentration of low affinity sites amidst relatively low concentrations of high affinity sites gives binding behavior, based on equilibrium models, which leads to an estimation of bonding site concentrations which is higher than that due solely to the high affinity sites. It can also be seen that the magnitude of this overestimation decreases as the high affinity site concentrations increase. Finally, the limiting slope of the Scatchard plots also decreases with an increase in the high affinity site concentration.

Precisely these trends, with similar magnitudes, are observed in the data of Table I. Figure 2 gives a comparison of theoretical and experimental results. As the concentration of the high affinity immunospecific sites ($[Ab]_t$) increases with respect to those of low affinity, the concentration range of antigen assessed must also be increased. A decrease in the limiting affinity, K_L', results, a trend which is seen both in experimental results and in the simulations; this is attributed to the increasing contributions to the overall binding from nonspecific sites at increasing Ag concentrations. The influ-

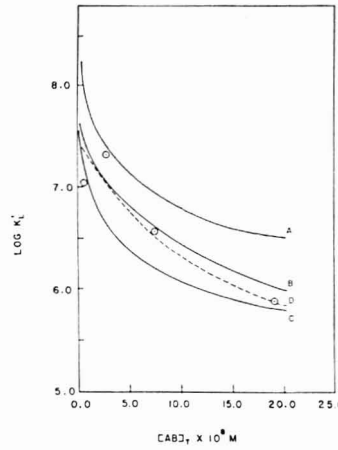


Figure 2. Effect of nonspecific binding on apparent affinity constants: (A) $K_1 = 10^{11}$, $K_2 = 10^{9}$ L/mol, $[B] = 1 \times 10^{-3}$ M; (B) $K_1 = 10^{11}$, $K_2 = 10^{9}$ L/mol, $[B3] = 2 \times 10^{-3}$ M; (C) $K_1 = 10^{10}$, $K_2 = 10^{8}$ L/mol, $[B3] = 1 \times 10^{-3}$ M; (D) line drawn through experimental data (circled points). Other conditions are as given in Table II.

ence of the low affinity sites is markedly illustrated by comparing curves A and B of Figure 2. Here, a doubling of the concentration of low affinity sites causes the theoretical curve to shift downward as shown; this is to be compared with the shift (curve C) caused by a 10-fold reduction in the antibody binding constants.

From a comparison of experimental and theoretical results we conclude that the change in K_L' seen in Table I is one predictable by equilibrium arguments. Furthermore, the assumptions made regarding the relative values of the various binding parameters are qualitatively consistent with the chosen model. It is also predicted from this model that the error in assessing the value of $[Ab]_t$ from equilibrium binding data is a function of both the concentration [B3] and affinity K_3 of the nonspecific site. Figure 3 shows that as the product of these two values increases relative to those of the high affinity interactions $[Ab]_t \times K_0$, where $\log K_0 = (\log K_1 + \log K_2)/2$, a point is reached after which the error in $[Ab]_t$ becomes intolerable. Using the approximate values of the parameters for our experimental data, we calculate an overestimation of about 10% in $\log [Ab]_t$, which agrees with the experimental error observed.

It seems reasonable therefore to assume that a quasi-equlibrium model for HPIC provides a simple but effective conceptual basis for understanding the individual contributions of matrix and antibody to the observed binding of antigen. It should be noted that these errors in estimation of binding parameters would not be expected to show up as concomitant errors in an immunoassay based on HPIC, since a calibration curve may still be generated with appropriate standards. However, when the extent of nonspecific binding (e.g., $[B3]K_3$) becomes large enough relative to specific binding ($[Ab]_tK_0$), the precision or steepness of the standard curve will be adversely affected and the accuracy will become sensitive to interferences from the analyte matrix.

That genuine biospecific interactions predominate in the present study is indicated by the low value of $(B/F)_0$, the B/F ratio of labeled antigen alone, when only diol bonded phase is present, as shown in Table I. Further, since these values

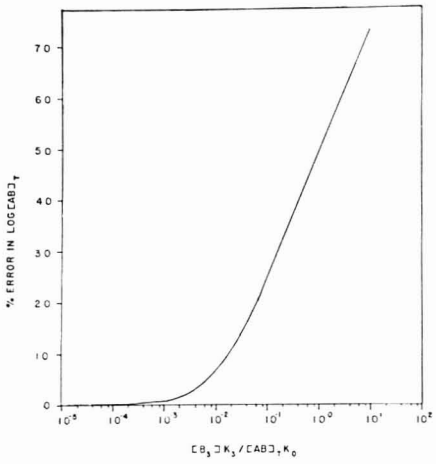


Figure 3. Effect of nonpspecific binding on determination of antibody concentration: $[Ab]_t = 2 \times 10^{-8}$ M; $K_0 = 1 \times 10^9$ M^{-1}.

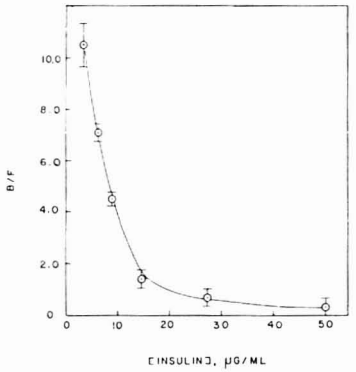


Figure 4. Standard curve for insulin immunoassay by HPIC: column, 5 mm × 6 mm i.d., CP2-G23 mixture (see text for composition); flow rate, 0.5 mL/min; volume injected, 50 μL; T, 33 °C. Bound to free ratio (B/F) is based on activity of tracer [^{125}I]insulin recovered in each fraction. Points shown represent average of duplicate determinations.

are obtained at the concentration of labeled antigen which is roughly equal to 1×10^{-11} M, the ability of the HPIC technique to perform extremely sensitive assays is indicated.

Figures 4 and 5 are standard curves for an insulin immunoassay at two different ranges of antigen concentration. In Figure 4, the standard curve covers the range of 0.1–2 μg/mL, and here the HPIC column is packed with 75 mg of immunosorbent only. In Figure 5, the standard curve covers the range 10–300 ng/mL, and the column has been packed with a mixture of 1 mg of immunosorbent and 70 mg of diol bonded phase.

Kinetic Studies. The approximation of equilibrium implies that the kinetics of HPIC are rapid. The range of flow rates over which analytical measurements may be made will depend on these kinetics as well. The rate of formation of the antibody–antigen complex in HPIC may be estimated by

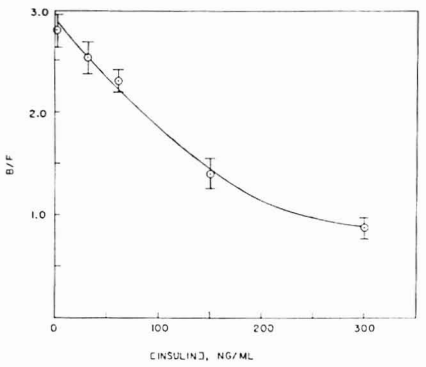


Figure 5. Standard curve for insulin immunoassay by HPIC. Conditions as in Figure 4. Column: see text for composition.

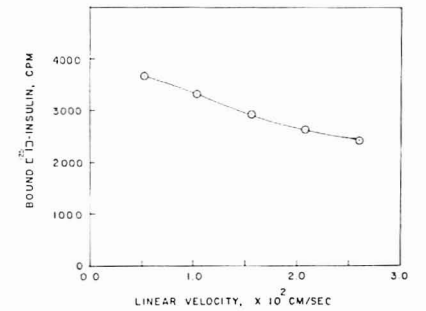


Figure 6. Flow rate dependence for the binding of [^{125}I]insulin to HPIC column. Column and other conditions are as given in Figure 4. Flow rates = 0.1–0.5 mL/min.

varying the flow rate and hence residence time of the antigen in the column.

Figure 6 is a plot of the flow rate dependence of the extent of [^{125}I]insulin binding to an HPIC column. It can be seen that a 5-fold decrease in flow rate results in only a 50% increase in the total number of counts bound; this would seem to indicate that at least two kinetically distinct binding processes are occurring: one fast, possibly diffusion limited, the other considerably slower. Assuming reversible second-order kinetics, one can treat the data of Figure 6 to obtain an apparent forward rate constant, k_f', for this slower process of 3.6×10^6 M^{-1} s^{-1}. This is to be compared with the results of the batch kinetics experiment whose results are shown graphically in Figure 7. In both cases the data are plotted according to the integrated form of a second-order reversible rate expression

$$f(X) = \frac{1}{(\bar{X}' - \bar{X})} \ln \left(\left| \frac{X}{\bar{X}'} \right| \cdot \left| \frac{\bar{X}' - X}{\bar{X} - X} \right| \right) = k_f' t \qquad (3)$$

where $\bar{X}$ is the equilibrium value of bound antigen concentraton and X is the value at any time T; $\bar{X}'$ is given by

$$\bar{X}' = \frac{K([Ag]_0 + [Ag]_0) + 1}{K} - \bar{X} \qquad (4)$$

where $[Ag]_0$ and $[Ab]_0$ are initial antigen and antibody concentrations, respectively (*11*).

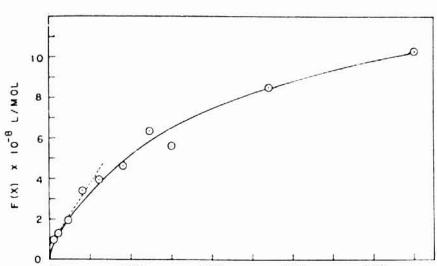


Figure 7. Batch mode kinetics of [^{125}I]insulin binding to CP2-G23 immunosorbent. Dashed line is the initial slope referred to in text.

It can be seen that the slope of this plot is clearly not a straight line. Since the kinetics of antibody–antigen reactions in both heterogeneous and homogeneous reaction phases are known to follow a second-order rate law (*12, 13*) the curvature of this plot evidently is due to heterogeneity of antigenic binding sites and reflects the contribution of several separate forward rates (*14*) some of which may be due to nonspecific binding. Taking the initial slope ($10 \text{ s} < t < 120 \text{ s}$), a value for k_f' of $3.4 \times 10^6 \text{ M}^{-1} \text{ s}^{-1}$ is obtained, comparable to the value obtained for the "slower" process alluded to above in the description of flow rate dependence of antigen binding.

The nonzero intercept of this line suggests that still faster reactions (greater than $10^7 \text{ M}^{-1} \text{ s}^{-1}$) are occurring which cannot be measured by present techniques. Studies at higher flow rates were then undertaken to observe these faster kinetics. The results of such studies at 0.5–3.0 mL/min gave a linear relationship when plotted according to eq 2 and a forward rate of $3 \times 10^7 \text{ M}^{-1} \text{ s}^{-1}$. It has been noted that the forward step of many antigen- and hapten–antibody reactions proceeds at diffusion-limited rates (*7*). The observed "fast" kinetics are consistent with such processes.

Affinity chromatography has been proposed as a method for the determination of rapid forward rate constants on the basis of a statistical treatment of band broadening of an isocratically eluted peak (*15*). Such a model assumes relatively low affinity and fast reverse rate constants. As we have shown here, an apparent forward rate constant k_f' of $3 \times 10^7 \text{ M}^{-1} \text{ s}^{-1}$ is obtained by kinetic assessment of the flow rate dependence of antigen binding. If the average affinity K_0 of the immunosorbent is conservatively estimated to be $5 \times 10^9 \text{ M}^{-1}$, a value of $6 \times 10^{-3} \text{ s}^{-1}$ is obtained for k_r', the apparent reverse rate constant. On the time scale of these experiments, an essentially irreversible reaction thus results, and the error due to dissociation of specific complexes can be considered negligible. Indeed, the irreversible nature of insulin binding to high affinity antisera has already been reported (*16*). We have observed that the recovery of bound [^{125}I]insulin is not measurably affected by long (10 min) delays between adsorption and desorption, consistent with the above calculations.

In this study it has been assumed that the rate-limiting step in binding is the intrinsic forward rate of the antibody–antigen reaction, and that the effect of changing the flow rate is merely one of changing the residence or reaction time of the antigen in the column. Horvath has demonstrated that the major factor leading to nonequilibrium in high-performance liquid chromatography (HPLC) is the kinetic limitation of solute–stationary phase interaction and not mass transport phenomena, provided that particle size and flow rates are of magnitudes similar to those employed in this work (*17*). High affinity interactions with fast forward rate kinetics should show behavior approximating equilibrium at diminishing flow rates, an observation which we have noted previously (2).

We have observed in the course of this work that the nonspecific interactions of insulin with immunosorbents and unmodified silica proceed at much lower rates than those for the specific binding by immobilized antibody. This suggests that HPIC may be advantageously used in an isokinetic fashion to discriminate between biospecific and nonspecific binding on the basis of the slower rates of the latter. The ability to determine relatively rapid kinetics of antibody–antigen reactions by HPIC is indicated. This should prove useful in many areas of immunochemical research.

In conclusion it can be said that the theory of HPIC provides a model for assessing the effects of changes in binding site concentration. That this theory holds for systems utilizing such low concentrations as reported here bodes well for the development of rapid protein-binding assays by HPIC. The data shown here demonstrate that equilibrium is very nearly approached in HPIC as in other forms of chromatography and hence a quasi-equilibrium theory is appropriate and adequate to describe the binding behavior within the limits prescribed by the extent and nature of any competing nonspecific adsorptive processes.

Registry No. Insulin, 9004-10-8.

LITERATURE CITED

(1) Ruoslahti, E., Ed. "Immunoadsorbents in Protein Purification"; University Park Press: Baltimore, MD, 1976.
(2) Sportsman, J. R.; Wilson, G. S. *Anal. Chem.* **1980**, *52*, 2013–2018.
(3) Yalow, R. S.; Berson, S. A. In "Principles of Competitive Protein Binding Assays"; Odell, W. D., Daughaday, W. H., Eds.; Lippincott: Philadelphia, PA 1977; p 1.
(4) Schuurmann, H. J; de Liguy, C. L. *Anal. Chem.* **1979**, *51*, 2–7.
(5) Adams, E. C.; Layman, K. M.; Hartnagel, R. *Ann. Clin. Lab. Sci.* **1974**, *4*, 19–28.
(6) Peterson, G. L. *Anal. Biochem.* **1977**, *83*, 346–356.
(7) Richard, R. F.; Rosenstein, R. W.; Varga, J. M.; Konigsberg, W. H. In "Immunoglobulins"; Litman, G. W., Good, R. A., Eds.; Plenum: New York, 1978; pp 138–141.
(8) Farr, R. S. *J. Infect. Dis.* **1958**, *103*, 239.
(9) Zettner, A. *Clin. Chem.* (*Winston-Salem, N.C.*) **1973**, *19*, 699–705.
(10) Line, W. E.; Siegel, S. J.; Kwong, A.; Frank, C.; Ernst, R. *Clin. Chem.* (*Winston-Salem, N.C.*) **1973**, *19*, 1361–1365.
(11) Emanuel, N. M.; Knorre, D. G. "Chemical Kinetics"; Wiley: New York, 1969; pp 174–179.
(12) Day, E. D. "Advanced Immunochemistry"; Williams and Wilkins: Baltimore, MD, 1972; pp 183–217.
(13) Hertl, W.; Odstrchel, G. *Mol. Immunol.* **1979**, *16*, 173–178.
(14) Berson, S. A.; Yalow, R. S. *J. Clin. Invest.* **1959**, *38*, 1996–2016.
(15) Denizot, F. C.; Delaage, M. A. *Proc. Natl. Acad. Sci. U.S.A.* **1975**, *72*, 4840–4843.
(16) Keane, P. M.; Walker, W. H. C.; Gauldie, J.; Abraham, G. E. *Clin. Chem.* (*Winston-Salem, N.C.*) **1976**, *22*, 70–73.
(17) Horvath, C.; Lin, H. *J. Chromatogr.* **1978**, *149*, 43–70.

RECEIVED for review April 19, 1982. Resubmitted October 5, 1982. Accepted January 18, 1983. This research was supported in part by National Science Foundation Grant CHE 80-22286.

Determination of Rate Constants of Pseudo-First-Order Electrocatalytic Reactions from Overlapped Voltammetric Data

James F. Rusling* and Thomas F. Connors

Department of Chemistry, U-60, University of Connecticut, Storrs, Connecticut 06268

A method based on nonlinear regression is described for determination of rate constants of rate-determining solution electron-transfer reactions in kinetically controlled redox electrocatalytic processes from linear-sweep voltammograms severely overlapped with the current for direct reduction of the substrate. The five-parameter regression equation employed one term to describe the catalytic current and a second term to describe the background. The method gave accurate rate constants from simulated voltammograms with varying degrees of overlap. Regression analysis gave more precise rate constants than direct background subtraction for electrocatalytic reduction of 4,4′-dichlorobiphenyl in DMF with anthracene as the catalyst. Severely overlapped catalytic voltammograms could be distinguished from those obtained from noncatalytic systems using deviation-pattern recognition.

Redox electrocatalytic reductions involve electron transfer to a substrate in solution through mediation of a soluble catalyst (*1*, *2*). Electrocatalysis lowers the overpotential for reduction of the substrate and amplifies the cathodic current. This amplification has been used as a basis for sensitive analytical methods (*1*, *3*). Recently, reports of new electrocatalytic transformations (*4–9*) and advances in theory (*10–13*) have revived interest in redox electrocatalysis.

Equations 1 and 2 show the scheme for redox electrocatalysis. The product of reaction 1, Q, reacts with substrate A

$$P + e \rightleftharpoons Q \quad E^\circ \tag{1}$$

$$Q + A \underset{k_{-1}}{\overset{k_1}{\rightleftharpoons}} P + B \tag{2}$$

in reaction 2, yielding B and regenerating P. When $C^*_A \gg C^*_P$, where C^*'s are bulk concentrations, reaction 2 is pseudo first order in catalyst. Linear-sweep voltammetry (LSV) is frequently used to study such reactions (*11–16*). The current and curve shape in LSV are controlled by the dimensionless kinetic parameter $\lambda = (k_1 C^*_A/\nu)(RT/F)$, where ν is the scan rate, k_1 is the forward rate constant in reaction 2, and the other symbols have their usual meanings. At large λ, reaction 2 is the rate-determining step (RDS) and the current is said to be under pure kinetic control. The current–potential curve then becomes sigmoid shaped, in contrast to the usual peak shape in LSV, and is described by (*12*, *14–16*)

$$i = i_{l,c}/(1 + \theta) \tag{3}$$

where $\theta = \exp[(F/RT)(E - E^\circ)]$, i is the current at potential E, and $i_{l,c}$ is the limiting catalytic current. The rate constant k_1 can be obtained from $i_{l,c}$ through

$$i_{l,c} = FAC^*_P D_P^{1/2} (C^*_A \sigma k_1)^{1/2} \tag{4}$$

where A is the area of the electrode, D_P is the diffusion coefficient of P, and σ is a stoichiometric factor allowing for additional reactions of Q (*16*) following eq 2. As k_1 increases, the difference between E° of the catalyst and the potential for direct reduction of the substrate decreases (*13*). Thus, linear-sweep voltammograms of such systems show severe overlap of the catalytic wave with the peak for direct reduction of substrate. The resulting uncertainty in $i_{l,c}$ leads to a large uncertainty in the calculated value of k_1.

We felt that the application of modern methods of data analysis to resolve the overlapped voltammograms would result in better precision and accuracy in $i_{l,c}$ and thus k_1. One approach, which has been used with other electrochemical techniques (*17*, *18*), is to subtract the separately recorded current–potential curve of the substrate from the unresolved catalytic voltammograms. This method assumes that the background current is unaffected by the electrocatalyst and its reduction product, that the area and nature of the electrode surface are identical in both experiments, and that no drift occurs in the potential of the reference electrode. These assumptions are not valid in many cases. Furthermore, such background subtraction causes an increase in noise in the resulting subtractive voltammograms. In 1973, Meites and Lampugnani (*19*) used nonlinear regression analysis with a six-parameter model to determine limiting currents from dc polarographic waves severely overlapped with the reduction wave of the supporting electrolyte. We have applied a modification of their technique to the determination of $i_{l,c}$ and E° from severely overlapped linear-sweep voltammograms for pseudo-first-order, kinetically controlled, electrocatalytic reactions. The method was tested with simulated data and applied to the electrocatalytic carbon–chlorine cleavage of 4,4′-dichlorobiphenyl. Although all simulated and experimental examples are reductions, the method is easily transposable to oxidations.

EXPERIMENTAL SECTION

A PARC 174A polarographic analyzer with a three-electrode cell was used for LSV as described previously (*20*). The cell contained a PARC Model 9323 hanging-drop mercury electrode (HDME) with a drop of area 0.0184 cm^2, a Ag/AgI reference electrode, and a platinum wire counterelectrode. Anthracene and 4,4′-dichlorobiphenyl (4,4′-DCB) from Aldrich Chemical Co. and reagent grade *tert*-butylammonium iodide (TBAI) were used as received. *N,N′*-Dimethylformamide (DMF), distilled-in-glass grade from Burdick and Jackson Laboratories, was passed through a column of neutral alumina (Activity I, 70–230 mesh) and purged with purified nitrogen before use. Supporting electrolyte solutions were prepared directly in the electrochemical cell by passing the required volume of DMF into the cell through a column of alumina, purging with nitrogen, and adding TBAI to obtain a final concentration of 0.1 M. Alumina was added directly to the cell to scavenge remaining water and impurities (*21*). Before each voltammetric scan, solutions were stirred and purged with nitrogen which had passed through, in succession, a purification train to remove oxygen (*20*), a drying tower, and DMF containing alumina. The final concentration of anthracene was 0.10 mM; that of 4,4′-DCB was 4.0 mM.

Nonlinear regressions and pointwise analyses of variance (ANOVA) were performed with general programs for those purposes (*22*, *23*). The regression program provides a least-squares estimate of the "best" values in a mathematical model describing the experimental data. Pointwise ANOVA is based on the non-

0003-2700/83/0355-0776$01.50/0 © 1983 American Chemical Society

Table I. Comparison of Five- and Six-Parameter Regression Analyses

parameter	units	error in estimated initial param	theory	found[a] 6-param	found[a] 5-param
E°	V	±0.01	−1.366	−1.364	−1.367
RT/F	V	0	0.0257	0.0257	0.0257
$i_{l,c}$	μA	±0.80	2.500	2.312	2.515
$\alpha n_a F/RT$	V^{-1}	±4	33.3	25.7	34.7
i'	μA	±0.02	1.600	1.86	1.62
E'	V	±0.02	−1.460	1.483	fixed

[a] Average of seven curve fits on simulated data with 0.5% $i_{l,c}$ noise. Initial parameters were varied over ranges defined by the errors listed.

linear regression program (*23*). Preliminary computations employed the Radio Shack Level II BASIC language and a TRS-80 microcomputer. Most of the final calculations were carried out in FORTRAN (WATFIV) in double precision with an IBM System/370 computer.

Simulated voltammograms were generated with the appropriate theoretical equation. An absolute amount of normally distributed noise was added to the theoretical currents. Noise, expressed here as a percentage of the limiting catalytic current, was generated by using the method of Box and Müller (*24*) to obtain N normally distributed numbers z_j with zero means and unit variance. N theoretical currents i_j were also generated. Currents $i_{j,f}$ containing noise at a fraction, f, of the catalytic limiting current were obtained from

$$i_{j,f} = i_j + f z_j i_{l,c} \quad (5)$$

Currents from experimental voltammograms of 4,4′-DCB/anthracene, anthracene alone, and 4,4′-DCB alone were measured from a linear extrapolation of the residual current line observed at potentials more positive than the reduction waves. These currents were digitized at 5.0-mV intervals. In the background subtraction method, currents from a separately obtained voltammogram of 4.0 mM 4,4′-DCB were subtracted from the overlapped voltammograms obtained at the same scan rate. Thirty data points, as i,E pairs with currents between 5 and 95% of the estimated $i_{l,c}$, were generally used in the regression analyses. In all computations, the absolute, rather than the relative, error in the current was assumed to be randomly distributed.

RESULTS AND DISCUSSION

Equation 6, similar to that employed for polarographic data by Meites and Lampugnani (*19*), adequately described overlapped voltammograms when the catalytic process was pseudo first order and kinetically controlled. The first term

$$i = i_{l,c}/(1 + \theta) + i' \exp[(\alpha n_a F/RT)(E' - E)] \quad (6)$$

on the right-hand side gives the catalytic current, as in eq 3. The second term describes the background current caused by direct reduction of the substrate, where E' is an arbitrary potential at which the background current i' flows, α is the electrochemical transfer coefficient, and n_a is the number of electrons in the rate-determining step of the irreversible reduction (*25*).

Simulated Voltammograms. Data with normally distributed noise were generated by using eq 6 and 5. By examination of standard deviations of regressions of well-resolved catalytic voltammograms (*26*) onto eq 3 and comparison of these to standard deviations obtained in the same way with simulated data, it was concluded that 0.5 to 1.0% noise gave a good representation of experimental data obtained with commercial instruments under optimum conditions. Initially, both five- and six-parameter curve fits were investigated. The parameters used and their values for the simulated data (Figure 1a) are listed in Table I. Since we wished to evaluate possible errors in the calculated parameters caused by realistic errors in the initial parameters, we estimated the probable error in the initial value of each parameter. The estimated error in the initial value of $i_{l,c}$ is greatest (Table I), since its

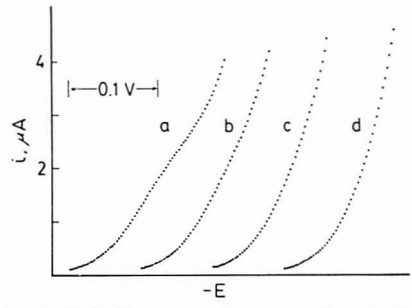


Figure 1. Simulated linear-sweep voltammograms. Parameters from Table I, except E°: (a) E° = −1.366 V, ΔE = 94 mV; (b) E° = −1.400 V, ΔE = 60 mV; (c) E° = −1.420 V, ΔE = 40 mV; (d) E° = −1.440 V, ΔE = 20 mV.

choice involves a large amount of judgement. Based on the initial $i_{l,c}$, estimates of the half-wave potential (E°) and its error were obtained. The initial value of RT/F was always its theoretical value at 25 °C. Errors in the initial estimates of $\alpha n_a F/RT$ and i' were made by assuming the availability of a separate voltammogram for reduction of the substrate. Once E' is fixed, i' can be measured from the current–potential curve. $\alpha n_a F/RT$ was estimated from a two-parameter fit of data on the rising portion of the curve to eq 7. The second

$$i = i' \exp[(\alpha n_a F/RT)(E' - E)] \quad (7)$$

parameter was i'. These estimates of errors in the initial parameters (Table I) were then used as limits within which the initial estimates of the parameters were varied in fitting the simulated data to eq 6. Initial values of $i_{l,c}$ were 1.7, 2.1, 2.3, 2.4, 2.7, 2.9, and 3.3 μA. The other parameters, for which errors in initial estimates are smaller, were varied in an arbitrary manner over their error ranges. Seven regression analyses in single precision were performed in both the five- and six-parameter modes.

Average calculated parameters (Table I) showed the five-parameter regression to be more accurate for determination of $i_{l,c}$. The average $i_{l,c}$ for the five-parameter fits was 2.515 μA, while that for six-parameter fits was 2.312 μA. The latter value was significantly different from the theoretical value of 2.500 μA at the 95 and 99% confidence levels, as shown by t tests. All other average parameter values for both six- and five-parameter fits gave t tests which indicated no significant differences from their theoretical values at the 95% confidence level. It was later found that more precise values for the parameters and better standard deviations of regression were obtained by carrying out the five-parameter fits in double precision. It was concluded that the best values of $i_{l,c}$ would be obtained from the overlapped voltammograms using the five-parameter regression in double precision.

Table II. Results of Pointwise ANOVA[a]

$E - E^\circ$, mV	E°	RT/F	$i_{l,c}$	$\alpha n_a F/RT$	i'	overall
			ΔE = 94 mV: Relative Weights			
76	0.39	0.12	0.007	0.078	2×10^{-5}	0.25
61	0.47	0.17	0.023	0.061	3×10^{-5}	0.31
46	0.17	0.14	0.008	0.035	1×10^{-5}	0.15
31	0.003	0.066	4×10^{-5}	0.011	1×10^{-6}	0.033
16	0.006	1.00	1.00	0.073	2×10^{-5}	0.89
1	0.77	0.012	0.014	0.043	1×10^{-6}	0.36
−14	0.51	0.064	5×10^{-4}	0.008	1×10^{-7}	0.25
−29	1.00	0.057	0.15	0.002	6×10^{-5}	0.52
−44	0.28	0.043	0.018	1.00	1.00	1.00
−59	0.053	0.017	6×10^{-4}	0.032	0.42	0.22
parameters[b]	−1.366	0.02563	2.473	31.69	1.604	
std error, %	0.019	0.75	0.71	3.16	204	
			ΔE = 40 mV: Relative Weights			
85	0.22	0.43	0.013	0.007	0.16	0.37
70	0.26	0.64	0.034	0.007	0.17	0.50
55	0.18	0.70	0.022	0.006	0.16	0.48
40	0.066	0.56	0.016	0.003	0.077	0.32
25	0.093	0.076	7×10^{-4}	0.002	0.017	0.084
10	0.74	0.075	0.002	0.011	0.35	0.53
−5	1.00	0.10	0.085	0.005	0.37	0.70
−20	0.55	1.00	0.002	0.006	0.23	0.80
−35	0.021	0.069	0.138	1.00	1.00	1.00
−50	0.007	0.008	1.00	0.010	0.64	0.75
parameters[b]	−1.420	0.02565	2.577	33.86	1.534	
std error, %	0.026	0.51	0.19	3.24	0.68	

[a] Carried out using the program VARPAR (22). Standard errors were calculated by using an estimated absolute standard error in current of 0.0034 μA, obtained as the standard deviation of regression at 0.5% noise. [b] Theoretical value used to simulate voltammograms.

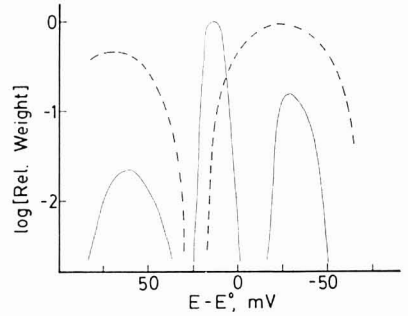


Figure 2. Pointwise ANOVA plot showing how relative weights in determining $i_{l,c}$ (—) and E° (—) vary with potential for simulated data with ΔE = 94 mV.

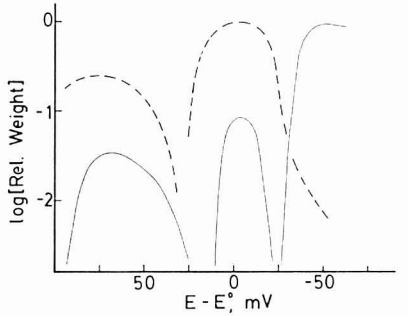


Figure 3. Pointwise ANOVA plot showing how relative weights in determining $i_{l,c}$ (—) and E° (– –) vary with potential for simulated data with ΔE = 40 mV.

Pointwise ANOVA. This method (22, 23) was used to evaluate the relative weight of data in various potential ranges in determining the final values of each parameter. The program used (22) also supplied estimates for standard errors of the parameters. Two sets of noise-free, simulated data were analyzed (Table II). The first had parameters close to those in Table I; the second had similar parameters except E° was −1.420 V. The difference in these two simulated voltammograms can be characterized by using $\Delta E = E^\circ - E'$, where E' is fixed and E° can be varied. The first set of simulated data has ΔE = 94 mV (Figure 1a). The second has ΔE = 40 mV and corresponds to more severe overlap of the catalytic wave with the direct reduction peak of the substrate (Figure 1c).

The value of the limiting current is of greatest interest in our work, since it enables calculation of k_1. For the data with ΔE = 94 mV, a sharp maximum in the relative weight (Figure 2) occurred between $E - E^\circ$ of 0 to 20 mV. Thus, data in this region are the most significant in determination of $i_{l,c}$. Secondary maxima occurred at $E - E^\circ$ of 61 and −29 mV. For the data with ΔE = 40 mV, the largest maxima (Figure 3) was at $E - E^\circ$ of −50 mV and two secondary maxima occurred at $E - E^\circ$ of −5 and 70 mV.

Determination of E° is also important in studies of electrocatalytic reactions (12). The dependence of relative weight in determining E° on potential showed two broad maxima for each data set (Figures 2 and 3). The positions of these maxima were similar for each ΔE. For both sets of data, the potentials of maximum relative weight for $i_{l,c}$ coincided with a region of low relative weight for E°. In general, evaluation of $i_{l,c}$ and E° would be required in situations where ΔE changes

Table III. Influence of Shift in E° for Simulated Voltammograms[a] with Fixed Background

			average calculated values[b]					
N^c	$-E^\circ$, theory	% noise	$-E^\circ$	RT/F	$i_{l,c}$	$\alpha n_a F/RT$	i'	std dev[d] × 10^3
5	1.366	0.5	1.367 ± 0.001	0.02583 ± 0.00011	2.545 ± 0.042	34.7 ± 1.8	1.59 ± 0.01	3.41
5	1.400	0.5	1.400 ± 0.001	0.02570 ± 0.00023	2.500 ± 0.080	32.9 ± 1.1	1.60 ± 0.06	3.30
5	1.420	0.5	1.420 ± 0.002	0.02571 ± 0.00048	2.595 ± 0.171	34.0 ± 1.3	1.53 ± 0.11	3.34
7	1.440	0.5	1.441 ± 0.003	0.02579 ± 0.00079	2.631 ± 0.380	33.6 ± 1.8	1.53 ± 0.18	3.13
5	1.366	1.0	1.366 ± 0.001	0.02546 ± 0.00028	2.425 ± 0.095	30.4 ± 3.7	1.63 ± 0.02	6.05
2	1.400	1.0	1.400	0.02550	2.420	31.6	1.67	6.42
4	1.420	1.0	1.419 ± 0.001	0.02534 ± 0.00028	2.456 ± 0.106	32.9 ± 0.9	1.61 ± 0.07	8.28
2	1.440	1.0	1.440	0.02552	2.467	32.8	1.62	4.96

[a] Values of the simulation parameters were RT/F = 0.02569 V, $i_{l,c}$ = 2.50 μA, $\alpha n_a F/RT$ = 33.33 V^{-1}, i' = 1.60 μA. The value of E° varied as shown in the table. E' was −1.46 V. [b] Values given with standard deviations. Initial parameters were varied over the ranges given in Table I. [c] Number of curve fits. [d] Standard deviation of the regression.

from experiment to experiment, by changing the scan rate, for example. On the basis of the above considerations, we concluded that the best values of $i_{l,c}$ and E° would be obtained by using data in the range $-75 \text{ mV} \leq (E - E^\circ) \leq 70 \text{ mV}$ for the regression analyses. In practice, this was attained by taking the first data point to be about 5% of the estimated $i_{l,c}$. Twenty-nine successive data points were then used at intervals spaced −5.0 mV along the potential axis, giving a good approximation to the desired range of potentials.

Pointwise ANOVA indicated standard errors in E°, RT/F, and $i_{l,c}$ of less than 1% (Table II). However, $\alpha n_a F/RT$ had a standard error of 3.4% for both sets of data. The standard error in i' was 204% for ΔE = 94 mV and 0.7% for ΔE = 40 mV. The errors in $\alpha n_a F/RT$ and i' are larger than those of the other parameters for ΔE = 94 mV because the relative weights for these parameters at $(E - E^\circ) > -40$ mV are low (Table II). Thus, only a small portion of the data is significant in determining $\alpha n_a F/RT$ and i'. For the data set with ΔE = 40 mV, the contribution of the background to the total current is larger, relative weights for i' increase throughout the potential range, and the standard error of i' decreases to 0.7%. Relative weights for $\alpha n_a F/RT$ were not significantly affected by changing ΔE.

Influence of ΔE and of Errors in Initial Parameters on Accuracy and Precision. Sets of simulated data were generated using four values of E° from −1.366 to −1.440 V (Table III) and keeping the other parameters at their values in Table I. The negative shift in E° corresponds to moving the catalytic wave closer to the peak for direct reduction of substrate and can be characterized by ΔE values of 94, 60, 40, and 20 mV (Figure 1). A series of curve fits on these data were carried out with variation of the initial estimates of parameters over the error ranges listed in Table I. Two levels of noise were studied—0.5% $i_{l,c}$ and 1.0% $i_{l,c}$. For the data with 0.5% noise, average values of the parameters (Table III) did not differ significantly from their theoretical values at the 95% confidence level, as shown by t tests. Standard deviations for E°, RT/F, $i_{l,c}$, and i' increased as ΔE decreased. The standard deviation of the regression was independent of ΔE. Deviation plots (*23*) for all sets of data were random.

The accuracy of the results was not seriously affected by an increase in noise in the data to 1.0%. Average values of all parameters (Table III) at this higher noise level showed no significant differences from their theoretical values at the 95% confidence level using t tests. Standard deviations of the regression were about twice those obtained for data with 0.5% noise.

The limiting current, $i_{l,c}$, is subject to a large error in its initial estimate. We wanted to determine if this error influenced the final calculated value of $i_{l,c}$. A plot of the error in the initial $i_{l,c}$ vs. the error in its final value (Figure 4) shows no correlation between these two quantities for the 35 regression analayses summarized in Table III. Furthermore, linear regression of the data in Figure 4 gave a correlation coefficient of 0.18, indicating essentially no correlation.

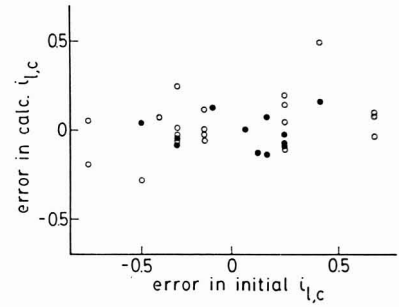


Figure 4. Influence of the error in the initial estimate of $i_{l,c}$ on the error in its final value calculated from five-parameter regression analysis. Data were simulated with 0.5% $i_{l,c}$ noise (O) and 1.0% $i_{l,c}$ noise (●).

The above results show that using initial estimates of parameters within realistic limits, nonlinear regression provides good values for $i_{l,c}$ and E° from overlapped voltammograms. However, the precision in these calculated parameters decreases as the overlap in the voltammograms becomes more severe (Table III). Nevertheless, accurate values of $i_{l,c}$ are obtainable, even at ΔE = 20 mV, where the catalytic wave cannot be seen on the current–potential curve (Figure 1d).

Application to Electrocatalytic Reduction of 4,4′-Dichlorobiphenyl. With anthracene, 9,10-diphenylanthracene, or α-naphthonitrile as catalysts, 4,4′-dichlorobiphenyl (4,4′-DCB) undergoes a two-electron electrocatalytic reduction to 4-chlorobiphenyl (*26*). The catalyst is reduced to its anion radical at the electrode and the anion radical then reduces 4,4′-DCB. With anthracene as the catalyst in DMF, catalytic linear-sweep voltammograms are severely overlapped (Figure 5) with those for direct, irreversible reduction of 4,4′-DCB (*27, 28*). Voltammetric data for the 4,4′-DCB/anthracene system was obtained at scan rates (ν) of 50, 100, and 200 mV s^{-1}. E' was fixed at −1.46 V vs. Ag/AgI. Data on the rising portions of voltammograms of 4,4′-DCB alone were fit to eq 7 to estimate $\alpha n_a F/RT$ and i', yielding an average $\alpha n_a F/RT$ of 32.9 ± 4.2 V^{-1} and values of i' of 0.84, 1.34, and 1.18 μA at 50, 100, and 200 mV s^{-1}, respectively. The latter were in good agreement with the values of 0.85, 1.30, and 1.15 μA read directly from the current–potential curves.

Sixteen sets of data for the 4,4′-DCB/anthracene system were used to compare the five-parameter regression analysis to the background subtraction method for determination of

Table IV. Average Values of Parameters and Rate Constant Determined from Regression Analysis of Voltammograms of 4,4′-DCB and Anthracene

scan rate, mV s^{-1}	N^a	$-E°$	RT/F	$i_{l,c}$	$\alpha n_a F/RT$	i'	std dev^b × 10^3	k_1, L mol^{-1} s^{-1}	log k_1
				5 Parameter Fits					
50	3	1.362 ± 0.013	0.0242 ± 0.0009	2.20 ± 0.12	36.6 ± 5.6	1.45 ± 0.57	8.8	1300 ± 230	3.11 ± 0.08
100	6	1.369 ± 0.008	0.0243 ± 0.0008	2.49 ± 0.40	36.3 ± 6.6	1.33 ± 0.25	9.5	1240 ± 310	3.08 ± 0.12
200	7	1.368 ± 0.009	0.0250 ± 0.0005	2.53 ± 0.20	31.8 ± 3.4	1.34 ± 0.30	8.4	1590 ± 340	3.19 ± 0.09
means		1.367 ± 0.009	0.0246 ± 0.0008	2.46 ± 0.29	34.4 ± 5.4	1.36 ± 0.32	8.9	1410 ± 340	3.14 ± 0.11
				Background Subtraction Method					
50	3	1.363 ± 0.008	0.0246 ± 0.0024	2.21 ± 0.18			20.0	1370 ± 540	3.11 ± 0.20
100	6	1.367 ± 0.007	0.0240 ± 0.0010	2.43 ± 0.45			18.1	1210 ± 390	3.06 ± 0.18
200	7	1.368 ± 0.008	0.0255 ± 0.0014	2.62 ± 0.29			14.2	1720 ± 535	3.22 ± 0.13
means		1.368 ± 0.008	0.0248 ± 0.0015	2.47 ± 0.36			16.8	1460 ± 512	3.14 ± 0.17

[a] Number of individual voltammograms. [b] Standard deviation of the regression.

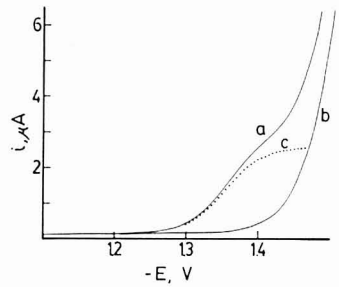


Figure 5. Linear-sweep voltammograms at 200 mV s^{-1} for reduction of 4,4′-DCB: (a) electrocatalytic reduction with 0.10 mM anthracene as catalyst and 4.0 mM 4,4′-DCB; (b) direct reduction of 4.0 mM 4,4′-DCB; and (c) catalytic reduction wave after resolution by five-parameter regression analysis.

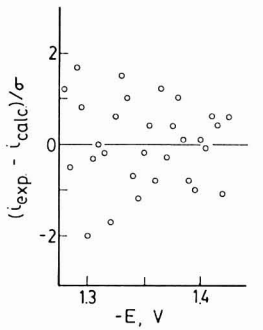


Figure 6. Deviation plot obtained after regression analysis of data in Figure 5a.

rate constant k_1. In the former, data were regressed directly onto eq 6. Deviation plots (*23*) of residuals vs. E were featureless (Figure 6), showing the validity of the model used. The same 16 current–potential curves were subjected to background subtraction followed by three-parameter nonlinear regression onto eq 3. Mean values of $E°$, RT/F, and $i_{l,c}$ (Table IV) at the three scan rates were subjected to t tests at the 95% confidence level, which showed that these parameters were independent of scan rate. This is consistent with the mechanism of pseudo-first-order electrocatalytic reduction under pure kinetic control of reaction 2 (*12–16, 26*). Overall means for each parameter from each method showed no significant differences by t-tests at the 95% confidence level. Similarly, means of $\alpha n_a F/RT$ and i' from five-parameter fits were not significantly different at the 95% confidence level from the values obtained from direct reduction of 4,4′-DCB.

Rate constants for the reaction of the anthracene radical anion with 4,4′-DCB were calculated from values of $i_{l,c}$ obtained by both methods. Dividing eq 4 with $\sigma = 2$ by the Randles–Ševčik equation (*25*) gives

$$i_{l,c}/i_d = 0.447^{-1}(RT/F)^{1/2}(2k_1C^*_A/\nu)^{1/2} \quad (8)$$

where i_d is the peak current of the catalyst alone. On rearrangement and combination of constant terms, the rate constant k_1 at 25 °C becomes

$$k_1 = (i_{l,c}/i_d)^2(7.778\nu/2C^*_A) \quad (9)$$

No significant differences at the 95% confidence level were found between any values of k_1. The average values of log k_1 found by both methods were identical, but the standard deviation for log k_1 from the five-parameter regression was lower. An F-test showed that the variances of the two methods were significantly different at the 95% confidence level. Furthermore, the average standard deviation of regression for the five-parameter fits was about half that obtained by background subtraction. These results are consistent with the earlier discussion of the disadvantages of background subtraction. The relative standard deviation of log k_1 of ±3.5% obtained from the five-parameter regressions was the same as the average value (±3.5%) obtained in log k_1 for 24 electrocatalytic reactions (*13*) of halobenzenes and halopyridines ($1.0 \leq \log k_1 \leq 5.5$) with well-separated catalytic waves.

In situations where the catalytic wave is not evident on the voltammogram (Figure 1d), a way to recognize the presence or absence of electrocatalysis is necessary. To simulate the case in which a potential catalyst and substrate are present in solution, but where no catalysis occurs, current–potential curves for the reversible reduction of 0.10 mM anthracene in DMF were shifted by −80 mV and added to the current for direct reduction of a 40-fold excess of 4,4′-DCB. Four overlapped voltammograms with $E°$ of −1.446 ± 0.004 V and ΔE between 20 and 35 mV were constructed in this way, using data obtained at scan rates between 50 and 200 mV s^{-1}. When these data were regressed onto eq 6, deviation plots showed a maxima and two minima (Figure 7). Furthermore, calculated values of $E°$ ranged from −1.58 to −2.05 V, while those for RT/F were between 0.041 and 0.078 V, all much greater than the respective theoretical values. Regression analysis of the background current alone using eq 6 gave similar de-

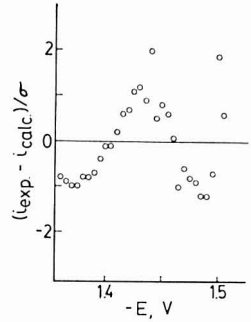


Figure 7. Deviation pattern for overlap of reversible linear-sweep voltammogram with background current (ΔE = 25 mV) corresponding to noncatalytic case fit to eq 6. See text for details.

viation patterns and unrealistic parameters. Clearly, these data do not fit eq 6. On the other hand, simulated catalytic voltammograms with ΔE = 20 and 40 mV gave random deviation plots and accurate values for parameters (Table III). Thus the catalytic and noncatalytic cases are easily distinguished.

In conclusion, nonlinear regression using eq 6 can be used to determine the forward rate constant for the chemical step in pseuso-first-order electrocatalytic processes if conditions can be found where the voltammetric response is under pure kinetic control of reaction 2. Adherence of the experimental data to this model can be tested by observation of deviation plots, which should be random if eq 6 is followed (cf. Figure 6). When the unresolved catalytic wave is observable as a shoulder on the catalytic current–potential curve (cf. Figures 1a,b and 5), precision of the rate constant is comparable to that obtained from well-resolved catalytic waves. The five-parameter regression analysis gives better precision than the background subtraction method. Although precision in k_1 decreases with an increasing contribution of background to the total current (i.e., as ΔE gets smaller), results of acceptable accuracy are obtainable even when the catalytic wave cannot be visually observed on the voltammograms.

Registry No. 4,4′-Dichlorobiphenyl, 2050-68-2; anthracene, 120-12-7.

LITERATURE CITED

(1) Heyrovsky, J.; Kuta, J. "Principles of Polarography"; Academic Press: New York, 1966.
(2) Malranovskii, S. G. "Catalytic and Kinetic Waves in Polarography"; Plenum Press: New York, 1968.
(3) Meites, L. "Polarographic Techniques"; 2nd ed.; Wiley: New York, 1965.
(4) Saveant, J. M. *Acc. Chem. Res.* **1980**, *13*, 323–329.
(5) Margel, S.; Levy, M. *J. Electroanal. Chem.* **1974**, *56*, 259–267.
(6) Lund, H.; Michel, M.-A.; Simonet, J. *Acta Chem. Scand., Ser. B* **1975**, *B28*, 900–904.
(7) Lund, H.; Simonet, J. *J. Electroanal. Chem.* **1975**, *65*, 205–218.
(8) Simonet, J.; Michel, M.-A.; Lund, H. *Acta Chem. Scand., Ser. B* **1975**, *B29*, 489–498.
(9) Dumas-Bouchiat, J. M.; Kitani, A.; Miller, L. L. Electrochemical Society Spring Meeting, Extended Abstract No. 530, Montreal, Canada, 1982.
(10) Andrieux, C. P.; Dumas-Bouchiat, J. M.; Saveant, J. M. *J. Electroanal. Chem.* **1978**, *87*, 39–53.
(11) Andrieux, C. P.; Dumas-Bouchiat, J. M.; Saveant, J. M. *J. Electroanal. Chem.* **1978**, *87*, 55–65.
(12) Andrieux, C. P.; Blocman, C.; Dumas-Bouchiat, J. M.; M'Halla, F.; Saveant, J. M. *J. Electroanal. Chem.* **1980**, *113*, 19–40.
(13) Andrieux, C. P.; Blocman, C.; Dumas-Bouchiat, J. M.; Saveant, J. M. *J. Am. Chem. Soc.* **1979**, *101*, 3431–3441.
(14) Saveant, J. M.; Vianello, E. In "Advances in Polarography"; Longmuir, I., Ed.; Pergammon Press: London, 1960; Vol. I, pp 367–374.
(15) Nicholson, R. S.; Shain, I. *Anal. Chem.* **1964**, *36*, 706–723.
(16) Saveant, J. M.; Vianello, E. *Electrochim. Acta* **1965**, *10*, 905–920.
(17) Bond, A. M. "Modern Polarographic Methods in Analytical Chemistry"; Marcel Dekker: New York, 1980.
(18) He, P.; Avery, J. P.; Faulkner, L. R. *Anal. Chem.* **1982**, *54*, 1313A–1326A.
(19) Meites, L.; Lampugnani, L. *Anal. Chem.* **1973**, *45*, 1317–1323.
(20) Rusling, J. F. *J. Electroanal. Chem.* **1981**, *125*, 447.
(21) Jenson, B. S.; Parker, V. D. *J. Chem. Soc., Chem. Commun.* **1974**, 367.
(22) Meites, L. "The General Multiparametric Curve-Fitting Program CFT4A"; Computing Laboratory, Clarkson College of Technology: Potsdam, NY, 1976.
(23) Meites, L. *Crit. Rev. Anal. Chem.* **1979**, *8*, 1–53.
(24) Bard, Y. "Nonlinear Parameter Estimation"; Academic Press: New York, **1974**; pp 316–317.
(25) Bard, A. J.; Faulkner, L. R. "Electrochemical Methods"; Wiley: New York, 1980.
(26) Connors, T. F.; Rusling, J. F. *J. Electrochem. Soc.*, in press.
(27) Maruyama, M.; Murakami, K. *Nippon Kagaku Kaishi* **1976**, 536–539.
(28) Arena, J.; Rusling, J. F., unpublished work, University of Connecticut, 1982.

RECEIVED for review October 21, 1982. Accepted January 11, 1983. This work was supported by the University of Connecticut Research Foundation.

Software for Quantitative Analysis by Carbon-13 Fourier Transform Nuclear Magnetic Resonance Spectrometry

Christopher H. Sotak, Charles L. Dumoulin, and George C. Levy*

NIH Resource for Multi-Nuclei NMR and Data Processing, Department of Chemistry, Syracuse University, Syracuse, New York 13210

Computational aspects of quantitative analysis by ^{13}C NMR are examined. A simple mixture of high dynamic range and neat octanol-2-*d* were employed to investigate the accuracy and precision of results as functions of residual base line abnormalities, signal to noise, and spectral data point density. Components of a high dynamic range mixture present at mole ratios of 88.83%, 5.59%, 1.08%, 0.27%, and 0.13% were determined, using a high level spectroscopic data analysis software package, as 87.50% (0.57), 5.43% (0.17), 1.04% (0.09), 0.28% (0.12), and 0.12% (0.07), respectively. The values in parentheses denote ±1 standard deviation. Accuracy and precision of determination for minor components in the mixture were found to decrease with signal to noise. A similar trend was also observed for neat octanol-2-*d* spectra of decreasing signal to noise. Increasing the spectral data point density was found to improve analytical results for neat octanol-2-*d*; however, satisfactory results were obtained even at relatively low digital resolution.

The usefulness of ^{13}C Fourier transform (FT) NMR spectrometry as an analytical technique stems from the potential direct relationship between the area under an NMR peak and the number of the particular type of nuclei which give rise to that signal. In addition, the sensitivity of ^{13}C chemical shifts to small differences in molecular environment, coupled with a large chemical shift range (~220 ppm), gives a "chromatographic" separation of resonances of interest and has made ^{13}C NMR an attractive method for analyzing complex mixtures (*1–9*).

Unfortunately, extracting the desired quantitative information from a ^{13}C NMR analysis is hampered by several experimental limitations. These complications have been discussed previously in some detail (*7–10*) and will therefore only briefly be recounted for clarity. To avoid partial saturation of ^{13}C resonances, the relaxation period between successive observe pulses must be at least five times the longest spin–lattice time, T_1, of interest in the sample. The nuclear Overhauser enhancement (NOE) of the carbon signal must also be nullified in order to obtain quantitative results. Spin-relaxation reagents (*11–15*) have been used to shorten and equalize ^{13}C T_1's and to suppress NOE's by circumventing normal carbon–hydrogen dipolar relaxation. The use of paramagnetic sample additives, however, does not alone ensure effective NOE suppression (*16*) and the gated decoupling method (*17*) is generally chosen to eliminate the NOE.

Software Considerations. In conjunction with experimental considerations, care must be taken to avoid subjecting the analysis to additional inaccuracies in the course of processing the data. The integrity of peak intensity measurements can suffer from: (1) insufficient spectral data point density; (2) poor base line characterization; and (3) improper integration limits. The spectral data point density is dictated by the number of computer words used to digitize the free induction decay (FID). This should be sufficient to resolve the narrowest feature in the transformed spectrum. Additional improvements in peak definition may be obtained by zero-filling. The precision and accuracy of peak integrations obtained on discrete data can be shown to increase with the number of points integrated.

Analytical accuracy is also strongly dependent on the correct identification of the base line around and under the peak. Lengthy signal averaging and instrumental artifacts contribute to base line distortions which must be compensated for, through software, to make high accuracy integrations meaningful.

Finally, an often overlooked aspect of integration in NMR is the choice of integration limits. If limits of integration are consistently chosen as a function of the peak line width, then the ratio of individual integrals within a spectrum will remain constant. This is an important consideration if the concentration of an unknown sample is determined from a calibration curve based on an internal standard.

The above data processing considerations have been incorporated as part of a spectral data processing system developed for FT-NMR called ORACLE (*O*ptimized *R*ealtime *A*nalysis in the *C*hemical *L*aboratory *E*nvironment). This software is designed to provide a high degree of flexibility and control over spectral data analysis while at the same time minimizing the user's ability to bias the data. The basic method used to achieve this goal is to use sophisticated algorithms which base decisions on statistical methods. A block diagram of the software modules employed in quantifying a spectrum is shown in Figure 1. The FID is zerofilled, multiplied by an appropriate exponentially decaying function, and Fourier transformed. The resulting spectrum is carefully phased, and base line distortions are removed through an iterative base line flattening algorithm. Resonances are identified by the peak analysis module and pertinent peak information, such as, position, intensity, and line width are tabulated. Peak areas are then calculated with a floating point Simpson's rule algorithm, with integration limits chosen as a constant multiple of peak line width. An integration module allows the user to manipulate or repeat peak integrations obtained automatically in the peak analysis module. Partially resolved peaks can be integrated by modifying the number of peak line widths used to determine the limits of integration or may be deconvoluted by using a curve fitting algorithm. In addition, the integration module allows the data to be corrected for signal attenuation due to nonuniform excitation and filter roll-off.

Two chemical systems were chosen to investigate the analytical results that can be obtained by adhering to the above data processing considerations. The first system demonstrates the accuracy of determination for a minor component in a mixture of high dynamic range. Four-component mixtures having dynamic ranges varying in mole ratio from 10:1 to approximately 600:1 were employed for this purpose. The second system, neat octanol-2-*d*, having eight lines of equal area, was used to evaluate the effects of signal to noise and spectral data point density on the accuracy and precision of ^{13}C analyses.

EXPERIMENTAL SECTION

Materials. Components of mixtures consisted of reagent grade tetrahydrofuran (Fisher Scientific), 2-propanol (Fisher Scientific),

0003-2700/83/0355-0782$01.50/0 © 1983 American Chemical Society

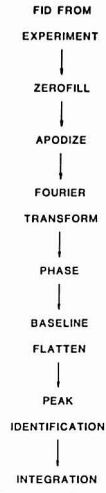


Figure 1. Data processing protocol.

1,2-dimethoxyethane (Eastman), and 1,3-propanediol (Aldrich Chemical Co.). These compounds were used without further purification. Mixtures were prepared from the neat components by weighing out the appropriate quantities of each compound (to the nearest 0.1 mg) corresponding to the desired mole ratio (approximately THF:2-PrOH:1,2-DME:1,3-Pr(OH)$_2$ = 100.00:10.00:1.00:0.30). Samples were prepared just prior to obtaining their ^{13}C spectra and were quickly stoppered to minimize evaporation. Acetone-d_6 was added to the mixture in a volume ratio of approximately 10%, to serve as field frequency lock solvent. Spectra were acquired from samples in 10-mm tubes fitted with Teflon vortex plugs.

Spectra of neat octanol-2-*d* (Aldrich Chemical Co.) were obtained in 10-mm sample tubes fitted with a 3-mm coaxial inner tube containing D_2O as the field frequency lock solvent.

Instrumentation. All spectra were obtained on a Bruker WM-360 wide bore (^{13}C frequency equal to 90.56 MHz) NMR spectrometer equipped with an Aspect 2000 minicomputer.

Spin–Lattice Relaxation Time Measurements and Suppression of the Nuclear Overhauser Effect. Spin–lattice relaxation times for an equivolume mixture of tetrahydrofuran, 2-propanol, 1,2-dimethoxyethane, and 1,3-propanediol were measured by using the fast-inversion-recovery technique (*18*). This method was also employed to measure the T_1 values of neat octanol-2-*d*. Chemical shifts of spectral resonances were assigned from published spectra (*19*). The spin–lattice relaxation times were calculated, using ORACLE, from a least-squares, three-parameter fit to an exponential function of intensity vs. τ values. The T_1 values for each component in the mixture are given in Table I. The T_1 values (in seconds) for neat octanol-2-*d* are as follows:

$$\overset{1.1}{\mathrm{CH_3}}\text{-}\overset{1.2}{\mathrm{CH(OH)}}\text{-}\overset{1.2}{\mathrm{CH_2}}\text{-}\overset{1.4}{\mathrm{CH_2}}\text{-}\overset{1.9}{\mathrm{CH_2}}\text{-}\overset{2.4}{\mathrm{CH_2}}\text{-}\overset{2.7}{\mathrm{CH_2}}\text{-}\overset{3.6}{\mathrm{CH_3}}$$

To avoid saturation of the nuclear spins, pulse intervals were chosen to be greater than five times the longest T_1 in the sample.

The nuclear Overhauser effect was suppressed by the gated decoupling method. The criterion for suppression, a waiting period between pulses in excess of five times the longest T_1 in the sample, was previously satisfied by the relaxation delay employed to avoid saturation. Furthermore, the FID acquisition periods employed, 1.64 s for the high dynamic range mixture and 1.36 s for neat octanol-2-*d*, resulted in decoupling duty cycles of less than 5%.

Acquisition and Processing Parameters. For the mixture analysis, 16384 (16K) data point FID's spanning a spectral region of 5000 Hz were accumulated for a total of 64 scans. Analog filters were chosen as twice the spectral width. A pulse width of 12.5 μs was utilized corresponding to a 90° tip angle of the macroscopic magnetization. Each accumulated FID was transferred to a Data General MV-8000 32-bit computer running the ORACLE software package. The FID's were zerofilled to 32K and multiplied by an exponentially decaying function, equivalent to 1.0 Hz line broadening, prior to Fourier transformation. The resulting spectra had four to five data points above half maximum intensity for each resonance of interest.

Neat octanol-2-*d* spectra of relatively high signal-to-noise ratio (approximately 800:1) were obtained from the sum of 64, 16K FID's covering a spectral width of 6024 Hz. Neat octanol-2-*d* spectra of varying signal-to-noise ratio were derived from addition of a noise FID (multiplied by an appropriate scaling factor) to a 16-scan neat octanol-2-*d* FID. The coadded FID's were each of 16K and covered a spectral width of 6024 Hz; other conditions were as above except that 2.0-Hz line broadening was applied prior to Fourier transformation.

To determine the effect of spectral data point density on the accuracy of integration, a set of five replicate neat octanol-2-*d* FID's was obtained at each of the following spectral sizes: 1K, 2K, 4K, 8K, 16K, and 32K. Each replicate was composed of 64 scans. All other conditions were as above.

Table I. Carbon-13 T_1 Data for an Equivolume Mixture of Tetrahydrofuran, 2-Propanol, 1,2-Dimethoxyethane, and 1,3-Propanediol

compound	^{13}C T_1, s C-1	C-2	OCH$_3$
	14.9	17.1	
$\overset{1}{\mathrm{CH_3}}\overset{2}{\mathrm{CH(OH)CH_3}}$	4.5	9.2	
$\overset{1}{\mathrm{CH_3OCH_2CH_2OCH_3}}$	7.9		10.2
$\overset{1}{\mathrm{HOCH_2}}\overset{2}{\mathrm{CH_2CH_2OH}}$	3.2	2.6	

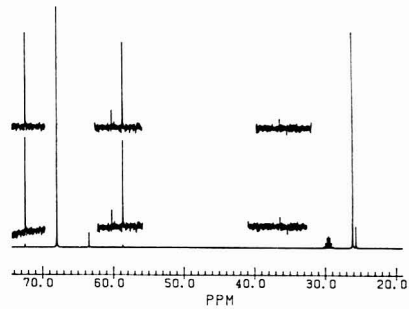


Figure 2. Carbon-13 spectrum of a high dynamic range mixture of mole ratio THF:2-PrOH:1,2-DME:1,3-Pr(OH)$_2$ = 330:41.5:3.98:1.00. Vertical expansions are ×32 scale and were obtained before (lower) and after (upper) base line flattening. Spectral assignments are given in Table II.

RESULTS AND DISCUSSION

Mixture Analysis. A high dynamic range mixture of tetrahydrofuran, 2-propanol, 1,2-dimethoxyethane, and 1,3-propanediol was investigated to evaluate the accuracy to which the minor component in the sample could be determined. The ^{13}C spectrum of this mixture, Figure 2, having a mole ratio of THF:2-PrOH:1,2-DME:1,3-Pr(OH)$_2$ = 330:41.5:3.98:1.00, shows eight resonances, each component giving rise to two peaks. It should be noted that because of molecular symmetry,

Table II. Quantitative Results of Seven Replicate Analyses of a Sample of Mole Ratio THF:2-PrOH:1,2-DME:1,3-Pr(OH)$_2$ = 330:41.5:3.98:1.00

peak no.	shift, ppm	component	S/N (RMS)	expected integral[a]	mean integral ORACLE[a]	rel % error
1	72.5	1,2-DME	38:1	1.08	1.04 (0.08)[b]	−3.7
2	68.0	THF	2260:1	88.83	87.50 (0.57)	−1.5
3	63.5	2-PrOH	156:1	5.59	5.43 (0.17)	−2.9
4	60.3	1,3-Pr(OH)$_2$	5:1	0.27	0.28 (0.12)	3.7
5	58.7	1,2-DME	25:1	1.08	1.04 (0.11)	−3.7
6	36.4	1,3-Pr(OH)$_2$	3:1	0.13	0.12 (0.07)[c]	−7.7
7, 8	26.2/25.7	THF/2-PrOH	2030:1	100.00	100.00	

[a] Percent of the peak areas of THF/2-PrOH. [b] Values in parentheses denote ±1 standard deviation. [c] Based on six replicates (due to insufficient S/N in remaining spectrum).

Table III. Quantitative Results of Eight Replicate Analyses of a Sample of Mole Ratio THF:2-PrOH:1,2-DME:1,3-Pr(OH)$_2$ = 293:31.4:3.26:1.00

peak no.	shift, ppm	component	S/N (RMS)	expected integral[a]	mean integral ORACLE[a]	rel % error
1	72.5	1,2-DME	28:1	1.00	0.99 (0.12)[b]	−1.0
2	68.0	THF	2500:1	90.31	89.3 (1.0)	−1.1
3	63.5	2-PrOH	144:1	4.85	7.76 (0.23)	−1.9
4	60.3	1,3-Pr(OH)$_2$	6:1	0.31	0.22 (0.11)	−29
5	58.7	1,2-DME	24:1	1.00	1.01 (0.08)	−1.0
6	36.4	1,3-Pr(OH)$_2$	5:1	0.16	0.08 (0.06)	−50
7, 8	26.2/25.7	THF/2-PrOH	2840:1	100.00	100.00	

[a] Percent of the peak areas of THF/2-PrOH. [b] Values in parentheses denote ±1 standard deviation.

Table IV. Quantitative Results of Five Replicate Analyses of a Sample of Mole Ratio THF:2-PrOH:1,2-DME:1,3-Pr(OH)$_2$ = 263:26.1:4.22:1.00

peak no.	shift, ppm	component	S/N (RMS)	expected integral[a]	mean integral ORACLE[a]	rel % error
1	72.5	1,2-DME	40:1	1.45	1.38 (0.09)[b]	−4.8
2	68.0	THF	2250:1	91.03	89.22 (0.63)	−2.0
3	63.5	2-PrOH	113:1	4.48	4.19 (0.07)	−6.5
4	60.3	1,3-Pr(OH)$_2$	7:1	0.35	0.39 (0.06)	11
5	58.7	1,2-DME	37:1	1.45	1.33 (0.09)	−8.3
6	36.4	1,3-Pr(OH)$_2$	4:1	0.17	0.09 (0.04)	−47
7, 8	26.2/25.7	THF/2-PrOH	2380:1	100.00	100.00	

[a] Percent of the peak areas of THF/2-PrOH. [b] Values in parentheses denote ±1 standard deviation.

carbon-2 of 2-PrOH and 1,3-Pr(OH)$_2$ are present at only half the molar concentration of other carbons in the sample. Thus, the true dynamic range of the mixture (carbon-1 or carbon-2 of THF:carbon-2 of 1,3-Pr(OH)$_2$) is 660:1. The integrated intensity of each peak was normalized to the area of the partially resolved THF/2-PrOH pair at 26.2 and 25.7 ppm, respectively. Seven consecutive replicate analyses were performed on the sample to facilitate estimation of the precision of the analysis. The results are shown in Table II. The mean integral for all components is in good agreement with the actual composition. In addition, excellent internal precision is observed for peaks 1 and 5. Component peaks with lower signal-to-noise ratio exhibit a concomitant decrease in accuracy and precision of determination.

The above analysis was repeated for two additional mixtures of similar mole ratios to estimate the precision between runs. These data are given in Tables III and IV. Although the number of replicates and concentration ratios is not identical, the data still illustrate good run-to-run reproducibility for components of even moderate signal-to-noise ratio. However, the precision is seen to decrease with signal to noise. The authors are aware that an additional significant figure is not warranted in some of these data.

Neat Octanol-2-*d*. Neat octanol-2-*d*, Figure 3, was employed to probe the accuracy and precision of ^{13}C analyses as a function of signal-to-noise (S/N) ratio and spectral data point density. To evaluate to the effect of S/N, a preliminary

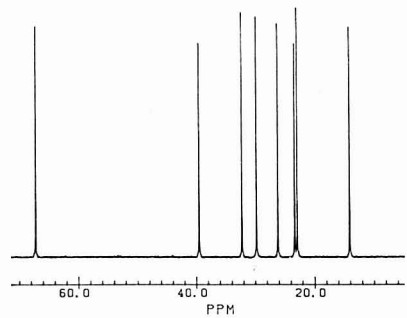


Figure 3. Carbon-13 spectrum of neat octanol-2-*d*. Spectral assignments are given in Table V.

experiment was conducted which had sufficient S/N (approximately 800:1) so as to minimize its effect on the analysis. Five successive replicate analyses of neat octanol-2-*d* were performed. Each spectrum was integrated with and the resulting peak areas were normalized to the unresolved carbon-1/carbon-7 pair at 23.4 and 22.9 ppm, respectively. These data are given in Table V. The accuracy and precision of the

Table V. Quantitative Results for Five Replicate Analyses of Neat Octanol-2-*d*

peak no.	carbon no.	shift, ppm	mean integral ORACLE[a]	rel % error[b]
1	2	67.3	48.76 (0.59)[c]	−2.5
2	3	39.6	49.26 (0.36)	−1.5
3	6	32.3	48.59 (0.35)	−2.8
4	5	29.8	49.24 (0.53)	−1.5
5	4	26.2	48.83 (0.42)	−2.3
8	8	14.1	48.57 (0.37)	−2.9

[a] Percent of peak areas of C-1 and C-7. [b] The "true value" of the integral is assumed to be 50.00%. [c] Values in parentheses denote ±1 standard deviation.

Table VI. Effect of Signal-to-Noise Ratio on Accuracy and Precision of Integrations of Neat Octanol-2-*d*

S/N (RMS)	mean integral ORACLE[a]	rel % error[b]
303:1	48.0 (0.8)[c]	−3.4
202:1	47.1 (1.2)	−4.0
123:1	46.2 (1.7)	−5.7
66:1	45.1 (3.0)	−7.6
45:1	43.4 (4.2)	−9.8
27:1	40.7 (6.3)	−13
14:1	36.2 (11)	−28
7:1	29.2 (19)	−42

[a] Percent of peak areas of C-1 and C-7. [b] The "true value" of the integral is assumed to be 50.00%. [c] Values in parentheses denote ±1 standard deviation.

mean integral for each carbon show good consistency. The internal precision of the mean integral is also observed to be slightly better than the precision between runs. If all carbons in each replicate are considered equivalent, then the mean integral for the analysis, based on 30 values, is 48.88 ± 0.49% (1 standard deviation) which yields a relative percent error of 2.2.

Neat octanol-2-*d* spectra of decreasing *S/N* were obtained from an FID to which was added noise of progressively increasing magnitude. Each spectrum was integrated and the resulting peak areas were normalized to carbon-1/carbon-7 pair as before. The mean integral for the six peaks in each spectrum was calculated and is tabulated in Table VI with the corresponding spectral *S/N*. Precision of determination decreases with *S/N*, corroborating the trend observed in the analysis of the high dynamic range mixtures. It is not clear why the relative accuracy of the data in Table VI shows a systematic trend to lower values with decreasing *S/N*. This may be due to the use of a noise spectrum which was not white, or to some degree of misphasing in the spectra of lower *S/N*, or to a combination of the two effects. The combined integral of the carbon-1/carbon-7 peaks is used as an arbitrary standard; this integral, at twice the size of the remaining integrals, is less prone to error.

Neat octanol-2-*d* was also studied to ascertain the effect of spectral data point density on analytical results. The results obtained for each spectral density were calculated from 30 values, five spectra of six peak areas each, and are tabulated in Table VII. Analytical accuracy increases with spectral resolution since the accuracy with which the integral is approximated is enhanced as the number of data points defining the line shape increases. The precision of the analysis also increases with spectral density. It is noteworthy that the case of 2K real data points accuracy is good (albeit with poor precision) with individual peaks being defined by as few as two points above half height.

Quantitative Determination of Overlapping Component Peaks by Deconvolution. In spite of the high spectral

Table VII. Effect of Spectral Data Point Density on the Accuracy and Precision of Integrations of Neat Octanol-2-*d*

spectral data set size (K)	no. of real pts[a]	Hz/pt	mean integral ORACLE[b]	rel % error[c]	av fwhh, Hz
1	512	11.8	*d*	*d*	*d*
2	1024	5.9	47.1 (11)[e]	−5.8	7.6
4	2048	2.9	49.4 (4.3)	−1.1	3.7
8	4096	1.5	49.1 (0.6)	−1.8	4.0
16	8192	0.7	48.9 (0.5)	−2.2	3.8
32	16384	0.4	48.8 (0.4)	−2.4	3.8
64[f]	32768	0.2	48.8 (0.4)	−2.3	3.8

[a] The number of displayed points (Reals) is half the spectral data set size. [b] Percent of peak areas of C-1 and C-7. [c] The "true value" of the integral is assumed to be 50.00%. [d] Unable to determine due to spectral distortions. [e] Values in parentheses denote ±1 standard deviation. [f] Derived from 32K spectral data sets which were zerofilled to 64K.

dispersion of resonances in ^{13}C NMR, peaks of quantitative interest frequently overlap. This situation presents little difficulty if resolved resonances for the overlapping components exist elsewhere in the spectrum which can be used in the determination. However, this is not always the case, and methods must be employed to separate the individual contributions to an overlapping line shape in order to quantify the components.

Resolving integrals for closely spaced peaks is achieved in ORACLE by either manipulating the integration limits using the line width criterion or curve fitting. If the peak overlap occurs only near the base line, limits of integration for the overlapping bands are chosen such that they do not overlap. This method is limited in accuracy since the wings of the normally Lorentzian NMR line shape extend a considerable distance and can contribute significant area to adjacent peaks, as in the case of a small peak which lies on the wing of a much larger peak.

A more accurate approach is to determine the individual components of a composite profile by fitting the curve based on an appropriate function. Lorentzian curves approximate most NMR line shapes adequately (except near the base line, in practice). The coefficients of the individual Lorentzians contained in the composite profile are then determined by a least-squares optimization method.

The least-squares method was applied to deconvolute the the partially resolved THF/2-PrOH pair in the high dynamic range mixtures. For the data in Table II, a value for 2-PrOH (normalized to THF as 100%) of 11.7 ± 0.1% (1 standard deviation) was obtained resulting in a relative percent error of −7.3 (actual value 12.55%). The procedure was repeated for the data in Tables III and IV, yielding values for 2-PrOH of 9.75 ± 0.07% (relative percent error of −9.1) and 9.61 ± 0.12% (relative percent error of −2.4), respectively. Although the precision of the above values is generally better than those obtained for carbon-2 of 2-PrOH, the accuracy is lower. This may be due to a poorer least-squares fit of the minor 2-PrOH component relative to the large THF component of the composite profile.

The curve fitting procedure was also used to resolve the carbon-1/carbon-7 pair of neat octanol-2-*d*. From the data in Table V, the area of the carbon-7 peak (normalized to carbon-1 as 100%) was found to be 99.0 ± 0.7% (1 standard deviation) resulting in a relative percent error of −1.0. The peaks are of approximately the same intensity and line shape and hence should be fit to similar degrees of accuracy. This would account for the improvement in the relative percent error over that obtained in the high dynamic range mixtures.

Details of Processing Methods. By observing the appropriate experimental conditions, ^{13}C NMR spectra can usually be measured such that individual peak intensities are proportional to the concentration of the corresponding component in the sample. If all of the spectral line widths and line shapes are *identical*, then the relative peak heights will represent the relative concentrations of the species giving rise to each signal. However, line widths and line shapes within a spectrum frequently vary due to a variety of chemical and instrumental influences, and therefore relative peak areas must be measured to obtain quantitative results.

Several numerical integration methods are available for approximating the area under a peak defined by discrete data points. The use of a particular technique depends on the degree of accuracy desired in determining the integral. The simplest numerical integration technique is to sum all the data points contained within the peak. The total area under the curve is simply the combined area of a set of rectangles, each having equal width. The "rectangle rule" gives a fairly crude approximation of the integral, especially in cases where the number of data points on the peak is relatively small. As the number of points defining the peak increases, however, the integration errors of individual rectangles (rectangle area – true area) are decreased. Thus, the accuracy of the integral increases with the number of data points defining the peak.

A more accurate method of approximating the area under the peak is to linearly interpolate between adjacent data points. The total area is now given by the combined area of a set of trapezoids of equal width. This technique is called the "trapezoidal rule". The integration errors for individual trapezoids are less than those obtained by summation; therefore, the accuracy of integration is increased.

Further increases in accuracy are possible if three data points rather than two are used for interpolation. A common three-point interpolation scheme for integration is "Simpson's rule". With this method, a parabolic function is defined by three consecutive points and the area underneath the function is calculated. The integration errors using "Simpson's rule" are smaller than those obtained by either the "rectangle" or "trapezoidal" rule because a parabola is a better approximation to the peak curvature (over small ranges) than rectangles or trapezoids.

Regardless of the method of integration employed, two aspects of the data can introduce large systematic errors in integrals: base line distortion and base line offset. Base line distortions can be caused by a variety of instrumental and processing considerations. Lengthy experiments containing a large number of acquisitions frequently suffer from broad distortions that are not apparent in shorter experiments. Minor anomalies such as imperceptible pulse breakthrough, probe background, and amplifier distortions are additive and become serious only after many acquisitions. Formidable distortions can also occur where the data overflow or are truncated prior to Fourier transformation.

Correction of these distortions is possible with a method proposed by Pearson (*20*), as long as they are broad with respect to the spectral information which is to be retained. The algorithm fits a function to the signal-free portion of the spectrum. The function is then subtracted from the data set to give a partially corrected spectrum. The process if repeated until the base line is flat. Almost any function can be used for the fitting procedure; however, since most distortions manifest themselves as continuous curves, fitting a multiorder polynomial is appropriate.

We have extended Pearson's method to be more versatile by allowing the user to specify the order of the correction and further to select multiple spectral regions to be independently corrected. Very complex distortions can be removed by applying the fitting procedure to small portions or blocks of the data set. Thus, a fourth-order correction on four individual blocks of data can be as effective as an sixteenth-order correction on the entire spectrum. Perhaps the most important aspect of method, however, is that line shape and integrals are preserved for narrow features and, thus, the integrity of quantitative data is maintained.

Table VIII. Accuracy of Integration for Lorentzian Lines as a Function of Integration Range

accuracy (fraction of total integral)	integration range (in units of line width)
99.99%	6366
99.90%	636
99.00%	63.6
90.00%	6.31
80.00%	3.08
50.00%	1.00

Another consideration in processing quantitative data is the proper choice of integration limits. Their importance can be demonstrated by evaluating the theoretical line shape of an NMR signal. The line shape can be derived from the Bloch equations and has been shown to be a Lorentzian function

$$f(\nu) = A\frac{\alpha}{\alpha^2 + (2\nu)^2}$$

in which α is the full width at half maximum height and A is the peak intensity times α. Integration between the limits $-\nu_1$ and $+\nu_1$ gives

$$\int_{-\nu_1}^{+\nu_1} f(\nu)\,d\nu = 2A\alpha\int_0^{\nu_1}\frac{d\nu}{\alpha^2 + (2\nu)^2} = A\tan^{-1}\frac{(2\nu_1)}{\alpha}$$

When ν_1 is infinite, the total integrated intensity becomes

$$\int_{-\infty}^{\infty} f(\nu)\,d\nu = \frac{A\pi}{2}$$

It is unreasonable to integrate digitally over all frequencies, so an approximation must be made by choosing limits. Fortunately, if this approximation is consistently implemented, the ratio of individual integrals within a spectrum will remain constant. Table VIII shows how the limits can be chosen as a function of peak width to obtain various accuracies of integration for a Lorentzian line. Since most of the integrated intensity lies within a few multiples of the line width, small errors in the determination of the line width or in the line shape will have very little effect on the integral if the limits are consistently chosen as several line widths.

Integration as a function of line width facilitates automatic integrations. The default limit criterion can be changed, however, in order to integrate partially resolved peaks. The number of integrated points can be increased without changing the limit criterion by zerofilling the data set while in the Fourier codomain. This action increases the digital resolution, or number of points per peak, thus increasing the accuracy of a peak's integration. Convolution techniques, such as line broadening, also increase digital resolution, but will not affect integrals when the integration limits are chosen as a function of line width.

Although the above data processing considerations have been applied to NMR, they are in no way limited to NMR. Modular design provides for easy adaptation of pertinent features to other spectroscopies as well as chromatography. The ORACLE software package is currently configured for the Data General MV-8000 and DEC VAX 32-bit computers and will soon be implemented on other laboratory computers.

ORACLE is available at no charge to academic laboratories. Inquiries may be addressed to the corresponding author.

ACKNOWLEDGMENT

The authors thank Anil Kumar for technical assistance.

LITERATURE CITED

(1) Carman, C. J.; Wilkes, C. E. *Macromolecules* **1974**, *7*, 40–43.
(2) O'Neill, I. K.; M. A. Pringuer *Org. Mag. Reson.* **1974**, *6*, 398–399.
(3) Sarneski, J. E.; Reilley, C. N. *Anal. Chem.* **1976**, *48*, 1303–1308.
(4) Levy, G. C.; Hewitt, J. M. *J. Assoc. Off. Anal. Chem.* **1977**, *60*, 241–243.
(5) Abidi, S. L. *Anal. Chem.* **1982**, *54*, 510–516.
(6) Forsyth, D. A.; Hediger, M.; Hahmoud, S. S.; Giessen, B. C. *Anal. Chem.* **1982**, *54*, 1896–1898.
(7) Shoolery, J. N. *Prog. NMR Spectros.* **1977**, *11*, 79–93.
(8) Marecl, T. H.; Scott, K. N. *Anal. Chem.* **1977**, *49*, 2130–2136.
(9) Thiault, B.; Mersseman, M. *Org. Mag. Reson.* **1976**, *8*, 28–33.
(10) Blunt, J. W.; Munro, M. H. G. *Aust. J. Chem.* **1976**, *29*, 975–986.
(11) LaMar, G. N. *J. Am. Chem. Soc.* **1971**, *93*, 1040–1041.
(12) LaMar, G. N. *Chem. Phys. Lett.* **1971**, *10*, 230–232.
(13) Freeman, R.; Pachler, K. G. R.; LaMar, G. N. *J. Chem. Phys.* **1971**, *55*, 4586–4593.
(14) Natusch, D. F. S. *J. Am. Chem. Soc.* **1971**, *93*, 2566–2567.
(15) Levy, G. C.; Cargioli, J. D. *J. Magn. Reson.* **1973**, *10*, 231–233.
(16) Levy, G. C.; Edlund, U. *J. Am. Chem. Soc.* **1975**, *97*, 4482–4485.
(17) Freeman, R.; Hill, H. D. W.; Kaptein, R. *J. Magn. Reson.* **1972**, *7*, 327–329.
(18) Canet, D.; Levy, G. C.; Peat, I. R. *J. Magn. Reson.* **1975**, *18*, 199–204.
(19) "Sadtler Standard ^{13}C NMR Spectra"; Sadtler Research Laboratories, Inc.: Philadelphia, PA: 1976, Vol. 1; 1977, Vol. 10, Vol. 15.
(20) Pearson, G. A. *J. Magn. Reson.* **1977**, *27* (2), 265–272.

RECEIVED for review October 12, 1982. Accepted January 3, 1983. Financial support from the National Science Foundation (Grant CHE 81-05109) and the Division of Research Resources, National Institutes of Health (Biotechnology Research Resource, RR 01317), is gratefully acknowledged.

CORRESPONDENCE

Study of Chromatographic Retention with Spectroscopic Bandwidths

Sir: An improved understanding of chromatographic retention behavior has been provided from statistical thermodynamic descriptions of solute distribution coefficients (*1–3*). Also, spectroscopic measurements have been developed to obtain specific structural information about bonded stationary phases (*4, 5*). The link between these two areas of study is the determination of the relationship between distribution coefficients and the structures of the chromatographic phases. The purpose of this work is to establish a first step toward developing an understanding of the intermolecular interactions giving rise to the molecular shape dependence of solute retention.

The fundamental mechanisms that determine the structure dependence of chromatographic retention are presently not well understood. It is widely accepted that the polar mobile phase gives rise to the retention selectivity for polycyclic aromatic hydrocarbrons using *n*-alkylsilane stationary phases (*6*). The selectivity is thought to arise from hydrophobic exclusion in the mobile phase, with the stationary phase being inert. This idea is consistent with the observations that the selectivity decreases markedly upon changing mobile phase composition and less upon changing the nonpolar stationary phase. A mobile phase origin of PAH selectivity is also consistent with the inverse correlation between retention time and molecular size (*7*). On the other hand, there are recent chromatographic data that are more consistent with the stationary phase as the origin of selectivity. These data show that the retention indexes of polycyclic aromatic hydrocarbons (PAH) correlate with length-to-breadth ratio in LC separations employing a C_{18} stationary phase with an acetonitrile–water mobile phase (*8*). The fact that solutes having higher length-to-breadth ratios are retained longer by the *n*-octadecyl stationary phase suggests that the shape selectivity originates from the stationary phase rather than the mobile phase.

Chromatographic retention measurements alone are insufficient to identify unambiguously the contributions to selectivity from each phase because retention inherently senses the difference between two phases. Spectroscopy allows study of the phases individually. It can potentially provide information pertinent to chromatographic retention mechanisms because the intermolecular interactions that determine retention also control the positions and widths of spectroscopic bands. The relation between spectroscopic and chromatographic measurements is thus the attractive and repulsive intermolecular interactions that influence both measurements.

The observed molecular shape selectivity of chromatographic retention suggests that steric interactions between the solute and its environment are controlling selectivity among isomers. Steric interactions for nonpolar molecules occur through short-range repulsive forces between molecules. Spectroscopic bandwidths are known to be affected by repulsive and attractive forces that cause modulations of the quantum states of the molecule. The relation of these interactions to vibrational line shapes is the subject of vibrational dephasing theory (*9–11*). Vibrational spectra are not studied in this application because a large, unknown contribution from lifetime broadening diminishes the reliability of such measurements. Since the same interactions operate on electronic spectra, the ideas developed in vibrational dephasing theory are adapted to this discussion. Both the temporal properties and the strengths of the attractive and repulsive interactions contribute to spectroscopic bandwidths. For nonpolar molecules, where the interaction strengths are weak, it is likely that the repulsive, steric interactions largely control the bandwidths; for polar phases, both attractive and repulsive interactions contribute. The fact that the steric interactions are evident in the spectroscopic bandwidths is the principle behind this work.

The purpose of this work is 2-fold: first, the existence of a relationship between spectroscopy and chromatography is explored, and second, the spectroscopic measurements are applied to the study of the origin of retention in the reverse-phase separation of polycyclic aromatic hydrocarbons. To study the shape dependence of the solute–solvent steric interactions, the retention times and the electronic spectral bandwidths of solutes having varying shapes were measured. The bandwidths for the solute in each solvent should thus reveal the extent to which the corresponding phase contributes to shape selectivity in chromatographic retention. A series of dimethylnaphthalene derivatives was chosen to achieve a

0003-2700/83/0355-0787$01.50/0 © 1983 American Chemical Society

Table I. Correlation of Spectroscopic and Chromatographic Data

naphthalene derivative	retention time[a]	bandwidth difference,[b] cm^{-1}	*n*-dodecane bandwidth, cm^{-1}	85% AN-W bandwidth, cm^{-1}	L/B[d]
1,4-dimethyl	0.917	6.8 ± 1.7[c]	230	237	1.10
2,3-dimethyl	0.932	10.2 ± 1.0	213	223	1.38
1,3-dimethyl	0.961	27.2 ± 2.5	190	217	1.30
2,6-dimethyl	1.000	50.0 ± 2.0	170	220	1.53

[a] Relative to 2,6-dimethylnaphthalene. [b] Difference between the bandwidth in 85% acetonitrile–water and that in *n*-dodecane. [c] 75% confidence limits. [d] Length-to-breadth ratio.

variety of molecular shapes without significantly perturbing the polarizabilities of the ground and excited states. The electronic 0–0 bands of the first excited singlet states were studied in order to minimize lifetime relaxation effects on the bandwidths. The difference between the bandwidth in the polar phase and that in the nonpolar phase was used to represent the additional repulsive contribution from the polar phase over that from the nonpolar phase. Polar solvents acetonitrile–water and methanol, and nonpolar solvents *n*-dodecane and benzene were used in the spectroscopic experiments. The results are compared with chromatographic retention measurements on comparable phases. The same octadecylsilane column used to determine the shape correlation of ref 7 was used in this work for the chromatographic measurements. It is assumed that the steric interactions between the solutes and the bulk nonpolar phase approximate those between the solute and the bonded stationary phase consisting of the same type of functional group.

EXPERIMENTAL SECTION

Absorption spectra were obtained on a Cary 118C UV/visible absorption spectrometer operating with an approximate spectral bandwidth of 20 cm^{-1} in the spectral region of interest. The spectra consist of several bands which are overlapped by different amounts for the different compounds. The 0–0 bands were used in all cases, with the assignments of the 0–0 bands for the various compounds obtained from published work (*12*). The bandwidths for the 0–0 bands were quantified as the half-width at half-height, taken from the band center to the low frequency side. This procedure minimizes the effect of overlap with higher frequency bands on the measured bandwidths. The spectra for the four dimethylnaphthalene compounds used are given in Figure 1 to illustrate the degree of band overlap. Hot bands do not appear to contribute significantly to the widths at half-height. All bandwidths reported are estimated to be precise to ±5 cm^{-1}, and the bandwidth differences to ±7 cm^{-1}, except as otherwise noted. The fwhm of the bands are typically 400 cm^{-1}. To estimate the sytematic error on the bandwidths from the 20 cm^{-1} instrument band-pass, the convoluted bandwidth can be approximated to be a Gaussian of half-width $[A^2 + B^2]^{1/2}$, where A is 20 cm^{-1} and B is 400 cm^{-1}, and both the bandwidth and band-pass are approximated to be Gaussians (*13*). The systematic error due to band-pass is therefore less than 1 cm^{-1}, which is negligible.

Liquid chromatographic separations were performed with a Separations Group Vydac 201TP polymeric octadecylsilane column. Two different mobile phases were used: 85% (v/v) acetonitrile–water and methanol. A Waters Associates Model M-45 solvent delivery system was used with a Waters Model U6J loop injector and a Waters Model 400 absorption detector operating at 254 nm. 2,6-Dimethylnaphthalene was used as an internal standard for the naphthalene derivatives, which were not well resolved. The accuracy of the relative retention times is estimated to be ±0.2%.

RESULTS AND DISCUSSION

The data plotted in Figure 2 show that there is a strong correlation between reversed-phase chromatographic retention and the differences in spectroscopic bandwidth between 85% acetonitrile–water and *n*-dodecane phases. The four dimethylnaphthalene derivatives occur in the same order in spectroscopy as in chromatography. The shape factor is also shown to correlate reasonably well with retention time; however, the order for the close-lying 1,3- and 2,3-derivatives is predicted correctly by spectroscopy, whereas the shape factor predicts the wrong order in this case. The correlation is consistent with the prediction that the spectroscopic bandwidths describe the repulsive interactions controlling retention selectivity. A quantitative evaluation of the relation between bandwidth difference and retention, based upon these data, would not be realistic due to the small range of possible shapes obtainable by rearranging methyl groups. Other systems are to be studied in future work.

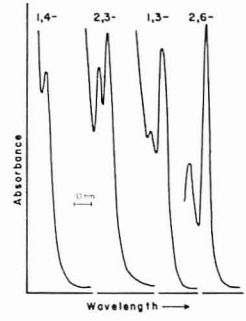


Figure 1. Electronic spectra of the four dimethylnaphthalene compounds illustrating the extent of band overlap. The 0–0 band is the lowest energy band in each case.

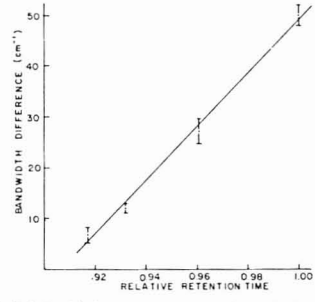


Figure 2. Relationship between spectroscopic bandwidth difference and chromatographic retention time. The error bars represent 75% confidence levels.

The data of Table I show that the retention correlates with the spectroscopic bandwidths themselves in *n*-dodecane but not with the bandwidths in 85% acetonitrile–water. The bandwidths in the latter solvent are nearly equal for all solutes except 1,4-dimethylnaphthalene, which is possibly due to the

Table II. Effect of Polar and Nonpolar Phase on the Bandwidth Differences (cm^{-1})

naphthalene derivative	bandwidth differences					retention time (MeOH)
	benzene	100% AN-W	85% AN-W	60% AN-W	methanol	
1,4-dimethyl	−15	−11	7	8	0	0.979
2,3-dimethyl	−9	−6	10	19	12	0.975
1,3-dimethyl	3	11	27	34	5	0.972
2,6-dimethyl	17	40	50	44	22	1.000

unusually strong band overlap for the 1,4-derivative. That the correlation holds for the *n*-dodecane bandwidths alone indicates that the nonpolar phase provides most of the retention selectivity. This assumes that any differences in bandwidths among the derivatives arises only from repulsive interactions rather than from (1) attractive interactions, (2) inhomogeneous broadening due to a distribution of solvation environments, (3) inherent differences in polarizability, or (4) lifetime contributions to the bandwidths. The last two contributions have been minimized by our selection of compounds. The importance of the first two contributions may be determined from a band-shape analysis of the spectroscopic bands because the repulsive contribution is the only one that imparts a Lorentzian shape to the bands. The attractive contribution is expected to be Gaussian; the distribution of environments is not known but it would be fortuitous if it were a Lorentzian. While a quantitative band-shape analysis is currently under way, the profiles all appear to be Voigt. The bandwidths are of comparable magnitude for both solvents. The profiles for the solutes in *n*-dodecane appear to be nearly Lorentzian, thus supporting the conclusion that the bandwidth differences, and hence the chromatographic selectivity, arise from steric repulsive interactions. The profiles for the solutes in acetonitrile–water are nearly Gaussian, suggesting that steric repulsions are much smaller than for *n*-dodecane and that, of course, attractive contributions are much larger. These considerations of the data in Table I strongly support the conclusion that the steric interactions in the stationary phase give rise to selective retention of PAH.

One limitation to the applicability of electronic bandwidth measurements in probing solute–solvent steric interactions is that the spectra only sense the repulsions at the aromatic part of the molecule, while much of the repulsion related to selectivity may occur at the methyl groups. It is likely that the methyl groups, which are only a few angstroms from the center of the ring, sufficiently disrupt the structure of the solvation environment that the increased repulsive interaction is sensed by the ring.

Chromatographic retention behavior is strongly dependent upon the choice of phases, and the band broadening differences should exhibit the same strong dependences. Studies of bandwidths were undertaken for these same solutes in polar and nonpolar phases where chromatographic data were available. The effect of varying the nonpolar phase composition on the spectroscopic bandwidth differences is shown in the data of Table II. For solvent benzene, the bandwidth differences for the solute molecules are less distinguishable than those for *n*-dodecane. This is consistent with the report that benzyl bonded phases provide poorer chromatographic resolution for substituted naphthalenes than do octadecyl bonded phases (*6*).

Measurements for two types of polar phases were made: acetonitrile–water mixtures of different compositions and methanol. The data of Table II show the effects of these polar phases on the spectroscopic behavior of the dimethylnaphthalenes. Changes in the composition of water in acetonitrile–water does not affect the range of bandwidth differences but does shift the values. This is consistent with the report that the water composition has little effect upon the chromatographic selectivity of PAH with the C_{18} stationary phase (*14*).

The data show that the use of methanol as a polar phase results in bandwidth differences that are closer together and probably arranged in a slightly different order. The 2,6-derivative has a distinctly different bandwidth from the others. The low spectroscopic resolution predicts low chromatographic resolution, according to the arguments made earlier. In chromatography, methanol does give lower resolution, as shown in Table II. In addition, the 2,6-derivative is distinguished from the other three, as it was in the spectroscopic data. The retention order among the three other compounds does not agree with the bandwidth order. The small quantitative disageement can be attributed to the failure of one of the assumptions that has been made, although the particular assumption is not identifiable without further experiments.

The similar behavior of the solute molecules with respect to their bandwidths in methanol and *n*-dodecane suggests that similar steric interactions take place in each phase. It is thought from theoretical (*15*) and X-ray diffraction studies (*16*) that the bulk liquid structure of methanol consists of short, straight chains. The fact that both stationary and mobile phases are comprised of chains is consistent with the low steric selectivity for mobile phase methanol with C_{18} stationary phase.

The agreement between the spectroscopic and chromatographic selectivity supports the predicted relation of these two measurements; however, caution must be used in quantitatively comparing different solvents. Attractive forces also contribute to spectroscopic band broadening and this contribution can be large for polar solvents due to large dipole-induced dipole interactions. Hypothetically, the solutes in acetonitrile–water could have a larger bandwidth contribution from attractive forces than they do in methanol, thus minimizing the fraction of the acetonitrile bandwidths due to repulsive forces. While this situation could diminish the apparent shape selectivity of acetonitrile–water to hamper quantitative comparison, it is not likely to be so large as to change the interpretation of the results because the attractive interactions are approximately independent of the position of the methyl group. To accomplish quantitative comparisons among chromatographic phases, a more detailed analysis of the band shapes providing separation of the attractive and repulsive contributions is currently under way.

The experimental results show that spectroscopic bandwidth measurements are sensitive to the subtle solvation interactions that control selective chromatographic retention and can thus be used to probe the fundamental retention processes. The approach in this work of using behavior in bulk solvents to infer bonded phase behavior is an approximation because, first, the bonded phase structures are not known but are unlikely to be the same as the bulk liquid structures, and second, the bonded phase structures may be altered by the mobile phase. Since the bulk and bonded *n*-alkanes are comprised of the same molecular structures, which determine the overall phase structure, the approximation is thought to be adequate for defining the relationship between the spectroscopic and chromatographic measurements. With further

characterization, spectroscopy can provide valuable information about the processes controlling selectivity to aid in enhancing selectivity of chromatographic separations.

LITERATURE CITED

(1) Snyder, L. R. *Anal. Chem.* **1974**, *46*, 1384.
(2) Jaroniec, M.; Rozylo, J. K.; Golkiewicz, W. *J. Chromatogr.* **1979**, *178*, 27.
(3) Boehm, R. E.; Martire, D. E. *J. Phys. Chem.* **1980**, *84*, 3620.
(4) Lochmuller, C. H.; Marshall, D. B.; Wilder, D. R. *Anal. Chim. Acta* **1980**, *130*, 31.
(5) Lochmuller, C. H.; Marshall, D. B.; Harris, J. M. *Anal. Chim. Acta* **1981**, *131*, 263.
(6) Colin, H.; Guiochon, G. *J. Chromatogr.* **1977**, *141*, 289.
(7) Sleight, R. B. *J. Chromatogr.* **1973**, *83*, 31.
(8) Wise, S. A.; Bonnett, W. J.; Guenther, F. R.; May, W. E. *J. Chromatogr. Sci.* **1981**, *19*, 457.
(9) Schweizer, K. S.; Chandler, D. *J. Chem. Phys.* **1982**, *76*, 2296.
(10) Oxtoby, D. W. *J. Chem. Phys.* **1981**, *74*, 5371.
(11) George, S. M.; Auweter, H.; Harris, C. B. *J. Chem. Phys.* **1980**, *73*, 5573.
(12) Petruska, J. A. In "Systematics of Electronic Spectra of Conjugated Molecules"; Platt, J. R., Ed.; Wiley: New York, 1964.
(13) Bracewell, R. N. "The Fourier Transform and its Applications"; McGraw-Hill: New York, 1978.
(14) Ogan, K.; Katz, E.; Slavin, W. *Anal. Chem.* **1979**, *51*, 1315.
(15) Jorgensen, W. L. *J. Am. Chem. Soc.* **1980**, *102*, 543.
(16) Magini, M.; Paschina, G.; Piccaluga, G. *J. Chem. Phys.* **1982**, *77*, 2051.

Mary J. Wirth*
David A. Hahn
Ronald A. Holland

Department of Chemistry
University of Wisconsin—Madison
Madison, Wisconsin 53706

RECEIVED for review September 3, 1982. Accepted December 22, 1982. We gratefully acknowledge the research support of the National Science Foundation.

Investigation of Adsorption of Benzene on Nickel(001) by Secondary Ion Mass Spectrometry

Sir: It is now possible, using secondary ion mass spectrometry (SIMS) or fast atom bombardment (FAB), to form gas-phase molecular ions directly from organic and inorganic solids (*1–3*). This ionization scheme, where the sample is bombarded by a particle with 1–5 keV of kinetic energy, has proven particularly useful for the analysis of thermally labile organic solids such as amino acids (*1*, *4*) and for the characterization of biomolecules with molecular weights in the 1000–10 000 dalton range (*5*). The mechanism of ejection of these large molecular species has been the subject of numerous speculations since it appears improbable at first thought that a large organic molecule held together by tens of electronvolts of energy could withstand impact by a 1000-eV primary particle.

Although no rigorous approach has been developed to fully explain the observations, a number of conceptual advances in understanding the ejection mechanism have been made utilizing classical dynamics calculations to model the dissipation of energy of the primary particle (*6*). For benzene adsorbed on Ni(001) for example, molecular ejection is favored since (i) the primary ion energy is rapidly dissipated in the solid such that atomic collisions with the benzene molecule are often only a few electronvolts, (ii) the organic molecule possesses many internal vibrational modes which can absorb excess energy from a violent collision, and (iii) the metal substrate atom is larger than a carbon atom which allows it to strike two or three carbon atoms simultaneously, pushing the entire molecule in one direction (*6*). It remains to be shown how many of these concepts are extendable to molecules of much higher molecular weight.

In this paper, we present preliminary SIMS experimental results for the adsorption of benzene on Ni(001) with the goal of comparing our observation to the previous benzene/Ni(001) classical dynamics calculations (*6*, *7*). The results show that, in agreement with studies by other techniques, that the adsorption occurs molecularly at room temperature reaching monolayer coverage after approximately 1 langmuir benzene exposure. In this environment, the only molecular ion that is observed with significant intensity is $NiC_6H_6^+$, in contrast to the very complex spectra found from Ni surfaces exposed to much higher quantities of benzene. We also present evidence for the mechanism of cationization of benzene by Ni, which is predicted to occur via recombination of benzene with Ni^+ ions over the surface of the solid. In general, this model system is utilized to better understand the SIMS spectra of organic solids and to evaluate the importance of various experimental parameters on the quality of the mass spectra.

EXPERIMENTAL SECTION

Experiments were performed in an ion-pumped stainless steel vacuum chamber with base pressure of 3.0×10^{-10} torr after bakeout. The primary ion was generated by a Physical Electronics sputter gun that had been modified to be differentially pumped by a 6-in. trapped diffusion pump. The gun could produce an ion beam with energies ranging from 75 to 1500 eV. With this arrangement we could perform SIMS measurements at an operating pressure of 1.0×10^{-8} torr with the ion gun normally operated at 3×10^{-6} torr of Ar. An Extranuclear 162-8 quadrupole mass spectrometer was employed to perform the secondary ion detection. The spectrometer was fitted with a Bessel box type energy analyzer with energy resolution typically between 1 and 2 eV. In addition, the filter could be electrically scanned for use in observing secondary ion energy distributions. The primary ion was incident on the sample at 45° and the analyzer was positioned to detect ejected ions at 45° with a half-angle acceptance of 16°. The signal was amplified by a Channeltron electron multiplier coupled to a PAR 1120 amplifier–discriminator.

The nickel(001) crystal was cut and finally polished with 0.05-μm alumina to ±0.5° orientation. Before the crystal was mounted, it was etched in a 3:1:1:5 mixture of concentrated HNO_3, H_2SO_4, H_3PO_4, and CH_3COOH and rinsed in deionized water and ethanol. The crystal was then mounted on a sample holder that could be resistively heated to 1300 K as monitored by a chromel–alumel thermocouple.

The sample gas consisted of spectra grade benzene (Fischer) which had been degassed through a series of freeze–pump–thaw cycles. The benzene was admitted through a variable leak valve, with the pressure measured by a nude Bayard-Alpert ionization gauge calibrated for air.

Crystal cleaning was restricted to cycles of heating in oxygen (5×10^{-7} torr, 1200 K, 10 min) and hydrogen (1×10^{-6} torr, 1200 K, 10 min) followed by sputtering and annealing at 1200 K. The surface was considered clean when no O^+ and NiO^+ peaks could be observed in the SIMS spectra and when the Ni_2^+/Ni^+ ratio approached 0.25 (*8*).

RESULTS AND DISCUSSION

The SIMS spectrum of the clean Ni surface is given in Figure 1a. Note that the only peaks other than Ni^+ and Ni_2^+ are the ubiquitous Na^+ and K^+ contamination peaks. This

0003-2700/83/0355-0790$01.50/0 © 1983 American Chemical Society

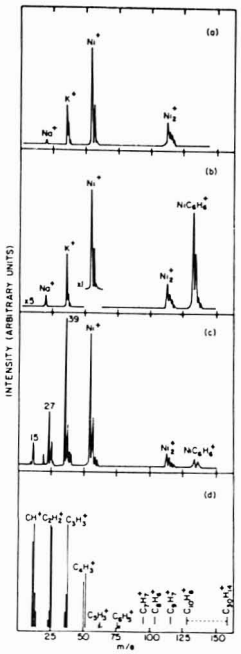


Figure 1. SIMS spectra for various coverages of benzene: (a) clean Ni(001); (b) 3 langmuir benzene exposure; (c) 4500 langmuir benzene exposure; (d) frozen benzene from ref 12. All spectra except (d) were obtained at 298 K using 3 nA/cm^2 of 1 keV Ar^+ ions.

surface was then exposed to a dose equal to 3 L of benzene at room temperature resulting in the SIMS spectrum shown in Figure 1b. As a result of the chemisorption of benzene, the Ni^+ and Ni_2^+ signals are greatly enhanced with respect to the clean surface. In addition, peaks beginning at mass 136 are also observed and are assigned to the cationized species $NiC_6H_6^+$. No other significant ions in the mass spectrum are found below mass 200.

These spectra persist in a qualitatively similar way for all exposures between zero and several hundred Langmuir exposure. As illustrated in Figure 2, the Ni^+ and $NiC_6H_6^+$ ion yields both exhibit a rapid initial rise followed by a saturation near 1.0 langmuir. A saturation point at 3 langmuir exposure has been observed for benzene on Ni(001) by electron energy loss spectroscopy (EELS) and corresponds to the $c(4 \times 4)$ ordered overlayer structure observed by LEED (*9*, *10*). The EELS measurements as well as chemical measurements which show (*11*) that molecular benzene is displaced from Ni(001) by $P(CH_3)_3$ at room temperature suggest that the adsorption occurs associatively. Thermal desorption studies associated with our SIMS experiments show loss of benzene from the surface at ~500 K, further suggesting that the same benzene overlayer is being characterized by all three methods.

Although there are no major changes in the types of observable cluster ions ejected from the benzene surface at monolayer coverage or below, the situation alters dramatically as the coverage is increased beyond the monolayer point. After exposures of Ni(001) to 4500 langmuir benzene, for example, as shown in Figure 1c, the $NiC_6H_6^+$ peak is strongly attenuated, while fragment peaks at mass 15 (CH_3^+), 27 ($C_2H_3^+$), 29 ($C_2H_5^+$), 39 (K^+, $C_3H_3^+$), 41 (K^+, $C_3H_5^+$), and 43 ($C_3H_7^+$) become quite prominent. The presence of $C_3H_3^+$ and $C_3H_5^+$ fragments at mass 39 and 41, respectively, is suggested by the change in the isotopic ratio normally expected for K^+ alone. Note that the spectrum obtained at 2100 langmuir (*7*) is nearly identical with the one shown in Figure 1c except that the weak $NiC_6H_6^+$ ion signal not observed previously has now been extracted from the noise. The exact nature of the surface composition is not clear at this stage. Apparently, several layers of benzene condense on the Ni surface. This condensation does not proceed indefinitely, however, since Ni^+ and Ni_2^+ ion signals are still observed. The increased complexity of the mass spectrum is perpetuated as the amount of benzene is increased further as illustrated by Lancaster and co-workers (*12*) who have reported the spectrum of frozen benzene, reproduced in Figure 1d. This spectrum, obtained at 77 K, exhibits intense fragment peaks, the parent ion $C_6H_5^+$, and numerous clusters containing greater than six carbon atoms. Many of the low mass fragmentation peaks are of different relative intensity than those in Figure 1c. The series of spectra shown in Figure 1b–d, then, clearly reveal that there is a dramatic, matrix-dependent alteration in the fundamental character of the benzene SIMS spectrum.

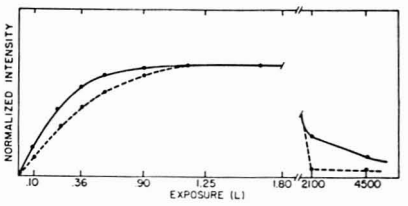


Figure 2. Normalized intensity plot for (—) Ni^+ and (---) $NiC_6H_6^+$ vs. benzene exposure.

It is possible to gain a certain level of understanding of the molecular ejection mechanism by focusing on the $c(4 \times 4)$ structure and by comparing our results to results of recent classical dynamics calculations for the same system (*7*). At the initial level of comparison, the classical dynamics model appears to be quite helpful. It predicts that the major species which ejects, other than Ni, is the molecular benzene itself with very small contributions from the C_nH_z (with $n < 6$) fragments. In addition, a sizable component of the spectrum is predicted to be NiC_6H_6. This organometallic species is found to form via a recombination of ejected Ni atoms and benzene molecules above the surface while still interacting with the solid. In addition, the model predicts that most of the benzene molecules (~75%) do not have sufficient internal energy to decay unimolecularly during the several microsecond passage to the detector.

As shown in Figure 1b, our experimental spectrum agrees in many respects with the predicted spectrum. The major difference is that the molecular ions $C_6H_6^+$ or $C_6H_6^-$ are not observed. A similar observation was made for CO adsorbed on Ni(001) where no CO^+ (or CO^-) could be detected but where a large $NiCO^+$ signal was observed (*13*). This discrepency is due in part to the relatively large difference in ionization potential between Ni and C_6H_6. This difference implies that the number of $C_6H_6^+$ ions ($I_{C_6H_6^+}$) relative to the number of Ni^+ ions (I_{Ni^+}) will be very small as indicated by an expression of the form (*14*)

$$I_{C_6H_6^+}/I_{Ni^+} = \exp[(IP_{Ni} - IP_{C_6H_6})/\epsilon_0]$$

where IP_{Ni} and $IP_{C_6H_6}$ are the respective ionization potentials of 7.6 and 9.3 eV, and ϵ_0 is a parameter generally between 0.25 eV and 0.5 eV (*15*). For this case, assuming that the yields

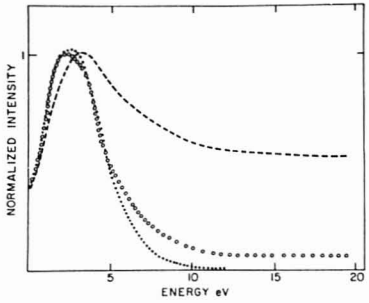


Figure 3. Normalized secondary ion energy distributions for: (---) Ni^+ clean surface: (O) Ni^+ 3 langmuir benzene; (●) $NiC_6H_6^+$ 3 langmuir benzene.

of Ni and C_6H_6 are of the same order, $I_{C_6H_6^+}/I_{Ni^+} \simeq 10^{-3} - 10^{-2}$, so that virtually all the C_6H_6 molecules should be ejected as neutrals. A similar agreement applies to the ejection of negative ions. By following the predictions of the classical dynamics calculations and by considering experimental evidence from other systems (*16*), the cationization product is almost certainly formed between an ionized Ni atom and a neutral benzene molecule as

$$Ni^+ + C_6H_6 \xrightarrow[\text{surface}]{} NiC_6H_6^+$$

Also, in agreement with the calculations, there is very little fragmentation observed in the experimental spectrum.

With this insight, it is possible to speculate about the reasons for the strong matrix effects observed when the benzene concentration is increased beyond the monolayer point. In this case, the benzene matrix itself, rather than the metal lattice, must dissipate all of the kinetic energy of the incident particle. It is reasonable to assume that these energetic collisions will lead to numerous fragments which further scramble by recombination reactions above the surface. For metallic systems these collisions occur mainly between metal atoms and only a few actually involve the benzene molecule itself.

The argument that the classical dynamics calculations provide a reasonable description of the nuclear motion that leads to benzene ejection is also enhanced by examining the kinetic energy distributions of the ejected species. To make a comparison between the calculated distributions of the neutrals and the measured distributions of the ions, it is necessary to consider the influence of the image charge created in the metal by the departing ion. For the clean surface, the Ni^+ ion distribution, as shown in Figure 3, is much broader than that calculated for the neutrals as presented in ref 7. The broadening has been shown to arise, in part, from the increased attraction of ~3.6 eV between the ion and the metal due to the image force (*17*). When the Ni surface is exposed to benzene, the calculated neutral energy distributions for both Ni and NiC_6H_6 are very similar to the measured distributions (see Figure 6b of ref 7) for Ni^+ and $NiC_6H_6^+$ assuming an image energy of 1.8 eV. The decrease in this value presumably arises due to screening of the image charge by the benzene overlayer. This effect also provides an explanation for the sharpness of the energy distributions of the benzene covered surface relative to the clean surface. Further, the fact that the experimental energy distributions for Ni^+ and $NiC_6H_6^+$ are very similar to the corrected calculated distributions provides additional evidence that the cationization reaction occurs via a recombination process.

Finally, it is important to note that the $NiC_6H_6^+$ ion maximum intensity corresponds to the $c(4 \times 4)$ structure. Presumably at lower coverages, the Ni^+ ion yield has not attained its maximum value and hence limits the intensity of the $NiC_6H_6^+$ species. At greater than monolayer coverages, the Ni yield is diminished since Ni atoms cannot penetrate through the overlayer to eject. This result is important to consider when utilizing cationization to enhance the yield of molecular ions of solid compounds by preparing thin films of the sample on a metal foil.

CONCLUSIONS

From this SIMS investigation of the adsorption of benzene on Ni(001) at room temperature we have found (i) the chemisorption of benzene on Ni(001) appears to form a stable superstructure on the surface as indicated by the saturation of the $NiC_6H_6^+$ signal. From the presence of this adsorbed structure we observe a SIMS spectrum with very different character to that reported in a previous study for frozen benzene. (ii) A condensed phase of benzene can be initiated at room temperature on the surface by increasing the dose. From this we see a spectrum approaching the spectrum of frozen benzene. (iii) Preliminary evidence from the comparison of experimental energy distributions of $NiC_6H_6^+$ and Ni^+ with the classical dynamics model of this system implies that the formation of $NiC_6H_6^+$ proceeds via Ni^+ and C_6H_6 recombination above the surface to produce the cationized species $NiC_6H_6^+$.

Registry No. Benzene, 71-43-2; nickel, 7440-02-0.

LITERATURE CITED

(1) Benninghoven, A.; Jaspers, D.; Sichtermann, W. K. *Appl. Phys.* **1976**, *11*, 35.
(2) Pierce, J.; Busch, K. L.; Walton, R. A.; Cooks, R. G. *J. Am. Chem. Soc.* **1981**, *103*, 2583.
(3) Barber, M.; Bordoli, R. S.; Sedgewick, R. D.; Tyler, A. N. *J. Chem. Soc., Chem. Commun.* **1981**, 325.
(4) Grade, H.; Winograd, N.; Cooks, R. G. *J. Am. Chem. Soc.* **1977**, *99*, 7725.
(5) Williams, D. H.; Bradley, C.; Bojesen, G.; Santikarn, S.; Taylor, L. C. E. *J. Am. Chem. Soc.* **1981**, *103*, 5700.
(6) Garrison, B. J. *J. Am. Chem. Soc.* **1980**, *102*, 6553.
(7) Garrison, B. J. *J. Am. Chem. Soc.* **1982**, *104*, 6211.
(8) Fleisch, T.; Winograd, N.; Delgass, W. N. *Surf. Sci.* **1978**, *78*, 141.
(9) Bertolini, J. C.; Rousseau, J. *Surf. Sci.* **1979**, *89*, 467.
(10) Bertolini, J. C.; Dalmai-Imelik, G.; Rousseau, J. *Surf. Sci.* **1977**, *67*, 478.
(11) Friend, C. M.; Muetterties, E. L. *J. Am. Chem. Soc.* **1981**, *103*, 773.
(12) Lancaster, G. M.; Honda, F.; Fukuda, Y.; Rabalais, J. W. *J. Am. Chem. Soc.* **1979**, *101*, 1951.
(13) Fleish, T.; Ott, G. L.; Winograd, N.; Delgass, W. N. *Surf. Sci.* **1978**, *78*, 141.
(14) Nørskov, J. K.; Lundquist, B. I. *Phys. Rev. B: Condens. Matter* **1979**, *19*, 5661.
(15) Yu, M. L. *Phys. Rev. Lett.* **1981**, *47*, 1325.
(16) Winograd, N.; Garrison, B. J.; Fleisch, T.; Delgass, W. N.; Harrison, D. E. Jr., *J. Vac. Sci. Technol.* **1979**, *16*, 629.
(17) Gibbs, R. A.; Holland, S. P.; Foley, K. E.; Garrison, B. J.; Winograd, N. *Phys. Rev. B: Condens. Matter* **1981**, *24*, 6178.

Nicholas Winograd*
E. J. Karwacki

The Pennsylvania State University
152 Davey Laboratory
Department of Chemistry
University Park, Pennsylvania 16802

RECEIVED for review October 25, 1982. Accepted January 11, 1983. The financial support of the National Science Foundation, the Office of Naval Research, the Air Force Office of Scientific Research, and the donors of the Petroleum Research Fund, administered by the American Chemical Society, is greatly acknowledged.

Karl Fischer Titration Equation on Mass Basis

Sir: In a recent paper (*1*) on the application of automatic Karl Fischer titration to the determination of water in solids, an equation used to calculate percent H_2O was presented. In this equation advantage was taken of the precision and convenience of use of calibrated syringes for measuring the quantity (volume) of solvent used for extraction, the quantity of the specimen of solvent–H_2O mixture, and the quantity of the solvent blank. Since publication of the paper, it has become evident that it would be desirable to also develop a similar equation in which these quantities are expressed on a mass, rather than volume, basis. It is the purpose of this correspondence to present such an equation. The equation, similar in form to that of eq 1 in ref 1, is

$$\% \ H_2O = (MC/m_g)[(A_s/m_s) - (A_b/m_b)]/[1 - (CA_s/m_s)]] \times 100 \quad (1)$$

where M is the mass of solvent used for extraction, C is the standardization factor of the titrator, m_g is the mass of the sample of solid substance to be analyzed for H_2O, A_s is the titration value (mass of H_2O or volume of Karl Fischer reagent) for the specimen of solvent-extracted H_2O mixture, m_s is the mass of the specimen, A_b is the titration value for the solvent blank, and m_b is the mass of the blank.

The presence of any extraneous substance in the specimen that significantly affects the mass necessitates a correction to eq 1. The corrected equation is

$$\% \ H_2O = \mathrm{RHSI} \times [1 + (m_0/M)/[1 - (A_b/m_b)/(A_s/m_s)]] \quad (2)$$

where RHSI is the right-hand side of eq 1 and m_0 is the mass of the extraneous substance.

Registry No. Water, 7732-18-5.

LITERATURE CITED

(1) Jones, F. E. *Anal. Chem.* **1981**, *53*, 1957.

Frank E. Jones

Center for Chemical Engineering
National Engineering Laboratory
National Bureau of Standards
Washington, D.C. 20234

RECEIVED for review December 6, 1982. Accepted December 27, 1982.

Comments on Sorption Capacities of Graphitized Carbon Black in Determination of Chlorinated Pesticide Traces in Water

Sir: We have been using graphitized carbon black (GCB) for trace enrichment of organics from water for several years (*1–3*). However, we have obtained results which, in certain instances, differ markedly from those reported by others (*4*). The main conflict is with adsorption of *n*-alkanes and methyl esters, which are reportedly not adsorbed at all (*4*). We have performed a wide variety of experiments which demonstrate that these compounds are indeed adsorbed from water by GCB and which provide possible explanations for the inaccuracy of the previous data. We also describe alternate procedures for studying the adsorption/desorption properties of GCB which allow optimization of trace enrichment parameters.

EXPERIMENTAL SECTION

Procedures and equipment were similar to those reported previously (*1, 2*). Adsorption traps were prepared from Soxhlet extracted GCB (Carbopack B, 60/80 mesh, Supelco, Inc., Bellefonte, PA) and small diameter (4–5 mm) glass or stainless steel tubes (*1*) or large diameter (10 mm) glass tubes (*2*). Two general types of adsorption/elution experiments were performed. The first type involved passing a specific volume of water, which had been spiked with a solution of the test substance, through the GCB trap, and then eluting the trap with a solvent or solvent series (*2*). The second type involved application of a small volume of a solution of the test substance directly to the top of a trap, followed by elution (*1*). Recoveries of test substances were determined by GLC, using external standards. Trap eluents were analyzed either directly or after concentration or dilution. Container surfaces and effluent water were tested by extracting with organic solvent and analyzing the extract.

RESULTS AND DISCUSSION

Previous work (*2*) indicated that adequate preparation of aqueous solutions of nonpolar organics required the use of a water miscible cosolvent. Since Lagana et al. (*4*) had used hexane solutions of hydrocarbons and ether solutions of esters

Table I. Hydrocarbon Adsorption on GCB and Container Surfaces[a]

	% recovered					
	pentadecane		hexadecane		octadecane	
solvent	trap	reservoir	trap	reservoir	trap	reservoir
acetone	94	0	95	0	96	0
hexane	20	72	15	76	11	79

[a] Percent of added amount of each hydrocarbon eluted from GCB trap or solution reservoir with 2:1 petroleum ether:toluene. A 50-μg sample of each hydrocarbon in 0.5 mL of either acetone or hexane added to 1 L of water in a reservoir and passed through a 10 × 150 mm trap.

0003-2700/83/0355-0793$01.50/0 © 1983 American Chemical Society

Table II. Percent Adsorption of Esters by GCB[a]

ester	% recovery
methyl hexanoate	95
methyl heptanoate	94
methyl decanoate	95

[a] A 50-μg sample of each ester in 0.5 mL of acetone added to 1 L of water and passed through a 10 × 150 mm GCB trap. The trap was eluted with 2:1 petroleum ether:toluene.

Table III. Hydrocarbon Adsorption on GCB and Container Surfaces

amt added[a]	% recovered[b] pentadecane trap	pentadecane reservoir	hexadecane trap	hexadecane reservoir	octadecane trap	octadecane reservoir
800	13	88	13	86	13	86
400	79	20	65	34	59	40
200	81	18	74	26	79	19
100	85	10	81	15	77	20
50	94	0	95	0	96	0

[a] Amount of each *n*-paraffin added (μg in acetone solution) to 1 L of water in reservoir. [b] Percent recovered after passing the aqueous test mixture through the 10 × 150 mm trap and extracting the trap and reservoir with 2:1 petroleum ether:toluene.

to prepare their aqueous test solutions, it seemed likely that this could be a major reason for the anomalous results. We tested this possibility by preparing 1 L aqueous test solutions of three *n*-paraffins from both acetone and hexane stock solutions, passing the aqueous solutions through 10 × 150 mm GCB traps, and determining the residual amounts of hydrocarbons on both the GCB trap and in the solution reservoir (2:1 petroleum ether:toluene elution). The results are shown in Table I. Additional experiments with the hexane stock solution showed the amounts of hydrocarbons retained on the walls of the reservoir to vary considerably, over a range of about 20 to 80% of the total recovered, with factors such as method of combining solutions (organic to aqueous or vice versa), mixing conditions (time, temperature, vigor), and "settling" time (time after mixing, before adsorption) all contributing to the variability.

Similarly, use of an acetone stock solution of methyl esters to prepare an aqueous test solution gave the adsorption results listed in Table II. The results reported in reference 4 show zero adsorption for both the *n*-paraffins and the methyl esters. A close examination of the experimental procedures of Lagana et al. provides a possible explanation for their results. Taking the hydrocarbon case as an example, the aqueous test solution was prepared by adding a hexane solution containing 50 μg of each *n*-paraffin to 500 mL of water, shaking the mixture, and allowing it to stand for 10 min. The mixture was transferred to another container and then pumped through the GCB trap. Adsorption was determined by analyzing aliquots of the aqueous influent and the effluent from the trap and comparing the values. In order to reach the conclusion that zero adsorption had occurred, the amount of hydrocarbon measured in the influent and the effluent must be equal. Since, based on our experience, we would expect to find no hydrocarbon in the effluent, the amount determined in the influent would also have to have been zero. These data were not provided in ref 4 but were probably the case, as the following estimate of the expected amount indicates. On the basis of the data in Table I, the actual hydrocarbon concentration in the aqueous test solution after mixing and standing would be about 15 ng/mL. If a 20-mL aliquot of this solution

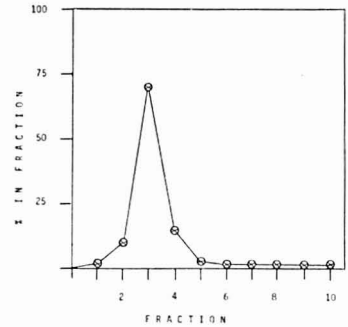


Figure 1. Elution curve for *p,p'*-DDT from 10 × 150 mm GCB trap (1 mL fractions): (O) DDT applied in acetone solution directly to trap; (X) DDT dissolved in 1 L of water and then passed through the trap.

Table IV. Elution of Octadecane from GCB[a]

fraction no.	eluent	amt, mL	% recovered[b]
1	methanol	5	0
2	methylene chloride	1.5	0
3	methylene chloride	2	100
4	methylene chloride	2	0

[a] A 50-μg sample of octadecane in 50 μg of hexane applied to a 5 × 100 mm trap. [b] Fraction concentrated to about 100 μL before analysis.

were extracted and the extract evaporated to 1 mL (the actual volumes were not specified in ref 4), a sample having a final hydrocarbon concentration of 300 ng/mL would be obtained. A 5-μL injection aliquot of this solution would contain only 1.5 ng of hydrocarbon, a virtually undetectable peak on most GC systems. Thus, the conclusion of zero adsorption of hydrocarbons (and esters) by GCB was quite likely based on negative findings.

Even when acetone solutions are used to prepare aqueous test solutions, care must be taken not to exceed the aqueous solubilities of the test substances. The results of a series of adsorption experiments, using a range of added hydrocarbon amounts, are presented in Table III.

In order to overcome these and other difficulties inherent in using aqueous test solutions, to improve accuracy, and to simplify the process of determining adsorption/desorption characteristics of GCB, we have developed an alternate procedure. The procedure involves the direct application of an accurately known quantity of the test substances to an adsorption trap, followed by elution of the trap first with water and then with organic solvent (*1*). This allows the trap capacity to be quickly and accurately determined without resorting to over saturated or large volume test solutions. It also allows breakthrough volumes to be determined more accurately, since the test substance will emerge in a more concentrated, and thus more readily detectable, form. In addition, the desorption characteristics of compounds are very quickly ascertained with this method (*1*), and the optimum recovery solvent(s) and volume can be readily determined.

The direct application method was compared to the aqueous test solution method by means of elution curves (*2, 5*). Thus, identical curves were obtained for a sample of *p,p'*-DDT whether it was applied directly as an acetone solution followed by a 2-mL water rinse or as a trace constituent adsorbed from 1 L of water (2:1 petroleum ether:toluene trap elution) (Figure 1).

Additional experiments with hydrocarbon test substances were performed by using the direct application method. Thus, when *n*-octadecane (50 μg in 0.5 μL of ethyl acetate) was applied to a 4 × 50 mm trap and the trap flushed with 500 mL of water at 6 mL/min, no hydrocarbon (<1%) appeared in the aqueous effluent (methylene chloride extraction). Elution with methanol followed by methylene chloride resulted in complete recovery of the hydrocarbon. Repeating this experiment with a hexane solution of octadecane applied to a 5 × 100 mm trap gave the results shown in Table IV. Similar experiments using 11-, 12-, 13-, and 14-carbon normal alkanes and ether trap elution are reported in ref 1.

From the above evidence we must conclude that inadequate experimental procedures led Lagana et al. to the incorrect results regarding hydrocarbons and esters reported in ref 4 and that these substances are definitely adsorbed by and can easily be recovered from GCB.

Registry No. *p,p'*-DDT, 50-29-3; octadecane, 593-45-3; water, 7732-18-5.

LITERATURE CITED

(1) Petty, Robert L. *Anal. Chem.* **1981**, *53*, 1548.
(2) Mangani, F.; Crescentini, G.; Bruner, F. *Anal. Chem.* **1981**, *53*, 1627.
(3) Petty, Robert L. Pacific Conference on Chemistry and Spectroscopy, San Francisco, CA, 1978; Paper No. 84. Abstracts published by California Section, ACS, Berkeley, CA.
(4) Bacaloni, Alessandro; Goretti, Giancarlo; Lagana, Aldo; Petronio, Bianca Maria; Rotatori, Mauro *Anal. Chem.* **1980**, *52*, 2033.
(5) Smith, L. M. *Anal. Chem.* **1981**, *53*, 2152.

Fabrizio Bruner*
Giancarlo Crescentini
Filippo Mangani

Istituto di Scienze Chimiche
Universita di Urbino
Piazza Rinascimento, 6-61029 Urbino, Italy

Robert Petty*

Marine Science Institute
University of California
Santa Barbara, California 93106

RECEIVED for review January 28, 1982. Resubmitted August 30, 1982. Accepted January 6, 1983.

AIDS FOR ANALYTICAL CHEMISTS

Semiquantitative Screening Test for Cocaine

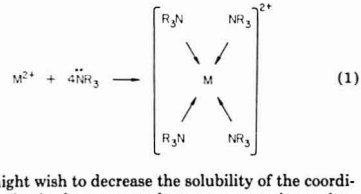
Basil Travnikoff

P.O. Box 287, Lodi, California 95241

This method describes a simple, rapid, and highly specific presumptive identification test for cocaine, in either its salt or free base forms, which is virtually unaffected by diluents, fillers, or excipients and which gives a fair estimation of the purity of cocaine by color comparison.

THEORY

As ion pair extraction is often used to isolate a cationic or anionic radical from an aqueous phase by addition of a select ionogen, so too may a particular weak ionogen, such as an organic base, form a coordination complex with a metallic ion as illustrated by the following:



(1)

If one might wish to decrease the solubility of the coordination complex in the aqueous phase, an appropriate anion, A^-, could be added to favor extraction into the organic phase

$$M(NR_3)_4^{2+} + 2A^- \rightarrow M(NR_3)_4A_2 \quad (2)$$

Cocaine, in dilute acid solution, appears to exhibit these properties with iron or copper ions, and the addition of thiocyanate ion appears to decrease the solubility of the coordination complex in the acid phase making it easy to extract the complex into chloroform while giving the chloroform a characteristic color, the intensity of which is proportional to the amount of cocaine in the sample.

EXPERIMENTAL SECTION

Approximately 10 mg of a sample suspected of containing cocaine is placed into a small test tube. Add to the test tube about 1 mL of 2% cupric sulfate pentahydrate (in 0.1 N HCl). Add about 1 mL of 2% potassium thiocyanate (aqueous). Add about 2 mL of chloroform. Stopper and shake the test tube.

RESULTS AND DISCUSSION

If cocaine or any of its optical isomers is present, the lower chloroform layer will display the brown color of the complex salt. By use of 10 mg of sample in the test, a 10% cocaine mixture will show a light brown color and a 100% cocaine sample will cause the chloroform to turn very dark brown. Thus, it is possible to estimate the purity of cocaine in the sample by comparing the color in the chloroform with a color scale or other known samples of cocaine.

As in screening tests where smaller amounts of cocaine are often encountered, a large sample may be easily tested to increase the sensitivity of the test. For example, a 20 mg sample will detect a 5% cocaine mixture. A 100 mg sample will detect a 1% cocaine mixture, and so on. Should an emulsion occur due to use of a sample larger than 10 mg in the test, it should easily be broken by adding additional chloroform. Of course, the semiquantitative characteristics of the test should be adjusted for variation in sample size or volume of reagents.

0003-2700/83/0355-0795$01.50/0 © 1983 American Chemical Society

The experimental procedure was checked with several other drugs including heroin, methaqualone, PCP, quinine, methamphetamine, barbiturates, procaine, benzocaine, tetracaine, lignocaine, butacaine, and methapyrilene. None of these drugs gave a positive test. However, the study of possible interfering compounds was by no means exhaustive, and because the reaction is generally applicable to organic bases, interfering substances may be encountered in the future.

Registry No. Cocaine, 50-36-2.

RECEIVED for review December 10, 1982. Accepted January 13, 1983.

Determination of Bromine in Blood Serum by Epithermal Neutron Activation Analysis

Zeev B. Alfassi*

Department of Nuclear Engineering, Ben-Gurion University of the Negev, Beer-Sheva 84121, P.O.B. 653, Israel

Nathan Lavi

Soreq Nuclear Research Center, Yavne, Israel

The determination of trace amounts of elements by neutron activation analysis (NAA) has been a standard technique for many years. Usually, the amount of the produced radionuclides has been measured by γ-ray spectrometry either without any chemical treatment, i.e., instrumentally, or after chemical separation. In some cases (*1*), there are advantages to measure the activated nuclides by their emission of X-rays due to electron capture or internal conversion processes. The main advantage of X-ray spectrometry is that many elements do not emit X-rays, thus reducing the background; this is in addition to the small number of lines in the characteristic X-ray spectrum of each element and the direct correlation between the element and the energies of its X-rays. Shenberg et al. (*2*) were the first to recommend X-ray spectrometry for the nondestructive determination of bromine. Rapaport et al. (*3*) determined the bromine content of blood serum by neutron activation analysis followed by X-ray spectrometry reducing the background due to the β-electrons by a magnetic field (*4*, *5*). The advantage of X-ray spectrometry is that in γ-ray spectrometry the Compton effect of the more abundant ^{38}Cl and ^{24}Na interferes with the measurement of the short-lived ^{80g}Br (17.8 min) and force the use of longer lived ^{82m}Br (35.3 h) after long decay (*6*–*8*). Nakahara et al. (*9*) determined Br by the 617-keV γ line of the 17.8 min ^{80g}Br in instrumental neutron activation analysis (INAA); however, they do not give their spectra while other works were not able to detect Br in short-time irradiation followed by short decay (*10*, *11*).

Another way to get rid of the interferences of the more abundant elements in biological tissues, Na and Cl, is by using epithermal neutrons. Guinn and Miller (*12*) determine the bromine content in biological material by using Cd-lined irradiation and by measuring the short-lived ^{79m}Br from the ^{79}Br(n,n')^{79m}Br reaction. Epithermal neutron activation analysis is advantageous in the case when the desired element has a nuclide with a high I/σ_0 (resonance activation integral/thermal neutron cross section) ratio while the major interfering activities in the sample have a lower ratio. This is the case for Br in a biological matrix, since Br has a ratio of 16.6 while the ratios for Cl and Na are 0.39 and 0.58, respectively (*13*). If a sample is irradiated within a suitable cadmium cover, the thermal neutrons are greatly attenuated and only neutrons with energies higher than about 0.4 eV will contribute significantly to the activation process. Na ions can be removed also by the use of chemical separation, as by HAP (hydrated antimony pentaoxide), or bromine can be oxidized and extracted by organic solvents. However, these are destructive methods.

This work was done to measure the detection limit of Br in this method and to compare with the other methods of NAA. For a representative biological sample we chose blood serum.

EXPERIMENTAL SECTION

Blood serum was prepared by centrifugation of blood samples. A 0.2-mL sample of the serum was transferred by a micropipet to a very thin Mylar sheet (0.006 mm) and left to dry in an under-vacuum desiccator containing P_2O_5, till complete dryness. After dryness, the samples were covered with another piece of Mylar sheet and were introduced to polyethylene bag which was heat-sealed.

Standards of bromine were prepared in the same way using dilute solutions of NH_4Br.

The samples were irradiated in the pneumatic tube of the IRR-1 reactor. For irradiation with epithermal neutrons, the polyethylene bag was inserted into a 0.5 mm thick cadmium box. After irradiation, the samples were taken from the plastic bag and measured directly.

The γ-rays of the activated samples were measured with a calibrated 100 cm^3 Ge(Li) detector connected to Cannbera 30 multichannel analyzer. The energy resolution (fwhm) of the system was 2.5 keV for 1332 keV. The samples were counted for 60–900 s after 5–10 min of cooling time necessary for the transfer of the irradiated sample to the counting room. The irradiation and counting times for the Cd-lined irradiated samples were usually longer than for the thermal neutron activated samples due to the higher activity of the second ones. The X-ray spectra of the activated samples were measured with a Si(Li) detector of 100 mm^2 area, 4 mm depth, and resolution (fwhm) of 320 eV for 6.4 keV (Fe k X-rays). A 1.5-mm plastic absorber was used to reduce interference from β decay electrons for both γ-ray and X-ray measurements.

RESULTS AND DISCUSSION

Figure 1 shows the spectra obtained from the irradiated blood serum, irradiated with a Cd cover (Epithermal Neutrons) and without a Cd cover (Reactor Neutrons), in the range of 400–1500 keV. As can be seen in Figure 1a, the Compton effect of the ^{24}Na covers all the peaks when using reactor neutrons. Figure 1b shows that when using only epithermal neutrons, bromine is seen very clearly and its amount can be measured from several peaks which increases the accuracy.

Figure 2 shows the X-ray spectrum measured after irradiation with reactor neutrons (2a) and with epithermal neutrons (2b). For reactor neutrons, the peaks of Br are masked with the activity of electrons due to ^{24}Na and ^{36}Cl. It is possible to remove this interference by magnets (*3*–*5*). However, Figure 2b shows that by use of epithermal neutrons, bromine can be determined quite easily and the use of a magnet is not necessary.

A calibration curve for 0.1–1.5 μg of bromine, irradiating with epithermal neutrons and measuring the 617-keV activity,

0003-2700/83/0355-0796$01.50/0 © 1983 American Chemical Society

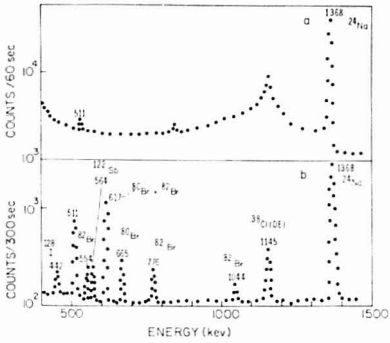


Figure 1. γ-Ray spectra of irradiated human blood serum: (a) 0.2 mL irradiated without Cd for 1 min and counted for 1 min after a cooling time of 10 min; (b) 0.2 mL irradiated under Cd for 20 min and counted for 5 min after a cooling time of 10 min.

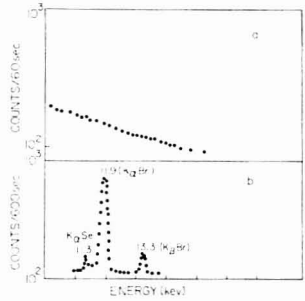


Figure 2. X-ray spectra of irradiated human blood serum: (a) 0.2 mL irradiated for 1 min without Cd and counted for 60 s after a cooling time of 10 min; (b) 0.2 mL irradiated under Cd for 20 min counted for 10 min after a cooling time of 10 min.

was found to be linear with the amount of bromine. The sensitivity obtained from this curve is 19931 ± 150 counts/μg Br (20 min irradiation, 5 min cooling, and 15 min counting). An almost identical line is obtained for the Kα + Kβ X-rays where the sensitivity is 20432 ± 180 counts/μg of Br. When counting is done without the 1.5 mm absorber, the sensitivity increases to 39940 ± 350 counts/Br, but however the ratio of peak to background is worse. Table I gives the amount of bromine measured both by γ-ray and X-ray spectrometry. The average value, 6.66 ± 0.21 μg/mL is in a good agreement with the published data (*3*, *14–16*).

The detection limit of a radionuclide is usually defined as the smallest photopeak which can be detected with a certain confidence above the background continuum. Currie (*17*) has shown the detection limit for the case of radioactivity to be given by the equation

$$L_D(\text{counts}) = 2.71 + 4.65\sqrt{\mu_B}$$

where μ_B is the true mean of the blank. The minimum detected mass is given by

$$M_D = L_D/K$$

where K is the sensitivity factor (counts per milligram).

Table I. Determination of Bromine in Human Blood Serum by Epithermal Neutron Activation followed by γ-Ray (618 keV ^{80}Br) and X-ray Spectrometry (K_α + K_β of ^{80}Br)

γ-ray		X-ray	
sample	amt of Br, μg/mL	sample	amt of Br, μg/mL
1	6.45	1	6.40
2	6.40	2	6.51
3	6.85	3	6.86
4	6.96	4	6.80
5	6.70	5	6.90
6	6.60	6	6.80
7	6.80		
8	6.40		
9	6.83		
av	6.66 ± 0.21	av	6.71 ± 0.20

For a 0.2-mL sample irradiated for 20 min and counted for 5 min after a decay time of 5 min the detection limits for determination of Br by γ-ray and X-ray spectrometry is 37 and 46 ng/mL, respectively.

Since γ-ray measurement has a lower detection limit and X-ray measurement has a drawback of self-absorption, it is clear that for epithermal neutron activation it is preferable to use γ-ray spectrometry.

When the concentration of bromine is very low, too low to be detected by this method, the use of longer irradiation with thermal neutrons followed by a long decay and a long counting time can enable the measurement the bromine content. In this case, the ^{82m}Br is used. The advantage in this case is the higher flux (Cd ratio for bromine is about 7) and the longer intensity—7% for 618 keV of ^{80}Br, compared to 66% for 554 keV and 41% for 619 keV of ^{82}Br. Since the cross section is about the same, this can lead to an advantage of about 65 for ^{82}Br. However, in this case, long irradiation and counting times are required, which is inconvenient for routine measurement.

Registry No. Bromine, 7726-95-6; bromide, 24959-67-9.

LITERATURE CITED

(1) Mantel, M.; Amiel, S. *Anal. Chem.* **1972**, *44*, 548.
(2) Shenberg, C.; Gilat, J.; Finston, L. H. *Anal. Chem.* **1967**, *39*, 780.
(3) Rapaport, M. S.; Mantel, M.; Nothmann, R. *Anal. Chem.* **1979**, *51*, 1356.
(4) Amiel, S.; Mantel, M.; Alfassi, Z. B. *J. Radioanal. Chem.* **1977**, *37*, 189.
(5) Mantel, M.; Alfassi, Z. B.; Amiel, S. *Anal. Chem.* **1978**, *50*, 441.
(6) Stella, R.; Genova, N.; Di Casa, M. *Radiochem. Radioanal. Lett.* **1977**, *30*, 65.
(7) Behne, D.; Diel, F. In "Nuclear Activation Techniques in the Life Sciences"; IAEA: Vienna, 1972; IAEA-SM-157, p 41.
(8) Behne, D.; Jurgensen, H. *J. Radioanal. Chem.* **1978**, *42*, 447.
(9) Nakahara, H.; Nagame, Y.; Yashizawa, Y.; Oda, H.; Gotoh, S.; Murakami, Y. *J. Radioanal. Chem.* **1979**, *54*, 183.
(10) Guzzi, G.; Pietra, R.; Sabioni, E. *Comm. Eur. Communities*. [*Rep*] *EUR* **1974**, *EUR 5282e*.
(11) Spyrou, N. M.; Fricker, M. E.; Robertson, R.; Gilboy, W. B. In "Symposium on Nuclear Techniques in Comparative Studies of Food and Environmental Contamination"; IAEA: Vienna, 1973; IAEA/SM-175.
(12) Guinn, V. P.; Miller, D. A. *J. Radioanal. Chem.* **1977**, *37*, 313.
(13) "Handbook on Nuclear Activation Cross-Section, Technical Reports No. 156"; IAEA: Vienna, 1974.
(14) Altman, P. L., Dittmer, D. S., Ed. "Biology Data Book"; Federation of American Societies for Experimental Biology: Bethesda, MD, 1974; Vol. 3, p 1752.
(15) Barrette, M.; Lamoureux, G.; Lebel, E.; Lecomte, R.; Paradis, P.; Monara, S. *Nucl. Instrum. Methods* **1976**, *134*, 189.
(16) Rapaport, M. S.; Mantel, M.; Shenberg, C. *Med. Phys.* **1982**, *9*, 194.
(17) Curie, L. A. *Anal. Chem.* **1968**, *40*, 586.

RECEIVED for review August 23, 1982. Accepted November 22, 1982.

Determination of Quantum Yields of Fluorescence by Optimizing the Fluorescence Intensity

Clifford L. Renschler* and Larry A. Harrah

Sandia National Laboratories, Albuquerque, New Mexico 87185

One of the most important spectroscopic measurements is the determination of fluorescence quantum yields, ϕ_F, of molecules in solution. We report here a simple, rapid method for determining ϕ_F values, using either a fluorimeter with dual detectors or a standard fluorimeter and an absorption spectrophotometer. We begin with a brief review of the equations which apply to the most common method of quantum yield determination.

The fluorescence quantum yield is defined as

$$\phi_F = I_F/I_a \tag{1}$$

where I_F is the number of fluorescence photons emitted per unit time and I_a is the number of photons of the excitation beam absorbed per unit time. For right angle fluorescence, when the entire length of the cell is viewed by the detector, the value of I_a is given by

$$I_a = I_0(1 - 10^{-\epsilon bc}) \tag{2}$$

where I_0 is the intensity of the excitation beam in photons per second, a is the molar absorptivity of the fluorophore, b is the length of the sample cell in centimeters, and c is the fluorophore concentration in moles per liter (*1*). For dilute solutions, where $abc < 0.02$, eq 2 can be approximated by

$$I_a = I_0(\epsilon bc)(\ln 10) \tag{3}$$

Because geometric and instrumental response factors are not known for most fluorimeters, I_F is difficult to determine directly. For this reason, quantum yields are usually determined by comparing the fluorescence response of the unknown to that of a standard whose quantum yield is known, as given by (*2*)

$$\phi_u = \phi_s\left(\frac{B_s}{B_u}\right)\left(\frac{I(\lambda_s)}{I(\lambda_u)}\right)\left(\frac{n_u^2}{n_s^2}\right)\left(\frac{D_u}{D_s}\right) \tag{4}$$

where ϕ is the quantum yield, B is the fraction of incident light absorbed, $I(\lambda)$ is the relative intensity of the excitation beam at the wavelength of excitation, n is the refractive index of the solvent, and D is the integrated area under the emission spectrum, corrected for monochromator and detector response. The subscripts u and s refer to unknown and standard, respectively.

Of course, if the same solvent and excitation wavelength are used for both unknown and standard solutions, the I and n^2 ratios each become unity. Since $B = I_a/I_0$, and the absorbance of the solution, A, is from Beer's law equal to (abc), eq 4 becomes

$$\phi_u = \phi_s\left(\frac{A_s}{A_u}\right)\left(\frac{I(\lambda_s)}{I(\lambda_u)}\right)\left(\frac{n_u^2}{n_s^2}\right)\left(\frac{D_u}{D_s}\right) \tag{5}$$

The use of eq 5 is limited to solutions of low absorbances for two reasons. First, as mentioned above, eq 3 is only valid for absorbances less than 0.02. Secondly, eq 2 strictly applies only to right angle fluorescence measurements in which the entire length of the cell is viewed by the detector, a condition not met with most fluorimeters (*3*).

BASIS FOR THE METHOD

Our technique for determining quantum yields is based on the more common instrumental condition shown in Figure 1, where the detector views a part of the interior of the cell, symmetrical about the midplane. For a cell of length $2w$ and a viewed length of $2s$, the detector views the solution from a depth of $w - s$ to $w + s$. It should be noted that the situation depicted in Figure 1 is somewhat idealized, since the edges of the viewed region will seldom, if ever, be absolutely parallel to the midplane. However, since most fluorimeters have small acceptance angles, Figure 1 represents a good approximation to the true viewed region.

The transmittance of the excitation beam at the edge of the viewed region closest to the excitation source is given by

$$T_1 = 10^{-\epsilon(w-s)c} = 10^{-\epsilon wc}10^{\epsilon sc} \tag{6}$$

while the transmittance at the opposite edge of the viewed region, T_2, is given by

$$T_2 = 10^{-\epsilon(w+s)c} = 10^{-\epsilon wc}10^{-\epsilon sc} \tag{7}$$

since

$$I_a = I_0(T_1 - T_2) \tag{8}$$

and the integrated fluorescence intensity D is proportional to I_a, then

$$D = KI_0 10^{-\epsilon wc}(10^{\epsilon sc} - 10^{-\epsilon sc}) \tag{9}$$

where K is a constant of proportionality which includes factors for geometric and instrumental response. Under these conditions, the fluorescence intensity seen by the detector will first rise with increasing fluorophore concentration and then fall again as the solution absorbs most of the excitation beam at solution depths less than $w - s$. To find the solution absorbance at which D is at a maximum, one differentiates the expression for D with respect to concentration and sets this equal to zero, thus obtaining

$$2\epsilon c = \frac{\log\left(\frac{w+s}{w-s}\right)}{s} \tag{10}$$

Multiplying both sides by w

$$A = \epsilon(2w)c = \frac{w\log\left(\frac{w+s}{w-s}\right)}{s} \tag{11}$$

where A is the absorbance developed by the solution over the entire length of the cell for the fluorophore concentration giving the maximum fluorescence intensity. With this expression and the definition of absorbance as $A = -\log T$, the transmittance at which fluorescence intensity is maximized, T_{max}, was found for several different combinations of cell lengths and viewed lengths, as shown in Table I. Clearly, the value of T_{max} shifts very little as $2s$ goes from 50% to 5% of $2w$. The limit of T_{max} as $2s$ approaches zero is 0.135. A derivation similar to the preceding one has been presented for the quantification of inner filter effects (*4*).

Theoretical values of D, normalized to 1.0 at T_{max}, are drawn as a function of T for $(2s/2w) = 0.050$ in Figure 2 (continuous line). For the range of $(2s/2w)$ values from 0.125 to near 0.0, the graphs would be essentially identical. Experimental data for $(2s/2w)$ approaching zero are plotted as discrete points on the same graph. Clearly, the experimental and predicted

0003-2700/83/0355-0798$01.50/0 © 1983 American Chemical Society

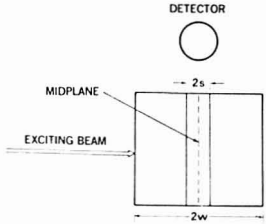


Figure 1. Cell of length $2w$ viewed normal to the exciting beam over length $2s$.

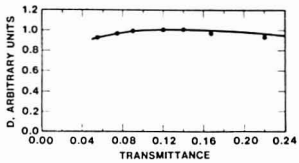


Figure 2. Relative fluorescence intensity vs. solution transmittance. Solid line is theoretical curve for $(2s/2w) = 0.050$. Discrete points are experimental values for $(2s/2w)$ nearly zero.

Table I. Values of T for Maximum Fluorescence, T_{max}[a]

width viewed by detector ($2s$), cm	T_{max}
0.500	0.111
0.300	0.127
0.125	0.134
0.050	0.135

[a] All values given for a cell width ($2w$) of 1.0 cm.

values agree quite well. Since D varies by less than 3% from $T = 0.10$ to $T = 0.20$, quantum yields can be quickly and easily determined with good accuracy, using the simple instrument schematically represented in Figure 3. The transmittance detector, usually a photomultiplier tube, is used to measure the relative intensity of the excitation beam after passing through the cell which contains a solvent blank. Quantum yield standard is then added to the cell until the transmittance detector registers an intensity ca 0.13 times that observed with the blank. Alternatively, the solution transmittance can be obtained by using a separate absorption spectrophotometer. Fluorescence is then measured with the other detector over the appropriate wavelength range. This emission spectrum is corrected for monochromator and detector response (*5*) and the area under the spectrum determined. The procedure is then repeated for the fluorophore of unknown quantum yield and ϕ_u is determined by

$$\phi_u = \phi_s\left(\frac{D_u}{D_s}\right) \tag{12}$$

Correction factors for changes in intensity of the excitation beam and refractive index can be applied as in eq 5, if necessary.

RESULTS AND DISCUSSION

This method has been applied to the determination of the quantum yield of 2-phenyl-5-(4-biphenylyl)-1,3,4-oxidazole (PBD) and *p*-quaterphenyl. The standard used was *p*-terphenyl, with a literature value for the quantum yield of 0.93 in cyclohexane (*6*). The quantum yield for PBD was determined to be 0.84 in cyclohexane, as compared with Berlman's value of 0.83 (*7*). For *p*-quaterphenyl, the quantum yield in cyclohexane was found to be 0.81, as compared with Berlman's value of 0.89 (*8*). The agreement of both of these values with those reported by Berlman demonstrates the viability of the method.

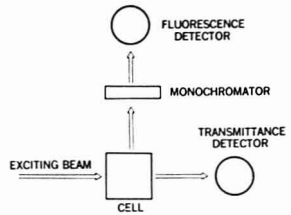


Figure 3. Instrument for measuring T and D.

Several advantages accrue from this method of quantum yield determination. The measurement can be performed rapidly, so long-term drift in both detectors is minimized. Experience in the authors' laboratory has shown that, with practice, the proper amount of fluorophore can be placed in the cell with two or three additions requiring only a few minutes. Of course, small drifts in the transmittance detector lead only to very small errors due to the flatness of the curve in Figure 2.

Since the spectra are taken in the transmittance region of maximum fluorescence intensity, signal-to-noise ratios are increased, leading to better precision.

Finally, transmittance values in the range of 0.13 can be measureed easily and accurately. In contrast, the transmittance values required for the optically dilute methods ($A \leq 0.02$, $T \geq 0.95$) are instrumentally difficult to measure and often require the use of long pass cells. Special care must then be taken that no turbidity is present in the solutions, since this could cause an error in the absorbance determinations. It should be noted that the higher absorbances used with this method make the measurement quite sensitive to cell positioning. For this reason, a solidly mounted cuvette holder which allows for reproducible positioning should be used.

Equations 6 and 7 require that Beer's law be obeyed for both standard and unknown solutions. While instrumental and chemical factors can sometimes lead to apparent deviations, Beer's law usually holds up to absorbances of at least 1.0. If one suspects deviations in a given system, this can easily be checked.

With any fluorescence measurement requiring significant solution absorbance, the possibility of errors due to reabsorption and/or reemission must be considered. Both effects increase with increased overlap between the absorption and emission spectra of the fluorophore of interest. For many fluorophores, including those discussed above, self-overlap is small and reabsorption and reemission effects are usually not problems. For fluorophores for which self-overlap is significant, these errors can be experimentally minimized, e.g., by moving the cell so that the excitation beam passes close to the edge of the cell nearest the fluorescence detector (*2*). If reabsorption and reemission effects are still significant, suitable mathematical correction can be made for them (*1*, *2*).

LITERATURE CITED

(1) Parker, C. A.; Rees, W. T. *Analyst (London)* **1960**, *85*, 587.
(2) Demas, J. N.; Crosy, G. A. *J. Phys. Chem.* **1971**, *75*, 991.
(3) Parker, C. A. "Photoluminescence of Solutions"; Elsevier: New York, 1968; Chaper 3.
(4) DeJersey, J.; Morley, P. J.; Martin, R. B. *Biophys. Chem.* **1981**, *13*, 223.

(5) Drushel, H. V.; Sommers, A. L.; Cox, R. C. Anal. Chem. 1963, 35, 2166.
(6) Berlman, I. B. "Handbook of Fluorescence Spectra of Aromatic Molecules", 2nd ed.; Academic: New York, 1971; p 220.
(7) Berlman, I. B. "Handbook of Fluorescence Spectra of Aromatic Molecules", 2nd ed.; Academic: New York, 1971; p 306.
(8) Berlman, I. B. "Handbook of Fluorescence Spectra of Aromatic Molecules", 2nd ed.; Academic: New York, 1971; p 238.

RECEIVED for review October 1, 1982. Accepted December 23, 1982. This work was supported by the U.S. Department of Energy.

Hydrogen–Tritium Exchange between Glass-Fiber Filters and Tritiated Water

William P. Bryan

Department of Biochemistry, Indiana University School of Medicine, Indianapolis, Indiana 46223

Hydrogen exchange between glass and water is an occasional problem in analytical procedures. For example, work on the infrared spectra of solutions of D_2O in CCl_4 was complicated by the presence of HOD bands due to hydrogen exchange between D_2O and borosilicate glass present in the infrared cell (*1*). Our own measurements of hydrogen–tritium exchange between biological membranes and tritiated water involved filtration of exchanged samples onto Whatman GF/C glass fiber filters, thorough washing with very dry tetrahydrofuran to remove all water, and liquid scintillation counting of residual tritium exchanged into the membranes. Because the amount of membrane preparation which could be filtered was limited, unacceptably high blank counts due to tritium exchange into the glass fiber filters were observed. This exchange occurred during the brief period between filtration and washing. The problem was largely eliminated by preheating the GF/C filters at 500 °C for at least 1 day.

It was thought that this hydrogen exchange between water and glass might be of sufficient interest to warrant further study.

EXPERIMENTAL SECTION

The general method involved incubation of GF/C filters with tritiated water for varying periods followed by freezing and freeze-drying to remove the water. Nonradioactive water was then added. This was followed by a period of back-exchange long enough for complete uptake of tritium by the water. The water was then liquid scintillation counted. Contact of the tritiated filters with air was avoided since exchange between tritium in the glass and atmospheric water vapor can occur. The procedure is based on a freeze-drying method for studying hydrogen exchange between proteins and water (*2*).

Whatman glass microfiber filters are made from borosilicate glass microfibers of circular cross section. They have a mean diameter of 0.05 μm upward. No binder is present. The filters can be heated up to 500 °C without adverse effects. The GF/C grade has a medium retention efficiency (*3*).

Pieces of GF/C filters (3–6 mg) were placed in borosilicate glass "minivials" used for liquid scintillation counting. These vials had been preheated at 500 °C for at least 1 day to minimize blank counts. To start exchange, 0.2 or 0.4 mL of deionized tritiated water (10^{-4} Ci/mL) was added to each vial, which was then tightly capped. Constant temperature for exchange at 1 °C was maintained with a constant temperature bath. A Scientific Products Temp-Blok module heater was used for constant temperatures above ambient. Several blank vials, not containing GF/C filters, were included in each run so that a blank correction curve could be established.

After various periods of exchange, samples were frozen in dry ice, caps were removed, and the "minivials" placed in holders (11 cm closed tubes with 24/25 standard taper female joints) for freeze-drying. The linear vacuum manifold had a number of 24/25 male joints directly attached through stopcocks, so it was only necessary to add a holder and open a stopcock to start freeze-drying a sample. Vacuum was obtained with a Cenco 7 mechanical pump. Two dry ice–ethanol traps, in series between the manifold and pump, were used to collect the tritiated water. Pressures below 10^{-3} torr were obtained with this system. Samples were freeze-dried and then dried overnight so that no physically adsorbed tritiated water was present.

After drying, the samples and manifold were closed off and very dry CO_2 was passed into the manifold until a pressure somewhat above that of the atmosphere was attained. The gas was dried by passage through Aquasorb (Mallinckrodt Chemical Works). Special precautions were used to ensure that the water content of the gas was very low (*4*). The heavier than air CO_2 acts as a protective blanket and eliminates any hydrogen exchange between the glass and atmospheric water vapor. Water was added to each sample by admitting CO_2 to the sample, removing the holder from the manifold, adding 0.50 mL of water directly to the "minivial", and capping it tightly. After water had been added to all the samples, they were set aside for back-exchange. All samples were allowed to back-exchange for a period at least three times the duration of the exchange run at a temperature greater than or equal to that of the run.

A sample for determining the radioactivity of the 10^{-4} Ci/mL tritiated water used in an exchange run was prepared by diluting 0.100 mL of this water to 100.0 mL with ordinary water and adding 0.100 mL of this dilution along with 0.40 mL of water to a "minivial". Five milliliters of Bray's solution was added to each sample. In order to ensure that each sample was counted with the same efficiency, pieces of GF/C filters were added to the blank vials and the vial used for water activity determination. After the samples were counted, a blank curve was prepared so that blank values due to tritium exchange with the glass of the vials could be subtracted from the total counts given by GF/C filter sample vials.

Results were calculated from the expression

$$h_{\text{calcd}} = \frac{0.0111C}{1000C_0w} \tag{1}$$

where C is the corrected counts per minute in a GF/C filter sample, C_0 is the counts per minute in the sample for water radioactivity determination, w is the weight of the GF/C filter in grams, 0.0111 represents the grams of hydrogen present in 0.100 mL of water, and h_{calcd} is the apparent number of grams of hydrogen per gram of glass which have exchanged with water. Equation 1 takes no account of isotope effects. After complete exchange each chemically equivalent group of hydrogens in the glass will show an equilibrium isotope effect given by

$$I_i = \frac{(\text{GT})_i(\text{H}_2\text{O})}{(\text{GH})_i(\text{HTO})} \tag{2}$$

where $(\text{GT})_i$ and $(\text{GH})_i$ correspond to concentrations of tritium and hydrogen in the group and (HTO) and (H_2O) correspond to concentrations of tritium and hydrogen in the water. Upon attainment of equilibrium for each equivalent group of hydrogens

$$h_i = h_{\text{calcd},i}/I_i \tag{3}$$

where h_i represents the true number of grams of hydrogen per gram of glass in the group (*2*).

RESULTS AND DISCUSSION

Hydrogen exchange curves at several temperatures are shown in Figure 1. At 1 °C there is an immediate exchange of surface hydrogens. The 1 °C curve also shows a slight slope which is presumably due to exchange of interior hydrogens.

0003-2700/83/0355-0800$01.50/0 © 1983 American Chemical Society

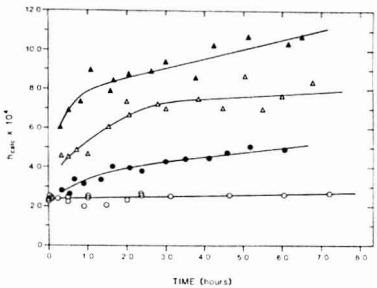


Figure 1. Exchange curves between GF/C filters and tritiated water at various temperatures: 1 °C, open circles; 50 °C, filled circles; 80 °C, open triangles; 100 °C, filled triangles.

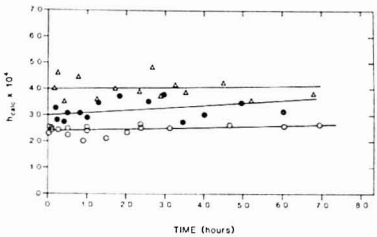


Figure 2. Exchange curves between GF/C filters and tritiated water at 1 °C: no prior treatment, open circles; 1 h prior treatment with water at 100 °C, filled circles; 7 h prior treatment with water at 100 °C, open triangles.

Additional exchange of interior hydrogens is shown at 50 °C, 80 °C, and 100 °C. The scatter in data points at higher temperatures is at least partly due to uncertainties in the relatively large blank corrections. The curves show no indication of leveling off due to complete exchange of all preexisting hydrogens in the glass.

The appearance of the samples run at higher temperatures is interesting. A surprisingly large amount of fluffy lyophilized material was seen in both filter-containing and blank vials. This material is freeze-dried solubilized glass. It immediately dissolved upon readdition of water. Since solubilization is accompanied by hydrolysis (*5*), some part of h_{calcd} at 80 and 100 °C and perhaps also at 50 °C is due to reaction of the glass with water rather than to exchange of preexisting hydrogens in the glass with water.

The production of new hydrogens in the glass due to reaction with water is clearly demonstrated by the data shown in Figure 2 where exchange curves at 1 °C are shown for untreated GF/C filters and filters which were heated with water at 100 °C for 1 h or 7 h and then freeze-dried prior to the start of the exchange run. The rapid exchange values obtained by extrapolating the curves to zero time are 2.4×10^{-4} g of H/g of glass for untreated filters, 3.0×10^{-4} g of H/g of glass for filters pretreated with water for 1 h, and 4.0×10^{-4} g of H/g of glass for 7 h of pretreatment. The higher values for the pretreated filters are due to rapidly exchangeable hydrogens in the solubilized glass and the production of additional rapidly exchangeable hydrogens at the glass surface.

Pretreatment of the GF/C filters at 500 °C for 20 h results in a dramatic decrease in h_{calcd} as shown in Figure 3. The extrapolated value for 1 °C exchange drops from 2.4×10^{-4} g of H/g of glass to 0.27×10^{-4} g of H/g of glass. Far less exchange is also observed at 100 °C. The average value for

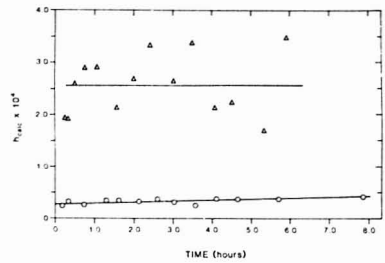


Figure 3. Exchange curves between GF/C filters preheated at 500 °C for 20 h and tritiated water at various temperatures: 1 °C, open circles; 100 °C, open triangles.

the exchange points at 100 °C is 2.55×10^{-4} g of H/g of glass and there is no clear indication of any additional exchange in the period from 20 min to 7 h after the start of exchange (compare with Figure 1). This loss of hydrogens from the glass is due to removal of water by heating (*6*, *7*).

Experiments at 50 and 100 °C in which exchange was carried out in the presence of 10^{-3} M HCl instead of deionized water gave points which fall on the corresponding curves in Figure 1. This shows that the exchange is not acid catalyzed.

Hydrogens in glass are mainly present as silanol (≡Si—OH) groups (*8*). In the glass interior such groups can be either free or hydrogen bonded. It is also possible that molecular water might be present to some extent in the glass interior. Free and hydrogen bonded silanol groups are also present on the glass surface, but water adsorbed on the surface is removed by vacuum drying in the present experiments. It would be expected that surface hydrogens would exchange more rapidly than interior hydrogens and that hydrogen bonding would slow the rate of exchange.

Water can react with glass by hydrolysis of silicon–oxygen bonds or by ion exchange of hydrogen ions for alkali ions in the glass (*5*). Water could also diffuse into the glass interior. All these processes would give rise to the production of additional glass hydrogens during exchange experiments.

Not much work has been done on the use of tracers in the study of glass–water hydrogen exchange. A study of hydrogen exchange between D_2O vapor and silica gels at room temperature and 1200 °C has been reported (*9*). Surface and interior silanol groups could be distinguished. Tritiated water vapor at temperatures from 700 to 1300 °C has been used to determine tritium penetration profiles into silica glass under conditions where rapidly exchanging tritiums are washed out prior to measurement (*10*).

The present study of hydrogen exchange between liquid water and borosilicate glass fibers allows a determination of h_{calcd} for preexisting surface hydrogens, but exchange of preexisting interior hydrogens cannot be distinguished from the production of additional hydrogens due to reaction with water. Some preexisting interior hydrogens may only exchange if they are sufficiently exposed to water by hydrolytic processes (*5*, *11*).

Whatman GF/C glass filters show a relatively large number of preexisting hydrogens. Normally borosilicate glass shows a water content of 0.07% or less (*12*). The surface hydrogens of untreated GF/C filters (2.4×10^{-4} g of H/g of glass) correspond to an apparent water content of 0.22% alone. The large apparent water content of these glass fibers may be due to the manufacturing process. However, some of this apparent water content may be due to equilibrium isotope effect values greater than 1.0. It has been shown that deuterium is preferentially taken up over hydrogen at a glass surface (*1*).

The dramatic reduction of the hydrogen content of GF/C filters by heating at 500 °C shows that heat treatment is a useful way of reducing problems due to the presence of hydrogen in glass. Most of the water lost by heating probably results from two silanol groups which are sufficiently close for hydrogen bonding rather than from isolated silanol groups. Isolated silanol groups cannot be removed by heating silica at 500 °C (*13*). The results in Figure 3 also show that heat treatment may be useful in reducing the reactivity of glass with water.

The freeze-drying method described here would be useful in conjunction with surface area measurements, since the apparent surface density of hydrogens exchangeable with water in various insoluble solid materials could then be obtained.

Registry No. Water, 7732-18-5; hydrogen, 1333-74-0.

LITERATURE CITED

(1) Glasoe, P. K.; Bush, C. N. *Anal. Chem.* **1972**, *44*, 833-834.
(2) Byrne, R. H.; Bryan, W. P. *Anal. Biochem.* **1970**, *33*, 414-428.
(3) "Glass Microfiber Filters"; Bull. No. 400, Whatman, Inc.: Clifton, NJ, 1976.
(4) Bryan, W. P.; Rao, P. B. *Anal. Chim. Acta* **1976**, *84*, 149-155.
(5) Doremus, R. H. "Glass Science"; Wiley: New York, 1973; pp 242-248.
(6) Todd, B. J. *J. Appl. Phys.* **1955**, *26*, 1238-1243.
(7) Todd, B. J. *J. Appl. Phys.* **1956**, *27*, 1209-1210.
(8) Boulos, E. N.; Kreidl, N. J. *J. Can. Ceram. Soc.* **1972**, *41*, 83-90.
(9) Davydov, V. Y.; Kiselev, A. V.; Zhuravlev, L. T. *Trans. Faraday Soc.* **1964**, *60*, 2254-2264.
(10) Burn, I.; Drury, T.; Roberts, J. P. *Silic. Ind.* **1965**, *30*, 403-407.
(11) Lanford, W. A.; et al. *J. Non-Cryst. Solids* **1979**, *33*, 249-266.
(12) Williams, J. P.; et al. *Am. Ceram. Soc. Bull.* **1976**, *55*, 524-527.
(13) Armistead, C. G.; et al. *J. Phys. Chem.* **1969**, *73*, 3947-3953.

RECEIVED for review September 27, 1982. Accepted January 17, 1983.

Thermal Vaporization for One-Drop Sample Introduction into the Inductively Coupled Plasma

Eiichi Kitazume

Central Research Laboratory, Hitachi Ltd., Kokubunji, Tokyo 185, Japan

Inductively coupled plasma (ICP) atomic emission spectrometry has become one of the most useful techniques for determining multielement traces. However, the nebulizer commonly used for sample introduction is inefficient and requires a solution of at least 0.1 mL. More efficient sample introduction systems are required that can provide an analysis using less solution. If only one drop of sample could be effectively introduced into the ICP, absolute detection limits and analytical capability would be greatly improved.

Recently, electrothermal vaporization techniques that use a tantalum filament (*1*) and graphite rod (*2*, *3*) were investigated. However, their evaporation chambers were above 100 mL in volume because of the structure of the large electric current devices used for the thermal vaporization systems. Large chamber dead volumes will lead to temporal peak broadening due to vapor diffusion mechanisms. For improved detection limits, a smaller evaporation chamber volume is better for preventing sample aerosol dilution by the carrier gas. In addition, it is necessary to provide a sufficiently high heating rate to the filament to ensure a rapid rate of removal of analyte from the surface (*2*).

This paper describes the application of a wire filament electrothermal vaporization technique for introducing samples into the ICP. In this technique, a microliter sample solution is vaporized on a filament heated by momentary condenser discharge (*4*) in a small evaporation chamber. Detection limits for six elements were measured and the effects of sodium, potassium, and lithium on analyte emissions were studied.

EXPERIMENTAL SECTION

Apparatus. A block diagram of the overall apparatus is shown in Figure 1. The ICP atomic emission spectrometer system is a Jarrell-Ash Model 975 plasma spectrometer which has 40 fixed-wavelength channels, and an additional variable-wavelength channel. For observation of the signal profile, a 1-m grating monochromator (Nippon Jarrell-Ash, M-1, 1200 grooves/mm) and a storage oscilloscope (Hitachi, Model V-038) were mainly used. The wire filament vaporization apparatus employed is shown in Figure 2. The filament was platinum or tungsten wire, 0.25–0.30 mm in diameter, and was placed in a small quartz evaporation chamber (about 4.5 mL in volume). The regular operating conditions are described in Table I. The filament temperature was measured by an optical pyrometer.

Table I. Operating Conditions

coolant gas flow rate	18 L of Ar/min
plasma gas flow rate	1.0 L of Ar/min
carrier gas flow rate	1.0 L of Ar/min
generator forward power	1.1 kW
generator reflected power	5 W
observation height	16 mm above load coil
desolvation current	3.0–4.0 A
condenser charging voltage	9.75 V for Pt filament 8.00 V for W filament
sample volume	10 μL
integration time	3 s

Procedure. After the plasma was generated and stabilized, the argon flowing through the filament chamber was adjusted to the value established as optimal. The monochromator was set at the desired wavelength for the emission profile that was observed.

A 10-μL sample was deposited at the top of the wire filament with an Eppendorf microliter pipet. The sample was dried slowly by passing a 3–4 A current through the filament and vaporized by pulse heating from a high capacity condenser (0.22 F, 16 V). The condenser had been charged to an appropriate voltage that was determined experimentally, and the filament temperature quickly increased to approximately 1400 °C for the platinum filament and to more than 1500 °C for the tungsten filament.

The vaporized specimen was introduced into the ICP torch through polypropylene tubing and a three-way stopcock. The emission intensities of elements of interest were then integrated in the polychromator system and printed. (The condenser was discharged immediately after integration was started.) At the same time, the emission signal of the element of interest could be observed by the monochromator and storage oscilloscope. After the measurement, the condenser was discharged twice with no sample on the filament to clean the filament.

Standard Solutions. A boron standard solution was prepared by dissolving reagent grade potassium tetrafluoroborate in water, because boron in samples prepared from boric acid was apt to evaporate when the solution was dried on the filament. A phosphorus standard solution was prepared by dissolving reagent grade potassium dihydrogenphosphate in water. Other standard

0003-2700/83/0355-0802$01.50/0 © 1983 American Chemical Society

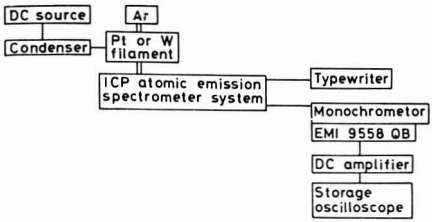


Figure 1. Block diagram of apparatus.

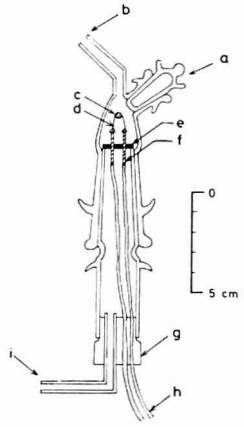


Figure 2. Wire filament vaporization apparatus: (a) sample injection port; (b) sample introduction orifice, connected through polypropylene tubing (20 cm) with the torch; (c) sample; (d) platinum or tungsten filament; (e) acrylic resin; (f) brass screw; (g) silicon rubber stopper; (h) cord to condenser; (i) argon gas inlet.

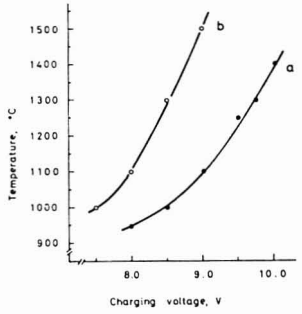


Figure 3. Relationship between charging voltage and filament temperature: (a) platinum filament, 0.30 mm in diameter; (b) tungsten filament, 0.25 mm in diameter.

solutions were prepared from commercially available standard solutions for atomic absorption spectrometry.

RESULTS AND DISCUSSION

Temperature Profile of Filament. Figure 3 shows the relationship between the charging voltage of the condenser and the temperature of the filament. The platinum filament

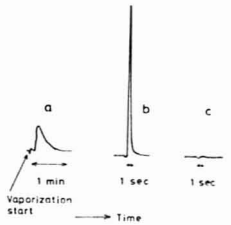


Figure 4. Emission signals of boron 249.68 nm: (a) 1 μg/mL B, in 500-mL chamber; (b) 0.1 μg/mL B, in 4.5-mL chamber; (c) blank signal, in 4.5-mL chamber.

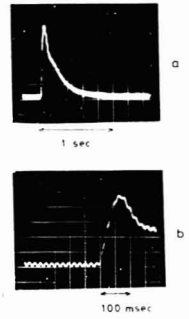


Figure 5. Oscillograms of signal of boron 249.68 nm for solution containing 1 μg/mL B: carrier gas flow rate, 1.0 L/min; time base, (a) 200 ms/division; (b) 50 ms/division.

was quite firm below 1400 °C, and the platinum emission intensity at 269.95 nm was not detected until platinum fusion occurred (above 10.5 V charging voltage). The tungsten filament temperature could be raised above 1500 °C, however, tungsten began to vaporize from 1300 °C. The following experiments were mainly made using a platinum filament. A tungsten filament was used when a rectilinear calibration curve was not obtained with a platinum filament.

Vaporization Chamber Volume. Figure 4 shows boron emission signals measured while using a platinum filament. The signal was obtained through the profile mode of a computer program. Figure 4a was obtained when a 500-mL chamber for a conventional nebulizer was used. With a large volume sample evaporation chamber, the signal appeared slowly, and the peak width was about 1 min. Figure 4b was obtained with a 4.5-mL chamber as shown in Figure 2. Figure 4c shows a blank signal of filament "firing" using a 4.5-mL chamber. The peak intensity increased remarkably, and the peak width was about 1 s. For more exact measurement of the signal profile, a storage oscilloscope connected with the monochromator was used. Figure 5 shows the oscillograms. The signal appeared about 250 ms after the discharge and finished before 1 s had elapsed.

Sample vapor condensation losses on chamber walls were not studied in this paper. Although it is possible that such losses may be more significant with an unusually small chamber where the cold wall is in closer proximity to the hot expanding vapor cloud, further studies are needed to establish whether or not this is a significant problem. If it is a problem, Figure 4 clearly shows that any such condensation disadvantage is at least heavily counterbalanced by elimination of dead volume, peak broadening, vapor diffusion, and gas di-

Table II. Detection Limits

element	line,[a] nm	filament	detection limit, μg/mL	pg	TFV-ICP,[c] pg	graphite rod atomizer-ICP,[d] pg
B	249.68	Pt	0.0004	4	10	
Ge	199.82	Pt	0.006	60		
P	214.91[b]	Pt	0.01	100	2000	200
Pb	220.35	W	0.002	20	300	100
Sn	189.99	W	0.002	20	2000	
Zn	206.20	Pt	0.003	30		20

[a] Wavelengths used for present work. [b] Second-order line. [c] From ref 1. [d] From ref 2.

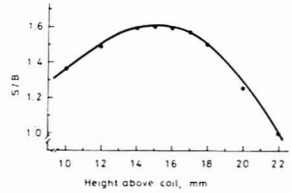


Figure 6. Relationship between observation height and S/B ratio: boron concentration, 0.1 μg/mL; carrier gas flow rate, 0.8 L/min.

lution effects with the present smaller chamber. In fact, the smaller chamber is seen to give a much narrower, more intense signal profile.

Optimization of Observation Height and Carrier Gas Flow Rate. Figure 6 shows the relationship between the observation height above the load coil and the ratio of signal to background. The maximum signal to background was obtained between 15 and 16 mm above the load coil. The following measurement was made at a height of 16 mm. This height was also optimum for a conventional nebulizer introduction system. Figure 7 shows the relationship between the carrier gas flow rate, and the ratio of signal to background. The relationship between the carrier gas flow rate and the emission intensity is also shown. The emission intensity proved to be maximum at a flow rate of 0.4 L/min. However, as the carrier gas flow rate decreased, the background level increased. Consequently, the maximum signal to background ratio was obtained at a flow rate of 1.0 L/min. The measurements that follow were made at a flow rate of 1.0 L/min.

Figure 8 shows the oscillograms observed when the carrier gas flow rate was changed from 0.75 L/min to 0.85 L/min. In these regions, double peaks appeared. Below 0.75 L/min, the second peak was the larger of the two, but above 0.85 L/min, the reverse was true. If the sample changes to two or more different compounds when vaporized from the filament, boron arrival time to the plasma may differ because of the difference in the evaporation rates for these compounds. Presumably, at high carrier gas flow rate, all boron will be removed quickly enough to prevent any secondary compound formation. In all cases, as the emission signal is ordinarily integrated, the integrated signal would not change even if the double peak appeared.

Effect of Coexisting Elements. The effect of alkali metals on the emission intensities of boron, germanium, and phosphorus (each 1 μg/mL) was measured. Generally, signals were suppressed with an increase in alkali metal concentration. When 0.5 mg/mL of potassium or sodium was present in the solution, 10–15% decreases in germanium and 30–50% decreases in boron and phosphorus intensities were observed. The presence of potassium and sodium did not change the maximum emission intensity position in each oscillogram.

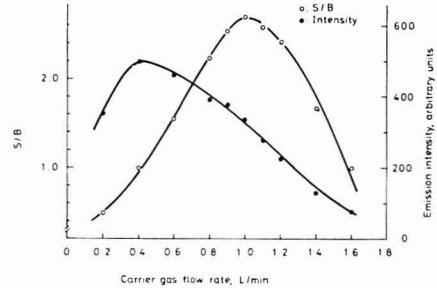


Figure 7. Effect of carrier gas flow rate: boron concentration, 0.1 μg/mL.

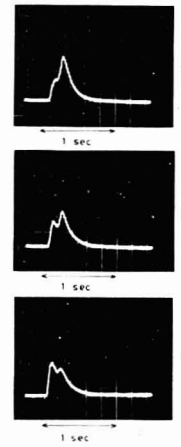


Figure 8. Oscillograms of signal of boron 249.68 nm for solution containing 1 μg/mL B. Carrier gas flow rate was as follows: (a) 0.75 L/min; (b) 0.80 L/min; (c) 0.85 L/min.

However, the presence of 0.5 mg/mL of lithium delayed the attainment of maximum boron emission intensity.

Detection Limits. Table II shows the detection limits for six elements when a 10-μL sample was injected. The detection limit was defined as the concentration required to produce a net emission intensity equivalent to twice the standard deviation of the background noise. Literature values with use of a tantalum filament vaporization system (*1*) and graphite

rod vaporization system (2) are also shown in Table II. A comparison of the absolute detection limits expressed as analyte mass shows that in most cases a superior power of detection was obtained with the present method. The relative standard deviation was 2–4% for boron, lead, phosphorus, and tin, and 5–10% for germanium and zinc with a 1 μg/mL concentration. A rectilinear calibration curve was obtained from 0.001 μg/mL over 4 orders of magnitude for boron, from 0.01 μg/mL over 3 orders of magnitude for phosphorus, lead, tin, and zinc, and from 0.01 μg/mL over 2 orders of magnitude for germanium.

The author acknowledges that the present study is limited to relatively volatile elements. It is not known whether the same advantages of this small chamber system would also occur with less volatile elements. This will be the subject of future investigation in this laboratory.

ACKNOWLEDGMENT

The author is grateful to Atsushi Mizuike, Hiroshi Kawaguchi, Fumio Nagata, and Hisao Kojima for their helpful suggestions.

Registry No. B, 7440-42-8; Ge, 7440-56-4; P, 7723-14-0; Pb, 7439-92-1; Sn, 7440-31-5; Zn, 7440-66-6.

LITERATURE CITED

(1) Nixon, D. E.; Fassel, V. A.; Kniseley, R. N. *Anal. Chem.* **1974**, *46*, 210–213.
(2) Gunn, A. M.; Millard, D. L.; Kirkbright, G. F. *Analyst (London)* **1978**, *103*, 1066–1073.
(3) Millard, D. L.; Shan, H. C.; Kirkbright, G. F. *Analyst (London)* **1980**, *105*, 502–508.
(4) Kawaguchi, H.; Vallee, B. L. *Anal. Chem.* **1975**, *47*, 1029–1034.

RECEIVED for review April 13, 1982. Accepted December 9, 1982.

Breath Analysis by Atmospheric Pressure Ionization Mass Spectrometry

Frank M. Benoit*

Environmental Health Directorate, Health and Welfare Canada, Tunney's Pasture, Ottawa, Ontario K1A 0L2, Canada

W. R. Davidson, A. M. Lovett, Sabatino Nacson, and Angie Ngo

Sciex Inc., 55 Glencameron Road, Thornhill, Ontario L3T 1P2, Canada

The value of human breath analysis in medical, forensic, and environmental applications has long been recognized. Sampling techniques have consisted of the collection of large volumes of breath in Teflon (*1*), Mylar (*2–5*), or Plastigas (*6*) bags, in glass tubes (*4, 5, 7–9*), or in cryogenic traps (*10, 11*) followed by concentration of the volatiles onto Tenax (*1, 11*), charcoal (*3*), silica gel (*6*), or cryogenic (*2*) traps prior to analysis by infrared spectrometry, gas chromatography, or gas chromatography/mass spectrometry. A recent report (*12*) suggested that direct introduction of expired breath into the ion chamber of API/MS system would allow the extraction of the organics directly from the gaseous mixture by ion–molecule ionization. However, direct breath introduction into the ion source caused difficulties due to interferences from ammonia (*12*). In the present study a novel breath inlet system which allows the direct sampling of exhaled human breath for analysis by API/MS is described.

EXPERIMENTAL SECTION

Breath Inlet. The breath inlet shown in schematic form in Figure 1 consisted of a mouthpiece, filter tube, manifold, and mixing chamber mounted on a metal frame. The disposable polyethylene mouthpiece (Inspiron, Rancho Cucamonga, CA) was separated from the glass filter tube (22 mm o.d. × 270 mm, Sovirel, France) by a diaphragm one way valve (Inspiron, Rancho Cucamonga, CA). The filter tube could be filled with filter material contained between two loose fitting glass wool plugs, if required. The filter tube was fitted with a port (Swagelok fittings) though which carrier gas could be directed, if required, to simulate an exhalation for calibration purposes. The filter tube assembly was attached to the stainless steel manifold via a tee connection of which one arm, fitted with an adjustable valve, led to the atmosphere and the second arm, containing a replaceable glass capillary, led to a stainless steel manifold. The manifold was connected to a mixing chamber containing perforated macor disks to ensure mixing of the breath sample with the carrier gas prior to introduction into the ion chamber. The manifold and filter tube assembly were fitted with outlets for the pressure transducers such that the pressure differential across the capillary was measured by two manometers connected in parallel. One manometer (Magnehelic, range 0–2 in. of water, Dwyer Instruments, Michigan City, IN) provided a visual reading to the subject who was required to maintain a prescribed constant pressure differential across the capillary during exhalation. The second manometer (Robinson Halpern, range 0–10 in. of water, Plymouth Meeting, PA) controlled the scan of the TAGA ion analyzer and provided a reading of the pressure differential during each scan period. The carrier gas, zero grade air (Matheson) was passed through a filter (molecular sieves Linde 13X and Linde 4A) to remove impurities in the air prior to introduction into the manifold. The carrier gas flow was controlled by a Lee Jet orifice such that the flow could be set by adjusting the regulator pressure.

RESULTS AND DISCUSSION

Atmospheric Pressure Ionization. In the positive mode of operation a series of protonated water clusters $H^+(H_2O)_n$ are generated from the moisture in the ambient air following a series of ion–molecule reactions (*13*) initiated by the ionization of molecular nitrogen in a point to plane corona discharge. Ionization of a sample molecule (T) produces protonated molecule–water clusters of varying size depending on n (reaction 1).

$$T + H^+(H_2O)_n \rightarrow TH^+(H_2O)_n \quad (1)$$

$$TH^+(H_2O)_n + N_2 \rightarrow TH^+ + (n)H_2O + N_2 \quad (2)$$

Upon passage of a clustered target ion through a gas (N_2) curtain located between the ion chamber and the mass analyzer (*14*) collisions with the neutral nitrogen molecules activate the ion sufficiently to strip the loosely held water molecules from the ion and a protonated molecule, (eq 2) is transmitted to the analyzer. One consequence of the "declustering" is that the distribution of ions collected at the detector does not necessarily correspond to the original distribution of ions generated in the ion source at the moment of ionization.

In the negative mode of operation the reagent ion O_2^- is generated by point to plane corona discharge ionization of oxygen in ambient air. Some of the observed reactions with

0003-2700/83/0355-0805$01.50/0 © 1983 American Chemical Society

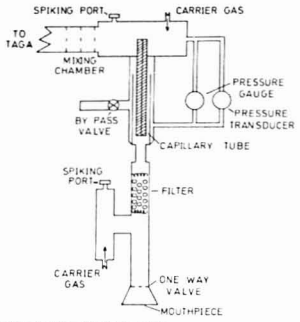


Figure 1. Schematic of breath inlet.

the sample molecule are charge transfer (reaction 3) and proton abstraction (reaction 4) depending upon the relative electron and proton affinities, respectively, of the sample molecule and the reagent ion.

$$T + O_2^- \rightarrow T^- + O_2 \quad (3)$$

$$T + O_2^- \rightarrow (T\text{-}H)^- + HO_2 \quad (4)$$

One problem associated with the API ion source is ion signal saturation at relatively low (low parts per million) sample molecule concentrations. In the positive mode the usual total abundance of protonated water clusters is ca 10^6 counts/s. However, reagent ion clusters are not all equally reactive. As the size of the cluster increases, the proton affinity of the cluster increases and the reactivity of the protonated cluster by proton transfer decreases. Hence only a portion of the reagent ions may be reactive toward a particular sample molecule and the maximum concentration of sample molecule ions that may be generated is limited by the concentration of reagent ions clusters that have a proton affinity lower than the proton affinity of the sample molecule. A complicating factor is that a water cluster has a higher proton affinity than the water molecule alone and the initial sample ion formed is a water clustered sample ion (reaction 1); therefore the prediction of the reactivity of a sample molecule based on the proton affinities of the simple water and sample molecules may not be valid. However, the proton affinities of water clustered molecules are unavailable at present; hence the use of the proton affinities of the simple molecules represents the best compromise. In addition, when analyzing mixtures, the ion signal may be partitioned among the various components which in effect further reduces the concentration of reagent ions available for a particular reaction. Consequently the number of sample molecules entering the ion source may exceed the number of reagent ions available for reaction, in which case the target ion signal is no longer proportional to the target molecule concentration in the ion source. A plot of ion abundance vs. molecule concentration shows onset of curvature at the low parts per million (20 ppm) level (Figure 2) which is generally the upper concentration limit for quantitative work. It is essential therefore in quantitative work to establish the concentration range for linear response for the particular reaction under study. Fortunately for samples of high concentrations it is always possible to dilute the sample to lower concentrations that fall within the linear response range.

A second problem associated with the API ion source is interference from extraneous compounds in a multicomponent gas mixture, in which individual ionization reactions will be dependent upon the proton affinities of the sample molecules

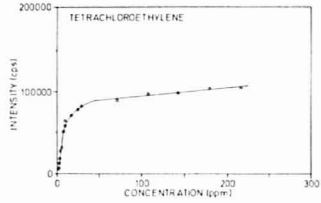


Figure 2. Ion abundance vs. concentration (ppm range).

relative to that of the reagent ion. During the residence time in the ion chamber the ionized species undergo numerous collisons with the neutral molecules from the air matrix. However, should there be present in the gaseous mixture species of higher proton affinity, a collision could be reactive and proton transfer between sample molecules (reaction 5)

$$T_1H^+ + T_2 \rightarrow T_2H^+ + T_1 \quad (5)$$

deplete the ion signal for T_1H^+. In the limit, at "higher" T_2 concentrations, T_1H^+ may "disappear". Problems of interferences are generally eliminated by dilution of the sample although the limit of detection of components of lower concentration is raised when dilution of the sample is required.

Breath Inlet System. The direct introduction of exhaled human breath into the ion chamber of the API/MS produced both the saturation and interference effects; although not the major component of breath, ammonia was present in sufficiently high concentrations in breath and had a higher proton affinity than the other breath components which resulted in a saturated signal at m/z 18, NH_4^+ (*12*). In order to overcome these problems a novel inlet was designed with the aim of diluting and filtering (if desired) the sample of breath prior to introduction into the ion source. The breath inlet, which is described in the Experimental Section, achieved controlled dilution of the breath sample by bleeding a portion of the breath sample through a capillary of known bore and length into a stream of carrier gas (N_2) of known flow prior to mixing and introduction into the ion source. The excess breath was dumped to the atmosphere via a variable valve. The volume of breath transmitted through the capillary was determined by the pressure differential across the capillary which was measured with a manometer in view of the subject.

With a capillary of 0.50 mm i.d. and of 5 cm length, an exhalation pressure of ca. 0.2 in. of water and a carrier gas flow of 90 cm^3/s, a dilution factor of ca. 1000 was obtained. Under these conditions the difficulties with saturation and interferences were eliminated.

Performance of Breath Inlet System. To enhance the sensitivity of the API/MS the electron multiplier was operated in the ion counting mode in which the analyzer, under computer control, remained "open" at a mass window until either a selected number of ions (set by operator within narrow limits) had been detected or a preset time limit (from $^1/_{15}$ s to 1 s) had expired. Even with the fastest scan speed ($^1/_{15}$ s per amu) a complete scan over 200 amu could not be obtained during one exhalation. In fact two to three exhalations were usually required. To obtain meaningful results, it was therefore necessary to suspend the scan between exhalations. This was achieved by initiating and maintaining the scan only when the inlet pressure exceeded a selected preset value (usually 0.2 in. of water). The spectra presented were then obtained by subtraction of background carrier gas spectra from the exhaled breath spectra.

In previously reported (*1*, *10*) profiles of human breath, acetone was observed as the most abundant organic species. In Figure 3 a full scan (positive mode) of a breath sample using

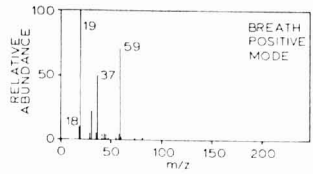


Figure 3. Full scan (positive mode) of human breath.

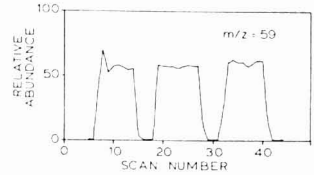


Figure 4. Acetone (MH^+, m/z 59) as a function of exhalations.

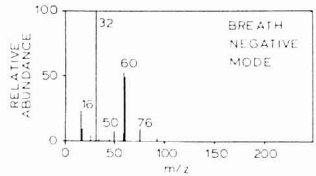


Figure 5. Full scan (negative mode) of human breath.

the breath inlet system exhibited a prominent peak at m/z 59 corresponding to the protonated acetone molecule. The peaks at m/z 19 and m/z 37 corresponded to protonated water clusters $H^+(H_2O)$ and $H^+(H_2O)_2$, respectively. The peak at m/z 18 due to NH_4^+ which dominated the spectrum of nondiluted breath despite its low concentration is no longer the most prominent peak when the breath sample is diluted via the breath inlet system prior to introduction into the ion source; thus the dilution technique successfully eliminated the interferences from ammonia and, despite the dilution factor of ca. 1000, the system retains sufficient sensitivity to detect volatile organic vapors on breath. Other minor peaks observed include m/z 33 and m/z 47, corresponding to protonated methanol and ethanol, respectively.

In Figure 4 $(M + H)^+$ of acetone, m/z 59 is shown as a function of time over several exhalations with the instrument operating in the selected ion mode. The observed response of the system to an exhalation is rapid as shown by the sharp onset when the exhalation is swept into the ion source. Further, at the end of an exhalation there is a sharp decrease in the ion signal to background levels. There is no evidence of contamination from one exhalation to another at least for the compound under study.

In the negative ion mode the breath spectrum (Figure 5) contained large peaks at m/z 16, m/z 59, m/z 60, and m/z 61 in addition to the reagent ion peak at m/z 32. The negative ion spectrum of expired breath differed markedly from the positive ion spectrum. Compounds of high proton affinities (ionized in positive mode) generally do not have high electron affinities (ionized in negative mode) and vice versa. The largest peak, other than the reagent ion peak, corresponded to CO_3^- m/z 60 which resulted from reaction of O_2^- with CO_2 in expired breath. The peak at m/z 61 corresponding to HCO_3^- likely originated from the interaction of CO_3^- and moisture in the breath. Endogenous organics contributed to a few minor peaks at m/z 26 (CN^-) and m/z 93 ($C_6H_5O^-$).

Registry No. Acetone, 67-64-1; methanol, 67-56-1; ethanol, 64-17-5; tetrachloroethylene, 127-18-4.

LITERATURE CITED

(1) Krotoszynski, B.; Gabriel, G.; O'Neill, H. *J. Chromatogr. Sci.* **1977**, *15*, 239.
(2) Levey, S.; Balchum, O. J.; Medrano, V.; Jung, R. *J. Lab. Clin. Med.* **1964**, *63*, 574.
(3) Jansson, B. O.; Larsson, B. T. *J. Lab. Clin. Med.* **1969**, *74*, 961.
(4) Stewart, R. D. In "Essays in Toxicology"; Hayes, W., Ed.; Academic Press: New York, 1974; Vol. 5, Chapter 5.
(5) Stewart, R. D.; Hake, C. L.; Wu, A. *Scand. J. Work, Environ. Health* **1976**, *2*, 57.
(6) Gage, J. C.; Lagesson, V.; Tunek, A. *Ann. Occup. Hyg.* **1977**, *20*, 127.
(7) Stewart, R. D.; Hake, C. L.; Peterson, J. E. *Arch. Environ. Health* **1974**, *6*, 29.
(8) Pasquini, D. A. *Am. Ind. Hyg. Assoc. J.* **1978**, *39*, 55.
(9) Verberk, M. M.; Scheffers, T. M. L. *Environ. Res.* **1980**, *21*, 432.
(10) Conkle, J. P.; Camp, B. J.; Welch, B. E. *Arch. Environ. Health* **1975**, *30*, 290.
(11) Gearhart, H. L.; Pierce, S. K.; Payne-Bose, D. *J. Chromatogr. Sci.* **1977**, *15*, 480.
(12) Lovett, A. M.; Reid, N. M.; Buckley, J. A.; French, J. B.; Cameron, D. M. *Biomed. Mass Spectrom.* **1979**, *6*, 91.
(13) Good, A.; Durden, D. I.; Kebarle, P. *J. Chem. Phys.* **1970**, *52*, 212.
(14) French, J. B.; Reid, N. M.; Poon, C. C. Twenty-Fifth Annual Conference on Mass Spectrometry and Allied Topics, Washington, DC, 1977.
(15) Carroll, D. I.; Dzidic, I.; Stillwell, R. N.; Horning, M. G.; Horning, E. C. *Anal. Chem.* **1974**, *46*, 706.

RECEIVED for review October 8, 1982. Accepted December 20, 1982. This work was carried out by Sciex, Inc., under contract with Health and Welfare Canada.

Modification of a Centrifugal Filtration Device for Direct Filtration into an Autosampler Vial

I. A. Elseman and L. A. Pachla*

Warner-Lambert/Parke-Davis Pharmaceutical Research Division, Warner-Lambert Company, Ann Arbor, Michigan 48105

Samples for high-performance liquid chromatography are frequently derived directly from biological materials, pharmaceutical preparations, or TLC spots. Often the analytical sample requires filtration to remove suspended matter. Presently there is commercially available a centrifugal microfilter which is capable of filtering microliter volumes with greater than 95% recovery (Bioanalytical Systems, MF-1 centrifugal mirofilter). This filtration device has been successfully applied to the analysis of phenolics (*1*). This device is an excellent tool when samples are manually injected into

0003-2700/83/0355-0807$01.50/0 © 1983 American Chemical Society

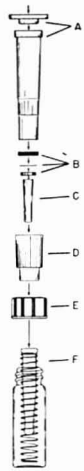


Figure 1. Modified centrifugal filtration apparatus for direct filtration into an autosampler vial: (A) receiving tube and cap; (B) O-ring, filter membrane, and filter support disk; (C) glass microfunnel; (D) filter support compartment; (E) autosampler vial cap; (F) microvial insert assembly.

the chromatographic system. However, an extra sample transfer step is required when samples are injected with an autosampler. This extra transfer step (from receiver tube to autosampler microvial) results in loss of sample and increased processing time.

An approach to minimizing this loss in sample volume is to filter the sample directly into the autosampler microvial (Waters Associates, No. 73030). Figure 1 illustrates the necessary modifications required to allow direct filtration from a centrifugal microfilter into an autosampler microvial. The filter support compartment is first press-fitted into the cap of a sample vial (Waters Associates). The microfunnel which is fitted into the filtration device (Bioanalytical Systems Inc., Model MF-1) is a borosilicate ground glass joint (Lab Glass Co. No. LG0015-inner member) that has been cut and ground to fit into the filter support compartment. The device is then assembled as illustrated in Figure 1.

Samples are placed in the sample compartment and the sample is centrifuged at high speed. After replacement of the filter assembly with an autosampler cap, the sample can be directly injected into the HPLC. The modified filtration device is easily disassembled for cleaning.

We have used the above modified centrifugal filter for several months and found it to be helpful in methods development and bioavailability studies where final filtration of the sample is required. The modified centrifugal filter was designed to be used with one type of autosampler vial (Waters Associates No. 73030). The modified filter assembly can be adapted to other types of vials by using a 13 mm × 8.0 mm i.d. Nalgene tube (Scientific Products, No. R5365-90) to connect the filter support compartment directly to the autosampler vial.

LITERATURE CITED

(1) Rosten, D. A.; Kissinger, P. T. *Anal. Chem.* **1981**, *53*, 1695-1699.

RECEIVED for review October 12, 1982. Accepted December 17, 1982.

Purification of Nitric Acid at Trace Metal Levels

Richard P. Maas*[1] and Steven A. Dressing

Department of Environmental Sciences and Engineering, School of Public Health, University of North Carolina, Chapel Hill, North Carolina 27514

Concentrated nitric acid has been used increasingly in recent years in the field of trace metal analysis for digestion or preservation of both organic and inorganic environmental samples. The presence of significant levels of trace metals in both commercial reagent grade and expensive ultrapurity nitric acid creates problems such as large reagent blanks in digested samples. This paper describes a rapid, inexpensive method for purifying commercial reagent grade nitric acid.

Several investigators have reported methods for purifying nitric acid and other acids, but unfortunately all of these have proved to be very time-consuming or expensive. Coppola and Hughes (*1*) first used a polyethylene subboiling still for preparing pure hydrofluoric acid. Mattinson (*2*) refined the procedure by constructing an apparatus which consisted of two Teflon bottles threaded to a Teflon block. The apparatus is kept nearly airtight, and heat is applied to the feed bottle. The collecting bottle is immersed in cold water and acid gradually condenses in the collection bottle. High-purity nitric, hydrochloric, and hydrofluoric acids were obtained from reagent grade acids, although the maximum rate with room-temperature cooling water is about 100 mL/day.

The highest purity acids have been obtained by Kuehner et al. (*3*). They used a pure quartz subboiling still with a Teflon collector bottle. The distillation was performed in a clean air chamber with commercial reagent grade acids.

Table I. Metal Concentrations in 70% Nitric Acid in Parts per Billion (10^{-9} g of Metal/g of Acid)

method	Zn	Cd	Cr	Pb
boiling glass still (this paper)	0.70	0.01	0.10	0.20
starting material (reagent ACS grade nitric acid)	10.0	1.60	106.7	7.2
two-bottle subboiling Teflon still (*2*)				0.049
subboiling quartz still in clean air chamber (*3*)	0.04	0.01	0.05	0.01

DESCRIPTION AND OPERATION

The still consisted of a 500-mL triple-necked Pyrex distilling flask which was connected to a glass condenser (Figure 1). The condenser was connected to a linear polyethylene collection bottle

[1] To whom correspondence should be addressed at: Department of Biological and Agricultural Engineering, National Water Quality Evaluation Project, 1300 St. Mary's St., Raleigh, NC 27605.

0003-2700/83/0355-0808$01.50/0 © 1983 American Chemical Society

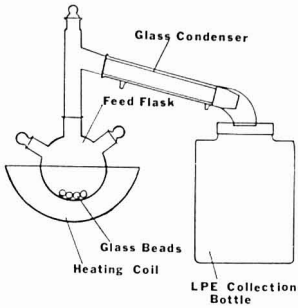


Figure 1. Diagram of boiling glass distillation apparatus.

by polyethylene tubing which was inserted through a hole in the top of the collection bottle. The connection was left unsealed to prevent pressure buildup in the apparatus. Following distillation the collection bottle was sealed and used for storage of the distilled acid. Reagent grade nitric acid (metal content shown in Table I) was added to the distilling flask, and a heating coil was used to boil the acid. A slow, steady boiling rate was attained by using several small glass beads and by carefully adjusting the current to the heating coil.

Prior to use the apparatus was thoroughly cleaned and soaked in concentrated nitric acid. The still was given a final cleaning by operating the apparatus continuously for 1 week. Metal concentrations of the distilled acid were monitored daily during this time and, although initially quite high, reached a constant low level after 5 days.

RESULTS AND DISCUSSION

The metal concentrations reached a constant level after about 1500 mL of nitric acid had been distilled through the apparatus. The distilled nitric acid and the reagent grade nitric acid used as starting material were analyzed for zinc, cadmium, chromium, and lead by heated graphite furnace AAS. The results show that highly pure acid can be prepared by this simple and rapid method (Table I). Silicate was determined in the distilled and reagent grade acid to be 3.98 and 4.12 mg/L, respectively, indicating that glass matrix materials such as silicate are not significantly removed during distillation.

The still can produce up to 800 mL/day although we found that a slower boiling which produced about 500 mL/day gave acid of slightly higher purity. Also it should be noted that the metal concentrations reported here are from the collection bottle. Use of polyethylene or Teflon collecting bottles might be preferable to the linear polyethylene (LPE) collecting bottle used here since the production of LPE uses catalysts containing metals. Since the collecting bottle was not airtight, the laboratory air may also be a source of at least some of the metals remaining in the distilled acid, especially lead, in which case a clean air chamber such as that used by Kuehner et al. might further improve results.

Registry No. Nitric acid, 7697-37-2.

LITERATURE CITED

(1) Coppola, P. P.; Hughes, R. C. *Anal. Chem.* **1952**, *24*, 768.
(2) Mattinson, J. M. *Anal. Chem.* **1972**, *44*, 1715-1716.
(3) Kuehner, E. C.; Alvarez, R.; Paulsen, P. J.; Murphy, T. J. *Anal. Chem.* **1972**, *44*, 2050.

RECEIVED for review May 12, 1980. Resubmitted and accepted January 14, 1983.

Room-Temperature Gas Chromatography/Mass Spectrometry of Volatile Solids and of Volatiles Trapped in Solids

John R. Sutter,* James W. Wheeler, Arnold S. Collier, William M. Jackson, and Thomas Rush

Department of Chemistry, Howard University, Washington, D.C. 20059

Recently we required a knowledge of the compounds in coal that were volatile at room temperature. This requires an analysis that does not involve extraction of the sample or other technique that would enhance the yield, such as heating the sample. The following should be applicable to any analysis of this sort.

The electrodes of self-sealing Parr oxygen bomb (Parr 1108 oxygen combustion bomb) were removed and a one-piece sample of fresh coal weighing 25-50 g was introduced with two 20-g brass weights. The bomb was sealed, flushed with helium (or nitrogen), and finally pressurized to slightly less than 1 atm gauge. The bomb and contents were then shaken vigorously by hand in order to pulverize the sample, the brass weights acting as pestles, thus releasing whatever volatiles were trapped in the coal. At the end of the experiment, the bomb was opened and the coal sieved. It was found that most of the coal would pass through a 120 mesh sieve (A.S.T.M. E-11 specification), ensuring maximum yield of volatiles. With a short length of rubber tubing fitted with a hypodermic needle, the entire volatile contents of the bomb in the helium stream were led through the septum of a Finnigan 3200 GC/MS onto the room-temperature GC column, the vacuum diverter being held open. By use of a 1.6-m column packed with 10% SP-1000 or A-71 Polypak I and a heating rate of 10 °C/min from 40 to 200 °C, several GC peaks were observed. Through the use of comparison spectra (*1*), the mass spectral assignments were made. Two of the compounds found were butane and pentane.

In order to show that this technique is applicable to any mixture of solids containing volatile components, synthetic mixtures of compounds of various room-temperature vapor pressures were analyzed in the above fashion. Naphthalene and anthracene were chosen to represent a reasonable range of vapor pressures. These solids were placed in the bomb in approximately equal amounts and analyzed as above. The results were as expected, we found what we put in. The only limitation seems to be whether a compound has sufficient vapor pressure so that enough sample will be generated in the 340-mL bomb volume.

If one uses the Parr bomb, although this is not required, the bomb can be heated to moderately high temperatures, thus extending the method.

This method, then, offers a way of simplifying the analysis of complex solid mixtures by analyzing the volatiles first and

0003-2700/83/0355-0809$01.50/0 © 1983 American Chemical Society

separate from the nonvolatiles.

ACKNOWLEDGMENT

Coal sample supplied by Pennsylvania State University Coal Data Base Sample No. PSOC-371.

Registry No. butane, 106-97-8; pentane, 109-66-0.

LITERATURE CITED

(1) Stenhagen, E., Abrahamsson, S., McLafferty, F. W., Eds. "Registry of Mass Spectral Data"; Wiley: New York, 1974; Vol. 1.

RECEIVED for review June 10, 1982. Resubmitted August 5, 1982. Accepted January 5, 1983. Supported in part by D.O.E Contract DEF 79ET 6003.

Removal of Oxygen from Solvents for Liquid Chromatography with Electrochemical Detection

Fred Senftleber,* Daniel Bowling, and M. Sonia Stahr

Department of Chemistry, Murray State University, Murray, Kentucky 42071

In the development and application of electrochemical detection for use in liquid chromatographic procedures, the oxidative mode of detection has dominated the literature to date (*1–4*). High background current from the reduction of oxygen impurities in the mobile phase has been a major deterrent to the use of reductive detection (*4, 5*). To decrease the magnitude of this background current, investigators have commonly employed one of three approaches. The most popular technique is to remove dissolved oxygen from the eluent solvent with an inert gas purge (*6–9*). Although moderately effective, this technique is beset with several problems. Time requirements can be excessive. Lund et al. (*10*), for example, suggest bubbling argon through the mobile phase for at least 4 h before introducing the eluent into the chromatograph. Voluminous inert gas consumption and loss of eluent through evaporation can be additional problems. When mixed solvents or salt solutions are employed, solvent evaporation can lead to significant change in the mobile phase composition. Other investigators (*11, 12*) have suggested continuously refluxing the mobile phase as a means to remove dissolved oxygen. In our laboratory, we have not found this technique to be entirely successful. Significant background currents were generally still observed. Recently, Hanekamp et al. (*5*) introduced a two-electrode on-line "scrubber" to electrochemically remove oxygen and other reducible impurities from the eluent solvent. This system appears to be very efficient but requires a stable high current potentiostat for operation. Ironically, to minimize current levels, the authors suggest that a nitrogen purge be used to "preclean" oxygen from the solvent. In choosing a mobile phase for use in this system, care must be exercised to ensure that products from the oxidation and reduction processes in the scrubber do not react chemically with sample molecules subsequently injected into the eluent stream.

In this paper an apparatus is described which overcomes the disadvantages associated with other mobile phase deoxygenating techniques. By use of a series of alternating evacuation–refill cycles, the system minimizes the consumption of inert gas, the evaporation of solvent, and the formation of bubbles in the detector due to outgassing. A typical deaeration procedure using the present system requires less than 15 min.

EXPERIMENTAL SECTION

System Description. A schematic representation of the apparatus is given in Figure 1. The main body of the system (A), constructed from borosilicate glass, consists of two halves joined via 25 mm i.d. O-ring joints (e) to provide a greaseless vacuum-tight seal (Ace Glass, O-ring Seal ǂ Joints, Catalog No. 7648, work equally as well). The bottom section of the apparatus is a 500-mL Erlenmeyer-shaped flask (f) equipped with a Teflon-coated magnetic bar (i). The top half of the system contains vacuum and inert gas inlet ports (a) and (b), respectively, and a Teflon needle valve (d) through which mobile phase can be removed. The oblique bore, three-way stopcock (c) prevents opening of the system to the vacuum and inert gas ports simultaneously. Connection between the apparatus and a liquid chromatograph is made with $^1/_8$ in. stainless steel tubing (not shown). A $^1/_4 \times ^1/_8$ in. stainless steel reducing union (Swagelok Fitting 400-6-2) employing a Teflon ferrule on the $^1/_4$ in. side provides an airtight connection between the stainless steel tubing and the glass outlet of the needle valve.

Section (B) of the system serves as a safety bubbler. Through the incorporation of a liquid-seal check valve (n), air and bubbler oil cannot be inadvertently drawn into the system. For correct operation, the oil level in the bubbler must be above the seat on the valve.

System Operation. The apparatus is first assembled as discussed above and purged with an inert gas. No eluent is present in flask (f) during this procedure. By opening needle valve (d) and correctly positioning stopcock (c), one can permit inert gas to flow through the system displacing the air in the stainless steel tubing connecting the apparatus to the liquid chromatograph. In our laboratory where a Waters Associates (Melford MA) Model M6000A chromatographic pump is used, the inert gas is also permitted to purge the input manifold and solvent takeoff valve on the pump. After closing stopcock (c), needle valve (d), and the solvent takeoff valve, flask (f) is removed and the system is ready for operation.

Approximately 300 mL of filtered mobile phase is placed in the flask (f) and the flask is reconnected to the apparatus. With the magnetic bar stirring, stopcock (c) is positioned to evacuate the system. The magnitude of the vacuum and its duration are described in the Results and Discussion section. After the appropriate time, stopcock (c) is turned to permit inert gas to enter the flask. The system is then cycled alternately between vacuum and inert gas until the desired oxygen level is attained.

To start the solvent into the liquid chromatograph, temporarily cover outlet (l) on the safety bubbler and open needle valve (d) on the apparatus. When the solvent takeoff valve on the liquid chromatograph is opened, a positive inert gas pressure forces the mobile phase to the chromatograph's input manifold. Uncover safety bubbler outlet (l) and adjust the inert gas flow to a rate sufficient to keep a blanket over the solvent.

Instrumentation. Electrochemical experiments were performed with an IBM Model EC/225 voltammetric analyzer equipped with a Bausch & Lomb Series 100 Omnigraphic X-Y recorder.

Materials. Argon and nitrogen employed in the experiments contained less than 5 ppm and 10 ppm oxygen, respectively. Aqueous solutions were prepared with doubly distilled water. All chemicals were reagent grade and used without further purification.

RESULTS AND DISCUSSION

The effectiveness of the present system to remove dissolved oxygen from an eluent solvent was demonstrated through two

0003-2700/83/0355-0810$01.50/0 © 1983 American Chemical Society

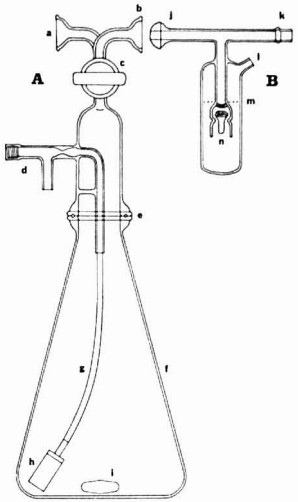


Figure 1. (A) Solvent deaeration apparatus: (a) size 18/9 ground-glass ball joint (connection to vacuum source); (b) size 18/9 ground-glass socket joint (connection to bubbler); (c) three-way 3 mm ground-glass stopcock; (d) Teflon needle valve, 0–3 mm; (e) O-ring joint, 25 mm; (f) 500-mL flask; (g) Teflon tubing, $^1/_8$ in. o.d.; (h) stainless steel filter, 2 μm porosity; (i) Teflon-coated magnetic stirring bar. (B) Safety bubbler: (j) size 18/9 ground-glass ball joint (connection to deaeration apparatus); (k) inert gas inlet tube; (l) bubbler outlet tube; (m) oil level; (n) ground-glass liquid-seal check valve.

sets of experiments. In the first series, the oxygen in a pH 7.8, 0.10 M sodium phosphate solution was monitored as a function of the evacuation time in the deaeration cycle. Each experiment involved placing a 75-mL aliquot of phosphate solution into the apparatus, evacuating to 45 torr pressure with a water aspirator for a set period of time, and backfilling the apparatus with argon. A portion of the solution was then transferred through the needle valve on the apparatus to a three-electrode electrochemical cell using a positive argon pressure developed by temporarily covering the outlet tube (l, Figure 1) on the safety bubbler. To minimize the possible introduction of oxygen from other sources, we excluded a chromatographic column and pump from the evaluation system. Oxygen levels in the solvent were measured at a mercury drop electrode using linear sweep voltammetry. The voltammetric technique allowed us to discriminate between oxygen and other possible reducible impurities in the test solutions.

Results from a typical series of experiments are shown in Figure 2. As illustrated by the reduction in peak current, both the oxygen level in the phosphate solution and the rate of oxygen removal were a function of the evacuation time. After the apparatus was evacuated for 1 min, the oxygen level decreased to about 15.7% (curve b) of its original value (curve a). Increasing the time to 2.0 and 4.0 min resulted in a reduction of the level to 9.5% (curve c) and 2.9% (curve d), respectively. Although higher percentages of oxygen were removed by using the longer evacuation times, the greatest reduction in oxygen concentration per unit time was achieved during the first minute.

A second series of experiments involved repeatedly cycling a single 300-mL aliquot of phosphate solution through the evacuation–refill sequence. Each evacuation period was 1.0

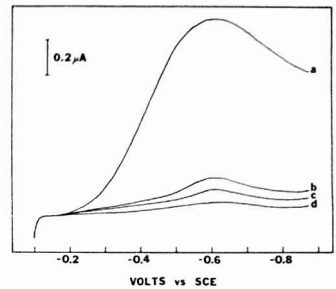


Figure 2. System evaluation: linear sweep voltammogram of pH 7.8, 0.10 M phosphate solution; scan rate, 200 mV/s; (a) before deaeration; (b) after 1.0 min of evacuation, O_2 concentration = 15.7% of curve (a); (c) after 2.0 min of evacuation, O_2 concentration = 9.5% of curve (a); (d) after 4.0 min of evacuation, O_2 concentration = 2.9% of curve (a).

min in length and nitrogen was used as the inert refill gas. After the system was cycled once, the oxygen level in the phosphate solution was found to be 20.5% of the original concentration. This somewhat higher concentration, as compared with the 15.7% observed in the first series of experiments (Figure 2, curve b), can probably be attributed to the larger volume of solvent used in this experiment. The use of nitrogen instead of argon as the refill gas should have had little, if any, influence on the efficiency of the system. Cycling the system a second time reduced the oxygen concentration in the solution to 4.3% of its original level. The third cycle decreased the level to 1.6% and the fourth cycle to 0.3%. The removal of dissolved oxygen by repeatedly cycling the system was a cumulative process. Each cycle reduced the oxygen concentration to an average 24% of the level existing before that cycle. After five consecutive 1-min evacuation–refill cycles, the current measured in the voltammogram was indistinguishable from background.

The ability of the present system to deoxygenate the eluent solvent can be examined in terms of Henry's law. According to this law, the solubility of oxygen in the mobile phase is directly proportional to the partial pressure of oxygen above the solvent. Through the use of the evacuation–inert gas refill cycle, the present apparatus reduces the oxygen pressure above the mobile phase, and thus the oxygen solubility, to a fraction of that existing before the cycle. The most effective use of the system, as illustrated by our experiments, is achieved through repetitive cycling of the apparatus rather than by employing a single lengthy evacuation period. Four 1-min cycles, for example, reduced the oxygen level in the phosphate solution to 0.3% of its original concentration as compared with a reduction to 2.9% using one 4-min evacuation. If one assumes an initial dissolved oxygen concentration of 2.5×10^{-4} mol L^{-1} (*13*) and a reduction to 24% in each cycle, four 1-min cycles would reduce the oxygen level in the solution to less than 1×10^{-6} M. With additional cycles, assuming a leak-free system and the use of an inert gas containing less than 0.1 ppm O_2, it should be possible to reduce the oxygen concentration in the solvent to the nanomolar level, a level well below the detection limit of the voltammetric technique utilized in the present study.

The apparatus described in the present paper has been successfully employed in deaerating mobile phases which have been utilized in the liquid chromatographic separation and reductive electrochemical detection of derivatized polyamines (*14*). The system is efficient, relatively inexpensive, and minimizes the solvent evaporation and inert gas consumption

difficulties experienced with previous techniques described in the literature. In addition, the rapid deaerating capabilities of the present apparatus allows for the rapid change of solvents during method developments.

Registry No. Oxygen, 7782-44-7.

LITERATURE CITED

(1) Heineman, William R.; Kissinger, Peter T. *Anal. Chem.* **1978**, *50*, 166R-175R.
(2) Heineman, William R.; Kissinger, Peter T. *Anal. Chem.* **1980**, *52*, 138R-151R.
(3) Majors, Ronald E.; Barth, Howard G.; Lochmüller, Charles H. *Anal. Chem.* **1982**, *54*, 323R-363R.
(4) Ryan, Michael D.; Wilson, George S. *Anal. Chem.* **1982**, *54*, 20R-27R.
(5) Hanekamp, H. B.; Voogt, W. H.; Bos, P.; Frei, R. W. *Anal. Chim. Acta* **1980**, *118*, 81-86.
(6) MacCrehan, W. A.; Durst, R. A. *Anal. Chem.* **1978**, *50*, 2108-2112.
(7) Eggli, R.; Asper, R. *Anal. Chim. Acta* **1978**, *101*, 253-259.
(8) Hanekamp, H. R.; Voogt, W. H.; Bos, P.; Frei, R. W. *Anal. Lett.* **1979**, *12*, 175-189.
(9) Funk, Max. O.; Keller, Maggie B.; Levison, Bruce *Anal. Chem.* **1980**, *52*, 771-773.
(10) Lund, Walter; Hannisdal, Merete; Greibrokk, Tyge *J. Chromatogr.* **1979**, *173*, 249-261.
(11) Brunt, K.; Bruins, C. H. P. *J. Chromatogr.* **1978**, *161*, 310-314.
(12) Michel, L.; Zatza, A. *Anal. Chim. Acta* **1979**, *105*, 109-117.
(13) Lange, Norbet Adolph, Ed., "Handbook of Chemistry", 9th ed.; Handbook Publishers: Sandusky, OH, 1956; p 1091.
(14) Senftleber, Fred; Bowling, Daniel; Stahr, Sonia 33rd Annual Pittsburgh Conference, March 8, 1982, Atlantic City, NJ, paper 077.

RECEIVED for review August 3, 1982. Accepted December 10, 1982. This work was funded by the Committee for Institutional Studies and Research, Murray State University, under Grant Numbers 454 and 212724.

Determination of Lead in Plant Ash by X-ray Fluorescence Spectrometry

Mark L. Dietz and Stanford L. Tackett*

Department of Chemistry, Indiana University of Pennsylvania, Indiana, Pennsylvania 15705

The use of X-ray fluorescence spectrometry for the analysis of plant tissue is well established. First introduced in 1958 by Brandt and Lazar (*1*) for the determination of manganese, cobalt, zinc, and molybdenum, the technique has since been expanded to permit the determination of a number of major and trace elements in plant material. At the same time, a variety of sampling methods have been introduced, thereby permitting the material to be analyzed in any one of several forms. Typically, plant tissue is analyzed as a compressed disk or pellet of the dried material (*2-5*). Alternately, a sample may be analyzed in the form of a loosely packed dry powder (*6*), as an aqueous solution (*7*), or as an ash, after deposition upon a filter paper disk (*8*). All of these methods, however, suffer from shortcomings which make them not entirely satisfactory. For example, not all types of samples may be compressed into self-supporting disks or pellets. In such cases, binders such as cellulose must be added to increase the rigidity of the sample disk. This, however, often precludes further use of the sample (*9*). Loose packing of dry samples, while simple and rapid, is generally not precise enough for quantitative work (*3*). Aqueous solution methods can involve tedious sample preparation steps, such as digestion of samples in nitric acid (*7*). Lastly, analysis of ash after deposition on a paper disk offers an accuracy of only ±15% for many elements (*8*).

In conjunction with our studies of the uptake of heavy metals by plants, we have sought a simple technique for use with plant tissue specimens not readily converted to self-supporting disks or pellets, a technique more precise and accurate than loose-packed dry sample or deposited ash methods, but without the tedious sample preparation associated with aqueous solution methods. The present paper describes such a technique. Specifically, it describes a new sample holder and illustrates its use in the determination of lead in spinach leaves.

EXPERIMENTAL SECTION

Apparatus. The sample holder consisted of an XRF polyethylene sample cup (Chemplex Industries, Inc.) modified by the authors by fitting it with a core of cast acrylic monomer into which a depression (1.50 cm, diameter and 0.46 cm. maximum depth) had been bored with a radius generator. Samples were held in this depression by a thin Mylar film cover secured with a polyethylene ring. The holder is shown in Figure 1.

Analyses were performed with a Picker solid-state X-ray fluorescence spectrometer comprised of a Model 6238 X-ray geenrator, a Model 6239 spectrodiffractometer, and a Model 6245 radiation analyzer. A tungsten target X-ray tube operated at 50 kV and 30 mA was used in conjunction with a LiF diffracting crystal and a scintillation detector. Instrument settings were those recommended as optimum by the manufacturer (*10*).

Dry ashing of plant material took place in a Hoskins FD 204 C electric furnace.

Reagents. Deionized water was used in the preparation of all solutions. The stock solutions of lead were prepared by dilution of a 1000 μg/mL lead reference solution (Fisher Scientific Co.). The ashing aid was prepared by addition of concentrated sulfuric acid (Ultrex, J. T. Baker Chemical Co.) to an equal volume of deionized water.

Procedure. Oven-dried spinach leaf samples were prepared for analysis by dry ashing overnight at 430 °C (*11*). A 2-mL aliquot of the ashing aid was added to each sample prior to ashing to ensure complete recovery of lead (*12*) and to reduce the amount of unoxidized carbon remaining. Once prepared, a 0.3000-g portion of each sample ash was weighed into the sample holder and the intensity of its Pb Lα1 emission measured by accumulating counts for a period of 120 s at 33.92° 2θ. During measurement, samples were rotated at a rate of 30 rpm. Each sample was counted three times, and the emission intensities were averaged. Background radiation was measured by counting at two values of 2θ, one on either side of the Pb Lα1 peak. The background count for the sample was then determined from these values by interpolation. This background was subtracted from the average peak count rate to obtain the net count rate for the sample. The lead content of each was then determined from a calibration curve obtained by evaluation of a series of ash standards. These standards were prepared by addition of various aliquots of a 100 μg/mL lead stock solution to weighed portions of commercially obtained spinach. The method used for the ashing and for the evaluation of the standards was identical with that described for the samples.

RESULTS AND DISCUSSION

For evaluation of the accuracy of the lead determinations performed by using the new sample holder, the lead contents of a series of spinach samples which had been spiked with various aliquots of a 500 μg/mL lead stock solution were determined. The aliquot added was, in each case, chosen so that the lead content of the ash would be less than 1.00% by weight, as above this the calibration curve is nonlinear. The results of these determinations are presented in Table I. It can be readily seen from these results that there is good agreement between the amounts of added lead and those determined experimentally over the entire range of concentrations examined.

0003-2700/83/0355-0812$01.50/0 © 1983 American Chemical Society

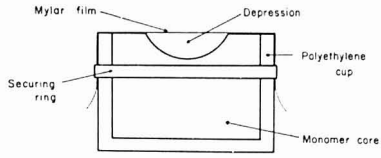


Figure 1. Cross section of the sample holder.

Table I. Comparison of Added and Experimentally Determined Lead Levels in Spinach Leaves

% added lead	% determined lead	% difference
0.797	0.838	+5.14
0.413	0.436	+5.57
0.201	0.194	−3.48
0.100	0.101	+1.00
0.0494	0.0477	−3.44
0.0101	0.00956	−5.35
0.00600	0.00602	+0.33

The precision of the sampling method was evaluated by repeated analysis of a series of standards. Ten replicate determinations using a sample containing 9.89×10^{-4}% lead by weight produced an average fluorescent emission intensity of 1319 counts/s with a standard deviation of 10.2 counts/s. This corresponds to a relative standard deviation of 0.776%. Similar determinations with standards containing 2.18×10^{-3}% and 2.50×10^{-2}% lead by weight yielded relative standard deviations of 0.726% and 1.18%, respectively.

It is important to note that the precision of the sampling method is very dependent upon the sample size. For optimum precision, it is essential that the amount of ash taken just fills the depression in the sample holder. Lesser amounts are free to tumble about within the holder, resulting in some loss of reproducibility. Larger amounts, on the other hand, produce some creasing and bulging of the Mylar cover, again resulting in a loss of reproducibility.

CONCLUSIONS

The proposed sampling method offers several definite advantages over the other methods available, among them excellent precision and accuracy, as well as minimal operator involvement in sample preparation. It would seem then, that this method offers the best available alternative in cases where it is not possible to prepare a self-supporting disk or pellet from dried plant tissue.

Registry No. Pb, 7439-92-1.

LITERATURE CITED

(1) Brandt, C. Stafford; Lazar, Victor A. *J. Agric. Food. Chem.* **1968**, *6*, 306-309.
(2) Handley, Raymond. *Anal. Chem.* **1960**, *32*, 1719-1720.
(3) Ball, D. F.; Perkins, D. F. *Nature (London)* **1962**, *194*, 1163-1165.
(4) Fieldes, M.; Furkert, R. J. *N. Z. J. Sci.* **1971**, *14*, 280-291.
(5) Reuter, F. W. *Anal. Chem.* **1975**, *47*, 1763-1766.
(6) Whittig, L. D.; Buchanan, J. R.; Brown, A. L. *J. Agric. Food Chem.* **1960**, *8*, 419-421.
(7) Champion, K. P.; Whittem, R. N. *Analyst (London)* **1967**, *92*, 112-114.
(8) Florkowski, T.; Kuc, T.; Piorek, S. *Int. J. Appl. Radiat. Isot.* **1977**, *28*, 679-686.
(9) Evans, C. C. *Analyst (London)* **1970**, *95*, 919-929.
(10) "Radiation Analyzer Manual"; Picker Instruments: Cleveland, OH, 1968; p 59.
(11) Webber, M. D. *Can. J. Soil Sci.* **1972**, *52*, 282-284.
(12) Feinberg, Max; Ducauze, Christian *Anal. Chem.* **1980**, *52*, 207-209.

RECEIVED for review August 30, 1982. Accepted November 22, 1982.

Mass Spectrometer Polymer Membrane Sample Introduction Device

George J. Kallos and Nels H. Mahle*

Analytical Laboratories, Dow Chemical U.S.A., Midland, Michigan 48640

In recent years attention has been given to the evaluation and use of semipermeable membranes for the determination of contaminants in air and drinking water (*1-3*). Hollow fiber probes, constructed of different permeable materials, were designed and evaluated as mass spectrometric sampling devices by Westover and co-workers (*4*). These hollow fiber devices have been applied to the routine monitoring of trace levels of toxic contaminants in aqueous solution and in air (*5, 6*). Eustache and Histi have described a membrane device which is coupled to a mass spectrometer through a vacuum leak assembly (*7*).

The development of a new membrane device for use with a mass spectrometer was prompted by the general unavailability of hollow fibers which constitute an obstacle to the application of these devices. The new membrane sampling device described in this paper is simple and easy to construct from readily available components.

EXPERIMENTAL SECTION

Construction of Metal Probe. The metal probe was constructed from a 1 in. × $^1/_4$ in. fine mesh stainless steel screen tube that was silver soldered to a 4 in. × $^1/_4$ in. stainless steel tube as shown in Figure 1. A $^1/_8$ in. × $^1/_4$ in. diameter solid stainless steel disk was soldered (soft silver solder) on the other end of the screened tubing to serve as a plug. The screen was obtained from Newark Wire Cloth Co., Newark, NJ (0.003 in. diameter steel wire with 100 × 100 meshes per linear in.). All metal pieces were thoroughly rinsed with water, methanol, methylene chloride, and acetone before silver soldering and also before polymer coating.

Chemicals. Experimental block copolymers of poly(α-methylstyrene–dimethylsiloxane) [X4-2541 (75% PDMS), X9-6317 (60% PDMS), and X4-2517 (40% PDMS)] were obtained from Dow Corning Corp., Midland, MI, and have been previously described (*8-10*).

Membrane Coating of the Probe. The polymer to be coated on the probe screen was dissolved in a solvent, preferably toluene or xylene for siloxane polymers, at concentration levels of 10-15 wt %. The precleaned metal probe was dipped into the solution for 1 min, removed and then immediately rotated 180° so that the solution drained through the opening of the $^1/_4$ in. tube. Any solution left inside the screen portion of the probe would leave an uneven coating of the polymer after evaporation of the solvent. The probe was allowed to dry overnight. A Varian-MAT CH4B mass spectrometer was used for evaluating the membrane probe.

RESULTS AND DISCUSSION

Only polymers which are highly permeable, selective, and possess a high degree of chemical and physical stability can be used for mass spectrometer probes. High permeability minimizes area and pressure requirements for direct sampling with a mass spectrometer. Although many polymers were coated for evaluation, the poly(dimethylsiloxanes) and in particular the organo–siloxane block copolymers were found

0003-2700/83/0355-0813$01.50/0 © 1983 American Chemical Society

Table I. Comparison of Siloxane Membrane Probe to Hollow Fiber Probe Responses (50 ppm (v/v))

	peak height, mm		ion source pressure,[a] torr
	acrylonitrile m/z 53	methylene chloride m/z 84	
(1) membrane probe prepared from 10% polymer solution	22	105	0.6×10^{-6}
(2) membrane probe prepared from 15% polymer solution	14	77	0.45×10^{-6}
(3) siloxane hollow fiber probe	6	60	0.55×10^{-6}

[a] Background pressure for water blanks was 0.4×10^{-6} torr for all three cases.

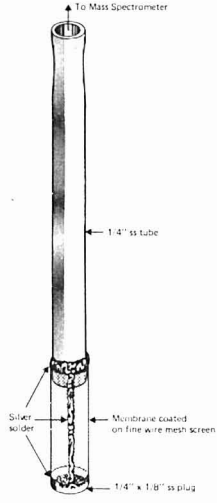


Figure 1. Diagram of membrane probe.

to be more widely applicable for a variety of organic components.

To demonstrate the usefulness of the membrane probe device as compared to the siloxane hollow fiber probe made from the same block copolymer, we prepared two membrane probes of siloxane block copolymer (X4-2517, 40% poly(dimethylsiloxane), 60% α-methylsytrene) using two solutions of 10% and 15% copolymer in toluene. Fifty part-per-million (v/v) standards of acrylonitrile and the common industrial solvent, methylene chloride, were made up in water. As shown in Table I equal or better response was obtained with the membrane probe at comparable source pressures. The effective membrane probe surface area was calculated to be 1.14 cm^2 which was very close to the 1.06 cm^2 for the 15-element siloxane hollow fiber probe. Organo–siloxane block copolymers with higher siloxane content, such as X4-2541 (75% poly(dimethylsiloxane), 25% α-methylstyrene) provided good permeability for many compounds but lower enrichment factors. The enrichment factor of chloroform in aqueous solution with this membrane probe was determined to be 0.6×10^4 as compared to 1.1×10^4 reported by Westover et al. (*4*) with the use of the siloxane hollow fiber probe. Other polymer membrane probes, including poly(vinyl alcohol), poly(cyanoacrylate), and poly(styrene–α-methylstyrene) were found to be much less permeable than the organo–siloxane block copolymer. This new membrane probe possesses the following advantages over other sampling devices: (1) It is easy to construct. (2) There is no need for gasket seals or adhesives which could lead to vacuum leaks or memory effects. (3) A large number of polymers can be tested for applications of tailor-made separations for mass spectrometer or other instrument probes. (4) The membrane probe can be heated through the metal by heat conduction to study permeability of polymers at higher temperatures. (5) It is easy to evaluate permeation properties of polymers that cannot be fabricated as hollow fibers.

Registry No. Water, 7732-18-5.

LITERATURE CITED

(1) Klein, E.; Eichelberger, J.; Eyer, C.; Smith, J. *Water Res.* **1975**, *9*, 807.
(2) Reiszner, K. D.; West, P. W. *Environ. Sci. Technol.* **1973**, *7*, 526.
(3) Hardy, J. K.; Dasgupta, P. K.; Reiszner, K. D.; West, P. W. *Environ. Sci. Technol.* **1979**, *13*, 1090.
(4) Westover, L. B.; Tou, J. C.; Mark, J. H. *Anal. Chem.* **1974**, *46*, 568.
(5) Tou, J. C.; Kallos, G. J. *Anal. Chem.* **1974**, *46*, 1866.
(6) Tou, J. C.; Kallos, G. J. *Am. Ind. Hyg. Assoc. J.* **1974**, *33*, 419.
(7) Eustache, H.; Histi, G. J. *Membr. Sci.* **1981**, *8*, 105.
(8) Saam, J. C.; Ward, A. H.; Fearon, F. W. G. "Advances in Chemistry Series"; American Chemical Society: Washington, DC 1973; Adv. Chem. Ser. No. 129, p 239.
(9) Monroe, C. M.; Ward, A. H.; Abstracts, Rubber Division of the American Chemical Society, Toronto, Canada, May 7, 1974, No. 15.
(10) Ward, A. H.; Kendrick, T. C.; Saam, J. C. "Advances in Chemistry Series", No. 142, American Chemical Society: Washington, DC, 1975; Adv. Chem. Ser. No. 142, p 300.

RECEIVED for review July 21, 1982. Accepted December 14, 1982.

Determination of Carbon Isotope Ratios in Plant Starch via Selective Enzymatic Hydrolysis

Arndt Schimmelmann* and Michael J. DeNiro[1]

Department of Earth and Space Sciences, University of California, Los Angeles, California 90024

Previous determinations of the stable carbon isotopic composition of biopolymers involved isolation and purification of the intact polymers from complex organic mixtures, followed by their combustion and isotopic analysis of the resulting carbon dioxide (e.g., ref 1–3). We present here a method based on the selective enzymatic hydrolysis of a biopolymer. The resulting monomer is collected after passage through a dialysis membrane which serves to separate it from other components present in the original biological material. The monomer is then combusted prior to isotopic analysis.

[1] Also Program in Archaeology.

0003-2700/83/0355-0814$01.50/0 © 1983 American Chemical Society

Table I. δ ^{13}C Values and Yields for Starch Prepared by the Chemical Purification Method and for Glucose Obtained from Starch by the Enzymatic Method[a]

	enzymatic method		chemical purification	
sample	δ ^{13}C, ‰	yield,[b] %	δ ^{13}C, ‰	yield,[b] %
potato starch	−25.8 ± 0.1 (n = 4)	98 (n = 1)	−26.0 ± 0.1 (n = 2)	79 (n = 1)
corn starch	−10.0 ± 0.1 (n = 4)	96 ± 2 (n = 5)	−10.1 ± 0.4 (n = 4)	62 ± 7 (n = 4)
bean powder	−23.9 ± 0.3 (n = 4)	n.a.[c]	−24.1 ± 0.0 (n = 3)	n.a.[c]

[a] The number of replicates is indicated by n. [b] Expressed as percentage of amount of starch present initially. [c] Not applicable.

Although we chose to develop the method to determine the carbon isotope ratios of starch, this approach should find general applicability to biopolymers that can be degraded quantitatively to monomers and/or oligomers by using specific hydrolytic enzymes.

EXPERIMENTAL SECTION

Corn starch, potato starch, and amyloglucosidase (exo-1,4-α-glucosidase, E.C. 3.2.1.3) from *Aspergillus niger* (*4*) were obtained from Sigma Chemical Co. Dried beans (*Phaseolus vulgaris*) were purchased from a grocer. Dialysis tubing Spectrapor No. 6, with a 2000 molecular weight cutoff, was obtained from Spectrum Medical Industries, Inc.

Starch was isolated from powdered beans and from the commerical starch samples by a standard chemical purification method (*5*). One of the last steps in this procedure involves removal of iodine from a precipitated starch–iodine complex with alcoholic NaOH solution which has a pH of 12. At this pH, the wet precipitated starch may trap atmospheric carbon dioxide. To avoid contaminating the starch carbon with inorganic carbon in the form of carbonates, we used either freshly precipitated starch or starch that had been dialyzed one day against running distilled water for the isotopic measurements on chemically purified starch.

In the enzymatic method, starch in the beans and the commerical starch samples were hydrolyzed with amyloglucosidase and the resulting glucose separated from the other components present in the starting mixture by passage through a dialysis membrane, according to the following procedure. First, the commercial starches were dissolved in quantities of 100 mg in 10 mL of distilled water by boiling the mixture for 10 min. The solutions were transferred quantitatively into dialysis bags. Next, 200-mg aliquots of finely pulverized bean were heated with 10 mL of distilled water to 100 °C for 10 min; after being cooled, the supernatant solutions were transferred into dialysis bags. A few drops of toluene (approximately 0.1 mL) were added to all solutions undergoing dialysis to prevent microbial degradation. The starch solutions were dialyzed one day against running distilled water at room temperature to remove all water-soluble components with molecular weights below 2000. Next, 1 mL of amyloglucosidase solution (approximately 100 units of enzyme) that had been predialyzed for 1 day against running distilled water was added to the dialysis bags containing the starch solutions and toluene. The dialysis bags were then incubated at 40 °C for 2 days in flasks containing 40 mL of distilled water. The completeness of the enzymatic hydrolysis of starch at the end of 2 days was verified by the absence of an iodine–starch reaction (*5*) on small samples from the inside of the bags. The presence of glucose in the 40-mL solution was verified by the positive reaction with Fehling's solution (*6*).

Freeze–dried starch and glucose samples were combusted by a modified version of the Stump and Frazer (*7*) method and the $^{13}C/^{12}C$ ratios of the resulting carbon dioxide measured as described in ref 8. The results are expressed in the usual $\delta^{13}C$ notation, where

$$\delta^{13}C = \left[\frac{(^{13}C/^{12}C)_{sample}}{(^{13}C/^{12}C)_{std}} - 1 \right] \times 1000‰$$

The standard is the Peedee belemnite carbonate (PDB).

Chemically purified starch contains some sodium chloride from the alcoholic NaCl washing solution. Thus the yield for the chemical purification of starch was calculated from the amount of CO_2 formed during the combustion of an aliquot of the starch/NaCl mixture. The yield for the enzymatic method was calculated from the glucose content of an aliquot of the solution against which the starch and enzyme mixture had been dialyzed. The glucose content of this solution was determined gravimetrically.

RESULTS AND DISCUSSION

The results of the yield and isotope ratio measurements are given in Table I. The $\delta^{13}C$ values for both the chemically purified commercial potato and corn starches and the glucose produced enzymatically from them are in good agreement with each other. Comparisons of yield determinations on both starches show that the enzymatic approach has the advantage of an almost complete conversion of the starch to glucose, whereas the chemical purification causes 21% and 38% losses of starch for the commercial potato and corn starches, respectively. These losses probably occur during the numerous washings and centrifugations using alcoholic–aqueous solutions in which starch has a noticeable solubility. The results for the whole bean powder show the same good agreement between the $\delta^{13}C$ values of the chemically purified starch and the enzymatically obtained glucose.

Some enzymatically produced oligomers with molecular weights less than 2000 may have passed through the dialysis membrane and escaped complete conversion to glucose. This possibility does not affect the results or interpretations presented here.

CONCLUSIONS

The enzymatic method described here is especially useful for the preparation of purified glucose from small amounts of starch in a complex organic mixture because the method has a quantitative yield.

The enzymatic approach should be generally applicable to biopolymers for which a hydrolytic enzyme converts the polymer quantitatively to monomers or oligomers small enough to permeate through dialysis tubing or filtration membranes. Quantitative conversion of polymer to monomer and/or oligomer is required to avoid introduction of artifacts relating to isotope effects during enzymatic reactions (*9*). Hydrolases such as chitinases, proteases, and cellulases are capable of hydrolysis of their respective substrates to monomers or oligomers (*10–12*) and thus appear to be good candidates for use in the enzymatic method described here. The enzymatic approach could be adapted for use in the study of isotopic differences among biopolymers of the same kind but with different molecular weights by using a series of dialysis tubings with increasing molecular weight exclusion limits.

Finally, we note that many enzymes require special pH ranges to develop their maximum activity. For example, the enzyme used in this study shows maximum activity in the pH range of 4–6. A carbon-free buffer system with pH 6 (saturated solution of molybdic acid adjusted with dilute sodium molybdate solution) was developed and did not inhibit the enzymatic activity. While amyloglucosidase showed sufficient activity without the buffer system to hydrolyze starch quantitatively, other enzymes might require buffered conditions.

In such cases, carbon-free buffer systems such as the one described here should be employed to avoid the added step of having to separate the monomer and/or oligomer from a carbon-containing buffering component prior to combustion and isotopic analysis.

ACKNOWLEDGMENT

We thank Leo Sternberg for his valuable advice and criticism. Dave Winter performed the stable isotope ratio determinations.

Registry No. Carbon-12, 7440-44-0; carbon-13, 14762-74-4; starch, 9005-25-8; E.C. 3.2.1.3, 9032-08-0; hydrolase, 9027-41-2.

LITERATURE CITED

(1) DeNiro, M. J.; Epstein, S. *Geochim. Cosmochim. Acta* **1978**, *42*, 495–506.
(2) Hsu, J. D.; Smith, B. N. *Plant Cell Physiol.* **1972**, *13*, 689–694.
(3) Deleens, E.; Garnier-Dardart, J. *Planta* **1977**, *135*, 241–248.
(4) Marshall, J. J.; Whelan, W. J. *FEBS Lett.* **1970**, *9*, 85–88.
(5) Purcher, G. W.; Leavenworth, C. S.; Vickery, H. B. *Anal. Chem.* **1948**, *9*, 850–853.
(6) Stanek, J.; Cherný, M.; Kocourek, J.; Pacák, J. "The Monosaccharides"; Academic Press: New York, 1963; p 868.
(7) Stump, R. K.; Frazer, J. W. *Nucl. Sci. Abstr.* **1973**, *28*, 746.
(8) Northfelt, D. W.; DeNiro, M. J.; Epstein, S. *Geochim. Cosmochim. Acta* **1981**, *45*, 1895–1898.
(9) O'Leary, M. H. In "Isopote Effects on Enzyme-Catalyzed Reactions"; Cleland, W. W., O'Leary, M. H., Northrop, D. B., Eds.; University Park Press: Baltimore, MD, 1976; pp 233–251.
(10) Stirling, J. L.; Cook, G. A.; Pope, A. M. S. In "Fungal Walls and Hyphal Growth"; Burnett, J. H., Trinci, A. P., Eds.; Cambridge: London, 1979; pp 169–188.
(11) Cowling, E. B.; Kirk, T. K. *Biotechnol. Bioeng. Symp.* **1976**, *6*, 95–123.
(12) Fruton, J. S. In "The Proteases and Biological Control"; Reich, E., Rifkin, D. B., Shaw, E., Eds., Cold Spring Harbor Laboratory: Cold Spring Harbor, NY, 1975; pp 33–50.

RECEIVED for review October 4, 1982. Accepted November 22, 1982. The research was funded by a grant from the Academic Senate Committee on Research at UCLA and NSF Grant ATM 79-24591.

CORRECTIONS

Determination of Diffusion Coefficients by Flow Injection Analysis

Greg Gerhardt and Ralph N. Adams (*Anal. Chem.* 1982, *54*, 2618–2620).

There is an unfortunate error in eq 1, appearing on page 2618. The terms a^2f were omitted from this equation of Vanderslice and the definition of a is also missing. The correct equation should read

$$\Delta t_B = \frac{35.4a^2f}{D^{0.36}}\left(\frac{L}{q}\right)^{0.64} \quad (1)$$

and the sentence following should read: L is the distance between the injection port and the detector in centimeters, q is the flow rate in milliliters per minute, D is the diffusion coefficient, a is the radius of the flow path tubing in centimeters, f is a concentration and detector sensitivity factor, and Δt_B is the peak width in seconds.

Circuit for Constant Current Operation of an Electron Capture Detector

W. B. Knighton and E. P. Grimsrud (*Anal. Chem.* 1982, *54*, 1892–1893).

There is an error in Figure 1 appearing on page 1893. The 2.7 kΩ resistor at the bottom of Figure 1A was inadvertently shown as being connected between pin 3 of the CD 4011B IC (the output of the first NAND gate) and ground. This resistor should be placed on the other side of the 470-pF capacitor so that it is connected to pins 5 and 6 of the IC (the inputs of the second NAND gate) and ground. The resulting configuration is then consistent with the pulse width control shown in Figure 2.

AUTHOR INDEX

Adams, F. C., 671
Adams, R. N., 816
Alfassi, Z. B., 796
Andreae, M. O., 608
Aoki, K., 604
Attari, S. A., 659

Bacon, J. R., 653
Balfanz, E., 599
Barnard, W. R., 608
Bauer, D., 662
Benoit, F. M., 805
Biemann, K., 758
Blakley, C. R., 750
Blotcky, A. J., 677
Bond, A. M., 718
Boudeville, P. E. A., 612
Bowling, D., 810
Bramston-Cook, R., 626
Bromba, M. U. A., 648
Brown, R. S., 723
Brumleve, T. R., 698
Bruner, F., 793
Bryan, W. P., 800
Bursey, M. M., 744
Buydens, L., 738
Byers, W. A., 615, 620

Capizzi, T. P., 638
Collier, A. S., 809
Connors, T. F., 776
Cooks, R. G., 762
Crescentini, G., 793
Crow, F. W., 677

Davidson, W. R., 805
Demas, J. N., 653
DeNiro, M. J., 814
Deutsch, E., 708
De Waele, J. K., 671
Dietz, M. L., 812
Dorsey, J. G., 730
Dressing, S. A., 808
Dumoulin, C. L., 782

Eiseman, I. A., 807

Fassett, J. D., 765
Foley, J. P., 730
Fourré, P., 662
Freiser, B. S., 620
Freiser, H., 656
Funcke, W., 599

Geerlings, P., 738
Gerhardt, G., 816
Gillette, P. C., 630
Grimsrud, E. P., 713, 816

Hahn, D. A., 787
Haraguchi, K., 656
Harrah, L. A., 798
Hass, J. R., 744
Heineman, W. R., 708
Hites, R. A., 594
Holland, R. A., 787

Ishii, K., 604

Jackson, W. M., 809
Janini, G. M., 659
Jensen, T. E., 594
Jones, F. E., 793

Kallos, G. J., 813
Karwacki, E. J., 790
Kitazume, E., 802
Knighton, W. B., 713, 816
Koenig, J. L., 630
König, J., 599
Kormos, D. W., 633
Kosinski, M. A., 688

Lafleur, A. L., 758
Lando, J. B., 630
Lavi, N., 796
Lea, R. E., 626
Leary, J. A., 758
Lemerle, J., 662
Levy, G. C., 782
Lewis, J. Y., 708
Liber, H. L., 758
Liddil, J. D., 771
Lindberg, W., 643
Lovett, A. M., 805
Lovrić, M., 704
Lytle, F. E., 765

Maas, R. P., 808
Macklin, J. W., 684
Mahle, N. H., 813
Mangani, F., 793
Massart, D. L., 738
Mehta, H., 638
Miller, A. G., 684
Moore, L. J., 765
Munson, B., 754
Murthy, R. S. S., 682

Nacson, S., 805
Ngo, A., 805

O'Dea, J. J., 704
Opelanio, L. R., 677
Oppenheimer, L., 638
Osteryoung, J., 698, 704
Osteryoung, R. A., 698

Pachla, L. A., 807
Perone, S. P., 615, 620
Persson, J.-Å., 643
Petty, R., 793
Polley, C. W., Jr., 754

Rack, E. P., 677
Renschler, C. L., 798
Romanowski, T., 599
Rush, T., 809
Rusling, J. F., 776
Ryan, D. E., 682

Saari, L. A., 667
Schimmelmann, A., 814
Seitz, W. R., 667
Senftleber, F., 810
Siemer, D. D., 692
Singleton, K. E., 762
Sotak, C. H., 782
Sovocool, G. W., 744
Sportsman, J. R., 771
Stahr, M. S., 810
Sutter, J. R., 809

Tackett, S. L., 812
Taylor, L. T., 723
Travis, J. C., 765
Travnikoff, B., 795
Tschida, J., 626

Uchida, H., 688

Van Espen, P., 671
Vansant, E. F., 671
Vestal, M. L., 750
Voyksner, R. D., 744

Wallace, G. G., 718
Waugh, J. S., 633
Weppelman, R. M., 638
Wheeler, J. W., 809
Wilson, G. S., 771
Winefordner, J. D., 688
Winograd, N., 790
Wirth, M. J., 787
Wold, S., 643
Wood, K. V., 762

Ziegler, H., 648
Zodda, J. P., 708

Future Articles

Solid-Phase Reagent Strips for Detection of Therapeutic Drugs in Serum by Substrate-Labeled Fluorescent Immunoassay
Bert Walter, Alfred C. Greenquist, and Willis E. Howard, III

Modeling of Experimental Data with Interactive Graphics
David J. Balaban, Julia L. Wang, and Jack W. Frazer

Determination of Free Silica and Manganese in Airborne Particles by Flameless Atomic Absorption Spectrometry
H. G. Chen and T. H. Risby

Efficiency Enhancement in Micellar Liquid Chromatography
John G. Dorsey, Maria T. DeEchegaray, and John S. Landy

Polychromator System for Multielement Determination by Gas Chromatography with Helium Plasma Atomic Emission Spectrometric Detection
Michael E. Eckhoff and Joseph A. Caruso

Acid-Vapor Decomposition for Determination of Zinc in Brain Tissue by Isotope Dilution Mass Spectrometry
M. A. Kiltenick, C. J. Frederickson, and W. I. Manton

Sartorius accuracy in 0.1 second flat!



Sartorius Series 1400 Toploading Balances

High-technology electronics, faster weighing, new built-in keyboard capabilities, unique "Autocheck" ...starting at $1,150.

Great things come in these small packages: Sartorius Series 1400 toploaders, bringing you the latest technology...very large-scale integration in low-profile electronic weighing systems. Now new microprocessors, MP-7 and soon-to-come-MP-8, control weighing functions previously done by many integrated circuit components.

While size has decreased, speed and reliability have improved. Electronic weighing has never been faster (with an update time as little as 0.1 second in the MP-8) or had fewer components. And decreasing the size has decreased the cost of owning a 1400 MP-7/MP-8...perfect for all your weighing needs even in less than perfect conditions.

The new 1400 Series toploaders simplify many weighing operations—counting, conversions, and animal weighing. These optional program capabilities are all accessed through a new, convenient, built-in keyboard—another exclusive from Sartorius.

Convenience, in this case, means confidence. A unique "Autocheck" feature reviews and verifies the functioning of all electronic circuits *automatically*. Convenience and confidence in a compact, affordable weighing system from the company that brought you the first microprocessor-controlled balance—Sartorius.

For more information or a demonstration, call or write: Brinkmann Instruments Co., Division of Sybron Corporation, Cantiague Road, Westbury, NY 11590. Tel: 800-645-3050; in New York: 516-334-7500.



Sartorius electronic weighing systems

Brinkmann

SYBRON

Circle 28 For information. Circle 29 For a demonstration.